A Multiscale Approach towards the Characterisation of Upper Crustal Deformation at Passive Continental Margins: A Case Study on the Otway Basin, Australia

By

Hugo Bonython Burgin

The Australian School of Petroleum

THE UNIVERSITY of ADELAIDE

This thesis is submitted in fulfilment of the requirements for the degree of

Doctorate of Philosophy

in the Faculty of Engineering, Computer and Mathematical Science,

At The University of Adelaide

The 29th Day of March, 2019

Table of Contents

Thesis Abstract

This thesis presents a multiscale structural analysis of upper crustal deformation at a passive continental margin, using the Jurassic - Quaternary Otway Basin along Australia's southern margin as a case study.

Techniques of structural analyses across the micro (calcite twin, magnetic and porefabric analyses), meso (wellbore and outcrop natural fracture analysis) and macroscales (three-dimensional seismic interpretation) providing an effective means of characterising stress and strain across space and time.

The integration of these investigative methods at a passive continental margin for the first time, has assisted in reducing structural uncertainty for basin evolution models, delivering original insights into the evolution of stress within these tectonic environments. The results of this study show magnitudes of maximum differential stress as high as 69MPa during extension and continental breakup, in contrast to magnitudes as low as 13MPa during basin inversion. The influence of high extensional stresses during continental break up, resulting in layer parallel stretching (LPSt), a microstructural strain which may develop in layered rock, characterised by an azimuth of stretching or thinning, orthogonal to the orientation of regional extensional faults. LPSt occurs in the early stages of extension, prior to the development of calcite twins, natural fractures, and faults which occur progressively as the intensity and duration of extension increases.

This is evidenced in the Otway Basin, where Late Cretaceous aged NE-SW and N-S oriented LPSt is co-axial with extensional azimuths during that time, derived from the stress inversion of seismic scale faults, calcite twins and natural fractures from the outcrop and wellbore. The neotectonic preservation of LPSt in the Otway Ranges, an uplifted section of Early Cretaceous sediments in the Otway Basin, suggests that early grain-scale extensional strain can be

preserved during ensuing phases of inversion at continental margins. As during the process of inversion, stress is primarily released through the reactivation of previously formed extensional fault and detachment systems. A process of deformation that results in low levels of coupling between the basement and cover, an observation that is supported by the low magnitudes of compressional stress (13MPa) calculated during the same period.

Additionally, the results of this study have improved our understanding of sub-surface fluid flow in the Otway Basin. Geomechanical modelling demonstrating that low contemporary magnitudes of effective normal stress, acting on NW-SE oriented faults, striking parallel to the orientation of maximum horizontal stress, results in a high risk of fault dilation. This suggests that future efforts of exploration for conventional oil and gas systems within the Otway Basin, are best focused where E-W, N-S and NE-SW striking faults interact with the major NW-SE fabric, or where the influence of basin inversion is most pronounced.

A major outcome of this study is a new structural framework for the Otway Basin, one that is defined by a consistent pattern of NW-SE striking faults across much of the basin, in contrast to the previous structural model of opposing fault trends in the west and east. The new framework characterises a structural trend that is consistent with faulting patterns in sedimentary provinces to the west and east along Australia’s southern margin.

Declaration

I certify that this work contains no material which has been accepted for the award of any other degree or diploma in my name, in any university or other tertiary institution and, to the best of my knowledge and belief, contains no material previously published or written by another person, except where due reference has been made in the text. In addition, I certify that no part of this work will, in the future, be used in a submission in my name, for any other degree or diploma in any university or other tertiary institution without the prior approval of the University of Adelaide and where applicable, any partner institution responsible for the joint-award of this degree.

I acknowledge that copyright of published works contained within this thesis resides with the copyright holder(s) of those works.

I also give permission for the digital version of my thesis to be made available on the web, via the University's digital research repository, the Library Search and also through web search engines, unless permission has been granted by the University to restrict access for a period of time.

I acknowledge the support I have received for my research through the provision of an Australian Government Research Training Program Scholarship.

Hugo Bonython Burgin **28/03/2019**

Statement of Author's Contribution

The research summarised within the papers and manuscripts that constitute this thesis was undertaken at the Australian School of Petroleum (ASP) at the University of Adelaide and the University of Cergy Pontoise, Paris, France.

As such, some research involved collaboration with my fellow PhD students within the ASP and research staff from other institutions, outside my supervisory team. The contribution of these individuals is evidenced in the author sequence and percentage contribution found within the statement of authorship forms prior to each section.

The research was supported by contributions from the Endeavour Research Fellowship scheme, the American Association of Petroleum Geologists (AAPG), Beach Energy and Santos.

Acknowledgements

Dr Khalid Amrouch: When we met in 2015 your enthusiasm for geology and eagerness to question everything helped me reignite my own love for science. Having you as my supervisor has presented me with many fantastic opportunities: the field trip to Oman, making new friends and connections in Vienna, working towards my PhD in Paris... I never would have imagined geology would allow me to do the things that I have done, and I have you to thank for much of it. I am happy to not only call you my supervisor, but my mentor and friend. Thank you!

Dr Simon Holford: Thanks, for co-supervising my project and providing brief but important input on my study area and feedback on my writing.

Dr Philippe Robion: Thank you, for essentially acting as a third supervisor, **f**or welcoming me to the University of Cergy-Pontoise and guiding me through an integral part of my thesis.

Dr David Kulikowski: Thank you for teaching me how to click.

Dr Tayallen Velathanthem: Thank you for your friendship and support during my thesis and for making the dungeon of the ASP that little bit brighter.

Dad: Thanks for always encouraging me to get the most out of myself and to continue to open new doors and pursue new opportunities.

Mum: Thank you for your love, kindness and un-wavering support throughout my entire life.

Posters, Publications and Manuscripts

Poster Presentations

Burgin, H. B., Amrouch, K. and Rajabi, M. (2016) 4D Fracture Distribution as a Signature of Structural Evolution in the Otway Basin. Poster presentation as part of the Australian Earth Sciences Convention, Adelaide, Australia

Burgin, H.B., Amrouch, K. and Holford, S. (2017) Paleostress Reconstruction from 3D seismic, Natural Fracture and Calcite Twin Analyses: Structural Insights into the Otway Basin, Australia. Poster presentation as part of The European Geological Union (EGU) General Assembly, Vienna, Austria.

Burgin, H. B., Amrouch, K., Kulikowski, D., Rajabi, M. and Holford, S. (2018) Determining Paleo-structural Environments through Natural Fracture and Calcite Twin Analyses: A Case Study in the Otway Basin, Australia. Poster presentation as part of Australian Petroleum Production and Exploration Association conference, Adelaide, Australia.

Burgin, H. B., Amrouch, K., Robion, P. and Kulikowski, D. (2019). An integrated approach to determining 4D stress development at Castle Cove. Poster Presentation as part of the Australian Petroleum Production and Exploration Association conference, Brisbane Australia.

Burgin, H. B., Amrouch, K., Kulikowski, D., Robion, P. (2019) Geomechanical modelling and consequences for fluid-flow in complex rifted settings: A case study in the Otway Basin, Australia. Poster presentation as part of The European Geological Union (EGU) General Assembly, Vienna, Austria.

First Author Peer Reviewed Journal Articles

Burgin, H. B., Amrouch, K., Rajabi, M., Kulikowski, D., & Holford, S. P. (2018). Determining paleo-structural environments through natural fracture and calcite twin analyses: a case study in the Otway Basin, Australia. The APPEA Journal, 58(1), 238-254 (published)

Burgin, H. B., Amrouch, K., Robion, P. and Kulikowski, D. (2019) An integrated approach to determining 4D stress development at Castle Cove. The Australian Petroleum Production and Exploration Association (APPEA) Journal (accepted)

Burgin, H. B. and Amrouch, K. (2019a). Reducing structural uncertainty in complex extensional settings: New insights into the evolution of Australia's South Eastern Passive Margin. (In Prep)

Burgin, H. B. and Amrouch, K. (2019b). 4D structural evolution of Australia's Great Ocean Road Region: The first quantification of paleostress magnitudes at a Passive Continental Margin (In Prep).

Burgin, H. B., Robion, P. and Amrouch, K. (2019). Layer Parallel Stretching? Characterising magnetic and pore fabric styles at a rifted continental margin: New insights from the Otway Ranges, Australia. (In Prep)

Burgin, H. B. and Amrouch, K. (2019c). Exploring the complexities of sub-surface fluid flow at passive continental margins: A case study using geomechanical modelling from the Otway Basin Australia. (In Prep).

Burgin, H. B. and Amrouch, K., (2019d). The structural framework of the Otway Basin: New insights from the Torquay sub-Basin. (In Prep).

Co-Authored Peer Reviewed Journal Articles

Kulikowski, D., Amrouch, K., & **Burgin, H. B.** (2018). Mapping permeable subsurface fracture networks: A case study on the Cooper Basin, Australia. Journal of Structural Geology.

Kulokowski, D., Amrouch, K., Pokalai, K., Mackie, S. I., Gray, M. and **Burgin H. B.** (2019) The intracratonic Cooper and Eromanga Basins, Australia: A Comprehensive Review (in – prep)

Awards and Scholarships

Much of the research within this thesis was made possible due to a number of scholarship schemes and awards for which I am very thankful.

- The Australian Postgraduate Award Scholarship (2016 – 2019)

- The Australian Endeavour Research Fellowship (2017)

- The American Association of Petroleum Geologists (AAPG) Grants in Aid funding scheme (2018)

- The Australian School of Petroleum Award for Postgraduate Research (2018)

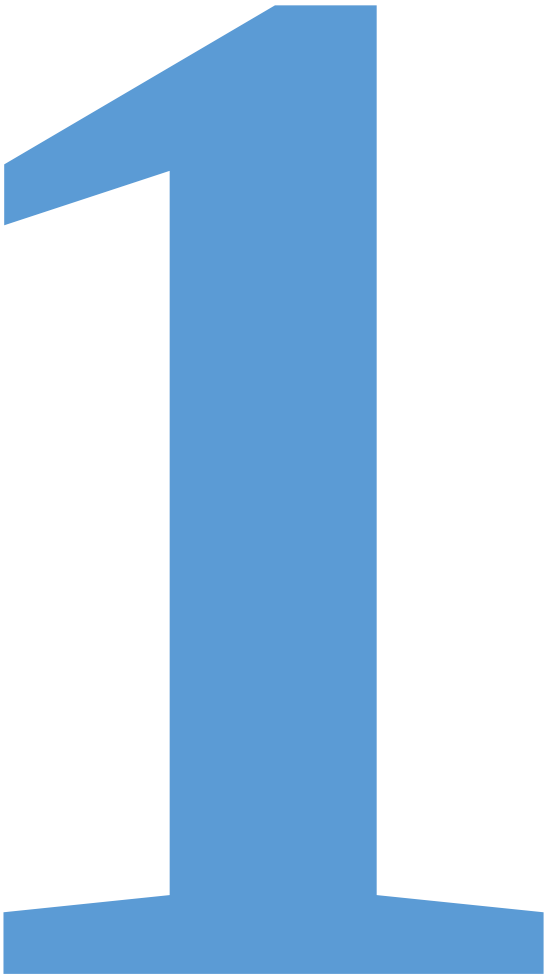

Chapter 1: Contextual Statement of research

The aim of this thesis was to undertake a multiscale structural study of upper crustal deformation at a passive continental margin. The aim being to increase our understanding of how stress of strain evolve across time and space within these tectonic environments.

Previous research using many of the same methods, including calcite twin, natural fracture and petrophysical analysis, have been successful in constraining the tectonic evolution of other plate settings. Especially in stable foreland basins and fold-and-thrust belts such as the Paris Basin (France) (e.g. Rocher et al., 2004) and the Rocky Mountains (North America), (e.g. Amrouch et al., 2010), in many cases redefining the structural understanding of the respective study areas. The integration of these techniques with three dimensional seismic (3D) data, has also proved to be a powerful tool for constraining the structural evolution of subsurface, intra-cratonic sedimentary basins, such as The Cooper-Eromanga Basin (Australia) (Kulikowski and Amrouch, 2017).

In this thesis the chosen case study is the Otway Basin, a Jurassic – Quaternary sedimentary province located along Australia's southern continental margin. A region of great significance to Australia's natural resource sectors; prospective for oil and gas, geothermal energy and hosting Australia's largest carbon capture and storage experiment.

The Otway Basin has seen a significant amount of geological research, however most studies to date that have focused on constraining its structural evolution have been limited to the macroscale (seismic data). The current structural framework of the basin (Krassay et al., 2004) is enigmatic, especially in the eastern Otway Basin where NW-SE striking faults, representative of the main structural trend in the west, supposedly intersect with orthogonal NE-SW striking faults in the Otway Ranges and Torquay Sub-Basin.

The occurrence of these two orthogonally striking sets of faults has resulting in a number of conflicting models for early basin evolution and extension. Which broadly speaking tend to favour either a large scale NE-SW oriented branched rift system (e.g. Etheridge et al., 1987) or oblique styles of rifting where fault strike has not developed orthogonal to the direction of tectonic transport, under NW-SE and N-S azimuths of extension (e.g. Cooper and Hill et al., 1997).

An additional point of debate with respect to the history of the Otway Basin, is the timing and influence of any compressional and inversional tectonic events. With episodes of inversion and subsequent structuring proposed mainly during the Mid-Cretaceous (e.g. Cooper and Hill, 1997) and the Miocene – recent (Holford et al., 2014). Time periods which do not align well with some thermochronological datasets that indicate cooling during the Latest Cretaceous and Early Palaeogene, and that the source rocks of the basin are currently at their maximum burial temperatures (Duddy and Erout, 2001).

This study aims to address the uncertainties with respect to both tectonic extension and compression in the Otway Basin, taking a multiscale approach to structural analysis. Simultaneously demonstrating the effectiveness of this style of investigation at continental margins. The outcomes of this study may have potential consequences for the timing, development and critical moment of petroleum systems within the basin, in addition to future efforts of carbon capture and storage and geothermal energy projects.

Manuscript 1

As prior to this thesis, there were no studies investigating the paleostresses of the study area on the meso (wellbore/outcrop) and micro (grain/crystal) scale, it was necessary to undertake a brief pilot study. Particularly as calcite twin analysis had not been attempted within the basin,

there was a need to ensure that calcite veins were suitable for use with Etechecopar's calcite stress inversion technique. Containing crystals of ample size to measure visually with a universal stage microscope and sufficient levels of twinning to derive a statistically accurate stress tensor.

Natural fractures were interpreted from nine geophysical wellbore image logs in the western basin, and 13 field sites within the Otway Ranges, an outcropping section of Early Cretaceous sediments in the eastern basin. A single paleostress tensor was derived from the use of calcite twin analysis from an outcrop sample, also within the Otway Ranges.

The results of this study indicated that mesoscale fracture evidence for multiple post-Albian structural events, was more complex than previously thought. In particular suggesting the occurrence of a ~NE-SW oriented compressional stress regime, at some point during the basins evolution following the deposition of the Aptian – Albian Eumeralla Formation. A tectonic event, which was inexplicable given the current structural framework of the basin. This study also indicated calcite veins within the Otway Ranges were suitable for further calcite twin analysis studies.

Manuscript 2

As the Otway Basin covers almost 150,000 square kilometres, it was necessary to divide our analysis between the western and eastern portions. In the western Otway Basin, stress inversion of natural fracture data from 11 geophysical borehole image logs was combined with oriented calcite twin samples from the sub-surface, and fault data from four 3D seismic surveys.

Results from this study assisted in constraining the multiscale patterns of deformation across the western Otway Basin, indicating that successive paleostress events were reflected across fault, fracture and calcite twin data. The results essentially refining a previously proposed

model of structural evolution, to include a Post-Albian – Pre Late Creataceous stage of ~NW-SE extension and thermal subsidence, isolated onshore.

A lack of macroscale geological evidence for compressional deformation, such as fault inversion structures, reverse offset or low angle thrust faulting also indicated that the influence of compressional deformation throughout the history of the western Otway Basin is negligible. The results from this study, also providing potential insights into the degree to which plate boundary forces dissipate within intraplate settings, as well as the nature of inversion within the Otway Basin. Which the results suggest is unlikely to have occurred in a ~NW-SE oriented manner, given the high degree of non-co-axiality between horizontal stresses of that orientation and dip directions of major faults.

The study also highlights the degree of structural and spatial uncertainty when working with 2D rather than 3D seismic data, and how a multiscale approach to structural analysis can assist in reducing this. Drawing contrasts between the 3D seismic data interpreted within the results, and a previous study utilising nearby 2D seismic lines, which strike ~NW-SE, parallel to the orientation of major extensional faults.

Manuscript 3

The outcomes detailed within manuscript 1, particularly those indicating a possible NE-SW compressional event, suggested that further fieldwork within the eastern section of the basin, may reveal more about its structural history. During this work a notable outcropping calcite vein, ~5cm in apperture with two generations of calcite crystals, was discovered in the Eumeralla Formation at Castle Cove. A location supposedly characterised by the Castle Cove Fault, a ~NE-SW trending inverted normal fault that has shaped the evolution of the cove (Debenham et al., 2018). The discovery of this vein provided a unique opportunity to undertake

a local case study, integrating multiple techniques of structural analysis across the micro and mesoscale.

Stress inversion of stylolites, calcite twins and natural fractures were paired with three samples of magnetic fabric analysis to investigate the nature of paleostress and strain at Castle Cove. As a consequence, the study determined 5 phases of stress development at Castle Cove, including the influence of an early ~NW-SE oriented maximum horizontal stress during the Mid Cretaceous, two stages of ~N-S and NE-SW oriented extension during the Late Cretaceous and a ~NE-SW oriented strike slip or compressional phase at some point between the end of Late Cretaceous rifting, and stress reorganisation in the Late Miocene.

The findings also showed a lack of multiscale evidence for the presence of the ~NE-SW trending inverted Castle Cove Fault. Characterised by the preservation of extensional, petrophysical rock fabrics, a lack of low angle fractures and thrust faults and no evidence of ~NW-SE oriented compression within calcite twin data, which is highly sensitive. Raising further questions with regard to the structural style of the eastern Otway Basin and in particular the nature of basin inversion.

Manuscript 4

This study addresses the findings of manuscript 1 and manuscript 3, further integrating outcrop fracture data with geophysical image logs, 3D seismic and calcite twin analysis. The results of this manuscript provide original insights into the evolution of stress at passive continental margins.

The structural analysis of three 3D seismic surveys, positioned immediately SW from the outcropping Otway Ranges, provided the opportunity to study what is essentially the offshore continuation of the structure. This was combined with natural fracture and fault analysis in five

geophysical image logs and 31 field sites throughout the Otway Ranges. In addition to the application of Etchecopar's calcite stress inversion technique on 12 calcite vein samples from throughout the Otway Ranges.

From 3D seismic interpretation, structures that had previously been interpreted as ~NE-SW trending anticlinal folds were revealed to actually comprise a ~NE-SW trending network of inverted, ~NW-SE striking detachment faults. Structural evidence for fault inversion within the system being most obvious above sections of underlying shallow basement.

These observations were supported with natural fracture analysis from the outcropping section of the structure, within the Otway Ranges. Fracture analysis showing a complex network of 11 fracture sets (6 major and 5 minor) characterising five main phases of basin evolution. Phase 1 and phase 2, defining ~NE-SW and radial continental rifting at the start of the Late Cretaceous. Phase 3 outlining a period of ~NE-SW oriented strike slip and compressional basin inversion, beginning in the ~Mid-Maastrichtian. With phases 4 and 5 defining compressional relaxation, continental separation and eventual reorganisation to the environment of in situ stress.

Paleostress tensors derived through calcite stress inversion further support this model, with calculated stress magnitudes displaying a distinct pattern. One that is defined by magnitudes of maximum differential extensional stress, as high as 69MPa, during continental separation and as low as 13MPa during basin inversion. When compared to previous studies in foreland basins and fold-and-thrust belts, the magnitudes calculated in this study represent some of the highest extensional paleostress values determined to date. Suggesting that extensional paleostresses of this magnitude, may uniquely define the evolution of stress at passive continental margins.

The high extensional stresses are explained due to the intensity of extensional deformation during continental break up, especially when rifting occurs following a period of tectonic

quiescence and minimal faulting. In contrast, the low compressional stresses during basin inversion are attributed to the release of stress through the reactivation of the extensional detachment surface, and existing network of extensional faults and fractures. In the Otway Ranges, this effect corresponds to low levels of compressional deformation on the mesoscale.

With respect to the framework of the Otway Basin, the structural model suggested within this study proposes that ~NW-SE striking faults dominate the structural framework of the eastern basin and Otway Ranges. The results suggesting that no orthogonal change in fault strike occurs from west to east within the sediments of Otway Basin. The NE-SW trend of the Otway Ranges explained by its isolation above an enigmatic section of shallow underlying basement, which assisted in isolating the release of stress during basin inversion.

Manuscript 5

Given the nature of the proposed model for basin inversion in manuscript 4, it was pertinent to apply two microstructural techniques of analysis within the Otway Ranges. In an attempt to constrain the nature and orientation of internal deformation and link its development to the evolution of stress within the region.

The anisotropy of magnetic susceptibility (AMS) and anisotropy of P-wave velocity (APWV) was determined on 16 outcropping samples within the Otway Ranges. The results showing a well-defined magnetic and pore fabric, indicative of ~N-S and ~NE-SW oriented extensional tectonic deformation. Of particular note in the results, is the defined phase of layer parallel stretching (LPSt) an extensionally driven counterpart to the well documented phenomenon of layer parallel shortening (LPS).

It is proposed in this paper that LPSt occurs during the first stage of extensional deformation, prior to the development of mesoscale features – such as fractures - and the tilting of the

bedding. In the Otway Ranges these extensional petrofabrics were preserved during inversion, as stress was released mainly through the reactivation of the top basement decollement zone. A feature that is well documented in compressional settings (e.g. Robion et al., 2007) and typical of low levels of coupling between the basement and cover. An insight which provides further evidence for the presence of a top basement detachment zone within the eastern Otway Basin, and the structural model of evolution presented in manuscript 4.

As this study represents the first characterisation of grain-scale strain at a rifted margin, there is no basis for comparison. That being said given the intensity of extensional deformation documented within manuscript 4, which is defined by values of maximum differential stress as high as 69MPa. It is suggested that the development LPSt may be dependent upon high extensional stress magnitudes, especially in basin units that are largely unaffected by faulting prior to the onset of extensional deformation and continental break up.

The results also support the occurrence of ~NW-SE striking faults within the Otway Ranges, suggested by the findings of manuscript 4. Making a significant contribution towards redefining the structural architecture of the Otway Ranges and the eastern Otway Basin.

Manuscript 6

As the Otway Basin is an important natural resource for Australia and given the vast amount of geophysical data interpreted within manuscripts 2, 4 and 5. It was pertinent to investigate the complexity of sub surface fluid flow within the basin, and attempt to use the region as a case study for other passive margin sedimentary basins. In doing so, taking into account the debate surrounding the in situ stress regime of the basin, which has been interpreted as compressional, strike slip and extensive in recent times (Tassone et al., 2017).

The geomechanical modelling of dilation tendency on faults, from eight 3D seismic surveys was completed alongside the stability of natural fractures, extracted from 7 well bore image logs. Modelling of fault dilation tendency indicated that high angle (50-90º) ~NW-SE striking faults, trending parallel to the orientation of maximum horizontal stress are at a high risk of dilation, largely irrespective of the regime of in situ stress. This is due to low levels of effective normal stress in the horizontal plane under strike slip and extensional regimes of in situ stress. Under a compressional stress regime, this window of risk increases to include ~NW-SE striking faults of all dip angles. While under an extensional stress regime, low angle (10-30º) ~NW-SE striking faults are at a low risk of dilation. The complimentary modelling of fracture stability in this study also indicated that increases in pore pressure required for fracture reactivation, are lowest under a strike slip stress regime. Requiring less than 5MPa in order to be reactivated.

The results of the modelling were contrasted with the style of successful and unsuccessful hydrocarbon fields within the Otway Basin, and the distribution of volcanic material and shallow cave systems. Displaying good correlation in both cases and suggesting that the results of the modelling may be reflected by geological evidence.

The outcomes of this study also have specific implications for any future unconventional hydrocarbon production within the Otway Basin. As the low reactivation pressure of natural fracture networks and the high likelihood of dilated faults, suggests a potentially high risk of up-dip contamination of regional groundwater systems, which are important in the region. Additionally, this case study in the Otway Basin may provide lessons for other frontier continental margin basins, such as the Ceduna Sub-Basin, which displays a similar relationship between in situ stress and fault geometry.

Manuscript 7

Because of the insights provided in the preceding manuscripts, and other recent studies the structural framework of the Otway Basin required revising. This study presents the final piece of the "structural puzzle," in the interpretation of the Torquay 3D seismic within the Torquay Sub-Basin, at the eastern margin of the Otway Basin.

The results from this study support theories from manuscript 4 and manuscript 5, that ~NW-SE striking faulting continues to dominate the structural architecture of Otway Basin sediments, into its eastern most sections. Characterising a structural trend that is more consistent from east to west within the basin, and between the neighbouring sedimentary provinces along Australia's southern margin. An insight that suggests the existing structural framework, incorporating two orthogonally striking fault networks that intersect within the Otway Ranges is unlikely.

As a result, a new structural map of the basin was produced, incorporating the multiscale evidence from the preceding manuscripts and other modern works within the region.

References

Amrouch, K., Lacombe, O., Bellahsen, N., Daniel, J. M., & Callot, J. P. (2010). Stress and strain patterns, kinematics and deformation mechanisms in a basement-cored anticline: Sheep Mountain Anticline.

Cooper, G. T., & Hill, K. C. (1997). Cross-section balancing and thermochronological analysis of the Mesozoic development of the eastern Otway Basin. The APPEA Journal, 37(1), 390-414Wyoming. Tectonics, 29(1).

Duddy, I. R., & Erout, B. (2001). AFTA-calibrated 2-D Modelling of Hydrocarbon Generation and Migration Using Temispack: Preliminary Results from the Otway Basin. Eastern Australasian Basins Symposium (485-497).

Etheridge, M. A., Branson, J. C., & Stuart-Smith, P. G. (1987). The Bass, Gippsland and Otway basins, southeast Australia: a branched rift system formed by continental extension

Holford, S. P., Tuitt, A. K., Hillis, R. R., Green, P. F., Stoker, M. S., Duddy, I. R. and Tassone, D. R. (2014). Cenozoic deformation in the Otway Basin, southern Australian margin: implications for the origin and nature of post-breakup compression at rifted margins. Basin Research, 26(1), 10-37. doi: 10.1111/bre.12035

Krassay, A. A., Cathro, D. L., & Ryan, D. J. (2004). A regional tectonostratigraphic framework for the Otway Basin.

Kulikowski, D., & Amrouch, K. (2017). Combining geophysical data and calcite twin stress inversion to refine the tectonic history of subsurface and offshore provinces: A case study on the Cooper-Eromanga Basin, Australia. Tectonics, 36(3), 515-541.

Robion, P., Grelaud, S., & de Lamotte, D. F. (2007). Pre-folding magnetic fabrics in fold-and-thrust belts: Why the apparent internal deformation of the sedimentary rocks from the

Minervois basin (NE—Pyrenees, France) is so high compared to the Potwar basin (SW—Himalaya, Pakistan). Sedimentary Geology, 196(1-4), 181-200.

Rocher, M., Cushing, M., Lemeille, F., Lozac'h, Y., & Angelier, J. (2004). Intraplate paleostresses reconstructed with calcite twinning and faulting: improved method and application to the eastern Paris Basin (Lorraine, France). Tectonophysics, 387(1-4), 1-21.

Tassone, D. R., Holford, S. P., King, R., Tingay, M. R., & Hillis, R. R. (2017). Contemporary stress and neotectonics in the Otway Basin, southeastern Australia. Geological Society, London, Special Publications, 458, SP458-10.

2

Chapter 2: Literature Review of the Study Area: Australia's Otway Basin – Tectonic Setting, Structural Evolution and Hydrocarbon Systems

2.1 Introduction – The Otway Basin

Australia's southern margin underwent its first extensional event during the breakup of the super continent Gondwana, from approximately 164-145 Ma (Leven et al., 1990), responsible for the formation of the en-echelon series of sedimentary basins straddling its coast line, the Bight, Otway and Gippsland Basins (Boeuf & Doust, 1975; Leven et al., 1990; Norvick & Smith, 2001; Perincek et al 1994a). Rifting along the southern margin began in the west, in the Bight Basin, during the Callovian (Mid-Late Jurassic), having propagated east towards the Otway Basin by the Tithonian (Late Jurassic – Early Cretaceous) (Lyon et al. 2007; Norvick & Smith, 2001) (**fig. 1**).

The Otway Basin (**fig. 2**) trends largely NW-SE and extends within on and offshore parts of South Australia, Victoria and Tasmania (Krassay et al, 2004) over a geographical area of approximately 60,000km^2 from Cape Jaffa in the west, to the Mornington Peninsula in the east (Gallagher and Holdgate, 2000). To the SE the basin is continuous with the Sorrell Basin (Moore et al. 2000), to the east with the Bass Basin (Hill et al. 1995), to the west by the Bight Basin (Wilcox and Stagg, 1990) and is bound to the north and north east by the Paleozoic and Proterozoic basement rocks of Victoria's ancient fold belts (Cayley et al. 2002: Krassay et al. 2004).

Since the early commercial discovery of hydrocarbons within the North Paaratte-1 well in 1979 in Victoria (Geoscience Australia, 2014) the Otway Basin has been one of the most explored basins in Australia. Over 200 wells have been drilled within on and offshore sections of the basin and at least 35,000km of 2D seismic and 10,000km^2 of 3D seismic has been acquired,

concentrated mainly within South Australia and Victoria. Despite these efforts, commercial discoveries have been limited to isolated dry gas fields totalling close to two trillion cubic feet (O'Brien et al. 2009) well beneath the scale of Australia's other basins such as the Cooper, Gippsland and Carnarvon.

This literature review outlines the tectonic setting of the Otway Basin, with a focus on its structural evolution and hydrocarbon prospectively.

2.2 Geological Setting of the Otway Basin

2.2.1 Evolution and Tectonic History of the Otway Basin

Initial rifting along the southern margin of the Australian continent began during the Callovian (Mid-Late Jurassic) at the western edge of the Bight Basin, with rifting having propagated east into the Otway Basin by the Tithonian (Late Jurassic – Early Cretaceous) (Norvick & Smith, 2001). In the past, the southern margin of the Otway Basin was confined by Antarctica and a 'triple point plate' junction, a boundary that is now marked by Western Tasmania and the West Tasman Rise (Gibson, Morse, Ireland, & Nayak, 2011). Along its northern edge, the basin includes thin aprons of sediment of which small outcrops are visible today (e.g. Marino High) bounded by Paleozoic and Proterozoic basement (Ball et al., 2013; Krassay, 2004). Within the deepest sections of the basin sediment thickness is approximately 12km composed of ~6km of Early Cretaceous units, ~4km of Late Cretaceous units and ~2km of Tertiary deposits (Birch, 2003). The western margin of the basin in South Australia is bounded by the N-E trending Trumpet Fault near the town of Robe (Drexel & Preiss, 1995; Morton & Dextral, 1995). The Eastern margin is marked by the highly faulted Sorell Zone east of the Torquay Sub-basin and the Mornington Peninsula.

The majority of studies within the Otway Basin (**fig.3**) divide its tectonic history into five main phases which are generally agreed upon within most of the current literature. They include; initial rifting during the Early Cretaceous, a post-rifting event of basin compression and inversion during the Mid-Cretaceous (post Albian), renewed rifting in the Late Cretaceous, a and a "recent" change to a tectonic environment of compression from the Miocene to the present day (Holford et al. 2014).

2.2.1.1 Late Jurassic to Early Cretaceous Initial Rifting

Early rifting within the Otway Basin was primarily isolated onshore (Krassay et al. 2004; Lyon et al. 2007) and was responsible for the formation of a series of half-grabens continuous with the regional coastline, mainly defined by landward dipping faults (**fig.4**) (Palmowski et al. 2001; Lyon et al. 2007; Briguglio et al. 2015). Despite a large amount of research, the orientation and extensional lineation of the initial rifting event within the Otway Basin remains under debate. Early works suggest an extensional lineation oriented ~NW-SE, producing ~NW-SE and ~W-E striking faults as a product of oblique extension (Wilcox and Stagg, 1990: O'Brien et al. 1994), others propose a ~NE-SW lineation more normal to regional fault patterns (Perincek et al 1994b; Teasdale et al. 2003) in addition to ~N-S rifting (Hill et al. 1994; Finlayson et al. 1998; Lyon et al. 2007). Much of the regional debate on rifting orientation can be attributed to the paradox of near-orthogonal structural grains within the Otway Basin, particular in the eastern half of the Basin and the Otway Ranges (**fig. 5**) (Cooper, 1995).

Briguglio et al. (2015) has presented the most detailed insight into the evolution of basin wide depocentres during the Early Cretaceous to date. Through the use of extensive 2D seismic mapping across much of the onshore basin, the study shows that the deposition of many early basin units were controlled by the displacement, linkage and growth rate of faults, which varied

significantly across the basin. Extension during the Early Cretaceous was as much as 21% in the western basin and far less in the east (Cooper and Hill, 1997; Briguglio et al. 2015).

Initial rifting within the Otway Basin came to a close at the end of the Hauterivian (Early Cretaceous), when rifting is believed to have shifted offshore and south of the Tartwauop Fault Zone. Thus leaving many of the Early Cretaceous depocentres, such as the Penola Trough, as failed rift structures (Palmowski et al. 2001; Lyon et al. 2007). The influence of post-rift subsidence across the basin increased into the Berremain and Albian periods replacing fault growth as the main driver behind the creation of accommodation space (Palmowski et al. 2001; Lyon et al. 2007).

2.2.1.2 Mid Cretaceous Basin Inversion

Following the cessation of initial extension and the deposition of the widespread Eumeralla Formation, the Otway Basin is believed to have experienced basin wide ~NW-SE compression (**fig. 6**). Resulting in uplift and erosion responsible for an unconformity at the top of the Eumeralla Formation (Krassay et al. 2004). This uplift was originally attributed to thermal uplift accompanied by compression by Smith (1988) based on the analysis of 2D seismic reflection data in the eastern basin. Although is now known to be synonymous with regional uplift and denundation across much of eastern Australia (Noll and Hall 2003; Hill et al. 1995; Palmowski et al. 2004; Norvick and Smith 2001).

In this period it has been proposed that reverse reactivation along basin forming normal faults was responsible for accommodating inversion (Hill et al. 1995; Krassay et al. 2004) there is very little evidence for fault inversion as few present day faults display reverse offsets along with a distinct lack of thrust faulting, especially within the western basin (Lyon et al. 2007). Within this period, the Otway Ranges was possibly uplifted due to 8-10% shortening, isolating

the Torquay Sub Basin from the more western sectors of the basin (Hill et al. 1995; Hill and Cooper 1996; Cooper and Hill, 1997). This period along with the Miocene – recent inversional event is discussed in greater detail in the coming section.

2.2.1.3 Renewed Late Cretaceous Rifting

Although sea floor spreading was slow (Veevers et al. 1991) rifting and the creation and growth of normal fault networks recommenced during the Late Cretaceous (Palmowski et al. 2001; Noll and Hall 2003; Robson et al. 2016, 2017, 2018). The creation of a hinge zone, south of the initial Early Cretaceous fault zones produced a series of ~NW-SE trending offshore depocentres along with the creation of wide-spread seaward dipping fault networks (Palmowski et al. 2001). As with the lineation of initial rifting, extensional directions within this period have also been debated with N-S to NE-SW (Perincek et al. 1994b), exclusive N-S (Miller et al. 2002) and more oblique ~NE-SW (Schneider et al. 2004) rifting all proposed.

Stages of fault growth within this period have been studied in detail by a series of works by Robson et al. (2016, 2017 and 2018). In the western basin, ~NW-SE striking normal faults were found to have nucleated at the start of the Late Cretaceous, linked to deeper ~W-E striking basement fabrics, experienced a period of dormancy during the middle-Late Cretaceous followed by additional fault nucleation and growth into the latest Cretaceous along with continued growth into the Cenozoic (Robson et al. 2017). In the eastern basin, highly variable fault growth of ~NW-SE striking basement linked faults, began in the early Turonian, continuing into the latest Maastrichtian resulting in the development of a series of hard linked fault arrays (Robson et al. 2016). Additionally, the presence of wide-spread sinistral transtensional features within the Shipwreck Trough (Robson et al. 2018) has shown this sector

of the basin experienced a significant degree of strike slip influence through this stage of rifting, as suggested by earlier works (Palmowski et al. 2004; Stacey et al. 2013).

This secondary phase of rifting led to continental break up to the west, within the Bight Basin (Norvick and Smith, 2001) and was eventually deflected southward, beneath Tasmania within the Otway Basin, leaving the Torquay Sub Basin and the Bass Basin as failed rift structures (Hill et al. 1995).

2.2.1.4 A Shift to Fast Seafloor Spreading

The first creation of oceanic crust between Australia and Antarctica in the Mid Eocence at approximately ~44Ma marked a shift to faster spreading and a continental drift regime (**fig. 2**) (Royer and Rollet 1997; Norvick and Smith 2001). In the Otway Basin, this faster environment of drift led to thermal subsidence wide spread marine transgression and the collapse of continental margins (Norvick and Smith, 2001). Due to this increase in drift, the Sorrel Fault Zone in the eastern basin saw thousands of kilometres of transform strike-slip motion (Moore et al. 2000; Miller et al. 2002; Palmowski et al. 2004).

2.2.1.5 Stress Reorganisation and Miocene to Present Day Compression

The mid Miocene is believed to have represented a period of stress reorganisation to ~NW-SE compression throughout much of south east Australia, resulting in fault inversion, folding and uplift all most pronounced within the eastern Otway Basin within the Otway Ranges (Perincek et al. 1994b) Krassay et al. 2004; Palmowski et al. 2001; Hill et al. 1995). Many studies have used the analysis of petroleum industry data, largely borehole break out and drilling induced tensile fracture data, which support a ~NW-SE maximum horizontal stress orientation (**fig. 7**)

as evidence for this compressional environments of stress (Tassone et al. 2017). This state of compressional stress within south east Australia has been attributed to changes in plate motion between the Pacific and Indo-Australian Plate (Dickinson et al. 2002; Sandiford 2003a).

This is largely due to the arc collision of Australia with SE Asia at Australia's northern plate boundary combined with southern ridge push forces from the spreading centre and collisional forces at the eastern plate boundary with New Zealand (Hill et al. 1995; Sandiford 2003a; Nelson et al. 2006). In the Otway Basin uplift of the Otway Ranges has also been attributed to igneous under plating due to large scale extension and detachment faulting along upper plate boundaries has also been suggested by Lister et al. (1991), although this theory is has not been explored by any other authors. In contrast to fault related uplift, which is the favoured model by most authors, it has been suggested that late Pliocene and Quaternary uplift and sea level changes were caused by Quaternary glacial episodes resulting in an unconformable relationship between Quaternary and Pliocene strand line systems (Wallace et al. 2005). These uplift and compressional events will be discussed in greater detail in section 3.3

2.2.2 Stratigraphy of the Otway Basin

Since 1962 (McQueen, 1962) the stratigraphy of the Otway Basin has been subjected to numerous studies (e.g. Leslie 1966; White 1968; Reynolds et al. 1966) with these early works based mainly on palynological, palaeontological and petrographic data from on-shore petroleum wells, outcrop data and limited off-shore samples (Moore et al. 2000; Tassone, 2014). Prior to the establishment of a basin wide tectonostratigraphic framework through extensive 2D seismic mapping by Krassay et al. (2004), the stratigraphy of the basin was highly confusing, with almost 200 formation names and the on-going changing of unit names (Boult et al. 2002) likely due to units being correlated on their palaeontology rather than their lithology

(Glenie, 1971). Substantial structural variations between the basin's western and eastern portions have led to studies based in South Australia and Victoria placing varying emphasis on different stratigraphic divisions (Birch, 2003).

The effort to redefine basin wide stratigraphy by Krassay et al. (2004) (**fig. 3**) was largely successful with the majority of recent works adopting the framework. This work divided basin wide sedimentary succession into eight super-sequence scaled stratigraphies across seven varying tectonic basin phases. From oldest to youngest, the super sequences include the Crayfish Supersequence, which includes the reservoir and source rocks of the Pretty Hill Formation, Sawpit Shale and Sandstones and Laira and Casterton Formation. The Eumeralla Supersequence, which includes the Eumeralla Formation, recognised as the major source rocks within eastern parts of the basin (O'Brien et al. 2009). The Shipwreck Supersequence, containing the reservoir Flaxman and Waarre formations along with the Belfast Mudstone, Sherbrook, Wangerrip, Nirranda, Heytesbury and Whalers Bluff Supersequences. This work differs from other recent studies as it includes sediments within the "Gambier Basin" as being within the greater Otway Basin, while they were identified as a separate basin by Boult and Hibburt (2002). Though widely used, improvements to the framework can still be made as the identification of a number of units within the Sherbrook Supersequence, especially the Belfast Mudstone, remains a challenge (Tassone, 2014). Partridge (2001) gives a descriptive revised stratigraphy of the Sherbrook Group which in part addresses this shortcoming (Tassone, 2014).

As the works within this thesis are largely focussed upon the structure of the Otway Basin, rather than the stratigraphy, it is not discussed further. For detailed lithological descriptions of various units and more in depth chronological distributions it is recommended that the reader consult Krassay et al. (2004).

2.2.4 In-situ Stress of the Otway Basin

The in-situ stress tensor is composed of both the orientations and magnitudes of the three principal stresses (Anderson, 1951). Maximum horizontal stress orientation within the Otway Basin has been constrained by many scientific works (eg: Hillis and Williams, 1992, 1993; Hillis 1995; Hillis and Reynolds, 2000; Mildren and Hillis, 2000; Reynolds and Hillis, 2000; Reynolds et al. 2003; Nelson et al. 2006; Van Ruth et al. 2006; Bailey et al. 2014. 2016; Rajabi et al. 2017; Tassone et al. 2017) and has shown to be approximately ~135° NW-SE (Tassone et al. 2017), which is believed to primarily reflect the increased coupling of the Australian and Pacific plate boundaries associated with uplift in southern New Zealand since the late Miocene to early Pliocene (Sandiford et al. 2004).

Within the central and eastern Otway Basin the magnitude of maximum horizontal stress has been determined on two occasions, both through the application of the expanded frictional limit theory. Nelson et al. (2006) determined a value of approximately 29MPa/km within the western basin increasing to 37MPa/km in the east. While Vidal-Gilbert et al. (2010) determined a value of 27MPa/km and Berard et al. (2008) a much lower gradient of 18.75MPa/km down to depths of 2km.

Due to the large amount of petroleum industry data within the Otway Basin, the magnitude of minimal horizontal stress has been published on a number of occasions (Nelson et al. 2006; Vidal-Gilbert et al. 2010; Hillis 1995) including a thorough central and eastern basin regional review by Tassone et al. (2017) using eighty-nine LOTs (**fig. 8**) from 73 vertical wells with all data of D quality. This review showed that σh values vary significantly with lithology and depth within the basin, the highest best-fit gradients present within the marl and carbonate formations at 20.3 MPa/km and 21.2MPa/km for the central and eastern basin respectively and

the lowest gradients within the sands and undifferentiated sands/shale formations at gradients of 15.4MPa/km and 17.9MPa/km for the central and eastern regions. These values were relatively consistent with the gradients determined by Nelson et al (2006) of 18.5MPa/km with a lower limit of 15.5MPa/km, Van-Ruth (2007) of 14.5MPa/km and Berard et al. (2008) of 15.98MPa/km. Vertical stress gradients (**fig. 9**) have also been determined within a number of these studies. Drawing on the most recent review of regional neotectonics by Tassone et al. (2017) it was found that as with minimum horizontal stress, vertical stress gradients vary across the basin, but in general the regional gradients are between 22MPa/km and 24MPa/km with evidence for gradients as high as ~26MPa/km where older, denser rocks have been exhumed. This range is slightly higher than the result determined by Vidal-Gilbert et al. (2010) of 21.45 MPa/km and that of Berard et al. (2008) of 20.7MPa/km.

Pore pressure gradients reviewed from Tassone et al. (2017) within the Otway Basin show considerable variation with geographic location and are consistently above the hydrostatic gradient assumed by Nelson et al. (2006). In the central Otway Basin, gradients lie between 10MPa/km and 14MPa/km and in the case of one well, as high as ~16.5MPa/km, in the eastern basin pore pressure are on the whole, lower, lying between ~10MPa/km and ~12.5MPa/km. Vidal-Gilbert et al. (2010) determined a pore pressure gradient of approximately 8.64MPa/km at the CO2 CRC site in February 2008, prior to the injection of CO2 but following the production of gas within the unit.

Whilst the orientation of maximum horizontal stress, and the orientation of the entire tensor has been consistently interpreted, the stress regime has been interpreted as normal, strike slip and reverse across most of the basin. Determining the relative magnitudes of the in-situ stresses, and the in-situ stress regime has been a complex problem, especially when stress data from the petroleum industry related datasets is compared to neotectonic evidence of faulting and folding (Tassone et al. 2017).

As this thesis is predominantly concerned with the analysis of paleo stresses, although the proposed in-situ stress regimes for the basin are often considered, more detailed descriptions are not provided here. For a detailed analysis of both neotectonic deformation and petroleum industry data it is recommended the reader consult Tassone et al. (2017) which provides a comprehensive insight into the neotectonics of the Otway Basin.

2.3 Structural Framework of the Otway Basin

2.3.1 Extensional Origins

Typically speaking many recent structural studies within the Otway Basin are concerned with structuring associated with the accumulation of hydrocarbons (e.g. Lyon et al. 2007; Schneider et al. 2004; Robson et al. 2016) although other studies have analysed basin wide evolution (Etheridge 1985; Moore et al. 2000; Teasdale et al. 2003; Krassay et al. 2004; Stacey et al. 2013; Briguglio et al. 2015). Generally speaking the basin is recognised to have a variable structural style from the west (**fig. 5, fig. 10)**, within South Australia to the east within Victoria and Tasmania (Krassay et al. 2004) generally divided by the differing structural trends identified within Early Cretaceous sedimentary units (Hill et al. 1995; Finlayson et al. 1996; Miller et al. 2002). Onshore in the western basin high angled ~NW-SE and W-E striking normal faults that dip northward dominate the structuring (Miller et al. 2002; Lyon et al. 2007), while offshore high angle normal faults that dip towards the south are most obvious (Robson et al. 2017). In the eastern basin NE-SW striking NW dipping normal faults and N-S striking extensional and sinistral strike slip faults dominate basin architecture, a number of which are thought to have been inverted during compressional events (Perincek et al. 1994b; Miller et al. 2002; Debenham et al. 2018) although it is worth noting, few inversional structures have been

clearly observed in 3D and have been published, although Holford et al. (2011; 2014) assumed a model where normal offset along reactivated faults was maintained.

A number of early works suggested that basement terranes (**fig. 11**) have played a significant role in shaping the structural architecture of the basin. For example Hill et al. (1995) used 2D seismic data to essentially show the variation of fault systems across two distinct basement provinces in the eastern basin, while Teasdale et al. (2003) modelled the effect of basement terranes using a multitude of large scale geophysical data including, gravity, aeromagnetic and seismic data. Basement influence has been studied at a higher resolution in the western basin, where Lyon et al. (2007) used 2D and 3D seismic analysis to investigate the influence of deep seated basement faults on the evolution of Early and Late Cretaceous normal faults in the Penola Trough. Miller et al. (2002) also attributed the variation in fault strike across the basin to rheological differences between neighbouring basement terranes, especially as they respond to crustal extension.

Gibson et al. (2011) proposed that architectural basement features left over from the late Neoproterozoic, such as the Avoca-Sorrell Fault were re-activated during the mid-late Mesozoic, heavily influencing continental rifting and basin development during this period. Gibson and Totterdell et al. (2013) expand on this concept and present a convincing case for early basement controlled faulting at the time of basin formation within the Otway Basin proposing that the varying structural trends in basin sediments, from west to east across the basin are a result of differential environments of stress throughout its sectors, which they attribute to basement architecture. The authors propose that the predominantly NW – SE structural fabric in the western half of the Basin and the almost orthogonal NNE – SSW fabric in the eastern half have been heavily influence by the compartmentalisation of strain within the

Coorong Shear Zone (west) and Avoca-Sorrell Fault Zone (east) (**fig. 12**). In particular they give additional evidence to the theory that basement rocks beneath the Western half of the Otway Basin are similar to that of the Gawler Craton remaining from the breakup of the Rodinia supercontinent.

The concept of the reactivation of basement features by Gibson et al. (2011) coincides with studies by other authors that show evidence for significant sinistral transtension along this fault zone – also known as the Sorrell Fault Zone. Miller et al. (2002), Hill et al. (1994)and Krassay et al. (2004) all agree that this zone was responsible for the significant partitioning of high angle N-S strike-slip faulting with the perhaps the best evidence coming from Robson et al. (2018) who observed sinistral releasing jog structures typical of transtension (**fig. 13**). This zone essentially marks the transition from a typical passive margin environment in the western most basin to the failed rift structuring of the Bass Basin and uplifted highlands to the east (Hill et al. 1994; Robson et al. 2018). Irrespective of their origins, the varying structural features across the Otway Basin have been well mapped (e.g. Gloe et al. 1998; Smith, 1998) although the first most major study, labelling numerous sub-basins and fault zones was Moore et al. (2002) (**fig. 14)** which employed extensive 2D seismic analysis, dividing the basin into six provincial depocentres including the inner Otway Basin, Beach Port Sub-Basin, Morum Sub-Basin, Discovery Basin high, Hunter Sub-Basin and Nelson Sub-Basin neighbouring the Sorell Basin off the western coast of Tasmania. This initial work was then updated as part of the extensive tectonostratigraphic framework by Krassay et al. in 2004. Using Moore et al. (2000) as a basis the study identified additional structural features that required individual identification including the Penola Trough, Shipwreck Trough and Torquay Sub-Basin. In addition to a variation of structural styles from west to east, it has also been shown by Palmowski et al. (2004) that whilst in both cases, sedimentation rates were equal to extensional rate, suggesting subsidence as the main driver, rates of extension were almost double in the

eastern Shipwreck Trough during the Late Cretaceous than what they were within the Penola Trough. Suggesting that throughout the basins history extension rates have varied spatially across the basin (Palmowski et al. 2004).

2.3.2 Basin Inversion and Exhumation

Generally speaking there is a widespread consensus within much of the current literature that the Otway Basin has experienced two periods of uplift, which in general have both been attributed to ~NW-SE compressional forces resulting in the inversion of basin forming normal faults (**fig. 15**) (Hill et al. 1995; Cooper and Hill, 1997; Krassay et al. 2004 Edwards, 1996; Debenham et al. 2018). Whilst they have largely been considered to have affected the entire Otway Basin (Krassay et al. 2004) differences in vertical motions and resulting exhumation between the west and east have been identified (Palmowski et al. 2001; Tassone et al. 2014). Early evidence from Gloe et al. (1988) suggested that the presence of Palaeocene-Eocene coals at 300-360m within the 600m Otway Range, that sit unconformable on top of the outcropping Eumeralla Formation provided evidence for a limited amount (e.g. <300m) of exhumation (Hill et al. 1994). As scientific works progressed in detail so did the estimated degree of uplift. Aside from exhumation additional evidence for these events of compression affecting the basin has been presented using the 2D seismic analysis of a number of low wave length fold structures within the offshore basin, with Holford et al. (2014) presenting evidence for multiple periods of post break up compression (**fig. 16**). These events have been generally thought to be responsible for the formation of the Otway Ranges, Minerva Anticline, Crowes Anticline, Loch Ard Anticline, Pecten Anticline and Curdi Monocline (Holford et al 2014, Tassone et al.2014). Additional work utilising 2D seismic restoration techniques have been used by Hill and Cooper

(1996) who constructed a balanced cross section across the Otway Ranges, in the eastern part of the basin, also incorporating thermochronological virtinite reflectance data.

A series of other studies have used similar techniques incorporating vitrinite reflectance studies (e. g. Duddy et al. 1993; Cooper and Hill, 1997; Green et al. 2004) in order to constrain events of exhumation and uplift. These works suggest a cooling events occurring during the mid-Cretaceous, and post Campanian – pre-Miocene. The degree of removed section across the basin varies considerably with estimates ranging from 3.5km (Cooper and Hill, 1997) in the east to 1.5km across the Mussel Terrace (Duddy and Erout, 2001; Duddy et al. 2003), with major exhumation believed to be concentrated around the eastern most coastline of the Otway Ranges (Hill et al. 1995).

More recent work by Tassone et al. (2014) (**fig. 17**) and Tassone (2014) has continued to explore the theme of exhumation. Tassone et al. (2014) utilized sonic transit time analyses in order to produce estimates of net exhumation across the entire Otway Basin. Applying this technique to Early Cretaceous fluvial shales within 110 onshore and offshore petroleum wells, the authors suggested >1500m of exhumation within much of the eastern basin and minor exhumation, <200m, across the central and western portions, suggesting that uplift has been concentrated around the eastern Otway Ranges section. This model for basin development has recently been integrated as part of a cast study at Castle Cove by Debenham et al. (2018) who undertook highly detailed fracture mapping producing a chronological model for regional fracture development assuming the reserve reactivation of ~NE-SW trending normal faults.

Whilst the afore mentioned studies suggest there is obvious evidence for exhumation, the driving forces and timing behind the creation and timing of structuring of these events is less well constrained. The growth of offshore fold structures attributed to both NW-SE compressive plate boundary forces (Sandiford et al. 2003; Holford et al. 2014) in addition to transpressive

forces surrounding the Sorrel Fault Zone (Schnieder et al. 2004). Holford et al. (2014) used 2D seismic analysis along ~W-E striking lines in order to interpret the compressive growth of low amplitude fold, while a similar earlier study was conducted by Hill et al. (1995). While these two studies, in addition to others (e.g. Edwards et al. 1996) present interpretations of thrust faulting and inversion, they lack detail. Additionally the most comprehensive mapping of the Otway Ranges to date (**fig. 18**) conducted by Medwell (1971) includes no outcropping ~NE-SW thrusts or inversional structures within the basin, which raises certain questions as to the driving force behind basin exhumation and uplift.

In contrast to compressive based -fault inversion models for uplift and exhumation in the Miocene, Wallace et al. (2005) use a geomorphological approach interpreting strandlines in order to estimate post-depositional uplift, implying between 175-240m of Early Pliocene uplift when sea level changes are also considered (Sandiford et al. 2003). Although this evidence has been viewed as questionable as Late Neogene magnitudes for uplift from these studies (Wallace et al. 2005; Sandiford et al. 2003) give estimate of roughly 500m less than thermochronological data.

To summarise this section, the history of uplift and compression within the Otway Basin, remains confusing. As whilst many different studies postulate uplift and exhumation, estimations vary considerably and the exact drivers behind this uplift remain relatively unknown.

2.4. Petroleum Systems, Carbon Capture, Geothermal and Unconventional in the Otway Basin

2.4.1 Petroleum Systems

The hydrocarbon systems of the southern Australian margin consist of a series of subdivisions belonging to the Austral Petroleum Super-system (APS), catalogued by the age of their individual source rocks and similar tectonic history (Bradhshaw, 1993). In total, three subdivisions of the APS have been recognised for the Otway Basin, relating to various types of source rock depositional environment, and can be correlated geochemically to separate oil families (Edwards et al. 1999). Furthermore Edwards et al. (1999) divided these subdivisions into smaller groups, four of which are known to occur within the Otway Basin (**fig. 19**), surmising that in total; six oil families are present within the Basin. Although, work by Boreham et al. (2004) showed that this may be an overestimation due to drilling contaminants.

While commercial oil is yet to be discovered, commercial gas discoveries have been made within the Port Campbell Embayment/Shipwreck Trough in Victoria and the Penola Trough in South Australia (Geoscience Australia, 2014). Due to a series of oil shows that demonstrate good medium-gravity, waxy oil proneness the presence of oil within the region should not be ruled out, although many have been classed as under mature or leaked off (Mehin & Kamel, 2002). A number of these oil shows have been described to have a strong geochemical association with their respectful natural gases suggesting the two share similar a similar source (Boreham et al. 2004). Additionally, strong stratigraphic and geographic relationships between oil and gas shows and their respective source rocks suggest that the hydrocarbons of the Otway Basin are likely to have short to medium range migration pathways from source rock to trap (Boreham et al., 2004; Morton & Dextral, 1995) This also suggests that within the Otway Basin, reservoir proximity to actively generating source kitchens is the principal control on the

distribution of significant accumulations of hydrocarbons. As a consequence the basin is still considered an active target for hydrocarbon exploration. Whilst poor fault seal within the Otway Basin has long been suggested as a significant hindrance to the discovery of significant hydrocarbon plays (O'Brien et al. 2009), a secondary factor of a narrow window for present day maturity for source rocks has also been suggested (O'Brien et al. 2009).

It is also worth noting that accumulations of natural gas within the Otway Basin vary in their composition, showing clear chemical differences between fields in the west and eastern regions (Mehin and Kamel,2002; O'Brien et al. 2009). Gas from some wells appears high in methane and low in carbon dioxide (e.g. North Paaratte-1: 96.0%/0.1%) while others display an almost opposite trend (e.g. Boggy Creek-1: 9.0%/88.7%) (O'Brien et al. 2009). Mehin and Kamel (2002) suggested that the presence of wet gas and carbon dioxide within some wells was not a product of thermal cracking of gas in place, this was supported by helium isotope analysis by Watson et al. (2004) confirming a mantle derived source for carbon dioxide within the basin.

Within the ASP, three subdivisions have been recognised within the Otway Basin (Edwards et al. 1999). They are primarily related to the deposition environment of source rock and can be correlated to three distinct families of oil. Table 1 displays a summary of hydrocarbon volumes within the basin and subsystems.

2.4.1.1 Austral 1 (A1) Petroleum System

Source rocks of the A1 petroleum system are those present within Late Jurassic interbedded mudstones of the early rift phase Casterton Formation and the lacustrine shales of the Crayfish Subgroup (O'Brien et al. 2009). Recognised as an excellent source rock by a number of early studies (Lovibond et al. 1995; Lsvin and Muscatello, 1997), the Casterton Formation was deposited within Early Cretaceous half-grabens, thickest in the western basin and has an

average total organic carbon (TOC) of approximately 2.6% with mainly type II-III kerogens. The unit is potentially generative for oil and gas (Mehin and Constantine, 1999; O'Brien et al. 2009) and with early geochemical studies (Padley et al. 1995; Edwards et al. 1999) identifying the unit as the most probable source for much of the oil and gas accumulations within the Pretty Hill reservoir unit in South Australia (O'Brien et al. 2009).

Within the eastern Victorian sector of the basin, the distribution of the Crayfish group is largely restricted to the portions closest to South Australia. Although within this portion of the basin The Pretty Hill Formation has been found to have a "fair" source rock potential (Mehin and Constantine, 1999) with average TOC levels of 1.7% with typically type III kerogens, with minor levels of type II and type IV (O'Brien et al. 2009). Where it is thermally mature within the basin, the Laira Formation is also potentially generative for both oil and gas (Mehin and Constantine, 1999).

Effectively all of the discovered hydrocarbons within the onshore South Australian Otway Basin are derived from the A1 petroleum system and reservoired within the Crayfish Subgroup sediments (O'Brien et al. 2009). This is likely due to the fact that A1 source rocks are optimally located with respect to windows of highest maturity, within the western basin, the Eumeralla Formation is far less mature than in the east (O'Brien et al. 2009). It has been suggested that equivalent members to the Crayfish Group within the eastern basin are now over mature, having experienced far greater levels of burial and now no longer generating hydrocarbons (O'Brien et al. 2009). Peak maturity within the Otway Basin for this system has been modelled by O'Brien et al. (2009) (**fig. 20**).

2.4.1.2 Austral 2 (A2) Petroleum System

Lying uncomfortably above the members of the A1 systems, the members of the A2 petroleum system are largely responsible for the majority of economical hydrocarbon discoveries within the eastern and offshore Otway Basin (Edwards et al. 1999; Boreham et al. 2004). The Early Cretaceous Eumeralla Formation, has been recognised as the primary source rock within this system, in particulary within the Port Campbell Embayment and the Shipwreck Trough, which contain the Thylacine, Geographe, Casino, Halladale and Iona gas fields (Mehin and Link, 1994; Foster and Hodgson, 1995; Luxton et al. 1995; Boreham et al. 2004), with gas shows outside these regions also being attributed to this system (O'Brien et al. 2009). The Eumeralla Formation was deposited throughout the Albian to Aptian and coincides with a major anoxic oceanic event, with a very strong intra-formational spike in TOC at ages of approximately 113Ma which correlates in age with the proposed Seli anoxic oceanic event of early Aptian in age (O'Brien et al. 2009).

Gas has been considered to have been sourced primarily from two coaly facies within the Eumeralla Formation, the first of Early Aptian age, the second of Early Albian age (O'Brien et al. 2009). These facies have been described as approximately 200m in thickness, consisting of repeating successions of 2-3m seams with interlaced mudstones rich in disseminated organic matter (O'Brien et al. 2009). Data from BHP Petroleum (1992), suggest that these two facies extend across most of the basin with excellent potential for the generation of gas and light oil (Preston, 1992; Geary and Reid, 1998). Interbedded organic rich mudstones within the Eumeralla Formation have also been thought to have contributed to discoveries made within this system (O'Brien et al. 2009). Whilst there is recognised potential for the generation of liquid hydrocarbons within the A2 system in the Otway Basin, discoveries to date consist entirely of gas prone source rocks, with limited quantities of condensate and liquid production.

2.4.1.3 Austral 3 (A3) Petroleum System

The Late Cretaceous to Early Paleogene, Latrobe Group sediments have been acknowledged as the major source rock interval for the oil and gas systems of the offshore Gippsland Basin, and some of Australia's first major oil and gas fields. There have been no significant discoveries within this system in the Otway Basin (O'Brien et al. 2009). Neither the tertiary sediments nor any members of the Sherbrook Group have reached thermal maturity within many of the wells drilled within the onshore or inner continental shelf region (O'Brien et al. 2009). As of 2009, further exploration was recommended in order to assess the ability of the A3 petroleum system to produce economic volumes of hydrocarbons, although that being the case, from extensive modelling by O'Brien et al. (2009) it seems that if any liquid hydrocarbons are present it will be within Turonian, Waarre and Flaxman sections, deposited within anoxic oceanic conditions.

2.4.2 Geothermal energy and Carbon Capture and Storage

The geothermal potential of the Otway Basin is currently under assessment. The most recent volcanic activity on the Australian continent is thought to have occurred in the Mt Gambier region of south eastern South Australia, within the confines of the Otway Basin (Geoscience Australia, 2014). Additionally the region has been found to contain higher heat flow than surrounding areas making it a potential target for hot dry rock geothermal technology (Geoscience Australia, 2014).

The Otway Basin is also host to Australia's largest and longest running, operating, carbon capture and storage project: CO2 CRC, within the onshore Port Campbell Embayment (**fig. 21**). To date it is the world's largest carbon capture and storage project with over 80,000 tonnes of CO2 injected and stored across multiple Late Cretaceous formations. The site was chosen for a number of reasons including access to previously established oil and gas infrastructure, a nearby source of carbon dioxide from the Naylor-1 well and a large amount of available oil and gas data.

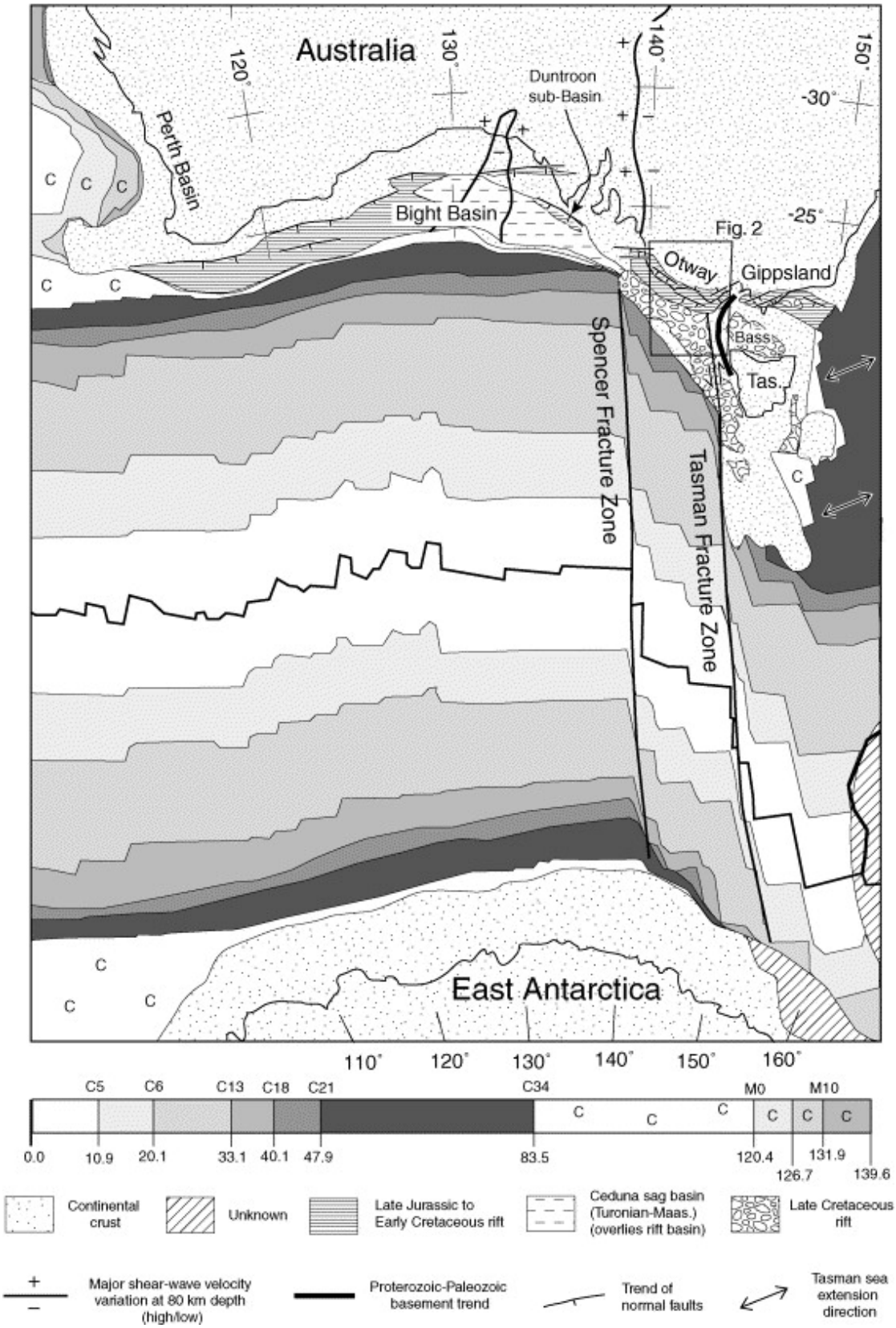

Fig. 1: *A geological map of the southern margin of the Australian continent and the location of the Bight, Otway, Bass and Gippsland Basins. Note that here the Tasman Fracture Zone is synonymous with the Sorell Fault Zone. Additionally sea floor isochrons between Australia and Antarctica are also displayed. Taken from Miller (2000) (Miller et al., 2002).*

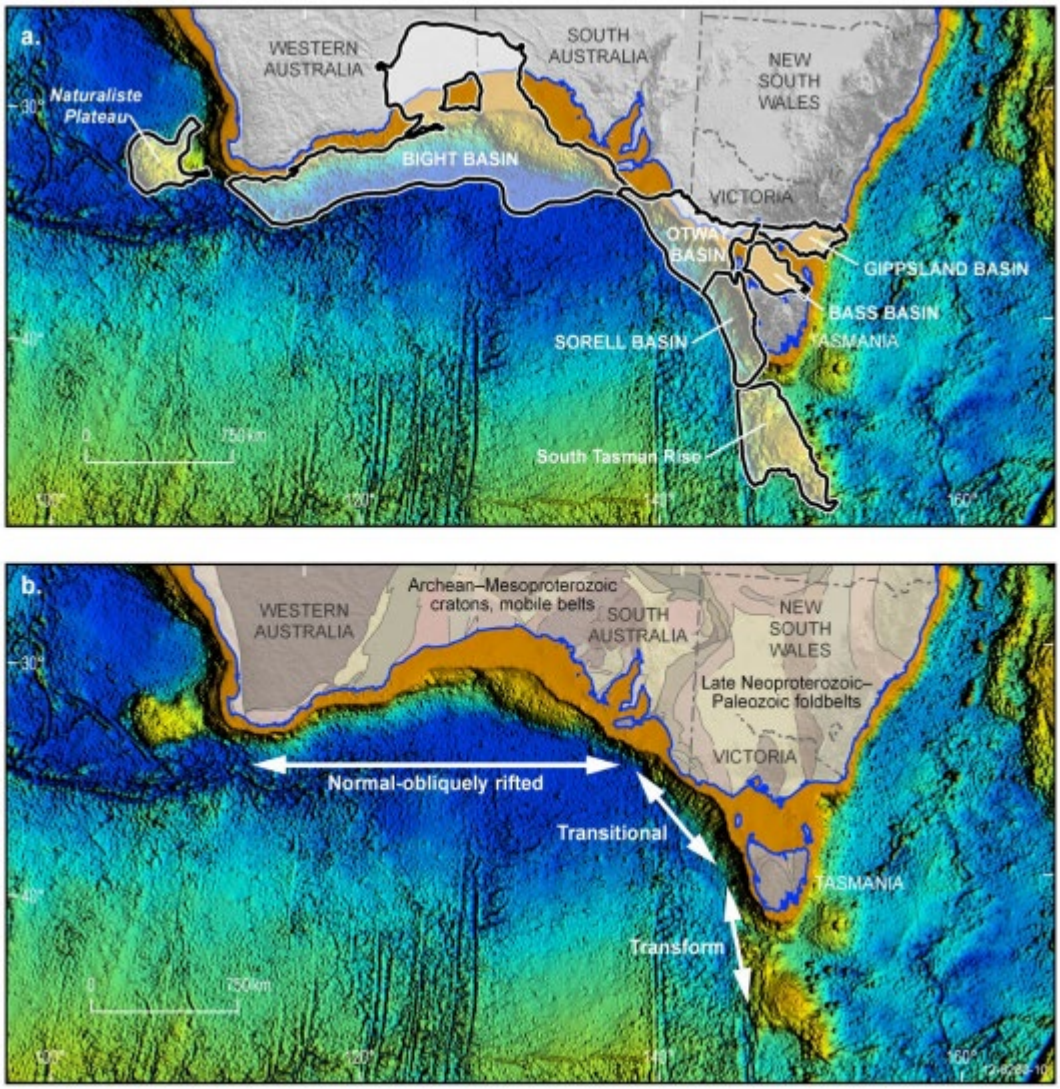

Fig. 2 *A second map of Australia's southern rifted margin with (a) more clearly outlining the extent of the Otway Basin and (b) noting the changes in rift nature from normal rifting in the west, where continental separation began along the southern margin, to a transitionally rifted margin in the Otway Basin. Taken from Stacey et al. (2013).*

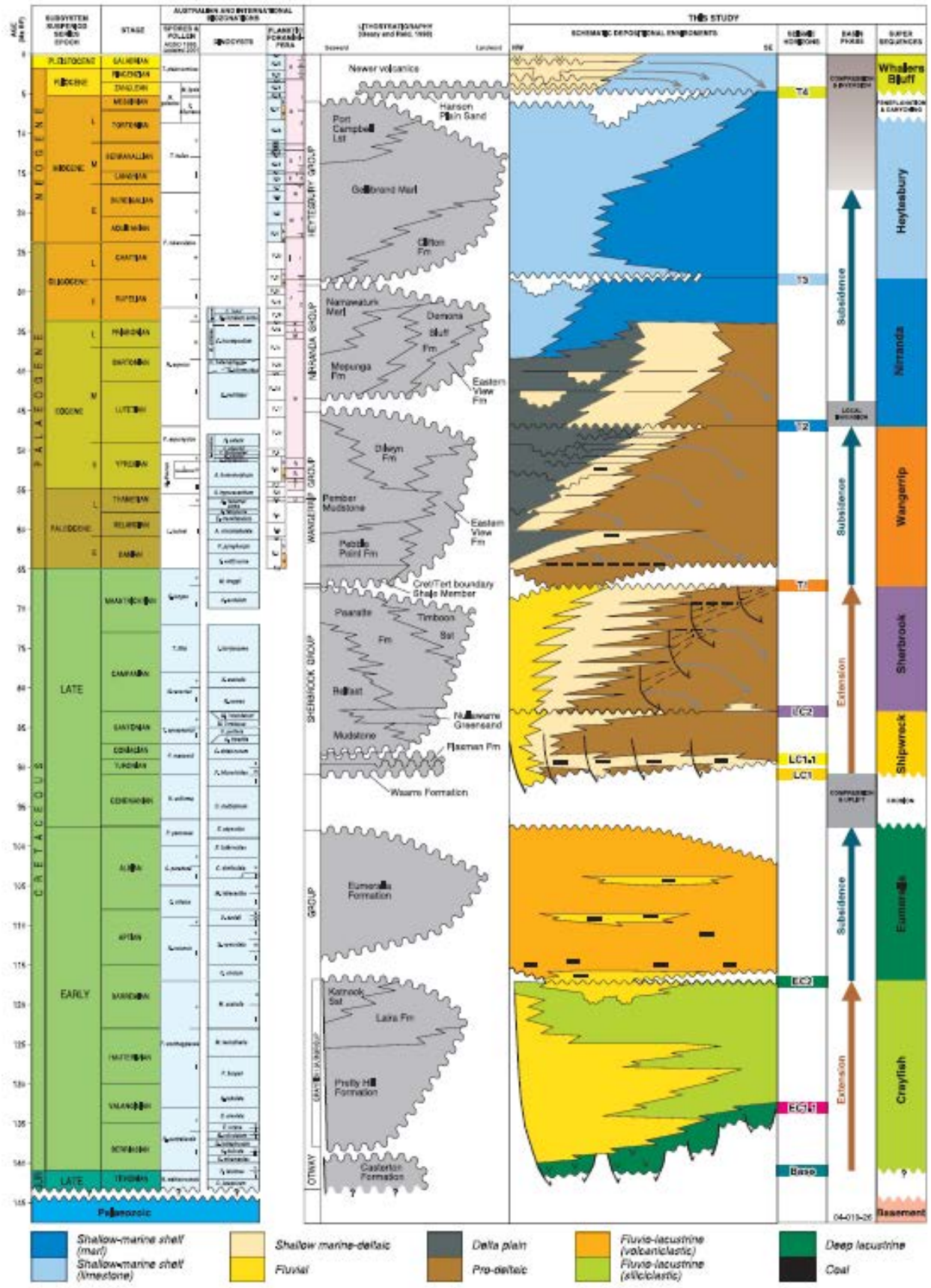

Fig. 3: *A stratigraphic section of the Otway Basin taken from Krassay et al (2004) which shows the main lithological units and rift phases.*

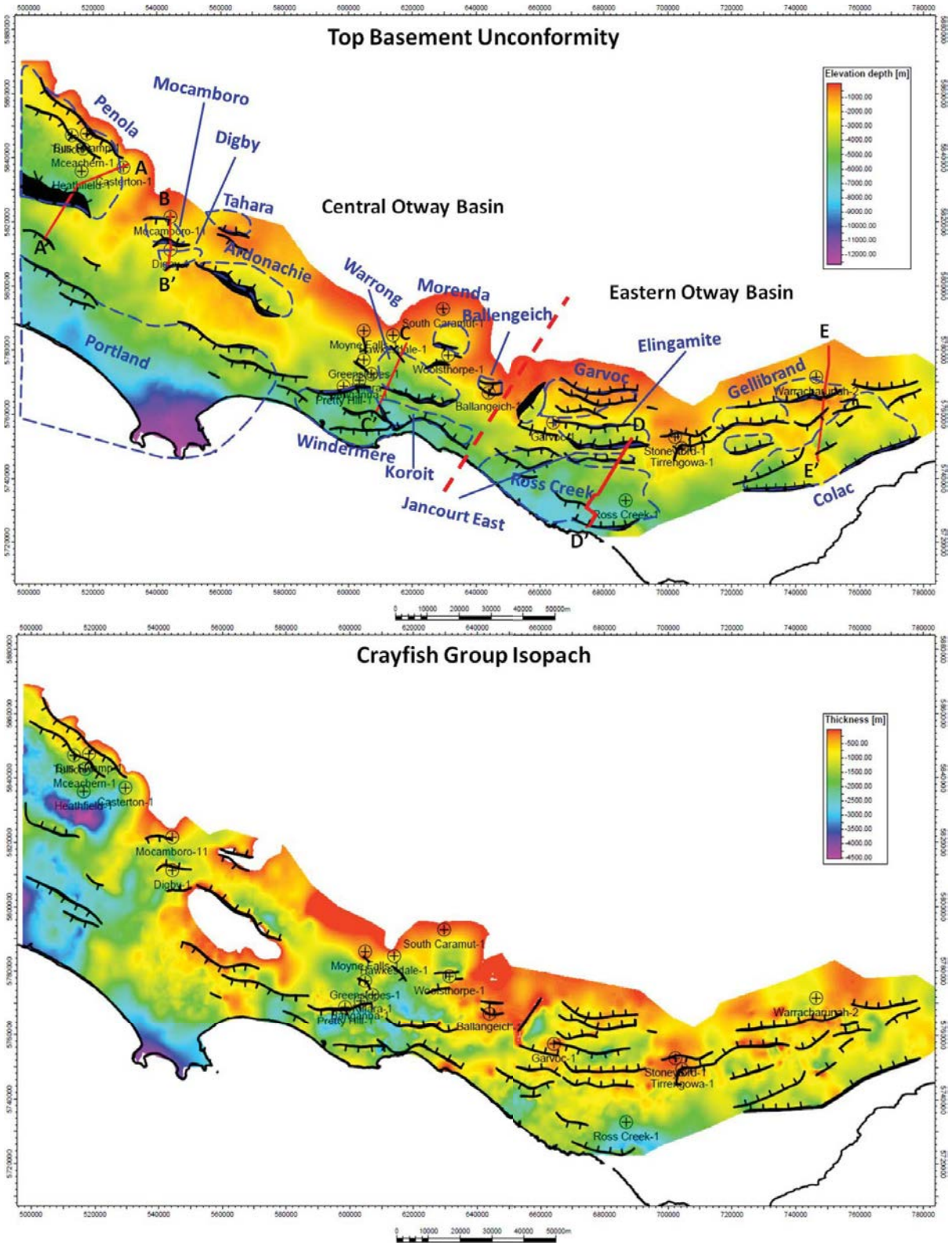

Fig. 4*: The Otway Basin (a) showing the location of of major Early Cretaceous depocentre bounding faults as well as the depth to basement (b) an isopach map for the Crayfish group. (Briguglio et al. 2015). Note the high thickness of the Crayfish Group in the west where early extension rates were higher.*

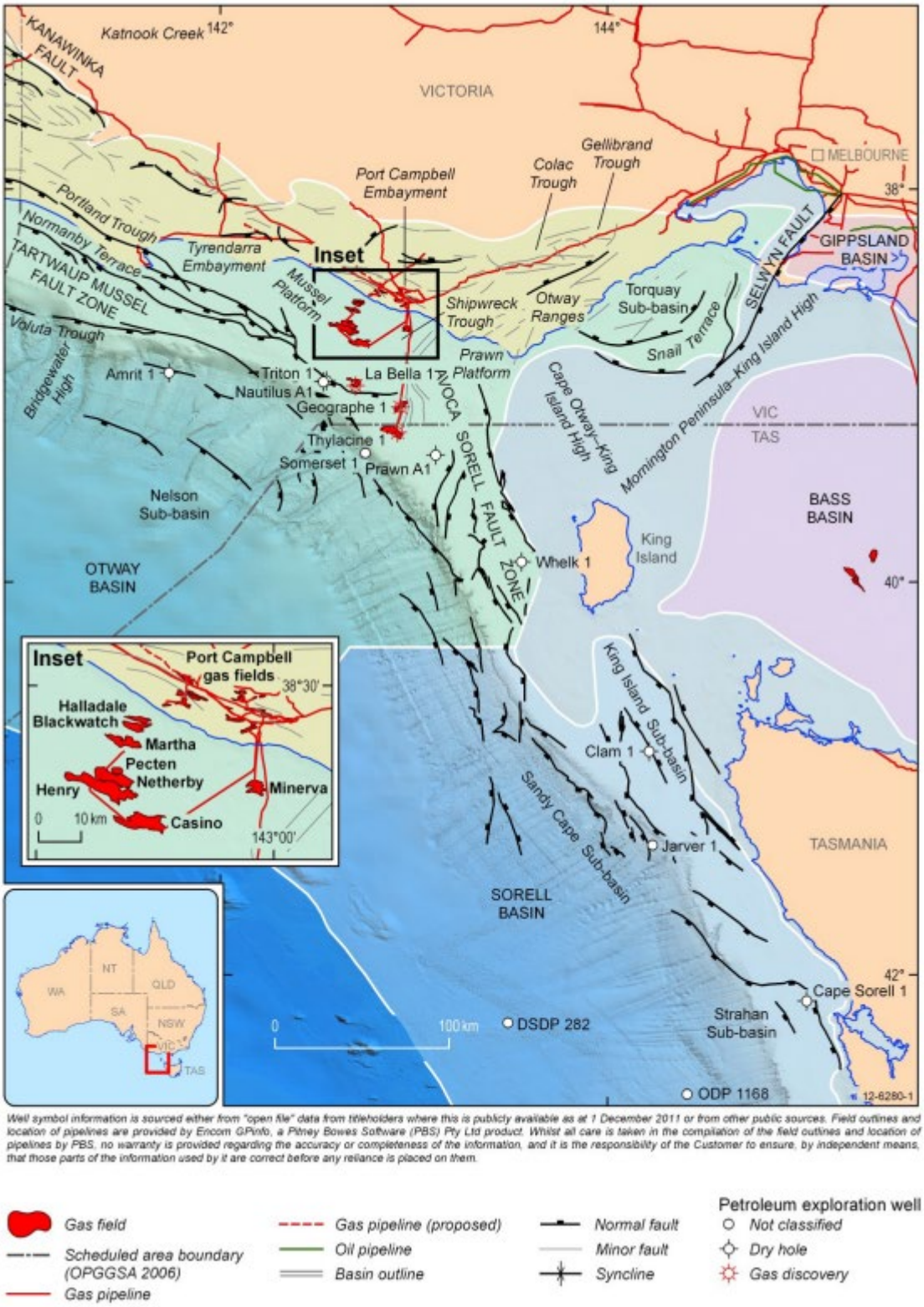

Fig. 5*: A structural elements map of the eastern most Otway Basin taken from Stacey et al. (2013). Note the change in structural trend from ~NW-SE to ~NE-SW across the Prawn Platform at ~143ºE. This feature has considerably contributed to different models for basin evolution.*

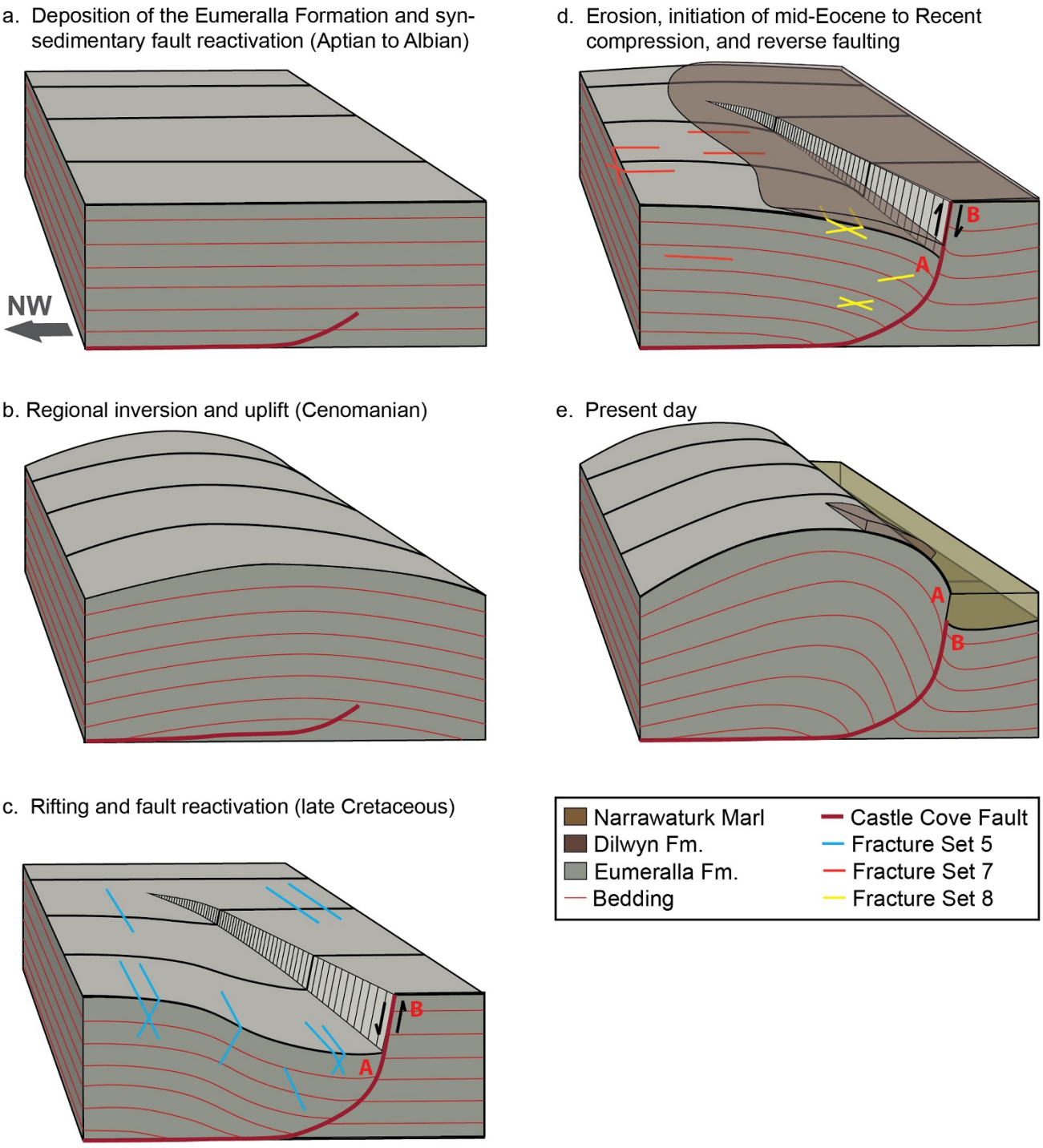

Fig. 6 *A schematic example of the Castel Cove Fault, within the Otway Ranges which has been interpreted as an inverted normal fault. This diagram simply outlines the general basin phases; rifting, compression, renewed rifting, and the onset of compression, which are agreed upon within the literature. Taken from Debenham et al. (2018).*

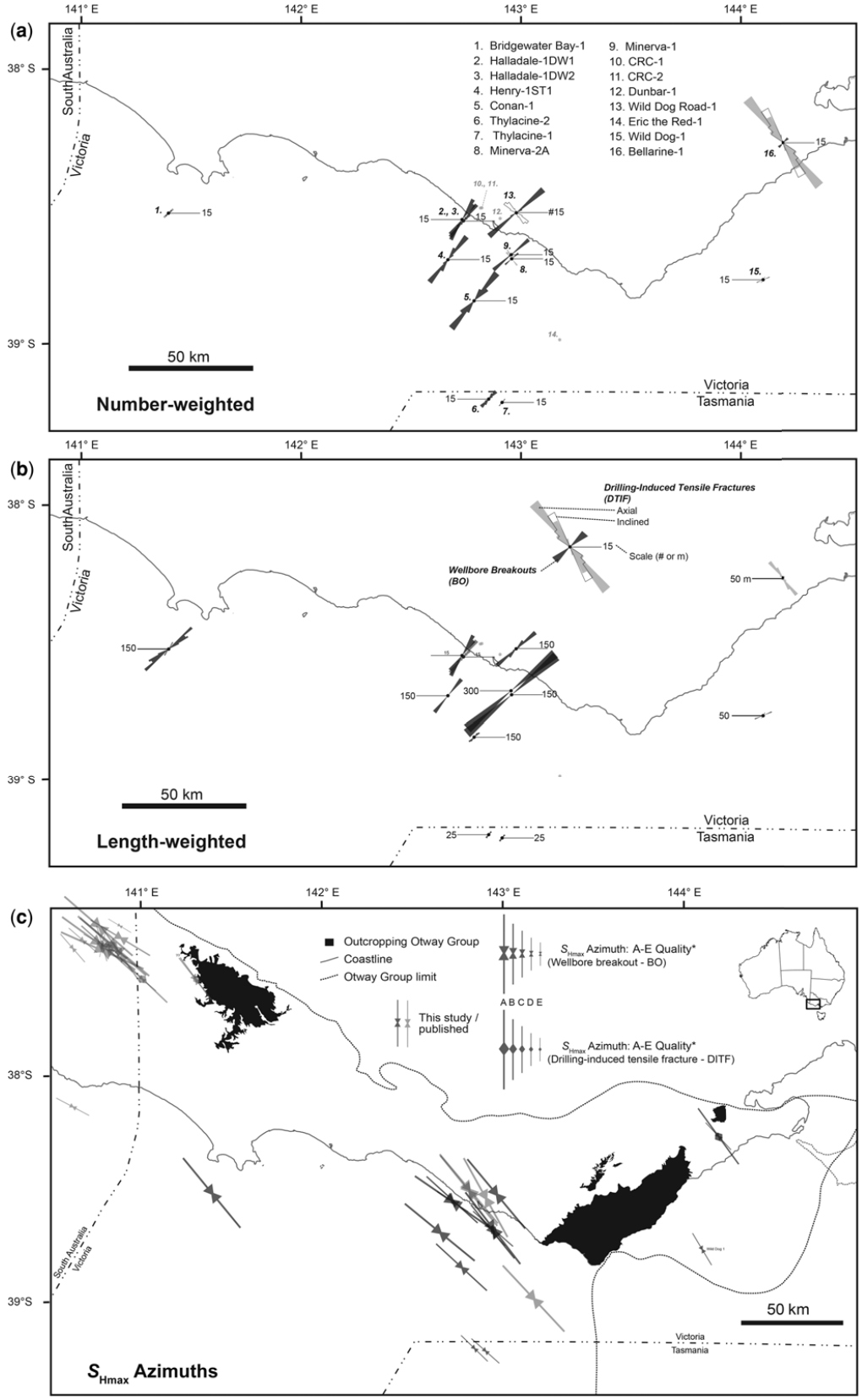

Fig. 7*: An example of results from the most recent in-situ stress study by Tassone et al. (2017) showing (a) the orientation of well-bore failure features (b) the same features length weighted and (c) The determined orientations on maximum in-situ stress. Taken from Tassone et al. (2017).*

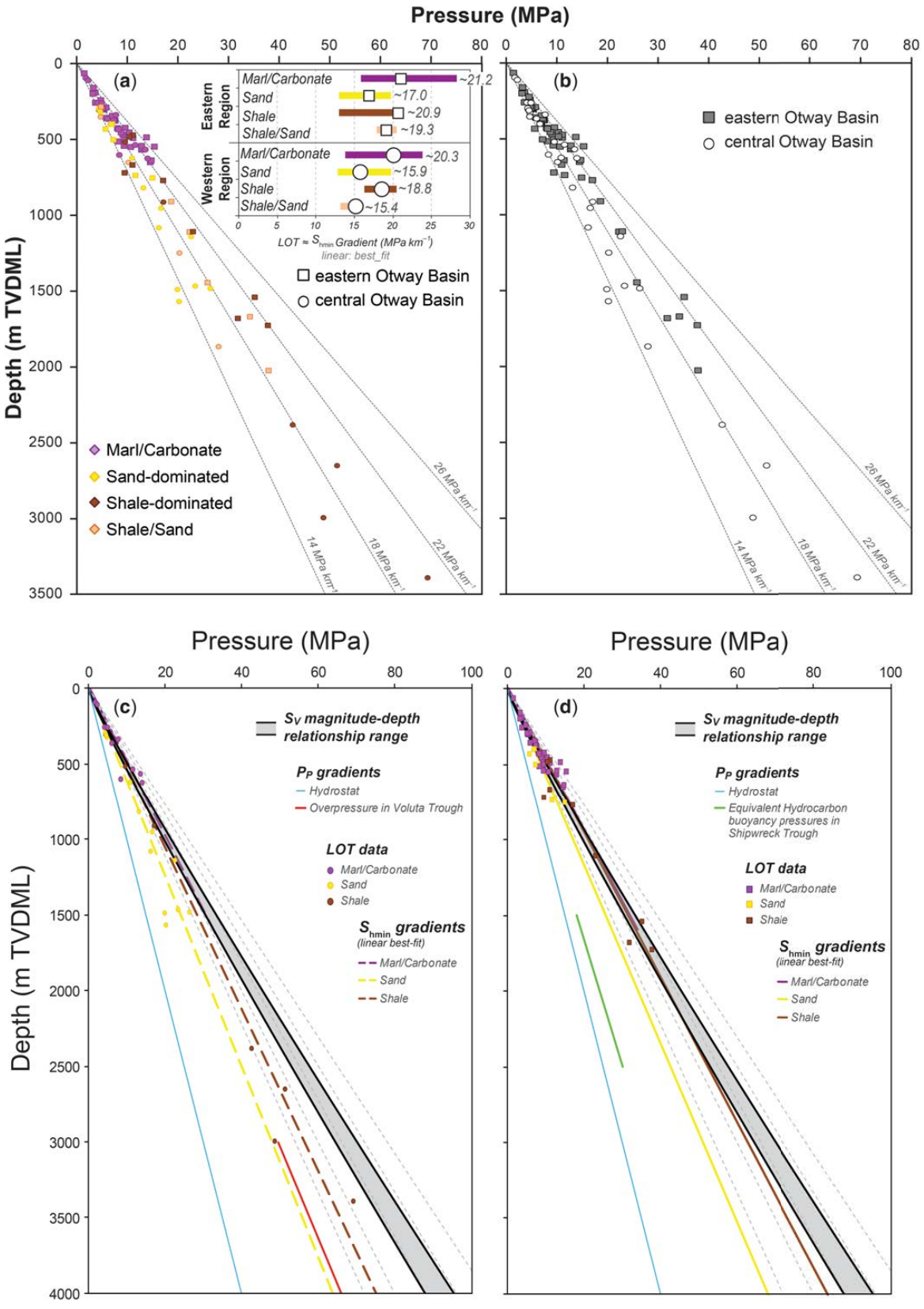

***Figure 8**: Leak off test data for the Otway Basin compiled by Tassone et al. (2017). Note the variations between central and eastern regions and by formation. A good example as to why the regime of in-situ stress is still debated.*

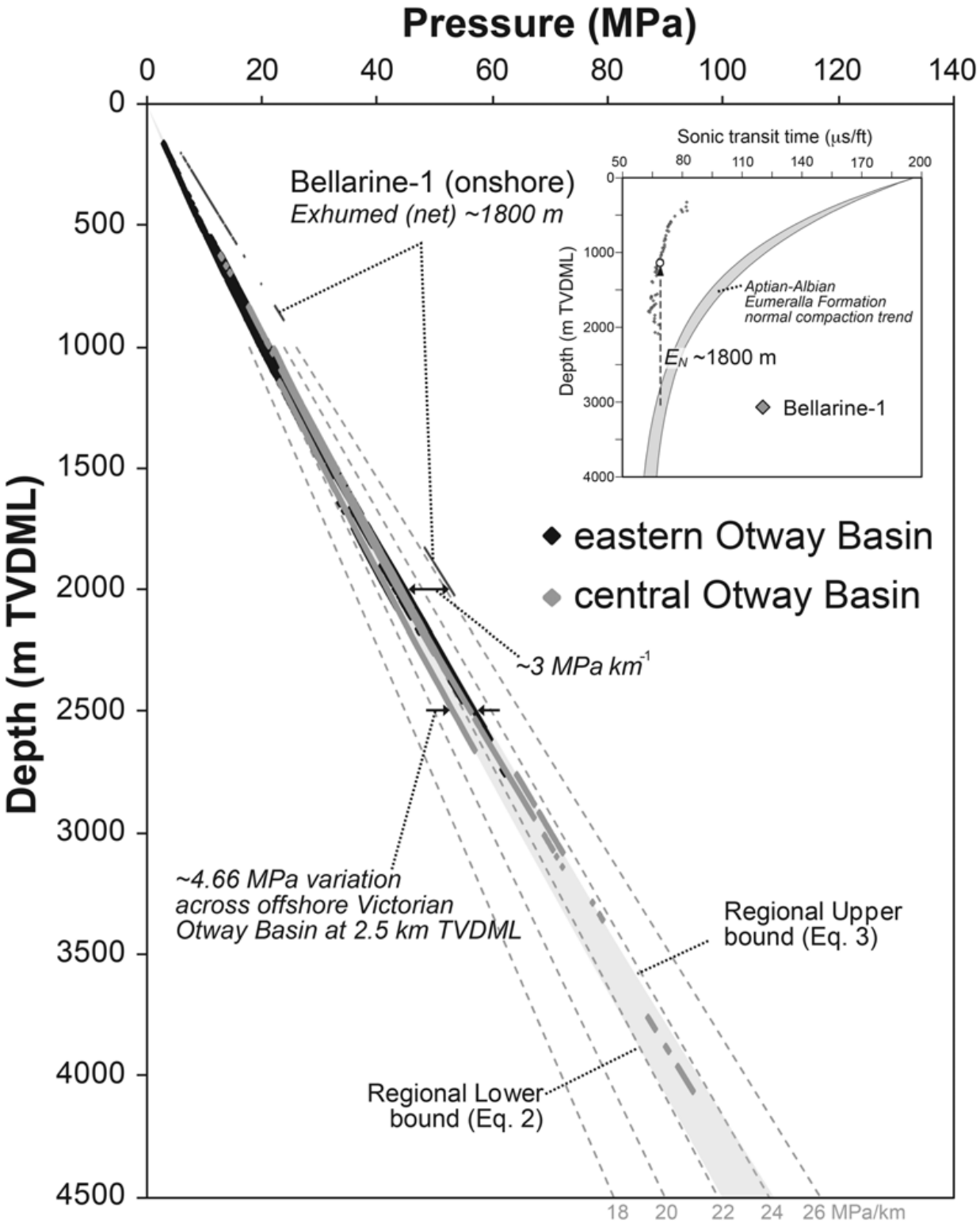

Fig.9*: Vertical stress gradients determine from 24 wells within the Otway Basin by Tassone et al. (2017). Again, note the changes in gradient between the central and eastern Otway Basin which contributed to challenges when attempting to constrain the in-situ stress tensor on the basin scale.*

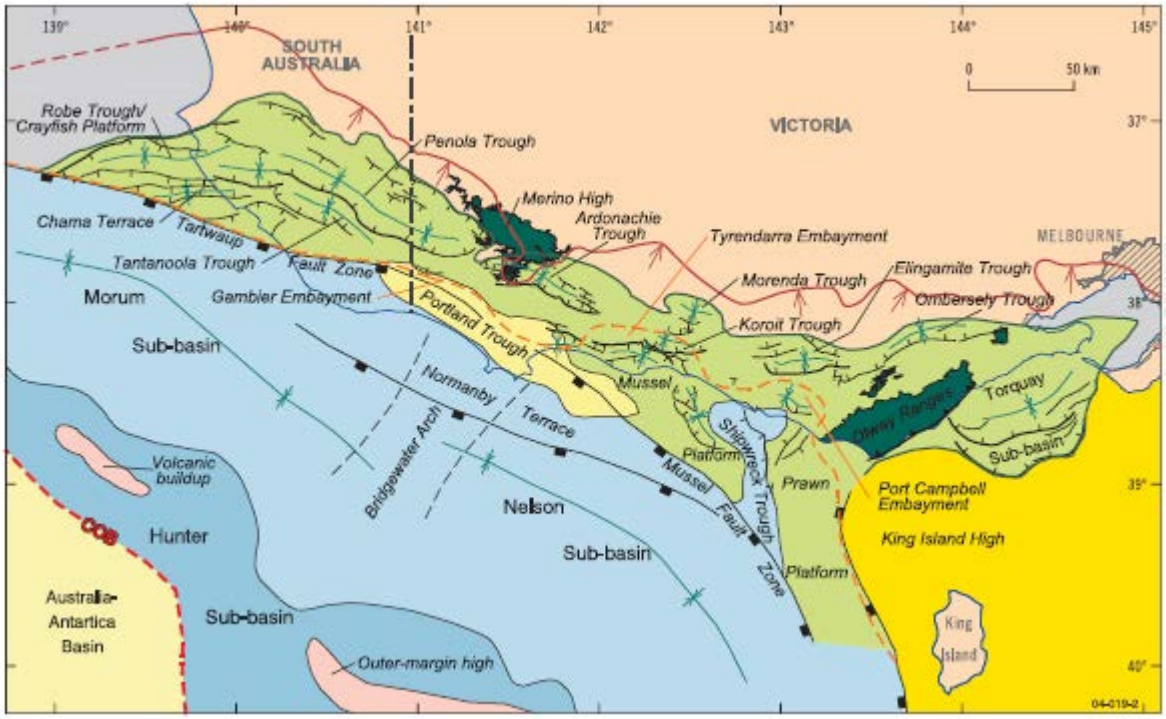

Fig 10: *A basin wide structural elements map of the Otway Basin, taken from Krassay et al. (2004) modified Alley and Lindsay (1995) and Moore et al. (2000).*

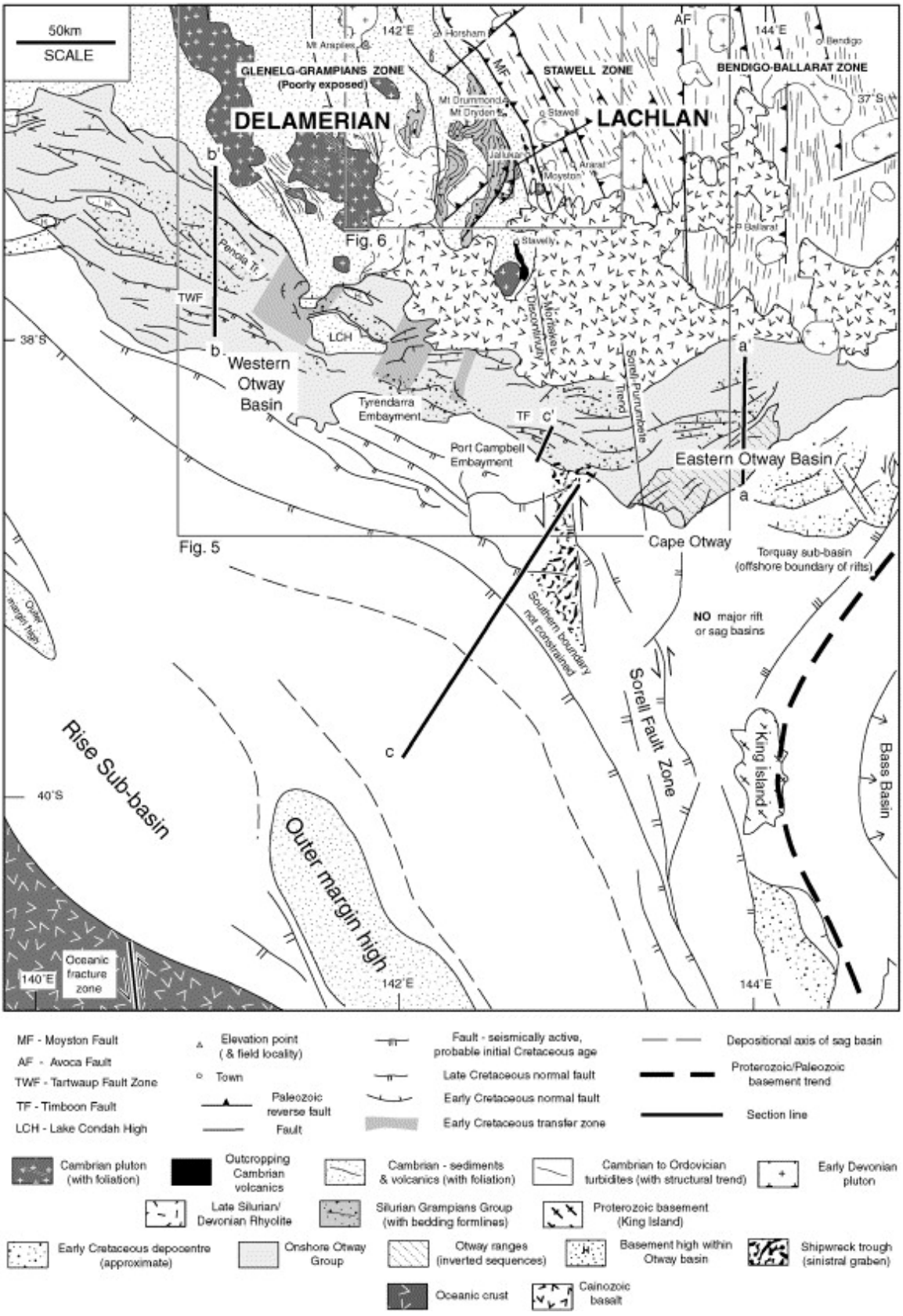

Fig. 11: *A geological basement map of the Otway region. Showing the western Lachlan Fold Belt, eastern Delamerian Fold Belt and structural trends across the basin, which have suggested to influence the nature of fault development. Taken from Miller (2002).*

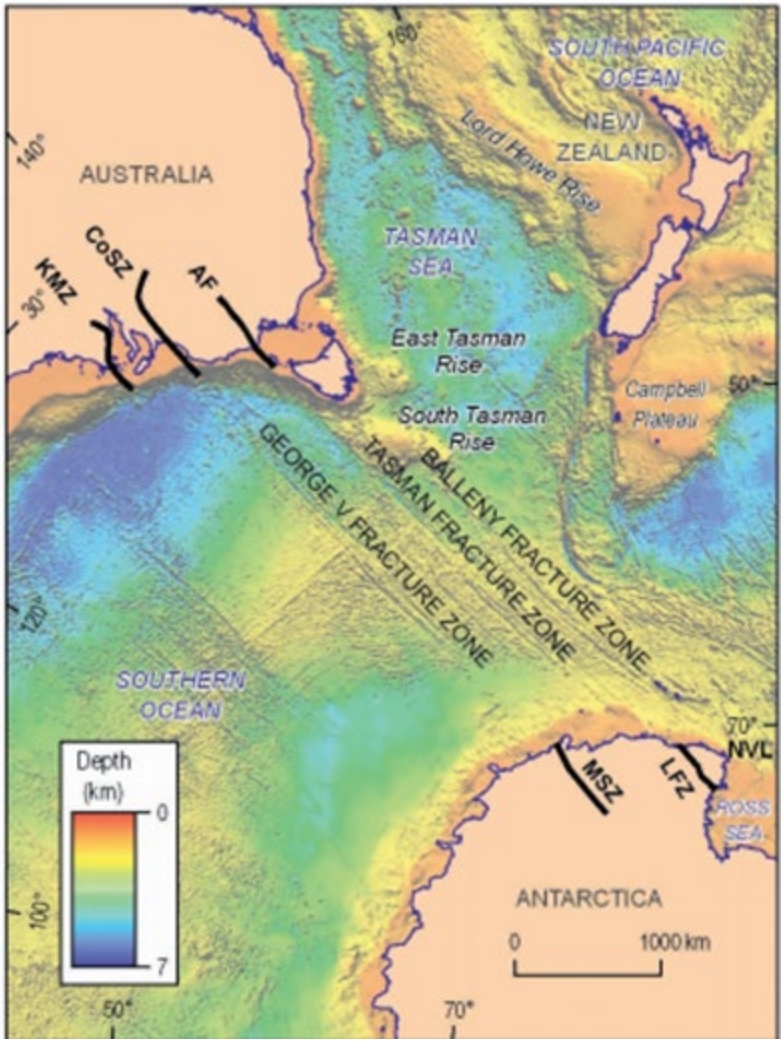

***Fig 12**: A geographical map showing the location of the Avoca Fault (AF) in addition to the Coorong Shear Zone (CoSZ) and the Kalinjala Mylonite Zone (KMZ), which have been suggested to have accommodated strain and influence the development of fault networks within the Otway Basin. Taken from Gibson et al. (2013).*

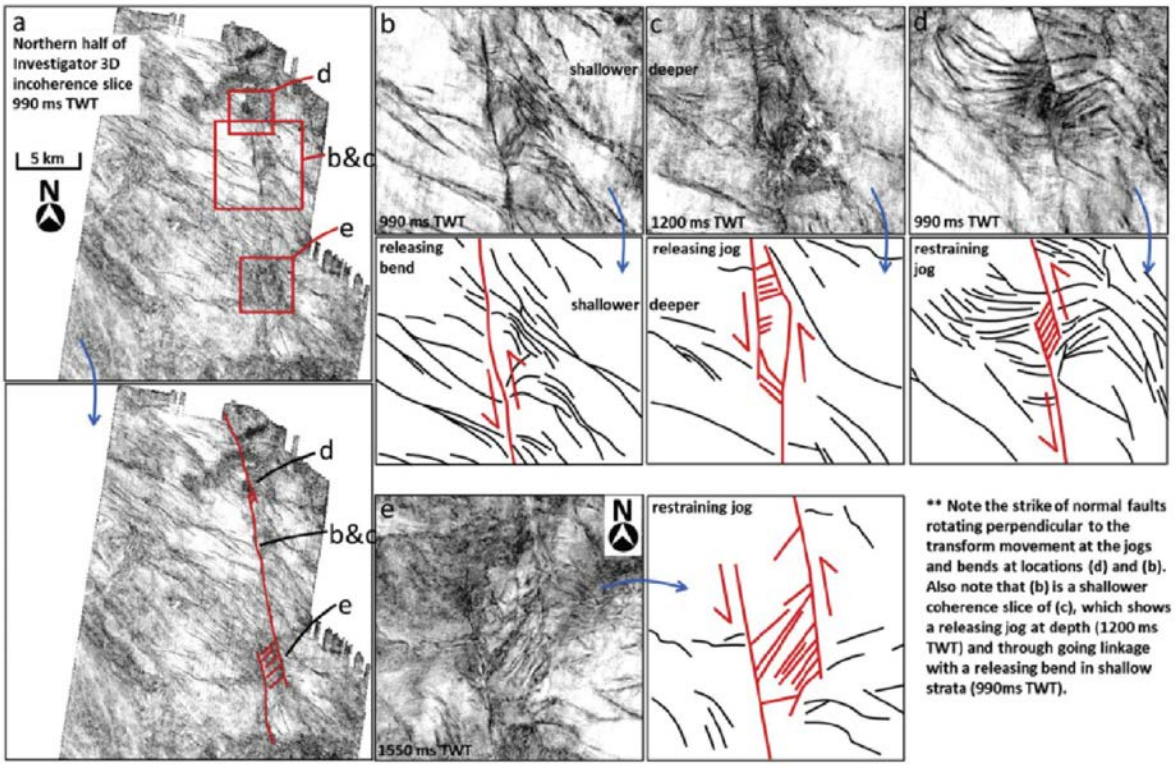

Fig. 13: *Documented evidence of sinistral transtension along the Sorell Fault Zone within the the Shipwreck Trough, taken from Robson et al. (2018).*

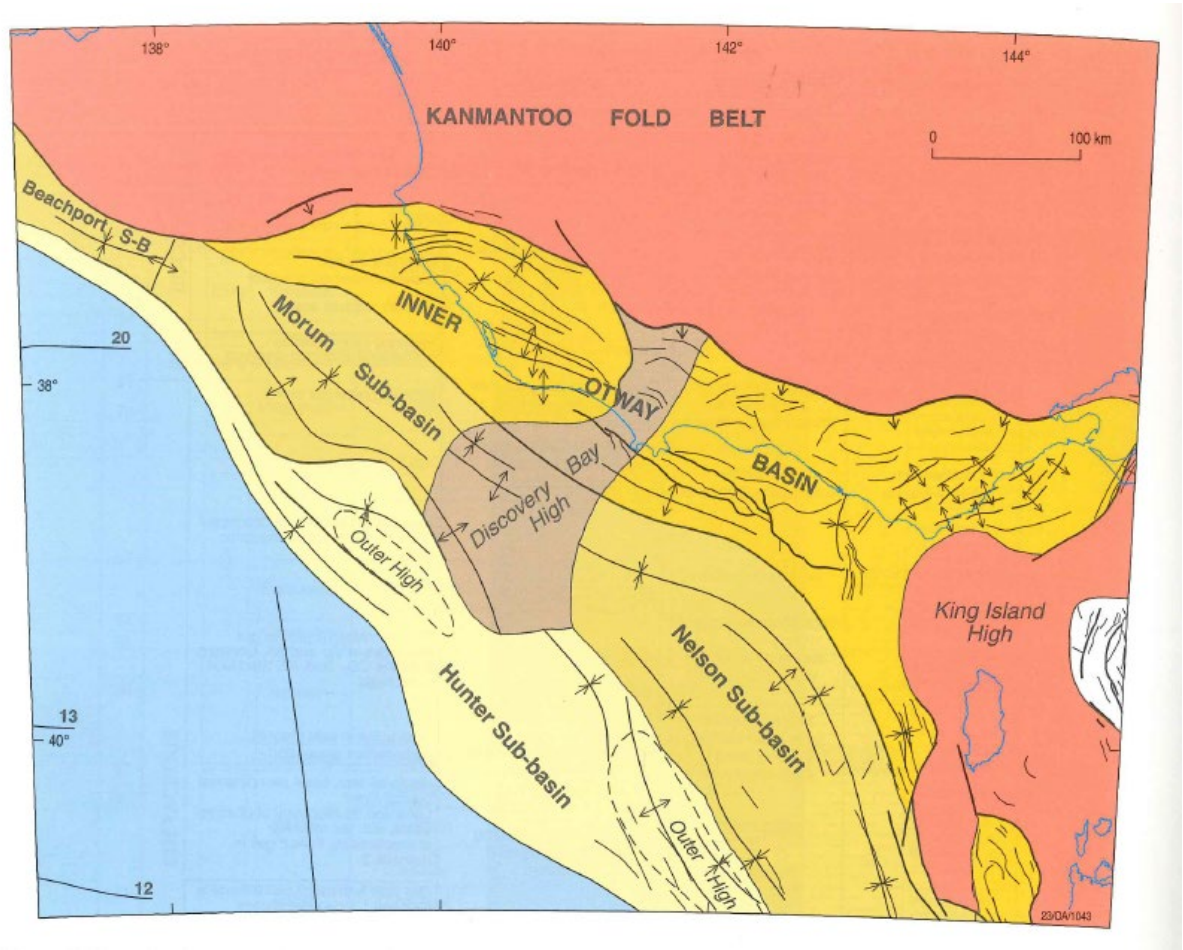

***Fig 14**: A geological map showing the division of off-shore late-phase rift structures from the Mid Cretaceous within the Otway Basin. Taken from Moore et al. (2000).*

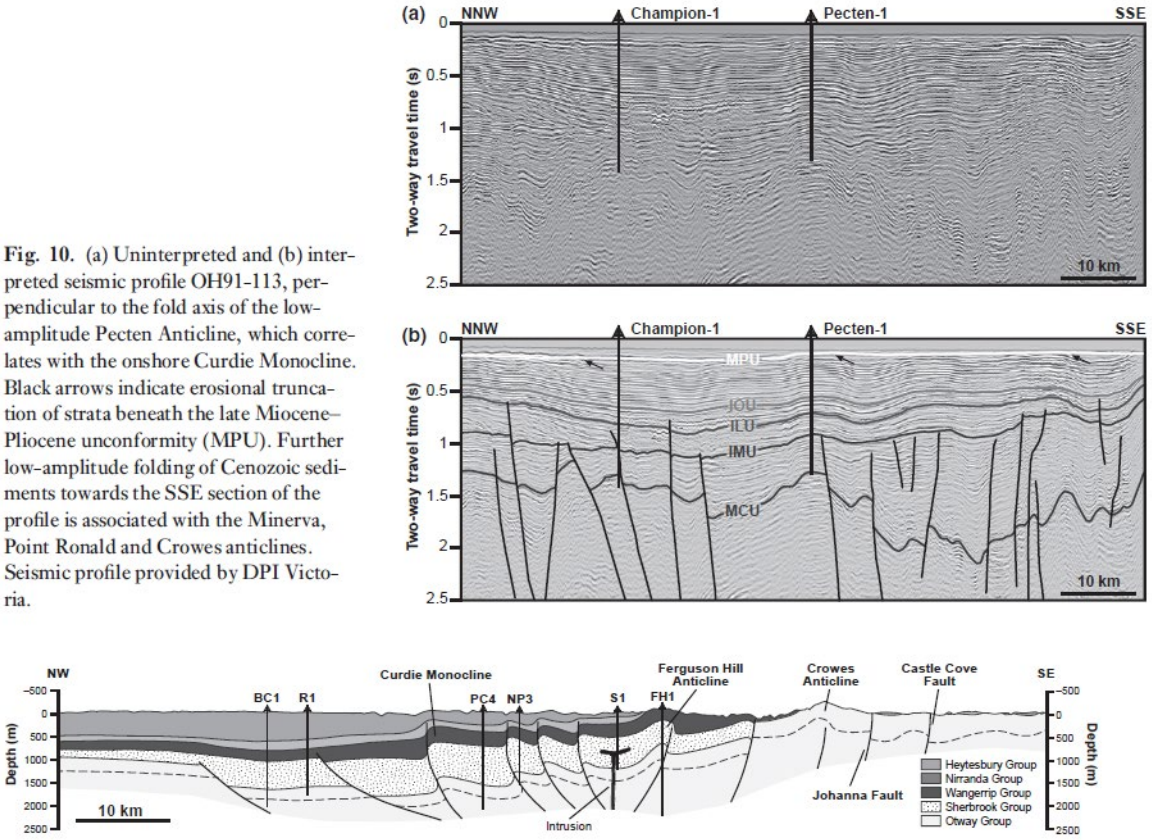

Fig. 10. (a) Uninterpreted and (b) interpreted seismic profile OH91-113, perpendicular to the fold axis of the low-amplitude Pecten Anticline, which correlates with the onshore Curdie Monocline. Black arrows indicate erosional truncation of strata beneath the late Miocene–Pliocene unconformity (MPU). Further low-amplitude folding of Cenozoic sediments towards the SSE section of the profile is associated with the Minerva, Point Ronald and Crowes anticlines. Seismic profile provided by DPI Victoria.

Fig. 15*: A figure taken from Holford et al (2014), based largely on a model for basin development outline by Edwards et al. (1996). The top figures display an un-interpreted and interpreted seismic section through low wavelength folding attributed to the reactivation of NE-SW striking faults which is outlined in the cross section below modified from Edwards et al. (1996*

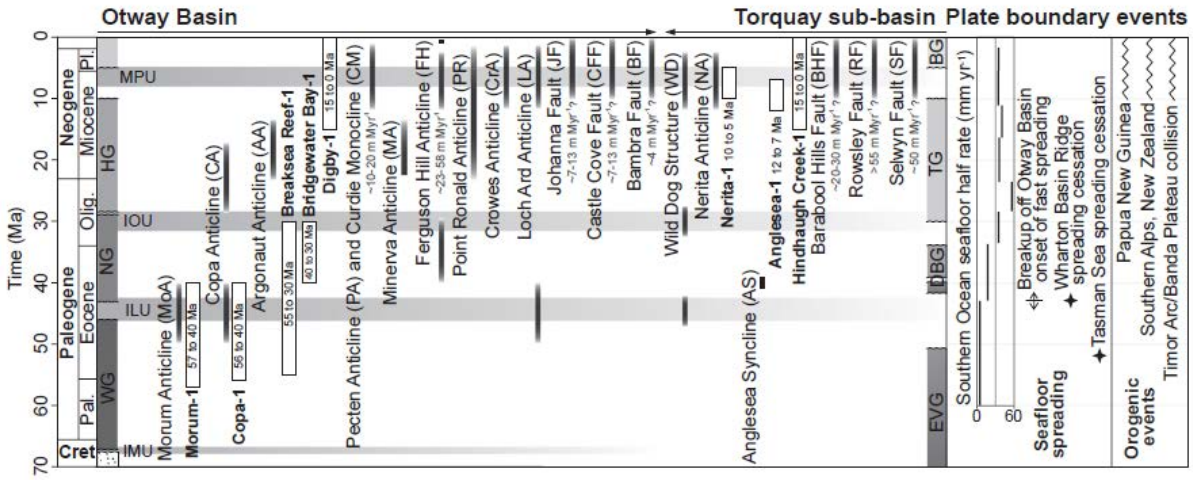

Fig. 16: *The chronology of post-breakup inversion structures within the Otway Basin. Taken from Holford et al. (2014).*

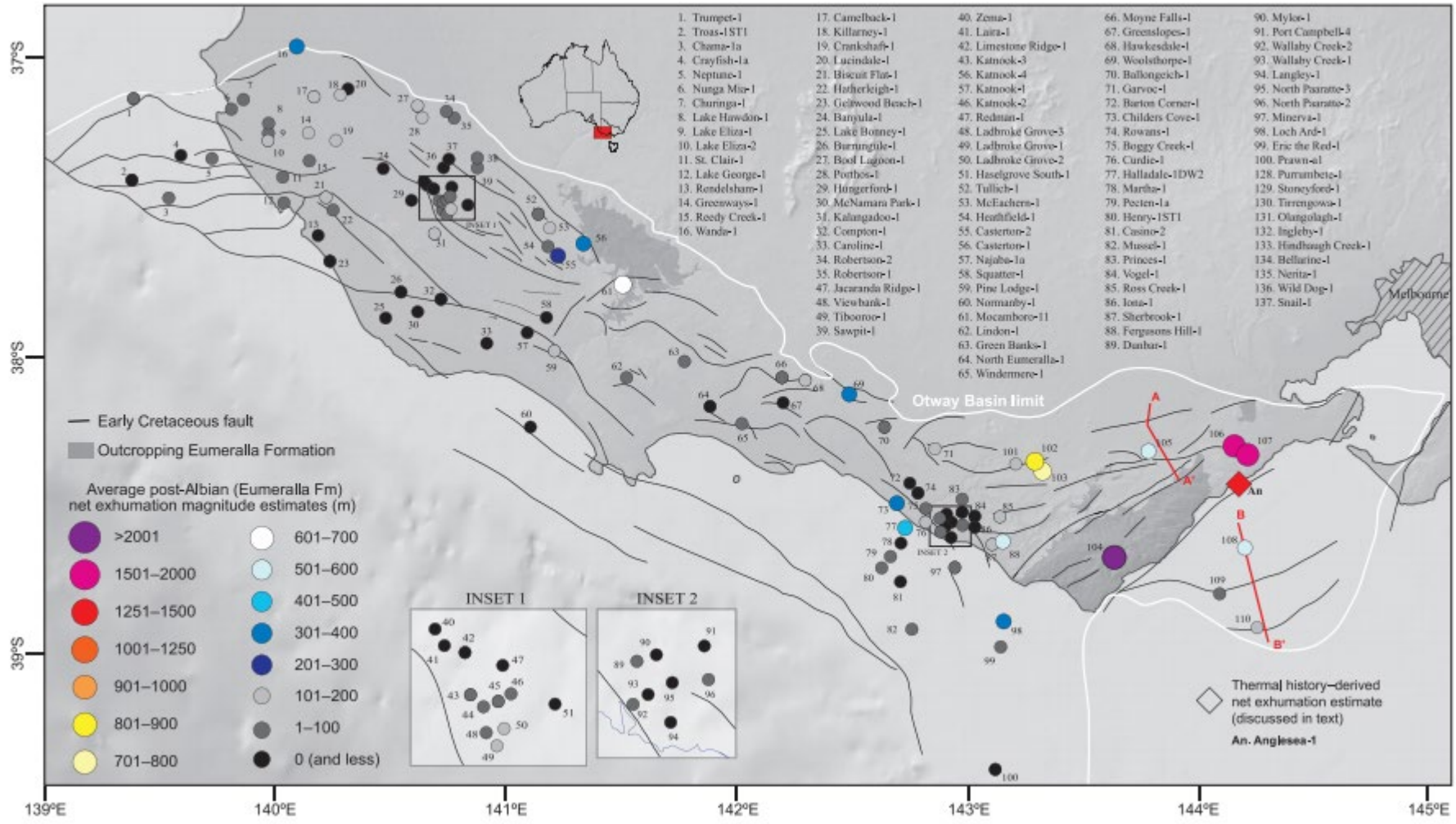

***Fig. 17**: A figure taken from Tassone et al. (2014) which outlines the distribution of post-Albian net exhumation across the Otway Basin.*

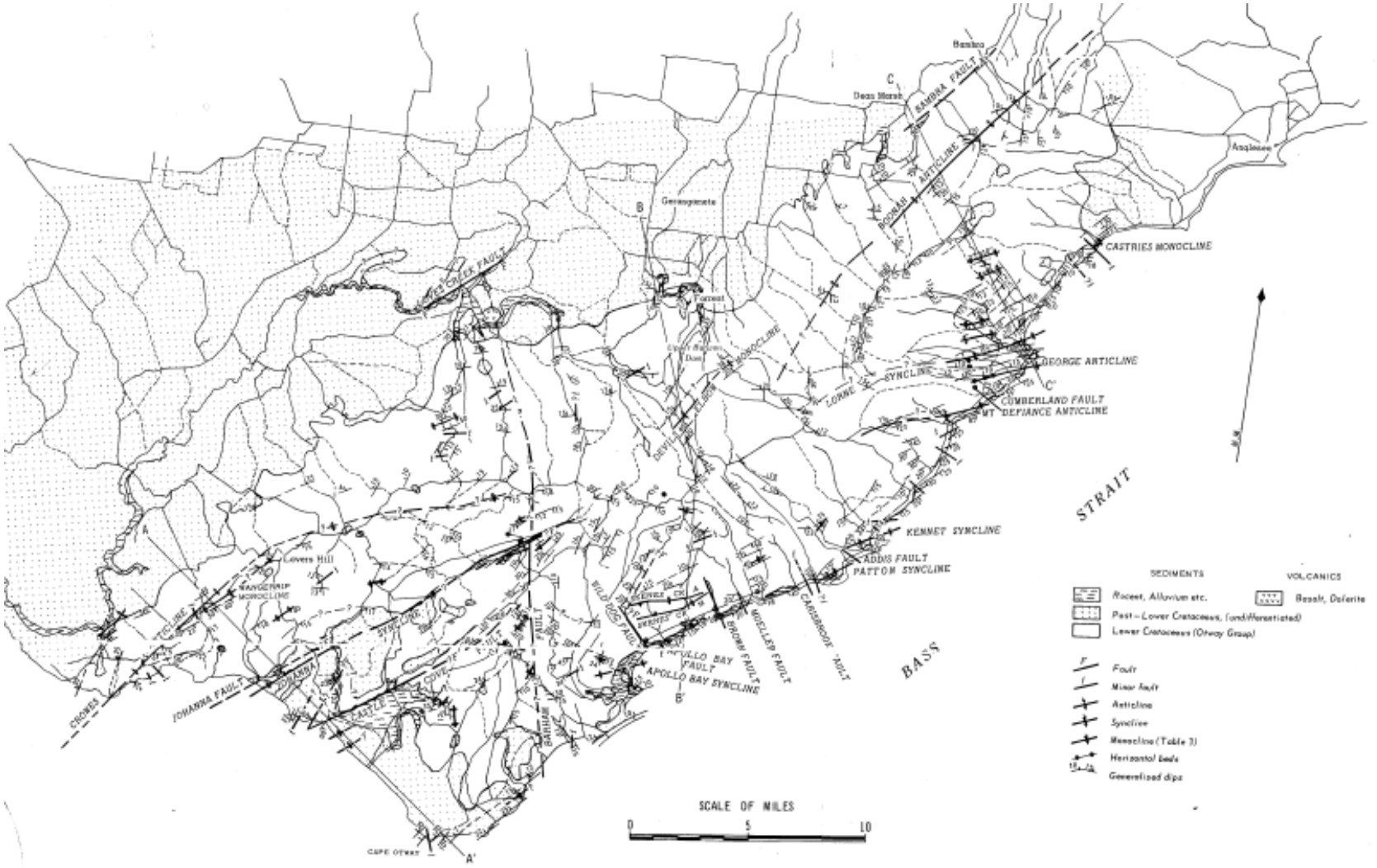

(*b*) Structural map of Otway Ranges showing generalized dips.

Fig. 18*: Detailed structural map of the Otway Ranges, note the lack of thrust faulting. Taken from Medwell (1968*).

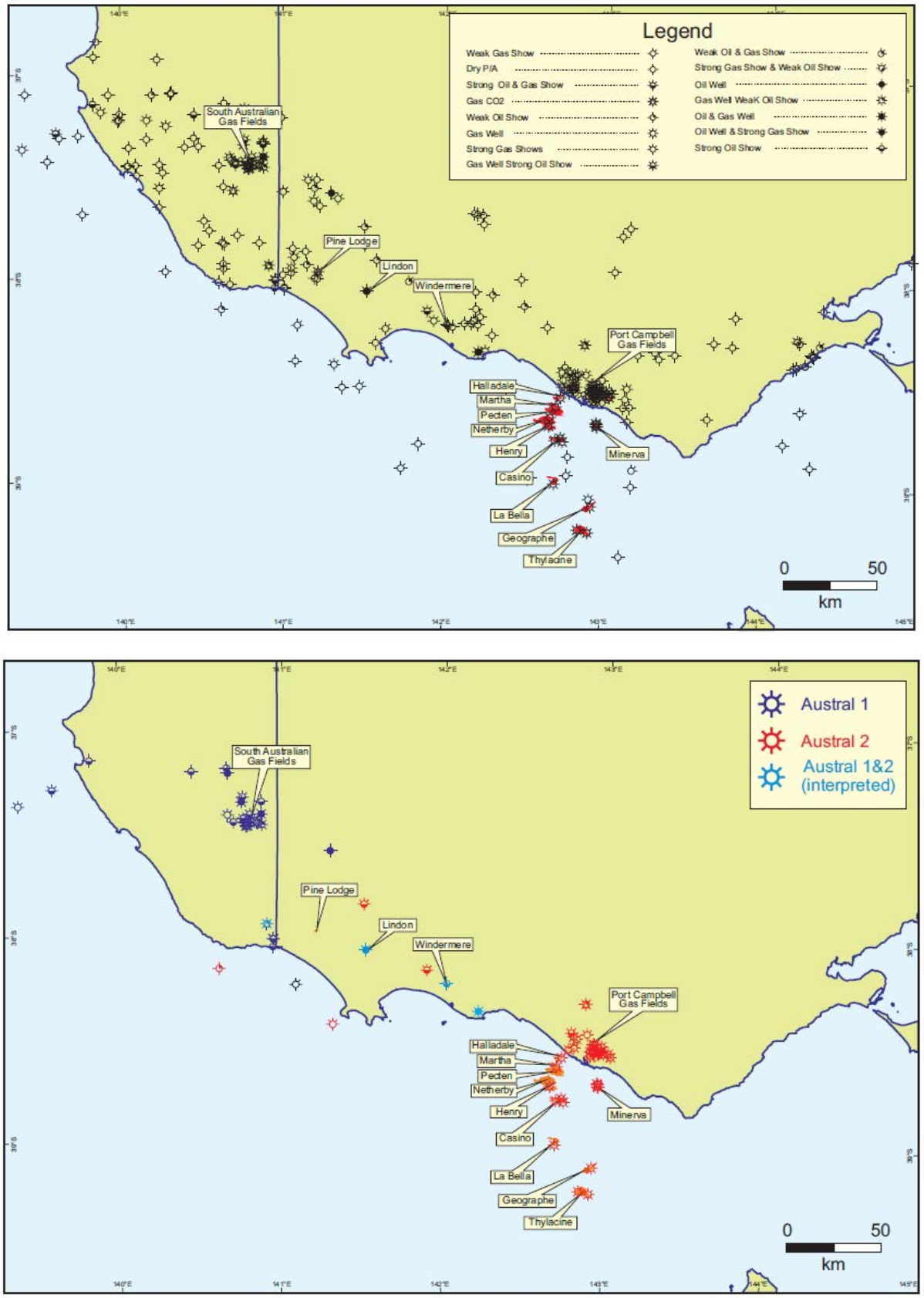

***Fig. 19**: Two figures taken from O'Brien et al. (2009). Top represents well drilled in the OB classified according to their hydrocarbon shows. Bottom represents wells that intersected strong shows within the different petroleum systems.*

State	Field	Reserves (Bcf)	Petroleum system
Victoria offshore			
	Minerva	300	Austral 2
	Casino	290	Austral 2
	Thylacine	532	Austral 2
	Geographe	286	Austral 2
	Martha/Halladale	153	Austral 2
	Labella	150	Austral 2
	Henry	160	Austral 2
Victoria onshore			
	North Paratte	10.9	Austral 2
	Iona	19	Austral 2
	Wild Dog Road	0.6	Austral 2
	Wallaby Creek	11.9	Austral 2
	Skull Creek	1.3	Austral 2
	Fenton Creek	3.2	Austral 2
	Mylor	7.9	Austral 2
	Penryn	2.4	Austral 2
	Boggy Creek	13.9	Austral 2
	Grumby	0.7	Austral 2
	Langley	3.4	Austral 2
	Dunbar	2.5	Austral 2
	Butress (CO_2)	1.1	
	McIntee		Austral 2
	Tregony	7.3	Austral 2
	Lavers	0.6	Austral 2
	Naylor	5.8	Austral 2
	Croft	5.8	Austral 2
	TOTAL	**1969.3**	
South Australia onshore			
	Caroline	89.6 (CO_2)	?Austral 1 & 2
	Haselgrove	17.4	Austral 1
	Jacaranda Ridge	0.026	Austral 1
	Katnook PHFm	26	Austral 1
	Katnook WSMr	4.41	Austral 1
	Katnook Intra-EuFm	0.001	Austral 1
	Ladbroke Grove PHF	61.62	Austral 1
	Redman	17.8	Austral 1
South Australia offshore			
	Troas	24.7	Austral 1
	TOTAL	**151.957**	

Table 1: *Taken from O'Brien et al. (2009) displays a list of approximate volumes of hydrocarbons present in fields in (in billion cubic feet or Bcf), classified by the (interpreted) petroleum system that sourced them.*

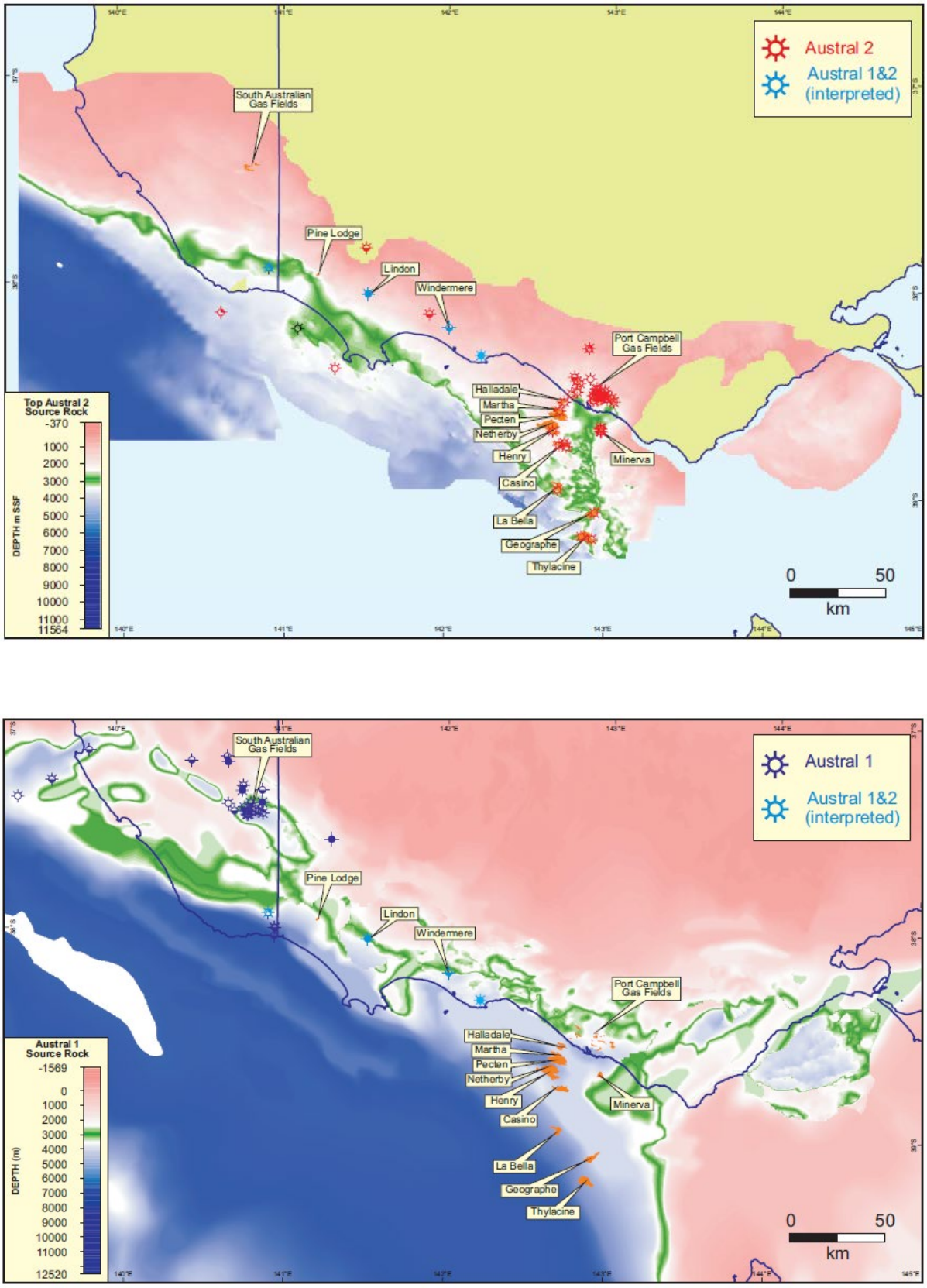

Fig. 20: *Peak maturity for the A1 (top) and A2 (bottom) petroleum systems within the Otway Basin. Taken from O'Brien et al. (2009).*

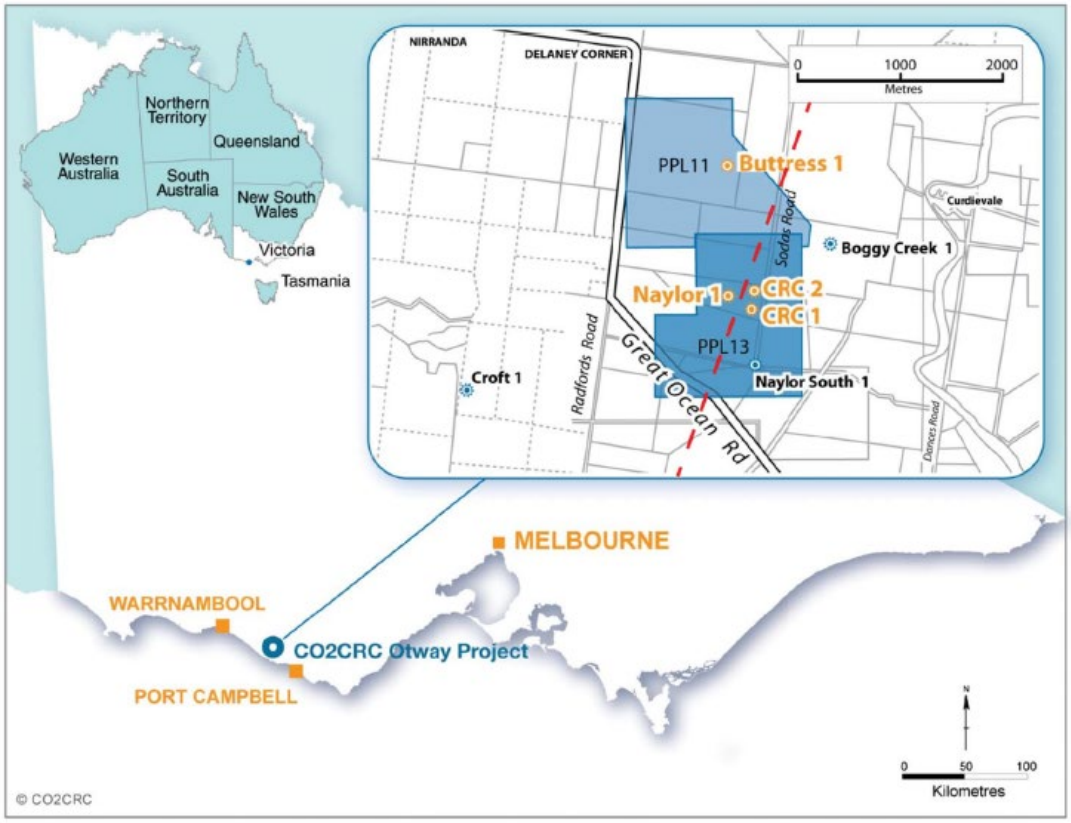

***Fig. 21**: A map showing the location of the CO2 CRC project in the Otway Basin. Taken from Aruffo et al. (2014)*

References

Alley N. F. and Lindsay J. M. 1995. The Phanerozoic, South Australia: In: Drexel J. F. & Preiss W. V. eds. The geology of South Australia Vol. 2. The Phanerozoic. South Australian Department of Minerals and Energy Bulletin 54, 151–218. Adelaide SA

Anderson, E. M. (1951). The dynamics of faulting and dyke formation with applications to Britain. Hafner Pub. Co..

Aruffo, C. M., Rodriguez-Herrera, A., Tenthorey, E., Krzikalla, F., Minton, J., & Henk, A. (2014). Geomechanical modelling to assess fault integrity at the CO2CRC Otway Project, Australia. Australian Journal of Earth Sciences, 61(7), 987-1001.

Bailey, A., King, R., Holford, S., Sage, J., Backe, G., & Hand, M. (2014). Remote sensing of subsurface fractures in the Otway Basin, South Australia. Journal of Geophysical Research: Solid Earth, 119(8), 6591-6612.

Bailey, A. H., King, R. C., Holford, S. P., & Hand, M. (2016). Extending interpretations of natural fractures from the wellbore using 3D attributes: The Carnarvon Basin, Australia. Interpretation, 4(1), SB107-SB129.

Ball, P., Eagles, G., Ebinger, C., McClay, K., & Totterdell, J. (2013). The spatial and temporal evolution of strain during the separation of Australia and Antarctica. Geochemistry, Geophysics, Geosystems, 14(8), 2771-2799.

Berard, T., Sinha, B. K., van Ruth, P., Dance, T., John, Z., & Tan, C. P. (2008, January). Stress estimation at the otway CO 2 storage site, Australia. In SPE Asia Pacific Oil and Gas Conference and Exhibition. Society of Petroleum Engineers.

BHP PETROLEUM, 1992—Farm-out proposal, VIC/P30 and VIC/P31, Otway Basin, unpublished.

Birch (Editor) W. D., G. S. o. V. (2003). Geology of Victoria. Special Publication, 23.

Boeuf, M. G., & Doust, H. (1975). Structure and Development of the Southern Margin of Australia. The APPEA Journal, 15(1), 33-43.

Boreham, C. J., Hope, J. M., Jackson, P., Davenport, R., Earl, K. L., Edwards, D. S., ... & Krassay, A. A. (2004). Gas-oil-source correlations in the Otway Basin, southern Australia.

Boult, P., & Hibburt, J. E. (2002). The petroleum geology of South Australia. In Otway Basin (Vol. 1). Department of Primary Industries and Resources South Australia.

Boult, P. J., Camac, B. A., & Davids, A. W. (2002). 3D fault modelling and assessment of top seal structural permeability—Penola Trough, onshore Otway Basin. The APPEA Journal, 42(1), 151-166.

Bradshaw, M. (1993). Australian petroleum systems. PESA Journal, 21, 43-53

Briguglio, D., Hall, M., & Keetley, J. (2015). Structural evolution of the Early Cretaceous depocentres, Otway Basin, Victoria. Australian Journal of Earth Sciences, 62(6), 717-733.

Cayley, R. A., Taylor, D. H., VandenBerg, A. H. M., & Moore, D. H. (2002). Proterozoic–Early Palaeozoic rocks and the Tyennan Orogeny in central Victoria: the Selwyn Block and its tectonic implications. Australian Journal of Earth Sciences, 49(2), 225-254.

Cooper, G. T. (1995). Seismic Structure and Extensional Development of the Eastern Otway Basin-Torquay Embayment. APEA.

Cooper, G. T., & Hill, K. C. (1997). Cross-section balancing and thermochronological analysis of the Mesozoic development of the eastern Otway Basin. The APPEA Journal, 37(1), 390-414.

Debenham, N., King, R. C., & Holford, S. P. (2018). The influence of a reverse-reactivated normal fault on natural fracture geometries and relative chronologies at Castle Cove, Otway Basin. Journal of Structural Geology, 112, 112-130.

Drexel, J. F., & Preiss, W. V. (Eds.). (1995). The Geology of South Australia (Vol. Volume 2: The Phanerozoic)

Dickinson, J. A., Wallace, M. W., Holdgate, G. R., Gallagher, S. J., & Thomas, L. (2002). Origin and timing of the Miocene-Pliocene unconformity in southeast Australia. Journal of Sedimentary Research, 72(2), 288-303.

Duddy, I. R., & Erout, B. (2001). AFTA-calibrated 2-D Modelling of Hydrocarbon Generation and Migration Using Temispack: Preliminary Results from the Otway Basin. Eastern Australasian Basins Symposium (485-497).

Duddy, I. R. (2003). Mesozoic, a time of change in tectonic regime. Geology of Victoria, 23, 239-286.

Edwards, J., Leonard. J. G., Pettifer, G. R. McDonald, P. A. (1996). Colac 1: 250 000 map geological report. Geological Survey of Victoria.

Edwards, D. S., Struckmeyer, H. I. M., Bradshaw, M. T., & Skinner, J. E. (1999). Geochemical characteristics of Australia's southern margin petroleum systems. The APPEA Journal, 39(1), 297-321.

Espurt, N., Callot, J.-P., Totterdell, J., Struckmeyer, H., & Vially, R. (2009). Interactions between continental breakup dynamics and large-scale delta system evolution: Insights from the Cretaceous Ceduna delta system, Bight Basin, Southern Australian margin. Tectonics, 28(6), n/a-n/a. doi: 10.1029/2009TC002447

Etheridge, M. A., Branson, J. C., & Smith, P. G. S. (1985). Extensional Basin-forming Structures in Bass Strait and their Importance for Hydrocarbon Exploration. The APPEA Journal, 25, 344-361.

Finlayson, DM (compiler), NGMA/Petroleum Exploration Society of Australia Otway Basin Symposium, Melbourne (Vol. 20, pp. 7-12).

Finlayson, D. M., Johnstone, D. W., Owen, A. J., & Wake-Dyster, K. D. (1996). Deep seismic images and the tectonic framework of early rifting in the Otway Basin, Australian southern margin. Tectonophysics, 264(1-4), 137-152.

Finlayson, D. M., Collins, C. D. N., Lukaszyk, I., & Chudyk, E. C. (1998). A transect across Australia's southern margin in the Otway Basin region: crustal architecture and the nature of rifting from wide-angle seismic profiling. Tectonophysics, 288(1-4), 177-189.

Foster, J. D., & Hodgson, A. J. (1995). Port Campbell reviewed: methane and champagne. The APPEA Journal, 35(1), 418-435.

Gallagher, S. J., & Holdgate, G. (2000). The palaeogeographic and palaeoenvironmental evolution of a Palaeogene mixed carbonate–siliciclastic cool-water succession in the Otway Basin, Southeast Australia. Palaeogeography, Palaeoclimatology, Palaeoecology, 156(1-2), 19-50.

Geary, G. C. and Reid, I. S. A. (1998) Geology and prospectivity of the offshore eastern Otway Basin, Victoria. Victorian Initiative for Minerals and Petroleum Report, 55

Geoscience Australia (2014). The Otway Basin. 25/06/2016. http://www.ga.gov.au/scientific-topics/energy/province-sedimentary-basin-geology/petroleum/offshore-southern-australia/otway

Gibson, G. M., Morse, M. P., Ireland, T. R., & Nayak, G. K. (2011). Arc–continent collision and orogenesis in western Tasmanides: Insights from reactivated basement structures and formation of an ocean–continent transform boundary off western Tasmania. Gondwana Research, 19(3), 608-627. doi: http://dx.doi.org/10.1016/j.gr.2010.11.020

Gibson, G. M., Totterdell, J. M., White, L. T., Mitchell, C. H., Stacey, A. R., Morse, M. P., & Whitaker, A. (2013). Pre-existing basement structure and its influence on continental rifting and fracture zone development along Australia's southern rifted margin. Journal of the Geological Society, 170(2), 365-377.

Glenie, R. C. (1971). Upper Cretaceous and Tertiary rock-stratigraphic units in the central Otway Basin. The Otway Basin of Southeastern Australia, 193-214.

Gloe, C. S., Barton, C. M., Holdgate, G. R., Bloger, P. F., King, R. L., & George, A. M. (1976). Brown coal. Geology of Victoria: Geological Society of Australia, Special Publication, 5, 378-389.

Green, P. F., Crowhurst, P. V., & Duddy, I. R. (2004). Integration of AFTA and (U-Th)/He thermochronology to enhance the resolution and precision of thermal history reconstruction in the Anglesea-1 well, Otway Basin, SE Australia.

Hill, K. C., & Cooper, G. T. (1996). A strategy for palinspastic restoration of inverted basins: thermal and structural analyses in SE Australia. Geological Society, London, Special Publications, 99(1), 99-115.

Hill, K. A., Cooper, G. T., Richardson, M. J., & Lavin, C. J. (1994). Structural framework of the eastern Otway Basin: inversion and interaction between two major structural provinces. Exploration Geophysics, 25(2), 79-87.

Hillis, R. R., & Reynolds, S. D. (2000). The Australian stress map. Journal of the Geological Society, 157(5), 915-921.

Hillis, R. R., & Williams, A. F. (1992). Borehole breakouts and stress analysis in the Timor Sea. Geological Society, London, Special Publications, 65(1), 157-168.

Hillis, R. R., & Williams, A. F. (1993). The contemporary stress field of the Barrow-Dampier Sub-Basin and its implications for horizontal drilling. Exploration Geophysics, 24(4), 567-576.

Hill, K. C., Hill, K. A., Cooper, G. T., O'Sullivan, A. J., O'Sullivan, P. B., & Richardson, M. J. (1995). Inversion around the Bass basin, SE Australia. Geological Society, London, Special Publications, 88(1), 525-547.

Hillis, R. R. (1995). The contemporary stress field of the Otway Basin, South Australia: implications for hydrocarbon exploration and production. APEA Journal.

Holford, S. P., Tuitt, A. K., Hillis, R. R., Green, P. F., Stoker, M. S., Duddy, I. R., . . . Tassone, D. R. (2014). Cenozoic deformation in the Otway Basin, southern Australian margin: implications for the origin and nature of post-breakup compression at rifted margins. Basin Research, 26(1), 10-37. doi: 10.1111/bre.12035

Holford, S., Hillis, R., Duddy, I., Green, P., Stoker, M., Tuitt, A., ... & MacDonald, J. (2011). Cenozoic post-breakup compressional deformation and exhumation of the southern Australian margin. The APPEA Journal, 51(1), 613-638.

Krassay, A. A., & Totterdell, J. M. (2003). Seismic stratigraphy of a large, Cretaceous shelf-margin delta complex, offshore southern Australia. AAPG bulletin, 87(6), 935-963.

Krassay, A. A., Cathro, D. L., & Ryan, D. J. (2004). A regional tectonostratigraphic framework for the Otway Basin.

Lavin, C. J., & Muscatello, T. (1997). The Petroleum Prospectivity Pf the Casterton Petroleum System in the Victorian Onshore Otway Basin. Department of Natural Resources & Environment.

Leslie, R. L. (1966). Petroleum Exploration in the Otway Basin. Paper presented at the Proceedings of the 8th Commonwealth and Metallurgical Congress, Australia and New Zealand.

Leven, J. H., Finlayson, D. M., Wright, C., Dooley, J. C., Kennett, B. L. N., Willcox, J. B., & Stagg, H. M. J. (1990). Siesmic Probing of Continents and their MarginsAustralia's southern margin: a product of oblique extension. Tectonophysics, 173(1), 269-281

Lister, G. S., Etheridge, M. A., & Symonds, P. A. (1991). Detachment models for the formation of passive continental margins. Tectonics, 10(5), 1038-1064.

Lovibond, R., & Aburas, R. J. S. J. E. S. A. N. (1995). The Hydrocarbon Potential of the Penola Trough. Australian Petroleum Exploration Association Journal, 35(1), 358-371.

Luxton, C. W., Horan, S. T., Pickavance, D. L., & Durham, M. S. (1995). The La Bella and Minerva gas discoveries, offshore Otway basin. The APPEA Journal, 35(1), 405-417.

Lyon, P. J., Boult, P. J., Hillis, R. R., & Bierbrauer, K. (2007). Basement controls on fault development in the Penola Trough, Otway Basin, and implications for fault-bounded hydrocarbon traps. Australian Journal of Earth Sciences, 54(5), 675-689.

McQueen, A. F. (1962). The Geology of the Otway Basin. Australian Oil and Gas Journal, 8(2), 8-12.

Medwell, G. J. (1971) Structures of the Otway Ranges. Geological Survey of Victoria. Special Bulletin. 339-359.

Mehin, K., & Constantine, A. E. (1999). Hydrocarbon potential of the western onshore Otway Basin in Victoria: 1999 Acreage Release. Victorian Initiative for Minerals and Petroleum Report, 62.

Mehin, K., & Kamel, M. (2002). Gas resources of the Otway Basin in Victoria.

Mehin, K., & Link, A. G. (1994). Source, migration and entrapment of hydrocarbons and carbon dioxide in the Otway Basin, Victoria. The APPEA Journal, 34(1), 437-459.

Mildren, S. D., & Hillis, R. R. (2000). In situ stresses in the Southern Bonaparte Basin, Australia: Implications for first-and second-order controls on stress orientation. Geophysical research letters, 27(20), 3413-3416.

Miller, J. M., Norvick, M. S., & Wilson, C. J. (2002). Basement controls on rifting and the associated formation of ocean transform faults—Cretaceous continental extension of the southern margin of Australia. Tectonophysics, 359(1-2), 131-155.

Moore, A. M. G., Stagg H. M. J., Norvick M. S. . (2000). Deep-water Otway Basin: A New Assessment of the Tectonics and Hydrocarbon Prospectively. The APPEA Journal, 40, 66-85.

Morton, J. G. G., & Drexel, J. F. (Eds.). (1995). The petroleum geology of South Australia. Petroleum Division, SA Department of Mines and Energy.

Nelson, E., Hillis, R., Sandiford, M., Reynolds, S., & Mildren, S. (2006). Present-day state-of-stress of southeast Australia. The APPEA Journal, 46(1), 283-306.

Noll, C. A., & Hall, M. (2003). Fluvial architecture and the tectonic control on deposition of onshore Eumeralla Formation, Otway Ranges, Victoria: implications for exploration in the Early Cretaceous Otway Basin. The APPEA Journal, 43(1), 99-116.

Norvick, M. S., & Smith, M. A. (2001). Mapping the plate tectonic reconstruction of southern and southeastern Australia and implications for petroleum systems. The APPEA Journal, 41(1), 15-35.

O'Brien, G. W., Reeves, C. V., Milligan, P. R., Morse, M. P., Alexander, E. M., Willcox, J. B., ... & Brodie, R. C. (1994). New ideas on the rifting history and structural architecture of the western Otway Basin: evidence from the integration of aeromagnetic, gravity and seismic data. The APPEA Journal, 34(1), 529-554.

O'Brien, G., Boreham, C., Thomas, H., & Tingate, P. (2009). Understanding the critical success factors determining prospectivity—Otway Basin, Victoria. The APPEA Journal, 49(1), 129-170.

Padley, D., McKirdy, D. M., Skinner, J. E., Summons, R. E., & Morgan, R. P. (1995). Crayfish Group hydrocarbons—implications for palaeoenvironment of Early Cretaceous rift fill in the western Otway Basin. The APPEA Journal, 35(1), 517-537.

Palmowski, D., Hill, K. C., Hoffman, N., & Bernecker, T. (2001). Otway Basin Rifting to sea-floor spreading-hydrocarbon implications.

Palmowski, D., Hill, K. C., & Hoffman, N. (2004). Structural-Stratigraphic Styles and Evolution of the Offshore Otway Basin-A Structural Seismic Analysis.

Partridge, A. D. (2001). Revised stratigraphy of the Sherbrook Group, Otway Basin.

Cockshell, D. P. C. (1995). The Otway basin: early Cretaceous rifting to Neogene inversion. The APPEA Journal, 35(1), 451-466.

Perincek, D., Simons, B., & Pettifer, G. R. (1994a). THE TECTONIC FRAMEWORK AND ASSOCIATED PLAY TYPES OF THE WESTERN OTWAY BASIN, VICTORIA, AUSTRALIA. The APPEA Journal, 34(1), 460-478.

Perincek, D., Cockshell, C. D., Finlayson, D. M., & Hill, K. A. (1994b). The Otway Basin: Early Cretaceous Rifting to Miocene Strike Slip. In Proceedings NGMA/PESA Otway Basin Symposium Abstracts, AGSO Record (pp. 27-33).

Presnton, J., 1992a—Geochemical evaluation of cuttings samples from Fergusons Hill-1, Otway Basin, Victoria, Southern Australia. BHP Petroleum report, June, unpub-lished.

Rajabi, M., Tingay, M., Heidbach, O., Hillis, R., & Reynolds, S. (2017). The Present-day stress field of Australia. Earth-Science Reviews, 168, 165-189.

Reynolds, S. D., & Hillis, R. R. (2000). The in situ stress field of the Perth Basin, Australia. Geophysical Research Letters, 27(20), 3421-3424.

Reynolds, M. A., Evans, P. R., Bryan, R., & Hawkins, P. J. (1966). The stratigraphic nomenclature of Cretaceous rocks in the Otway Basin. Australian Oil and Gas Journal, 13(3), 2-33.

Reynolds, S. D., Coblentz, D. D., & Hillis, R. R. (2003). Influences of plate-boundary forces on the regional intraplate stress field of continental Australia. SPECIAL PAPERS-GEOLOGICAL SOCIETY OF AMERICA, 59-70.

Robson, A. G., Holford, S. P., & King, R. C. (2017). Structural evolution of a normal fault array in the Gambier Embayment, offshore Otway Basin, South Australia: insights from 3D seismic data. Australian Journal of Earth Sciences, 64(5), 611-624.

Robson, A. G., King, R. C., & Holford, S. P. (2017). Structural evolution of a gravitationally detached normal fault array: Analysis of 3D seismic data from the Ceduna Sub-Basin, Great Australian Bight. Basin Research, 29(5), 605-624.

Robson, A. G., Holford, S. P, King. R. C, and D. Kulikowski (2018). Structural evolution of horst and half-graben structures proximal to a transtensional fault system determined using

3D seismic data from the Shipwreck Trough, offshore Otway Basin, Australia, Marine and Petroleum Geology, 89(3), 615-634, doi:10.1016/j.marpetgeo.2017.10.028.

Royer, J. Y., & Rollet, N. (1997). Plate-tectonic setting of the Tasmanian region. Australian Journal of Earth Sciences, 44(5), 543-560.

Sandiford, M., Wallace, M., & Coblentz, D. (2004). Origin of the in situ stress field in south-eastern Australia. Basin Research, 16(3), 325-338.

Sandiford, M. I. K. E. (2003). Neotectonics of Southeastern Australia: linking the Quaternary faulting record with seismicity and in situ stress. SPECIAL PAPERS-GEOLOGICAL SOCIETY OF AMERICA, 107-120.

Schneider, C. L., Hill, K. C., & Hoffman, N. (2004). Compressional growth of the Minerva Anticline, Otway Basin, Southeast Australia—evidence of oblique rifting. The APPEA Journal, 44(1), 463-480.

Smith, G.C. 1988. Oil and Gas. In: Douglas, J. G., Ferguson, J. A., & Douglas, J. G. (1988). Geology of Victoria. Melbourne, Australia: Geological Society of Australia.

Stacey, A., Totterdell, J., Heike, I. S., & Mitchell, C. (2013). Geology and Hydrocarbon Prospectivity of the Deepwater Otway and Sorell Basins, Offshore Southeastern Australia [h][online Resource]/[c] Andrew Stacey, Cameron Mitchell, Heike Struckmeyer and Jennifer Totterdell. Geoscience Australia.

Basins of the Great Australian Bight region: geology and petroleum potential

Tassone, D. R. (2014). Compressional deformation and exhumation in sedimentary basins at ‘passive’continental margins, with implications for hydrocarbon exploration and development (Doctoral dissertation).

Tassone, D. R., Holford, S. P., Duddy, I. R., Green, P. F., & Hillis, R. R. (2014). Quantifying Cretaceous–Cenozoic exhumation in the Otway Basin, southeastern Australia, using sonic transit time data: Implications for conventional and unconventional hydrocarbon prospectivity. AAPG Bulletin, 98(1), 67-117.

Tassone, D. R., Holford, S. P., King, R., Tingay, M. R., & Hillis, R. R. (2017). Contemporary stress and neotectonics in the Otway Basin, southeastern Australia. Geological Society, London, Special Publications, 458, SP458-10.

Teasdale, J. P., Pryer, L. L., Stuart-smith, P. G., & Loutit, M. A. E. T. S. (2003). Structural framework and basin evolution of Australia's southern margin. The APPEA Journal, 43, 12-35.

Thompson, B. R., & Walker, G. M. (1985). Development of a stratigraphic data file for the Otway Basin. Otway 85, earth resources of the Otway Basin: summary papers and excursion guides, Mount Gambier, South Australia, 7th-10th February, 1985, 23.

Totterdell, J. M., Blevin, J. E., Struckmeyer, H. I. M., Bradshaw, B. E., Colwell, J. B., & Kennard, J. M. (2000). A NEW SEQUENCE FRAMEWORK FORTHE GREAT AUSTRALIAN BIGHT: STARTING WITH A CLEAN SLATE. The APPEA Journal, 40(1), 95-118.

Van Ruth, P. (2007). CRC-1 extended leak-off test report. CO2CRC Report RPT07-0608, 8.

Van Ruth, P. J., Nelson, E. J., & Hillis, R. R. (2006). Fault reactivation potential during CO2 injection in the Gippsland Basin, Australia. Exploration Geophysics, 37(1), 50-59.

Veevers, J. J., Powell, C. M., & Roots, S. R. (1991). Review of seafloor spreading around Australia. I. Synthesis of the patterns of spreading. Australian journal of earth sciences, 38(4), 373-389.

Vidal-Gilbert, S., Tenthorey, E., Dewhurst, D., Ennis-King, J., Van Ruth, P., & Hillis, R. (2010). Geomechanical analysis of the Naylor Field, Otway Basin, Australia: Implications for CO2 injection and storage. International Journal of Greenhouse Gas Control, 4(5), 827-839.

Wallace, M. W., Dickinson, J. A., Moore, D. H., & Sandiford, M. (2005). Late Neogene strandlines of southern Victoria: a unique record of eustasy and tectonics in southeast Australia. Australian Journal of Earth Sciences, 52(2), 279-297.

Watson, M. N., Boreham, C. J., & Tingate, P. R. (2004). Carbon dioxide and carbonate cements in the Otway Basin: implications for geological storage of carbon dioxide. The APPEA Journal, 44(1), 703-720.

White, A. H. (1968). Exploration in the Otway Basin. The APPEA Journal, 8(78-87).

Willcox, J. B., & Stagg, H. M. J. (1990). Australia's southern margin: a product of oblique extension. Tectonophysics, 173(1-4), 269-281.

Chapter 3: Literature Review of Methods Used in this Study

Foreword

The aim of this thesis is to integrate a number of proven methods of structural analysis, from the micro to the macroscale, in order to provide a complete understanding of the evolution of stress within passive margin sedimentary basins. This work represents the most comprehensive structural analysis, in addition to the first study of paleostress evolution within such a setting to date. Providing insights that are applicable to all industries that utilise sub-surface resources (e.g. oil, gas, geothermal energy, carbon capture and storage) within these provinces. The chosen case study is the Otway Basin, Australia. A sedimentary province that provides outcropping rift sections, along with a large amount of petroleum industry data, both on and offshore, which has allowed for traditional outcrop and laboratory techniques to be combined with cutting edge industry geophysical and well data. As a result, this study also represents the first time many of these techniques have been used, and integrated, within a predominantly offshore sedimentary basin.

The methods used in this study can be broken down to the various spatial scales they are concerned with:

Microscale: A*pplication of calcite twin and petrophysical analysis, including the anisotropy of magnetic susceptibility and the anisotropy of P-wave velocity.*

Mesoscale: *Geophysical (well bore image log), core and outcrop analysis of natural fracture data.*

Macroscale: *The analysis of three dimensional (3D) seismic datasets.*

The following section provides outlines of these analytical methods, beginning with calcite twin stress inversion, in many senses, the key microscale method of this study.

3.1 Calcite Twin Stress Inversion Technique

3.1.1 The nature of twinning within calcite crystal

The occurrence of twinning within calcite crystals is a mechanism of plastic deformation and a response to gliding along particular crystal planes (Amrouch, 2010). First studied by Turner (1953), twinning in calcite occurs primarily at low confining pressures and temperatures of typically between 25Cº and 400ºC with levels of critical resolved shear stress (RSS) of 10±4 MPa (Turner et al., 1954; Lacombe and Laurent, 1996; Laurent et al., 2000; Amrouch, 2010; Lacombe, 2010; Kulikowski, 2018; Beaudoin and Lacombe, 2018). The development of twins within calcite crystals of varying size follows well constrained geometric laws (**fig. 1**) with each twin representing a dislocation wedge (**fig. 2**) which has migrated along a sliding plane, defined as an *e* twin (Amrouch, 2010). Each calcite crystal contains three *e* planes, configured around the optical axis of the crystal (Turner and Orozco, 1976) with the direction of twinning along each plane, defined as the orientation of the straight line that connects the initial and final position of a given atom or the direction of simple shear (Amrouch, 2010; Kulikowski, 2018). Twinning with calcite crystals is limited to these three *e* planes due to the atomic structure of calcite (Turner and Orozco, 1976). Each twin lamella within a crystal can be compared to a fault plane, which as a result of the critical RSS, experiences reactivation and subsequent slip in a certain orientation, in the case of a vertical optical crystal axis, this reactivation is towards the centre, much like a reverse fault (Turner et al., 1954).

Twinning will only occur under shear stresses above a critical values, defined as the critical resolved shear stress (CRSS) or the twinning threshold $\tau_{s.}$

$$Equation\ 1: \tau_a = \sigma * S$$

Equation 1, represents how the value of CRSS can be obtained, where σ represents the stress applied to the critical point of the twin plane and *S* represents the Schmid factor (Amrouch, 2010; Kulikowski, 2018) defined below.

$$Equation\ 2\text{: } S = \cos(\alpha) * \cos(\beta)$$

Where α represents the angle between the direction normal to the twin plane and the direction of the applied compressional stress and β, the angle between the compression and the twin displacement vector. High Schmid values have been shown to be analogous with high volumes of twinning (Rowe and Rutter, 1990). A value or CRSS of 10MPa is typically used for grains sized between 300-400μm (Turner et al., 1954, Laurent, 1984; Lacombe and Laurent, 1996) the value is largely independent of temperature, and can vary, especially with grain size and distribution (Newman, 1994) and internal deformation (Laurent et al., 2000). The magnitude of CRSS also depends on internal crystal strain or strain hardening, fluctuating between 5-7MPa for weakly (~1%) deformed crystals and 13-15MPa for zones of higher (4%) deformation (Laurent et al., 2000).

3.1.2 External effects which can influence results

3.1.2.1 Grain Size

Work by Rowe and Rutter (1990) and a number of previous studies (Schmid and Paterson, 1977; Casey et al., 1978; Spiers, 1982; Spiers and Rutter, 1984) showed that the occurrence and volume fraction of twinning within a crystal increases with grain size. As such, given constant conditions of differential stress, larger crystals will contain a higher incidence of twins than smaller crystals (Kulikowski et al., 2018) mainly due to the relationship between grain boundary and grain volume. Therefore, as grain size increases values of CRSS decrease which

has consequences for understanding variations in grain size within samples when using techniques of calcite twin stress inversion (Kulikowski et al., 2018).

3.1.2.2 Internal Deformation

It has been shown that due to strain hardening affects within heavily deformed or twisted calcite crystals, values of CRSS are often higher than within undeformed crystals (Amrouch, 2010). The more deformed a crystal, the more difficult it is to twin (Amrouch, 2010). Indeed, at higher temperatures of deformation or simply higher deformation in general, other mechanisms for absorbing stress can intervene such as sliding along cleavage planes within the crystal, which can result in the distortion or curving of twins (Amrouch, 2010).

3.1.2.3 Temperature

Temperature can have a significant effect on the appearance of twins within calcite crystals (Burkhard, 1994) but as twinning is not thermally activated it is not directly dependant on temperature. Amrouch (2010) shows that twin density can be highly affected by temperature as especially below 170 ºC -200 ºC it is far easier to widen existing twin planes than to create new ones. The opposite is also true; at temperatures exceeding ~200 ºC, it is easier to create new twins than to widen existing ones (Amrouch, 2010) and as such high temperature twinning conditions are reflective of thick, low density twins (Burkhard, 1994; Ferrill, 1998; Janssen et al., 2007). Resulting relationships between twin density, twinning temperature, twinning intensity and thickness can be used to provide indications as to the paleotemperature conditions that rocks were exposed to (Amrouch, 2010)

3.1.2.4 Pressure

Both isotropic and fluid pressures have been found to increase the normal stress acting on twin planes, increasing the CRSS value required to induce twinning. Although this increased value is <1% of the value of normal stress (Turner et al., 1954). This was confirmed by Friedman and Heard (1974) who showed that twinning will not occur if samples are exposed to simple isotropic environments of stress (Amrouch, 2010).

3.1.2.5 Differential Stress Magnitude

It has been shown for any constant grain size, temperature or confining pressure, the maximum differential stress ($\sigma_1 - \sigma_3$) can significantly influence twin density (**fig. 3**) and the volume fraction of twinning within the crystal (Rowe and Rutter, 1990; Amrouch, 2010). Given a constant grain size, increases in maximum differential stress will result in higher twin volumes, density and incidence (Kulikowski, 2018).

3.1.2.6 The appearance of calcite twins

As the measurement of calcite twins within this study has been completed manually – using a universal stage - it is important to recognise how the above factors can influence the appearance of twin planes within calcite crystals. Much work on this was completed by Burkhard (1994). **Fig. 4** displays a modified table which assists in classifying calcite twins based upon their appearance.

.

3.1.3 Determining Paleostress Tensors from Calcite Twins

3.1.3.1 Background

Since the pioneering work of Turner (1953) 65 years ago, there have been several methods developed to determine paleo-stress orientations from calcite twin data (Spang, 1972; Jamison and Spang, 1976; Laurent, 1984; Laurent et al., 1990; Etchecopar, 1984; Sperner and Ratschbacher, 1994; Nemcok et al., 1999; Lacombe, 2010). All these methods of paleostress analysis founded on calcite twin analysis share a fundamental assumption that crystal twins were formed under a homogenous stress field and have not been subject to passive rotations following deformation (Lacombe, 2010). These methods work best when applied to small strains which can easily be approximated by coaxial conditions of stress and strain (Burkhard, 1993; Lacombe, 2010), in this case the orientation of twinning along *e* planes can be correlated with principal paleostress orientations.

Amongst these different methods, Etchecopar's (1984) calcite stress inversion technique (CSIT) has emerged as the most useful and regularly used, applied in a number of tectonic environments including the thrust belts of Zagros [Iran] (Amrouch et al., 2010), Khao Khwang [Thailand] (Arboit et al., 2017), The Albanides [Albania] (Lacombe et al., 2009) and the Rocky Mountains [Wyoming] (Craddock and Van Der Pluijm, 1999; Amrouch et al., 2010a, 2010b; Beaudoin et al., 2012, 2016) and more recently in the Cooper and Eromanga Basins of Australia (Kulikowski and Amrouch, 2017). While early techniques of calcite twin analysis such as Turner's (1953) which can only be applied to uniaxial stress ellipsoids and yields only the orientation of the maximum and minimum principal stresses, and Jamison and Spang's (1976) which provides only the maximum differential stress and no orientations, the computerised CSIT provides five of the 6 parameters needed to constrain the complete stress tensor (Lacombe, 2010). To date, CSIT (Etchecopar, 1984; Laurent, 1984) is the only technique which

allows for the simultaneous calculation of principal stress orientation and differential stress magnitudes from a single set of twin data (Lacombe, 2010). The method is tried and proven (Beaudoin and Lacombe, 2018) and although the last three years has seen the emergence of new methods (Parlangeau et al., 2018; Yamaji, 2015) CSIT continues to be the most widely used (Beaudoin and Lacombe, 2018).

3.1.3.2 Etchecopar's Calcite Stress Inversion Technique

The CSIT technique contains a number of assumptions:

1) *The state of stress is homogeneous at the grain scale*
2) *A constant critical resolved shear stress is responsible for twinning*
3) *Tangential forces applied to any material cause parallel displacement*
4) *The stress tensor is symmetrical, i.e no torque.*

The inversion process is very similar to that used to determine paleostress orientations from fault slip data (Etchecopar, 1984), as twin gliding in the direction of twinning is geometrically comparable to slip along a slickenside lineation within a fault plane (Lacombe, 2010). In addition to accounting for deformed – twinned - planes, CSIT also takes into account undeformed – untwinned - planes (Etchecopar, 1984). The inverse problem consists of finding the appropriate stress tensor that best fits the distribution of both twinned and untwinned planes within the crystal (Lacombe, 2010). Theoretically, the derived stress tensor must meet the major requirements that all twinned planes have sustained RSS larger than that exerted upon all the untwinned planes (Lacombe, 2010).

The initial inversion of slip data along calcite twin planes produces what is defined as the reduced stress tensor, **T'**, which contains only four of the six parameters needed for a complete tensor (Lacombe, 2010).

These four parameters include:

1) Orientation of the maximum principal stress ($\boldsymbol{\sigma_1}$)

2) Orientation of the intermediate principal stress ($\boldsymbol{\sigma_2}$)

3) Orientation of the minimum principal stress ($\boldsymbol{\sigma 3}$)

4) The ellipsoid shape ratio for the stress tensor ($\boldsymbol{\phi}$) (equation 3)

$$Equation\ 3\text{: } \phi = \frac{(\sigma 2 - \sigma 3)}{(\sigma 1 - \sigma 3)}$$

These four parameters define **T'** which at this point is simply a function of **T, –**the complete stress tensor, such that:

$$Equation\ 4\text{: } T = kT' + l\boldsymbol{I}$$

Where both ***k*** and ***l*** represent scalar values [k = (σ1 – σ3) > 0; l = σ3)] and **I** the unit matrix. From this point forward the solution to the inversion is searched for as the reduced tensor **T'**, while the maximum differential stress (σ1 – σ3) is scaled to a value of 1 (Etchecopar, 1984; Lacombe, 2010). For this reduced and normalised tensor, the RSS acting along any twin plane can therefore only vary between -0.5 and 0.5 (Lacombe, 2010).

The inversion process can then take place, in two steps: Firstly, a solution is obtained by applying a series of completely random stress tensors and calculating the components with respect to all the twinned and untwinned planes (**fig. 5**) (Lacombe, 2010). Following this step it is possible that the RSS exerted on some untwinned planes may exceed that exerted along

twinned planes that are compatible with the tensor, the second stage of the process requires the application of a penalization function, $\boldsymbol{f}$ (equation 5) ideally reduced to zero, in order to minimise this effect.

$$\textit{Equation 5: } f = \sum_{i=1}^{N}(\tau_{sj} - \tau_a{}')$$

Where **τa'** is the smallest RSS applied on compatible twinned planes and **τsj** are the resolved shear stresses applied to the **N** number of untwinned planes **j** such that **τsj** > **τa'** (Etchecopar, 1984). The optimisation of this process allows for a best fit solution to the reduced stress tensor, including the largest amount of twinned planes whilst simultaneously achieving the lowest possible value for ***f***. From this the orientations of the three principal stresses σ1, σ2, and σ3 (σ1 ≥ σ2 ≥ σ3, compression being positive) are calculated, in addition to the value of the shape ratio, Φ [$\Phi = (\sigma2 - \sigma3)/(\sigma1 - \sigma3)$, $0 \leq \varphi \leq 1$] indicating the magnitude of σ2 relative to σ1 and σ3 (Etchecopar, 1984; Lacombe, 2010). In the case of polyphase tectonic events, once a given tensor is resolved, and if sufficient data remains (>30% of the original twinned data) the process can be re-run incorporating all untwinned planes in addition to the remaining twinned planes from the resolution of the first tensor (Etchecopar, 1984; Kulikowski, 2018). This ability has been proven an a number of occasions (Lacombe et al., 1990; Lacombe, 2007) and can also be applied to single phase stress tensors in order to solidify the results, this is of particular importance in complex basin settings which have under gone successive phases of tectonic development (Kulikowski, 2018).

At this point given an assumed constant and known CRSS, the absolute magnitude of maximum differential stress can be calculated. In addition to the magnitude of the principal stresses if accurate rock mechanics data is available.

3.1.4 Sample collection, preparation and analysis within this study

The initial goal of this study was to undertake the first integration of calcite twin analysis from an offshore sample obtained from well core, and reoriented using the technique and method described within Kulikowski and Amrouch (2017). After promising expectations within the planning phase of the project these efforts were hindered due to a number of reasons including: 1) A small amount of oriented wells that also contained core samples within the appropriate intervals 2) Long time frames organising core inspections as a number of core samples 3) The misidentification of both drilling mud and quartz for calcite from core photographs, which provided the best was to initially plan sampling (**fig. 6**). 4) Insufficient calcite to produce a stress tensor using the CSIT method within a number of sampled intervals 5)

While two sub-surface samples were collected and analysed, as a result of the difficulties described above, sampling for CSIT for this study was conducted primarily within outcropping sections of the Eumeralla Formation within the Otway Ranges. Samples were collected from oriented outcropping veins mainly from cliff faces and shortcut platforms along the coast. Samples were then prepared using the method outlined in **fig. 7** and thin sections were created in three orientations in order to measure twinning orientations in 3D. All measurements were completed using a universal stage microscope (**fig. 7**) which was available for use at the Australian School of Petroleum, at the University of Adelaide, allowing for the complete measurement of all twinned and untwinned planes within each calcite crystal, in addition to the optical axes Following their measurement, a number of rotations were required in order to reorient the sample back to the field orientation.

3.2 Analyses of Rock Physical Properties

3.2.1 Introduction

The rationale behind the inclusion of the following analyses techniques as part of this thesis accounts for the contribution that petrophysical rock heritage has upon ongoing deformation, to quantify grain-scale strain and to compare it with results from our other datasets. When combined with other methods including calcite twin analyses, the interpretation of multi-scale geophysical data and natural fault and fracture mapping in the field, techniques of petrophysical analyses allow us to more fully "complete the picture," in terms of the relationship between induced stress and perceived strain. Such comparisons and insights are particularly important within the petroleum industry as structural deformation on the micro-scale can have large scale implications and consequences with regard to porosity and permeability.

In the next section the fundamentals of the two techniques of petrophysical analysis used within this study are outlined; the anisotropy of magnetic susceptibility (AMS) and the anisotropy of P-wave velocity (APV).

3.2.2 Rock Magnetism

3.2.2.1 Introduction to techniques

There are a number of methods used to measure the anisotropy of rocks. They differ from each other by measuring either the induced or the remanent magnetisations:

> **Anisotropy of Magnetic Susceptibility (AMS):** measures the weak field anisotropy of rock fabrics (Borradaile, 1988; Rochette et al., 1992; Borradaile and Henry, 1997)

Anisotropy of Remanent Magnetism (ARM): measures the magnetisation of isothermal remanent anisotropy, which is linked to the ferromagnetic fraction of the rock (Amrouch, 2010).

In this thesis, we use AMS, which has been successfully applied within a number of previous structural studies, especially those within orogenic belts (e.g. Jackson, 1991; Robion, 2007; Amrouch, 2010b: Robert et al., 2018). Ideally this method is combined with an analysis of the magnetic mineralogy of the rock, which assists in identifying the main carrier of the magnetic signal. Although due to time constraints, it was not possible in this study.

3.2.2.2 Magnetic Mineralogy

The magnetic mineralogy of a material is generally define by:

1) The magnetic moment, **M** ($A.m^{-1}$)
2) Its magnetisation, **J** ($A.m^{-1}$)
3) Its magnetic susceptibility, **K**

Magnetisation of any material contains two components, the remanent magnetisation which is always present in the rock, without the presence of an external field or applied field, **H** and the magnetisation induced by the applied field, which is absent without it. Applying a field to any material results in the development of an induced magnetisation, **J** which is directly proportional to the material's susceptibility along with the strength of the applied field (equation 6):

$$Equation\ 6: J = K * H$$

In this case, magnetic susceptibility **K**, is a dimensionless ratio, between **H** and **J**. It is controlled mainly by the crystallographic composition of the minerals within any material.

In general magnetic mineralogy can be divided into three types:

Diamagnetic Materials: Diamagnetism is characterised by a very low magnetic susceptibility within any given material. This susceptibility is negative and also independent of temperature. The minerals responsible for diamagnetic behaviour are those with zero magnetic moments. For example, many rare earth elements, alkaline earths, rare gases and lead. The magnetic field induced by these materials is proportional to the induced field but aligned in a negative manner (Langevin, 1905).

Paramagnetic Materials: Paramagnetic behaviour is exhibited when these materials dominated the magnetic signal of the rock. This partial signal can be attributed to the spin of electrons within the incomplete outer shells of a number of elements. In a latent fashion these materials act in a similar manner to diamagnetic materials, however when subjected to an imposed field they align in a positive manner. The strength of this magnetism is reliant on the strength of the implied field, though in this case is inversely proportional to the applied temperature (Langevin, 1905).

Ferromagnetic Materials: Ferromagnetic behaviour is characterised by a very strong and reasonably stable magnetic susceptibility, approximately 1000 times stronger than diamagnetic materials. Therefore such materials have a strong influence over the average of the signal, even if they are present in extremely small amounts. Unlike other forms of magnetic behaviour Ferromagnetism is strongly related to temperature (Langevin, 1905).

3.2.2.3 Magnetic Susceptibility

The magnetic susceptibility of a material is simply a measure of its overall response to an applied magnetic field (Borradaile, 1988). This characteristic behaviour in rocks can be can be considered as one of the three main classes described previously, as determined by their mineralogical composition.

Magnetic susceptibility is defined by equation 7, where **J** is the induced magnetisation of the material and **H** is the applied, external magnetic field. Both **H** and **M** within this equation are expressed in amperes per meter. Volumetric susceptibility is dimensionless, or written as SI units.

$$Equation\ 7: K = \frac{J}{H}$$

Magnetic susceptibility varies in the general case, according to both applied field and temperature values, and may also vary according to the measurement direction, possibly resulting in a non-parallelism between the **H** and **M** vectors. That being the case, it is standard practice to measure **K** at room temperature with low field strength (≤ 1mT) conditions:

1) Experimental procedures are simple, safe and allow for a high turnover of samples and high sensitivity.

2) Magnetic susceptibility, **K** is a good estimate of the in situ induced magnetization of a rock in the Earth's field and can therefore also serve as a good estimate for magnetic anomaly interpretations.

3) The value of **K** can be correctly approximated for by a second order (magnitude and two directions), symmetrical tensor. A factor that greatly facilities the measurement of the anisotropy of susceptibility.

For both paramagnetic and diamagnetic minerals, the anisotropy of magnetic susceptibility is controlled by the crystallographic orientations of the mineral grains within the crystal lattice and not sizable influenced by the overall grain shape (Borradaile, 1988). The anisotropies of paramagnetic, matrix forming minerals are quite high when compared to other minerals of different classes (Amrouch, 2010).

The contributions of ferromagnetic minerals to the overall susceptibility are important, as such it is best to know whether or not they are present within any given material prior to investigating its susceptibility. The susceptibilities of these minerals are sensitive to overall rock composition and grain organisation but at the same time are much stronger and more positive than those of the para and diamagnetic classes. For example, typical **K** values are up to 5 SI units/unit volume for magnetite. For minerals like magnetite, the response can be heavily controlled by grain shape and grain spacing within the rock. Hematite, like the paramagnetic and diamagnetic rock-forming minerals, yields a component of magnetic fabric to the rock that is primarily influenced by the crystallographic alignment of the anisotropic grains. As such, even if present in very small quantities ferromagnetic minerals have the ability to drastically influence the susceptibility of a material with an even larger effect on its anisotropy.

3.2.3 The Anisotropy of Magnetic Susceptibility (AMS)

3.2.3.1 Introduction to AMS

The Anisotropy of Magnetic Susceptibility (AMS) is one of the most widely used methods of analyses, used to measure the orientation of magnetic fabric within the rock (Borradaile, 1988; Borradaile and Jackson, 2004). Previous work has also shown that AMS can be applied to structural geology as a tool for the analyses of micro-deformation. Through the microscale

analyses of both mineral and tectonic fabrics (eg: Amrouch et al., 2011; Borradaile and Henry, 1997; Jackson and Tauxe, 1991; Robion et al., 2014; Tarling and Hrouda, 1993).

Measuring AMS in rock samples is a non-destructive technique for quantifying the average magnetic fabric (Amrouch, 2010). AMS analyses is rapidly completed and can be done on a wide range of rocks and specimens. Its most attractive feature being that it sums the magnetic contributions of multiple components of the rock, presenting an average bulk fabric description (Borradaile, 1988) from the use of induced magnetisation within an applied field. Under these conditions measurements along a minimum of six suitably oriented axes through a specimen provide us with a quantification of the AMS. As all induced magnetisations are ephemeral responses to applied field susceptibility can be defined as the ratio of the induced magnetisation to the inducing field. Susceptibility is controlled almost exclusively by the combined orientation distribution of 100% of the minerals within a single sample. When measured properly at low fields within rocks that contain a strong permanent magnetisation, the AMS is unaffected. Conversely, for samples that contain a very weak signal the equipment requires careful and precise calibration in order to penetrate through the typical surrounding noise (Sagnotti et al., 2003).

The beauty of the AMS technique is that within a ~3 minute time period the method can provide a measure of the orientation distribution within a 10.5cm3 core-plug sample (**fig. 8**).

AMS has been widely used within earth science disciplines for a number of years. In the early 1990s especially, the technique was used more commonly due to:

1) Applicability to almost every rock and soft sediments type.

2) High sensitivity which allows fabrics that were once considered isotropic to be re-analysed, opening up new research fields.

3)Timely operation of approximately 15 minutes per sample allowing, for statistically significant fabric investigations, particularly applicable to the mapping of large scale structures such as those in magmatic bodies or tectonic units.

4) Opening new possibilities for semi-quantitative and quantitative application in terms of fabric deformation, intensity and symmetry.

5) Prevalence as a new tool to aid in paleomagnetic interpretations in terms of age of the natural remanence magnetism and a better correction for structural influences on the fabric.

3.2.3.2 Technique Background

AMS analysis can be completed on a wide range of rocks and specimens (Borradaile, 1988). Its most attractive feature being that it sums the magnetic contributions of multiple components of the rock, presenting an average bulk fabric description (Borradaile, 1988) which, like in this study, can be linked to larger environments of stress and strain (Amrouch, 2010).

The principle directions of the susceptibility ellipsoid (**fig. 9)** derived from AMS, commonly show orientations consistent with that of rock kinematic history (strain). This relationship arises as most magnetically susceptible minerals have distributions or shape orientations that are easily influenced by kinematic deformation within the rock lattice. Due to this, AMS is a physical property of rocks which has been used extensively for petrofabric and structural studies (Rochette et al., 1992). Its governing principle is simple: AMS arises from preferred bulk, orientation of anisotropic magnetic minerals or the magnetic fabric. The orientation of the crystallographic axes themselves, often controlling grain shape, determine the AMS for the vast majority of rock forming minerals (Borradaile, 1988).

The output for typical AMS measurements are given in the form of an ellipsoid of magnetic susceptibility, (**fig. 9**) defined by a second order tensor of length and orientation of the three principle axes K1 > K2 > K3.

In addition to the tensor values and the ellipsoid of magnetic susceptibility a number of additional parameters are also used as part of the data measurement and analysis, including Mean susceptibility (**equation 8**) to give an overall estimate of bulk susceptibility in addition to three main ratios of the anisotropy in different directions (**table 1**). Known as the lineation, foliation and degree of anisotropy.

$$Equation\ 8: K(mean) = \frac{(k1 + k2 + k3)}{3}$$

Parameter	Formula	Source
Magnetic Lineation	$L = \frac{K1}{K2}$	Balsley and Buddington, 1960
Magnetic Foliation	$F = \frac{K2}{K3}$	Stacey et al., 1960
Degree of Anisotropy (P)	$P = \frac{K1}{K3}$	Nagata, 1961
Degree of Anisotropy (Corrected)	$P' = exp\sqrt{2}[\,(n_1 - n_m)^2 + (n_2 - n_m)^2 + (n_3 - n_m)^2]$ Where $n_1 = lnK1, n_2 = lnK2, n_3 = lnK3$	Jelinek, 1981
Shape Parameter (T)	$T = \frac{2n_2 - n_1 - n_3}{n_1 - n_3}$	Jelinek, 1981

Table 1: *Different parameters used to define the shape of the ellipsoids of anisotropy. K1, K2 and K3 are respectively the maximum, intermediate and minimum main axes, after Amrouch (2010) and cited sources.*

Following data acquisition, using the appropriate equipment, statistical treatment of AMS data from a set of specimens is required in order to define a mean site AMS tensor. This treatment can be in the form of either numerical or analytical techniques (Rochette, 1992). Additionally, early use of the AMS technique contained a number of specific assumptions, which have shown to still generally apply today (Rochette et al., 1992).

They are as follows:

1) The assumption the AMS ellipsoid is co-axial to the major petrofabric of the rock. This can be the bedding plane within sedimentary rocks, the magmatic foliation plane for magmatic rocks or the flattening plane for solid state deformed rocks. **K1** is parallel to the foliation, whichever form it may take. The **K3** axis is perpendicular to the foliation. Therefore, we name **K1** the magnetic lineation direction and **K3** the pole of magnetic foliation. Though this assumption is on the whole, valid, inverse AMS fabrics have been found within samples where susceptibility is carried by a certain group of minerals, including iron bearing carbonates, tourmaline, cordierite, goethite and SD magnetite (Rochette et al., 1992).

2) The shape of the AMS ellipsoid is directly related to the rock fabric. In most rock types there is a simple relationship between the **F** and **L** parameters and the intensities of linear or planar preferred orientations. In the case of deformation in the solid state, this implied a direct relationship between the resolved AMS tensor and strain within the rock sample. Therefore, a

quantitative application of AMS is possible once the exact relationship with strain has been determined (Borradaile, 1991).

3) The assumption that the obtained AMS measurement is not effected by natural or artificial remanent magnetisations. On the whole this is valid, although structurally based AMS tensors can be biased by the presence of magnetic remanence. As such it is best not to use samples that have previously been used for ARM or IRM acquisition or those that have been submitted to static field demagnetisation.

3.2.3.3 Measuring the AMS signal

The actual acquisition of AMS data is a rapid procedure, with magnetic anomalies within 10 cubic cm sample able to be measured in period less than 5 minutes (Graham, 1954). While this technique can yield important information regarding the magnetic fabric within the rock. It is not always a simple and easy process to link the fabric resolved from AMS with any specific deformation (Robion et al., 2014).

The measurements themselves within this study gave been made within a KLY-3 Kappabridge susceptometer (f**ig. 10**) that operates under a low A.C field of 4x10-4T. This was free available for use at the University of Cergy-Pontoise, Paris, France.

While individual mineral grains will possess their own unique degree of AMS due to their shape, size, crystal lattice or state of stress, a sample composed of roughly 105 grains randomly distributed anisotropic grains, will, present as isotropic. This means the actual degree of AMS in a measured sample can be attributed to mainly other, non-granular factors (Amrouch, 2010). Additionally, anisotropy is controlled strongly by both the magnetocrystalline properties and the overall form of the crystal. For example, Stacey et al., (1960) showed that induced

magnetisation is easier when parallel to the orientation of easy magnetisation within the crystal lattice structure, especially in highly anisotropic crystal systems. A relationship between the percentages of shape anisotropy as a function of measured susceptibility (**fig. 11**) can be observed within different crystal shape ratios (Amrouch et al., 2011; Bathal, 1971) as evidence for grain shape having a significant effect on susceptibility.

3.2.3.4 Interpreting the Magnetic Fabric

A petrofabric shown within a completed AMS measurement should reflect the mean orientation of the three axes of anisotropy within the magnetic field (**fig. 9**). The overall shape of the anisotropy can be classed as one of three broad categories according the relationship between the different axes; planar, linear or triaxial. Both planar and linear fabrics can be heavily influenced by the presence of either complimentary or highly-adverse mineral grain shapes (**fig. 12**).

As sedimentary rocks often contain their own natural fabric (e.g: bedding) the study of AMS fabrics within them can at times become complex, as discerning between such fabrics and relevant tectonic magnetic ones can be difficult. While sedimentary fabrics are affected by all types of depositional processes including gravity, currents in addition to grain shape and condition. The more sediments have been subjected to consolidation and mechanical compaction the more difficult it is to record a new anisotropy relating to tectonics (Robion et al., 2007). It is also possible for processes such as diagenesis to create new paramagnetic minerals which may slightly alter the initial sedimentary fabric.

A challenge of working with AMS data within sedimentary rocks is distinguishing between the original sedimentary fabric and those imposed by any form or degree of tectonic deformation. The three major styles of magnetic fabrics are sedimentary, intermediate and tectonic.

Sedimentary fabrics: Initial magnetic fabrics within sedimentary rocks are dependent upon a number of factors, including grain shape, size and weight, in addition to gravity, paleocurrents and the orientation of the earth's magnetic field (Amrouch, 2010). In the case of a sedimentary rock deposited in calm terrestrial conditions, gravity is the major factor, and a planar rock fabric (Rees, 1965) is developed. In this case **K1** and **K2** lie within the depositional plane and **K3** is parallel to the pole of the bedding plane. The presence of weak or strong currents of deposition can alter this fabric (King, 1955; Rusnak, 1957; Granar, 1958; Hecht, 1962) although in general **K3** remains perpendicular to the depositional plane or slightly rotated in the direction of the current (Granar, 1958) with **K1** remaining in the bedding. In all cases sedimentary fabrics display planar or oblate fabrics (**fig. 13**), with a **T** value of ~1 and **F** greater than 1. Depending on the degree of compaction, burial or dissolution, this fabric may be difficult to alter throughout the process of deformation (Robion et al., 2007).

Intermediate fabrics: During compressional events it has been shown that the magnetic lineation of **K1** develops parallel to the relevant fold axis, an effect known as layer parallel shortening (Graham, 1966; Frizon DeLamotte et al., 2002). This fabric is referred to as intermediate and not wholly tectonic in nature, as though the **K1** lineation has shifted parallel to the folding, the pre-existing sedimentary fabric remains defined by the **K3** lineation. As such, the very first effect of shortening that can be observed in such fabrics is the shift of the **K1** lineation parallel to the shortening direction (Kissel et al., 1986) (**fig. 14**).

Tectonic fabrics: As deformation due to tectonic forces increases, so does their influence on magnetic fabrics (**fig. 14**). Strictly speaking we define a fabric as tectonic, rather than intermediate, if the plane containing the **K1** and **K2** linitations is perpendicular or oblique to the sedimentary fabric, resulting in a shift of **K3** away from a position perpendicular to the bedding fabric (**fig. 14**). As a rule, these are present, mainly in highly deformed and metamorphic rocks. Much work has been done comparing magnetic fabrics of different origins

[Graham (1966), Kligfield et al. (1981), Averbuch et al. (1993), Lüeneburg et al. (1999) and Frizon DeLamotte et al. (2002)] with a consensus, magnetic fabrics and their nature are highly related to the overall degree of tectonic influence.

In addition to sedimentary, intermediate and tectonic fabrics, shear and inverse magnetic fabrics also exist. Though they are not discussed herein. For information regarding their nature, the reader should refer to: Lamarche and Rochette (1987) and Borradaile and Jackson (2009).

3.2.3.5 Using AMS to constrain and environments of paleostress

A number of studies have successfully compared AMS results with the structural analysis of brittle structures on the micro and mesoscale, at low levels of deformation (Kissel et al., 1986; Sagnotti et al., 1994, 1999; Mattei et al., 1997; Faccenna et al., 2002; Borradaile and Hamilton, 2004; Cifelli et al., 2004, 2005; Amrouch et al., 2010b). Although the process is not easily completed as brittle strucutes – especially fracture networks- can record polyphase deformation events, while AMS often records strain in an area close to the stress field and during shorter periods of time (Amrouch, 2010). Where AMS measurements have recorded tectonic compression, the magnetic lineation of **K1** has typically been found to be perpendicular to the orientation of compression (Kissel et al., 1986; Mattei et al., 1997; Sagnotti et al., 1998; Pares et al., 1999, Amrouch, 2010b; Robert et al., 2018). Interpretation of magnetic fabrics on this basis provide a reliable indicator of the orientations of paleostresses, especially compression. Additionally it has been shown that in weakly deformed sediments within extensional settings, the lineation of **K1** coincides will with the direction of maximum stretching ($\sigma 3$) or extension (Cifelli et al., 2005) (**fig. 16**).

3.2.4 Anisotropy of P-wave Velocity (APV)

In contrast to AMS, the analysis of the anisotropy of the P-wave velocity (APV) is more sensitive to porosity and void arrangement (Amrouch, 2010) in addition to the form and individual structure of the minerals constituting the rock (Bhathal, 1971) and the nature of inter-granular arrangements. Structural studies that have utilised elastic properties and the propagation velocity of P waves to study microstructural anisotropy in rocks are limited, although in sedimentary rocks notable studied include; King, 1966, Hrouda, 1993; Louis et al., 2003; 2004; Amrouch, 2010. In this study, with inspiration from Amrouch (2010) we compare the results of these two methods of AMS with APV in order to gain a more complete insight into the anisotropy of pore fabric within our samples (Louis et al., 2004).

3.2.4.1 Principles of APV

For any sedimentary rock, its physical properties are dependent upon a number of factors, including:

1) *The shape of the crystal lattice of minerals within the rock.*
2) *The shape of individual grains and their orientation within the rock matrix.*
3) *Structural or mechanical damage of the rock or the alteration of intergranular contact surfaces.*
4) *The structure of the porosity network within the rock.*
5) *The nature of the bedding plane.*

All the above factors can vary through space within the rock meaning that they are responsible for varying degrees of anisotropy. As such varying style of rock anisotropy can be defined or

approximated using a second rank tensor, where the three dimensional representation is a simple ellipsoid, generally known as ***K***:

$$\mathbf{K}=\begin{pmatrix} K_{11} & K_{12} & K_{13} \\ K_{21} & K_{22} & K_{23} \\ K_{31} & K_{32} & K_{33} \end{pmatrix}$$

Converting **K**, to the (XYZ) reference plane, the tensor is simplified to:

$$\mathbf{K}=\begin{pmatrix} K_{max} & 0 & 0 \\ 0 & K_{int} & 0 \\ 0 & 0 & K_{min} \end{pmatrix}$$

As with AMS, the shape and nature of the ellipsoid, **K**, is dependent upon the relative magnitudes of **K*max***, **K*min*** and **K*int***. This makes the analysis of rock microstructures though the use of this method possible (Amrouch, 2010), allowing for a high sensitivity of measurement but the characterisation and estimation of the general structural condition of the rock. Amrouch (2010) showed the existence of a link between multiple rock physical properties, including AMS and APV with the microstructural nature of the rock, including the orientation of microfracture networks.

As APV measures the speed of P-waves through the rock sample the results are predominantly a function of rock density (Louis et al., 2003, 2004; Amrouch, 2010). The varying anisotropy of P-wave speed through the sample provides good indications with respect to the texture of the matrix, the arrangement of the grains and the connectivity of the pore fabric within the rock. By comparing P-wave velocity between dry and saturated rock samples it is possible to gain

an insight into the permeability of the rock and its influence of anisotropy. It is also possible to combine these results with other analytical methods including the measurement of porosity using mercury and the impregnation of ferro fluid into the rock to gain an even more accurate constrain on the nature of pore the porefabric.

3.2.4.2 Controls on APV

Within sedimentary rocks, such as those measured in this study, APV is controlled by a number of factors, including:

1) Shape of the pore fabric within the sample; due to the presence of void spaces within the rock, generally the orientation of maximum velocity following the measurement of APV is parallel to the direction of maximum pore length, with the minimum speed perpendicular to it (Louis et al., 2003; 2004).

2) The shape of individual grains within the sample. As grain shape directly controls the shape of the pore fabric, a similar influence is observed. The maximum speed in the longest grain orientation and the minimum speed perpendicular to it.

3) The distribution and nature of intergranular contacts; two granular contact zones are considered, vertical and horizontal. Louis et al (2003) showed that deformation under horizontally oriented loading is mechanically easier than vertical loading. Additionally, uniaxial compaction upon a set of spherical grains will reorient the contact surfaces and harden the deformed medium, parallel to the orientation of compaction. Resulting in increased P-wave speed in this orientation.

4) As shown by Sayers and Kachanov (1995) patterns of micro fractures within the rock can have a significant effect on velocity anisotropy. For example in a non-porus media with a set of sub-parallel micro fractures, P-wave speed will be significantly reduced in the orientation perpendicular to the micro fractures. For more information regarding the effect of micro fractures on P-wave velocity see Hudson (1981) and Kachanov (1993).

3.2.4.3 Rock Fabric Styles in APV

Prior to experiencing deformation, – for example horizontal shortening – sedimentary rocks, as with AMS, are characterised by a sedimentary fabric associated with the bedding plane. These fabrics can be either derived to simple horizontal deposition or their vertical compaction (Louis et al., 2003). For depositional style fabrics, lower P-wave speeds associated with orientations parallel with the bedding plane (Louis et al., 2003). For compaction style sedimentary fabrics – vertical compaction results in grain scale alterations to intergranular contact surfaces (Louis et al., 2003). As such for compaction style fabrics, the maximum velocity is generally parallel to the pole of bedding, usually parallel with vertical compaction. For example, following deformation in the case of horizontal shortening, it is possible for a fabric similar to that of a compaction style to develop, once again, with the maximum P-wave speed parallel to the bedding plane.

3.2.4.4 Measuring APV

In this study APV is measured using an experimental protocal and device described within David et al. (2017). In contrast to other methods, that require manual rotation of individual samples, in order to measure P-wave velocity at varying orientations (**fig. 17**) this device (**fig.**

18) is responsible for manually rotating the specimen and acquiring measurements at 10º intervals, resulting in 36 measurements per specimen. The device utilises a pair of ultra-sonic P-wave sensors in addition to a digital oscilloscope HP54603B (**fig. 18**).

Samples for APV were measured under dry conditions, following 24 hours in an oven at 60° after saturation with distilled water in order to control for the effect of pore space on travel time. P-wave velocity values were then calculated from the measured travel time, first; by automatic detection using the AIC method and second, controlled through the use of in house scilabTM routine developed by P. Robion.

3.2.5 Preparation of Rock Samples for AMS and APV

As this study involved the transportation of rock samples from the Victorian Coast, within the eastern most OB, to the University of Cergy-Pontoise in Paris, the preparation of samples was a long process. In all but one sample case, both AMS and APV was completed on all samples. As field sampling was not possible, and in order to study the petrophysical characteristics of our samples in 3D, it was essential to have specimens within varying orientations. This required the use of a protocal designed by Louis et al. (2003) in which an oriented field sample is used to collect multiple cylindrical samples in three orthogonal orientations (**fig. 17**). As such, large blocks were collected from the field (**fig. 19**) and cut down to cubes using a large saw. Cyclindrical plugs were taken from three faces – X, Y, Z – and trimmed down to the standard size for AMS measurement, which closely approximate a sphere (22.5mm long and 25mm in diameter). This resulted in a total of 271 specimens for AMS and APV across a total of 18 samples. In the case of APV we used a method outlined by Louis et al. (2004) as although seismic velocities are generally described by a fourth rank tensor, they can be approximated

using a second rank velocity tensor, construction the measurements in the three orthogonal planes.

3.3 Natural Fracture Analysis

3.3.1 Introduction

Within this study, the analysis of natural fracture composes the mesoscale component of structural analysis, providing a proven method for linking the upscaling of microscale techniques, such as CSIT, AMS and APV to the macroscale (Amrouch, 2010a, 2010b; Kulikowski and Amrouch, 2017). Natural fracture and fault data was acquired from outcropping formations, primarily, the Early Cretaceous Eumeralla Formation, which outcrops in the Otway Ranges and in the sub-surface through the analysis of geophysical resistivity based wellbore image logs.

For subsurface analysis, the introduction of modern imaging tools has presented fundamentally new methods, providing a nearly continuous record of the in situ chemical and physical properties of the penetrated formations (Prensky, 1999). Wellbore imaging tools are one of the fastest, easiest and most precise methods for the collection of subsurface formation specific data (Prensky, 1999; Poppelreiter et al., 2010; Pokalai et al., 2016; Kulikowski et al., 2016c). Wellbore imaging tools measure either the electrical conductivity / resistivity of the borehole wall or the sonic travel time and amplitude of the reflected acoustic signal (Prensky,1999; Gaillot et al., 2007). Conductivity/resistivity based borehole instruments used to record the analysed imaged logs in this study are the Simultaneous Acoustic and Resistivity Images (STAR) by Baker Atlas, and the Fullbore Formation Micro Imager (FMI) and Formation Micro

Scanner (FMS) developed by Schlumberger. The interpretation of wellbore image logs (**fig. 20**) was carried out using cutting edge software (Geolog by Paradigm and RockDok by Ikon Science) which allowed for the 3D orientation of structural features, including natural fractures, faults and bedding planes to be resolved. In outcrop natural fracture and other outcrop data (**fig. 21**), was collected in 3D using a compass clinometer and the freely available electronic app, FieldMoveClino, developed by Midland Valley.

3.3.2 Processing and Analysis Natural Fractures

In both the surface and subsurface, once measured sets of natural fractures can be identified based upon common angles of dip and strike, in addition to lithological unit of occurrence. As part of this processing natural fractures are sorted into bins, based up their 3D geometry and spatial distribution, which allows for the distinct trends to be revealed which are not easily observed within large data dumps of planes or poles on stereonets (Kulikowski, 2018). At this point, depending on the nature of bedding, data may be "back tilted" in order to distinguish sets that may have occurred prior to the tectonic event responsible for tilting the bedding (Hancock, 1985; Bellahsen et al., 2006). It is important to consider the mode of fracturing as different sets may also be distinguished based upon their mode of nucleation (**fig . 22**). Once natural fracture sets have been distinguished, they are analysed based upon their geometry and assigned conjugate sets and paleostress tensors based upon their 3D characteristics and relationship to the three principal stresses (Anderson, 1951). This process can be assisted by inversion software such as Win-Tensor that simulates paleostress tensors based upon the 3D geometry of fracture sets (Kulikowski, 2018).

3.3.3 Stress Inversion of Natural Fracture Data

The nucleation of natural fractures within a rock mass requires a magnitude of differential stress that is equal or greater to the rock strength, that in the field are typically derived from natural structural activity (Zoback et al. 1989; Sibson, 2003; Zoback et al. 2003; Kulikowski, 2017). Failure can also be induced as a result of increases in pore pressure within the rock matrix, which essentially reduces the effective normal stress acting on the rock mass, resulting in tensile failure (**fig. 22**) shifting the Mohr's circle to the left, potentially intersecting the failure or reactivation curves (Kulokowski, 2017).

The orientation of the three principal stresses (Anderson, 1951) which define the stress tensor are the primary control on the development of fracture geometries. An an understanding of the patterns of deformation which form under each type of stress regimes (e.g. normal, strike slip, reverse) can allow for stress tensor and nucleation relationships to be formed (Anderson, 1951), with changes in dip, intensity and strike often indicating a change in structural activity or tectonic regime (Seeburger and Zoback, 1982; Amrouch, 2010; Kulikowksi, 2017). While not possible in the sub-surface, the observation of cross cutting relationships can assist in discerning relative chronologies between fracture sets (Amrouch, 2010). The 3D geometry of natural fractures within outcropping formations and subsurface data can be used to provide significant insights into the paleostresses responsible for their formation in addition to complex regional structural histories (Price and Cosgrove, 1990; Bellahsen et al., 2006; Amrouch, 2010; Amrouch et al., 2010a, Arboit et al., 2015; Kulikowski and Amrouch, 2017; Kulikowski, 2017).

One aspect that is key to the stress inversion of natural fractures is identifying the mode of fracture formation (**fig. 22**). Conjugate mode 2 fractures, the most common in subsurface provinces (Kulikowski, 2017) will develop with ~60˚ of separation between them, bisected by the plunge orientation of the maximum principle stress (σ1). With the minimum principle stress (σ3) bisecting the complimentary 120˚ arc in the same plane as the intermediate principle stress (σ2) (Anderson, 1951; Zoback, 2003). While extensional (mode 1) fractures will develop

parallel to the plane of σ1, dilating in the direction of σ3 (Anderson, 1951). As such understanding both tensile and shear modes of failure requires different approaches, which can be challenge when working in large regional setting (Kulikowski, 2017). Challenges with this method can arise due to stress perturbations created by local pre-existing faults, folds or fractures (Tavani et al., 2015) and as such care must be taken in order to precisely distinguish regional fracture trends from local ones.

As per the method of Kulikowski and Amrouch (2017) this style of natural fracture stress inversion can be undertaken within successive stratigraphic units within sedimentary basins, in order to distinguish polyphase stress evolutions that can then be confirmed using quantitative multiscale methods (Amrouch et al., 2010a, 2010b; Kulikowski, 2017).

3.4 Three Dimensional (3D) Seismic Analysis

3.4.1 Introduction

The analysis of three dimensional (3D) seismic surveys is common place within the petroleum industry, providing for an effective means of imaging and mapping the subsurface. In Australia, the large amount of open file datasets of this nature provide a unique opportunity for the combination of multiple, large datasets in order to constrain the structural and tectonostratophic framework of sedimentary basins (e.g. Krassay et al., 2004; Kulikowski, 2017). In this study, as with previous work completed in the Cooper Basin (Kulikowksi, 2017) 3D seismic data allows for the upscaling of micro and mesoscale techniques of structural analysis to a regional scale. Basic techniques of seismic analysis such as fault and horizon picking in cross section provide the foundations for more advanced techniques of analysis such as the use of seismic attributes, providing insights intro structural trends which would otherwise not be available (Kulikowksi, 2017).

This thesis utilises the analysis of multiple 3D seismic surveys completed at varying degrees of detail depending on their location and the use of their data within the scope of this study. The following section briefly outlines the main methods of seismic analysis used in this study.

3.4.2 3D Seismic Time to Depth Conversion

One obstacle that must be overcome during the use of seismic datasets is the conversion of the dataset from the two way time (TWT) domain, to the depth domain. This is important as the geometries of faults and structures within TWT are not reflective of the true geometry, and as such analysis purely within the time domain is insufficient for the degree of structural insight required in this study. Whilst there are many methods for converting from TWT to depth (see Kulikowski, 2017 for a good summary), to date their varying accuracy has not been assessed within the Otway Basin, and as such within this study a single method of depth conversion has been used across all datasets.

Well control within the data in this study is sufficient to control conversion from time to depth with all but two surveys, containing checkshot data from wells, which provides time and depth pairs. Depth conversion was undertaken using the time-depth-trend method, which utilises a relationship between the TWT domain of seismic data and the true depths of horizons from wells, a method which has been successfully used in the region before (**fig. 23**) (Lyon et al., 2007). Time and depth pairs from wells within each survey were plotted on a graph and their relationship defined by either a linear or exponential trend such as equation 11, where *y* is equal to depth, *x* equal to time, and *a, b* and *c* constants.

$$Equation\ 11: y = ax^2 + bx + c$$

This time-depth equation was then used to extrapolate time depth pairs beyond the available well data and convert the entire 3D survey to depth. This process was undertaken with cutting edge industry software Down Under Geosolutions: Insight v4.4 (DUG Insight). Where well checkshot data was not available, a linear time-depth trend from Petkovick (2004) was used in order to undertake the process.

3.4.3 Techniques of Seismic Analysis

3.4.3.1 Overview

The interpretation of 3D seismic surveys is not a complicated process, with modern software packages allowing for an easy and integrated approach, although it can become a challenge amidst areas of complex structuring or low data resolution. In this study, 3D surveys were converted from time to depth and interpreted using the standard techniques (Mitchum et al., 1977; Vail et al., 1977) incorporating fault identification, reflector tracing and attribute mapping. In particular the seismic attributes of incoherence and curvature proved to be the most valuable as they can be used to visually enhance structuring along reflectors that are difficult to distinguish within the depth volume (Neves et al., 2004; Basir et al., 2013; Kulikowski, 2017). Seismic interpretation within this project was completed using the industry standard software DUG: Insight.

3.4.3.2 Fault Interpretation using 3D seismic

The approach used for interpreting faults within the datatsets was fundamentally guided by the current understanding of basin evolution for the region. The presence of extensional, strike slip and compressional faults were all thought to be possible. Particular care was taken with respect

to the analysis of fault inversion. Faults were interpreted at line spacing's that varied from survey to survey, depending on the size and degree of structural complexity. Faults were predominantly recognised in cross sections along survey inlines and crosslines, with arblines being employed in a number of regions where structural complexity was high and the orientation of survey lines was not ideal for the resolution of the structural trend (e.g fault strike is W-E and crossline strike is also W-E). In cross section, faults were typically identified due to the offset of seismic reflectors along their length (**fig. 24**).

3.4.3.2 Reflector Identification

The interpretation of seismic reflectors within the datasets was guided by well ties in addition to the current basin framework, which outlines major periods of rifting occurring throughout the Early and Late Creteaceous Period. Each reflector was traced along survey lines where possible to establish a broad framework and then traced in further detail along various line spacings. Interpretation was significantly aided by a built in amplitude snapping feature within DUG: Insight in addition to propagator guided picking at survey extremities and where structuring was less complex. Finally each interpretation was interpolated between lines in order to create complete 3D surface.

3.4.3.4 Seismic Attribute Mapping

The most useful seismic attribute, employed throughout this study were incoherence and curvature.

Useful for identifying faults, incoherency (also known as coherency or similarity) was introduced by Bahorich and Farmer (1995) and later developed by Gersztenkorn and Marfurt

(1999). In this instance DUG: Insight was used to re-process the original 3D volume into an incoherency volume for which amplitudes were then extracted along particular horizons of interest or depth slices to visually enhancing lateral discrepancies (**fig. 25**). Incoherency was often used with this study to provide a "first pass" which greatly assisted in identifying major fault networks and trends.

The mapping of curvature along specific horizons assisted in providing potential insights into the distribution of natural fractures attributed to folding or bending within our datasets.

For more information on curvature, it is recommended the reader consult (Kulikowski, 2017)

3.5 Integrating Multiscale Data

There are a number of cases involving the integration of many of the methods outlined within this chapter to date.

For example CSIT has been combined with natural fracture data on a number of occasions in order to constrain consistent evidence for various regimes of paleostresses (e.g. Amrouch et al., 2010a; Beaudoin et al., 2012) whilst Amrouch et al. (2010b) have shown to the usefulness of combining techniques of petrophysical analysis such as AMS and APV with such datasets in order to more fully constrain the 4D evolution of stress and strain, although this was completed on a single anticline at Sheep Mountain, Wyoming, not across an entire sedimentary basin.

The most recent example of this style of multiscale integration comes from the Cooper Basin (Kulikowski, 2017) where the first integration of sub-surface CSIT data was combined for the first time with geophysical well and seismic datasets (Kulikowski and Amrouch, 2017). This was done through coordinating paleostress regimes from the microscale to the macroscale, and

proved effective in constraining the 4D evolution of one of Australia's most importance sedimentary basins.

In this study, we build on these works, with the aim to combine the proven out comes of Amrouch (2010) (multiscale methods of stress and strain analysis) and Kulikowski (2017) (multiscale methods of stress analysis in the subsurface) in order to undertake the first study within a passive margin sedimentary basin.

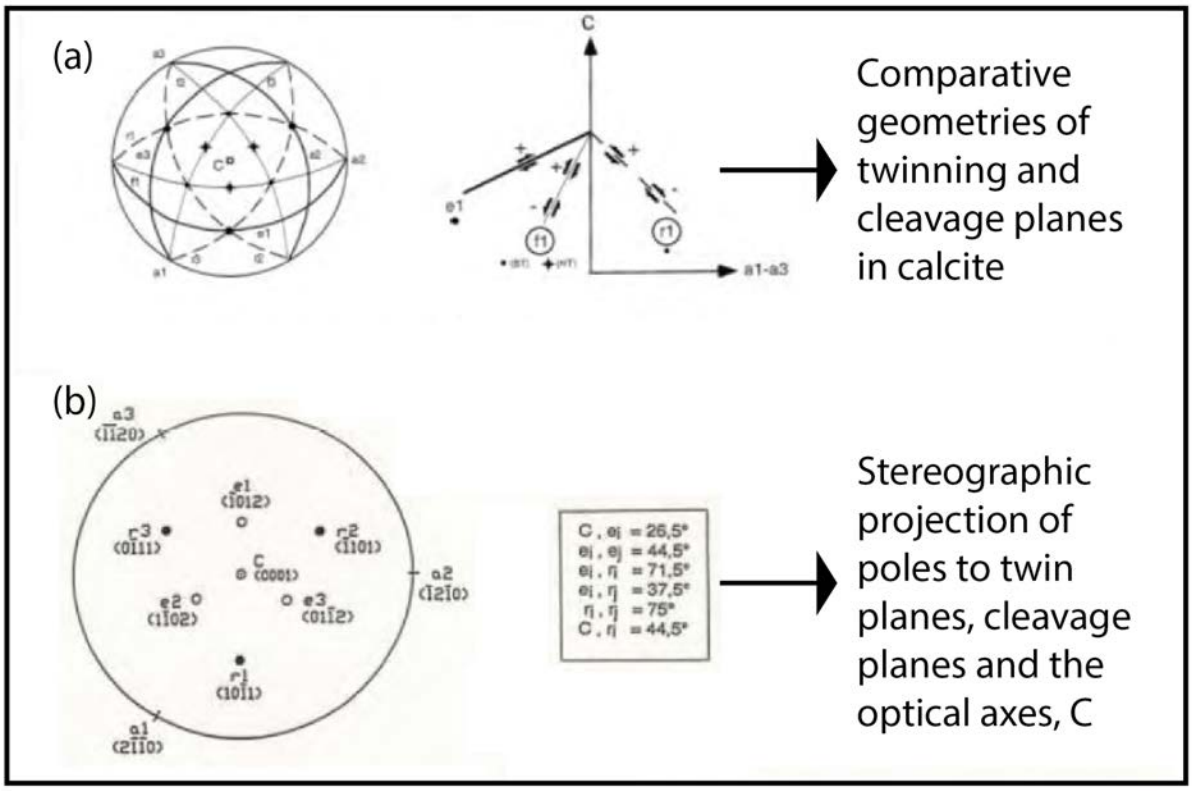

Fig. 1: *The geometric laws that define twinning with calcite crystals (a) displays a stereographic projection of twin and cleavage planes in addition to their shear orientation in relation to the optical axis, C. From Amrouch (2010) after Turner and Weiss (1976).*

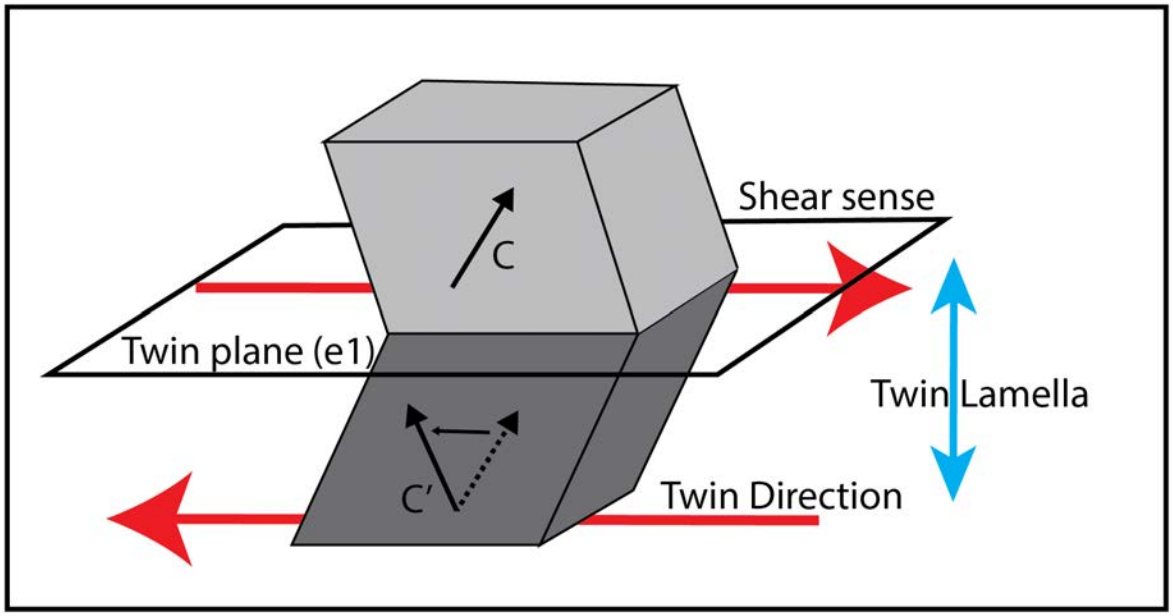

Fig. 2: *Schematic diagram of a twin plane, showing the change in optical axis, C, between the host crystal (light grey) and twin (dark grey) with the shear sense oriented towards the host crystal. Modified after Lacombe et al. (1990) and Amrouch, (2010).*

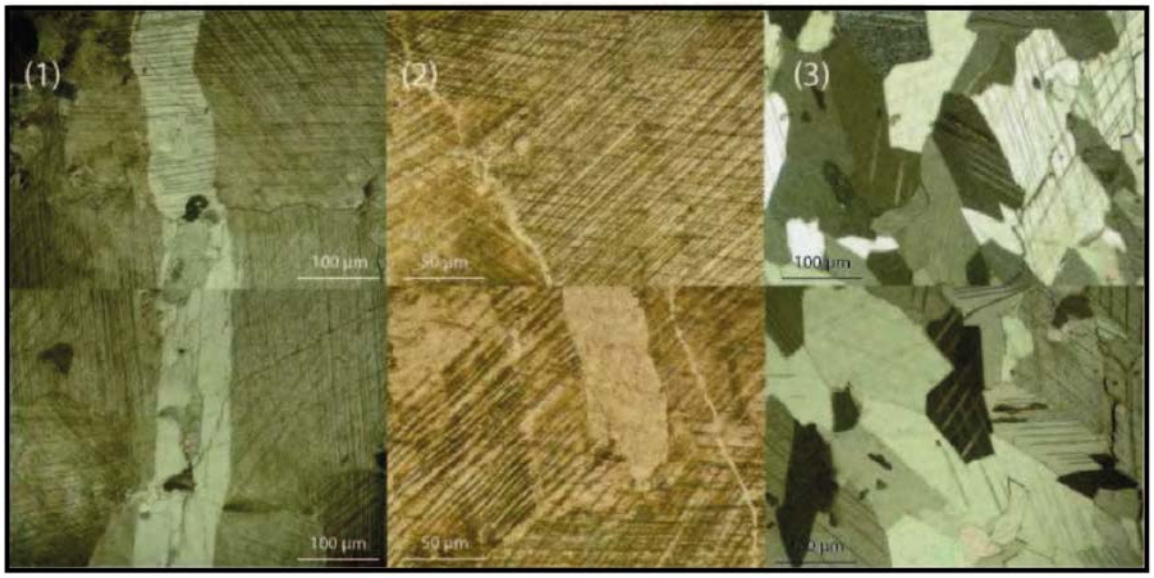

Fig 3: *Examples of varying twin density from Amrouch (2010) high density to the left and low density to the right*

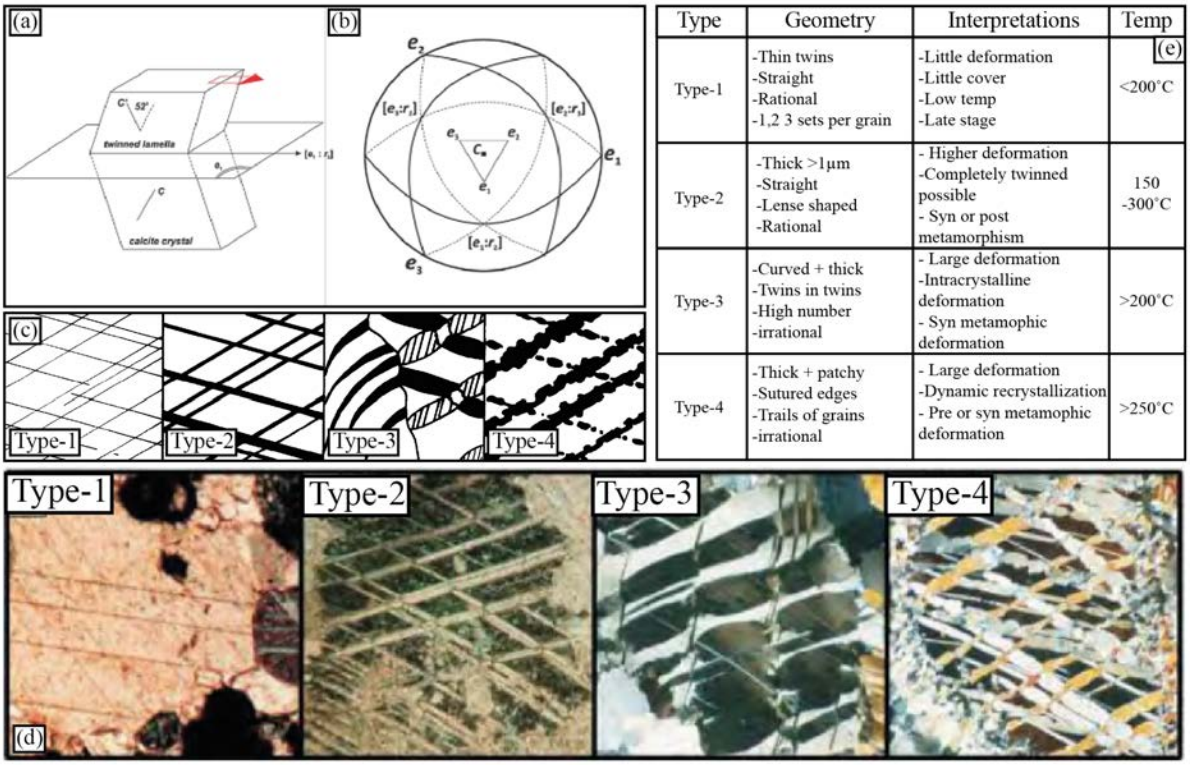

Type	Geometry	Interpretations	Temp
Type-1	-Thin twins -Straight -Rational -1,2 3 sets per grain	-Little deformation -Little cover -Low temp -Late stage	<200°C
Type-2	-Thick >1µm -Straight -Lense shaped -Rational	- Higher deformation -Completely twinned possible - Syn or post metamorphism	150 -300°C
Type-3	-Curved + thick -Twins in twins -High number -irrational	- Large deformation -Intracrystalline deformation - Syn metamophic deformation	>200°C
Type-4	-Thick + patchy -Sutured edges -Trails of grains -irrational	- Large deformation -Dynamic recrystallization - Pre or syn metamophic deformation	>250°C

Fig. 4: *A figure focusing on the different types of calcite twins after Burkhard (1994). (a) and (b) schematic diagrams showing the geometry of twinning in relation to the optical axis (c) sketches of twin types taken from Burkhard (1994) (d) real world examples of the different types of calcite twins taken from Amrouch (2010) (e) a table modified from Burkhard (1994) summarising the geometry, interpretations and temperatures of the different twin types.*

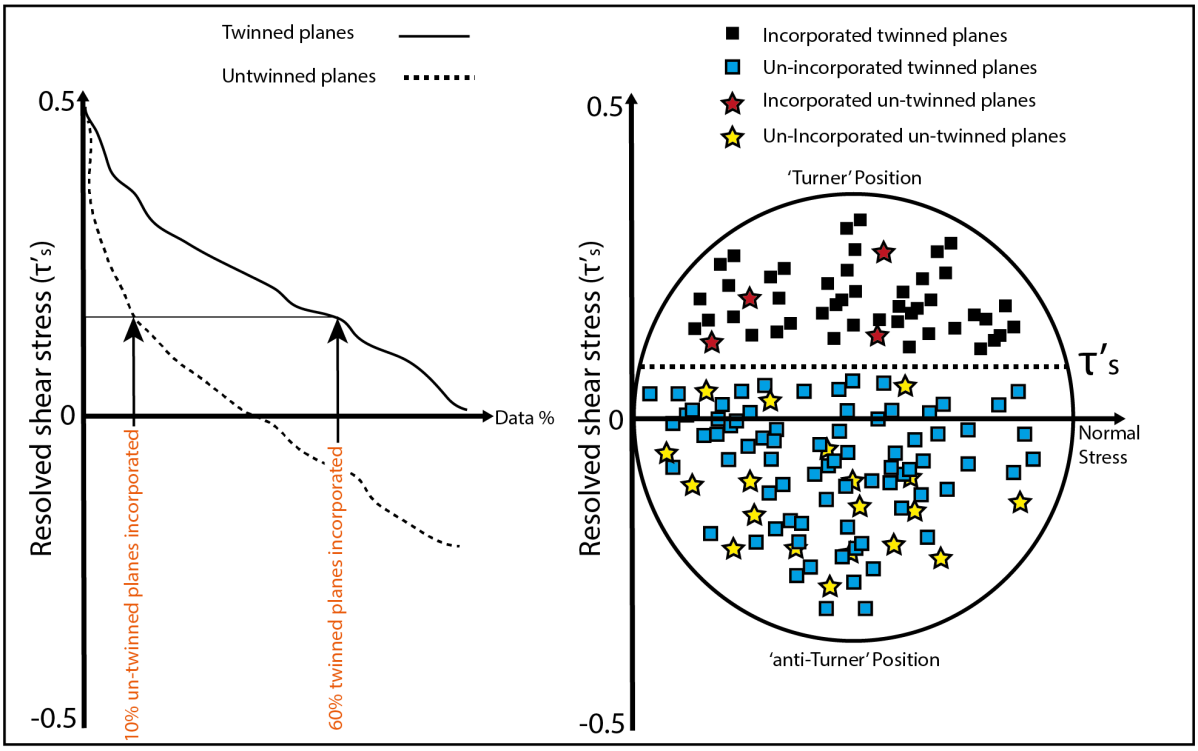

Fig. 5: *Left: Aa schematic graphical representation of the normalised shear stress within both twinned and untwinned planes. Right: Pseudo Mohr's circle that illustrates the compatible and incompatible twin data for a given stress tensor, modified after Lacombe and Laurent (1995).*

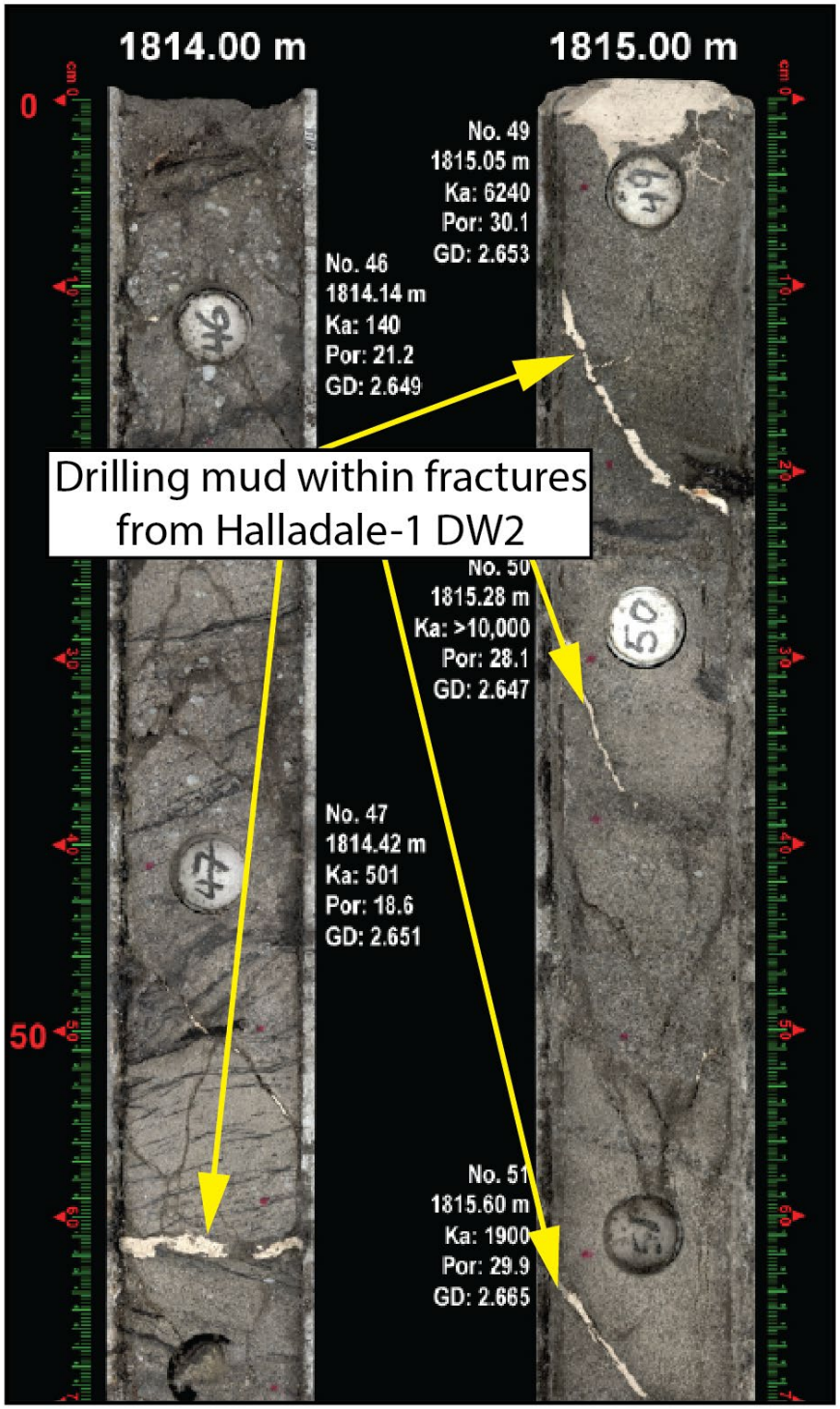

Fig. 6: *An example of filled fractures within off-shore core sections from wells Halladale-1DW1 and Halladale-1DW2. Fracture fill was mistakenly identified as calcite from core photographs. Upon inspection, the fractures are filled with drilling mud or cement. During the planning stage these two wells were identified as the primary target for the first offshore sampling of CSIT.*


(a)
(b)
(x,y)
(x,z)
(z,y)
(c)
(d)
(e)
(f)
(g)
100µm
(h)
100µm

***Fig.7**: A series of photographs outlining the sampling process for CSIT. (a) an oriented sample is collected from the field (b) small sections are cut from the sample in x,y / x,z / z,x planes in order to measure the sample in 3D (c) thin sections are created (d – f) samples are measured using the universal stage microscope, where slides are placed on the stage between thin layer of glycerine. See how the stage can be moved in order to measure the orientation of the twin planes in (f). (g) and (h) examples of twinning under the microscope, with (g) focused around a small vein and (h) from a large crystalline sample.*

***Fig. 8**: Photo of the 10.5cm^3 core specimens used to measure AMS and APV*

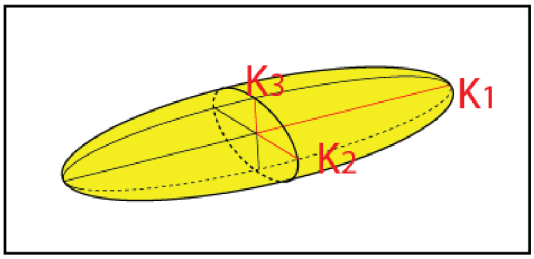

***Fig. 9:** The ellipsoid of magnetic susceptibility, defined by the maximum (K1), intermediate (K2) and minimum (K3) susceptibility.*

Fig. 10: *Photograph of the KLY-3 Kappabridge Susceptometer used to complete the AMS measurements in this study.*

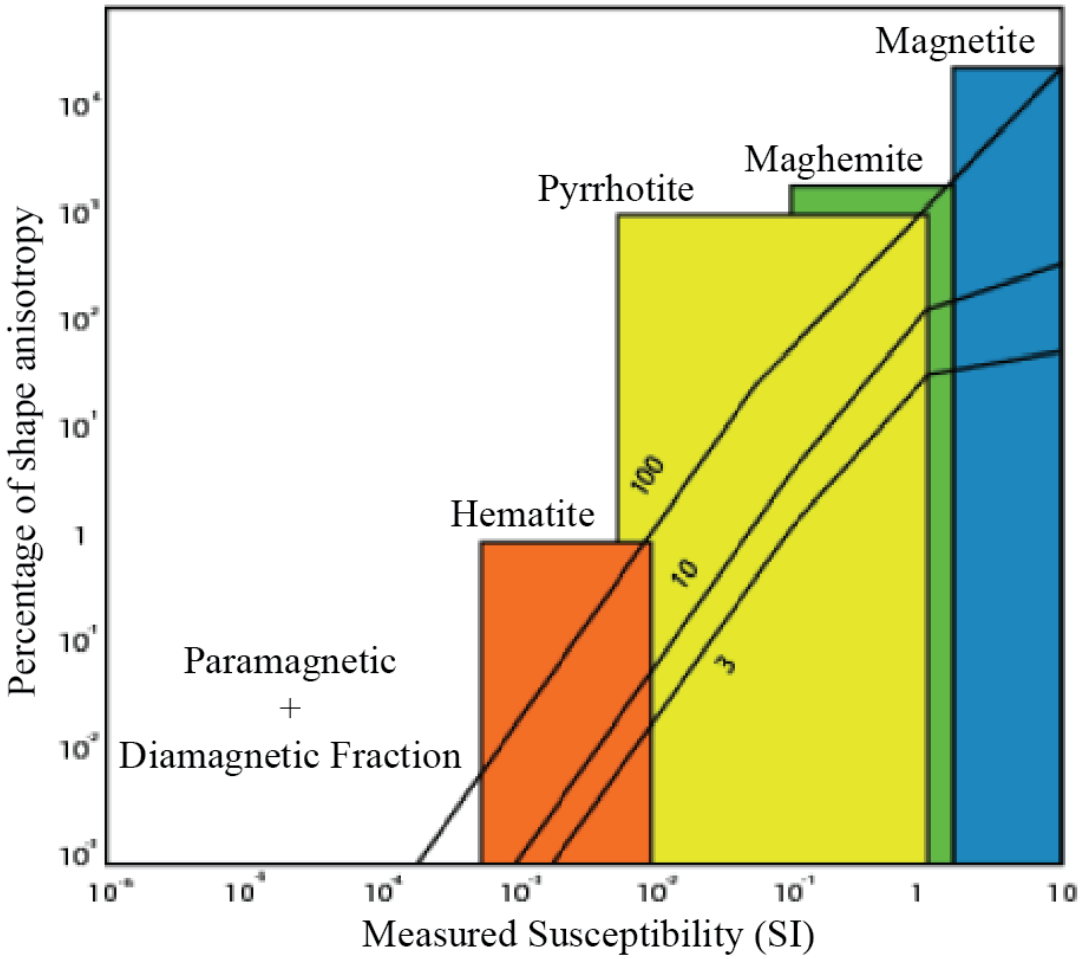

Fig. 11: *Graph displaying the evolution of shape anisotropy as a percentage of the total signal as a function of the overall susceptibility with different mineralogical contributions highlighted. Modified from Amrouch (2010)*

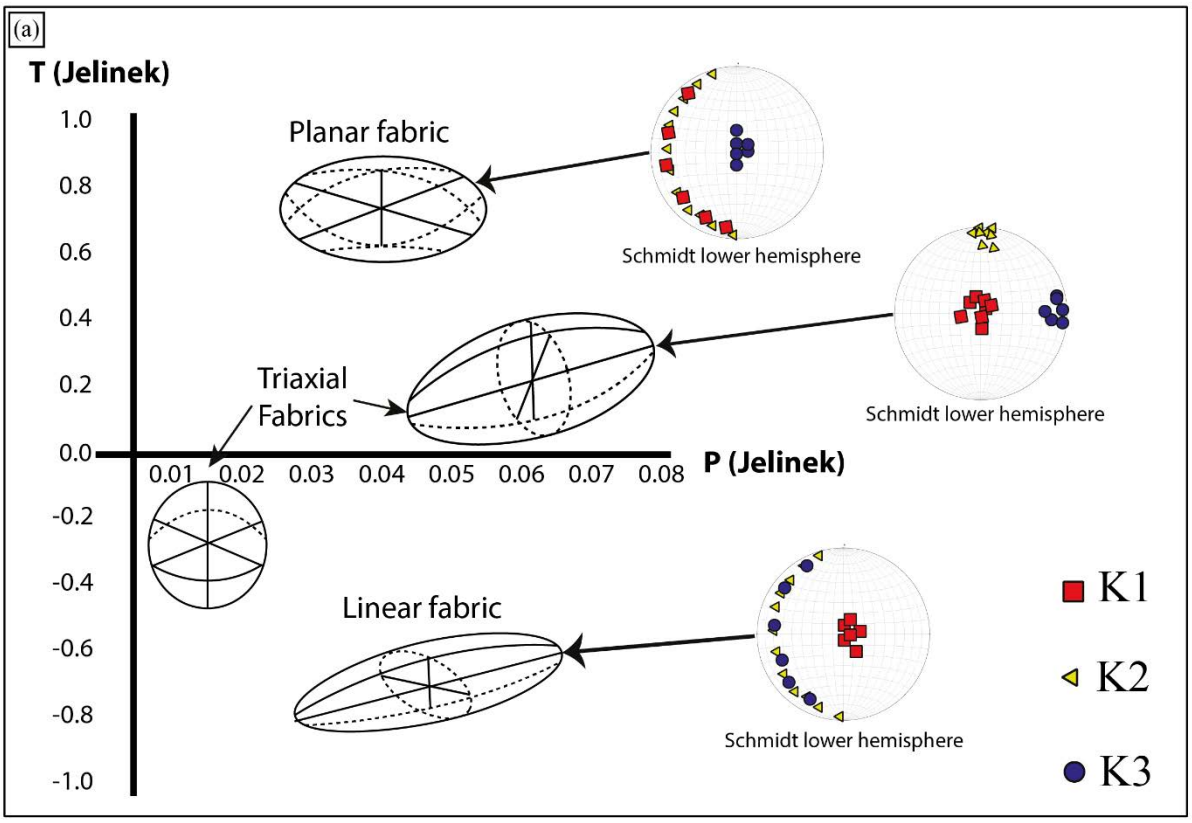

Fig. 12: *Graphical diagram of shape parameters T vs P; (Jelinek, 1981) with the different styles of magnetic fabrics annotated, planar, triaxial and linear.*

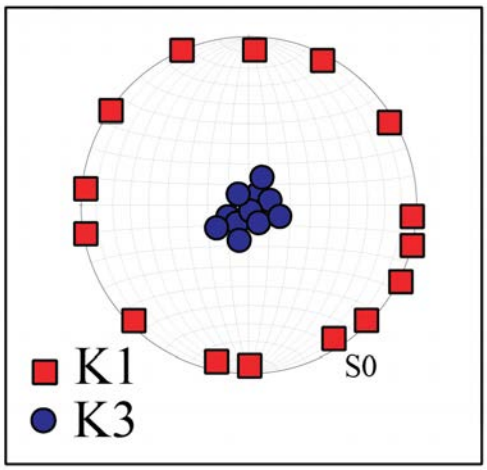

Fig. 13: *A lower hemisphere projection, displaying an example of a sedimentary fabric, with S0 (the bedding) in the horizontal plane, containing K1 and K3, clustered vertically.*

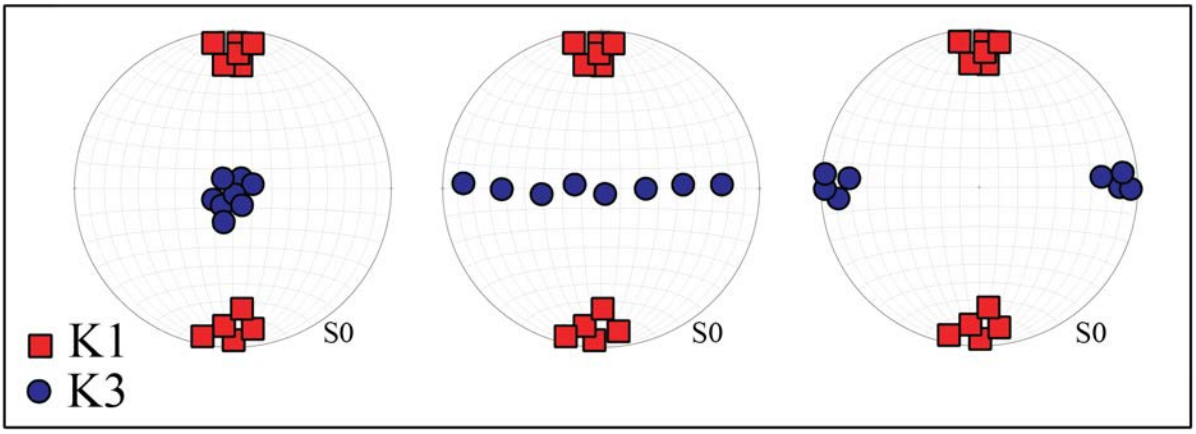

***Fig. 14**: A lower hemisphere steronet plot displaying the transition from sedimentary fabric (left) to intermediate fabric (middle) to finally a tectonic fabric (right).*

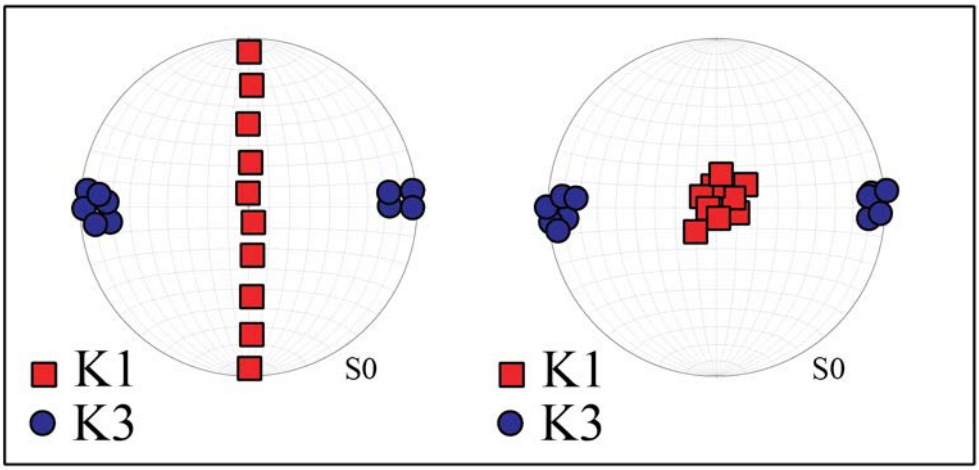

***Fig. 15:** Lower hemisphere stereonet projections showing two different styles of tectonic fabric. With S0 (bedding) in the horizontal plane. Note how K3 lies within it S0.*

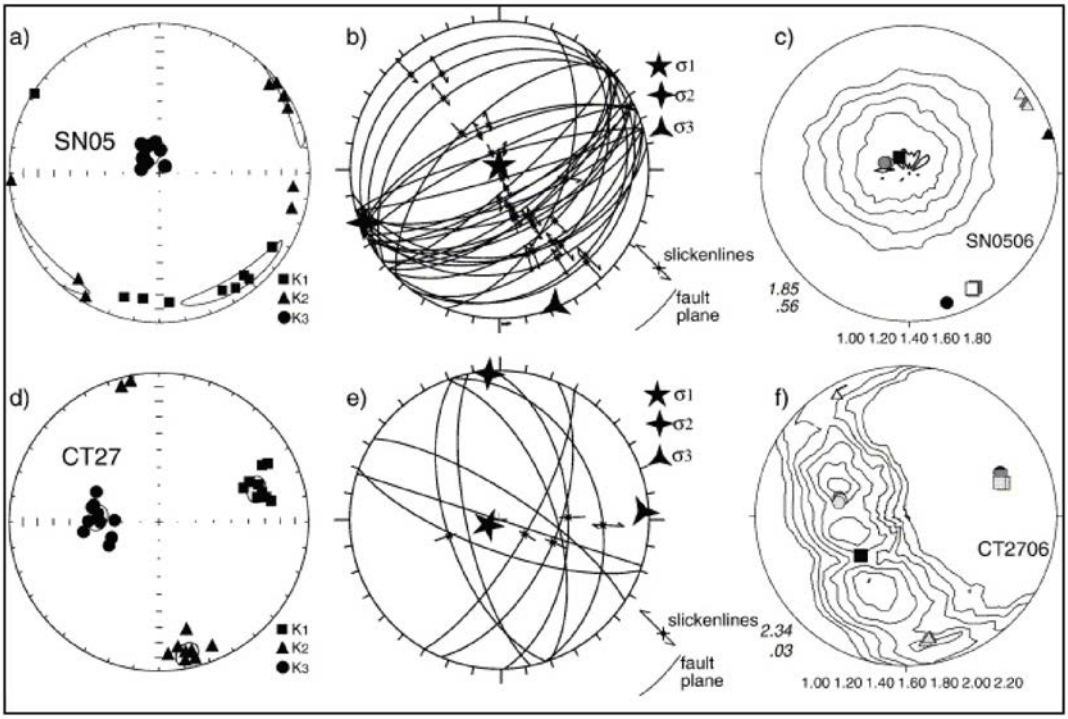

Fig 16: *From Cifelli et al. (2005), using AMS within "undeformed clays" steronets on the left display the AMS fabric, while stereonets in the middle show the orientation of extensional stresses resolved from fault plane solutions. The two show good agreement*

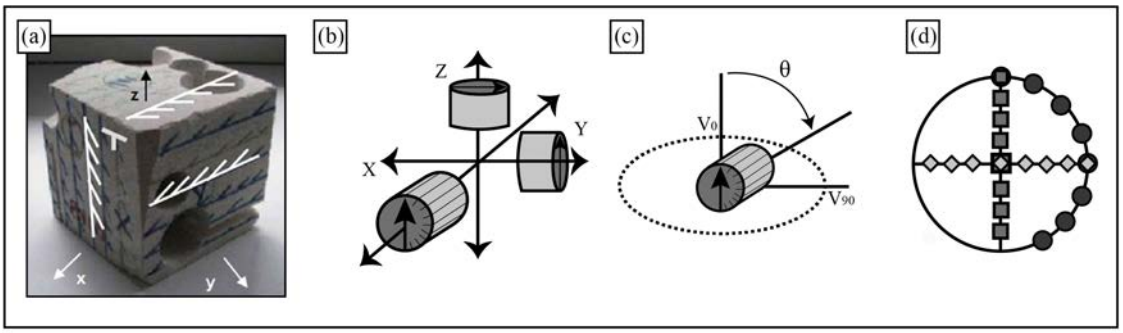

Fig. 17: *Sampling method for the APWV and AMS samples within this study. (a) Coring scheme showing the sampling of three orthogonal samples cored from a single block. Where one of the faces, in this case X, corresponds to precise geographic coordinates. After David et al. (2017) (b) Position of the three oriented cores with the inferred measurement directions (in this case 26) (c) example of the measurement path around the sample and (d) Measurement scheme represented on sample and on a lower hemisphere stereonet, with the investigated directions for this schematic scenario. Azimuth angles measured from the north and dip angles from the horizontal plane.*

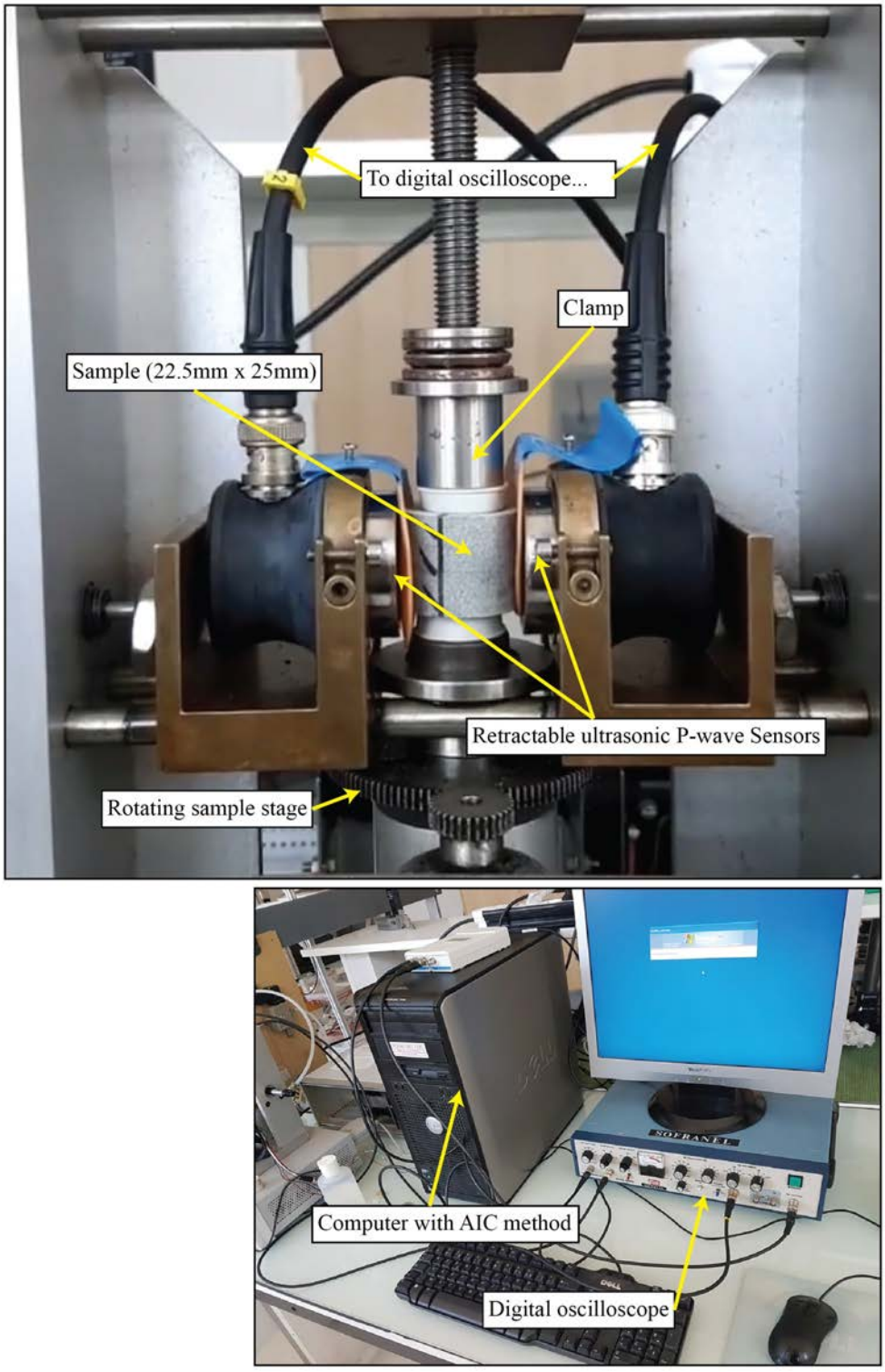

Fig. 18: *Annotated photographs of the experimental device used to measure APV (top) and the linked computer and oscilloscope. This is advantageous and easier as the used does not need to manually rotate the sample as in previous studies e.g. Amrouch (2010).*

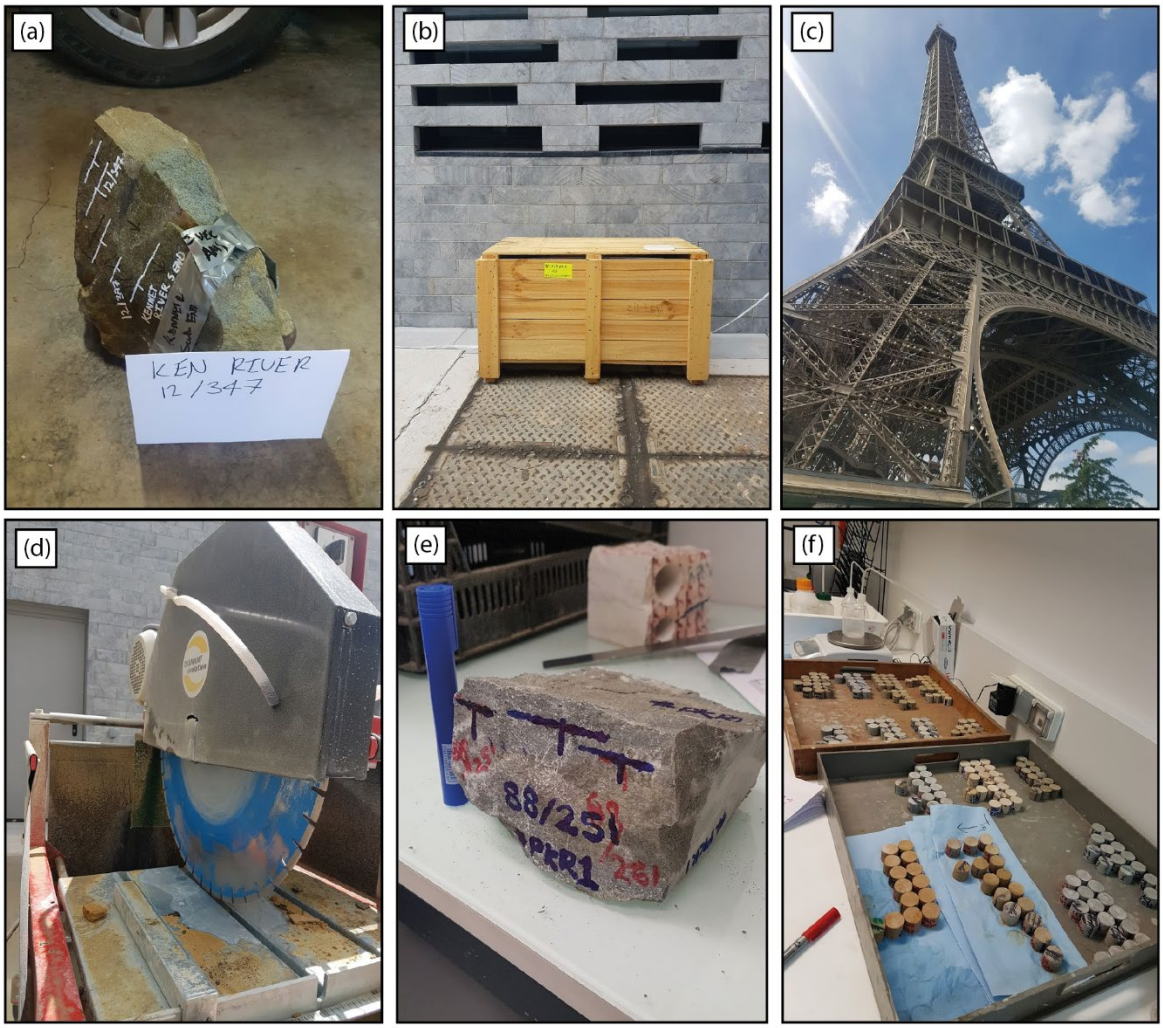

Fig. 19: *A series of photographs showing how the samples for AMS and APV were prepared in this study. (a) Oriented samples were taken from the field from sites within the Otway Ranges (b) Samples were packaged carefully and shipped to (c) Paris in France for analysis at the University of Cergy-Pontoise (d) uneven samples were cut into even cubes in order for the three orthogonal plugs to be taken (e) faces on each cube are annotated to ensure the correct orientation of the plugs following the sampling (f) Plug speicmens used for both AMS and APV are prepared totalling 253 across 18 sites.*

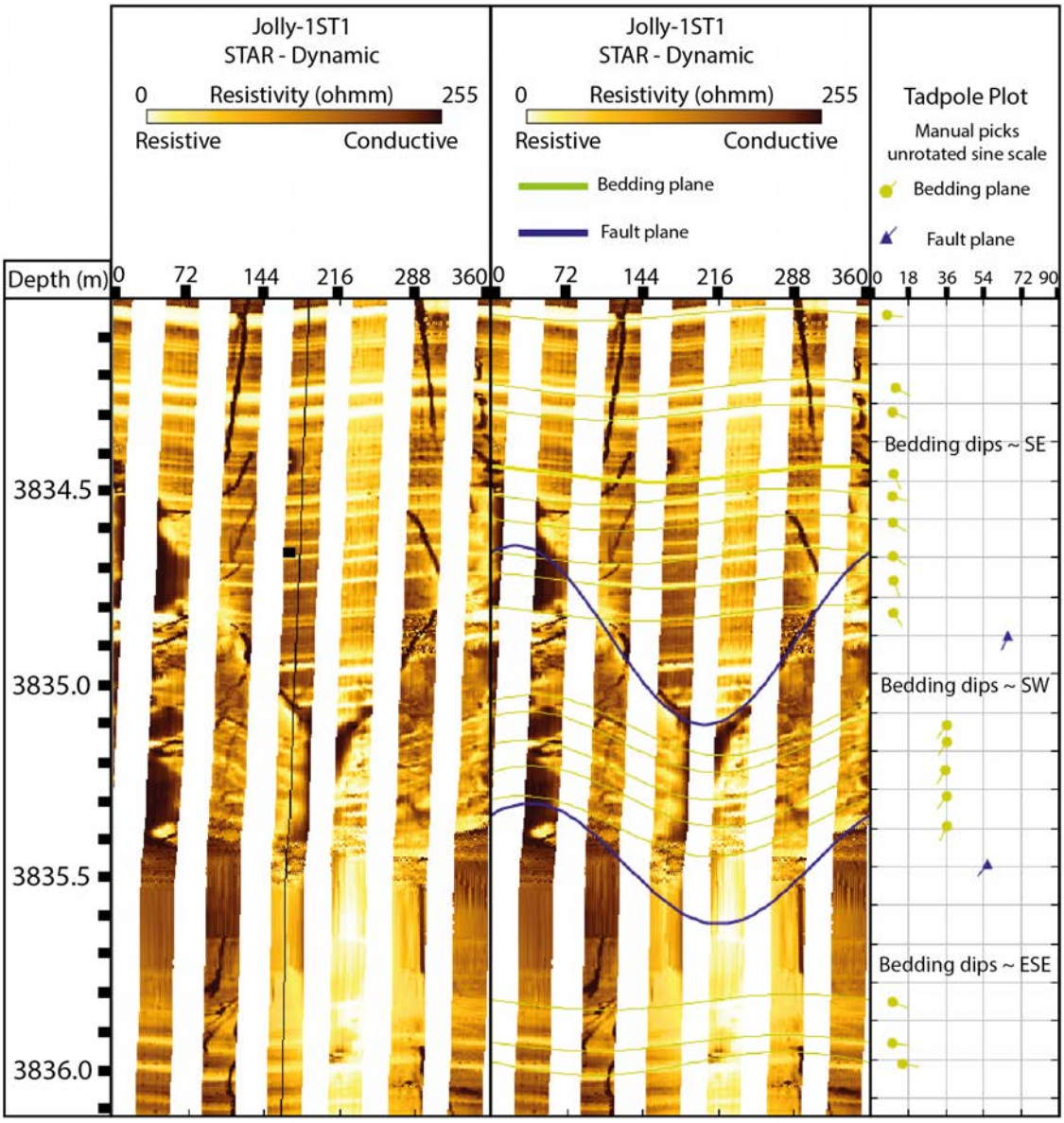

Fig. 20: *An example of an interpreted image log from Jolly-1ST1 within this study, showing the nature of the bedding and an interpreted fault zone, which is distinguished by a change in bedding nature.*

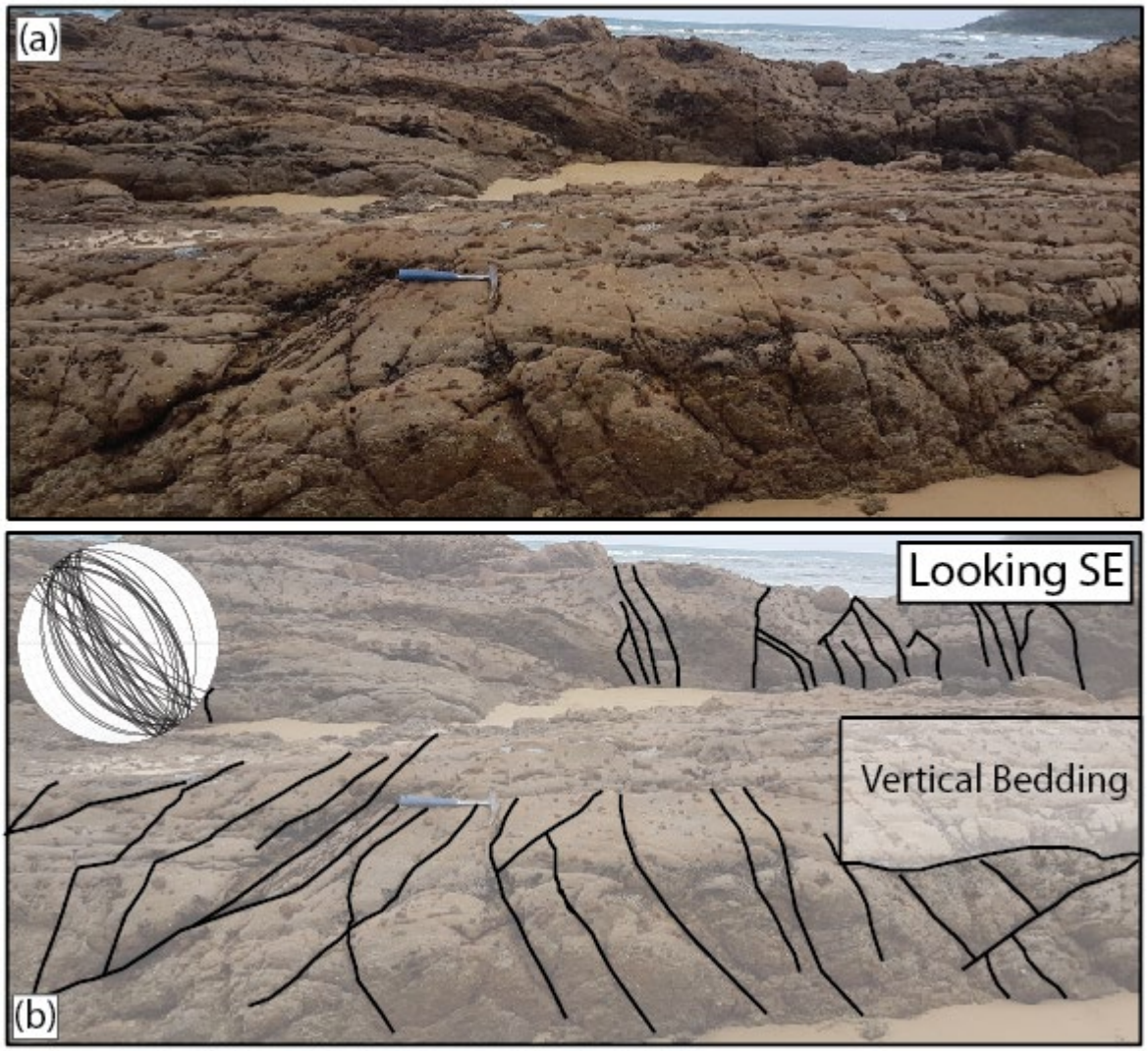

Fig. 21: *An example of natural fracture data acquired from outcropping formations(a) unannotated (b)annotated photograph showing the nature of the bedding and a stereonet showing general fracture orientations.*

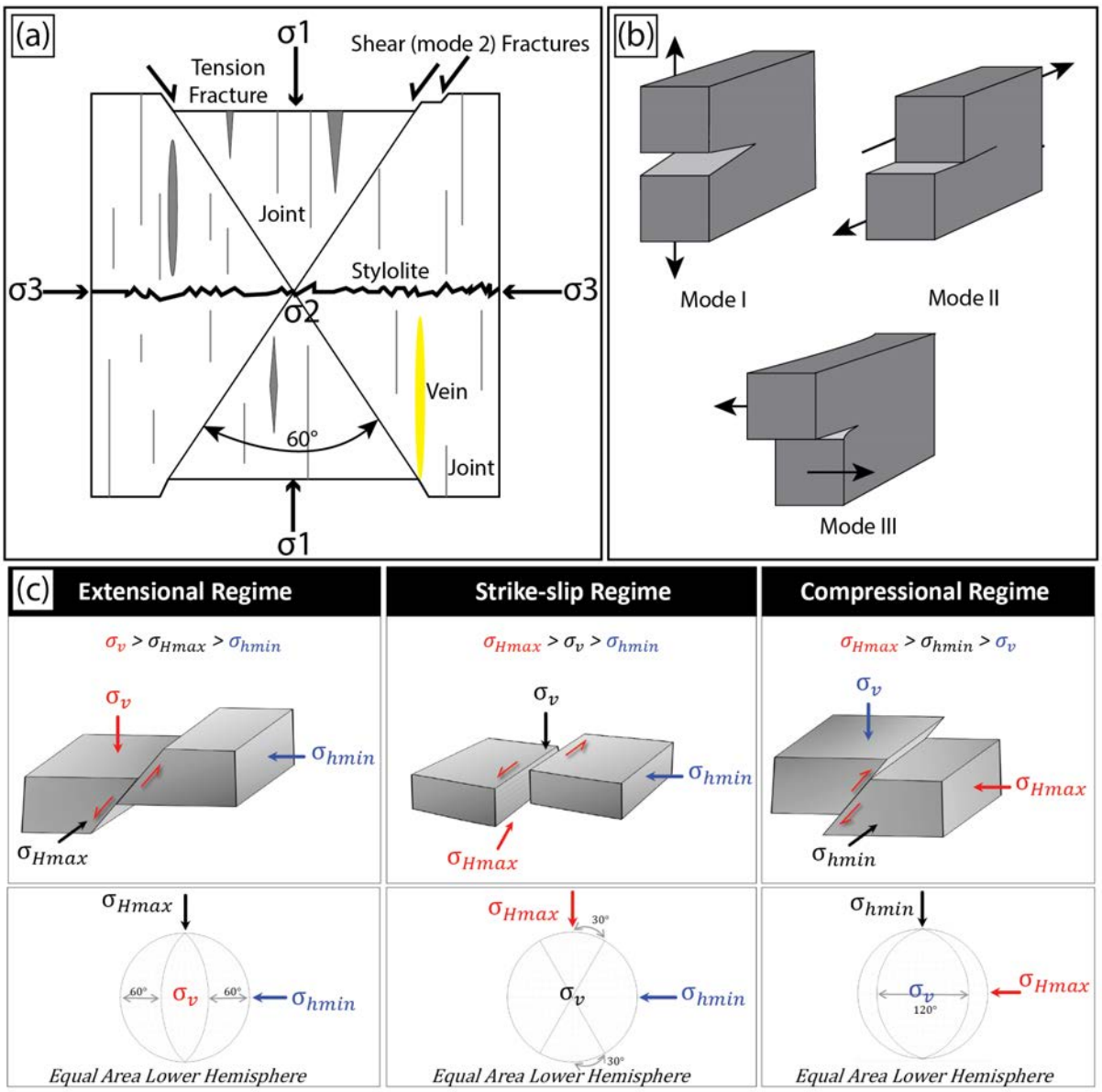

Fig. 22: *(a) Schematic digram modified from Fossen (2016) showing the relationship of various deformation features with the three principal stresses (b) Schematics displaying the three main modes of fracture formation (c) Schematics showing the orientation of the three principal stresses under the three regimes of stress, including lower hemisphere projections of conjugate (mode 2) fractures.*

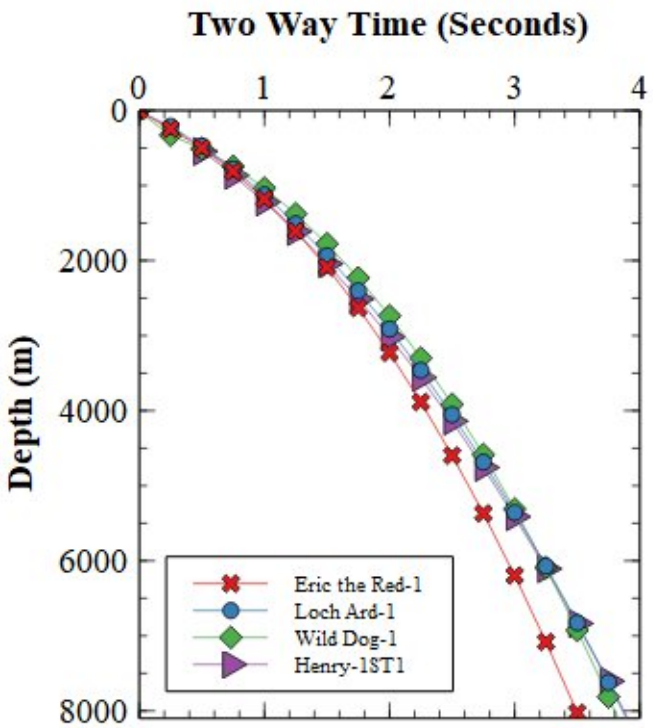

***Fig. 23**: Time vs depth plot example from this study showing how time depth relationships can be derived from velocity well checkshot data by fitting a polynomial trend.*

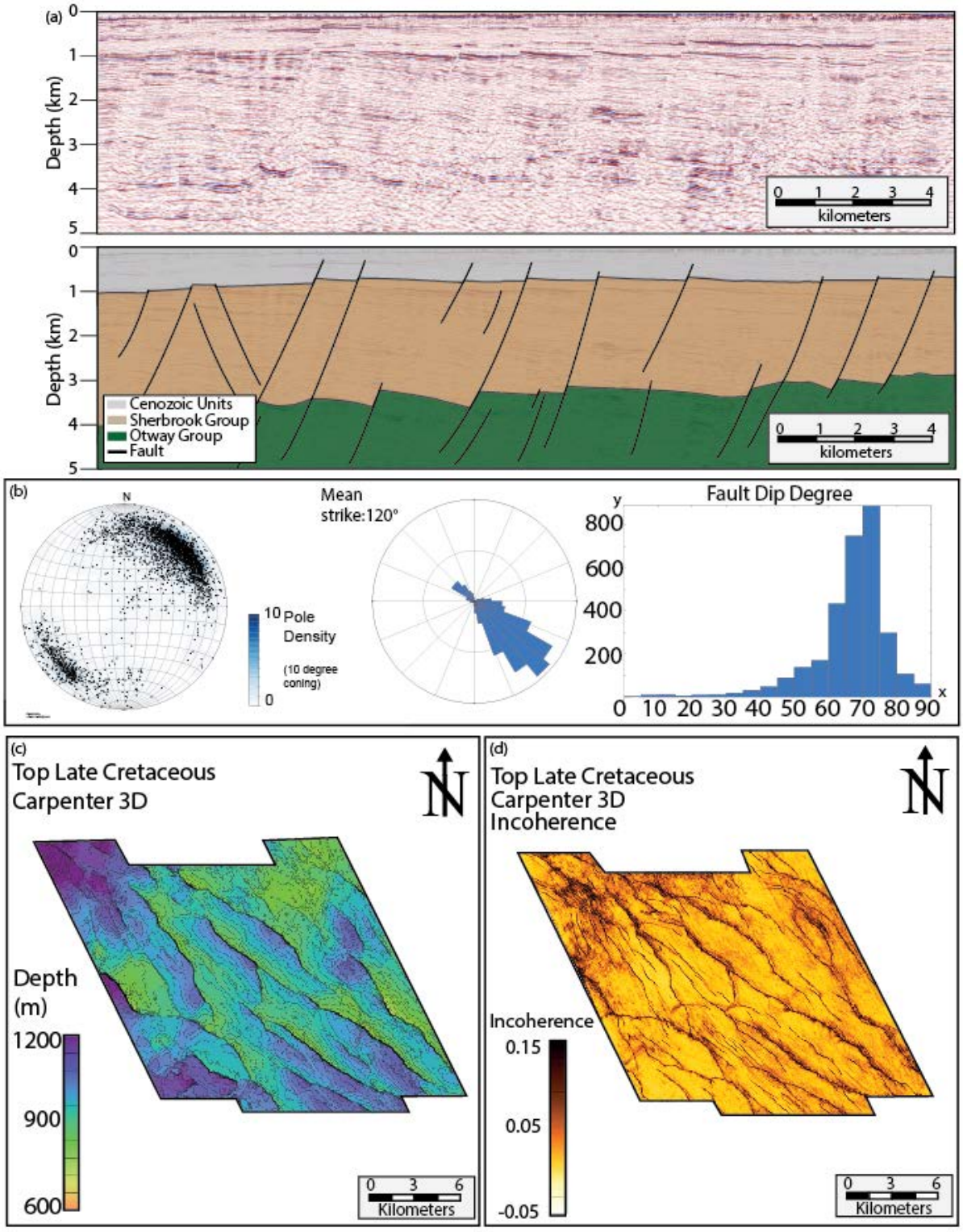

Fig. 24: *(a) An example of an uninterpreted seismic section from the Carpenter 3D used in this study (b) interpreted section showing faults and horizons (c) stereonet and rose diagram showing geometry of interpreted faults (d) dip angles of interpreted faults in the survey.*

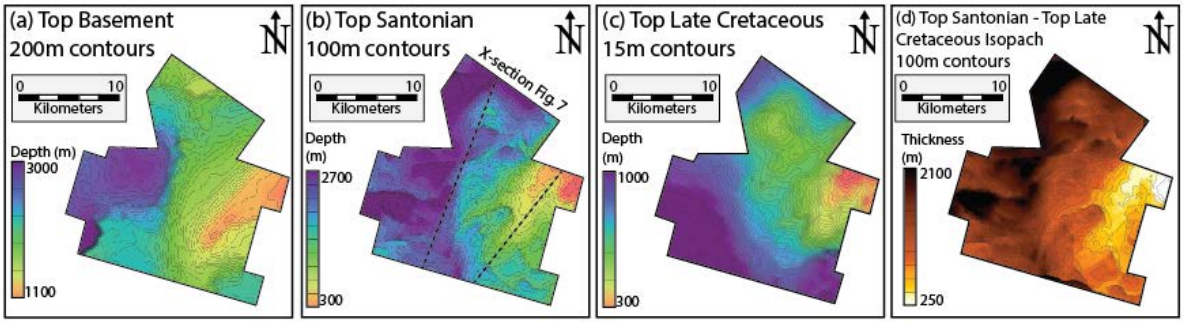

Fig. 25: *Examples of reflectors interpreted (a),(b),(c) and isopachs (d) and (h)interpreted within this study.*

References

Amrouch, K., Lacombe, O., Bellahsen, N., Daniel, J. M., & Callot, J. P. (2010). Stress and strain patterns, kinematics and deformation mechanisms in a basement-cored anticline: Sheep Mountain Anticline, Wyoming. *Tectonics*, 29(1).

Amrouch, K. (2010). Contribution of microstructural analysis to the understanding of folding mechanisms: Examples of folded structures in the USA (Wyoming) and in Iran (Zagros)

Anderson, E. M. (1951). The dynamics of faulting and dyke formation with applications to Britain. Hafner Pub. Co.

Amrouch, K., Beaudoin, N., Lacombe, O., Bellahsen, N., & Daniel, J. M. (2011). Paleostress magnitudes in folded sedimentary rocks. *Geophysical Research Letters*, 38(17).

Arboit, F., Amrouch, K., Collins, A. S., King, R., & Morley, C. (2015). Determination of the tectonic evolution from fractures, faults, and calcite twins on the southwestern margin of the Indochina Block. *Tectonics*, 34(8), 1576-1599.

Arboit, F., Amrouch, K., Morley, C., Collins, A. S., & King, R. (2017). Palaeostress magnitudes in the Khao Khwang fold-thrust belt, new insights into the tectonic evolution of the Indosinian orogeny in central Thailand. *Tectonophysics*, 710, 266-276.

Averbuch, O., de Lamotte, D. F., & Kissel, C. (1992). Magnetic fabric as a structural indicator of the deformation path within a fold-thrust structure: a test case from the Corbières (NE Pyrenees, France). *Journal of Structural Geology*, 14(4), 461-474.

Bahorich, M. S., & Farmer, S. L. (1995). 3-D seismic discontinuity for faults and stratigraphic features: The coherence cube. *In SEG Technical Program Expanded Abstracts* 1995 (pp. 93-96). Society of Exploration Geophysicists.

Basir, H. M., Javaherian, A., & Yaraki, M. T. (2013). Multi-attribute ant-tracking and neural network for fault detection: a case study of an Iranian oilfield. *Journal of Geophysics and Engineering*, 10(1), 015009.

Beaudoin, N., & Lacombe, O. (2018). Recent and future trends in paleopiezometry in the diagenetic domain: Insights into the tectonic paleostress and burial depth history of fold-and-thrust belts and sedimentary basins. *Journal of Structural Geology*, 114, 357-365.

Beaudoin, N., Leprêtre, R., Bellahsen, N., Lacombe, O., Amrouch, K., Callot, J. P. & Daniel, J. M. (2012). Structural and microstructural evolution of the Rattlesnake Mountain Anticline (Wyoming, USA): new insights into the Sevier and Laramide orogenic stress build-up in the Bighorn Basin. *Tectonophysics*, 576, 20-45.

Beaudoin, N., Koehn, D., Lacombe, O., Lecouty, A., Billi, A., Aharonov, E., & Parlangeau, C. (2016). Fingerprinting stress: Stylolite and calcite twinning paleopiezometry revealing the complexity of progressive stress patterns during folding—The case of the Monte Nero anticline in the Apennines, Italy. *Tectonics*, 35(7), 1687-1712.

Bellahsen, N., Fiore, P. E., & Pollard, D. D. (2006). From spatial variation of fracture patterns to fold kinematics: A geomechanical approach. *Geophysical Research Letters*, 33(2).

Bhathal, R. S. (1971). Magnetic anisotropy in rocks. Earth-Science Reviews, 7(4), 227-253.

Borradaile, G. J. (1988). Magnetic susceptibility, petrofabrics and strain. *Tectonophysics*, 156(1-2), 1-20.

Borradaile, G. J. (1991). Correlation of strain with anisotropy of magnetic susceptibility (AMS). *Pure and Applied Geophysics*, 135(1), 15-29.

Borradaile, G. J., & Hamilton, T. (2004). Magnetic fabrics may proxy as neotectonic stress trajectories, Polis rift, Cyprus. *Tectonics*, 23(1).

Borradaile, G. J., & Henry, B. (1997). Tectonic applications of magnetic susceptibility and its anisotropy. *Earth-Science Reviews*, 42(1-2), 49-93.

Borradaile, G. J., & Henry, B. (1997). Tectonic applications of magnetic susceptibility and its anisotropy. *Earth-Science Reviews*, 42(1-2), 49-93.

Burkhard, M. (1993). Calcite twins, their geometry, appearance and significance as stress-strain markers and indicators of tectonic regime: a review. *Journal of structural geology*, 15(3-5), 351-368.

Burkhard, M. (1993). Calcite twins, their geometry, appearance and significance as stress-strain markers and indicators of tectonic regime: a review. *Journal of structural geology*, 15(3-5), 351-368

Cifelli, F., Rossetti, F., Mattei, M., Hirt, A. M., Funiciello, R., & Tortorici, L. (2004). An AMS, structural and paleomagnetic study of quaternary deformation in eastern Sicily. *Journal of Structural Geology*, 26(1), 29-46.

Cifelli, F., Mattei, M., Chadima, M., Hirt, A. M., & Hansen, A. (2005). The origin of tectonic lineation in extensional basins: combined neutron texture and magnetic analyses on “undeformed” clays. *Earth and Planetary Science Letters*, 235(1-2), 62-78.

Cifelli, F., Mattei, M., Chadima, M., Hirt, A. M., & Hansen, A. (2005). The origin of tectonic lineation in extensional basins: combined neutron texture and magnetic analyses on “undeformed” clays. *Earth and Planetary Science Letters*, 235(1-2), 62-78.

Craddock, J. P., & van der Pluijm, B. A. (1999). Sevier–Laramide deformation of the continental interior from calcite twinning analysis, west-central North America. *Tectonophysics*, 305(1-3), 275-286.

Etchecopar, A. (1984). Etude des états de contrainte en tectonique cassante et simulations de déformations plastiques: approche mathématique (Doctoral dissertation).

Faccenna, C., Speranza, F., Caracciolo, F. D. A., Mattei, M., & Oggiano, G. (2002). Extensional tectonics on Sardinia (Italy): insights into the arc–back-arc transitional regime. *Tectonophysics*, 356(4), 213-232.

Ferrill, D. A. (1998). Critical re-evaluation of differential stress estimates from calcite twins in coarse-grained limestone. *Tectonophysics*, 285(1-2), 77-86.

Fossen, H. (2016). Structural geology. Cambridge University Press.

Friedman, M., & Heard, H. C. (1974). Principal stress ratios in Cretaceous limestones from Texas Gulf Coast. *AAPG Bulletin*, 58(1), 71-78.

De Lamotte, D. F., Souque, C., Grelaud, S., & Robion, P. (2002). Early record of tectonic magnetic fabric during inversion of a sedimentary basin Short review and examples from the Corbieres transfer zone (France). *Bulletin de la Société Géologique de France*, 173(5), 461-469.

Gaillot, P., Brewer, T., Pezard, P., & Yeh, E. C. (2007). Borehole imaging tools—principles and applications. *Scientific Drilling*, 5, 1-4.

De Lamotte, D. F., Souque, C., Grelaud, S., & Robion, P. (2002). Early record of tectonic magnetic fabric during inversion of a sedimentary basin Short review and examples from the Corbieres transfer zone (France). *Bulletin de la Société Géologique de France*, 173(5), 461-469.

Graham, J. W. (1954). Magnetic anisotropy, an unexploited petrofabric element. *Geol. Soc. Am. Bull.*, 65, 1257-1258.

Graham, J. W. (1996). Significance of magnetic anisotropy in Appalachian sedimentary rocks. The Earth Beneath the Continents: A Volume of Geophysical Studies in Honor of Merle A. Tuve, 627-648.

Granar, L. (1958). Magnetic measurements on Swedish varved sediments. Ark. Geofys, 3(1), 1-40.

Hancock, P. L. (1985). Brittle microtectonics: principles and practice. *Journal of structural geology*, 7(3-4), 437-457.

Borradaile, G. J., & Jackson, M. (2004). Anisotropy of magnetic susceptibility (AMS): magnetic petrofabrics of deformed rocks. *Geological Society, London, Special Publications*, 238(1), 299-360.

Hecht, K. (1962). Magnetic susceptibility anisotropy of beach sand (Doctoral dissertation, Brown University).

Hrouda, F. (1993). Theoretical models of magnetic anisotropy to strain relationship revisited. *Physics of the Earth and Planetary Interiors*, 77(3-4), 237-249.

Hudson, J. A. (1981). Wave speeds and attenuation of elastic waves in material containing cracks. *Geophysical Journal International*, 64(1), 133-150.

Jackson, M. (1991). Anisotropy of magnetic remanence: a brief review of mineralogical sources, physical origins, and geological applications, and comparison with susceptibility anisotropy. *Pure and Applied Geophysics*, 136(1), 1-28.

Jackson, M., & Tauxe, L. (1991). Anisotropy of magnetic susceptibility and remanence: developments in the characterization of tectonic, sedimentary and igneous fabric. *Reviews of Geophysics*, 29(S1), 371-376.

Jamison, W. R., & Spang, J. H. (1976). Use of calcite twin lamellae to infer differential stress. *Geological Society of America Bulletin*, 87(6), 868-872.

Janssen, C., Hoffmann-Rothe, A., Bohnhoff, M., Wetzel, H. U., Matar, A., Khatib, M., & DESERT Research Group. (2007). Different styles of faulting deformation along the Dead Sea Transform and possible consequences for the recurrence of major earthquakes. Journal of *Geodynamics*, 44(1-2), 66-89.

Jelinek, V. (1981). Characterization of the magnetic fabric of rocks. *Tectonophysics*, 79(3-4), T63-T67.

Kachanov, M. (1993). Elastic solids with many cracks and related problems. In *Advances in applied mechanics* (Vol. 30, pp. 259-445). Elsevier.

King, R. F. (1955). The remanent magnetism of artificially deposited sediments. *Geophysical Supplements to the Monthly Notices of the Royal Astronomical Society*, 7(3), 115-134.

King, R. F., & Rees, A. I. (1966). Detrital magnetism in sediments: An examination of some theoretical models. *Journal of Geophysical Research*, 71(2), 561-571.

Kissel, C., Barrier, E., Laj, C., & Lee, T. Q. (1986). Magnetic fabric in “undeformed” marine clays from compressional zones. *Tectonics*, 5(5), 769-781

Kligfield, R., Owens, W. H., & Lowrie, W. (1981). Magnetic susceptibility anisotropy, strain, and progressive deformation in Permian sediments from the Maritime Alps (France). *Earth and Planetary Science Letters*, 55(1), 181-189.

Kissel, C., Barrier, E., Laj, C., & Lee, T. Q. (1986). Magnetic fabric in “undeformed” marine clays from compressional zones. *Tectonics*, 5(5), 769-781.

Kulikowski, D., & Amrouch, K. (2017). Combining geophysical data and calcite twin stress inversion to refine the tectonic history of subsurface and offshore provinces: A case study on the Cooper-Eromanga Basin, Australia. *Tectonics*, 36(3), 515-541.

Kulikowski, D. (2017). Modern Structural Analysis of Subsurface Provinces: A Case Study on the Cooper and Eromanga Basins, Australia (Doctoral dissertation, Doctoral dissertation, unpublished). Adelaide, SA: The Australian School of Petroleum, the University of Adelaide).

Kulikowski, D., & Amrouch, K. (2017). Combining geophysical data and calcite twin stress inversion to refine the tectonic history of subsurface and offshore provinces: A case study on the Cooper-Eromanga Basin, Australia. *Tectonics*, 36(3), 515-541.

Kulikowski, D., Amrouch, K., & Cooke, D. (2016). Geomechanical modelling of fault reactivation in the Cooper Basin, Australia. *Australian Journal of Earth Sciences*, 63(3), 295-314.

Lacombe, O. (2010). Calcite twins, a tool for tectonic studies in thrust belts and stable orogenic forelands. *Oil & Gas Science and Technology–Revue d'IFP Energies nouvelles*, 65(6), 809-838.

Lacombe, O., & Laurent, P. (1996). Determination of deviatoric stress tensors based on inversion of calcite twin data from experimentally deformed monophase samples: preliminary results. *Tectonophysics*, 255(3-4), 189-202.

Lacombe, O., Angelier, J., Laurent, P., Bergerat, F., & Tourneret, C. (1990). Joint analyses of calcite twins and fault slips as a key for deciphering polyphase tectonics: Burgundy as a case study. *Tectonophysics*, 182(3-4), 279-300.

Lacombe, O., Malandain, J., Vilasi, N., Amrouch, K., & Roure, F. (2009). From paleostresses to paleoburial in fold–thrust belts: Preliminary results from calcite twin analysis in the Outer Albanides. *Tectonophysic*s, 475(1), 128-141.

Lamarche, G., & Rochette, P. (1987). Microstructural analysis and origin of lineations in the magnetic fabric of some Alpine slates. *Tectonophysics*, 139(3-4), 285-293.

Langevin, P. (1905). Sur la théorie du magnétisme. J. Phys. Theor. Appl., 4(1), 678-693.

Laurent, P. (1984). Les macles de la calcite en tectonique: nouvelles méthodes dynamiques et premières applications (Doctoral dissertation).

Laurent, P., Kern, H., & Lacombe, O. (2000). Determination of deviatoric stress tensors based on inversion of calcite twin data from experimentally deformed monophase samples. Part II. Axial and triaxial stress experiments. *Tectonophysics*, 327(1-2), 131-148.

Laurent, P., Kern, H., & Lacombe, O. (2000). Determination of deviatoric stress tensors based on inversion of calcite twin data from experimentally deformed monophase samples. Part II. Axial and triaxial stress experiments. *Tectonophysics*, 327(1-2), 131-148.

Laurent, P., Bernard, P., Vasseur, G., & Etchecopar, A. (1981). Stress tensor determination from the study of e twins in calcite: a linear programming method. *Tectonophysics*, 78(1-4), 651-660.

Louis, L. (2003). Composite microstructural anisotropies in reservoir rocks: consequences on elastic properties and relation with deformation; Anisotropies microstructurales composites dans les roches reservoir: consequences sur les proprietes elastiques et relation a la deformation.

Louis, L., David, C., & Robion, P. (2003, December). Composite Anisotropies Revealed by P-Wave Velocity Data Under the Approximation of 2nd Rank Tensor. In AGU Fall Meeting Abstracts.

Louis, L., Robion, P., & David, C. (2004). A single method for the inversion of anisotropic data sets with application to structural studies. *Journal of Structural Geology*, 26(11), 2065-2072.

Lüneburg, C. M., Lampert, S. A., Lebit, H. D., Hirt, A. M., Casey, M., & Lowrie, W. (1999). Magnetic anisotropy, rock fabrics and finite strain in deformed sediments of SW Sardinia (Italy). *Tectonophysics*, 307(1-2), 51-74.

Mattei, M., Sagnotti, L., Faccenna, C., & Funiciello, R. (1997). Magnetic fabric of weakly deformed clay-rich sediments in the Italian peninsula: relationship with compressional and extensional tectonics. *Tectonophysics*, 271(1-2), 107-122.

Mitchum Jr, R. M., Vail, P. R., & Thompson III, S. (1977). Seismic stratigraphy and global changes of sea level: Part 2. The depositional sequence as a basic unit for stratigraphic analysis: Section 2. Application of seismic reflection configuration to stratigraphic interpretation.

Nemcok, M., Kovác, D., & Lisle, R. J. (1999). A stress inversion procedure for polyphase calcite twin and fault/slip data sets. *Journal of Structural Geology*, 21(6), 597-611.

Neves, F. A., Zahrani, M. S., & Bremkamp, S. W. (2004). Detection of potential fractures and small faults using seismic attributes. *The Leading Edge*, 23(9), 903-906.

Newman, J. (1994). The influence of grain size and grain size distribution on methods for estimating paleostresses from twinning in carbonates. *Journal of Structural Geology*, 16(12), 1589-1601.

Parés, J. M., & Van Der Pluijm, B. A. (2002). Evaluating magnetic lineations (AMS) in deformed rocks. *Tectonophysics*, 350(4), 283-298.

Parlangeau, C., Lacombe, O., Schueller, S., & Daniel, J. M. (2018). Inversion of calcite twin data for paleostress orientations and magnitudes: A new technique tested and calibrated on numerically-generated and natural data. *Tectonophysics*, 722, 462-485.

Pokalai, K., Kulikowski, D., Johnson, R. L., Haghighi, M., & Cooke, D. (2016). Development of a new approach for hydraulic fracturing in tight sand with pre-existing natural fractures. *The APPEA Journal*, 56(1), 225-238.

Poppelreiter, M., Garcia-Carballido, C., & Kraaijveld, M. (2010). Borehole image log technology: application across the exploration and production life cycle.

Prensky, S. E. (1999). Advances in borehole imaging technology and applications. *Geological Society, London, Special Publications*, 159(1), 1-43.

Price, N. J., & Cosgrove, J. W. (1990). Analysis of geological structures. Cambridge University Press.

Rees, A. I. (1965). THE USE OF ANISOTROPY OF MAGNETIC SUSCEPTIBILITY IN THE ESTIMATION OF SEDIMENTARY FABRIC 1. *Sedimentology*, 4(4), 257-271.

Robert, R., Robion, P., Souloumiac, P., David, C., & Saillet, E. (2018). Deformation bands, early markers of tectonic activity in front of a fold-and-thrust belt: Example from the Tremp-Graus basin, southern Pyrenees, Spain. *Journal of Structural Geology*, 110, 65-85.

Robion, P., David, C., Dautriat, J., Colombier, J. C., Zinsmeister, L., & Collin, P. Y. (2014). Pore fabric geometry inferred from magnetic and acoustic anisotropies in rocks with various mineralogy, permeability and porosity. *Tectonophysics*, 629, 109-122.

Robion, P., Grelaud, S., & de Lamotte, D. F. (2007). Pre-folding magnetic fabrics in fold-and-thrust belts: Why the apparent internal deformation of the sedimentary rocks from the Minervois basin (NE—Pyrenees, France) is so high compared to the Potwar basin (SW—Himalaya, Pakistan). *Sedimentary Geology*, 196(1-4), 181-200.

Robion, P., Grelaud, S., & de Lamotte, D. F. (2007). Pre-folding magnetic fabrics in fold-and-thrust belts: Why the apparent internal deformation of the sedimentary rocks from the Minervois basin (NE—Pyrenees, France) is so high compared to the Potwar basin (SW—Himalaya, Pakistan) *Sedimentary Geology*, 196(1-4), 181-200.

Rowe, K. J., & Rutter, E. H. (1990). Palaeostress estimation using calcite twinning: experimental calibration and application to nature. *Journal of Structural Geology*, 12(1), 1-17.

Rusnak, G. A. (1957). The Orientation of Sand Grains under Conditions of" Unidirectional" Fluid Flow: 1. Theory and Experiment. *The Journal of Geology*, 65(4), 384-409.

Sayers, C. M., & Kachanov, M. (1995). Microcrack-induced elastic wave anisotropy of brittle rocks. *Journal of Geophysical Research: Solid Earth*, 100(B3), 4149-4156.

Rowe, K. J., & Rutter, E. H. (1990). Palaeostress estimation using calcite twinning: experimental calibration and application to nature. *Journal of Structural Geology*, 12(1), 1-17.

Sagnotti, L., Faccenna, C., Funiciello, R., & Mattei, M. (1994). Magnetic fabric and structural setting of Plio-Pleistocene clayey units in an extensional regime: the Tyrrhenian margin of central Italy. *Journal of Structural Geology*, 16(9), 1243-1257.

Sagnotti, L., & Winkler, A. (1999). Rock magnetism and palaeomagnetism of greigite-bearing mudstones in the Italian peninsula. *Earth and Planetary Science Letters*, 165(1), 67-80.

Seeburger, D. A., & Zoback, M. D. (1982). The distribution of natural fractures and joints at depth in crystalline rock. *Journal of Geophysical Research: Solid Earth*, 87(B7), 5517-5534.

Sibson, R. H. (2003). Thickness of the seismic slip zone. Bulletin of the Seismological Society of America, 93(3), 1169-1178.

Spang, J. H. (1972). Numerical method for dynamic analysis of calcite twin lamellae. *Geological Society of America Bulletin*, 83(2), 467-472.

Sperner, B. & Ratschbacher, L. (1994). A Turbo Pascal program package for graphical presentation and stress analysis of calcite deformation. Z. Dtsch. Geol. Ges, 145, 414-423.

Spiers, C. J. (1982). The development of deformation textures in calcite rocks.

Spiers, C. J., & Rutter, E. H. (1984). A calcite twinning palaeopiezometer. *In Progress in Experimental Petrology* (Vol. 25, pp. 241-245)

Tarling, D., & Hrouda, F. (Eds.). (1993). Magnetic anisotropy of rocks. *Springer Science & Business Media.*

Tavani, S., Storti, F., Lacombe, O., Corradetti, A., Muñoz, J. A., & Mazzoli, S. (2015). A review of deformation pattern templates in foreland basin systems and fold-and-thrust belts: Implications for the state of stress in the frontal regions of thrust wedges. *Earth-Science Reviews*, 141, 82-104.

Tarling, D., & Hrouda, F. (Eds.). (1993). Magnetic anisotropy of rocks. *Springer Science & Business Media.*

Turner, F. J., & Orozco, M. (1976). Crystal bending in metamorphic calcite, and its relations to associated twinning. *Contributions to Mineralogy and Petrology*, 57(1), 83-97.

Weiss, T. F., Mulroy, M. J., Turner, R. G., & Pike, C. L. (1976). Tuning of single fibers in the cochlear nerve of the alligator lizard: relation to receptor morphology. *Brain research*, 115(1), 71-90.

Turner, F. J., Griggs, D. T., & Heard, H. (1954). Experimental deformation of calcite crystals. *Geological Society of America Bulletin*, 65(9), 883-934.

Vail, P. R., Mitchum Jr, R. M., & Thompson III, S. (1977). Seismic stratigraphy and global changes of sea level: Part 4. Global cycles of relative changes of sea level: Section 2. Application of seismic reflection configuration to stratigraphic interpretation.

Yamaji, A. (2015). Generalized Hough transform for the stress inversion of calcite twin data. *Journal of Structural Geology*, 80, 2-15.

Zoback, M. L., Zoback, M. D., Adams, J., Assumpcao, M., Bell, S., Bergman, E. A.& Fuchs, K. (1989). Global patterns of tectonic stress. *Nature*, 341(6240), 291.

Zoback, M. D., Barton, C. A., Brudy, M., Castillo, D. A., Finkbeiner, T., Grollimund, B. R.,& Wiprut, D. J. (2003). Determination of stress orientation and magnitude in deep wells. *International Journal of Rock Mechanics and Mining Sciences*, 40(7-8), 1049-1076.

Chapter 4.1: Manuscript 1

Determining paleo-structural environments through natural fracture and calcite twin analyses: a case study in the Otway Basin, Australia

This paper was accepted as part of the proceedings of the Australian Petroleum Production and Exploration Association (APPEA) conference in Adelaide in 2018, published in the association's journal following presentation.

Statement of Authorship

Title of Paper: Determining paleo-structural environments through natural fracture and calcite twin analyses: a case study in the Otway Basin, Australia

Publication Status: Published

Publication Details: Burgin, H. B., Amrouch, K., Rajabi, M., Kulikowski, D., & Holford, S. P. (2018). Determining paleo-structural environments through natural fracture and calcite twin analyses: a case study in the Otway Basin, Australia. The APPEA Journal, 58(1), 238-2

Principal Author: Hugo Bonython Burgin

Contribution: Field work and image log interpretation. Data analysis. Writing of paper. (55%)

Certification: This paper reports predominantly on original research I conducted during the period of my Higher Degree by Research candidature and is not subject to any obligations or contractual agreements with a third party that would constrain its inclusion in this thesis. I am the primary author of this paper.

Signed: **Date:** 05/03/2019

Co-Author Contributions

By signing the Statement of Authorship, each author certifies that:

- **i.** The candidate's stated contribution to the publication is accurate (as detailed above);
- **ii.** Permission is granted for the candidate to include the publication in the thesis; and
- **iii.** The sum of all co-author contributions is equal to 100% less the candidate's stated contribution.

Name of Co-Author: Dr Khalid Amrouch

Contribution to Paper: Supervised project. Assisted with field work and data interpretation (15%)

Signed: **Date:** 05/03/2019

Name of Co-Author: Dr Mojtaba Rajabi

Contribution to Paper: Supervised project. Assisted with image log interpretation and data fracture set identification (15%)

Signed: **Date:** 21/03/2019

Name of Co-Author: Dr Simon Holford

Contribution to Paper: Co-supervised project. Assisted with paper and Otway basin background (10%)

Signed: **Date:** 25/03/2019

Name of Co-Author: Dr David Kulikowski

Contribution to Paper: Assisted with paper writing and fracture set identification (5%)

Signed: **Date:** 13/03/2019

The APPEA Journal 2018, **58**, 000–000
https://doi.org/10.1071/AJ17099

Peer reviewed paper

Determining paleo-structural environments through natural fracture and calcite twin analyses: a case study in the Otway Basin, Australia

Hugo B. Burgin[A,B], *Khalid Amrouch*[A], *Mojtaba Rajabi*[A], *David Kulikowski*[A] *and Simon P. Holford*[A]

[A]Australian School of Petroleum, University of Adelaide, North Terrace, Adelaide, SA 5005, Australia.
[B]Corresponding author. Email: hugo.burgin@adelaide.edu.au

Abstract. The structural history of the Otway Basin has been widely studied; however, previous works have focussed on large kilometre scale, basin and seismic structures, or have over-simplified natural fracture analysis with an excessive focus on fracture strike direction and a disregard for 3D geometry, a crucial characteristic when considering states of stress responsible for natural fracture formation. In this paper, we combine techniques of natural fracture analysis and calcite twin stress inversion to investigate the meso (outcrop and borehole) and micro (crystal) scale evidence for structural environments that have contributed to basin evolution. Our results indicate that basin evolution during the post-Albian may be markedly more complex than the previously thought stages of late Cretaceous inversion, renewed rifting and long-lived mid-Eocene to recent compression, with evidence for up to six structural environments detected across the basin, including; NE–SW and NW–SE extension, NW–SE compression, a previously undetected regime of NE–SW compression, and two regimes of strike-slip activity. By constraining structural environments on the meso- and micro-scale we can deliver higher levels of detail into structural evolution, which in turn, provides better-quality insights into multiple petroleum system elements, including secondary migration pathways and trap formation. Our research also shows that the Otway Basin presents a suitable environment for additional micro-scale structural investigations through calcite twin analyses.

Additional keywords: basin analysis, tectonic, paleo-stress, structure.

Received 11 December 2017, accepted 30 January 2018published online dd mmm yyyy

Introduction

The use of natural fractures as a tool for paleo-stress and structural analyses is well established (Bellahsen *et al.* 2006; Amrouch 2010; Arboit *et al*. 2015) and is becoming increasingly more popular for basin analysis studies (Beaudoin *et al*. 2012; Kulikowski *et al*. 2015; Kulikowski *et al.* 2016*a*; Kulikowski and Amrouch 2017). Historically, paleo-stress analysis has relied on natural fracture data obtained from rock outcrops within onshore provinces; with recent studies beginning to expand these methods of interpretation and analysis to subsurface data (Kulikowski and Amrouch 2017). Borehole image log interpretation is a well documented process, and is often used to quantify *in situ* states of crustal stress (Zoback *et al.* 1985; Pokalai *et al.* 2016; Rajabi *et al.* 2017*a*) and to identify the presence of natural fractures and faults. While these techniques yield important information concerning local and instantaneous crustal stress fields, our scientific knowledge of stress fields sustained by rocks throughout their history, especially in Australian sedimentary basins, remains poor. Determining these ancient states of stress and the associated spatial and temporal distribution and density of natural fractures can have significant implications for exploration, improved recovery and economic feasibility of projects (Kulikowski *et al.* 2016*a*, 2016*b*, 2017; Kulikowski and Amrouch 2017), while also providing 'mechanical checkpoints' - quantified specific states of stress - during basin evolution (Amrouch *et al*. 2010*b*; Arboit *et al*. 2017).

The field of paleo-stress analysis is the understanding of ancient states of stress and their relative or absolute chronologies and magnitudes from the interpretation of deformation features within the rock (Lacazette 2009; Amrouch *et al*. 2010*b*). Traditional conceptual models for fracture deformation relationships have several shortcomings, which include: (1) an over-simplistic emphasis on fracture strike; (2) minimal emphasis on dip

angle; and (3) a failure to account for the spatial and temporal evolution of deformation (Bellahsen *et al.* 2006; Amrouch *et al.* 2010*a*). By considering fracture networks in four-dimensions (4D), as opposed to two- (2D) or even three-dimensions (3D), the accuracy of tectonic deformation understanding and the structural interpretation of data can be greatly improved (Kulikowski and Amrouch 2017). The integration of calcite twin analysis with methods of natural fracture interpretation in the subsurface and outcrop has been shown to provide another level of depth and confidence to structural interpretations (Amrouch *et al.* 2010*a*; Kulikowski and Amrouch 2017). In recent times, Kulikowski and Amrouch (2017) have made innovative inroads into quantitatively determining the structural evolution of subsurface provinces, by using calcite samples from re-oriented petroleum core in combination with natural fracture and fault analyses, providing the first paleo-stress tensors in an Australian case study, in the Cooper–Eromanga Basin.

Following on from these recent works, paleo-stress inversion is performed on natural fractures and calcite twins from a dataset in the Otway Basin, Australia, to provide insights into the structural history and provide the first quantitative measurement of specific orientations of paleo-stress within the region. The Jurassic to Quaternary Otway Basin (Fig. 1) is a large NW–SE trending sedimentary basin that spans the onshore and offshore parts of South Australia, Victoria and offshore Tasmania. This basin contains hydrocarbon accumulations, geothermal energy potential, and CO_2 storage capabilities, all of which require an understanding of subsurface natural fracture distributions and accurate basin development models. Current models show that initial rifting commenced during the Late Jurassic with multiple phases of extension and compression, responsible for the formation of stratigraphic and structural complexities (Norvick and Smith 2001). Although the region has been extensively studied, this paper presents a pilot study for the Otway Basin using a similar approach to Kulikowski and Amrouch (2017) in the Cooper Basin. For the first time the meso- and micro-scale structural history of the Otway Basin is investigated through the 4D analysis of natural fractures obtained from geophysical well data located in the Penola Trough (west) and from outcrop located in the Otway Ranges (east), with a calcite twin stress inversion technique that is performed on a sample obtained from the Otway Ranges. This study provides valuable information on the: (1) spatial distribution of natural fractures; (2) the temporal distribution

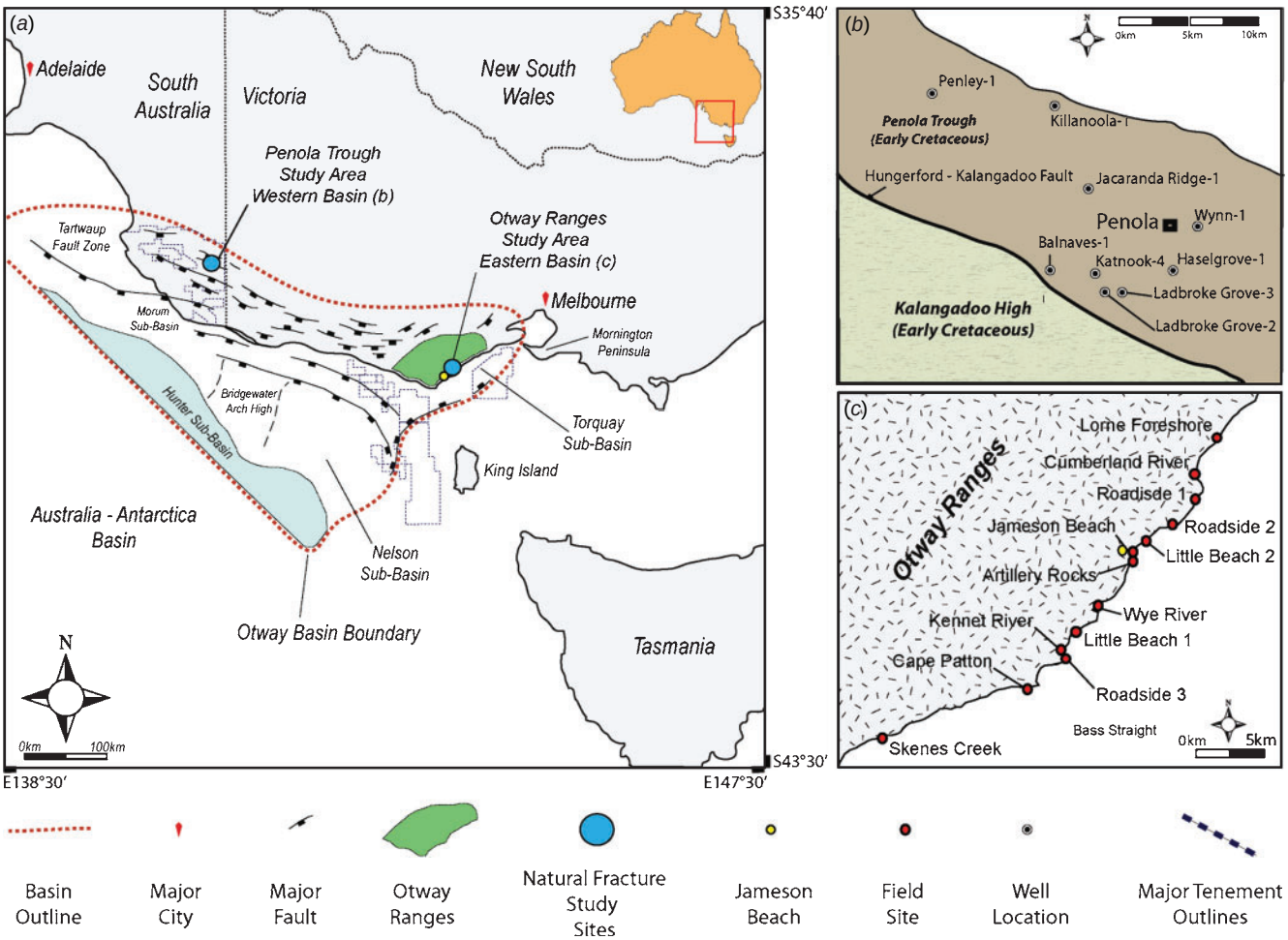

Fig. 1. (*a*) A map of Australia's southern margin showing the location of the Otway Basin, along with some major structural elements, after Alley and Lindsay (1995), Moore *et al.* (2000) and Krassay *et al.* (2004). (*b*) Locations of sub-surface image logs in the Penola Trough. (*c*) Field sites in the Otway Ranges.

of regional natural fracture sets; and (3) constraints on the stress orientation and regime of structural events.

Geological setting

Tectonic history

The structural evolution of the Otway Basin (Fig. 1) has been widely studied (e.g. Boeuf and Doust 1975; Willcox and Stagg 1990; Hill *et al.* 1994; Perincek *et al.* 1994*a*, 1994*b*; Moore *et al.* 2000; Holford *et al*. 2011, 2014; Norvick and Smith 2001; Lyon *et al.* 2007; Gibson *et al.* 2011, 2013; Robson *et al.* 2018) though there continues to be a large degree of uncertainty with respect to the nature of structural episodes that have shaped its development. For example initial rifting within the basin has been proposed as N–S (Lyon *et al*. 2007) N–S to NE–SW (Hill *et al.* 1994), NW–SE (Willcox and Stagg 1990) and NE–SW (Perincek *et al*. 1994*a*). Varying Structural trends from west to east are further highlighted by the presence of multiple directions of fault dip and strike – mainly NW dipping NE–SW trending faults in the east (Perincek and Cockshell 1995) and E–W to NW–SE trending faults in the west (Miller *et al*. 2002; Lyon *et al.* 2007) and a lack of sub-seismic scale structural investigations. More recent studies suggest that for a significant portion of its early history, the Otway Basin experienced local tectonic stress variations occurring simultaneously in different parts of the basin as a result of basement controlled rifting (Gibson *et al.* 2013). Following the major basin forming tectonic activity of the Jurassic and Cretaceous, a regional shift to a NW–SE compressional regime as early as the mid-Eocene was responsible for fault reactivation, right lateral wrenching, folding and uplift (Perincek and Cockshell 1995; Hill *et al.* 1994; Krassay *et al.* 2004; Palmowski *et al*. 2004; Holford *et al.* 2014). At present, the maximum horizontal stress component of this theory is supported by borehole breakout data in the offshore Otway Basin (Hillis and Reynolds 2000; Nelson *et al.* 2006). This significant shift in stress orientation during the Eocene can be attributed to the development of an intraplate stress field in south-eastern Australia, in addition to the ongoing evolution of the tectonic boundaries of the Indo-Australian plate (Sandiford *et al.* 2004; Rajabi *et al.* 2017*a*, 2017*b*). The influence of these boundaries is evident in several compressional structures within the basin, including the Otway Ranges, Barongarook High, Barrabool Hills and the Bellarine High (Krassay *et al.* 2004).

Stratigraphic record

From mid-way through the 20th century, the Otway Basin has been the focus of several stratigraphic studies (e.g. McQueen 1962; White 1968; Moore *et al.* 2000; Duddy 2003; Krassay *et al.* 2004). The most prevalent issue surrounding the stratigraphy of the Otway Basin is the definition of the Otway Group (or Otway Supergroup) and the boundary between the Lower Cretaceous Eumeralla Formation and the Crayfish Group (or Crayfish Subgroup), in addition to the nomenclature of many of the smaller formations. The nomenclature within the basin has been further confused by the conversion of the original nomenclature from litho-stratigraphic to chronostratigraphic based upon palynological divisions (Birch 2003). Substantial structural variations between the western and eastern portions of the basin have also led to studies from South Australia and Victoria placing varying emphasis on different stratigraphic divisions, which has led to further confusion across state lines. Fig. 2 displays the most current stratigraphic chart for the basin, in addition to complimentary tectonic histories from Lyon *et al.* (2007) and Krassay *et al*. (2004).

Hydrocarbon systems, geothermal energy and CO_2 capture and storage

The Otway Basin is of particular interest due to its significance as both a hydrocarbon producing province and a major global CO_2 sequestration project. The hydrocarbon systems of the southern Australian margin consist of a series of subdivisions belonging to the Austral Petroleum Super-system (APS), catalogued by the age of their individual source rocks and similar tectonic history (Bradshaw 1993). In total, two subdivisions of the APS have been recognised for the Otway Basin and can be correlated geochemically to the Austral 1 and Austral 2 oil families (Edwards *et al.* 1999). While commercial oil is yet to be discovered, commercial gas discoveries have been made within the Port Campbell Embayment/Trough in Victoria and the Penola Trough in South Australia (Geoscience Australia 2016). Due to a series of oil shows that demonstrate good, medium-gravity, waxy oil proneness the presence of oil within the region should not be ruled out, although many have been classed as under mature or leaked off (Mehin and Kamel 2002). Several these oil shows have been described to have a strong geochemical association with their respectful natural gases suggesting that the two share a similar source (Boreham *et al.* 2004).

Additionally, strong stratigraphic and geographic relationships between oil and gas shows and their respective source rocks suggest that the hydrocarbons in the Otway Basin are likely to have short to medium range migration pathways from source rock to trap (Morton and Dextral 1995; Boreham *et al.* 2004) This also suggests that within the Otway Basin, reservoir proximity to actively generating source kitchens is the principal control on the distribution of significant accumulations of hydrocarbons. As a consequence, the basin is still considered an active target for hydrocarbon exploration (Geoscience Australia 2016), with Beach Energy poised to drill the Haselgrove-3 well in late 2017. At present, hydrocarbon exploration and production are banned in onshore regional Victoria.

The geothermal potential of the Otway Basin is currently under assessment. The most recent volcanic activity on the Australian continent is thought to have occurred in the Mt Gambier region of south-eastern South Australia, within the confines of the Otway Basin (Geoscience Australia 2016), theoretically making the region an excellent target. Additionally, inland sectors of the basin have been found to contain higher heat flow than surrounding areas making it a potential target for hot dry rock geothermal technology (Geoscience Australia 2016). Several efforts have been made to successfully harness geothermal power from the region, however most have failed due to a lack of economic feasibility and fluid loss.

Lastly, the Otway Basin plays host to Australia's first demonstration of geological carbon storage as part of the 'CO_2 CRC – Otway Project'. The project is of global significance and involves leading Australian and international researchers working

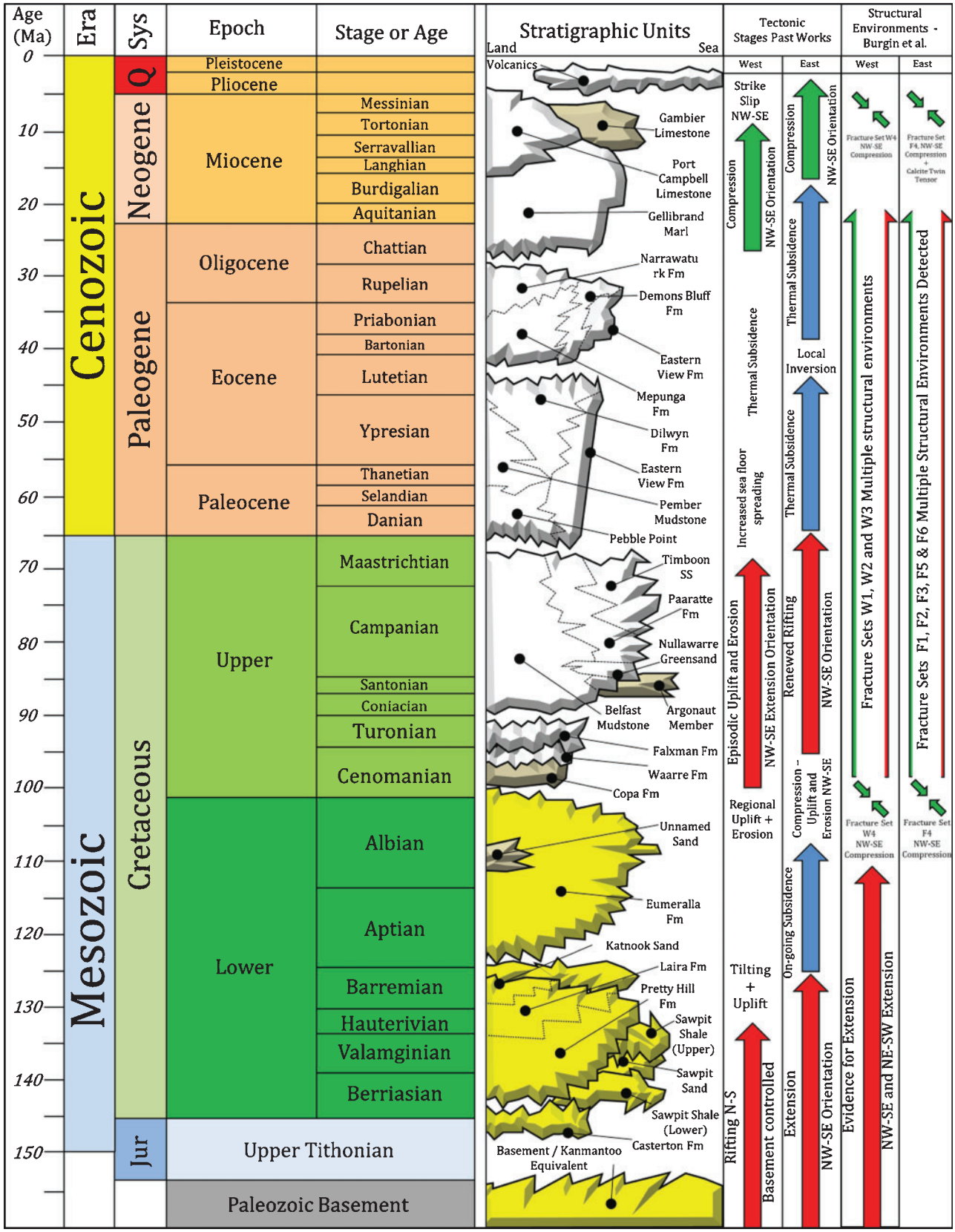

Fig. 2. A stratigraphic chart of the Otway Ranges showing lithostratigraphy taken from Krassay *et al.* (2004) and Lyon *et al.* (2007). Major tectonic events from both studies – in addition to evidence from this study – are also included. Stratigraphic units with natural fracture data in this study are highlighted in yellow.

to develop and implement rigorous monitoring and verification research complimenting the demonstration of subsurface CO_2 storage. Stage one of the project has seen over 65 000 tonnes of CO_2 injected and monitored in a depleted gas reservoir within the Late Cretaceous to Turonian Waarre Formation (CO_2 CRC 2016).

Methodology

To gain an insight into the meso-scale structural deformation of the basin, our approach was divided between the most easily accessible data for subsurface analysis – image log data within the South Australian Penola Trough – and the only sizeable outcropping portion of pre-Miocene sediments in the basin – the Otway Ranges. This approach allowed the structural environments of the western and eastern parts of the region to be analysed at the meso-scale. While drawing broad conclusions on the overall evolution of the basin from sparse (thousands of kilometres) structural data can overlook local variations, such an approach has provided a platform for the identification of regionally pervasive natural fracture sets. The study has also reiterated the importance of sub-seismic scale data analysis, particularly within complex basin settings that can have economic significance on valuable industries (e.g. petroleum, geothermal, and CO_2).

Natural fracture interpretation in the subsurface

The introduction of modern imaging tools has presented fundamentally new methods for subsurface analysis and data collection (Prensky 1999). Wellbore imaging tools are one of the fastest and most precise methods for gathering interval specific subsurface data. Natural fractures can be easily identified in wellbore electrical resistivity image logs as sinusoids, appearing either resistive (closed) or conductive (open) (Fig. 3). Distinguishing natural fractures from induced fractures and

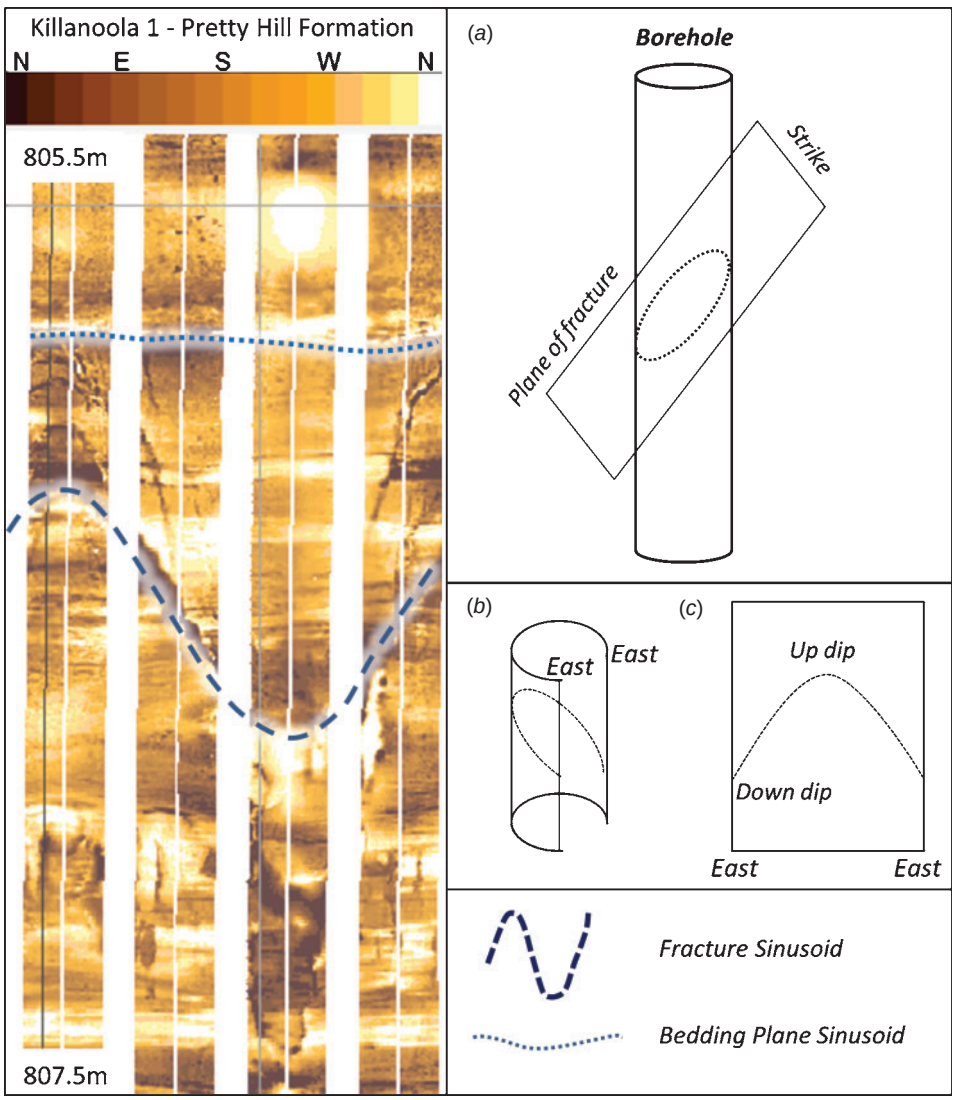

Fig. 3. A schematic showing how wellbore image logs, in this case a Formation Micro Imager (FMI) (*a*) can be 'unfolded,' and interpreted in 2D (*b*, *c*). Modified from Brown *et al*. (2015).

other rock features, such as faults, bedding, cross-bedding and other sedimentary structures, can be a challenge, especially as well inclination increases. As mode 2 (shear) natural fractures in subsurface logs are the most commonly encountered (Fig. 4), we use the term fractures in a general sense to describe slide-mode discontinuous measures on the borehole scale. With respect to the subsurface component of this study, a total of nine down-hole image logs were analysed from the South Australian portion of the Otway Basin in the Penola Trough. The total image log length amounted to 11.94 km and covered formations ranging in age from the Upper Jurassic to the Upper Cretaceous. Well information is displayed in Table 1.

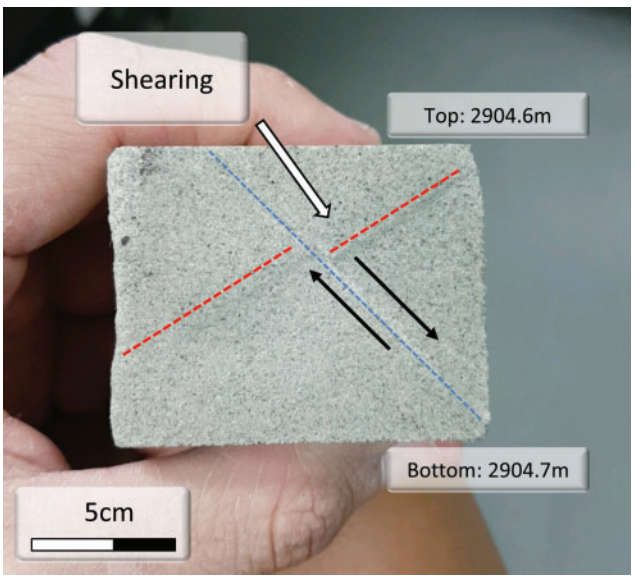

Fig. 4. A photograph taken from a subsurface core sample from Haselgrove-2 within sandstone of the Pretty Hill Formation. Red dashed line indicates a primary calcite vein; blue dashed line indicates secondary calcite vein formed through shearing or mode 2, determined through the apparent displacement of vein 1. Bedding within the formation is massive and not visible at this scale but is oriented at 10°/345°.

Natural fracture interpretation from rock outcrops

Fracture data was also collected at 14 sites within outcrops of the Lower Cretaceous syn-rift Eumeralla Formation, along the coast of the Otway Ranges in western Victoria. This formation crops out mainly as shore platforms, that are easily accessible by beaches, and as cliff faces along the road side. Structural data was collected via traditional methods, involving the use of a compass clinometer aided by Digital Field Mapping Software.

Natural fracture processing and analysis

Within this study, our interpretation of natural fracture data is based upon the statistical analyses of fracture strike and dip angles, in combination with fracture-bedding relationships. Once obtained, fracture data were divided initially by their stratigraphic unit of occurrence, in an attempt to chronologically constrain their incidence. Within these groups, major fracture sets were identified based upon the statistical analyses of common strike and dip angles. Pre-tilting and post-tilting of the bedding and its effect on fracture orientation and dip was also considered, however in most subsurface cases, bedding dip was on average less than 11°. Additionally, the principal stress orientation tool, Win-Tensor (Delvaux and Sperner 2003), was used to constrain the specific sets and assign regional directions of the three principal stresses. Outlying fractures that did not fall within one of our sets (less than 20% of total fracture data) were excluded from our final interpretations. The excluded fracture data likely represents local stress perturbations, rock heterogeneities, or measurement error and do not align with the regional paleo-principal stresses (Faulkner *et al.* 2010; Kulikowski and Amrouch 2017).

Our approach was based upon the fundamental principles of rock failure, with a heavy emphasis on the three Andersonian environments of stress (Anderson 1905) (Fig. 5). The occurrence of natural fractures is dependent on the critical failure strength of the given rock unit. This strength, and the corresponding conditions of stress responsible for inducing failure, are normally associated with structural events (Zoback *et al.* 1989; Dresen 1991; Sibson 2003; Zoback *et al.* 2003) and often lead

Table 1. A table displaying well information for the nine image Formation Micro Imager (FMI) and Formation Micro Scanner (FMS) log intervals used as part of this study. Maximum borehole deviations do not necessarily align with image log intervals, virtually all natural fracture data was gathered from near-vertical well sections

Well name	Latitude	Longitude	Type of image log	Image log depth (MD)	Fracture count	Maximum borehole deviation
Killanoola 1	37°12′ 42.20″	140°40′03.02″	FMI	788 m	163	4.40°
Balnaves 1	37°26′ 50.50″	140°42′16.10″	FMI	1894 m	177	56.07°
Jacaranda Ridge 1	37°20′ 57.19″	140°45′10.72″	FMS	2207 m	17	8.50°
Wynn 1	37°24′ 32.99″	140°52′19.84″	FMS	1621 m	23	5.97°
Ladbroke Grove 2	37°27′ 54.75″	140°47′24.49″	FMS	997 m	13	31.00°
Ladbroke Grove 3	37°24′ 56.32″	140°46′49.42″	FMI	874 m	124	11.54°
Katnook 4	37°27′ 18.92″	140°46′32.22″	FMS	1248 m	11	6.99°
Penley 1	37°12′ 07.63″	140°26′49.53″	FMS	1437 m	109	5.50°
Haselgrove 1	37°26′ 30.94″	140°49′49.78″	FMS	393 m	40	4.69°

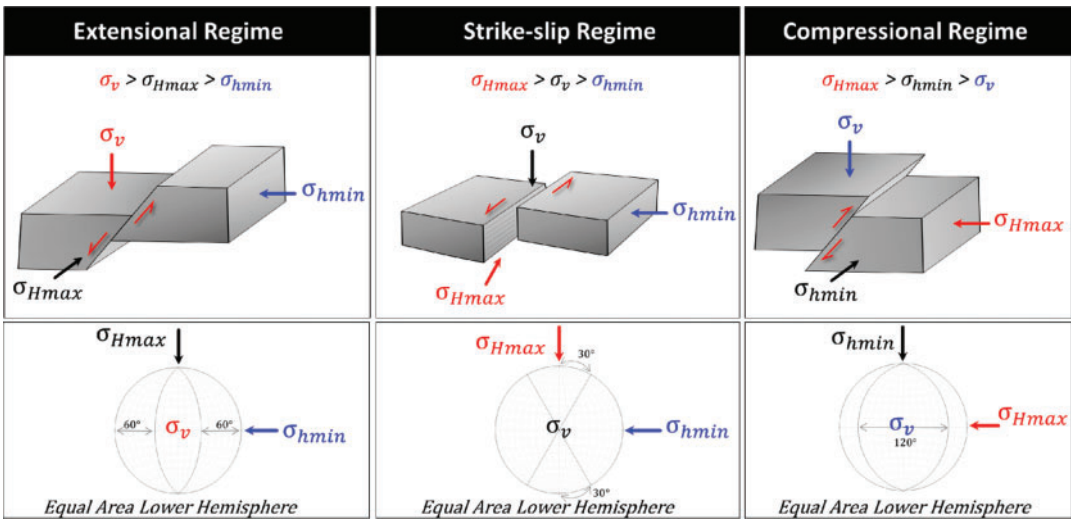

Fig. 5. A schematic diagram showing the three Andersonian stress environments (Anderson 1905) in addition to text book fracture sets formed under their conditions. Row 1 represents orientations of fault displacement, while row 2 displays approximate angles of conjugate fracture formation for each regime.

to the formation of highly distinguishable fracture set geometries and characteristics. The geometry of these regional natural fracture sets are dependent on the relationship between the three principal stresses (σ_1, σ_2 and σ_3) and the precise mode of fracturing (I, II or III). Under an ideal and 'text book' environment of stress, conjugate natural fracture sets will develop with ~60° of separation and bisected by the maximum principal stress (σ_1). In this case the minimum principal stress (σ_3) will bisect the corresponding angle of 120° formed by the conjugate pair, and be orthogonal to the orientation of the intermediate principal stress (σ_2) (Anderson 1905) (Fig. 5). An understanding of these fracture geometries, in addition to their relationship with the bedding, allows us to gain insights into the likely stress environment responsible for their development and relative chronology. That being said, when making such structural inferences, it is important to keep in mind that that perturbations to 'text book' stress environments and pre-existing deformation such as folds, faults or fractures can have a significant influence on fracture geometries, especially in environments of non-coaxial deformation (Healy *et al.* 2006; Tavani *et al.* 2015).

Calcite twin analysis

Mechanical twinning within calcite is a plastic deformation that occurs at low temperatures (25−400°C) and low confining pressures. The process of e-twinning – twinning along the 'e' plane of the crystal lattice – is easily compared with a zone of simple shear. Three 'e-planes' exist for calcite and are geometrically centred on the optical axis of the crystal. The analyses of these twins through calcite twin inversion, has been proven to accurately measure five of the six parameters needed to define a complete paleo-stress tensor, and is capable of providing evidence for poly-phase tectonic events (Rocher *et al.* 2004; Lacombe *et al.* 2007; Amrouch *et al.* 2010*a*; Amrouch 2010). The calcite twin stress inversion technique is similar to the technique used to analyse slickensides on a fault plane (Etchecopar 1984). The technique consists of developing the best fit tensor for the distribution of twinned and untwinned *e*-planes within the sample. Within this study, the use of calcite twin analysis is to: (1) compare the quantitative results with those from natural fracture analysis; and (2) test the regions suitability for more extensive calcite twin analysis. This study uses Etchecopar's calcite stress inversion technique (CSIT) (Etchecopar 1984) on a sample taken from a shore platform of outcropping Eumeralla Formation at Jameson Beach (Fig. 6).

Results and interpretation

Subsurface natural fracture analysis and categorisation

When dealing with large amounts of structural data, it is inherently difficult to divide results and interpretation, as the categorisation of fracture sets is in itself an interpretation. Over 600 natural fractures were interpreted within the subsurface of the Penola Trough, in the South Australian portion of the Otway Basin (Fig. 7). Across the nine wells, fracture data was collected within all the penetrated formations, although the fracture density (fractures/metre) was variable between formations. Our initial treatment of data divided these fractures into eight major sets with evidence for a total of four structural environments. Natural fracture count per well can be seen in Table 1, while Table 2 displays fracture density by well and formation. All the fractures interpreted within the subsurface have dip angles less than 85°. This may be due to the fact that in a generally vertical well, naturally formed vertical fractures are difficult to intersect and distinguish due to their common orientation with the well bore and the fact that their presence is easily concealed by the occurrence of borehole break outs and/or drilling induced tensile fractures.

The first major fracture group (W1) contains two conjugate sets of NW–SE striking fractures with dip angles greater than 45° (Fig. 8). Consequently, fractures were categorised to have nucleated under an extensional regime ($\sigma_1 = \sigma_V$), with the direction of extension (σ_3) oriented NE–SW. Evidence for this set was detected within all penetrated formations that contained image logs, including the Palaeozoic basement. The second major

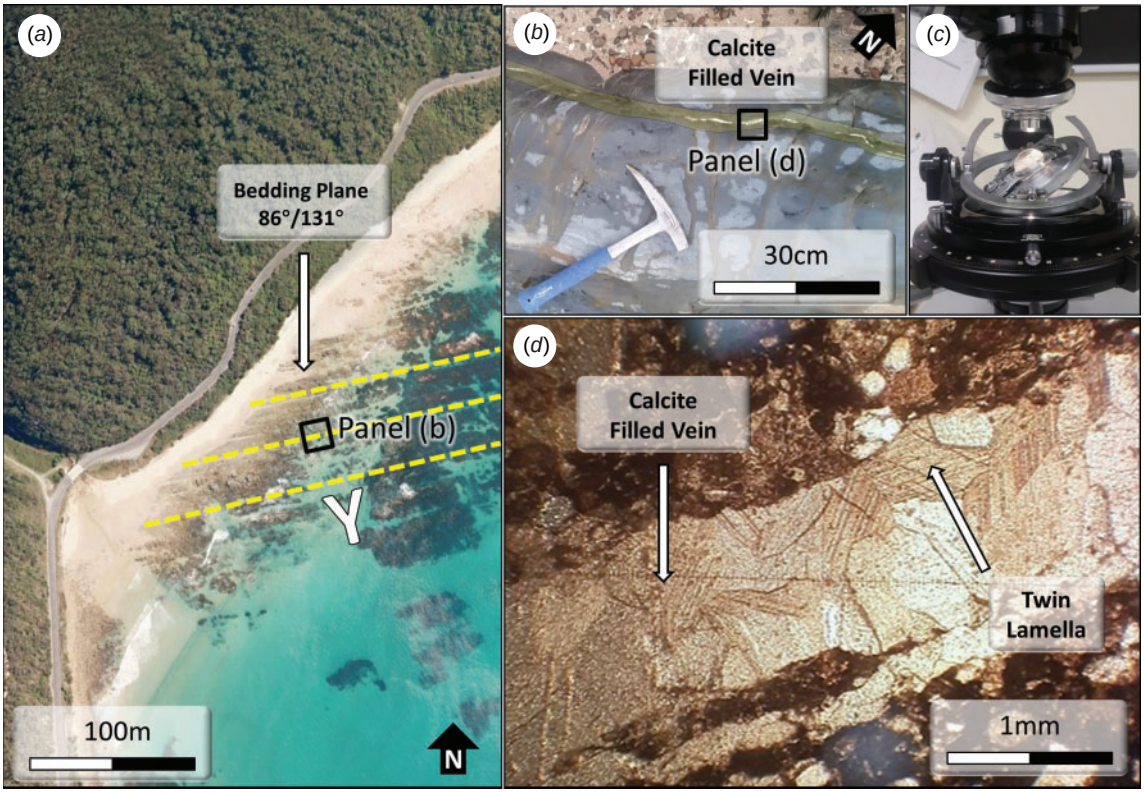

Fig. 6. (*a*) A satellite image (Google Earth 2018) showing the orientation of the vertical bedding within a wave platform at Jameson Beach. The Great Ocean Road can be seen running past on the left (*b*) A photograph taken in the field showing the sampled vein at Jameson Beach in the Otway Ranges. (*c*) A universal stage microscope used to measure the spatial orientation of the twinned and untwinned planes within the crystal and angles of extinction of the calcite crystals. (*d*) The calcite filled vein – in the Z orientation – from Jameson Beach. The sample is within the Eumeralla Formation.

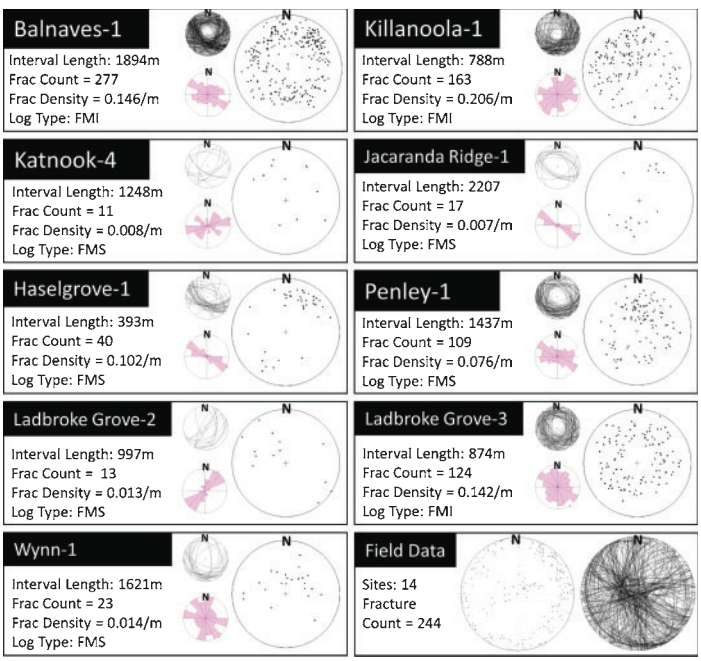

Fig. 7. Equal area lower hemisphere stereonet plots displaying natural fracture data collected from the nine wells within multiple formations in the western Otway Basin and fracture data gathered in the field. For wells, large steronets represent poles to fracture planes, with small steronets displaying fracture planes and fracture strike as rose diagrams. For field data, at the bottom right, all poles to planes and fracture planes are displayed for the 13 field sites.

Table 2. This table displays fracture densities from each well by their formation. Average fracture density (frac/m) within each formation is also displayed. Values were calculated by dividing fracture count per interval by interval length in metres

NP, not penetrated; *PNL*, penetrated no log

Well / Formation	Sawpit Formation	Pretty Hill Formation	Laira Formation	Katnook Sandstone	Windermere Sandstone	Eumeralla Formation
Killanoola 1	0.1	0.07	*NP*	*PNL*	*NP*	*PNL*
Balnaves 1	NP	0.28	0.18	NP	0.09	0.09
Jacaranda Ridge 1	0.05	*PNL*	*PNL*	*PNL*	*PNL*	*PNL*
Wynn 1	0.09	*NP*	*PNL*	*PNL*	*NP*	*PNL*
Ladbroke Grove 2	*NP*	0.03	0.01	*PNL*	*PNL*	*PNL*
Ladbroke Grove 3	*NP*	0.05	0.04	0.05	0.22	0.03
Katnook 4	*NP*	0.02	*PNL*	*PNL*	*PNL*	*PNL*
Penley 1	0.04	*NP*	0.006	*NP*	*NP*	0.12
Haselgrove 1	*NP*	0.22	*PNL*	*PNL*	*PNL*	*PNL*
Formation Average	**0.07**	**0.11**	**0.059**	**0.05**	**0.15**	**0.08**

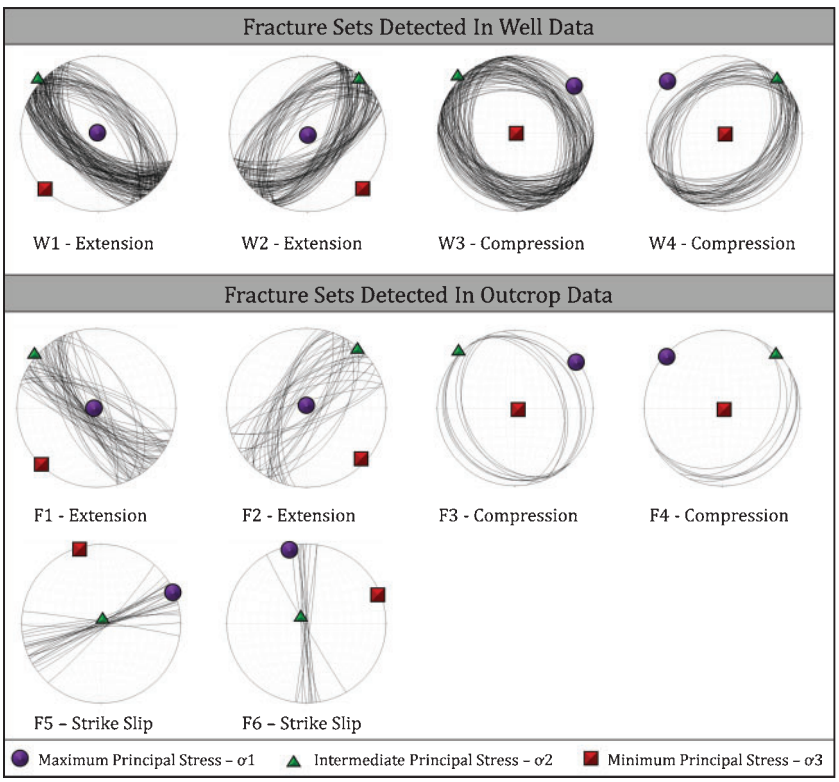

Fig. 8. Orientation of the major fracture sets categorised by dip degree and dip direction as part of this study. For well data, these sets include all detected fractures across all penetrated formations with image logs. Field data includes fractures from all 13 localities studied within the Eumeralla Formation. See Fig. 1 for location of wells and field sites.

group (W2) included those striking almost orthogonal to set one, with similar angles of dip above 45° and striking towards the NW and the SE (Fig. 8). As such, these fractures were categorised under a NW–SE extensional regime. Once again, this major set was detected within all penetrated formations that contained borehole image log data, including the basement. The third (W3) and fourth (W4) major fracture groups detected within the well data are fractures with dip angles less than 45°. As such these fractures were categorised to have nucleated under compressive regimes of paleo-stress ($\sigma_3 = \sigma_V$). Group W3 is composed of NW–SE striking fractures dipping towards the NE or the SW with $\sigma_1 = \sigma_H$ and oriented towards the NE or SW. Fractures within this group were found in four of the six formations penetrated with image logs. Evidence for their

occurrence did not occur within either the Windermere or Katnook sandstones, as they were detected in formations both above and below these two units. The final set (W4) is composed of fractures striking orthogonal to group 3, and once again categorised to have formed under a compressive regime with $\sigma_1 = \sigma_H$, and oriented NW–SE.

Outcrop fracture analysis and categorisation

Field data were collected from a total of 14 localities within the Otway Ranges. All data were collected from portions of the Lower Cretaceous Eumeralla Formation outcrops, which appears as grey coloured sandstone exposed on elongated platforms parallel to the coast line. Honeycomb style weathering within the unit is abundant and at times made the collection of accurate fracture data difficult. In total, fracture data for seven major fracture sets were gathered during the field work, with evidence for a total of five paleo-tectonic structural environments. Similar to the well data, major fracture sets F1 and F2 were comprised of conjugate fracture sets striking NW–SE (F1) and NE–SW (F2) with dips greater than 45°. As such, these were classified to have nucleated under extensive conditions and categorised as evidence for NW–SE and NE–SW extensional events. Fracture sets F3 and F4 each contained only one minor fracture set each, meaning that no conjugate fractures were detected. That being the case fracture set F3 contains NW–SE striking fractures with dip angles lower than 45°, while fracture set F4 contains those striking NE–SW with a similar angle of dip. These were categorised to have formed under compressive conditions. Additionally, fracture evidence for two strike-slip environments was detected; fracture set F5, contains near-vertical fractures (>85°) striking approximately NNW–SSE while set F6 contains a set striking NE–SW.

In addition to fracture geometry, regular cross cutting relationships were observed. Fractures categorised as part of set F2 were regularly observed to terminate upon those categorised as part of set F1 (Fig. 9). All major fracture sets and their paleo-stress regimes are outlined in Fig. 8.

Jameson Beach – paleo-stress tensor from calcite twin data

With a bedding dip angle of almost 90° providing a good potential control on pre-tilting and post-tilting structural events, Jameson Beach on the eastern edge of the Otway Ranges provided an interesting environment within which to complete calcite twin analyses (Fig. 6). A total of 95 calcite crystals of similar sizes (400–500 μm) were measured within the X, Y and Z planes, with moderately thin, type 1 twins being the most prevalent implying a low temperature (<200°C) and low deformation environment (Burkhard 1993). Table 3 presents the determined calcite paleo-stress tensor in detail.

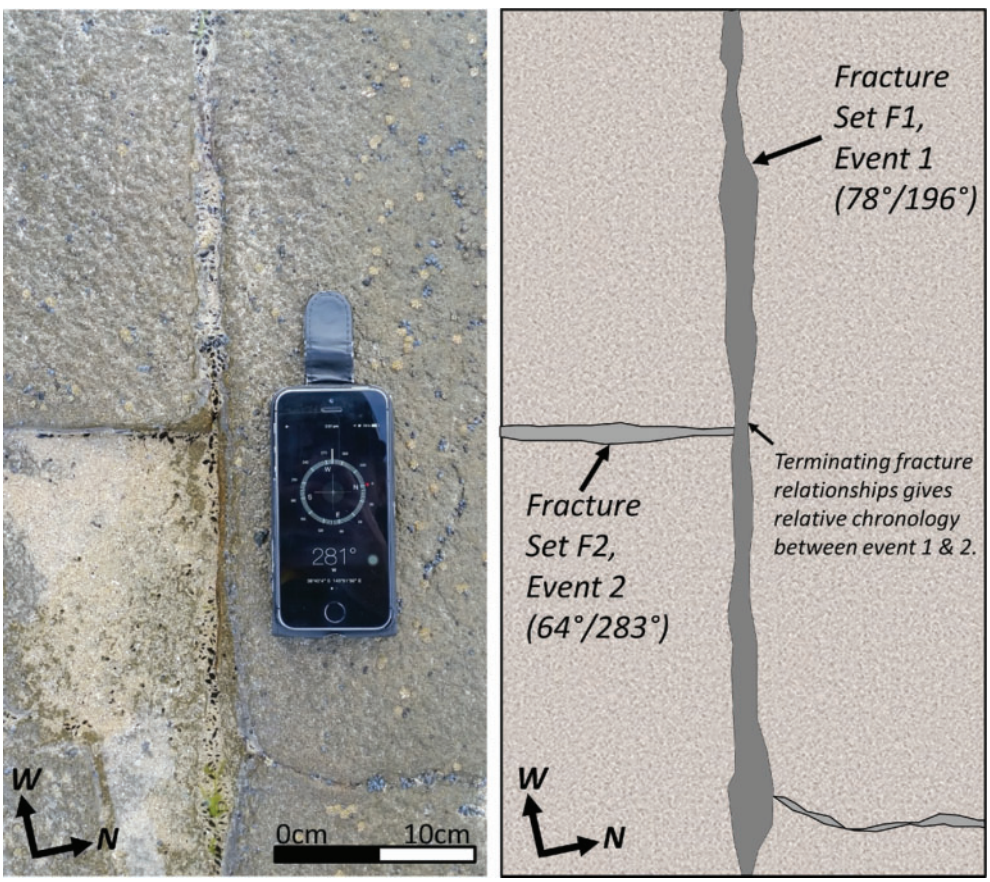

Fig. 9. Natural fracture cross cutting relationships observed on a bedding plane upon a wave cut platform within the Eumeralla Formation. Fractures appear unfilled and suggest a distinct chronology between structural environments. Fracture set F2 is regularly observed to terminate on Fracture Set F1.

Table 3. A table displaying the calcite twin data from the sample at Jameson Beach displayed in the bedding 'raw' format. Under this scenario $\sigma 1$ represents maximum horizontal stress, $\sigma 2$ minimum horizontal stress and $\sigma 3$ vertical stress. *R* value represents the shape ratio of the derived stress tensor. Total data **represents the total number of twinned and untwinned planes measured for the sample.** Penalisation Function **represents a numerical consideration of untwinned planes that lie within the derived stress tensor for the twinned planes (see Etchecopar 1984 and Amrouch 2010; for greater detail), reducing this value as close to zero as possible is ideal**

Sample name	Latitude	Longitude	Formation	Age period	Sample vein	Mean bedding	Calcite crystal size	σ1 (plunge/ plunge direction)	σ2 (plunge/ plunge direction)	σ3 (plunge/ plunge direction)	R	Total data (twinned/ untwinned)	Penalisation function
Jameson Beach S-01	38°35′44.50″	143°55′19.06″	Eumeralla Formation	Early Cretaceous	36/243	86/131	460 µm	06/337	03/68	83/181	0.7	216/68	0.92

The determined tensor, in combination with the extremely high angle of dip, allows for two possible paleo-stress scenarios (Fig. 10). First, interpreted using the present-day sub-vertical bedding, we see evidence for a compressional regime ($\sigma_3 = \sigma_v$) with an almost horizontal σ_1, plunging towards to NNW. Second, if we analyse the tensor using a pre-tilted bedding plane (rotation of stereonet to horizontal bedding), we observe a rotation between σ_1 and σ_3 with evidence for an extensional stress regime with $\sigma_1 = \sigma_v$ and σ_3 horizontal and plunging towards the NNW.

Discussion

Although the structural evolution of the Otway Basin has been studied in several works (e.g. McQueen 1962; White 1968; Hill *et al.* 1994; Moore *et al.* 2000; Krassay *et al.* 2004; Palmowski *et al*. 2004; Lyon *et al.* 2007; Holford *et al.* 2014), complex structural geometries and conflicting studies (e.g. Lyon *et al*. 2007; Willcox and Stagg 1990; Hill *et al.* 1994; Perincek *et al.* 1994*a*) mean that to date basin evolution remains controversial. Krassay *et al*. (2004) provide a comprehensive regional tectonostratigraphic framework for the Otway Basin, dividing basin evolution into seven basin phases which compliment varying structural styles throughout the region. This includes two early stages of rifting from the Tithonian–Barremian and Aptian–Albian, subsequent uplift in the Cenomanian and renewed rifting from the Turonian–Middle Eocene driven by varying rates of sea floor spreading, followed by the onset of compression. However, even with such a comprehensive stratigraphic framework a detailed structural analysis, supported by quantitative data below the seismic resolution, remains unavailable.

Additionally, the variation in structural style from west to east within the basin has been identified by several authors (Hill *et al.* 1994; Palmowski *et al*. 2004; Gibson *et al.* 2013). Rates of extension are known to have been significantly higher in the eastern portions of the basin along with a greater influence of compression and inversion during the later stages of the Cretaceous (Palmowski *et al*. 2004). The combination of well and outcrop data from different localities within the basin, gathered as part of this study, give us further insight into these longitudinal structural variations. While this study is not the first to analyse natural fractures within the Otway Basin (Bailey *et al.* 2014) it is the first to account for their spatial distribution and 3D geometry that attempts to link their development to structural events.

Extensional structural environments

From the natural fracture results presented as part of this study, three inferences can be drawn regarding the structural evolution of the Otway Basin. First, in the eastern portion of the basin, following the deposition of the Lower Cretaceous Eumeralla Formation (~95 Ma), the basin may have experienced multiple extensional events, as shown by fracture sets F1 and F2 (Fig. 8). This hypothesis, for multiple periods and orientations of extension, is supported by Perincek and Cockshell (1995) and Teasdale *et al*. (2003) who proposed oblique NE–SW extension within the early periods of basin development. Perincek and Cockshell (1995) measured the strike and dip angle of regional

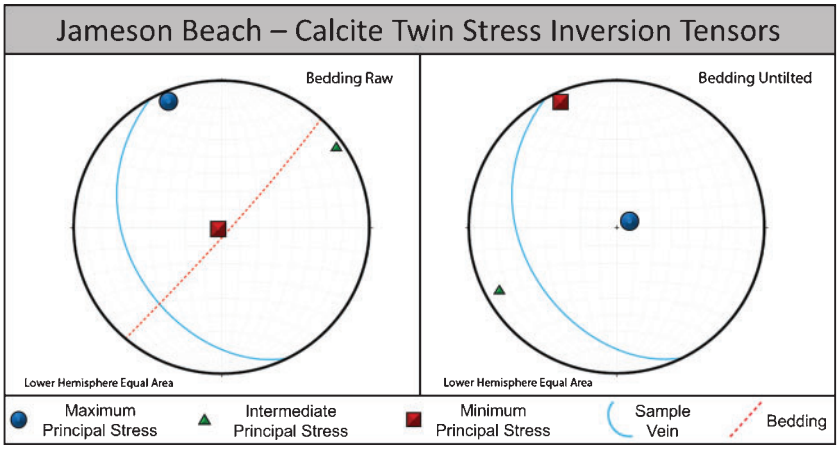

Fig. 10. Lower hemisphere equal area stereonet plots displaying the paleo-stress tensors derived from Etchecopar's (Etchecopar 1984) calcite twin stress inversion technique (CSIT) measurements at Jameson Beach. See Fig. 1 for location.

basement faults throughout the region using seismic data, which support a NE–SW extensional event during the Early Cretaceous, as does a series of NW–SE elongate troughs within the Otway Basin that are believed to have developed during this period. Teasdale *et al*. (2003) also employed basement seismic interpretation to determine that Early Cretaceous extension within the Otway Basin was focussed along a large NW trending fault zone within the region, complementing the theory of basin forming NE–SW extension. As the basin-wide deposition of the Eumeralla Formation postdates initial extension within the Otway, insights into the embryonic period of basin evolution are not possible from this dataset. However, fracture sets F1 and F2 suggest that the structural environments of extension within the eastern sector of the basin may have undergone greater variations of tectonic stress orientation, particularly following the deposition of the Eumeralla, than previously thought. This is further supported with the consistent cross cutting relationship evident between the two fracture sets (Fig. 9).

A large amount of extensional fractures were categorised into the conjugates fracture groups W1 and W2 in subsurface formations as young as 95 Ma, which infers that the western Otway Basin has experienced significant extensional structural environments oriented NE–SW and NW–SE (Fig. 8). This hypothesis is once again supported by Perincek and Cockshell (1995) and Teasdale *et al*. (2003). Fracture evidence for N–S extension as proposed by Lyon *et al*. from the analysis of basement fault geometry (2007) was not found. Due to the lack of chronological evidence from the well analysis, we are unable to determine the chronology of events between fracture set W1 and W2.

What is clear with respect to the extensional origins of the Otway Basin, is that the basin experienced significant longitudinal variations in structural environment from west to east. As suggested by the macro-scale studies of Hill *et al*. (1994), Palmowski *et al*. (2004) and Gibson *et al*. (2011). A variation was likely due to disparities in basin terrane fabric across the region. In the case of the West African and Brazilian break-up (a similar scenario to the break-up of Australia and Antarctica), basement control has been proven to exert a strong influence on the development and evolution of the margin during later active extension (de Castro *et al.* 2012). From simple fault trend analyses, it is clear that evidence for extension in all proposed directions is visible. Hill *et al*. (1994) was the first to recognise this and proposed that this scattering of fault trends may be due to the orientation of pre-existing basement faults and fabric. Miller *et al*. (2002) advocated for strong basement control on extensional orientations within the Otway Region, attributing them to 'substantial rheological differences in the lithosphere' across the boundary between the Lachlan and Delamerian Fold Belts, which lies within the central basin region. Additionally, the authors also suggested that extension within the eastern most portion of the basin was stalled in the Mid-Cretaceous by the presence of underlying Proterozoic and Paleozoic basement structures, which may explain the lower occurrence of extensional fractures found within the field data in this study. Additionally, in the western portion of the basin (Penola Trough), Lyon *et al*. (2007) expanded on how basement faults may control syn- and post-rift sedimentation and faulting.

We stress that the most important element of our evidence presented here is not that various extensional structural environments have shaped the basin – as this has already been shown on numerous occasions by multiple authors – but that from our meso-scale investigations, these variations and overall rifting may have continued to occur following the deposition of the Lower Cretaceous Eumeralla Formation, as the formation contains structural evidence for their occurrence. This poses new questions for basin development from the Late Cretaceous onwards and in particular the cessation of rifting at the end of the Albian. A higher level of extensional tectonic development, forward from this point in time, would have considerable implications on fault sealing and additional petroleum system elements, especially as the source rocks are believed to have been mature and over mature during the Middle to Late Cretaceous (Hill 2002).

Compressional structural environments

Through the categorisations of natural fractures in this study we were able to detect structural indications for two compressional

events within the basin, in both the western and eastern regions. While evidence for the NW–SE inversion event in fracture sets W4 and F4 is unsurprising, especially given the nature of the field study area within the uplifted Otway Ranges, of particular note is that both the well data and field data suggest that at some point in time both sectors of the Otway Basin experienced compression in a NE–SW orientation. Given that many previous studies within the basin have primarily focussed on large, basin and seismic scale structures, or have simply grouped fractures based upon their direction of strike, ignoring 3D geometry, it is not surprising that these signs have been overlooked until now, especially as large scale movement within this structural regime may have been overprinted by the significant amount of extensional features within the basin and the dominating presence of the NW–SE inversion event. What is questionable is when this event occurred relative to the other events within the history of the Otway Basin.

Strike-slip structural environments

Considering that under a typical strike-slip stress regime, natural fractures often developed near vertical, the fact that they were not detected within the multiple image logs in the western portion of the basin is not surprising as these near-vertical fracture sets are notoriously difficult to detect in a near-vertical well. However, as not a single high angle fracture was detected in the subsurface, our data suggest this region has been minimally affected by strike-slip stress conditions. We cannot rule out that some less steeply-dipping fractures we observe may be Riedel shears that are rooted in deeper, more-steeply-dipping strike-slip faults, but consider this unlikely.

Fracture data gathered from the Otway Ranges show signs for two strike-slip stress environments, in fracture sets F5 and F6 (Fig. 8). Determining the specific chronology of these sets from within one formation is difficult and evidence was not possible in outcrop. That being said, given the current maximal horizontal stress orientation within the region (Rajabi *et al.* 2017*a*) it is possible that fractures in set F6 have been formed under conditions similar to the present-day environment. This is entirely dependent on the rock mechanical properties, and the current stress magnitudes affecting the region which are presently un-constrained (Rajabi *et al*. 2017*a*).

Jameson Beach – interpretation of calcite twin and natural fracture data

The results from the calcite twin inversion are promising, especially in regard to planning additional studies of this nature within the Eumeralla Formation. The initial calcite twin analysis found a good number of quality calcite crystals, which is important to maintain statistical confidence in the derived tensor. That being said, the interpretation of the derived tensor is not so straight forward. Analysing the tensor data using a pre- and post-tilted bedding plane gives us two possible structural conditions. The post-tilting compressional tensor, with σ_1 plunging towards the NW and parallel to the present-day stress, coincides well with low angle fracture set F4, which is present on a regional scale, but was not detected at Jameson Beach. Additionally, the orientation of σ_1 in this case aligns very well with *in situ* stress orientations from recent studies conducted by Rajabi *et al*. (2017*a*) who showed that the maximum horizontal stress orientation within the Victorian Otway Basin trends NW–SE at 137°N. Lastly, the near-vertical orientation of the bedding striking NE–SW is almost certainly evidence for large scale NW–SE compression. Using the un-tilted bedding plane, the σ_1 becomes sub-vertical and presents an extensional tensor oriented NNW–SSE. This environment coincides with regional fracture set F2, which is present at most field sites and within the un-tilted fracture data detected at Jameson Beach. While direct fracture evidence at Jameson Beach is lacking for a NW–SE compressional environment, meso-scale evidence is present on a regional scale in the form of fracture set F4. While on the macro-scale, the mere presence of the uplifted Otway Ranges conclusively shows the region has been subjected to a NW–SE compressional environment. Additionally, given the low angle of compressional fractures and the limited vertical exposure at the site, it is very possible they may not have been detected by our field sampling. These things considered, we believe the correct interpretation of this data is in its present-day form as evidence for a NW–SE compression event occurring post-tilting of the bedding.

Bedding analysis from image log data

Throughout the course of assigning paleo-stress regimes, all conjugate fracture sets were analysed with the bedding plane in the present-day geometry and in the un-tilted form. This additional analysis is key to determining whether fractures developed before, during, or post-tilting of the bedding plane, and in constraining relative timing of fracture development. During this process fracture pairs within W1, classified under a NE–SW extensional regime, were found to contain a series of data that appeared more Andersonian in nature with the bedding un-tilted. Average bedding dip direction within the well data were found to be SSW (195°). This dip direction, parallel to the implied direction of extension as suggested by fracture group W1, suggests the western portion of the basin may have undergone substantial and multiple periods of NE–SW extension during the early basin history.

Implications for hydrocarbon exploration

A complete understanding of natural fracture networks within hydrocarbon reservoirs is fundamental to elements of both hydrocarbon exploration and production. Work in the Big Horn Basin in the United States (Amrouch 2010) and the Cooper Basin in Australia (Kulikowski and Amrouch 2017, 2018) has shown that a complete 4D understanding of natural fracture networks, and the stress regimes responsible for their inception, together with a regional tectonostratigraphic model have the potential to greatly enhance hydrocarbon exploration and production. In the case of the Otway Basin, this complete 4D picture is yet to be pieced together. Reservoir and source rocks of the relevant petroleum systems display strong stratigraphic and geographic relationships suggesting that migration from source to trap occurs over a short to medium distance in a vertical orientation and although migration pathways are thought to be simple, major economic discoveries are yet to be made. A possible explanation lies in the lack of a complete and comprehensive 4D model for the basin, especially throughout

the Late Cretaceous period during which the majority of the basins' source rocks (exact timing is dependent on the sub-system) are believed to have entered into the oil window (Hill 2002). Therefore, the nature of the structural events controlling basin evolution during this time period is of particular importance for hydrocarbon exploration and why the possible unknowns suggested herein should be taken into account. What is certain is that, the Otway Basin clearly underwent significant tectonic activity during the time the source rocks of its major petroleum systems were entering, and well within the oil window. Therefore, grounding any exploration efforts around incomplete or over-simplified knowledge of these events in particular should be done with great caution, as we have shown here, they are not fully constrained.

The possible presence of previously undetected compressional events within the basin, responsible for the formation of low angle and closed fracture networks, should also be cause for concern during the exploration and production process. As part of a wider fracture network these low-angled fractures may appear conductive under present-day stress conditions, but may remain closed simply due to their low dip angle geometry that is not critically oriented relative to the *in situ* stress to undergo reactivation (Kulikowski *et al.* 2016*c*). These geological factors have significance outside of the petroleum industry and in particularly can impact the effectiveness of current CO_2 storage and geothermal energy programs.

Conclusions and future work

Following the analysis of subsurface and outcrop natural fracture data, the structural evolution of both the western and eastern Otway Basin may be considerably more variable and complex than previously thought, especially from the Late Cretaceous until present, which is the most important window for hydrocarbon exploration and production. In this paper we have presented some of the first meso-scale structural evidence for different structural environments of paleo-stress in regions of the basin that are far removed from one another. Within both regions, we have presented natural fracture evidence for multiple paleo-stress regimes including several episodes of extension, strike-slip and compression. With four structural environments present within both the western and eastern portions of the basin and strike-slip environments unique to the eastern sector. Additionally, we have shown the first evidence for the presence of a possible compressional event oriented NE–SW within the study area. Lastly by completing the first calcite twin analysis on a sample collected from outcrop in the Australian continent, we have shown that the region is suitable for an expanded study of this nature, as calcite filled fractures are not only commonly found throughout multiple formations, but they are appropriately deformed to obtain sufficient data to quantitatively define the paleo-stress conditions throughout basin development.

Conflicts of interest

The authors declare no conflicts of interest.

Acknowledgements

The authors would like to thank Paradigm for their generous contribution of an academic licence for Geolog software, the Australian Renewable Energy Agency (ARENA) for their financial support and Natalie Debenham for her assistance in the field.

References

Alley, N. F., and Lindsay, J. M. (1995). Tertiary. In '*The geology of South Australa*'. Vol. 2, Geological Survey of South Australia. Geological Survey Bulliten **54**, 150–217.

Amrouch, K. (2010). Apport de l'analyse microstructurale à la compréhension des mécanismes de plissement. Exemples de structures plissées aux USA (Wyoming) et en Iran (Zagros), *Th*ése, Université Pierre et Marie Curie – Paris 6, 2010–03, 477p.

Amrouch, K., Lacombe, O., Bellahsen, N., Daniel, J., and Callot, J. P. (2010*a*). Stress/strain patterns, kinematics and deformation mechanisms in a basement-cored anticline: Sheep Mountain anticline (Wyoming, USA). *Tectonics* **29**, TC1005. doi:10.1029/2009TC002525

Amrouch, K., Robion, P., Callot, J. P., Lacombe, O., Daniel, J. M., Bellahsen, N., and Faure, J. L. (2010*b*). Constraints on deformation mechanisms during folding provided by rock physical properties: A case study at Sheep Mountain Anticline (Wyoming, USA). *Geophysical Journal International* **182**, 1105–1123. doi:10.1111/j.1365-246X.2010.04673.x

Anderson, E. (1905). The dynamics of faulting. *The Journal of Geology* **14**(3), 254–257.

Arboit, F., Amrouch, K., Collins, A. S., King, R., and Morely, C. (2015). Determination of the tectonic evolution from fractures, faults and calcite twins on the southwestern margin of the Indochina Block. *Tectonics* **34**, 1576–1599. doi:10.1002/2015TC003876

Arboit, F., Amrouch, K., Morley, C., Collins, A. S., and King, R. (2017). Paleostress magnitudes in the Khao Khwang fold-thrust belt, new insights into the tectonic evolution of the Indosinian orogeny in central Thailand. *Tectonophysics* **710–711**, 266–276. doi:10.1016/j.tecto.2017.01.008

Bailey, A., King, R., Holford, S., Sage, J., Backe, G., and Hand, M. (2014). Remote sensing of subsurface fractures in the Otway Basin, South Australia. *Journal of Geophysical Research. Solid Earth* **119**(8), 6591–6612. doi:10.1002/2013JB010843

Beaudoin, N., Lepretre, R., Bellahsen, N., Lacombe, O., Amrouch, K., Callot, J. P., Emmanuel, L., and Daniel, J. M. (2012). Structural and microstructural evolution of the Rattlesnake Mountain Anticline (Wyoming, USA): New insights into the Sevier and Laramide orogenic stress build-up in the Bighorn Basin. *Tectonophysics* **576–577**, 20–45.

Bellahsen, N., Fiore, P., and Pollard, D. D. (2006). The role of fractures in the structural interpretation of Sheep Mountain Anticline, Wyoming. *Journal of Structural Geology* **28**, 850–867. doi:10.1016/j.jsg.2006.01.013

Birch, W. D. (2003). Geology of Victoria: Special Publication. The Geological Survey of Victoria. Volume 23.

Boeuf, M. G., and Doust, H. (1975). Structure and Development of the Southern Margin of Australia. *The APPEA Journal* **15**, 33–43. doi:10.1071/AJ74004

Boreham, C. J., Hope, J. M., Jackson, P., Logan, G. A., and Krassay, A. A. (2004). Gas-oil-source correlations in the Otway Basin, Southern Australia, *in* Boult, P. J., Johns, D.R. and Lang, S.C, ed., *Eastern Australasian Basins Symposium II*, Petroleum Exploration Society of Australia, Special Publication, 603–627.

Bradshaw, M. T. (1993). Australian Petroleum Systems. *PESA Journal* **21**(1), 43–53.

Brown, J. D. B., Gawankar, K., Kumar, A., Li, B., Miller, C. K., Laronga, R., and Schlicht, P. 2015, Imaging: Getting the Down Hole Picture, *in* Schlumberger, ed., Oilfield Review, **27**.

Burkhard, M. (1993). Calcite twins, their geometry, appearance and significant as stress-strain markers and indicators of tectonic regime: a review. *Journal of Structural Geology* **15**, 351–368. doi:10.1016/0191-8141(93)90132-T

CO_2 CRC, 2016, CO_2 CRC: Otway Project.

de Castro, D. L., Bezerra, F. H. R., Sousa, M. O. L., and Fuck, R. A. (2012). Influence of Neoproterozoic tectonic fabric on the origin of the Potiguar Basin, northeastern Brazil and its links with West Africa based on gravity and magnetic data. *Journal of Geodynamics* **54**, 29–42. doi:10.1016/j.jog.2011.09.002

Delvaux, D., and Sperner, B. (2003). Stress tensor inversion from fault kinematic indicators and focal mechanism data: the TENSOR program. In New Insights into Structural Interpretation and Modelling (D. Nieuwland Ed.). Geological Society, London, Special Publications, 212: 75–100.

Dresen, G. (1991). Stress distribution and the orientation of Riedel shears. *Tectonophysics* **188**, 239–247. doi:10.1016/0040-1951(91)90458-5

Duddy, I. R. (2003) Mesozoic: A time of change in tectonic regime. In Birch, W. D. (Ed) The Geology of Victoria. GSA Special Publication **23**, 239–286.

Edwards, D. D., Struckmeyer, H. I. M., Bradshaw, M. T., and Skinner, J. E. (1999). Geochemical Characteristics of Ausralia's Southern Margin Petroleum Systems. *The APPEA Journal* **39**, 297–321. doi:10.1071/AJ98017

Etchecopar, A., (1984). Etude des états de contraintes en tectonique cassante et simulation de déformations plastiques (PhD thèse): Montpellier, France, Université Montpellier. 270 pp.

Faulkner, D. R., Jackson, C. A. L., Lunn, R. J., Schlische, R. W., Shipton, Z. K., Wibberley, C. A. J., and Withjack, M. O. (2010). A review of recent developments concerning the structure, mechanics and fluid flow properties of fault zones. *Journal of Structural Geology* **32**(11), 1557–1575. doi:10.1016/j.jsg.2010.06.009

Geoscience Australia, 2016, Geoscience Australia: The Otway Basin, Volume 2015.

Gibson, G. M., Morse, M. P., Ireland, T. R., and Nayak, G. K. (2011). Arc–continent collision and orogenesis in western Tasmanides: Insights from reactivated basement structures and formation of an ocean–continent transform boundary off western Tasmania. *Gondwana Research* **19**(3), 608–627. doi:10.1016/j.gr.2010.11.020

Gibson, G. M., Totterdell, J. M., White, L. T., Mitchell, C. H., Stacey, A. R., Morse, M. P., and Whitaker, A. (2013). Pre-existing basement structure and its influence on continental rifting and fracture zone development along Australia's southern rifted margin. *Journal of the Geological Society* **170**(2), 365–377. doi:10.1144/jgs2012-040

Google Earth (2018). V. 7.3.0.3832 (December 23 2016). Jameson Beach, Great Ocean Road, Victoria Australia. 38°35'45.49"S, 143°55'.16.85"E, Eye Alt 894m. Aibus / CNES, 2018. https://www.google.com.au/earth/ (23 January 2018)

Healy, D., Jones, R. R., and Holdsworth, R. E. (2006). Three-dimensional brittle shear fracturing by tensile crack interaction. *Nature* **439**, 64–67. doi:10.1038/nature04346

Hill, A. J. (2002). Maturity modelling, hydrocarbon occurrences and shows. *Petroleum Geology of South Australia* **1** Otway Basin, South Australia, no. 2, 9.

Hill, K. A., Cooper, G. T., Richardson, M. J., and Lavin, C. J. (1994). Structural framework of the eastern Otway Basin: inversion and interaction between two major structural provinces. *Exploration Geophysics* **25**(2), 79–87. doi:10.1071/EG994079

Hillis, R. R., and Reynolds, S. D. (2000). The Australian Stress Map. *Journal of the Geological Society* **157**(5), 915–921. doi:10.1144/jgs.157.5.915

Holford, S. P., Tuitt, A. K., Hillis, R. R., Green, P. F., Stoker, M. S., Duddy, I. R., Sandiford, M., and Tassone, D. R. (2014). Cenozoic deformation in the Otway Basin, southern Australian margin: implications for the origin and nature of post-breakup compression at rifted margins. *Basin Research* **26**(1), 10–37. doi:10.1111/bre.12035

Holford, S., Hillis, R., Duddy, I., Green, P., Stoker, M., Tuitt, A., Backé, G., Tassone, D., and MacDonald, J. (2011). Cenozoic post-breakup compressional deformation and exhumation of the southern Australian margin. *The APPEA Journal* **51**, 613–638. doi:10.1071/AJ10044

Krassay, A. A., Cathro, D. L., and Ryan, D. J. (2004). A Regional Tectonostratigraphic Framework for the Otway Basin. *PESA Eastern Australian Basins Symposium II*.

Kulikowski, D., and Amrouch, K. (2017). Combining Geophysical Data and Calcite Twin Stress Inversion to Refine the Tectonic History of Subsurface and Offshore Provinces: A Case Study on the Cooper-Eromanga Basin, Australia. *Tectonics* **36**(3), 515–541. doi:10.1002/2016TC004366

Kulikowski, D., and Amrouch, K. (2018). 3D seismic analysis investigating the relationship between stratigraphic architecture and structural activity in the intra-cratonic Cooper and Eromanga basins, Australia. *Marine and Petroleum Geology* **91**, 381–400. doi:10.1016/j.marpetgeo.2018.01.019

Kulikowski, D., Amrouch, K., Al Barwani, K.H.M., Liu W. and Cooke, D. (2015). Insights into the Tectonic Stress History and Regional 4-D Natural Fracture Distribution in the Australian Cooper Basin Using Etchecopar's Calcite Twin Stress Inversion Techbique, 2-D/3-D Seismic Interpretation and Natural Fracture Data From Image Logs and Core. *Search and Discovery, Article* 41752

Kulikowski, D., Cooke, D., and Amrouch, K. (2016*a*). Constraining the distribution and relationship between overpressure, natural fracture density and temperature in the Cooper Basin. *The APPEA Journal* **56**, 11–28. doi:10.1071/AJ15002

Kulikowski, D., Hochwald, C., Cooke, D., and Amrouch, K. (2016b). A Statistical Approach to Assessing Depth Conversion Uncertainty on a Regional Dataset: Cooper-Eromanga Basin, Australia. *ASEG-PESA-AIG 2016 Conference, Adelaide*. Extended Abstract #200, 484–490.

Kulikowski, D., Amrouch, K., and Cooke, D. (2016*c*). Geomechanical Modelling of Fault Reactivation in the Cooper Basin, Australia. *Australian Journal of Earth Sciences* **63**(3), 295–314. doi:10.1080/08120099.2016.1212925

Kulikowski, D., Amrouch, K., Cooke, D., and Gay, M. E. (2017). Basement Structural Architecture and Hydrocarbon Conduit Potential of Polygonal Faults in the Cooper-Eromanga Basin, Australia. *Geophysical Prospecting*, In press.

Lacazette, A. (2009). Paleostress analysis from image logs using pinnate joints as slip indicators. *AAPG Bulletin* **93**(11), 1489–1501. doi:10.1306/08110909087

Lacombe, O., Amrouch, K., Mouthereau, F., and Dissez, L. (2007). Calcite twinning constraints and deformation mechanisms in the active Zagros collision belt. *Geology* **35**(3), 263–266. doi:10.1130/G23173A.1

Lyon, P. J., Boult, P. J., Hillis, R. R., and Bierbrauer, K. (2007). Basement controls on fault development in the Penola Trough, Otway Basin, and implications for fault-bounded hydrocarbon traps. *Australian Journal of Earth Sciences* **54**(5), 675–689. doi:10.1080/08120090701305228

McQueen, A. F. (1962). The Geology of the Otway Basin. *Australian Oil and Gas Journal* **8**(2), 8–12.

Mehin, K., and Kamel, M. (2002). 'Gas resources of the Otway Basin in Victoria'. (The Department of Natural Resources).

Miller, J. M., Norvick, M. S., and Wilson, C. J. L. (2002). Basement controls on rifting and the associated formation of ocean transform faults—Cretaceous continental extension of the southern margin of Australia. *Tectonophysics* **359**(1–2), 131–155. doi:10.1016/S0040-1951(02)00508-5

Moore, A. M. G., Stagg, H. M. J., and Norvick, M. S. (2000). Deep-water Otway Basin: A New Assesment of the Tectonics and Hydrocarbon Prospectivity. *The APPEA Journal* **40**, 66–85. doi:10.1071/AJ99005

Morton, J. G. G., and Dextral, J. F. (1995). The Petroleum Geology of South Australia, Volume 1: Otway Basin, Volume 1: South Australia, SA Department of Mines and Energy.

Nelson, E., Hillis, R., Sandiford, M., Reynolds, S., and Mildren, S. (2006). Present Day State of Stress of South East Australia. *The APPEA Journal* **41**(1), 15–35.

Norvick, M. S., and Smith, M. A. (2001). Mapping the Plate Tectonic Reconstruction of Southern and Southeastern Australia and Implications for Petroleum Systems. *The APPEA Journal* **41**, 15–35. doi:10.1071/AJ00001

Palmowski, D., Hill, K. C., and Hoffman, N. (2004). Structure and hydrocarbons in the Shipwreck Trough, Otway Basin: half-graben gas fields abutting a continental transform. *The APPEA Journal* **44**, 417–440. doi:10.1071/AJ03016

Perincek, D., and Cockshell, C. (1995). The Otway Basin: Early Cretaceous Rifting to Neogene inversion. *The APPEA Journal* **35**, 451–466. doi:10.1071/AJ94029

Perincek, D., Cockshell, C. D., Finlayson, D. M., and Hill, K. A. (1994*a*). The Otway Basin: Early Cretaceous Rifting to Miocene Strike Slip, *in* Proceedings NGMA/PESA Otway Basin Symposium Abstracts, AGSO Record, 27–33.

Perincek, D., Simons, B. A., and Pettifer, G. (1994*b*). The Tectonic Framework and associated Play Types of the Western Otway Basin, Victoria Australia. *The APPEA Journal* **35**, 451–466.

Pokalai, K., Kulikowski, D., Johnson, R. L. Jr, Haghighi, M., and Cooke, D. (2016). Development of a new approach for hydraulic fracturing in tight sand with pre-existing natural fractures. *The APPEA Journal* **56**, 225–238. doi:10.1071/AJ15017

Prensky, S. E. (1999). Bibliography of well-log applications; 1999 annual update. *Petrophysics* **41**, 41–109.

Rajabi, M., Tingay, M., Heidbach, O., Hillis, R., and Reynolds, S. (2017*a*). The Present-day stress field of Australia. *Earth-Science Reviews* **168**, 165–189. doi:10.1016/j.earscirev.2017.04.003

Rajabi, M., Heidbach, O., Tingay, M., and Reiter, K. (2017*b*). Prediction of the present-day stress field in the Australian continental crust using 3D geomechanical-numerical models. *Australian Journal of Earth Sciences* **64**(4), 435–454. doi:10.1080/08120099.2017.1294109

Rocher, M., Baize, S., Angelier, J., Lozac'h, Y., Lemeille, F., and Cushing, M. (2004). Intraplate paleostresses reconstructed with calcite twinning and faulting: improved method and application to the Lorraine platform area (eastern France). *Tectonophysics* **387**, 1–21.

Robson, A. G., Holford, S. P., King, R. C., and Kulikowski, D. (2018). Structural evolution of horst and half-graben structures proximal to a transtensional fault system using a 3D seismic dataset from the Shipwreck Trough, offshore Otway Basin, Australia. *Marine and Petroleum Geology* **89**, 615–634. doi:10.1016/j.marpetgeo.2017.10.028

Sandiford, M., Wallace, M., and Coblentz, D. D. (2004). Origin of the in situ stress field in south-eastern Australia. *Basin Research* **16**, 325–338. doi:10.1111/j.1365-2117.2004.00235.x

Sibson, R. H. (2003). Brittle-failure controls on maximum sustainable overpressure in different tectonic regimes. *AAPG Bulletin* **87**(6), 901–908. doi:10.1306/01290300181

Tavani, S., Storti, F., Lacombe, O., Corradetti, A., Muñoz, J. A., and Mazzoli, S. (2015). A review of deformation pattern templates in foreland basin systems and fold-and-thrust belts: Implications for the state of stress in the frontal regions of thrust wedges. *Earth-Science Reviews* **141**, 82–104. doi:10.1016/j.earscirev.2014.11.013

Teasdale, J. P., Pryer, L. L., Stuart-smith, P. G., and Loutit, M. A. E. T. S. (2003). Structural framework and basin evolution of Australia's southern margin. *The APPEA Journal* **43**, 13–35. doi:10.1071/AJ02001

White, A. H. (1968). Exploration in the Otway Basin. *The APPEA Journal* **8**, 78–87. doi:10.1071/AJ67011

Willcox, J. B., and Stagg, H. M. J. (1990). Australia's Southern Margin: A Product of Oblique Extension. *Tectonophysics* **173**, 269–281. doi:10.1016/0040-1951(90)90223-U

Zoback, M., Moos, D., Mastin, L., and Anderson, R. N. (1985). Well bore breakouts and in situ stress. *Journal of Geophysical Research* **90**, 5523–5530. doi:10.1029/JB090iB07p05523

Zoback, M. L., Zoback, M. D., Adams, J., Assumpcao, M., Bell, S., Bergman, E. A., Blumling, P., Brereton, N. R., Denham, D., Ding, J., Fuchs, K., Gay, N., Gregersen, S., Gupta, H. K., Gvishiani, A., Jacob, K., Klein, K., Knoll, P., Magee, M., Mercier, J. L., Muller, B. C., Paquin, C., Rajendran, K., Stephansson, O., Suarez, G., Suter, M., Udias, A., Xu, Z. H., and Zhizhin, M. (1989). Global patterns of tectonic stress. *Nature* **341**(6240), 291–298. doi:10.1038/341291a0

Zoback, M. D., Barton, C. A., Brudy, M., Castillo, D. A., Finkbeiner, T., Grollimund, B. R., and Wiprut, D. J. (2003). Determination of stress orientation and magnitude in deep wells. *International Journal of Rock Mechanics and Mining Sciences* **40**(7–8), 1049–1076. doi:10.1016/j.ijrmms.2003.07.001

The authors

Hugo Burgin is a PhD candidate at the Australian School of Petroleum. An awardee of an Australian Endeavour Research Fellowship in 2017, his PhD is focussed on paleo-stress analyses within Australia's Otway Basin. His interests include structural geology, petrophysics and geomechanics.

Khalid Amrouch is a structural geologist with expertise in geomechanics. He graduated from the University of Pierre and Marie Curie (Paris VI) with an MSc and a PhD in structural geology. His main interest relates to brittle tectonics, fracture characterisation and 4D stress analyses. Khalid started his career in 2005 at the Institut Français du Pétrole (IFP), which sponsored his studies, followed in 2010 by a position as research engineer at Mines PariTech. In 2012, Khalid spent 1 year working for BHP as an exploration geologist in Chile, before joining the Australian School of Petroleum in February 2013. Since then, Khalid has been an active member of the S3 Research Group, one of the largest geoscience research groups at the University of Adelaide.

Mojtaba Rajabi is a research associate at the Australian School of Petroleum, University of Adelaide. He is currently the Deputy Head of the World Stress Map project. His research interests are petroleum geomechanics, petrophysics and tectonic evolution of sedimentary basins. Mojtaba graduated with a PhD in Petroleum Geoscience from the Australian School of Petroleum in 2016. He has worked on the Australian Stress Map and the World Stress Map projects in Australia and Germany since 2012. Member: AAPG, ASEG, EAGE, EGU, IAMG, PESA, SEG, SPE and SPWLA.

David Kulikowski recently completed his PhD in structural geology and geophysics from the Australian School of Petroleum, University of Adelaide. His PhD was entitled 'Modern Structural Analysis of Subsurface Provinces: A Case Study on the Cooper and Eromanga Basins, Australia' and involved the analysis of micro-, meso- and macros-scale data obtained through geophysics or core analysis. He produced nine first author papers (published in highly respected journals, such as Tectonics, Marine & Petroleum Geology, Journal of Structural Geology, Australian Journal of Earth Sciences, and Geophysical Prospecting to name a few) and contributed to several other papers as a co-author. He was awarded the Dean's commendation for doctoral thesis excellence and nominated by both of his PhD reviewers for the University Doctoral Research Medal. David currently works at Woodside Energy in an Exploration role.

Simon Holford is an Associate Professor at the Australian School of Petroleum, the University of Adelaide. He graduated with a BSc (Hons) from Keele University (2001) and a PhD from the University of Birmingham (2006). His research interests are in the deformation, uplift and magmatic evolution of rifted margins, sedimentary basins, and continental interiors and their impact on hydrocarbon exploration. Member: AAPG, AGU, GSA, GSL, PESA.

Chapter 4.2: Manuscript 2

Reducing structural uncertainty in complex extensional settings: New insights into the evolution of Australia's South Eastern Passive Margin

This manuscript will be submitted to the interactive open-access peer reviewed journal *Geophysical Prospecting*

Statement of Authorship

Title of Paper: Reducing structural uncertainty in complex extensional settings: New insights into the evolution of Australia's South Eastern Passive Margin

Publication Status: Unpublished and Unsubmitted work written in a manuscript style

Publication Details: Burgin, H. B. and Amrouch, K. (2019a). Reducing structural uncertainty in complex extensional settings: New insights into the evolution of Australia's South Eastern Passive Margin. (In Prep)

Principal Author: Hugo Bonython Burgin

Contribution: 3D seismic and image log interpretation. Calcite twin analysis. Stress inversion. Paper writing (60%)

Certification: This paper reports on original research I conducted during the period of my Higher Degree by Research candidature and is not subject to any obligations or contractual agreements with a third party that would constrain its inclusion in this thesis. I am the primary author of this paper.

Signed: **Date:** 05/03/2019

Co-Author Contributions

By signing the Statement of Authorship, each author certifies that:

- **i.** The candidate's stated contribution to the publication is accurate (as detailed above);
- **ii.** Permission is granted for the candidate to include the publication in the thesis; and
- **iii.** The sum of all co-author contributions is equal to 100% less the candidate's stated contribution.

Name of Co-Author: Dr Khalid Amrouch

Contribution to Paper: Supervision of project. Assisted with all stress inversion and structural interpretation (40%)

Signed: **Date:** 05/03/2019

Reducing structural uncertainty in complex extensional settings: New insights into the evolution of Australia's South Eastern Passive Margin

*Hugo B. **BURGIN**[a] (hugo.burgin@adelaide.edu.au)

Khalid **AMROUCH**[a] (khalid.amrouch@adelaide.edu.au)

[a]Australian School of Petroleum, University of Adelaide, North Tce, 5005, Adelaide, Australia

*Corresponding Author: Hugo B. Burgin (08 8313 8000)

Abstract

Deciphering the structural history of sedimentary basins that lack outcrop or are predominantly offshore is a processes rife with uncertainty. Especially as early models for basin evolution in such settings are often reliant on isolated seismic data sets, insufficient for the analysis of complex and regional structural trends. A solution to this problem is the integration of multi-scale structural data, which allow for comprehensive models to be produced in both three and four dimensions. Using calcite twin, core samples, geophysical image logs and 3D seismic surveys, we show the benefit of this integrated approach in South East Australia, within the western Otway Basin. Multiple paleostress environments were responsible for the creation of an intricate network of faults, across four main phases: (1) N-S oriented initial rifting (2) post-rift ~NW-SE extension, isolated onshore (3) renewed, ~NE-SW rifting, predominantly off-shore resulting in the long lived growth of ~NW-SE and E-W striking faults and (4) a shift to a passive margin, gravitationally dominated setting. Where ~NW-SE striking extensional faults likely remain active, especially along the continental shelf. Evidence for a compressional stress regime is limited to the micro and mesoscale, constrained by calcite twin and natural fracture data. Our findings indicate that it is possible the structural influence of basin inversion within the western Otway Basin has been over estimated in the past. This study also illustrates that

while such an approach is “more comprehensive,” no model is without potential short comings, which must be understood in the context of the local the structural framework.

1.0 Introduction

When working in complex sub-surface basin provinces, establishing an accurate model of structural evolution can be a challenge. Access to outcropping structures is often limited, and structural analysis is restricted to mesoscale (well) and macroscale (seismic) datasets with microscale techniques of analysis rarely included (e.g. Teasdale et al., 2003; Krassay et al., 2004; Lyon et al., 2007). While the analysis of seismic datasets is a powerful tool, it is not without its shortcomings. Especially when restricted to two dimensions (2D) as 1) only a slither of data is available for interpretation that may or may not be representative of the regional or even local structural trend. 2) Structural analysis is highly dependent upon the domain (i.e. two way time or depth) in which the data is interpreted, as the angles of faults and folds may drastically change. 3) The relative angle between subsurface structures and the acquired dataset can have a significant impact on the nature of the 2D lines with some structures often invisible in certain line orientations. In complex rifted settings, these problems are often emphasised by the high number of faults, large spatial distribution of rift-units, on and off-shore scattering of datasets and unknowns regarding the nature of in situ stresses (Tassone et al., 2017). Which results in a high degree of uncertainty for models of structural evolution.

The analysis of mesoscale natural fracture data (Bellahsen et al., 2006) and microscale calcite twin data (Lacombe et al., 2007; Amrouch et al 2010; Arboit et al., 2017; Kulikowski et al., 2017) represent well-established means of constraining stress (Etchecopar, 1984; Burkhard, 1993; Lacombe and Laurent, 1996) and strain (Groshong, 1972; Craddock and Van Der Pluihm, 1999; Amrouch 2010) patterns. However, only recently have they been integrated with modern geophysical tools (Kulikowski and Amrouch, 2017) and never before have they been applied in the sub-surface at a passive margin setting.

In this study we present an integrated approach to reducing the level of structural uncertainty when working in complex rifted settings. Our chosen case study being the Otway Basin (**fig. 1**) a sedimentary province along Australia's southern margin, which has been the focus of continued exploration for oil and gas and geoscience research for 40 years. Also hosting carbon capture and storage and geothermal energy projects.

Efforts to constrain the structural evolution of the region have varied in success, with most past studies focusing mainly on isolated portions of the basin (e.g: The Penola Trough: Lyon et al., 2007; Bailey et al., 2014, The Shipwreck Trough: Robson et al., 2017, Schnieder et al., 2004, The Torquay Sub Basin: Hill et al., 1995, Trupp et al., 1994; Holford et al., 2011a) particularly within the off-shore eastern section, and only in a few cases (eg: Krassay et al., 2004; Briguglio et al., 2015) has basin wide analysis been completed.

Past works utilise mainly macroscale two dimensional (2D) (e.g Hill et al., 1995, Krassay et al., 2004; Holford et al., 2014) and three dimensional (3D) seismic data in isolation (Lyon et al., 2007; Schneider et al., 2004; Robson et al., 2016, 2017, 2018). Providing structural descriptions of fault networks often limited to the time domain, and interpretations using lines of restricted orientation. The contribution that micro and mesoscale deformation can make towards establishing a more comprehensive model for structural evolution (Amrouch et al., 2010a, 2010b; Robion et al., 2007; Arboit et al., 2015; Kulikowski and Amrouch, 2017) has been ignored until now.

In this paper, we integrate the multiscale analyses of calcite twin, fault and fracture data in order to analyse both the spatial and temporal distribution of structural deformation within the study area. Focused on the western, subsurface portion of the basin this study is the most

spatially inclusive of to date, incorporating micro, meso and macroscale data. Providing an insight into fault and fracture populations within the sub-surface, which are of consequence for conventional and unconventional models of hydrocarbon explorations and production, geothermal energy and carbon capture and storage projects.

2.0 Geological Setting

2.1 Geological Background and Structural Evolution

The Otway Basin (**fig. 1**) is a large ~NW-SE striking sedimentary basin, that formed as part of an en-echelon series of sedimentary provinces along the southern margin of the Australian continent during the separation of Gondwana (Norvick and Smith, 2001; Krassay et al 2004). It is continuous with the Bight Basin to the west and the Sorrell and Bass Basins to the east (**fig. 1**). Covering close to 150,000 km^2 , with almost 80% of the basin located in offshore provinces.

While the series of basin forming events is generally well agreed upon (Krassay et al., 2004), there is uncertainty regarding the environments of paleostress. Recent work highlighting this complexity (Burgin et al., 2018). Initial rifting during the Early Cretaceous was concentrated onshore (Norvick and Smith, 2001), producing rift segments such as the Penola Trough (**fig 1**), which trend broadly NW-SE. Sedimentary fill during this period is defined by the Crayfish Subgroup member of the Otway Group (**fig. 2**), early rifting continuing until the late Barremian (Krassay et al 2004). Extensional azimuths during this period have been proposed as N-S (Lyon et al., 2007), and ~NW-SE (Williamson et al., 1990; O'Brien et al 1994).

A basin-wide cessation in active rifting resulted in a significant period of subsidence and cooling during the Aptian – Albian, during which the Eumeralla Formation, the top most

member of the Otway Group, was deposited. The top of the formation is marked by a basin-wide unconformity, representing a period of stress-reorganisation, compression, and the inversion of faults across the basin (Hill et al., 1995; Duddy, 2003). Rifting recommenced from the Turonian to Late Maastrichtian without the creation of oceanic crust at the rifting centre (Krassay et al., 2004).

Extensional azimuths during this period have been proposed as N-S, following initial N-S rifting (Miller et al., 2002) and NE-SW following NW-SE (O'Brien et al 1994; Lyon et al., 2007). The influence of large-scale transtension and sinistral strike slip movements within the eastern portion of the basin has also been suggested during this period (Robson et al., 2017; Schneider et al 2004). Further subsidence following ~Mid Eocene break up is believed to have initiated a significant transgressive event throughout the entire basin (Bernecker et al., 2003). Growth wedges in the eastern portion of the basin suggesting that extension may have continued as far as the Paleogene (Holford et al., 2014).

There is a consensus that from the mid-Eocene much of southeastern Australia has been subjected to ~NW-SE compressional stresses due to plate boundary forces, and coupling with New Zealand (Sandiford et al., 2003; 2004). In the Otway Basin, this reorganisation has supposedly led to faulting, folding and the reverse reactivation of existing normal faults (Hill et. al., 1005; Hillis et. al., 2008a, 2008b; Holford et al., 2011a; 2011b; 2014),(Etheridge et. al., 1991; Dickenson et al., 2002; Holford et al., 2014). Producing a number of broad amplitude anticlines within the offshore basin (e.g. Holford et al., 2014). That being said, there is a degree of uncertainty as to the interpretation of these inversion structures as 1) evidence for thrust faulting and inversion is limited to the interpretation of poor quality 2D lines, containing little reverse offset. 2) Early Cretaceous, petroleum source rocks are at their maximum burial

temperature (Duddy and Erout, 2001; Tassone et al., 2014) suggesting recent exhumation is unlikely. 3) The azimuth of suggested Miocene inversion is non-coaxial with the overall extensional trend of the basin, meaning that any fault inversion would be highly oblique (**fig. 1**). Further questions with respect to the nature of basin inversion have been raised recently, with mesoscale evidence for a ~NE-SW compressive event on the mesoscale (Burgin et al., 2018).

3.0 Methodology

This study is based on the integration of calcite twinning, natural fracture and fault analysis and 3D seismic interpretation.

3.1 Macroscale Fault Structural Analyses Using 3D Seismic Data

3.1.1 3D Seismic Data

Structural analysis was completed on four 3D surveys, three onshore and one offshore (**fig. 1**), in the western Otway Basin. The primary aim being to determine fault strike, dip angle and spatial distribution.

Onshore this study utilises: The St George 3D seismic, acquired in 2001 with a vertical resolution of 41m and a maximum penetration of 8s TWT. The Balnaves-Haselgrove 3D, acquired and merged in 2000, with a resolution of 44m and a penetration of 5s TWT. The Tillbooroo 3D, acquired in 1993, with a resolution of 42m and a penetration of 3.9s. All surveys are situated over the NW-SE trending Early Cretaceous Penola Trough.

Off-shore we utilise the Carpenter 3D survey, positioned in shallow waters, approximately 35km south the Australian coastline. Acquired in 2002, the survey has a resolution of 51m and a maximum depth of 6.0s TWT.

3.1.2 Seismic Interpretation

To assist with seismic interpretation we exploit a common seismic attribute known as incoherency, demonstrated as an effective tool for 3D seismic interpretation (Basir et al., 2013; Kulikowski et al., 2017). Seismic interpretation began with the identification of a series of regional reflectors, primarily the Top Sherbrook and Top Otway Group reflectors as they represent the top of rift units within the basin (Krassay et al., 2004).

Faults were interpreted at various line spacing's throughout each survey, according to structural complexity. Seismic analysis was completed in the depth domain; with conversion from time to depth for onshore surveys completed using check-shot data and polynomial model from Bungaloo-1 (**fig. 3**). The offshore Carpenter 3D seismic was converted to depth using time-depth relationships for the Central Otway Basin derived from Petkovic (2004) (**fig. 3**).

3.2 Mesoscale Natural Fracture and Fault Analyses

In this study we use the categorisation of natural fracture and fault data throughout the sub-surface of the basin to develop deformation-fracture relationships (Stearns, 1968; Price and Cosgrove, 1990). Relationships that assist in the interpretation of paleostress tensors and the nature of sub-surface fault and fracture networks, providing a link between micro and macroscale data.

3.2.1 Natural fracture data in the sub-surface

Modern imaging tools have allowed for new methods of subsurface analysis and structural interpretation (Prensky, 1999) (**fig. 4**). Natural fractures can be identified in resistivity based image logs as sinusoidal features that appear either conductive or resistive (Bailey et al., 2014). In this study we integrate the analysis of 11 well-bore image logs within the Penola Trough, in the western Otway (**table 1**) within regional basement and the sediments of the Otway Group.

3.2.2 Natural Fracture Processing and Analysis

Following image log interpretation fracture sets were defined based upon their degree of dip and common dip azimuth, in addition to their spatial relationships with each other and the bedding (**fig. 5**). As mode of opening is difficult to distinguish from resistivity based image logs (**fig. 6**), core inspections were carried out to ensure mode-2 formation (**fig. 7**). Fracture measurements outside of the major regional sets (~20%) were not included in the processing and analysis. Classed as outliers representing stress perturbations, rock heterogeneities or measurement errors that cannot be correlated to the orientations of the principal stresses (Faulkner et al., 2010).

The analytical approach is based on the fundamental principles of rock failure that describe the relationship between Anderson's three stress regimes and nucleated fracture geometry (**fig. 5**), which develops once the point of mechanical failure has been reached (Zoback et al., 1989; Dresen, 1991; Sibson, 2003; Zoback et al., 2003). Aided by paleostress orientation tool wintensor (Delvaux and Sperner, 2013) specific geometries of fractures were distinguishable based upon their relationship to the principal stress orientation, and the mode of fracture formation (Anderson, 1951).

Conjugate fracture sets are assumed to develop with ~50˚-70˚ of separation between them, bisected by the plunge orientation of the maximum principle stress (σ1) (**fig. 5**). With the minimum principle stress (σ3) bisecting the complimentary 120˚ arc in the same plane as the intermediate principle stress (σ2) (Anderson, 1951; Zoback, 2003). This understanding of natural fracture geometry, and consideration of pre and post tilting relationships, allows for the determination of most likely regime of paleostress responsible for fracture nucleation (Anderson, 1951).

3.2.3 Fault Interpretation

Mesoscale faults were interpreted in well-bore image logs where distinguishable offset was visible along the sinusoidal feature, and where bedding dip varied significantly and consistently across a damage zone sinusoid (**fig. 6**). Fault planes were also identified in re-oriented core samples from Jolly-1 (**fig. 7**) and Jacaranda Ridge-1 (**fig. 7**), to derive the regime of faulting and the sense of movement along the fault plane.

3.3 Measuring microscale deformation with calcite twin analysis

Pioneered by Turner (Turner, 1953) several methods of calcite twin stress inversion exist. All of which can be employed to produce meaningful paleostress orientation and magnitude data (Etchecopar, 1984; Tourneret and Laurent, 1990; Lacombe, 2001; Lacombe et al., 1992; 2007; Rocher et al., 2004; Parlangaeu et al., 2018) Mechanical twinning in calcite crystals is plastic-style deformation in response to dislocation gliding along the “e-planes,” of the crystal lattice (Burkhard, 1993). Twinning in calcite occurs at temperatures between <25 and 400˚C and in environments of low-confining pressure and resolved shear stress (RSS). The component of stress that is aligned with the direction of twinning. Twinning can be compared to a zone of

perfect simple shear, due to a shift in the position of the atoms within the lattice. Three e-planes exist in each crystal and are geometrically centered on the optical axis, C (**fig. 8**). Etchecopar's calcite stress inversion technique (CSIT), used herein consists of developing the best fit tensor for the distribution of twinned and un-twinned e planes, and is capable of discerning polyphase structural events. CSIT can be applied to small twinning deformation which is able to be approximated under co-axial conditions (stress = strain).

We use CSIT to determine four of the six parameters of a complete stress tensor: maximum principal stress orientation: (σ1), intermediate principal stress orientation (σ2), minimum principal stress orientation (σ3) and the differential stress ratio, (ϕ; where $\phi = [(\sigma 2 - \sigma 3)]/[(\sigma 1 - \sigma 3])$). These four values comprise what is defined as the reduced stress sensor, T'.

The technique begins with a trial and error process of applying several experimental tensors to the dataset. The total components of T' being calculated for each scenario. A perfect tensor is found when all twined planes are consistent with a given tensor, each twinned plane sustaining a shear stress value larger than the maximal one exerted upon any un-twinned plane. The best tensor is found when the penalization function, (f) is reduced as close to zero as possible. This function is defined as:

$$f = \sum_{j=1}^{N} \left(\tau_{sj} - \tau_{a'}\right)$$

Where $\tau a'$ is the smallest RSS applied to the twinned planes that are compatible with the experimental stress tensor, and τsj is the RSS applied upon the N of untwinned planes j such that $\tau sj > \tau a'$ (Etchecopar, 1984; Laurent, 1984).

The optimal tensor is found by incorporating the maximum amount of twinned planes in the sample, while ensuring the value of the penalization function remains as low as possible. Due to local heterogeneities, perturbations, and measurement uncertainties, a small percentage (~10-15%) of un-twinned planes can be included within the tensor as having received a RSS greater than the τa'. We combine CSIT with subsurface methods of sampling and integration from Kulikowski and Amrouch (2017) in order to obtain paleostress tensors from re-oriented petroleum core samples from the subsurface Otway Basin.

3.4 Previous studies using similar datasets

While previous works have utilised the same datasets [e.g. Lyon et al., 2007 – St George and Balnaves 3D, Robson et al., (2016) – Carpenter 3D, Bailey et al., 2014; Burgin et al., 2018 (image log data – except Jolly-1ST1 and Bungaloo-1)]. This study is the first to comprehensively integrate their analysis with high order fault data. The dataset having been re-interpreted from all previous works.

Additionally, in comparison to previous studies in the region (Bailey et al., 2014) we place a far greater level of importance on complete 3D fracture geometry and take the further step of linking fracture geometry with paleostress regimes.

4.0 Results and Interpretation

In any study involving the use of geophysical data, such as image logs and seismic surveys, the separation of results and interpretation is difficult, as the interpretation of faults within seismic data, is itself the result. In this section we present our 'results' and interpretation of the 3D seismic and wellbore image logs in parallel, followed by a discussion.

4.1 Macroscale: Structural Analysis using 3D seismic

In all 3D surveys, fault dips were predominantly high (**fig. 9**, **fig. 10**, **fig. 14**) and where low angle faulting is displayed it is representative of a gradual transition towards a lower angle at depth (**fig. 10**).

4.1.1 On Shore 3D Surveys

Multiple fault sets are present within the onshore surveys, which are linked to varying orientations of extension. They are best observed along the Top Sherbrook Group reflector within each survey (**fig. 11**).

Consistent across all three surveys is a NW-SE ~145°N striking fault set (**fig. 9** and **fig. 10**). Faults in this set occur in a number of ways including, isolated planes and laterally linked arrays (**fig. 10**). Relay ramps were also interpreted in St George 3D and Balnaves-Haselgrove 3D. This fault set is pervasive throughout most of the seismic section, penetrating all units of the Sherbrook and Otway Group and is characterised by concave extensional faults (**fig. 12**), that dip at high angles towards the southwest and northeast (**fig. 9** and **fig. 10**). Thickening of the Sherbrook Group sediments and Early Otway Group Units, in the hanging wall of these faults can be observed within all three surveys. Offset along these faults is normal, with their upwards propagation (**fig. 9** and **fig. 10**) into Palaeogene and Neogene sediments visible within all datasets.

A second major set of ~E-W striking normal faults was detected in the Balnaves-Haselgrove 3D, defined by a large listric fault that dips towards the south (**fig. 10**). The fault has controlled the formation of synthetic and antithetic faults of the same style, with faulting seeming to sole

out along the basement surface (**fig. 10)**, although this was difficult to accurately constrain due to decreasing seismic quality with depth. Thickening within the Sherbrook Group is apparent within the hanging walls of these faults with minor thickening also evident in the early members of the Otway Group (**fig. 10**). In many cases along strike in either direction, these faults are linked to NW-SE and NE-SW striking normal faults (**fig 11**).

A minor ENE-WSW (**fig. 9** and **fig. 10**) striking set of faults was interpreted within the Balnaves-Haselgrove 3D and the Tillbooroo 3D. In both surveys, these faults are mainly isolated to the Eumerella Formation, terminating at the top Otway unconformity boundary, and showing no vertical linkage with deeper faults. The largest faults in this set dip towards the south, and are responsible for the formation of a small series of ENE-WSW striking horst and graben structures which are particularly evident within incoherency depth slices (**fig. 13**). In the Balnaves-Haselgrove 3D these faults are soft-linked to NW-SE and E-W striking faults along strike to the west. The formation of this fault set post-dates the deposition of the Otway Group as thickness is uniform between the foot and hanging walls.

4.1.2 Offshore 3D Survey – Carpenter 3D

Offshore, the Carpenter 3D is dominated by high-angle ~NW-SE (135°N) striking normal faults that dip towards the southwest. The faults are best observed along the Top Sherbrook Group reflector (**fig. 15**) where soft and hard linkage of parallel striking faults can be seen.

As discussed by Krassay et al., (2004) the offshore western Otway Basin contains a far thicker sector of the Sherbrook Group in comparison to the onshore portion, which was also observed (**fig. 14**). Considerable thickening of the Sherbrook Group sediments within the hanging walls of some faults can be seen, though this is not consistent throughout the survey, suggesting that

multiple episodes of similarly oriented faulting have occurred. Large faults in the survey penetrate upwards into undifferentiated Palaeogene units, in a number of cases displaying significant normal offset (**fig. 14**).

4.1.3 Fault division by unit of occurrence

Grouping faults from all surveys between on and off-shore sectors, and dividing them according to their characteristics: basement involved, isolated to the Otway Group, or non-basement involved Otway and Sherbrook Group Faults – provides another degree of insight (**fig. 16**).

Basement linked faults strike primarily E-W or ~NW-SE in both on and off-shore sections of the basin. Onshore ~NE-SW striking faults are isolated within the Otway Group sediments. Non-basement involved, ~NW-SE and E-W striking faults extend throughout the Sherbrook and Otway Group sediments. Representing a broad pattern of faults that dip towards the north (**fig. 16**).

4.2 Mesoscale: Natural Fracture and Fault Analyses

4.2.1 Natural Fracture and Fault Interpretation from Wellbore Image Logs

Lower hemisphere stereographic projections of fracture data with present day geometries, sorted by well are presented in **fig. 17**. Poles to planes cluster at NNW-SSE, N-S and NE-SW with natural fracture dip angles varying from ~25° to ~ 88° within a single well. High angle fractures dominate (**fig. 18**) with very few low angle and vertical fractures detected (**fig. 19**). However, in most cases well deviation from vertical was minimal, meaning vertical fractures were difficult to detect. Killanoola-1DW1 contained a high amount of ~NE-SW striking fractures and it's impact on the overall trend within our data is observed within **fig. 19**.

Fault extracted from wellbore image logs strike ~NW-SE and ~NE-SW with dip angles between ~40° and ~80°. Offset along many of these faults was also visible, making it possible to classify their nature and regime of nucleation based on their sinusoidal geometry, which was mainly normal.

4.2.3 Core Analysis

Analysis from the Casterton member of the Otway Group in Jolly-1 ST1 at a depth of 3850.5m yielded the successful measurement of a high-angle extensional ~NNW-SSE striking fault (**fig. 7**) showing slight oblique movement. Analysis within Jacaranda Ridge-1 at a depth of 2639.4 m also showed evidence for small scale extensional faulting within the Upper Sawpit member of the Otway Group sediments, though in this case it was not possible to reorient the sample.

4.3 Paleostress Regimes from Fault and Fracture Data

Due to the highly faulted nature of the datasets, paleostress regimes were assigned to fault data using idealistic models and pure dip-slip normal movement on the fault planes. ~NE-SW striking normal faults were categorised under a NW-SE extensional stress regime as part of set FLT-A. ~NW-SE striking faults under a NE-SW extension regime FLT-B, and E-W striking faults under a N-S extensional stress regime, FLT-C (**fig. 21**). As all fracture data was obtained from the Otway Group units, discerning their relative chronologies based on their vertical distribution was not possible. Additionally, as in all wells bedding dip degree was negligible, generally ~10º, the analysis of pre and post tilting events was not possible.

More than 80% of mesoscale fracture data was categorised under our method of analysis, with a diverse spread of mainly high angled fractures, classified into various sets and assigned

paleostress regimes. Fractures striking NE-SW were assigned to fracture set FRC-A an extensional paleostress regime, with σ3 trending broadly towards the SE. Fractures striking NW-SE were assigned to a second extensional regime, FRC-B, with σ3 trending broadly NE. Arguably both FRC-A and FRC-B could be further reduced to a total of 4 extensional fracture sets, as both can be seen to contain two sub-sets of natural fractures (**fig. 21**). However, we have chosen to categorise them under only two sets as we believe that given the meso-scale nature of the data, the subsets likely reflect small variations within a large scale extensive stress regime which is defined by FLT-A and FLT-B. Fractures striking E-W were assigned to set, FRC-C, a N-S extensive regime with σ3 plunging towards the south.

In addition to the extensional fracture sets, two lower angle compressional sets were visible within the data. Fractures striking NE-SW with low angles of dip were assigned to a compressive stress regime fracture set, COMP-A, with σ1 trending towards the NW. Low angle, NW-SE striking fractures only present within the penetrated basement units in Killanoola 1 and Penley 1 were assigned to set COMP-B, with σ1 trending towards the NE.

Faults from image log data were assigned to two environments of paleostress: NE-SW striking faults were assigned to a NW-SE extensive stress regime in set ILF-A. Faults striking NW-SE were assigned to set ILF-B under a NNE-SSW extensional stress regime.

4.4 Stress tensors from Etchecopar's CSIT

Two calcite samples from high angle, extensive fractures within the Sawpit Sandstone and Pretty Hill members of the Otway Group were analysed using Etchecopar's CSIT. Producing a single stress tensor from each sample.

Sample JR-1 recorded a stress tensor, with a horizontal σ1 trending ~NW-SE and a low differential stress ratio (ϕ= 0.2) (**fig. 22**), σ1 plunging at 03º towards 135º. Sample HSG-2 produced a ~NW-SE extensional stress tensor under back-tilted bedding conditions (**fig. 22**), σ1 plunging and 43º towards 120ºN. JR-1 was re-oriented using image log data from the same well, while the HSG-2 samples was re-oriented using well bore image log from surrounding wells in combination with dip data from 3D seismic Kulikowski and Amrouch (2017). Data for each tensor is presented in **table 2**.

5.0 Discussion

5.1 An integrated approach to determining extensional origins and paleostress evolution

This study shows a distinct correlation between micro, meso and macroscale data, with a number of paleostress environments consistently present across all scales. Given that most basement involved faults strike E-W and the presence of a possible deep E-W fabric within both on and off-shore provinces (Lyon et al., 2007; Robson et al 2016), initial rifting within the western Otway Basin was likely oriented ~N-S. With the growth of E-W striking faults and more oblique ~NW-SE basement involved faults continuing throughout most of the Early Cretaceous. Evident in the thickening of all Crayfish sub-group units within the hanging walls of these faults, supporting evidence from Lyon et al., (2007). Mesoscale evidence for this paleostress event comes from FRC-C, in addition to the small scale faulting interpreted within the Jolly-1 core. This period also saw the development of a number of antithetic ~NW-SE and E-W striking syn-rift faults develop in conjunction with larger basement involved structures.

Following deposition of the complete Otway Group during the Early Cretaceous, ~NE-SW striking faults isolated within the early onshore units suggest the western Otway Basin experienced a minor ~NW-SE oriented extensional event. Supported by FRC-A, along with

the CSIT tensor from HSG-2 and image log fault set ILF-A. As there is no evidence for this fault set within our offshore dataset it is likely that this paleostress field was isolated onshore, possibly due to thermal relaxation or subsidence. This is a likely cause, especially as early rifting was concentrated onshore (Krassay et al., 2004; Brugiglio et al., 2015) and these faults show little penetration into the deeper sections, no syn-deposition growth and are restricted to the upper sections of the Otway Group (**fig. 13**)

Renewed rifting began at the start of the Late Cretaceous, moving mainly offshore, marked by a higher thickness of Sherbrook Group sediments compared to the onshore region (**fig. 9** and **fig. 10**). From the high amount of non-basement linked ~NW-SE striking faults onshore, and the presence of recently active ~NW-SE striking faults within the off-shore sector of the basin, this renewed period of rifting was likely oriented ~NE-SW. Supported by the mesoscale fracture and fault data from FRC-B and ILF-B. This period also saw the reactivation of early E-W striking faults, evident in their continued growth within on-shore sections of the basin and in very few cases ~NE-SW striking minor fault sets linked to ~E-W striking fault sections. From the presence of post rift faulting within the Sherbrook Group (**fig. 14**) and propagation of NW-SE striking faults within Palaeogene units, both on and off-shore, it is likely that this extensional regime of paleostress persisted well into the Palaeogene.

5.2 Basin Inversion and Compressional History of the Western Otway Basin

From the presence of broad wavelength folding within Palaeogene and Neogene units, previous studies suggest the Otway Basin has experienced multiple episodes of ~NW-SE compression and inversion throughout its evolution (Hill et al., 1994; Duddy et al., 1994; Krassay et al., 2004; Holford et al., 2011a; Holford et al., 2014). These are generally believed to have been responsible for the multiple unconformities throughout the sedimentary succession (Krassay et

al., 2004; Holford et al., 2014) with inversion accommodated through the ~NW-SE reverse reactivation of basin forming normal faults.

Two periods of ~NW-SE oriented compression have been proposed, firstly, following the deposition of the Otway Group, in the Mid-Cretaceous due to a rearranging of plate boundary forces. Secondly, from ~Late Miocene to recent due to stress transfer from the eastern plate margin (Sandiford et al 2003; 2004). To date the most substantial evidence for any significant compression within our study area, is the analysis of the broad amplitude Morum and Copa Anticlines (**fig. 23**), although the structures have only been imaged using scarcely spaced 2D seismic lines, interpreted in TWT (Holford et al., 2014).

Considering the data from Carpenter 3D survey, it is possible the Morum and Copa structures have been misinterpreted, due to a parallel geometry between 2D line and regional fault strike (**fig. 23**). Especially as interpreted anticline hinges trend near orthogonal to the strike of underlying extensional faults (**fig. 1**), meaning they could not have accommodated ~NW-SE oriented inversion (**fig. 23**). However, if these structures do represent topographic highs, it is possible they were formed by a means other than ~NW-SE oriented fault inversion. Such as long-term compaction over a basement high, detachment folding within deep rift units or even co-axial inversion oriented ~NE-SW. For which mesoscale fracture evidence has been suggested by Burgin et al., (2018) in the eastern Otway Ranges.

In the results from this study on the macroscale, there is no evidence for compressional environments of stresses, past or present. All faults are high-angle and display normal off-set, while ~NE-SW striking faults within the Tillbooroo 3D and Balnaves-Haselgrove 3D, which are ideally oriented for inversion under a ~NW-SE oriented compressional stress regime, show no evidence for reactivation. Suggesting that compressional neotectonic structuring within the

western Otway Basin has been minimal. Further evidence against the influence of large scale ~NW-SE oriented compression, at the end of the Early Cretaceous, is the horizontal nature of seismic reflectors (**fig. 8**) between the Otway Group and Sherbrook Group. A feature which suggests that, though an unconformity may be present, there is no structural evidence to support that erosion was driven by fault inversion and tectonic compression. Lastly, very low levels of post-Albian exhumation in many wells, determined from sonic-log analysis (Tassone et al., 2014) suggest minimal uplift following the deposition of the Otway Group echoing the results of the structural interpretations within this study.

Although evidence on the macroscale for environments of compression is lacking, two paleostress environments of compression are present within the natural fracture and CSIT datasets. Suggesting that the influence of compressional stresses is not entirely absent from the western Otway Basin, but is limited to the micro and mesoscale. The presence of fracture set COMP-B, exclusively within the Paleozoic basement, suggests that at some point prior to initial rifting the region experienced ~NE-SW oriented compressional forces. While fracture set COMP-A and the stress tensor from JR-1 suggest that following the deposition of the Otway Group, the western Otway Basin may have experienced mild-compressive forces. Although the low ϕ value of 0.2 in tensor JR-1 suggests that $\sigma 2$ and $\sigma 3$ were interchangeable, meaning that a strike slip stress regime is also possible.

Given the large amount of evidence for Miocene- recent ~NW-SE oriented compressional forces throughout much of South East Australia (Sandiford et al., 2003; 2004; Holford et al., 2011a; 2014; Tassone et al., 2017) we believe the ~NW-SE compressional paleostress regimes detected within data from this study to be associated with this event. However, local stress perturbations – possibly due to previously formed structures - may also be responsible.

5.3 Neotectonic compression along Australia's Southern Margin

There is almost irrefutable evidence that plate boundary forces exert a first order control on the orientation of in-situ stresses within intra-plate settings such as the Australian continent, (Reynolds et al., 2003; Sandiford et al., 2004; Holford et al., 2014). However there is little in-sight into the degree to which stress is released moving in-wards from plate boundaries (Rajabi et al., 2017b) and how regimes of in-situ stress are affected. Especially with respect to evidence from geological structures and not petroleum industry data, which may contradict each other, especially in the Otway Basin (Tassone et al., 2017).

Evidence for neotectonic activity along Australia's southern margin is at its most intense at the eastern boarder (Clark et al., 2011; Sandiford et al., 2004; Holford et al., 2011a; Tassone et al., 2017), in the Gippsland Basin, where significant neotectonic normal fault inversion has occurred. The structures defining some of Australia's pre-eminent oil fields of the late 20th century (e.g. the Snapper Anticline (Glenton, 1991). Moving progressively west, away from the "front," of compression, despite, high levels of seismicity within the Bass Basin and possible uplift concentrated around the Otway Ranges (**fig. 24**). There seems to be a lack of widespread thrusting and inversion structures. Suggesting that the influence of plate-boundary compressive forces significantly decreases from east to west (**fig. 24**) along the southern margin of Australia.

This is supported by evidence from this study, concentrated in the western Otway Basin, where the influence of ~NW-SE compression is limited to the micro and mesoscale (**fig. 24**) and post-Albian exhumation is very low (Tassone et al., 2014). This insight has possible implications

for considering the structural evolution of intra-plate sedimentary basins and assists in providing further geological evidence for comparison with petroleum industry datasets.

5.4 Comparisons with the intra-cratonic settings

This study represents the second integration of multiscale datasets throughout the sub-surface, the first located within Australia's intra-cratonic Cooper Basin (Kulikowski and Amrouch, 2017). Whilst we have been able to apply this approach to our study area with some success - reducing the uncertainty surrounding a number of basin forming events - it is worth noting distinct challenges to the method when working in a passive margin, rather than intra-cratonic basin setting. In contrast to intra-cratonic sedimentary basins, which show lower levels of mesoscale extensional deformation (Kulikowski and Amrouch, 2017), passive margin settings such as the Otway Basin are controlled heavily by the influence of gravity as a vertical principal stress throughout their history. This is reflected in our dataset by the high amount of extensional faults and natural fractures – that all share a vertically oriented principal stress – and which, when viewed as a single group show evidence for environments of extension across almost 360º (**fig. 19**).

This made distinguishing individual fracture sets a challenge, especially when all formations were of similar age, and would have been impossible without the aid of fault and calcite twin data, highlighting the necessity for a multi-scale approach. Additionally, in such a gravitationally controlled province it is possible that extensional fracture sets may develop due to intermittent periods of thermal subsidence or flexural relaxation, which are not directly linked to large-scale paleo stresses, and are impossible to distinguish form those that are. In such a highly extended sub-surface province like the Otway Basin, it is also possible that low-angle compressional fracture sets or twinning data may record local stress perturbations or stress "deflections," (King et al., 2012; Debenham et al 2018). Resulting in compression within

or in close proximity to large extensional faults within the hanging wall section, especially when wide spread faulting is present within younger (higher) stratigraphic units. Within our dataset, this may be an alternative explanation for fracture sets COMP-A and COMP-B, especially as orientation of σ1 within both fracture sets are parallel to azimuths of σ3 from fault sets FLT-A and FLT-C, respectively. Additionally, the stress tensor derived from the JR-1 sample, which with a differential stress ratio of 0.2 indicates the value of σ2 and σ3 were interchangeable (Lacombe et al., 2007) meaning any compression was not well defined.

5.3 Implications for in-situ stress and present day sub-surface permeability

A number of assessments of the in-situ stresses in the western Otway Basin using petroleum industry data, consider the region to be either within a strike-slip or compressional stress regime (Nelson et al 2006; King et al., 2012). With ~NW-SE, trending maximum horizontal stress considered as the maximum principal stress.

Despite these suggestions, as discussed, evidence from this study shows that macro-scale geological evidence for both of these regimes is lacking. No strike slip faults or fractures have been detected, (although these are difficult to detect within vertical wells) and evidence for compression limited to the micro and mesoscale. Suggesting the influence of compressional stresses has been minimal during the structural evolution of the basin.

In contrast, the propagation of extensional faulting into Palaeogene - Neogene sediments visible within all of our surveys (**fig. 9** – **fig. 14**) suggests that extension within the region may have persisted until at least the Neogene. The on-going growth of extensional structures and their reactivation at depth required to accommodate continuing growth, is most likely under an extensional stress regime. Suggested by Rajabi et al., (2017b) who modelled a shallow

transition at ~3km from a shallow strike slip stress regime to an extensional stress regime in the Otway Basin.

The presence of this transitional zone of stress within the shallower sections of the basin has significant consequences for current geomechanical models. While, Bailey et al., (2014) modelled fracture reactivation it was only completed under strike-slip and reverse conditions. Whereas evidence from this study suggests these regimes are unlikely, especially at depths of interest to petroleum exploration. As such, using similar stress conditions, we have briefly modelled fracture susceptibility for natural fractures from Jolly-1 under a present day extensional stress (**fig. 25**).

The modelling indicates that under a normal stress regime almost all high angle fractures, especially those striking ~NW-SE within FRC-B, have very low pressures needed for reactivation. Meaning they are ideally oriented for fracture stimulation through hydraulic fracturing to assist in the production of potential oil and gas targets. This current uncertainty, affects not only the models for subsurface permeability of petroleum systems within the basin, but is of high importance for geothermal and carbon dioxide sequestration which involve the injection of material into subsurface networks.

Additional evidence for present day extension within the western Otway Basin, especially within the off-shore sector, may be the presence of seismic activity concentrated around the continental shelf. Whilst there are no focal mechanism solutions available for any of these earthquakes, their clustering along the shelf (**fig. 26**), suggests they are likely extensional in nature and gravitationally controlled. As the influence of gravity, acting a vertical principal

stress, is particularly high along the continental shelf. However, this cannot be confirmed without focal mechanism solutions.

This warrants further investigation as it suggests that passive margin basins, which extend throughout on and offshore provinces like the Otway Basin may experience somewhat of a "hybrid," environment of in-situ stress between their onshore and offshore sections. As the local influence of gravitationally driven extension interacts with plate boundary forces, especially in offshore sections of the basin surrounding the continental shelf. As such, while the results of this study has successfully refined much of the regional structural evolution, they have also emphasised possible contradictions between geological evidence and petroleum industry data, with respect to the environment of in situ stress within the region.

6.0 Summary and future work

This study demonstrates how the use of an integrated approach to conducting structural analysis within a complex rifted setting, can assist in reducing the uncertainty behind models of structural development. Especially those that rely predominantly on the interpretation of seismic datasets. By combining methods of structural analyses across the micro, meso and macro scale we have presented new insights into the multi-scale structural framework of Otway Basin and the nature of post-break up compression along Australia's southern margin. The first integration of these techniques within a passive margin sedimentary basin have produced a more comprehensive history of basin evolution than any previous study (**fig. 27**), one that accounts for deformation across both time and space.

Basin evolution is constrained to four main phases: (1) ~N-S oriented initial rifting, wherein E-W basement fabric highly influenced fault development, supported by Lyon et al., (2007) and Robson et al., (2018). (2) minor, post-rift ~NW-SE extension, isolated onshore, possibly due to thermal relaxation or subsidence, which has not been previously discussed and was

resolved predominantly due to the integrated approach of this study. (3) Renewed, ~NW-SE rifting, mainly offshore, resulting in the long-lived growth of ~NW-SE and ~E-W striking faults during the deposition of the Late Cretaceous and Palaeogene sedimentary units. (4) A shift to a passive margin, gravitationally dominated setting, where ~NW-SE striking extensional faults may remain active. Especially surrounding the continental shelf.

The results provide the most comprehensive distribution of natural fracture and fault data to date along Australia's southern margin, assisting on-going efforts for hydrocarbon exploration and production. Future work should involve the application of these techniques within the eastern Otway Basin, to assess the true nature of basin inversion and post-break up ~NW-SE oriented compression which has been questioned in this study.

Acknowledgments

The authors appreciate the financial contributions provided from Australian Postgraduate Award Scholarship through the University of Adelaide. Thank you to Richard Allmendinger for Stereonet 8.8.8, and Carlos H. Grohmann and Ginaldo A.C. Campanha for "OpenStereo 0.1.2". Thank you to Down Under Geosolutions for the use of D.U.G insight v4.4. Additional information is available by contacting the lead author: hugo.burgin@adelaide.edu.au.

676

677

678

Well Name	Latitude	Longitude	Type of Image Log	Image log Depth	Fracture Count	Maximum Borehole Deviation
Killanoola 1/DW1	37°12’ 42.20”	140°40’03.02”	FMI	788m	330	4.40°
Balnaves 1	37°26’ 50.50”	140°42’16.10”	FMI	1894m	316	56.07°
Bungaloo 1	37°19’ 34.70”	140°44’08.50”	STAR	3712m	190	6.68°
Jolly 1/ST1	37°24’ 03.30”	140°50’54.50”	STAR	2390m	258	7.65°
Jacaranda Ridge 1	37°20’ 57.19”	140°45’10.72”	FMS	2207	735	8.50°
Wynn 1	37°24’ 32.99”	140°52’19.84”	FMS	1621m	23	5.97°
Ladbroke Grove 2	37°27’ 54.75”	140°47’24.49”	FMS	997m	243	31.00°
Ladbroke Grove 3	37°24’ 56.32”	140°46’49.42”	FMI	874m	1	11.54°
Katnook 4	37°27’ 18.92”	140°46’32.22”	FMS	1248m	16	6.99°
Penley 1	37°12’ 07.63”	140°26’49.53”	FMS	1437m	109	5.50°
Haselgrove 1	37°26’ 30.94”	140°49’49.78”	FMS	393m	0	4.69°

679 **Tables**

680 ***Table 1:*** *Well bore image logs interpreted as part of this study.*

681

682

683

684

Table 2: *Paleostress tensors derived from calcite twin analysis as part of this study.*

Sample Name	Depth	Formation	Age Period	Reference Bedding	σ1	σ2	σ3	Differential Stress Ratio *R*	Total Data (T/UT)	F-Function
JR1	2637.6m	Sawpit Sandtone	Early Cretaceous	17°/308°	03°/135°	32°/043°	57°/229°	0.2	172/56	0.71
HSG2	2905.8m	Pretty Hill Sandstone	Early Cretaceous	20°/308°	43°/120°	15°/224°	43°/328°	0.6	158/31	0.2

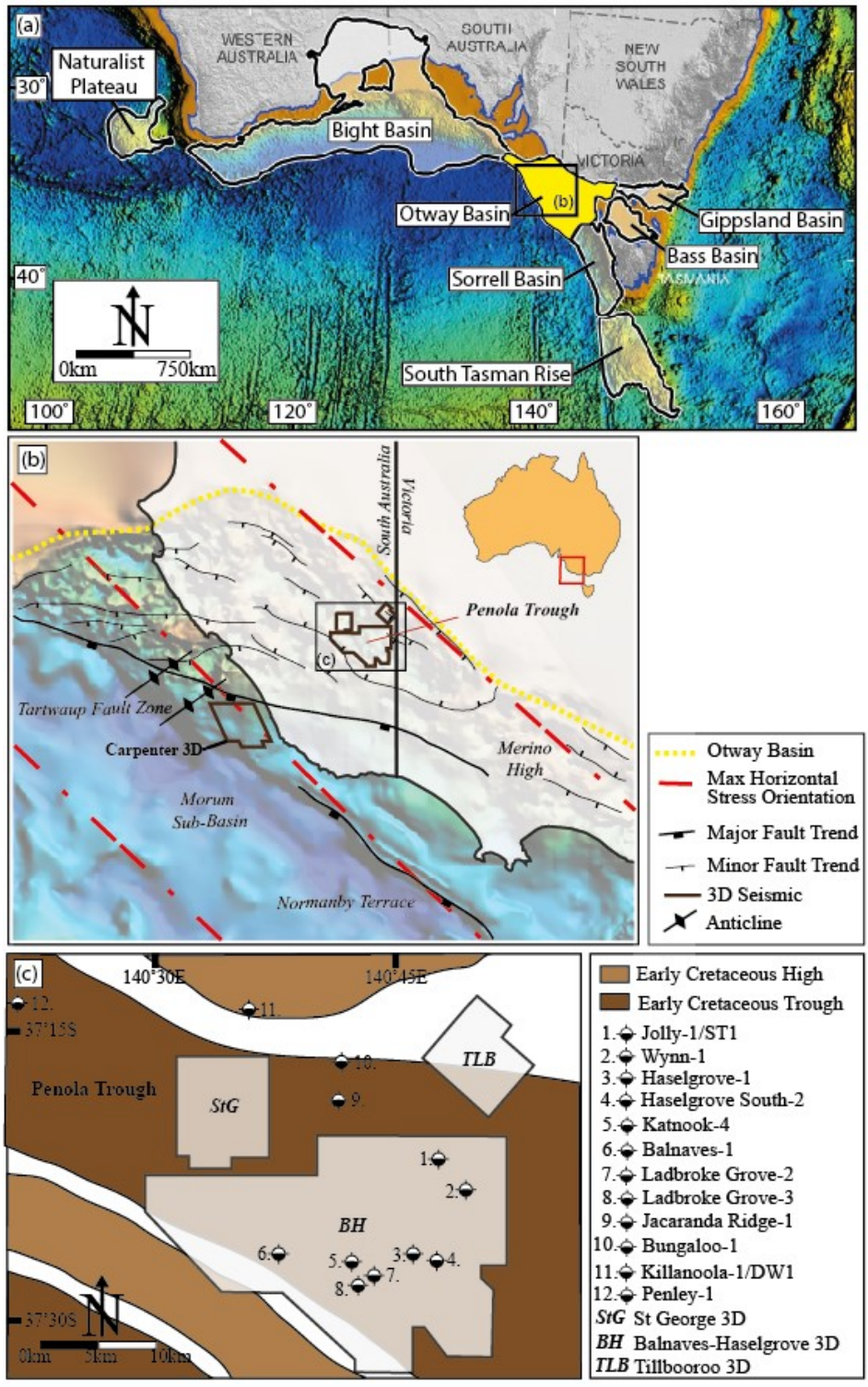

Fig. 1: *(a) Map of Australia's southern margin displaying the location of the Otway Basin (modified from Stacey et al. (2013)* ***(b)*** *A regional map of the Western Otway Basin draped over a SEEBASE depth to basement model (Krassay et al. 2009). Local structures from Moore et al., (2000) and Holford et al. (2014). The locations of the four seismic surveys used within this study are also outlined (c) A close up map of the Penola Trough modified from Bailey et al. (2014), displaying the location of the Balnaves-Haselgrove 3D, Tilbooroo 3D and the St George 3D in addition to the 12 image logs used as part of this study.*

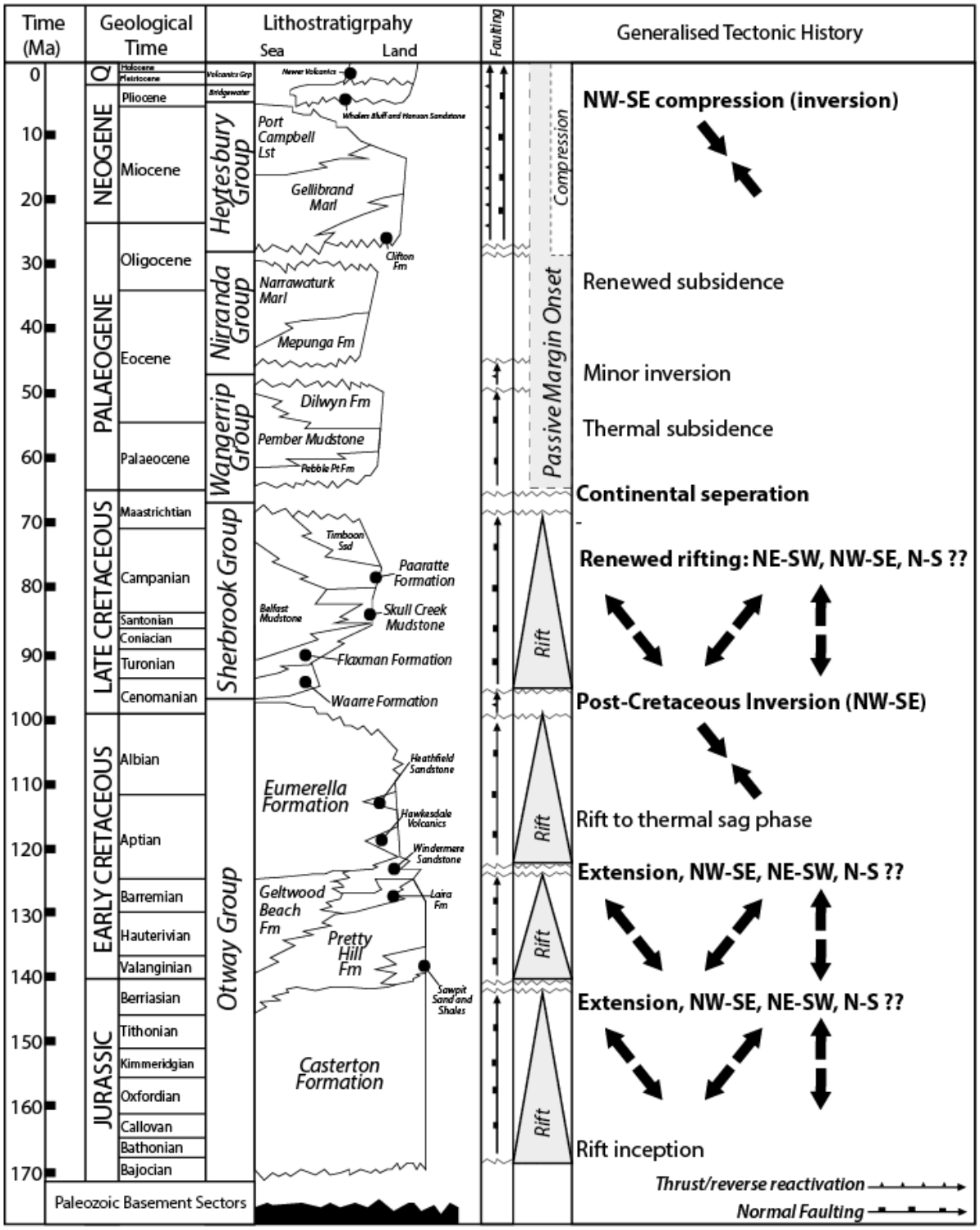

Fig. 2: *A stratigraphic column for the Otway Basin, including the major groups of sediments interpreted as part of this study. Modified from Tassone et al (2017) after Geary and Reid (1998) to include the confusion regarding many of the basin forming rift events. Note:the formations between the top Casterton Formation and the bottom Eumeralla Formation represent the Crayfish Subgroup of Early Cretaceous Units.*

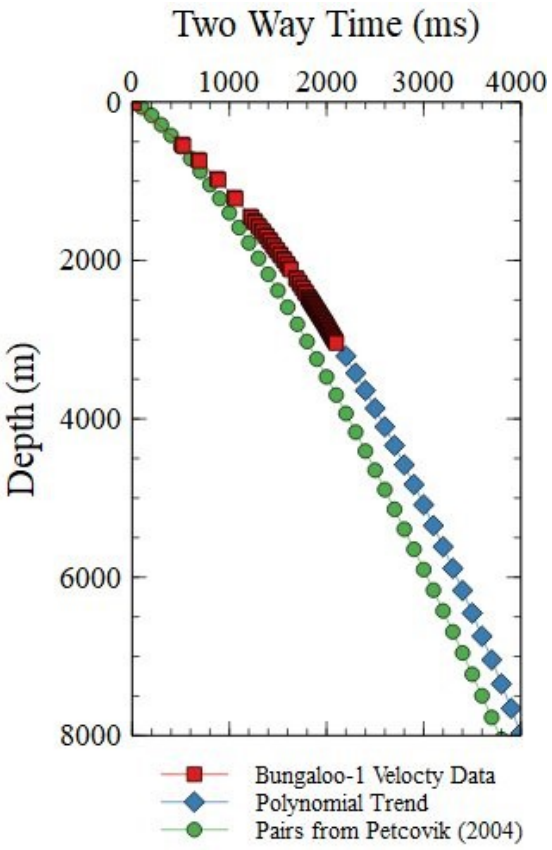

Fig. 3: *Time depth relationships used to convert 3D seismic data from the time to depth domain in the western Otway Basin.*

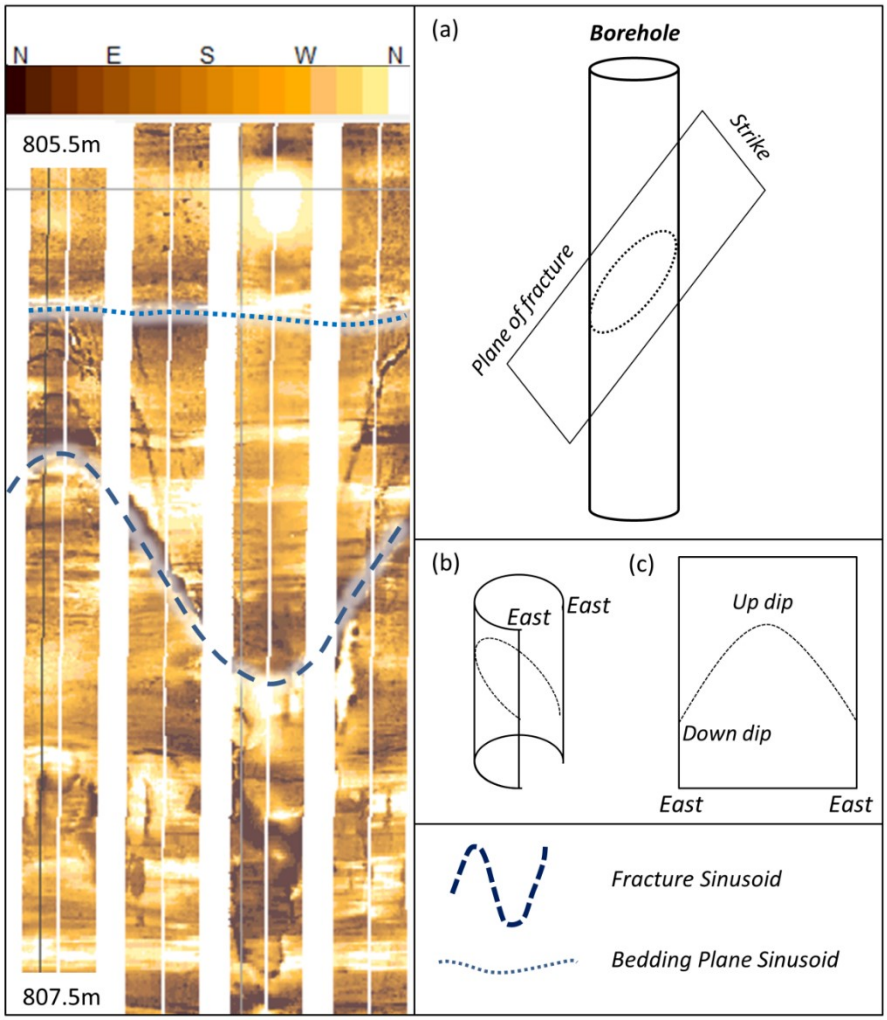

Fig. 4: *A schematic showing how wellbore image logs, in this case a Formation Micro Imager (FMI) (a) can be 'unfolded,' and interpreted in 2D (b and, c). After Burgin et al (2018).*

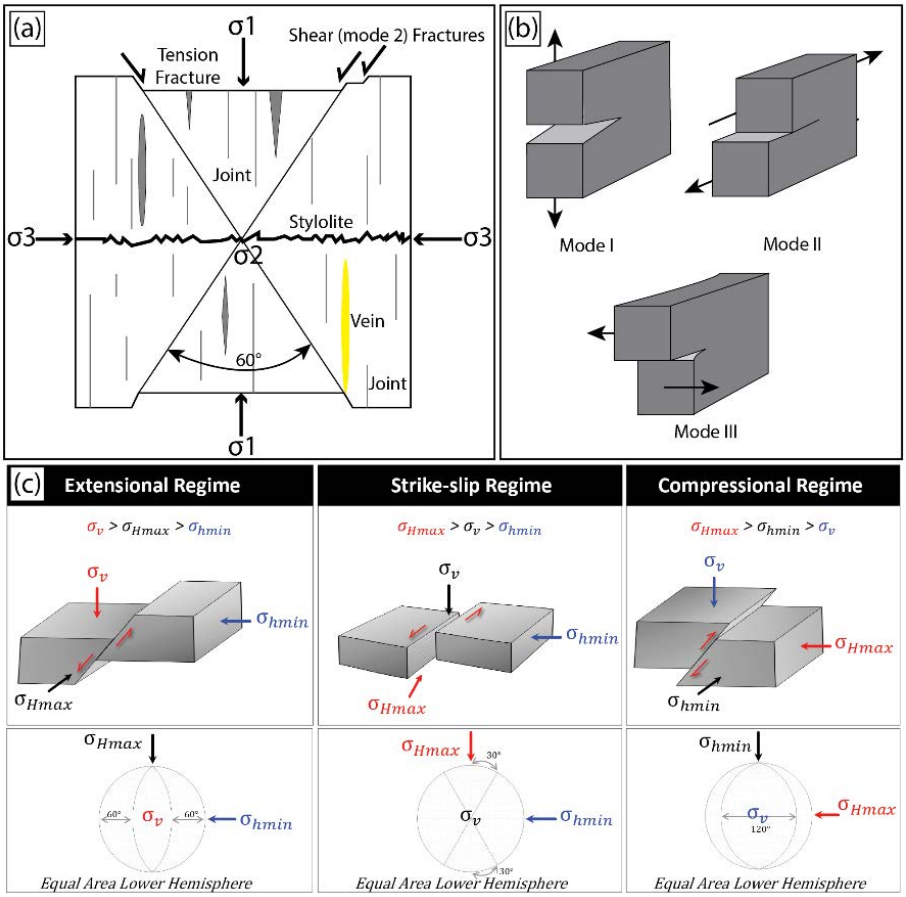

Fig. 5: *(a) A schematic diagram after Burgin et al., (2018) displaying the relationship between structural deformation features and the three principle stresses (b) The three primary modes of fracture formation (c) Text book relationships between Anderson's three principle stresses (Anderson, 1951) and fault and fracture formation.*

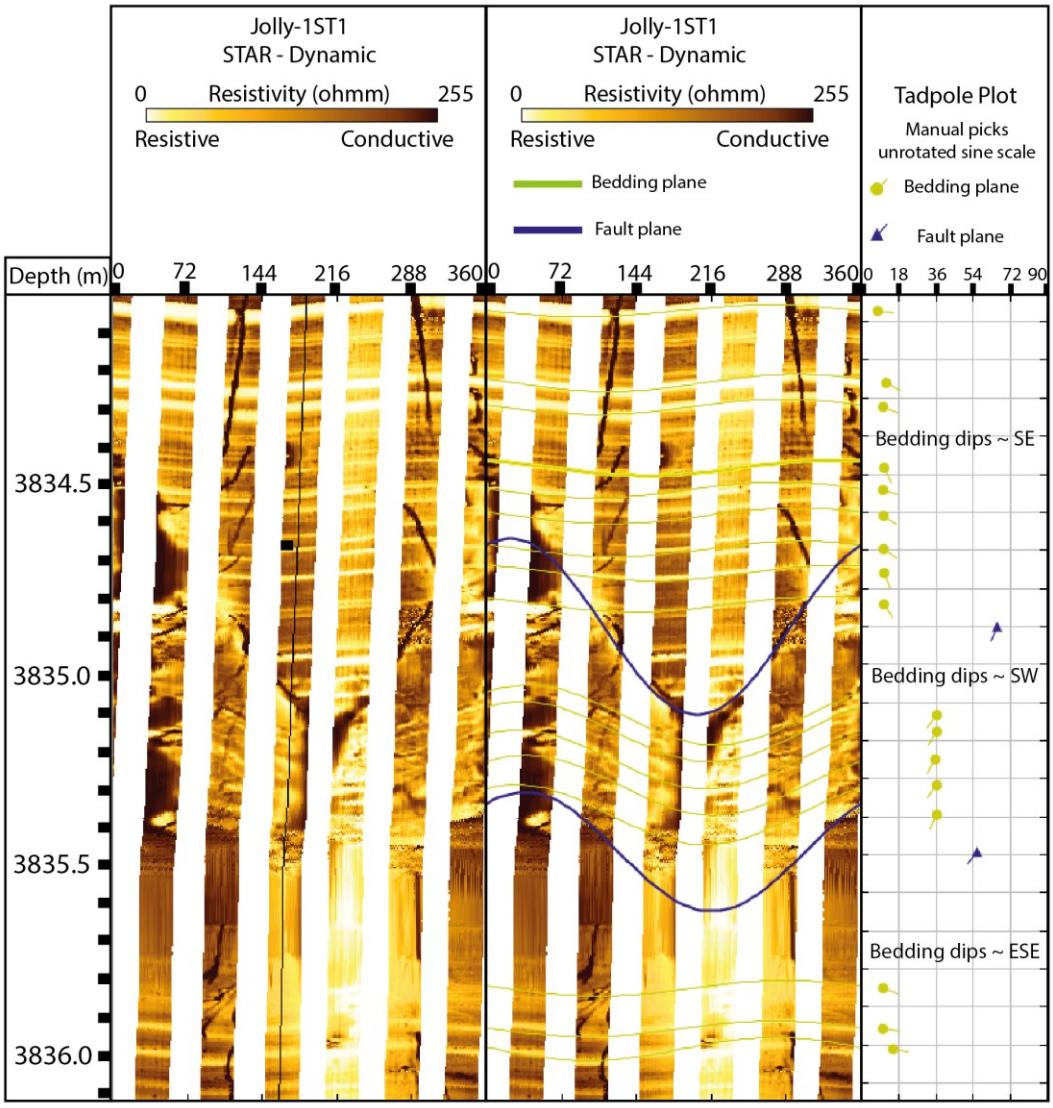

Fig.6: *Example of an interpreted fault within this study from Jolly-1/ST1. A fault zone is identified, not only along a sinusoidal features but by abrupt and distinct changes in bedding nature across the sinusoid. Bedding dips ~SE above the fault zone ~SW within it and then back to ~SE below.*

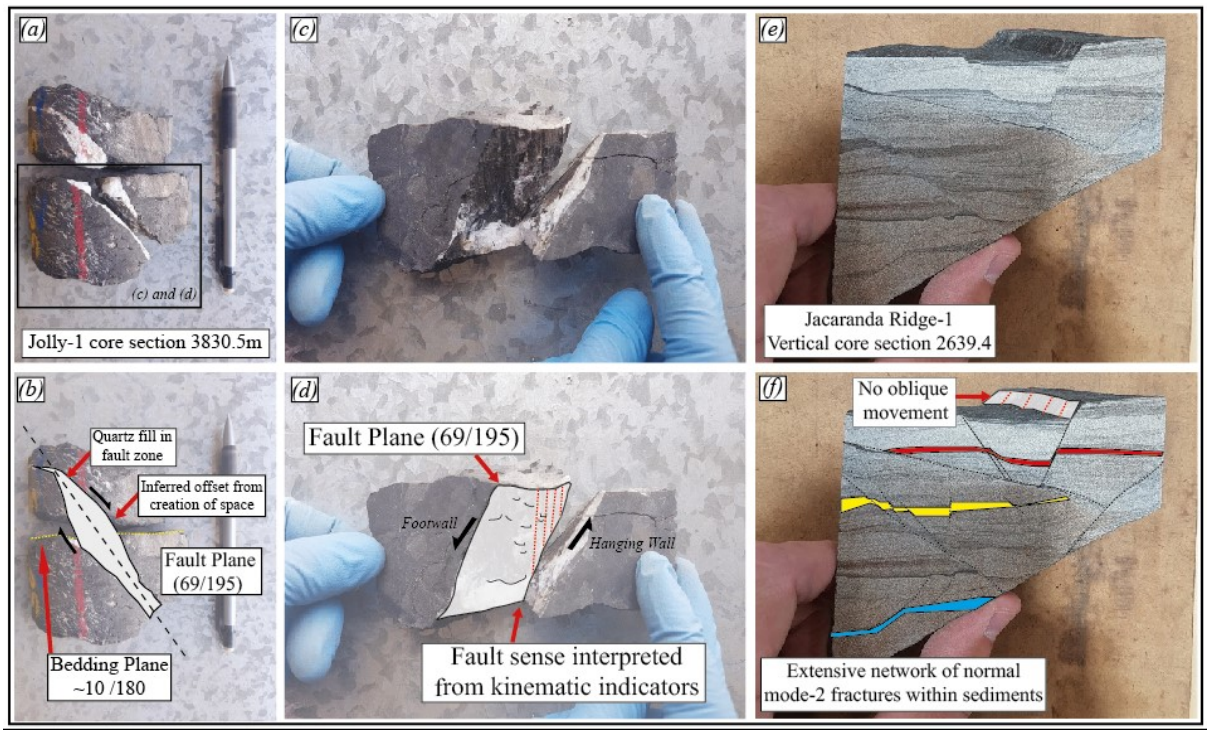

Fig. 7: *Jolly-1 ST1: (a) A picture of the filled fault plane within the Casterton member of the Otway Group with a mechanical pencil inserted for scale (b) annotation of the fault including the movement sense inferred from where space was created. The bedding plane used for re-orientation is also included (c) Kinematic indicators on the fault plane with fingers for scale (d) annotations of kinematic indicators (slickenlines and slickenslides) assisting us in inferring the sense of movement. Jacaranda Ridge-1: (e) An uninterrupted vertical core section from Jacaranda Ridge-1 within the Sawpit Shale member of the Otway Group (f) interpreted core section showing significant mode-2 style normal offset within the core. As this section is well above the image log interval within the well it was not able to be precisely reoriented but nevertheless displays significant evidence for complex extension.*

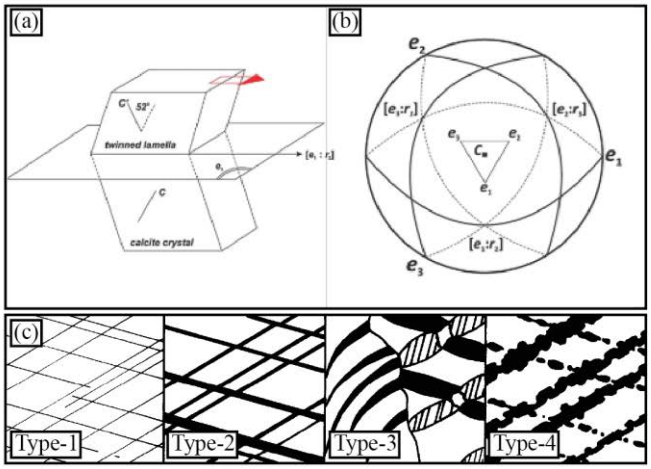

Type	Geometry	Interpretations	Temp
Type-1	-Thin twins -Straight -Rational -1,2 3 sets per grain	-Little deformation -Little cover -Low temp -Late stage	<200°C
Type-2	-Thick >1µm -Straight -Lense shaped -Rational	- Higher deformation -Completely twinned possible - Syn or post metamorphism	150 -300°C
Type-3	-Curved + thick -Twins in twins -High number -irrational	- Large deformation -Intracrystalline deformation - Syn metamophic deformation	>200°C
Type-4	-Thick + patchy -Sutured edges -Trails of grains -irrational	- Large deformation -Dynamic recrystallization - Pre or syn metamophic deformation	>250°C

Fig. 8: (a) Schematic diagram of a twin lamella in a calcite crystal (b) Stereographic projection (lower hemisphere, equal area) of the calcite twin planes. The central optical axis is vertical with poles to planes at 26.5º to the C axis. Planes of twinning are the three great circles. (c) Schematic illustrations of calcite twin types 1 -4 along with type descriptions in the neighboring table. (a) and (b) modified from Arboit et al. (2015) from Burkhard (1993) (c) along with table descriptions from Burkhard (1993).

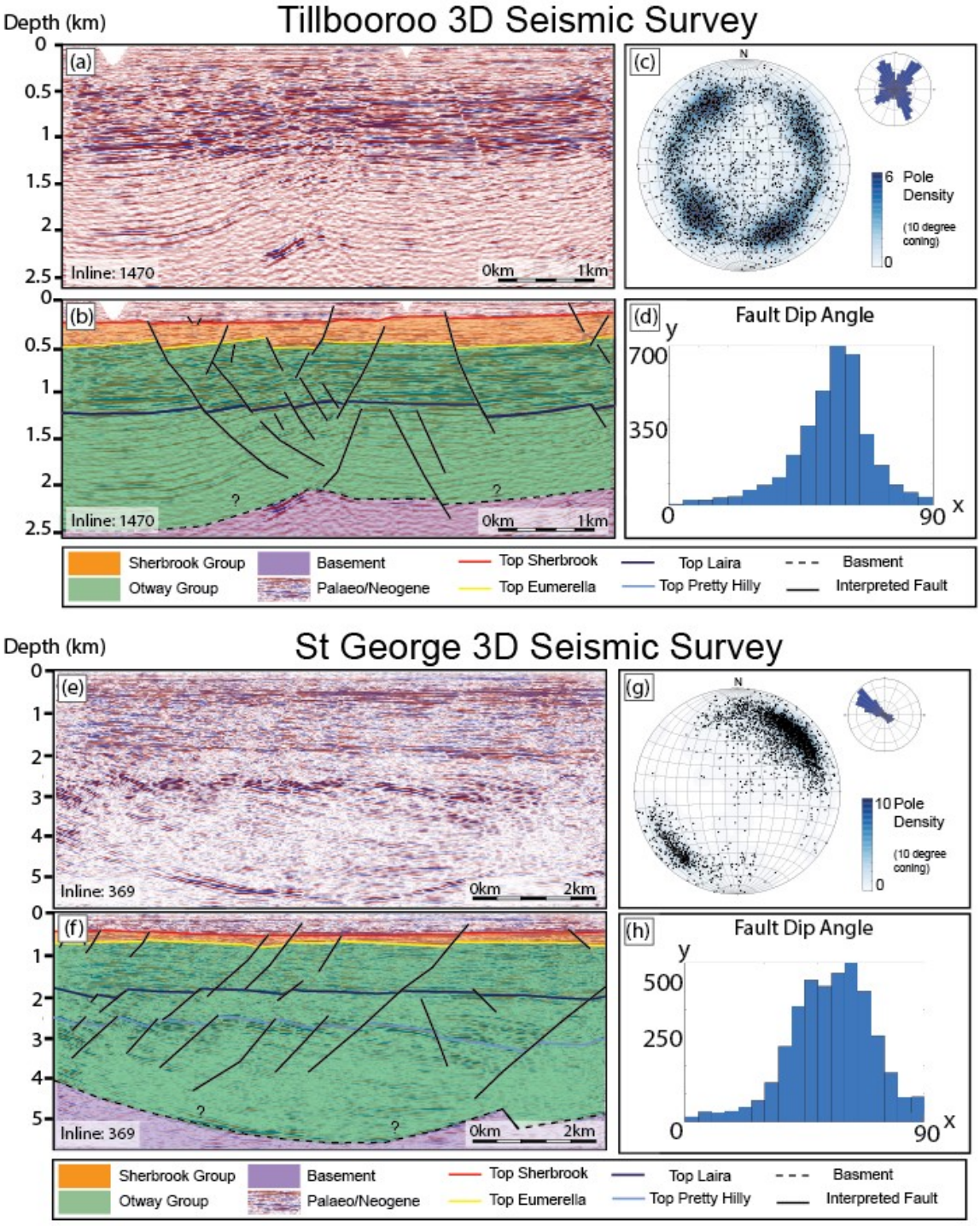

Fig. 9: *Seismic cross section and the results of our interpretation of the Tillbooroo 3D (a – d) and St George 3D (e –f). Of note is the clustering of poles within (c) and (g) that indicate the major fault sets within each survey. Also note the predominantly high angle nature of faults visible within the histogram displays in (d) and (h) an likely indicator, along with fault offset as to the extensive nature of the faults. x/y axes in histograms represent fault dip angles and fault count.*

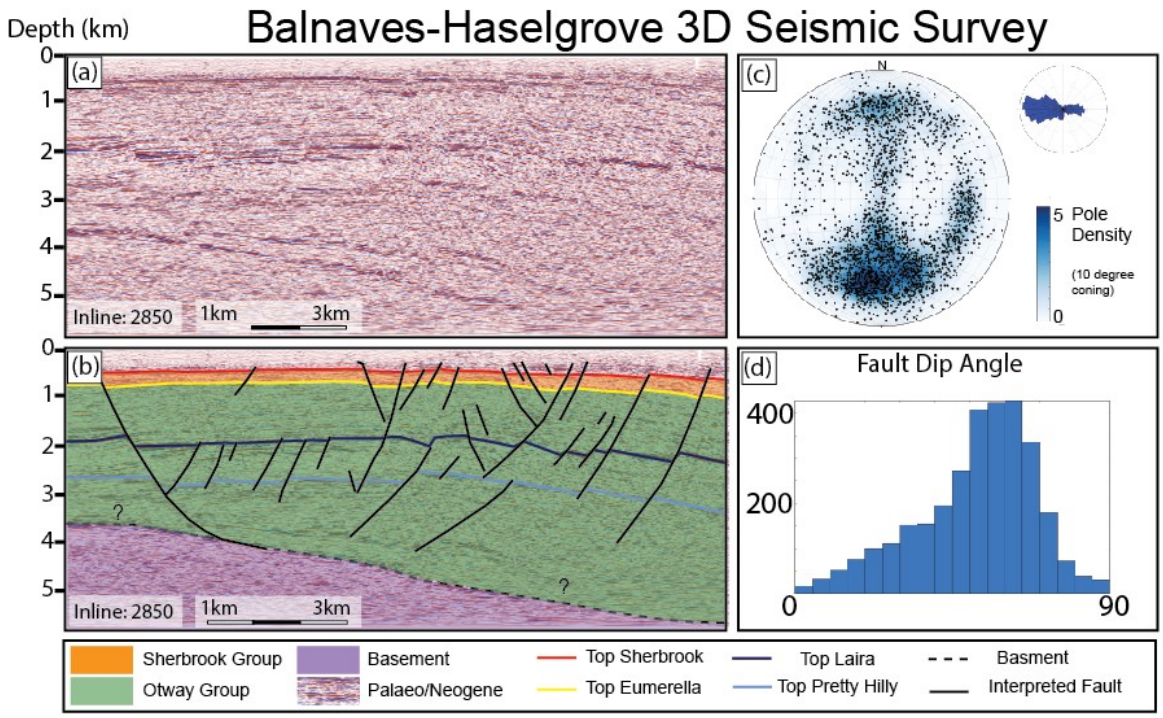

Fig. 10: *Un-interpreted (a) and interpreted (b) sections through the Balnaves-Haselgrove 3D survey. Showing the thickening of units within the hanging wall sections of faults (c) Poles to planes projection of interpreted faults displaying major sets where pole density is highest and (d) fault dip angle histogram. Low angle faults within this survey are interpreted as part of a gradual transition towards a low angle listric fault (b) and not a result of compressional paleostress environments. x/y axes in histograms represent fault dip angles and fault count.*

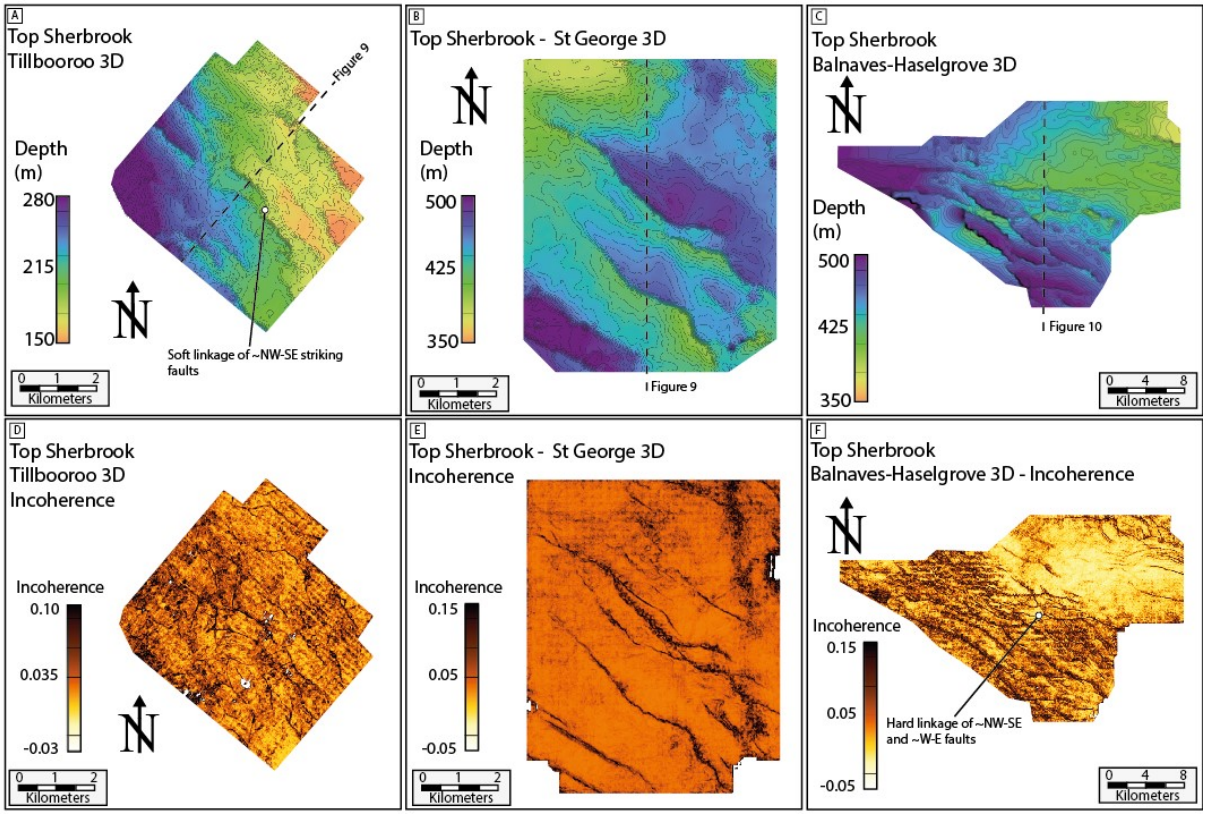

Fig. 11: *Depth to structure maps (a), (b), (c) and the incoherence attribute (d), (e), (f) of the Top Sherbrook group reflector within the Tillbooroo 3D, St George 3D and Balnaves-Haselgrove 3D surveys. Linkage between ~NW-SE and W-E striking faults can be seen within (f).*

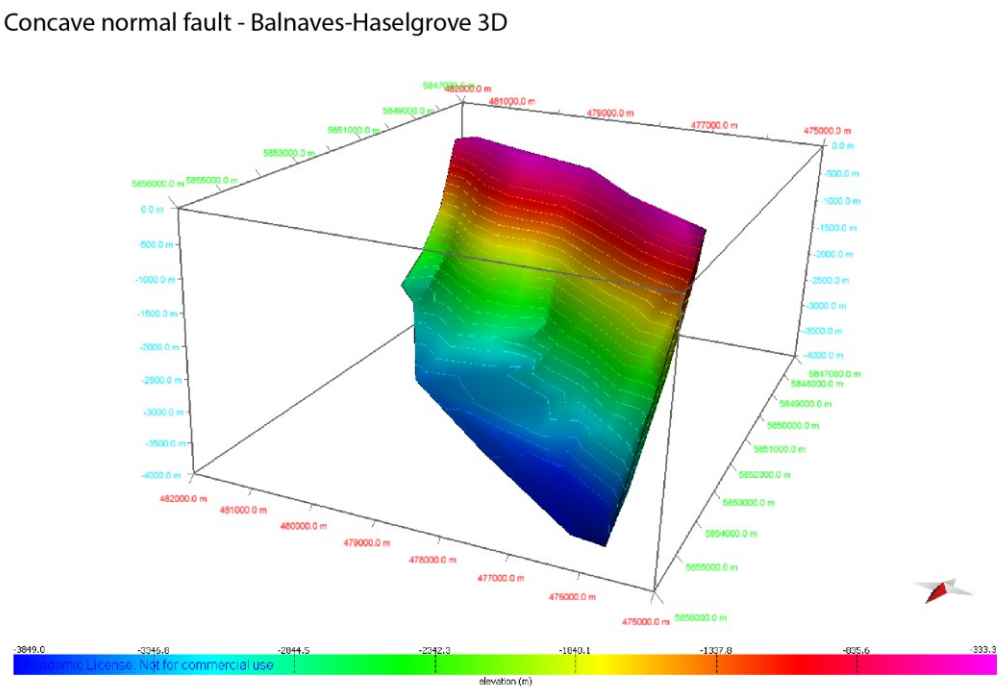

Fig. 12: *An example of an interpreted~ NW-SE striking fault plane taken from the Balnaves-HaselGrove 3D. Note the concave nature of the fault, the high angle and the ~ NE dip direction.*

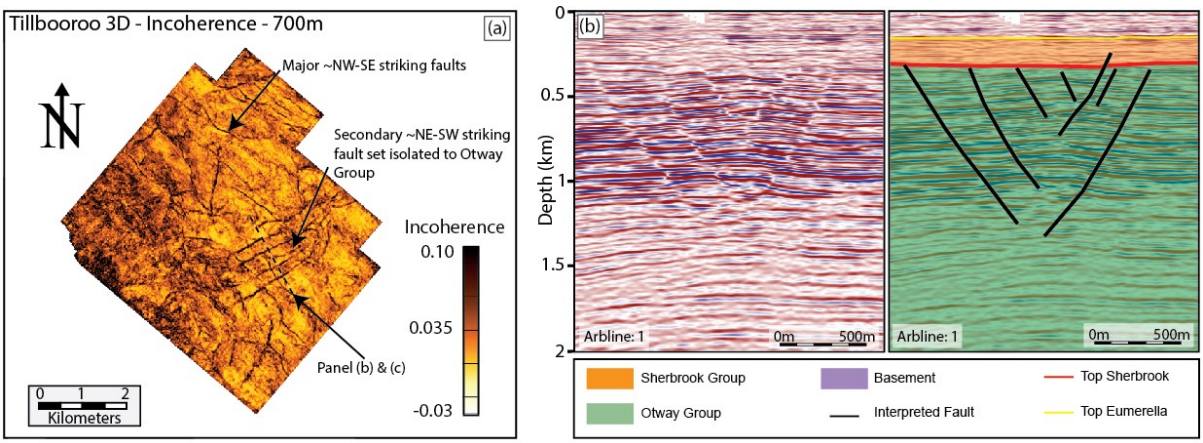

Fig. 13: *(a) A depth slice at 700m displaying the incoherence attribute through the Tillbooroo 3D survey, highlighting the tightly spaced NE-SW oriented fault network which cross cuts the major NW-SE faulting (b) un-interpreted arbitrary line through the survey (c) interpreted arbline through the survey showing the interpretation of the ~NE-SW trending fault network.*

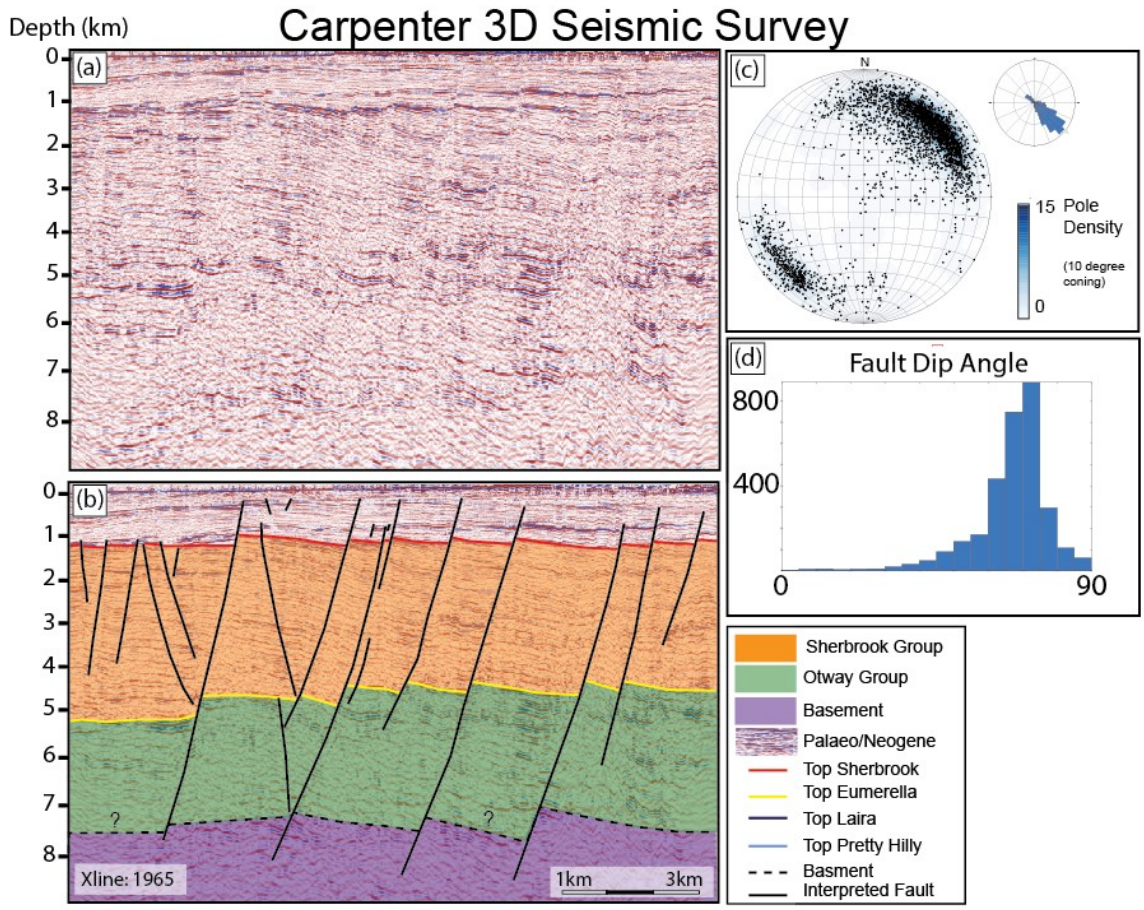

Fig. 14: Un-interpreted (a) and interpreted (b) sections through the Carpenter 3D survey. (c) Poles to planes projection of interpreted faults displaying the major ~NW-SE fault trend (d) Dip angles of fault interpreted within the survey. Of note is the extension of faults within panel (b) above the Top Sherbrook horizon and into Palaeogene sedimentary units in addition to the thickening of the Sherbrook Group within the hanging wall of large faults. Note the presence of both synrift faults – that show thickening of the unit, and post rift faults – which do not.

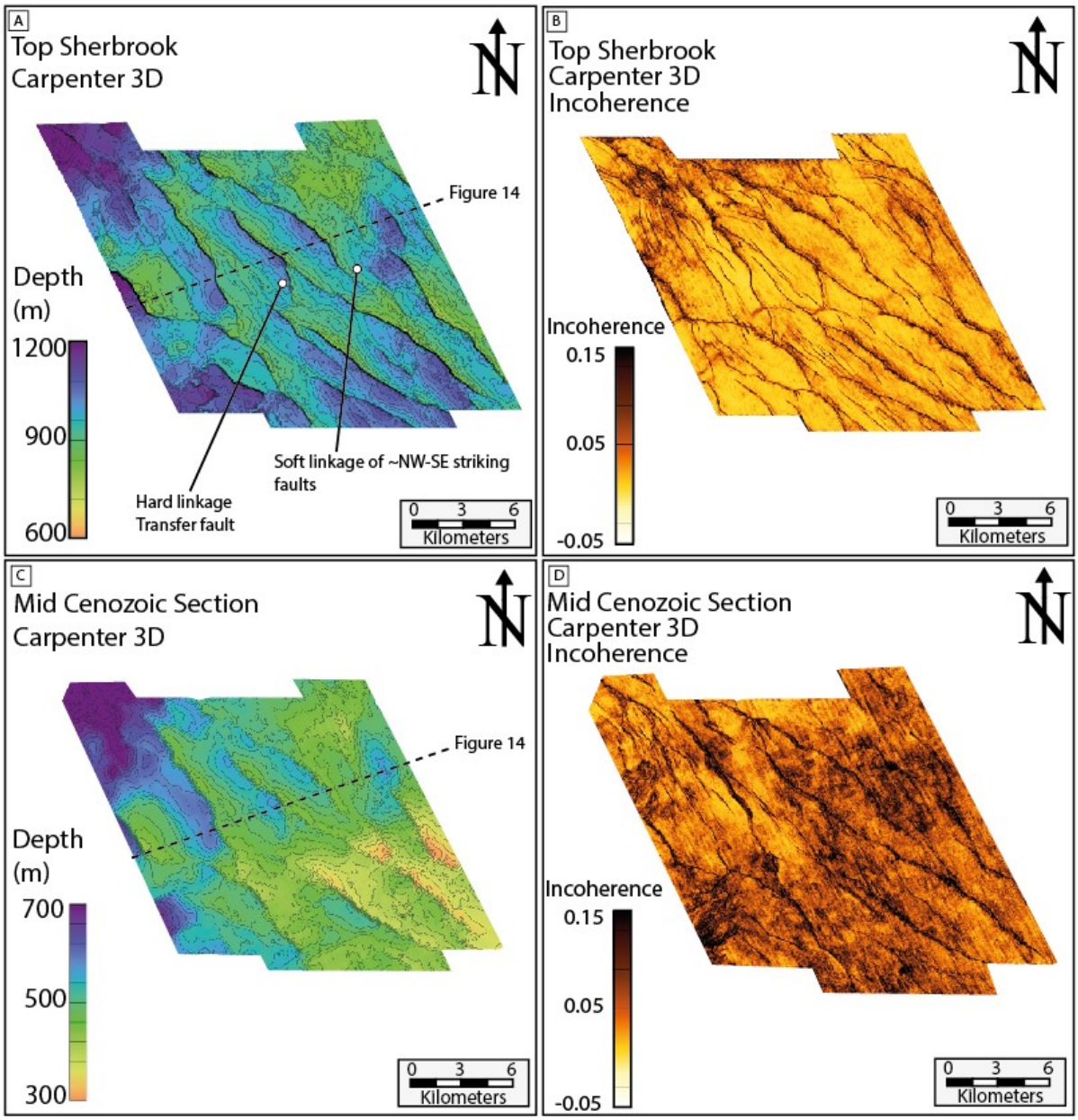

Fig. 15: *The Top Sherbrook and Mid Cenozoic reflector from the Carpenter 3D survey displayed as depth (a) and (c) and incoherence (b) and (d) which allows for a more distinct visualization of fault the major ~NW-SE striking fault trend. Note that in contrast to the on-shore surveys faults almost exclusively dip towards the SW.*

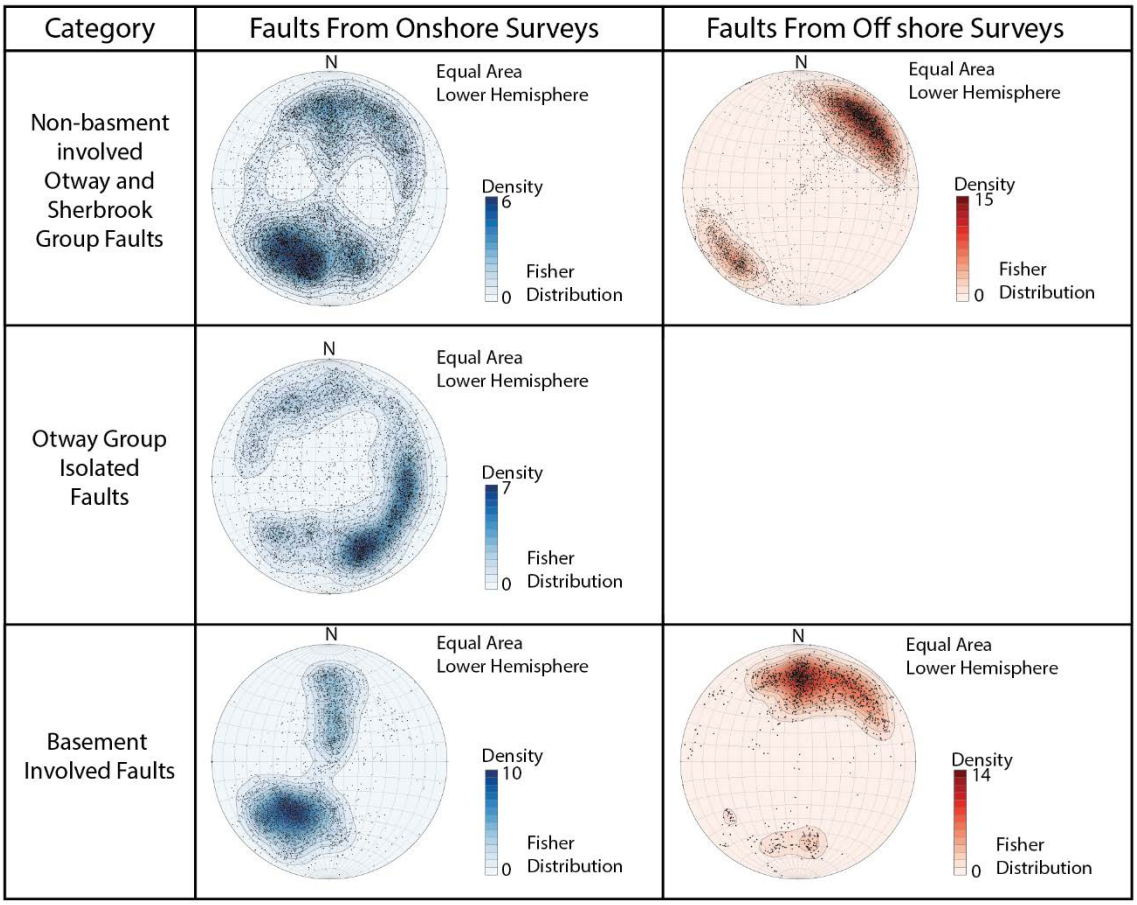

Fig. 16: *Amalgamated fault data from onshore and offshore sections of the western Otway Basin, divided into three formation specific categories. E-W striking and ~NW-SE striking fault comprise the majority of basement linked faults. NE-SW striking faults are largely isolated onshore, within the Otway Group sediments.*

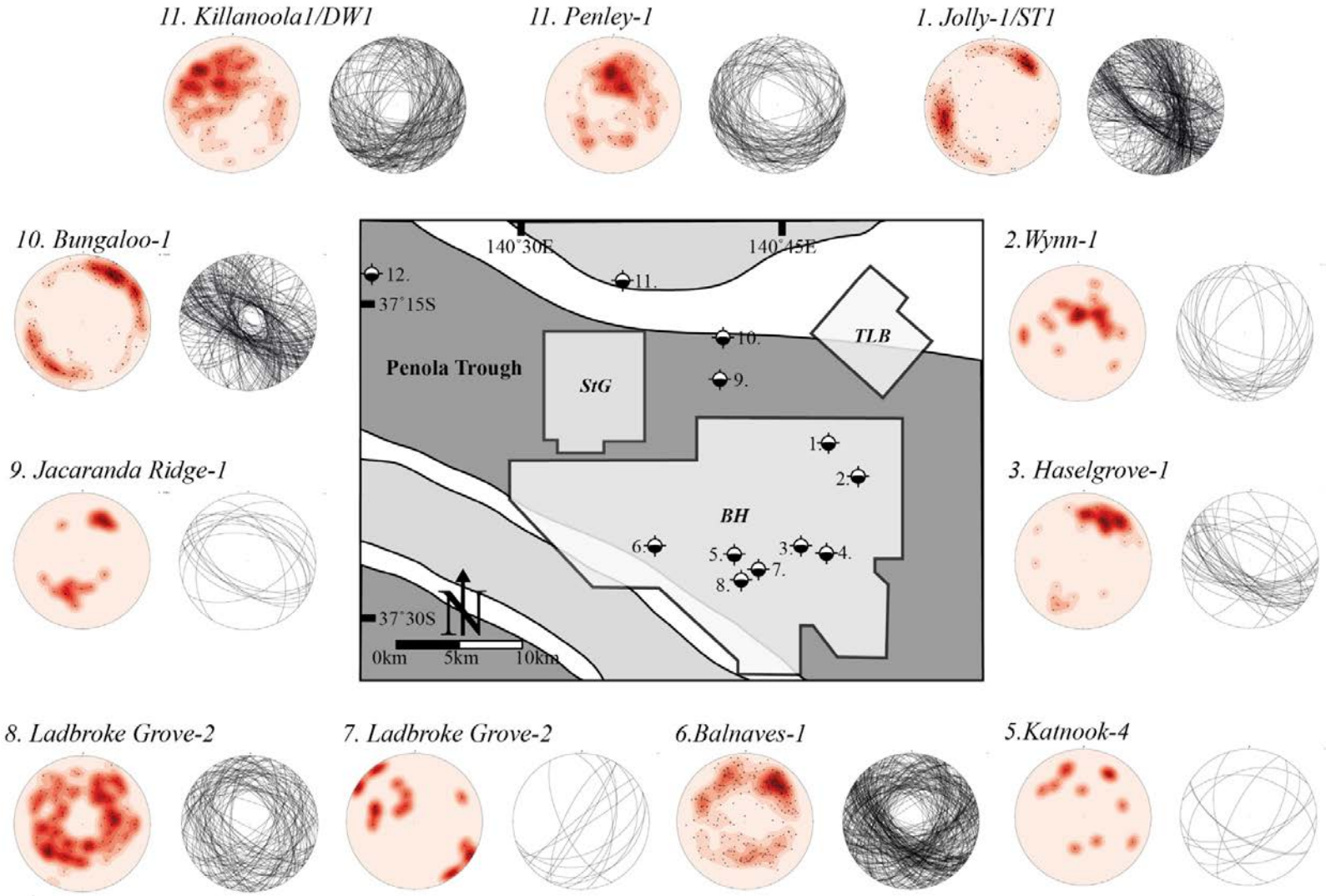

Fig. 17: Lower hemisphere stereonets displaying poles to planes and planes of all natural fracture data obtained from our image log interpretation.

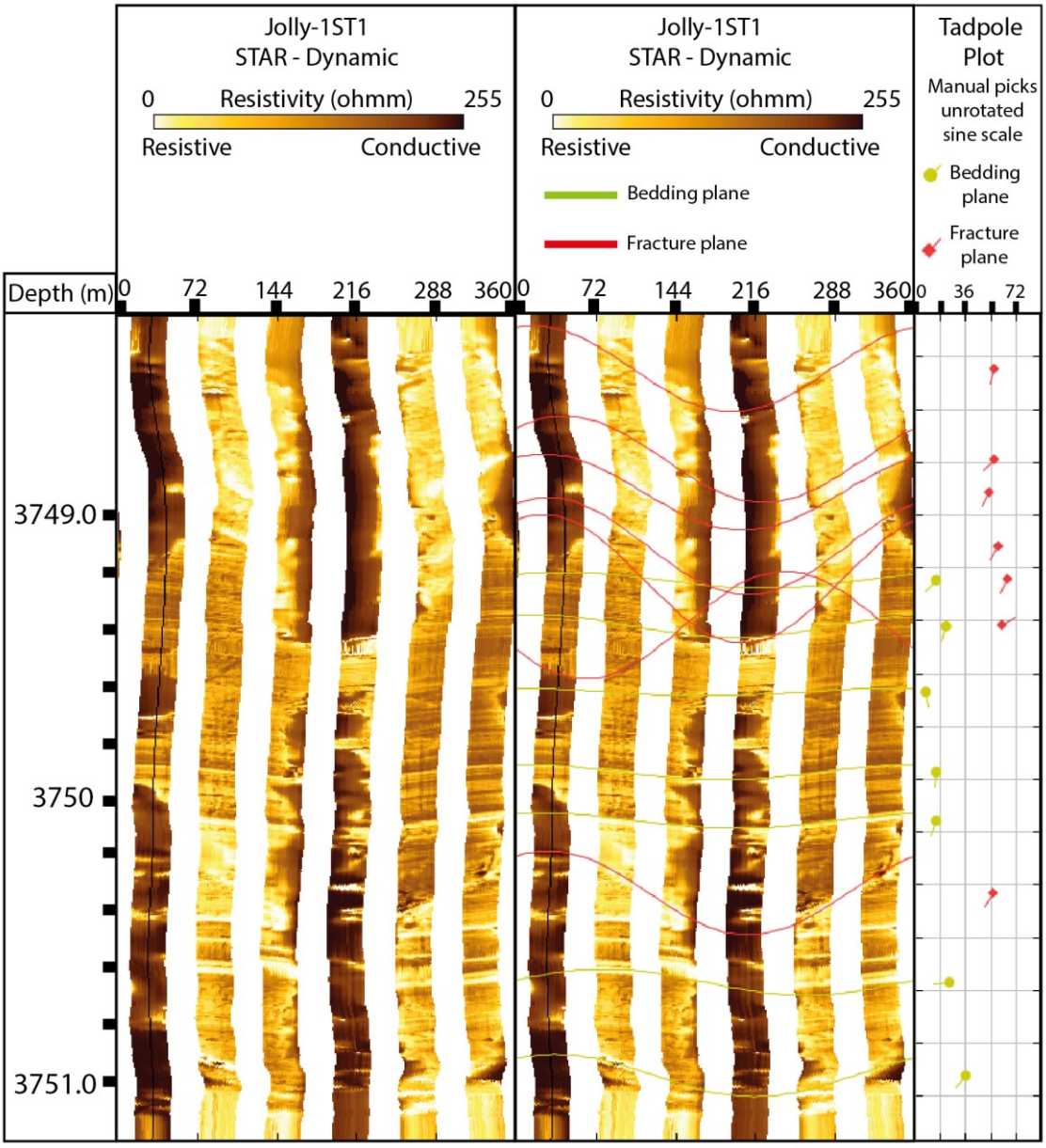

Fig. 18: An example of high angle, predominantly NW-SE striking natural fractures interpreted within the Jolly-1/ST1 well bore image log. There fractures are categorised as part of fracture set FRC-B and have been assigned a paleostress regime of ~NE-SW extension.

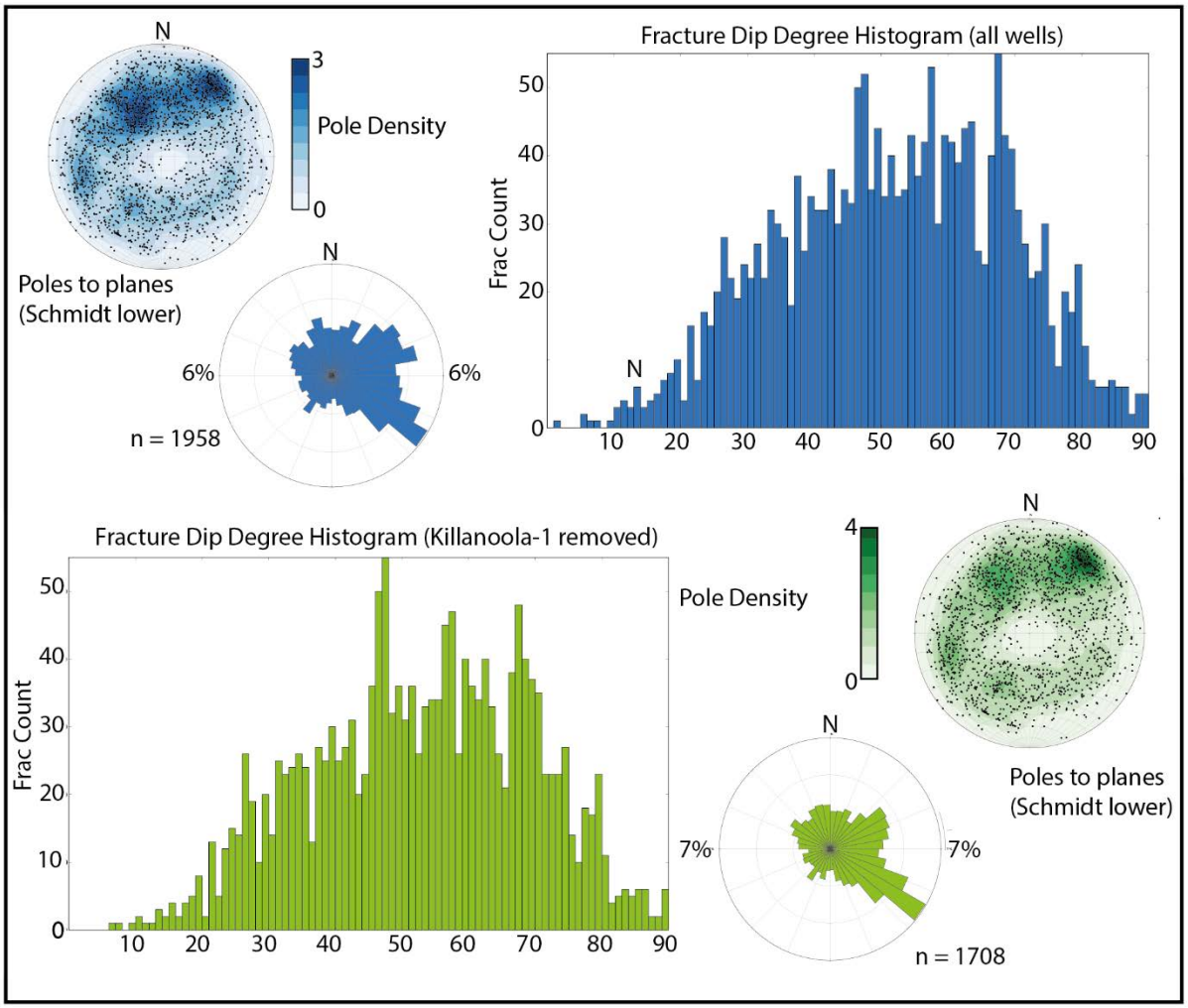

Fig. 19: Blue: All natural fractures from our interpretation. Green: All wells with fractures from Killanoola-1 removed. Note the high number of extensional fractures, from which determining individual sets would have been impossible without out structural data.

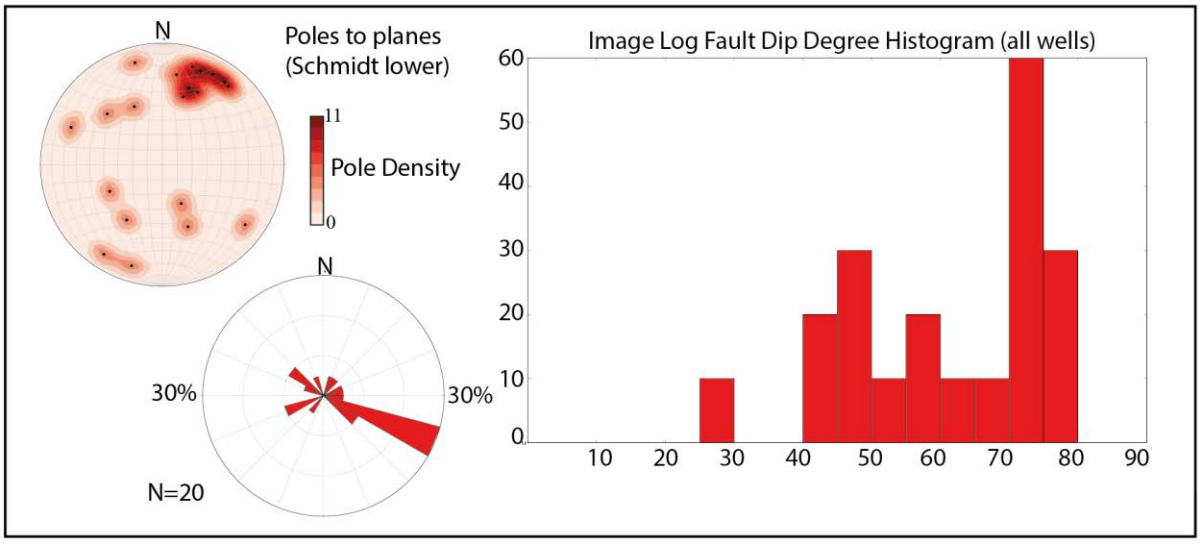

716
717
718 **Fig. 20:** All faults interpreted within the image log data of this study. Not the predominantly
719 high angle of most faults in addition to the mean ~NW-SE strike.

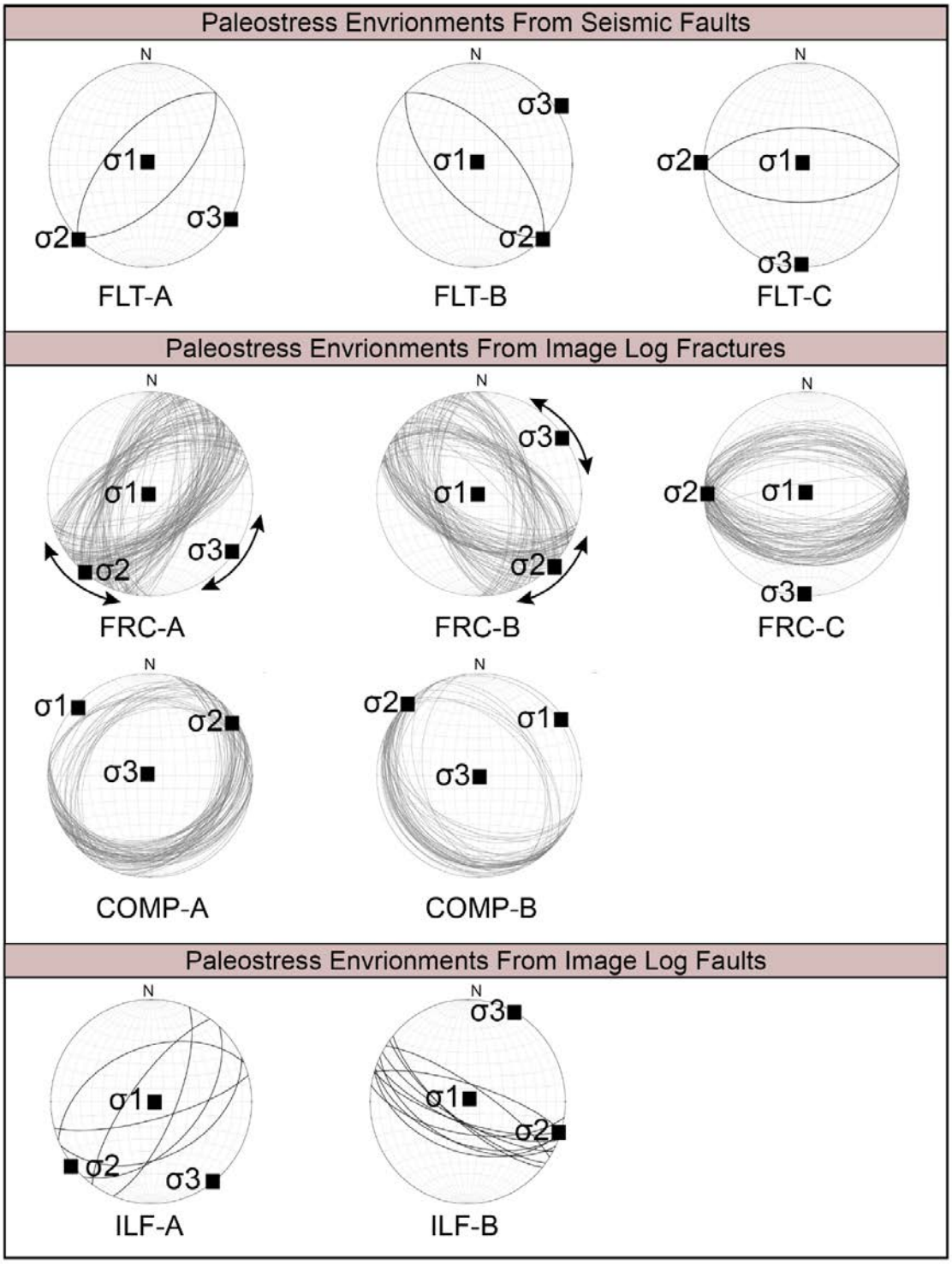

Fig. 21: *Paleostress tensors attributed to the formation of seismic scale faulting, natural fractures and faults from image logs determined through the method of analysis. For all fractures bedding is horizontal.*

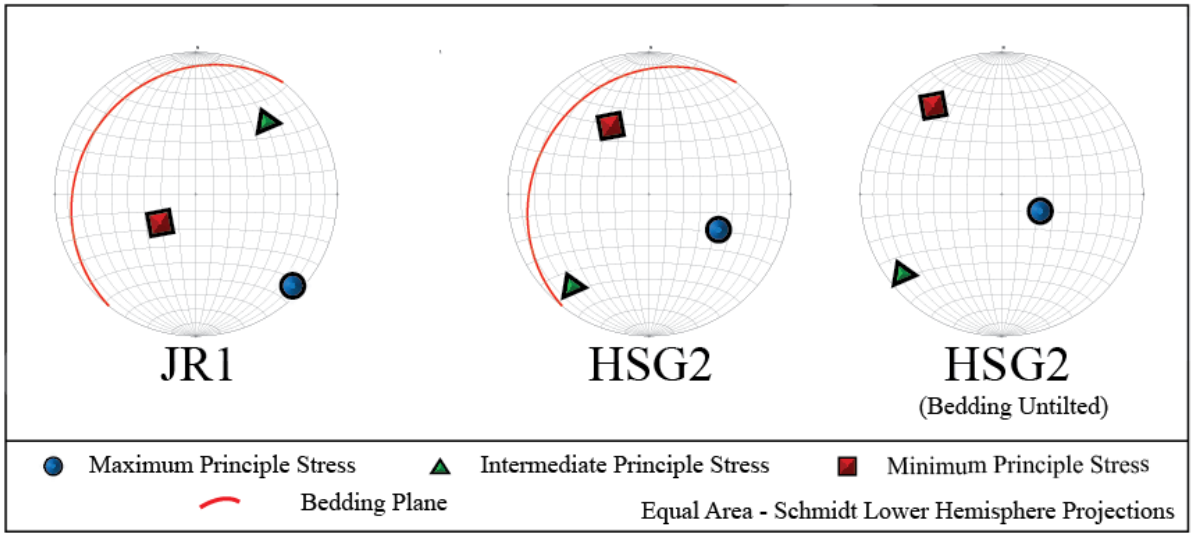

Fig. 22: *The two stress tensors produced from CSIT in this study. JR-1, a ~NW-SE compressional stress tensors and HSG-2 a ~NW-SE extensional stress tensor interpreted under backtilted bedding conditions.*

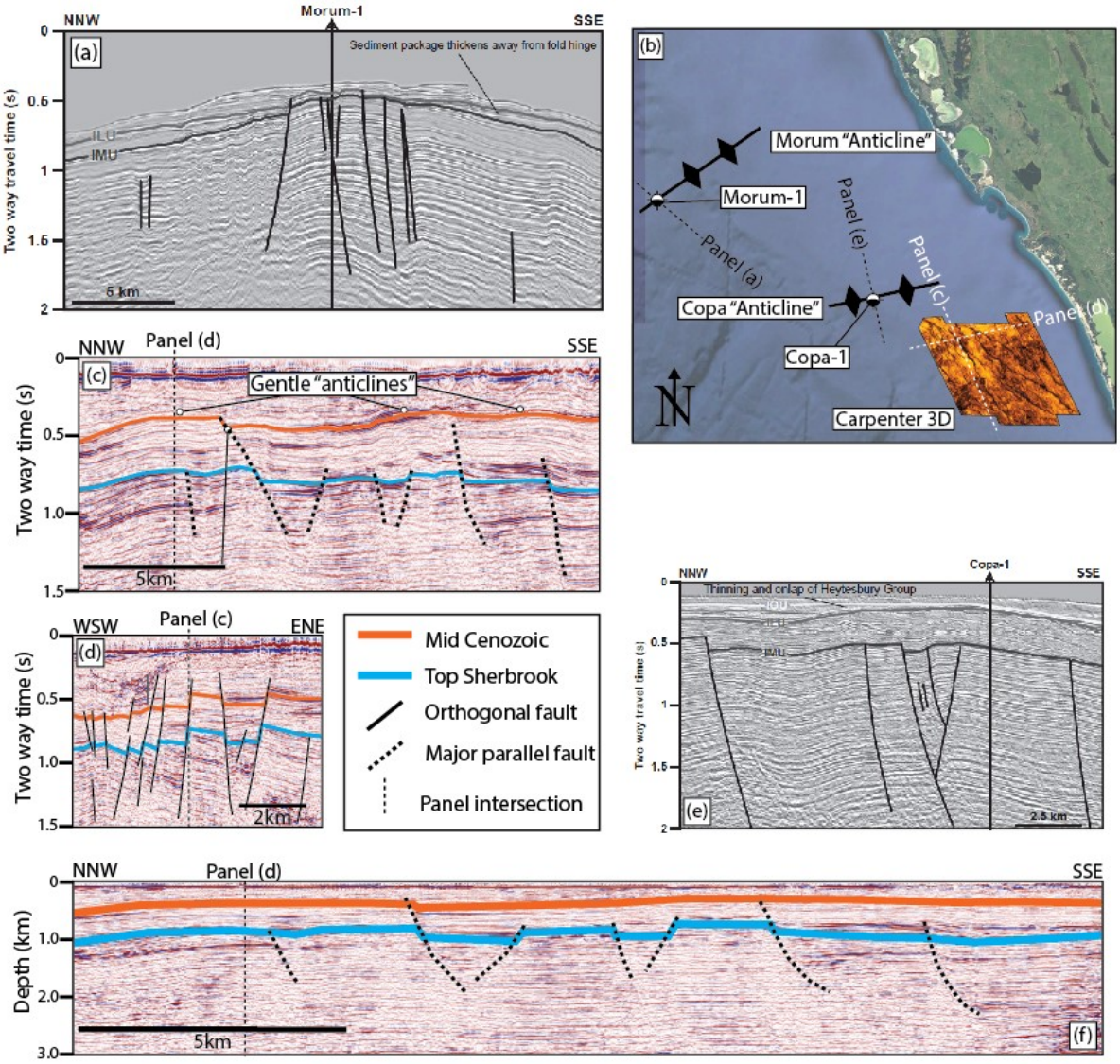
NNW
Morum-1
SSE
(a)
Sediment package thickens away from fold hinge
Two way travel time (s)
ILU
IMU
5 km
(b)
Morum "Anticline"
Morum-1
Panel (a)
Panel (e)
Panel (c)
Panel (d)
Copa "Anticline"
Copa-1
Carpenter 3D
N
NNW
Panel (d)
SSE
(c)
Gentle "anticlines"
Two way time (s)
5km
WSW
Panel (c)
ENE
(d)
2km
Mid Cenozoic
Top Sherbrook
Orthogonal fault
Major parallel fault
Panel intersection
NNW
Copa-1
SSE
Thinning and onlap of Heytesbury Group
TOU
ILU
IMU
Two way travel time (s)
(e)
2.5 km
NNW
Panel (d)
SSE
Depth (km)
5km
(f)

Figure 23: *A compilation of figures illustrating an example of the possible misinterpretation of offshore "anticlines" within previous studies. (a) interpreted cross section from Holford et al. (2014) showing the interpretation of the low amplitude Morum anticline (b) map showing the location of this line in addition to the local fold axes (Holford et al. 2014) along with the incoherence attribute displayed along the mid-Cenozoic horizon from this study (c) Inline through the Carpenter 3D parallel to the major fault trend, showing how line parallel faulting can cause apparent folding, especially in non-depth converted datasets which do not constrain the vertical to horizontal ratio (d) crossline through the Carpenter 3D showing the true structural architecture of the sub-surface and the "unfortunate" orientation of panel (c). (e) A second example from Holford et al. (2014) which likely represents the same scenario, interpretations from this study were likely greatly hindered by the inability to comprehensively determine fault geometry using only 2D data. (f) Depth converted version of panel (c) showing the drastic change in geometry of structures in the true geometry, where even apparent folds barely exist.*

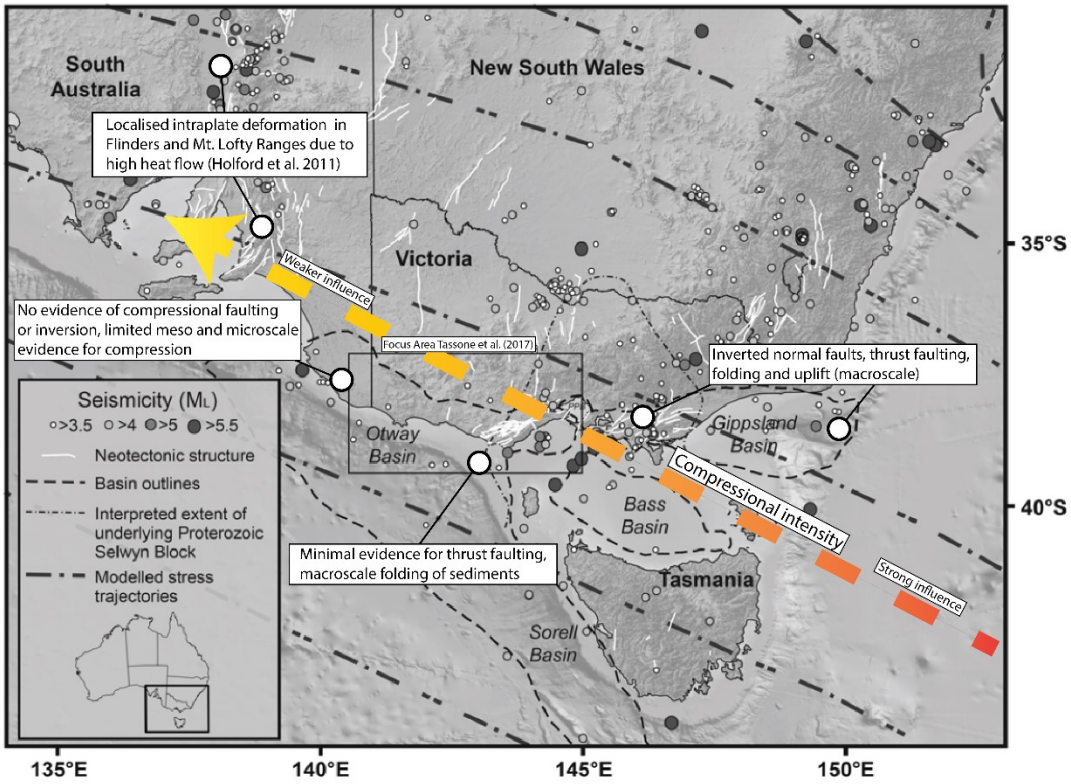

Fig. 24: *Stress and neotectonic map of south eastern Australia, showing the weaker influence of plate boundary compression moving from east to west. Modified from Tassone et al., (2017).*

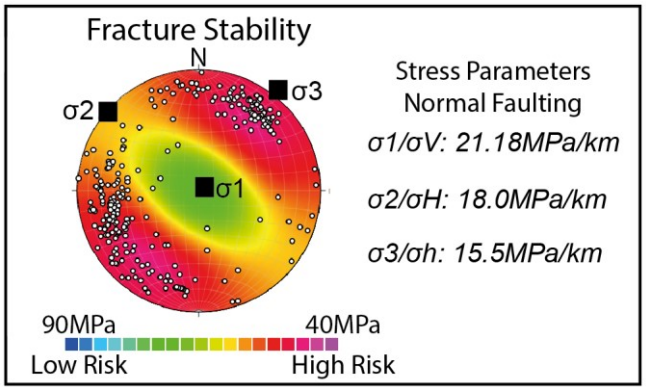

Fig. 25: *Results from the geomechanical modelling of natural fractures interpreted within the Jolly-1 well. Stress parameters were derived from Nelson et al. (2006) and Bailey et al. 2014, although the value of maximum horizontal stress was adjusted to reflect a possible over estimation and reflect a resultant extensive regime of in-situ stress. High angle fractures striking ~NW-SE such as those within FRC-B are found to be most susceptible to reactivation.*

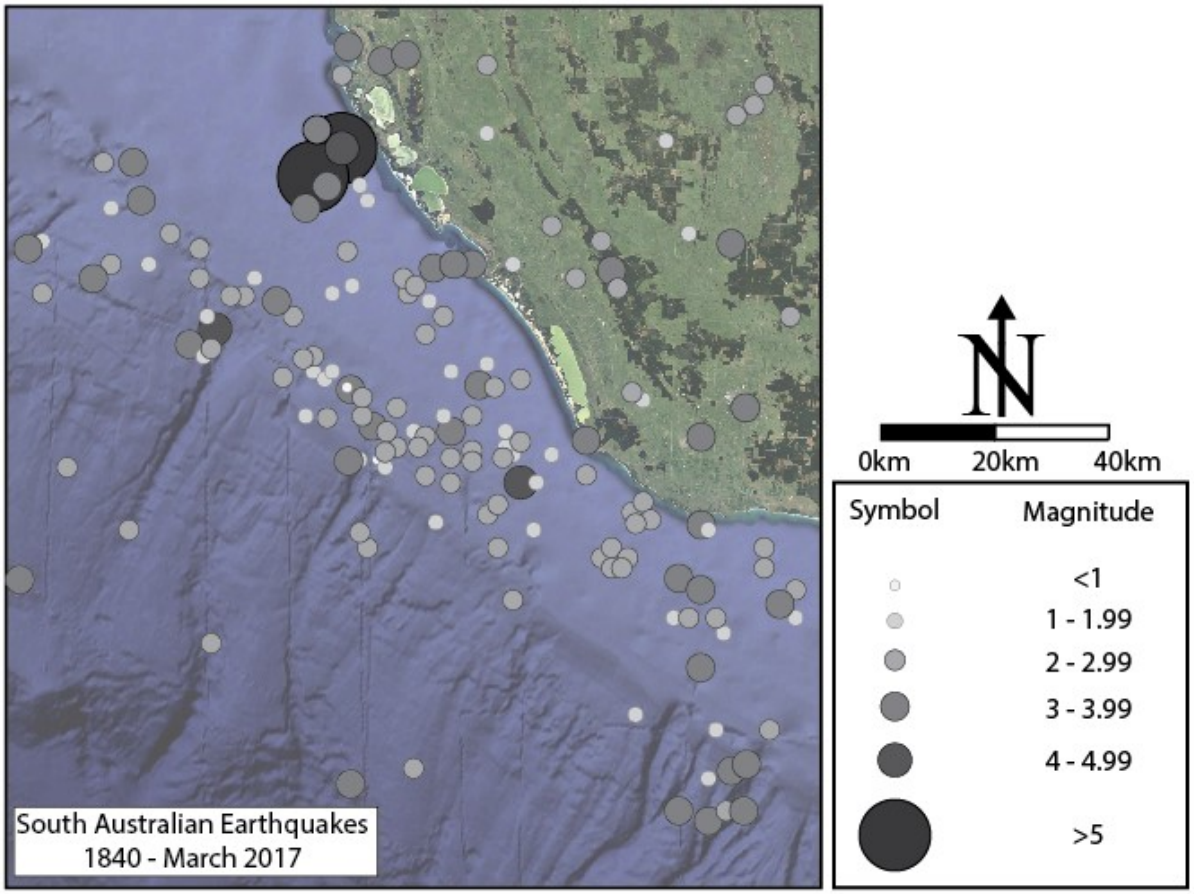

Fig. 26: *Map showing earthquakes within the western Otway Basin from 1840 to March 2017. Note the concentration of seismic activity in this sector of the basin around the continental shelf. While focal mechanisms have not been determined, the clustering around the shelf break suggests that many of these earthquakes may be controlled by downward gravitational extension. Earthquake data from Department of Energy and Mining (2019).*

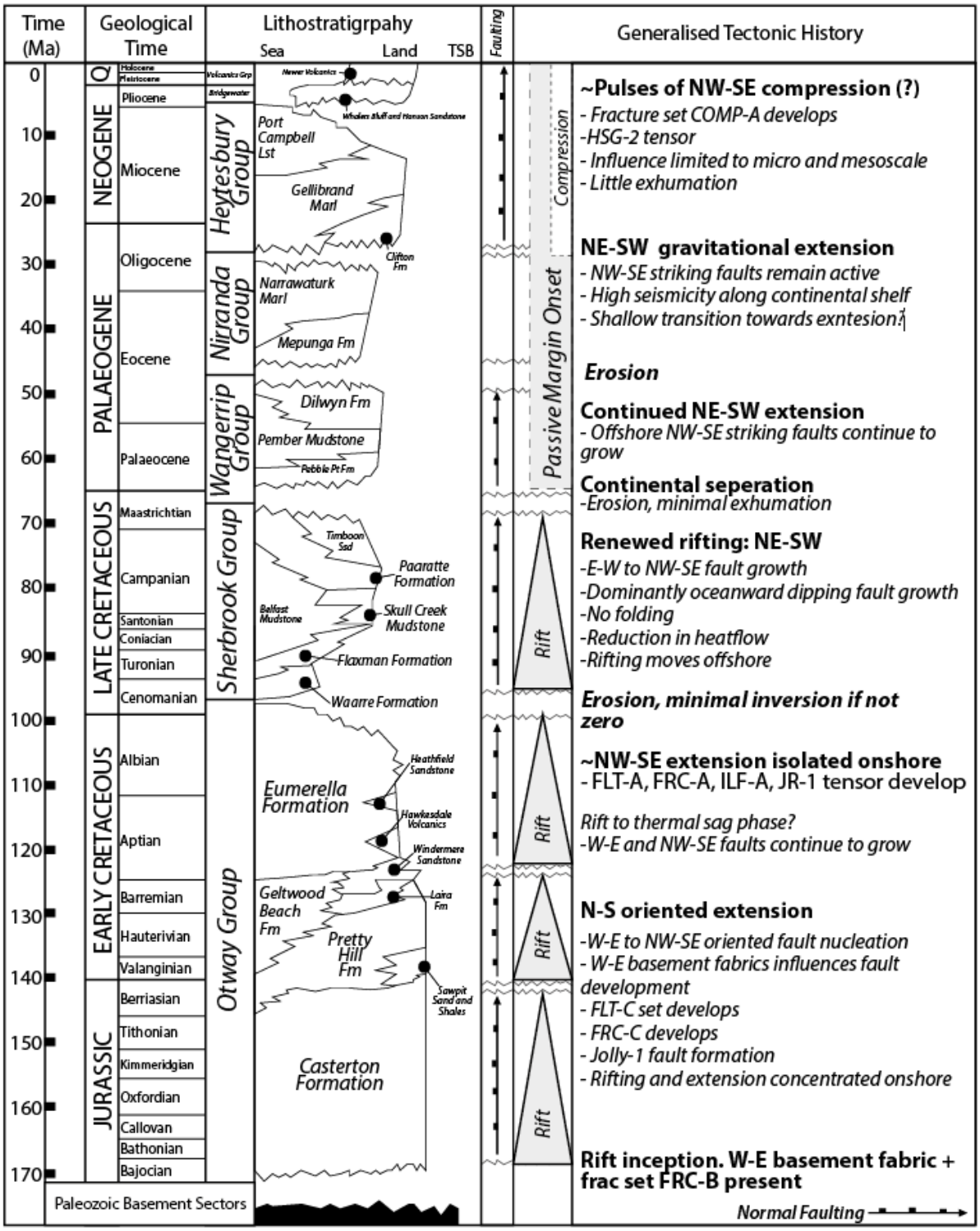

Fig. 27: *A stratigraphic column for the western Otway Basin after Tassone et al., (2017) after Geary and Reid (1998), including a revised generalised tectonic history based on the outcomes of this study.*

References

Amrouch, K., Lacombe, O., Bellahsen, N., Daniel, J. M., & Callot, J. P. (2010). Stress and strain patterns, kinematics and deformation mechanisms in a basement-cored anticline: Sheep Mountain Anticline, Wyoming. Tectonics, 29(1).

Amrouch, K. (2010). Contribution of microstructural analysis to the understanding of folding mechanisms: Examples of folded structures in the USA (Wyoming) and in Iran (Zagros) (Doctoral dissertation, University Pierre and Marie Curie-Paris VI).

Anderson, E. M. (1951). The dynamics of faulting and dyke formation with applications to Britain. Hafner Pub. Co.

Arboit, F., Amrouch, K., Collins, A. S., King, R., & Morley, C. (2015). Determination of the tectonic evolution from fractures, faults, and calcite twins on the southwestern margin of the Indochina Block. Tectonics, 34(8), 1576-1599.

Arboit, F., Amrouch, K., Morley, C., Collins, A. S., & King, R. (2017). Palaeostress magnitudes in the Khao Khwang fold-thrust belt, new insights into the tectonic evolution of the Indosinian orogeny in central Thailand. Tectonophysics, 710, 266-276.

Bailey, A., King, R., Holford, S., Sage, J., Backe, G., & Hand, M. (2014). Remote sensing of subsurface fractures in the Otway Basin, South Australia. Journal of Geophysical Research: Solid Earth, 119(8), 6591-6612.

838 Basir, H. M., Javaherian, A., & Yaraki, M. T. (2013). Multi-attribute ant-tracking and neural
839 network for fault detection: a case study of an Iranian oilfield. Journal of Geophysics and
840 Engineering, 10(1), 015009.
841
842 Bellahsen, N., Fiore, P., & Pollard, D. D. (2006). The role of fractures in the structural
843 interpretation of Sheep Mountain Anticline, Wyoming. Journal of structural Geology, 28(5),
844 850-867.
845
846 Briguglio, D., Hall, M., & Keetley, J. (2015). Structural evolution of the Early Cretaceous
847 depocentres, Otway Basin, Victoria. Australian Journal of Earth Sciences, 62(6), 717-733.
848
849 Burgin, H. B., Amrouch, K., Rajabi, M., Kulikowski, D., & Holford, S. P. (2018). Determining
850 paleo-structural environments through natural fracture and calcite twin analyses: a case study
851 in the Otway Basin, Australia. The APPEA Journal, 58(1), 238-254.
852
853 Burkhard, M. (1993). Calcite twins, their geometry, appearance and significance as stress-
854 strain markers and indicators of tectonic regime: a review. Journal of structural geology, 15(3-
855 5), 351-368.
856
857 Craddock, J. P., & van der Pluijm, B. A. (1999). Sevier–Laramide deformation of the
858 continental interior from calcite twinning analysis, west-central North America.
859 Tectonophysics, 305(1-3), 275-286.
860
861 Department for Energy and Mining, the Government of South Australia, Geoscientific Data,
862 Sourced on 7 January 2019, https://map.sarig.sa.gov.au/

Delvaux, D. (2012, April). Release of program Win-Tensor 4.0 for tectonic stress inversion: statistical expression of stress parameters. In Geophysical research abstracts (Vol. 14). EGU General Assembly Vienna.

Dresen, G. (1991). Stress distribution and the orientation of Riedel shears. Tectonophysics, 188(3-4), 239-247.

Duddy, I. R. (1994, April). The Otway Basin: thermal, structural, tectonic and hydrocarbon generation histories. In Extended abstracts, NGMA/PESA Otway Basin Symposium, Melbourne (Vol. 20, pp. 35-42).

Duddy, I. R. (2003). Mesozoic, a time of change in tectonic regime. Geology of Victoria, 23, 239-286.

Duddy, I. R., & Erout, B. (2001). AFTA-calibrated 2-D Modelling of Hydrocarbon Generation and Migration Using Temispack: Preliminary Results from the Otway Basin. Eastern Australasian Basins Symposium (485-497).

Etchecopar, A. (1984). Etude des états de contrainte en tectonique cassante et simulations de déformations plastiques: approche mathématique (Doctoral dissertation).

Etheridge, M., McQueen, H., & Lambeck, K. (1991). The role of intraplate stress in Tertiary (and Mesozoic) deformation of the Australian continent and its margins: a key factor in petroleum trap formation. Exploration Geophysics, 22(1), 123-128.

888 Faulkner, D. R., Jackson, C. A. L., Lunn, R. J., Schlische, R. W., Shipton, Z. K., Wibberley,
889 C. A. J., & Withjack, M. O. (2010). A review of recent developments concerning the structure,
890 mechanics and fluid flow properties of fault zones. Journal of Structural Geology, 32(11),
891 1557-1575.
892
893 Dickinson, J. A., Wallace, M. W., Holdgate, G. R., Gallagher, S. J., & Thomas, L. (2002).
894 Origin and timing of the Miocene-Pliocene unconformity in southeast Australia. Journal of
895 Sedimentary Research, 72(2), 288-303.
896
897 Finlayson, D. M., Cockshell, C. D., Finlayson, B., Johnstone, D. W., Reeves, C. V., Morse, M.
898 P., & Milligan, P. R. (1993). The Western Otway Basin? a tectonic framework from new
899 seismic, gravity and aeromagnetic data. Exploration Geophysics, 24(4), 493-500.
900
901 Gibson, G. M., Totterdell, J. M., White, L. T., Mitchell, C. H., Stacey, A. R., Morse, M. P., &
902 Whitaker, A. (2013). Pre-existing basement structure and its influence on continental rifting
903 and fracture zone development along Australia's southern rifted margin. Journal of the
904 Geological Society, 170(2), 365-377.
905
906 Glenton, P. N. (1991). Snapper Field--Australia Offshore Gippsland Basin, Southeast
907 Australia.
908
909 Groshong Jr, R. H. (1972). Strain calculated from twinning in calcite. Geological Society of
910 America Bulletin, 83(7), 2025-2038.
911

912 Hill, K. A., Cooper, G. T., Richardson, M. J., & Lavin, C. J. (1994). Structural framework of
913 the eastern Otway Basin: inversion and interaction between two major structural provinces.
914 Exploration Geophysics, 25(2), 79-87.
915
916 Hill, K. C., Hill, K. A., Cooper, G. T., O'Sullivan, A. J., O'Sullivan, P. B., & Richardson, M.
917 J. (1995). Inversion around the Bass basin, SE Australia. Geological Society, London, Special
918 Publications, 88(1), 525-547.
919
920 Holford, S., Hillis, R., Duddy, I., Green, P., Stoker, M., Tuitt, A., ... & MacDonald, J. (2011a).
921 Cenozoic post-breakup compressional deformation and exhumation of the southern Australian
922 margin. The APPEA Journal, 51(1), 613-638.
923
924 Holford, S. P., Hillis, R. R., Hand, M., & Sandiford, M. (2011b). Thermal weakening localizes
925 intraplate deformation along the southern Australian continental margin. Earth and Planetary
926 Science Letters, 305(1-2), 207-214.
927
928 Holford, S. P., Tuitt, A. K., Hillis, R. R., Green, P. F., Stoker, M. S., Duddy, I. R., Tassone, D.
929 R. (2014). Cenozoic deformation in the Otway Basin, southern Australian margin: implications
930 for the origin and nature of post-breakup compression at rifted margins. Basin Research, 26(1),
931 10-37. doi: 10.1111/bre.12035
932
933 King, R., Holford, S., Hillis, R., Tuitt, A., Swierczek, E., Backé, G., ... & Tingay, M. (2012).
934 Reassessing the in-situ stress regimes of Australia's petroleum basins. The APPEA Journal,
935 52(1), 415-426.
936

King, R., Backé, G., Tingay, M., Hillis, R., & Mildren, S. (2012). Stress deflections around salt diapirs in the Gulf of Mexico. Geological Society, London, Special Publications, 367(1), 141-153.

Krassay, A. A., Cathro, D. L., & Ryan, D. J. (2004). A regional tectonostratigraphic framework for the Otway Basin.

Kulikowski, D., & Amrouch, K. (2017). Combining geophysical data and calcite twin stress inversion to refine the tectonic history of subsurface and offshore provinces: A case study on the Cooper-Eromanga Basin, Australia. Tectonics, 36(3), 515-541.

Kulikowski, D., Amrouch, K., & Cooke, D. (2016). Geomechanical modelling of fault reactivation in the Cooper Basin, Australia. Australian Journal of Earth Sciences, 63(3), 295-314.

Lacombe, O. (2001). Paleostress magnitudes associated with development of mountain belts: Insights from tectonic analyses of calcite twins in the Taiwan Foothills. Tectonics, 20(6), 834-849.

Lacombe, O., Amrouch, K., Mouthereau, F., & Dissez, L. (2007). Calcite twinning constraints on late Neogene stress patterns and deformation mechanisms in the active Zagros collision belt. Geology, 35(3), 263-266.

960 Lacombe, O., & Laurent, P. (1996). Determination of deviatoric stress tensors based on
961 inversion of calcite twin data from experimentally deformed monophase samples: preliminary
962 results. Tectonophysics, 255(3-4), 189-202.
963
964 Lacombe, O., & Laurent, P. (1992). Determination of principal stress magnitudes using calcite
965 twins and rock mechanics data. Tectonophysics, 202(1), 83-93.
966
967 Lyon, P. J., Boult, P. J., Hillis, R. R., & Bierbrauer, K. (2007). Basement controls on fault
968 development in the Penola Trough, Otway Basin, and implications for fault-bounded
969 hydrocarbon traps. Australian Journal of Earth Sciences, 54(5), 675-689.
970
971 Moore, A. M. G., Stagg, H. M. J., & Norvick, M. S. (2000). Deep-water Otway Basin: a new
972 assessment of the tectonics and hydrocarbon prospectivity. The APPEA Journal, 40(1), 66-85.
973
974 Nelson, E., Hillis, R., Sandiford, M., Reynolds, S., & Mildren, S. (2006). Present-day state-of-
975 stress of southeast Australia. The APPEA Journal, 46(1), 283-306.
976
977 Norvick, M. S., & Smith, M. A. (2001). Mapping the plate tectonic reconstruction of southern
978 and southeastern Australia and implications for petroleum systems. The APPEA Journal, 41(1),
979 15-35.
980
981 O'Brien, G. W., Reeves, C. V., Milligan, P. R., Morse, M. P., Alexander, E. M., Willcox, J. B.
982 & Brodie, R. C. (1994). New ideas on the rifting history and structural architecture of the
983 western Otway Basin: evidence from the integration of aeromagnetic, gravity and seismic data.
984 The APPEA Journal, 34(1), 529-554.

Parlangeau, C., Lacombe, O., Schueller, S., & Daniel, J. M. (2018). Inversion of calcite twin data for paleostress orientations and magnitudes: A new technique tested and calibrated on numerically-generated and natural data. Tectonophysics, 722, 462-485.

Petkovic, P. and Geoscience Australia. (2004). Time-depth functions for the otway basin. Geoscience Australia Record, 2(2).

Prensky, S. E. (1999). Advances in borehole imaging technology and applications. Geological Society, London, Special Publications, 159(1), 1-43.

Price, N. J., & Cosgrove, J. W. (1990). Analysis of geological structures. Cambridge University Press.

Rajabi, M., Tingay, M., Heidbach, O., Hillis, R., & Reynolds, S. (2017). The Present-day stress field of Australia. Earth-Science Reviews, 168, 165-189.

Rajabi, M., Heidbach, O., Tingay, M., & Reiter, K. (2017). Prediction of the present-day stress field in the Australian continental crust using 3D geomechanical–numerical models. Australian Journal of Earth Sciences, 64(4), 435-454.

Reynolds, S. D., Coblentz, D. D., & Hillis, R. R. (2003). Influences of plate-boundary forces on the regional intraplate stress field of continental Australia. SPECIAL PAPERS-GEOLOGICAL SOCIETY OF AMERICA, 59-70.

1010 Robion, P., Grelaud, S., & de Lamotte, D. F. (2007). Pre-folding magnetic fabrics in fold-and-
1011 thrust belts: Why the apparent internal deformation of the sedimentary rocks from the
1012 Minervois basin (NE—Pyrenees, France) is so high compared to the Potwar basin (SW—
1013 Himalaya, Pakistan) Sedimentary Geology, 196(1-4), 181-200.
1014
1015 Robson, A. G., Holford, S. P., & King, R. C. (2017). Structural evolution of a normal fault
1016 array in the Gambier Embayment, offshore Otway Basin, South Australia: insights from 3D
1017 seismic data. Australian Journal of Earth Sciences, 64(5), 611-624.
1018
1019 Robson, A. G., Holford, S. P., & King, R. C. (2017). Structural evolution of a normal fault
1020 array in the Gambier Embayment, offshore Otway Basin, South Australia: insights from 3D
1021 seismic data. Australian Journal of Earth Sciences, 64(5), 611-624.
1022
1023 Robson, A. G., S. P. Holford, R. C. King, and D. Kulikowski (2018). Structural evolution of
1024 horst and half-graben structures proximal to a transtensional fault system determined using 3D
1025 seismic data from the Shipwreck Trough, offshore Otway Basin, Australia, Marine and
1026 Petroleum Geology, 89(3), 615-634, doi:10.1016/j.marpetgeo.2017.10.028.
1027
1028 Rocher, M., Cushing, M., Lemeille, F., Lozac'h, Y., & Angelier, J. (2004). Intraplate
1029 paleostresses reconstructed with calcite twinning and faulting: improved method and
1030 application to the eastern Paris Basin (Lorraine, France). Tectonophysics, 387(1-4), 1-21.
1031
1032 Sandiford, M. I. K. E. (2003). Neotectonics of southeastern Australia: linking the Quaternary
1033 faulting record with seismicity and in situ stress. SPECIAL PAPERS-GEOLOGICAL
1034 SOCIETY OF AMERICA, 107-120.

Sandiford, M., Wallace, M., & Coblentz, D. (2004). Origin of the in situ stress field in south-eastern Australia. Basin Research, 16(3), 325-338.

Schneider, C. L., Hill, K. C., & Hoffman, N. (2004). Compressional growth of the Minerva Anticline, Otway Basin, Southeast Australia—evidence of oblique rifting. The APPEA Journal, 44(1), 463-480.

Sibson, R. H. (2003). Thickness of the seismic slip zone. Bulletin of the Seismological Society of America, 93(3), 1169-1178.

Stearns, D. W., & Friedman, M. (1972). Reservoirs in fractured rock: Geologic exploration methods.

Tassone, D. R., Holford, S. P., Duddy, I. R., Green, P. F., & Hillis, R. R. (2014). Quantifying Cretaceous–Cenozoic exhumation in the Otway Basin, southeastern Australia, using sonic transit time data: Implications for conventional and unconventional hydrocarbon prospectivity. AAPG Bulletin, 98(1), 67-117.

Tassone, D. R., Holford, S. P., King, R., Tingay, M. R., & Hillis, R. R. (2017). Contemporary stress and neotectonics in the Otway Basin, southeastern Australia. Geological Society, London, Special Publications, 458, SP458-10.

1058 Teasdale, J. P., Pryer, L. L., Stuart-smith, P. G., & Loutit, M. A. E. T. S. (2003). Structural
1059 framework and basin evolution of Australia's southern margin. The APPEA Journal, 43, 12-
1060 35.
1061
1062 Tourneret, C., & Laurent, P. (1990). Paleo-stress orientations from calcite twins in the North
1063 Pyrenean foreland, determined by the Etchecopar inverse method. Tectonophysics, 180(2-4),
1064 287-302.
1065
1066 Trupp, M. A., Spence, K. W., & Gidding, M. J. (1994). Hydrocarbon prospectivity of the
1067 Torquay Sub-basin, offshore Victoria. The APPEA Journal, 34(1), 479-494.
1068
1069 Tarling, D., & Hrouda, F. (Eds.). (1993). Magnetic anisotropy of rocks. Springer Science &
1070 Business Media.
1071
1072 Williamson, P. E., Swift, M. G., O'Brien, G. W., & Falvey, D. A. (1990). Two-stage Early
1073 Cretaceous rifting of the Otway Basin margin of southeastern Australia: Implications for rifting
1074 of the Australian southern margin. Geology, 18(1), 75-78.
1075
1076 Zoback, M. L., Zoback, M. D., Adams, J., Assumpcao, M., Bell, S., Bergman, E. A., ... &
1077 Fuchs, K. (1989). Global patterns of tectonic stress. Nature, 341(6240), 291.
1078
1079 Zoback, M. D., Barton, C. A., Brudy, M., Castillo, D. A., Finkbeiner, T., Grollimund, B. R., ...
1080 & Wiprut, D. J. (2003). Determination of stress orientation and magnitude in deep wells.
1081 International Journal of Rock Mechanics and Mining Sciences, 40(7-8), 1049-1076.

Chapter 4.3.1: Manuscript 3

An integrated approach to determining 4D stress development at Castle Cove

This manuscript has been accepted as part of the proceedings of the Australian Petroleum Production and Exploration Association (APPEA) conference in 2019. It will be published in the association's journal following presentation at the conference in Brisbane in May, 2019.

Statement of Authorship

Title of Paper: An integrated approach to determining 4D stress development at Castle Cove

Publication Status: Accepted

Publication Details: Burgin, H. B., Amrouch, K., Robion P. and Kulikowski, D. (2019). An integrated approach to determining 4D stress development at Castle Cove. The APPEA Journal (Accepted)

Principal Author: Hugo Bonython Burgin

Contribution: Field work, calcite twin measurements, fracture measurements. AMS measurement. Data analysis. Writing of paper. (60%)

Certification: This paper reports on original research I conducted during the period of my Higher Degree by Research candidature and is not subject to any obligations or contractual agreements with a third party that would constrain its inclusion in this thesis. I am the primary author of this paper.

Signed: **Date:** 05/03/2019

Co-Author Contributions

By signing the Statement of Authorship, each author certifies that:

- **i.** The candidate's stated contribution to the publication is accurate (as detailed above);
- **ii.** Permission is granted for the candidate in include the publication in the thesis; and
- **iii.** The sum of all co-author contributions is equal to 100% less the candidate's stated contribution.

Name of Co-Author: Dr Khalid Amrouch

Contribution to Paper: Supervised project. Assisted with calcite twin, natural fracture and AMS and data interpretation (20%)

Signed: **Date:** 05/03/2019

Name of Co-Author: Dr Philippe Robion

Contribution to Paper: Assisted with AMS analysis interpretation (20%)

Signed: **Date:** 13/03/2019

Name of Co-Author: Dr David Kulikowski

Contribution to Paper: Assisted with field work (10%)

Signed: **Date:** 13/03/2019

The APPEA Journal 2019, **000**, 000–000
https://doi.org/10.1071/AJ18173

Peer reviewed paper

An integrated approach to determining 4D stress development at Castle Cove

Hugo B. Burgin[A,D], *Khalid Amrouch*[A], *Philippe Robion*[B] *and David Kulikowski*[A,C]

[A]Australian School of Petroleum, University of Adelaide, North Tce, 5005, Adelaide, Australia.
[B]Geosciences et Environnement University of Cergy-Pontoise, 33 Boulevard du Port, 95000 Cergy-Pontoise, France.
[C]Woodside Energy, Perth, Australia.
[D]Corresponding author. Email: hugo.burgin@adelaide.edu.au

Abstract. Models for basin evolution and natural fracture development often contain many uncertainties. Multiscale approaches to structural analysis assist in reducing these by providing checkpoints for structural evolution to better constrain the development of palaeostress phases through time. In this study, we integrate the analysis of calcite twins, magnetic fabrics, stylolites and natural fractures at Castle Cove in the eastern Otway Basin, producing a five-phase model for stress evolution consisting of: phase 1 ~NW–SE Mid-Cretaceous strike-slip or compression; phases 2 and 3 Late Cretaceous extension, coinciding with the development of ~NW–SE and ~NE–SW striking extensional fracture sets; phase 4 ~NE–SW strike-slip and compression, representing an enigmatic period of stress evolution with respect to the current understanding of the Otway Basin; and phase 5 present day ~NW–SE strike-slip stress. The results contribute to a 4D structural history construction for the eastern Otway Basin and suggest that the evolution of the region may require reassessing in order to determine the timing and nature of the detected ~NE–SW oriented compressional event. This study also demonstrates how the use of a calcite stress inversion technique can assist in providing mechanical checkpoints for the evolution of complex natural fracture networks, which can easily be expanded within the sub-surface.

Keywords: calcite, fracture, Otway Basin, palaeostress, tectonic.

Received 7 December 2018, accepted 1 March 2019, published online dd mmm yyyy

Introduction

When establishing models for basin evolution and fracture development, there are many unknowns; taking a multiscale approach by using microscale techniques, such as calcite twin and petrophysical analysis, assists in refining these models. Quantifying stress and strain through time and space has been extensively used to reduce these unknowns, providing quantitative palaeostress and strain checkpoints (e.g. Amrouch *et al*. 2010*a*, 2010*b*, 2011). Etchecopar's (1984) calcite stress inversion technique (CSIT) has by far been the most dominant method of calcite twin analysis over the last 40 years (Tavani *et al*. 2015; Beaudoin and Lacombe 2018).

The ability of calcite twin analysis to determine palaeostress (Etchecopar 1984; Laurent 1984; Burkhard 1993; Lacombe 2001; Lacombe *et al*. 2007) and palaeostrain (Groshong 1972, 1974; Groshong *et al*. 1984) has been proven in several tectonic environments, including the major fold-and-thrust belts of Zagros (Iran) (Amrouch *et al*. 2005; Lacombe *et al*. 2007; Amrouch *et al*. 2010*a*), Khao Khwang (Thailand) (Arboit *et al*. 2015), the Albanides (Albania) (Lacombe *et al*. 2009), the Rocky Mountains (Wyoming) (Craddock and van der Pluijm 1999; Amrouch *et al*. 2010*a*, 2010*b*; Beaudoin *et al*. 2012, 2016) and, more recently, in the Cooper and Eromanga basins of Australia (Kulikowski and Amrouch 2017). The integration of CSIT with petrophysical and natural fracture data has also been shown to provide a good constraint on rock physical strain (Amrouch *et al*. 2010*b*). Resultantly, the ability to upscale stress data from CSIT with higher order basin models and modern interpretations of geophysical well, 2D and 3D seismic data allows basin evolution models to be created with even greater accuracy and extrapolated in higher detail throughout the sub-surface (Kulikowski *et al*. 2018)

In this study, we present a multiscale analysis that integrates CSIT, magnetic fabric and natural fractures alongside a structural analysis from a special oriented sample 'Alice-18' (A-18) taken from Castle Cove in the eastern Otway Basin. In the scope of

previous research, we highlight the relevance of palaeostress inversion techniques in investigating sedimentary basins, emphasising the effectiveness of a multiscale approach as a useful tool for constraining fracture development and structural models for use within the petroleum industry, in both onshore and offshore provinces.

Geological setting

The Otway Basin (Fig. 1) trends largely NW–SE and occupies the onshore and offshore regions of South Australia, Victoria and Tasmania. It is of particular significance due to its status as one of Australia's commercial oil and gas provinces, in addition to hosting one of the country's major CO_2 burial experiments with additional potential for geothermal energy. Structural trends vary from west to east across the Otway Basin, a characteristic possibly explained by variations in basement architecture (Lyon *et al*. 2007; Gibson *et al*. 2011), with much of the western portion underlain by geological terranes comprising the regional Cambrian–Ordovician fold belt and the Mid-Palaeozoic Lachlan fold belt with a N–NNW striking boundary (Gibson *et al.* 2011). The eastern portion of the basin overlays the Neoproterozoic–Cambrian Selwyn-Taswegia Block, and the major N–S striking Avoca Shear Zone continues offshore as the Sorrel Fracture Zone (Gibson *et al*. 2011).

Initial rifting within the Otway Basin began during the Late Jurassic and gradually propagated eastwards during the break-up of Gondwana (Perincek and Cockshell 1995; Norvick and Smith 2001; Krassay *et al.* 2004). Extensional azimuths for this period of rifting have varied across a 90° arc, as suggested by numerous authors over the last 30 years, and include azimuths of NW–SE (Wilcox *et al*. 1992; O'Brien *et al.* 1994), N–S (Cooper and Hill 1997; Lyon *et al*. 2007) and NE–SW extension (Etheridge *et al.* 1985; Perincek *et al*. 1994). This period is characterised by NW–W striking elongate depocentres in the western portion of the basin with almost orthogonal N–E striking structures in the east (Fig. 1*b*).

A significant period of tectonic subsidence following the conclusion of early rift activity during the Aptian–Albian led to the deposition of the volcaniclastic and fluvio-lacustrine Eumeralla Formation, which outcrops at Castle Cove (Fig. 2*b*) and throughout the Otway Ranges (Fig. 2*a*). The Eumeralla is the host formation for this study, and with its intra-formational coal units, it is believed to be the key source for gas accumulations in the eastern Otway Basin (Edwards *et al*. 1999; Boreham *et al*. 2004). The Otway Basin is believed to have been subjected to a significant period of NW–SE compression, resulting in the inversion of the basin and fault formation during the Cenomanian and a basin wide unconformity that marks the top of the Eumeralla Formation, with no Cenomanian units preserved within the region (Krassay *et al*. 2004).

The Mid-Eocene (~43 Ma) marked the onset of an increase in the seafloor-spreading rate between Australia and Antarctica (Veevers 2000; McGowran *et al.* 2004). Most studies indicate that after this time period, the Otway Basin, along with most of the continent, was subjected to compressional stresses as a result of stress transfer from the Indo-Australian plate boundary (Sandiford and Quigley 2009; Holford *et al.* 2014). This compression is believed to have caused widespread inversion throughout multiple sedimentary basins in Australia (Dickinson *et al.* 2002; Holford *et al.* 2014), including the Otway Basin. The most significant later-stage compressional structures occur in the eastern section of the basin, in and around the Otway Ranges (Fig. 2) (Hill *et al.* 1995; Sandiford *et al.* 2004; Tassone *et al.* 2014), and comprise mostly ~NE–SW striking anticlinal structures, with most studies labelling them as either Miocene or Pliocene in age (Hill *et al*. 1995; Hillis *et al*. 2008).

It is worth noting that while this period of Miocene–Recent compression and fault inversion is widely accepted, there are a few cases where reverse fault offset or thrust faulting has been directly observed, which has puzzled many previous researchers (e.g. Schneider *et al*. 2004). As such, the reactivation of faults, in some cases, has often been inferred from surface geology or the presence of folding (e.g. Edwards *et al.* 1996).

Methodology

Our structural analysis at Castle Cove took place at four sites (Fig. 2*b*). Anisotropy of magnetic susceptibility (AMS) data was gathered from sites 1, 2 and 3, in addition to natural fracture data, while our CSIT sample, A-18, was gathered from site 4 at the western most end of cove. Due to difficult conditions accessing the fourth site, no AMS sample was able to be collected from this location.

Measuring palaeostress orientations with CSIT

Mechanical twinning within calcite crystals is a plastic-style deformation response to dislocation gliding along 'e-planes' within the crystal lattice (Fig. 3*a*) (Burkhard 1993). Twinning is the most common deformation mechanism of calcite and occurs at temperatures between 25°C and 400°C and in environments of low-confining pressure. It occurs at a resolved shear stress (RSS) of 10 ± 4 MPa (Amrouch 2010). The RSS is defined as the component of stress that is aligned with the direction of twinning, with its threshold dependent upon both grain size and previous internal deformation (Rowe and Rutter 1990; Laurent *et al.* 2000; Amrouch 2010; Parlangeau *et al*. 2019). The process of 'e-twinning' within the calcite crystal can be compared with a zone of perfect simple shear, due to the shift in position of the atoms within the lattice along the e-plane. For unmetamorphosed calcite, three of these planes exist within each crystal and are geometrically centred on the optical axis, 'C' (Fig. 3*b*).

The CSIT provides five of the six parameters needed for a complete tensor:

(1) Maximum principal stress orientation ($\sigma1$),
(2) Intermediate principal stress orientation ($\sigma2$),
(3) Minimum principal stress orientation ($\sigma3$),
(4) Differential stress ratio, (R; where $R = [\sigma2 - \sigma3]/[\sigma1 - \sigma3]$), and
(5) The peak differential stress ($\sigma1 - \sigma3$).

In this study, we restrict our analysis to the first four parameters, known as the reduced stress tensor, T′. CSIT begins with a process of trial and error, applying multiple experimental stress tensors to the dataset, with the total components of T′ being calculated for each scenario. Theoretically, a 'perfect' tensor is found for any sample when all twined planes are consistent with a given tensor, although the

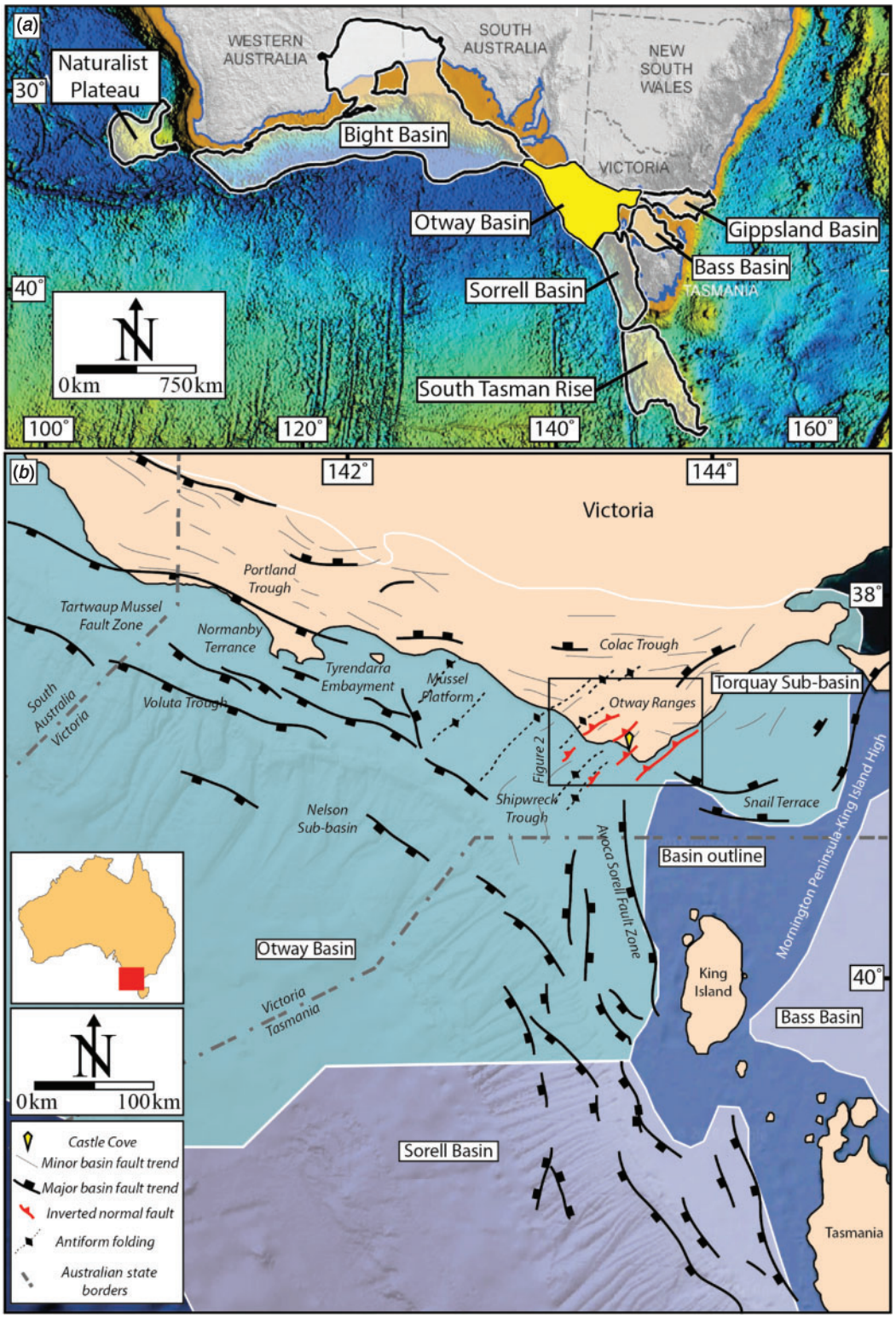

Fig. 1. (*a*) A map of the Australian southern margin showing the location of the Otway Basin (modified from Stacey *et al*. (2013)). (*b*) Structural map of the eastern Otway Basin (modified from Stacey *et al*. (2013)) showing the presence of two distinct structural fabrics within the region. Inverted normal faults are taken from Debenham *et al*. (2018) and Holford *et al*. (2014). Location of Fig. 2 is also inserted.

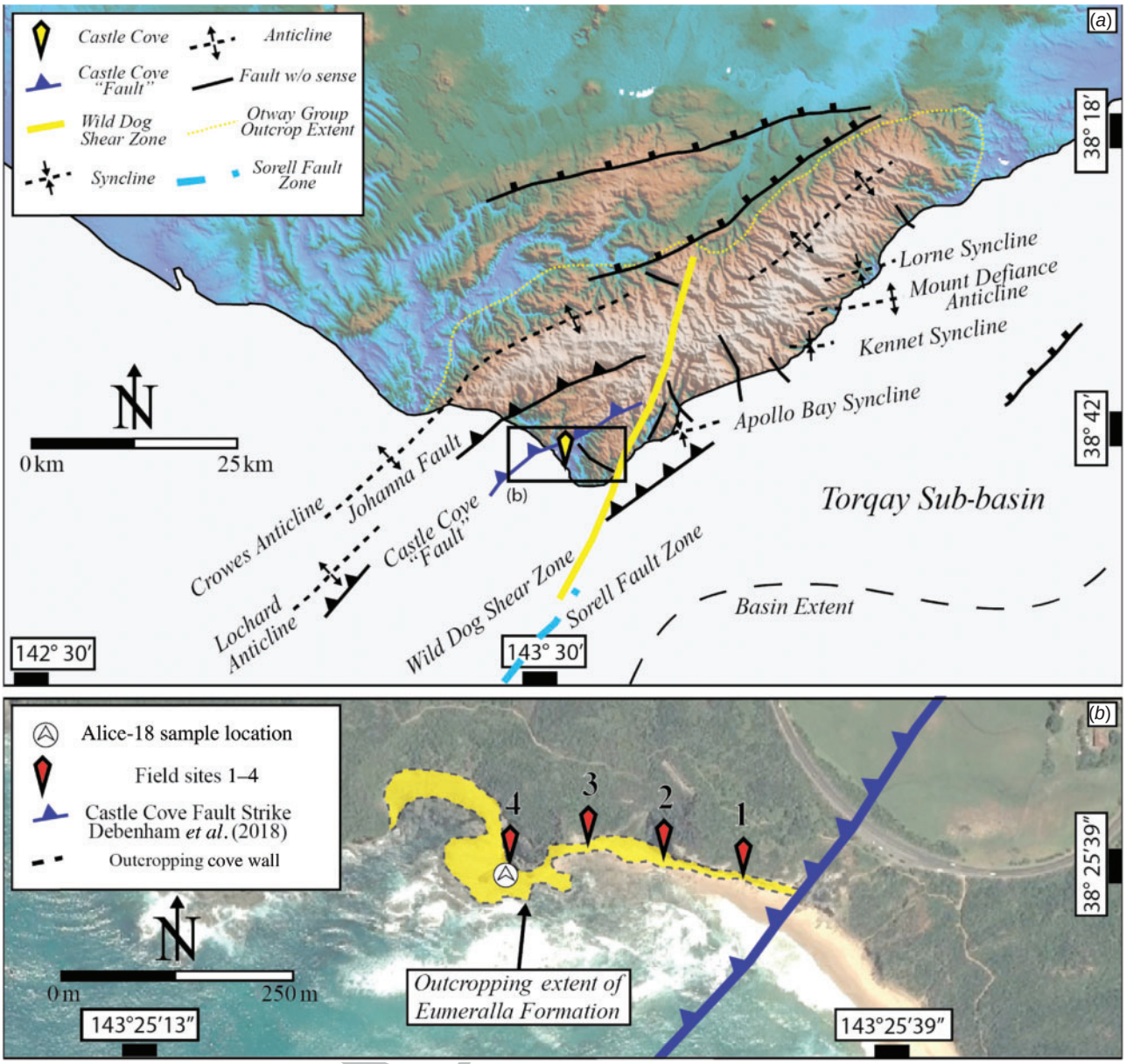

Fig. 2. (*a*) A structural map of the Otway Ranges (after Debenham *et al.* (2018)) showing major structural patterns along with the location of Castle Cove. (*b*) A satellite image (Map data: Google Earth, CNES/Airbus 201) of Castle Cove (38° 47′ 03.65″S, 143° 25′ 27.05″W, Eye alt 1.83 km) showing the outcropping location of the Eumerella Formation and the inferred location of the Castle Cove Fault (from Debenham *et al.* (2018)).

determination of a perfect tensor is unlikely, as untwinned planes are often incorporated. As such, the best tensor solution is found when the penalisation function, *f*, is reduced as close to zero as possible. The *f* function is described by:

$$f = \sum_{j=1}^{N} (\tau_{sj} - \tau_{a'})$$

where $\tau_a{}'$ is the smallest RSS applied to the twinned planes that are well matched with the experimental stress tensor, and τ_{sj} is the RSS applied upon the N number of untwinned planes, j, such that $\tau_{sj} > \tau_a{}'$ (Etchecopar 1984; Laurent 1984). The optimal stress tensor is found by incorporating the maximum amount of twinned planes in the sample while ensuring the minimal incorporation of untwined planes. Due to local heterogeneities, perturbations and measurement uncertainties, a small number of untwinned planes could be included within the tensor as having received a RSS greater than the $\tau_a{}'$ but not twinned. In this sense the *f* function describes both the arrangement of twin planes to the experimental tensor, in addition to its quality. The successful execution of this process leads to the determination of T′ (Etchecopar 1984; Laurent 1984). Calcite twins measured within our oriented outcrop sample A-18 were type 1 or 2 twins (Fig. 4) (Burkhard 1993). For more information regarding CSIT, we recommend the reader consult Amrouch (2010).

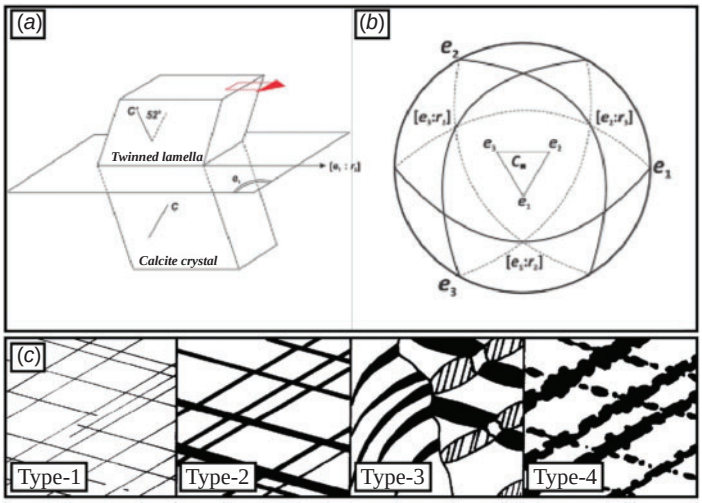

Type	Geometry	Interpretations	Temp
Type-1	- Thin twins - Straight - Rational - 1,2 3 sets per grain	- Little deformation - Little cover - Low temp - Late stage	<200°C
Type-2	- Thick >1µm - Straight - Lense shaped - Rational	- Higher deformation - Completely twinned possible - Syn-or post-metamorphism	150 –300°C
Type-3	- Curved + thick - Twins in twins - High number - Irrational	- Large deformation - Intracrystalline deformation - Syn-metamophic deformation	>200°C
Type-4	- Thick + patchy - Sutured edges - Trails of grains - Irrational	- Large deformation - Dynamic recrystallisation - Pre-or syn-metamophic deformation	>250°C

Fig. 3. (*a*) Schematic diagram of a twin lamella in a calcite crystal showing how deformation can occur along certain 'e-planes' (modified from Arboit *et al.* (2015)). (*b*) Stereographic projection (lower hemisphere, equal area) of the calcite twin planes. The central optical axis is vertical with poles to planes at 26.5° to the 'C' axis. Planes of twinning are the three great circles (modified from Burkhard (1993)). (*c*) Schematic illustrations of calcite twin types 1–4 along with type descriptions in the neighbouring table (modified from Burkhard (1993)).

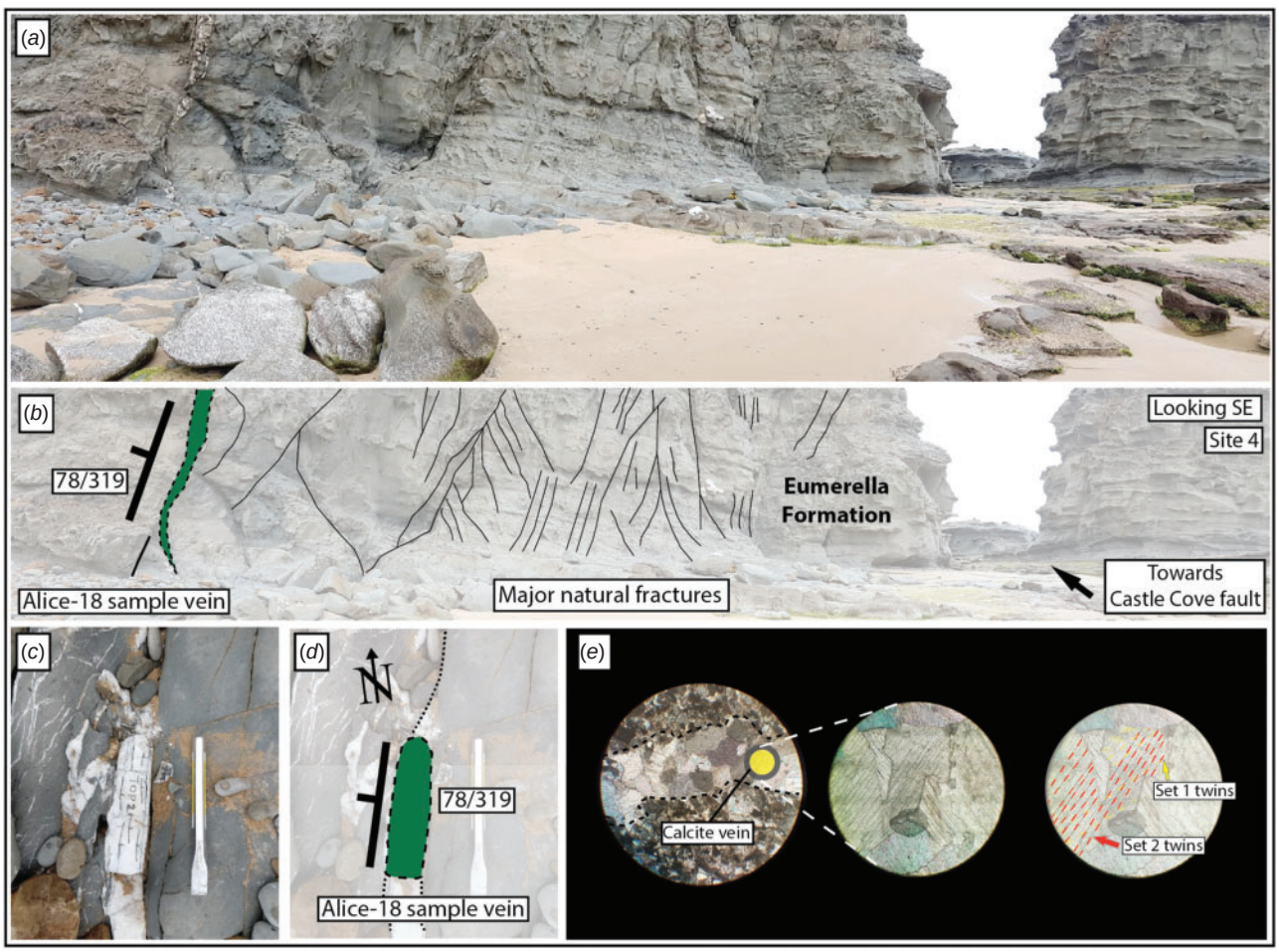

Fig. 4. Photographs (*a*) and annotations (*b*) of the western most part of Castle Cove, near site 4, where the 'Alice-18' (A-18) sample was obtained and the wall strikes to the south-west. Photograph (*c*) and annotated photo (*d*) of the sample itself in-situ. (*e*) An example of type-1 calcite twins under the microscope and how multiple sets of twin planes can be measured using the universal stage microscope.

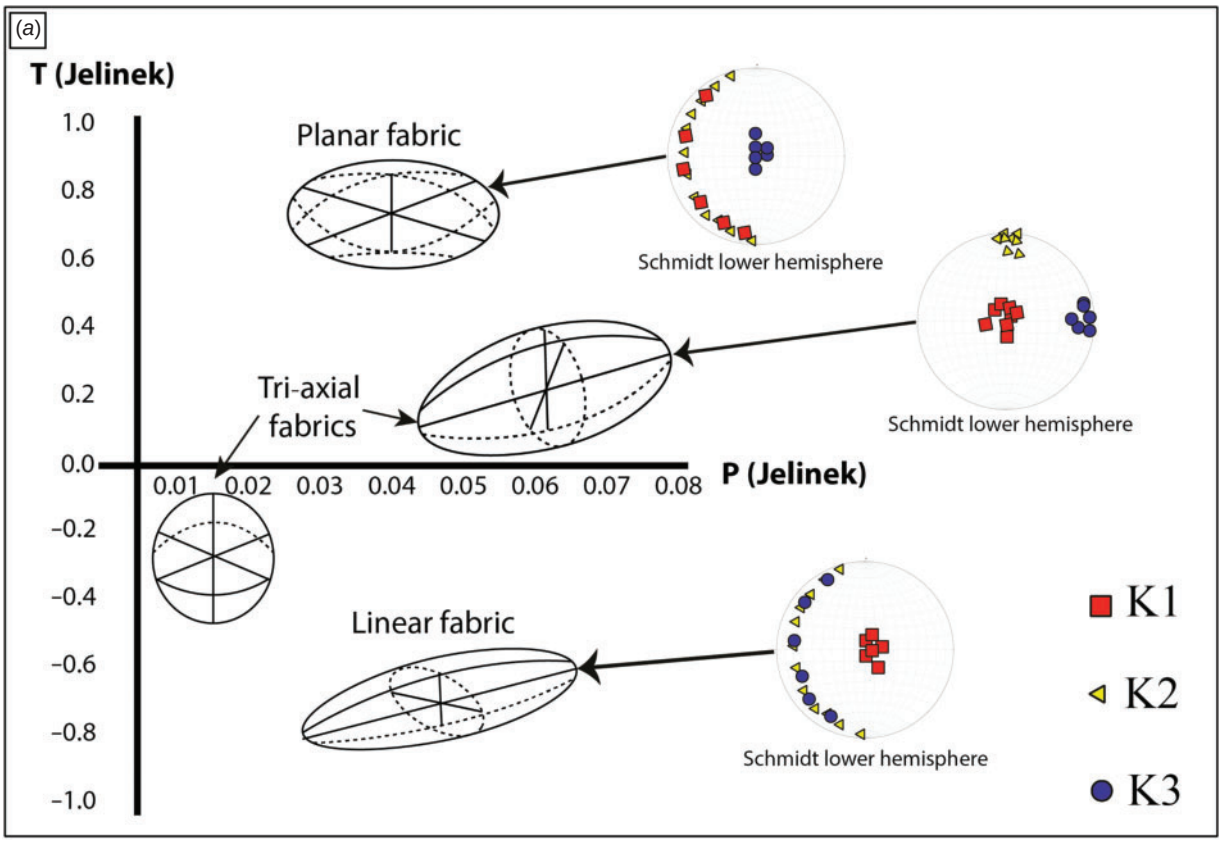

Fig. 5. Shape parameter (T) vs anisotropy (P_J) plot for Jelinek statistics (Jelinek 1981) displaying the three types of ellipsoid fabrics along with stereographic examples: planar, tri-axial (this study) and linear fabrics (modified from Amrouch (2010)).

Strain analysis using AMS

The measurement of the AMS within sedimentary rocks has been commonly used as a petrofabric tool to define weak deformation (Hrouda 1991; Tarling and Hrouda 1993; Borradaile and Henry 1997). Described by a second order tensor with three principal vectors defined by maximum susceptibility (K1), intermediate susceptibility (K2) and minimum susceptibility (K3), where K1 > K2 > K3 and their corresponding eigenvalues, the mathematical representation is an ellipsoid of varying shape and magnitude (Fig. 5) (Jelinek 1981). With a high sensitivity to even a slight preferred orientation of magnetic minerals, this method can be used to characterise very weak anisotropy in sedimentary rocks and allows for the deciphering of sedimentary to tectonic rock fabrics in compressional (Kissel *et al*. 1986; Averbuch *et al*. 1992; Grelaud *et al*. 2000; Frizon De Lamotte *et al*. 2002; Robion *et al*. 2007; Amrouch et al., 2010*b*; Robert *et al*. 2018) and extensional settings (Mattei *et al*. 1997; Cifelli *et al*. 2004, 2005; Soto *et al*. 2007; García-Lasanta *et al*. 2014, 2015).

The magnetic fabric within a rock is typically defined through the orthogonal orientations of K1, K2 and K3 (Fig. 5) and their varying spatial distributions. To assess the magnitude and character of the form of anisotropy within our samples, we have analysed three common parameters of AMS after Jelinek (1981). First, we calculated the corrected degree of anisotropy, P_J. Ranging between a value of one, (indicating a perfect sphere) and infinity, P_J provides a measure of the degree of ellipticity. It can be defined as:

$$P_J = \sqrt{2[(n1-n)^2 + (n2-n)^2 + (n3-n)^2]}$$

where n1, n2 and n3 represent natural logarithms of the tensor eigenvalues and $n = (n1 + n2 + n3)/3$. Second, we calculated the shape parameter, T; if the susceptibility ellipsoid is prolate or rod shaped, then $t = -1$. If magnetic foliation is dominant, then $t = 1$ with an oblate fabric style. Transitional values denote the various interactions between both factors. T is defined by:

$$T = (2n2 - n1 - n3)/(n1 - n3)$$

Lastly, the mean eigenvalues of the produced tensor, K, are defined by:

$$Kmean = (Kmax + Kint + Kmin)/3$$

As part of our analysis of AMS at Castle Cove, a total of 48 cores from three sample sites were analysed within the Eumeralla Formation. Our analysis of AMS took place at the University of Cergy-Pontoise in Paris, France, using a spinner kappabridge KLY-4S with a sensitivity of 0.5×10^{-8} SI units.

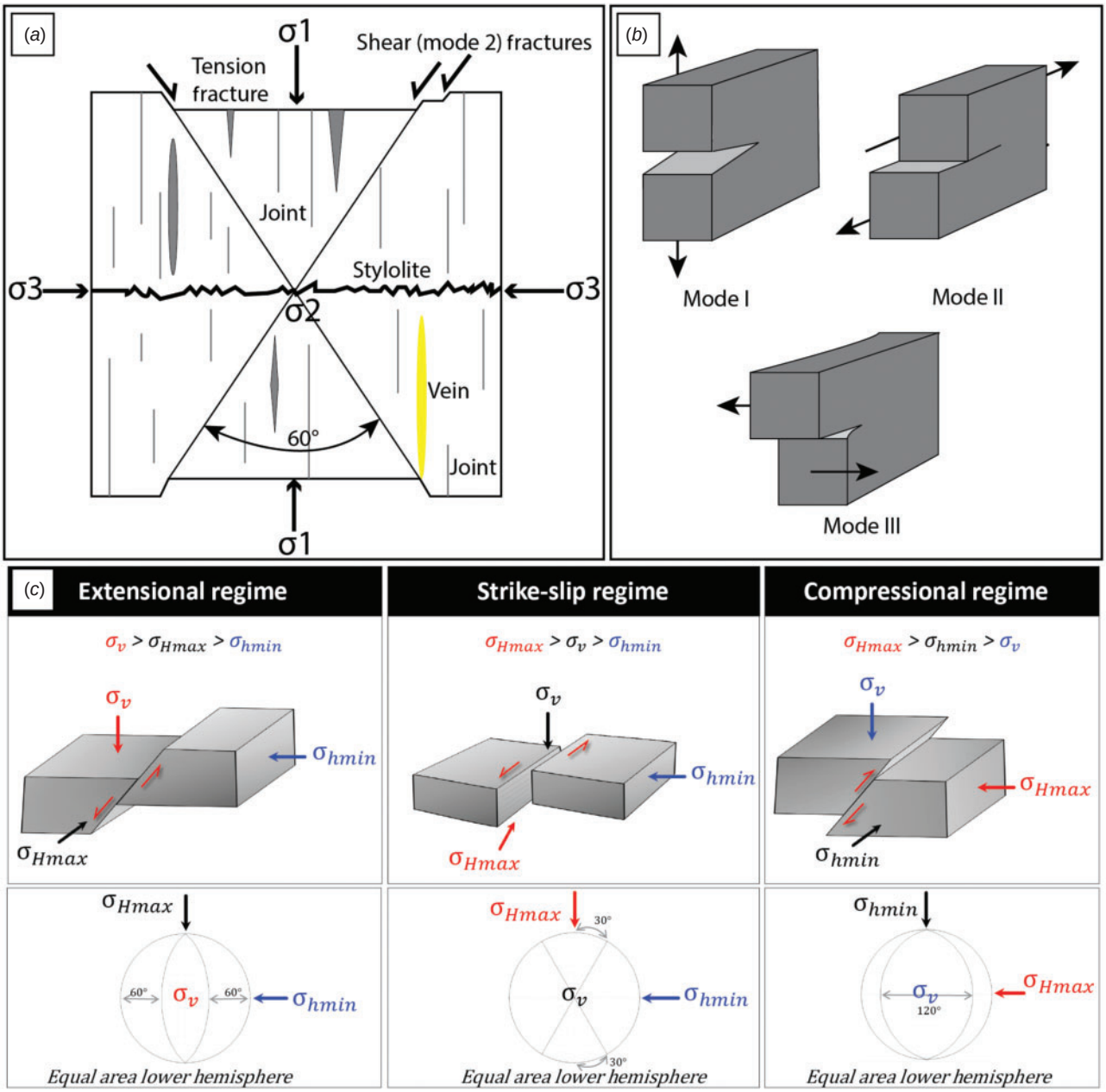

Fig. 6. (*a*) A schematic cross-section displaying the relationship of the three principal stresses and various features of structural deformation (modified from Fossen (2010)). (*b*) The three modes of fracture formation. (*c*) Anderson's (Anderson 1951) three environments of stress and the 'text book' nature of fracture and fault formation within them.

Natural fracture analysis

Fracture populations were sampled from the outcropping Eumeralla Formation at Castle Cove (Fig. 4*b*). Fracture dip and dip direction were recorded, in addition to cross-cutting relationships and/or evidence for fracture reactivation, though these were minimal. The fundamental principles of rock failure that describe the relationship between principal stress orientation and fracture geometry formed the basis of our analytical technique for this study (Fig. 6).

Natural fractures of certain geometry form under specific conditions of stress once the point of rock failure has been surpassed (Zoback *et al.* 1989). These specific geometries are distinguishable based on their 3D relationship to the principal stress orientation and the mode of fracture formation (Anderson 1951; Zoback *et al.* 2003). Conjugate shear (mode 2) fracture sets will develop with ~60° of separation between them, bisected by the plunge orientation of the σ1, with the σ3 bisecting the complimentary 120°–140° arc. The σ2 is centred at the intersection point of the two conjugate fractures (Fig. 6) (Anderson 1951; Zoback *et al.* 2003). This understanding of natural fracture geometry, combined with consideration of the bedding plane, allows for the prediction of the most likely regime

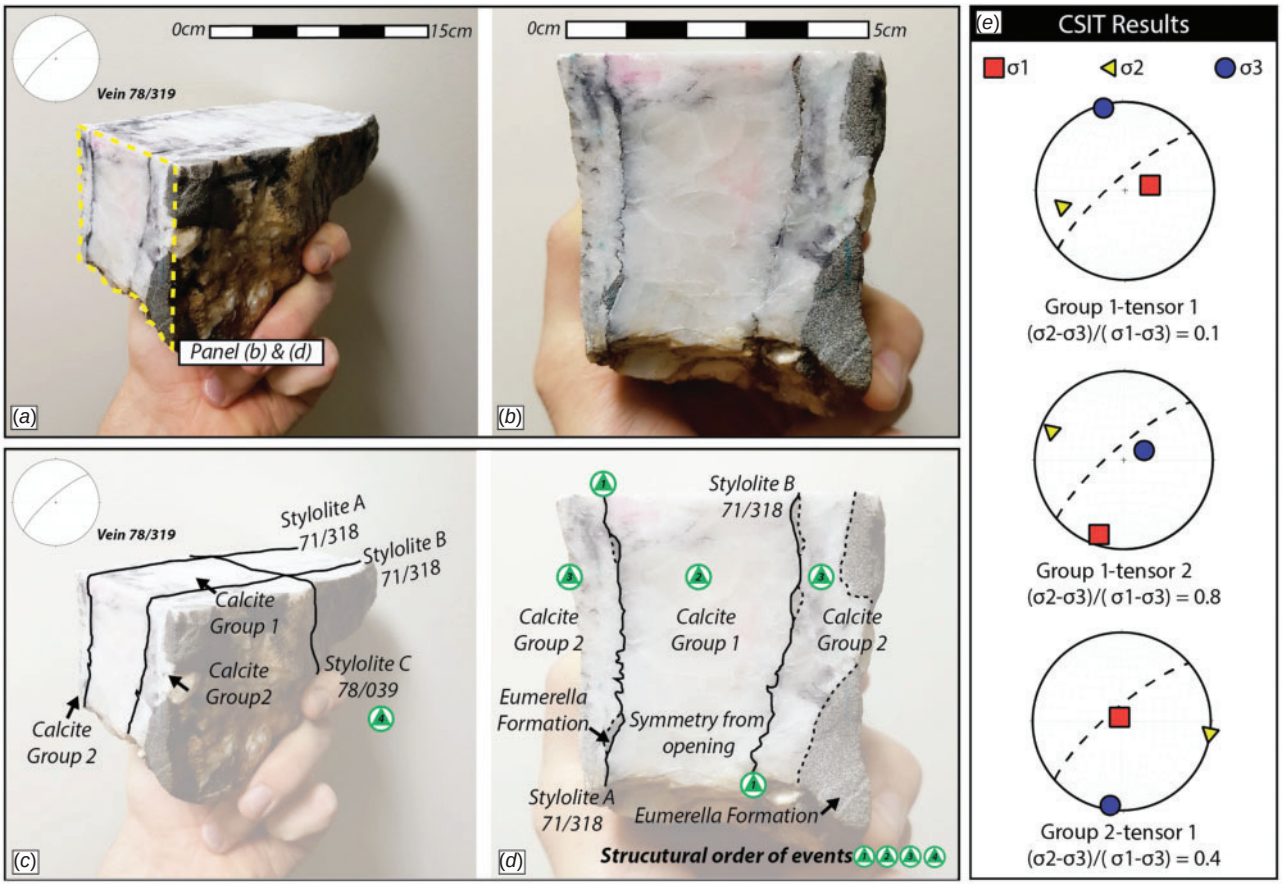

Fig. 7. (*a*) and (*b*) Cross-sections through the Alice-18 sample from site 4 at Castle Cove. (*c*) Annotated cross-section through the sample showing stylolites A, B and cross-cutting stylolite C in addition to the two groups of calcite and their relationships to the overall strike of the vein. (*d*) Another annotated cross-section displaying the symmetry between stylolites A and B and sections of the Eumerella Formation between the two groups of calcite. This led us to deduce there were multiple opening events of the vein and the interpreted order of structural events within the sample. Stylolite C is included in panel (*c*). (*e*) The three palaeostress tensors derived from calcite stress inversion technique analysis on the A-18 sample.

of palaeostress responsible for fracture nucleation (Anderson 1951). Stereonet v8.0 (Allmendinger 2013), along with the palaeostress orientation tool Wintensor (Delvaux 2012), was used for the identification of major fracture sets and the assigning of palaeostress regimes.

Analysis was conducted at four sites within Castle Cove (Fig. 2), coinciding with the locations of the AMS and CSIT samples. In order to reduce noise, data were only collected from fractures where a complete 3D geometry was able to be clearly observed – a defining feature of our method – within a 10 × 10 m spacing at each site. This meant that many of the fractures within the horizontal shore-cut platforms and near vertical cliff face at the cove were not considered, as there was no way to accurately constrain their angle of dip and dip direction.

Results

Stress inversion

Initial field analysis of A-18 showed a complex series of structural events. Within the sample (Fig. 7) that dips at 78° towards 319°N, we found three stylolites and two groups of calcite crystals of distinctly different sizes, separated by a thin section of the host rock (Fig. 7). Stylolite A and B strike parallel to each other and the strike of the vein and dip 71° towards 318°N; stylolite C cross-cuts stylolites A and B in addition to both generations of calcite crystals and dips at 78° towards 039°N.

CSIT results from calcite group one (G1) determined two stress tensors, (Fig. 7*e*) (Table 1) derived from the measurement of type-1 and type-2 calcite twins (Burkhard 1993). The first tensor (T1) from G1 (G1-T1) is indicative of an extensional stress regime under backtilted bedding conditions, with a σ1 plunging 78° towards the 058°N and a σ3 plunging at 02° towards 345°N, with a low R value $(\sigma2 - \sigma3)/(\sigma1 - \sigma3) = 0.1$.

The second tensor (T2), recorded within calcite G1 (G1-T2), indicates a compressional stress regime under backtilted bedding conditions, with a shallow σ1 plunging at 13° towards 199°N and a σ3 plunging at 71° towards the 067°N, with an R value of 0.8.

CSIT results from smaller crystals of calcite group two (G2) (Fig. 7*e*) produced a single stress tensor (G2-T1), indicating a second extensional stress regime under backtilted bedding conditions. In this case, σ1 plunges at 85° towards 353°N and a σ3 plunges at 04° towards the 189°N, with an R value of 0.4.

Table 1. Table one presents the four calcite stress inversion technique tensors produced from the analysis on the A-18 sample. All tensors are presented under backtilted conditions

Sample name	Sample vein	Site bedding	σ1 (Plunge direction/plunge)	σ2 (Plunge direction/plunge)	σ3 (Plunge direction/plunge)	R	Penalisation function	Palaeostress regime
A-18G1-T1	78/319	16/145	058/78	254/31	345/02	0.1	0.8	Extension
A-18G1-T2	78/319	16/145	199/13	292/15	067/71	0.8	0.95	Compression
A-18G2-T2	78/319	16/145	353/85	098/01	189/04	0.4	0.84	Extension

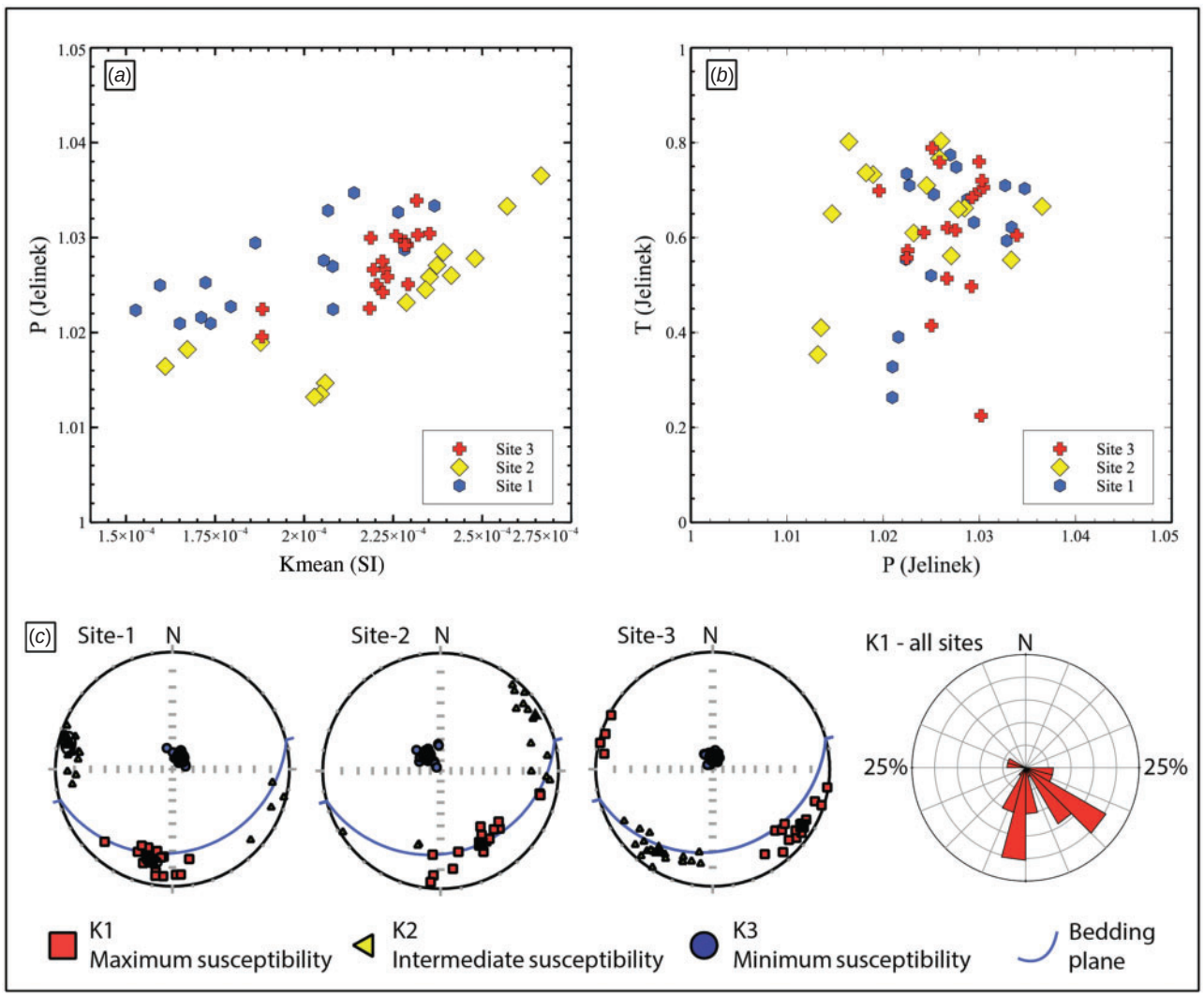

Fig. 8. (*a*) Measured anisotropy (P_J) vs mean susceptibility (Kmean) plot of our anisotropy of magnetic susceptibility (AMS) results from sites 1, 2 and 3 at Castle Cove. We observe slight increases in anisotropy with increasing susceptibility. Note that Kmean values are typical of either diamagnetic or ferromagnetic minerals. (*b*) P_J vs T plots of our AMS results aid in the identification of oblate to tri-axial magnetic fabrics, further assisting in our identification of the influence of extensional tectonics. (*c*) AMS results from sites 1, 2 and 3 projected onto equal area lower hemisphere stereonets. In general, the maximum magnetic susceptibility (K1) trend towards the down-dip direction of the bedding. Note the red rose diagram showing the trends of K1 between the three sites.

Grain scale strain from AMS analysis

The low-field AMS results (Fig. 8) present Jelinek (1981) P_J and T values that are consistent with those of weakly deformed sediments. At all sites and for all measured specimens, P_J values are between 1.0 and 1.05, presenting magnetic ellipsoids that are oblate to tri-axial in nature. All sites show similar trends, with K1 roughly parallel to the down-dip direction of the bedding (Fig. 8*c*) and K3 parallel to the pole to bedding in each case. These fabrics are typical of an extensive environment (Cifelli *et al.* 2005), with K1 clustering in our case, suggesting extensional azimuths oriented to the ~NE–SW and NNW–SSE (Fig. 8*c*). Correlations between the values of P_J and Kmean

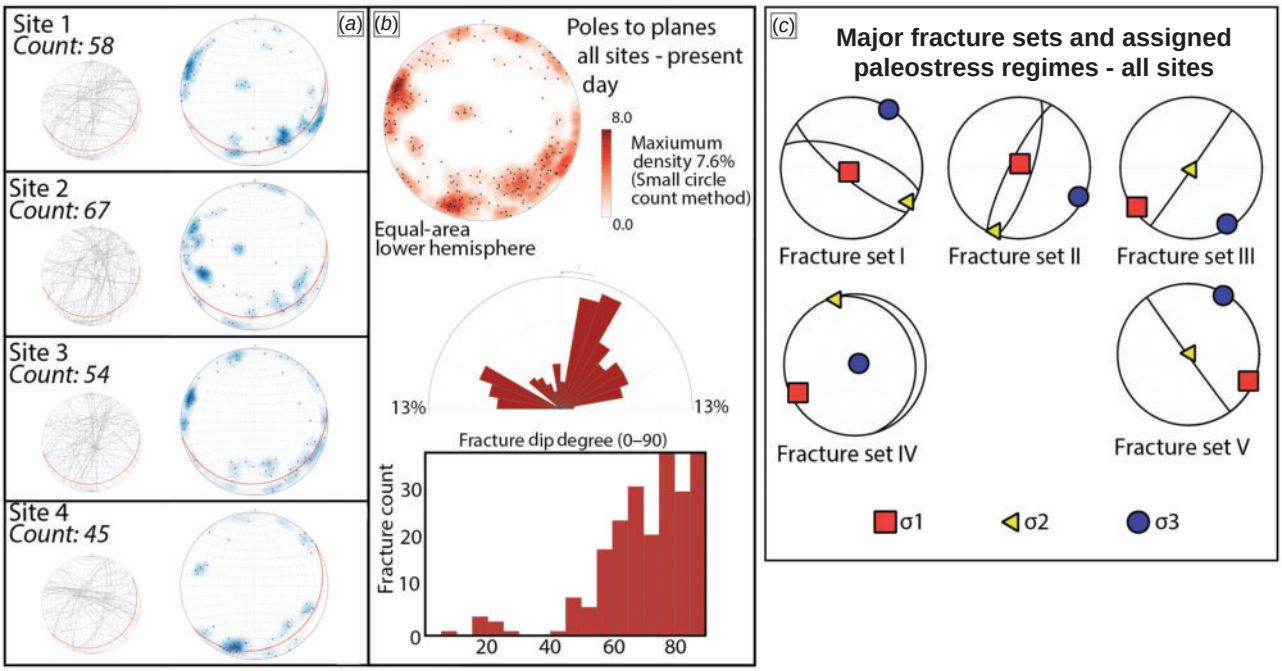

Fig. 9. (*a*) Our natural fracture measurement from sites 1–4. All stereonets represent lower hemisphere projections. (*b*) All sites grouped together under present day bedding conditions with an average strike of ~006°N. (*c*) Major fracture sets from our outcrop analysis. Fracture sets I–IV are displayed under backtilted conditions.

(Fig. 8*a*) suggest that the AMS signal within our samples is derived from different contributions (Rochette *et al*. 1992).

Natural fracture sets from outcrop analysis

A total of 234 natural fractures were measured across the four sample sites (Fig. 9). Under present day conditions, natural fracture dip is mainly 60° and 90°, with very few low angle fractures detected, while mean fracture strike is 006°.

Bedding dip and dip direction varied slightly from site to site, although, in general, beds were dipping between 16° and 19° towards the SE. Our understanding of natural fracture geometry, combined with consideration of the plane of bedding, allows for the prediction of the most likely regime of palaeostress responsible for fracture nucleation (Bellahsen *et al*. 2006; Amrouch *et al*. 2010*a*; Beaudoin *et al*. 2012). Our method has resulted in the categorisation of five major fracture sets across the four sites, accounting for more than 80% of data (Fig. 9*c*).

Fracture sets I, II, III and IV have been interpreted as having formed with the bedding backtilted, under more Andersonian (Anderson 1951) conditions of stress. Fracture set V was interpreted as having formed under present day conditions of stress. Fracture sets are in good agreement with those from Burgin *et al*. (2018) along the north-eastern margin of the Otway Ranges.

Interpretation and discussion

We begin this section of the paper with some brief comments regarding the structure at Castle Cove, then we continue forwards by analysing the palaeostress evolution from the A-18 sample. We then expand these solutions by correlating them with our other datasets to produce a multiscale model.

Comments on the Castle Cove structure

Castle Cove displays what is essentially a gentle fold structure with bedding progressively steepening gently towards the ~SE. Although subjected to numerous studies, the exact nature of the structure remains unclear: Duddy (1994) suggests the local structuring represents a reactivated ~NE–SW striking normal fault that extends to the surface, Edwards *et al*. (1996) describes a monocline structure overlying a high-angle inverted normal fault present at greater depths, while Debenham *et al*. (2018) describe a 'greater than 80 m in half-wavelength' anticline forming inversion structure. All studies associate the structure at the cove with neotectonic, Miocene–Pliocene compression and inversion, with a ~NW–SE oriented σ1.

In this study, we approach this model of development with some reserve due to several reasons: (1) no fault plane is actually visible at the surface and seismic imaging of the structure has not been possible; (2) complimentary structural evidence for fault inversion and compression is minimal within the cove with no visible accompanying back-break, shortcut thrusts, or horsetail splays, which may be expected during the inversion of a steeply dipping normal fault; and (3) the nearby offshore framework, particularly within the Shipwreck Trough, largely reflects extensive faults that typically strike ~NW–SE and N–S (Schneider *et al*. 2004; Robson *et al*. 2018), with little evidence for ~NE–SW striking normal faults within the sediments of the Otway Basin.

Palaeostress evolution within the A-18 sample

From our analyses of the stylolites and CSIT within A-18 (Fig. 7), we propose a chronological sequence of palaeostress events. Stylolites A and B mark the first structural event and, in actual fact, represent a single stylolite that was subjected to 'opening'

during a later stage of deformation. This is due to the symmetry of stylolites A and B bordering the edge of the large crystals of the calcite G1 (Fig. 7). Adjusted for backtilted bedding at site 4, this original stylolite – referred to as stylolite AB henceforth – was likely formed under a stress regime with a ~NW–SE trending σ1 with an original spatial orientation dipping 78° towards 319°N.

The second palaeostress phase from A-18 involves the opening of the stylolite forming the G1 calcite within the resulting vein. Adjusted for backtilted bedding, stylolite AB was subjected to reactivation and opening, resulting in the formation of the host vein with an original dip and dip direction of 86° towards 318°N and the first generation of calcite crystals. Due to the geometry of the vein, opening likely occurred under a ~NNW–SSE extensional stress regime with the orientation of paleo-σ3 inferred to be at ~90° to the strike of the vein. This coincides well with CSIT tensor G1-T1, with a vertical σ1, supporting ~NNW–SSE opening of the vein and suggesting that first generation of calcite in the sample recorded the initial opening event. The third stress phase recorded within the sample represents a second phase of extension, resulting in another episode of reactivation and the influx of calcite G2 into the vein. As with G1-T1, CSIT tensor G2-T1 from within the G2 crystals recorded this event.

The fourth phase of stress recorded within the A-18 sample represents stylolite C (Fig. 7), which cross-cuts both calcite groups and stylolites A and B. Under backtilted bedding conditions, this vertical stylolite formed with a ~NE–SW (039°N) trending σ1. Such a palaeostress regime is recorded in A-18, within G1-T2, as a ~NE–SW compressive stress regime with σ1 trending parallel to the orientation of σ1 from stylolite C.

Magnetic fabrics and extensional strain at Castle Cove

In fold-and-thrust belt environments, AMS studies have been extensively used to show that, during significant shortening events, magnetic fabrics evolve from sedimentary fabrics towards intermediate and tectonic fabrics (e.g. Frizon De Lamotte *et al*. 2002; Amrouch *et al*. 2010*b*; Robert *et al*. 2018). Additionally, as sedimentary rocks often contain their own natural fabric (e.g. bedding), the study of AMS within weakly deformed units can become complex, as discerning between such fabrics and relevant tectonic ones can be difficult. In basin environments, all types of depositional processes can affect sedimentary fabrics, including gravity and palaeocurrents. It is also possible for processes such as diagenesis to create new paramagnetic and/or ferromagnetic minerals, which may slightly alter the initial sedimentary fabric.

During compressional and inversion events, it has been shown that the magnetic lineation of K1 develops parallel to the relevant fold axis (Kissel *et al*. 1986; Averbuch *et al*. 1992, Frizon De Lamotte *et al*. 2002; Robion *et al*. 2007; Amrouch *et al*. 2011). In our case, the implied regional axis of folding of the Otway Ranges from previous studies (Duddy 1994; Edwards *et al*. 1996; Krassay *et al*. 2004; Holford *et al*. 2014), and the subsequent proposed axis of inversion for the Castle Cove fault, strikes roughly NW–SE. As our results are tri-axial in nature, with K1 plunging towards the SW and SSE (Fig. 8*c*), our results do not show any evidence for ~NW–SE oriented compressional stresses at Castle Cove, but they do suggest that ~NE–SW to NNW–SSE extensional fabrics have been preserved throughout the recent structuring – if indeed any has occurred.

Although the magnetic fabrics characterised at Castle Cove are not reflective of tectonic shortening, they display good co-axiality with our extensional palaeostress data from CSIT and natural fracture analysis, particularly stress tensors G1-T1 and G2-T2, which show radial and ~N–S oriented extension. What is unclear from the data at Caste Cove, and warrants further investigation, is whether such fabric developed during or post Eumeralla Formation deposition.

Natural fracture sets and successive palaeostress development at Castle Cove

Using data from A-18 and previous works, we integrated the outcrop fracture sets and inferred palaeostress with stress tensors derived from our CSIT results and stylolites. This allowed us to produce a comprehensive model for the development of five main phases of stress at Castle Cove (Fig. 10).

The first phase of palaeostress evolution at Castle Cove is defined by the stylolite AB, which, under backtilted bedding conditions, formed vertically under an early phase of ~NW–SE oriented shortening during the Mid-Cretaceous, as suggested by previous studies (e.g. Cooper and Hill 1997; Krassay *et al*. 2004). Given that most extensional petrofabrics are syn-depositional, we suggest that our detected fabrics had already formed at this point in time (Cifelli *et al*. 2005).

It was not possible to discern the chronological order between fractures sets I and II from cross-cutting relationships, as set I fractures were mainly measured within uneven sections of the wave cut platform and the ~NE-–SW trending wall at site 4 (Fig. 4), while set II fractures were measured in the main ~NW–SE striking wall of the cove at sites 1, 2 and 3. That being the case for phase 2, we combine the two fracture sets as both having occurred along with tensor G1-T1, which, with a vertical σ1 and low R value, supports extension in a radial manner, most likely at some point during the Late Cretaceous when the Otway Basin saw significant deposition and growth of ~NW–SE and ~W–E striking faults (Robson et al. 2018). Burgin *et al*. (2018) present evidence along the eastern margin of the Otway Ranges for ~NE–SW striking extensional fractures, typical of our set II fractures, that terminated on ~NW–SE striking fractures typical of our set I fractures, suggesting that initial extension during the Late Cretaceous may have occurred with a slightly more ~NE–SW oriented azimuth. Phase 4 represents continuing extension and further reactivation of the A-18 vein, resulting in the influx of calcite G2 (Fig. 10)

For phase 4, we combine fracture set IV with palaeostress tensor G1-T2, as both are representative of a ~NE–SW oriented compressional stress regime at Castle Cove. Fracture set III represents the earliest phase of ~NE–SW oriented contraction, indicated by strike-slip stresses that likely preceded the pure compressional event, as ~NE–SW oriented horizontal stresses progressively increased in intensity. As discussed above, the formation of stylolite C is also attributed to this regime of stress and was likely formed during the early strike-slip phase of the shortening event due to increases in fluid pressure. Though detected in Burgin *et al*. (2018), this regime of palaeostress is more obvious at Castle Cove and enigmatic with respect to the

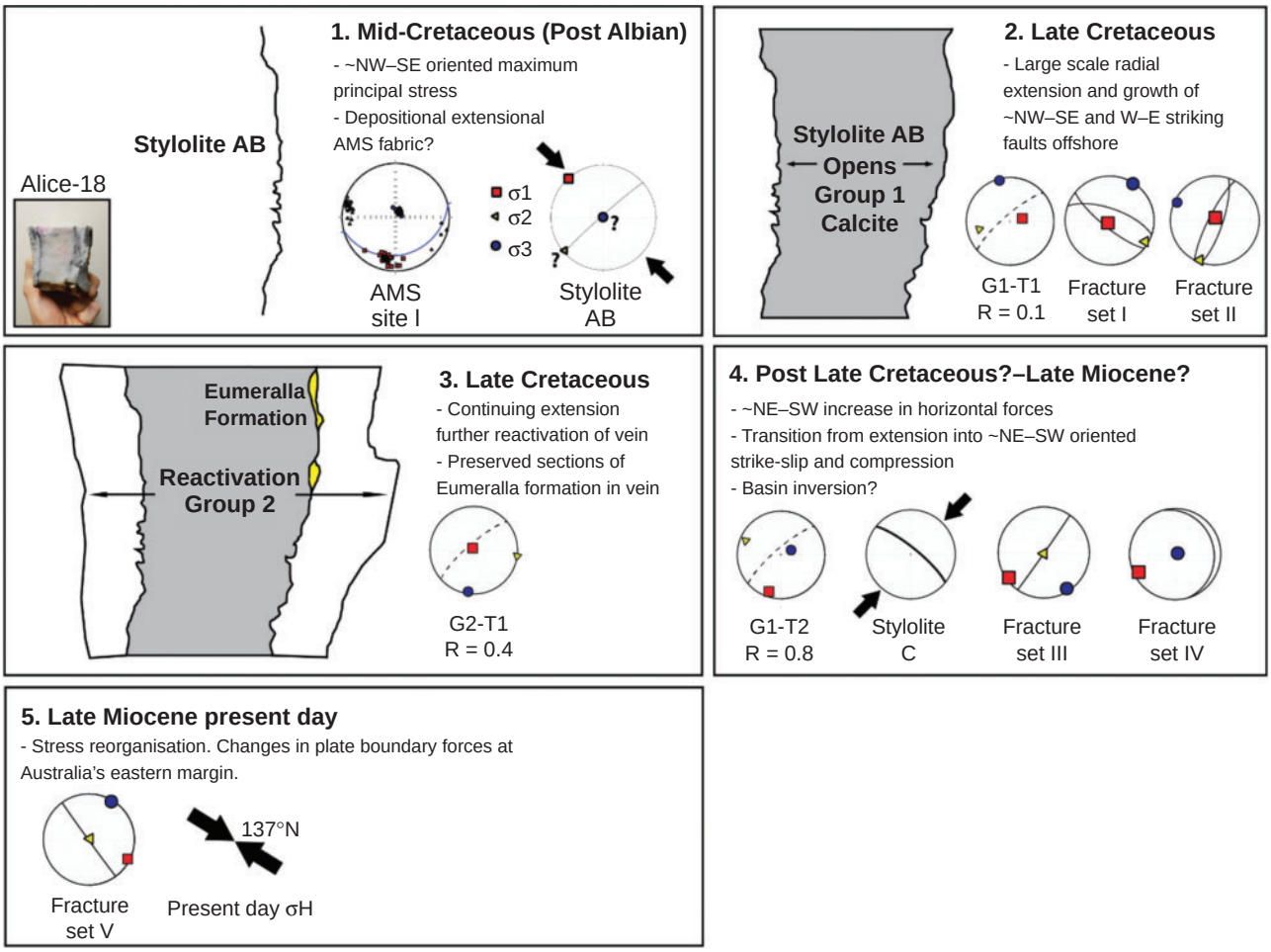

Fig. 10. Our progressive five-phase model of stress development for the Alice-18 sample and natural fracture network at Castle Cove.

current understanding of the Otway Basin's structural development, as at present, all studies that advocate for inversion within the basin favour ~NW–SE oriented compression (Hill *et al*. 1995; Cooper and Hill 1997; Holford *et al*. 2011; Holford *et al*. 2014; Debenham *et al*. 2018). Given that ~NW-–SE oriented horizontal forces have dominated much of south-eastern Australia from the Late Miocene (Sandiford *et al*. 2004), our findings lead us to suggest that the Otway Basin may have experienced ~NE–SW oriented structuring and stress reorganisation at some point between the Late Cretaceous extension phase and the stress re-organisation and coupling of the Late Miocene, which is currently under investigation.

Although fracture set V is unable to be integrated with any paleostress data from Castle Cove, we integrate it with the present day orientation of maximum horizontal stress within the Otway Basin, which trends approximately ~NW–SE (137°N) (Rajabi *et al*. 2017*b*). As such, phase 5 represents a late phase of strike-slip stresses oriented broadly ~NW–SE within the eastern Otway Basin, coinciding with estimates that the basin may currently be within a strike-slip stress regime (Rajabi *et al*. 2017*a*).

Reassessing the structural framework of the eastern Otway Basin

In our opinion, the dominance of extensional palaeostress phases and strain at Castle Cove, along with the lack of multiscale evidence for structural data representing a ~NE–SW striking zone of compression, raises significant questions with respect to the nature of the Castle Cove structure. Given the multiscale evidence we have detected in this study for ~NE–SW oriented compressional forces in lieu of those oriented ~NW–SE, it is possible that, at present, the current model for basin inversion and major structuring within the Otway Basin and Otway Ranges is inaccurate, and requires reassessment. This may especially be the case within the eastern Otway Basin where orthogonally striking ~NW–SE and ~NE–SW structural fabrics are thought to interact with one another. Such a reassessment of the timing and orientation of inversion within the Otway Basin may have significant consequences with respect to the current models for petroleum systems development, which currently support the Mid-Cretaceous and Late Miocene as the most significant periods of trap development (O'Brien *et al*. 2009).

Conclusions and future work

Through the integration of CSIT, AMS data and natural fracture analysis we have demonstrated how a relative chronology for fracture development can be established (Fig. 10). In addition, we have provided a measureable insight into the local stress development at Castle Cove. We believe the use of such techniques are relevant to both exploration and production within the oil and gas, geothermal and carbon capture and storage industries, as they assist in reducing the unknowns when establishing a structural model for regional and local evolution. These improved understandings can affect how we approach analysing migration pathways in 4D and how we predict natural fracture formation and distribution within the subsurface. This can significantly affect both conventional and unconventional hydrocarbon production. Additionally, the co-axiality of extensional environments within our results raise new questions as to the degree to which previously proposed events of compression and inversion have shaped the structural framework of the Otway Basin and the source and timing of the petrofabrics within the Eumeralla Formation. These questions will be addressed in coming works that will further integrate these techniques with widespread datasets from across the eastern Otway Basin, including 3D seismic surveys.

Conflicts of interest

The authors declare no conflicts of interest.

Acknowledgements

We appreciate the financial contribution provided from the Endeavour Scholarship through the University of Adelaide. Additionally, we wish to thank the staff of the Geosciences and Environment Laboratory at the University of Cergy-Pontoise, Paris, for their welcoming attitude and assistance with AMS sample preparation. Thank you to field assistants Natalie Debenham, David Kulikowski and Annabel Gibson. Thank you to Richard Allmendinger for Stereonet 8.8.8 and Carlos H. Grohmann and Ginaldo A.C. Campanha for 'OpenStereo 0.1.2'. Additional information is available by contacting the lead author: hugo.burgin@adelaide.edu.au.

References

Allmendinger, R. W. (2013). Stereonet Help–the user's manual for Stereonet 8. Available at http://funnel.sfsu.edu/students/frankv/gcourses/E620/Stereonet.app/Contents/Resources/Stereonet%20Help/

Amrouch, K., Lacombe, O., Mouthereau, F., and Dissez, L. (2005). Quantification of orientations and magnitudes of the late Cenozoic paleostresses in the Zagros folded belt from calcite twin analysis. In 'International Meeting on Thrust Belts and Foreland Basins, Rueil-Malmaison, December 2005. pp. 31–35. (Institut Français du Pétrole: Rueil-Mailmaison, France)

Amrouch, K. (2010). Contribution of microstructural analysis to the understanding of folding mechanisms: Examples of folded structures in the USA (Wyoming) and in Iran (Zagros). PhD Thesis, University Pierre and Marie Curie-Paris VI, Paris.

Amrouch, K., Lacombe, O., Bellahsen, N., Daniel, J. M., and Callot, J. P. (2010*a*). Stress and strain patterns, kinematics and deformation mechanisms in a basement-cored anticline: Sheep Mountain Anticline, Wyoming. *Tectonics* **29**, TC1005doi:10.1029/2009TC002525

Amrouch, K., Robion, P., Callot, J. P., Lacombe, O., Daniel, J. M., Bellahsen, N., and Faure, J. L. (2010*b*). Constraints on deformation mechanisms during folding provided by rock physical properties: a case study at Sheep Mountain anticline (Wyoming, USA). *Geophysical Journal International* **182**(3), 1105–1123. doi:10.1111/j.1365-246X.2010.04673.x

Amrouch, K., Beaudoin, N., Lacombe, O., Bellahsen, N., and Daniel, J. M. (2011). Paleostress magnitudes in folded sedimentary rocks. *Geophysical Research Letters* **38**, L17301 doi:10.1029/2011GL048649

Anderson, E. M. (1951). 'The dynamics of faulting and dyke formation with applications to Britain'. (Oliver and Boyd: Edinburgh, Scotland).

Arboit, F., Amrouch, K., Collins, A. S., King, R., and Morley, C. (2015). Determination of the tectonic evolution from fractures, faults, and calcite twins on the southwestern margin of the Indochina Block. *Tectonics* **34** (8), 1576–1599. doi:10.1002/2015TC003876

Averbuch, O., de Lamotte, D. F., and Kissel, C. (1992). Magnetic fabric as a structural indicator of the deformation path within a fold-thrust structure: a test case from the Corbières (NE Pyrenees, France). *Journal of Structural Geology* **14**(4), 461–474. doi:10.1016/0191-8141(92)90106-7

Beaudoin, N., and Lacombe, O. (2018). Recent and future trends in paleopiezometry in the diagenetic domain: Insights into the tectonic paleostress and burial depth history of fold-and-thrust belts and sedimentary basins. *Journal of Structural Geology* **114**, 357–365. doi:10.1016/j.jsg.2018.04.001

Beaudoin, N., Leprêtre, R., Bellahsen, N., Lacombe, O., Amrouch, K., and Callot, J. P. (2012). Structural and microstructural evolution of the Rattlesnake Mountain Anticline (Wyoming, USA): new insights into the Sevier and Laramide orogenic stress build-up in the Bighorn Basin. *Tectonophysics* **576-577**, 20–45. doi:10.1016/j.tecto.2012.03.036

Beaudoin, N., Koehn, D., Lacombe, O., Lecouty, A., Billi, A., Aharonov, E., and Parlangeau, C. (2016). Fingerprinting stress: Stylolite and calcite twinning paleopiezometry revealing the complexity of progressive stress patterns during folding—The case of the Monte Nero anticline in the Apennines, Italy. *Tectonics* **35**(7), 1687–1712. doi:10.1002/2016TC004128

Bellahsen, N., Fiore, P. E., and Pollard, D. D. (2006). From spatial variation of fracture patterns to fold kinematics: A geomechanical approach. *Geophysical Research Letters* **33**(2), L02301 doi:10.1029/2005GL024189

Boreham, C. J., Hope, J. M., Jackson, P., Davenport, R., Earl, K. L., Edwards, D. S., and Krassay, A. A. (2004). Gas-oil-source correlations in the Otway Basin, southern Australia. In 'PESA Eastern Australasian Basins Symposium II, Adelaide, 19–22 September 2004.'(Eds K. C. Hill, T. Bernecker.) pp. 603–627. (PESA)

Borradaile, G. J., and Henry, B. (1997). Tectonic applications of magnetic susceptibility and its anisotropy. *Earth-Science Reviews* **42**(1–2), 49–93. doi:10.1016/S0012-8252(96)00044-X

Burgin, H. B., Amrouch, K., Rajabi, M., Kulikowski, D., and Holford, S. P. (2018). Determining paleo-structural environments through natural fracture and calcite twin analyses: a case study in the OB, Australia. *The APPEA Journal* **58**(1), 238–254. doi:10.1071/AJ17099

Burkhard, M. (1993). Calcite twins, their geometry, appearance and significance as stress-strain markers and indicators of tectonic regime: a review. *Journal of Structural Geology* **15**(3–5), 351–368. doi:10.1016/0191-8141(93)90132-T

Cifelli, F., Rossetti, F., Mattei, M., Hirt, A. M., Funiciello, R., and Tortorici, L. (2004). An AMS, structural and paleomagnetic study of quaternary deformation in eastern Sicily. *Journal of Structural Geology* **26**(1), 29–46. doi:10.1016/S0191-8141(03)00092-0

Cifelli, F., Mattei, M., Chadima, M., Hirt, A. M., and Hansen, A. (2005). The origin of tectonic lineation in extensional basins: combined neutron texture and magnetic analyses on "undeformed" clays. *Earth and Planetary Science Letters* **235**(1–2), 62–78. doi:10.1016/j.epsl.2005.02.042

Cooper, G. T., and Hill, K. C. (1997). Cross-section balancing and thermochronological analysis of the Mesozoic development of the eastern OB. *The APPEA Journal* **37**(1), 390–414. doi:10.1071/AJ96024

Craddock, J. P., and van der Pluijm, B. A. (1999). Sevier–Laramide deformation of the continental interior from calcite twinning analysis, west-central North America. *Tectonophysics* **305**(1–3), 275–286. doi:10.1016/S0040-1951(99)00008-6

Debenham, N., King, R. C., and Holford, S. P. (2018). The influence of a reverse-reactivated normal fault on natural fracture geometries and relative chronologies at Castle Cove, Otway Basin. *Journal of Structural Geology* **112**, 112–130. doi:10.1016/j.jsg.2018.05.004

Delvaux, D. (2012). Release of program Win-Tensor 4.0 for tectonic stress inversion: statistical expression of stress parameters. In 'European Geosciences Union General Assembly, Vienna, 22–27 April 2012. EGU2012-5899. (EGU: Munich, Germany).

Dickinson, J. A., Wallace, M. W., Holdgate, G. R., Gallagher, S. J., and Thomas, L. (2002). Origin and timing of the Miocene-Pliocene unconformity in southeast Australia. *Journal of Sedimentary Research* **72**(2), 288–303. doi:10.1306/082701720288

Duddy, I. R. (1994, April). The Otway Basin: thermal, structural, tectonic and hydrocarbon generation histories. In 'NGMA/PESA Otway Basin Symposium, Melbourne, 20 April 1994'. pp. 35–42 (Australian Geological Survey Organisation: Canberra, ACT).

Edwards, J., Tickell, S. J., Willocks, A. J., Eaton, A. R., King, R. L., and Bourton, S. (1996). Colac 1: 250 000 geological map (Second edition). Geological Survey of Victoria. Department of Natural Resources and Environment, Victoria.

Edwards, D. S., Struckmeyer, H. I. M., Bradshaw, M. T., and Skinner, J. E. (1999). Geochemical characteristics of Australia's southern margin petroleum systems. *The APPEA Journal* **39**(1), 297–321. doi:10.1071/AJ98017

Etchecopar, A. (1984). Etude des états de contrainte en tectonique cassante et simulations de déformations plastiques: approche mathématique. Thése d'Etat (Doctoral dissertation), Université de Montpellier, Montpellier. [In French]

Etheridge, M. A., Branson, J. C., and Smith, P. G. S. (1985). Extensional Basin-forming Structures in Bass Strait and their Importance for Hydrocarbon Exploration. *The APPEA Journal* **25**, 344–361. doi:10.1071/AJ84030

Fossen, H. (2010). 'Structural Geology'. (Cambridge University Press: Cambridge, UK).

Frizon De Lamotte, D., Souque, C., Grelaud, S., and Robion, P. (2002). Early record of tectonic magnetic fabric during inversion of a sedimentary basin Short review and examples from the Corbieres transfer zone (France). *Bulletin de la Société Géologique de France* **173**(5), 461–469. doi:10.2113/173.5.461

García-Lasanta, C., Oliva-Urcia, B., Román-Berdiel, T., Casas, A. M., and Hirt, A. M. (2014). Understanding the Mesozoic kinematic evolution in the Cameros basin (Iberian Range, NE Spain) from magnetic subfabrics and mesostructures. *Journal of Structural Geology* **66**, 84–101. doi:10.1016/j.jsg.2014.05.013

García-Lasanta, C., Oliva-Urcia, B., Román-Berdiel, T., Casas, A. M., Gil-Peña, I., and Sánchez-Moya, Y. (2015). Evidence for the Permo-Triassic transtensional rifting in the Iberian Range (NE Spain) according to magnetic fabrics results. *Tectonophysics* **651–652**, 216–231. doi:10.1016/j.tecto.2015.03.023

Gibson, G. M., Morse, M. P., Ireland, T. R., and Nayak, G. K. (2011). Arc–continent collision and orogenesis in western Tasmanides: Insights from reactivated basement structures and formation of an ocean–continent transform boundary off western Tasmania. *Gondwana Research* **19**(3), 608–627. doi:10.1016/j.gr.2010.11.020

Grelaud, S., Buil, D., Hardy, S., and Frizon de Lamotte, D. (2000). Trishear kinematic model of fault-propagation folding and sequential development of minor structures; the Oupia Anticline (NE Pyrenees, France) case study. *Bulletin de la Société Géologique de France* **171**(4), 441–449. doi:10.2113/171.4.441

Groshong, R. H. Jr (1972). Strain calculated from twinning in calcite. *Geological Society of America Bulletin* **83**(7), 2025–2038. doi:10.1130/0016-7606(1972)83[2025:SCFTIC]2.0.CO;2

Groshong, R. H. Jr (1974). Experimental test of least-squares strain gage calculation using twinned calcite. *Geological Society of America Bulletin* **85**(12), 1855–1864. doi:10.1130/0016-7606(1974)85<1855:ETOLSG>2.0.CO;2

Groshong, R. H. Jr, Teufel, L. W., and Gasteiger, C. (1984). Precision and accuracy of the calcite strain-gage technique. *Geological Society of America Bulletin* **95**(3), 357–363. doi:10.1130/0016-7606(1984)95<357:PAAOTC>2.0.CO;2

Hill, K. C., Hill, K. A., Cooper, G. T., O'Sullivan, A. J., O'Sullivan, P. B., and Richardson, M. J. (1995). Inversion around the Bass basin, SE Australia. *Geological Society of London, Special Publications* **88**(1), 525–547. doi:10.1144/GSL.SP.1995.088.01.27

Hillis, R. R., Sandiford, M., Reynolds, S. D., and Quigley, M. C. (2008). Present-day stresses, seismicity and Neogene-to-Recent tectonics of Australia's 'passive'margins: intraplate deformation controlled by plate boundary forces. *Geological Society of London, Special Publications* **306**(1), 71–90. doi:10.1144/SP306.3

Holford, S. P., Hillis, R. R., Duddy, I. R., Green, P. F., Tassone, D. R., and Stoker, M. S. (2011). Paleothermal and seismic constraints on late Miocene–Pliocene uplift and deformation in the Torquay sub-basin, southern Australian margin. *Australian Journal of Earth Sciences* **58** (5), 543–562. doi:10.1080/08120099.2011.565074

Holford, S. P., Tuitt, A. K., Hillis, R. R., Green, P. F., Stoker, M. S., and Duddy, I. R. (2014). Cenozoic deformation in the OB, southern Australian margin: implications for the origin and nature of post-breakup compression at rifted margins. *Basin Research* **26**(1), 10–37. doi:10.1111/bre.12035

Hrouda, F. (1991). Models of magnetic anisotropy variations in sedimentary thrust sheets. *Tectonophysics* **185**(3–4), 203–210. doi:10.1016/0040-1951(91)90444-W

Jelinek, V. (1981). Characterization of the magnetic fabric of rocks. *Tectonophysics* **79**(3–4), T63–T67. doi:10.1016/0040-1951(81)90110-4

Kissel, C., Barrier, E., Laj, C., and Lee, T. Q. (1986). Magnetic fabric in "undeformed" marine clays from compressional zones. *Tectonics* **5**(5), 769–781. doi:10.1029/TC005i005p00769

Krassay, A. A., Cathro, D. L., and Ryan, D. J. (2004). A regional tectonostratigraphic framework for the Otway Basin. In 'Eastern Australasian Basins Symposium II. Petroleum Exploration Society of Australia, Special Publication.' (Eds P. J. Boult, D. R. Johns and S. C. Lang.) pp. 97–116. (PESA: Adelaide, SA).

Kulikowski, D., and Amrouch, K. (2017). Combining geophysical data and calcite twin stress inversion to refine the tectonic history of subsurface and offshore provinces: A case study on the Cooper-Eromanga Basin, Australia. *Tectonics* **36**(3), 515–541. doi:10.1002/2016TC004366

Kulikowski, D., Amrouch, K., and Burgin, H. B. (2018). Mapping permeable subsurface fracture networks: A case study on the Cooper Basin, Australia. *Journal of Structural Geology* **114**, 336–345. doi:10.1016/j.jsg.2018.02.009

Lacombe, O. (2001). Paleostress magnitudes associated with development of mountain belts: Insights from tectonic analyses of calcite twins in the Taiwan Foothills. *Tectonics* **20**(6), 834–849. doi:10.1029/2001TC900019

Lacombe, O., Amrouch, K., Mouthereau, F., and Dissez, L. (2007). Calcite twinning constraints on late Neogene stress patterns and deformation mechanisms in the active Zagros collision belt. *Geology* **35**(3), 263–266. doi:10.1130/G23173A.1

Lacombe, O., Malandain, J., Vilasi, N., Amrouch, K., and Roure, F. (2009). From paleostresses to paleoburial in fold–thrust belts: Preliminary results from calcite twin analysis in the Outer Albanides. *Tectonophysics* **475**(1), 128–141. doi:10.1016/j.tecto.2008.10.023

Laurent, P. (1984). Les macles de la calcite en tectonique: nouvelles méthodes dynamiques et premières applications. Thése d'Etat (Doctoral dissertation), Université de Montpellier, Montpellier. [In French]

Laurent, P., Kern, H., and Lacombe, O. (2000). Determination of deviatoric stress tensors based on inversion of calcite twin data from experimentally deformed monophase samples. Part II. Axial and triaxial stress experiments. *Tectonophysics* **327**(1–2), 131–148. doi:10.1016/S0040-1951(00)00165-7

Lyon, P. J., Boult, P. J., Hillis, R. R., and Bierbrauer, K. (2007). Basement controls on fault development in the Penola Trough, OB, and implications for fault-bounded hydrocarbon traps. *Australian Journal of Earth Sciences* **54**(5), 675–689. doi:10.1080/08120090701305228

Mattei, M., Sagnotti, L., Faccenna, C., and Funiciello, R. (1997). Magnetic fabric of weakly deformed clay-rich sediments in the Italian peninsula: relationship with compressional and extensional tectonics. *Tectonophysics* **271**(1-2), 107–122. doi:10.1016/S0040-1951(96)00244-2

McGowran, B., Holdgate, G. R., Li, Q., and Gallagher, S. J. (2004). Cenozoic stratigraphic succession in southeastern Australia. *Australian Journal of Earth Sciences* **51**(4), 459–496. doi:10.1111/j.1400-0952.2004.01078.x

Norvick, M. S., and Smith, M. A. (2001). Mapping the plate tectonic reconstruction of southern and southeastern Australia and implications for petroleum systems. *The APPEA Journal* **41**(1), 15–35. doi:10.1071/AJ00001

O'Brien, G. W., Reeves, C. V., Milligan, P. R., Morse, M. P., Alexander, E. M., and Willcox, J. B. (1994). New ideas on the rifting history and structural architecture of the western OB: evidence from the integration of aeromagnetic, gravity and seismic data. *The APPEA Journal* **34**(1), 529–554. doi:10.1071/AJ93042

O'Brien, G., Boreham, C., Thomas, H., and Tingate, P. (2009). Understanding the critical success factors determining prospectivity—Otway Basin, Victoria. *The APPEA Journal* **49**(1), 129–170. doi:10.1071/AJ08009

Parlangeau, C., Dimanov, A., Lacombe, O., Hallais, S., and Daniel, J. M. (2019). Uniaxial compression of calcite single crystals at room temperature: insights into twinning activation and development. *Solid Earth* **10**(1), 307–316. doi:10.5194/se-10-307-2019

Perincek, D., and Cockshell, C. D. (1995). The OB: early Cretaceous rifting to Neogene inversion. *The APPEA Journal* **35**(1), 451–466. doi:10.1071/AJ94029

Perincek, D., Simons, B., and Pettifer, G. R. (1994). The tectonic framework and associated play types of the western Otway Basin, Victoria, Australia. *The APPEA Journal* **34**(1), 460–478. doi:10.1071/AJ93038

Rajabi, M., Heidbach, O., Tingay, M., and Reiter, K. (2017*a*). Prediction of the present-day stress field in the Australian continental crust using 3D geomechanical–numerical models. *Australian Journal of Earth Sciences* **64**(4), 435–454. doi:10.1080/08120099.2017.1294109

Rajabi, M., Tingay, M., Heidbach, O., Hillis, R., and Reynolds, S. (2017*b*). The present-day stress field of Australia. *Earth-Science Reviews* **168**, 165–189. doi:10.1016/j.earscirev.2017.04.003

Robert, R., Robion, P., Souloumiac, P., David, C., and Saillet, E. (2018). Deformation bands, early markers of tectonic activity in front of a fold-and-thrust belt: Example from the Tremp-Graus basin, southern Pyrenees, Spain. *Journal of Structural Geology* **110**, 65–85. doi:10.1016/j.jsg.2018.02.012

Robion, P., Grelaud, S., and de Lamotte, D. F. (2007). Pre-folding magnetic fabrics in fold-and-thrust belts: Why the apparent internal deformation of the sedimentary rocks from the Minervois basin (NE—Pyrenees, France) is so high compared to the Potwar basin (SW—Himalaya, Pakistan)? *Sedimentary Geology* **196**(1–4), 181–200. doi:10.1016/j.sedgeo.2006.08.007

Robson, A. G., Holford, S. P., King, R. C., and Kulikowski, D. (2018). Structural evolution of horst and half-graben structures proximal to a transtensional fault system determined using 3D seismic data from the Shipwreck Trough, offshore OB, Australia *Marine and Petroleum Geology* **89**(3), 615–634. doi:10.1016/j.marpetgeo.2017.10.028

Rochette, P., Jackson, M., and Aubourg, C. (1992). Rock magnetism and the interpretation of anisotropy of magnetic susceptibility. *Reviews of Geophysics* **30**(3), 209–226. doi:10.1029/92RG00733

Rowe, K. J., and Rutter, E. H. (1990). Palaeostress estimation using calcite twinning: experimental calibration and application to nature. *Journal of Structural Geology* **12**(1), 1–17. doi:10.1016/0191-8141(90)90044-Y

Sandiford, M., and Quigley, M. (2009). TOPO-OZ: Insights into the various modes of intraplate deformation in the Australian continent. *Tectonophysics* **474**(1–2), 405–416. doi:10.1016/j.tecto.2009.01.028

Sandiford, M., Wallace, M., and Coblentz, D. (2004). Origin of the in situ stress field in south-eastern Australia. *Basin Research* **16**(3), 325–338. doi:10.1111/j.1365-2117.2004.00235.x

Schneider, C. L., Hill, K. C., and Hoffman, N. (2004). Compressional growth of the Minerva Anticline, Otway Basin, Southeast Australia—evidence of oblique rifting. *The APPEA Journal* **44**(1), 463–480. doi:10.1071/AJ03018

Soto, R., Casas-Sainz, A. M., Villalaín, J. J., and Oliva-Urcia, B. (2007). Mesozoic extension in the Basque–Cantabrian basin (N Spain): contributions from AMS and brittle mesostructures. *Tectonophysics* **445**(3–4), 373–394. doi:10.1016/j.tecto.2007.09.007

Stacey, A., Mitchell, C., Struckmeyer, H., and Totterdell, J. (2013). Geology and hydrocarbon prospectivity of the deepwater Otway and Sorell Basins, offshore southeastern Australia. Geoscience Australia, Canberra. Available at: https://d28rz98at9flks.cloudfront.net/74603/Rec2013_002.pdf [verified 12 March 2019]

Tarling, D., and Hrouda, F. (1993). 'Magnetic anisotropy of rocks'. (Springer Science & Business Media: Berlin, Germany).

Tassone, D. R., Holford, S. P., Duddy, I. R., Green, P. F., and Hillis, R. R. (2014). Quantifying Cretaceous–Cenozoic exhumation in the Otway Basin, southeastern Australia, using sonic transit time data: Implications for conventional and unconventional hydrocarbon prospectivity. *AAPG Bulletin* **98**(1), 67–117. doi:10.1306/04011312111

Tavani, S., Storti, F., Lacombe, O., Corradetti, A., Muñoz, J. A., and Mazzoli, S. (2015). A review of deformation pattern templates in foreland basin systems and fold-and-thrust belts: Implications for the state of stress in the frontal regions of thrust wedges. *Earth-Science Reviews* **141**, 82–104. doi:10.1016/j.earscirev.2014.11.013

Veevers, J. J. (2000). Change of tectono-stratigraphic regime in the Australian plate during the 99 Ma (mid-Cretaceous) and 43 Ma (mid-Eocene) swerves of the Pacific. *Geology* **28**(1), 47–50. doi:10.1130/0091-7613(2000)28<47:COTRIT>2.0.CO;2

Wilcox, J. B., Colwell, J. B., and Constantine, A. E. (1992). New Ideas on Gippsland Basin Regional Tectonics. In 'Energy, Economics and Environment, Gippsland Basin Symposium, Melbourne, 22–23 June 1992'. (Eds .M. Barton, K. Hill, C. Abele, J. Foster, N. Kempton) pp. 93–110. (AusIMM and PESA: Melbourne, VIC).

Zoback, M. L., Zoback, M. D., Adams, J., Assumpcao, M., Bell, S., Bergman, E. A., Blumling, P., Brereton, N. R., Denham, D., Ding, J., Fuchs, K., Gay, N., Gregersen, S., Gupta, H. K., Gvishiani, A., Jacob, K., Klein, K., Knoll, P., Magee, M., Mercier, J. L., Muller, B. C., Paquin, C., Rajendran, K., Stephansson, O., Suarez, G., Suter, M., Udias, A., Xu, Z. H., and Zhizhin, M. (1989). Global patterns of tectonic stress. *Nature* **341**(6240), 291–298. doi:10.1038/341291a0

Zoback, M. D., Barton, C. A., Brudy, M., Castillo, D. A., Finkbeiner, T., and Grollimund, B. R. (2003). Determination of stress orientation and magnitude in deep wells. *International Journal of Rock Mechanics and Mining Sciences* **40**(7–8), 1049–1076. doi:10.1016/j.ijrmms.2003.07.001

The authors

Hugo Burgin is a PhD candidate at the Australian School of Petroleum and an awardee of the Australian Endeavour Research Fellowship in 2017 and the AAPG Grants in Aid Scheme in 2018. His interests include structural geology and petroleum geoscience. He is entering the Australian oil and gas industry in 2019 as a Graduate Geoscientist with ExxonMobil.

Dr Khalid Amrouch is a structural geologist with expertise in geomechanics. He graduated from the University of Pierre and Marie Curie (Paris VI) with a MSc and a PhD in structural geology. His main interests relate to brittle tectonics, fracture characterisation and 4D stress analyses. Khalid started his career in 2005 at the Institut Français du Pétrole, which sponsored his studies, followed in 2010 by a position as a Research Engineer at Mines PariTech. In 2012, Khalid spent one year working for BHP as an Exploration Geologist in Chile, before joining the Australian School of Petroleum in February 2013. Since then, Khalid has been an active member of the S3 Research Group, one of the largest geoscience research groups at the University of Adelaide.

Dr Philippe Robion is a Senior Lecturer in Geoscience at the Department of Geosceience and Environment at the Université of Cergy-Pontoise in Paris. He has skills and expertise within structural geology, tectonics and basin analysis, with a focus on microstructural analysis techniques and the anisotropy of physical and mechanical properties of geomaterials.

Dr David Kulikowski recently completed his PhD in structural geology and geophysics from the Australian School of Petroleum, University of Adelaide. His PhD was titled "Modern Structural Analysis of Subsurface Provinces: A Case Study on the Cooper and Eromanga Basins, Australia" and involved the analysis of micro-, meso- and macros-scale data obtained through geophysics or core analysis. He produced nine first author papers (published in highly respected journals, such as Tectonics, Marine & Petroleum Geology, Journal of Structural Geology, Australian Journal of Earth Sciences and Geophysical Prospecting, to name a few) and contributed to several other papers as a co-author. He was awarded the Dean's Commendation for Doctoral Thesis Excellence and was nominated by both of his PhD reviewers for the University Doctoral Research Medal. David currently works at Woodside Energy in an exploration role.

Chapter 4.3.2: Manuscript 4

4D structural evolution of Australia's Great Ocean Road Region: The first quantification of paleostresses at a Passive Continental Margin

This finalised manuscript will be submitted to the peer reviewed journal *Tectonics*.

Statement of Authorship

Title of Paper: 4D structural evolution of Australia's Great Ocean Road Region: The first quantification of paleostresses at a Passive Continental Margin

Publication Status: Unpublished and Unsubmitted work written in a manuscript style

Publication Details: Burgin, H. B. and Amrouch, K. (2019b). 4D structural evolution of Australia's Great Ocean Road Region: The first quantification of paleostresses at a Passive Continental Margin (In Prep)

Principal Author: Hugo Bonython Burgin

Contribution: 3D seismic interpretation. Field work. Calcite twin analysis. Stress inversion. Paper writing (80%)

Certification: This paper reports on original research I conducted during the period of my Higher Degree by Research candidature and is not subject to any obligations or contractual agreements with a third party that would constrain its inclusion in this thesis. I am the primary author of this paper.

Signed: **Date:** 05/03/2019

Co-Author Contributions

By signing the Statement of Authorship, each author certifies that:

- **i.** The candidate's stated contribution to the publication is accurate (as detailed above);
- **ii.** Permission is granted for the candidate in include the publication in the thesis; and
- **iii.** The sum of all co-author contributions is equal to 100% less the candidate's stated contribution.

Name of Co-Author: Dr Khalid Amrouch

Contribution to Paper: Supervision and guidance with structural interpretation and stress inversion (20%)

Signed: **Date:** 05/03/2019

4D structural evolution of Australia's Great Ocean Road Region: The first quantification of paleostress at a Passive Continental Margin

*Hugo B. **BURGIN**[a] (hugo.burgin@adelaide.edu.au)

Khalid **AMROUCH**[a] (khalid.amrouch@adelaide.edu.au)

[a]Australian School of Petroleum, University of Adelaide, North Tce, 5005, Adelaide, Australia

*Corresponding Author: Hugo B. Burgin (hugo.burgin@adelaide.edu.au)

Abstract

This paper presents the first quantification of stress patterns across space and time at a passive continental margin, through the use of a multi-scale structural analysis. The case study: Australia's Southern Margin and the Otway Basin, which is traversed by the country's famous Great Ocean Road, a major tourist attraction.

We investigate the chronological relationship of paleostress events, derived from the interpretation of three 3D seismic datasets, surface and subsurface natural fractures and stress tensors calculated from calcite twins. The multi-scale data defining five phases of Late Cretaceous – recent, basin evolution: 1) ~NE-SW oriented rifting 2) on-going radial style extension, during what should have been the final stages of continental breakup 3) strike-slip, followed by compressional, ~NE-SW inversion during the Latest Cretaceous (Mid-Maastrichtian) 4) relaxation of the system, renewed extension and continental break up followed by 5) tectonic reorganisation and an increase in ~NW-SE oriented horizontal stresses in the Late Miocene. The proposed ~NE-SW extension and inversion of the system is reflected across kinematic and chronological datasets on the macro (seismic), meso (outcrop/wellbore)

and microscale (crystal). Quantification of paleo-differential stress magnitudes from calcite twins show a phase-to-phase variation throughout basin evolution, with some of the highest extensional stress magnitudes calculated to date using calcite twin analysis, attributed to phases of continental break up. In addition to re-defining the structural framework of one of Australia's most studied basins, this work provides original insights into the nature of stress evolution at inverted passive continental margins.

1.0 Introduction

Studying the mechanical relationship between stress magnitudes and the brittle deformation of rocks is a challenge. Even so, the analysis of features such as faults (Angelier, 1989), stylolites (Ebner et al., 2009; Beaudoin et al., 2016; Ebner et al., 2010) and calcite twins (Jamison and Span, 1976; Rowe and Rutter, 1990; Lacombe and Laurent, 1996; Amrouch et al., 2011) in brittlely deformed rocks has allowed for the determination and quantification of various elements of the paleostress tensor.

Though fruitful, a drawback of studies utilising these methods is that – barring the rare case of densely spaced geophysical and oriented core data (e.g. Kulikowski and Amrouch, 2017) – they typically rely on a hands on approach to structural analysis. Involving the systematic collection of mesoscale (outcrop) and microscale (crystal) datasets, leading to the construction of a three or four dimensional model of stress evolution (e.g. Lacombe et al., 2007; Beaudoin et al., 2012; Amrouch et al., 2010). Due to this requirement, the majority of these studies, especially those using calcite twins have been focused in tectonic settings associated with high levels of easily accessible brittle deformation. Typically, fold-and-thrust belts [Zagros – Iran, (Amrouch et al., 2005; Lacombe et al.,2007; Amrouch, 2010), Khao Khwang-Thailand, (Arboit et al., 2015; 2017), The Albanides - Albania, (Lacombe et al., 2009), The Apenines – Italy, (Beaudoin et al., (2016), Parlangeau et al., 2018), SW Taiwan Foothills – Taiwan, (Lacombe, 2001), Rocky Mountains – Canada, (Jamison and Spang, 1976)] and stable foreland basins [Big Horn Basin – Wyoming, (Craddock and Van Der Pluijm, 1999; Amrouch et. al., 2010a, 2010b; Beaudoin et al., 2012, 2016), Paris Basin – France, (Lacombe and Laurent, (1992), Tourneret and Laurent, (1990), Lacombe et al., (1990; 1994), Rocher et al.,2004) associated with neighbouring orogenic belts.

Comparatively, the contribution techniques of paleostress determination and quantification can make towards the study of more "passive," tectonic settings, such as continental margins, has not been explored. As a result, our knowledge of how crustal stresses develop during episodes of plate scale tension, is vastly exceeded by our understanding of deformation driven by tectonic compression (Lacombe, 2006).

In order to better constrain the complete pathway of deformation within the upper crust it is important to continue to complement our knowledge of in situ stresses, and neotectonic activity with the study of paleostress. Having matured over the last 20 years, paleostress analysis is moving into the 21st century (Beaudoin and Lacombe, 2018; Parlangeau et al., 2018; 2019), with the integration of modern geophysical datasets and traditional methods now possible (Kulikowski and Amrouch, 2017). Alongside freely available software packages utilising the approaches (e.g. Wintensor [Delvaux, 2010]) and the continued refinement of traditional analytical methods (e.g Yamaji, 2015a; 2015b; Parnlangeau et al., (2019). Given these advances, we must take care not to limit our investigations to the most convenient tectonic settings, and the reliable and consistent nature of the datasets they present.

Passive margin sedimentary basins are often characterised by complex histories of rifting, and episodic periods of basin inversion (Ziegler, 1982; Van Hoorn, 1987; Koopman et al., 1987; Garcia-Lasanta et al., 2018). Periods of deformation that are not easily defined simply through the use of geophysical datasets, especially as their influence extends within both on and offshore provinces. Even so, understanding the stress pathway with regard to the evolution of paleostress orientations, and magnitudes in these settings is valuable, and an opportunity to test the limits of our investigative techniques. Especially as many ocean facing passive margin basins present scientific, environmental and industrial value.

Though the scale of deformation is far below the high pressure and high temperature levels of near ductile deformation within many major fold-and-thrust belts. Fortunately, many passive margin sedimentary basins have been subjected to episodic inversion. Resulting in the reverse reactivation of space-creating normal faults, allowing for early rift units to be up-lifted and exposed within coastal shallow water environments. These scenarios representing a unique opportunity for the integration of predominantly onshore techniques of multiscale analysis, such as the stress inversion of faults, fractures and calcite twins. Alongside the interpretation of cutting edge geophysical datasets and the complimentary opportunities they contain.

This study presents an effort to expand the field of paleostress beyond its tectonic comfort zone. Undertaking the first multiscale assessment of paleostress orientations and magnitudes at a passive continental margin. The chosen case study; the Otway Basin (**fig. 1**) represents one of Australia's most important natural resources, hosting a number of oil and gas fields, geothermal energy projects and the largest functional carbon capture and storage project in the southern hemisphere.

The basin has experienced varying degrees of extensional (Lyon et al., 2007; Robson et al., 2016; 2017; 2018) and compressional (Holford et al., 2014) deformation. With neotectonic compressive stresses (**fig. 2a**) suggested to have formed a series of ~NE-SW trending anticlines, through the reactivation of ~NE-SW striking faults, concentrated within the eastern section of the basin (**fig. 2c,d**) striking ~90º to the present day orientation of maximum horizontal stress (Edwards et al., 1996; Holford et al., 2014). This model is considered problematic by some (Burgin and Amrouch, 2019a; Burgin et al., 2019). Due to no kinematic

evidence for the existence of these faults and the fact they have never been viewed in three dimensions in the subsurface or outcrop.

Taking the Otway Basin as a case study, this paper demonstrates the applicability of a multiscale approach to structural analysis at passive continental margins. Reassessing the framework of the study area, whilst simultaneously providing the first insight into the multi-phase evolution of paleostresses during continental breakup. The discussed industrial importance of the basin exists in parallel to a delicate ecosystem and agricultural industry, dissected by the Great Ocean Road. One of the Australia's most famous tourist attractions. With outcropping Early Cretaceous rift units in the Otway Ranges (**fig. 2**) and an abundance of regional geophysical data, the basin is the perfect natural laboratory to undertake this study. Pushing the analysis of paleostresses into a new frontier.

2.0 Geological Setting of the Otway Basin

2.1 Structural Framework

The Otway Basin (**fig. 1b**) is located along the southeastern margin of the Australian continent. The basin covers approximately 150,000km^2 within on and offshore provinces, trending ~NW-SE having formed due to the Late Jurassic to Early Paleogene break up of Gondwana and the resulting separation of Australia and Antarctica (Norvick and Smith, 2001; Krassay et al., 2004). The axis for extension within the region is debated with multiple interpretations having been suggested including NW-SE (Wilcox and Stagg, 1990), NE-SW (Perincek et al., 1994), N-S (Lyon et al., 2007; Burgin and Amrouch, 2019a) in addition to other more intermediate directions (Etheridge et al., 1985; Hill et al., 1994).

While the basin has seen a large amount of structural studies, many of them have focused on either individual structures, surveys (e.g; Schnieder et al., 2004; Robson et al., 2016; 2017; 2018, Luxton et al., 1995; Holford et al., 2011) or sections (e.g. Onshore Western Basin: Lyon et al., 2007, Eastern Basin: Hill et al, 1995), which means their outcomes are often limited to the local scale. Many of these studies have also exclusively used two dimensional (2D) seismic analysis (e.g. Hill et al., 1995; Krassay et al., 2004; Holford et al., 2014), a powerful and popular tool, but one with limitations, especially when interpreting complex geological structures (Burgin and Amrouch, 2019a).

Under the current structural framework, the basin is divided into western, central and eastern portions (Tassone et al., 2017). The western and central section's consisting of mainly ~NW-SE and ~E-W striking fault networks (Lyon et al., 2007; Burgin and Amrouch, 2019a). The eastern basin, including the Otway Ranges and Torquay Sub-Basin (**fig. 2**) supposedly dominated by ~NNE-SSW striking normal and strike slip faults. A number of studies suggesting that this second set of faults have been subjected to reverse reactivation and inversion during the Miocene – recent, as a result of neotectonic, ~NW-SE trending maximum horizontal stresses (Edwards et al., 1996; Dickenson, 2002; Holford et al., 2014 Debenham et al., 2018). As such, most studies describe the Otway Ranges, where much of our analysis is based, as a ~NE-SW trending series of anticlines subjected to uplift and inversion from the Late Miocene – recent (Medwell, 1971; Edwards et al., 1996; King et al., 2012; Holford et al., 2014; Debenham et al., 2018). The Shipwreck Trough (**fig. 1b**) to the south east of the Otway Ranges, contains N-S trending strike slip faults (Robon et al., 2018).

2.2 Stratigraphy of the Eastern Otway Basin

Initial rifting within the Otway Basin was concentrated onshore in the north (Lyon et al., 2007; Bruigiglo et al., 2014; Burgin and Amrouch, 2019a), taking place between the Late Jurassic (Berriasian) to the mid-Early Cretaceous (Barremian). A period characterised by the syn-depositional basin fills of the Casterton Formation and Crayfish Sub-Group (**fig. 3a**). Extension in this phase was most intense in the western Otway Basin, estimated at ~21%, compared to only ~12% in the east (Cooper and Hill, 1997; Brugiglo et al., 2014).

During a cessation of rifting, and a period of subsidence during the Aptian – Albian, the post-rift-sag Eumerella Formation was deposited, largely unaffected by initial rift (Berriasian – Barremian) faults (Krassay et al., 2004; Lyon et al., 2007; Burgin and Amrouch, 2019a). The formation is thickest in the offshore sections of the eastern Otway Basin and forms the majority of the Otway Ranges (**fig. 2c**). It is comprised of interbedded clays, sands, siltstones and coals and outcrops mainly along the coast of the Otway Ranges, in weathered wave-cut platforms. The Eumeralla Formation is the source rock for the hydrocarbon systems and natural gas accumulations within the eastern Otway Basin (O'Brien et al., 2009; Bernecker et al., 2013) and is marked at its top by an unconformity. A boundary that is thought to be caused by uplift and inversion, during an episode of ~NW-SE compression during the Mid Cretaceous (~100Ma). However, there is no evidence for this event in the western Otway Basin (Burgin and Amrouch, 2019a).

Active rifting recommenced at the start of the Late Cretaceous, major faulting moving offshore, to the south (Krassay et al., 2004; Lyon et al., 2007). Defining a stage of continental separation, which coincided with the deposition of the Late Cretaceous Sherbrook Group (**fig. 3a**) (Geary and Reid, 1998). A formation which is also marked at its top by an unconformity due to erosion

and uplift in the Mid Maastrichtian. Identified as a major period of cooling by Duddy and Erout (2002) and their thermo-chronological analysis (**fig. 3c**) of the Mussel Terrace (**fig. 1b**). The cooling episode beginning at ~60Ma, coinciding with the commencement of a regional increase in denudation rates across much of south eastern Australia (Kohn et al., 2002) (**fig. 3b**). Eventual continental break up was followed by a period of subsidence and the deposition of the Wangerrip and Nirranda Groups during the early Palaeogene (**fig. 3a**) (~60 -30Ma). As well as a shift to fast seafloor spreading and the rapid northward movement of Australia, beginning in the Mid Eocene (Muller et al., 2002).

Two distinct styles of continental break up have been proposed in the Otway Basin, characterised by the presence or absence of detachment style faulting. Etheridge et al., (1987) describing a branched rift system dependent upon upper and lower plate geometries (Lister et al., 1986), consisting of ~NW-SE striking normal listric faults, proposed by the authors to sole out along shallow dipping detachment surfaces. A pattern that characterises broadly ~NE-SW extension across much of southeastern Australia. On the other hand, Cooper and Hill (1997), suggest that under the influence of a pre-existing basement fabric, local stress perturbations may occur and fault strike will not develop perpendicular to the direction of tectonic transport and the azimuths of stretching. Proposing an oblique rift model where faults of multiple orientations form coincidentally under ~NNW-SSE and N-S extensional azimuths during continental separation. Citing ~NE-SW striking faults within the Otway Ranges and surrounding ~NW-SE striking faults as their primary evidence.

2.3 Basement Units of the Eastern Otway Basin

Basement style varies significantly throughout the Otway Basin (Vendenberg et al., 2000) (**fig. 2b**). From pre-Permian basement terranes taken from Vandenberg et al., (2000) it can be seen that the eastern most sector of the Otway Basin is underlain by the Palaeozoic Selwyn Block (**fig. 2b**), its extent within the onshore basin being analogous with the location of the Otway Ranges (**fig. 2b**). Data taken from a basin wide study (Krassay et al., 2009) employing multiple advanced approaches to map basement depth in the same region, show that this sector of basement marks a regional transition towards a basement high that underlies the Otway Ranges, and much of the nearby Bass Basin (**fig. 2b**).

Detailed regional analysis of the Selwyn Block has shown that its influence has had a lasting effect on the development of post-Palaeozoic units throughout nearby parts of onshore eastern Australia. Cayley et al., (2002) noted that the Otway Ranges are underlain by some of the shallowest portions of the Selwyn Block, and that its presence beneath this sector of the basin likely explains why the region has remained a structural high throughout time. Although no substantial connection between this basement high and the development of the Otway Ranges has been made to date.

3.0 Data sets and methodology

In order to extrapolate the results across space and time, and produce a high resolution structural model we use analytical techniques across multiple scales (**fig. 4a**).

Microscale data is highly sensitive to even far field stresses (Amrouch et al., 2010a; Kulikowski and Amrouch, 2017) and allows for the quantification of paleostress and strain magnitudes and orientations. However, such data is almost pointless without higher order information to

provide a local structural context and ensuring that stress perturbations are not influencing the results.

While mesoscale approaches allow for detailed mapping of faults and fractures to occur, in most cases they require vast outcropping sections or densely spaced well data for data collection. Also requiring a high number of outcrop faults (>15) per site for accurate stress inversion to take place (Angelier, 1984; 1990; Lacombe, 2012), a distinguishing characteristic that limits their applicability to mainly highly deformed settings. As with microscale data, when used in isolation mesoscale approaches also provide little regional context.

Modern macroscale techniques of analysis are powerful, but used in isolation they provide no insight into paleostress magnitudes or micro and mesoscale deformation. Additionally as they only provide the final structure, there is no way to determine the presence of early or subtle phases of stress, whose effects have been overprinted by later stages of deformation. A distinction which is possible on the micro and the meso scale.

As such, the combination of techniques across all three scales, provides all of their strengths, while simultaneously eliminating their individual weaknesses. Allowing for a quantified and spatially comprehensive structural model to be constructed. This approach has recently been used in Australia's intra-cratonic Cooper Basin, with much success (Kulikowski and Amrouch, 2017).

3.1 Macroscale - Structural analysis of 3D seismic datasets and Elementary Stress Pathway

3.1.1 Datasets

This study uses the Champion-Hercules 3D, Minerva-Schomberg 3D and Crows Foot 3D seismic surveys positioned in the offshore eastern Otway Basin, parallel to the coastline and directly orthogonal to the NE-SW trend of the Otway Ranges (**fig. 2c**).

3.1.1.1 The Champion-Hercules 3D

The Champion-Hercules merged 3D seismic reflection survey covers an area of ~517km^2 and has a maximum penetration of 4.0s two-way time. The northern edge of the 3D survey is positioned ~10km from the southern coast of Australia. Inlines strike NW-SE and are spaced at 25m with crosslines striking NE-SW spaced at 12.5m. Multiple wells are present within the survey area including, Champion-1, Halladale-1[DW-1, 2, 3], Pecten 1 and 1A, Henry-1 and Henry-1ST1. Processing artefacts inhibit the use of seismic attributes within the top 1.5s TWT.

The survey has a vertical resolution conservatively calculated at 65m with a dominant frequency of 16.5Hz at 3 seconds TWT. Detailed horizon interpretation of the Top Late Cretaceous and Top mid-Eocene was completed, with the Top Early Cretaceous also identified. Interpretations were tied to data from Henry-1, Henry-1ST11, and Pecten-1 and 1A, the structural analysis focused on the region of the Pecten Anticline (Holford et al., 2014) (**fig. 2c**) to determine the true geometry of the structure. Velocity check-shot data from Henry-1 was used for depth conversion as part of a standard windowing velocity model.

3.1.1.2 *The Schomberg-Minerva 3D*

The Schomberg-Minerva merged 3D seismic reflection survey covers ~457km^2 with a maximum penetration of 6.1s two-way time. The northern edge of the 3D survey is positioned only ~1km from the southern coast of Australia and the Great Ocean Road. Inlines strike NE-

SW and are spaced at 25m with crosslines striking NW-SE spaced at 12.5m. Multiple wells are present within the survey area including, Minerva-1, Minerva-2 (**fig.1**).

The survey has particularly good vertical resolution of 63m at 3 seconds TWT, with a dominant frequency of 14.8Hz, with the regular definition of the regional basement – interpreted as the Selwyn Block (**fig. 2b**) - possible. Horizon interpretation for the Top Basement (Selwyn Block), Top Santonian and Top Late Cretaceous was tied to data from Minerva-1 and Minerva-2. The main goal being to investigate the style of faulting, and the nature of the Minerva and Point Ronald Anticlines (Holford et al., 2014).Velocity check-shot data from Minerva-2 was used for depth conversion, as part of a standard windowing velocity model.

3.1.1.3 The Crows Foot 3D

The Crows Foot 3D seismic reflection survey was acquired in 2016 and covers an area of ~656 km^2 with a maximum penetration of 7.0s two-way time. The northern edge of the 3D survey is positioned only ~8km from the southern coast of the Otway Ranges, covering what is essentially the offshore continuation of the structure, within a previously poorly mapped section of the Prawn Platform (**fig. 1b**). Inlines strike N-S and are spaced at 25m with crosslines striking E-W spaced at 12.5m. Two wells are present within the survey, Eric the Red-1 and Loch Ard-1.

Vertical resolution is poor in comparison with the other surveys, calculated at approximately 126m at 3 seconds TWT, with a dominant frequency of 9.9Hz. Seismic quality decreasing rapidly with depth past ~2km. Horizon interpretation of the Top Early Cretaceous, Top Santonian and Top Late Cretaceous was completed, and tied to well data from both Eric the Red-1 and Loch Ard-1. However, complex structuring, poor resolution and the isolated nature

of the well data made this a challenge, especially within the western section of the survey. Analyses of the Crowes and Loch Ard anticlines (Holford et al., 2014) as well as the first interpretation of fault trends within the offshore Otway Ranges was the main goal. Velocity check-shot data from both wells was used for depth conversion, as part of a standard windowing velocity model.

3.1.*2 An elementary stress pathway from 3D seismic interpretation*

Many studies use the analysis of 3D seismic datasets to construct a model of basin evolution, or as we term it an "elementary stress pathway," (ESP) (e.g. Lyon et al., 2007; Teasdale et al., 2003) which essentially reflects a basic understand of the evolution of stress within the study area.

Recently, work by Kulikowski and Amrouch (2017), has expanded these techniques utilising macroscale geophysical datasets alongside a basic stress inversion on faults extracted from 3D seismic. We adopt a similar technique, constructing an ESP that relies on both the seismic interpretation of the data alongside a basic stress inversion of faults within each survey. During this process, faults interpreted during 3D seismic interpretation are broken down into polygons using a triangular dislocation theory within Move 2017.2 (Midland Valley Exploration Ltd., 2017). Each polygon is represented by a single plane, upon which we assume dip-slip movement and paleostress orientations are then calculated for the grouped planes, with the assistance of stress orientation tool Wintensor (Delvaux and Sperner, 2003).

3.2 Natural fracture analysis

Fracture and microscale fault data (offset on the scale of 2-5cm) were collected from 31 locations across the Otway Ranges within the Early Cretaceous Eumeralla Formation (e.g. **fig.**

352 **5** and **fig. 6**). Analysis was restricted to where 3D geometry was observable, recording the
353 orientation, modes of deformation and cross cutting relationships (Bellahsen et al., 2006a;
354 Amrouch et al., 2010; Beaudoin et al., 2012).
355
356 Major fracture sets were defined based on their 3D geometry, mode of opening and relationship
357 with the bedding and other fractures. Evidence for fracture modes of formation was mainly
358 mode-2, supported by centimeter scale faulting in the same sense (**fig. 6a**) and the presence of
359 text-book style Andersonian (Anderson, 1951) conjugate sets of a similar geometry (**fig. 5a, b,**
360 **e**). Mode-1 opening was interpreted in some cases (Engelder, 1987; Pollard and Aydin, 1988)
361 due to the preservation of plume structures. The process of fracture categorization was assisted
362 by paleostress orientation tool Wintensor (Delvaux and Sperner, 2003). A software digitizing
363 the approach of Angelier (1989) that allows for fracture sets to be assigned stress regimes for
364 integration with paleo-σ3 orientations derived from 3D seismic and calcite twin analysis.
365
366 Furthermore natural fracture data were collected from geophysical image logs, with lengths
367 between 259-1151m, from five wells in the eastern Otway Basin (**fig. 1**) (**table 1**). The wells
368 penetrating sedimentary units both Early and Late Cretaceous in age. In the sub-surface mode
369 of formation was controlled from examples of previous mode-2 fracturing within the same
370 sequences at other locations within the basin (Burgin and Amrouch, 2019). Allowing for the
371 assigning of paleostress regimes in the same manner as outcrop data, assuming shear modes of
372 nucleation. Sub-surface natural fractures were divided into major sets based upon common
373 orientation and geometry and their corresponding paleo-σ3 orientations (Engelder, 1987).
374
375 Fracture data were assessed with pre and post-folding fracture-bedding relationships,
376 determined on a site by site basis, though this was not possible in the subsurface as bedding

dip was minimal across most intervals. The variation of natural fracture geometry and their paleostress conditions -due to variations from pre-existing faults and fractures- was also considered. Fracture cluster determination was completed using Stereonet v9.3.2 (Almendinger, 2013) and the 1% area contouring algorithm. This approach considers each contouring interval within the lower hemisphere stereogram to be constrained to 1% of the total net area, with fracture clusters determined as poles to planes based upon their grouping patterns as indicated by the contouring method.

3.3 Quantification of Maximum Differential Stress Magnitudes with Calcite Twin Inversion

Since 1953 (Turner, 1953) there have been several methods of calcite twin analysis and inversion employed to produce meaningful paleostress tensor orientations and magnitudes (Etchecopar, 1984; Tourneret and Laurent, 1990; Lacombe et al., 1992, 2007; Lacombe, 2001; Parlangeau et al., 2018). Mechanical twinning within calcite crystals is a plastic deformation in response to dislocation gliding along "e-planes," within the crystal lattice (**fig.4b**) (Burkhard, 1993). Twin lamella are commonly thin (≤1 μm) below ~200˚C becoming thicker with increasing temperatures for a given amount of twinning strain (e.g. Ferril et al., 2004).

The occurrence of twinning is also dependent upon the value of a threshold or critical stress. Defined as the critically resolved shear stress (CRSS - τ_a) (Tullis, 1980; Ferrill, 1988) for which questions as to the correct value have been raised (Rocher et al.,2004; Amrouch 2010; Parlangeau et al.,2019). The factor likely controlled by grain size and the degree of internal deformation, as following initial twinning calcite grains harden (Turner et al.,1954). e-*twinning* within the calcite crystal can be compared to a zone of simple shear. For un-metamorphosed

calcite, three of these planes exists within each crystal and are geometrically centered on the optical axis, C (**fig. 4b**).

Accounting for both twinned and untwinned planes, the analysis of calcite twins has been proven to accurately measure five of the six parameters needed to define a complete paleo-stress tensor:

1) *Maximum principal stress orientation (σ1)*
2) *Intermediate principal stress orientation (σ2)*
3) *Minimum principal stress orientation (σ3)*
4) *Differential stress ratio, (ϕ; where ϕ = [σ2 − σ3]/[σ1 − σ3]).*
5) *The peak differential stress (σ1 − σ3)*

Capable of providing evidence for poly-phase tectonic events and paleostress orientations in addition to mono-phase events (Lacombe et al., 1992; Rocher et al., 2004; Lacombe, 2007, 2010; Amrouch et al., 2010a). When combined with brittle deformation and rock mechanics data the method can also provide the complete paleostress tensor (Amrouch et al., 2011). And when associated with methods of absolute dating it can also assist in constraining highly detailed models of stress evolution (Beaudoin et al., 2018).

The calcite stress inversion technique is similar to that used to analyze slickenslide data present along a fault plane (Etchecopar, 1984), consisting of developing the best fit tensor for the distribution of twinned and un-twinned *e* planes within the sample. Polyphase events are likely if more than 30% of twinned planes within a sample cannot be explained by a single tensor. In this case, the initial correlated twinned planes are removed and the process is repeated a second time, with the uncorrelated twinned planes and the entire set of un-twinned planes. The process

assumes that analysed *e* planes developed under a homogenous field of paleostress, and that they have not been subjected to rotation following their deformation (Lacombe et al., 2007).

For this study we use Etchecopar's calcite stress inversion technique (CSIT) (Etchecopar, 1984) in order to obtain the paleostress tensors. Though effective, the method may have its limitations with small variations between the computed principal stress orientations and the imposed directions in experimentally deformed samples (5-7˚ for monophase data and 7-11º for polyphase data) (Lacombe and Laurent, 1996; Laurent et al., 2000). Recent works also suggesting that the penalization function used in the approach is too restrictive, especially during optical measurement (Rez and Melichar, 2010; Yamaji, 2015b).

As a result other studies have modified the method (e.g. Rocher et al., 2004; Yamaji, 2015; Parlangeau et al., 2018) but the approach of the original CSIT is generally considered accurate, being the most commonly used technique in the past (Rocher et al., 1996; Rocher et al., 2000; Lacombe, 2001; Lacombe, 2007; Lacombe et al., 2009; Amrouch et al., 2010; Beaudoin et al., 2012; Beaudoin et al., 2016). Proving effective in constraining paleostress data for integration with meso and macroscale data, where small errors in the approach likely have minimal impact (Kulikowski and Amrouch, 2017).

CSIT can be applied to small twinning deformation which is able to be approximated under co-axial conditions (stress = strain) and requires a universal stage microscope for completion. The process is broken down into a number steps, working with the hypothesis that a potential *e*-plane is only twinned if the resolved shear stress (τ_s) along the gliding direction of the e-plane is higher than the CRSS (equation 1).

$$Equation\ 1: If\ \tau_s \geq \tau_a, \text{ then the plane will be twinned}$$

The technique then finds a stress tensor, which includes the largest possible number of twinned planes while simultaneously verifying the entire set of untwinned planes. As such a reduced stress tensor is produced (T'), consisting of the orientations of the maximum (σ1); intermediate (σ2) and minimum principal stresses (σ3) and the stress ratio (ϕ) (equation 2) with the maximum differential stress normalized to 1.

$$Equation\ 2: 1 \geq \frac{(\sigma 2 - \sigma 3)}{(\sigma 1 - \sigma 3)} \geq 0$$

The actual inversion process entails finding the stress tensor that best describes the distribution of both twinned and untwinned planes throughout the sample. Theoretically, a perfect stress tensor should be reached when the spatial distribution of twinned and untwinned planes is accounted for. All twin planes having sustained a τ_s value that exceeds that exerted on all untwinned planes. The best tensor solution is found when the penalization function (equation 3) is reduced as close to zero as possible. This function is defined as:

$$\text{Equation 3: } f = \sum_{j=1}^{N} \left(\tau_{sj} - \tau_{a'}\right)$$

Where τa ′ is the smallest RSS applied to the twinned planes that are compatible with the tensor, and τsj is the resolves shear stress applied upon the *N* of untwinned planes (*j)* such that Tsj> Ta' (Etchecopar, 1984; Laurent, 1984). The optimal stress tensor is therefore found by incorporating the maximum amount of twinned planes in the sample, while ensuring the value of the penalization function remains as low as possible. Due to local heterogeneities, perturbations, and measurement uncertainties, a small percentage (~10-15%) of un-twinned

planes can be included within the tensor as having received a RSS greater thanτ_a. In this sense the f function describes both the arrangement of twin planes to the experimental tensor, in addition to its quality. The orientation of the three principal stresses are consequently produced, however the value of differential stress is dimensionless (equation 4) and as such given an assumed constant and known CRSS, the absolute magnitude of maximum differential stress can be calculated (equation 5).

$$Equation\ 4\text{: } \frac{(\sigma1-\sigma3)}{\tau_a} = \frac{(\sigma1-\sigma3)normalised}{\tau_{smin}} = \frac{1}{\tau_{smin}}$$

$$Equation\ 5\text{: } (\sigma1-\sigma3) = \frac{\tau_a}{\tau_{smin}}$$

4.0 Results

Results are presented from the macroscale to the microscale, beginning with the interpretation of the three seismic datasets and the establishment of an ESP. Followed by supporting evidence from fracture data and derived paleostress orientations and magnitudes from the CSIT results.

4.1 Macroscale structural analysis of 3D seismic datasets and elementary stress pathway

When working with seismic datasets, the interpretation of the dataset, is itself the result. As such, these two sections are difficult to divide and are discussed together in the following section.

4.1.1 Champion-Hercules 3D – Structural Interpretation

The Champion-Hercules 3D is dominated by broadly ~NW-SE striking normal faults (**fig. 7a**) parallel in geometry to the inline orientation. Structural analysis was focused on a central and eastern section of the survey in close proximity to the Pecten Anticline (Holford et al., 2014) (**fig. 8a, c**). Faulting within the survey is responsible for the formation of a series of ~NW-SE striking horst and graben structures, which show downwards rotation towards the SW and evidence for inversion in the presence of fault bend folding in their hanging walls sections and bulging of collapsed graben structures (**fig. 8a**).

Two generations of faulting, confined to the Early and Late Cretaceous rift units are identified. One that shows thickening of hanging wall sediments within the Late Cretaceous, – implying they were active during the deposition of the formation – and one that does not. Indicating the formation of the second set post-dates the deposition of the unit (**fig. 8a**). Faulting style is characteristic of detachment faulting, major faults, showing almost identical dip angles and the presence of rotated blocks suggesting detachment at depth (**fig. 8a**).

The Pecten Anticline (Holford et al., 2014) structure is well imaged within the survey. However, rather than appearing as an anticline, the structure – which is penetrated by the well Pecten-1 - is associated with crestal bulge within a mildly inverted collapsed graben, viewed along the Top Late Cretaceous. While a broad dome structure is present along the Top Mid-Eocene (Nirranda Group) (**fig. 8b**), due to the lack of faulting in the unit and the geometry of the "fold," (~ 9,000m wavelength and an amplitude of 70m, equating to a vertical difference of 0.78% from trough to trough) the structure likely formed due to differential compaction across the underlying high within this unit.

There is no evidence for ~NE-SW striking faults within the survey suggested to permeate the region by previous works (e.g. Edwards et al., 1996; Holford et al., 2014; Tassone et al., 2017).

4.1.2 The Schomberg-Minerva 3D survey – Structural analysis

The Schomberg-Minerva survey is the deepest penetrating survey used as part of the study, allowing for the top basement to be clearly interpreted, ~NW-SE striking faults (**fig. 7b)** dominating the structural architecture. Top Basement, Top Mid Late Cretaceous (Santonian) and Top Late Cretaceous (Maastrichtian) reflectors were mapped throughout the survey (**fig. 9**) the Top Early Cretaceous being difficult to map consistently due to a reduction in signal quality from 4 – 7km depth.

A depth map along the Top Santonian (**fig. 9b**) displays the NE-SW trending Minerva and Point Ronald "Anticlines" (Holford et al., 2014). As with the Pecten "anticline," it is clear that both structures reflect the inversion of underlying ~NW-SE trending faults. Though in this case, the two can clearly be seen to have been isolated above underlying basement highs trending ~NE-SW (**fig. 9**). Structural features that are bordered by ~NE-SW trending faults along their margins, which do not propagate upwards into the Otway Basin sediments.

Listric extensional faults, show evidence for growth in the Late Cretaceous and are interpreted at the very north eastern edge of the survey, revealed only through the use of arblines trending ~NE-SW (**fig 8c**). These faults exert a strong control on deformation within the northern edge of the survey, accommodating the main inversion of the Minerva and Point Ronald Structures, with multiple synthetic and antithetic faults present. Many of them showing syn-depositional growth identified by the thickening of units in their hanging walls. These faults sole out at

depth along the underlying basement highs in the presence of a likely décollement, especially visible in the case of the Point Ronald structure (**fig. 8d**)

A majority of faults within the survey display normal offset, however evidence for their inversion is obvious, with fault parallel folding in the hanging walls of large faults, tightening of fault angles and bulging of collapsed graben structures (**fig. 8c, d**). Minor reverse faulting is also present, as is the beginning of a back thrusting harpoon inversion structure, typical of inverted listric faults (Buchanan and McLay, 1994).

Isopach maps of the Campanian – Maastrichtian succession of Late Cretaceous sediments show thinning over the crest of both the Minerva and Point Ronald structures (**fig. 9d**) suggesting growth of the structure may have begun during the mid-Maastrichtian. Early Palaeogene sediments onlap onto the Top Late Cretaceous in an angular unconformity (**fig. 8c**). Additionally a minor trend of ~NE-SW striking faults are present, although they are limited to the basement, showing no growth within the sediments of the Otway Basin.

4.1.3 Crows Foot 3D survey – Structural analysis

The structure of the Crows Foot 3D is highly deformed. Mapping of the Top Early Cretaceous, Top Santonian and Top Late Cretaceous was completed (**fig. 9**) although differentiation of the last was difficult due to poor well control. Igneous intrusions identified by their characteristic hard seismic kicks, made interpretation within some sections a challenge.

The Crowes and Loch Ard “anticlines,” Holford et al., (2014) dominate the northern half of the survey. As with the “anticlines” in the previous surveys they reflect NE-SW trending chains of

inverted horst and graben structures, bound by orthogonally striking normal faults (**fig. 7c**) and not the folds described by previous works.

Both structures are highly faulted and broken into a series of well-defined horst and graben structures that trend ~NW-SE. Bound by major ~SW and ~NE dipping normal faults that in some cases display ~600m offset of the Top Early Cretaceous (**fig. 8e**). The largest faults within the survey show distinct evidence for syn-rift growth during the Late Cretaceous, due to thickening of the units within their hanging walls. Other smaller faults do not, once again implying two generations of faulting, one major syn-rift and one minor, post deposition during the Late Cretaceous.

Though basement is not visible within the survey, fault geometries especially viewed along the hinge-line of the Crows Anticline (**fig. 8e**), indicate faulting is likely influenced by a décollement at depth. An observation that is supported by the presence of low angle listric normal faults (**fig. 7c**).

The interpretation is further suggested by the presence of similar ~NE-SW trending basement highs in the Minerva-Schomberg 3D and associated evidence for ~NE-SW inversion of the extensional system upon them. Inversion is most pronounced along the hinge line of the Crowes Anticline (**fig. 8e**) where fault bend folding, inner rim tightening and bulging of collapsed grabens can be observed.

4.1.4 Summary of seismic analysis

Seismic interpretation indicates that ~NW-SE listric faulting dominates this section of the Otway Basin. Observations that support very early evidence from Etheridge et al., (1987) and Lister et al., (1986).

Across all surveys, the strike of major faults is broadly ~NW-SE, with evidence for syn-depositional and minor post depositional normal faulting throughout Late Cretaceous. Faulting is minimal within Paleogene and Neogene sediments, except where minor reactivation has occurred along the most major faults (**fig. 8**).

Though still displaying normal offset, many of these faults have been inverted. For which evidence is most obvious above underlying basement highs in the form of inverted half grabens, collapsed grabens and fault bend folds. Features that are concentrated in ~NE-SW inverted chains extending in a finger like style, from the ~NE-SW (**fig. 9**). This hypothesis is supported by the interpretation of basement highs in the Minerva-Schomberg 3D and by a regional depth to basement model from Krassay et al., (2009) (**fig. 2b**).

With respect to the timing of inversion, the interpretation suggests contraction began during the final stages of deposition of the Latest Cretaceous units, in the ~Mid-Maastrichtian. Suggested by the thinning of Campanian – Maastrichtian within the Minerva structure and the overall geometry of the fold. That being the case, improved well control within the Crowes Foot 3D, particularly along the hinge line of the Crowes “anticline,” would significantly assist refining this estimate, particularly as it is the most highly structured section within all the datasets. From the on lap of Palaeogene units along the Top Late Cretaceous inversion was certainly finished by the Palaeogene. Given these insights, we propose a period of ~NE-SW oriented basin inversion beginning during the Latest Cretaceous (~Mid Maastrichtian)

coinciding with an unconformity between the Late Cretaceous and Early Palaeogene units. For ease of discussion, we term the network of inverted listric faults and inverted chains interpreted within the surveys the Great Ocean Fault System (GOFS).

4.1.5 Elementary Stress Pathway from 3D seismic data

Seismic interpretation and the stress inversion of faults extracted from the seismic datasets, allow us to construct an ESP (**fig. 10**). The ESP consists of three major structuring events, from the start of the Late Cretaceous until the early Palaeogene. Following the deposition of the Early Cretaceous Eumeralla Formation, which formed during a period of subsidence.

Stress inversion of seismic faults indicate event 1, occurring at the beginning of the Late Cretaceous, was an intense period of extension with regional paleo-σ3 orientations trending broadly ~NE-SW. Structures typical of inversion within both Early and Late Cretaceous units, absent from Palaeogene units, suggest event 2 was characterised by ~NE-SW inversion, during which uplift and contraction was isolated above underlying basement highs. The presence of an angular unconformity at the Top Late Cretaceous suggesting inversion peaked prior to the deposition of Palaeogene units. Basin inversion was followed by the deposition of Paleogene and Neogene units and the reactivation of large faults. Constituting, a third event of renewed minor extension with a ~NE-SW trending paleo-σ3.

4.2 Mesoscale Fracture set succession and other supporting outcrop evidence

Outcrop fracture analysis across the Otway Ranges reveals 6 major and 5 minor fracture sets (**fig. 7d**). Cross cutting relationships and pre/post bedding tilting geometries providing insight into their successive development. Fractures were sampled within the Eumeralla Formation,

642 the top member of Early Cretaceous sediments, which was deposited during a period of
643 subsidence, not active rifting.
644
645 The most pervasive set throughout the outcrop analysis is, set 1 fractures, a conjugate mode-2
646 set that dips on average towards ~038 ºN and ~218ºN at an average angle of ~68 º under back-
647 tilted conditions, representative of a ~NE-SW trending paleo-σ3 (**fig. 5a**). This set is integrated
648 with centimetre scale faulting detected at site 18 (**fig 6c**).
649
650 Set 2 fractures, a second conjugate mode-2 set, also back-tilted, dip towards ~007ºN and
651 ~185ºN at ~76º, represent a N-S trending paleo-σ3, they are observed alongside set 1,
652 terminating on the previous set (**fig. 6b**).
653
654 Set 3 also a back-tilted extensional conjugate mode-2 set (**fig. 5b)** dip at ~66º towards ~138ºN
655 and ~314ºN, reflecting a NW-SE paleo-σ3. They are observed in outcrop to terminate on set 1
656 fractures (**fig. 5f**).
657
658 Set 4 represents a high angle (~88 º) back-tilted mode-2 fracture set, corresponding with a
659 group of centimetre scale faults at site 26 that dip towards ~316ºN and ~132ºN, suggestive of
660 ~NE-SW oriented sinistral strike-slip stresses with a ~NE-SW trending σ1 (**fig. 6a**). Though
661 set 4 fractures strike parallel to set 3 fractures, the two sets were distinguished from each other
662 by observing their 3D geometry within uneven sections of the wave-cut platforms (**fig. 5g**).
663
664 Set 5 fractures, another back-tilted conjugate mode-2 set, dip at ~24º towards 048ºN and 214ºN
665 suggesting ~NE-SW compression with paleo-σ1 also ~NE-SW.
666

The only major set interpreted under present day conditions is set 6, a mode-2 set dipping at ~88º towards ~046ºN and ~232ºN, representative of a ~NW-SE paleo-σ. The set regularly cross cuts fracture set 4 (**fig. 5d**), producing two independent strike slip fracture sets that intersect with each other at 90º. This is integrated with evidence for a vertical fault at site 31, striking ~NW-SE showing strike slip movement (**fig. 5c**).

Outcrop analysis also showed five minor fracture trends (**fig. 7d**), including set 7, a mode-2 back-tilted set, dipping towards 091ºN at ~ 73º. A mode 1 (set 8) and a mode 2 (set 9) of ~NE-SW trending strike slip fractures. Both dipping at ~88º towards ~146ºN and ~º317N º. Set 10, an extensional mode-2 conjugate set. Dips at ~67º towards ~020ºN and ~229ºN and is only present where set I fractures are not. Set 11 is defined by low angle (~18º) compressive fractures that dip towards 135ºN.

Two stylolites were also interpreted during outcrop analysis at site 28 (**fig. 6d**): Stylolite A, which has been reactivated as a vein, suggests a back-tilted ~NW-SE trending (319ºN) σ1. Stylolite B cross cuts stylolite A at 90 º and the opened vein, suggesting a later back-tilted 049º trending σ1.

Fracture categorisation in the subsurface showed similar patterns to outcrop data (**fig. 7e**), with four subsurface sets determined (**fig. 7e**): Set A, a conjugate set complimentary of outcrop set 1, fractures, set B and extensional set integrated with outcrop set 2, set C reflecting set 3 outcrop fracture geometries and set D, showing geometries typical of those within fracture set 5.

4.3 Microscale calcite twin analysis

4.3.1 Paleostress orientations from calcite twin data

CSIT results (**table 2**) reveal five main stages of paleostress evolution (**fig. 10**) defined by different stress regimes and varying tensor shape ratios. The first stage, corresponding to backtilted ~NE-SW extension includes one stress tensor 10T2 with a vertical σ1 and a ϕ value of 0.5.

The second stage is characterised by other backtilted extensional stress tensors – A-ST1, B-AT1 and C-T1, with σ3 plunging towards the ~N, and ~NW. These tensors have shape ratios of ϕ= 0.4 or lower.

The third stage, represents a backtilted compressional event, with a ~NE-SW oriented σ1, defined by tensors CT-2, A-LT2 and 10T1. Φ values for these tensors are between 0.2 (tensor: 10T1) and 0.8 (A-LT2).

Stage four stress tensors, under present day bedding conditions, outline a transition back to extensional paleostresses, defined by vertical σ1 trends and ~NW (tensor 10T3), S (tensor A-LT1) and SE (tensor 12T2) trending σ3 orientations. Shape ratios for these tensors are between ϕ values of 0.6 and 0.1

Stage five, represents a present day reorganisation defined by a vertical σ3 and a σ1 trending towards the NW and a ϕ= 0.8.

Transitional, strike slip stress stages are defined between stage two and three by tensor B-BT2 with a southerly trending σ1, and between stages three and four by B-BT1 with an easterly trending σ1.

4.3.2 Differential stress magnitudes during basin evolution

Quantified maximum paleo-differential stresses (**table 2**) defined throughout the stages of stress evolution as outlined by CSIT display a pattern. Characterised by high magnitudes during extension and low magnitudes during compression (**fig. 10**)

Stage one extensional tensor 10T2 displays the highest stress magnitude of 69MPa. Stage two begins with high magnitudes with tensor A-ST1 (66MPa). Followed by decreasing magnitudes in tensors B-AT1 (36MPa) and C-T1 (34MPa) as values of ϕ decrease from 0.4 to 0.2. Transitional tensor B-BT2, highlights decreasing magnitudes (32MPa) into stage three compressional tensors, defined by lower values of 12MPa (C-T2), 28MPa (A-LT2) and 31MPa (10-T1). Magnitudes increase again following transitional tensor B-BT1, (32MPa) into stage four tensors ranging between 43MPa (10T3) and 57MPa (12T2). Stage five tensor 12T1 suggests a value of 50MPa.

5.0 Discussion

5.1 Consistency of multiscale structural datasets

The results of this study show good consistency across all datasets (**fig. 7, fig. 10**). On the macroscale the style of faulting is consistent across all seismic surveys, as is the evidence for ~NE-SW oriented inversion. Though it is most pronounced within the Schomberg-Minerva and Crowes Foot 3D surveys.

Under a more traditional approach to the stress inversion of faults extracted from 3D seismic (Kulikowski and Amrouch, 2017) low angle faults (<45º) are attributed to compressional regimes of paleostress. In this study we are dealing with the inversion of listric faults, which decrease in dip with depth, as they transition towards the zone of décollement. In our case due to the style of the triangular dislocation method used to produce fault data, this results in the apparent occurrence of low angle fault planes (**fig. 7**), which in fact represent the lower angled sections of the listric faults as they shallow out with depth. Therefore, during the stress inversion of this dataset, we have assumed that all faults nucleated in an extensional style based on their shape, offsets and mass occurrence. As even where small reverse offset is observable, the extensional origin of the fault is obvious from its common angle with the surrounding network and the growth of sediments within its hanging wall. Additionally, where the beginnings of back thrusting are visible, it is not of a sufficient degree to interpret as a continuous fault plane.

Mesoscale fault and fracture data display good accordance with the macroscale results. This is especially so in fracture set 1 and set A, which though distributed across a broad strike (~105 - 165ºN) both show an almost identical correspondence with fault geometries extracted from 3D seismic (**fig. 7**). Additionally, although the low number of outcrop faults (less than 15) does not represent a large enough dataset for reliable inversion (Angelier, 1984, 1990; Lacombe, 2012), their analysis and derived paleostresses is in excellent correspondence with complimentary Andersonian natural fractures (**fig. 5**) throughout the system. Contributing a degree of reliability in the methods of fracture analysis used.

On the microscale, stress tensors derived from Etchecopar's CSIT are of good quality. With all but one tensor (12T1) displaying *f* values (a measure of quality) ranging between 0 and 0.95.

Most CSIT samples (except A-LT2 and 10T3) also containing more than the threshold of 90 twins required to reduce the likelihood of any inversion error (Lacombe et al., 1990). Further testament to the reliability of the CSIT results is their correspondence with the macro and especially mesoscale dataset, an element of the results that is particularly good, given the small amount of tensors within the study.

5.2 Tectonic Phase Progression

The results of this study show multiscale evidence for five main tectonic phases (**fig. 11 – 15**) throughout the evolution of the GOFS and the Otway Ranges. Prior to the main phases of structuring, the presence of stylolite A, striking ~NE-SW (**fig. 10**) suggests the minor influence of a ~NW-SE oriented σ1. A compression or strike slip event, likely concurrent with regional uplift across much of Australia during the mid-Cretaceous due to collisional stresses along the eastern margin (Norvick and Smith, 2001). Though evidence from this study suggests that structuring during this phase was minimal as there is no angular unconformity between the Top Early Cretaceous and Late Cretaceous unit (**fig. 8**).

Phase 1 (**fig. 11, fig. 16**) consists of a strong period of broadly ~NE-SW oriented extension, beginning at the start of the Late Cretaceous (**fig. 10**). Primary evidence for this phase comes from event 1 within the ESP and the nucleation of the substantial network of ~NW-SE striking extensional faults within the dataset. A fault set that grew in a syn-depositional nature during the deposition of Late Cretaceous units. On the meso and microscale, evidence for this tectonic phase is discernible under bedding back-tilted conditions, ~NW-SE striking extensional fracture sets 1 (outcrop) and A (well data) reflecting Andersonian conjugate fractures. With paleo-σ3 orientations trending broadly towards the NE and SW, in good agreement with macroscale fault data and centimetre scale faulting at site 18 (**fig. 6c**).

CSIT tensor 10T2 is also reflective of broad ~NE-SW extension under back tilted conditions, with σ3 plunging towards 236ºN. The sample itself comes from a natural fracture reflective of set 1 geometries, suggesting this phase of structuring continued for some time, allowing for the creation of the fracture, it's filling with calcite and the twinning of the calcite within. An observation that is consistent with the large growth of Cenomanian – Santonian Late Cretaceous units within the seismic datasets (**fig. 8)**. Paleostress quantification of magnitudes within tensor 10T2 suggests this phase was characterised by magnitudes of extensional stress as high as 69MPa. With a tensor ϕ value of 0.5, also indicating this phase of evolution was well defined with no perturbations.

The magnitude of extensional stress calculated as part of tensor 10T2 in phase 1, and the first tensor of phase 2 (AST-1), described below, represent some of the highest extensional stress magnitudes calculated to date using CSIT. As this study represents the first quantification of paleostress during continental break up, it suggests that these tectonic periods may be characterised by high magnitudes of extensional paleostress. Especially when compared to extensional stresses within stable foreland basins, such as the Paris Basin (Rocher et al., 2004). This phenomena is explored further within section 5.5.

Phase 2 (**fig. 12**) represents on going extension associated with the continued growth of ~NW-SE striking faults on the macroscale and the creation of post depositional extensional faults. On the meso and microscale, the phase is characterised by significant extensional evidence (**fig. 5b**) with the bedding backtilted. As extension progressed and increased in intensity, the results suggest a shift from a well-defined ~NE-SW extensional azimuth, to a poorly defined, radial style, resulting in the formation of ~E-W (set 2, set B), ~NE-SW (set 3, set C) and ~N-S (set

7) striking extensional fractures. This is particularly apparent in cross cutting relationships between fracture set 1 and fracture sets 2 and 3, which both terminate upon the former. Microscale evidence for this transition comes in the form of tensors A-ST1, B-AT1 and C-T1, which suggest ~N-S, ~NNW-SSE and ~NW-SE extension respectively, C-T1 recorded within a fracture of set 3 geometry and A-ST1 within the reactivated and opened vein of stylolite A. Also suggesting the length of this stage of extension was significant, as the tectonic event responsible for opening the stylolite was also recorded within the vein fill. Defining a tectonic period likely coinciding with the formation of post depositional faulting within the 3D datasets. Computed ϕ ratios of tensors within this phase are lower than phase 1, the first two tensors equal to 0.4 and the last equal to 0.2. Suggesting that in the final stages of this phase the values of $\sigma 2$ and $\sigma 3$ were similar (Lacombe et al., 2007). Indicating that switching between them may have occurred, and supporting the interpretation of a vast network of radial extensional fractures.

Similar to phase 1, paleostress magnitudes characterised from the CSIT tensors within phase 2 suggest an initially high level of extensional stress (66MPa, tensor A-ST1). With a reduction in magnitude as deformation increased and ϕ values become lower (36MPa, tensor, B-AT1; 34MPa, tensor C-T1). The progressive reduction in stress magnitude and ϕ value between the three tensors also allowing a specific order of occurrence to be constructed (**fig. 10**). Fracture set B striking ~E-W and fracture set C striking ~NE-SW within the subsurface are also indicative of this phase of deformation. Given the evidence for Late Cretaceous, Campanian – Maastrichtian, growth of extensional faults, within this study and others in the region (Robson et al., 2017; 2018), this phase likely extended into the very latest stages of deposition during the Late Cretaceous. During a period that should have been the final stages of continental

separation (**fig. 16**), as the creation of oceanic crust moved from west to east across Australia's southern margin (Mueller et al., 1997).

The progressive decrease in tensor shape ratios and magnitudes throughout phase 2 described in the paragraph above, is indicative of the coming compressional, phase 3. Especially as in tensor C-T1, decreasing differences between σ2, oriented ~NE-SW and σ3, oriented ~NW-SE suggest the beginnings of an equalisation between minimum and maximum horizontal stress.

Phase 3 (**fig. 13**) reflects a significant period of compressional deformation and basin inversion within the GOFS and the Otway Ranges. The phase is broken down into three components; early and late transitional phases of strike slip stress, connected by a main phase of compression. On the macroscale, this phase is characterised by the inversion of collapsed grabens and half grabens along ~NW-SE striking normal listric faults, and a contraction of the system towards the north east, concentrated above sections of shallow basement (**fig. 9**). The majority of micro and mesoscale evidence interpreted under bedding back tilted conditions.

On the microscale the beginnings of stress reorganisation is marked by the CSIT tensor B-BT2, taken from a set 1 fracture, the initial azimuth of inversion possibly coming from the SSW (**fig. 10**). Prior to the onset of compression, fracture set 4 (**fig. 13**) formed as stress reorganisation continued due to progressive increases in ~NNE-SSW oriented horizontal stresses. The set represents a vertical strike slip conjugate set of fractures, visible as Andersonian pairs at sites 14, 23 and 26 (**fig. 13**). Offset along micro-faults (**fig. 6a**) which cross cut fracture set 2 at site 26 integrated with the set, suggest sinistral strike slip movement, which is reflective of previously documented geometries within the nearby Shipwreck Trough (Robson et al., 2018). σ1 orientations derived from the analysis of stylolite B at site 28, also support the initial stages

of ~NE-SW oriented inversion following the opening of stylolite A, as the former cross cuts the latter (**fig. 6d**).

The microscale onset of ~NE-SW oriented compression is marked by CSIT tensors CT-2, A-LT2 and 10T1 and the creation of the ~NW-SE striking low angle fracture set 5 (**fig. 13**). A specific phase order between these tensors can be constructed using their ϕ values and stress magnitudes. The most well defined compressional tensor, CT-2, with a shape ratio of 0.5 and the lowest stress magnitude, occurring first. The low magnitude explained due to the ample opportunity to release stress through the reactivation of the existing extensional network of deformation during the early stages of compression. Occurring second, tensor A-LT2 marks a slight increase in stress magnitude as stress became more difficult to release through reactivation, following continuing inversion. The high shape ratio of the tensor, ϕ = 0.8, illustrating an increase in horizontal stresses, and a possible switching between $\sigma1$ and $\sigma2$. Occurring third in the phase, with another small increase in stress magnitude, tensor 10T1, with a low shape ratio of ϕ = 0.2 highlights the final peaking of compression, as values of $\sigma2$ and $\sigma3$ began to equalise given the scale of the vertical uplift and increases in vertical stresses. Fracture set D within the subsurface represents additional mesoscale evidence for this tectonic event. Following slight relaxation, CSIT tensor B-BT1 and strike slip fracture sets 8 and 9 represent post tilting events of ~WSW-ENE oriented strike slip stress. A period which was also characterised by low differences between $\sigma2$ and $\sigma3$, given the low ϕ value of 0.3 (**fig. 10**).

Paleostress magnitudes calculated during phase 3 display a pattern (**fig. 10**): The compressional stress tensors indicating low magnitudes of stress (13MPa, tensor: C-T2, 28MPa, tensor: A-LT2, 31MPa, tensor 10T1) and the strike slip tensor displaying intermediate values between the preceding and superseding phases (32MPa, tensor: B-BT2 and B-BT-1).

The estimated timing of basin inversion from 3D seismic analysis coinciding with the end of the Late Cretaceous - possibly as early as the mid-Maastrichtian - coincides well with previous studies. Thermal history estimates from the region from Duddy and Erout (2003; 2001) (**fig. 3c**) suggest a major cooling peak between ~60 and 52Ma in the Mussel Terrace (**fig. 1**). A period coinciding with a regional increase in denudation rates across South Eastern Australia from Kohn et al., (2002) (**fig. 3b**). Along with a major unconformity observed in the nearby Torquay sub-Basin (**fig. 1**) (Trupp et al.,1994) at the top of the Eastern View Group (the Late Cretaceous sub-unit within the basin). Late Cretaceous ~mid-Maastrichtian, inversion is also supported by Schneider et al., (2004) and their analysis of the Minerva "anticline," however, the authors favoured a ~NW-SE oriented maximum horizontal stress. Given the timing of phase 3 can be generally constrained, the question remains as to the source of stress for this ~NE-SW oriented stress reorganisation, which is enigmatic given the region was in the final stages of continental breakup.

From plate boundary reconstructions of Australia (Veevers et al.,1994; Muller et al.,2000; Norvick and Smith, 2001) it is clear that eastern Australia was subjected to complex far field stresses during the Late Cretaceous, Early Paleogene and even (**fig. 8**) Early Eocene (**fig. 16**). Not only was seafloor spreading propagating from west to east in the south (**fig. 16d**), but from north to south in the east within the Tasman Sea, and SE-NW in the north. Possibly placing SE Australia under complex ridge torque forces, which have been shown to sustain high levels of collisional stresses under the right conditions (Sandiford,et al., 2008). Coinciding with this complex environment of break-up in the east, was a deceleration in subduction rate and the arrival of Indian continental crust in the Himalayan collision zone, at the north western boarder of the Indo-Australian plate, as early as 58Ma (Zhu et al., 2018; Leech et al., 2005). Suggested

914 to have been responsible for stress reorganisation in central Australia around this time
915 (Kulikowski and Amrouch, 2017). As a result in seems that during the final part of the Late
916 Cretaceous, continental separation in the Otway Basin was interrupted by a period of plate
917 boundary driven ~NE-SW oriented compressional stress (**fig. 16**). Possibly explaining why the
918 creation of oceanic crust within the basin was delayed until the ~Mid Eocene, the contractional
919 event essentially postponing continental separation.
920
921 As with the transition between phase 2 and phase 3, the coming phase of renewed strike slip
922 and extension is suggested by the change in tensor shape ratios across the phase 3 and phase 4
923 boundary (**fig. 10**). Shape ratios of 0.2 (tensor: 10T1) and 0.3 (tensor: BT-T1) outlining
924 minimal differences between σ2 and σ3 predicting the switch from compression back to strike
925 slip. A shape ratio of 0.6 for tensor 10T3 also denoting the following switch between σ1 and
926 σ2 from strike slip into extension (**fig. 10**).
927
928 Phase 4 (**fig. 14**) dictates a relaxation of compressive stresses and a progressive return towards
929 an environment of ~NE-SW extension. On the microscale, post tilting evidence for phase 4 is
930 evident in tensors 10T3, A-LT1 and T12. Once again these can be assigned a unique order, as
931 the ~NW-SE and ~NNW-SSE extension suggested by 10T3 and A-LT1 occurred as a result of
932 a persisting ~NE-SW oriented maximum horizontal stress following inversion. Tensor T12,
933 representing a complete relaxation and a transition back to strong ~NE-SW oriented extension.
934 Given the scale of extensional deformation within phases 1 and 2, it is not surprising that meso
935 scale evidence for phase 4 is limited. Especially as following basin inversion, previously
936 formed extensional faults and fractures were likely reactivated during the deposition of early
937 Paleogene units. A concept that is supported with macroscale observations (**fig. 8**) in all 3D
938 seismic datasets and fracture set 10. A ~NW-SE striking extensional fracture set, which was

recorded at two of the field sites where set 1 fractures were not present and able to accommodate relaxation.

Stress magnitudes during phase 4 show the reverse trend of phase 2 (**fig. 10**). Extensional stress magnitudes increasing following inversion, culminating in a maximum differential stress of 57MPa derived from tensor 12T2. Timing of this phase coincides with the deposition of the early Palaeocene Wangerrip Group (**fig. 3a**), prior to first creation of oceanic crust offshore in the eastern Otway Basin during the mid-Eocene. An observation that is reflected in the high stress magnitudes of tensor 12T1, echoing the trend from phase 1, of high stress magnitudes associated with continental breakup and active rifting. Following continental separation, Australia began its fast northward movement, a period characterised by tectonic quiescence, thermal subsidence and the deposition of the Eocene – Oligocene Nirranda Group sediments.

Following continental separation (**fig. 16**) phase 5 (**fig. 15**) represents stress reorganisation, evident in numerous studies of regional contemporary stress (Sandiford et al., 2003; 2004). A restructuring that is defined by an increase in ~NW-SE oriented horizontal stresses during the Late Miocene, which now characterise the in situ stress regime of the Otway Basin (**fig. 2a**) (Tassone et al., 2017). Evidence for this is recorded in this study on the micro and the meso scale, CSIT tensor 12T1 suggesting post-tilting ~NW-SE oriented compression with σ1 horizontal, trending 337ºN and fracture set 6, along with accompanying faults (**fig. 5d**). That are observed to crosscut fracture set 4 at 90º at site 14 (**fig. 5d**). Fracture set 11, present at site 28 and fracture set E within the subsurface also suggest mesoscale evidence for a degree of compression as part of this phase, although strike slip evidence is far more common (**fig. 15**). There is no evidence for phase 5 on the macroscale, indeed, the geometry of faults within all three datasets strike parallel to the regime of in situ stress. Explaining the relatively high

964 magnitudes of stress within tensor 12T1, when compared to compressional tensors in phase 3.
965 As with σ1 in the plane of the regional faults, trending parallel to their strike, stress is unable
966 to be released through reactivation of the extensional network. **Fig. 16** displays the phases of
967 stress evolution described above and the plate scale settings during each period.
968
969 **5.3 The role of décollement during inversion**
970 Listric faults within the Otway Basin were noted in the 1980s (e.g. Etheridge et al., 1986; Lister
971 et al., 1986), though they were ignored or supposedly refuted by almost all following works
972 (e.g. Cooper and Hill, 1997). 3D seismic interpretations in this study highlight their occurrence
973 and the isolation of inverted structures above underlying shallow portions of basement (**fig. 9**).
974 This suggests that the nature of faulting and, in particular, the presence of a top basement
975 décollement has played a key role in the accommodation of stress and strain during basin
976 inversion in the Otway Basin.
977
978 Sandbox experiments (Buchanan and McClay, 1990; Bonini et al., 2012) indicate that during
979 the inversion of listric fault networks, normal offset is preserved along major faults up to 30%
980 shortening. With the initial ~10% of contraction accommodated mainly through the
981 reactivation of the underlying décollement. There is good correlation between the inversion
982 structures observed within the 3D seismic interpretation and sandbox models (**fig. 17**).
983 Additionally, the location of the Otway Ranges, directly ~NE along strike of the basement
984 highs overlain by the inverted structures in the 3D seismic (**fig. 17**), provides further evidence
985 for the deep accommodation of initial strain during the early stages of deformation. The initial
986 release of stress occurring primarily along the décollement zone and within pre-existing faults,
987 with the localisation of inversion likely concentrated onshore in the Otway Ranges. The
988 backstop of the system, situated somewhere around its highest point - Mt Cowley (**fig. 17i**).

This concentration of inversion towards the north east is also supported by increasing estimates of post-Cretaceous exhumation from Tassone et al.,(2014) moving from the ~SW to the ~NE (**fig. 17a**).

The partitioning of stress and the accommodation of strain through the reactivation of the extensional listric décollement also assists in explaining why normal offset has been maintained within the fault network to the degree that it has, a question that has puzzled previous studies (e.g. Schneider et al., 2004; Holford et al., 2014). It also clarifies why mesoscale evidence for compressional inversion is not more substantial within the region, as stress was likely released primarily through the reactivation of the extensional décollement and accompanying faults. Though this was likely not possible during the early strike slip component of the phase as σ2 remained vertical, evident from the high degree of strike slip fracturing and faulting. It also provides an explanation as to the low magnitudes of compressional stress during the inversion of the system in phase 3 (**fig. 10**), as there was ample opportunity for the release of stress via reactivation of the extensional fabric. Particularly evident at the beginning of the phase, within sample C-T2 (**fig. 10**). It is also possible that the reactivation of the décollement may have been assisted by high-thermal gradients (thermal weakening) within the Eumeralla Formation and Otway Ranges, due to its radiogenic nature (Holford et al., 2011). And/or by the shale and coaly inter-beds within the formation, which may have assisted in accommodating strain, suggested by bedding parallel failure and faulting (**fig. 6b)**.

5.4 New insights into the Otway Basin

The results from this study re-define the structural framework of the eastern Otway Basin and the Otway Ranges (**fig. 17a**). Of leading consequence from the results of this study is the lack

of a ~NE-SW striking fault fabric within the eastern Otway Basin. Fault patterns that have been favoured by previous studies to have accommodated mid-Eocene – recent, ~NW-SE oriented compressional stresses during the Neotectonic uplift of the Otway Ranges (see Debenham et al., 2018). As noted in section 5.2, given the near parallel nature of the faults interpreted within this study and the in-situ stress regime of the basin (**fig. 2a**), it is likely that the environment of neotectonic stress within the Otway Basin has had a minimal effect on the macro scale structuring of the region. This is echoed by the results of this study, which favour ~NE-SW oriented inversion and uplift, during the Latest Cretaceous (~Mid-Maastrichtian). A period where maximum horizontal stress was orthogonal to fault strike and the dip-slip inversion of ~NW-SE striking faults was possible, especially around sections of the underlying basement block that are anonymously shallow in comparison to the surrounding region (**fig. 2b**). The timing of Latest Cretaceous, rather than neotectonic uplift in the eastern Otway Basin is also supported by petroleum industry data (Duddy and Erout, 2001). Indicating source rocks within the surrounding region are currently at their maximum burial temperature, suggesting that recent uplift - which some estimates place in excess of 2000m (Tassone et al., 2014) is highly unlikely.

Contrasts can also be drawn between the nature of the data used in this study and those that advocate for mainly neotectonic structuring of the eastern Otway Basin and Otway Ranges. Previous studies (e.g. Holford et al., 2014; Tassone et al., 2017) have utilised mainly isolated 2D seismic lines that strike ~NW-SE within the off-shore eastern basin. Insights from this study indicate these lines were parallel to the major fault trend, and as such inappropriate for the interpretation of the structures. The interference out of plane faults causing apparent faulting and interpretation in the time domain exaggerating this “folded,” interpretation. Leading some authors to suggest impractical styles of deformation such as neotectonic folding isolated only

to the post break up sedimentary succession, due to neotectonic ~NW-SE compressional stresses (Tassone et al., 2017).

Lastly, as we have not imaged it in 3D we cannot conclusively determine that well studied structures such as the Castle Cove Fault (**fig. 17f**) exist. Though the evidence of this study support initial inferences regarding the structure from Burgin et al., (2019). That being said, from comparisons between the sub surface style of the Top Early Cretaceous and its outcropping nature within the Otway Ranges at Castle Cove (**fig. 17a**) it is clear the two share a similar structural heritage. As such the outcropping structure is likely defined by a series of ~NW-SE striking inverted normal faults (**fig. 17h**) isolated in a ~NE-SW trending structural chain above shallow basement. Under this framework, the NE-SW trending fault scarp that characterises the region, can be explained due to a combination of differential compaction across the edge of the basement high and gravitational collapse downwards towards the southeast (**fig. 17h**). Explaining the gentle tilting of beds towards the south east and the lack of an outcropping fault plane at the cove (Debenham et al., 2018).

Given this insight and using a detailed topographic map of the Otway Ranges (**fig. 17a**) we interpret a series of ~NW-SE striking faults throughout the ranges. A faulting pattern that is far more continuous with that interpreted offshore within the seismic datasets and other studies (Robson et al., 2016; 2017; 2018) in comparison to the previous model.

5.5 Comparison of rifted margin stress magnitudes with collisional settings

The quantification of maximum paleo-differential stresses within this study, represents the first attempt to quantify extensive stress during the process of progressive continental break up. Of

note within the results is that magnitudes of stress appear higher during periods of extension and rifting, than during those of compression and inversion in the Otway Basin (**fig. 18**).

When compared to previous works quantifying paleo-differential stress magnitudes, with similar margins for error (<20%) (Lacombe and Laurent, 1992; Lacombe, 2001; Rocher et al., 2004; Lacombe et al., 2007; Lacombe et al., 2009; Amrouch et al., 2010; Beaudoin et al., 2012; Arboit et al., 2017; Kulikowski and Amrouch, 2017; Parlangeau et al., 2018) within foreland, intracontinental and collisional settings, magnitudes of extensive differential stress in this study present some of the highest values of extensional stress to date. Additionally, within foreland basins, compressional and strike slip stresses generally exceed extensional stress, while at the passive margin, we have observed a reverse trend. Likely due to the release of stress through the reactivation of the extensional network of deformation, as discussed in section 5.3.

There are a number of possible reasons for this phenomenon: Firstly, in the case of many primarily collisional settings (Sheep Mountain, ZCB, Cooper Basin) the determined phases of deformation have been largely constrained to strike slip and compressive regimes of stress – except in the case of outer rim style extension (Amrouch et al., 2010a) is a separate process. In all cases, stages of horizontal shear and displacement have been preceded by an earlier events of extension, meaning that pre-existing faults and fractures exist, which can help to relive stress during inversion. However, in the case of many rifted margins, early extensional phases likely involve the deformation of largely un-deformed formations such as the Eumeralla Formation, deposited during periods of tectonic quiescence and subsidence (Krassay et al., 2004). As such during the first phase of deformation there is less release of stress, as creating new faults and fractures is more difficult than the reactivation of previously existing networks. Secondly, even in the case of previously un-deformed sedimentary rock, compressional stress regimes – where

(σ1- σ3) = (σH- σv) – are characteristic of higher magnitudes of horizontal shear stress, allowing for the reactivation of the bedding, décollement or other intra-formational sedimentary layers – say between sands and silts. In contrast during extension where (σ1- σ3) = (σV- σh), and σ1 has no component of shear stress on the horizontal plane (Anderson, 1951), the release of stress along horizontal layers is harder and as such the release of stress happens after the faulting, hence the higher accumulation of stress during the early stages.

It is also worth noting that from the compiled paleostress tensors in **fig. 18**, that within each setting and individual studies, there appears to be distinct peaks with a number of anomalously high magnitude stress tensors in comparison to the rest of the dataset. From the insights gained in this study, where the highest magnitudes of stress are present within the initial phases of deformation, we hypothesise that a pattern may exist between the first, and preceding phases of stress. Stress magnitudes possibly being anomalously high in the very first stages of deformation. However, a more detailed investigation is well beyond the scope of this study, though this may warrant further investigation.

6.0 Conclusions

In this paper we have presented the first multiscale investigation into the paleostress development of a passive continental margin. As part of this study we have provided the first insight into the magnitude of extensional paleostresses during continental break up. A phase of deformation that is characterised by high values of extensional stress (~69MPa) when compared to previous studies in other tectonic settings.

This work has also completely redefined the structural framework of one of Australia's most studied sedimentary basins and most famous tourist regions along the Great Ocean Road.

Acknowledgements

Thank you to Natalie Debenham, David Kulikowski, Ian Duddy and Colin Burgin for their assistance in the field. Thank you to Professor Mike Hall for use of his holiday house at Apollo Bay as a base during field work. Thank you to Down Under Geosolutions for the use of D.U.G Insight and to Midland Valley Exploration Ltd for the use of Move 2017.2. Thank you to Rick Almendinger for the use of Stereonet 8 and to Damien Delvaux for the use of Wintensor. Thank you to Beach Energy for supplying the Crowes Foot 3D. The authors appreciate the contribution of the Australian Postgraduate award from the University of Adelaide.

Table 1

Well	Tool Type	Bit Size (inches)	Max Borehold Deviation	Top of Log (m bKB)	Bottom of Log (m bKB)	Log Length	Fracture Count
Bellarine-1	FMI	8.5	1	278	978	700	24
Halladale-1DW2	STAR	8.5	21.72	1668	1927	259	25
Henry-1ST1	STAR	8.5	1	1725	2015	290	37
Wild Dog Road-1	FMI	8.5	34.5	1200	1676	476	27
Moreys-1	CMI	8.5	21.4	1700	2300	600	60
Glenaire-1	FMS	8.5	20.5	2996	3702	706	24

Table 2

Calcite stress inversion results from the Eumeralla Formation

Sample Name	Bedding (D/DD)	Vein (D/DD) present	Vein Set	σ1	σ2	σ3	Total Data (T/UT)	Compataible Planes (T/UT)	R value	F function	Pre/Post bedding tilting	Differential Stress (MPa)
10T2	45/00	77/216	1	61/143	29/328	02/236	117/60	60/49	0.5	0.69	Pre	69±14
A-ST1	16/145	78/319	sty	85/352	01/098	04/189	273/18	125/17	0.4	0.49	Pre	66±13
B-AT1	15/169	80/049	1	62/318	06/060	27/153	229/65	82/53	0.4	0.56	Pre	36±7
C-T1	15/169	75/289	3	84/359	04/225	04/135	238/50	109/36	0.2	0.72	Pre	34±7
B-BT2	15/169	80/048	1	08/182	81/359	01/092	168/67	50/45	0.8	0.39	Pre	32±6
C-T2	15/169	75/289	3	07/220	04/310	80/65	129/50	56/41	0.5	0.87	pre	13±3
A-LT2	16/145	78/319	sty	13/199	15/292	71/067	82/22	67/21	0.8	0.95	Pre	28±6
10T1	45/005	77/216	1	00/062	20/332	70/154	182/61	65/49	0.2	0.34	pre	31±6
B-BT1	15/169	80/048	1	16/088	58/205	28/350	245/67	88/57	0.3	0.15	Post	32±6
10T3	45/005	66/245	1	68/089	19/234	12/328	56/59	23/57	0.6	0.41	Post	43±9
A-LT1	16/145	78/319	sty	61/051	25/262	13/166	185/22	103/19	0.1	0.8	Post	46±9
12T2	86/131	36/243	1	59/244	05/146	34/052	118/68	51/61	0.6	1.15	Post	57±11
12T1	86/131	36/243	1	06/337	03/068	83/181	216/68	99/53	0.7	0.92	Post	50±10

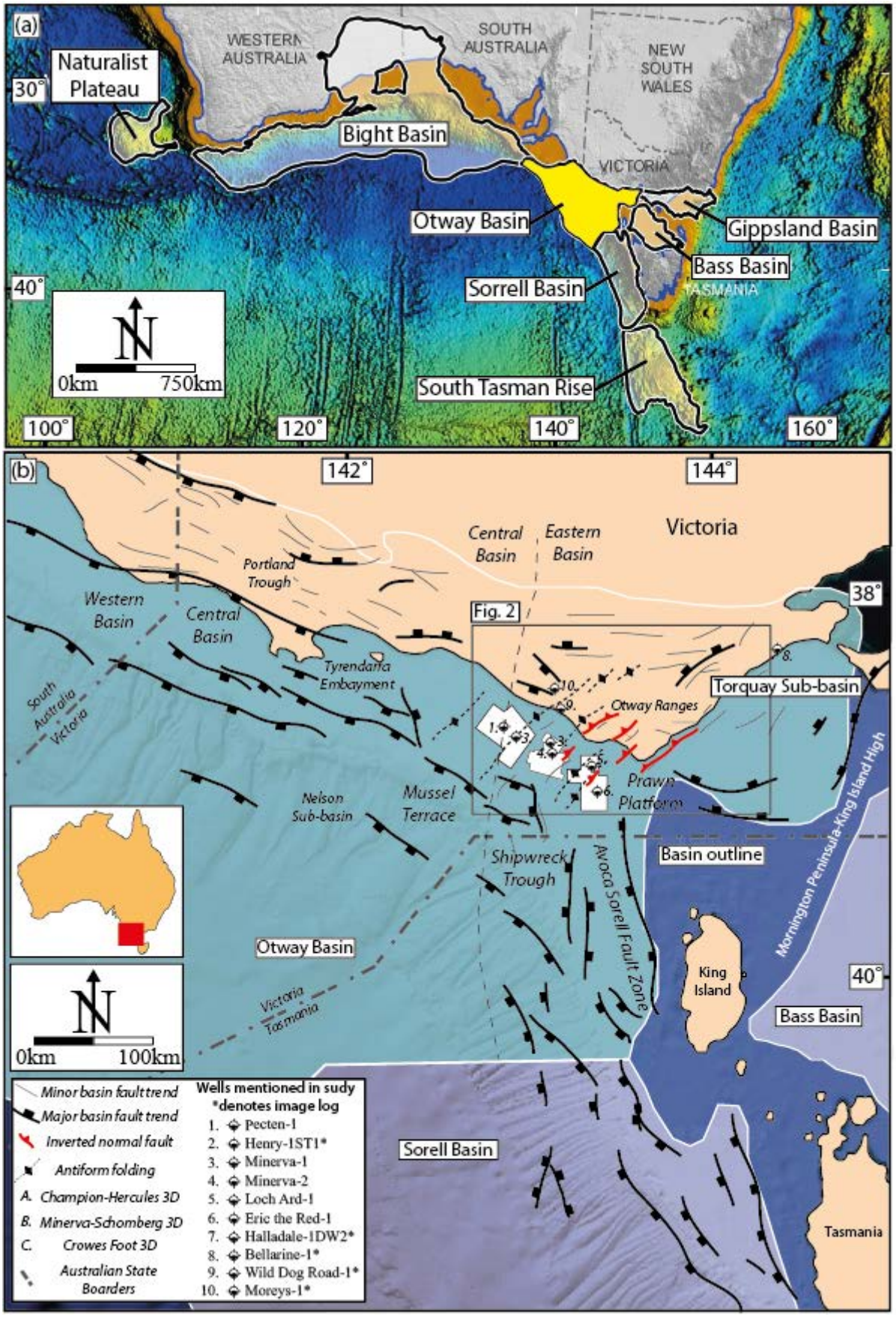
(a)
WESTERN AUSTRALIA
SOUTH AUSTRALIA
NEW SOUTH WALES
VICTORIA
TASMANIA
Naturalist Plateau
Bight Basin
Otway Basin
Gippsland Basin
Bass Basin
Sorrell Basin
South Tasman Rise
30°
40°
100°
120°
140°
160°
0km
750km
(b)
142°
144°
38°
40°
Victoria
Central Basin
Eastern Basin
Portland Trough
Western Basin
Central Basin
Tyrendarra Embayment
South Australia
Victoria
Fig. 2
Otway Ranges
Torquay Sub-basin
Prawn Platform
Nelson Sub-basin
Mussel Terrace
Shipwreck Trough
Avoca Sorell Fault Zone
Basin outline
Mornington Peninsula-King Island High
King Island
Otway Basin
Victoria
Tasmania
Bass Basin
Sorell Basin
Tasmania
0km
100km
Minor basin fault trend
Major basin fault trend
Inverted normal fault
Antiform folding
A. Champion-Hercules 3D
B. Minerva-Schomberg 3D
C. Crowes Foot 3D
Australian State Boarders
Wells mentioned in sudy
*denotes image log
1. Pecten-1
2. Henry-1ST1*
3. Minerva-1
4. Minerva-2
5. Loch Ard-1
6. Eric the Red-1
7. Halladale-1DW2*
8. Bellarine-1*
9. Wild Dog Road-1*
10. Moreys-1*

Fig. 1: (a) A map of Australia's southern margin showing the basins of the southern rift system and (b) The present day structural framework of the Otway Basin. Modified after Stacey et al., (2013) with inverted faults from Holford et al., (2014) and Debenham et al (2018).

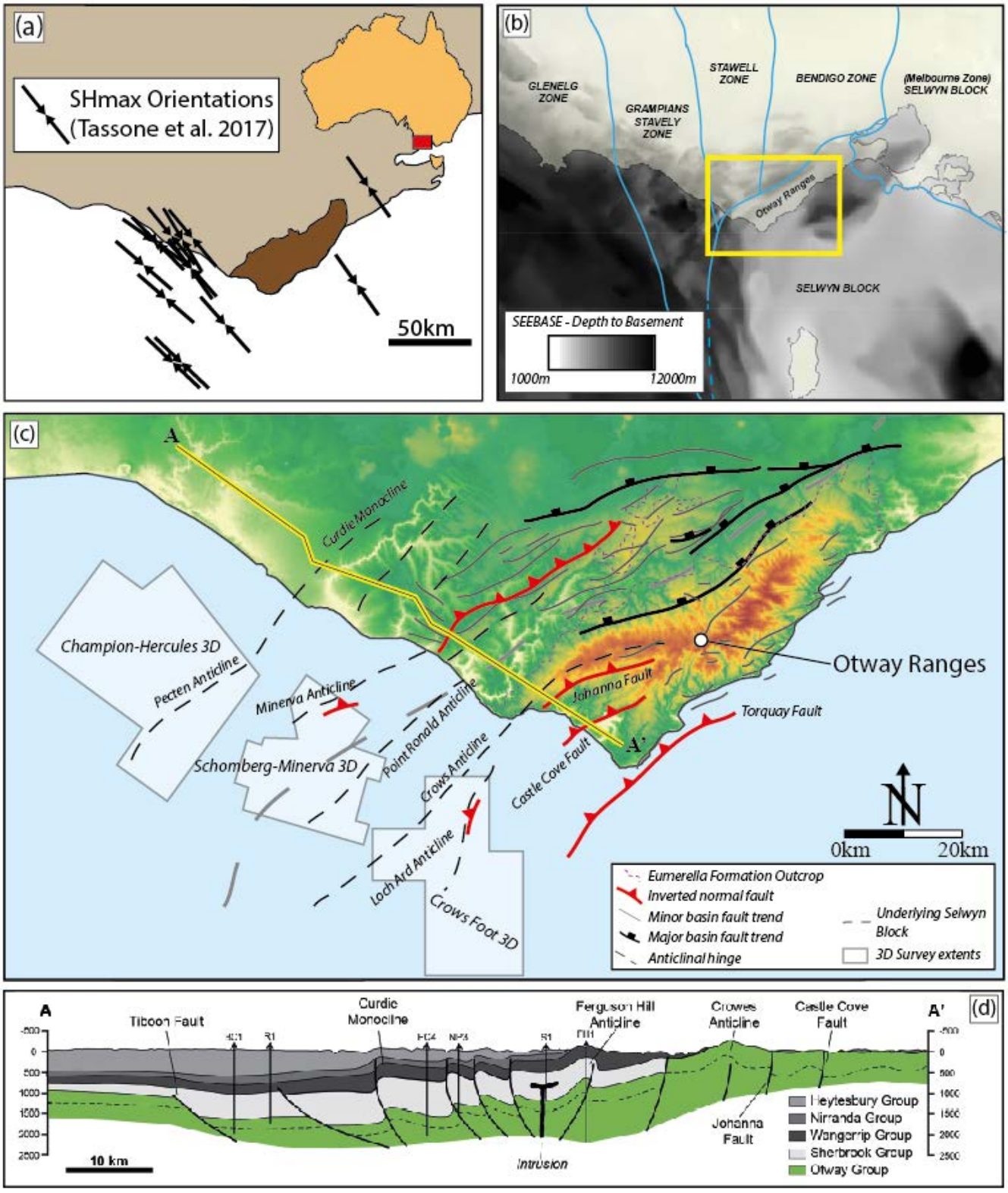
(a)
SHmax Orientations
(Tassone et al. 2017)
50km
(b)
GLENELG ZONE
GRAMPIANS STAVELY ZONE
STAWELL ZONE
BENDIGO ZONE
(Melbourne Zone) SELWYN BLOCK
Otway Ranges
SELWYN BLOCK
SEEBASE - Depth to Basement
1000m
12000m
(c)
A
A'
Curdie Monocline
Champion-Hercules 3D
Pecten Anticline
Minerva Anticline
Schomberg-Minerva 3D
Point Ronald Anticline
Crows Anticline
Loch Ard Anticline
Crows Foot 3D
Castle Cove Fault
Johanna Fault
Torquay Fault
Otway Ranges
N
0km
20km
Eumerella Formation Outcrop
Inverted normal fault
Minor basin fault trend
Major basin fault trend
Anticlinal hinge
Underlying Selwyn Block
3D Survey extents
(d)
A
A'
Tiboon Fault
Curdie Monocline
Ferguson Hill Anticline
Crowes Anticline
Castle Cove Fault
Johanna Fault
Intrusion
10 km
Heytesbury Group
Nirranda Group
Wangerrip Group
Sherbrook Group
Otway Group

Fig. 2: (a) In situ stress orientation in the eastern Otway Basin. (b) Basement units of the eastern Otway Basin after Krassay et al., (2009) (c) The present day structural framework of the study area and (d) Cross sections from Debenham et al (2018) after Edwards et al., (1996) showing the current structural framework of the Otway Ranges

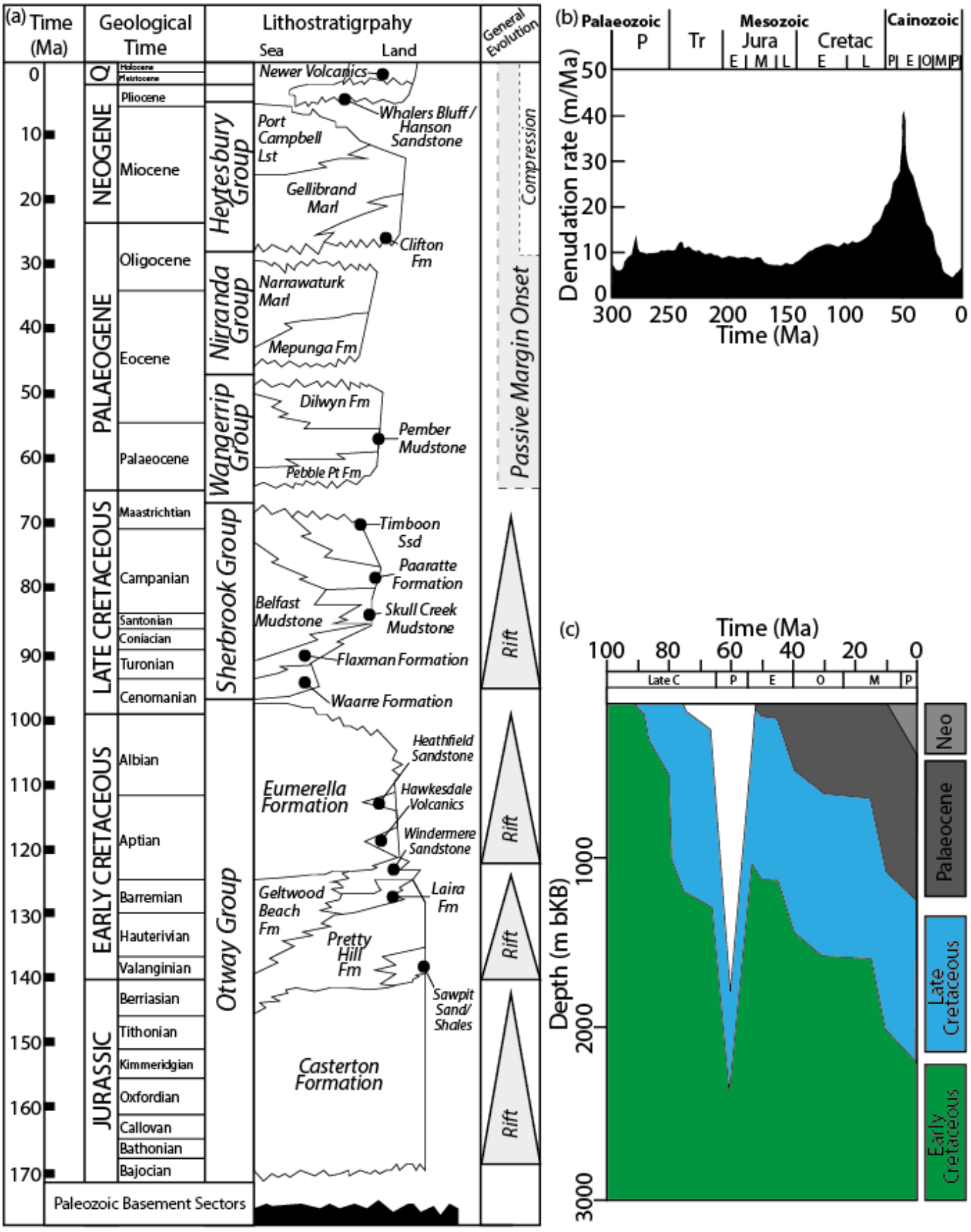
(a)
Time (Ma)
Geological Time
Lithostratigrpahy
Sea
Land
General Evolution
Q
Holocene
Pleistocene
NEOGENE
Pliocene
Miocene
PALAEOGENE
Oligocene
Eocene
Palaeocene
LATE CRETACEOUS
Maastrichtian
Campanian
Santonian
Coniacian
Turonian
Cenomanian
EARLY CRETACEOUS
Albian
Aptian
Barremian
Hauterivian
Valanginian
JURASSIC
Berriasian
Tithonian
Kimmeridgian
Oxfordian
Callovan
Bathonian
Bajocian
Heytesbury Group
Nirranda Group
Wangerrip Group
Sherbrook Group
Otway Group
Newer Volcanics
Whalers Bluff / Hanson Sandstone
Port Campbell Lst
Gellibrand Marl
Clifton Fm
Narrawaturk Marl
Mepunga Fm
Dilwyn Fm
Pember Mudstone
Pebble Pt Fm
Timboon Ssd
Paaratte Formation
Belfast Mudstone
Skull Creek Mudstone
Flaxman Formation
Waarre Formation
Heathfield Sandstone
Eumerella Formation
Hawkesdale Volcanics
Windermere Sandstone
Geltwood Beach Fm
Laira Fm
Pretty Hill Fm
Sawpit Sand/ Shales
Casterton Formation
Paleozoic Basement Sectors
Compression
Passive Margin Onset
Rift
Rift
Rift
Rift
(b)
Palaeozoic
Mesozoic
Cainozoic
P
Tr
Jura
Cretac
E M L
E L
P E O M P
Denudation rate (m/Ma)
Time (Ma)
(c)
Time (Ma)
Late C
P
E
O
M
P
Depth (m bKB)
Neo
Palaeocene
Late Cretaceous
Early Cretaceous

Fig. 3: (a) stratigraphic column of the Otway Basin, modified after Constantine and Liebermann (2002) (b) Denudation rates for South East Australia from Kohn et al., (2002) (c) Burial diagram from Mussel-1 well, suggesting ~60Ma major cooling, modified from Duddy and Erout (2001).

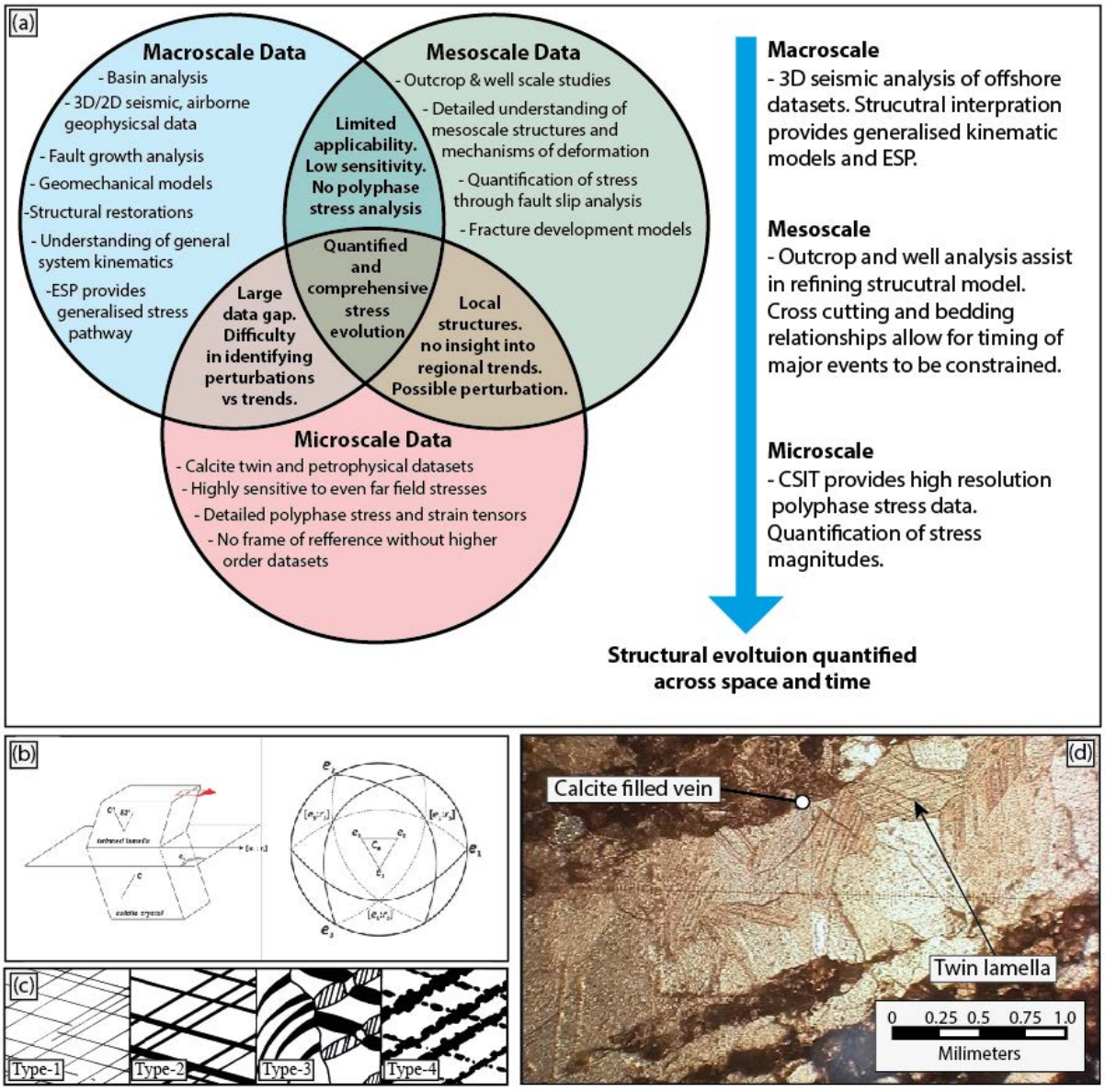

Fig. 4: (a) Venn-diagram showing the strengths of different scales of structural analysis and how they can be effectively combined to produce a quantified and comprehensive model for basin evolution. The specific multiscale pathway is shown alongside. (b) Schematic diagram of calcite twin lamella and the orientation of e-planes distributed with respect to the optical axes of the crystal (c) Types of twins modified from Burkhard (1994) (d) Calcite filled vein from sample 12T at site 12.

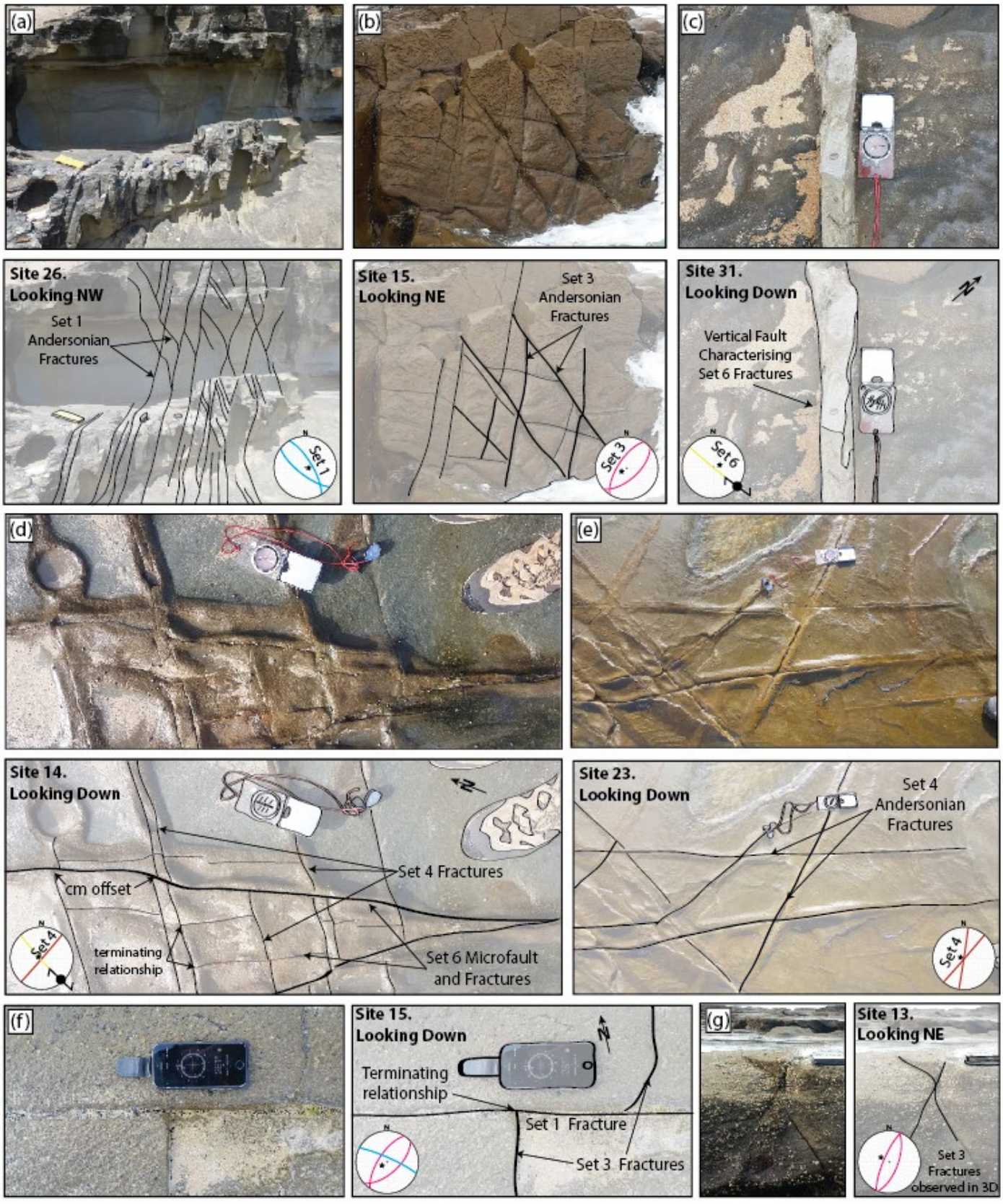
(a)
(b)
(c)
Site 26.
Looking NW
Set 1
Andersonian
Fractures
Set 1
Site 15.
Looking NE
Set 3
Andersonian
Fractures
Set 3
Site 31.
Looking Down
Vertical Fault
Characterising
Set 6 Fractures
Set 6
(d)
(e)
Site 14.
Looking Down
cm offset
Set 4 Fractures
terminating
relationship
Set 6 Microfault
and Fractures
Set 4
Site 23.
Looking Down
Set 4
Andersonian
Fractures
Set 4
(f)
Site 15.
Looking Down
Terminating
relationship
Set 1 Fracture
Set 3 Fractures
(g)
Site 13.
Looking NE
Set 3
Fractures
observed in 3D

Fig. 5: (a) Set 1 Andersonian ~NE-SW extensive fractures at site 26. (b) Set 3 Andersonian fractures at site 15. (c) A microfault showing ~NW-SE oriented strike slip movement at site 31. (d) Set 6 fractures and microfaults cross cutting and terminating on set 4 fractures at site 14. (e) Andersonian strike slip fractures interpreted at site 23. (f) Set 3 fractures terminating on set 1 fractures at site 15, providing a relative chronology. (g) Set 3 fractures observed in 3D, distingushing them from set 4 fractures by the extensional andersonian nature.

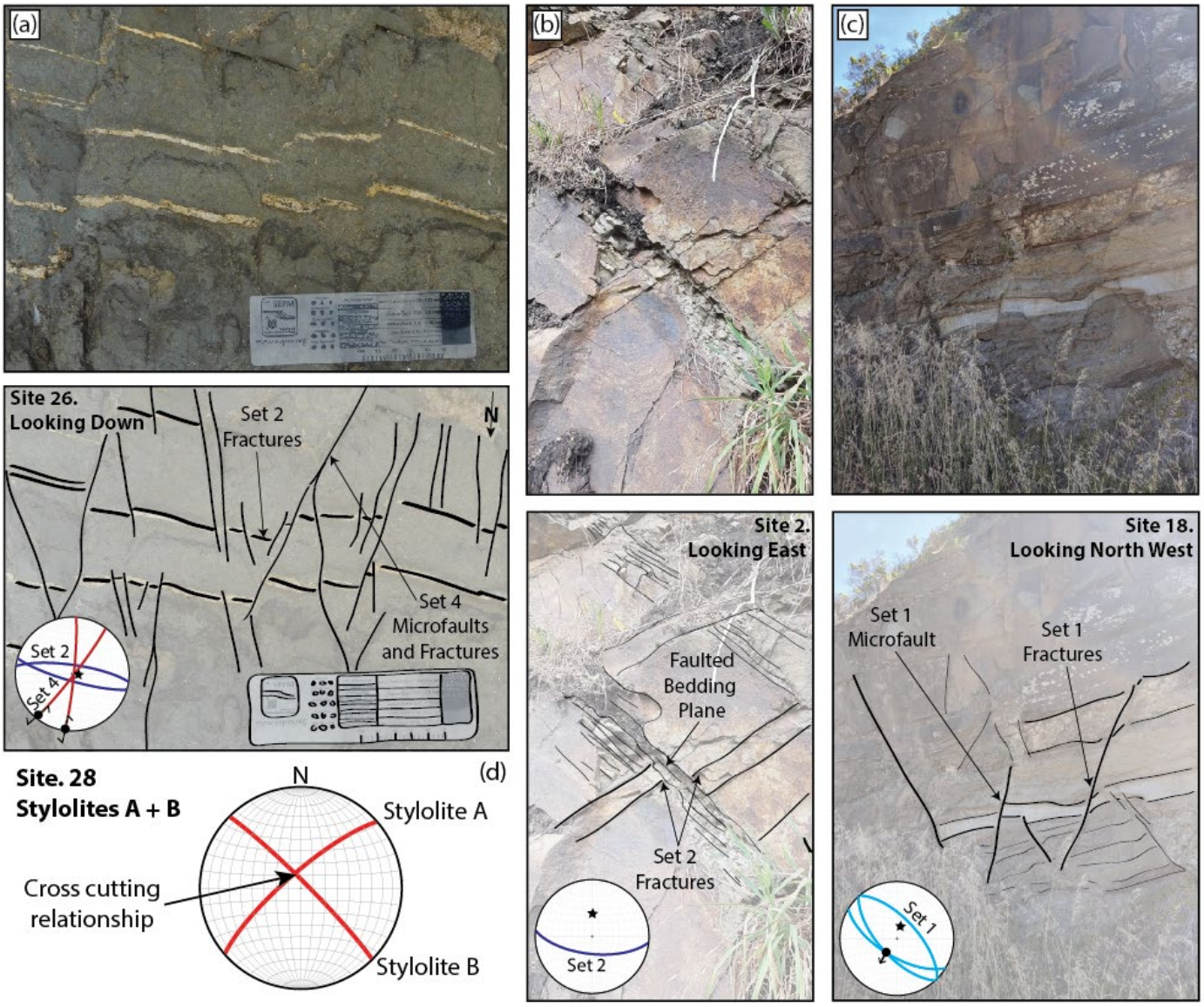

Fig. 6: (a) Set 4 microfaults and fractures crosscutting and offsetting set 2 fractures at site 26. (b) Set 2 fractures offset by slip along the bedding plane at site 2 (c) Microfault and extensive fractures integrated as part of fracture set 1 at site 18. (d) The two stlolites interpreted as part of this study at site 28. Stylolite B cross cuts stylolite A, which has been reactivation as a vein.

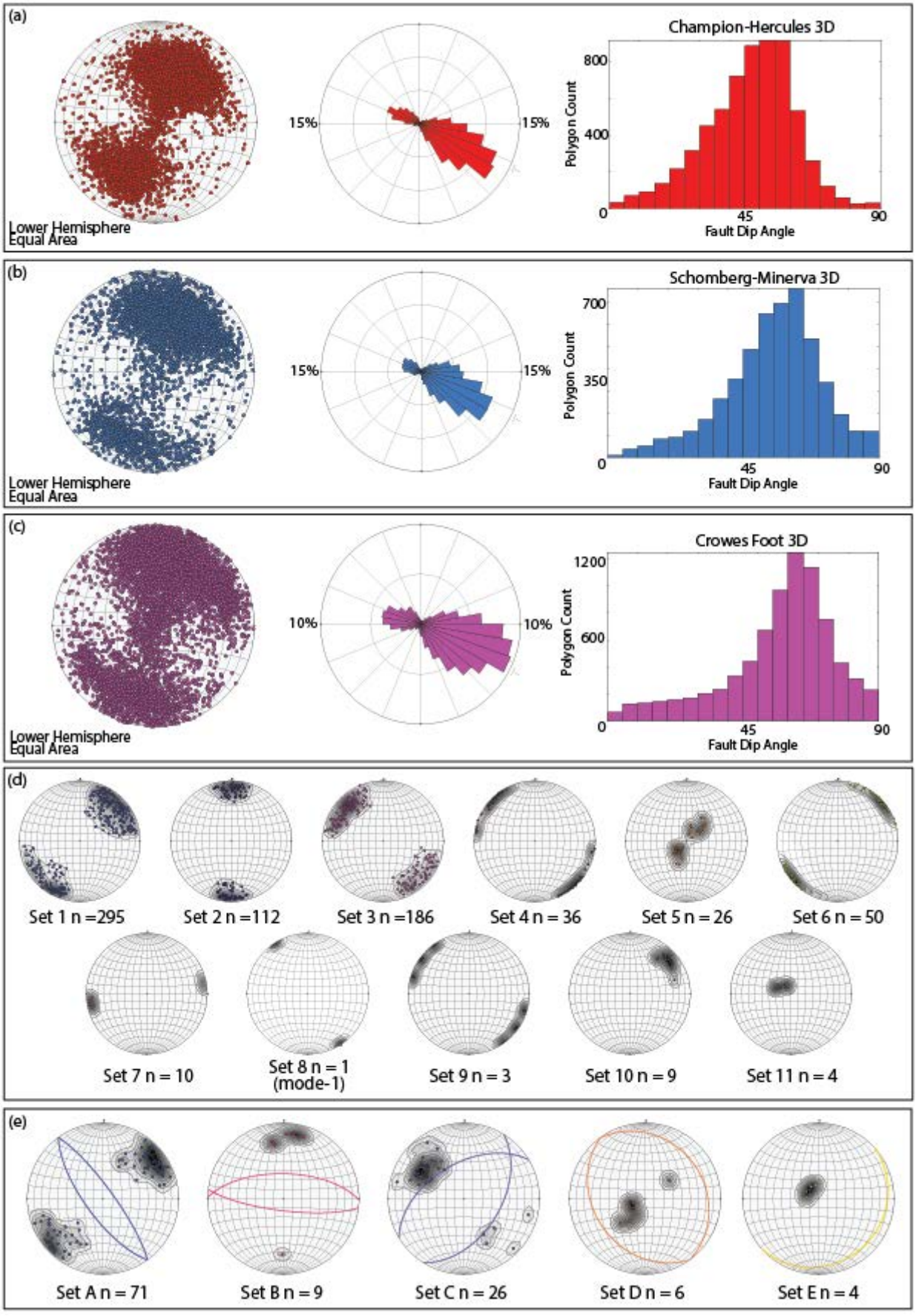
(a)
Lower Hemisphere
Equal Area
15%
15%
Champion-Hercules 3D
Polygon Count
800
400
0
45
90
Fault Dip Angle
(b)
Lower Hemisphere
Equal Area
15%
15%
Schomberg-Minerva 3D
Polygon Count
700
350
0
45
90
Fault Dip Angle
(c)
Lower Hemisphere
Equal Area
10%
10%
Crowes Foot 3D
Polygon Count
1200
600
0
45
90
Fault Dip Angle
(d)
Set 1 n =295
Set 2 n =112
Set 3 n =186
Set 4 n = 36
Set 5 n = 26
Set 6 n = 50
Set 7 n = 10
Set 8 n = 1
(mode-1)
Set 9 n = 3
Set 10 n = 9
Set 11 n = 4
(e)
Set A n = 71
Set B n = 9
Set C n = 26
Set D n = 6
Set E n = 4

Fig. 7: (a) poles to planes and rose diagrams from faults extracted from the Champion-Hercules 3D (b) the Schomberg-Minerva 3D and (c) the Crowes Foot 3D which includes a dip-angle histogram showing the low angle listric style faulting. (d) Poles to planes, showing the natural fracture data collected from outcrop sites within the Otway Ranges. Sets 1 – 6: major sets, sets 7-11: Minor sets (e) Poles to planes and rose showing all sub-surface natural fracture data and (f) major fracture sets established in the sub-surface.

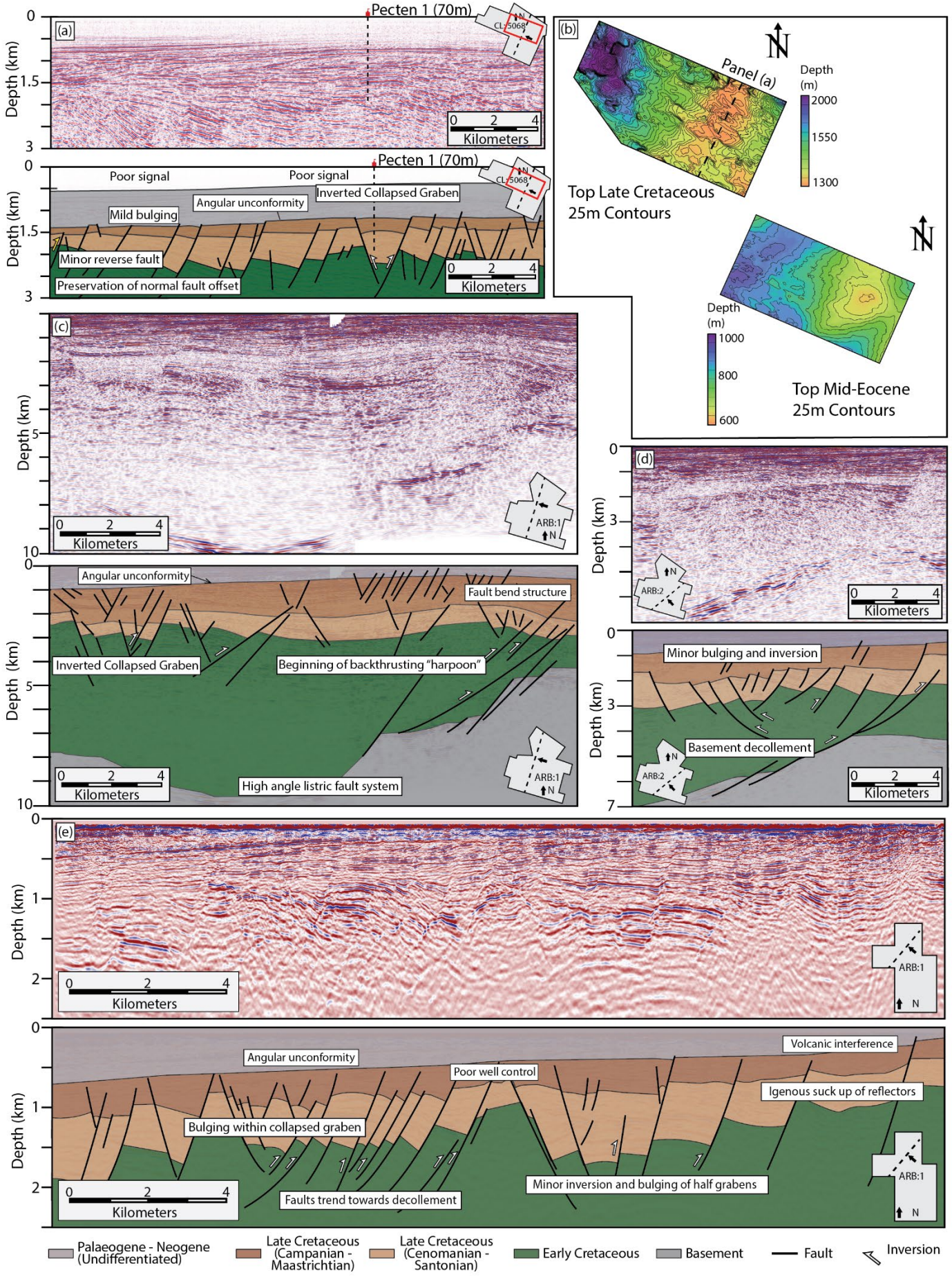
(a)
Pecten 1 (70m)
Depth (km)
0
1.5
3
0 2 4
Kilometers
(b)
Panel (a)
Depth (m)
2000
1550
1300
Top Late Cretaceous
25m Contours
Depth (m)
1000
800
600
Top Mid-Eocene
25m Contours
Poor signal
Poor signal
Inverted Collapsed Graben
Angular unconformity
Mild bulging
Minor reverse fault
Preservation of normal fault offset
(c)
5
10
ARB:1
(d)
ARB:2
Angular unconformity
Fault bend structure
Inverted Collapsed Graben
Beginning of backthrusting "harpoon"
High angle listric fault system
Minor bulging and inversion
Basement decollement
7
(e)
Volcanic interference
Poor well control
Igenous suck up of reflectors
Bulging within collapsed graben
Minor inversion and bulging of half grabens
Faults trend towards decollement
Palaeogene - Neogene (Undifferentiated)
Late Cretaceous (Campanian - Maastrichtian)
Late Cretaceous (Cenomanian - Santonian)
Early Cretaceous
Basement
Fault
Inversion

Fig. 8:(a) un-interpreted and interpreted section though the Champion-Hercules 3D survey (red box = interpreted section) showing the inverted collapsed graben penetrated by Pecten-1 (b) Top Late Cretaceous from the Champion-Hercules 3D showing the ~NW-SE trending fault pattern and Pecten structure visible due to differential compaction along Top Mid-Eocene horizon (c) un-interpreted and interpreted arbline from the Schomberg-Minerva 3D survey through the Minerva structure (d) un-interpreted and interpreted through the Point Ronald structure (e) Un-interpreted and interpreted arbline along the hinge of the Crowes inversion structure.

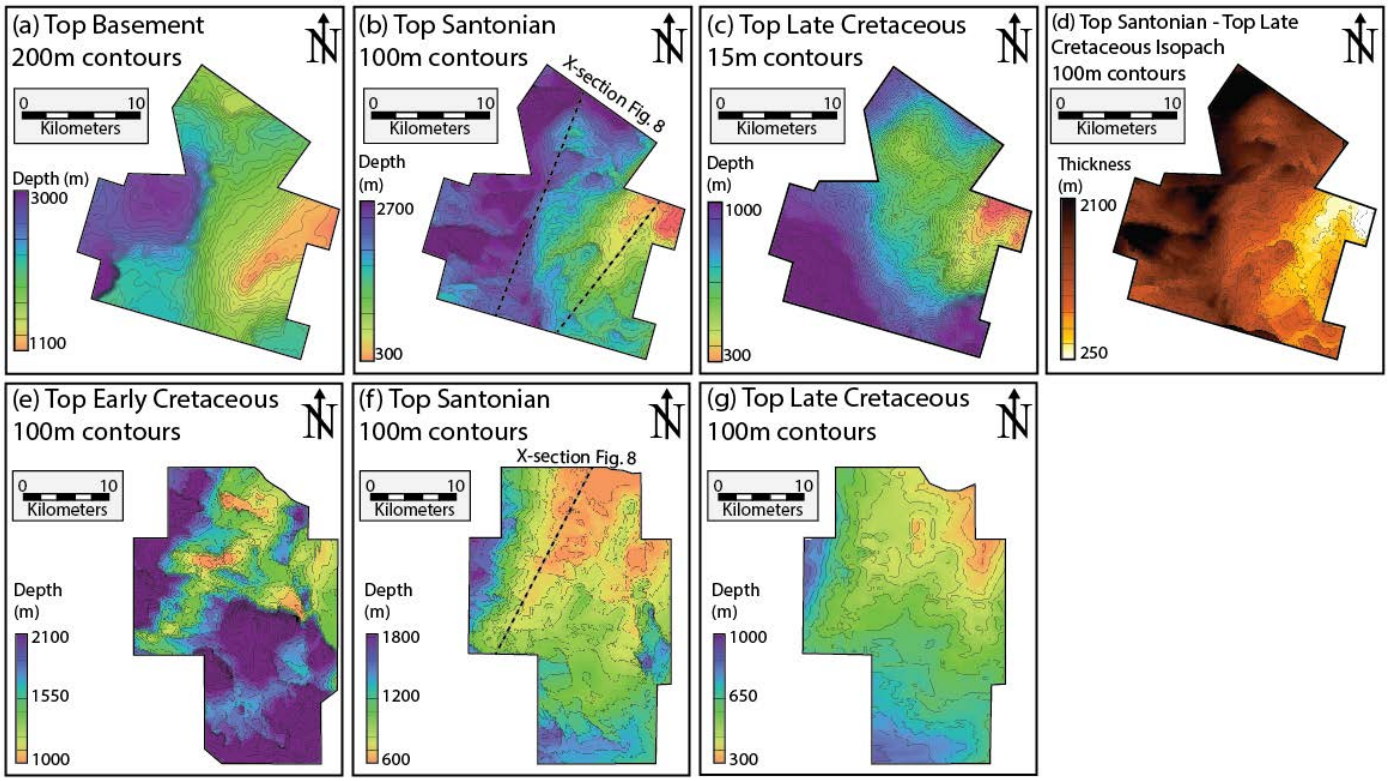

Fig 9. (a) – (c) horizons and Late Cretaceous isopach from the Schomberg-Minerva 3D. Note how highs within the Top Santonian and Top Late Cretaceous overlie sections of high basement. (e) – (h) Horizons for the Crowes Foot 3D.

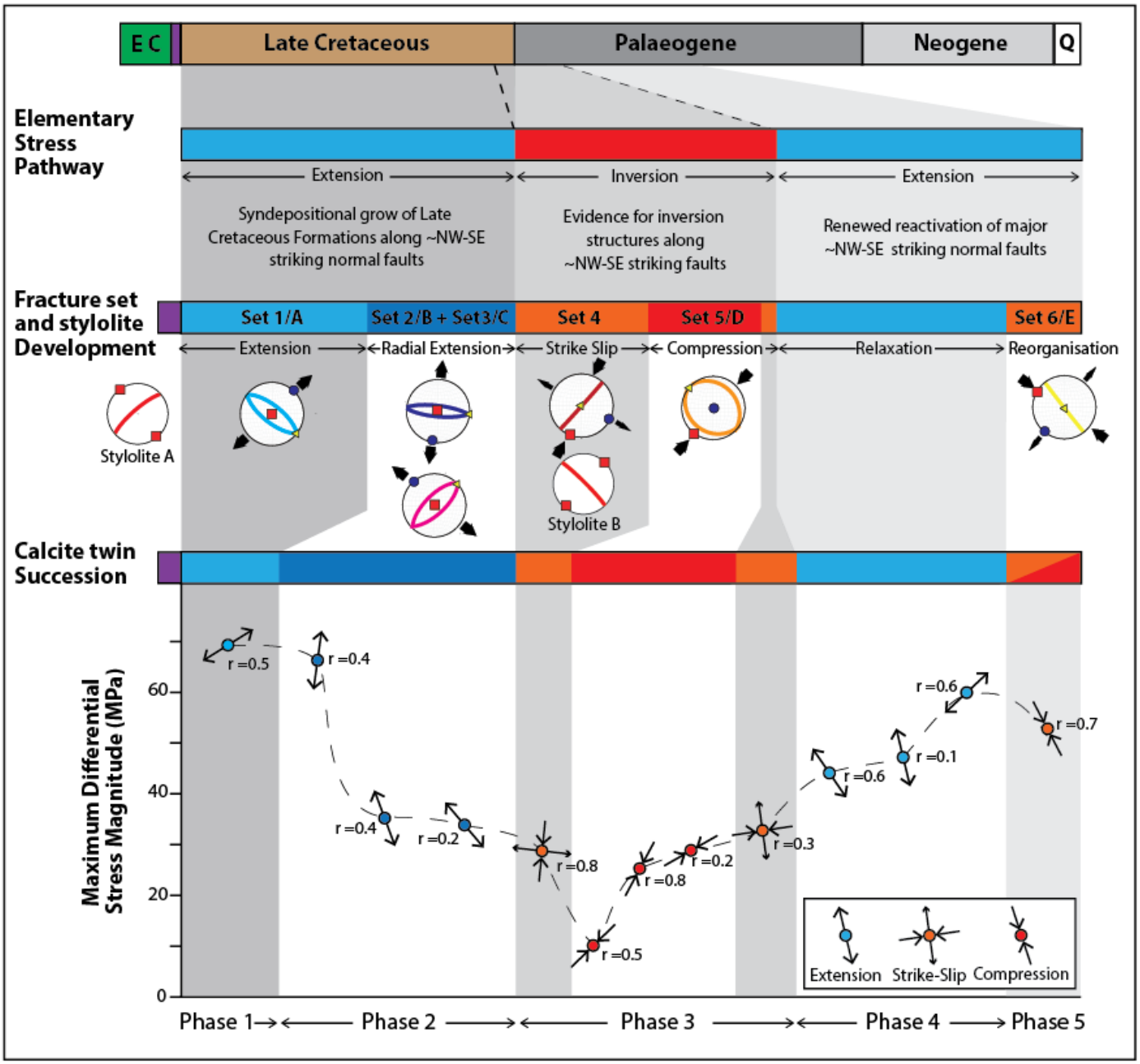

Fig. 10: The multiscale model for basin evolution, reflecting the ESP (top), fracture succession of major sets from outcrop and well data (middle) and calcite twin stress tensor data (bottom). Note the higher levels of differential extensional stress during the phases of extension and continental break up.

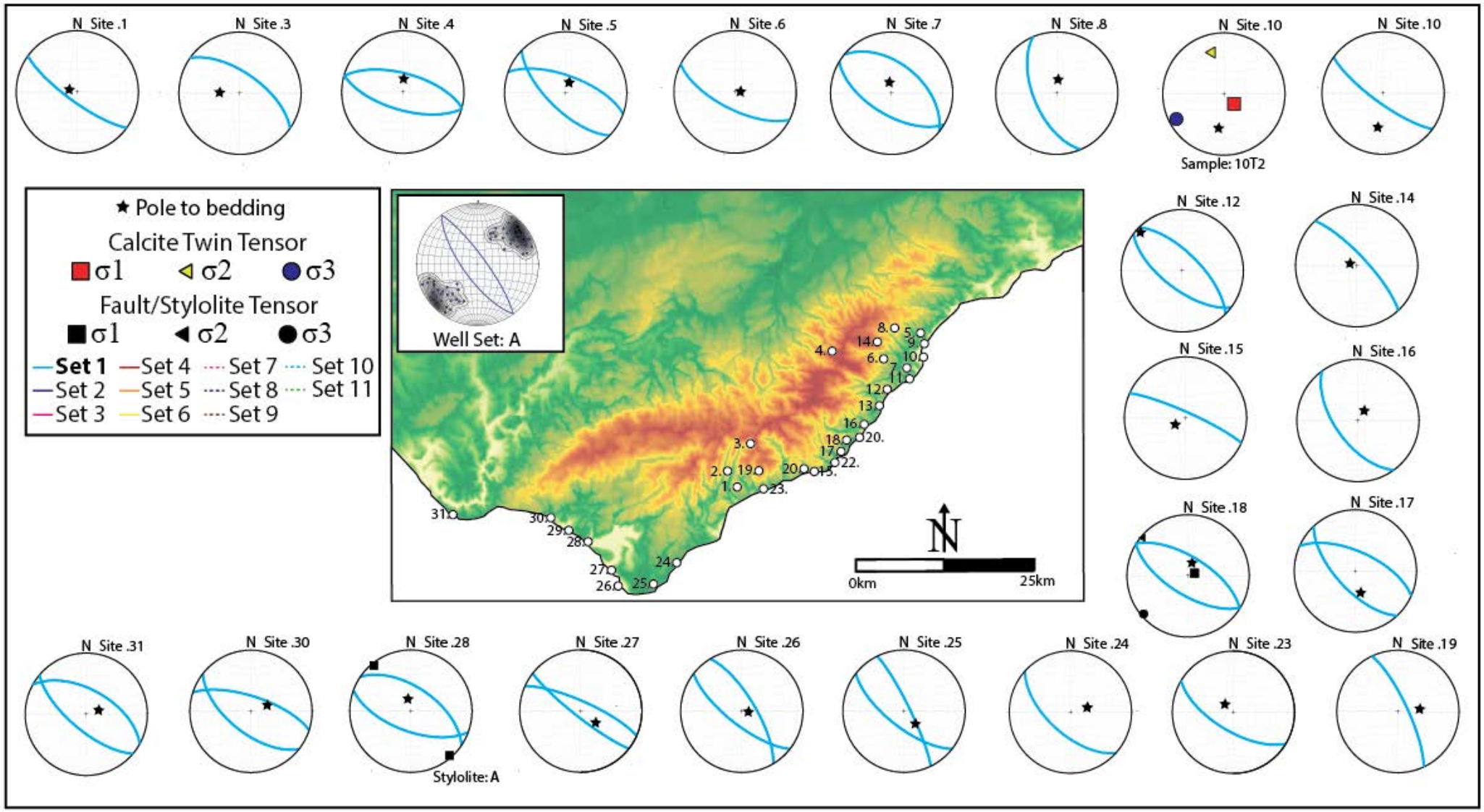
N Site .1
N Site .3
N Site .4
N Site .5
N Site .6
N Site .7
N Site .8
N Site .10
Sample: 10T2
N Site .10
★ Pole to bedding
Calcite Twin Tensor
σ1 σ2 σ3
Fault/Stylolite Tensor
σ1 σ2 σ3
Set 1 Set 4 Set 7 Set 10
Set 2 Set 5 Set 8 Set 11
Set 3 Set 6 Set 9
Well Set: A
N Site .12
N Site .14
N Site .15
N Site .16
N Site .18
N Site .17
N Site .31
N Site .30
N Site .28
Stylolite: A
N Site .27
N Site .26
N Site .25
N Site .24
N Site .23
N Site .19
0km
25km

Fig. 11: Fracture sets, micro faults and calcite twin tensors interpreted within basin phase 1. All data is presented with the bedding back tilted. Stylolite A is included at Site 28. Though this is attributed to a preceding event of, minor ~NW-SE compression or strike slip as discussed in text. All data is presented on lower hemisphere equal area stereonet plots

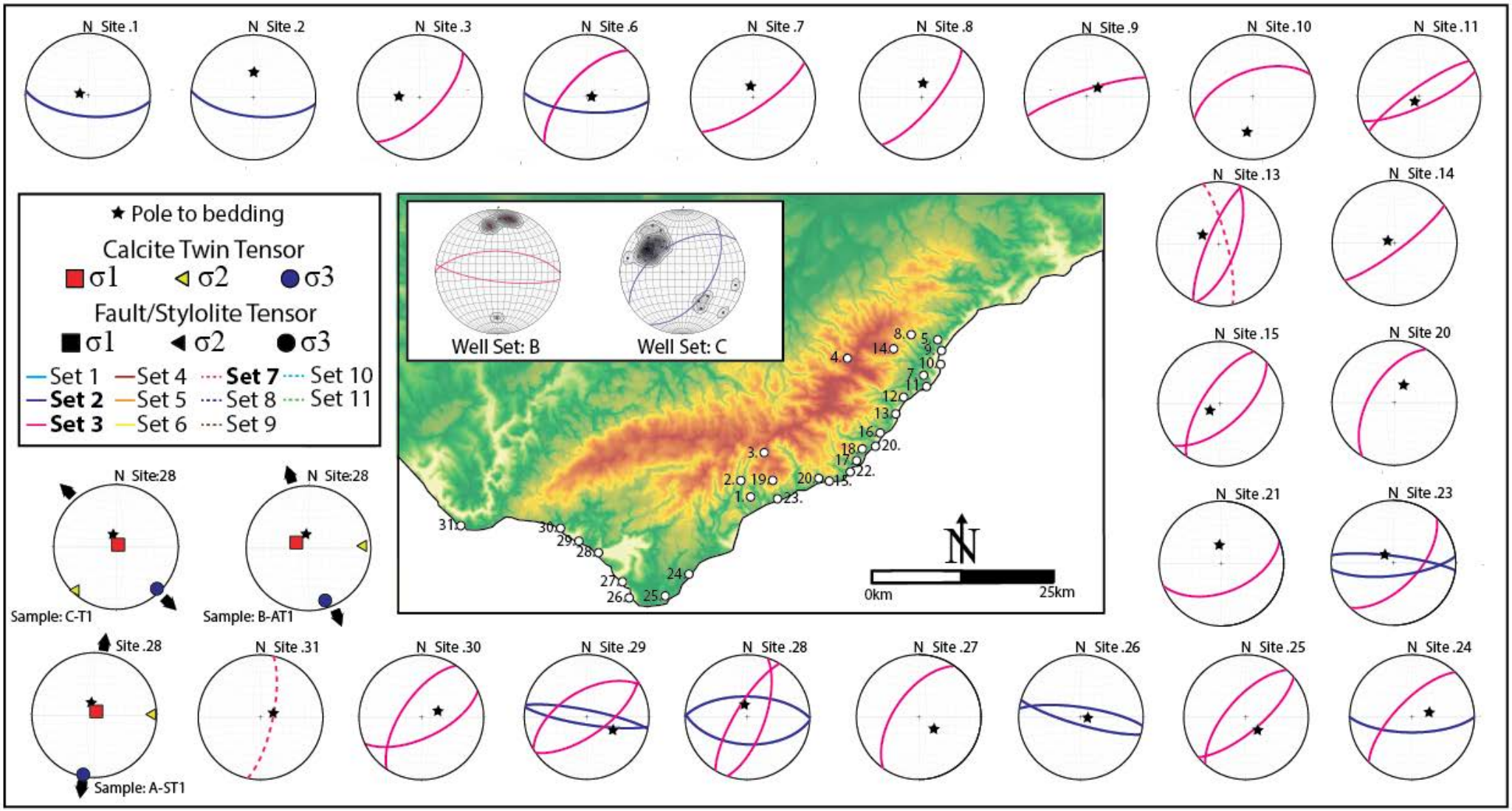
N Site .1
N Site .2
N Site .3
N Site .6
N Site .7
N Site .8
N Site .9
N Site .10
N Site .11
N Site .13
N Site .14
N Site .15
N Site 20
N Site .21
N Site .23
N Site .24
N Site .25
N Site .26
N Site .27
N Site .28
N Site .29
N Site .30
N Site .31
Site .28
N Site:28
N Site:28
Sample: C-T1
Sample: B-AT1
Sample: A-ST1
Pole to bedding
Calcite Twin Tensor
σ1 σ2 σ3
Fault/Stylolite Tensor
σ1 σ2 σ3
Set 1 Set 4 Set 7 Set 10
Set 2 Set 5 Set 8 Set 11
Set 3 Set 6 Set 9
Well Set: B
Well Set: C
0km
25km

Fig. 12: Fracture sets, micro faults and calcite twin tensors interpreted within basin phase 2. All data is presented with the bedding back tilted on lower hemisphere equal area stereonet plots.

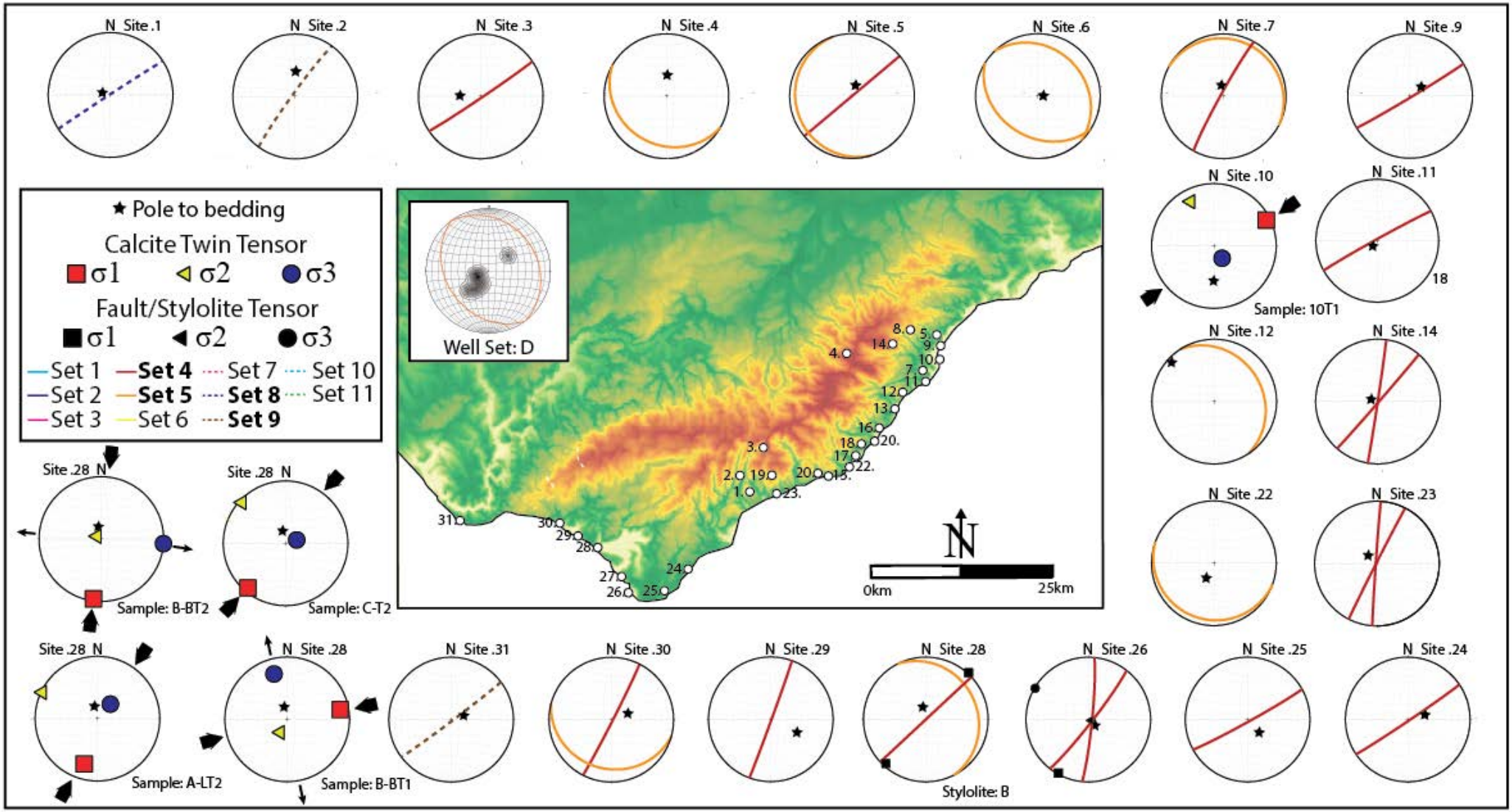
N Site .1
N Site .2
N Site .3
N Site .4
N Site .5
N Site .6
N Site .7
N Site .9
N Site .10
N Site .11
Sample: 10T1
N Site .12
N Site .14
N Site .22
N Site .23
N Site .24
N Site .25
N Site .26
N Site .28
N Site .29
N Site .30
N Site .31
Stylolite: B
Sample: B-BT1
Sample: A-LT2
Site .28 N
Site .28 N
Sample: C-T2
Sample: B-BT2
★ Pole to bedding
Calcite Twin Tensor
σ1 σ2 σ3
Fault/Stylolite Tensor
σ1 σ2 σ3
Set 1 Set 4 Set 7 Set 10
Set 2 Set 5 Set 8 Set 11
Set 3 Set 6 Set 9
Well Set: D
0km
25km

Fig. 13: Fracture sets, micro faults and calcite twin tensors interpreted within basin phase 3. All data is presented with the bedding back tilted on lower hemisphere equal area stereonet plots.

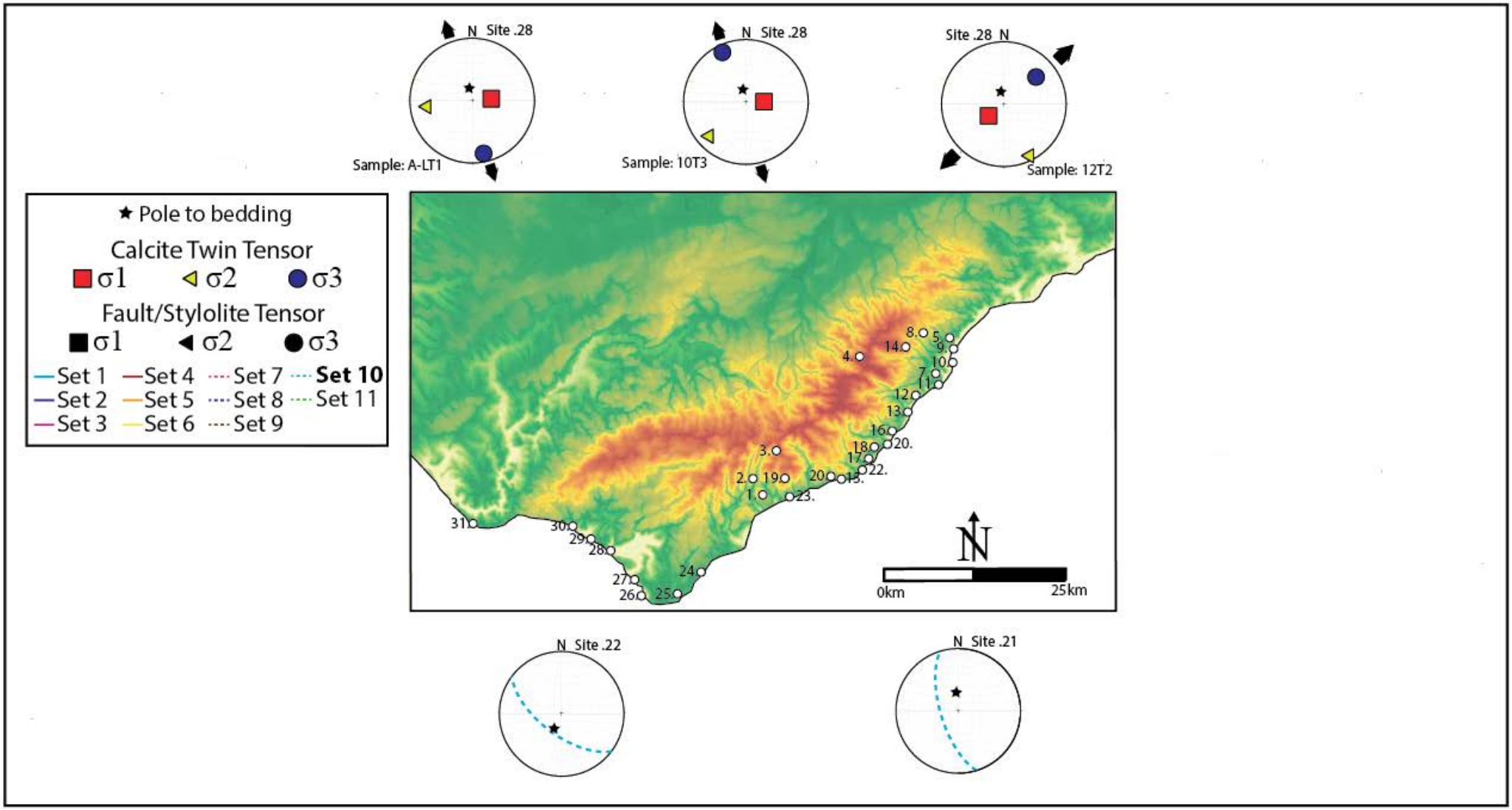
N Site .28
Sample: A-LT1
N Site .28
Sample: 10T3
Site .28 N
Sample: 12T2
★ Pole to bedding
Calcite Twin Tensor
σ1 σ2 σ3
Fault/Stylolite Tensor
σ1 σ2 σ3
Set 1 Set 4 Set 7 Set 10
Set 2 Set 5 Set 8 Set 11
Set 3 Set 6 Set 9
0km
25km
N Site .22
N Site .21

Fig. 14: Fracture sets, micro faults and calcite twin tensors interpreted within basin phase 4. All data is presented under present day bedding on lower hemisphere equal area stereonet plots.

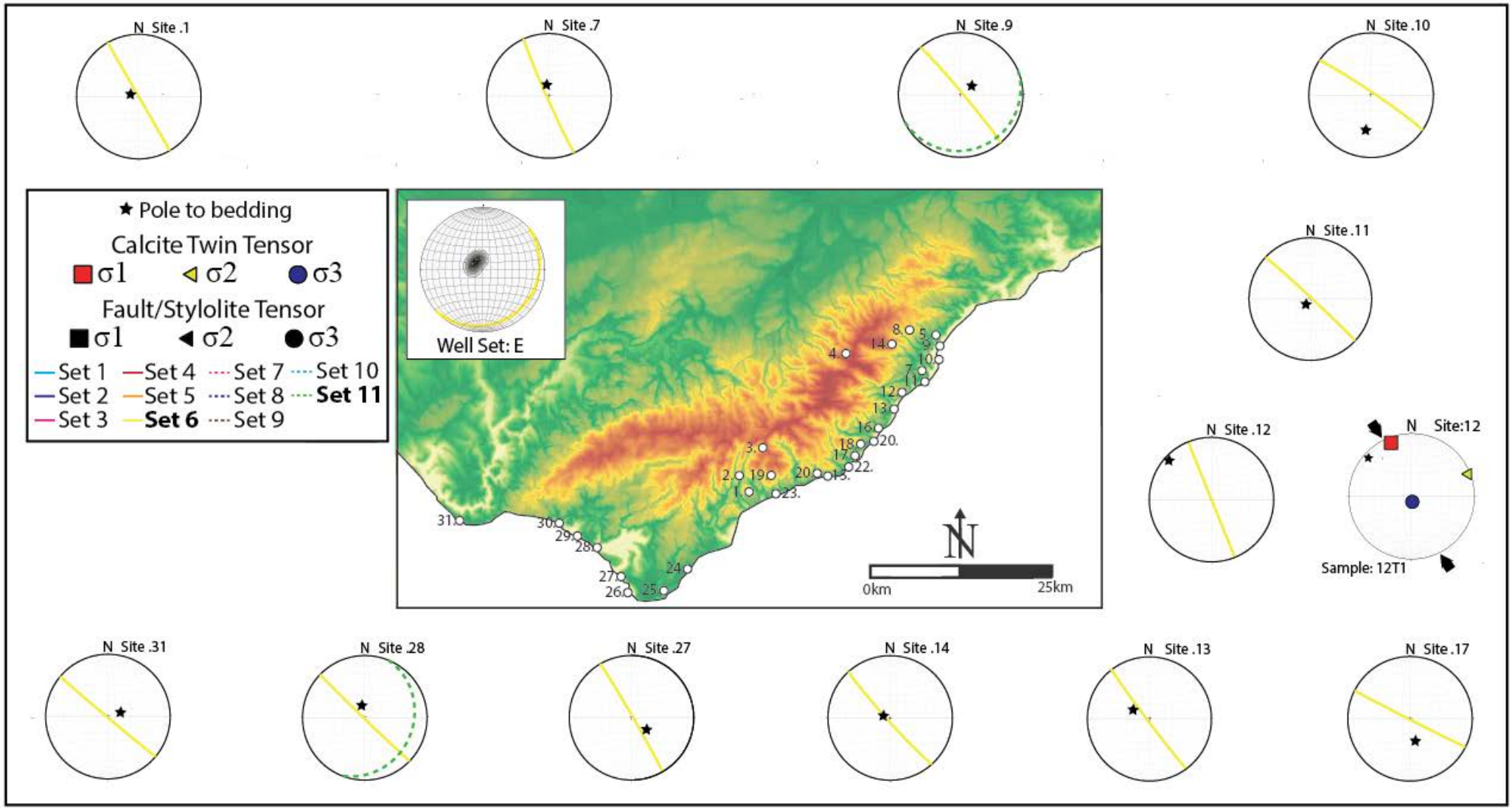
N Site .1
N Site .7
N Site .9
N Site .10
N Site .11
N Site .12
N Site:12
Sample: 12T1
N Site .31
N Site .28
N Site .27
N Site .14
N Site .13
N Site .17
★ Pole to bedding
Calcite Twin Tensor
σ1 σ2 σ3
Fault/Stylolite Tensor
σ1 σ2 σ3
Set 1 Set 4 Set 7 Set 10
Set 2 Set 5 Set 8 Set 11
Set 3 Set 6 Set 9
Well Set: E
0km
25km

Fig. 15: Fracture sets, micro faults and calcite twin tensors interpreted within basin phase 5. All data is presented under present day bedding on lower hemisphere equal area stereonet plots.

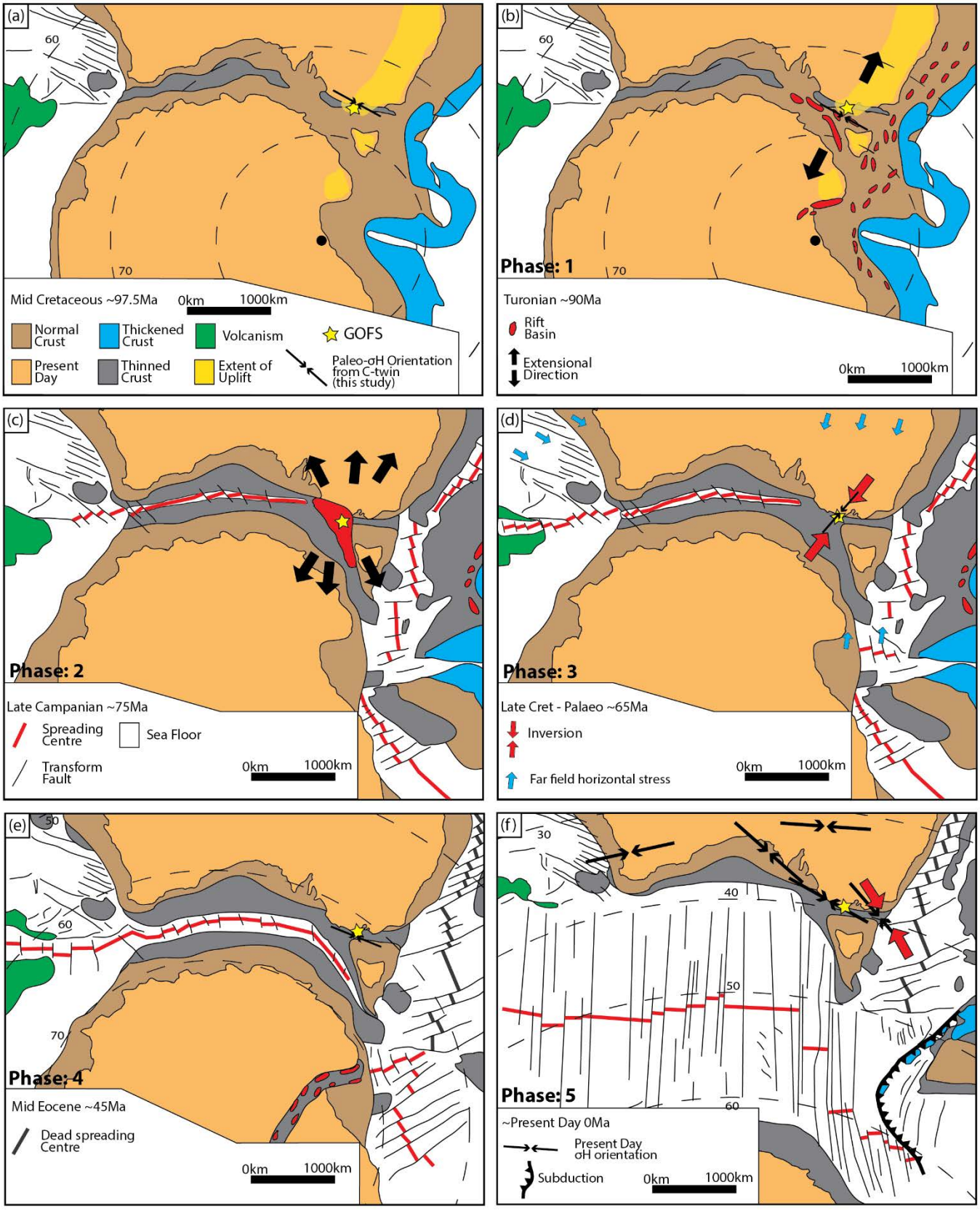
(a)
60
70
Mid Cretaceous ~97.5Ma
0km 1000km
Normal Crust
Thickened Crust
Volcanism
GOFS
Present Day
Thinned Crust
Extent of Uplift
Paleo-σH Orientation from C-twin (this study)
(b)
60
70
Phase: 1
Turonian ~90Ma
Rift Basin
Extensional Direction
0km 1000km
(c)
Phase: 2
Late Campanian ~75Ma
Spreading Centre
Sea Floor
Transform Fault
0km 1000km
(d)
Phase: 3
Late Cret - Palaeo ~65Ma
Inversion
Far field horizontal stress
0km 1000km
(e)
50
60
70
Phase: 4
Mid Eocene ~45Ma
Dead spreading Centre
0km 1000km
(f)
30
40
50
60
Phase: 5
~Present Day 0Ma
Present Day σH orientation
Subduction
0km 1000km

Fig. 16: (a) – (f) Progressive break up and stress evolution along Australia's southern margin, including approximate timing for the phases of stress outlined in this study. Note the complex interaction of ridge forces and plate boundary forces in panel (d), suggested to be responsible for the inversion of the GOFS in the Otway Basin. Figure modified after Norvick and Smith (2001).

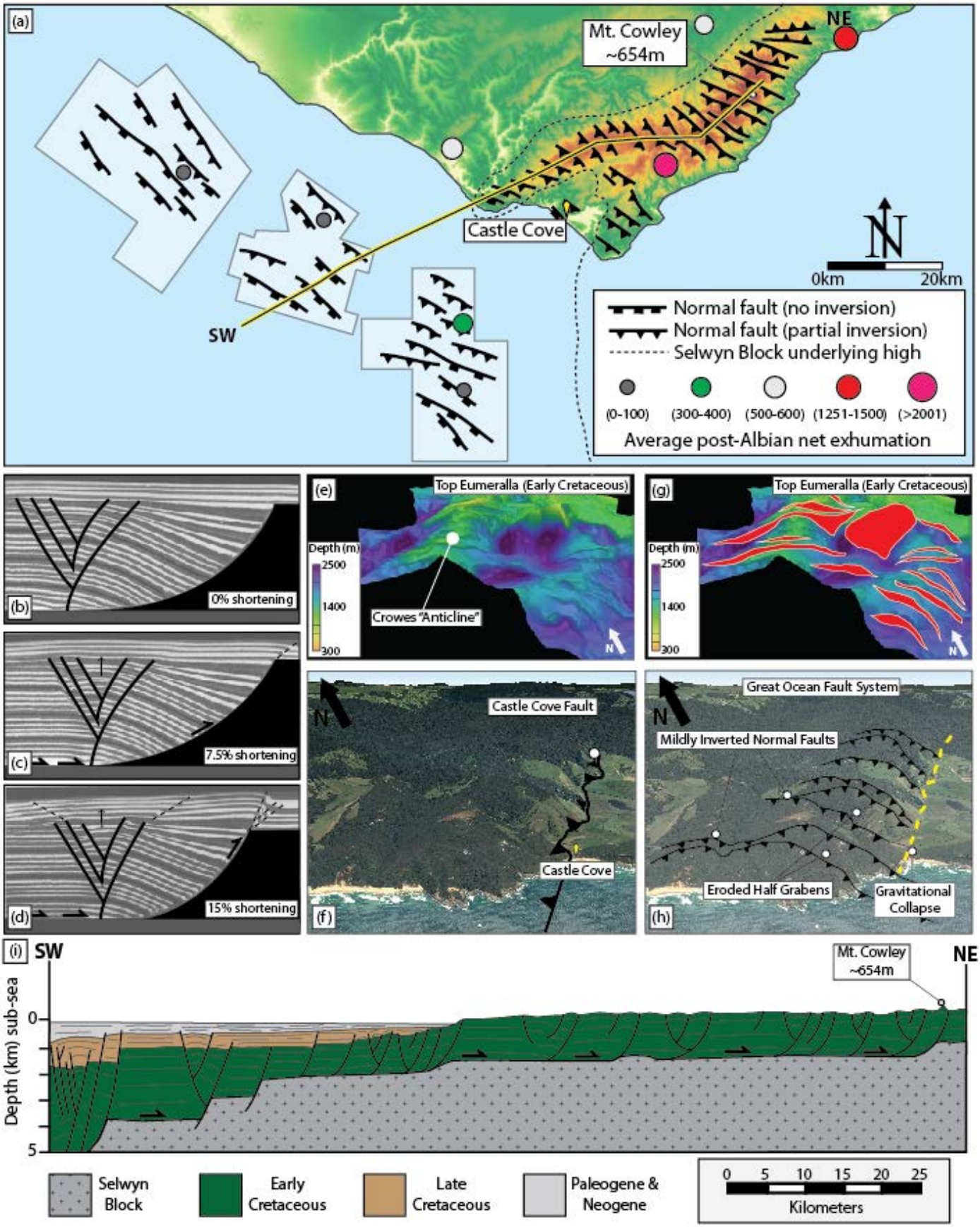
(a)
Mt. Cowley
~654m
NE
Castle Cove
SW
N
0km
20km
Normal fault (no inversion)
Normal fault (partial inversion)
Selwyn Block underlying high
(0-100)
(300-400)
(500-600)
(1251-1500)
(>2001)
Average post-Albian net exhumation
(b)
0% shortening
(c)
7.5% shortening
(d)
15% shortening
(e)
Top Eumeralla (Early Cretaceous)
Depth (m)
2500
1400
300
Crowes "Anticline"
(g)
Top Eumeralla (Early Cretaceous)
Depth (m)
2500
1400
300
N
Castle Cove Fault
Castle Cove
(f)
Great Ocean Fault System
Mildly Inverted Normal Faults
Eroded Half Grabens
Gravitational Collapse
(h)
(i) SW
NE
Mt. Cowley
~654m
Depth (km) sub-sea
0
5
Selwyn Block
Early Cretaceous
Late Cretaceous
Paleogene & Neogene
0 5 10 15 20 25
Kilometers

Fig. 17: (a) The new framework of the eastern Otway Basin and Otway Ranges, with onshore structure inferred from the multiscale results, exhumation magnitudes taken from Tassone et al.,(2014) increase towards the ~NE. (b) – (d) Sandbox modelling of inverted listric faults showing how inversion is accommodated through initial movement along the decollement surface. (e) and (f) the Top Early Cretaceous (Eumeralla) horizon from the Crowes Foot 3D with no faults mapped and annotated aerial photograph of the Otway Ranges near castle cove with the old framework and showing very similar ~NE-SW trending structures. (g) And (h) Top Early Cretaceous horizon with fault polygons mapped and this framework inferred onto the onshore structure, which fits well, the previous fault scarp attributed to gravitational collapse. (i) A new estimated cross section through the Point Ronald structure and the Otway Ranges showing a network of ~NE-SE striking listric style faults with the backstop located onshore near Mt Cowley, the highest point of the ranges.

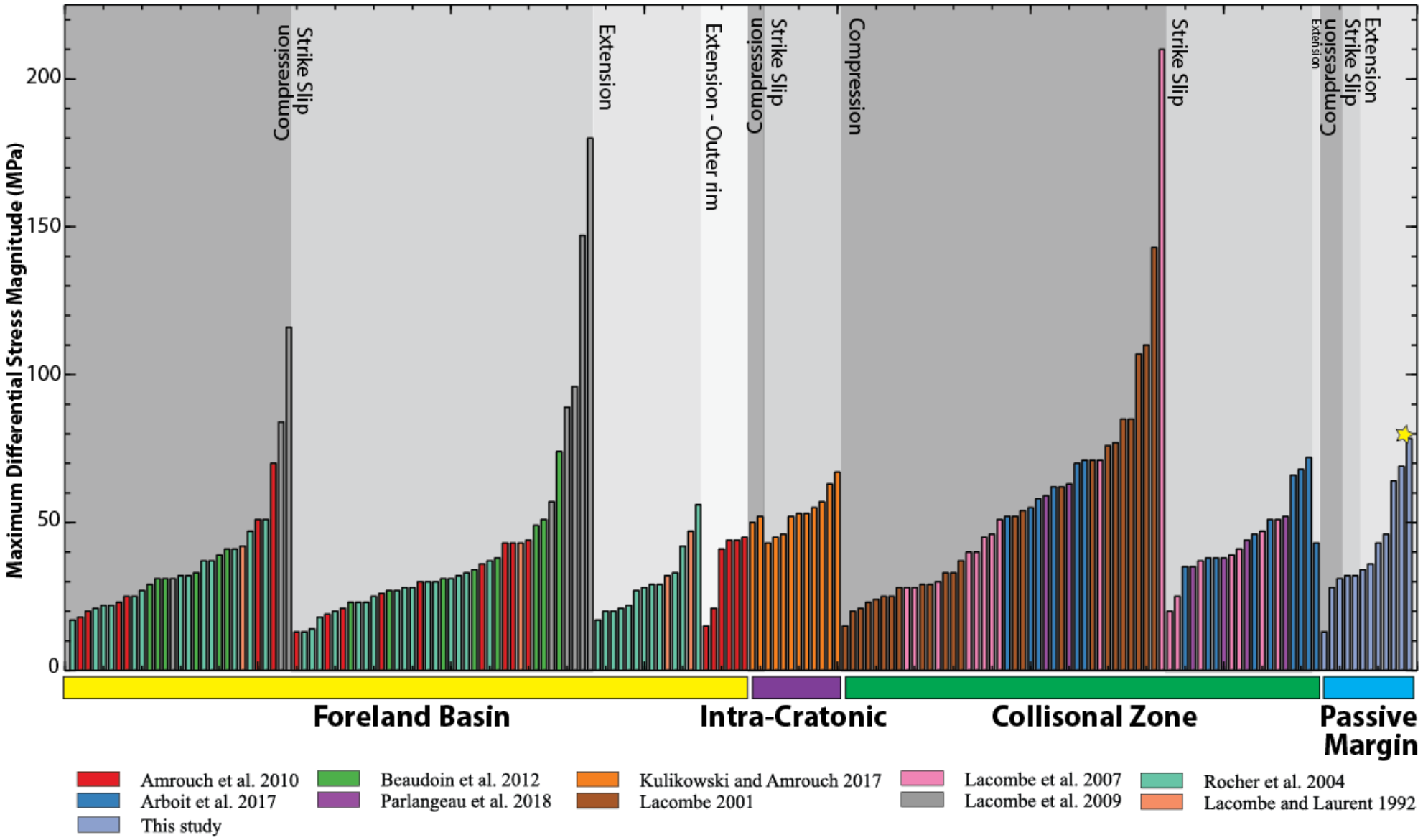
Maximum Differential Stress Magnitude (MPa)
0
50
100
150
200
Compression
Strike Slip
Extension
Extension - Outer rim
Compression
Strike Slip
Compression
Strike Slip
Extension
Compression
Extension
Strike Slip
Foreland Basin
Intra-Cratonic
Collisonal Zone
Passive Margin
Amrouch et al. 2010
Arboit et al. 2017
This study
Beaudoin et al. 2012
Parlangeau et al. 2018
Kulikowski and Amrouch 2017
Lacombe 2001
Lacombe et al. 2007
Lacombe et al. 2009
Rocher et al. 2004
Lacombe and Laurent 1992

Fig. 18: Over 170 paleostress tensors with approximately 20% error derived from the use of Etchecopar's CSIT within 11 studies, since 1992. Sorted by tectonic region and increasing magnitude from left to right within each stress regime. Note the high extensional stress magnitudes (star) computed as part of this study within a passive continental margin and that magnitudes of extensional stress exceed those of compressional and strike slip.

References

Allmendinger, R. W. (2013). Stereonet Help–the user's manual for Stereonet 8.

Amrouch, K. (2010). Contribution of microstructural analysis to the understanding of folding mechanisms: Examples of folded structures in the USA (Wyoming) and in Iran (Zagros)

Amrouch, K., Lacombe, O., Mouthereau, F., & Dissez, L. (2005, December). Quantification of orientations and magnitudes of the late Cenozoic paleostresses in the Zagros folded belt from calcite twin analysis. In Thrust Belts and Foreland Basins, International Meeting, Rueil-Malmaison (pp. 31-35).

Amrouch, K., Lacombe, O., Bellahsen, N., Daniel, J. M., & Callot, J. P. (2010). Stress and strain patterns, kinematics and deformation mechanisms in a basement-cored anticline: Sheep Mountain Anticline, Wyoming. Tectonics, 29(1).

Amrouch, K. (2010). Contribution of microstructural analysis to the understanding of folding mechanisms: Examples of folded structures in the USA (Wyoming) and in Iran (Zagros)

Anderson, E. M. (1951). The dynamics of faulting and dyke formation with applications to Britain. Hafner Pub. Co.

Amrouch, K., Beaudoin, N., Lacombe, O., Bellahsen, N., & Daniel, J. M. (2011). Paleostress magnitudes in folded sedimentary rocks. Geophysical Research Letters, 38(17).

Angelier, J. (1989). From orientation to magnitudes in paleostress determinations using fault slip data. Journal of structural geology, 11(1-2), 37-50.

Angelier, J. (1990). Inversion of field data in fault tectonics to obtain the regional stress—III. A new rapid direct inversion method by analytical means. Geophysical Journal International, 103(2), 363-376.

Arboit, F., Amrouch, K., Collins, A. S., King, R., & Morley, C. (2015). Determination of the tectonic evolution from fractures, faults, and calcite twins on the southwestern margin of the Indochina Block. Tectonics, 34(8), 1576-1599.

Arboit, F., Amrouch, K., Morley, C., Collins, A. S., & King, R. (2017). Palaeostress magnitudes in the Khao Khwang fold-thrust belt, new insights into the tectonic evolution of the Indosinian orogeny in central Thailand. Tectonophysics, 710, 266-276.

Beaudoin, N., & Lacombe, O. (2018). Recent and future trends in paleopiezometry in the diagenetic domain: Insights into the tectonic paleostress and burial depth history of fold-and-thrust belts and sedimentary basins. Journal of Structural Geology, 114, 357-365.

Beaudoin, N., Leprêtre, R., Bellahsen, N., Lacombe, O., Amrouch, K., Callot, J. P., ... & Daniel, J. M. (2012). Structural and microstructural evolution of the Rattlesnake Mountain Anticline (Wyoming, USA): new insights into the Sevier and Laramide orogenic stress build-up in the Bighorn Basin. Tectonophysics, 576, 20-45.

Beaudoin, N., Koehn, D., Lacombe, O., Lecouty, A., Billi, A., Aharonov, E., & Parlangeau, C. (2016). Fingerprinting stress: Stylolite and calcite twinning paleopiezometry revealing the complexity of progressive stress patterns during folding—The case of the Monte Nero anticline in the Apennines, Italy. Tectonics, 35(7), 1687-1712.

Beaudoin, N., Lacombe, O., Roberts, N. M., & Koehn, D. (2018). U-Pb dating of calcite veins reveals complex stress evolution and thrust sequence in the Bighorn Basin, Wyoming, USA. Geology, 46(11), 1015-1018.

Bellahsen, N., Fiore, P. E., & Pollard, D. D. (2006). From spatial variation of fracture patterns to fold kinematics: A geomechanical approach. Geophysical Research Letters, 33(2).

Bonini, M., Sani, F., & Antonielli, B. (2012). Basin inversion and contractional reactivation of inherited normal faults: A review based on previous and new experimental models. Tectonophysics, 522, 55-88.

Briguglio, D., Hall, M., & Keetley, J. (2015). Structural evolution of the Early Cretaceous depocentres, Otway Basin, Victoria. Australian Journal of Earth Sciences, 62(6), 717-733.

Buchanan, P. G., & McClay, K. R. (1991). Sandbox experiments of inverted listric and planar fault systems. Tectonophysics, 188(1-2), 97-115.

Burgin, H. B. and Amrouch, K. (2019b). 4D structural evolution of Australia's Great Ocean Road Region: The first quantification of paleostress magnitudes during continental break up. (In Prep).

Burgin, H. B., Amrouch, K., Rajabi, M., Kulikowski, D., & Holford, S. P. (2018). Determining paleo-structural environments through natural fracture and calcite twin analyses: a case study in the Otway Basin, Australia. The APPEA Journal, 58(1), 238-254.

Burkhard, M. (1993). Calcite twins, their geometry, appearance and significance as stress-strain markers and indicators of tectonic regime: a review. Journal of structural geology, 15(3-5), 351-368.

Cayley, R. A., Taylor, D. H., VandenBerg, A. H. M., & Moore, D. H. (2002). Proterozoic–Early Palaeozoic rocks and the Tyennan Orogeny in central Victoria: the Selwyn Block and its tectonic implications. Australian Journal of Earth Sciences, 49(2), 225-254.

Cooper, G. T., & Hill, K. C. (1997). Cross-section balancing and thermochronological analysis of the Mesozoic development of the eastern Otway Basin. The APPEA Journal, 37(1), 390-414.

Cifelli, F., Mattei, M., Chadima, M., Hirt, A. M., & Hansen, A. (2005). The origin of tectonic lineation in extensional basins: combined neutron texture and magnetic analyses on "undeformed" clays. Earth and Planetary Science Letters, 235(1-2), 62-78.

Debenham, N., King, R. C., & Holford, S. P. (2018). The influence of a reverse-reactivated normal fault on natural fracture geometries and relative chronologies at Castle Cove, Otway Basin. Journal of Structural Geology, 112, 112-130.

Dickinson, J. A., Wallace, M. W., Holdgate, G. R., Gallagher, S. J., & Thomas, L. (2002). Origin and timing of the Miocene-Pliocene unconformity in southeast Australia. Journal of Sedimentary Research, 72(2), 288-303.

Duddy, I. R., & Erout, B. (2001). AFTA-calibrated 2-D Modelling of Hydrocarbon Generation and Migration Using Temispack: Preliminary Results from the Otway Basin. Eastern Australasian Basins Symposium(485-497).

Ebner, M., Koehn, D., Toussaint, R., Renard, F., & Schmittbuhl, J. (2009). Stress sensitivity of stylolite morphology. Earth and Planetary Science Letters, 277(3-4), 394-398.

Edwards, J., & Edwards, J. (1996). Colac 1: 250 000 map geological report. Geological Survey of Victoria.

Engelder, T. (1987). Joints and shear fractures in rock. Fracture mechanics of rock, 27-69.

Etchecopar, A. (1984). Etude des états de contrainte en tectonique cassante et simulations de déformations plastiques: approche mathématique (Doctoral dissertation).

Etheridge, M. A., Branson, J. C., & Stuart-Smith, P. G. (1985). Extensional basin—forming structures in Bass Strait and their importance for hydrocarbon exploration. The APPEA Journal, 25(1), 344-361.

Etheridge, M. A. (1986). On the reactivation of extensional fault systems. Philosophical Transactions of the Royal Society of London. Series A, Mathematical and Physical Sciences, 317(1539), 179-194.

Etheridge, M. A., Branson, J. C., & Stuart-Smith, P. G. (1987). The Bass, Gippsland and Otway basins, southeast Australia: a branched rift system formed by continental extension.

Ferrill, D. A., Morris, A. P., Evans, M. A., Burkhard, M., Groshong Jr, R. H., & Onasch, C. M. (2004). Calcite twin morphology: a low-temperature deformation geothermometer. Journal of structural Geology, 26(8), 1521-1529.

Geary, G. C. and Reid, I. S. A. (1998) Geology and prospectivity of the offshore eastern Otway Basin, Victoria. Victorian Initiative for Minerals and Petroleum Report, 55

Hill, K. A., Cooper, G. T., Richardson, M. J., & Lavin, C. J. (1994). Structural framework of the eastern Otway Basin: inversion and interaction between two major structural provinces. Exploration Geophysics, 25(2), 79-87.

Hill, K. C., Hill, K. A., Cooper, G. T., O'Sullivan, A. J., O'Sullivan, P. B., & Richardson, M. J. (1995). Inversion around the Bass basin, SE Australia. Geological Society, London, Special Publications, 88(1), 525-547.

Holford, S., Hillis, R., Duddy, I., Green, P., Stoker, M., Tuitt, A., ... & MacDonald, J. (2011). Cenozoic post-breakup compressional deformation and exhumation of the southern Australian margin. The APPEA Journal, 51(1), 613-638.

Holford, S. P., Tuitt, A. K., Hillis, R. R., Green, P. F., Stoker, M. S., Duddy, I. R., Tassone, D. R. (2014). Cenozoic deformation in the Otway Basin, southern Australian margin: implications for the origin and nature of post-breakup compression at rifted margins. Basin Research, 26(1), 10-37. doi: 10.1111/bre.12035

Jamison, W. R., & Spang, J. H. (1976). Use of calcite twin lamellae to infer differential stress. Geological Society of America Bulletin, 87(6), 868-872.

King, R., Holford, S., Hillis, R., Tuitt, A., Swierczek, E., Backé, G., ... & Tingay, M. (2012). Reassessing the in-situ stress regimes of Australia's petroleum basins. The APPEA Journal, 52(1), 415-426.

Kohn, B. P., Gleadow, A. J. W., Brown, R. W., Gallagher, K., O'sullivan, P. B., & Foster, D. A. (2002). Shaping the Australian crust over the last 300 million years: insights from fission track thermotectonic imaging and denudation studies of key terranes. Australian Journal of Earth Sciences, 49(4), 697-717.

Koopman, A., Speksnijder, A., & Horsfield, W. T. (1987). Sandbox model studies of inversion tectonics. Tectonophysics, 137(1-4), 379-388.

Krassay, A. A., Cathro, D. L., & Ryan, D. J. (2004). A regional tectonostratigraphic framework for the Otway Basin.

Krassay, A et al., (2009). Otway Basin Hot Sedimentary Aquifers & SEEBASE Project, Confidential Report to PIRSA-GA-DPI Vic.

Kulikowski, D., & Amrouch, K. (2017). Combining geophysical data and calcite twin stress inversion to refine the tectonic history of subsurface and offshore provinces: A case study on the Cooper-Eromanga Basin, Australia. Tectonics, 36(3), 515-541.

Lacombe, O. (2001). Paleostress magnitudes associated with development of mountain belts: Insights from tectonic analyses of calcite twins in the Taiwan Foothills. Tectonics, 20(6), 834-849.

Lacombe, O. (2012). Do fault slip data inversions actually yield “paleostresses” that can be compared with contemporary stresses? A critical discussion. Comptes Rendus Geoscience, 344(3-4), 159-173.

Lacombe, O., & Laurent, P. (1992). Determination of principal stress magnitudes using calcite twins and rock mechanics data. Tectonophysics, 202(1), 83-93.

Lacombe, O., & Laurent, P. (1996). Determination of deviatoric stress tensors based on inversion of calcite twin data from experimentally deformed monophase samples: preliminary results. Tectonophysics, 255(3-4), 189-202.

Lacombe, O., Angelier, J., Laurent, P., Bergerat, F., & Tourneret, C. (1990). Joint analyses of calcite twins and fault slips as a key for deciphering polyphase tectonics: Burgundy as a case study. Tectonophysics, 182(3-4), 279-300.

Lacombe, O., Laurent, P., Angelier, J., & Roure, F. (1994). Calcite twins as a key to paleostresses in sedimentary basins: Preliminary results from drill cores of the Paris basin. Peri-Tethyan Platforms, 197-210.

Lacombe, O., Amrouch, K., Mouthereau, F., & Dissez, L. (2007). Calcite twinning constraints on late Neogene stress patterns and deformation mechanisms in the active Zagros collision belt. Geology, 35(3), 263-266.

Lacombe, O., Malandain, J., Vilasi, N., Amrouch, K., & Roure, F. (2009). From paleostresses to paleoburial in fold–thrust belts: Preliminary results from calcite twin analysis in the Outer Albanides. Tectonophysics, 475(1), 128-141.

Lacombe, O., Mouthereau, F., Kargar, S., & Meyer, B. (2006). Late Cenozoic and modern stress fields in the western Fars (Iran): implications for the tectonic and kinematic evolution of central Zagros. Tectonics, 25(1).

Laurent, P. (1984). Les macles de la calcite en tectonique: nouvelles méthodes dynamiques et premières applications(Doctoral dissertation).

Leech, M. L., Singh, S., Jain, A. K., Klemperer, S. L., & Manickavasagam, R. M. (2005). The onset of India–Asia continental collision: early, steep subduction required by the timing of UHP metamorphism in the western Himalaya. Earth and Planetary Science Letters, 234(1-2), 83-97.

Lister, G. S., Etheridge, M. A., & Symonds, P. A. (1986). Detachment faulting and the evolution of passive continental margins. Geology, 14(3), 246-250.

Lyon, P. J., Boult, P. J., Hillis, R. R., & Bierbrauer, K. (2007). Basement controls on fault development in the Penola Trough, Otway Basin, and implications for fault-bounded hydrocarbon traps. Australian Journal of Earth Sciences, 54(5), 675-689.

Medwell, G. J. (1971) Structures of the Otway Ranges. Geological Survery of Victoria. Special Bulletin. 339-359.

Müller, R. D., Gaina, C., & Clark, S. (2000). Seafloor spreading around Australia. Billion-year earth history of Australia and neighbours in Gondwanaland, 18-28.

Norvick, M. S., & Smith, M. A. (2001). Mapping the plate tectonic reconstruction of southern and southeastern Australia and implications for petroleum systems. The APPEA Journal, 41(1), 15-35.

O'Brien, G., Boreham, C., Thomas, H., & Tingate, P. (2009). Understanding the critical success factors determining prospectivity—Otway Basin, Victoria. The APPEA Journal, 49(1), 129-170.

Parlangeau, C., Lacombe, O., Schueller, S., & Daniel, J. M. (2018). Inversion of calcite twin data for paleostress orientations and magnitudes: A new technique tested and calibrated on numerically-generated and natural data. Tectonophysics, 722, 462-485.

Parlangeau, C., Dimanov, A., Lacombe, O., Hallais, S., & Daniel, J. M. (2019). Uniaxial compression of calcite single crystals at room temperature: insights into twinning activation and development. Solid Earth, 10(1), 307-316.

Perincek, D., Simons, B., & Pettifer, G. R. (1994). THE TECTONIC FRAMEWORK AND ASSOCIATED PLAY TYPES OF THE WESTERN OTWAY BASIN, VICTORIA, AUSTRALIA. The APPEA Journal, 34(1), 460-478.

Pollard, D. D., & Aydin, A. (1988). Progress in understanding jointing over the past century. Geological Society of America Bulletin, 100(8), 1181-1204.

Rez, J., & Melichar, R. (2010). Peek inside the black box of calcite twinning paleostress analysis. Trabajos de Geologia, 30(30).

Robion, P., Grelaud, S., & de Lamotte, D. F. (2007). Pre-folding magnetic fabrics in fold-and-thrust belts: Why the apparent internal deformation of the sedimentary rocks from the Minervois basin (NE—Pyrenees, France) is so high compared to the Potwar basin (SW—Himalaya, Pakistan). *Sedimentary Geology*, 196(1-4), 181-200.

Robson, A. G., Holford, S. P., & King, R. C. (2017). Structural evolution of a normal fault array in the Gambier Embayment, offshore Otway Basin, South Australia: insights from 3D seismic data. Australian Journal of Earth Sciences, 64(5), 611-624.

Robson, A. G., Holford, S. P., & King, R. C. (2017). Structural evolution of a normal fault array in the Gambier Embayment, offshore Otway Basin, South Australia: insights from 3D seismic data. Australian Journal of Earth Sciences, 64(5), 611-624.

Robson, A. G., S. P. Holford, R. C. King, and D. Kulikowski (2018). Structural evolution of horst and half-graben structures proximal to a transtensional fault system determined using

3D seismic data from the Shipwreck Trough, offshore Otway Basin, Australia, Marine and Petroleum Geology, 89(3), 615-634, doi:10.1016/j.marpetgeo.2017.10.028.

Rocher, M., Lacombe, O., Angelier, J., & Chen, H. W. (1996). Mechanical twin sets in calcite as markers of recent collisional events in a fold-and-thrust belt: Evidence from the reefal limestones of southwestern Taiwan. Tectonics, 15(5), 984-996.

Rocher, M., Cushing, M., Lemeille, F., Lozac'h, Y., & Angelier, J. (2004). Intraplate paleostresses reconstructed with calcite twinning and faulting: improved method and application to the eastern Paris Basin (Lorraine, France). Tectonophysics, 387(1-4), 1-21.

Rowe, K. J., & Rutter, E. H. (1990). Palaeostress estimation using calcite twinning: experimental calibration and application to nature. Journal of Structural Geology, 12(1), 1-17.

Sandiford, M. I. K. E. (2003). Neotectonics of southeastern Australia: linking the Quaternary faulting record with seismicity and in situ stress. SPECIAL PAPERS-GEOLOGICAL SOCIETY OF AMERICA, 107-120.

Sandiford, M., Coblentz, D. D., & Richardson, R. M. (1995). Ridge torques and continental collision in the Indian-Australian plate. Geology, 23(7), 653-656.

Sandiford, M., Wallace, M., & Coblentz, D. (2004). Origin of the in situ stress field in south-eastern Australia. Basin Research, 16(3), 325-338.

Schneider, C. L., Hill, K. C., & Hoffman, N. (2004). Compressional growth of the Minerva Anticline, Otway Basin, Southeast Australia—evidence of oblique rifting. The APPEA Journal, 44(1), 463-480.

Tassone, D. R., Holford, S. P., Duddy, I. R., Green, P. F., & Hillis, R. R. (2014). Quantifying Cretaceous–Cenozoic exhumation in the Otway Basin, southeastern Australia, using sonic transit time data: Implications for conventional and unconventional hydrocarbon prospectivity. AAPG Bulletin, 98(1), 67-117.

Tassone, D. R., Holford, S. P., King, R., Tingay, M. R., & Hillis, R. R. (2017). Contemporary stress and neotectonics in the Otway Basin, southeastern Australia. Geological Society, London, Special Publications, 458, SP458-10.

Tourneret, C., & Laurent, P. (1990). Paleo-stress orientations from calcite twins in the North Pyrenean foreland, determined by the Etchecopar inverse method. Tectonophysics, 180(2-4), 287-302.

Trupp, M. A., Spence, K. W., & Gidding, M. J. (1994). Hydrocarbon prospectivity of the Torquay Sub-basin, offshore Victoria. The APPEA Journal, 34(1), 479-494.

Turner, F. J., Griggs, D. T., & Heard, H. (1954). Experimental deformation of calcite crystals. Geological Society of America Bulletin, 65(9), 883-934.

Van Hoorn, B. (1987). Structural evolution, timing and tectonic style of the Sole Pit inversion. Tectonophysics, 137(1-4), 239-284.

Veevers, J. J. (2000). Change of tectono-stratigraphic regime in the Australian plate during the 99 Ma (mid-Cretaceous) and 43 Ma (mid-Eocene) swerves of the Pacific. Geology, 28(1), 47-50.

VandenBerg, A. H. M. (2000). The Tasman Fold Belt system in Victoria: geology and mineralisation of Proterozoic to Carboniferous rocks. Geological Survey of Victoria.

Willcox, J. B., & Stagg, H. M. J. (1990). Australia's southern margin: a product of oblique extension. Tectonophysics, 173(1-4), 269-281.

Yamaji, A. (2015). How tightly does calcite e-twin constrain stress?. Journal of Structural Geology, 72, 83-95.

Yamaji, A. (2015). Generalized Hough transform for the stress inversion of calcite twin data. Journal of Structural Geology, 80, 2-15.

Zhu, D. C., Wang, Q., Zhao, Z. D., Chung, S. L., Cawood, P. A., Niu, Y., & Mo, X. X. (2015). Magmatic record of India-Asia collision. Scientific Reports, 5, 14289.

Ziegler, P. A. (1982). Geological atlas of western and central Europe: The Hague, Shell Internat. Petroleum Maatschappij BV, 130p.

362

363

364

Chapter 4.4: Manuscript 5

Layer Parallel Stretching? Characterising magnetic and pore fabric styles at a rifted continental margin: New insights from the Otway Ranges, Australia

This finalised manuscript will be submitted to the peer reviewed journal *Geophysical Journal International*

Statement of Authorship

Title of Paper: Layer Parallel Stretching? Characterising magnetic and pore fabric styles at a rifted continental margin: New insights from the Otway Ranges, Australia

Publication Status: Unpublished and Unsubmitted work written in a manuscript style

Publication Details: Burgin, H. B., Robion, P. and Amrouch, K. (2019). Layer Parallel Stretching? Characterising magnetic and pore fabric styles at a rifted continental margin: New insights from the Otway Ranges, Australia (In prep)

Principal Author: Hugo Bonython Burgin

Contribution: Field sampling. Petrophysical measurements and analysis. Paper writing (55%)

Certification: This paper reports on original research I conducted during the period of my Higher Degree by Research candidature and is not subject to any obligations or contractual agreements with a third party that would constrain its inclusion in this thesis. I am the primary author of this paper.

Signed: **Date:** 05/03/2019

Co-Author Contributions

By signing the Statement of Authorship, each author certifies that:

- **i.** The candidate's stated contribution to the publication is accurate (as detailed above);
- **ii.** Permission is granted for the candidate in include the publication in the thesis; and
- **iii.** The sum of all co-author contributions is equal to 100% less the candidate's stated contribution.

Name of Co-Author: Dr Khalid Amrouch

Contribution to Paper: Guidance with analysis and sampling method (15%)

Signed: **Date:** 05/03/2019

Name of Co-Author: Dr Philippe Robion

Contribution to Paper: Guidance with AMS and APWV analysis and interpretation. Assistance with writing paper (30%)

Signed: **Date:** 13/03/2019

Layer Parallel Stretching? Characterising magnetic and pore fabric styles at a rifted continental margin: New insights from the Otway Ranges, Australia

*Hugo B. **BURGIN**[a] (hugo.burgin@adelaide.edu.au)

Philippe **ROBION**[b] (philippe.robion@u-cergy.fr)

Khalid **AMROUCH**[a] (khalid.amrouch@adelaide.edu.au)

[a]Australian School of Petroleum, University of Adelaide, North Tce, 5005, Adelaide, Australia

[b] Geosciences et Environment University of Cergy-Pontoise, 33 Boulevard du Port, 95000 Cergy-Pontoise, France

*Corresponding Author: Hugo B. Burgin (08 8313 8000)

Abstract

This study presents the first analysis of the anisotropy of magnetic susceptibility and anisotropy of P-wave velocity at a passive continental margin. In the Otway Ranges, Australia, Early Cretaceous sediments deposited during a period of tectonic quiescence, display triaxial magnetic fabrics typical of extensional deformation, which are supported by the orientation of the pore fabric. The inferred extensional azimuths, show good agreement with axes for renewed Late Cretaceous rifting and continental break up. A period of structural evolution in the Otway Basin which was characterised by abnormally high levels of paleostress. We suggest the influence of layer parallel stretching (LPSt), which represents the first phase of extensional deformation during periods of intense tectonic extension. These fabrics have been preserved during NE-SW oriented basin inversion, which involved the reactivation of the local detachment surface, the partitioning of strain, and resultantly low levels of coupling between the basement and the cover. The results from this study highlight the applicability of these methods for characterising rock anisotropy at passive continental margins and have distinct outcomes with respect to the structural framework of the study area.

1. Introduction

In models of structural evolution for sedimentary basins, the inclusion of multiscale datasets is often advantageous. The benefit being that analyses on the micro and mesoscale, typically offer insights into different or subtle patterns of deformation, reducing structural uncertainty and assisting in characterising the evolution of folded or faulted strata on the macroscale (Frizon de Lamotte et al., 1997; 2002; Sans et al., 2002; Louis et al., 2006; Robion et al., 2007; Robion et al., 2014; Robert et al., 2018). The anisotropic behaviour of sedimentary rocks with respect to specific individual properties (permeability, elasticity, magnetic susceptibility, electrical conductivity) is of great importance with respect to inferring the microstructural characteristics of potential reservoir units, and for understanding weak levels of deformation (Louis et al., 2003).

This study focuses on the characterization and description of two of these properties by means of two techniques of microstructural analysis, proven to constrain them. Firstly, the anisotropy of magnetic susceptibility (AMS) which has been successfully used to define magnetic fabrics, associated with varying degrees of deformation (Borradaile, 1989, Tarling and Hrouda, 1993, Borradaile and Henry, 1997). Secondly, the anisotropy of p-wave velocity (APWV) which is sensitive to porosity shape and/or microcracks within the rock. Assisting in providing direct insights into the presence of microstructural features within the rock (Louis et al., 2003; 2004; Robion et al., 2014, David et al., 2017).

The measurement of the anisotropy of low field magnetic susceptibility within sedimentary rocks has been commonly used to define petrofabrics and weak deformation (e.g. Graham, 1966, Kissel et al., 1986; Hrouda, 1991; Averbuch et al., 1992; Borradaile and Henry, 1997). The method is typically applied within fold and thrust belts to

demonstrate even the slight effect of layer parallel shortening (LPS), in rocks that have been weakly strained (e.g. Robion et al., 2007; Robion et al., 2014, Amrouch et al., 2010b; Robert et al., 2018). AMS has also been used abundantly in back-arc (Cifelli et al., 2004; 2005) and thrust-top extensional settings (Cifelli et al., 2009), where un-deformed sediments at the outcrop scale, carry magnetic fabrics reflective of the regional extensional pattern. This study represents the first time it will be used to characterise grain scale strain at a passive continental margin.

The beauty of combining AMS with APWV is that both techniques can be described by the use of a second rank tensor (Louis et al., 2004), which is easily visualised on a lower hemisphere stereonet. This can then be compared to other styles of structural data, such as fractures, faults, calcite twins and compaction bands (Robion et al., 2007; Amrouch et al., 2010; Robert et al., 2018). With this in mind, the results of this study are compared with paleostress patterns previously constructed by Burgin and Amrouch (2019b), from a multiscale analysis in the same study area. With the goal of deciphering the relative contribution of environments of stress towards its strain footprint, during the regions evolution.

The sedimentary basins of Australia's south eastern margin, such as the Otway Basin (**fig. 1**) provide a unique opportunity for a multiscale approach to structural analyses. Uplifted and outcropping rift sections deposited during the stages of continental separation – such as Otway Ranges – allow for considerable amounts of micro metre and centimetre-to-metre scale data (e.g. calcite twin, pore fabric and natural fracture analyses) to be combined with geophysical, well and seismic datasets from the petroleum industry. Recently, new insights from this style of investigation by Burgin and Amrouch (2019b)

and Burgin et al., (2018; 2019) has suggested that the structural framework of the Otway Ranges requires re-examining. Microscale calcite twin data and mesoscale fracture evidence from the study area suggesting co-axial ~NE-SW oriented extension and inversion occurred onshore within the ranges during the Late Cretaceous. These results are in contrast with most other works, which favour a ~NE-SW trending structural fabric, including faults such as the Castle Cove and Johanna Faults (e.g. Debenham et al., 2018) (**fig. 2**).

This paper aims to contribute to this debate, attempting to unravel the petrophysical heritage of the Otway Ranges (**fig. 2**) and attempting to characterise the chronological sequence of deformation across multiple scales. Simultaneously demonstrating the applicability of AMS and APWV to characterising weak deformation in these tectonic settings.

The Otway Ranges are a broadly ~NE-SW trending outcrop comprised predominantly of the Early Cretaceous Eumeralla Formation, the major Early Cretaceous unit within the basin, in addition to the source rock for ~99% of hydrocarbons discovered within the basin to date (O'Brien et al., 2009). The techniques used in this study are especially useful in the region, as macroscopic structural evidence is not visible or easily interpreted due to dense vegetation that covers much of the Otway Ranges.

2. Geological Setting

2.1 The Otway Basin

The Otway Basin forms part of Australia's southern rift system (**fig.1**) and is located along the south eastern margin of the Australian continent (**fig. 1**). The basin covers

approximately 150,000km^2 across on and off-shore provinces, and trends largely ~NW-SE, having been formed due to Late Jurassic to Early Paleogene rifting within Gondwana (Norvick and Smith, 2001; Krassay et al., 2004).

Historically the framework of the Otway Basin was divided into western, central and eastern portions (Miller et al., 2002; Tassone et al., 2017), with the western and central sections consisting of mainly ~NW-SE striking fault networks (Lyon et al., 2007; Burgin et al., 2018). A fault network that has been attributed to a large scale, broadly ~N-S extensional system. In contrast, the eastern basin was thought to be dominated by NNE-SSW striking sinistral and normal faults, where reverse reactivation and inversion during the Miocene – recent, resulted in the formation of the Otway Ranges (Duddy et al., 1994; Edwards et al., 1996; Debenham et al., 2018; 2019).

This idea has recently been challenged by Burgin and Amrouch (2019b), who completed a multiscale analysis of the region including 3D seismic analysis of fault and fold systems offshore, directly south west from the ranges (**fig. 2**). The results of the study indicating that while ~N-S striking faults are present within sections of the Shipwreck Trough (Robson et al., 2018), the dominant strike of faults across the Prawn Platform and much of the eastern Otway Basin is ~NW-SE, a continuation of the western and central trend. This analysis has two major consequences for the region: 1) In the absence of ~NE-SW striking faults, previous models of formation for the Otway Ranges and surrounding inversion structures (e.g. Pecten Anticline, Loch Ard Anticline and Crowes Anticline) requiring the inversion of faults in this orientation (Edwards et al., 1996; Holford et al., 2014; Debenham et al., 2018; Debenham et al., 2019) seems improbable. 2) Rather than

Miocene – recent ~NW-SE inversion and major uplift of the system, Late Cretaceous (~Mid-Maastrichtian) – Early Paleogene ~NE-SW inversion is more likely.

Complimentary evidence for this theory includes similar structures and timing in the Bight Basin (Macdonald et al., 2012) and a peak in regional denudations rates throughout much of south eastern Australia (Kohn et al., 2002) (**fig. 3**). Additionally, thermal history data from Duddy et al. (2003) and Duddy and Erout (2001) suggest a major cooling episode beginning in the Late Cretaceous within the offshore Otway Basin. The fact that source rocks within the basin are currently at their maximum burial temperature (Duddy and Erout, 2001) is also supportive of pre-Neotectonic structuring.

Azimuths for basin forming extension within the Otway Basin were likely broadly oriented ~N-S (Lyon et al., 2007; Burgin and Amrouch, 2019a) although other studies have suggested more oblique orientations and intermediate directions towards the ~NE (Etheridge et al., 1985; Hill et al., 1994). Subsidence during a period of structural quiescence and minimal fault growth, during the Aptian and Albian led to the deposition of the Eumerella Formation (**fig. 3**) (Krassay et al., 2004). A basin phase that was followed by a period of stress reorganisation in the Mid Cretaceous, and uplift across most of eastern Australia (Norvick and Smith, 2001). However, the effects of this event on the structural architecture of the Otway Basin are now considered minor (Burgin and Amrouch, 2019a; 2019b).

Renewed rifting during the early Late Cretaceous (~Cenomanian) was responsible for the deposition of the Sherbrook group sediments (Geary and Reid, 1988) (**fig. 3**) and resulted in the development of broadly ~NW-SE striking normal fault networks. The azimuth of

extension during this period is also debated as either ~NE-SW (Perincek et al., 1994a) or N-S (Miller et al., 2002) within the Otway Ranges region. Given the dominance of ~NW-SE striking fabrics within the offshore basin, the former seems the most likely (Lyon et al., 2007; Burgin and Amrouch, 2019a).

The Late Maastrichtian saw a period of rapid basin inversion, through the reverse reactivation of ~NW-SE striking normal faults and the likely uplift of the Otway Ranges described above. After which the shallow marine Nirranda and Wanggerrip Groups were deposited during the late Eocene (Krassay et al., 2004).

2.2 The Otway Ranges

The Otway Ranges (**fig. 2**) represent the most significant onshore evidence for inversion in the Otway Basin. Initial structural mapping of the ranges was completed almost 50 years ago by Medwell, (1971) who defined a large ~NE-SW trending anticline. A model which has been favoured by almost all following works (e.g. Duddy et al., 1993; Hill et al., 1994; Edwards et al., 1996; Moore et al., 2002; Krassay et al., 2004; Holford et al., 2011; King et al., 2012; Holford et al., 2014; Tassone et al., 2017; Debenham et al., 2018; 2019) advocating for mainly neotectonic formation of the structure.

This framework and timing has since been challenged by Burgin and Amrouch (2019b), where the ranges are designated as part of the Great Ocean Fault System. Having been uplifted due to stress reorganisation of the Australian plate during the Latest Cretaceous, resulting in the ~NE-SW oriented inversion of major ~NW-SE striking listric detachment faults. During this period, a large portion of contraction was accommodated through reverse movement and stress release along the Top Selwyn block decollement zone (**fig.**

198 **2**). While micro and mesoscale evidence for this theory is considerable, high resolution,
199 detailed structural mapping across much of the ranges is impossible, due to the dense
200 vegetation and steeply dipping cliffs that dominate the coastline.
201
202 Onshore, the ranges extend for approximately 90km from the ~NE to the SW, with similar
203 architecture visible for ~50km towards to NW. The extent of the Otway Ranges coincides
204 with the shallowest underlying extent of the Selwyn Block throughout the region (Cayley
205 et al., 2002) which was likely a primary contributing factor to isolated nature of the ranges
206 (Burgin and Amrouch, 2019b).
207
208 **3. 0 Methodology**
209 **3.1 Overview**
210 To achieve the goal of investigating the degree and nature of microstructural deformation
211 within the Otway Ranges, (**fig. 4**) two well-proven techniques of petrofrabric analysis–
212 AMS and APWV (Louis et al., 2003, 2004, 2008) were carried out.
213
214 **3.2 Sampling**
215 253 specimens were measured across 16 sample sites within the Otway Ranges
216 concentrated along the coast line, 4 samples within the Nirranda Formation and 12 within
217 the Eumerella Formation (**fig. 3**).
218
219 As it forms the majority of the Otway Ranges, sampling was concentrated within the
220 Early Cretaceous Aptian – Albian, Eumeralla Formation. A large sequence of sediments
221 made up of chloritic, micaceous, carbonaceous claystone and volcaniclastic and
222 feldspathic sandstones (Krassay et al., 2004). In some regions of the southwest coast of

the Otway Ranges, NE-SW trending depocentres - attributed to the reverse reactivation of ~NE-SW striking faults by some studies (Debenham et al., 2018)- have been in-filled with the Eocene Nirranda Group. The unit is a siliclastic-dominated low-stand to transgressive systems tract unit (Edwards et al., 1996), and contains minor sub-groups of sediments (**fig. 3**). However these are poorly differentiated throughout the Otway Ranges. As such we consider our sampling to be generally within the Nirranda Group succession, our samples representative of a well-sorted, moderately compacted clean sandstone.

3.3 Analysing petrofabrics in sedimentary rocks

Anisotropy of rock physical properties is dependent upon matrix properties along with void-space distributions and micro-scale deformation (Lo et al., 1986). Together these rock characteristics have been shown to be responsible for inducing anisotropic behaviour with respect to elasticity, magnetic susceptibility, electrical conductivity (Owens and Bamford, 1976; Hawton and Borradaile, 1989; Louis et al., 2003; Robion et al., 2014a; 2014b).

Anisotropic behaviour of the rock matrix can occur due to preferred mineral orientation related to paleo-current directions during deposition, extensional or compressional stresses, or pressure solution. Internal deformation of the rock forming in response to a non-isotropic stress environment during loading. While magnetic anisotropy is a well understood property within sedimentary rocks, and has been constrained on many occasions with laboratory based methods. Determining the style of petrofabric using seismic anisotropy is less commonly used, mainly due to the difficulty of determining the principal directions of the anisotropy.

A routine established by Louis et al. (2003 and 2004) (**fig. 5**) addresses this complexity, providing an advanced methodology for the comparison of elastic and magnetic anisotropy. Following the work of Thomsen (1986) and Tsvankin (1997), Louis et al. (2004) have shown, that for anisotropic sedimentary materials (i.e. those with orthotropic symmetry) P wave anisotropy can be measured in the laboratory, as a direct function of the angle of wave propagation. After which the direction of principal anisotropy can be described as a symmetric, second rank tensor, with an error <4%. Consequently, both magnetic and seismic anisotropy can be described by similar second rank tensors **K** and **V,** respectively, making them useful for integration with each other**.** The mathematical representation of each tensor is an ellipsoid of varying shape and magnitude (**fig. 6**) (Tarling and Hrouda, 1993) along with their corresponding eigenvalues (i.e maximum value of magnetic susceptibility =K1 [or V1 for maximum velocity] intermediate value of magnetic susceptibility =K2 [V2] and minimum value of magnetic susceptibility =K3 [V3]) and their associated three principal vectors.

In order to gauge the magnitude of, and consistently characterise the form of anisotropy within our samples we have analysed three common parameters of AMS after Jelinek (1981): Firstly, the corrected degree of anisotropy - P_J, ranging between a value of one, indicating a perfect sphere and infinity. P_J provides a good measure of the degree of ellipticity and is defined as $P_J = \sqrt{2[(n1-n)^2 + (n2-n)^2 + (n3-n)^2]}$ where $n1, n2, n3$ represent natural logarithms of the tensor eigenvalues and $n = (n1 + n2 + n3)/3$, (ni=Ki, Vi, with i=1, 2, 3).

Secondly, we use the tensor shape parameter T. If susceptibility within the ellipsoid is prolate or rod shaped, meaning only the magnetic lineation is developed, then $T = -1$. If

magnetic foliation is completely dominant then $T = 1$ with an oblate fabric style. Transitional values between -1 and 1 denoting various interactions between both factors (Jelinek, 1981). T is defined by $T = (2n2 - n1 - n3)/(n1 - n3)$.

Lastly, we use the mean eigenvalues of the produced tensor – K or V for both magnetic susceptibility and P-wave velocity respectively. Values that are defined by $Kmean = (K1 + K2 + K3)/3$ (in the case of susceptibility).

3.2.1 Magnetic anisotropy of sedimentary rocks

With a high sensitivity to even a slight preferred orientation of magnetic minerals, AMS can be used to characterise even the weakest levels of deformation and distinguish between sedimentary, intermediate and tectonic rock fabrics (**fig. 6**) (e.g. Fuller et al., 1964; Graham, 1966, Kissel et al., 1986; Borradaile and Tarling, 1981; Averbuch et al., 1992; Robion et al., 2007).

In sedimentary rocks, the relationship of the magnetic fabric with the bedding plane is also important, as it can assist in constraining the timing of the recorded event. Additionally, a correlation between the orientations of principal AMS axes and the principal axes of strain has been shown to exist. However this cannot be said for their relative magnitudes (e.g. Evans and Elmore, 2006; Latta and Anastasio, 2007).

For sedimentary rocks, the measured magnetic signal can stem from three sources; (1) dominant diamagnetic minerals – eg: quartz or calcite (2) paramagnetic minerals present as either grains or within rock matrix – eg: clays and ferromagnesian silicates and (3) diluted ferromagnetic minerals eg: oxides, hydroxides and sulfides such as magnetite,

hematite, goethite, and or pyrrhotite. In sedimentary rocks a mix between the three sources in different proportions is common and typical $Kmean$ values are between -10 x 10^{-6} and 10 x 10^{-3}SI units.

In the case of un-deformed sediments, the development of a magnetic ellipsoid is attributed to the depositional or compaction process, and is generally oblate in nature, with the plane of magnetic foliating roughly sub-parallel to the bedding plane. If sediments experience tectonic deformation, an AMS fabric typically develops, modifying the sedimentary fabric according to the intensity and style of deformation.

As this can be in the form of extensional of compressional deformation it is important to distinguish between these two scenarios: In primarily extensional environments, the magnetic lineation is typically acquired during the early phases of deposition and coincides with the azimuths of regional extension, parallel to the dip direction of regional faults. In this case K1 is generally aligned with the down dip direction of the bedding when it remains near horizontal (Mattei et al., 1999; Cifelli et al., 2005; 2004). In contrast, when subjected to tectonic compression, magnetic fabrics will evolve from sedimentary to tectonic through an initial migration of K1 parallel to the strike of the bedding (**fig. 6**), orthogonal to the axis of compression. A transition that is followed by an eventual habit of K1 parallel to the pole of the bedding, with K3 parallel to the shortening axis (**fig. 6**)

For this study the analysis of AMS took place at the University of Cergy-Pontoise using a spinner kappabridge KLY-4S with a sensitivity of 0.5 x 10^{-8} SI units.

3.2.2 APV – Anisotropy of P-Wave Velocity

In order to measure APWV we utilised an experimental device developed in-house at the University of Cergy-Pontoise, which is designed to automate the acquisition of elastic wave measurement on small core samples (**fig. 5**) (David et al., 2017). The accompanying method consists of combining a triplet of cylindrical plugs along three perpendicular directions. The APWV of each individual plug characterised by measuring P-wave travel time along multiple – in this case 36 – diameters (**fig. 5**), after which it is possible to approximate APWV in weakly anisotropic rocks (Louis et al., 2004). State of the art, the measurement of APWV in this fashion has been proven to compliment AMS studies on a number of occasions (Louis et al., 2003; 2004; 2006; 2008; Robion et al., 2007; 2014a; Humbert et al., 2012). Their combination proven to provide direct insights into the nature of the void space within the rock, which is controlled by grain orientation, contact and microstructures, complimentary magnetic fabric analysis.

Samples for APWV in this study were measured under dry conditions, following 24 hours in an oven at 60°C and after saturation with distilled water, to control for the effect of pore space on travel time and anisotropy. P-wave velocity values were then calculated from the measured travel time using the method outlined by David et al. (2017) the main objective being to investigate the orientation – if any – of the void space.

4.0 Results and Interpretation

4.1 Magnetic fabrics

4.1.1 Magnetic Fabrics from the Eumeralla Formation

Classical P_j vs T plots of results from the Eumeralla formation show T values between 0 and 1, suggesting triaxial magnetic fabrics (**fig. 7 a**), with varying degrees of anisotropy between P_j = 1 and 1.2.

Km vs P_j plots (**fig. 7b**) show classical trends with increasing levels of anisotropy accompanying increasing magnitudes of susceptibility. Mean susceptibility values across the formation varies, with some sites (KEN-1, KEN-2, JOH-1) displaying values above 500e-6 SI, suggesting the fabric is likely controlled by ferromagnetic fractions within the rock (Borradaile, 1988; 2000; Rochette et al., 1992). The remaining sites possibly controlled by para-diamagnetic or ferromagnetic fractions.

Prolate fabrics at most sites (CC-1, CC-2, CC-3, CR-1, KEN-1, KEN-2, SKC-1, SKC-2, JOH-1) correlate well with the clustering of each susceptibility axes (K3, K2 and K1) within the bedding plane (**fig. 8**), the azimuth of K3 near to or parallel to the pole of the bedding. In these cases the magnetic lineation K1, is close to or parallel to the down dip direction of the bedding (**fig. 8**), representing a fabric typical of those previously identified within extensional settings (e.g. Mattei et al., 1999; Cifelli et al., 2004; 2005).

Three sites display a deviation from this trend: LORNE-1, JAB-1 and JAB-2. LORNE-1 shows a planar fabric, with K1 distributed across the bedding plane and K3 parallel to the bedding pole, typical of a sedimentary fabric. JAB-1 and JAB-2 display poorly defined, transverse style fabrics with a girdle of Kmax across the E-W axis and a clustering of K3 unrelated to the bedding pole (**fig. 8**). In both cases despite a measurable susceptibility, the total anisotropy within the samples is very low (~1.01) suggesting the presence of diamagnetic, isotropic quartz and small amounts of magnetite.

The habit of K1 plunging down dip of the bedding in most samples represents the distinctive feature of magnetic fabrics typical of extensional environments (Mattei et al., 1999; 2004; Cifelli et al., 2004; Oliva-Urcia et al., 2010). In this case the magnetic fabric develops progressively, related to the reorientation of the basal planes of the phyllosilicate grains within the rock (Cifelli et al., 2005; 2007). These fabrics are characterised by the development of a magnetic lineation that is generally down dip of the bedding and orthogonal to the main extensive faults in the region (Sagnotti et al., 1994; Mattei et al., 1997; 2004; Cifelli et al., 2004). Current theories suggesting the fabric is acquired during the early stages of deformation, when bedding is still sub-horizontal (Mattei et al., 1997) and sediments are relatively soft (Borradaile, 1988).

Deposited during tectonic subsidence, the Eumeralla Formation represents the most significant Early Cretaceous unit in the eastern Otway Basin. As it is not a major syn-rift unit, rotation of the bedding away from the horizontal plane took place following deposition, coinciding either with a period of extension during the early Late Cretaceous or uplift inversion in the Latest Cretaceous (~Mid Maastrichtian). Therefore restoring the bedding to the horizontal plane is appropriate to discern the paleo-orientation of Kmax (**fig. 9**). Following this restoration (**fig. 9**), K1 azimuths appear clustered towards the N-S and NE-SW, orientations which are in good agreement with the regional offshore architecture, and the inferred onshore fault orientations from Burgin and Amrouch (2019b). The study also notes that this faulting pattern is suggested by the topographic nature of the ranges (**fig. 2**), which are defined by a series of ~NW-SE and ~E-W striking ridges and valleys.

In the case of JAB-1 and JAB-2, due to their near isotropic fabric and corresponding low levels of anisotropy we are more hesitant to interpret them as representative of typical extensional fabrics. Especially as K3 is significantly rotated away from the bedding pole in both cases, as such it is possible that measurement errors have occurred throughout the analytical process, resulting in a dislocation of the sample block orientation away from the bedding plane.

4.1.2 Magnetic Fabrics from the Nirranda Group

AMS fabrics measured in the Palaeogene, Nirranda Group at sites SBW-1, SBW-2, AR-1 and AR-2 display the lowest mean susceptibility values from our study, typically between 30x10-6 and 400x10-6 (**fig. 7b**) and remain below the threshold of 500e-6 SI. A characteristic which suggests the fabric is likely controlled by a mix of paramagnetic and ferromagnetic minerals.

T vs P_J plots (**fig. 7a**) show classical planar magnetic fabrics after Robion et al. (2007). In all cases these fabrics are correlated to a scattering of K1 and K2 throughout the bedding plane, with the lineation of Kmin generally parallel to the pole of the bedding (**fig. 10**). A feature which is typical of sedimentary fabrics in rocks that have not been subjected to any post-depositional deformation (Cifelli et al., 2005).

4.2 Anisotropy of P-wave Velocity

All samples subjected to AMS were analysed with APWV, firstly after drying in an oven for 24 hours and secondly, following saturation in distilled water for another 24 hours, during which porosity was also measured. This protocol allows us to distinguish between the matrix and void related anisotropy by comparing the two acoustic measurements

(Louis et al., 2003). During this process, the saturation of samples allows for differences between the matrix and void related anisotropy to be distinguished (Louis et al., 2003). As water is denser than air and virtually isotropic, saturation typically results in an increase of velocity and concomitant decrease of anisotropy within a sample. The difference is obtained by subtracting the velocity measured between saturated and dry conditions, in each direction of measurement. The resulting differential tensor is represented in a similar way as for velocities, with 3 principal axes, ie. ΔVmax, ΔVint, ΔVmin respectively for maximum, intermediate and minimum velocity difference. By subtracting the two tensors in this manner, we generate a representation of velocity variations due to the saturation. These variation, allows us to distinguish between the matrix and void related anisotropy and also determine the orientation of any differences, which is the most useful for comparison with AMS datasets (Louis et al., 2003; 2004).

For 253 samples across all sites, the measurement of APWV under wet and dry conditions in this study resulted in almost 19,000 individual velocity measurements.

4.2.1 APWV results from Eumeralla Samples

Under dry conditions, porosity vs velocity (**fig. 11a**) and P_J plots (**fig. 11b**) show classical trends, describing high P-wave velocities (up to 4.5km/s). Decreasing with increasing porosity, and lower levels of anisotropy (P= ~1.1) in low porosity (<5%) samples (e.g. CC-1, CC-2 and CC-3) in addition to the reverse trend.

P_J vs V_{mean} plots (**fig. 12a**) comparing dry and saturated conditions for the Eumeralla Formation (**fig. 10**) display mild increases in velocity between dry and saturated samples, accompanied by significant decrease in anisotropy. The exception in our case being JAB-

2, which displays no increase in velocity and only a minor decrease in anisotropy between dry and saturated conditions. This suggests that in the case of most samples (CC-1 and JAB-2 excepted) the measured velocity anisotropy is largely a function of the void space within the rock, rather than controlled by the presence of micro cracks.

Under dry conditions, most results within the Eumeralla formation display a V3 close to or parallel to the pole of the bedding (**fig. 13**), with the most anisotropic of the samples under dry conditions also displaying V1 orientations that trend parallel to the bedding strike (e.g. CR-1, KEN-1, KEN-2). However, this characteristic is less well defined with decreasing anisotropy (e.g. CC-1, CC-2 and CC-3).

Under saturated conditions for samples of higher anisotropy, V3 remains parallel to the bedding pole with V1 and V2 migrating to the bedding plane (**fig. 13**). Though this is not the case for KEN-1 and KEN-2. For samples with lower anisotropy under dry conditions (eg. CC-1, CC-2, CC-3) we observe a reduction on anisotropy, with V3 remaining parallel to the bedding (**fig. 13**), in which case the distribution of V1 and V2 remains similar to that under dry conditions.

With respect to the differential velocity tensors (**fig. 14**) within the Eumeralla Formation there are two types of results: 1) A case where the maximum velocity change (ΔV_{max}) is more or less parallel to V3 (CC-2, CC-3, CR-1, JOH-1, SKC-1, SKC-2, KEN-1, KEN-2, LRN-1). 2) Where any correlation is more unclear (CC-1 and JAB-1, JAB-2). Additionally, in the case where ΔV_{max} is parallel to V3 , ΔV_{min} is more or less parallel to the mean maximum susceptibility lineation orientation, i.e. the magnetic lineation.

From these differential tensors, and the visualised changes between the dry and wet stereonet plots (**fig. 14**), the results suggest that P-wave velocity and pore fabric are generally controlled by the void space within the rock. Thus, assuming that the ΔVmin mimics the long axis of porosity, these results also suggest that anisotropy of porosity is more or less coaxial to the magnetic fabric, allowing the latter to be used as a proxy of porosity orientation. However in the case of CC-1 micro-fractures trending ~NW-SE may be present (**fig. 13**), given the distribution of Δmax along a ~NE-SW trend (Louis et al., 2004), very low levels of porosity and no significant change following saturation.

4.2.2 APWV results from Nirranda Group

APWV results from the Nirranda Formation can be broken down into two categories based on differences in their velocity between dry and saturated conditions, which is likely directly linked to their porosity.

As with the Eumeralla Formation, under dry conditions, porosity vs velocity (**fig. 11a**) and P_J plots (**fig. 11b**) show classical trends, describing high P-wave velocities (up to 4.6km/s) decreasing with increasing porosity, and decreasing levels of anisotropy. Samples AR-1 and AR-2 display approximately half the porosity of samples SBW-1 and SBW-2, with ~1km/s increase in speed, and are characterised by lower velocities under dry conditions. Though the formation typically represents a clean porous sandstone, these velocity differences between our two sample groups suggest a higher contribution of cement, possibly in the form of calcite, within the samples from SBW-1 and SBW-2. However, the style of micro-structuring may also be an explanation.

P_J vs V_{mean} (**fig. 12b**) plots comparing dry and saturated conditions for samples from the Nirranda Formation also display two styles of results. Samples AR-1 and AR-2 show significant reductions in anisotropy along with increasing velocity between dry and saturated conditions. Samples SBW-1 and SBW-2 show no appreciable change in anisotropy between dry and saturated conditions, however small increases in velocity are present. This suggests that for samples AR-1 and AR-2 as with the Eumeralla Formation, void space is the main control on anisotropy, but for samples SBW-1 and SBW-2, a contribution from other microstructures to the anisotropy may be present, i.e, micro-cracks or grain contacts.

Though these differences in velocity are observed, spatially speaking, (**fig. 15**), there is little variation between dry and saturated conditions for all samples within the formation. V3 being consistently parallel with the bedding pole in all cases and essentially isotropic distributions of V1 and V2 along the bedding plane (**fig. 15**). That being the case, from differential tensors of the samples (**fig. 16**) we regard the measured fabrics as isotropic and associated with the bedding plane. This observation is supported by differential orientations of ΔVmax parallel to the pole of bedding and ΔVint and ΔVmin scattered throughout the plane.

5.0 Discussion

In the following section we begin with a synthesis of our two petrophysical datasets. We then integrate these outcomes, with respect to the timing of deformation in both sedimentary units with calcite twin, fault and fracture data obtained from Burgin and Amrouch (2019b).

519 **5.1 Synthesis and AMS and APV Datasets**

520 There is good agreement between the AMS and APWV results. This is especially evident
521 within the Nirranda Group, where both AMS and APWV suggest the presence of an
522 isotropic transverse sedimentary rock fabric. It is also the case for sample LORNE-1 from
523 within the Eumeralla Formation.

524

525 With respect to the other samples from the Eumeralla Formation, they are characterized
526 by a trend where the maximum velocity difference between dry and saturated conditions,
527 VΔmax, is well aligned with K3. Both of which are approximately parallel to the pole of
528 the bedding (CC-2, CC-3, CR-1, JOH-1, SKC-1, SKC-2).

529

530 This correlation is useful when considering our interpretation of the AMS data as
531 representative of extensional tectonics, providing us with supporting evidence for the
532 interpretation. The relationship between the two independent methods suggesting it is
533 unlikely that there is any inversion of the AMS fabric related to mineralogical effects. As
534 such for these samples APWV is supportive of the ~N-S to ~NE-SW extensional pore
535 fabrics interpreted within the AMS results (**fig. 9**) and is reflective of the direction of
536 porosity elongation which is roughly parallel to the AMS axes (**fig. 8** and **fig. 14**).

537

538 Samples which represent exceptions to the above trend are JAB-1, JAB-2 and CC-1. In
539 each case there is little correlation between differential velocity tensor and the fabric
540 determined from the AMS results. In the case of CC-1, as porosity was calculated to be
541 approximately 3%, APWV values are likely not reflective of the pore fabric but
542 everything else (grain orientation, contact, micro fractures). Analysis of the
543 corresponding velocity tensor under dry conditions (**fig. 13**), suggests the possible

presence of a microstructural feature trending ~NW-SE, which is defined by the distribution of V1 and V2 and has been shown to be possible in previous studies (Louis et al., 2004). We suspect that JAB-1 and JAB-2 (**fig. 13**) may represent a similar scenario, however as the AMS fabric is so poorly defined, it is not possible to accurately constrain to nature of the structure.

5.2 Timing and development of petrofabric: Layer Parallel Stretching?

Extensional magnetic fabrics are believed to be acquired during the early stages of deformation, when bedding is still sub-horizontal (Mattei et al., 1997) and sediments are relatively soft (Borradaile, 1988). Their formation characterised by the development of a magnetic lineation down dip of the bedding and parallel to the regional axis of stretching (Sagnotti et al., 1994; Mattei et al., 1997; 2004; Cifelli et al., 2004).

The Eumeralla Formation was deposited during a period of tectonic and extensional quiescence and subsidence during the Aptian – Albian (Krassay et al., 2004). With most studies focusing on the Early Cretaceous depocentres of the basin, presenting minimal evidence for structural growth along faults during this period (Lyon et al., 2007; Bruigiglo et al., 2015).

Extensional azimuths within the Eumeralla Formation suggested by AMS show good co-axiality with azimuths of early, Late Cretaceous extension in the Otway Ranges and surrounding area (Burgin and Amrouch, 2019b). Paleo-σ3 orientations derived from the stress inversion of calcite twins and natural fractures show an initial period of well-defined ~NE-SW oriented extension, defined by an unusually high magnitude of extensional maximum differential stress (**fig. 17**). As such, results from the Eumeralla

569 Formation therefore suggest the influence of an N-S to ~NE-SW extensional tectonic
570 stress very soon after deposition, azimuths which coincide well with the geometry of on
571 and offshore faults within the region inferred by Burgin and Amrouch (2019b).
572
573 Given the depositional style of the Eumeralla Formation described above and the co-
574 axiality of magnetic fabrics with early Late Cretaceous extensional events. We suggest
575 the results of this study represent an initial extensionally driven equivalent of layer
576 parallel shortening (LPS), in our case layer parallel stretching (**LPSt**) (**fig. 18**). In fold
577 and thrust belts LPS reflects a period of internal deformation that develops during the first
578 phase of deformation, prior to further brittle deformation structures such as fractures,
579 calcite twins, faults and folding (Averbunch et al., 1992; Amrouch, 2010b; Amrouch,
580 2011). We suggest LPSt develops in a similar manner, reflecting the first stage of
581 extensional deformation and the development of a stretching lineation parallel to the
582 azimuth of paleo-σ3 (**fig. 18**). In the case of the Otway Basin, high levels of extensional
583 differential stress proposed by Burgin and Amrouch (2019b) may suggest that LPSt
584 requires relatively high magnitudes of stress (~69MPa). Especially when compared to
585 paleostress magnitudes constrained during outer-rim style extension during folding,
586 where no such fabrics have been recorded (Amrouch, 2010b).
587
588 Given the high sensitivity of AMS to recording strain within sedimentary rocks, there
589 remains the possibility that the results record a period of very minor, ~N-S and ~NE-SW
590 extension during the deposition of the Eumeralla Formation. However, we believe this is
591 not the case due to the wide spread occurrence of ~NE-SW and ~N-S extensional
592 paleostresses throughout the Otway Ranges, under bedding backtilted (horizontal)
593 conditions (Burgin and Amrouch, 2019b). A feature that indicates that following

deposition, prior to the influence of Late Cretaceous extension, bedding was likely horizontal. In which case the development of extensional fabrics characterised by K1 down dip of the bedding would not have been possible, as the bedding had likely not yet rotated away from the horizontal plane.

The absence of any tectonic fabric within our samples from the Nirranda Group further supports arguments from Burgin and Amrouch (2019b) for Late Cretaceous (Mid ~Maastrichtian) basin inversion and structuring, prior to the deposition of the unit. A thesis that is in contrast to other studies in the region that have favoured Miocene – recent ~NW-SE compression and uplift of the Otway Ranges structure. Indeed, though few in number sampling within the Nirranda Group in this study took place in close proximity to these supposedly Neotectonic compressional structures (**fig. 2**). The petrofabric results showing no evidence for this structural style, and the absence of even an extensional fabric suggesting that during deposition the Nirranda Group, the Otway Ranges may still have been undergoing a degree of stress reorganisation. A hypothesis which is supported by a general lack of fault growth during the deposition of Palaeogene and Neogene sedimentary units in the eastern Otway Basin (Burgin and Amrouch, 2019b).

5.5 Insight into strain accommodation during inversion of listric fault extensional systems

In addition to a period of Late Cretaceous extension beginning in the Cenomanian, Burgin and Amrouch (2019b) also advocate for ~NE-SW inversion in the eastern Otway Basin, during the mid-Maastrichtian. A phase of deformation, that in contrast to the preceding extensional event, was characterised by low magnitudes of differential stress (**fig. 17**). This compressional phase of evolution interrupted the final stages of continental

separation, and coincides with a period of cooling and uplift identified by other studies (Duddy and Erout, 2001). In addition to the localisation of major uplift within the onshore Otway Ranges, concentrated towards the northeast (Tassone et al., 2014). The results from this study indicate that this inversional event has had little influence on the development of magnetic and pore fabric styles in the Eumeralla Formation.

This can be accounted for in the partitioning of strain within the decollement zone (Burgin and Amrouch, 2019b) beneath the Otway Ranges throughout the inversion process. A style of deformation that is reflected in low differential stress magnitudes during the compressive phase of basin evolution (**fig. 11**) and low levels of mesoscale compressional deformation throughout the ranges (Medwell, 1971). This is also supported by sandbox experiments (**fig. 2**) (Buchanan and McClay, 1990) that have shown that during the co-axial inversion of listric fault systems such as the Great Ocean Fault System, contractional forces are isolated along the deeper detachment surface, rather than to the fault succession within the overlying sedimentary layers. On the grain scale, our results support this inversion model, as from the offshore architecture there can be little doubt that some degree of ~NE-SW oriented contraction has occurred, due to the presence of inversion style structures, mainly in the form of bulging collapsed grabens and half grabens, concentrated above underlying basement highs (Burgin and Amrouch, 2019b).

This suggests that in contrast to more conventional compressional intraplate settings, (e.g. Sheep Mountain – Wyoming; Amrouch et al., 2010b) that involve the progressive accommodation of strain from the micro to the macro scale during shortening (a succession of deformation that includes an initial phase of LPS). At inverted continental

margins like the Otway Basin, strain patterns may evolve differently during the inversion of extensional detachment fault networks, as reactivation of the décollement surface and existing extensional faults, isolates and partitions the early effect of LPS. A phenomena which results in the partitioning of strain within the detachment zone, and the preservation of sedimentary and extensional fabrics within the uplifted section.

This phenomenon is also documented in results from Robion et al. (2007). A study that draws distinct contrasts between the Potwar Basin, located at the front of the south western Himalayan collision (Pakistan) and the Minervois Basin, at the north eastern tip of the Pyrenees (France). The first displaying low levels of internal deformation and the preservation of the sedimentary fabric, the second showing high levels of internal deformation and a complete loss of the sedimentary heritage of the rock. The primary tectonic difference between the two being large differences in the degree of coupling between the basement and the cover, which is notably higher within the rocks from the Minervois Basin.

As also noted by Robion et al. (2007) higher levels of compaction, burial, dissolution and dewatering, may also result in a depositional fabric that is difficult to alter during the deformation process. While estimates for exhumation within the Otway Basin vary significantly (Duddy et al., 1993; Holford et al., 2011; Tassone et al., 2014), sonic transit time analysis has suggested that exhumation within the eastern basin has been estimated in some cases to be >2000m (Tassone et al., 2014). Suggesting that the degree of compaction may have been significant enough to restrict a restructuring of the petrophysical fabric during inversion, which may also be supported by the unit's tight porosity in some samples (e.g. CC-1).

669

670 **5.2 Multi-scale co-axiality of structural datasets**

671 The integration of multiscale structural data also provides support for the presence of a
672 possible microstructural features detected within the CC1 sample at Castle Cove (**fig. 19**).
673 In this case the distribution of V1 and V2 may define a ~NW-SE striking microstructural
674 feature which integrates well with outcrop scale fracture and faults mapped throughout
675 the cove (**fig. 19**).

676

677 This is also indicative of the orientation of paleo-σ3 from nearby calcite twin tensors
678 (Burgin and Amrouch, 2019b), and the nature of offshore faults within the Crowes Foot
679 3D survey, and the inferred onshore architecture of the Top Eumeralla Formation (**fig.**
680 **19**). Further still supporting the model from Burgin et al., (2019a) that the ~NE-SW
681 trending Castle Cove and Johanna faults suggested by previous studies likely do not exist.
682 The outcropping nature of the structure at the cove likely representing the eastern edge of
683 an inverted half graben which is evident in the architecture at its western end (**fig. 19**).
684 The ~NE-SW depocentres boarding the cove simply representative of a basement low
685 point, where inversion did not occur, a style which is also evidence offshore (**fig. 19**).

686

687 **5.6 Implications for Regional Petroleum Systems**

688 In recent years there has been some discussion as to the unconventional resource potential
689 of the Otway Basin within the region of the Port Campbell and Tyrendarra Embayments
690 (**fig. 1**). As the source rock for the majority of hydrocarbons within the region the
691 Eumeralla Formation is the target formation, especially in the above areas, where the unit
692 is currently at its maximum burial temperature (Tassone et al., 2014).

693

694 It is likely that unconventional means associated with shale / tight gas likely represents
695 the only option for production directly from the Eumeralla Formation, which despite its
696 sandy intervals is relatively tight (Duddy, 2003; Debenham et al., 2018). A feature of the
697 unit that is highlighted by the porosity results of this study (**fig. 10**). That being said, this
698 potential is supported by drill stem test data from Moreys-1, in the Port Campbell
699 Embayment which briefly flowed gas and condensate from a sandy interval of the
700 Eumerella Formation between 1925 and 1935m depth (Campbell, 2012).
701
702 The results of this study are relevant to any future efforts to produce unconventionally
703 from the Eumeralla Formation. As the APWV results suggest that the formation may have
704 a preferential pore fabric aligned somewhat ~N-S and ~NE-SW, parallel to the dip
705 azimuth of major faults within the basin. An insight which may assist in plans for drilling,
706 completion and the placement of injection and production wells during unconventional
707 production.
708
709 Lastly, the results from CC-1 and comparisons with lower and higher orders of structural
710 data (**fig. 17**) suggest the presence of ~NW-SE striking microstructures are also relevant.
711 An observation that provides an insight into the degree to which multiscale networks of
712 structural permeability may be present within the Eumeralla Formation. Signifying that
713 while primary porosity within the unit may be low, networks of secondary, structural
714 permeability may be present, which could be further enhanced by hydraulic stimulation.
715
716 Additionally, the preservation of early extensional fabrics within reservoir units
717 throughout basin inversion is an important outcome of this study. As it suggests that even
718 in passive continental margins subjected to tectonic scale compression. Deformation on

719 the grain scale is likely still reflective of the early extensional style of deformation. An
720 insight which may have consequences with respect to models of reservoir connectivity
721 and internal damage.
722
723 **6.0 Conclusion**
724 The results of this study provide further supporting evidence for the presence of ~NE-SW
725 and ~N-S extension within the Otway Ranges and have significant consequences for
726 models of basin inversion in the region. In particular those that have advocated for the
727 presence and reactivation of ~NE-SW striking faults, which multiscale datasets suggest
728 do not exist.
729
730 The magnetic and pore fabric analysis of samples from within the Eumeralla and Nirranda
731 Formations support multiscale evidence from Burgin and Amrouch (2019b) and the
732 presence of the Great Ocean Fault System. A Cretaceous listric detachment fault system
733 subjected to co-axial inversion, likely during the Latest Cretaceous (~Mid Maastrichtian).
734
735 For future work, we recommend the application of ferro-fluid impregnation and analysis,
736 along with the study of the anisotropy of permeability within the more porous interval, to
737 further investigate the geometry of the pore fabric. Additionally, with respect to the local
738 geology, we recommend a detailed 3D seismic assessment of the Torquay Sub Basin to
739 determine the nature of the structural fabric to the east.
740
741 **Acknowledgements**
742 The authors appreciate the financial contributions provided from the Endeavour Research
743 Fellowship and the Australian Postgraduate Award Scholarship through the University of

744 Adelaide. Additionally we wish to thank the university and staff at the Geosciences and
745 Environment Laboratory at the University of Cergy-Pontoise, Paris, France. In particular
746 Eléonore Izquierdo and Christian David for their welcoming attitude and assistance with
747 sample preparation. Thank you to field assistants Natalie Debenham, David Kulikowski
748 and Annabel Gibson. Thank you to Richard Allmendinger for Stereonet 8.8.8, and Carlos
749 H. Grohmann and Ginaldo A.C. Campanha for “OpenStereo 0.1.2”. Additional
750 information is available by contacting the lead author: hugo.burgin@adelaide.edu.au.
751
752
753

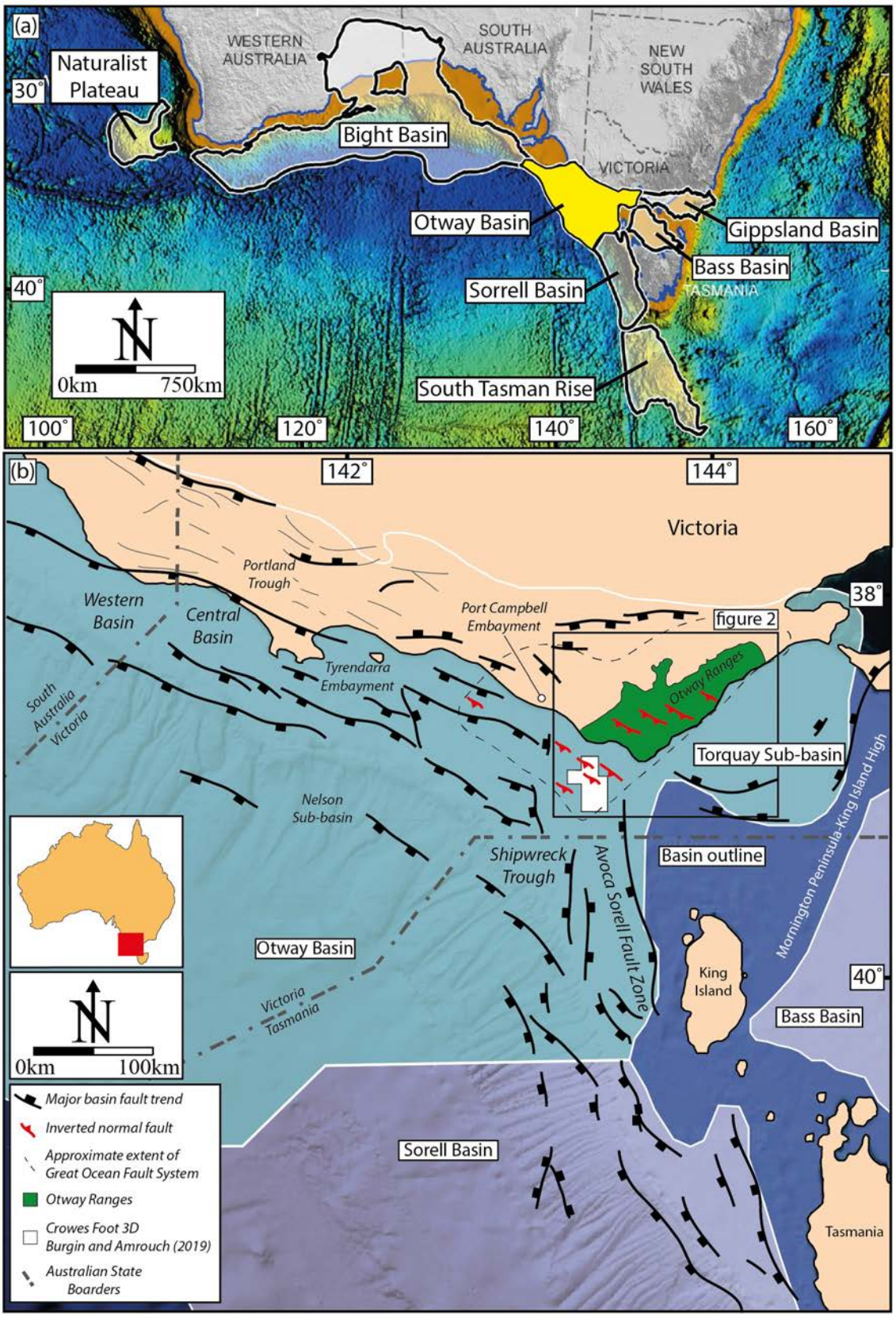
(a)
Naturalist Plateau
30°
WESTERN AUSTRALIA
SOUTH AUSTRALIA
NEW SOUTH WALES
Bight Basin
VICTORIA
Otway Basin
Gippsland Basin
Bass Basin
TASMANIA
Sorrell Basin
40°
0km
750km
South Tasman Rise
100°
120°
140°
160°
(b)
142°
144°
Victoria
Portland Trough
Western Basin
Central Basin
Port Campbell Embayment
figure 2
38°
Tyrendarra Embayment
Otway Ranges
South Australia Victoria
Torquay Sub-basin
Nelson Sub-basin
Shipwreck Trough
Avoca Sorell Fault Zone
Basin outline
Mornington Peninsula-King Island High
Otway Basin
Victoria Tasmania
King Island
40°
Bass Basin
0km
100km
Major basin fault trend
Inverted normal fault
Approximate extent of Great Ocean Fault System
Otway Ranges
Crowes Foot 3D Burgin and Amrouch (2019)
Australian State Boarders
Sorell Basin
Tasmania

754

755

Figure 1: (a) Map showing the location of the Otway Basin along the southern margin of Australia (b) Generalised structural map of the Otway Basin, Great Ocean Fault System and inverted faults modified from Burgin and Amrouch (2019b). Figure modified from Stacey et al., (2013)

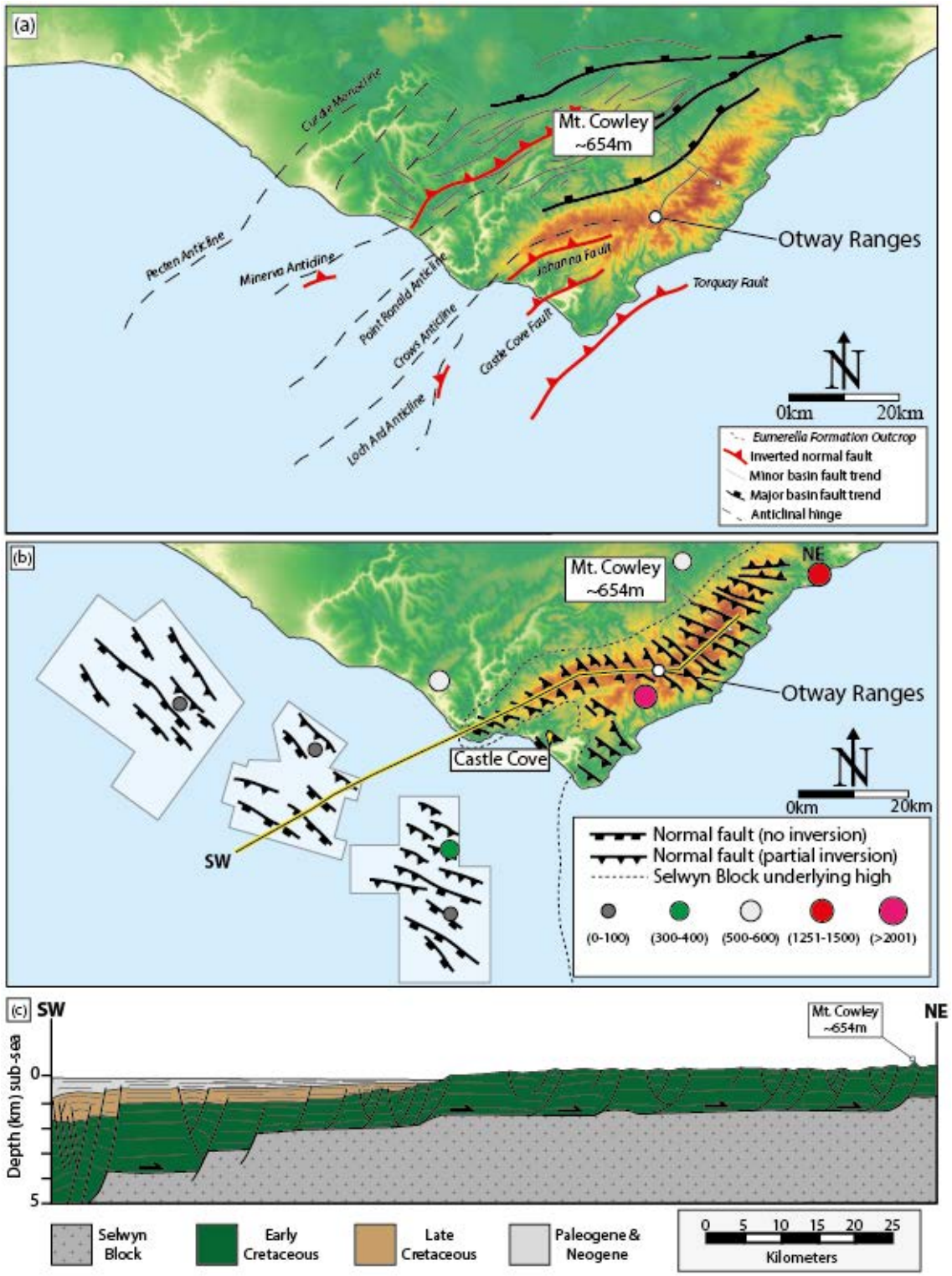

761

762

763

764

765 **Fig. 2:** (a) Structural model of the Otway Ranges after Debenham et al., (2018) after
766 Holford et al. (2014) (b) Structural model of the Otway Ranges after Burgin and
767 Amrouch (2019b) where on shore faults have been inferred from the topography and the
768 offshore architecture. 3D surveys from Burgin and Amrouch (2019b) also included. (c)
769 Approximated structural cross sections through the Otway Ranges (Burgin and
770 Amrouch, 2019b).
771
772

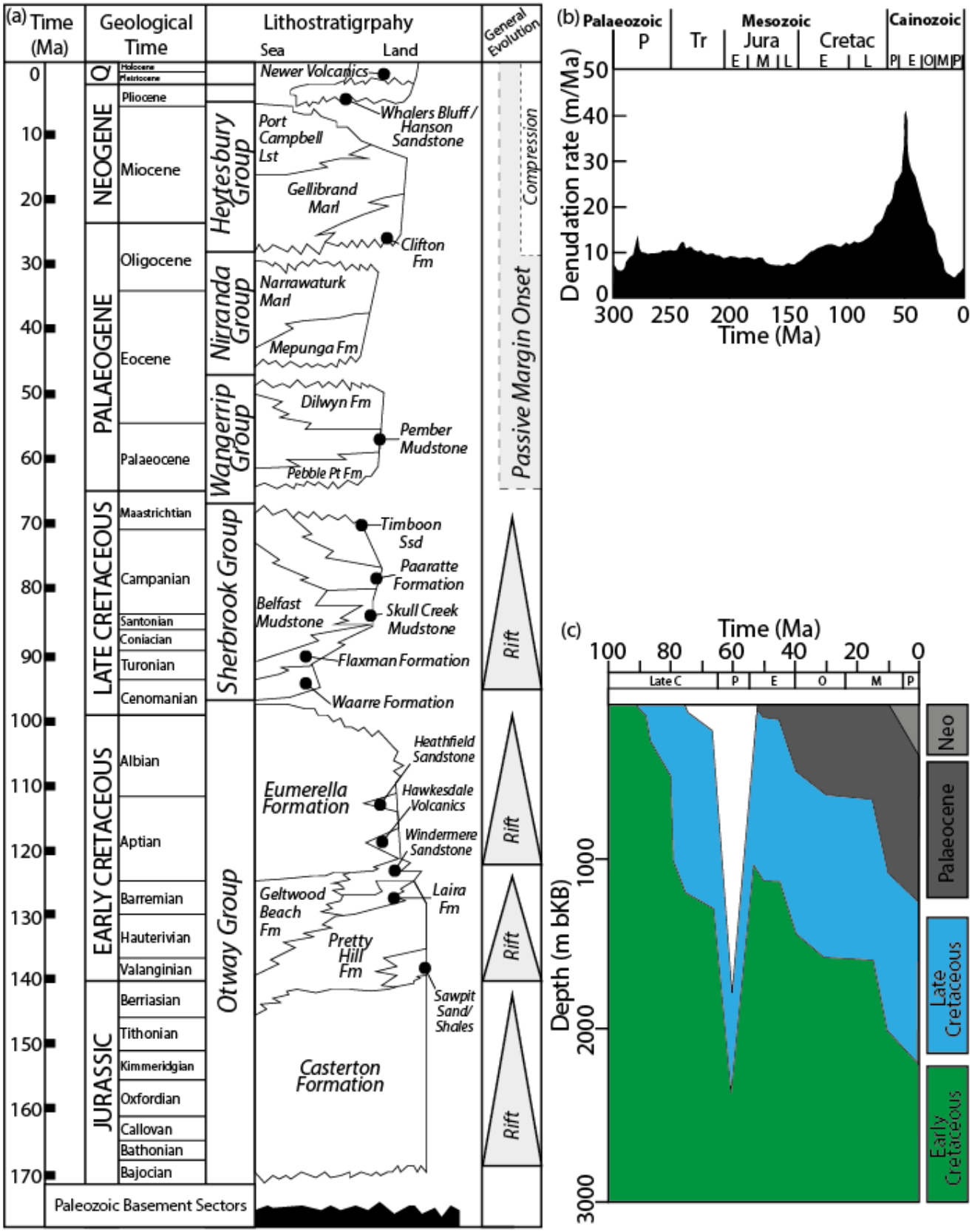
(a)
Time (Ma)
Geological Time
Lithostratigrpahy
Sea
Land
General Evolution
Q
Holocene
Pleistocene
NEOGENE
Pliocene
Miocene
PALAEOGENE
Oligocene
Eocene
Palaeocene
LATE CRETACEOUS
Maastrichtian
Campanian
Santonian
Coniacian
Turonian
Cenomanian
EARLY CRETACEOUS
Albian
Aptian
Barremian
Hauterivian
Valanginian
JURASSIC
Berriasian
Tithonian
Kimmeridgian
Oxfordian
Callovan
Bathonian
Bajocian
Heytesbury Group
Nirranda Group
Wangerrip Group
Sherbrook Group
Otway Group
Newer Volcanics
Whalers Bluff / Hanson Sandstone
Port Campbell Lst
Gellibrand Marl
Clifton Fm
Narrawaturk Marl
Mepunga Fm
Dilwyn Fm
Pember Mudstone
Pebble Pt Fm
Timboon Ssd
Paaratte Formation
Belfast Mudstone
Skull Creek Mudstone
Flaxman Formation
Waarre Formation
Heathfield Sandstone
Eumerella Formation
Hawkesdale Volcanics
Windermere Sandstone
Geltwood Beach Fm
Laira Fm
Pretty Hill Fm
Sawpit Sand/ Shales
Casterton Formation
Paleozoic Basement Sectors
Compression
Passive Margin Onset
Rift
Rift
Rift
Rift
(b)
Palaeozoic
Mesozoic
Cainozoic
P
Tr
Jura
Cretac
E M L
E L
Pl E O M P
Denudation rate (m/Ma)
Time (Ma)
(c)
Time (Ma)
Late C
P
E
O
M
P
Depth (m bKB)
Neo
Palaeocene
Late Cretaceous
Early Cretaceous

Figure 3: (a) Stratigraphic column modified from Tassone et al. (2017) after Geary and Reid (1998) (b) Denudation rates across south eastern Australia (c) Burial history data from Mussel-1 after Duddy and Erout (2001).

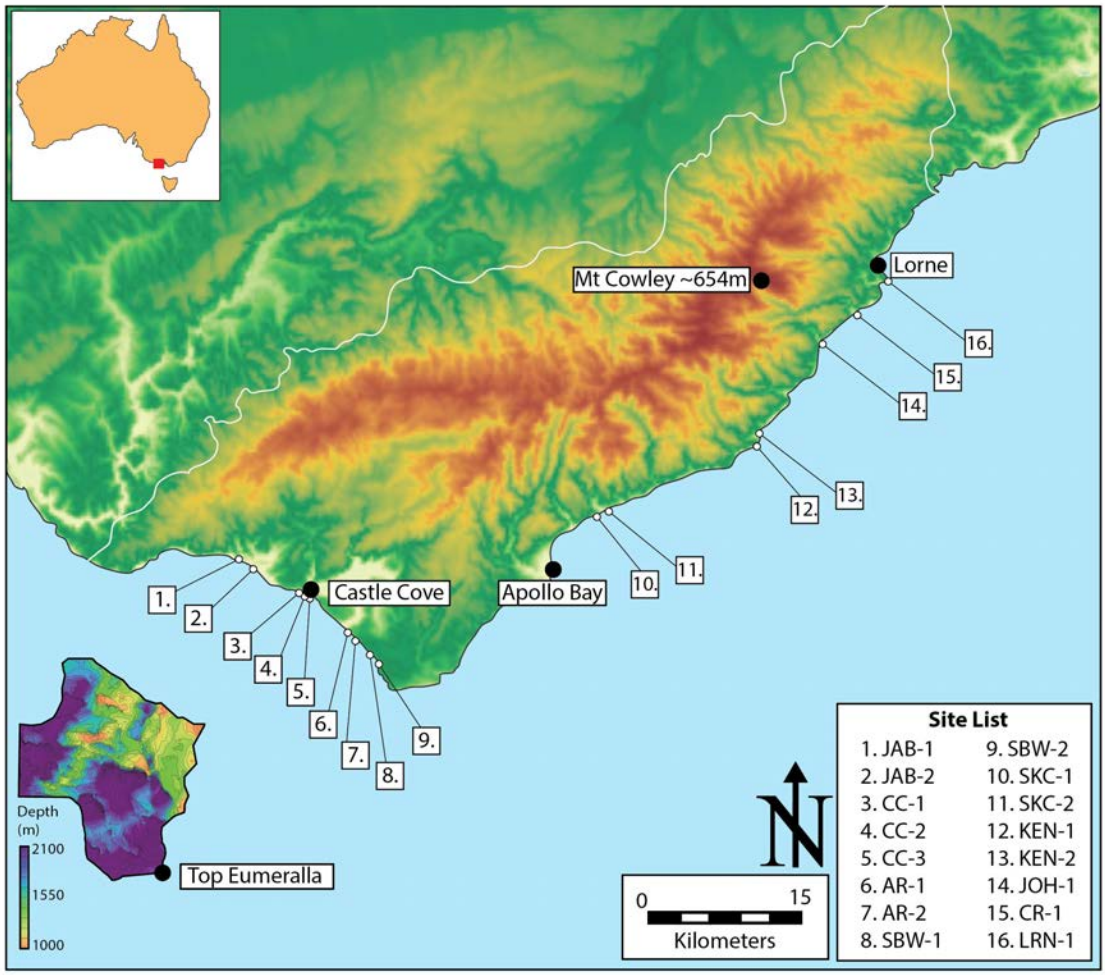

Figure 4: Topographic map of the Otway Ranges and the sample sites for the petrophysical analysis within this study. Inset is the Top Early Cretaceous (Eumeralla Formation) horizon – to scale - from Burgin and Amrouch (2019b) which shows the general continuation of the structure offshore as part of the Great Ocean Fault System.

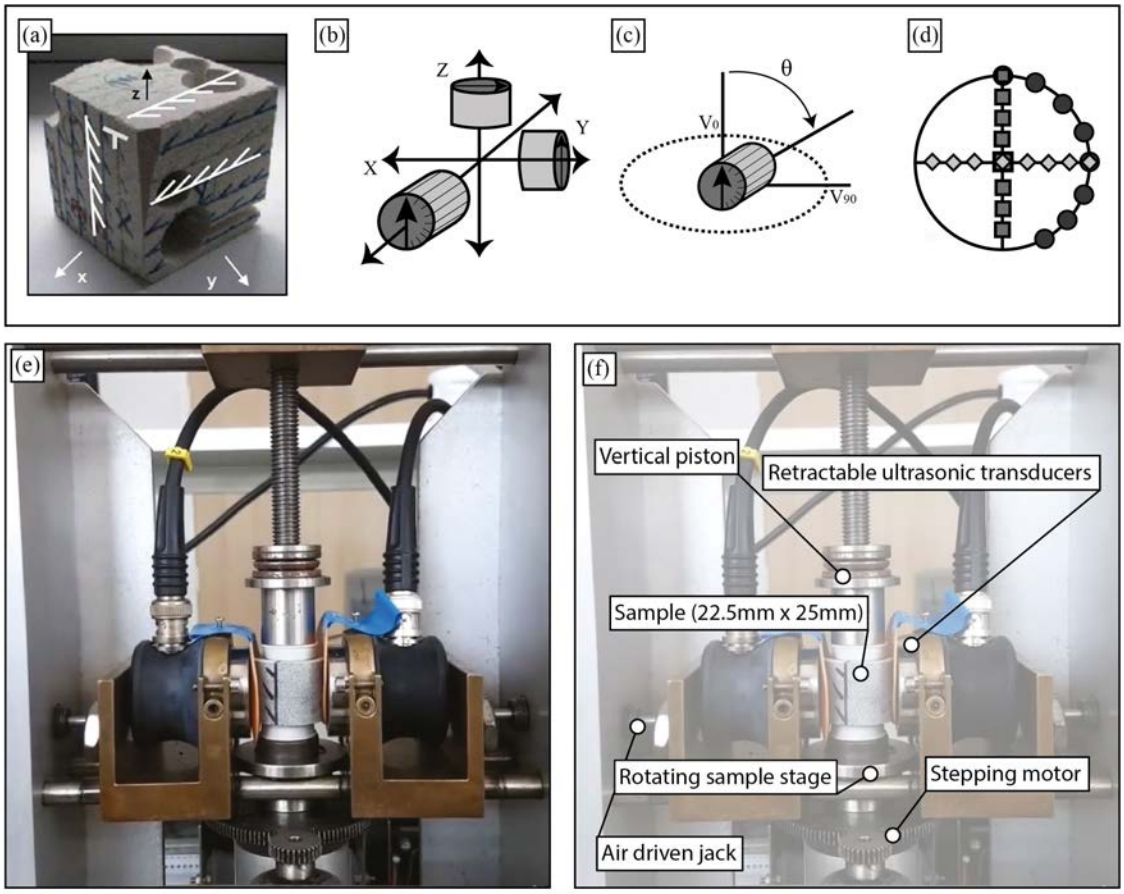

Fig. 5: Sampling method for the APWV and AMS samples within this study. (a) Coring scheme showing the sampling of three orthogonal samples cored from a single block. Where one of the faces, in this case X, corresponds to precise geographic coordinates. After David et al. (2017) (b) Position of the three oriented cores with the inferred measurement directions (in this case 26) (c) example of the measurement path around the sample and (d) Measurement scheme represented on sample and on a lower hemisphere stereonet, with the investigated directions for this schematic scenario. Azimuth angles measured from the north and dip angles from the horizontal plane. (e) and (f) unannotated and annotated photograph showing the experimental device after David et al. (2017). Sample in place for scale.

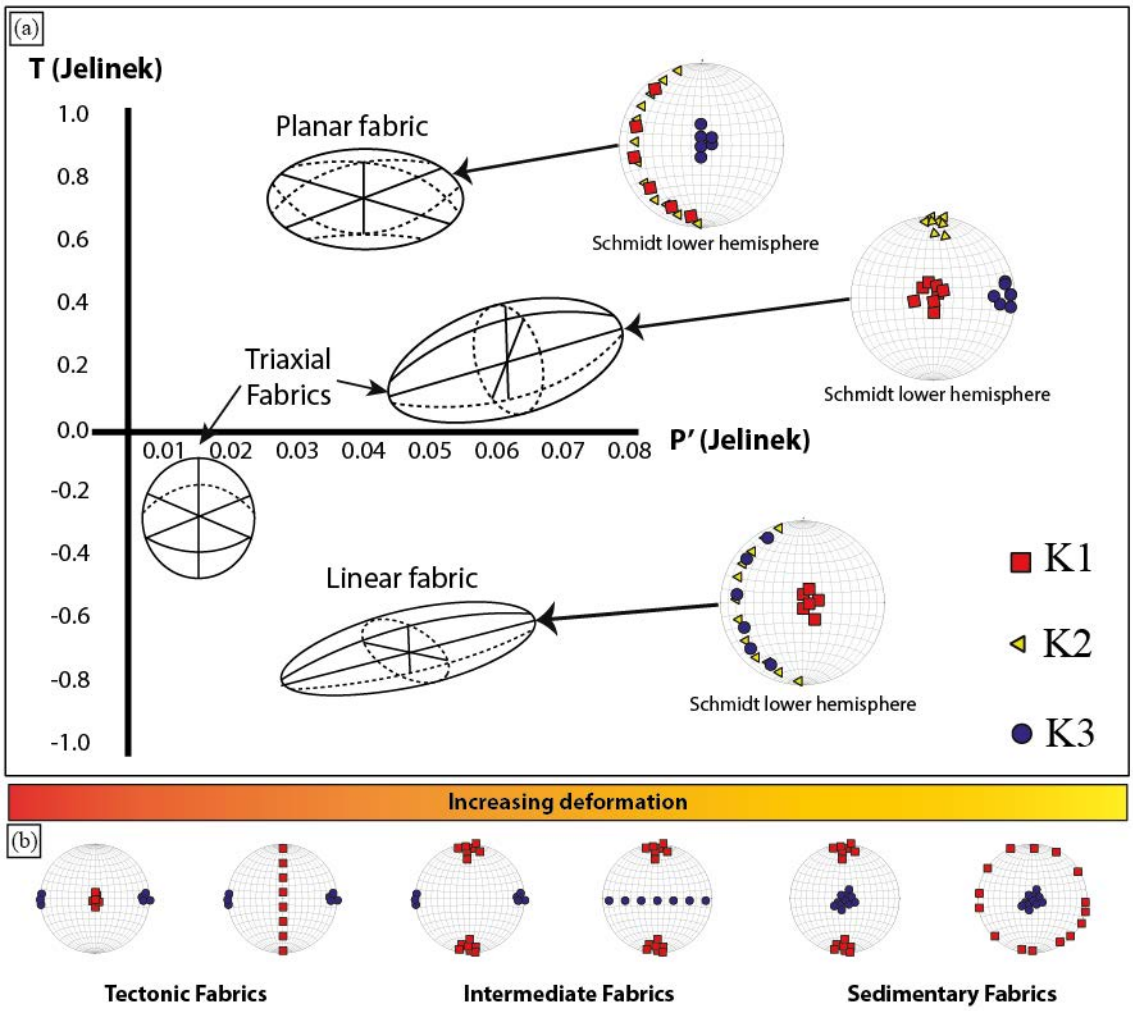

Figure 6: (a) T vs P' plot after Jelinek (1981) displaying the various distributions of magnetic fabrics and their possible natures (b) lower hemisphere stereonet projects of different fabric types, with increasing deformation from right to left. Bedding plane is horizontal and maximum shortening axis is oriented right /left. Type I is assumed to be the initial sedimentary fabric with isotropy in the bedding plane (after Robion et al. 2007).

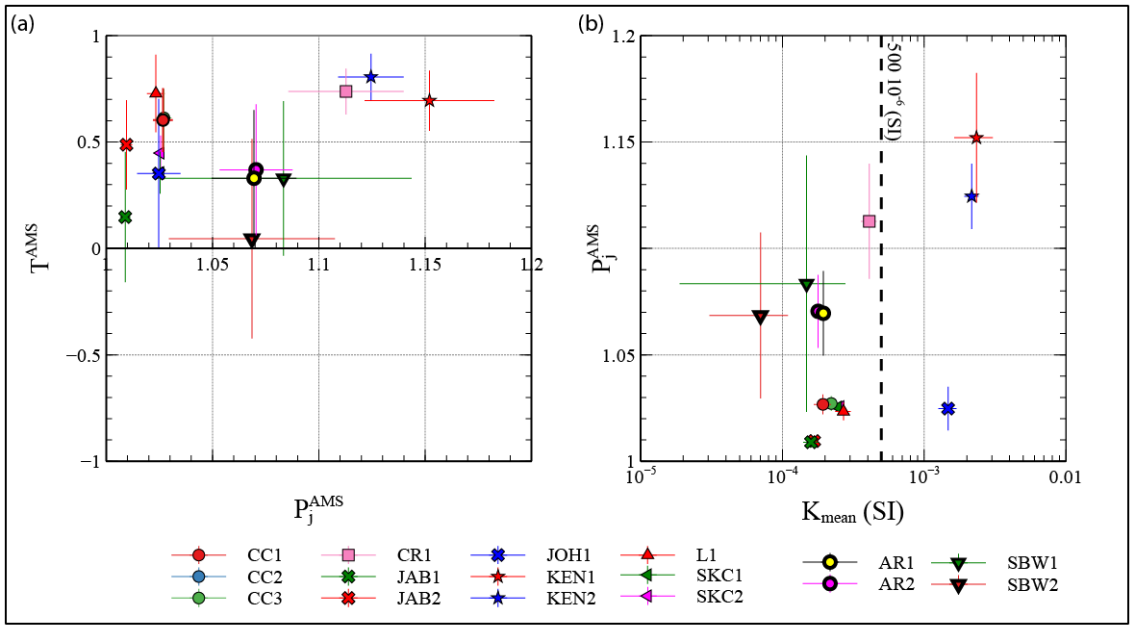

Fig. 7: P vs T (right) and Classical P vs Kmean (left) Jelinek (1981) plots for our AMS results within both sample formations.

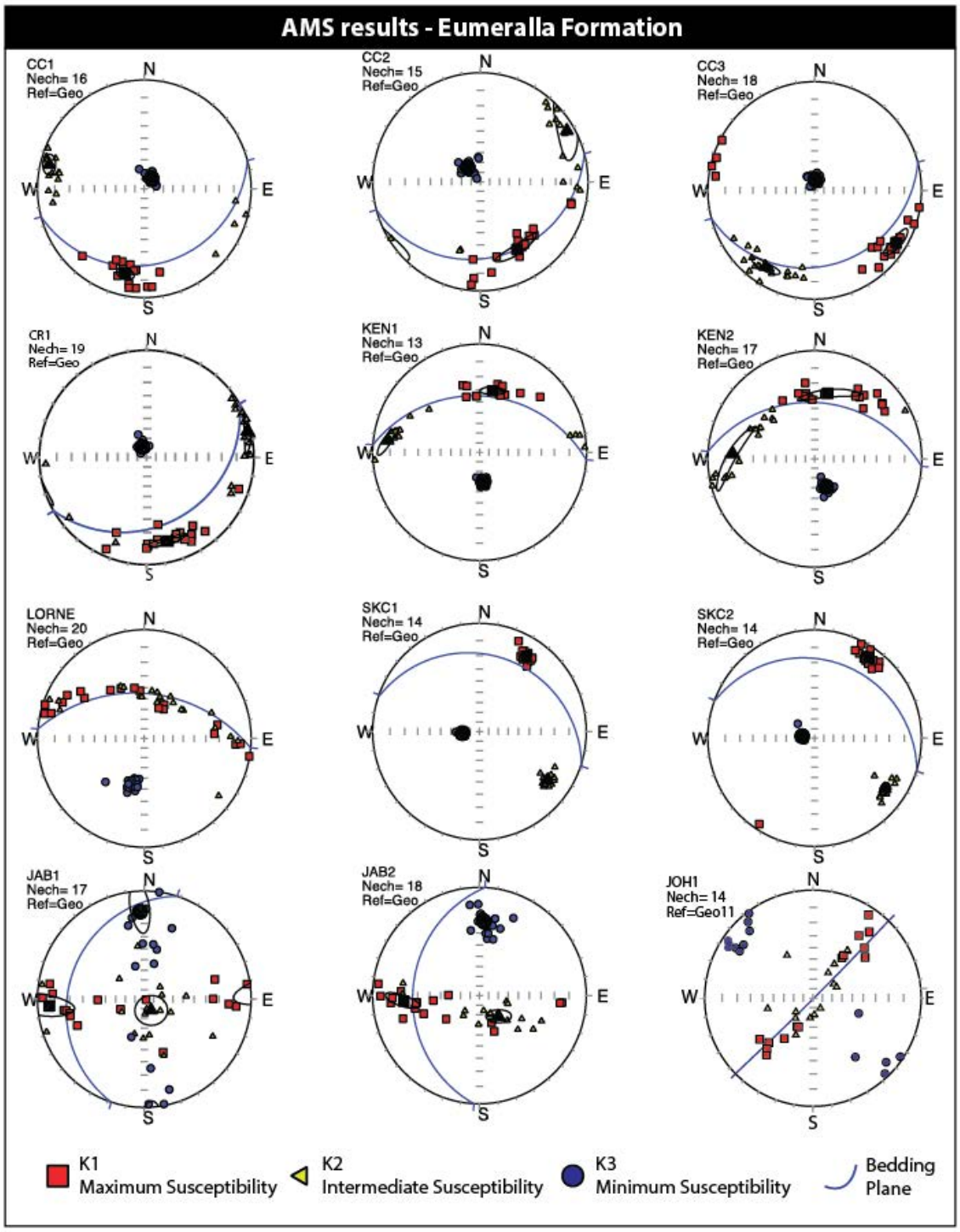

838

839

840 **Fig. 8:** AMS results from our 12 sites within the Eumeralla Formation. K1 is generally

841 aligned down dip of the bedding. Assisting our interpretation of extensional deformation.

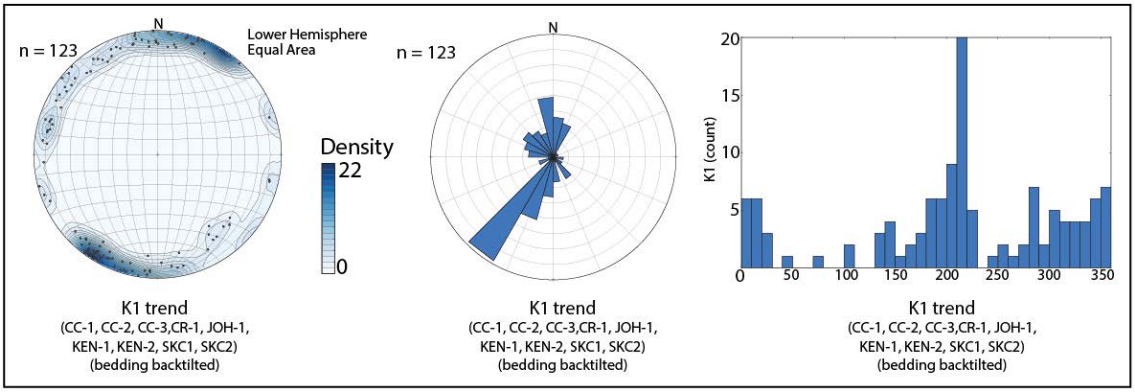

Fig. 9: Lower hemisphere stereonet, rose diagram and histogram showing the orientation and azimuths of K1 with bedding back tilted. Note the mainly NE-SW and N-S trends.

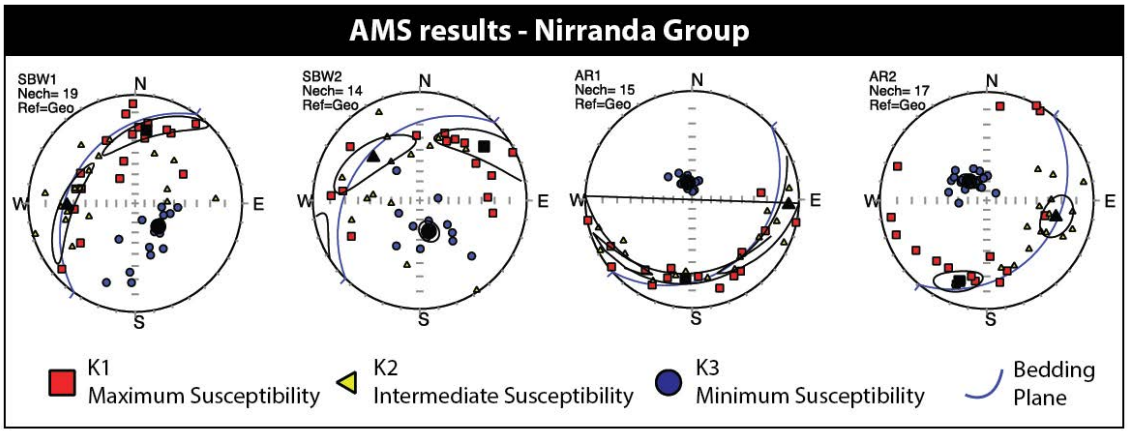

858

859 **Fig. 10:** AMS result from within the Nirranda Group sediments. Note that K3 is generally
860 parallel to the bedding with K1 and K2 distributed across the plane. Assisting our
861 interpretation of an isotropic sedimentary style fabric.

862

863

864

865

866

867

868

869

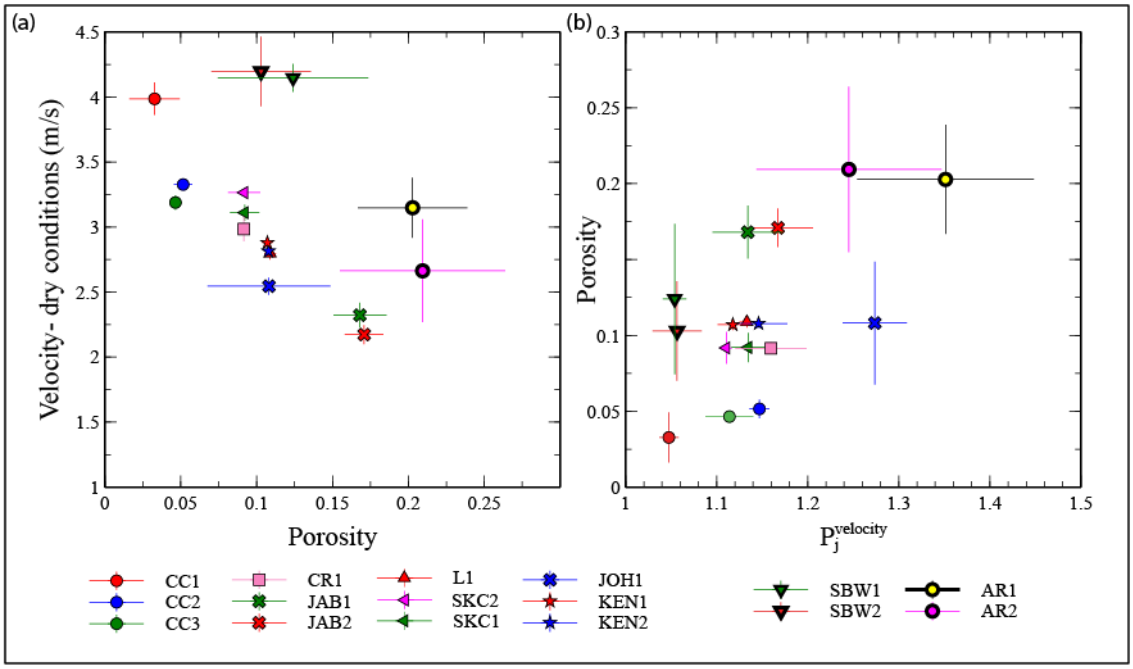

870

871 **Fig. 11:** Classical porosity vs velocity and porosity vs Pj for APWV under dry conditions.

872 Note the higher velocities and general lower levels of anisotropy with lower levels of

873 porosity

874

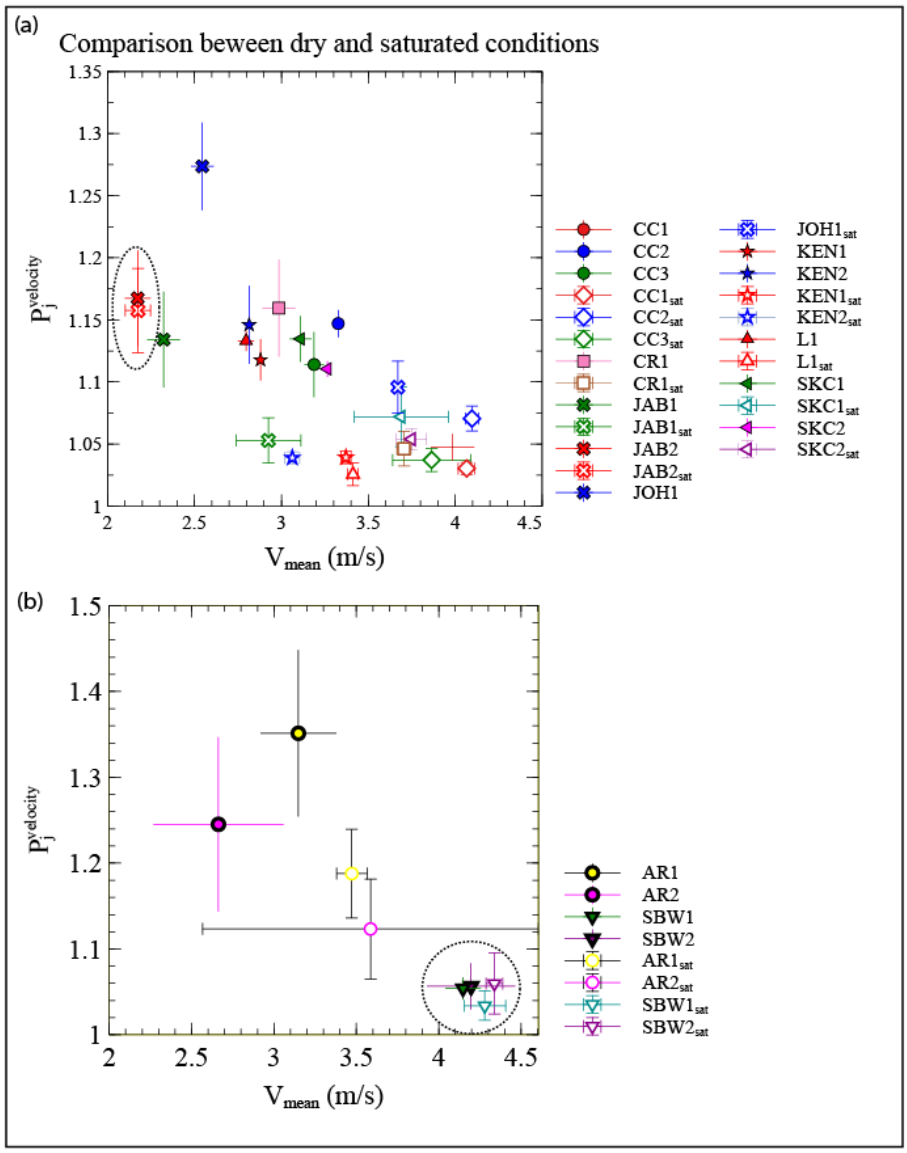

Fig. 12: Comparisons between dry and saturated conditions for the Eumeralla Formation samples (a) and the Nirranda Samples (b). Circles samples indicate where little change is observed. These are discussed in text.

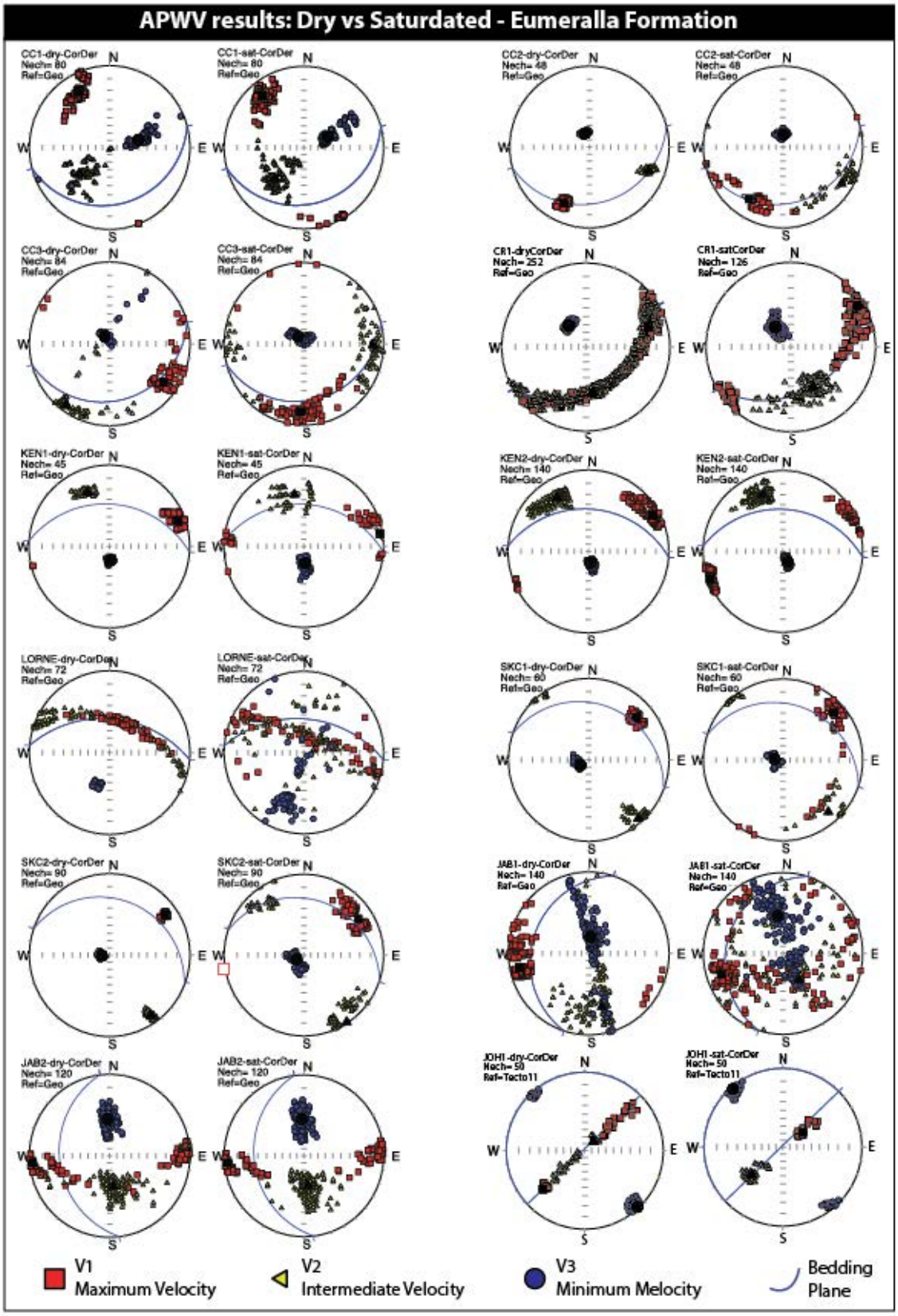

881

882 **Fig. 13:** APWV result pairs for dry (left) and saturated (right) conditions for the

883 Eumeralla formation.

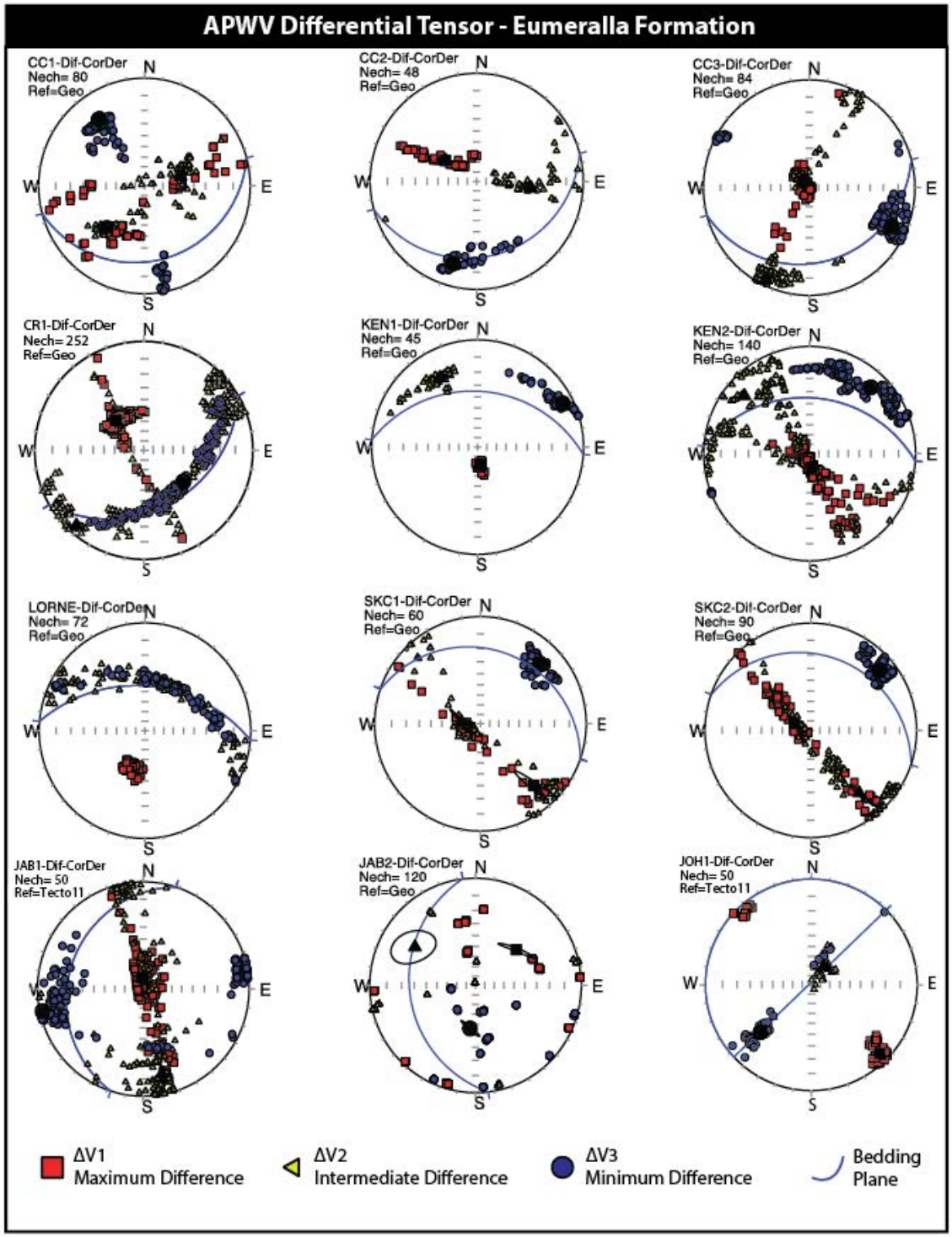

884

885 **Fig. 14:** APWV results for the differential tensors within the Eumeralla Formation.

886

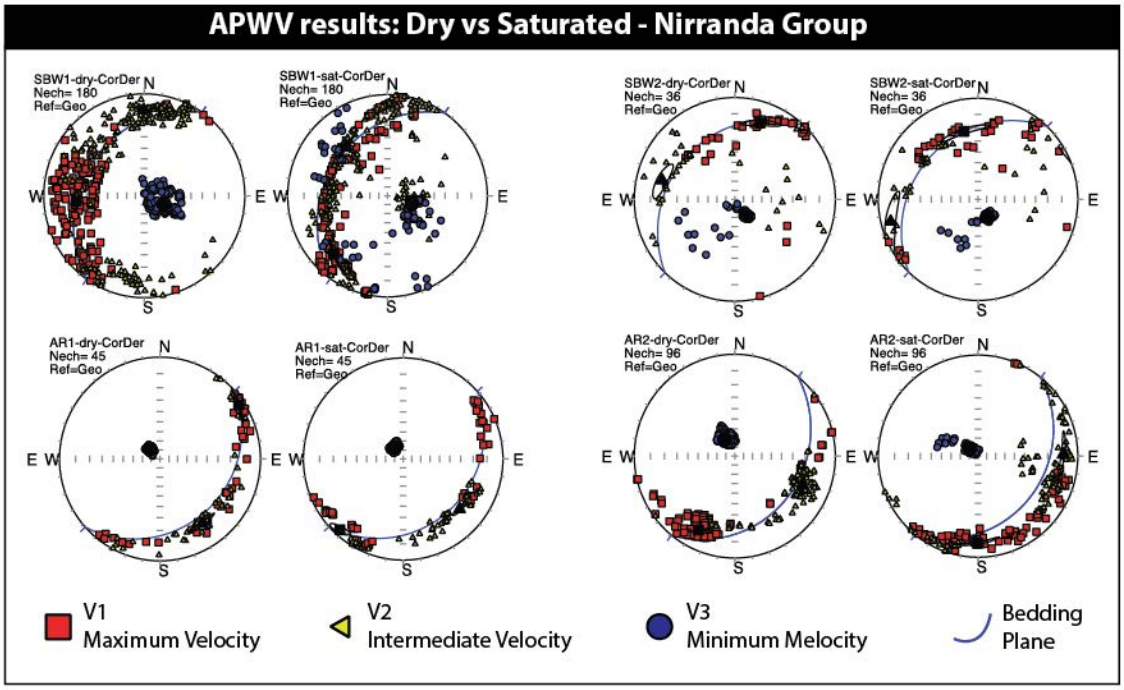

887

888 **Fig. 15:** APWV result pairs for dry (left) and saturated (right) conditions for the

889 Nirranda Group unit.

890

891

892

893

894

895

896

897

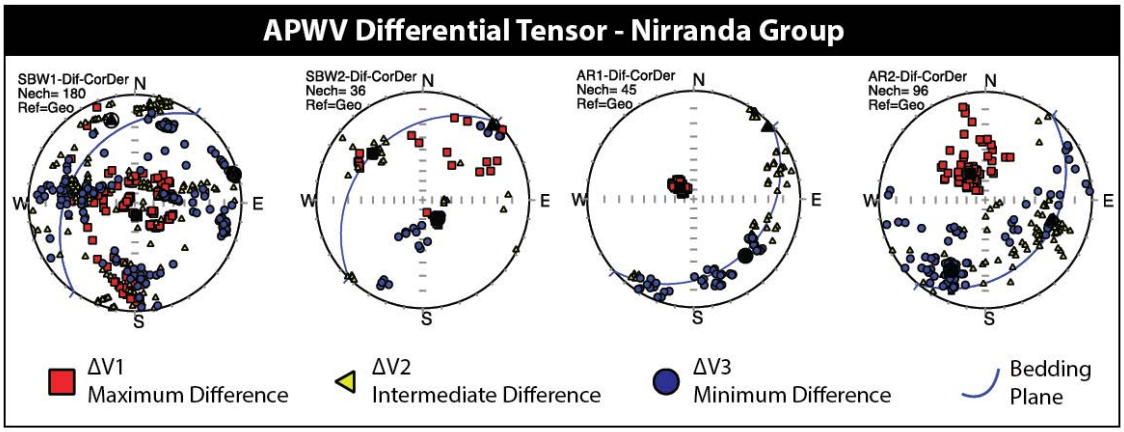

Fig. 16: APWV results for the differential tensors within the Nirranda Group.

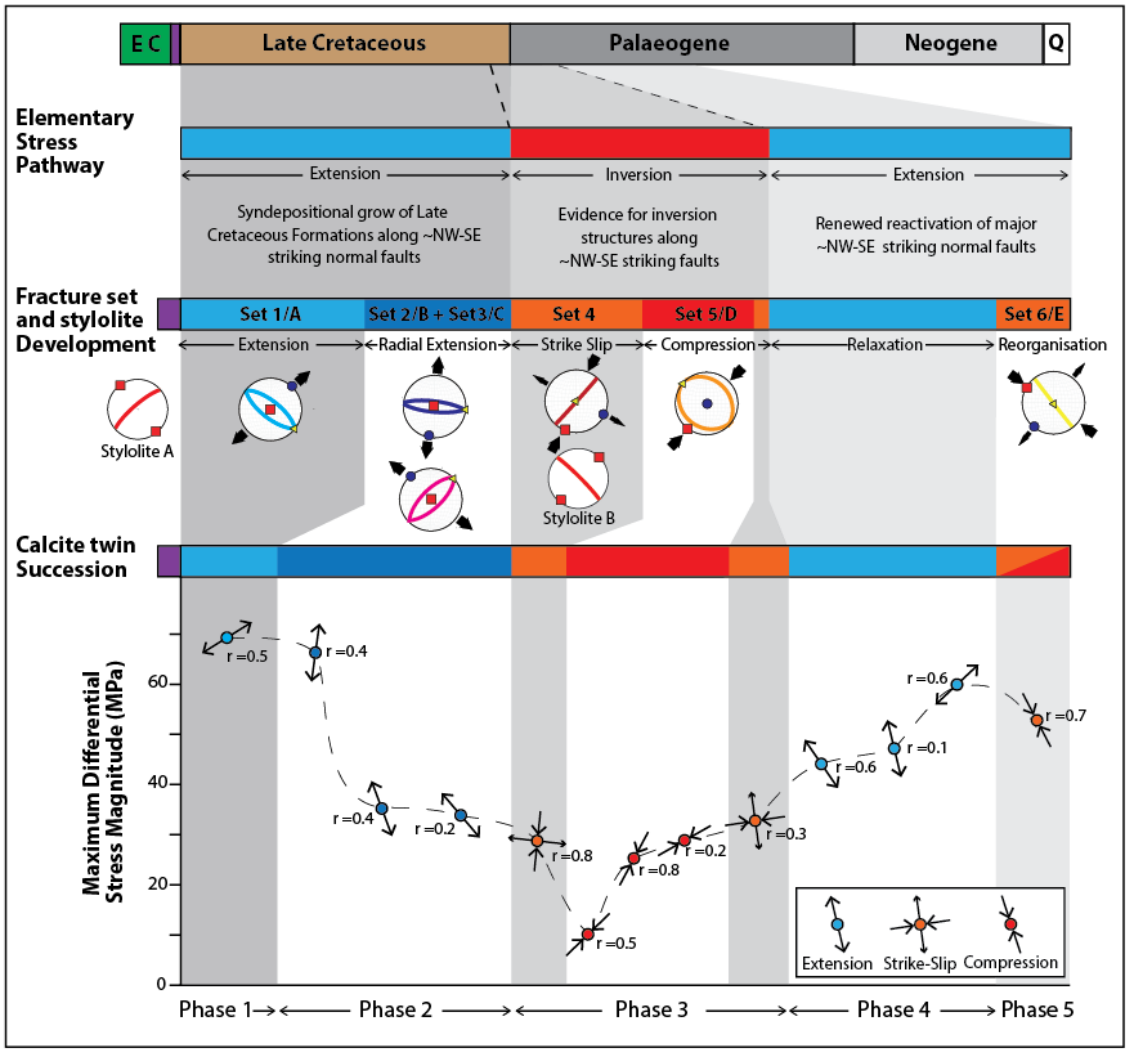

Fig. 17: (a) The multiphase evolution of the GOFS as outlined by multiscale results from Burgin and Amrouch (2019b) showing significant Late Cretaceous extension and subsequent inversion. Note the high values of differential stresses during phase 1 and 2 and the co-axiality of K1 azimuths with extensional orientations from calcite twin and natural fracture data.

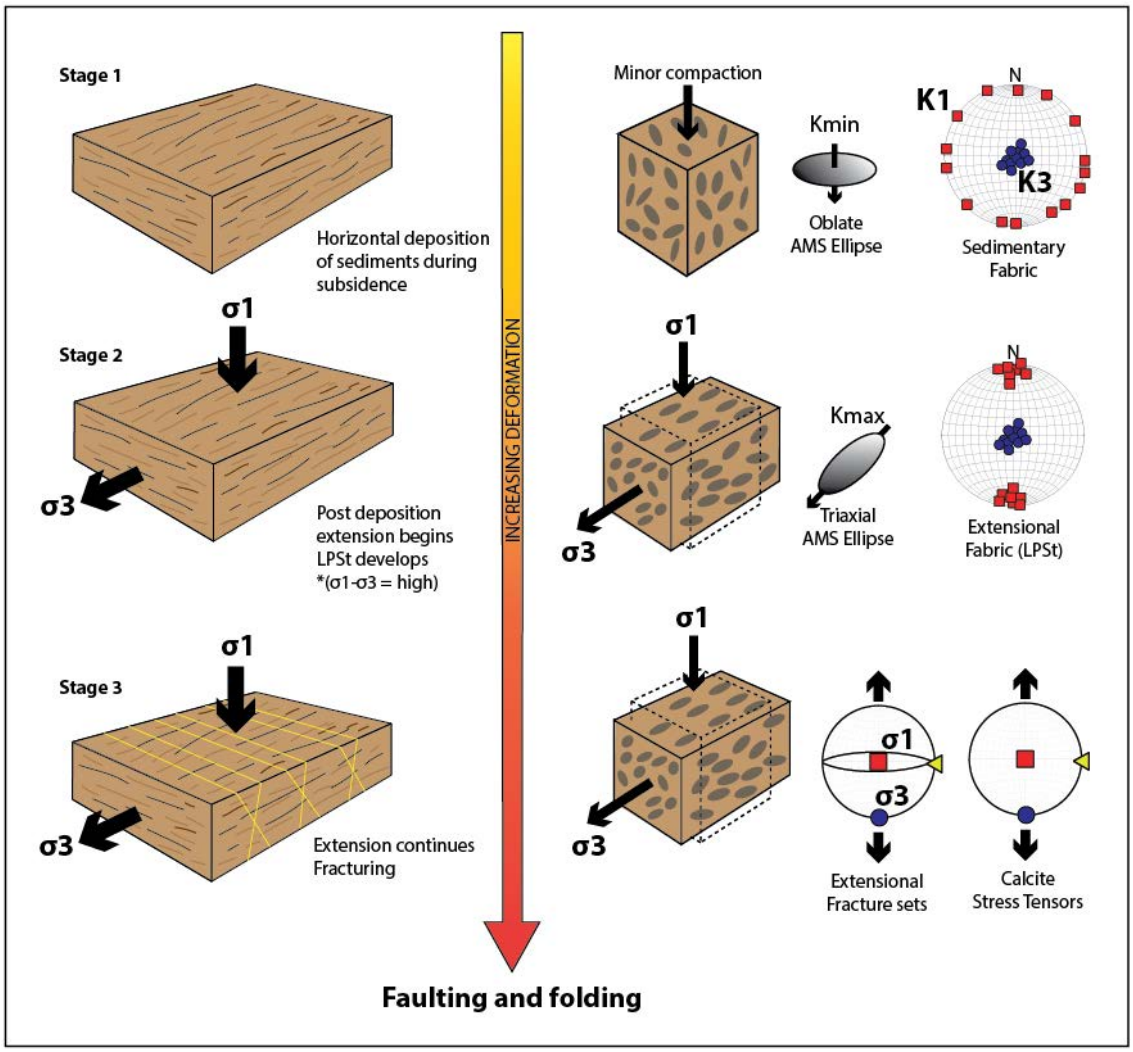

Fig. 18: Schematic diagram showing evolution of LPSt from horizontal deposition to increasing deformation associated with mesoscale fracturing. **Stage 1**: sediments deposited horizontally during a period of tectonic quiescence. Minor compaction characterised by oblate and sedimentary fabrics. **Stage 2**: LPSt, early, post depositional extension, elongation of pore fabric parallel to direction of stretching. Triaxial magnetic fabric develops. Bedding still horizontal. **Stage 3**: Deformation increases to mesoscale. Extensional fractures and calcite twins record extension with similar paleo-$\sigma 3$.

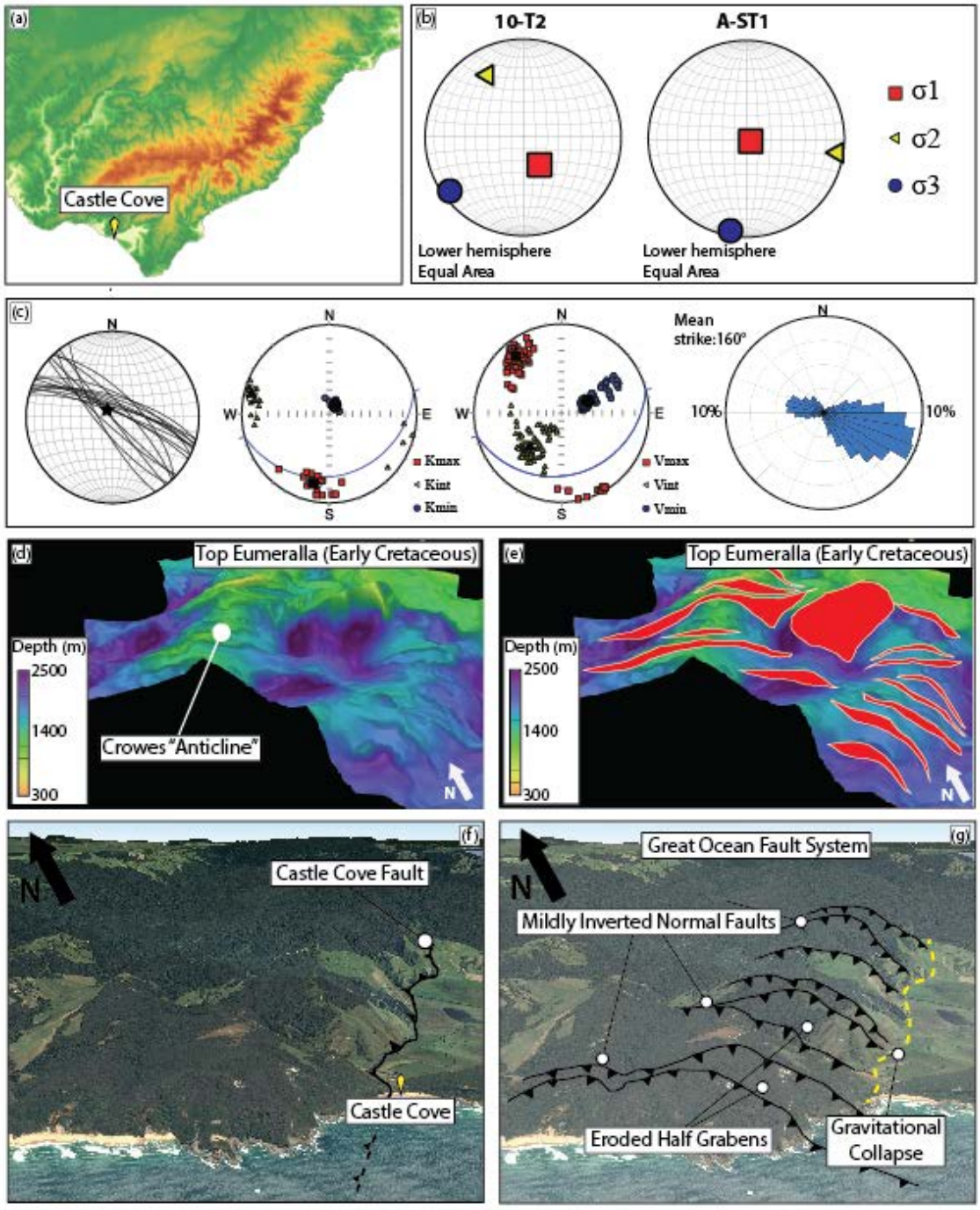

923

924

925

926

927

928

Fig. 19: Detailed integration of structural features across multiple scales at Castle Cove in the Otway Ranges (a). (b) Two early phase extensional calcite stress tensors from Burgin and Amrouch (2019b) displaying ~NE-SW and ~N-S extension (c) Multiscale datasets supportive of ~NE-SW extension, from left to right: ~NW-SE striking extensional fractures interpreted to have formed during ~NE-SW early extension at Castle Cove by Burgin and Amrouch (2019b), extensional AMS fabric from CC-1 with Kmax trending ~SSW, APWV under dry conditions suggesting the presence of a microstructural feature at the cove, a rose diagram of major extensional faults within the offshore Otway Basin ~20km due SW of Castle Cove (d) the top Eumeralla Formation from the Offshore Crowes Foot 3D (e) fault polygons showing ~NW-SE striking faults within the survey (f) the old local framework after Debenham et al. (2018) (g) The new framework after Burgin and Amrouch (2019b) for which CC-1 provides microstructural support.

Table 1: Calcite twin stress tensors derived from Etchecopars calcite twin stress inversion technique within the GOFS after Burgin and Amrouch (2019b).

Sample Name	Bedding (D/DD)	Vein (D/DD) present	Vein Set	σ1	σ2	σ3	Total Data (T/UT)	Compataible Planes (T/UT)	R value	F function	Pre/Post bedding tiliting	Differential Stress (Mpa)
10T2	45/00	77/216	1	61/143	29/328	02/236	117/60	60/49	0.5	0.69	Pre	69±14
A-ST1	16/145	78/319	sty	85/352	01/098	04/189	273/18	125/17	0.4	0.49	Pre	66±13
B-AT1	15/169	80/049	1	62/318	06/060	27/153	229/65	82/53	0.4	0.56	Pre	36±7
C-T1	15/169	75/289	3	84/359	04/225	04/135	238/50	109/36	0.2	0.72	Pre	34±7
B-BT2	15/169	80/048	1	08/182	81/359	01/092	168/67	50/45	0.8	0.39	Pre	32±6
C-T2	15/169	75/289	3	07/220	04/310	80/65	129/50	56/41	0.5	0.87	pre	13±3
A-LT2	16/145	78/319	sty	13/199	15/292	71/067	82/22	67/21	0.8	0.95	Pre	28±6
10T1	45/005	77/216	1	00/062	20/332	70/154	182/61	65/49	0.2	0.34	pre	31±6
B-BT1	15/169	80/048	1	16/088	58/205	28/350	245/67	88/57	0.3	0.15	Post	32±6
10T3	45/005	66/245	1	68/089	19/234	12/328	56/59	23/57	0.6	0.41	Post	43±9
A-LT1	16/145	78/319	sty	61/051	25/262	13/166	185/22	103/19	0.1	0.8	Post	46±9
12T2	86/131	36/243	1	59/244	05/146	34/052	118/68	51/61	0.6	1.15	Post	57±11
12T1	86/131	36/243	1	06/337	03/068	83/181	216/68	99/53	0.7	0.92	Post	50±10

948 **References**

949 Amrouch, K., Lacombe, O., Bellahsen, N., Daniel, J. M., & Callot, J. P. (2010a). Stress
950 and strain patterns, kinematics and deformation mechanisms in a basement-cored
951 anticline: Sheep Mountain Anticline, Wyoming. Tectonics, 29(1).
952
953 Amrouch, K., Robion, P., Callot, J. P., Lacombe, O., Daniel, J. M., Bellahsen, N., &
954 Faure, J. L. (2010b). Constraints on deformation mechanisms during folding provided by
955 rock physical properties: a case study at Sheep Mountain anticline (Wyoming, USA).
956 Geophysical Journal International, 182(3), 1105-1123.
957
958 Amrouch, K., Beaudoin, N., Lacombe, O., Bellahsen, N., & Daniel, J. M. (2011).
959 Paleostress magnitudes in folded sedimentary rocks. Geophysical Research Letters,
960 38(17).
961
962 Averbuch, O., de Lamotte, D. F., & Kissel, C. (1992). Magnetic fabric as a structural
963 indicator of the deformation path within a fold-thrust structure: a test case from the
964 Corbières (NE Pyrenees, France). Journal of Structural Geology, 14(4), 461-474.
965
966 Borradaile, G. J. (1988). Magnetic susceptibility, petrofabrics and
967 strain. Tectonophysics, 156(1-2), 1-20.
968
969 Borradaile, G. J., & Lagroix, F. (2000). Thermal enhancement of magnetic fabrics in high
970 grade gneisses. Geophysical Research Letters, 27(16), 2413-2416.
971

Borradaile, G. J., & Henry, B. (1997). Tectonic applications of magnetic susceptibility and its anisotropy. Earth-Science Reviews, 42(1-2), 49-93.

Briguglio, D., Hall, M., & Keetley, J. (2015). Structural evolution of the Early Cretaceous depocentres, Otway Basin, Victoria. Australian Journal of Earth Sciences, 62(6), 717-733.

Buchanan, P. G., & McClay, K. R. (1991). Sandbox experiments of inverted listric and planar fault systems. Tectonophysics, 188(1-2), 97-115.

Burgin, H. B., Amrouch, K., Rajabi, M., Kulikowski, D., & Holford, S. P. (2018). Determining paleo-structural environments through natural fracture and calcite twin analyses: a case study in the Otway Basin, Australia. The APPEA Journal, 58(1), 238-254.

Campbell I, 2012, Lakes Oil N.L. quarterly activities report. : For the three months, ended 30 June 2012. Lakes Oil N.L., Melbourne, Australia 19p.

Cayley, R. A., Taylor, D. H., VandenBerg, A. H. M., & Moore, D. H. (2002). Proterozoic–Early Palaeozoic rocks and the Tyennan Orogeny in central Victoria: the Selwyn Block and its tectonic implications. Australian Journal of Earth Sciences, 49(2), 225-254.

Cifelli, F., Mattei, M., & Rossetti, F. (2007). Tectonic evolution of arcuate mountain belts on top of a retreating subduction slab: The example of the Calabrian Arc. Journal of Geophysical Research: Solid Earth, 112(B9).

Cifelli, F., Mattei, M., Chadima, M., Lenser, S., & Hirt, A. M. (2009). The magnetic fabric in “undeformed clays”: AMS and neutron texture analyses from the Rif Chain (Morocco). Tectonophysics, 466(1-2), 79-88.

Cifelli, F., Rossetti, F., Mattei, M., Hirt, A. M., Funiciello, R., & Tortorici, L. (2004). An AMS, structural and paleomagnetic study of quaternary deformation in eastern Sicily. Journal of Structural Geology, 26(1), 29-46.

Cifelli, F., Mattei, M., Chadima, M., Hirt, A. M., & Hansen, A. (2005). The origin of tectonic lineation in extensional basins: combined neutron texture and magnetic analyses on “undeformed” clays. Earth and Planetary Science Letters, 235(1-2), 62-78.

David, C., Robion, P., & Louis, L. (2017). A single laboratory setup for investigating the anisotropy of both seismic and electrical properties in core samples. Geophysical Journal International, 210(3), 1595-1608.

Debenham, N., King, R. C., & Holford, S. P. (2018). The influence of a reverse-reactivated normal fault on natural fracture geometries and relative chronologies at Castle Cove, Otway Basin. Journal of Structural Geology, 112, 112-130.

Debenham, N., Farrell, N. J. C., Holford, S., King, R., & Healy, D. (2019). Spatial distribution of micrometre-scale porosity and permeability across the damage zone of a reverse-reactivated normal fault in a tight sandstone: insights from the Otway Basin, SE Australia. Basin Research.

Duddy, I. R., & Erout, B. (2001). AFTA-calibrated 2-D Modelling of Hydrocarbon Generation and Migration Using Temispack: Preliminary Results from the Otway Basin. Eastern Australasian Basins Symposium(485-497).

Duddy, I. R. (2003). Mesozoic, a time of change in tectonic regime. Geology of Victoria, 23, 239-286.

Duddy, I. (1994) In: Finlayson, D. M., Johnstone, D. W., Owen, A. J., & Wake-Dyster, K. D. (1994). NGMA/PESA Otway Basin Symposium, Melbourne, 20 April 1994: extended abstracts. AGSO, Record, 14.

Edwards, J., & Edwards, J. (1996). Colac 1: 250 000 map geological report. Geological Survey of Victoria.

Etheridge, M. A., Branson, J. C., & Smith, P. G. S. (1985). Extensional Basin-forming Structures in Bass Strait and their Importance for Hydrocarbon Exploration. The APPEA Journal, 25, 344-361.

Evans, M. A., & Elmore, R. D. (2006). Fluid control of localized mineral domains in limestone pressure solution structures. Journal of Structural Geology, 28(2), 284-301.

Frizon de Lamotte, D., Mercier, E., Dupre la Tour, A., Robion, P., & Averbuch, O. (1997). Cinématique du plissement et déformation interne des roches. L'exemple du pli

de Lagrasse (Aude, France). Comptes rendus de l'Académie des sciences. Série 2. Sciences de la terre et des planètes, 324(7), 591-598.

Frizon De Lamotte, D., Souque, C., Grelaud, S., & Robion, P. (2002). Early record of tectonic magnetic fabric during inversion of a sedimentary basin Short review and examples from the Corbieres transfer zone (France). Bulletin de la Société Géologique de France, 173(5), 461-469.

Fuller, M. D. (1964). On the magnetic fabrics of certain rocks. The Journal of Geology, 72(3), 368-376.

Geary, G. C. and Reid, I. S. A. (1998) Geology and prospectivity of the offshore eastern Otway Basin, Victoria. Victorian Initiative for Minerals and Petroleum Report, 55

Graham, J. W. (1996). Significance of magnetic anisotropy in Appalachian sedimentary rocks. The Earth Beneath the Continents: A Volume of Geophysical Studies in Honor of Merle A. Tuve, 627-648.

Hawton, M., & Borradaile, G. (1989). Dielectric determination of rock fabric anisotropy. Physics of the earth and planetary interiors, 56(3-4), 371-376.

Hill, K. C., Hill, K. A., Cooper, G. T., O'Sullivan, A. J., O'Sullivan, P. B., & Richardson, M. J. (1995). Inversion around the Bass basin, SE Australia. Geological Society, London, Special Publications, 88(1), 525-547.

Holford, S. P., Hillis, R. R., Duddy, I. R., Green, P. F., Tassone, D. R., & Stoker, M. S. (2011). Paleothermal and seismic constraints on late Miocene–Pliocene uplift and

deformation in the Torquay sub-basin, southern Australian margin. Australian Journal of Earth Sciences, 58(5), 543-562.

Holford, S. P., Tuitt, A. K., Hillis, R. R., Green, P. F., Stoker, M. S., Duddy, I. R., . . . Tassone, D. R. (2014). Cenozoic deformation in the OB, southern Australian margin: implications for the origin and nature of post-breakup compression at rifted margins. Basin Research, 26(1), 10-37. doi: 10.1111/bre.12035

Hrouda, F. (1991). Models of magnetic anisotropy variations in sedimentary thrust sheets. Tectonophysics, 185(3-4), 203-210.

Humbert, F., Robion, P., Louis, L., Bartier, D., Ledésert, B., & Song, S. R. (2012). Magnetic inference of in situ open microcracks in sandstone samples from the Taiwan Chelungpu Fault Drilling Project (TCDP). Journal of Asian Earth Sciences, 45, 179-189.

Jelinek, V. (1981). Characterization of the magnetic fabric of rocks. Tectonophysics, 79(3-4), T63-T67.

King, R., Holford, S., Hillis, R., Tuitt, A., Swierczek, E., Backé, G., ... & Tingay, M. (2012). Reassessing the in-situ stress regimes of Australia's petroleum basins. The APPEA Journal, 52(1), 415-426.

Kissel, C., Barrier, E., Laj, C., & Lee, T. Q. (1986). Magnetic fabric in "undeformed" marine clays from compressional zones. Tectonics, 5(5), 769-781.

Kohn, B. P., Gleadow, A. J. W., Brown, R. W., Gallagher, K., O'sullivan, P. B., & Foster, D. A. (2002). Shaping the Australian crust over the last 300 million years: insights from fission track thermotectonic imaging and denudation studies of key terranes. Australian Journal of Earth Sciences, 49(4), 697-717.

Krassay, A. A., Cathro, D. L., & Ryan, D. J. (2004). A regional tectonostratigraphic framework for the Otway Basin.

Latta, D. K., & Anastasio, D. J. (2007). Multiple scales of mechanical stratification and décollement fold kinematics, Sierra Madre Oriental foreland, northeast Mexico. Journal of Structural Geology, 29(7), 1241-1255.

Louis, L. (2003). Composite microstructural anisotropies in reservoir rocks: consequences on elastic properties and relation with deformation; Anisotropies microstructurales composites dans les roches reservoir: consequences sur les proprietes elastiques et relation a la deformation.

Louis, L., David, C., & Robion, P. (2003, December). Composite Anisotropies Revealed by P-Wave Velocity Data Under the Approximation of 2nd Rank Tensor. In AGU Fall Meeting Abstracts.

Louis, L., Robion, P., & David, C. (2004). A single method for the inversion of anisotropic data sets with application to structural studies. Journal of Structural Geology, 26(11), 2065-2072.

1121 Louis, L., Wong, T. F., Baud, P., & Tembe, S. (2006). Imaging strain localization by X-
1122 ray computed tomography: discrete compaction bands in Diemelstadt sandstone. Journal
1123 of Structural Geology, 28(5), 762-775.
1124
1125 Louis, L., Chen, T. M. N., David, C., Robion, P., Wong, T. F., & Song, S. R. (2008).
1126 Anisotropy of magnetic susceptibility and P-wave velocity in core samples from the
1127 Taiwan Chelungpu-Fault Drilling Project (TCDP). Journal of Structural Geology, 30(8),
1128 948-962.
1129
1130 Lyon, P. J., Boult, P. J., Hillis, R. R., & Bierbrauer, K. (2007). Basement controls on fault
1131 development in the Penola Trough, OB, and implications for fault-bounded hydrocarbon
1132 traps. Australian Journal of Earth Sciences, 54(5), 675-689.
1133
1134 Macdonald, J., Backé, G., King, R., Holford, S., & Hillis, R. (2012). Geomechanical
1135 modelling of fault reactivation in the Ceduna Sub-basin, Bight Basin,
1136 Australia. Geological Society, London, Special Publications, 367(1), 71-89.
1137
1138 Mattei, M., Sagnotti, L., Faccenna, C., & Funiciello, R. (1997). Magnetic fabric of weakly
1139 deformed clay-rich sediments in the Italian peninsula: relationship with compressional
1140 and extensional tectonics. Tectonophysics, 271(1-2), 107-122.
1141
1142 Mattei, M., d'Agostino, N., Zananiri, I., Kondopoulou, D., Pavlides, S., & Spatharas, V.
1143 (2004). Tectonic evolution of fault-bounded continental blocks: Comparison of
1144 paleomagnetic and GPS data in the Corinth and Megara basins (Greece). Journal of
1145 Geophysical Research: Solid Earth, 109(B2).

1146 Medwell, G. J. (1971) Structures of the Otway Ranges. Geological Survery of Victoria.
1147 Special Bulletin. 339-359.
1148
1149 Miller, J. M., Norvick, M. S., & Wilson, C. J. (2002). Basement controls on rifting and
1150 the associated formation of ocean transform faults—Cretaceous continental extension of
1151 the southern margin of Australia. Tectonophysics, 359(1-2), 131-155.
1152
1153 Moore, A. M. G., Stagg H. M. J., Norvick M. S. . (2000). Deep-water Otway Basin: A
1154 New Assesment of the Tectonics and Hydrocarbon Prospectivity. The APPEA Journal,
1155 40, 66-85.
1156 Norvick, M. S., & Smith, M. A. (2001). Mapping the plate tectonic reconstruction of
1157 southern and southeastern Australia and implications for petroleum systems. The APPEA
1158 Journal, 41(1), 15-35.
1159
1160 Oliva-Urcia, B., Roman-Berdiel, T., Casas, A. M., Pueyo, E. L., & Osacar, C. (2010).
1161 Tertiary compressional overprint on Aptian–Albian extensional magnetic fabrics, North-
1162 Pyrenean Zone. Journal of Structural Geology, 32(3), 362-376.
1163
1164 O'Brien, G., Boreham, C., Thomas, H., & Tingate, P. (2009). Understanding the critical
1165 success factors determining prospectivity—Otway Basin, Victoria. The APPEA
1166 Journal, 49(1), 129-170.
1167
1168 Owens, W. H., & Bamford, D. (1976). A Discussion on natural strain and geological
1169 structure-Magnetic, seismic, and other anisotropic properties of rock

fabrics. Philosophical Transactions of the Royal Society of London. Series A, Mathematical and Physical Sciences, 283(1312), 55-68.

Perincek, D., Simons, B., & Pettifer, G. R. (1994). THE TECTONIC FRAMEWORK AND ASSOCIATED PLAY TYPES OF THE WESTERN OTWAY BASIN, VICTORIA, AUSTRALIA. The APPEA Journal, 34(1), 460-478.

Robion, P., David, C., Dautriat, J., Colombier, J. C., Zinsmeister, L., & Collin, P. Y. (2014). Pore fabric geometry inferred from magnetic and acoustic anisotropies in rocks with various mineralogy, permeability and porosity. Tectonophysics, 629, 109-122.

Robert, R., Robion, P., Souloumiac, P., David, C., & Saillet, E. (2018). Deformation bands, early markers of tectonic activity in front of a fold-and-thrust belt: Example from the Tremp-Graus basin, southern Pyrenees, Spain. Journal of Structural Geology, 110, 65-85.

Robion, P., Grelaud, S., & de Lamotte, D. F. (2007). Pre-folding magnetic fabrics in fold-and-thrust belts: Why the apparent internal deformation of the sedimentary rocks from the Minervois basin (NE—Pyrenees, France) is so high compared to the Potwar basin (SW—Himalaya, Pakistan)?. Sedimentary Geology, 196(1-4), 181-200

Robson, A. G., S. P. Holford, R. C. King, and D. Kulikowski (2018). Structural evolution of horst and half-graben structures proximal to a transtensional fault system determined using 3D seismic data from the Shipwreck Trough, offshore Otway Basin, Australia, Marine and Petroleum Geology, 89(3), 615-634, doi:10.1016/j.marpetgeo.2017.10.028.

Robion, P., Grelaud, S., & de Lamotte, D. F. (2007). Pre-folding magnetic fabrics in fold-and-thrust belts: Why the apparent internal deformation of the sedimentary rocks from the Minervois basin (NE—Pyrenees, France) is so high compared to the Potwar basin (SW—Himalaya, Pakistan)?. Sedimentary Geology, 196(1-4), 181-200.

Sagnotti, L., Faccenna, C., Funiciello, R., & Mattei, M. (1994). Magnetic fabric and structural setting of Plio-Pleistocene clayey units in an extensional regime: the Tyrrhenian margin of central Italy. Journal of Structural Geology, 16(9), 1243-1257.

Sans, M., Vergés, J., Gomis, E., Parés, J. M., Schiattarella, M., Travé, A., ... & Doulcet, A. (2003). Layer parallel shortening in salt-detached folds: constraint on cross-section restoration. Tectonophysics, 372(1-2), 85-104.

Tarling, D., & Hrouda, F. (Eds.). (1993). Magnetic anisotropy of rocks. Springer Science & Business Media

Tassone, D. R., Holford, S. P., Duddy, I. R., Green, P. F., & Hillis, R. R. (2014). Quantifying Cretaceous–Cenozoic exhumation in the OB, southeastern Australia, using sonic transit time data: Implications for conventional and unconventional hydrocarbon prospectivity. AAPG Bulletin, 98(1), 67-117.

Tassone, D. R., Holford, S. P., King, R., Tingay, M. R., & Hillis, R. R. (2017). Contemporary stress and neotectonics in the Otway Basin, southeastern Australia. Geological Society, London, Special Publications, 458(1), 49-88.

Thomsen, L. (1986). Weak elastic anisotropy. Geophysics, 51(10), 1954-1966.

Tsvankin, I. (1997). Anisotropic parameters and P-wave velocity for orthorhombic media. Geophysics, 62(4), 1292-1309.

Zoback, M. L., Zoback, M. D., Adams, J., Assumpcao, M., Bell, S., Bergman, E. A., ... & Fuchs, K. (1989). Global patterns of tectonic stress. Nature, 341(6240), 291.

Chapter 4.5: Manuscript 6

Exploring the complexities of sub-surface fluid flow at passive continental margins: A case study using geomechanical modelling, from the Otway Basin, Australia

This unpublished manuscript will be submitted to the international and peer-reviewed journal *Marine and Petroleum Geology*.

Statement of Authorship

Title of Paper: Exploring the Complexities of Sub-Surface Fluid Flow at Passive Continental Margins: A case study using geomechanical modelling, from the Otway Basin, Australia

Publication Status: Unpublished and Unsubmitted work written in a manuscript style

Publication Details: Burgin, H. B. and Amrouch, K. (2019c). Exploring the Complexities of Sub-Surface Fluid Flow at Passive Continental Margins: A case study using geomechanical modelling, from the Otway Basin, Australia (in prep)

Principal Author: Hugo Bonython Burgin

Contribution: Extraction of faults and fractures. Modelling and interpretation. Writing of paper (80%)

Certification: This paper reports on original research I conducted during the period of my Higher Degree by Research candidature and is not subject to any obligations or contractual agreements with a third party that would constrain its inclusion in this thesis. I am the primary author of this paper.

Signed: **Date:** 05/03/2019

Co-Author Contributions

By signing the Statement of Authorship, each author certifies that:

- **i.** The candidate's stated contribution to the publication is accurate (as detailed above);
- **ii.** Permission is granted for the candidate to include the publication in the thesis; and
- **iii.** The sum of all co-author contributions is equal to 100% less the candidate's stated contribution.

Name of Co-Author: Dr Khalid Amrouch

Contribution to Paper: Assistance with paper writing. Providing constructive feedback on modelling scenarios and interpretations (20%)

Signed: **Date:** 05/03/2019

Exploring the complexities of sub-surface fluid flow at passive continental margins: A case study using geomechanical modelling, from the Otway Basin, Australia

*Hugo B. **BURGIN**[a] (hugo.burgin@adelaide.edu.au)

Khalid **AMROUCH**[a] (khalid.amrouch@adelaide.edu.au)

[a]Australian School of Petroleum, University of Adelaide, North Tce, 5005, Adelaide, Australia

*Corresponding Author: Hugo B. Burgin (08 8313 8000)

Abstract

Passive continental margins typically display parallel relationships between fault strike and the orientation of maximum horizontal stress. This study explores this relationship using techniques of geomechanical modelling on fault data from eight three dimensional (3D) seismic surveys, from the Otway Basin, Australia, where the regime of in situ stress is debated.

Fault dilation tendency is modelled on more than 900 faults from across the basin at varying depth, alongside the stability of natural fractures extracted from 7 wellbore image logs. High angle faults striking parallel to the maximum horizontal stress are at a high risk of dilation, irrespective of the regime of in situ stress, although shallow dipping faults have a reduced risk under strike slip and extension scenarios. Similarly striking fractures require very low increases in pore pressure in order to be reactivated (<5MPa under a strike slip scenario). The results of this study explain why fault seal in Otway Basin has historically been so poor and can be correlated with the nature of successful hydrocarbon fields within the basin. The results also indicate that while natural fracture networks may be optimally oriented for reactivation, there is a high associated risk with respect to up-dip contamination of regional aquifer systems along

steeply dipping ~NW-SE striking faults. Relationships between the distribution of volcanic material and the results of our modelling are in good accordance with each other. This work acts as a case study for frontier passive margin settings such as the Ceduna Sub-Basin. Where in situ stresses may be poorly defined, and has a number of consequences for the development of petroleum, geothermal and carbon storage industries within the basin.

1. Introduction

Passive margin sedimentary basins have long been identified as potential high-value areas for hydrocarbon exploration and production. With continental ocean-wards fronting settings accounting for in excess of 35% of the world's giant oil and gas fields (Mann et al., 2003), representing almost 67% of conventionally discovered global oil and gas reserves.

Their success is in part due to the fact they can host a plethora of prospective play styles, including; major deltaic depocentres (e.g. Cenozoic Gulf of Mexico; Venezuela, Brazil), slope by pass systems (Ghana, Equatorial Guinea; India) carbonate platforms and reefs (Pakistan, Senegal, Morocco), deep water fold belts (Mozambique, Nigeria), syn-rift sections (Gabon, India, Norway) and a variety of deep water petroleum systems (Norway, Australia, Brazil) (Levell et al., 2010). In addition to hosting petroleum systems, passive margin basins are often targets for carbon capture and storage and geothermal energy projects. Also often containing evidence for historic and active volcanism.

Good examples of these passive continental margin regions are the rift basins of Australia's Southern Rift System (Wilcox and Stagg, 1990). Characterising the well explored petroleum provinces of the Bight, Otway and Bass Basins where volcanic activity has also been documented in the form of dyke fed volcanoes and cones, sills, dykes and other less defined igneous features (Holt et al., 2013; Reynolds et al., 2018; Velayatham et al., 2019). In the Otway Basin, this recent volcanism and an elevated geothermal gradient has distinguished the region as one of the most favourable in Australia for Geothermal energy (Bahadori et al., 2013). While naturally occurring CO2 within shallow reservoirs marked the basin as an ideal target for Australia's largest and longest running CO2 storage project (CO2, CRC).

Although hydrocarbons, water, carbon dioxide and igneous materials are the result of distinctly separate processes, at their core they are all reliant on the movement of fluid within the sub-surface. Structural permeability, in the form of faults is of particular importance to this process as it controls migration pathways for hydrocarbons, which can contaminate natural aquifers, and igneous material.

The primary control on structural permeability is the regime of in-situ stress within the Earth's crust, which changes with depth. In situ stress not only governs the stability and likelihood of fault slip or reactivation due to increases in fluid pressure, but the likelihood of dilation. As such the relationship between in situ stress, depth and fault and fracture geometry is key with respect to any form of sub-surface fluid flow.

Utilising faults extracted from eight 3D seismic surveys and natural fracture data from 7 wells from the Otway Basin, Australia, the aim of this study is to explore how geomechanical modelling can be combined with petroleum industry and geological data to better constrain the movement of fluid within the sub-surface. Including; insights into the migration pathways of hydrocarbons into conventional reservoir systems, assessing fault and fracture reactivation risk during unconventional production and any relationships between fault geometry, depth and patterns of neotectonic volcanic activity.

As with the rest of south eastern Australia, the current stress field within the Otway Basin represents somewhat of an enigma. The general orientation of maximum horizontal stress, striking ~NW-SE, nearly orthogonal to the azimuth of plate motion, which is not to be expected, given the plates northwards movement (Sandiford et al., 2003). This has resulted in a parallel relationship between maximum horizontal stress and major fault strike that sets the

Otway Basin apart from the other sedimentary basins of Australia (**fig. 1**). While this correlation would suggest an extensional regime of in-situ stress, typical of passive margin sedimentary basins, assessments of in-situ stress within the basin favour a strike slip (Nelson et al., 2006; Rajabi et al., 2017b) or compressional regime (King et al., 2012; Tassone et al., 2017). As a result, this basin represents one of the final regions of Australia where the regime of in-situ stress is yet to be fully constrained (Rajabi et al., 2017b; Tassone et al., 2017).

Given this unknown environment of in situ stress, and the continued role that passive continental margins like the Otway Basin around the world will continue to play with respect to hydrocarbons, CO2 storage and geothermal energy. We find it pertinent to investigate how variations in in-situ stress may affect sub-surface fluid flow, using the distribution of igneous material at the end of the study, as geological evidence for our modelling results.

2. Geological Setting

2.1 Tectonic History

The Jurassic to Quaternary Otway Basin is an approximate NW-SE trending sedimentary province along the south-eastern margin of Australia, forming part of the Southern Rift System (Stagg et al., 1990) that developed as a result of the breakup of Gondwana. For many years, the basin was divided into two distinct portions on the basis of variable fault trends at approximately 143ºE. Although these discontinuities have been proven far less apparent of late, with ~NW-SE striking faults seen to dominate the structural framework across the basin (Burgin and Amrouch, 2019b). That being said, N-S striking fabrics are present within the basin, but predominantly isolated to the Shipwreck Trough (**fig.2**) (Robson et al., 2018).

In the Tithonian to Barremian ~N-S oriented rifting was concentrated on shore (Lyon et al., 2007; Burgin and Amrouch, 2019a) and led to the creation of significant accommodation space and the deposition of the Crayfish Sub-Group units (**fig. 3**). Formations which are of leading interest for geothermal projects, particularly in the western Otway Basin (Goldstein et al., 2009; Ryan et al., 1995; Krassay et al., 2004). Ensuing Aptian to Albian thermal subsidence resulted in the deposition of the laterally asymmetric Eumeralla Formation, which is thickest in the east (Hill et al., 1995; Krassay et al., 2004). Outcropping within the on-shore Otway Ranges, the formation, represents the main unconventional prospect and, contains extensive inter-beds of fluvio-lacustrine shales, coals, feldspathic and volcaniclastic sandstones (Hill et al., 1995; Duddy et al., 2003; Krassay et al., 2004). The unit is also the source rock for the gas accumulations in the eastern basin (O'Brien et al., 2009). The top of the Eumeralla Formation or Top Otway Group, is marked by a regional unconformity (Geary and Reid, 1998).

Renewed rifting oriented ~NE-SW, defined by magnitudes of extensional paleostress as high as 69MPa, (Lyon et al., 2007; Burgin and Amrouch, 2019a; 2019b) began at the start of the Late Cretaceous, coinciding with the deposition of the Sherbrook Group (Geary and Reid, 1998). This period of extension was followed by a brief and rapid phase of ~NE-SW oriented basin inversion beginning as early as mid-Maastrichtian, due to stress reorganisation across southern Australia (Burgin and Amrouch, 2019b). The cessation of active rifting and the retreat of the spreading centre towards the south, resulted in relaxation and the deposition of the post-break-up Wangerrip and Nirranda Groups in the Palaeocene and Late Eocene and Plio-Pleistocene Whalers Bluff Group (Krassay et al., 2004).

2.2 Miocene – Recent Stress Development

In-situ stress within southeastern Australia (**fig. 1**) has been studied a number of times (e.g. Sandiford et al., 2008: Tassone et al., 2017) and shown to be unusual due to the oblique nature between relative plate motion and the maximum horizontal stress (σH). Plate scale modelling suggests that the stress field reflects coupling at the Australian and Pacific Plate boundary, consistent since the late Miocene (Sandiford et al., 2003; Hillis et al., 2008). The in-situ stress orientation within the Otway Basin has been constrained by many studies (eg: Hillis and Williams, 1992, 1993; Hillis et al., 1995; Hillis and Reynolds., 2000; Reynolds and Hillis, 2000; Reynolds et al., 2003; Nelson et al., 2006; Van Ruth et al., 2007; Burgin 2015; Bailey et al., 2014. 2016; Rajabi et al., 2017a; Tassone et al., 2017) and shown to be approximately NW-SE. That being said, the orientations of maximum and minimum horizontal stress only assist in determining the regime of in-situ stress, as the component of vertical stress must also be considered, and the relative stress magnitudes of each principal stress also calculated. A process for which petroleum industry leak off test and density data, is commonly used. In the Otway Basin, dependant on their approach and location, studies completing this calculation suggest an extensive regime (Berard et al., 2008; Vidal Gilbert et al., 2009), strike slip regime (Hillis et al., 1995; Hillis and Reynolds, 2000; Nelson et al. ,2006; Vidal Gilbert et al., 2009; Rajabi et al., 2017b) and reverse stress regime (King et al., 2012; Tassone et al., 2017). The last most likely isolated in to the eastern basin, and the section surrounding the Otway Ranges.

Some neotectonic geological features within the Otway Basin indicate evidence for a ~NW-SE compressional stress regime (Cooper and Hill, 1997; Holdford et al., 2011; King et al., 2012; Tassone et al., 2017) although evidence from Burgin and Amrouch (2019b) reveals much of it may be misattributed, representing ~Latest Cretaceous, rather than Miocene – recent inversion. Other studies have cited the high levels of seismicity, especially along the continental shelf, as possible evidence for extensional stresses. It is apparent that more work needs to be completed,

to accurately constrain the in-situ stress regime of the Otway Basin. As such, in this study all three stress variations are explored.

2.3 Otway Basin petroleum systems, oil and gas fields

Based on their age, source rocks, and occurrence in time and space, hydrocarbons along Australia's southern margin have been assigned to the Austral Petroleum Supersystem (APS) (Bradshaw, 1993; Summons et al., 1998).

In the Otway Basin, hydrocarbons within two sub divisions of this system dominate (Edwards et al., 1999; O'Brien et al., 2009). The Austral-1 (A1) subdivision of the APS includes upper Jurassic to Cretaceous fluvio-lacustrine shales, present in the western Otway Basin within the Crayfish Sub group and the Casterton formation (Edwards et al., 1999). Economic discoveries in the A1 system have been limited to the Penola Trough (**fig. 2**).

The Austral 2 (A2) division of the APS is concentrated in the eastern sector of the basin, sourced from the lower Cretaceous coals towards the base of Eumerella Formation (Tupper et al., 1993). Multiple gas accumulations within the overlying Late Cretaceous formations are recognised in this division, including in the Waarre and Heathfield Sandstone members. The Minerva Gas field, located within the Schomberg-Minerva 3D used as part of this study was discovered in the mid-90s with approximately 575 BCF of gas in place (Luxton et al., 1995).

In the eastern Otway Basin, two distinct stages of hydrocarbon generation, one in the Early Cretaceous and the other during the tertiary are believed to be responsible for most hydrocarbon shows (Edwards et al., 1999). While generation occurred within the high heat flow rifting phase of the Early Cretaceous, most accumulations were likely devastated by successive and complex

tectonic evolution. It is now assumed most economic hydrocarbons were generated from the Eumerella Supersequence sometime within the Cenozoic (Duddy, 1997).

Discoveries at La Bella 1 (217 BCF GIP), Minerva 1 (558 BCF GIP), Geographe (500 BCF GIP) and Thylacine 1 (600 BCF) (**fig. 1**) coincide with a large number of dry wells and small shows (O'Brien et al., 2009). The basin's contribution towards Australia's overall hydrocarbon production and reserves remains minimal, compared to the continent's major producing regions such as the Cooper Eromanga Basin, Browse, Canarvon and Gippsland Basin.

Possible reasons for varying success across the basin may be differences in maturity levels of source rocks within the A1 and A2 systems (O'Brien et al., 2009). Structural styles may also play a role in success, as the most successful fields in the east (e.g. Minerva, La Bella) are present within a system that has been subjected to significant structural inversion (Burgin and Amrouch, 2019b). Reserves as of 2009 within the different systems and basin regions is outlined in table 1.

The Otway Basin has also been identified as having the potential for the development of unconventional petroleum plays, especially within the onshore section of the Part Campbell Embayment (**fig. 2**). Where source rocks within the Eumeralla Formation are likely at their maximum burial temperature (Tassone et al., 2014).

2.4 Geothermal Energy and Carbon Capture and Storage Projects

The Otway Basin is prospective for geothermal energy and carbon storage projects. Due to high geothermal gradients and the potential of latent heat distribution from recent volcanic events, Jurassic – Early Cretaceous sediments in the western Otway Basin have been identified

as potential geothermal plays. Especially where Palaeozoic granites dip beneath on lapping units, which have been identified by petroleum wells (Goldstein et al., 2009).

In the eastern basin, the CO2CRC Project is situated inland, within the Port Campbell Embayment (**fig. 2**). The project is of global significance involving the development and implementation of rigorous monitoring and verification research. Complementing the demonstration of subsurface CO_2 storage. Stage one of the project has seen over 65,000 tonnes of CO_2 injected and monitored in a depleted gas reservoir within the Late Cretaceous to Turonian Waarre Formation, with additional injections and monitoring planned for the future (CO_2 CRC, 2016).

2.5 Volcanism

In onshore parts of the Otway Basin the record of Cenozoic volcanism is relatively well studied (e.g. Price et al., 2003; Holt et al., 2013). The Newer Volcanics Province (**fig. 2**) represents a volumetric peak of between 5-0 Ma, although volcanic activity was likely near continuous throughout much of the Cenozoic. The province occupies roughly 15,000km^2 within the onshore Otway Basin, containing a variety of volcanic features including lava flows, cinder cones, shield volcanos and maars (Joyce, 1988; Holt et al., 2013). The most recent igneous activity in the region characterising the Gambier volcanic province in the western Otway Basin, suggesting an eruption as recent as 5 Ka (Demidjuk et al., 2007).

Identification of igneous material within the offshore Otway Basin is less well constrained, however sills, lava aprons, and possible hydrothermal vents have been identified, mainly concentrated around the central and eastern sectors (Holford et al., 2012). Their timing predates the Newer Volcanics Provinces, most likely occurring between ~45-37Ma, coinciding with

igneous events throughout southeastern Australia at that time (Holford et al., 2012). Volcanic activity within the neighbouring Bass and eastern Bight Basin has also been documented, with early to mid-Miocene (Reynolds et al., 2018) and Mid-Eocene (Schofield and Totterdell, 2008) timing. In the context of this study, the distribution of igneous material is investigated across the basin, exploring any potential relationship between the spatial distribution of material, and the results of the modelling.

3 Methodology

3.1 Seismic Reflection Data

This study uses fault data extracted from eight 3D seismic surveys from on and offshore parts of the western and eastern Otway Basin.

In the western basin, the Tillbooroo 3D, Balnaves-Haselgrove 3D, St George 3D are onshore while the Carpenter 3D lies less than 20km offshore. The onshore surveys overlie the Penola Trough ~NW-SE trending failed riff segment containing the Ladbroke, Redman, Haselgrove and Sawpit gas fields (**fig. 2**).

The Champion-Hercules, Schomberg-Minerva, Crowes Foot and Brandt 3D surveys lie within offshore areas of the eastern sector of the basin. The Champion-Hercules and Schomberg-Minerva surveys overlying portions of the Shipwreck Trough, containing the Casino, Halladale, La Bella, Geographe and Minerva gas fields (**fig. 2**).

All surveys were converted from two way time to depth using either checkshot velocity data from wells within the survey area, or time depth trends derived from Petokovic (2004) to limit the effect of time to space migration on the nature of fault geometry.

3.2 Geomechanical Fault and Fracture Modelling

3.2.1 Dilation Tendency

For any given present day stress environment, the relative risk of fault reactivation can be assed assuming that fault geometry, pore pressure and the rock failure envelope are well constrained. Such investigations have shown to be successful in Australia (Kulikowski et al., 2016; Kulikowski, 2017) and other basins around the world (Morris et al., 1996).

The capability of a fault plane to act as a conduit for fluid under in-situ stress or to undergo reactivation in a tensile fashion is modelled by the dilation tendency (Barton et al., 1995; Ferrill and Morris, 2003). The reactivation of faults and the consequential increase in fault permeability is undesirable within the oil and gas and carbon dioxide storage industries. As reactivation results in leakage and a subsequently reduced reservoir capacity, in addition to unwarranted tertiary migration and potential formation damage. For geothermal energy, an accurate constraint on fault permeability is needed to predict the movement of fluid within the system.

Modelling of dilation tendency (**fig. 4**) produces a relative value, governed by the effective normal stress acting on the fault plane when normalised to the differential stress. This directly impacts fault aperture (Barton et al., 1995; Ferrill and Morris, 2003; Jolie et al., 2015). Therefore, dilation tendency predicts the likelihood of migration along a potentially permeable pathway and is most applicable in environments that are fault sealing or have been penetrated by faults along with their overlying seal. An existing plane has an increased tendency towards dilation as the orientation of normal stress approaches the minimum in-situ stress orientation.

Move2017.2 was used to generate the results, separating each fault plane from the seismic interpretation into smaller polygons using a triangular dislocation theory. For the results of our modelling, each pole to plane represents a single polygon.

3.2.2 Fracture Stability

The analysis of fracture stability or FAST analysis differs from dilation tendency in a subtle manner. While, dilation tendency models a response within an effectively static system, FAST analysis provides an estimate of the increase in pore pressure, from the static modelled conditions, needed for reactivation (**fig. 4**). This can be understood in a straight forward fashion, as an increase in pore pressure (ΔP_P) will reduce the effective stress acting on the fault or fracture plane, shifting the Mohr's circle towards to the left until the reactivation curve is intersected.

Fracture stability is of particular important for carbon dioxide sequestration and unconventional production where the injection of fluids into the reservoir or source rock environment can directly influence reactivation by decreasing effective stress acting on the fracture (Hung and Wu, 2012).

3.3.3 Modelling Parameters

Modelling parameters were derived from the consideration of number of sources (**table 2**) that have defined both in-situ stress orientations and in-situ stress magnitudes (Hillis et al., 1995; Lyon et al., 2005; Nelson et al., 2006; Berard et al., 2008; Vidal-Gilbert et al., 2010; Bailey et al., 2014; Tassone et al., 2017) with different parameters for each basin region (western and eastern) selected on the basis of the current debate regarding the insitu stress regime.

Faults within each 3D survey were modelled with a unique water depth (if applicable) and profile depth typical of the regional target for hydrocarbon prospectivity (table 3).

4. Results

4. 1 Faults extracted from 3D seismic

The discussion of fault geometries used for modelling is divided between the western and eastern basin.

4.1.1 Western Basin

Faults extracted from the four 3D surveys within the western basin (Burgin and Amrouch, 2019a), show three major fault trends, including ~NW-SE, ~NE-SW and ~E-W striking networks (**fig. 5**).

Faults with a ~NW-SE strike are the most dominant. All faults within the western basin display normal offset of reflectors and mainly dip between 50° and 70° (**fig. 5**) with major faults dipping towards the south and south west accompanied by synthetic and antithetic faults. There is no evidence for normal fault inversion or compressional faulting.

The Tillbooroo 3D survey, shows a major ~NW-SE striking trend and a minor ~NE-SW striking set of faults. Forming a series of small horst and graben structures orthogonal to the major fault blocks within the survey.

The St George 3D, contains normal faults with a dominant ~NW-SE strike. That dip towards the NE. Although the influence of a minor E-W striking trend dipping north, is also evident within the survey area, particularly in the south.

The Balnaves-Haselgrove 3D contains two major interacting fault fabrics: ~NW-SE striking faults in the western and eastern sections of the survey that dip mainly NE, intersect a large ~E-W striking array of north and south dipping normal faults, dominated by a large southerly dipping listric fault.

Offshore, the Carpenter 3D survey (**fig. 6**), contains a complex array of high angled conjugate NW-SE striking normal faults that dip primarily towards the SW. The trend is especially obvious along horizon maps utilising the incoherence attribute (**fig.6**).

4.1.2 Eastern Basin

In the eastern basin, ~NW-SE striking faults continue to dominate the structural fabric.

The Brandt survey (**fig. 7**) is the most southerly of the data sets. Positioned almost directly over a section of the continental shelf NW of Tasmania (**fig. 2**). The survey is highly faulted, with a large network of mainly high-angled – 50° - 80° - normal faults that dip towards the southwest.

Covering the western edge of the Great Ocean Fault System (Burgin and Amrouch, 2010b), the Champion- Hercules survey also contains a major ~NW-SE striking fault trend. Fault dip is steep between 50-70° with southwest dipping faults more common that those dipping north east (**fig. 7**). The parallel interaction of multiple NW-SE striking faults controls the architecture of the survey, producing a series of tilted fault block structures.

The Schomberg-Minerva 3D (Burgin and Amrouch, 2019b) also displays a major ~NW-SE faulting fabric consistent with the other surveys. Fault dip is between 50-80° and dip direction

is primarily towards the south west defining a series of tilted fault blocks (**fig. 7**). The presence of a minor N-S and NNE-SSW striking sets of high angle faults were interpreted at the eastern edge of the survey.

As with our other datasets ~NW-SE striking normal faults dominate the architecture of the Crowes Foot 3D (Burgin and Amrouch, 2019b). The survey images the most comprehensive evidence for the Great Ocean Fault System as presented by Burgin and Amrouch, (2019b). Extensional networks of faults within the survey are pervasive and high angle (50-80º) (**fig. 8**) and where low angle faulting is defined, it is due to a gradual transition a low dip listric style, typical of continental margins and previously described within the region (Etheridge et al., 1986; Lister et al., 1989)

While ~NW-SE striking faults define the structural fabric of the surveys, in the case of the Champion-Hercules, Schomberg-Minerva and Crowes Foot 3D surveys, the lateral interaction of faults and concave nature produces a minor faulting trend that strikes more ~E-W rather than ~NW-SE. This is particularly evident within some deeper sections of the surveys and is reflected in our stereographic projections of poles to planes plunging towards the north and south (**fig. 7, 8**).

Though normal offset is maintained in most cases, the Champion-Hercules, Schomberg-Minerva and Crowes Foot 3D surveys all show evidence for ~NE-SW fault inversion structures, mainly in the form of inverted and bulging collapsed graben (**fig. 8**). Which are especially visible in the Schomberg-Minerva 3D, and the rotation and bulging of half grabens within the Crowes Foot 3D. For a detailed description of the Great Ocean Fault System and its inversion, it is recommended the reader consult Burgin and Amrouch (2019b).

4.2 Natural fractures from Image Log Data

Natural fractures were interpreted within the eastern Otway Basin, across seven well bore image logs (**table 4**), five interpretations extracted from Burgin and Amrouch (2019b). **Fig. 9** displays natural fracture data. High angle fractures striking ~NW-SE and ~NE-SW dominate the dataset, particularly onshore, where formation micro-imager (FMI) logs from both Wild Dog Road-1 and Bellarine-1 display sets of high angle, extensive fractures within image logs of particularly high quality (**fig. 10**). Fracture geometries within the dataset are reflective of those obtained from detailed outcrop mapping within the Otway Ranges (Burgin et al., 2019; Burgin and Amrouch, 2019b). However across the wells, fracture density varies significantly, suggesting that sub-surface natural fracture networks within the eastern offshore Otway Basin may not be distributed evenly.

4.3 Modelling of dilation tendency

In both sections of the basin, the three scenarios of stress are modelled (**table 3**). The dilation tendency results indicate the network of faults that define the basins major ~NW-SE fabric are at a high risk of dilation irrespective of stress regime. However, there are considerable differences between the dip angles of faults and their risk of dilation, which varies between stress regimes.

Modelling results (**fig. 11, fig. 12**) show that under a strike-slip stress regime, minor ~NE-SW striking faults are at a low risk of dilation. Especially those with dip angles between 50 and 80º. E-W striking faults are at moderate risk, although this increases too high for steeply dipping faults with a ~15º rotation in strike in a clockwise direction. Major ~NW-SE striking faults dipping between ~65º and 90 ˚ are at a high risk for all in-situ stress scenarios. The

window of high risk, characterising the ~NW-SE striking fault trend is wider for offshore than onshore surveys (**fig. 11**).

Under a compressional stress regime minor ~NE-SW striking faults are at a low risk of dilation, with risk increasing to moderate and high as fault dip angles decrease (**fig. 11**). Steeply dipping (>70˚) E-W striking faults are at a moderate risk of dilation, however as dip angle decreases under this threshold the risk of dilation rapidly increases to high. Again, dilation risk increases with minor rotations away from the E-W axis. Increasing with a ~15º degree clockwise rotation. Decreasing counter clockwise.

Under an extensive stress regime, minor NE-SW striking faults are at moderate risk of dilation, decreasing to low risk with a lower dip angle (**fig. 11**). In this case steeply dipping, E-W striking faults are at a high risk, becoming moderate then low, as dip angle decreases past 60º and 40º. A rotation of strike in a clockwise direction, results in a rapid increase to a wider window of high risk. Major ~NW-SE striking faults are at the highest risk of dilation, especially above dip angles of 50º.

This pattern between stress scenarios is largely the same between the western and eastern basin. A higher number of faults that define the ~NW-SE trend are present within the offshore sections of the eastern basin, suggesting that the overall risk of dilation increases from the west to the east, especially within intensely faulted ~NW-SE striking sections. Additionally risk under a compressional stress regime is slightly higher within the offshore eastern basin, due to shallower reservoir sections and lower magnitudes of vertical stress. This increased risk is particularly well highlighted within our modelling results from the Brand 3D survey, which overlies the continental shelf in the eastern basin. Where the results of our modelling suggesting

the entire succession of faults within the survey is at a high risk under a compressional stress regime. However, this decreases to moderate under strike slip conditions for faults dipping under 40º and transitions to low for the same angles under an extensive regime.

While there is some small variation between each individual dataset and scenario of stress, the results indicate that in general, the ~NW-SE striking faults that define much of the Otway Basins structural framework are at a high risk of experiencing dilation. A characteristic that is largely irrespective of the regime of in-situ stress.

4.4 Fracture stability modelling

Fractures from 7 wells were modelled, at a depth of 2000m (**fig. 13**), to coincide with the most mature intervals of the Eumerella Formation. Motivated by the recent renewed interest with respect to unconventional methods of production within the onshore Otway Basin (Tassone et al., 2014; 2017). Although not all borehole intervals intersected the Eumerella Formation, the formation is the oldest penetrated, and the presence of natural fracture geometries intersected within upper sedimentary units within it is likely (Kulikowski and Amrouch, 2017). Although as noted in the preceding sections, fracture density may vary significantly across the basin.

As with dilation tendency, modelling was conducted under all three regimes of stress for two environments of pore pressure: lithostatic and potentially mild-over pressure. As gradients exceeding lithostatic pressures are evident within the eastern Otway Basin, an insight gained from a wide spread summary of leak off test data compiled by a previous studies (Tassone et al., 2014; 2017).

Under strike slip conditions, high angle ~NW-SE striking natural fractures are at the highest

risk of reactivation, requiring less than ~10MPa under lithostatic pressure and ~5MPa with mild overpressure. While ~NE-SW striking fractures are at a lower risk, they still require less than ~15MPa. A similar trend is reflected in the results under a compressional regime, although stability pressures increase to ~ 20MPa, with a reduction in reactivation pressure with mild over pressure. In both cases a small window containing the most tightly spaced NW-SE striking fractures require higher pressures of ~25MPa.

Under an extensive stress regime, with lithostatic pressure ~NW-SE striking fractures generally require ~10MPa to undergo reactivation. With ~NE-SW striking fractures requiring moderately higher pressures between 15-20MPa. Under a scenario of mild overpressure; ~NW-SE striking fractures require an increase in ~5Mpa for reactivation while ~NE-SW striking fractures require between 10-15MPa.

5.0 Discussion

In the following section, insights provided by the geomechanical modelling are discussed. We begin with the implications with respect to conventional style hydrocarbon prospectivity. Progressing to those for unconventional methods, geothermal energy and carbon capture and storage projects. This is followed by a comparison of the results with geological evidence for other sub surface fluid flow features.

5.1 Implications for conventional hydrocarbon prospectively

5.1.1 Horizontal stress, fault dilation and sealing potential

Poor fault seal has hindered exploration efforts for conventional oil and gas in the Otway Basin since the early days of exploration (O'Brien et al., 2009). It is a defining feature of the basin that is supported by the results of our geomechanical modelling, which suggest that poor fault

seal, at reservoir depth and throughout the sedimentary succession, is possible under all scenarios of in-situ stress. Mainly due to the spatial relationship between the basins major ~NW-SE structural fabric and the orientation of the in-situ stress tensor.

With maximum horizontal stress near parallel to fault strike, it provides a minimal contribution towards the effective normal stress acting on the fault plane. In the Otway Basin the majority of the effective normal stress component is composed of the minimum horizontal stress, and as in most scenarios the magnitude of minimum horizontal stress is low, levels of effective normal stress acting on ~NW-SE striking faults are also low. This effect is magnified under a compressional stress regime, where the vertical component of stress is also low.

These results raise some concerns regarding the prospectivity of continental margins, especially those with a σH striking parallel to the coastline and the major fault pattern and low levels of minimum horizontal stress. It seems possible that for passive margin settings, that lack inversion or salt structures (which may provide different trap styles), there is a high likelihood that many faults will be at high risk for dilation.

With respect to sedimentary basins within Australia, the passive margin style of stress regime appears unique to the Otway Basin (**fig. 1**) and the immediate surrounding regions of the eastern Bight Basin and western Bass Basin. This is also reflected in the absences of any major ~NW-SE oriented Miocene – recent inversion structures, which is highlighted by Burgin and Amrouch (2019a; 2019b), as the regional σ_H striking parallel to most faults is unable to reactivate them in a reverse manner.

Given the close proximity of the Otway Basin to Australia's historically most successful oil and gas fields in the Gippsland Basin, the question of why petroleum exploration in the Otway Basin has not been more successful has been asked. Given the point raised concerning the relationship between in-situ stress orientation and fault strike above, the Gippsland Basin presents an almost opposite relationship to the Otway Basin. The Gippsland containing mainly ~NE-SW striking Late Cretaceous faults (Glenton, 1991) that trend near orthogonal to the orientation of maximum horizontal stress (Power et al., 2003; 2001) (**fig. 1**). As a result, not only have these major ~NE-SW faults been ideally oriented for reverse reactivation, since stress reorganisation in the Late Miocene, they have experienced far higher degrees of effective normal stress, in direct contrast to faults in the Otway Basin. Implying their dilatation tendency is likely very low and the effectiveness of fault seal is high. A good example of such a field is the Snapper Field and the associated Snapper Anticline (**fig. 14**) which is ~13km in length and 50km^2 in area. Initial reserves within the field being estimated at 2140 bcf of gas and 11 million STB of oil within the main reservoir and 6 million STB of oil within the surrounding small fields (Glenton, 1991).

That being the case, parts of the Gippsland Basin, including sections of the Snapper Anticline, are also permeated by ~NW-SE striking faults. However, in contrast to the Otway Basin in this case they do not penetrate the top reservoir seal, and act mainly as communication pathways between the units below (Glenton, 1991). A characteristic that further supports the modelled response of faults within this study.

The effect of fluid pressure increases towards a risk of dilation is also likely lower in the Gippsland Basin, mainly due to the shallower reservoir depth of ~1200m (Glenton, 1991), in contrast to depths of ~2500m+ in the Otway Basin.

547

548 *5.1.2 Structural setting of successful conventional fields within the Otway Basin*

549 The western sector of the Otway Basin is still considered an under explored province, and to
550 date average recoverable reserves have been low ~21bcf. While fault leakage has previously
551 been identified as a risk factor within the Penola Trough, this is mainly due to seal breaches on
552 a local scale, rather than regional in-situ stress conditions (Lyon et al., 2007). A number of
553 small fields have been discovered in the western basin (e.g. Katnook, Ladbroke Grove,
554 Haselgrove South and Redman). The Katnook and Ladbroke fields, lying within the Balnaves-
555 Haselgrove 3D survey utilised as part of this study (**fig. 2**). The local, A1 petroleum system,
556 consists of a regional reservoir within the Early Cretaceous Pretty Hill and Windermere
557 sandstone members of the Otway Group (**fig. 3**). With the Sawpit Shale and Laira Formation
558 acting as top seals, structural closure on the two fields is exerted mainly by E-W striking faults
559 (Lyon et al., 2007) a feature we suspect has played a major role in trap development, as the
560 modelling results suggest faults of this nature are generally at a lower risk than ~NW-SE
561 striking faults.

562

563 In contrast to the western Otway Basin, exploration has been more successful in the east, within
564 the A2 petroleum system, encompassing the Casino, Blackwatch and Henry fields. In addition
565 to the most prominent fields in the region; Minerva, La Bella and Thylacine. One example of
566 a successful structural play, the Minerva structure (**fig. 15**) formed as a result of Late
567 Cretaceous co-axial inversion of ~NW-SE faults representing a ~ broad ~NE-SW trending
568 dome of ~5km in length and ~4km in wavelength. And while, ~NW-SE trending faults are
569 present with the upper sedimentary succession Sherbrook Group units within the fold, and at
570 the back stop of the structure, a majority of them fail to penetrate to reservoir depth. The
571 topographic high of the inversion structure also providing closure and a top seal.

572

573 Within the same petroleum system, the La Bella and Geographe fields (**fig. 2**) to the southwest
574 and south of the Minerva structure represents similar, gentle ~NE-SW dome structures. Faulted
575 into gently rotated blocks by minor E-W striking faults that form part of a larger ~NW-SE
576 striking fault trend. As with the Minerva field, in both cases the high of the structure provides
577 the majority of closure for both plays and faults within upper portions of the Sherbrook and
578 Cenozoic sections fail to penetrate down to reservoir depth. Success of the plays is highlighted
579 at Geographe-1, which intersected a 233m gas column within the upper Sherbrook Group
580 sedimentary succession (Cliff et al., 2004). While these faulted inversion structures have been
581 successful on a number of occasions, this has not always been the case, as drilling of a similar
582 targets within the Triton-1 and Triton 1 ST1 wells (~10km west of the La Bella discovery) was
583 unsuccessful, producing only minor gas shows.

584

585 The Thylacine field (**fig. 2**) ~15km due south of the Geographe, represents a different structural
586 play to the other off-shore fields within the eastern basin, the structure (see Robson et al., 2018)
587 comprising a large composite E-W striking horst. That is fault bounded to the south and north
588 east by ~E-W striking faults, and in the east by ~N-S striking faults. The field sits on a large,
589 un-rotated portion of basement block, which assisted in isolating the field from the regional
590 extensional events (Origin Energy, 2003) during the Late Cretaceous. The field contains two
591 successful wells: Thylacine-1 which intersected a 277m gas column within the Flaxman and
592 Waarre members of the upper Sherbrook Group sediments and Thylacine 2, ~5km west from
593 the original well (**fig. 2**) which flowed gas at 28MMSCFD. (Cliff et al., 2004). While the
594 Thylacine structure is bound by high risk ~NW-SE striking faults on its south eastern edge,
595 they are not the primary control on the trap, only providing closure at its lowest sections. As a
596 result, in this case they have likely had a minimal effect on the success of the play. It is also

possible that all faults are non-sealing and that the rate of replacement exceeds leakage rate, which may be common within the Otway Basin (O'Brien et al., 2009).

In most cases the hydrocarbons within the eastern section of the basin are believed to be the result of a present day kitchen. Therefore, parallels can be drawn between the structural nature of the most successful fields, and the results of the modelling. Successful plays are centred on structures where seal is not fault dependant or that are structurally controlled by the minor ~E-W and ~N-S striking faults within the Shipwreck Trough and Sorell Fault Zone (**fig. 2**). Two faulting patterns that present lower risks of dilation when compared to the major ~NW-SE trending normal faults, that dominate the regions structural fabric.

To further illustrate this point, structures across the basin that have been drilled targeting ~NW-SE trending fault blocks and structures where closure is entirely dependent on sealing, parallel striking faults [western - (Pyrus 1, Zema-1, Wynn-1, Jacaranda Ridge-1; Penola Trough) central - (Fermat-1; Normanby Structure, Amrite-1; Amrite Structure) and east - (e.g. Champion-1; Champion Horst, Mussel-1; Tilted Block)] have been unsuccessful, almost without exception. In many cases producing small amounts of gas or oil or shows, but not sizeable fields.

Recent work by Burgin and Amrouch (2019a) in the western Otway Basin and Burgin and Amrouch (2019b) in the east, show distinct differences in the distribution of inversion structures across the basin. This distribution is echoed by the location of the most successful fields within the basin, which are located around the Otway Ranges and high sections of basement. Corresponding with areas that have been identified as those most likely to have

accommodate inversion through reactivation of the top basement decollement zone (Burgin and Amrouch, 2019b).

While the high likelihood of faults to dilate within the offshore sectors of the basin is a negative with respect to seal integrity, it can be viewed positively where structural closure is provided throughout other means, as conductive faults act as migration pathways for deeper generated hydrocarbons. This is especially the case in passive margin settings like the Otway Basin. Where peak generation windows for petroleum systems can occur beyond the continental shelf, due to higher levels of extension and burial that may be isolated offshore. Although there are no discoveries to date within the A3 petroleum system, this particular insight may be of importance for targeting hydrocarbon accumulations within it. Especially as hydrocarbons are most likely sourced from units within the Sherbrook Group occupying a zone of peak maturity isolated to a narrow section of the basin deep that is continuous with the continental shelf. A trend that is most apparent within the Tartwaup-Mussel Fault Zone (**fig. 2**) (O'Brien et al., 2009). As this zone trends largely ~NW-SE it is likely many of the faults along its section are at high risk of dilation, that being the case, it is plausible that migration from the A3 generative window has taken place along their length. Implying that accumulations may be present within sections of the upper shelf. A concept suggested by O'Brien et al. (2009). However, under an extensive stress regime, the results from this study suggest gently dipping, deeper fault sections may be the least likely to be dilated, illustrated in the results from the Brandt 3D. A characteristic which may influence the effectiveness of this model of migration. Further highlighting the importance of constraining the in situ stress regime of the basin accurately.

5.1.3 Recommendations for conventional hydrocarbon exploration

Recommendations for future conventional hydrocarbon exploration are as follows: Firstly within the A1 and A2 systems, efforts continue to be focused around portions of the Otway Basin, where the dominant ~NW-SE striking fault trend is dissected by other minor patterns on a local scale. Such as in the Penola Trough, Shipwreck Trough or further south along the Sorrel Fault Zone. Regions where ~E-W and ~N-S striking faults may influence the structural architecture and assist in providing structural closure along horst or anticlinal structures.

Additionally, sections of the eastern basin covered by the Crowes Foot 3D survey, show the presence of ~NE-SW striking inversion structures. Of which only one has been drilled, prior to the acquisition of the 3D survey. The survey covers the Crowes “anticline,” which reflects a series of ~NW-SE striking inverted structures many of which display four-way closure. Given that the Eumeralla Formation is likely at its highest burial temperature within this section of the basin (Tassone et al., 2014) we suggest the region is highly prospective for future efforts of conventional exploration.

Within the A3 system efforts along the upper Tartwaup-Mussel Fault Zone and the western Tasmanian shelf are recommended. As deeper seated faults may provide migratory pathways from within the basin deep, where the sediments of the Sherbrook Group are at their maximum burial temperature and within the generation window (O’Brien et al., 2009).

5.2 Implications for unconventional hydrocarbon prospectively

5.2.1 Structural permeability in the form of natural fracture networks

Since the expansion of tight and shale gas in the US, there has been renewed interest in unconventional style plays in Australia. As the Eumerella Formation is the source for ~99%

of discovered hydrocarbons within the basin (O'Brien et al., 2009), it is the likely target for these efforts in the Otway Basin. Especially where thick sections have been buried within the Port Campbell and Tyrendarra Embayment (Tassone et al., 2014) and the formation is currently at its maximal burial temperature.

Tassone et al. (2014) drew excellent comparisons between the Eumerella Formation and the major shale intervals of the US such as the Bakken and Barnett. Their results suggesting that despite significant differences in depositional environment, kerogen type and the style of exhumation the Eumerella contains potential for unconventional plays.

This is highlighted within DST data from Moreys-1, in the PCE, which flowed gas and condensate from a sandy interval of the Eumerella Formation between 1925 and 1935m depth (Campbell, 2012). Additionally more than 70% of wells drilled in the Port Campbell Embayment intersecting the Eumerella Formation, reported gas shows and fluorescence, with multiple wells displaying high gas and pure gas indications (O'Brien et al., 2009).

Petrographic and core analysis observations from Duddy (2003) indicate that the expulsion of hydrocarbons and migration throughout the Eumerella Formation, into conventional style structural traps is hindered by the units tight primary porosity, and permeability, resulting from early periods of diagenesis. Suggesting that efforts to produce directly from the unit will require high levels of secondary permeability, through the reactivation of natural fracture networks, for which the results of this study provide an original insight.

Fracture modelling at a depth of 2000m shows that in contrast to fault dilation, the stability of natural fracture networks within the eastern Otway Basin vary significantly with stress regime,

696 in addition to pore-pressure gradient. Low stability pressures (~5MPa) (ie. easily reactivation
697 fractures) for ~NW-SE striking fractures under both strike-slip and normal faulting conditions,
698 suggest that under such conditions of stress hydraulic stimulation of fracture networks would
699 require low injection pressures. In contrast, if a reverse stress regime is present within the
700 eastern Otway Basin, as alluded to by Tassone et al. (2017) then the same fracture networks
701 require almost four times (~20MPa) the pore pressure for reactivation.
702
703 Modelling suggests networks of natural fractures within the sub-surface eastern basin are well
704 oriented for reactivation at generally low pore-pressures (particularly if a strike slip or normal
705 stress regime is present). Especially those striking ~NW-SE, meaning that there is good
706 potential within the formation for the establishment of structural permeability networks. A
707 feature that may assist efforts to produce from tight sandy or shaley intervals, especially under
708 strike slip or normal faulting conditions.
709
710 As evident within the dataset, fracture density may vary considerable across the basin. In which
711 case we recommend a thorough assessment of subsurface fracture networks prior to any
712 unconventional efforts. Insight that could hypothetically be completed using further tightly
713 spaced image logs or the use of seismic attributes, such as curvature (Kulikowski et al., 2018).
714
715 The results of our fracture stability modelling highlight the importance of further detailed
716 assessments of in-situ reservoir stress within the eastern Otway Basin, especially if
717 unconventional methods of production are pursued. As variations between the conditions of in
718 situ stress considerably affect the required pressure increases needed for fracture stimulation.
719 This is especially the case in sections of the far east, where the exhumation of older and denser
720 rock may result in higher levels vertical stress gradients, to as much as 26MPa/km (Tassone et

al., 2014; 2017) increasing the likelihood of a vertically oriented minimum principal stress. That being said, the region has often been interpreted as experiencing a compressional stress regime (Tassone et al., 2014; 2017), a contradiction, which with respect to fracture reactivation, would be the least favourable.

5.2.2 Regional risks with fracture stimulation

Although low pore-pressure increases required for fracture stimulation is a plus for unconventional methods of production, as natural fracture networks can be reactivated to increase structural permeability, in the Otway Basin, it is a double-edged sword.

Fracture modelling results from this study may be used as a proxy for reactivation of fault planes, as faults can be reactivated in a similar manner due to increases in pore pressure within the sub-surface. As major fault networks also strike ~NW-SE and dip at high angles, our results indicate they too require low pore pressure increases, and as such are at a high risk for fault reactivation, due to minor increases in pore pressure. As such, hydraulic fracturing within the eastern Otway Basin and the Port Campbell Embayment, an important agricultural and tourist region, appears to be very high risk. As not only are major ~NW-SE striking faults at a high risk of dilation (**fig. 16**) but they may also be easily reactivated due to minimal increases in pore pressure. In a worst case scenario fault reactivation could result in up dip contamination of aquifer units within members of the Nirranda Group and Heytesbury Group sediments (e.g. Clifton Formation, Timboon Sand and Eastern View Formation) (Southern Rural Water, 2015) (**fig. 16**). Such contamination would be disastrous for the region, as ground water supply is of high importance to both the local agricultural industry and ecosystem, which supports one of Australia's most significant tourist attractions.

It is therefore recommended that any unconventional efforts within the Otway Basin are completed with the highest level of structural integrity. Proceeded by detailed assessments using both high resolution 2D and 3D seismic, and where possible undertaken in the absence of any ~NW-SE striking faults that are likely to act as fluid pathways.

5.3 Implications for other subsurface industries

5.3.1 Carbon capture and storage

Australia's largest carbon capture and storage effort to date; CO2 CRC, is located onshore at the Naylor field (**fig. 2**), a small depleted natural gas field, with an original gas cap size of approximately 40,000m^2 (Vidal Gilbert et al., 2010). Like the successful fields discussed in the previous section, the Naylor field is influenced by faults of multiple orientations. Bound to the west by a north-south trending fault that acts as an effective seal due to only partial off-set of the seal lithology, the Belfast Mudstone.

It is importance to note that CO2 storage differs from unconventional production as it involves the replacement of produced hydrocarbons with CO2, and thus the restoration of column pressures. However it still requires direct injection into the target formation, where changes in pore pressure can have negative effects on fault and seal integrity.

The results of our modelling suggest this may be especially relevant within the Otway Basin under either strike slip or extensional, conditions where high angle ~NW-SE striking fractures may require very low increases in pore pressure to undergo reactivation. As with unconventional projects the high propensity for ~NW-SE trending faults to be at high risk for dilation under both strike-slip and compressional conditions and the moderate risk of ~E-W striking faults under these regimes of stress, presents a possible risk. In the case of a

771 compressional regime of stress, essentially all faults dipping towards the N -S and E-W present
772 a high risk, as a result significant assessment of in situ stress conditions should take place prior
773 to the commencement of any project.
774
775 As such, ongoing efforts to pursue carbon capture and storage within the Otway Basin should
776 be approached with caution and focused in locations such as the Naylor field, where structural
777 closure is imposed mainly as a result of faults that strike ~N-S or E-W. Additionally,
778 approaching fields reliant on fault juxtaposition and seal, even along non-critically oriented
779 ~NE-SW striking faults should be approached with caution. As there is a risk for seal capacity
780 to be overcome and for fault integrity to respond differently under the varied conditions of
781 wettability and density of CO2 (Vidal Gilbert et al., 2010).
782
783 Lastly, while targeting depleted fields within the Otway Basin, may seem a “safe bet” as they
784 have likely supported hydrocarbon columns. Many fields within the eastern Otway Basin may
785 only contain economical volumes of hydrocarbons, as replacement rate is thought to exceed
786 leakage (O’Brien et al., 2009). Implying that the presence of in place reserves does not denote
787 a perfect seal, in which case assuming so during injection of CO2 may have negative
788 consequences.
789
790 *5.3.2 Geothermal energy*
791 While carbon storage projects require an understanding of subsurface permeability pathways,
792 they are less complex than geothermal energy projects as they require only injection. The
793 projects often also having the advantage of utilizing a depleted natural gas or oil field, where
794 the sub-surface structure is well constrained. In contrast, “hot rock” geothermal projects rely

on the circulation of fluids between two locations and as such require a more detailed understanding of sub surface migration pathways.

The results of our modelling suggest that constraining these pathways to the required degree within the Otway Basin may prove difficult. Especially as deeper fault sections within the basin are typically less steep, and from our modelling have the potential to behave very differently under strike slip, compressional and extensive stress regimes (**fig. 8b**).

As vertical stress increases most rapidly with depth, it may be acceptable to assume that the deepest sections of the basin may reflect an extensive stress regime. This poses a problem for geothermal projects within the Otway Basin, which are associated with deep basement units (Goldstein et al., 2009). Modelling results from this study suggest that at a depth of 3000m, within the western basin low angle faults of all orientation are at a low risk of dilation and likely closed. An insight that poses a significant hurdle for establishing the circulatory network required for geothermal energy projects.

5.4 Geological Evidence Supporting Modelling Results

5.4.1 Volcanism

As discussed in section 2.5, similar to many global passive margin settings, the Otway Basin has seen appreciable amounts of volcanism throughout its history. With extended eruption episodes interpreted throughout much of the Cenozoic (Price et al., 2003). In addition to intrusive and extrusive igneous rocks and volcanos within parts of the Otway Basin, very high levels of mantle sourced CO2 are present within a number of wells (Watson et al., 2004; O'Brien et al., 2009) (e.g. Boggy Creek-1 containing as much as 13.9Bcf of pure CO2).

In contrast to igneous material, mantle sourced gas migrates in a non-destructive fashion. Its presence within reservoir sections of the basin possibly suggesting that structural permeability networks in the Otway Basin have played an important part in the transportation of mantle material into the upper crust. We therefore propose that CO2 plumes within the region have migrated vertically along deep seated, conductive faults, to reservoir units within the upper sedimentary successions of the basin. Utilising migratory pathways that are largely defined by steeply dipping ~NW-SE trending faults that are at a high risk of dilation.

In the western Otway Basin, the distribution of eruption centres within the South Australian Quaternary Basalt province, part of the Newer Volcanics Province, displays a ~NW-SE trend as does the distribution of volcanic features in the central basin (**fig. 17**). Holt et al. (2013) suggest that the pattern of faulting and distribution may be related. An inference that is supported by the modelling results from this study, especially for ~NW-SE striking steeply dipping (>60º) faults, which are at a high risk of dilation, irrespective of the regime of in-situ stress (**fig. 17**). This relationship between the distribution of material and the structural fabric of the basin provides some insight in the possible nature of the deeper basement structural fabric within parts of the western Otway Basin. A province that may also reflect a ~NW-SE trend, more conducive for transporting mantle material into the upper sediments of the basin.

Volcanism can have a significant effect on petroleum systems, geothermal energy and natural occurring CO2 reservoirs, including the alteration of source material, the creation of traps and the destruction of in place hydrocarbons. As such, the likely presence of mantle derived volcanic material around deep seated, major NW-SE striking faults, should be considered during future subsurface industry projects. Especially as distinguishing between CO2 and hydrocarbon based gas prior to drilling is impossible.

5.4.2 Cavitonics and Shallow Fluid Flow

Although far shallower features than petroleum systems and geothermal energy, naturally formed cave systems on the margin of the western Otway Basin, likely also provide direct evidence as to the dilation of sub-surface fault and fracture networks.

As per Littva et al. (2015) the orientation of cave passages is approximately parallel to the orientation of maximum horizontal stress. The Naracoorte Cave system, ~ 30km north of the Penola Trough, lies within the Gambier Limestone, the South Australian equivalent of the Port Campbell Limestone and an upper most member of the Heytesbury Group (Moriarty et al., 2000). The cave system trends ~NW-SE at ~130ºN and has been shown to have formed recently within the Plio-Pleistocene. The system is bound by the ~NW-SE trending Kanawinka Scarp, a normal fault zone down thrown on the south western side (**fig. 17**).

The hypothesis here is that local ~NW-SE trending shallow faults and fractures, which have been imaged penetrating Cenozoic sediments in the western basin, (Burgin et al., 2019b) are experiencing dilation, and represent favourable pathways for ground water flow. This has led to increased levels of erosion overtime, within carbonaceous, and easily weathered formations such as the Gambier Limestone. The higher tendency of ~NW-SE trending fault and fracture networks to conduct groundwater has likely assisted in the evolution of the cave network (**fig. 17**). As a result, the caves now strike almost parallel to the local σH interpreted by Bailey et al. (2014).

5.6 The Otway Basin as a Regional Case Study

As mentioned previously, the Otway Basin and surrounding area within Australia represent the only truly passive margin regions of the Australian continent. Areas defined by a parallel relationship between maximum horizontal stress and major fault strike. This relationship may especially be the case within the Ceduna Sub-Basin, the eastern most section of the Bight Basin.

Unlike the Otway Basin, which contains some minor ~E-W and ~N-S structuring and uplifted basement blocks that are associated with many successful oil and gas fields, the Ceduna Sub-Basin reflects a more discrete ~NW-SE striking system of gravitationally driven listric faults (Robson et al., 2017). Though inversion structures are present in the sub-basin their closure is often still reliant upon fault seal along ~NW-SE striking faults (Macdonald et al., 2012).

From the insights gained from this study, it is possible that large normal faults within the Ceduna Sub Basin (**fig. 18**) may be at a high risk of being under dilation. In addition to the previously identified risk of reactivation due to increases in pore pressure (Reynolds et al., 2003; Macdonald et al., 2012). Indeed, the presence of paleo-fluid-flow features documented by (Velaytham et al., 2019) and the network of igneous bodies that strike parallel to major basin forming faults, suggest that leakage of fluids along major faults may have already occurred (**fig. 18**). As such, while there is much speculation that the Bight Basin may contain potential oil and gas reserves on the scale of some of the most successful fields in the world. The same may be said of the Otway Basin during its early phases of exploration, and the results of this study suggest efforts should be approached with caution.

6.0 Conclusions

In the Otway Basin and other passive continental margins, many faults may be at a high risk of dilation, due to low levels of effective normal stress acting on the fault plane. An affect that

can vary with depth and fault dip, depending on the regime of in-situ stress. Additionally, these environments are likely also characterised by low (<20MPa) reactivation pressures for natural fracture networks.

These insights into fluid flow pathways and fault dilations have a number of consequences with regard to subsurface industries within these settings:

- ~NW-SE trending normal fault networks are at a high risk of experiencing dilation especially under a compressional regime of stress, where all fault angles are at a high risk, and vertical stress magnitudes are low within shallow reservoir sections. A characteristic of their geometry that affects their ability to act as adequate seals to prospective hydrocarbon accumulations. However, this “risk” can also be viewed in a positive light as deeper seated faults within on the edge of the continental shelf may provide migration pathways from the basin deep to the upper sections of the continental shelf.

- ~NW-SE trending fracture networks in the Otway Basin require low (~5MPa in some cases) increases in pore pressure in order to be reactivated, which bodes well for the challenge of increasing secondary permeability within the tight Eumerella Formation, and has consequences for unconventional hydrocarbon production. For which the region has recently become a target. Additionally, there may be significant spatial variations in fracture density throughout the Otway Basin, which should be considered.

- High fault dilation risk and low fracture stability levels in the Otway Basin mean that any efforts for further storage of CO2, should be undertaken with caution. As many

major faults are critically oriented for dilation and likely to be reactivated, even with minimal increases in pore pressure. In which case, reactvation negatively affect aquifers within the upper sedimentary succession. Additionally, the likelihood of non-dilated faults within the deepest parts of the basin may pose a problem for geothermal energy projects.

- Geomechanical modelling results in this study are supported with geological evidence, with the occurrence of igneous activity and high concentrations of CO2 where faults have a high risk of dilation. An observation that is further supported by shallow surface cave systems that strike parallel with regional faults and σH.

Acknowledgements

The authors wish to acknowledge to contribution of the Australian Postgraduate Award Scholarship through the University of Adelaide. Additionally, thanks to Down Under Geosolutions and Midland Valley for the academic licensing of DUG: Insight and Move. Thank you to David Kulikowski for assisting with modelling and Associate Professor Simon Holford for guidance on the volcanic history of the basin.

Region/State	Field	Reserves (Bcf)	Petroleum Systems
Eastern Basin / Victoria offshore	Minerva	300	Austral 2
	Casino	290	Austral 2
	Thylacine	532	Austral 2
	Geographe	286	Austral 2
	Martha/Halladale	153	Austral 2
	Labella	150	Austral 2
	Henry	160	Austral 2
Eastern Basin /Victoria onshore	North Paratte	10.9	Austral 2
	Iona	19	Austral 2
	Wild Dog Road	0.6	Austral 2
	Wallaby Creek	11.9	Austral 2
	Skull Creek	1.3	Austral 2
	Fenton Creek	3.2	Austral 2
	Mylor	7.9	Austral 2
	Penryn	2.4	Austral 2
	Boggy Creek	13.9	Austral 2
	Grumby	0.7	Austral 2
	Langley	3.4	Austral 2
	Dunbar	2.5	Austral 2
	Butress (CO2)	1.1	Austral 2
	Tregony	7.3	Austral 2
	Lavers	0.6	Austral 2

	Naylor	5.8	Austral 2
	Croft	5.8	Austral 2
Western Basin /South Australia onshore	Caroline	89.6	Austral 1 and 2
	Haselgrove	17.4	Austral 1
	Jacaranda Ridge	0.026	Austral 1
	Katnook	30.411	Austral 1
	Lagbroke Grove	61.62	Austral 1
	Redman	17.8	Austral 1
Western Basin /South Australia offshore	Troas	24.7	Austral 1

943

944 **Table 1:** Displays approximate reserves of the fields within the western and eastern Otway
945 Basin as of 2009, which have not seen any appreciable increase. Modified from O Brien et al.
946 (2009).

Basin Region	σH Orientation	σh (MPa/km)	σH (MPa/km)	σV (MPa/km)	PP Gradient	Shape Ratio	Stress Regime	μ
Western Basin	131°N	15.5[a]	29[a]	21.18[a]	10MPa/km	0.42	Strike Slip	0.6
Western Basin	131°N	23[d]	29[a]	21.18[a]	10MPa/km	0.3	Compressional	0.6
Western Basin	131°N	15.5[a]	18.0[d]	21.18[a]	10MPa/km	0.4	Extensive	0.6
Eastern Basin	137°N	15.98[b]	18.75[b]	20.0[a]	10MPa/km	0.59	Extensive	0.6
Eastern Basin	137°N	14.5[c]	27[c]	21.45[b]	10MPa/km	0.56	Strike Slip	0.6
Eastern Basin	137°N	21.0[d]	27[c]	20.0[a]	10MPa/km	0.08	Compressional	0.6

Table 2: The modelling scenarios used within this study. Stress data taken from [a]Nelson et al. (2006), [b]Berard et al. (2008), [c]Vidal Gilbert et al. (2007) and [e]estimated to construct the scenario.

Seismic Dataset	Basin Region	On/off shore	Size (km2)	TWT Extent	Water Depth Modelled	Modelling Profile Depth (m)	Fault Count
Tillbooroo 3D	Western	Onshore	44	4.1s	-	-3000	98
St George 3D	Western	Onshore	66	4.1s	-	-3000	68
Balnaves-Haselgrove 3D	Western	Onshore	417	5s	-	-3000	72
Carpenter 3D	Western	Offshore	380	6s	55m	-3000	103
Crowes Foot 3D	Eastern	Offshore		6.5s	76m	-2500	
Champion-Hercules 3D	Eastern	Offshore	1560	5.5s	70m	-1750	181
Schomberg-Minerva 3D	Eastern	Offshore	457	5.5s	80m	-1700	126
Brandt 3D	Eastern	Offshore	150	5.1s	80m	-2000	125

Table 3: The modelling scenarios used for each individual seismic survey within this study. With scenario 1,2 and 3 from table 2 applied to each survey dependant on its location in the western or eastern basin.

Well	Tool Type	Bit Size (inches)	Max Borehold Deviation	Top of Log (m bKB)	Bottom of Log (m bKB)	Log Length	Fracture Count
[x]Bellarine-1	FMI	8.5	1	278	978	700	24
Halladale-1DW1	STAR	8.5	20.54	775	1916	1141	1
[x]Halladale-1DW2	STAR	8.5	21.72	1668	1927	259	25
[x]Henry-1ST1	STAR	8.5	1	1725	2015	290	37
[x]Wild Dog Road-1	FMI	8.5	34.5	1200	1676	476	27
[x]Moreys-1	CMI	8.5	21.4	1700	2300	600	60
Glenaire-1	FMS	8.5	20.5	2996	3702	706	24

Table 4: Image log fracture data from used for the modelling of fracture stability in this study. [x]Denotes taken from Burgin and Amrouch (2019b)

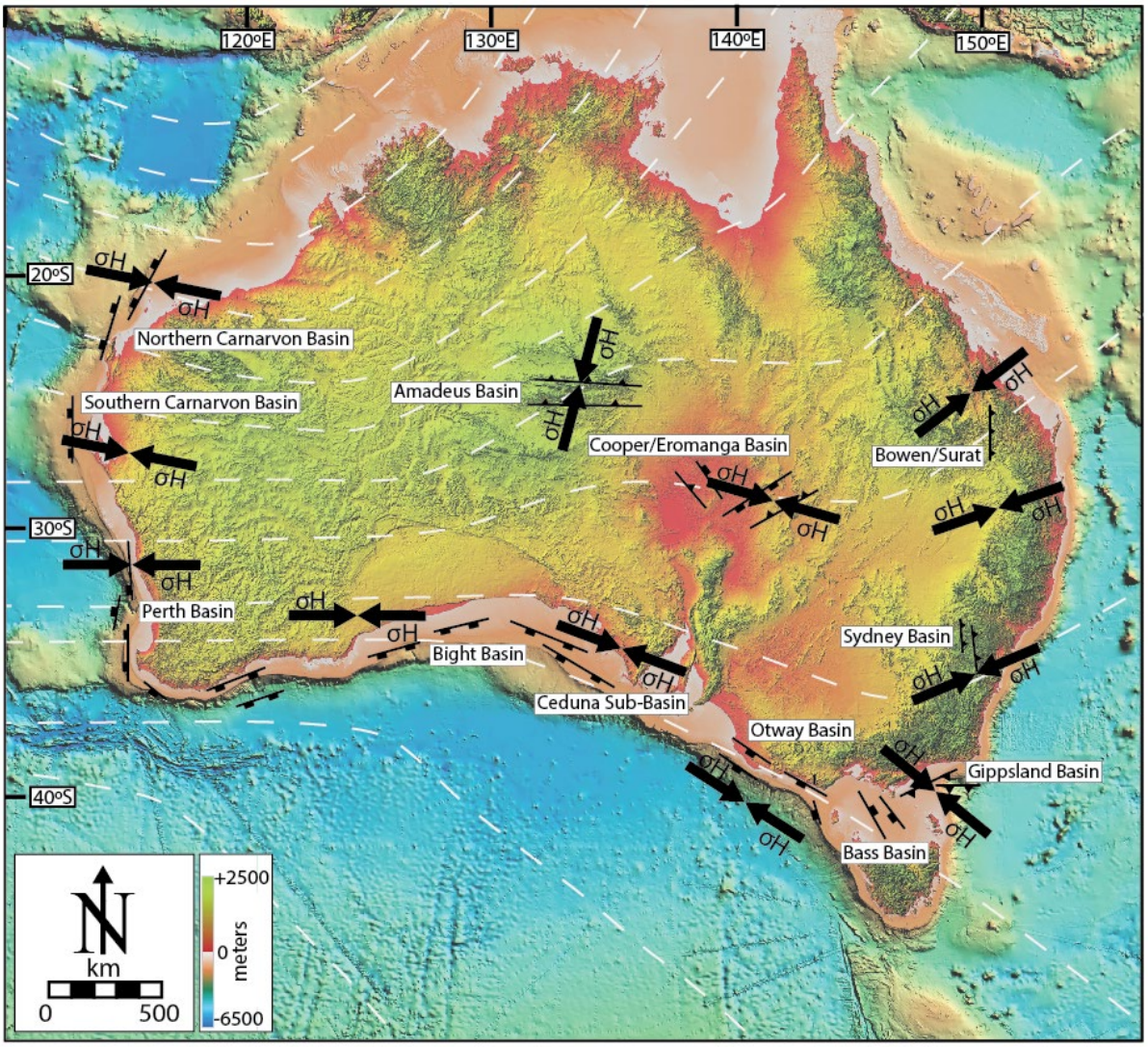

Fig. 1: A topographic map of Australia displaying σH data from Rajabi et al. (2017a) along with approximated regional fault trend data for Australia's major basins. White dashed lines represent modelled stress trajectories; black arrows represent averages within individual provinces after Rajabi et al. (2016a). Otway Basin fault trends from this study along with Burgin and Amrouch (2019a; 2019b), Bass Basin trends from Lennon et al. (1999), Gippsland Basin after Norvick et al. (2001), Perth and Bight Basin after Totterdell et al. (2000), Cooper/Eromanga from Kulikowski et al. (2016), Carnarvon Basin after Velayatham et al. (2018), Amadeus Basin after Shaw (1991), Sydney Basin after Glen and Beckett (1997), Bowen/Surat after Korsch et al. (2006)

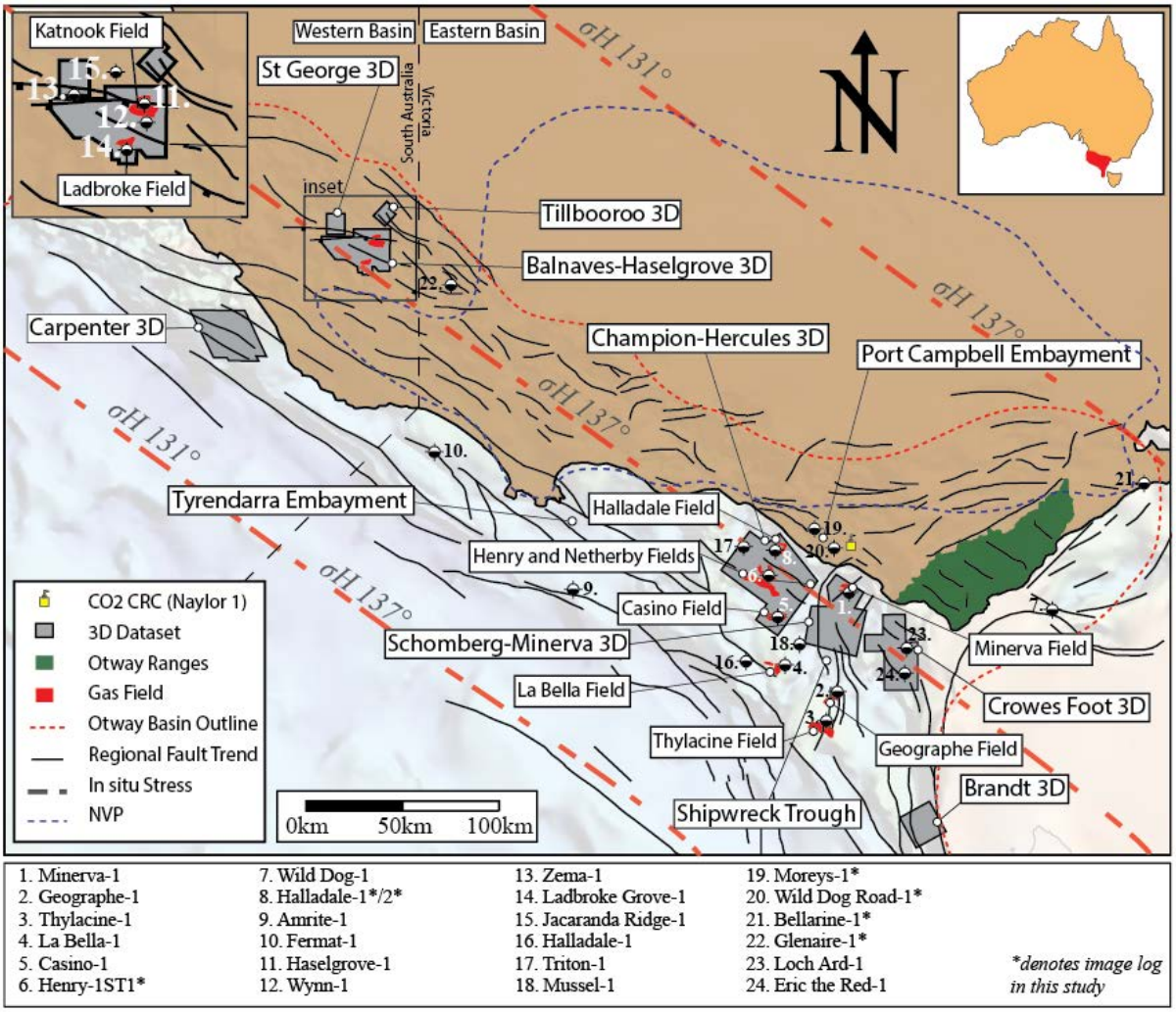

Fig. 2: A map of the Otway Basin, showing major fault trends after Krassay et al. (2004) and Burgin and Amrouch (2019b), in addition to the seismic surveys, wells and petroleum fields mentioned during this study. Newer Volcanics Province (NVP) after Boyce (2013).

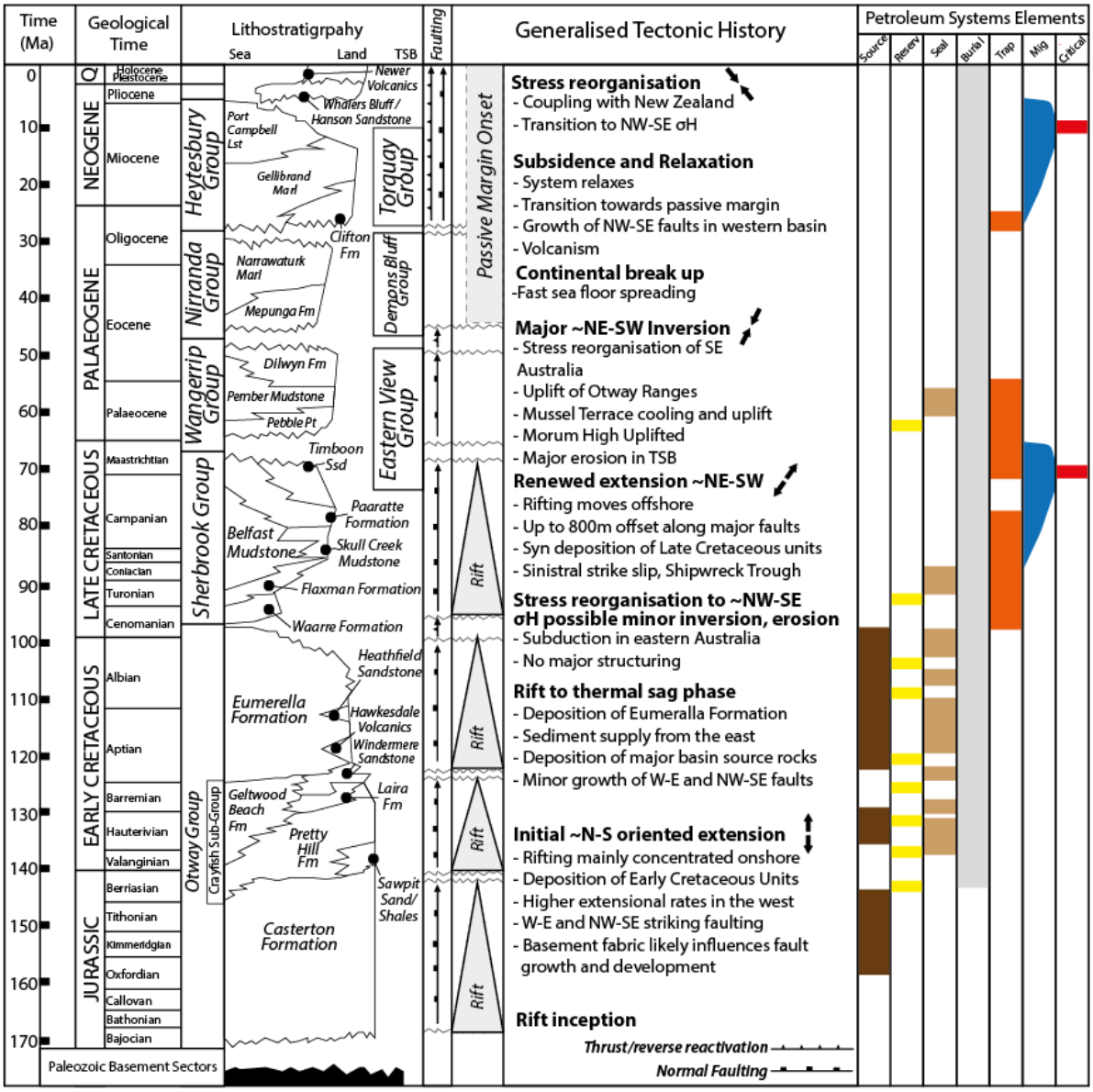

Fig. 3: A stratigraphic log and generalised model for basin evolution modified after Duddy (2003) and Geary and Reid (1998) with petroleum systems elements modified after O'Brien et al. (2009). Generalised tectonic history from Burgin and Amrouch (2019b).

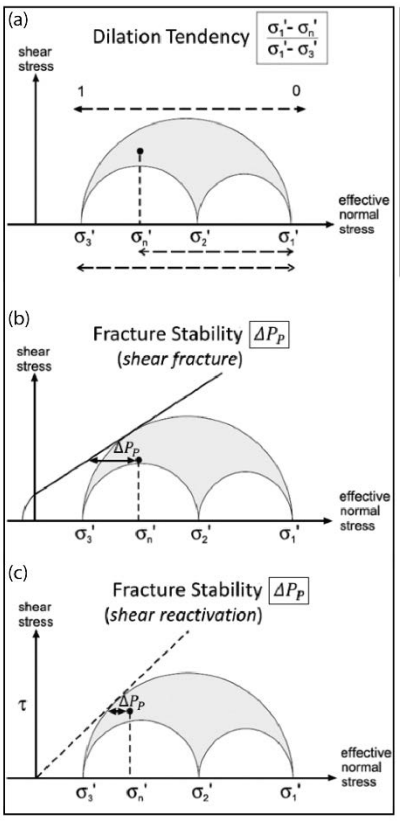

Fig 4: Schematic representation of modelling for (a) dilation tendency and (b) and (c) fracture stability. Modified from Kulikowski et al. (2016).

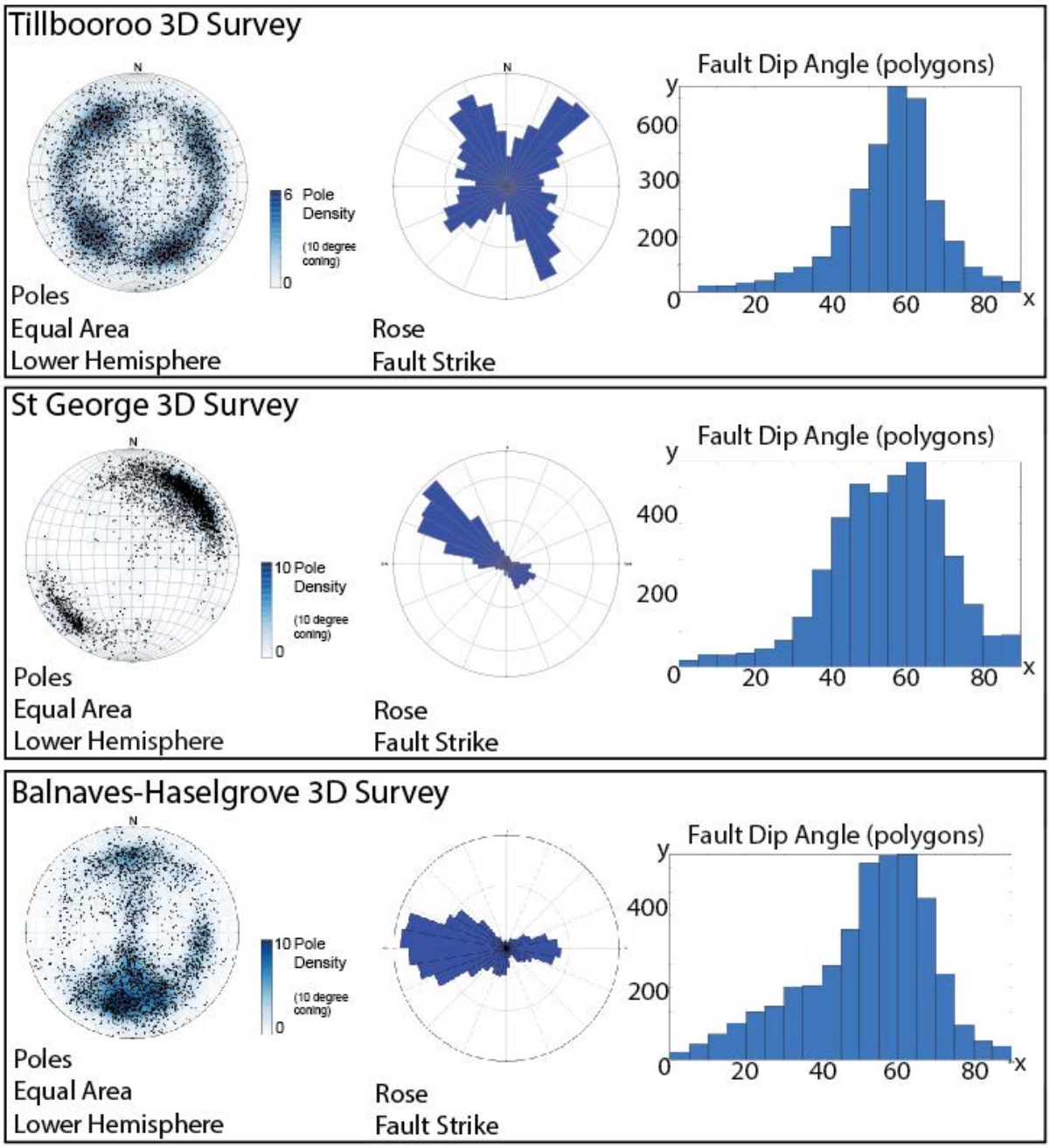

Fig. 5: Faults extracted and modelled within this study from the Tillbooro, St George and Balnaves Haselgrove 3D. Faults are largely high angle and in all cases are normal.(x,y) = fault dip angle and fault count.

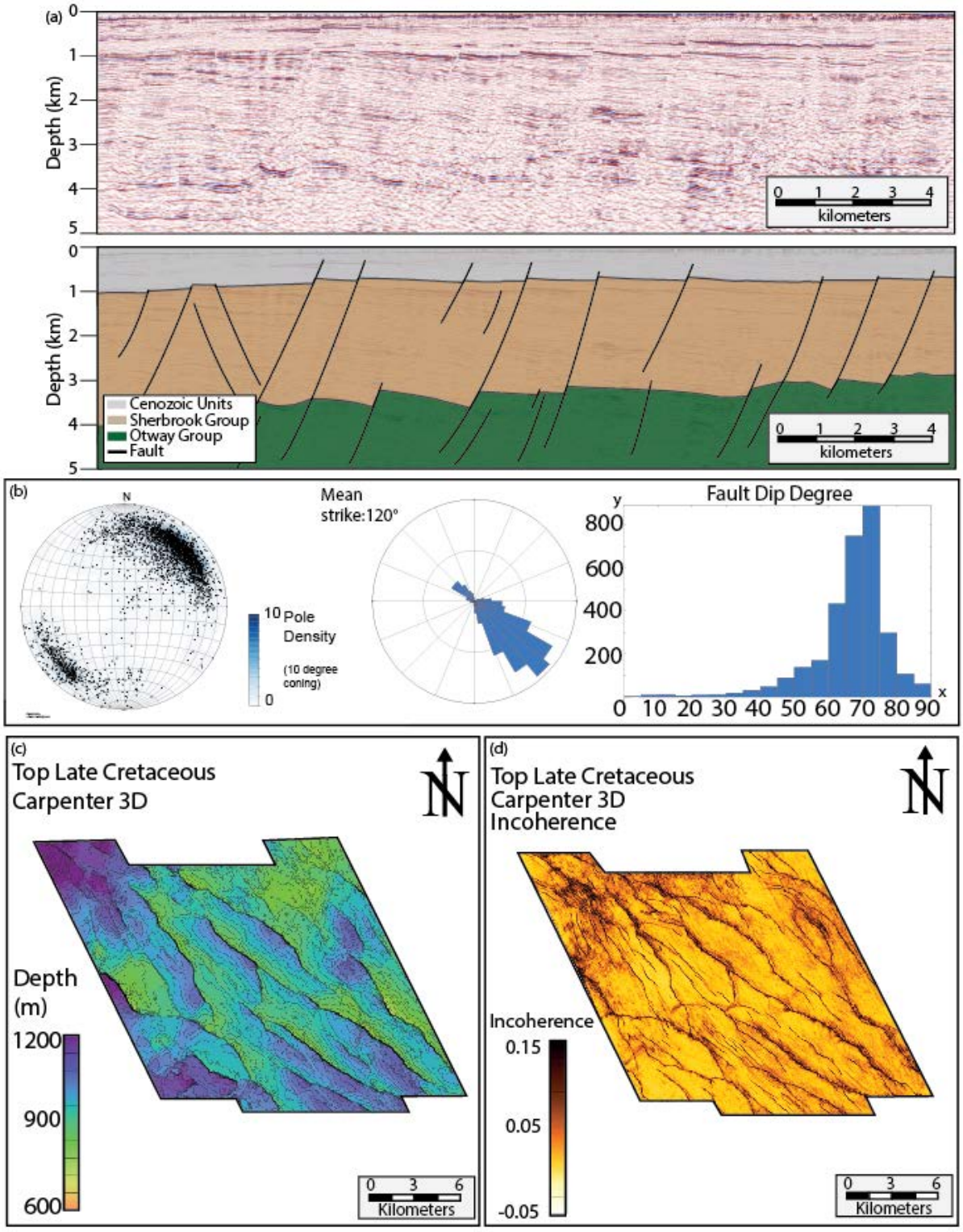

Fig. 6: (a) An example of an inline taken from the Carpenter 3D within the western Otway Basin (b) faults extracted from the survey and modelled as part of this study. (x,y) = fault dip angle and fault count. (c) A depth map of the Top Sherbrook formation within the Carpenter 3D as an example (d) The incoherence attribute displayed along the Top Sherbrook Formation that assists in highlighting the major ~NW-SE structural trend

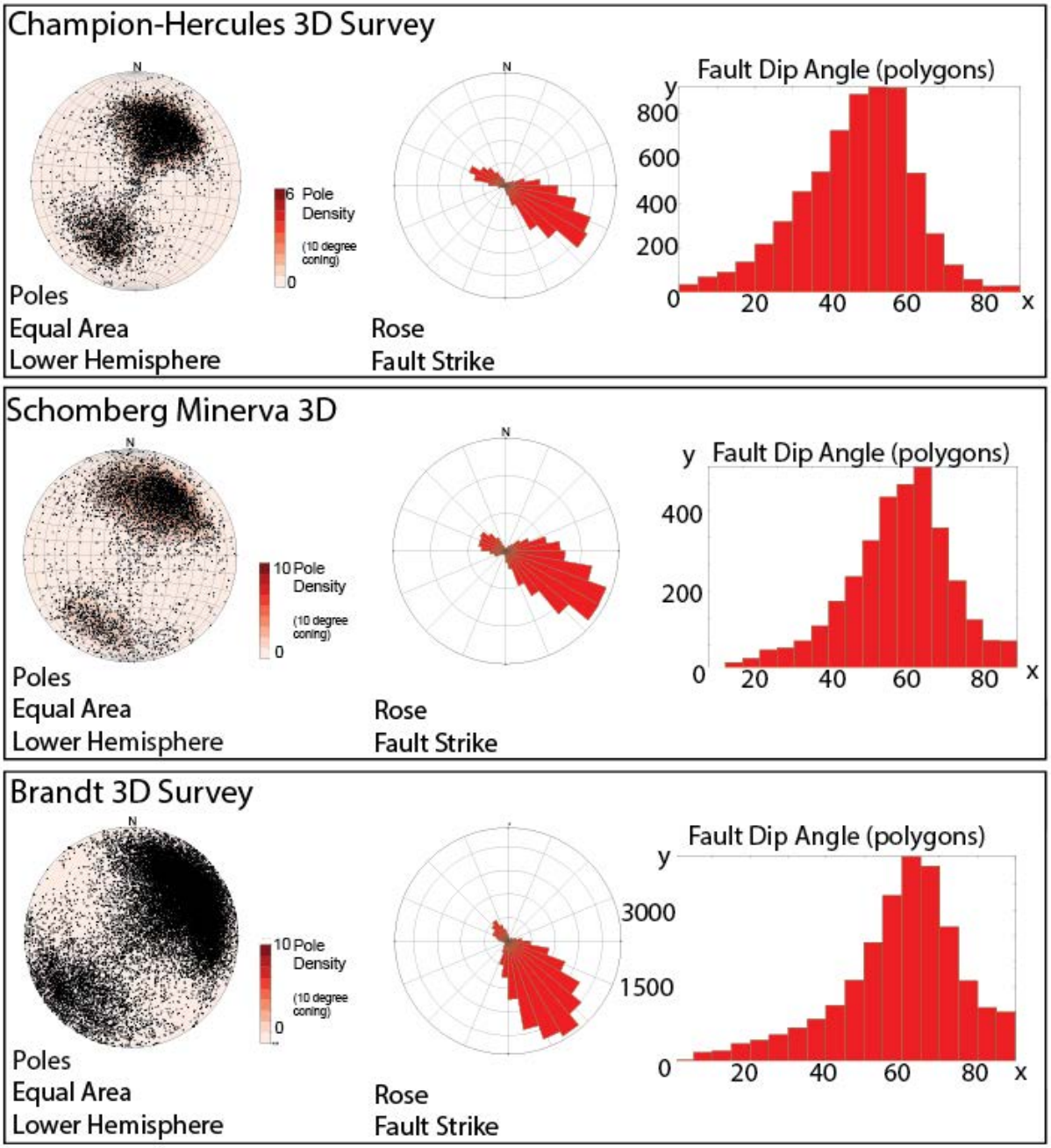

Fig. 7: Faults extracted and modelled within this study from the Champion-Hercules, Schomberg-Minerva, Brandt. Faults are largely high angle and in all cases are normal in nature. .(x,y) = fault dip angle and fault count.

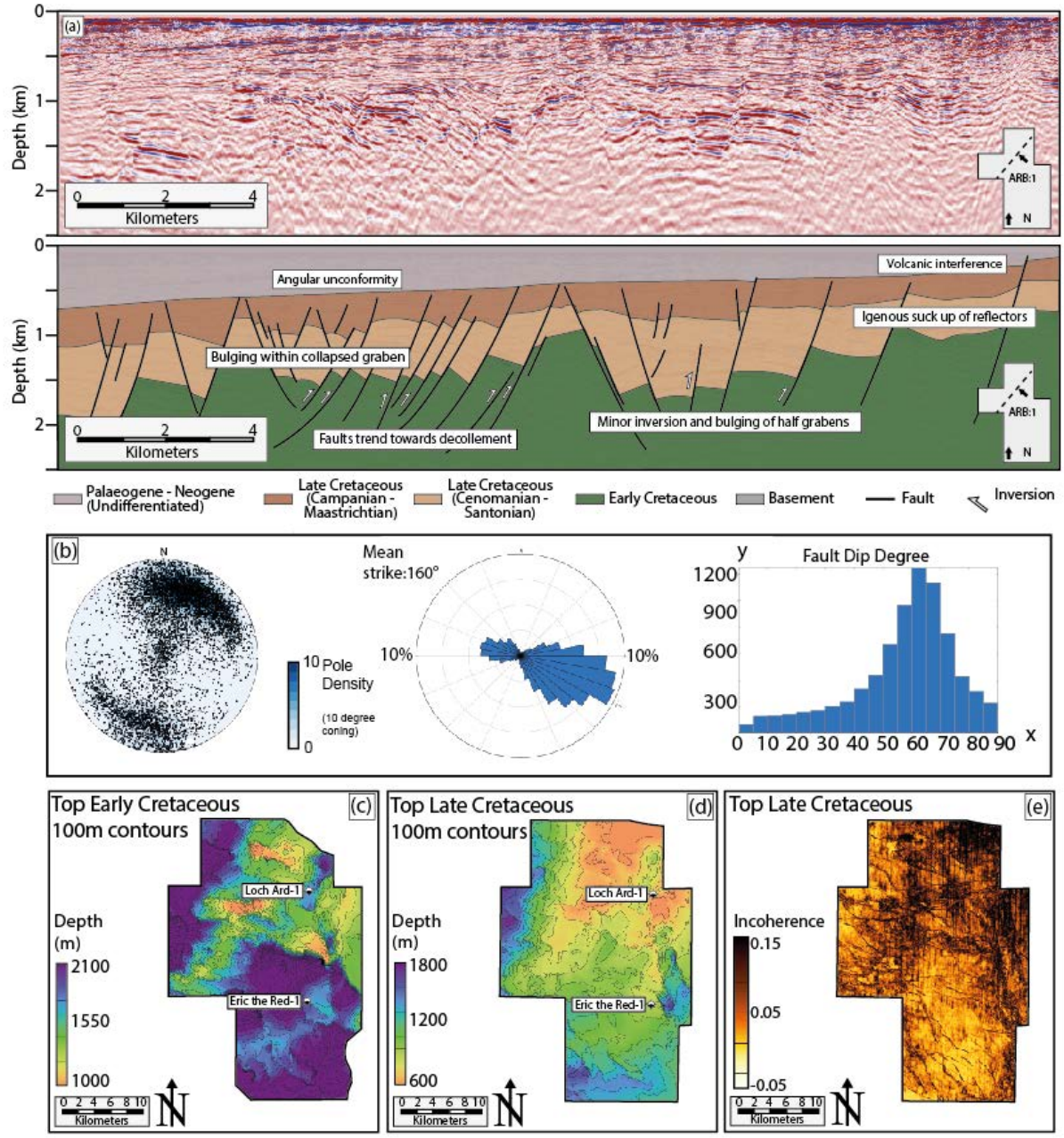

Fig. 8: (a) An example of an inline taken from the Crowes Foot 3D in the eastern Otway Basin (b) faults extracted from the survey and modelled as part of this study.(x,y) = fault dip angle and fault count. (c) A depth map of the Top Sherbrook formation within the Crowes Foot 3D as an example (d) The incoherence attribute displayed along the Top Sherbrook Formation that assists in highlighting the major ~NW-SE structural trend within the survey.

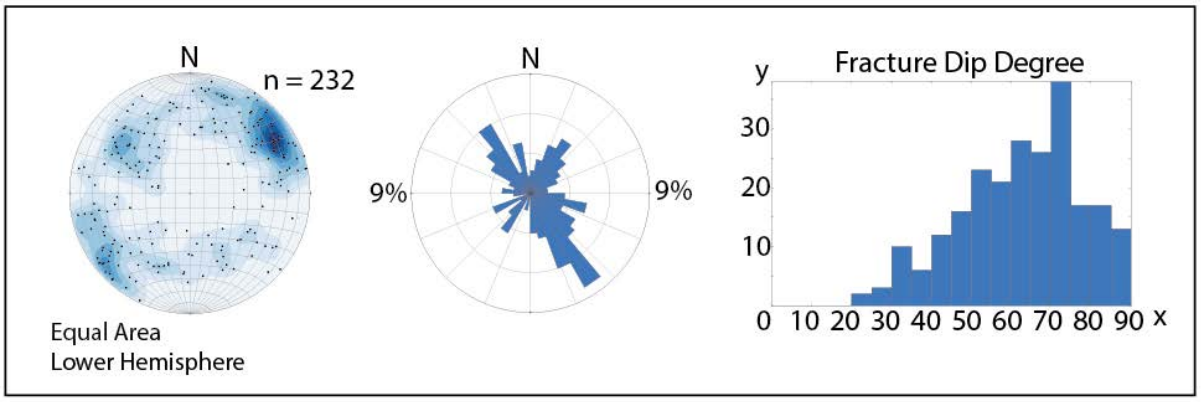

Fig. 9: Natural fracture extracted from well bore image log interpretations and modelled as part of this study. Fractures are mainly high angle ~50-90 degrees in dip and poles cluster mainly to the NE and SW.

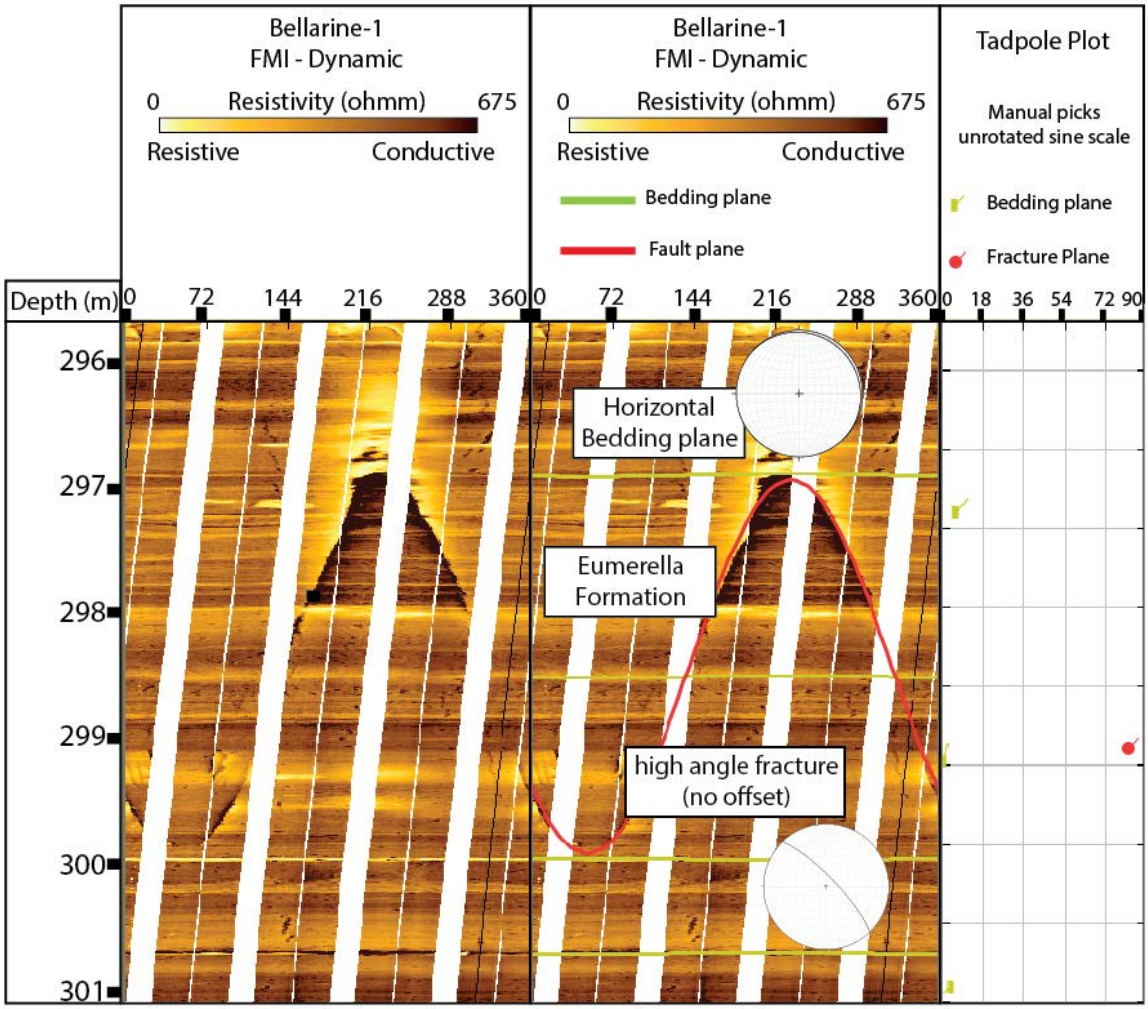

Fig. 10: An example of a high angle ~NW-SE striking fracture interpreted within the Bellarine-1 (Burgin and Amrouch, 2019b). This image log is of remarkable quality, with little tool stick, good correlation between image pads and a high resolution.

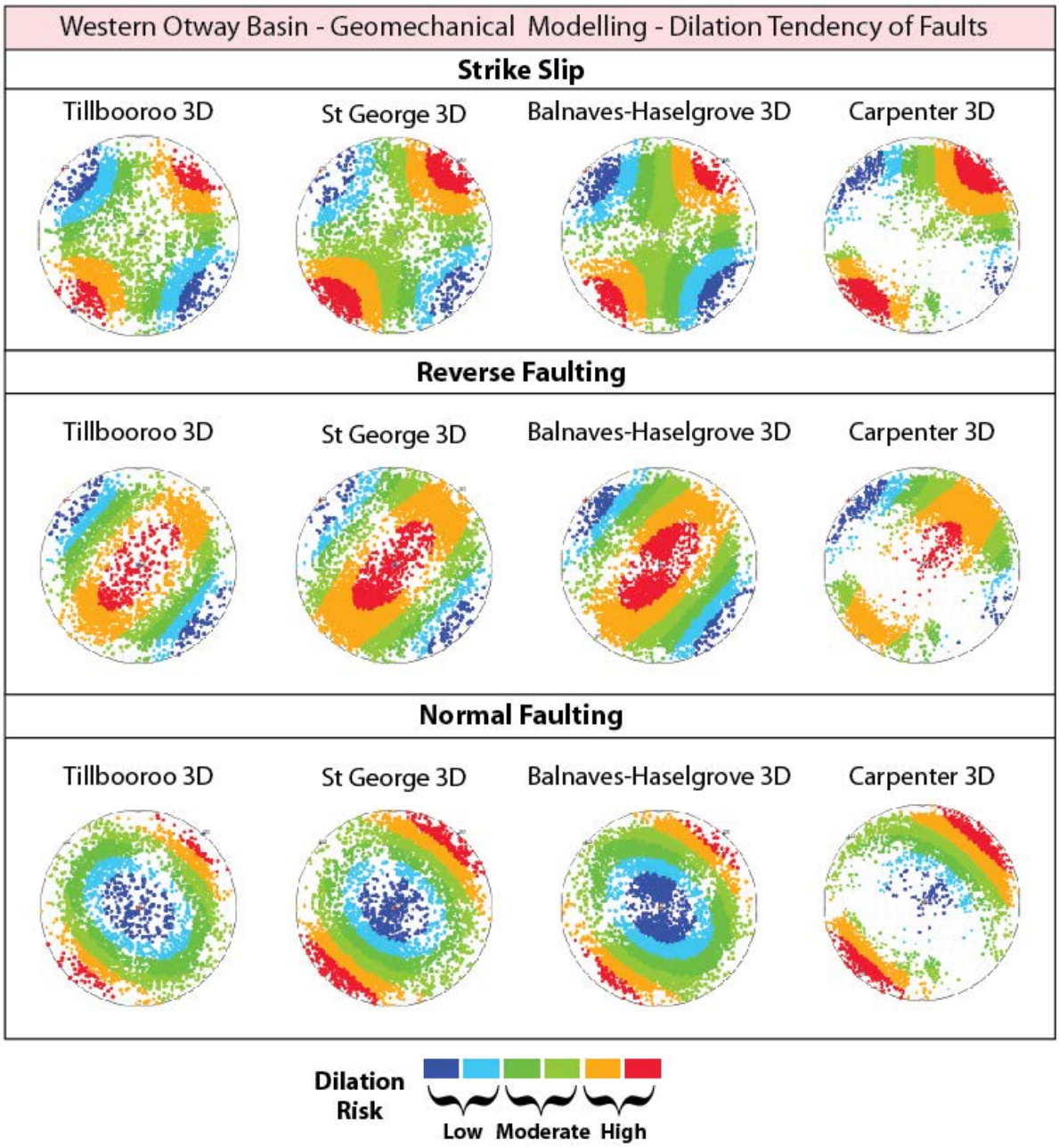

Fig. 11: The results from the modelling of dilation tendency within the western Otway Basin.

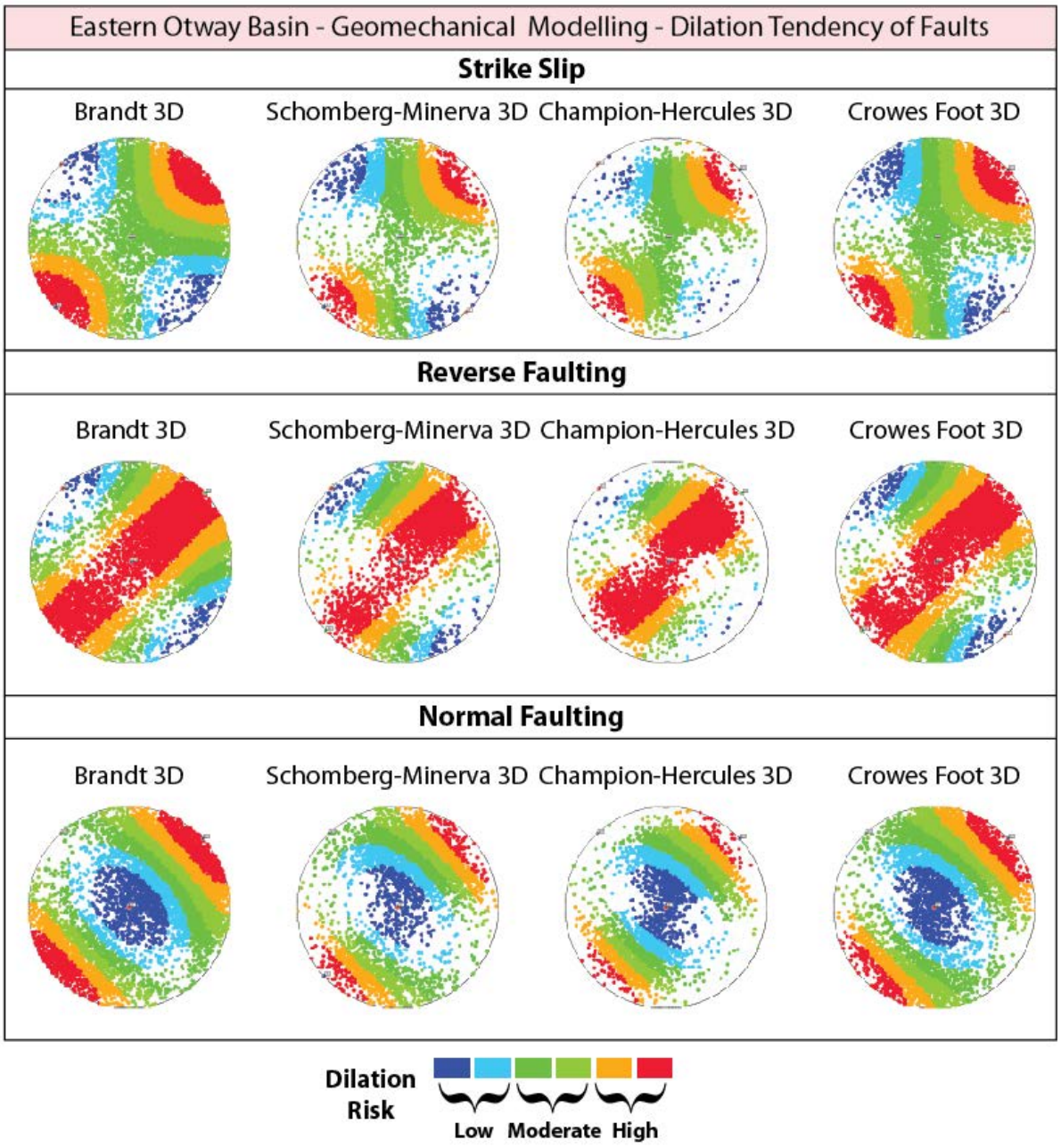

Fig. 12: The results from the modelling of dilation tendency in the eastern Otway Basin.

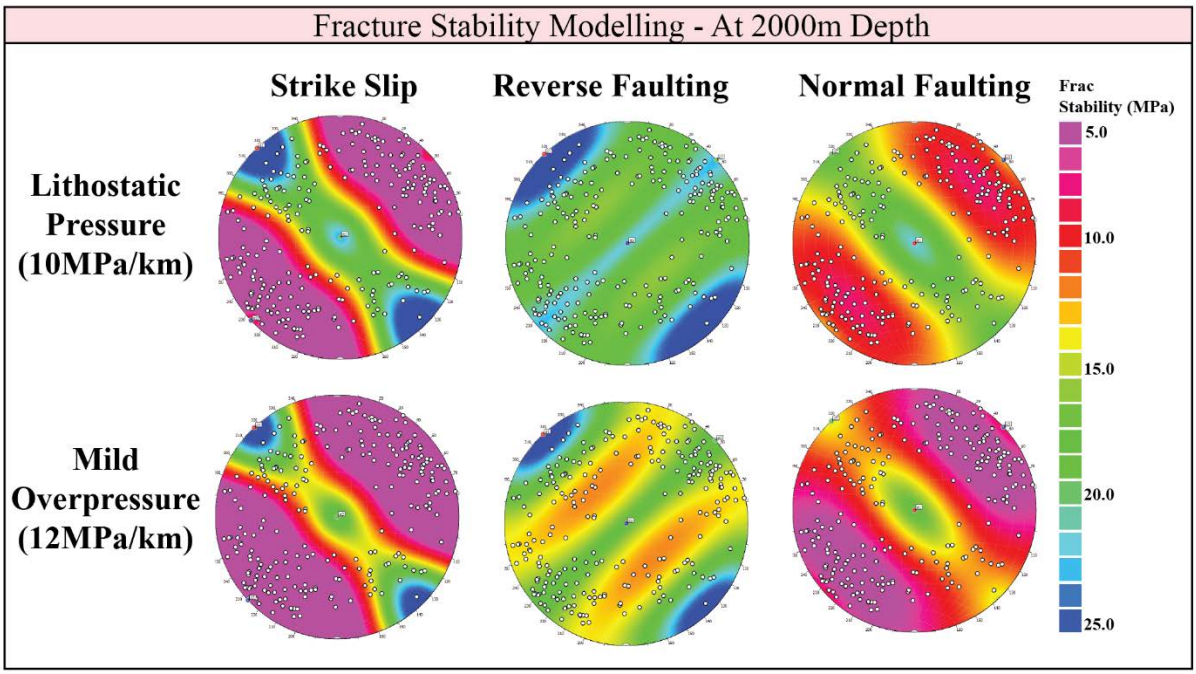

Fig. 13: The results from the modelling of natural fractures from seven wellbore image logs within the eastern Otway Basin.

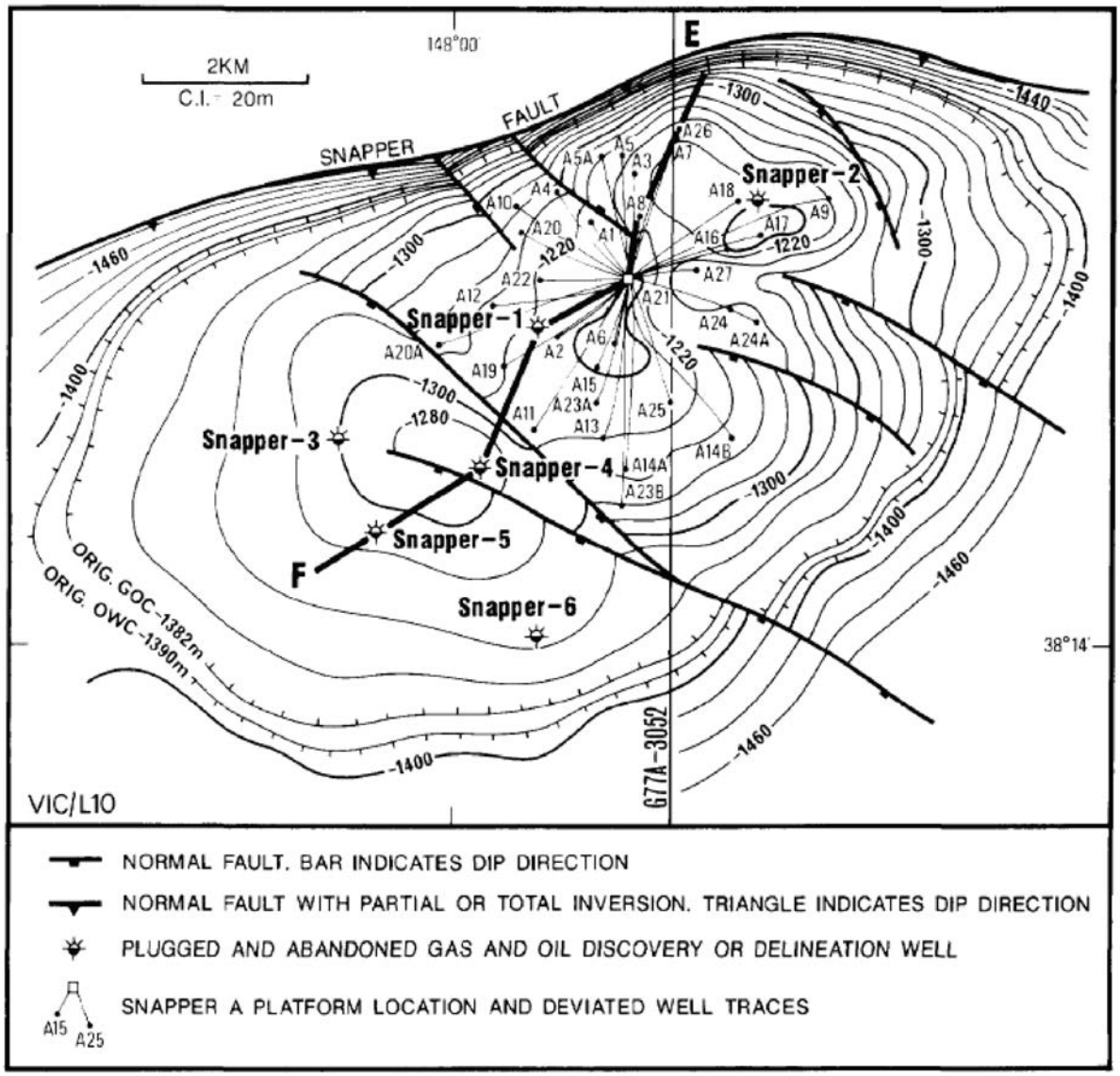

Fig. 14: A structural map taken from Glenton (1991) displaying the framework of the Snapper Anticline and Snapper Field in the Gippsland Basin. As can be seen significant inversion along ~ENE-WSW striking faults has resulted in the formation of a broad and long anticline, hosting one of Australia's first massive oil and gas fields

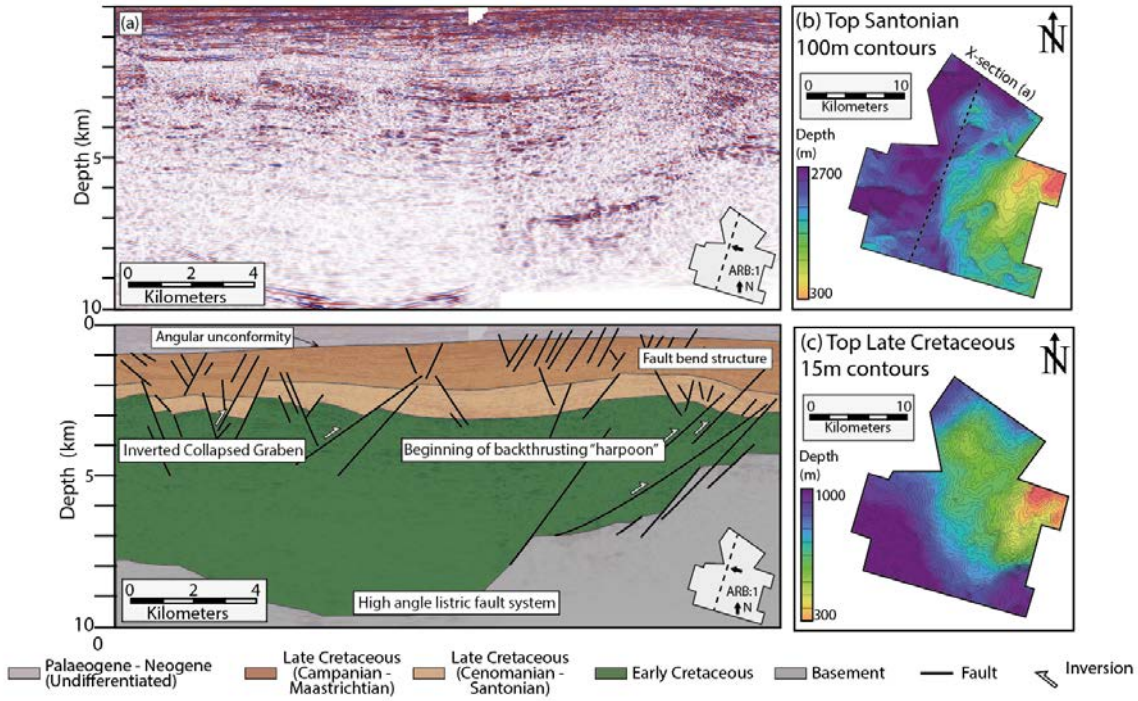

Fig. 15: (a) Arbitary line through the Minerva-Schomberg 3D, showing some of the modelled faults and the inversion structure that comprises the Minerva "anticline" penetrated by the well Minerva-1 (b) The Top Early Cretaceous surface through the survey. Modified from Burgin and Amrouch (2019b – in prep) (c) Top Late Cretaceous through the survey.

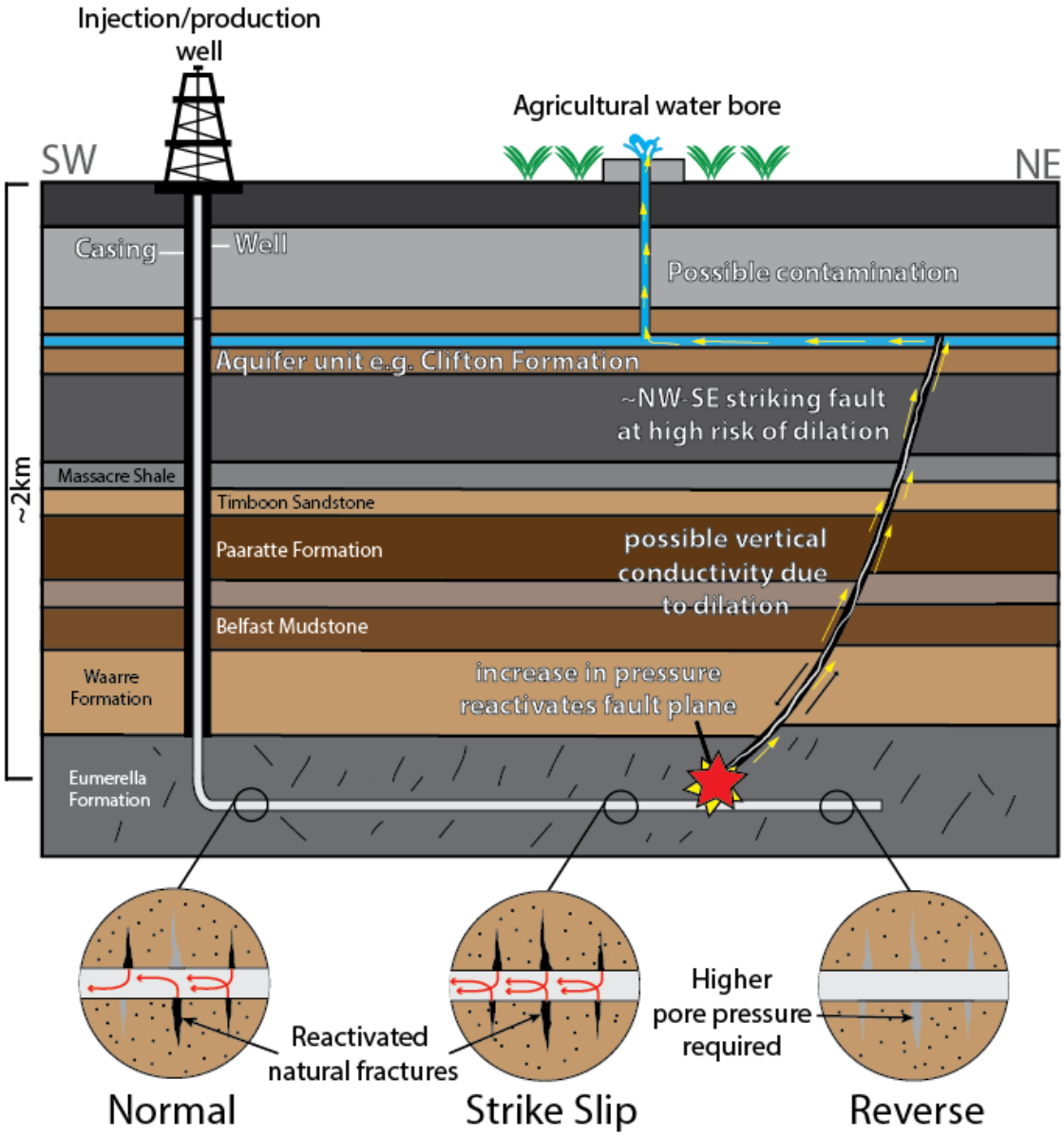

Fig. 16: A schematic diagram of the potential risks associated with unconventional production in addition to carbon capture and storage in the Otway Basin. ~NW-SE striking normal faults already at a high risk of dilation may be reactivated by even small increases in pore pressure at the reservoir depth, potentially acting as fluid conduits for either hydrocarbon, CO2, or drilling mud/hydraulic fluid which could contaminate aquifer units in the higher sedimentary succession, such as those within the Clifton Formation, which are of great importance to the agricultural industry within the region. Smaller schematics display the

approximate response of high angle fractures to different regimes of stress at a pore pressure increase of ~10MPa.

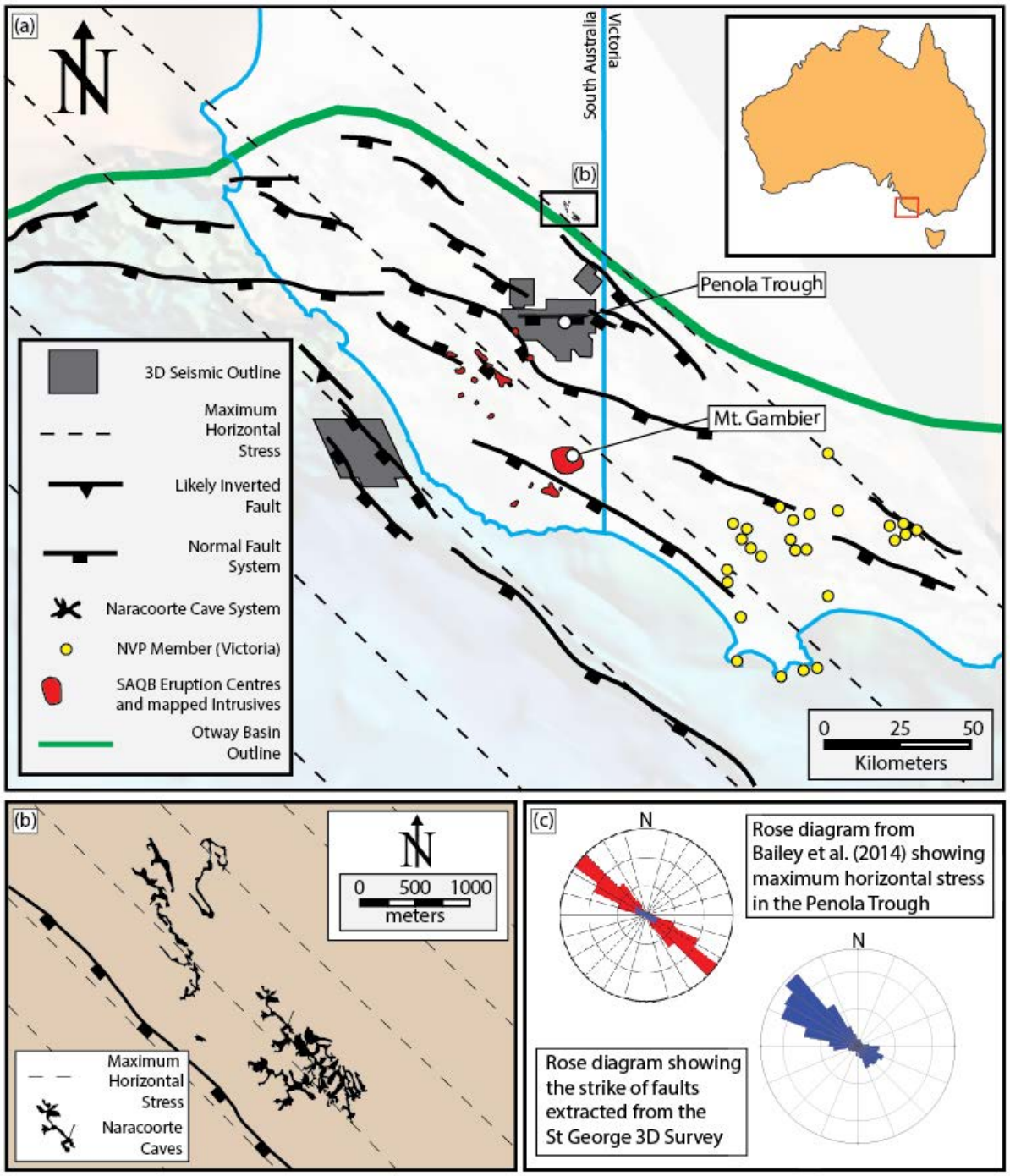

Fig. 17: (a) Map of the western Otway Basin showing the location of the 3D seismic surveys used for modelling in this region in addition to the major structural trend and regional evidence for recent volcanism (b) Schematic map from Moriarty et al. (2000) of the Naracoorte Cave systems which are parallel to the σH of the western Otway Basin (c) Red; a rose diagram showing the orientation of σH from Bailey et al .(2014). Blue; the strike of faults from the St George survey, closest to the caves which also strike parallel to the cave network and are at a high risk of dilation.

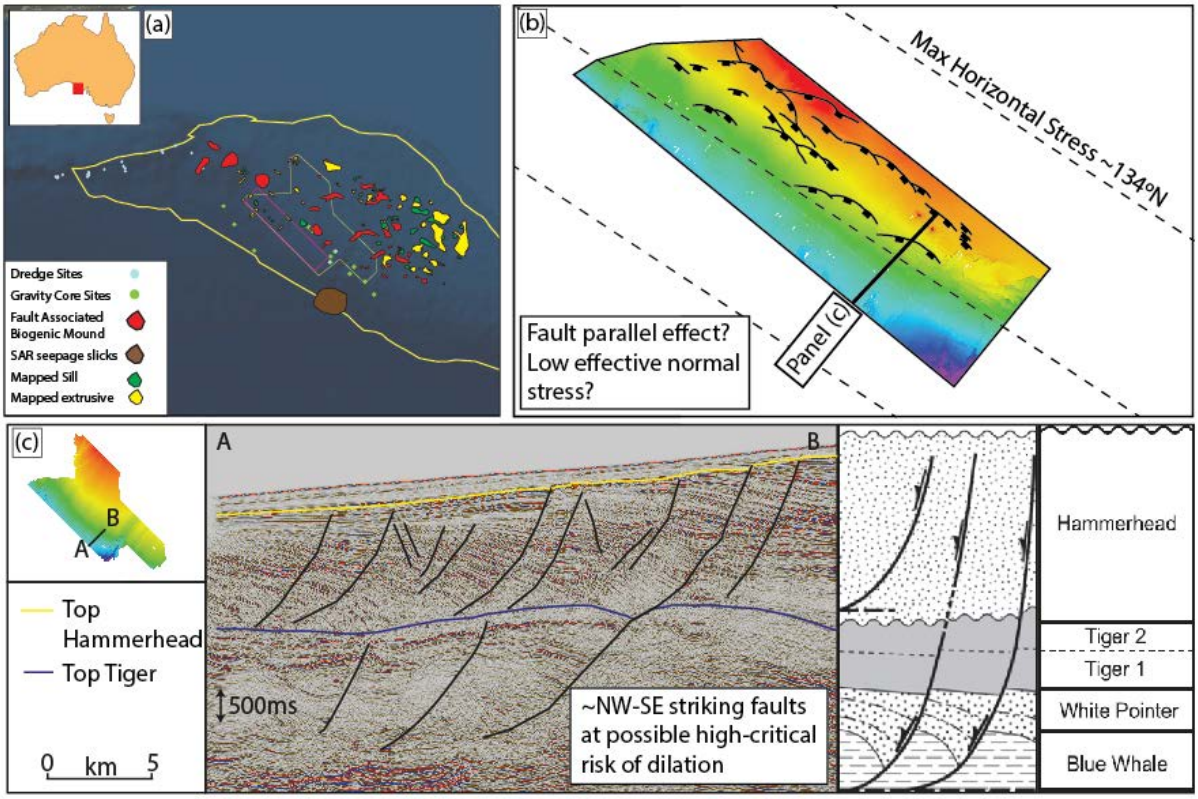

Fig. 18: a) Location of possible fluid flow associated features in the Ceduna Sub-Basin after Velatatham et al. (2019) (b) Time slice showing the orientation of major faults and their relationship to the in-situ stress field (c) cross section showing the listric style faults and minor fluid escape features.

References

Anderson, E. M. (1951). The dynamics of faulting and dyke formation with applications to Britain. Hafner Pub. Co..

Bailey, A., King, R., Holford, S., Sage, J., Backe, G., & Hand, M. (2014). Remote sensing of subsurface fractures in the Otway Basin, South Australia. *Journal of Geophysical Research: Solid Earth*, 119(8), 6591-6612.

Bailey, A. H., King, R. C., Holford, S. P., & Hand, M. (2016). Extending interpretations of natural fractures from the wellbore using 3D attributes: The Carnarvon Basin, Australia. *Interpretation*, 4(1), SB107-SB129.

Barton, C. A., Zoback, M. D., & Moos, D. (1995). Fluid flow along potentially active faults in crystalline rock. *Geology*, 23(8), 683-686.

Basir, H. M., Javaherian, A., & Yaraki, M. T. (2013). Multi-attribute ant-tracking and neural network for fault detection: a case study of an Iranian oilfield. *Journal of Geophysics and Engineering*, 10(1), 015009.

Bell, J. S. (1996). Petro Geoscience 1. In situ stresses in sedimentary rocks (part 1): measurement techniques. *Geoscience Canada*, 23(2).

Berard, T., Sinha, B. K., van Ruth, P., Dance, T., John, Z., & Tan, C. P. (2008, January). Stress estimation at the otway CO 2 storage site, Australia. *In SPE Asia Pacific Oil and Gas Conference and Exhibition*. Society of Petroleum Engineers.

Boreham, C. J., Hope, J. M., Jackson, P., Davenport, R., Earl, K. L., Edwards, D. S., ... & Krassay, A. A. (2004). Gas-oil-source correlations in the Otway Basin, southern Australia.

Bradshaw, M. (1993). Australian petroleum systems.

Braun, J., Burbidge, D. R., Gesto, F. N., Sandiford, M., Gleadow, A. J. W., Kohn, B. P., & Cummins, P. R. (2009). Constraints on the current rate of deformation and surface uplift of the Australian continent from a new seismic database and low-T thermochronological data. *Australian Journal of Earth Sciences*, 56(2), 99-110.

Broad, D. S., Jungslager, E. H. A., McLachlan, I. R., Roux, J., & Van der Spuy, D. (2012). South Africa's offshore Mesozoic basins. *In Regional Geology and Tectonics: Phanerozoic Passive Margins, Cratonic Basins and Global Tectonic Maps* (pp. 534-564).

Campbell, I., 2012, Lakes Oil N.L. quarterly activities report: For the three months, ended 30 June 2012: Lakes Oil N.L., Melbourne, Australia, 19 p.

Cliff, D. C. B., Tye, S. C., & Taylor, R. (2004). The Thylacine and Geographe gas discoveries, offshore eastern Otway Basin. *The APPEA Journal*, 44(1), 441-462.

CO2CRC (2016). CO2 CRC: Otway Project. Available at: http://www.co2crc.com.au/.

Cobbold, P. R., Meisling, K. E., & Mount, V. S. (2001). Reactivation of an obliquely rifted margin, Campos and Santos basins, southeastern Brazil. *AAPG bulletin*, 85(11), 1925-1944.

Constantine, A., & Liberman, N. (2001). Hydrocarbon prospectivity package for VIC/O-01 (1). VIC/O-01 (2) and VIC/O-01 (3), eastern onshore Otway Basin, Victoria, Australia: 2001 Acreage Release: Victorian Initiative for Minerals and Petroleum 70.

Cooper, G. T., & Hill, K. C. (1997). Cross-section balancing and thermochronological analysis of the Mesozoic development of the eastern Otway Basin. *The APPEA Journal*, 37(1), 390-414.

Dickinson, J. A., Wallace, M. W., Holdgate, G. R., Gallagher, S. J., & Thomas, L. (2002). Origin and timing of the Miocene-Pliocene unconformity in southeast Australia. *Journal of Sedimentary Research*, 72(2), 288-303.

Duddy, I. R., Erout, B., Green, P. F., Crowhurst, P. V., & Boult, P. J. (2003). Timing constraints on the structural history of the western Otway Basin and implications for hydrocarbon prospectivity around the Morum High, South Australia. *The APPEA Journal*, 43(1), 59-83.

Duddy, I. R. (2003). Mesozoic, a time of change in tectonic regime. Geology of Victoria, 23, 239-286.

Duddy, I. R. (1997). Focussing exploration in the Otway Basin: understanding timing of source rock maturation. *The APPEA Journal*, 37(1), 178-191.

Dyksterhuis, S., & Müller, R. D. (2008). Cause and evolution of intraplate orogeny in Australia. *Geology*, 36(6), 495-498.

Edwards, D. S., Struckmeyer, H. I. M., Bradshaw, M. T., & Skinner, J. E. (1999). Geochemical characteristics of Australia's southern margin petroleum systems. *The APPEA Journal*, 39(1), 297-321.

Etheridge, M., McQueen, H., & Lambeck, K. (1991). The role of intraplate stress in Tertiary (and Mesozoic) deformation of the Australian continent and its margins: a key factor in petroleum trap formation. *Exploration Geophysics*, 22(1), 123-128.

Ferrill, D. A., Winterle, J., Wittmeyer, G., Sims, D., Colton, S., Armstrong, A., & Morris, A. P. (1999). Stressed rock strains groundwater at Yucca Mountain, Nevada. GSA Today, 9(5), 1-8.

Ferrill, D. A., & Morris, A. P. (2003). Dilational normal faults. *Journal of Structural Geology*, 25(2), 183-196.

Gibson, G. M., Totterdell, J. M., White, L. T., Mitchell, C. H., Stacey, A. R., Morse, M. P., & Whitaker, A. (2013). Pre-existing basement structure and its influence on continental rifting and fracture zone development along Australia’s southern rifted margin. *Journal of the Geological Society*, 170(2), 365-377.

Glen, R. A., & Beckett, J. (1997). Structure and tectonics along the inner edge of a foreland basin: The Hunter Coalfield in the northern Sydney Basin, New South Wales. *Australian Journal of Earth Sciences*, 44(6), 853-877.

Glenton, P. N. (1991). Snapper Field--Australia Offshore Gippsland Basin, Southeast Australia.

Green, P. F., Crowhurst, P. V., & Duddy, I. R. (2004). Integration of AFTA and (U-Th)/He thermochronology to enhance the resolution and precision of thermal history reconstruction in the Anglesea-1 well, Otway Basin, SE Australia.

Hill, K. A., Cooper, G. T., Richardson, M. J., & Lavin, C. J. (1994). Structural framework of the eastern Otway Basin: inversion and interaction between two major structural provinces. *Exploration Geophysics*, 25(2), 79-87.

Hill, K. C., Hill, K. A., Cooper, G. T., O'Sullivan, A. J., O'Sullivan, P. B., & Richardson, M. J. (1995). Inversion around the Bass basin, SE Australia. *Geological Society, London, Special Publications*, 88(1), 525-547.

Hillis, R. R., & Reynolds, S. D. (2000). The Australian stress map. *Journal of the Geological Society*, 157(5), 915-921.

Hillis, R. R., & Williams, A. F. (1992). Borehole breakouts and stress analysis in the Timor Sea. *Geological Society, London, Special Publications*, 65(1), 157-168.

Hillis, R. R., & Williams, A. F. (1993). The contemporary stress field of the Barrow-Dampier Sub-Basin and its implications for horizontal drilling. *Exploration Geophysics*, 24(4), 567-576.

Hillis, R. R., Sandiford, M., Reynolds, S. D., & Quigley, M. C. (2008). Present-day stresses, seismicity and Neogene-to-Recent tectonics of Australia's 'passive'margins: intraplate deformation controlled by plate boundary forces. *Geological Society, London, Special Publications*, 306(1), 71-90.

Hillis, R. R. (1995). The contemporary stress field of the Otway Basin, South Australia: implications for hydrocarbon exploration and production. *The APPEA Journal.*

Holford, S. P., Tuitt, A. K., Hillis, R. R., Green, P. F., Stoker, M. S., Duddy, I. R., ... & Tassone, D. R. (2014). Cenozoic deformation in the Otway Basin, southern Australian margin: Implications for the origin and nature of post-breakup compression at rifted margins. *Basin Research*, 26(1), 10-37.

Holford, S., Hillis, R., Duddy, I., Green, P., Stoker, M., Tuitt, A., ... & MacDonald, J. (2011). Cenozoic post-breakup compressional deformation and exhumation of the southern Australian margin. *The APPEA Journal*, 51(1), 613-638.

Holford, S., Hillis, R., Duddy, I., Green, P., Tuitt, A., & Stoker, M. (2010). Impacts of Neogene-Recent compressional deformation and uplift on hydrocarbon prospectivity of the passive southern Australian margin. *The APPEA Journal*, 50(1), 267-286.

Hung, J. H., & Wu, J. C. (2012). In-situ stress and fault reactivation associated with LNG injection in the Tiechanshan gas field, fold-thrust belt of Western Taiwan. *Journal of Petroleum Science and Engineering*, 96, 37-48.

Jolie, E., Moeck, I., & Faulds, J. E. (2015). Quantitative structural–geological exploration of fault-controlled geothermal systems—A case study from the Basin-and-Range Province, Nevada (USA). *Geothermics*, 54, 54-67.

King, R., Holford, S., Hillis, R., Tuitt, A., Swierczek, E., Backé, G. & Tingay, M. (2012). Reassessing the in-situ stress regimes of Australia's petroleum basins. *The APPEA Journal*, 52(1), 415-426.

Korsch, R. J., Totterdell, J. M., Fomin, T., & Nicoll, M. G. (2009). Contractional structures and deformational events in the Bowen, Gunnedah and Surat Basins, eastern Australia. *Australian Journal of Earth Sciences*, 56(3), 477-499.

Krassay, A. A., Cathro, D. L., & Ryan, D. J. (2004). A regional tectonostratigraphic framework for the Otway Basin.

Kulikowski, D., Amrouch, K., Cooke, D., & Gray, M. E. (2018). Basement structural architecture and hydrocarbon conduit potential of polygonal faults in the Cooper-Eromanga Basin, Australia. *Geophysical Prospecting*, 66(2), 366-396.

Kulikowski, D., Amrouch, K., & Cooke, D. (2016). Geomechanical modelling of fault reactivation in the Cooper Basin, Australia. *Australian Journal of Earth Sciences*, 63(3), 295-314.

Kulikowski, D., Amrouch, K., & Cooke, D. (2016). Geomechanical modelling of fault reactivation in the Cooper Basin, Australia. *Australian Journal of Earth Sciences*, 63(3), 295-314.

Lennon, R. G., Suttill, R. J., Guthrie, D. A., & Waldron, A. R. (1999). THE RENEWED SEARCH FOR OIL AND GAS IN THE BASS BASIN: RESULTS OF YOLLA-2 AND WHITE IBIS-I. *The APPEA Journal*, 39(1), 248-262.

Leonard, M. (2008). One hundred years of earthquake recording in Australia. *Bulletin of the Seismological Society of America*, 98(3), 1458-1470.

Levell, B., Argent, J., Doré, A. G., & Fraser, S. (2010, January). Passive margins: overview. In Geological Society, London, Petroleum Geology Conference series (Vol. 7, No. 1, pp. 823-830). *Geological Society of London*.

Littva, J., Hok, J., & Bella, P. (2015). Cavitonics: Using caves in active tectonic studies (Western Carpathians, case study). *Journal of Structural Geology*, 80, 47-56.

Luxton, C. W., Horan, S. T., Pickavance, D. L., & Durham, M. S. (1995). The La Bella and Minerva gas discoveries, offshore Otway basin. *The APPEA Journal*, 35(1), 405-417.

Lyon, P. J., Boult, P. J., Hillis, R. R., & Bierbrauer, K. (2007). Basement controls on fault development in the Penola Trough, Otway Basin, and implications for fault-bounded hydrocarbon traps. *Australian Journal of Earth Sciences*, 54(5), 675-689.

Macdonald, J., Backé, G., King, R., Holford, S., & Hillis, R. (2012). Geomechanical modelling of fault reactivation in the Ceduna Sub-basin, Bight Basin, Australia. *Geological Society, London, Special Publications*, 367(1), 71-89.

Mann, P., Gahagan, L., & Gordon, M. B. (2003). Tectonic setting of the world's giant oil and gas fields.

McLean, C. E., Schofield, N., Brown, D. J., Jolley, D. W., & Reid, A. (2017). 3D seismic imaging of the shallow plumbing system beneath the Ben Nevis Monogenetic Volcanic Field: Faroe–Shetland Basin. *Journal of the Geological Society*, jgs2016-118.

Miller, J. M., Norvick, M. S., & Wilson, C. J. (2002). Basement controls on rifting and the associated formation of ocean transform faults—Cretaceous continental extension of the southern margin of Australia. *Tectonophysics*, 359(1-2), 131-155.

Moeck, I., Kwiatek, G., & Zimmermann, G. (2009). Slip tendency analysis, fault reactivation potential and induced seismicity in a deep geothermal reservoir. *Journal of Structural Geology*, 31(10), 1174-1182.

Moriarty, K. C., McCulloch, M. T., Wells, R. T., & McDowell, M. C. (2000). Mid-Pleistocene cave fills, megafaunal remains and climate change at Naracoorte, South Australia: towards a predictive model using U-Th dating of speleothems. *Palaeogeography, Palaeoclimatology, Palaeoecology*, 159(1-2), 113-143.

Morris, A., Ferrill, D. A., & Henderson, D. B. (1996). Slip-tendency analysis and fault reactivation. *Geology,* 24(3), 275-278.

Nelson, E., Hillis, R., Sandiford, M., Reynolds, S., & Mildren, S. (2006). Present-day state-of-stress of southeast Australia. *The APPEA Journal*, 46(1), 283-306.

Norvick, M. S., & Smith, M. A. (2001). Mapping the plate tectonic reconstruction of southern and southeastern Australia and implications for petroleum systems. *The APPEA Journal*, 41(1), 15-35.

O'Brien, G., Boreham, C., Thomas, H., & Tingate, P. (2009). Understanding the critical success factors determining prospectivity—Otway Basin, Victoria. *The APPEA Journal*, 49(1), 129-170.

Origin Energy. (2003). Well Completion Report - Interpretive: Thylacine-1. Unpublished

Cockshell, D. P. C. (1995). The Otway basin: early Cretaceous rifting to Neogene inversion. *The APPEA Journal*, 35(1), 451-466.

Perincek, D., Simons, B., & Pettifer, G. R. (1994). THE TECTONIC FRAMEWORK AND ASSOCIATED PLAY TYPES OF THE WESTERN OTWAY BASIN, VICTORIA, AUSTRALIA. *The APPEA Journal*, 34(1), 460-478.

Petkovic, P. & Geoscience Australia. (2004). Time-depth functions for the otway basin. Geoscience Australia Record, 2(2).

Power M. R., Hill K. C., Hoffman N., Bernecker T. & Norvick M. 2001. The structural and tectonic evolution of the Gippsland Basin: results from 2D section balancing and 3D structural modelling. In: Hill K.C. & Bernecker T. eds. Eastern Australasian Basins Symposium: a refocused energy perspective for the future, pp. 373–384. *Petroleum Exploration Society of Australia, Special Publication*. Melbourne Vic.

Power, M. R., Hill, K. C., & Hoffman, N. (2003). Structural inheritance, stress rotation, overprinting and compressional reactivation in the Gippsland Basin—Tuna 3D seismic dataset. *The APPEA Journal*, 43(1), 197-221.

Ebaugh, D. D., McClure, P. W., & Karduna, A. R. (2005). Three-dimensional scapulothoracic motion during active and passive arm elevation. *Clinical Biomechanics*, 20(7), 700-709.

Rajabi, M., Tingay, M., Heidbach, O., Hillis, R., & Reynolds, S. (2017). The Present-day stress field of Australia. *Earth-Science Reviews*, 168, 165-189.

Rajabi, M., Heidbach, O., Tingay, M., & Reiter, K. (2017). Prediction of the present-day stress field in the Australian continental crust using 3D geomechanical–numerical models. *Australian Journal of Earth Sciences*, 64(4), 435-454.

Reynolds, S. D., Coblentz, D. D., & Hillis, R. R. (2003). Influences of plate-boundary forces on the regional intraplate stress field of continental Australia. *SPECIAL PAPERS-GEOLOGICAL SOCIETY OF AMERICA*, 59-70.

Reynolds, S. D., & Hillis, R. R. (2000). The in situ stress field of the Perth Basin, Australia. *Geophysical Research Letters*, 27(20), 3421-3424.

Robson, A. G., Holford, S. P., King, R. C., & Kulikowski, D. (2018). Structural evolution of horst and half-graben structures proximal to a transtensional fault system determined using 3D seismic data from the Shipwreck Trough, offshore Otway Basin, Australia. *Marine and Petroleum Geology*, 89, 615-634.

Ryan, S., Knight, L., & Parker, G. (1995). The stratigraphy and structure of the Tyrendarra Embayment, Otway Basin, Victoria, Victorian Initiative for Minerals and Petroleum Report 15, Department of Agriculture. Energy and Minerals.

Sandiford, M., & Quigley, M. (2009). TOPO-OZ: Insights into the various modes of intraplate deformation in the Australian continent. *Tectonophysics*, 474(1-2), 405-416.

Sandiford, M., Quigley, M., de Broekert, P., & Jakica, S. (2009). Tectonic framework for the Cenozoic cratonic basins of Australia. *Australian Journal of Earth Sciences*, 56(S1), S5-S18.

Schmitt, D. R., Currie, C. A., & Zhang, L. (2012). Crustal stress determination from boreholes and rock cores: Fundamental principles. *Tectonophysics*, 580, 1-26.

Shaw, R. D. (1991). The tectonic development of the Amadeus Basin, central Australia. Geological and Geophysical Studies in the Amadeus Basin, Central Australia, *Bulletin 236.*

Sibson, R. H. (1996). Structural permeability of fluid-driven fault-fracture meshes. *Journal of Structural Geology*, 18(8), 1031-1042.

Basins of the Great Australian Bight region: geology and petroleum potential

Stoker, M. S., Praeg, D., Shannon, P. M., Hjelstuen, B. O., Laberg, J. S., Nielsen, T., ... & Evans, D. (2005, January). Neogene evolution of the Atlantic continental margin of NW Europe (Lofoten Islands to SW Ireland): anything but passive. *In Geological Society, London, Petroleum Geology Conference series* (Vol. 6, No. 1, pp. 1057-1076). Geological Society of London.

Summons, R. E., Bradshaw, M., Crowley, J., Edwards, D. S., George, S. C., & Zumberge, J. E. (1998). Vagrant oils: geochemical signposts to unrecognised petroleum systems.

Tassone, D. R., Holford, S. P., King, R., Tingay, M. R., & Hillis, R. R. (2017). Contemporary stress and neotectonics in the Otway Basin, southeastern Australia. *Geological Society, London, Special Publications*, 458, SP458-10.

Tassone, D. R., Holford, S. P., Duddy, I. R., Green, P. F., & Hillis, R. R. (2014). Quantifying Cretaceous–Cenozoic exhumation in the Otway Basin, southeastern Australia, using sonic transit time data: Implications for conventional and unconventional hydrocarbon prospectivity. *AAPG Bulletin*, 98(1), 67-117.

Totterdell, J. M., Blevin, J. E., Struckmeyer, H. I. M., Bradshaw, B. E., Colwell, J. B., & Kennard, J. M. (2000). A NEW SEQUENCE FRAMEWORK FORTHE GREAT

AUSTRALIAN BIGHT: STARTING WITH A CLEAN SLATE. The APPEA Journal, 40(1), 95-118.

Tupper, N. P., Padley, D., Lovibond, R., Duckett, A. K., & McKirdy, D. M. (1993). A key test of Otway Basin potential: the Eumeralla-sourced play on the Chama Terrace. *The APPEA Journal*, 33(1), 77-93.

Turner, J. P., Green, P. F., Holford, S. P., & Lawrence, S. R. (2008). Thermal history of the Rio Muni (West Africa)–NE Brazil margins during continental breakup. *Earth and Planetary Science Letters*, 270(3-4), 354-367.

Valle, P. J., Gjelberg, J. G., & Helland-Hansen, W. (2001). Tectonostratigraphic development in the eastern lower Congo Basin, offshore Angola, West Africa. *Marine and Petroleum Geology*, 18(8), 909-927.

van Ruth, P. J., Nelson, E. J., & Hillis, R. R. (2006). Fault reactivation potential during CO2 injection in the Gippsland Basin, Australia. *Exploration Geophysics*, *37*(1), 50-59.

Van Ruth, P. (2007). CRC-1 extended leak-off test report. CO2CRC Report RPT07-0608, 8.

Velayatham, T., Holford, S. P., & Bunch, M. A. (2018). Ancient fluid flow recorded by remarkably long, buried pockmark trains observed in 3D seismic data, Exmouth Plateau, Northern Carnarvon Basin. *Marine and Petroleum Geology*, 95, 303-313.

Vidal-Gilbert, S., Tenthorey, E., Dewhurst, D., Ennis-King, J., Van Ruth, P., & Hillis, R. (2010). Geomechanical analysis of the Naylor Field, Otway Basin, Australia: Implications for CO2 injection and storage. *International Journal of Greenhouse Gas Control*, 4(5), 827-839.

Watson, M. N., Boreham, C. J., & Tingate, P. R. (2004). Carbon dioxide and carbonate cements in the Otway Basin: implications for geological storage of carbon dioxide. *The APPEA Journal*, 44(1), 703-720.

Willcox, J. B., & Stagg, H. M. J. (1990). Australia's southern margin: a product of oblique extension. *Tectonophysics*, 173(1-4), 269-281.

Heidbach, O., Rajabi, M., Reiter, K., & Ziegler, M. (2016). World stress map 2016. *Science*, 277, 1956-62.

Zoback, M. L. (1992). First-and second-order patterns of stress in the lithosphere: The World Stress Map Project. *Journal of Geophysical Research: Solid Earth*, 97(B8), 11703-11728.

Chapter 4.6: Manuscript 7

The Structural Framework of the Otway Basin: New Insights from the Torquay Sub-Basin

This finalised manuscript will be submitted to the peer-reviewed journal *The Australian Journal of Earth Science.* Following the publication of all preceding manuscripts.

Statement of Authorship

Title of Paper: The Structural Framework of the Otway Basin: New Insights from the Torquay Sub-Basin

Publication Status: Unpublished and Unsubmitted work written in a manuscript style

Publication Details: Burgin, H. B. and Amrouch, K. (2019d). The Structural Framework of the Otway Basin: New Insights from the Torquay Sub-Basin. (In Prep)

Principal Author: Hugo Bonython Burgin

Contribution: 3D seismic interpretation. Writing of paper. Structural analysis. (85%).

Certification: This paper reports on original research I conducted during the period of my Higher Degree by Research candidature and is not subject to any obligations or contractual agreements with a third party that would constrain its inclusion in this thesis. I am the primary author of this paper.

Signed: **Date:** 05/03/2019

Co-Author Contributions

By signing the Statement of Authorship, each author certifies that:

- **i.** The candidate's stated contribution to the publication is accurate (as detailed above);
- **ii.** Permission is granted for the candidate to include the publication in the thesis; and
- **iii.** The sum of all co-author contributions is equal to 100% less the candidate's stated contribution.

Name of Co-Author: Dr Khalid Amrouch

Contribution to Paper: Assistance with structure and writing of paper. Assistance with regional interpretation (15%)

Signed: **Date:** 05/03/2019

The Structural Framework of the Otway Basin: New insights from the Torquay Sub Basin

*Hugo B. **BURGIN**[a] (hugo.burgin@adelaide.edu.au)

Khalid **AMROUCH**[a] (khalid.amrouch@adelaide.edu.au)

[a]Australian School of Petroleum, University of Adelaide, North Tce, 5005, Adelaide, Australia

*Corresponding Author: Hugo B. Burgin (08 8313 8000)

Abstract

The structural framework of the Otway Basin is well studied, with two distinct generations of work in the literature. The first, published during the early stages of hydrocarbon exploration from the 1980s to early 2000s, the second representing more modern assessments in the last ten years. The two generations of work, display distinct differences in approaches and available datasets and as a result, their ability to effectively constrain the framework of the basin has varied. Building on the modern body of work, through the structural interpretation of Torquay 3D seismic survey, this paper presents a revised structural framework for the Otway Basin. Simultaneously discussing a number of factors that may have hamstrung works within the first generation of studies, resulting in an enigmatic and inaccurate structural framework. The most notable revision for the new model is the absence of a ~NE-SW trending fault network within the eastern most basin, and the Otway Ranges. Though the exclusion of these faults is conflict with many past studies, the new framework is reliably defined by structural datasets from the micro to the macro scale. Characterising a more consistent framework, both within the basin and across Australia's southern margin.

1.0 Introduction

The Otway Basin (**fig.1**) represents a classic example of a passive continental margin basin and has seen many structurally focused investigations throughout the last fifty years. The basin is one of an en-echelon series of sedimentary provinces that line Australia's southern margin, comprising the Southern Rift System (SRS) (Wilcox and Stagg, 1990) (**fig. 1**), a region synonymous with some of Australia's most successful oil and gas fields.

Early research in the last decades of the 20th century within the Otway Basin, utilised petroleum industry datasets, mainly two-dimensional (2D) seismic. Studies of this era were focused on constraining the phases of early basin evolution (e.g. Etheridge et al., 1985; Wilcox and Stagg, 1990) and inversion (e.g. Hill et al., 1995; Cooper and Hill, 1997) and relating them to regional models of continental separation between Australia and Antarctica (e.g. Teasdale et al., 2003). A secondary focus was to discern how two seemingly orthogonally striking - ~NW-SE and ~NE-SW - structural fabrics developed simultaneously within the eastern sector of the basin (Duddy 1994; Hill et al., 1995; Finlayson et al., 1996; Cooper and Hill, 1997; Miller et al., 2002) and the degree and timing of inversional events (Duddy, 1994; Hill et al., 1994; Cooper and Hill, 1997).

This first generation of work, mainly between the 1980s and early 2000s, resulted in a variety of structural frameworks and theories for the nature of continental break up in the basin. Including; major ~NE-SW listric and planar detachment and transform systems (Etheridge et al., 1985; Etheridge et al., 1988; Lister et al., 1989), NW-SE oriented strike slip models (Willcox and Stagg, 1990; O'Brien et al., 1994), progressive N-S (Hill et al., 1994) and NE-SW (Perincek et al., 1994) rifting, oblique extension (Cooper and Hill, 1997) and progressive fault rotation from W to E (Miller et al., 2002).

Works using early datasets, such as 2D seismic, also present evidence for periodic inversion and uplift in the Otway Basin, particularly during the Mid Cretaceous (Duddy, 1994; Cooper and Hill, 1997), Late Cretaceous (Duddy and Erout, 2001; Duddy et al., 2003) and episodic, Miocene – recent (Holford 2011; Holford et al., 2014) which in all cases favour a ~NW-SE oriented compressional azimuth. As a result, through much of the early 21st century the structural framework of the basin remained confusing and poorly defined.

The past ten years has seen a resurgence of research within the basin, coming mainly from staff and students at the Australian School of Petroleum. These studies providing new, cutting edge insights into the evolution of the basin as well as complimentary fields at the forefront of geoscience, including: Detailed assessments of the stages of normal fault growth (Robson et al., 2016; 2017; 2018), the influence of basement architecture on fault development during rifting (Lyon et al., 2007), the quantification of exhumation and uplift using sonic log analysis (Tassone et al., 2014), detailed assessment of post break up compression (Holford et al., 2014), the introduction of novel techniques for fracture mapping in the sub-surface and outcrop (Bailey et al., 2014; Burgin et al 2018), comparing and contrasting in-situ stress environments from geological evidence and petroleum industry datasets (Tassone et al., 2017), investigations into the internal structure of faults (Debenham et al., 2018; 2019), the first application of microstructural techniques of petrophysical data at a passive continental margin (Burgin et al., 2019b), and the first quantification of differential stresses during continental break up (Burgin and Amrouch, 2019b).

Today, 11 3D cubes in the basin have seen detailed structural investigation across the Otway Basin (**fig. 2**), a significant increase in data resolution from the first generation of studies. Combining the insights from many of these studies, allows for detailed comparisons to be made

between the two generations of work. Contrasts that highlight the importance of viewing dated models for basin evolution with a degree of reserve, especially given the limited nature of the data available at the time.

As such, the aims of this paper are multi-faceted, to **1)** present new insights from a 3D seismic interpretation in the Torquay Sub-Basin (TSB) **2)** highlight the limitations of early studies, mainly surrounding the use of 2D datasets **3)** present a new structural framework for the Otway Basin and **4)** Discuss the consequences with respect to the in situ stress conditions of the region.

2.0 3D Seismic Analysis in the Torquay Sub Basin

This section outlines the interpretation of the Torquay 3D survey and how the results contribute to completing a refined model for the structural framework of the Otway Basin.

2.1 Geological Setting - The Torquay Sub Basin

The Torquay sub-basin (TSB) (**fig. 3**) formed due to off-shore extension within the north eastern most sector of the Otway Basin, the sub-basin contains a series of depocentres varying in age from the Early Cretaceous to the Neogene (Holford et al., 2011). With sediment thicknesses varying from 5-7km in the central deep, to 2 -5km in the surrounding Snail Terrance (Trupp et al., 1994).

The TSB has been the subject of a number of studies (e.g. Hill et al., 1995; Holford et al., 2011b; Holford et al., 2014) although detailed structural mapping using 3D seismic data has not been completed. The TSB is bound to the west by the outcropping Otway Ranges and to the east by the Mornington Peninsula (**fig. 3**). The sub-basin contains unconformities throughout the Paleogene and Neogene sedimentary succession, stratigraphic events that mark

a number of erosional events, including the widespread Miocene unconformity, which has been mapped throughout much of southeastern Australia (**fig. 4**).

Evidence for folding and faulting within Miocene sediments within the TSB has been presented in previous studies (Hill et al., 1994; Trupp et al., 2002; Holford et al., 2011; Dickenson et al., 2002). Many of which utilise predominately 2D seismic lines, which strike mainly ~NW-SE, to constrain the structural framework of the sub basin. In most cases these studies work with the assumption that the Otway Basin exhibits two contrasting distinct structural trends between the west and east (Tassone et al., 2017), which modern studies indicate it may not exist (Burgin and Amrouch (2019b). In light of recent findings by Burgin and Amrouch (2019b that suggest the presence of NW-SE, rather than NE-SW striking faults within the Otway Ranges, we believe the structural framework of the TSB requires a re-assessment.

Sedimentary successions within the TSB (**fig. 4**) are constrained by three wells, including Wild Dog-1, Snail-1 and Nerita-1 (**fig. 3**) and consist of Lower Paleozoic metasediments and volcanics units overlain by the Early Cretaceous Otway Group sediments, which encompasses the Eumeralla Formation. A major unconformity is present at the top of the Eastern View Group, which records exhumation and uplift constrained by a number of AFTA studies across much of southeastern Australia (Duddy, 1994, 2009; Hill et al., 1995; Duddy and Erout, 2001).

In the TSB, the Otway Group is overlain by the Eastern View Group (**fig. 4**), equivalent to the Sherbrook Group (Duddy et al., 2003) within other sectors of the eastern Otway Basin. The Eastern View Group is overlain by the Demon's Bluff Group, which is aged middle to late Eocene and represents an increasingly marine dominated environment of deposition (Messent et al., 1999). The Demons Bluff Group is overlain by the Late Oligocene-Miocene Torquay

Group which comprises mainly marine carbonate sections with a maximum thickness of 700m in the central deep of the sub-basin (Messent et al., 1999).

2.1 Dataset and Methodology

The Torquay 3D survey extends over ~245km^2 within the central TSB, covering the previously imaged Wild Dog-1 structure (Hill et al., 1994; Holford et al., 2014). The survey has a maximum penetration of 6.0s two-way time and was acquired in January 2013. The western most edge of the survey is ~36km due east from the sea side town of Apollo Bay in the Otway Ranges (**fig. 3**). Inlines within the survey strike N-S at a spacing of 25m, and crosslines E-W at 6.25m. Wild Dog-1 was used to tie horizon interpretations and to convert from the time to the depth domain using a standard windowing velocity model. Vertical resolution within the survey was calculated to be approximately 20m at 1s TWT with a dominant frequency of 32Hz.

2.2 Seismic interpretation and results

Igneous features exert a strong control over the structural fabric of the Torquay 3D survey, identified due to their high-amplitude nature and apparent discontinuity with surrounding seismic reflectors (**fig 5**).

Two sections of the survey are affected by the largest identifiable igneous features; the first, a dyke structure (IT-1) (**fig. 5b**) striking ~ENE-WSW, is confined to a fault plane within the Basement, Eumerella Formation, and sections of the Eastern View Group in the western half of the survey. IT-1 is visible at a depth slice of 1100m, and is almost 6km in length along strike (**fig. 5e**). In the eastern half of the survey, a buried volcano (EX-1) (**fig. 5b**), dominates the architecture, along with two associated intrusive bodies (IT-2 and IT-3) which are difficult to

discern due to the significant disruption of seismic reflectors. EX-1, IT-2 and IT-2 are best pictured at a depth slice of 700m (**fig. 5f**).

Interpretation of the regional basement was possible throughout most of the survey due to a hard seismic kick (**fig. 6**), that becomes less obvious in close proximity to the igneous events. The interpretation shows two basement structural fabrics (**fig. 3b**), the most dominant being a ~NW-SE striking series of faults, that define a series of similarly striking half grabens, extending upwards into the Eumeralla Formation. A second fault set striking ~ENE-WSW are isolated along the edge of a basement high and show minimal reactivation within the overlying sediments.

Due to poor data resolution within the Eumeralla Formation, only partial interpretation of the most extensive and continuous inter-formational reflector was possible. Even so, a partial depth map of the horizon (**fig. 6b**) displays a series of ~NW-SE striking domino style grabens – best viewed through a ~NE-SW striking arbline (**fig. 5c**) - that have been significantly rotated down towards the SW and panned off at the base Demons Bluff inconformity (**fig. 6c**). A feature that is suggestive of a major period of structuring and uplift prior to the deposition of the Demons Bluff Group.

Offset along most faults is normal, although reverse offset is visible in a few cases (**fig. 5d**), in combination with contracted fault angles, and bulging within collapsed graben structures. This structuring suggests the fault network has been subjected to ~NE-SW oriented inversion in a similar manner to faults within the Prawn Platform (Burgin and Amrouch, 2019b). ENE-WSW structuring is also evident within the Eumeralla Formation, although it is isolated to the fault plane hosting IT1-1.

The Eastern View Group is evident within the survey only within small half graben sections (**fig. 5d**) along ~NW-SE striking faults that penetrate the Eumeralla Formation and are downthrown to the SW. Due to removal it's throughout most of the survey and limited well control, differentiation between it and the Top Eumerella was difficult, as was its interpretation, and as such it was not completed in detail.

The base Demons Bluff Group was interpreted throughout all of the Torquay 3D survey (**fig. 6c**). The unit uncomfortably overlies both the Eumerella Formation and Eastern View Group, containing forced folding deformation (the folding of sediments due to the intrusion of igneous material) that is concentrated around the intrusive and extrusive bodies within the survey. This style of deformation is also visible along the top Demons Bluff reflector (**fig. 6e**) and to a lesser extent the mid-Torquay Group horizon (**fig 6g**). The Top Demons Bluff Group (**fig. 6e)** is un-faulted in cross section, throughout the survey, although minor deformation is evident utilising the incoherence attribute. The use of attribute highlighting the effect of the underlying intrusives as well as the extrusive volcano on the topography of the surface, in addition to the minor reactivation of underlying faults (**fig. 6f**).

To assess the deformation within the Torquay Group, an arbitrary and continuous reflector was interpreted throughout the survey at ~300m depth (**fig. 6g)**. Deformation of this surface is emphasised using the incoherency attribute, showing a dominant ~NW-SE striking pattern of small normal faults (**fig. 6h**). Polygonal style faulting is also seen within the unit, especially in sections overlying the igneous bodies (**fig. 6h**), and there is no direct dip linkage between NW-SE striking faults within the Torquay Group and those within underlying units. That being said many faults within the group occur directly up-dip from underlying faults within the basement,

Eumeralla and Demons Bluff Group, displaying the same dip degree and dip direction. Suggesting these deeper seated faults have accommodated minor reactivation, which has resulted in faulting propagating upwards into the overlying sediments. A structural feature that may have been exaggerated due to differential compaction.

With respect to the timing of igneous material within the survey: The presence of EX-1 at the top of the Demons Bluff Group and forced folding within the formations upper layers surrounding IT-1, the two events seem to have occurred within the late Palaeogene. With IT1 likely occurring mid deposition of the Demons Bluff Group and EX1 occurring post deposition of the unit (**fig. 5b**). This observation is supported by on-lap of the Torquay Group sediments and minor faults within the unit directly above the intrusions (**fig. 5b**)

2.4 Discussion of 3D seismic results

The interpretation of the Torquay 3D survey has a number of consequences with respect to revising the structural framework of the Otway Basin and aligns well with the recent insights from Burgin and Amrouch (2019b).

Firstly, it is apparent that the broadly ~NW-SE structural fabric present within almost all of the Otway Basin sediments to the west is also pervasive throughout the TSB. This observation, suggesting that if ~ENE-WSW faults are present within the region, they are likely confined to the basement, and defined by minimal reactivation into the Otway Group units, even during phases of extension. This supports Burgin and Amrouch's (2019b) thesis that no major structural change occurs within the eastern half of the Otway Basin. Also supporting the authors' model for ~NE-SW oriented, co-axial basin inversion and uplift in the Otway Ranges.

The interpretation also supports a major period of ~Latest Cretaceous basin inversion proposed by Burgin and Amrouch (2019b) an event that is characterised by the distinct erosional event following deposition of the Eastern View Group – the most angular unconformity observed within the basin to date - resulting in the panning off of the ~NW-SE striking grabens. Additionally, the style of inversional structures within the survey is similar to those observed within the Prawn Platform (Burgin and Amrouch, 2019b), implying a structural style of formation.

In contrast to previous works in the same region (Hill et al., 1995; Holford et al., 2014), the analysis, shows no evidence for ~NW-SE oriented Miocene – recent compression and inversion within the TSB around the Wild Dog structure (**fig. 3c**). In fact the noted correlation between deep seated ~NW-SE striking faults within the Eumeralla Formation and the Torquay Group (**fig. 6h**), suggest that if anything ~NE-SW extensional stresses may have continued dominate well into the Miocene and present day. Although the poorly imaged Nerita anticline may provide some evidence for regional Neotectonic uplift (Holford et al., 2011), the insights from this study suggest approaches using 2D data have likely been ineffective at constraining the true nature of the structure.

2.5 Section Summary

The results from the interpretation of the Torquay 3D are in contrast to the results from previous 2D seismic based studies within the TSB. 3D seismic interpretation revealing a structural trend that was predominantly hidden from previous datasets (**fig. 3c**). The insights gained within this study are due to the simple nature of the data, as all previous works used only 2D data and the degree of insight between it and 3D data is almost incomparable. That being said, it is our belief

that other factors also contributed to the misinterpretation of the structural framework within the TSB and eastern Otway Basin which we explore in the following section.

3.0 Contrasting dated and modern approaches

The Otway Basin and in particular studies within the TSB and the immediate surroundings, represent an excellent case study as to the importance of revising historic models of basin evolution. Highlighting the advantage of taking a modern and multiscale approach to basin analysis.

With the benefit of hindsight from many recent works, it is of use to briefly outline the distinct contrast in approaches and datasets between the two generations of work. These differences exist mainly between those studies utilising dated 2D datasets or in some cases single 2D lines, and those that have taken advantage of modern 3D methods of analysis including the integration of sub seismic datasets.

3.1 Paleostress or in-situ stress?

Investigations quantifying paleostress orientations and magnitudes in many regions around the globe (Zagros [Iran] (Amrouch et al., 2010), Khao Khwang [Thailand] (Arboit et al., 2017), The Albanides [Albania] (Lacombe et al., 2009) and the Rocky Mountains [Wyoming] (Amrouch et. al., 2010a, 2010b; Beaudoin et al., 2012, 2016) including Australia (Kulikowski and Amrouch, 2017), make it apparent that stresses within the earth are not static and evolve dynamically. As such when conducting structural investigations it is important to remember that in-situ stresses are not representative of paleostresses.

We suggest that in the Otway Basin, this distinction between paleostresses and in-situ stresses was often not recognised (**fig. 7**) at least to a high enough degree, when considering the region's structural evolution. From the commentary of many studies (Duddy 1994; Hill et al., 1995; Edwards et al., 1996; Cooper and Hill 1997; Krassay et al., 2004; King et al., 2012; Holford et al., 2011; 2014; Tassone et al., 2014; 2017) it is apparent an orthogonal orientation between the ~NE-SW striking Otway Ranges in the eastern sector of the basin, and the ~NW-SE trending maximum horizontal in situ stress, has biased their conclusions (**fig. 7**). Whilst in early studies these connections were often made with some reserve, alongside questions (such as to why the ranges were so isolated: Hill et al., 1995), these problems faded with time, the neotectonic model of formation becoming accepted in the late 90s (Cooper and Hill, 1997). In the Otway Ranges, this model of basin inversion resulted in the mapping of a number of ~NE-SW striking inverted faults, in the absence of any actual structural evidence for their existence (e.g. outcropping fault planes, reverse offset, kinematic indicators, seismic offset) even at the well-studied Castle Cove (Debenham et al., 2018; 2019; Burgin et al., 2019a). Indeed, one must only take a drive along the region's famous ~NE-SW trending Great Ocean Road to view the distinct lack parallel regional thrusting, which should be visible given the scale of the uplift, which has been estimated in excess of 2000m (Tassone et al., 2014).

3.2 Spatial limitations of 2D seismic datasets

The advantages of 3D seismic datasets over 2D seismic data are obvious, as 2D seismic lines, especially when used in isolation, only allow for a slither of information to be interpreted. While 3D seismic on the other hand, allows for the entire geometry of structures to be observed. A characteristic of the data that is of particular importance when completing structural analyses, especially when interpreting complex networks of faults. It is our belief that certain

limitations of 2D seismic data have played a key role in the history of establishing an accurate structural framework of the Otway Basin (**fig. 8**).

During 2D seismic analysis, it is difficult or impossible to discern true fault strike, or the presence of faults at all, if line orientation is parallel to fault strike (**fig. 3**). A drawback of the dataset that is further emphasised when only single 2D lines are used in isolation from the wider dataset (e.g. Dickenson et al., 2002; Hill et al., 1994). As even during the interpretation of complete survey set, characterised by tightly spaced 2D lines, changes in the structural nature of sediments is possible between the lines. In 2019, with the benefit of hindsight from many regional 3D studies, we believe these particular issues hamstrung early investigations in the Otway Basin and TSB. For instance Trupp et al., (1994), Hill et al., (1995) and Dickenson et al (2002) use the interpretation of 2D datasets to analyse the structural framework of the TSB. In all these cases, primarily ~NW-SE striking 2D lines were used for analysis, which from results presented in section *2* of this paper, means they were parallel to fault strike within the Eumeralla Formation. Making the interpretation of the large network of ~NW-SE striking faults in the formation a difficult task (**fig. 3**). We also suspect that in the case of Dickenson et al., (2002) oblique angles between faulting and line orientations have distorted the appearance of structures. Distinct differences between a study utilising 2D data and 3D data in the Otway Basin can also be drawn between Holford et al., (2014) and Burgin and Amrouch (2019b). The first study utilises the interpretation of a ~NW-SE striking 2D line along the prawn platform, interpreting the Crowes and Loch Ard anticlines. The second images these structures in 3D, displaying two ~NE-SW striking chains of horst and graben structures, defined by ~NW-SE striking faults, concentrated above a basement high (Burgin and Amrouch, 2019b).

3.3 Compounding Errors

Edwards et al., (1996) represents a Geological Report compiled by the Geological Survey of the Australian State of Victoria. The report is responsible for the construction of a series of structural cross sections through the on-shore Otway Basin and Otway Ranges. Despite containing an accurate and highly detailed map of the surface geology, the cross sections in this report, in particular those striking ~NW-SE are inaccurate. Their structural framework for the basin outlining the reverse reactivation of steeply dipping ~NE-SW striking faults under Miocene-recent, ~NW-SE compression. A model which has been largely refuted by later works (Schnider et al., 2004; Burgin and Amrouch, 2019b) (**fig. 9**). Although, the framework of ~NE-SW striking faults was present within the literature prior to the report by Edwards et al., in 1996 (e.g. Perincek et al., 1994) it is the cross sections within this study that have been most widely adopted by following works. Especially as they accompany a detailed surface map of the region, which made the report as a whole, an excellent resource.

These cross sections by Edwards et al., (1996) have been embraced by two major studies on the Australian neotectonic record including: Dickinson et al., (2002) who discuss the timing and origin of the Miocene-Pliocene unconformity and Clark et al., (2012) who present an extensive record of Australia's seismogenic record. Numerous other works throughout the literature have also directly adopted the Edwards et al., (1996) framework, including (Holford et al., 2014; Tassone et al., 2014; Debenham et al., 2018; Raiber et al., 2008) Stirling et al., (2011); Tassone et al., (2017); Clark et al., (2014); Clark et al., (2012) and King et al., (2012) with many of these studies using the flawed cross sections as a foundation for their own conclusions.

We also suspect that the first structural geological map of the Otway Ranges has had a significant influence on later works. The map was published by Medwell in 1971, prior to modern advances in topographic mapping and aerial photography and is the first study to describe the Otway Ranges as a series of ~NE-SW trending anticlines. An inference that was considerably built upon by Edwards et al., (1996), that led to many following works assuming inversion along NE-SW striking faults, parallel to the Otway Ranges as the most likely mode of formation.

3.4 The advantage of a multiscale structural analysis

Prior to recent work by Burgin et al., (2018), there had been no consideration of sub-seismic scale deformation and paleostresses within the Otway Basin, all preceding studies utilising 2D seismic data alongside other petroleum industry datasets. In the Otway Ranges and eastern Otway Basin, the integration of micro and mesoscale structural analysis with macroscale 3D seismic datasets has been key in revealing the true structural framework of the region.

The integration of microscale calcite twin datasets, a highly sensitive tool, which can be used to quantify paleostress magnitudes and orientations (e.g. Amroouch et al., 2010a; 2011), has contributed significantly to the revision of the structural framework. Its application, alongside microstructural investigations into the nature of internal deformation (Burgin et al., 2019b) has particularly assisted in characterising the nature of continental separation alongside the style of basin inversion. Two structural events which in the case of the Otway Basin, were most likely co-axial and oriented ~NE-SW (**fig. 9**).

Results from the applications of these multiscale studies (Burgin et al., 2018; 2019a; 2019b; Burgin and Amrouch, 2019b) also explain a number of phenomenon’s that have puzzled

preceding works. Such as the isolation of the Otway Ranges in contrast to the surrounding region (Hill et al., 1994) the preservation of normal offset during inversion (Holford et al., 2014) and the low levels of compressional mesoscale deformation within the Otway Ranges (Medwell, 1971). All of which can be explained through the co-axial nature of basin inversion and the presence of shallow basement beneath the Otway Ranges (Cayley et al., 2002; Burgin and Amrouch, 2019b). The formation of the ranges resulting due to the partitioning of strain during inversion to the reactivation of the detachment zone and vast network of ~NW-SE striking extensional faults. A feature that is well documented in sandbox experiments of inverted detachment faults (Buchanan and McLay, 1991) and in the study of detachment in collisional zones (e.g. Robion et al., 2007).

4.0 A Revised Structural Framework for the Otway Basin

Constructed with evidence from multiscale structural studies and work from this paper in the TSB, f**igure 10**, presents our revised structural framework for the Otway Basin. The framework builds on work by Moore et al., (2000) and Krassay et al., (2004) utilising their nomenclature for major basin provinces. Despite early studies that suggested otherwise, results from this study in the TSB along with other recent investigations have revealed that the overall nature of faulting is relatively consistent across most of the Otway Basin, although basement linked faults may reflect slight variations, especially in the Penola Trough (Lyon et al., 2007).

Onshore in the west, high angled ~NW-SE and E-W striking normal faults that dip northward dominate the structural trend in regions such as the Penola Trough, and Cray Fish Platform (Miller et al., 2002; Krassay et al., 2004; Lyon et al., 2007; Burgin and Amrouch, 2019a). Offshore, high angled normal faults that dip towards the south are most dominant (Krassay et al., 2004; Robson et al., 2017; Burgin and Amrouch, 2019a) within the Chanma Terrace and

Gambier Embayment, where ~NW-SE striking faults likely show evidence for minor ~NE-SW Late Cretaceous inversion, responsible for structures such as the Morum High (Duddy et al., 2003). In the central basin, ~NW-SE striking normal faults continue to dominate the architecture, within parallel striking depocentres such as the Portland and Voulta Troughs and regions surrounding the Tartwaup Mussel Fault Zone and the Tyrendarra Embayment.

In contrast to previous works (Cockshell, 1995; Miller et al., 2002; Debenham et al., 2018) offshore in the eastern basin, the new framework suggests that ~NW-SE striking fault patterns that dip mainly ocean ward persist within, and across the Shipwreck Trough and Port Campbell Embayment. Their structural influence continuing into the Prawn Platform, until the Cape Otway / King Island High, defining a fault pattern that is synonymous with the framework of the neighbouring Bass Basin in the east. Previously thought to be more regionally pervasive, N-S strike slip faults within the region are limited to the Shipwreck Trough and Shipwreck Fault Zone within the new structural framework.

Onshore, the Otway Ranges are most likely defined by a series of ~NW-SE and ~E-W striking listric faults subjected to minor inversion during the Latest Cretaceous (~Mid-Maastrichtian) having been well constrained with petrofabric data from Burgin et al., (2019b). Further north within the Colac and Gelibrand Troughs, faults strike broadly E-W, within the most poorly defined section of the basin, especially around the Bambra Deformation Zone (Edwards et al., 1996). Final evidence from the Torquay 3D (**fig. 3**) shows that ~NW-SE striking faulting continues within the TSB, while a similar pattern is also present to the south, along the continental shelf and the Sorell Fault Zone, as basin sediments transition into the Sorell Basin along Tasmania's western margin.

This updated framework results in far more consistent fault patterns along the southern margin of the Australian continent, and fault geometries that largely reflect the orientation of the continental shelf (**fig. 10**). As mentioned, faults in the eastern Otway echo those in the Bass Basin, where ~NW-SE striking normal faults define a series of parallel trending troughs (Cummings et al., 2004) and minor evidence for basin inversion is present within the Yolla Trough.

5.0 Impact on In Situ Stress

The orientation of the in-situ stress tensor in the Otway Basin has been well defined by many recent works (eg: Hillis and Williams, 1992, 1993; Hillis et al., 1995; Hillis and Reynolds, 2000; Reynolds and Hillis, 2000; Reynolds et al., 2003; Nelson et al., 2006; Van Ruth et al., 2007; Bailey et al., 2014. 2016; Rajabi et al., 2017a; Tassone et al., 2017). That being the case, the regime of stress has proven much more challenging to constrain, despite numerous efforts (see Tassone et al., 2017 and Burgin et al., 2019b for in depth discussion).

As discussed in section 3, many studies have interpreted the Otway Ranges and surrounding structures as evidence for Neotectonic deformation (**fig. 7a**) (e.g. King et al., 2012; Tassone et al., 2017). Favouring the presence of a compressional regime of in situ stress, and suggesting that estimates of a strike slip stress regime from petroleum industry datasets are inaccurate. Recent findings (Burgin and Amrouch, 2019b; Burgin et al., 2019b) suggest it is unlikely that the Otway Ranges and accompanying off shore structures represent neotectonic activity. Primarily because there is little evidence for ~NE-SW striking faults that have been suggested to have been reactivated. Encompassed within the new framework described in section 4, these structures likely formed in the Latest Cretaceous (Burgin and Amrouch, 2019b), just prior to final continental separation, due to the ~NE-SW inversion of ~NW-SE striking faults (**fig. 9**).

Furthermore evidence from these studies that advocate for neotectonic structuring is often conflicting, for example; Tassone et al., (2017) advocates for a Neotectonic compressional stress regime surrounding the Otway Ranges and the surrounding region. While the authors simultaneously presents an elevated vertical stress gradient in the immediate vicinity, within the well Bellarine-1 (26MPa/km). These two inferences are illogical as during compression, $\sigma V = \sigma 3$, and one would expect a lower value of vertical stress than the surrounding region if neotectonic compressional stresses were controlling the structural development, which is not the case.

As a consequence, it seems the "best," geological evidence for present day ~NW-SE compression within the Otway Basin is compressional faulting within the onshore Port Campbell Limestone (**fig. 11a**). However, evidence in this unit is also accompanied by normal and strike slip faulting (Bailey et al., 2017) (**fig. 11b, c**), observations which suggest that drawing any conclusions regarding the style of the in situ stress regime from the deformation of the unit would be unreliable. As multiple styles of deformation suggest it is likely affected by local perturbations and easily deformed.

In contrast to these isolated examples for compressional neotectonic stresses in the Port Campbell Limestone, recent field work in the Otway Ranges (Burgin and Amrouch, 2019b) shows consistent mesoscale evidence for a present day ~NW-SE oriented strike slip stress regime. Evidence that is defined by the presence of NW-SE striking vertical faults and fractures (**fig. 12**), that in many cases offset earlier NE-SW trending extensional, and strike slip, fracture sets (**fig. 12a**). The presence of a strike slip stress regime within the Otway Basin also seems

the most likely given plate scale modelling, conducted as part of the Australian Stress Map Project (Rajabi et al., 2017a; 2017b).

As such in the context of our new framework, the in situ stress regime within the Otway Basin may be less complex than previously thought, in light of the reduced conflict between petroleum industry data and geological evidence. Outcrop evidence for a strike slip stress regime in the Otway Ranges correlates well with a majority of works using petroleum industry data across the basin. Therefore we suggest that the within its upper ~3km, the Otway Basin can be generally described as being a strike slip stress province, with a transition towards an extensional, stress regime occurring at a depth of ~3km (Rajabi et al., 2017b; Burgin and Amrouch, 2019a). Though we note that this transition may occur at shallower depths along the continental shelf due to gravitational collapse (Burgin and Amrouch, 2019a) and within the Otway Ranges, where old dense rocks may have been exhumed.

6.0 Conclusions

This paper uses results from 3D seismic analysis in the TSB, integrated with results from other modern works, to present a new structural framework for the Otway Basin. In contrast to the previous model which was characterised by the presence of two orthogonally striking fault networks in the eastern Otway Basin. The new framework describes a far simpler structural framework, and one that is more consistent within the Otway Basin and across Australia's southern margin as a whole.

Acknowledgements

Thank you to Down Under Geosolutions (D.U.G) for the use of DUG Insights. Thank you to Associate Professor Simon Holford for his input on the history of the Otway Basin. The authors

also acknowledge the contribution of the Australian Postgraduate Award Scholarship through the University of Adelaide, alongside the work of the many staff and students of the Australian School of Petroleum.

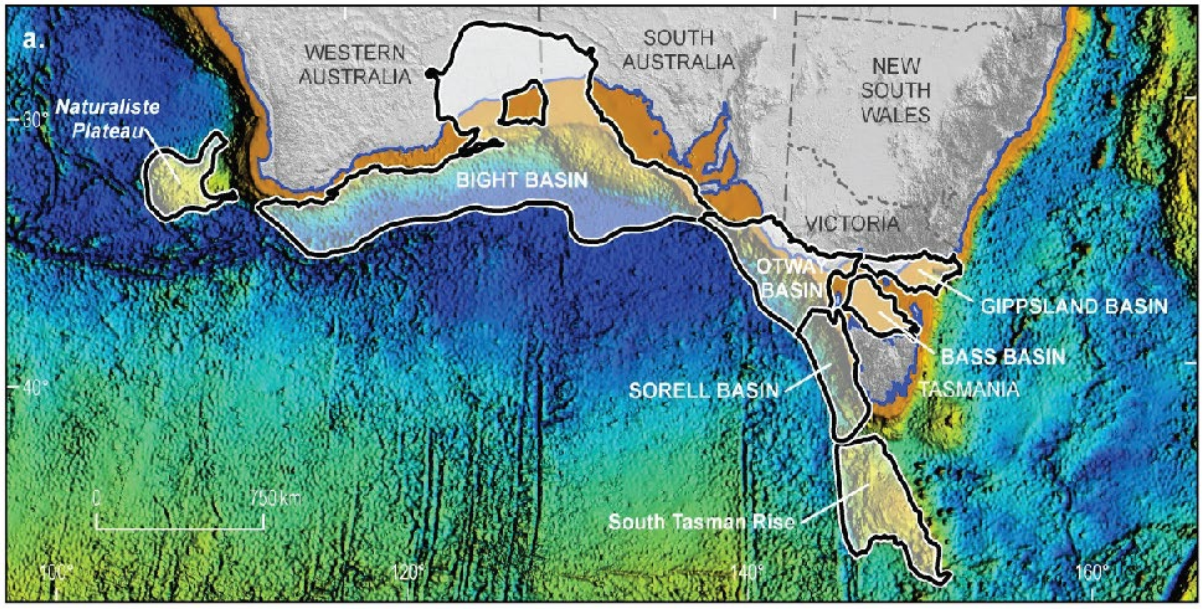

Fig. 1: Australia's southern margin and the sedimentary basins that comprise the southern rift system including the Otway Basin. Modified from Stacey et al., (2013).

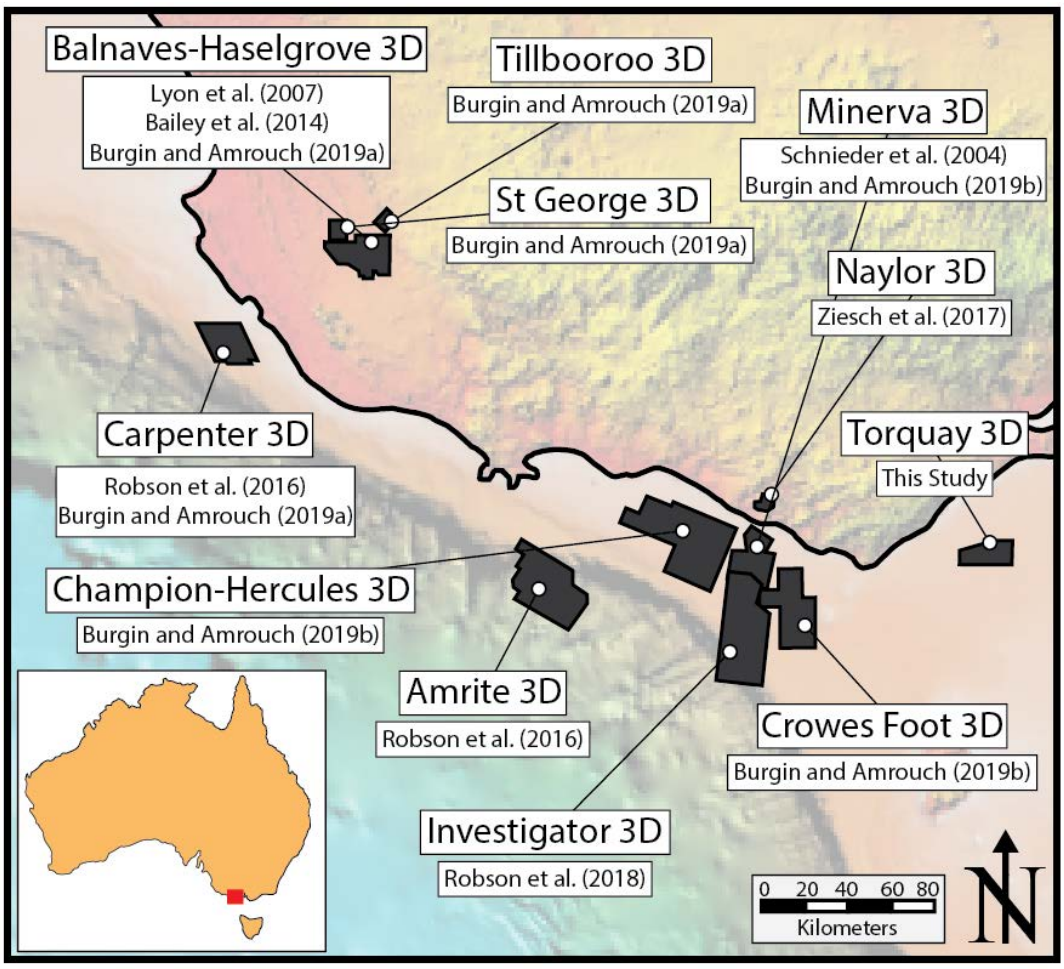

Fig. 2: Locations of 3D seismic datasets that have been analysed since the first generations of works in the 1990s and early 2000s.

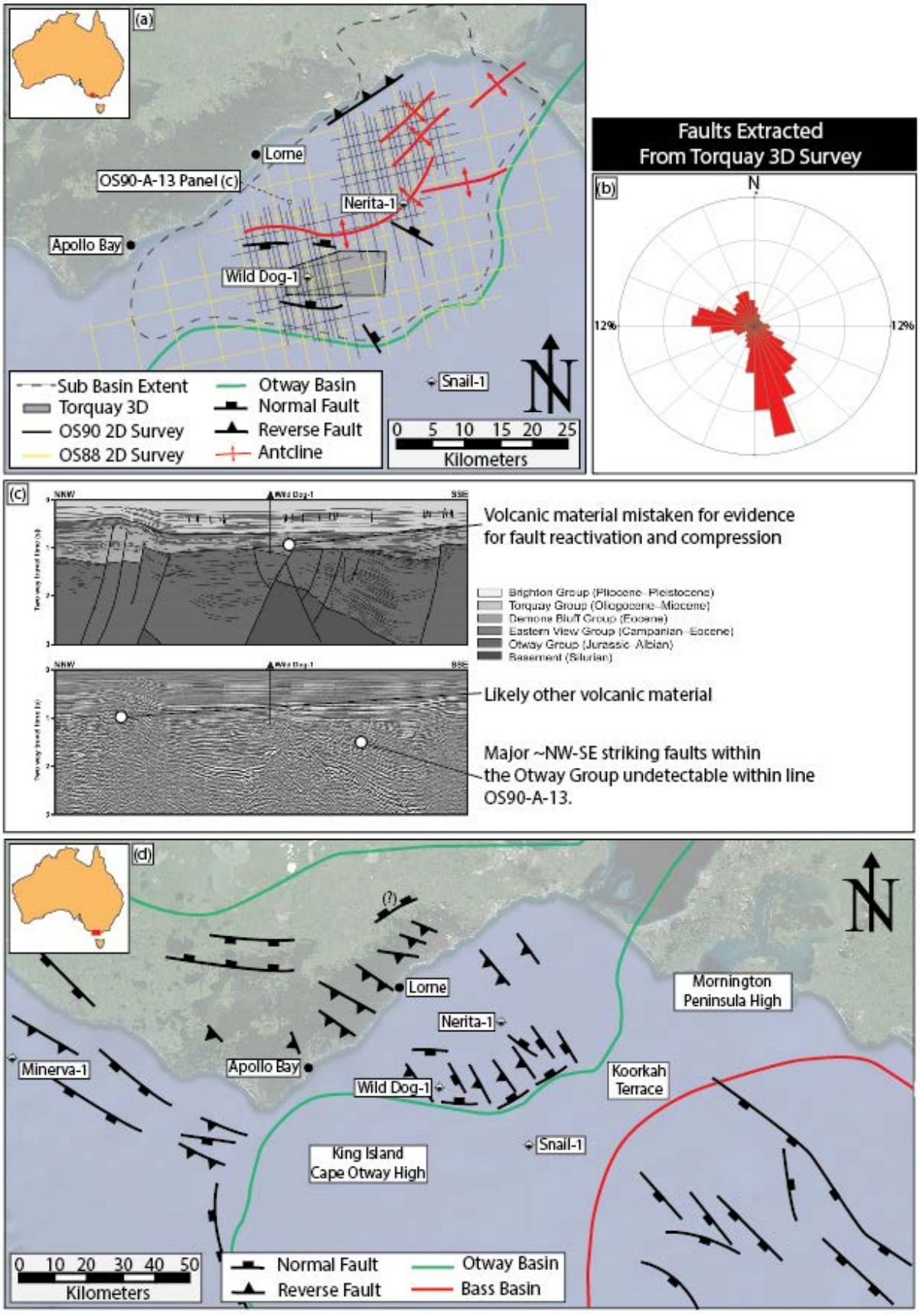
(a)
Lorne
OS90-A-13 Panel (c)
Nerita-1
Apollo Bay
Wild Dog-1
Snail-1
Sub Basin Extent
Torquay 3D
OS90 2D Survey
OS88 2D Survey
Otway Basin
Normal Fault
Reverse Fault
Antcline
0 5 10 15 20 25
Kilometers
Faults Extracted From Torquay 3D Survey
(b)
N
12%
12%
(c)
Volcanic material mistaken for evidence for fault reactivation and compression
Brighton Group (Pliocene–Pleistocene)
Torquay Group (Oligocene–Miocene)
Demons Bluff Group (Eocene)
Eastern View Group (Campanian–Eocene)
Otway Group (Jurassic–Albian)
Basement (Silurian)
Likely other volcanic material
Major ~NW-SE striking faults within the Otway Group undetectable within line OS90-A-13.
(d)
(?)
Lorne
Nerita-1
Mornington Peninsula High
Minerva-1
Apollo Bay
Wild Dog-1
Koorkah Terrace
Snail-1
King Island
Cape Otway High
0 10 20 30 40 50
Kilometers
Normal Fault
Reverse Fault
Otway Basin
Bass Basin

527

528

Fig. 3: (a) The location of the TSB and the current structural framework after Trupp et al., (1994). The location of 2D datasets within the basin are also included. (b) A rose diagram showing the strike of faults extracted from the Torquay 3D as part of this study. Note how fault strike is parallel to the majority of 2D displayed in panel (a). (c) Panel modified after Holford et al., (2011). Interpretation of line OS90-A-13 linking the growth of the Wild Dog structure to episodes of post break up compression (d) Likely structural framework of the TSB and surrounding region. Otway Ranges structural trend modified after Burgin and Amrouch (2019b – in prep).

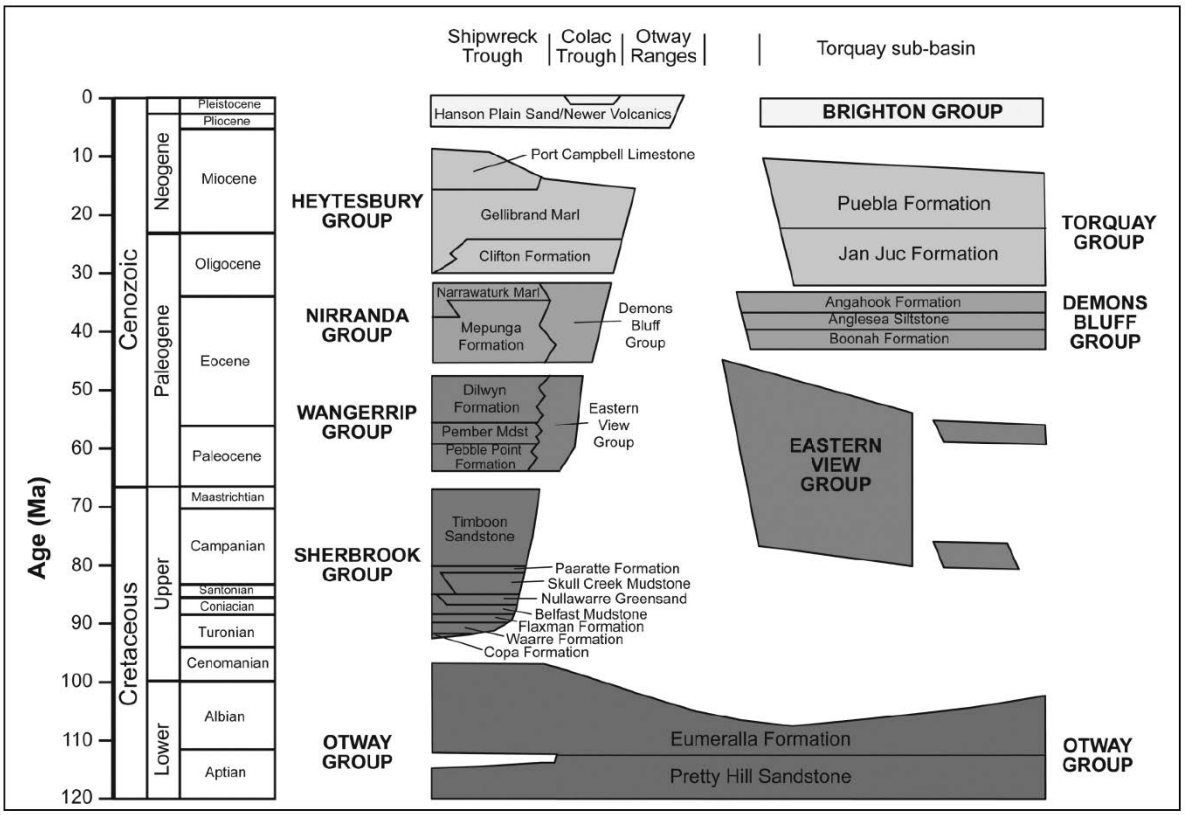

Fig. 4: The stratigraphic framework of the TSB in addition to comparative sections through the Otway Ranges, Colac and Shipwreck Trough. After Holford et al., (2011).

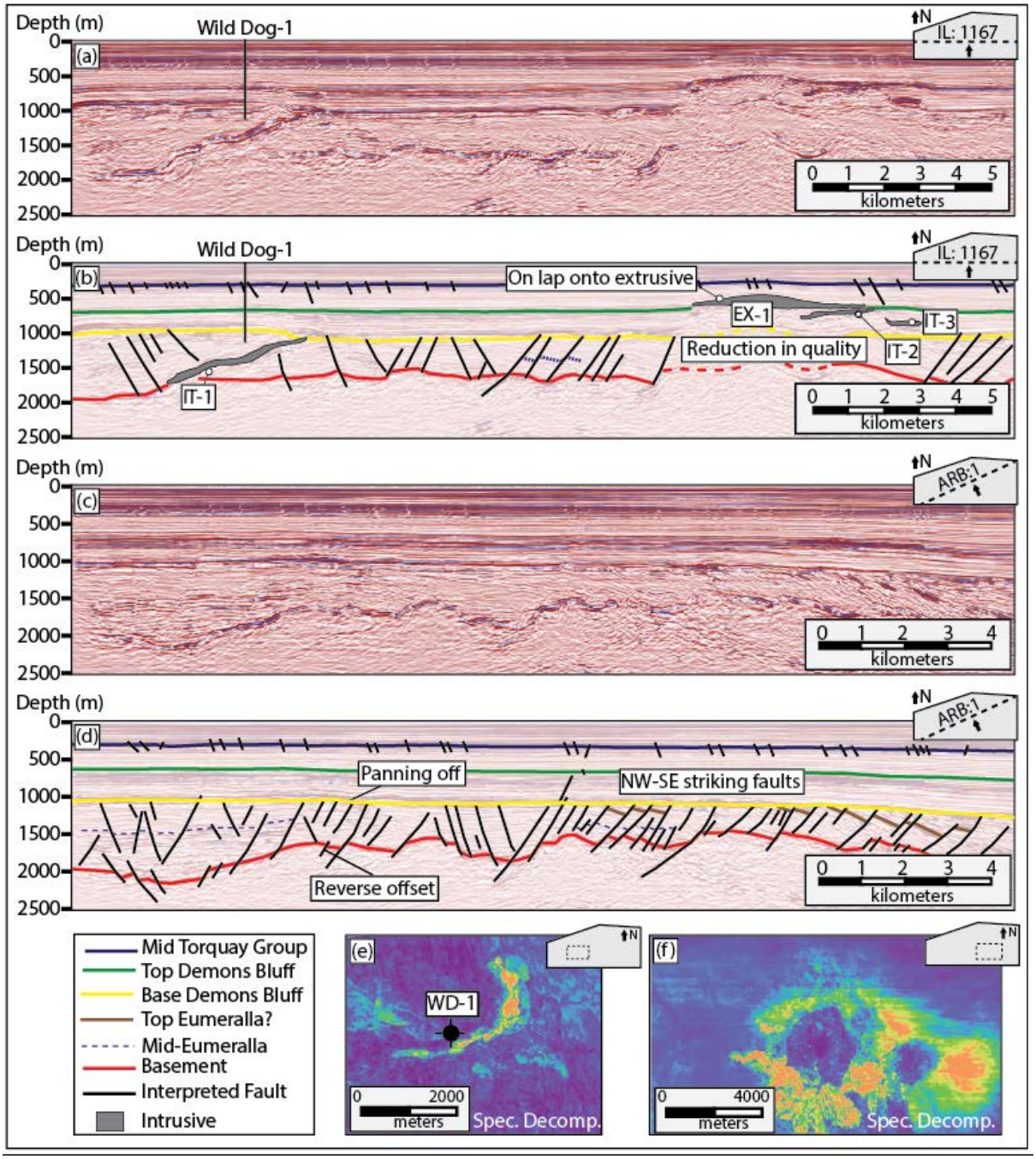
Depth (m)
Wild Dog-1
(a)
IL: 1167
N
0 1 2 3 4 5
kilometers
(b)
On lap onto extrusive
EX-1
IT-3
IT-2
Reduction in quality
IT-1
(c)
ARB:1
0 1 2 3 4
(d)
Panning off
NW-SE striking faults
Reverse offset
Mid Torquay Group
Top Demons Bluff
Base Demons Bluff
Top Eumeralla?
Mid-Eumeralla
Basement
Interpreted Fault
Intrusive
(e)
WD-1
0 2000
meters
Spec. Decomp.
(f)
0 4000
meters
Spec. Decomp.

Fig 5: (a) un-interpreted inline through the Torquay 3D, note the hard seismic kicks throughout the dataset (b) Interpretation of panel (a), note the presence of igneous bodies within the survey and the reduction in data quality surrounding the intrusive and extrusive events (c) Un-interpreted arbline through the Torquay 3D (d) interpreted panel (c) showing the dominant ~NW-SE striking structural fabric within the sediments of the Eumeralla and Otway Group sediments. Notice the panning of off structures at the Base Demons Bluff reflector (e) Spectral decomposition of a depth slice at 1100m showing IT1 (f) Spectral decomposition at a depth of 700m showing EX-1 and the surrounding intrusives which are poorly differentiated due to the disturbance of seismic reflectors.

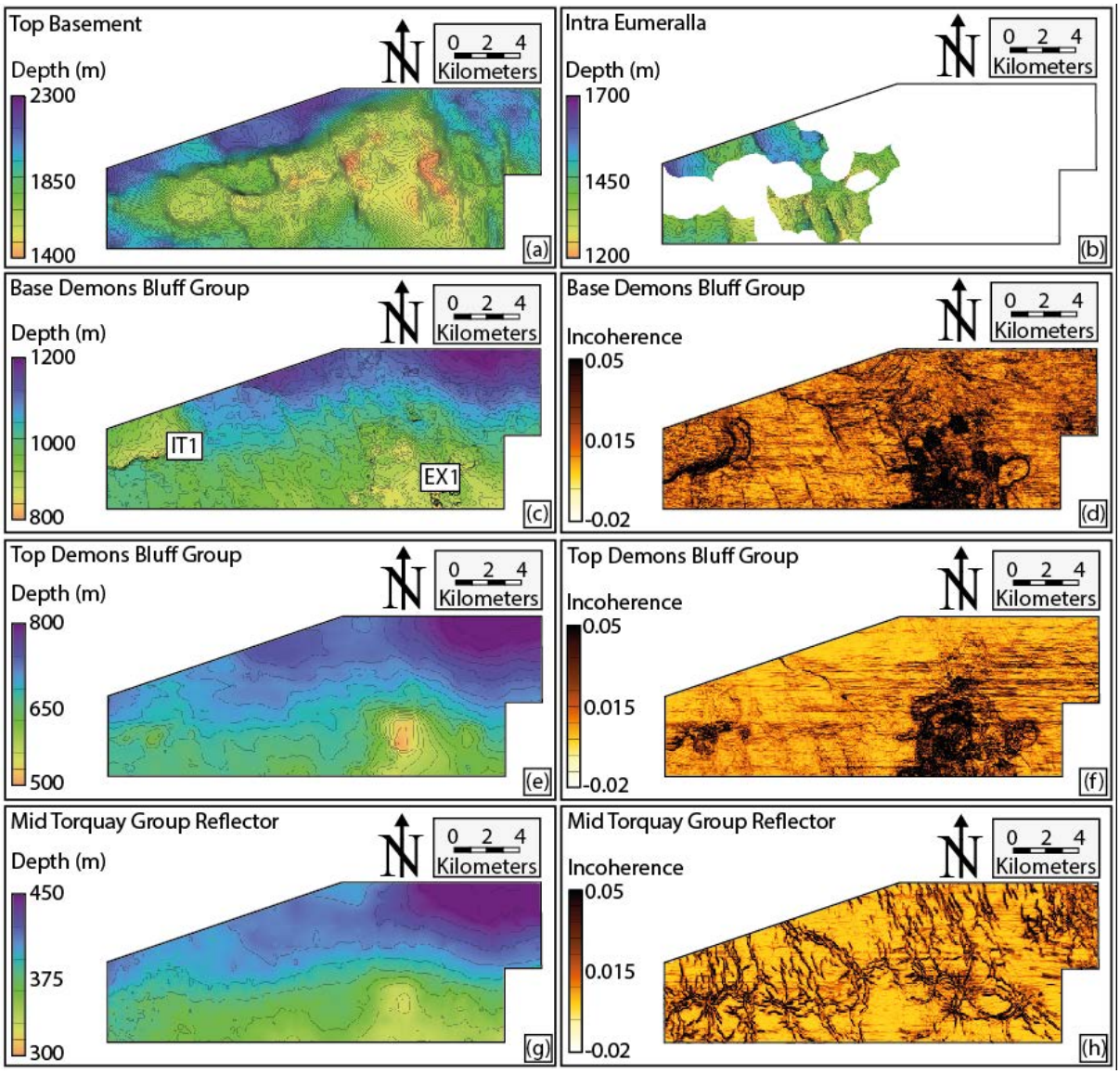

Fig 6: Reflectors interpreted as part of the interpretation of the Torquay 3D (a) Top Basement (b) Intra Eumeralla (c) Base Demons Bluff Group (d) Base Demons Bluff Group displaying the incoherence attributed, highlighting the presence of the igneous material and ~NW-SE trending faults. (e) Top Demons Bluff Group (f) Top Demons Bluff Group displaying the incoherence attribute (g) Mid Torquay Group reflectors showing what differential compaction over the deeper structures (h) Mid Torquay Group displaying the incoherence attribute highlighting the minor influence of ~NW-SE oriented minor faulting, reflective of the deeper pattern within the Otway Basin sediments,

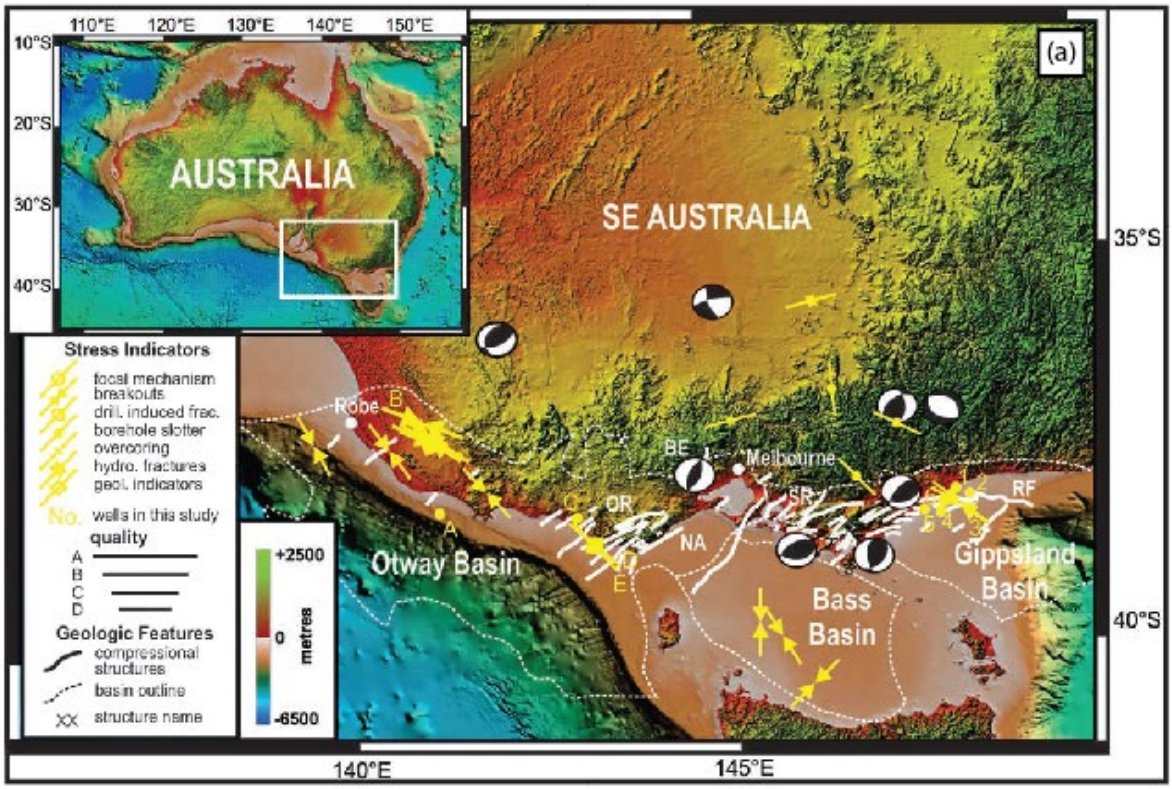

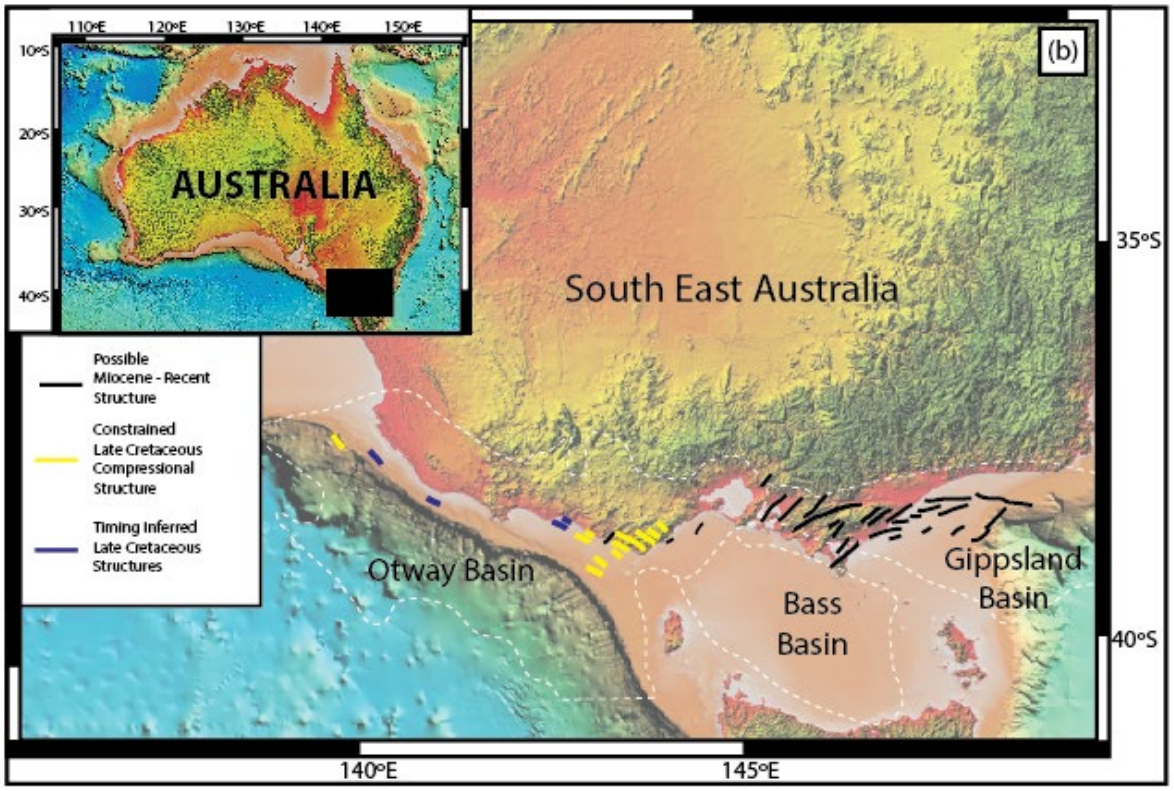

597

598

599

600

Fig 7: (a) Figure from King et al., (2012) showing supposed neotectonic structures and focal mechanisms in SE Australia. Note here the orthogonal strike between the orientation of in situ stress and the strike of the Otway Ranges. The interpreted structures within the Otway Basin are not representative of the regional framework (see Burgin and Amrouch, 2019b – in prep) (b) Modified record from the outcome of recent research. Neotectonic structuring is likely minimal.

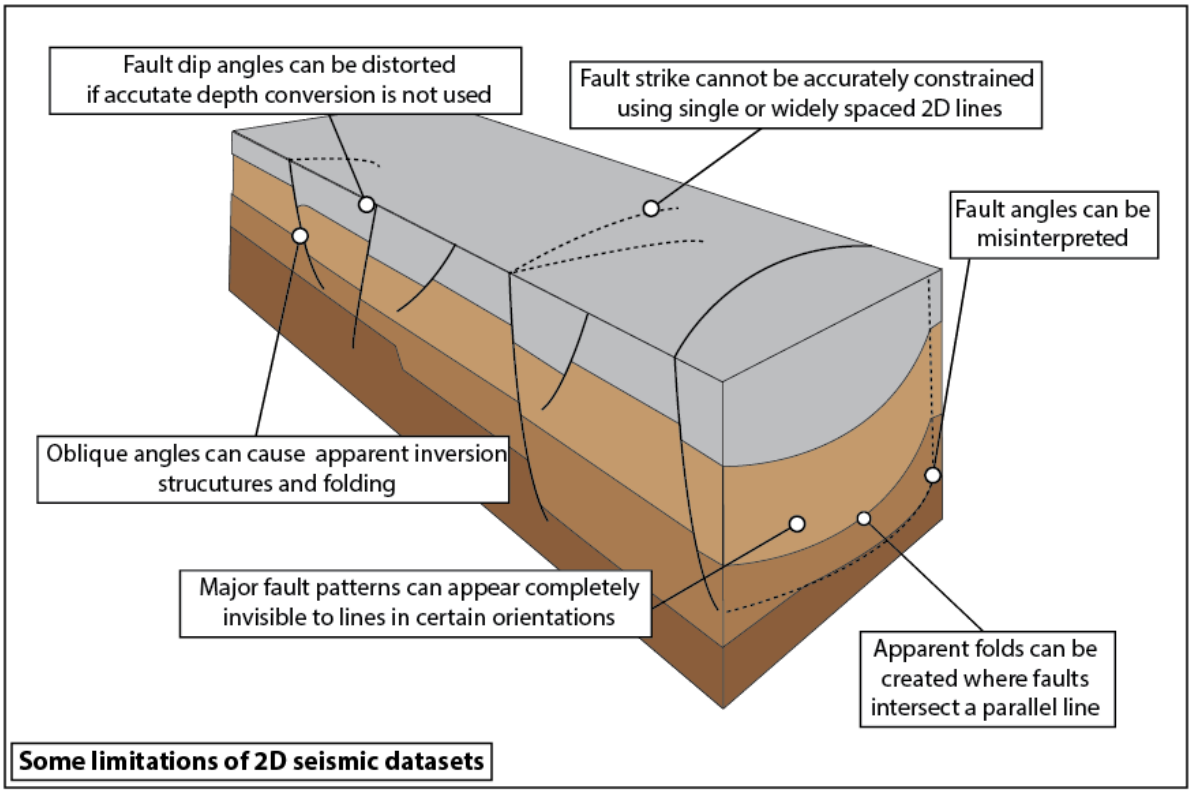

Fig 8: Schematic diagram displaying the limitations of 2D datasets. Of particular relevance to the Otway Basin is how 2D lines parallel to fault strike make the interpretation of faults difficult and distort the section creating apparent folds.

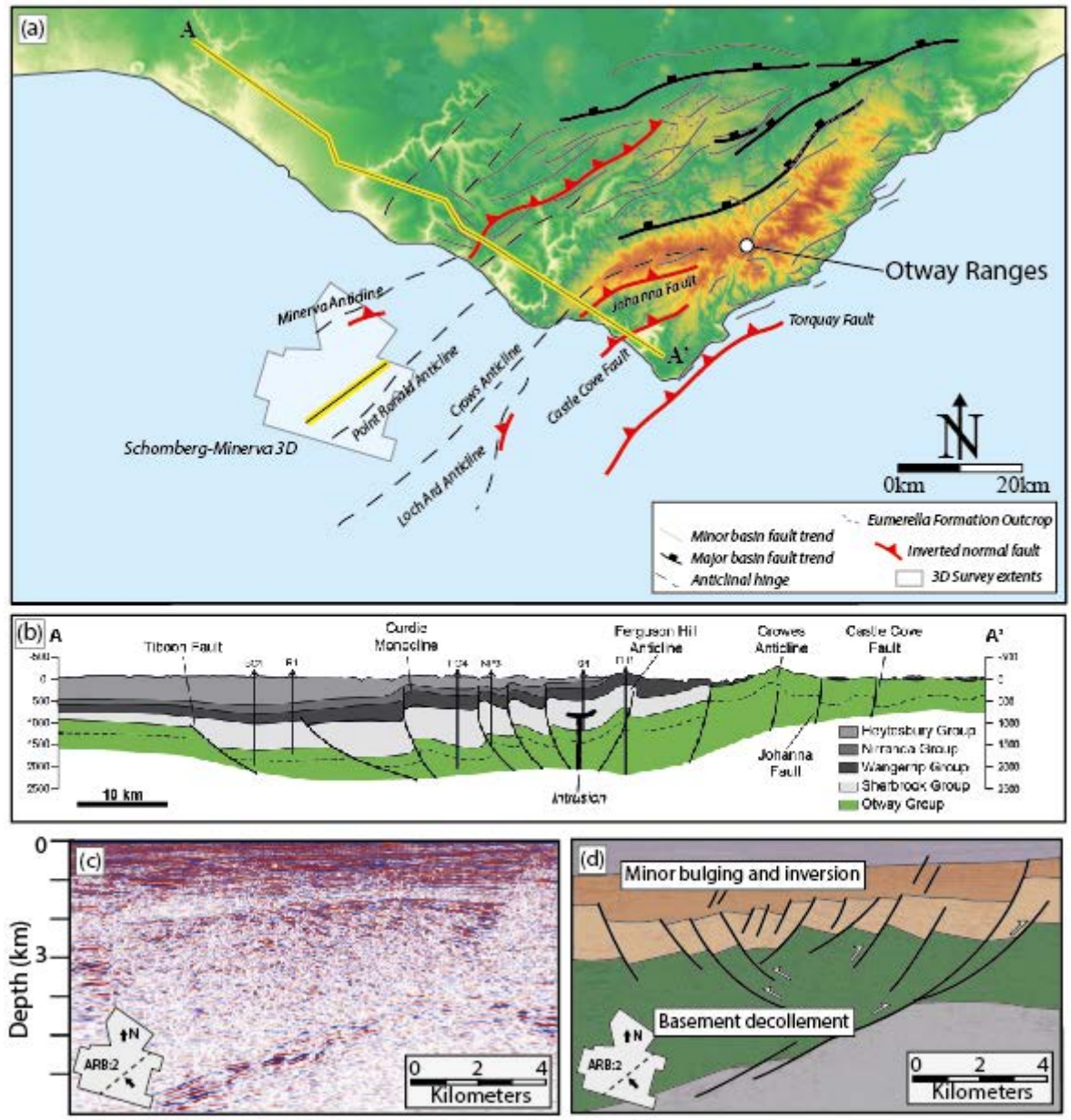

641

642

643 **Fig. 9:** (a) The old framework of the Otway Ranges region, modified from Debenham et al.,
644 (2018) after Edwards et al., (1996). (b) Cross section from Edwards et al., (1996) showing the
645 formation of ~NE-SW trending structures due to ~Miocene – recent inversion under ~NW-
646 SE compressive stresses. (c) Un-interpreted arbline through the Schomberg-Minerva 3D (d)
647 interpreted arbline through the Point Ronald Anticline, synonymous with the onshore
648 Fergurson Hill Anticline, showing how the regional framework represents co-axially inverted
649 ~NW-SE striking faults.

C

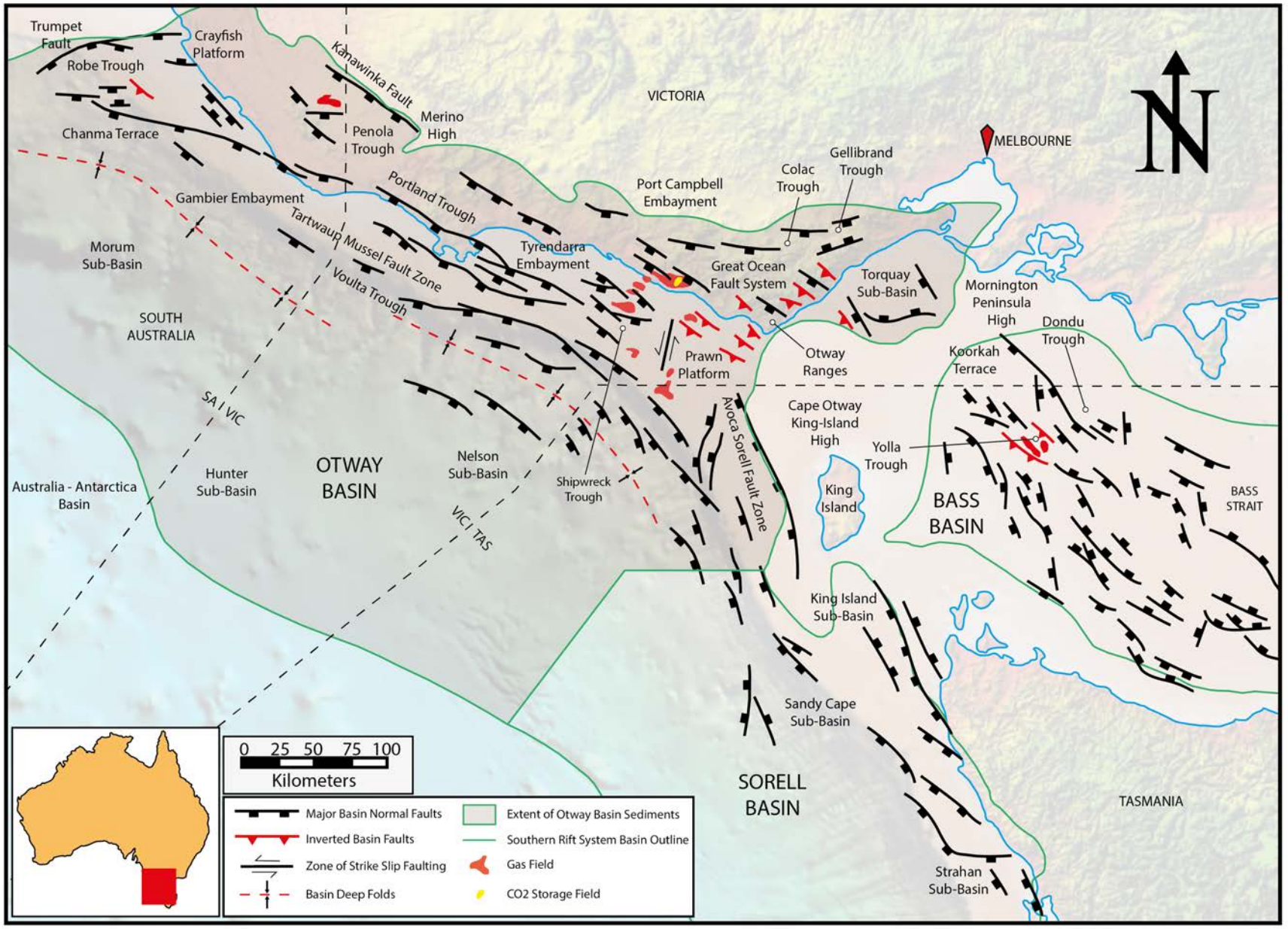
Trumpet Fault
Robe Trough
Crayfish Platform
Kanawinka Fault
Merino High
Penola Trough
Chanma Terrace
VICTORIA
MELBOURNE
Gellibrand Trough
Colac Trough
Port Campbell Embayment
Gambier Embayment
Portland Trough
Tartwaup Mussel Fault Zone
Voulta Trough
Tyrendarra Embayment
Great Ocean Fault System
Torquay Sub-Basin
Morum Sub-Basin
SOUTH AUSTRALIA
Mornington Peninsula High
Dondu Trough
Koorkah Terrace
Otway Ranges
Prawn Platform
SA I VIC
Cape Otway King-Island High
Avoca Sorell Fault Zone
Yolla Trough
Australia - Antarctica Basin
Hunter Sub-Basin
OTWAY BASIN
Nelson Sub-Basin
Shipwreck Trough
King Island
BASS BASIN
BASS STRAIT
VIC I TAS
King Island Sub-Basin
Sandy Cape Sub-Basin
SORELL BASIN
TASMANIA
Strahan Sub-Basin
0 25 50 75 100
Kilometers
Major Basin Normal Faults
Inverted Basin Faults
Zone of Strike Slip Faulting
Basin Deep Folds
Extent of Otway Basin Sediments
Southern Rift System Basin Outline
Gas Field
CO2 Storage Field

665

666 **Fig. 10:** The revised structural framework of the Otway Basin.

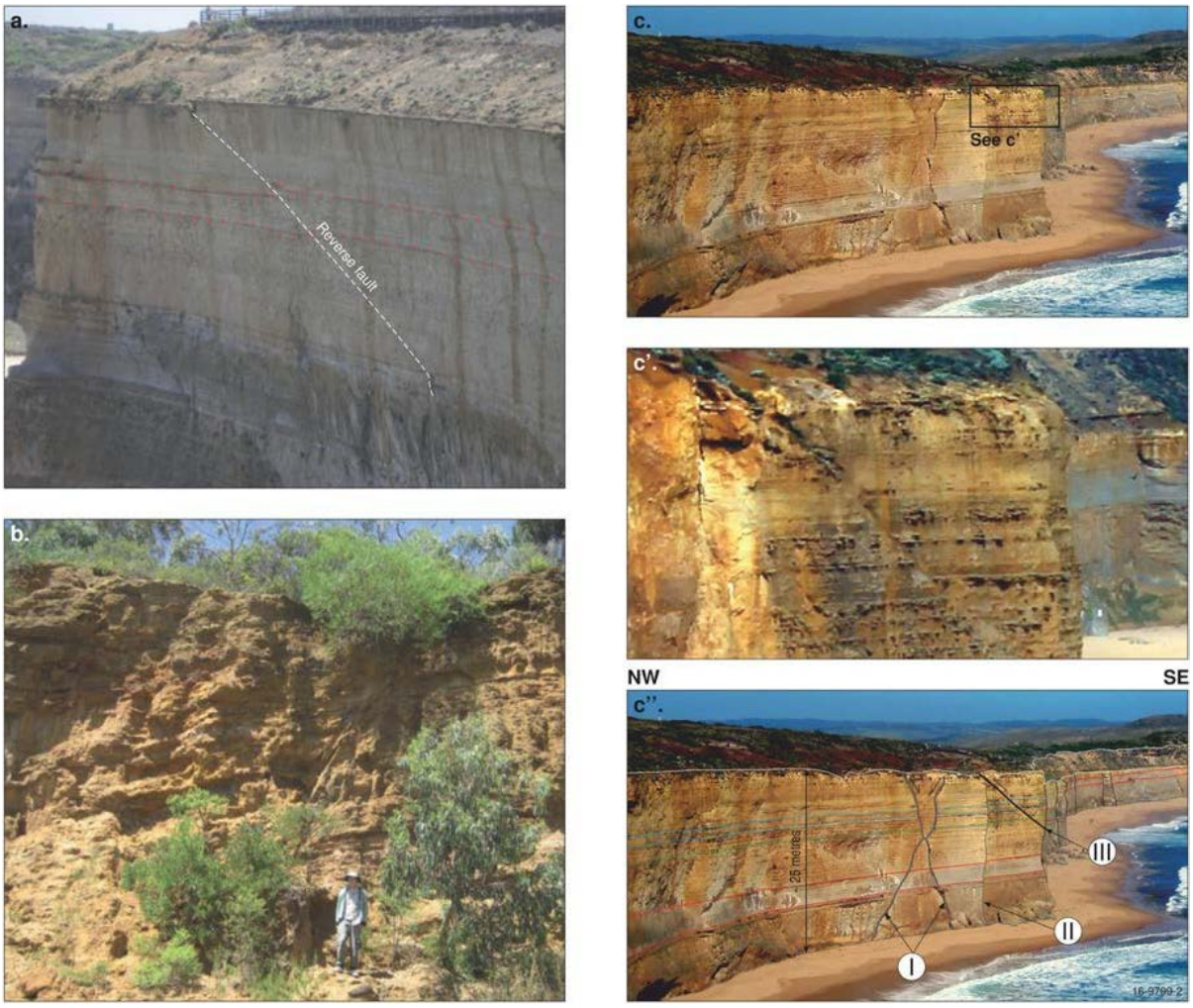

Fig. 11: Faults of different styles from the onshore Otway Basin after Bailey et al (2017). (a) The reverse fault at the 12 apostles along the Great Ocean Road within the Port Campbell Limestone, also discussed within Holford et al., (2011) and Tassone et al., (2017) (b) High angle reverse fault dipping north (c) Faulted cliff near the 12 Apostles. C' represents a close up of another reverse fault. C'' the interpretation of conjugate normal faulting and strike slip faulting within the same unit.

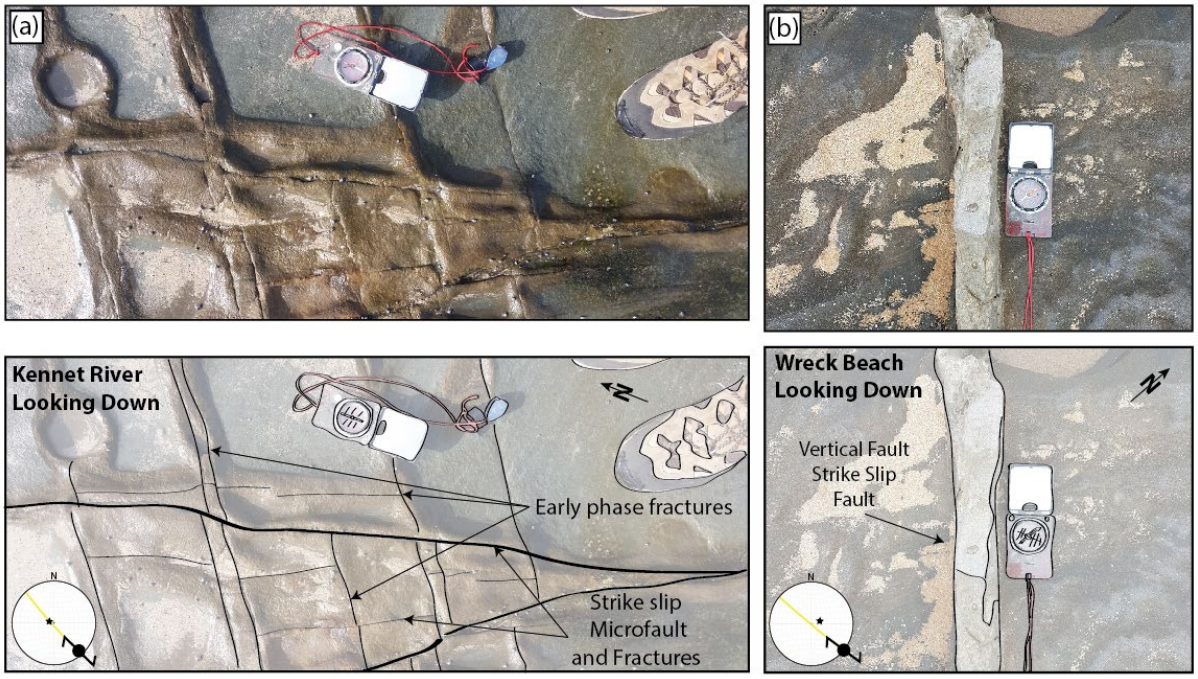

Fig. 12: Outcrop evidence for a ~NW-SE striking strike slip stress regime within the Otway Ranges including (a) NW-SE striking vertical fractures and microfaults cross cutting earlier fractures at Kennet River and (b) A vertical strike slip fault showing sinistral offset at Wreck Beach. Modified from Burgin and Amrouch (2019b).

695 **References**

696 Amrouch, K. (2010). Contribution of microstructural analysis to the understanding of folding
697 mechanisms: Examples of folded structures in the USA (Wyoming) and in Iran (Zagros)
698
699 Amrouch, K., Lacombe, O., Bellahsen, N., Daniel, J. M., & Callot, J. P. (2010). Stress and
700 strain patterns, kinematics and deformation mechanisms in a basement-cored anticline: Sheep
701 Mountain Anticline, Wyoming. *Tectonics*, 29(1).
702
703 Amrouch, K. (2010). Contribution of microstructural analysis to the understanding of folding
704 mechanisms: Examples of folded structures in the USA (Wyoming) and in Iran (Zagros)
705
706 Arboit, F., Amrouch, K., Morley, C., Collins, A. S., & King, R. (2017). Palaeostress
707 magnitudes in the Khao Khwang fold-thrust belt, new insights into the tectonic evolution of
708 the Indosinian orogeny in central Thailand. *Tectonophysics*, 710, 266-276.
709
710 Bailey, A., King, R., Holford, S., Sage, J., Backe, G., & Hand, M. (2014). Remote sensing of
711 subsurface fractures in the Otway Basin, South Australia. *Journal of Geophysical Research:*
712 *Solid Earth*, 119(8), 6591-6612.
713
714 Bailey, A. H. E., Pevzner, R., Urosevic, M., Popik, D., & Feitz, A. J. (2017). Shallow geology
715 of the CO2CRC Otway Site: Evidence for previously undetected neotectonic features?. *Energy*
716 *Procedia*, 114, 4424-4435.
717
718 Beaudoin, N., Leprêtre, R., Bellahsen, N., Lacombe, O., Amrouch, K., Callot, J. P., ... &
719 Daniel, J. M. (2012). Structural and microstructural evolution of the Rattlesnake Mountain

Anticline (Wyoming, USA): new insights into the Sevier and Laramide orogenic stress build-up in the Bighorn Basin. *Tectonophysics*, 576, 20-45.

Beaudoin, N., Koehn, D., Lacombe, O., Lecouty, A., Billi, A., Aharonov, E., & Parlangeau, C. (2016). Fingerprinting stress: Stylolite and calcite twinning paleopiezometry revealing the complexity of progressive stress patterns during folding—The case of the Monte Nero anticline in the Apennines, Italy. *Tectonics*, 35(7), 1687-1712.

Burgin, H. B. and Amrouch, K. (2019a). Reducing structural uncertainty in complex extensional settings: New insights into the evolution of Australia's South Eastern Passive Margin. (In Prep)

Burgin, H. B., Amrouch, K., Rajabi, M., Kulikowski, D., & Holford, S. P. (2018). Determining paleo-structural environments through natural fracture and calcite twin analyses: a case study in the Otway Basin, Australia. *The APPEA Journal*, 58(1), 238-254.

Burgin, H.B. and Amrouch, K. (2019a). Determining paleo-structural environments through natural fracture and calcite twin analyses: a case study in the Otway Basin, Australia. (In Prep).

Burgin, H. B. and Amrouch, K. (2019b). 4D structural evolution of Australia's Great Ocean Road Region: The first quantification of paleostress magnitudes during continental break up. (In Prep).

744 Cayley, R. A., Taylor, D. H., VandenBerg, A. H. M., & Moore, D. H. (2002). Proterozoic–
745 Early Palaeozoic rocks and the Tyennan Orogeny in central Victoria: the Selwyn Block and its
746 tectonic implications. *Australian Journal of Earth Sciences*, 49(2), 225-254.
747
748 Clark, D., McPherson, A., & Van Dissen, R. (2012). Long-term behaviour of Australian stable
749 continental region (SCR) faults. *Tectonophysics*, 566, 1-30.
750
751 Clark, D., & Leonard, M. (2014, November). Regional variations in neotectonic fault behaviour
752 in Australia, as they pertain to the seismic hazard in capital cities. In Australian Earthquake
753 Engineering Society 2014 Conference, Nov 21-23, Lorne, Vic.
754
755 Cockshell, D. P. C. (1995). The Otway basin: early Cretaceous rifting to Neogene
756 inversion. *The APPEA Journal*, 35(1), 451-466.
757
758 Cooper, G. T., & Hill, K. C. (1997). Cross-section balancing and thermochronological analysis
759 of the Mesozoic development of the eastern Otway Basin. *The APPEA Journal*, 37(1), 390-
760 414.
761
762 Cummings, A. M., Hillis, R. R., & Tingate, P. R. (2004, September). New perspectives on the
763 structural evolution of the Bass Basin: implications for petroleum prospectivity. In Eastern
764 Australasian Basins Symposium II'(Eds PJ Boult, DR Johns, and SC Lang) (pp. 133-149).
765
766 Debenham, N., King, R. C., & Holford, S. P. (2018). The influence of a reverse-reactivated
767 normal fault on natural fracture geometries and relative chronologies at Castle Cove, Otway
768 Basin. *Journal of Structural Geology*, 112, 112-130.

769 Debenham, N., Farrell, N. J. C., Holford, S., King, R., & Healy, D. (2019). Spatial distribution
770 of micrometre-scale porosity and permeability across the damage zone of a reverse-reactivated
771 normal fault in a tight sandstone: insights from the Otway Basin, SE Australia. *Basin Research*.
772
773 Dickinson, J. A., Wallace, M. W., Holdgate, G. R., Gallagher, S. J., & Thomas, L. (2002).
774 Origin and timing of the Miocene-Pliocene unconformity in southeast Australia. *Journal of*
775 *Sedimentary Research*, 72(2), 288-303.
776
777 Duddy, I. R., Mantilla, P. P., Hernández, C. A. M., & Trujillo, C. A. P. (2009, July). AFTA
778 apatite fission track analysis constraints on the Mesozoic to Quaternary thermal and tectonic
779 evolution of the Middle Magdalena Basin and Santander Massif, Eastern Cordillera,
780 Bucaramanga area, Colombia. In 10th Simposio Bolivariano-Exploracion Petrolera en las
781 Cuencas Subandinas.
782
783 Duddy, I. R. (1994, April). The Otway Basin: thermal, structural, tectonic and hydrocarbon
784 generation histories. In *Extended abstracts, NGMA/PESA Otway Basin Symposium,*
785 *Melbourne* (Vol. 20, pp. 35-42).
786
787 Duddy, I. R., Erout, B., Green, P. F., Crowhurst, P. V., & Boult, P. J. (2003). Timing constraints
788 on the structural history of the western Otway Basin and implications for hydrocarbon
789 prospectivity around the Morum High, South Australia. *The APPEA Journal*, 43(1), 59-83.
790
791 Edwards, J., & Edwards, J. (1996). Colac 1: 250 000 map geological report. Geological Survey
792 of Victoria.

Etheridge, M. A., Branson, J. C., & Smith, P. G. S. (1985). Extensional Basin-forming Structures in Bass Strait and their Importance for Hydrocarbon Exploration. *The APPEA Journal*, 25, 344-361.

Etheridge, M. A., Symonds, P. A., & Powell, T. G. (1988). Application of the detachment model for continental extension to hydrocarbon exploration in extensional basins. *The APPEA Journal*, 28(1), 167-187.

Finlayson, D. M., Johnstone, D. W., Owen, A. J., & Wake-Dyster, K. D. (1996). Deep seismic images and the tectonic framework of early rifting in the Otway Basin, Australian southern margin. *Tectonophysics*, 264(1-4), 137-152.

Hill, K. C., Hill, K. A., Cooper, G. T., O'Sullivan, A. J., O'Sullivan, P. B., & Richardson, M. J. (1995). Inversion around the Bass basin, SE Australia. *Geological Society, London, Special Publications*, 88(1), 525-547.

Hill, K. A., Cooper, G. T., Richardson, M. J., & Lavin, C. J. (1994). Structural framework of the eastern Otway Basin: inversion and interaction between two major structural provinces. *Exploration Geophysics*, 25(2), 79-87.

Hillis, R. R., & Reynolds, S. D. (2000). The Australian stress map. *Journal of the Geological Society*, 157(5), 915-921.

Hillis, R. R., & Williams, A. F. (1992). Borehole breakouts and stress analysis in the Timor Sea. *Geological Society, London, Special Publications*, 65(1), 157-168.

Hillis, R. R., & Williams, A. F. (1993). The contemporary stress field of the Barrow-Dampier Sub-Basin and its implications for horizontal drilling. *Exploration Geophysics*, 24(4), 567-576.

Hillis, R. R., Monte, S. A., Tan, C. P., & Willoughby, D. R. (1995). The contemporary stress field of the Otway Basin, South Australia: implications for hydrocarbon exploration and production. *The APPEA JOURNAL*, 35, 494-494.

Holford, S. P., Tuitt, A. K., Hillis, R. R., Green, P. F., Stoker, M. S., Duddy, I. R., Tassone, D. R. (2014). Cenozoic deformation in the Otway Basin, southern Australian margin: implications for the origin and nature of post-breakup compression at rifted margins. *Basin Research*, 26(1), 10-37. doi: 10.1111/bre.12035

Holford, S. P., Hillis, R. R., Duddy, I. R., Green, P. F., Tassone, D. R., & Stoker, M. S. (2011). Paleothermal and seismic constraints on late Miocene–Pliocene uplift and deformation in the Torquay sub-basin, southern Australian margin. *Australian Journal of Earth Sciences*, 58(5), 543-562.

King, R., Holford, S., Hillis, R., Tuitt, A., Swierczek, E., Backé, G., ... & Tingay, M. (2012). Reassessing the in-situ stress regimes of Australia's petroleum basins. *The APPEA Journal*, *52*(1), 415-426.

Krassay, A. A., Cathro, D. L., & Ryan, D. J. (2004). A regional tectonostratigraphic framework for the Otway Basin.

842 Kulikowski, D., & Amrouch, K. (2017). Combining geophysical data and calcite twin stress
843 inversion to refine the tectonic history of subsurface and offshore provinces: A case study on
844 the Cooper-Eromanga Basin, Australia. *Tectonics*, 36(3), 515-541.
845
846 Lacombe, O., Malandain, J., Vilasi, N., Amrouch, K., & Roure, F. (2009). From paleostresses
847 to paleoburial in fold–thrust belts: Preliminary results from calcite twin analysis in the Outer
848 Albanides. *Tectonophysics*, 475(1), 128-141.
849
850 Lister, G. S., Etheridge, M. A., & Symonds, P. A. (1986). Detachment faulting and the
851 evolution of passive continental margins. *Geology*, 14(3), 246-250.
852
853 Lyon, P. J., Boult, P. J., Hillis, R. R., & Bierbrauer, K. (2007). Basement controls on fault
854 development in the Penola Trough, Otway Basin, and implications for fault-bounded
855 hydrocarbon traps. *Australian Journal of Earth Sciences*, 54(5), 675-689.
856
857 Medwell, G. J. (1971) Structures of the Otway Ranges. Geological Survery of Victoria. Special
858 Bulletin. 339-359.
859
860 Messent, B. E., West, B. G., & Collins, G. I. (1999). Hydrocarbon prospectivity of the offshore
861 Torquay sub-basin, Victoria: gazettal area V99-1. Department of Natural Resources and
862 Environment.
863
864 Miller, J. M., Norvick, M. S., & Wilson, C. J. (2002). Basement controls on rifting and the
865 associated formation of ocean transform faults—Cretaceous continental extension of the
866 southern margin of Australia. *Tectonophysics*, 359(1-2), 131-155.

Moore, A. M. G., Stagg, H. M. J., & Norvick, M. S. (2000). Deep-water Otway Basin: a new assessment of the tectonics and hydrocarbon prospectivity. *The APPEA Journal*, 40(1), 66-85.

Nelson, E., Hillis, R., Sandiford, M., Reynolds, S., & Mildren, S. (2006). Present-day state-of-stress of southeast Australia. *The APPEA Journal*, 46(1), 283-306.

O'Brien, G. W., Reeves, C. V., Milligan, P. R., Morse, M. P., Alexander, E. M., Willcox, J. B. & Brodie, R. C. (1994). New ideas on the rifting history and structural architecture of the western Otway Basin: evidence from the integration of aeromagnetic, gravity and seismic data. *The APPEA Journal*, 34(1), 529-554.

Perincek, D., Simons, B., & Pettifer, G. R. (1994). THE TECTONIC FRAMEWORK AND ASSOCIATED PLAY TYPES OF THE WESTERN OTWAY BASIN, VICTORIA, AUSTRALIA. *The APPEA Journal*, 34(1), 460-478.

Rajabi, M., Tingay, M., Heidbach, O., Hillis, R., & Reynolds, S. (2017a). The Present-day stress field of Australia. *Earth-Science Reviews*, 168, 165-189.

Rajabi, M., Heidbach, O., Tingay, M., & Reiter, K. (2017b). Prediction of the present-day stress field in the Australian continental crust using 3D geomechanical–numerical models. *Australian Journal of Earth Sciences*, 64(4), 435-454.

Hillis, R. R., & Reynolds, S. D. (2000). The Australian stress map. Journal of the Geological Society, 157(5), 915-921.

Reynolds, S. D., Coblentz, D. D., & Hillis, R. R. (2003). Influences of plate-boundary forces on the regional intraplate stress field of continental Australia. SPECIAL PAPERS-GEOLOGICAL SOCIETY OF AMERICA, 59-70.

Robion, P., Grelaud, S., & de Lamotte, D. F. (2007). Pre-folding magnetic fabrics in fold-and-thrust belts: Why the apparent internal deformation of the sedimentary rocks from the Minervois basin (NE—Pyrenees, France) is so high compared to the Potwar basin (SW—Himalaya, Pakistan) *Sedimentary Geology*, 196(1-4), 181-200.

Robson, A., King, R., & Holford, S. (2016). Analysis of Gravity-Driven Normal Faults Using a 3D Seismic Reflection Dataset from the Present-Day Shelf-Edge Break of the Otway Basin, Australia. *ASEG Extended Abstracts*, 2016(1), 1-6.

Rajabi, M., Heidbach, O., Tingay, M., & Reiter, K. (2017). Prediction of the present-day stress field in the Australian continental crust using 3D geomechanical–numerical models. *Australian Journal of Earth Sciences*, 64(4), 435-454.

Robson, A. G., Holford, S. P., King, R. C., & Kulikowski, D. (2018). Structural evolution of horst and half-graben structures proximal to a transtensional fault system determined using 3D seismic data from the Shipwreck Trough, offshore Otway Basin, Australia. *Marine and Petroleum Geology*, 89, 615-634.

Schneider, C. L., Hill, K. C., & Hoffman, N. (2004). Compressional growth of the Minerva Anticline, Otway Basin, Southeast Australia—evidence of oblique rifting. *The APPEA Journal*, *44*(1), 463-480.

Tassone, D. R., Holford, S. P., Duddy, I. R., Green, P. F., & Hillis, R. R. (2014). Quantifying Cretaceous–Cenozoic exhumation in the Otway Basin, southeastern Australia, using sonic transit time data: Implications for conventional and unconventional hydrocarbon prospectivity. *AAPG Bulletin*, 98(1), 67-117.

Tassone, D. R., Holford, S. P., King, R., Tingay, M. R., & Hillis, R. R. (2017). Contemporary stress and neotectonics in the Otway Basin, southeastern Australia. *Geological Society, London, Special Publications*, 458, SP458-10.

Teasdale, J. P., Pryer, L. L., Stuart-Smith, P. G., Romine, K. K., Etheridge, M. A., Loutit, T. S., & Kyan, D. M. (2003). Structural framework and basin evolution of Australia's southern margin. *The APPEA Journal*, 43(1), 13-37.

Trupp, M. A., Spence, K. W., & Gidding, M. J. (1994). Hydrocarbon prospectivity of the Torquay Sub-basin, offshore Victoria. *The APPEA Journal*, 34(1), 479-494.

Van Ruth, P., Tenthorey, E., & Vidal-Gilbert, S. (2007). Geomechanical analysis of the Naylor structure, Otway Basin. Australia, Pre-Injection. Cooperative Research Centre for Greenhouse Gas Technologies, Canberra, Australia, *CO2CRC Publication Number* RPT07-0966. 27pp.

Willcox, J. B., & Stagg, H. M. J. (1990). Australia's southern margin: a product of oblique extension. *Tectonophysics*, 173(1-4), 269-281.

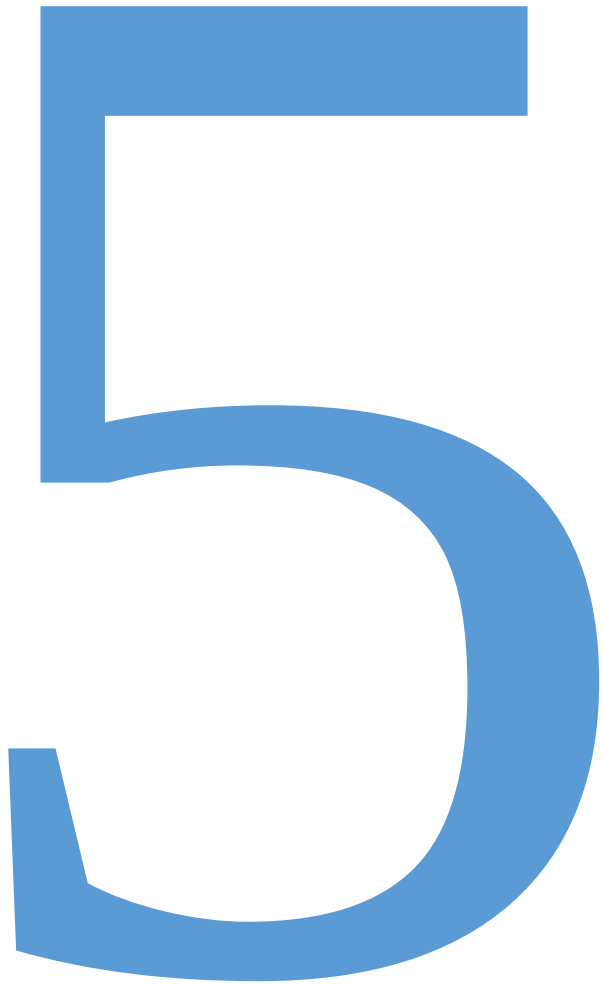

Chapter 5: Thesis Conclusions

Through the application of a multiscale structural analysis, this thesis provides original insights into the evolution and nature of upper crustal deformation at passive continental margins, using the Otway Basin, along Australia's southern margin as a case study.

On the microscale (grain/crystal), the use of Etchecopar's calcite stress inversion technique has proven to be a powerful tool, assisting in the identification of paleostress phases that are difficult to resolve when only macroscale techniques of analysis are used. The ability to quantify maximum paleo-differential stresses during phases of extension and inversion, has provided insights into how magnitudes of stress evolve through time during continental break up. Knowledge that represents the first step in increasing our understanding of the magnitudes of stress during tectonic extension, which the results of this study suggest are characterised by levels of maximum differential stress as high as 69MPa. This is contrasted against stress magnitudes as low as 13MPa during ensuing basin inversion, where stress is primarily released through the reactivation of the extensional network of deformation. In the Otway Basin, calcite twin stress tensors displaying these patterns define a period of NE-SW oriented extension and subsequent, co-axial compression and inversion.

The further use of microstructural analytical methods, such as the study of anisotropy of magnetic susceptibility and anisotropy of P-Wave velocity, have proven to be just as effective in characterising internal deformation at continental margins, as in fold-and-thrust belts. The methods providing insights into the early phases of strain acquisition during continental separation, which is characterised by layer parallel stretching. A style of homogenous strain and internal deformation that develops in layered rock, with a stretching azimuth parallel to the direction of tectonic extension. Layer parallel stretching has been identified in this study, by the presence triaxial magnetic and pore fabrics which correlate with the direction of porosity

elongation. These fabrics are in good agreement with paleo-σ3 orientations derived from the stress inversion of calcite twins, natural fractures and faults from 3D seismic, defining a period of Late Cretaceous, NE-SW and radial extension in the Otway Basin.

At passive continental margins like the Otway Basin, the extensional strain embodied by these fabrics, can be preserved during basin inversion, especially when the azimuth of compression is parallel to the earlier direction of extension. As in the case of the Otway Basin, compressional strain may be partitioned within the extensional detachment zone and existing faults, resulting in lower levels of deformation within the cover sediments of the basin.

On the mesoscale, the study of natural fractures at the outcrop and wellbore offers an effective means of integrating insights from the microscale. The study of fractures at the outcrop, and the capability to constrain cross cutting and pre/post bedding tilting relationships, prove just as effective in a passive margin setting, as is in regions of higher brittle deformation, such as fold-and-thrust belts. The study of natural fractures in the sub surface allows for mesoscale deformation to be studied in four dimensions. In the Otway Ranges, natural fracture analysis resulted in the definition of 11 fracture sets (6 major and 5 minor) which are correlated with five main phases of stress evolution and supported by paleostress orientations and extensional azimuths in the micro and macroscale datasets.

The integration of macroscale (seismic) geophysical datasets provides a powerful platform, to upscale structural insights from the micro and mesoscale, and produce a comprehensive model for basin evolution. This is particularly relevant with respect to episodes of basin inversion at passive continental margins like the Otway Basin, where macroscale evidence can be subtle, and disguised by the preservation of normal offset along major extensional faults. In which case the addition of micro and mesoscale datasets can provide sub-seismic, clues as to the possible stress phases that have shaped the basins structural evolution.

The use of macroscale geophysical datasets also allows for geomechanical models to be constructed, in order to better constrain the movement of fluids throughout subsurface fault and fracture networks. A phenomenon that can be complex at passive continental margins, due to the parallel nature of maximum horizontal stress and fault strike, resulting in low levels of effective normal stress acting on the fault planes.

In the case of the Otway Basin, high angle (50 – 90º) NW-SE striking faults that define the regions structural framework, are at a high risk of dilation, largely irrespective of the regime of in situ stress. The results of this modelling are supported by the distribution of volcanic material throughout the basin, in addition to the presence of shallow sub-surface cave networks that trend parallel to the orientation of maximum horizontal stress and major fault strike.

To conclude, in the Otway Basin Australia, the application of a multiscale approach towards characterising upper crustal deformation, has led to a complete revision of the basins structural framework. This approach has also produced original insights regarding the evolution of paleostress magnitudes and strain during tectonic scale extension, continental break up and basin inversion at passive continental margins.

Appendix I: Co-Authored Manuscripts

In addition to the main body of work within this thesis, contributions were made to two other pieces of work in the form of co-authored manuscripts.

Appendix I.I: Co-Authored Manuscript 1

Mapping permeable subsurface fracture networks: A case study on the Cooper Basin, Australia.

While based in the Cooper Basin, in central Australia, this manuscript draws on many of the elements fundamental to the main body of this thesis, in particular the distribution of sub-surface permeability networks.

This work investigates the distribution of high permeability sub-surface fracture networks. Utilising previous research that has shown the effectiveness of the seismic attribute curvature for mapping them.

The study demonstrates a relationship between natural fractures identified at the wellbore through image log analysis and those identified in 3D seismic using the curvature attribute. Providing insights into the location of high permeability "sweet spots," within the Patchawarra Formation, a hydrocarbon rich low permeability units within the Cooper Basin.

Citation: Kulikowski, D., Amrouch, K., & **Burgin, H. B**. (2018). Mapping permeable subsurface fracture networks: A case study on the Cooper Basin, Australia. Journal of Structural Geology.

Journal of Structural Geology 114 (2018) 336–345

Contents lists available at ScienceDirect

Journal of Structural Geology

journal homepage: www.elsevier.com/locate/jsg

Mapping permeable subsurface fracture networks: A case study on the Cooper Basin, Australia

David Kulikowski*, Khalid Amrouch, Hugo B. Burgin

Australian School of Petroleum, University of Adelaide, North Terrace, 5005, Adelaide, Australia

ARTICLE INFO

Keywords:
Cooper basin
Fracture
Fault
Seismic
Curvature
Geomechanics

ABSTRACT

The spatial distribution of permeable fracture networks is constrained in the subsurface Cooper Basin (Australia) through the integration of most positive curvature (K_+) analysis of five three dimensional (3D) seismic surveys, wellbore fracture data, and geomechanical modelling. The K_+ provides the likely distribution of subsurface extensional fractures based on the stress redistribution along the outer arc of an anticline. These results are reprocessed into the semblance (similarity) attribute to improve the signal-noise ratio prior to being extracted along the gas-rich and low permeability Patchawarra Formation. The subsurface fracture distribution maps show the geometry and density of extensional fractures that have been shown to facilitate fluid migration in this province, particularly those striking SE-NW and E-W, as these are properly oriented to undergo tensile re-activation. The density of these permeable SE-NW and E-W striking fracture sets is predicted to significantly increase along E-W elongate anticlines and may contribute to improved hydrocarbon recovery in this low permeability stratigraphic interval. We show that wellbore fracture data (n = 917) in the Patchawarra Formation presents a close relationship to K_+ results and can be used to generate high density structural data in this basin, with the methodology applicable to other subsurface and offshore provinces.

1. Introduction

Recent developments in three-dimensional (3D) seismic data analysis (Roberts, 2001; Chopra and Marfurt, 2007; Robson, 2017; Robson et al., 2018) have enabled high density structural information to be collected from subsurface and offshore provinces. Fractures detected from the most positive curvature (K_+) seismic attribute have been shown to correlate with outcrop and wellbore data in many provinces (e.g. Murray, 1968; Lisle, 1994; Stewart and Podolski, 1998; Hakami et al., 2004; Al-Dossary and Marfurt, 2006; Chopra and Marfurt, 2007; Bailey et al., 2014), and provides detailed constraints on the distribution of subsurface structures that can be highly beneficial in many industries related to carbon dioxide sequestration, low permeability hydrocarbon production, mining, and geothermal energy. As K_+ does not solely rely on reflector displacement, it can be used to predict the presence of extensional fractures based on the stress redistribution along the outer arc of an anticline (Murray, 1968; Ferrill and Groshong, 1993; Roberts, 2001). Understanding this concept, the distribution of extensional fractures can be selectively predicted. In the hydrocarbon-rich and low permeability Cooper Basin, Australia, these high angled fractures are critically oriented to facilitate fluid migration (Backe et al., 2011; Kulikowski, 2017; Kulikowski and Amrouch, 2017). There, the geometry and distribution of these regionally pervasive fractures are presently derived from wellbore locations, and due to their high angle nature, may not be accurately represented in vertical wellbores.

Using this basin as a case study, this research integrates K_+ analysis, wellbore fracture data, and geomechanical modelling to map the spatial distribution of the regionally pervasive and permeable high ($> 50^0$) angled fractures within the gas-rich and low permeability Patchawarra Formation (Kulikowski and Amrouch, 2017). Five 3D seismic surveys are time-to-depth converted, analysed using the K_+ attribute, processed into semblance attribute volumes to improve the signal-noise ratio before being extracted along the Patchawarra Formation, and finally compared to fracture data derived from 28 wellbores. Geomechanical modelling is incorporated into the methodology to determine the fracture sets that are critically oriented to undergo tensile reactivation and facilitate fluid migration under in-situ stress conditions. The connection between wellbore derived high ($> 50^0$) angle fractures and K_+ results is also discussed for this province. This integrated methodology is carefully applied and can benefit other subsurface or offshore provinces, given adequate geophysical data coverage, to extract important structural data that would otherwise be derived only from sparse wellbore locations.

* Corresponding author.
E-mail addresses: david.kulikowski@adelaide.edu.au (D. Kulikowski), khalid.amrouch@adelaide.edu.au (K. Amrouch), hugo.burgin@adelaide.edu.au (H.B. Burgin).

https://doi.org/10.1016/j.jsg.2018.02.009
Received 19 December 2017; Received in revised form 19 February 2018; Accepted 22 February 2018
Available online 23 February 2018
0191-8141/

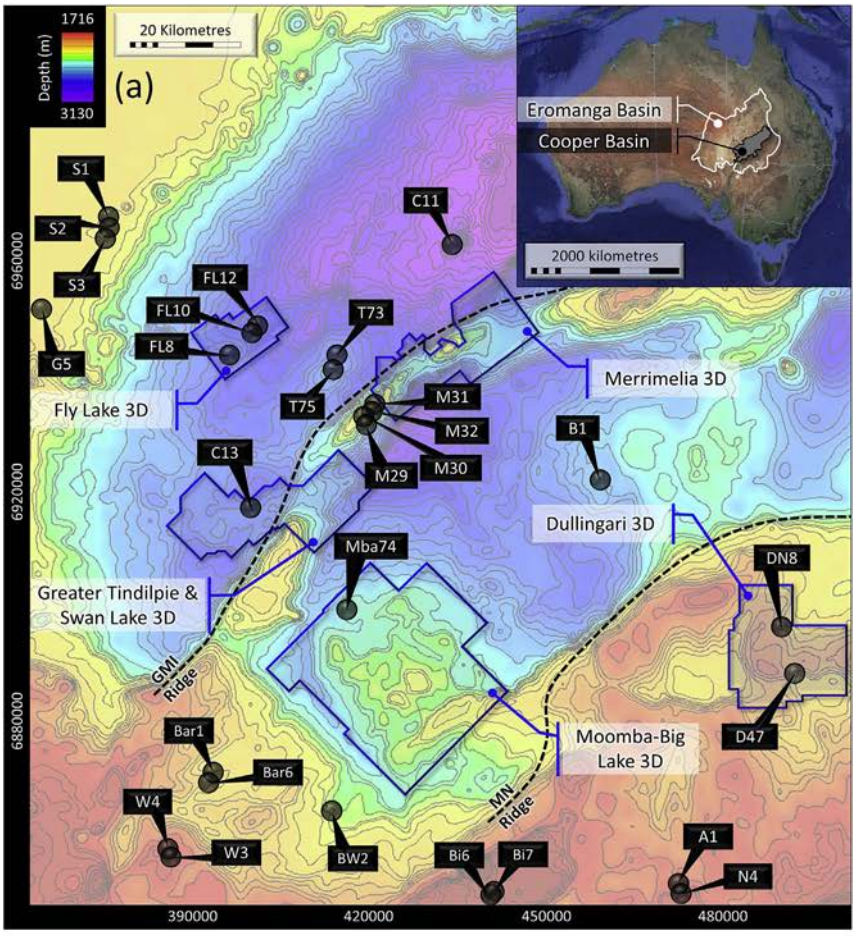

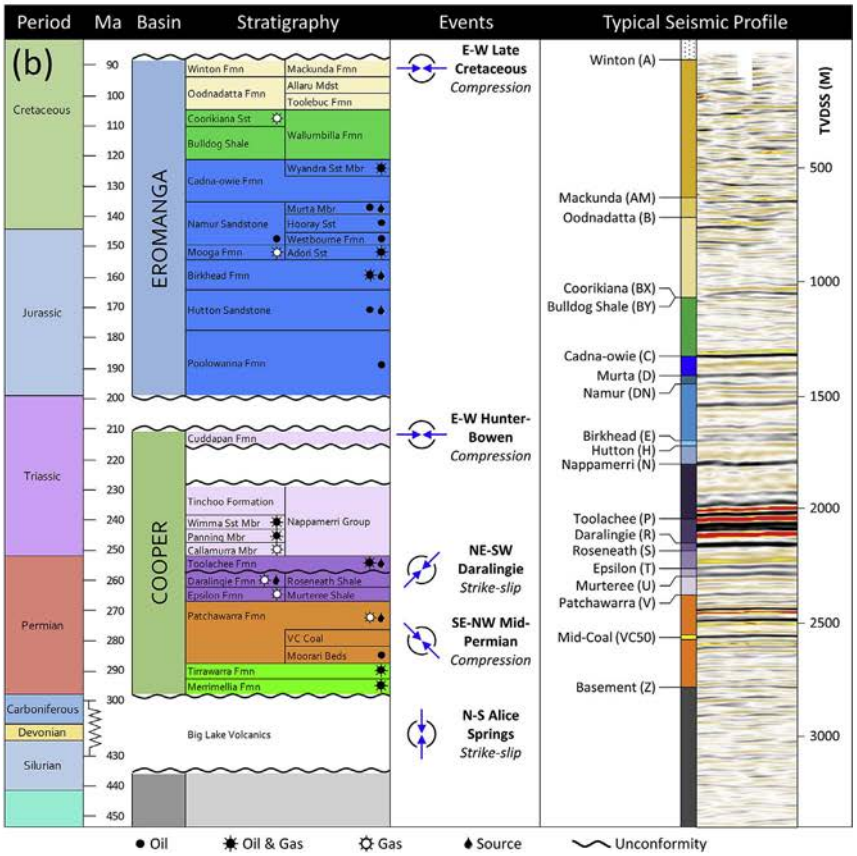

(caption on next page)

Fig. 1. (a) Location of 3D seismic surveys, borehole image logs, and the Gidgealpa-Merrimelia-Innamincka (GMI) and Murteree-Nappacoongee (MN) ridges within the South Australian Cooper Basin. Top Permian depth map shown (Kulikowski and Amrouch, 2017). Inset location of the Eromanga and Cooper basins, Australia (after Kulikowski et al., 2016). GDA94/MGA zone 54 coordinate system used and shown as X-Y locations. (b) Stratigraphic column of the Cooper and Eromanga Basins with a typical seismic reflection profile shown.

2. Geological setting

The Permian to Triassic intra-cratonic Cooper Basin is located in central Australia (Fig. 1a) and is unconformably overlain by the Jurassic to Cretaceous Eromanga Basin (Apak et al., 1997; Alexander et al., 1998). The South Australian portion of this region is defined by the NE-SW striking Gidgealpa-Merrimelia-Innamincka (GMI) and Murteree-Nappacoongee (MN) ridges that bound the NE-SW elongate Patchawarra, Nappamerri and Tenappera troughs (Fig. 1a) (Kulikowski et al., 2018). SE-NW extension during the Adelaidean (650-575 Ma) developed regionally extensive high angled ($> 50^0$) NE-SW striking basement normal faults that created early accommodation space for calcareous and siliciclastic Warburton Basin sediments to be deposited, before being inverted by subsequent compressional and strike-slip stress regime events (Fig. 1b) (Gatehouse, 1986; Apak et al., 1997; Kulikowski and Amrouch, 2017, 2018; Kulikowski et al., 2018).

The unconformity between the Warburton and Cooper basins was created by a N-S strike-slip stress regime belonging to the Carboniferous Alice Springs Event, which was later overlain by Upper Carboniferous glacial sediments (Merrimelia Formation) and Lower Permian braided fluvial sediments (Tirrawarra Formation) (Apak et al., 1997; Kulikowski and Amrouch, 2017). Repeated cycles of sands, shales and coals were deposited during the Middle Permian to form the low permeability and gas-rich Patchawarra Formation (Alexander et al., 1998; Gray, 2017). On-lapping and erosional features are present in the middle Patchawarra Formation along the GMI and MN ridges, and are a result of NW-SE compression during the Mid-Permian Event (Apak et al., 1997; Kulikowski and Amrouch, 2017, 2018). Compression from the Mid-Permian Event gradually eased, forming an east to west transgression, during which the Late Permian Murteree Shale, Epsilon Formation, Roseneath Shale, and Daralingie Formation were deposited (Apak et al., 1997). The Upper Permian Daralingie Formation was later eroded during NE-SW strike-slip stress regime conditions that were associated with the Daralingie Event (Kuang, 1985; Apak et al., 1997; Mavromatidis, 2006; Kulikowski and Amrouch, 2017, 2018). The Late Permian Toolachee Formation and the Triassic Nappamerri Group were deposited under meandering fluvial to deltaic, and floodplain, lacustrine and fluvial channel conditions, respectively (Apak et al., 1997; Alexander et al., 1998), which mark the top of the Cooper Basin stratigraphy.

An E-W compressional stress was present during the Late Triassic Hunter-Bowen Event, which eroded up to 500 m of Nappamerri Group sediments, creating the unconformity between the Cooper and overlying Eromanga basins (Alexander et al., 1998; Mavromatidis, 2006). Jurassic to Cretaceous deposition of Eromanga Basin sediments was uninterrupted, transitioning between fluvial, deltaic, lacustrine and shallow marine conditions (Alexander et al., 1998). Subsequent to this, E-W and N-S compression, associated with the Late Cretaceous Event and Paleogene Event, respectively, created folds and were succeeded by the present-day ESE-WNW strike-slip stress regime (Nelson et al., 2007).

3. Methodology

3.1. Curvature (K) attribute

The value for curvature (K) is the inverse of the radius of the oscillating circle (R) (Eq. (1)) (Roberts, 2001), such that for any point (P) the K is defined as the rate of change of the dip angle ($d\omega$) with respect to the arc length (dS) (Fig. 2a) (Roberts, 2001). The arc length (dS) is obtained from the osculating circle (Fig. 2a) that has a common tangent to P and makes the greatest possible contact with the curve (Roberts, 2001), where in two-dimensions K is defined as;

$$K = \frac{1}{R} \tag{1}$$

This provides unique K values depending on the location along a curve (Fig. 2b). When dealing with 3D data the curvature can be calculated in an infinite number of directions all with unique values. For any P a single intersecting plane normal to the surface that defines the largest absolute curvature value exists, which is termed the maximum curvature (K_{max}) (Roberts, 2001). Perpendicular to this plane, the minimum curvature (K_{min}) value is obtained, which defines the smallest absolute curvature value (Roberts, 2001). The K_{max} and K_{min} attributes are collectively termed the principal curvatures and can be used to derive any curvature value for planes that are normal to the given surface (normal curvature) (Roberts, 2001), such that;

$$K_i = (K_{max})cos^2\delta + (K_{min})sin^2\delta \tag{2}$$

Where δ is the angle between a normal curvature plane (K_i) and the K_{max} plane (Roberts, 2001). The distribution of extensional fractures along the anticlinal traps can be mapped by calculating the most positive curvature (K_+) (Eq. (3)), by incorporating a local quadratic surface with a 3 × 3 grid cell approach (Fig. 2c) (Murray, 1968; Roberts, 2001; Al-Dossary and Marfurt, 2006).

$$K_+ = (a + b) + \sqrt{(a - b)^2 + c^2} \tag{3}$$

where,

$$a = \frac{1}{2}\frac{\delta^2 z}{\delta x^2} = \left(\frac{Z_1 + Z_3 + Z_4 + Z_6 + Z_7 + Z_9}{12\Delta x^2}\right) - \left(\frac{Z_2 + Z_5 + Z_8}{6\Delta x^2}\right) \tag{4}$$

$$b = \frac{1}{2}\frac{\delta^2 z}{\delta y^2} = \left(\frac{Z_1 + Z_2 + Z_3 + Z_7 + Z_8 + Z_9}{12\Delta x^2}\right) - \left(\frac{Z_4 + Z_5 + Z_6}{6\Delta x^2}\right) \tag{5}$$

$$c = \frac{\delta^2 z}{\delta x \delta y} = \left(\frac{Z_3 + Z_7 - Z_1 - Z_9}{4\Delta x^2}\right) \tag{6}$$

Here, Z_i refers to the location of grid nodes along the local quadratic surface and Δx is the distance between grid nodes (Fig. 2c; Roberts, 2001). The equation for K_+ given in Eq. (3) uses the combination of Eqs. (4)–(6) (Roberts, 2001).

The theoretical relationship between K_+ and the presence of extensional fractures is in the stress re-distribution when a stratal-unit (or bed) is folded or bent (i.e. anticline). This folding creates extensional stresses along the outer arc, and compressional stresses in the inner arc (Murray, 1968; Ferrill and Groshong, 1993; Roberts, 2001; Amrouch et al., 2010a, 2010b). As the shape of reflectors can also be affected by mechanism other than folding, such as faulting, erosion, dunes, on-lapping, clinoforms, etc., an understanding of the structural and stratigraphic history of the region must be well understood. As the K_+ analysis predicts the location of fractures along a curved surface, the abrupt curvature associated with faulting is also captured in the results. A detailed fault model is therefore created for each seismic survey to help differentiate between the macro-scale faults and the meso-scale fractures.

3.2. Seismic dataset

The K_+ analysis was performed on five depth converted 3D seismic surveys from the South Australian portion of the Cooper Basin (Fig. 1a). These include the Moomba-Big Lake (acquired 1997), Dullingari (acquired 1997), Merrimelia (extension) (acquired 1998), Greater Tindilpie (GT)-Swan Lake (acquired 2000), and Fly Lake (acquired 2000)

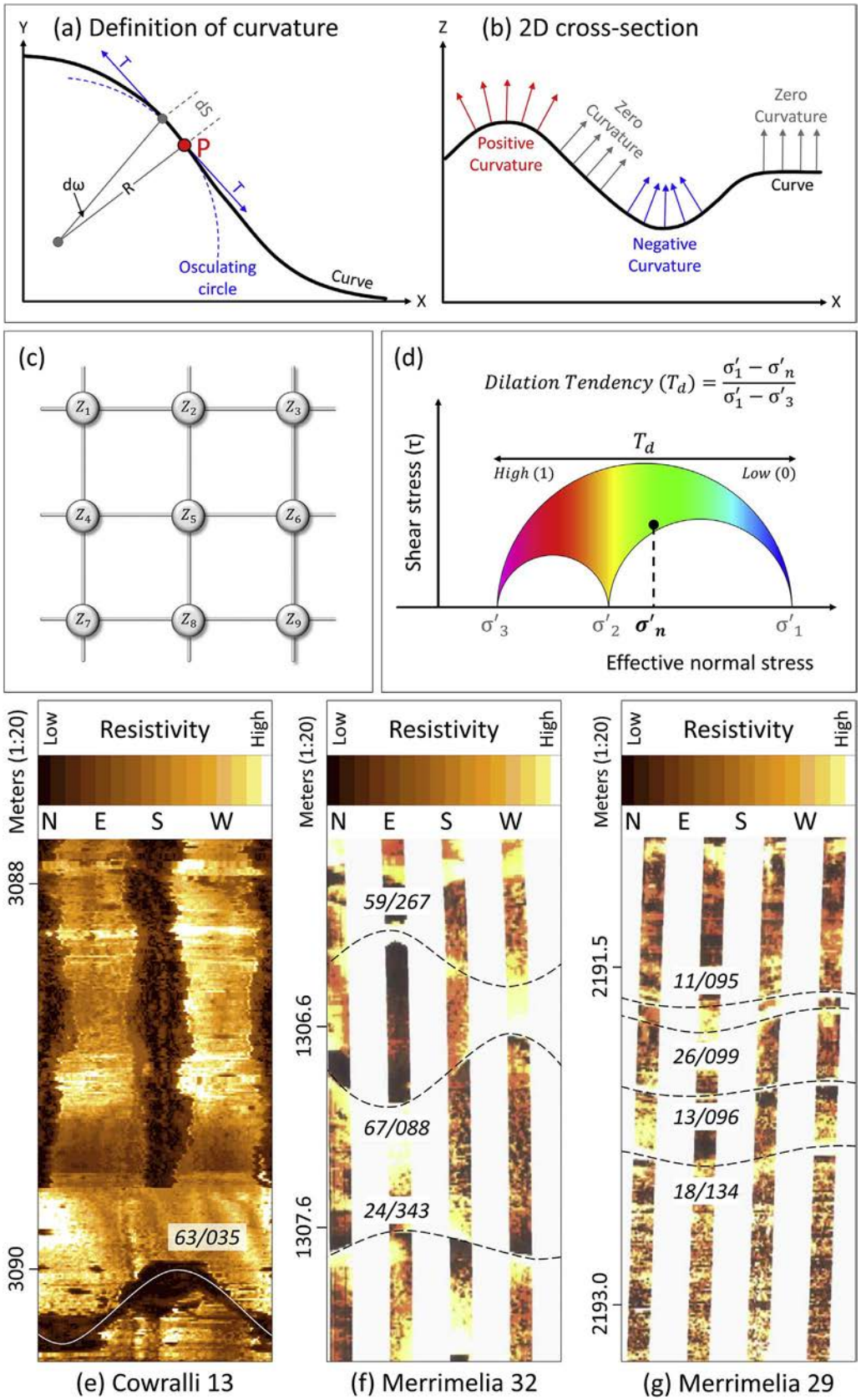

Fig. 2. (a) The definition of curvature where the value for curvature is defined as the rate of change of the direction of a curve, such that for any point (P) the curvature (K) is defined as the rate of change of the dip angle ($d\omega$) with respect to the arc length (dS) (after Roberts, 2001). (b) The change in curvature values along a curve (after Roberts, 2001). (c) Example of a 3 × 3 grid cell containing grid nodes (Z_i) used to compute curvature (Roberts, 2001); (b) The Dilation Tendency (T_d) in terms of maximum (σ'_1), minimum (σ'_3), and normal (σ'_n) effective stresses (Mildren et al., 2005). Conductive (solid line) and resistive (dashed line) natural fractures interpreted in borehole image logs from: (c) Cowralli 13; (d) Merrimelia 32; and (e) Merrimelia 29. See Fig. 1 for location.

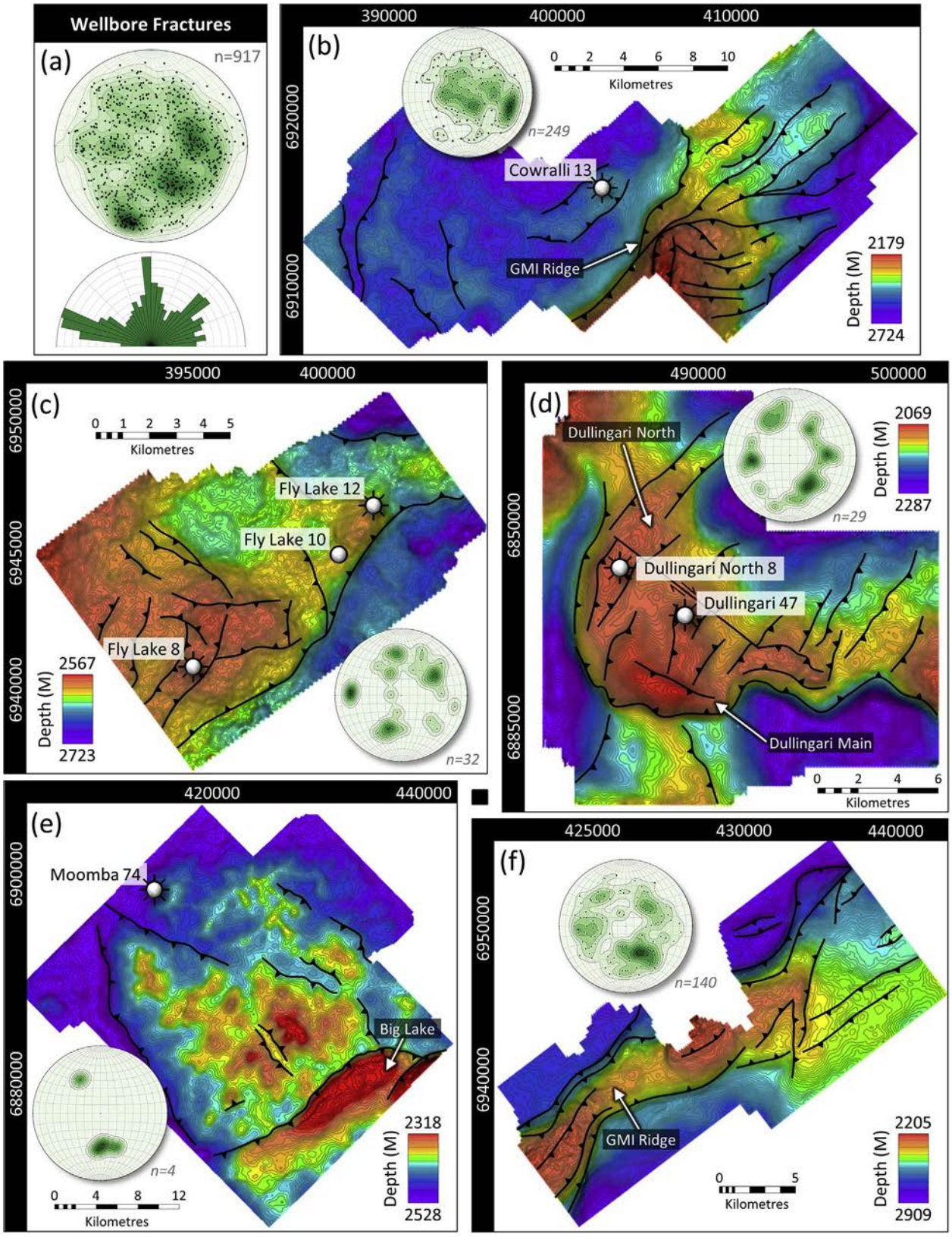

Fig. 3. Basement faults projected onto Top Permian depth maps and the geometry of natural fractures interpreted from image logs in (or adjacent to) the: (a) combined natural fracture data from all wells. See Fig. 1 for seismic survey location. (b) Greater Tindilpie-Swan Lake 3D (after Kulikowski et al., 2018). (c) Fly Lake 3D; (d) Dullingari 3D; (e) Moomba-Big Lake 3D; and (f) Merrimelia (ext) 3D (see Fig. 1 for well location). GDA94/MGA zone 54 coordinate system used and shown as X-Y locations.

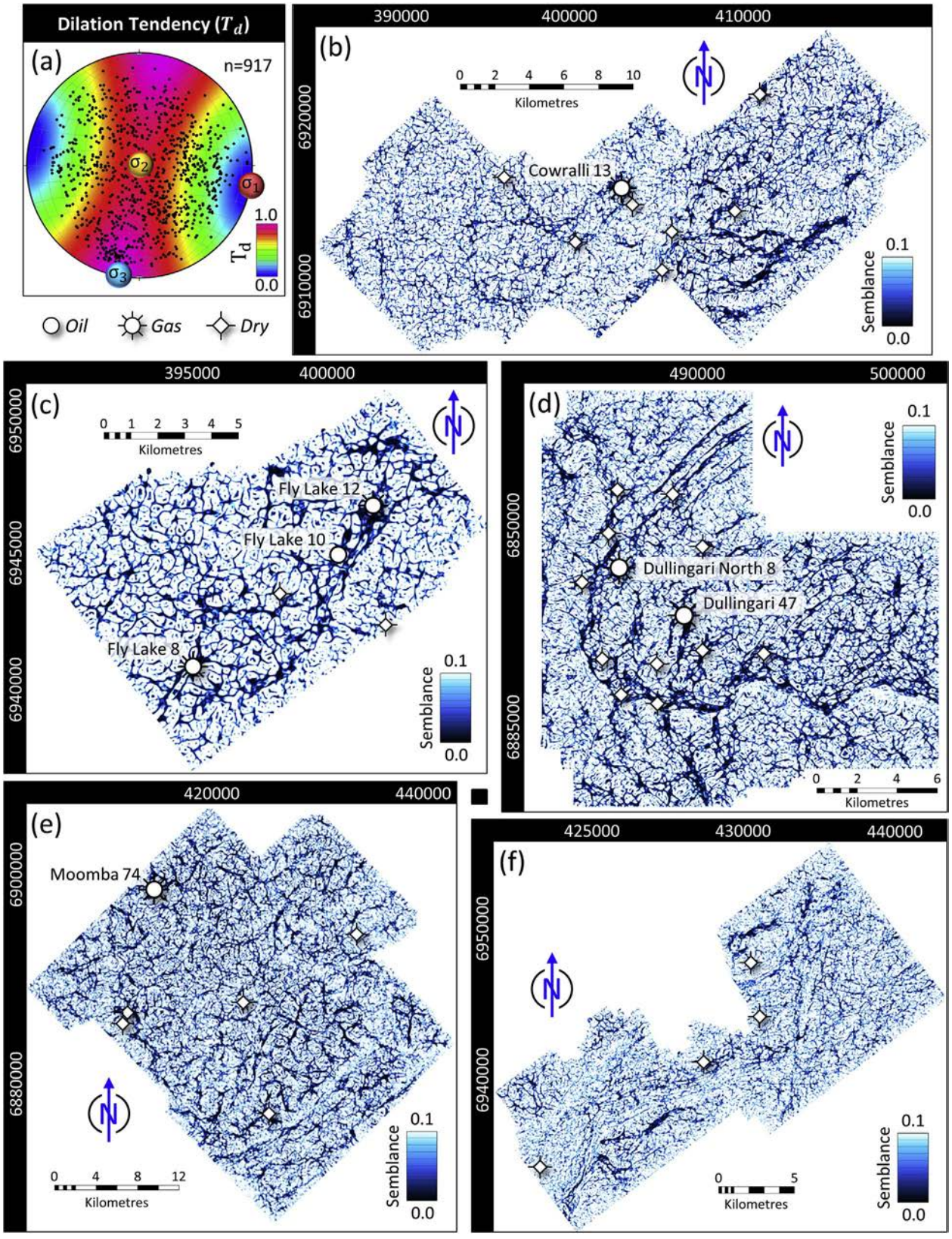

Fig. 4. Most positive curvature displayed as the semblance attribute (zero semblance = fractures) along the Middle Patchawarra Formation in: (a) Dilation Tendency results at 1500 m: equal-area lower hemisphere stereonet with stress data from Nelson et al. (2007). (b) Greater Tindilpie-Swan Lake 3D. (c) Fly Lake 3D; (d) Dullingari 3D; (e) Moomba-Big Lake 3D; and (f) Merrimelia (ext) 3D. See Fig. 1 for location. GDA94/MGA zone 54 coordinate system used and shown as X-Y locations.

3D seismic surveys. A total of 28 borehole image logs were used to measure natural fractures. These vertical wells are present throughout the study area, with 7 wells located within the 3D seismic data, and four wells (Merrimelia 29, 30, 31, and 32) located slightly outside of the Merrimelia (ext) 3D seismic survey (Fig. 1a). Prior to analysis, the seismic data were time-to-depth converted using the average velocity method, which is one of the more accurate methods for the basin (Kulikowski, 2017; Kulikowski et al., 2018). After depth conversion, a 3D subsurface dip field volume was created to provide the dip angle of all reflectors. The five 3D seismic volumes were individually analysed using the K_+ attribute, which was then processed into a semblance (similarity) attribute volume to improve the signal-noise ratio and finally extracted along the Middle Patchawarra Formation reflector. The semblance attribute volume measures the amount of similarity in the seismic curvature results in a local area, highlighting discontinuity trends, such as faults. A half-window vertical distance of 50 m was used, which visually emphasises the curvature results by removing noise (high semblance) and highlighting structural discontinuities (low semblance).

3.3. Dilation Tendency

To determine the likelihood of natural fractures undergoing tensile reactivation, and hence more likely to be hydraulically conductive under in-situ stresses, the Dilation Tendency (T_d) is measured from a geomechanical model using Eq. (8) and illustrated in Fig. 2d (Ferrill et al., 1999; Mildren et al., 2005; Jolie et al., 2015). This attribute is commonly used to determine the reactivation and fluid conduit potential of faults (Barton et al., 1995; Ferrill and Morris, 2003; Jolie et al., 2015; Kulikowski et al., 2016). The T_d is used in preference to measuring the Slip (shear) Tendency, as the latter predicts the shear potential and not the ability of natural fractures to remain open to fluid flow (Ferrill et al., 1999; Mildren et al., 2005). The T_d is governed by the effective normal stress acting on a plane, which directly affects the natural fracture aperture (Ferrill et al., 1999; Mildren et al., 2005). Therefore, the maximum (σ_1'), minimum (σ_3'), and normal (σ_n') effective stresses are used to measure the T_d (Ferrill et al., 1999; Mildren et al., 2005);

$$T_d = \left(\frac{\sigma_1' - \sigma_n'}{\sigma_1' - \sigma_3'} \right) \tag{8}$$

The T_d results are normalised to the differential stress, giving values that range from a maximum of one (high likelihood of tensile reactivation) to a minimum of zero (little to no tensile reactivation). To model the in-situ stress conditions, a present-day maximum horizontal stress orientation of 101°N was used together with a hydrostatic pore pressure gradient, a strike-slip stress regime with a low stress ellipsoid shape ratio (~0.10), and stress magnitude data from Nelson et al. (2007). Importantly, this model does not consider variables such as fracture plane roughness (texture), cementation, pressure variation, or the possibility of crystal bridging, which has been shown to enable fractures to remain open and permeable albeit not preferentially aligned with σ'_1 (Laubach et al., 2004). That being said, this model does show which fractures will be more opened, assuming the same type of fractures with the same parameters and with the same fluid pressures, with the only difference being the geometry. The present-day geomechanical model uses the assumption that hydrostatic pore pressure exists within the case study and is homogenously distributed. This can be an oversimplification and changes in local pore pressure can affect the stability of faults and fractures.

3.4. Borehole image logs

The Cooper Basin is an intra-cratonic subsurface basin, preventing direct measurements from outcrop; therefore, direct natural fracture measurements can only be made from borehole image logs or core. Images of the borehole are generated by measuring the electrical resistivity at the centimetre scale, which can provide information on whether fractures are fluid (conductive and open) or cement (resistive and closed) filled. These methods of obtaining natural fracture data can be selective in the natural fracture sets that are encounter, as high angled sets will be intersected less frequently by vertical wells than the low angle sets. This study uses 28 image logs (Fig. 1a) covering a total length of approximately 7.5 km in vertical wells. Theses were used to measure the natural fracture geometries present across the basin and to then determine which of the fracture sets is critically oriented to undergoes tensile reactivation and facilitate fluid flow (Fig. 2d). Both conductive (open to fluid flow) (Fig. 2e) and resistive (closed to fluid flow) (Fig. 2f and g) natural fractures were interpreted and geomechanically analysed based on the strike and dip angle.

4. Results

Natural fracture data measured from borehole image logs are presented on a stereonet and rose plot to show the regional natural fracture sets (Fig. 3a). The natural fracture data are projected onto the Dilation Tendency results (Fig. 4a) to identify the critically oriented sets.

4.1. Natural fractures at the wellbore

Borehole image log data were interpreted from 28 wells, which included 7 wells present within the 3D seismic data (Fig. 1a). These measured natural fractures (Fig. 3a) were used to: (1) compare the possible variation between the one-dimensional well data and three-dimensional seismic data results; and (2) generate an in-situ geomechanical model to determine the natural fracture geometry critically oriented to undergo tensile reactivation. The wellbore fracture data is dominantly N-S, NE-SW and E-W striking with a large number having a high ($> 50^0$) dip angle (Fig. 3a). This data is also presented for each group of wells that are present within the Greater Tindilpie-Swan Lake (Fig. 3b), Fly Lake (Fig. 3c), Dullingari (Fig. 3d), and Moomba-Big Lake (Fig. 3e) 3D seismic surveys. The fracture data presented for the Merrimelia (extension) 3D seismic survey (Fig. 3f) are located on the southwest border of the seismic survey (Fig. 1a). Important to note is that the statistical likelihood of intersecting high ($> 50^0$) angled fractures is reduced by drilling vertical wells, suggesting that the vertical wells used in this study may be underestimating the true fracture density.

The T_d results found that high angle ($> 50^o$) natural fractures striking 101°N (± 20°) are optimally oriented to dilate ($T_d = 1.0$) and act as potential fluid conduits (Fig. 4a), with natural fractures striking perpendicular to this geometry (011°N strike) being least likely to dilate ($T_d = 0$). This is also observed in borehole image logs, with examples of conductive (open) and resistive (closed) natural fractures presented from Cowralli 13 (Fig. 2e), and Merrimelia 32 (Fig. 2f) and Merrimelia 29 (Fig. 2g), respectively. These results infer that E-W striking high ($> 50^0$) angled natural fractures are critically oriented to undergo tensile reactivation and have potential to improve the hydraulic conductivity of low permeability reservoirs.

4.2. Natural fractures from seismic data

The K_+ results (reprocessed into the semblance attribute) are extracted along the Patchawarra Formation in each of the five seismic surveys (Fig. 4b–f). This allowed the extensional fracture networks to be clearly imaged in the subsurface. An example from the Greater Tindilpie and Swan Lake seismic survey shows the high density of extensional fractures interpreted from the borehole image log, which is reflected in the most positive curvature results (Fig. 5a). A close look at the curvature results (Fig. 5b) shows a dominant N-S strike, which coincides with the mean natural fracture strike interpreted from the

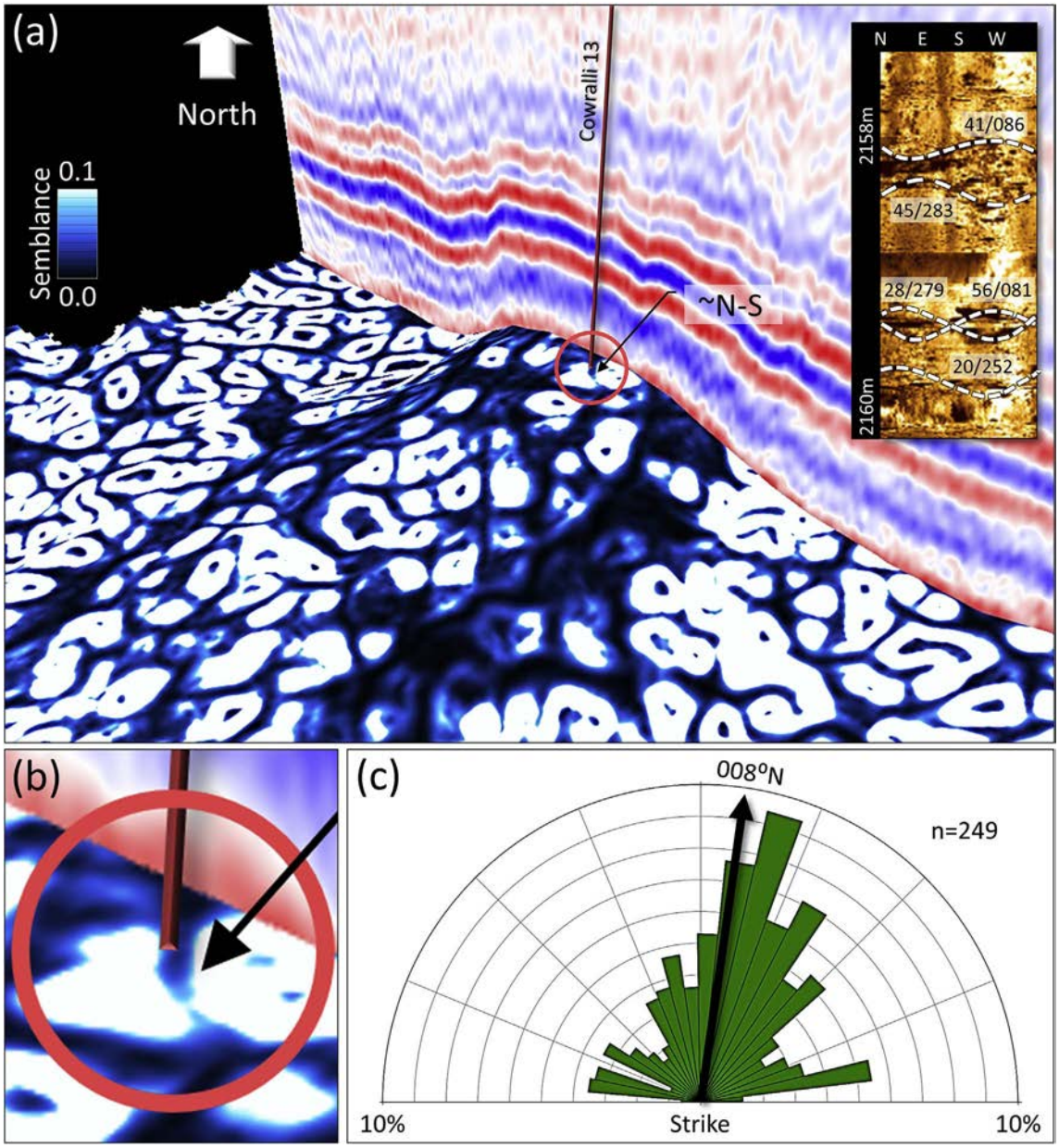

Fig. 5. (a) Seismic curvature (displayed as the semblance attribute) at the Cowralli 13 well location showing N-S striking results correlating well to interpreted N-S striking natural fractures. (b) Zoomed in image of the N-S striking seismic curvature results (displayed as the semblance attribute) at the Cowralli 13 well location. (c) Rose diagram of interpreted natural fractures from the Cowralli 13 borehole image log showing a mean N-S strike direction. See Fig. 1a for location.

borehole image log (Fig. 5c). Other wells that contain high ($> 50^0$) angled fractures also show this expected relationship, whereas wells with a low density of these fractures correspond to poor curvature results. The K_+ results (Fig. 4) also highlight the location of abrupt reflector curvature, or displacement, that is associated with interpreted basement-involved faults (Fig. 3).

4.2.1. Greater Tindilpie-Swan Lake 3D

The Greater Tindilpie-Swan Lake 3D seismic survey contains the Cowralli 13 well, which is located on a subtle NE-SW elongate anticlinal closure on the footwall side of the GMI Ridge (Fig. 3b). The K_+ analysis presents high fracture density (high K_+) within the Cowralli 13 well location, along the NE-SW striking GMI Ridge, and also along the approximately E-W striking splays in the east of the survey (Figs. 3b and 4b). The results present a dominant SE-NW and NE-SW striking network throughout the Middle Patchawarra Formation surface, that increase in density in regions of known basement faults (Figs. 3b and 4b).

4.2.2. Fly Lake 3D

Structural interpretation of Fly lake 3D shows a structural high in the west that is bound from the east by a NE-SW striking fault (Fig. 3c). The K_+ results present lineaments striking NE-SW, E-W, and N-S, with fewer striking SE-NW (Fig. 4c). The results along the Middle Patchawarra Formation show high K_+ values in the northeast of the survey within the vicinity of Fly Lake 10 and Fly Lake 12. Strong K_+ results are also present above known basement faults (Figs. 3c and 4c).

4.2.3. Dullingari 3D

The Dullingari 3D seismic survey contains two well controls; Dullingari North 8 and Dullingari 47, which are in the Dullingari North and Dullingari Main culminations, respectively (Figs. 3d and 4d). The K_+ analysis delineates a NE-SW and SE-NW striking network present throughout the survey (Fig. 4d), with secondary N-S striking features present within the Dullingari Main area (Figs. 3d and 4d). E-W striking K_+ lineaments are found in regions with known E-W striking basement

faults, and increases in density along E-W elongate anticlines (Figs. 3d and 4d). The results along the Middle Patchawarra Formation shows the detailed distribution of structural lineaments, such as the NE-SW striking features in Dullingari North and the saw-tooth-like geometry of the E-W striking fault bounding Dullingari Main from the south (Figs. 3d and 4d).

4.2.4. Moomba-Big Lake 3D

The Moomba 74 borehole image log is located on the outer edge of the Moomba-Big Lake 3D seismic survey, along the flank of a small Permian structure that corresponds to low K_+ (Figs. 3e and 4e). E-W trending K_+ lineaments are present within the Moomba 74 well location, with large SE-NW trending lineaments present elsewhere in the seismic survey that are subparallel to the basement faults (Figs. 3e and 4e). The major NE-SW elongate Big Lake structure is expressed with high K_+ values in the southeast of the survey along the Middle Patchawarra Formation horizon (Figs. 3e and 4e). The K_+ results in this area have a wide distribution of strikes and appears highly complex.

4.2.5. Merrimelia (extension) 3D

Three borehole image logs are located slightly outside of the Merrimelia (extension) 3D seismic survey, but remain along the GMI Ridge (Fig. 1a). The Merrimelia structure is a NE-SW elongate anticline bound from the west by the GMI Ridge fault (Fig. 3f). Significantly high K_+ values are present along this structure and increase to the northeast and southwest (Fig. 4f). The general trend of this dense K_+ network is mostly NE-SW, with secondary N-S, SE-NW, and E-W striking features also present (Fig. 4f). The results present a large N-S striking feature along the Middle Patchawarra Formation in the centre of the survey (Fig. 4f), which coincides with basement faults and an abrupt increase in depth (Fig. 3f).

5. Discussion

Although borehole image logs and cores can provide the natural fracture distribution at the wellbore, assuming this data is representative of the basin can be unrealistic. For one, the sampling of fractures is statistically biased in vertical wells to intersect more low angle fractures than high angle, and coupled with local stress perturbations and lateral changes in geology, the 1D well data can be wholly unrepresentative. An effective means of obtaining high density structural data from subsurface provinces is through the careful application of seismic curvature analysis (e.g. Murray, 1968; Lisle, 1994; Al-Dossary and Marfurt, 2006; Chopra and Marfurt, 2007; Bailey et al., 2014). By understanding that most positive curvature (K_+) analysis selectively presents high ($> 50^o$) angled fractures based on the extensional stress distribution along the outer arc of an anticline, this research is able to constrain the distribution of permeable fracture networks along the gas-rich Patchawarra Formation, Cooper Basin.

Borehole image log interpretation found resistive (closed) natural fractures typically striking N-S and NE-SW with high dip angle ($> 50^o$), with examples shown from Merrimelia 32 (Fig. 2f) and Merrimelia 29 (Fig. 2g). Alternatively, conductive fractures typically strike SE-NW and E-W with high dip angles ($> 50^o$), as shown in Cowralli 13 (Fig. 2e). Regional NE-SW and SE-NW striking faults and fractures have been shown to preferentially shear reactivate under present-day stress (Kulikowski et al., 2016; Kulikowski, 2017); however, it is important to understand whether they will remain open after shearing. We examine this by developing a geomechanical model of the in-situ stress to measure the T_d of fracture sets, with results aligning well with borehole image log interpretation of conductive and resistive fractures, showing that near vertical E-W striking fractures will preferentially dilate ($T_d = 1.0$), as will the pervasive SE-NW striking fracture set ($T_d = 0.7 - 0.8$) (Fig. 4a).

Previous research on the regional natural fracture distribution in the basin found that NE-SW and SE-NW striking high ($> 50^o$) dip angle sets dominate the region and likely developed through extensional stresses (Kulikowski, 2017; Kulikowski and Amrouch, 2017). These fracture sets are present within the Patchawarra Formation together with low angle ($< 30^o$) sets striking NE-SW, N-S, and E-W. The subsurface fracture distributions in each of the five seismic surveys shows a dominant NE-SW and SE-NW strike in the curvature (semblance attribute) results, supporting previous works that suggested their regional presence (Kuang, 1985; Apak et al., 1997; Kulikowski, 2017; Kulikowski and Amrouch, 2017). Amongst this dominant fracture network, N-S and E-W striking lineaments are also identified in each seismic survey. The geomechanical modelling results show that high angled fractures, particularly if striking E-W to SE-NW, are optimally oriented to undergo tensile reactivation. These E-W to SE-NW striking conductive fracture sets are present in each seismic survey and most pervasive within the Fly Lake (Fig. 4c), Dullingari (Fig. 4d), and Moomba-Big Lake (Fig. 4e) 3D seismic surveys. The density of these sets increases rapidly along SE-NW and E-W elongate anticlines, such as those found in the Moomba-Big Lake (Figs. 3e and 4e) and Dullingari (Figs. 3d and 4d) 3D seismic surveys.

Wells that were drilled in regions of high K_+ were found to have an increased number of high ($> 50^o$) angle natural fractures present in the wellbore image logs. This relationship is also found in wells that were drilled in low seismic curvature regions, which have relatively less high ($> 50^o$) angle natural fractures. A low fracture density in the Cooper Basin has previously been described and can potentially be attributed to the inability of vertical wells to intersect the high angled ($> 50^o$) fracture sets that dominate the province (Kulikowski, 2017; Kulikowski and Amrouch, 2017). Seismic K_+ analysis combats this limitation to widely present the fracture density within the five seismic surveys, suggesting that the density may be much higher than previously thought. Once the subsurface distribution of the regionally pervasive and critically oriented high ($> 50^o$) angle E-W and SE-NW striking fractures is defined, these can be exploited and become highly beneficial for many industries including, petroleum, geothermal, and carbon sequestration.

The additional processing of K_+ results into the semblance (similarity) attribute has better defined the fracture networks by improving the signal-noise ratio. High density fracture zones are compared with the location of known dry wells in each of the seismic surveys (Fig. 4), showing a noticeable absence of dry wells from high density locations in all cases. Although drilling within high fracture density zones may not be the single factor involved in a well failing to produce hydrocarbons, it can have a significant impact on the efficiency of hydraulic fracture stimulation treatments and in well design.

The remote sensing of fractures and faults has become an important tool in many industries (e.g. petroleum, geothermal, carbon dioxide capture and storage, hydrology, and mining) because of their potential for enhanced fluid/gas flow. A study that focused on a local area in the Penola Trough, Otway Basin, presented a large 3D subsurface fracture network that appeared to show good connectivity from curvature results; however, through core and image log analysis, and stress modelling, Bailey et al. (2014) concluded that this network was likely to be a poor hydraulic conductor. This reiterated the need for a careful approach when exploiting subsurface fracture networks. Following on from this work, we used the Cooper Basin as a case study to highlight the potential of integrating seismic curvature analysis with wellbore data and geomechanical modelling to constrain the distribution of permeable subsurface fracture networks, that would otherwise be limited to one-dimensional well data. Although we focus on one stratigraphic interval within the basin, future work should consider the changing fracture distribution between stratigraphic intervals and attempt to investigate the vertical persistency of fractures and its relationship to vertical hydraulic conductivity.

The careful application of this approach would be most beneficial to other important subsurface or offshore provinces that have a known regional distribution of high ($> 50^o$) angle extensional fractures and

faults, such as the Otway Basin in Australia (Bailey et al., 2014; Burgin et al., 2018), Piceance Basin in Colorado (Lorenz and Finley, 1991), East Texas Basin in the Gulf of Mexico (Laubach, 1988), Ordos Basin in China (Lianbo and Xiang-Yang, 2009), and frontier basins, such as the Ceduna Sub-basin in Australia (Robson, 2017), the group of basins in offshore Columbia (Beltrán Rivas and Vargas Jiménez, 2014), the Congo Basin in offshore West Africa (Brownfield and Charpentier, 2006), Zagros collision belt (Lacombe et al., 2007), and the Big Horn Basin in Wyoming (Amrouch et al., 2011; Beaudoin et al., 2012).

6. Conclusion

This research uses the intra-cratonic subsurface Cooper Basin (Australia) as a case study to carefully apply an approach that maps the distribution of permeable fracture networks through the integration of most positive curvature (K_+) seismic analysis, wellbore fracture data, and in-situ geomechanical modelling. Five three-dimensional seismic surveys were analysed using the K_+ seismic attribute to constrain the distribution of critically oriented high ($> 50^0$) angle permeable fracture networks within the gas-rich and low permeability Patchawarra Formation. The regionally pervasive high angle ($> 50^o$) SE-NW and E-W striking fracture sets were identified to be critically oriented to undergo tensile reactivation and act as fluid conduits under in-situ stresses. These sets are identified in each of the five seismic surveys and found to increase in density along E-W elongate anticlines. The well fracture data in the Cooper Basin presents a close relationship to K_+ results, which can be important for generating representative high density structural data that would otherwise be restricted to sparse well locations. Careful application of this approach to other subsurface or offshore provinces can provide important high density structural information between sparse one-dimensional well data.

Acknowledgements

We thank the financial contribution made by the GeoFrac Consortium, which includes the sponsoring companies: Santos, Beach Energy, Chevron, Halliburton and BG Group (QGC). Thank you to Midland Valley (MOVE), DownUnder Geosolutions (DUG Insight), and Paradigm (Geolog) for academic licencing. Thank you to Carlos H. Grohmann and Ginaldo A.C. Campanha for the “OpenStereo 0.1.2” stereonet software.

References

Al-Dossary, S., Marfurt, K.J., 2006. 3D volumetric multispectral estimates of reflector curvature and rotation. Geophysics 71 (5), 41–51.
Alexander, E.M., Gravestock, D.I., Cubitt, C., Chaney, A., 1998. Lithostratigraphy and environments of deposition. In: In: Gravestock, D.I., Hibburt, J.E., Drexel, J.F. (Eds.), The Petroleum Geology of South Australia, vol. 4. Cooper Basin, South Australia. Department of Primary Industries and Resources, pp. 69–116 Report Book, 98/9.
Amrouch, K., Lacombe, O., Bellahsen, N., Daniel, J.M., Callot, J.P., 2010a. Stress and strain patterns, kinematics and deformation mechanisms in a basement-cored anticline: sheep Mountain Anticline, Wyoming. Tectonics 29http://dx.doi.org/10.1029/2009TC002525. TC1005.
Amrouch, K., Robion, P., Callot, J.P., Lacombe, O., Daniel, J.M., Bellahsen, N., Faure, J.L., 2010b. Constraints on deformation mechanisms during folding provided by rock physical properties: a case study at Sheep Mountain anticline (Wyoming, USA). Geophys. J. Int. 182 (3), 1105–1123.
Amrouch, K., Beaudoin, N., Lacombe, O., Bellahsen, N., Daniel, J., 2011. Paleostress magnitudes in folded sedimentary rocks. Geophys. Res. Lett. 38 (17). http://dx.doi.org/10.1029/2011GL048649. L17301.
Apak, S.N., Stuart, W.J., Lemon, N.M., Wood, G., 1997. Structural evolution of the permian-triassic Cooper Basin, Australia: relation to hydrocarbon trap styles. AAPG (Am. Assoc. Pet. Geol.) Bull. 81, 533–555.
Backe, G., Khair, H.A., King, R., Holford, S., 2011. Fracture mapping and modelling in shale-gas target in the Cooper basin, South Australia. APPEA J. 51, 397–410.
Bailey, A., King, R.C., Holford, S.P., Sage, J., Backe, G., Hand, M., 2014. Remote sensing of subsurface fractures in the Otway Basin, South Australia. J. Geophys. Res.: Solid Earth 119 (8), 6591–6612. http://dx.doi.org/10.1002/2013JB010843.
Barton, C.A., Zoback, M.D., Moos, D., 1995. Fluid flow along potentially active faults in crystalline rock. Geology 23, 683–686.
Beaudoin, N., Lepretre, R., Bellahsen, N., Lacombe, O., Amrouch, K., Callot, J., Emmanuel, L., Daniel, J., 2012. Structural and microstructural evolution of the rattlesnake mountain anticline (Wyoming, USA): new insights into the sevier and laramide orogenic stress build-up in the Bighorn Basin. Tectonophysics 576–577, 20–45. http://dx.doi.org/10.1016/j.tecto.2012.03.036.
Beltrán Rivas, J.D., Vargas Jiménez, C.A., 2014. Hydrocarbon production scenarios in Colombia. Review of field sizes, hydrocarbon reserves and expectations of conventional and unconventional resources. Earth Sci. Res. J. 18 (1), 77–83.
Brownfield, M.E., Charpentier, R.R., 2006. Geology and Total Petroleum Systems of the West-Central Coastal Province (7203), West Africa. U.S. Geological Survey Bulletin 2207-B.
Burgin, H.B., Amrouch, K., Rajabi, M., Kulikowski, D., Holford, S.P., 2018. Determining structural environments through natural fracture and calcite twin analysis: a case study in the Otway Basin. APPEA J. 58 (accepted).
Chopra, S., Marfurt, K., 2007. Curvature attribute applications to 3D surface seismic data. Lead. Edge 26 (4), 404–414.
Ferrill, D.A., Groshong, R.H., 1993. Kinematic model for the curvature of the northern Subalpine Chain, France. J. Struct. Geol. 15 (3–5), 523–541.
Ferrill, D.A., Winterle, J., Wittmeyer, G., Sims, D., Colton, S., Armstrong, A., Morris, A.P., 1999. Stressed rock strains groundwater at Yucca Mountain, Nevada. GSA Today (Geol. Soc. Am.) 9 (5), 1–8.
Ferrill, D.A., Morris, A.P., 2003. Dilational normal faults. J. Struct. Geol. 25, 183–196.
Gatehouse, C.G., 1986. The geology of the Warburton Basin in South Australia. Aust. J. Earth Sci. 33 (2), 161–180.
Gray, M.E., 2017. Analytical Techniques for Evaluating Seal Capacity for Carbon Dioxide Storage in Selected Australian Basins (Doctoral dissertation). The Australian School of Petroleum, the University of Adelaide, Adelaide, Australia.
Hakami, A.M., Marfurt, K.J., Al-Dossary, S., 2004. Curvature attribute and seismic interpretation: case study from Fort Worth Basin, Texas, USA. In: 2004 SEG Annual Meeting. Society of Exploration Geophysicists.
Jolie, E., Moeck, I., Faulds, J.E., 2015. Quantitative structural geological exploration of fault-controlled geothermal systems—a case study from the Basin-and-Range Province, Nevada (USA). Geothermics 54, 54–67.
Kuang, K.S., 1985. History and style of Cooper-Eromanga Basin structures. Explor. Geophys. 16, 245–248.
Kulikowski, D., Amrouch, K., Cooke, D., 2016. Geomechanical modelling of fault reactivation in the Cooper Basin, Australia. Aust. J. Earth Sci. 63 (3), 295–314. http://dx.doi.org/10.1080/08120099.2016.1212925.
Kulikowski, D., 2017. Modern Structural Analysis of Subsurface Provinces: a Case Study on the Cooper and Eromanga Basins, Australia (Doctoral dissertation). The Australian School of Petroleum, the University of Adelaide, Adelaide, Australia.
Kulikowski, D., Amrouch, K., 2017. Combining geophysical data and calcite twin stress inversion to refine the tectonic history of subsurface and offshore provinces: a case study on the Cooper-Eromanga Basin, Australia. Tectonics 36 (3), 515–541. http://dx.doi.org/10.1002/2016TC004366.
Kulikowski, D., Amrouch, K., 2018. 3D seismic analysis investigating the relationship Between stratigraphic architecture and structural activity in the intra-cratonic cooper and Eromanga Basins, Australia. Mar. Petrol. Geol. 91, 381–400. http://dx.doi.org/10.1016/j.marpetgeo.2018.01.019.
Kulikowski, D., Amrouch, K., Cooke, D., Gray, M.E., 2018. Basement structural architecture and hydrocarbon conduit potential of polygonal faults in the Cooper-Eromanga Basin, Australia. Geophys. Prospect. 66 (2), 366–396. http://dx.doi.org/10.1111/1365-2478.12531.
Lacombe, O., Amrouch, K., Mouthereau, F., Dissez, L., 2007. Calcite twinning constraints on late Neogene stress patterns and deformation mechanisms in the active Zagros collision belt. Geology 35 (3), 263–266. http://dx.doi.org/10.1130/G23173A.1.
Laubach, S.E., 1988. Subsurface fractures and their relationship to stress history in East Texas Basin sandstone. Tectonophysics 156 (1/2), 37–49.
Laubach, S.E., Olson, J.E., Gale, J.F., 2004. Are open fractures necessarily aligned with maximum horizontal stress? Earth Planet Sci. Lett. 222 (1), 191–195.
Lianbo, Z., Xiang-Yang, L., 2009. Fractures in sandstone reservoirs with ultra-low permeability: a case study of the upper triassic Yanchang Formation in the Ordos Basin, China. AAPG (Am. Assoc. Pet. Geol.) Bull. 93 (4), 461–477.
Lisle, R.J., 1994. Detection of zones of abnormal strains in structures using Gaussian curvature analysis. AAPG (Am. Assoc. Pet. Geol.) Bull. 78 (12), 1811–1819.
Lorenz, J.C., Finley, S.J., 1991. Regional fractures II: Fracturing of mesaverde reservoirs in the Piceance Basin, Colorado. AAPG (Am. Assoc. Pet. Geol.) Bull. 75 (11), 1738–1757.
Mavromatidis, A., 2006. Burial/exhumation histories for the Cooper-Eromanga Basins and implications for hydrocarbon exploration, Eastern Australia. Basin Res. 18, 351–373.
Mildren, S.D., Hillis, R.R., Dewhurst, D.N., Lyon, P.J., Meyer, J.J., Boult, P.J., 2005. FAST: a new technique for geomechanical assessment of the risk of reactivation-related breach of fault seals. In: In: Boult, P., Kaldi, J. (Eds.), Evaluating Fault and Cap Rock Seals, vol. 2. AAPG Hedberg Series, Barossa Valley, South Australia, pp. 73–85.
Murray, G.H., 1968. Quantitative fracture study-Spanish pool, McKenzie county, North Dakota. AAPG (Am. Assoc. Pet. Geol.) Bull. 52 (1), 57–65.
Nelson, E.J., Chipperfield, S.T., Hillis, R.R., Gilbert, J., McGowen, J., 2007. Using geological information to optimize fracture stimulation practices in the Cooper Basin, Australia. Petrol. Geosci. 13 (1), 3–16.
Roberts, A., 2001. Curvature attributes and their application to 3D interpreted horizons. First Break 19 (2), 85–100.
Robson, A.G., 2017. Normal fault Growth Analysis Using 3D Seismic Datasets Located along Australia's Southern Margin (Doctoral dissertation). School of Physical Sciences, the University of Adelaide, Adelaide, Australia.
Robson, A.G., Holford, S.P., King, R.C., Kulikowski, D., 2018. Structural evolution of horst and half-graben structures proximal to a transtensional fault system determined using 3D seismic data from the Shipwreck Trough, offshore Otway Basin, Australia. Mar. Petrol. Geol. 89, 615–634. http://dx.doi.org/10.1016/j.marpetgeo.2017.10.028.
Stewart, S.A., Podolski, R., 1998. Curvature analysis of gridded geological surfaces. Geol. Soc. Lond. Spec. Publ. 127 (1), 133–147.

Appendix I.II: Co-Authored Manuscript 2

The intracratonic Cooper and Eromanga Basins, Australia: A Comprehensive Review

The finalised version of this manuscript will be submitted to the *Australian Journal of Earth Science.*

As with section I.I while based in the Cooper Basin, in central Australia. This manuscript draws on many of the elements fundamental to the main body of this thesis.

Much of the new contributions to the framework of the basin within the manuscript were made using the same approach as applied within the preceding pages of this thesis.

This study is further testament to what can be achieved when a multiscale approach to basin analysis is completed. Comprehensively summarising many geological aspects of the basin and its structural evolution.

The intracratonic Cooper and Eromanga Basins, Australia: A Comprehensive Review

David **Kulikowski**[a] (drdavidkulikowski@gmail.com)
Khalid **Amrouch**[a] (khalid.amrouch@adelaide.edu.au)
Kunakorn **Pokalai**[a] (kunakorn.pokalai@adelaide.edu.au)
Steve I. **Mackie**[b] (steve.mackie@geosimconsulting.com.au)
Michael E. **Gray**[a] (michael.gray2@woodside.com.au)
Hugo B. **Burgin**[a] (hugo.burgin@adelaide.edu.au)

[a]Australian School of Petroleum, University of Adelaide, North Terrace, 5005, Adelaide, Australia.

[b]Geosim Consulting Pty Ltd, 112b Sydenham Rd, Norwood, 5067, Adelaide, Australia.

Citation: Kulokowski, D., Amrouch, K., Pokalai, K., Mackie, S. I., Gray, M. and **Burgin H. B**. (2019) The intracratonic Cooper and Eromanga Basins, Australia: A Comprehensive Review (in – prep)

Abstract

This review focuses on integrating old literature with present-day models to provide a modern summary of Australia's largest onshore hydrocarbon province, the Cooper-Eromanga basins, with a focus on structural geology and geophysics. A rapid rise in cutting-edge research has been facilitated by exploration companies transitioning away from the nearly extinct anticlinal theory, to technically more challenging plays within the basin. The purpose of this review is to provide new and existing operating companies, and researchers, with a summary of the recent research developments, together with the fundamentals of the basin, to ensure that the tremendous unconventional hydrocarbon potential is effectively explored for and appropriately developed. A modern tectonostratigraphic evolution model is presented alongside the stress magnitude, regime and orientation of the six events that have affected the province (N-S Carboniferous Alice Springs Event; SE-NW Mid-Permian Event; NE-SW Late Permian Daralingie Event; E-W Triassic Hunter-Bowen Event; E-W Late Cretaceous Event; N-S Paleogene Event). Integration of these complete paleo-stress tensors with geomechanical models has constrained the dynamic reactivation (shear and tensile) of faults through time to find that since the critical moment (90 Ma), N-S and E-W striking high angle (50-70^{o}) faults were most likely to facilitate hydrocarbon migration. These form the major topics of discussion; however, the temporal and spatial distribution of natural fractures away from the wellbore, seismic time-to-depth conversion methods and accuracies, petroleum systems elements and processes, current and future exploration programs, common hydraulic fracturing and well surveillance programs, and recommendations for future research are also discussed. The methodologies, cutting-edge research and novel approaches presented here form a framework that can be applied to other hydrocarbon provinces around the world while also providing a knowledge platform for this highly prospective hydrocarbon province.

1. Introduction

The Cooper-Eromanga basins are Australia's largest onshore hydrocarbon province (Fig. 1) and have been producing oil and gas from tight reservoirs since the first natural gas discovery at Gidgealpa in 1963 (Gravestock, Alexander, Morton & Sun, 1998; Radke, 2009; Mackie, 2015). The basins are oil and gas saturated and require the simplest of structural traps, an anticline, for effective petroleum accumulation and preservation (Apak, Stuart, Lemon & Wood, 1997; Gravestock et al., 1998; Mackie, 2015). As such, much of the early research has focused on basic structural interpretation of sparse two-dimensional (2D) seismic data that remained in the time-domain, with the primary focus of identifying these anticlinal closures (e.g. Senior, Galloway, Ingram, & Senior, 1968; Stuart, 1976; Veevers, Jones & Powell, 1982; Kuang, 1985; Stanmore, 1989; Elliot, 1993; Apak et al., 1997; Sun, 1997; Gravestock & Jensen-Schmidt, 1998). The lack of detailed research has been further compounded by the limited exposure of rocks at surface, particularly within the South Australian portion of the basin, which has ultimately restricted much of the research to wellbore derived data. However, recent advancements in seismic data acquisition and processing, coupled with novel software applications and approaches, have enabled researchers to better constrain the structural geology and tectonic evolution of the Cooper-Eromanga basins. A detailed and modern synthesis of this prospective province, with a focus on the structural geology and geophysics, will provide fundamental and up to date understandings that will benefit future hydrocarbon exploration and development programs and highlight the present-day research gaps that can be further investigated.

The significantly reduced seismic resolution below Permian coal measures has made research difficult in the past. As a result, the structural and stratigraphic evolution of the province has received conflicting arguments through time, evolving from original models that display normal faults (Gravestock & Jensen-Schmidt, 1998), followed by researchers interpreting the

same structures as reverse faults (Kuang, 1985; Apak et al., 1997; Sun, 1997), to most recent studies that have presented evidence for extensive, compressional, and strike-slip faulting (Radke, 2009; Grant-Wooley, Kong, Schoemaker, Nasreddin & Montague, 2014; Kulikowski, Amrouch & Cooke, 2016c; Kulikowski, 2017; Kulikowski, Amrouch, Cooke & Gray, 2017; Kulikowski & Amrouch, 2017, 2018a, 2018b). These models are discussed and integrated with recent research to provide a modern tectonostratigraphic evolution model, which includes paleo-stress orientations, magnitudes and stress regimes that have affected the province through time.

This transition of structural models can also be linked to the improvement, and the use, of seismic time-to-depth conversion methods, which can have a significant impact on: (1) the true measurable fault dip angle; (2) the presence or absence of shallow low relief structures; and (3) pseudo structures resulting from high or low velocity heterogeneities. To promote the use and accuracy of high resolution 3D seismic data in future research, we describe the most commonly used seismic time-to-depth conversion methods, discuss their individual limitations and accuracies, identify the key seismic reflectors, and highlight the importance of accurate seismic time-to-depth conversion for future hydrocarbon exploration and research purposes.

Similarly, the improvement of petrophysics, drilling, and hydraulic fracture stimulation technologies has fostered exciting new research on geomechanics, optimisation of drilling programs, and in modelling the intrinsic relationship between hydraulic fracture stimulations and pre-existing natural fractures and faults (Chipperfield & Britt, 2000; Roberts, Chipperfield, & Miller, 2000; Johnson, Aw, Ball, & Willis, 2002; Johnson and Greenstreet, 2003; McGowen, Gilbert, & Samari, 2007; Scott et al., 2013; Johnson et al., 2015; Pokalai, Kulikowski, Johnson, Haghighi, & Cooke, 2016; Pokalai, 2018). Understanding the growth of hydraulic fractures, both temporally and spatially away from the wellbore, has been a strongly debated topic within the province (Scott et al., 2013; Cooke et al., 2015). The high stress environment, the effect of

pre-existing natural fractures, the influence of near wellbore pressure loss, and the complexity of intra-formational heterogeneity have contributed to ineffective hydraulic fracture programs in the past (Scott et al., 2013; Cooke, Tyiasning, & Abul Khair, 2016; Pokalai et al., 2016; Pokalai, 2018). These issues, together with current hydraulic fracturing practises and well surveillance programs, are discussed to provide fundamental background information for companies, both existing and new, that are investing in the basin.

This recent influx of high quality detailed research has been driven by the transition to a more technically challenging hydrocarbon exploration strategy. Few undrilled anticlinal traps remain within the basin, facilitating the shift to technically more challenging exploration that is focused on identifying new targets such as stratigraphic traps, basin centred gas, deep coals and polygonal fault related accumulations (Lowe-Young, Mackie, & Heath, 1998; Morton, 1998; Watterson, Walsh, Nicol, Nell, & Bretan, 2000; Hillis, Morton, Warner, & Penney, 2001; Radke, 2009; Mackie, 2015). This paradigm shift has tremendous opportunities for new investors and existing companies targeting hydrocarbons within this prolific basin. To facilitate this transition, the purpose of this research is to collate and critically discuss published works and integrate the key findings into a single document that provides: (1) a modern tectonostratigraphic evolution model; (2) a summary of geomechanical modelling results that predict fault and fracture reactivation (tensile and shear) through time to better understand hydrocarbon migration pathways; (3) a synthesis of the petroleum system processes and elements; (4) the spatial and temporal distributions of permeable natural fracture networks; (5) common hydraulic fracturing and well surveillance programs contrasted with the common difficulties and risks; (6) a discussion of the seismic time-to-depth conversion methods that are being used and their accuracies and limitations; (7) current and future hydrocarbon exploration and development targets; and (8) a discussion on the future research opportunities that can impact the success of future hydrocarbon programs.

This review collates and integrates previous research with modern understandings that can be disseminated within companies operating in the Cooper-Eromanga basins, Australia. The detailed methodologies, cutting-edge research and novel approaches form a research framework that can be applied to other subsurface or offshore provinces around the world.

Insert Fig. 1

2. Modern tectonostratigraphic evolution model

Unique to this province, the Silurian to Cambrian Warburton Basin, Triassic to Permian Cooper Basin, Cretaceous to Jurassic Eromanga Basin, and Paleogene to Quaternary Lake Eyre Basin are separated in time by regional unconformities that were developed through successive reactivation of pre-existing faults (Fig. 2) (Kantsler, Prudence, Cook, & Zwigulis, 1984; Bradshaw, 1993; Apak, 1997; Gravestock & Jensen-Schmidt, 1998; Mavromatidis, 2006). These vertically stacked basins have unique spatial extents and unique stratigraphy and hydrocarbon potential. The Warburton Basin is considered basement within this region and consists of volcanic, shallow shelf, deltaic and prograding shoreline deposits (Gatehouse, 1986). The Cooper Basin is the most hydrocarbon-rich, with a large volume of Permian coals that cycle with intra-formational sandstone and shale (Kantsler et al., 1984; Apak et al., 1997; Alexander, Gravestock, Cubitt, & Chaney, 1998). The Cooper Basin consists mostly of sediments deposited by fluvial, lacustrine, and swamp conditions. The Eromanga Basin is also hydrocarbon-rich with many of the present-day exploration programs targeting oil-rich Jurassic and Early Cretaceous sediments primarily along the western flank of the basin (Heath, McIntyre, & Gibbins, 1989). The depositional environment during this time transitioned from fluvial, lacustrine, deltaic, shoreface marine, and open shallow marine, with fluvial conditions returning to deposit one of the youngest and thickest units of the Eromanga Basin; the Winton

Formation (Lowe-Young et al. 1998). The Lake Eyre Basin is presently exposed at surface with no hydrocarbon potential.

The Permian coals are the major hydrocarbon source rock of the basin, and increase in thickness in the South Australian portion of the basin. As such, the major exploration and development targets are located within South Australia (Reynolds, Mildren, Hillis, & Meyer, 2004, 2006; Mackie, 2015). This portion of the basin contains two NE-SW striking ridges; the Gidgealpa-Merrimelia-Innamincka (GMI) Ridge and the Nappacoongee-Murteree (NM) Ridge (Fig. 3b) (Kuang, 1985; Apak et al., 1997; Gravestock & Jensen-Schmidt, 1998; Kulikowski, 2017). These prominent ridges form the major hydrocarbon fields in this sector of the basin and also separate the NE-SW elongate Patchawarra, Nappamerri and Tenappera troughs (Fig. 3). In the following sections, the structural and stratigraphic evolution of this intra-cratonic region will be discussed, with emphasis on the most up-to-date research.

Insert Fig. 2

Insert Fig. 3

2.1 Pre-Cambrian Extension (650-575 Ma)

During the Late Proterozoic much of the world's landmass was submerged by ocean with a relatively small landmass exposed at surface, consisting of portions of what is now Antarctica, India, South Africa, Congo, and the western portion of Australia (Fig. 4a) (Myers, Shaw, Tyler, 1996; Boger & Miller, 2003; Collins & Pisarevsky, 2005; Kulikowski and Amrouch, 2017). The ancient Australian landmass was in a similar geometry to present-day; slightly rotated in a clockwise direction and bisected in an NNE-SSW direction by the paleo-tectonic plate boundary (Myers et al., 1996; Boger & Miller, 2003; Collins & Pisarevsky, 2005). This boundary is now referred to as the Tasman Line that separates the younger land mass in eastern Australia from the rest of the continent (Haines, Hand, & Sandiford, 2001). Rifting within the

Panthalassic Ocean, east of the ancient plate, began in the Late Proterozoic (650 Ma) in an approximately SE-NW direction. This regional rifting event affected the then Centralian Superbasin as well as the Warburton Basin, developing SE-NW striking strike-slip faults and NE-SW striking normal faults within the Igneous Meta-sedimentary Willyama Supergroup (Veevers & Powell, 1984; Evan, 1988; Apak et al., 1997). These basin- to continent-scale SE-NW strike-slip faults are present within many other Australian provinces (Myers et al., 1996; Gibson et al., 2013).

Deep fault development during the Early Cambrian was concurrent with exhumation of the Mooracoochie Volcanics, which marks the base of the Warburton Basin stratigraphy (Gatehouse, 1986; Sun, 1997; Meixner et al., 2000). Continued extension developed accommodation space for the deposition of shallow shelf sediments that became the Diamond Bog Dolomite (~510 Ma), Coongie Limestone Member (~505-497 Ma), and Kalladeina Formation (~508-485 Ma) (Gatehouse, 1986). As relative sea levels rose, the depositional environment transitioned into low-stand fan, deltaic, and prograding shoreline, which deposited the Narcoonowie Formation (~490 Ma), Pando Formation (~488 Ma), and Innamincka Formation (~485-435 Ma) (Gatehouse, 1986; Rezaee & Sun, 2007). Regional erosion of the upper Innamincka Formation represents the unconformable boundary to the overlying Permian to Triassic Cooper Basin.

Insert Fig. 4

2.2 Carboniferous Alice Springs Event (450-300 Ma)

The Alice Springs Event (ASE) has had a significant influence on the tectonic development of central and northern Australia (Haines et al., 2001). Its effect has been recorded in a number of petroleum basins and structural provinces, including the Amadeus, Ngalia, Georgina, Wiso, Officer, and Warburton basins, as well as the Arunta and Musgrave inliers (Haines et al., 2001).

Calcite twin, natural fracture and fault data from within the South Australian portion of the Warburton Basin has constrained this regional tectonic event to have occurred under a strike-slip stress regime with maximum principal stress in an N-S direction in this region (Fig. 4b) (Kulikowski & Amrouch, 2017). The effective maximum principal stress magnitude was also calculated (49 MPa) through calcite twin stress inversion (Fig. 4i) (Kulikowski & Amrouch, 2018b). Geomechanical modelling of fault reactivation under this paleo-stress tensor identified N-S and NE-SW striking high angle (50-70^{o}), and SE-NW striking strike-slip faults to be the most likely to reactivate (Kulikowski & Amrouch, 2018b). A NNE-SSW and SE-NW striking vertical conjugate natural fracture set was developed during this event and is present only within the Warburton Basin stratigraphy (Kulikowski & Amrouch, 2017).

As mentioned earlier, the stratigraphy of this region contains a regional unconformity that separates the Warburton and Cooper basins and is a result of basement fault reactivation, exhumation and erosion of upper Warburton Basin sediments. Carboniferous Big Lake Granodiorite was also exhumed during this event in local regions south of the GMI Ridge and provides elevated contemporary temperature gradients due to their high uranium content (Meixner et al., 2000; Kulikowski, Cooke, & Amrouch, 2016a). The Australian continent remained connected to Antarctica during this time and exposed to plate scale glaciation (Collins & Pisarevsky, 2005; Gray & Foster, 2004; Metcalfe, 2013).

As the continent began to escape glaciation during the Late Carboniferous to Early Permian, the glacial Merrimelia Formation (~290 Ma) was deposited onto the regional unconformity, marking the base of the Cooper Basin. The overlying Tirrawarra Formation (~287 Ma) was deposited in a postglacial outwash to braided fluvial depositional environment (Lowe-Young et al., 1998; Mavromatidis, 2006). The Tirrawarra Formation is produced for oil, albeit being deeper and under higher temperatures and pressures than the gas-rich middle to upper Permian and Triassic reservoirs (Gravestock et al., 1998). The depositional environment transitioned

into fluvio-deltaic, lacustrine and swamp during the middle Permian, and deposited repeated cycles of sandstone, shale, and coal to compose the predominantly gas-rich Patchawarra Formation (~285-260 Ma) (Kantsler et al., 1984; Apak et al., 1997; Alexander et al., 1998).

2.3 Mid-Permian Event (290-270 Ma)

During deposition of the Patchawarra Formation, intra-formational on-lapping is observed from seismic data along paleo-structural highs, which are more often than not also the present-day structures (Apak et al., 1997; Gravestock & Jensen-Schmidt, 1998). On-lap is observed between 273 and 270 Ma, inferring that structural highs were present during the Mid-Permian and limited the accommodation space (Apak et al., 1996; Kulikowski & Amrouch, 2017, 2018a). Seismic interpretation aligns with stress inversion of calcite twin, natural fracture and fault data, which demonstrate a compressional SE-NW oriented event with an effective maximum principal stress magnitude of 56 MPa (Fig. 4i) (Kulikowski & Amrouch, 2017, 2018b). The far-field stresses likely originated from the approximately NE-SW to N-S striking subduction line along the eastern margin of Australia (Fig. 4c). The paleo-stress conditions likely reactivated E-W, NE-SW and N-S striking high angle (50-70^{o}) faults and developed a regional NE-SW striking low dip angle (30^{o}) conjugate natural fracture set within the Patchawarra, Tirrawarra and Merrimelia formations and also within basement (Kulikowski, 2017; Kulikowski & Amrouch, 2017, 2018b).

As compression from the short lived Mid-Permian Event eased, the upper Patchawarra Formation became finer grained and more shale dominated (Apak et al., 1997). An east to west transgression ended the deposition of the Patchawarra Formation, transitioning into a shoreface and lacustrine dominated environment that deposited the Murteree Shale (~264 Ma), Epsilon Formation (~262 Ma), Roseneath Shale (~260 Ma), and Daralingie Formation (~258 Ma) (Bradshaw, 1993; Apak et al., 1997; Gravestock & Jensen-Schmidt, 1998; Lowe-Young et al.,

1998; Mavromatidis, 2006). The Roseneath-Epsilon-Murteree (REM) stratal unit represents the major shale gas play in the region with total organic carbon (TOC) values ranging between 1.0 and 4.1% (Jadoon, Roberts, Blenkinsop, Raphael, & Shah, 2016).

2.4 Late Permian Daralingie Event (258 Ma)

Following the deposition of the Daralingie Formation, an erosional unconformity was first identified in 2D seismic data (Apak et al., 1996) and later confirmed through calcite twin stress inversion analysis (Kulikowski, 2017; Kulikowski & Amrouch, 2017). This SE-NW oriented strike-slip stress regime event recorded an effective maximum principal stress magnitude of approximately 56 MPa (Fig. 4i) that reactivated NE-SW striking high angle (50-70^{o}) faults (Kulikowski & Amrouch, 2018b). This event is most notable along the NE-SW striking GMI and NM ridges, as a significant portion of the Daralingie Formation was eroded from these areas (Kuang, 1985; Apak et al. 1997; Mavromatidis, 2006). New fracture and fault development was absent during this time, with the stress preferentially accommodated along pre-existing faults (Kulikowski et al., 2017). The far-field stress was likely related to the N-S striking subduction zone east of Australia during this time (Fig. 4d) (Kulikowski & Amrouch, 2017).

2.5 Upper Triassic Hunter-Bowen Event (245-190 Ma)

Post-compressional flexural relaxation, or sag, followed the Daralingie Event and generated accommodation space for the deposition of the Toolachee Formation (~250 Ma) that consists of sands, shales and coals deposited under meandering fluvial to deltaic conditions (Kantsler et al. 1984; Apak et al. 1997; Lowe-Young et al., 1998). The depositional environment transitioned to a floodplain, lacustrine and fluvial channel system in the Triassic, depositing the Nappamerri Group, which includes the Callamurra Member (~245 Ma), Panning Member (~243 Ma), Wimma Sandstone Member (~241 Ma), Tinchoo Formation (~238 Ma), and the

Cuddapan Formation (~210 Ma) (Kantsler et al., 1984; Apak et al., 1997; Alexander et al., 1998; Lowe-Young et al., 1998; Mavromatidis, 2006). The early Nappamerri Group was likely charged with oil and gas from the underlying Toolachee Formation, and perhaps along fault conduits from the deeper early Permian source rocks (Lowe-Young et al., 1998).

A regional erosional unconformity is carved into the upper Tinchoo Formation and the majority of the Cuddapan Formation, which is only present in local areas of the basin (Lowe-Young et al., 1998). This unconformity separates the Cooper and Eromanga basins and marks the timing of the Hunter-Bowen Event. The maximum principal stress was horizontal and in an E-W direction (Fig. 4e) (Kuang, 1985; Apak et al., 1997; Gravestock & Jensen-Schmidt, 1998; Kulikowski & Amrouch, 2017). The regional erosional boundary was first interpreted from 2D seismic data (Kuang, 1985; Apak et al., 1997) and later confirmed through calcite twin stress inversion, and natural fracture and fault stress inversion (Kulikowski & Amrouch, 2017). Calcite twin stress inversion results identified an E-W oriented compressional event with an effective maximum principal stress magnitude of 60 MPa (Fig. 4i) corresponding to the Hunter-Bowen Event (Kulikowski & Amrouch, 2017, 2018b). Geomechanical modelling using this stress tensor identified that NE-SW striking high angle (50-70^{o}) faults were most likely to shear reactivate at this time (Kulikowski & Amrouch, 2018b). Reactivation of predominantly this fault set exhumed and eroded up to 500 meters of Nappamerri Group sediments (Apak et al., 1997; Kantsler et al., 1983; Alexander et al., 1998; Mavromatidis, 2006).

2.6 Late Cretaceous Event (95-55 Ma)

As the Hunter-Bowen Event subsided, flexural relaxation generated accommodation space and a fluvial depositional environment transcended, which deposited the Poolowanna Formation (~200-180 Ma) onto the regional unconformity (Green, Brain, & John, 1989;

Hoffman, 1989; Lowe-Young et al., 1998). Tectonic quiescence continued with the deposition of the braided fluvial Hutton Sandstone (~178-160 Ma), fluvial to lacustrine Birkhead Formation (~157 Ma), and braided fluvial to lacustrine Adori Sandstone (~152 Ma) (Lowe-Young et al., 1998). The braided fluvial to lacustrine depositional environment continued in the region, depositing the Namur Sandstone (~152-140 Ma), Westbourne Formation (~150 Ma), and the oil-rich Murta Member (~140 Ma) (Lowe-Young et al., 1998). Jurassic units contain abundant oil (and gas) reservoirs at a shallower depth than Permian reservoirs, and currently primarily targeted on the western flank of the Cooper Basin (Heath et al., 1989).

The depositional environment transitioned into fluvial to shallow marine conditions and deposited the Cadna-owie Formation (~140-126 Ma) (Lowe-Young et al., 1998). The overlying Wyandra Sandstone Member (~125 Ma) was deposited under deltaic to shoreface marine conditions and contains some oil and gas potential (Lowe-Young et al., 1998). Following this, the Bulldog Shale (~125-108 Ma) and Wallumbilla Formation (~125-104 Ma) were deposited in restricted open marine conditions, which transitioned into a shoreface depositional environment to deposit the Coorikiana Sandstone (~105 Ma), in which some gas discoveries have been recently made (Lowe-Young et al., 1998). Shallow open marine conditions developed and deposited the Oodnadatta Formation (~104-98 Ma), Toolebuc Formation (~103 Ma), and Allaru Mudstone (~100 Ma) (Lowe-Young et al., 1998). Finally, the Winton Formation (~97-93 Ma) and Mackunda Formation (~97 Ma) were deposited by fluvial-lacustrine conditions to mark the final period of sediment deposition within the Eromanga Basin (Lowe-Young et al., 1998). These Middle to Late Cretaceous marine sediments also host the regionally extensive polygonal fault system that presents a new target for future exploration (Watterson et al., 2000). The critical moment in the Cooper-Eromanga basins hydrocarbon system, which marks the time of major hydrocarbon generation, migration, accumulation and preservation, occurred around 90 Ma (Lowe-Young, et al., 1998).

The Winton and Mackunda formations were significantly eroded following their exhumation by the E-W Late Cretaceous compressional Event (Fig. 4f) (e.g. Kuang, 1985; Green et al., 1989; Hoffman, 1989; Apak et al., 1997; Gravestock & Jensen-Schmidt, 1998; Lowe-Young et al., 1998; Mavromatidis, 2006; Kulikowski & Amrouch, 2017, 2018a). Folding related to pre-existing NE-SW striking faults, rather than reactivation, facilitated the development of this erosional boundary, which separates the Eromanga and Lake Eyre basins (Fig. 2). An effective maximum principal stress magnitude of 59 MPa was measured from calcite twin stress inversion analysis (Fig. 4i) (Kulikowski & Amrouch, 2018b). N-S striking low angle (30^{o}) conjugate natural fractures were developed during this time (Kulikowski & Amrouch, 2017). Considering that this event occurred during and after the critical moment, understanding the dilation and shear tendency of faults is vital for accurate migration pathway modelling. Under these stress conditions, E-W and NE-SW striking high angle (60^{o}) faults were the most likely to act as hydrocarbon conduits (Kulikowski & Amrouch, 2018b).

2.7 Paleogene Event (33-23 Ma)

During deposition of the Lake Eyre Basin, which is presently at surface, an N-S oriented Paleogene compressional event developed E-W striking low angle (30^{o}) conjugate natural fractures throughout the stratigraphic column (Kulikowski & Amrouch, 2017). This event is attributed to the northwards movement of the Australian plate (Fig. 4g). The effective maximum principal stress magnitude of this event was calculated from calcite twin stress inversion analysis and found to be 64 MPa (Fig. 4i) (Kulikowski & Amrouch, 2018b). Interestingly, this event does not appear to have reactivated or developed faults; however, N-S and NE-SW striking high angle (50-70^{o}) faults are considered to have been likely to dilate and act as permeable hydrocarbon conduits (Kulikowski & Amrouch, 2018b).

3. Petroleum Systems Elements

3.1 Hydrocarbon Source Rocks

Hydrocarbons in the Cooper Basin are principally sourced from intra-formational Permian coals and Permian to Jurassic carbonaceous shales, and reservoired within fluvial sandstones (Fig. 5) (Boreham & Hill, 1998). The petroleum system is largely gas saturated with small volumes of liquids found in localised areas (Kantsler et al., 1984). As such, the isotopic composition of intra-formational coals and carboniferous shales indicates fresh water origin and dominated by high order plants (Kantsler et al., 1984; Boreham & Hill, 1998). The Toolachee, Daralingie, Epsilon and Patchawarra formations contain an average total organic content (TOC) of 3.9% and 6.9 kg/tonne of hydrocarbon (Smyth, 1983; Boreham and Hill, 1998). The most organic-rich source rock is within the Toolachee Formation, averaging 214 kg/tonne (Hydrogen index) across the Cooper Basin (Boreham & Hill, 1998). Liquid hydrocarbon yields are low in Permian reservoirs due to high vitrinite and inertinite (Type III kerogens) composition in shale and coal measures, and are absent within the over mature Nappamerri Trough, which contributes only dry gas (Kantsler et al., 1984; Boreham & Hill, 1998).

Insert Fig. 5

The hydrocarbon source for the overlying Eromanga Basin is more uncertain, and likely to be sourced from: (1) non-marine Jurassic aged rocks (Powell et al., 1989; Lowe-Young et al., 1998); (2) Permian shales and coals with migration through reactivated faults (Heath et al., 1989; Lowe-Young et al., 1998); and (3) a combination of both Jurassic and Permian source rocks (Fig. 6c) (Kantsler et al., 1984; Jenkins, 1989; Lowe-Young et al., 1998). Jurassic aged units contain oil and gas; however, only gas has been discovered in Cretaceous aged reservoirs in the Strzelecki, Packsaddle and Nappacoongee regions (Kantsler et al., 1984). Permian aged

source rocks are currently within the gas window, with Jurassic to Cretaceous source rocks currently at peak oil generation in the deep basin centres (Kantsler et al., 1984).

Insert Fig. 6

3.2 Hydrocarbon Generation

Permian and Triassic source rocks reached the hydrocarbon generation window as early as the Permian to Middle Triassic during maximum burial (Fig. 6), and peaked during a secondary sag period in the Middle Cretaceous (Deighton & Hill, 1998; Mavromatidis, 2006). Relatively minor hydrocarbon generation and expulsion commenced in the Permian to Middle Triassic, before peaking in the Middle to Late Cretaceous and potentially continues today (Fig. 6a & 6b) (Pitt, 1986; Duddy, 1987; Gallagher, 1988; Lowe-Young et al., 1998; Mavromatidis, 2006; Deighton & Hill, 2009). Minor volumes of hydrocarbons were also generated in the Nappamerri Trough during the Permian, and, given sufficient residual kerogen, the effect of Late Tertiary elevated temperatures and Tertiary deposition may have led to secondary (late-stage) hydrocarbon generation and expulsion in certain parts of the basin (Fig. 6b) (Deighton & Hill, 2009).

Although a rare phenomenon, the concentration of carbon dioxide (CO_2) within the Cooper-Eromanga basins is significantly higher (10-30 v/v%) than typical sedimentary basins (Rigby & Smith, 1981; Kantsler et al., 1984; Wycherley, Fleet, & Shaw, 1999). However, the origin remains somewhat questionable, but could be related to: (1) an increase in coal thickness, with regions containing thick coal deposits, such as the Patchawarra Trough, containing the highest CO_2 concentrations; or (2) magmagenesis or metamorphic reactions, which is also supported by the correlation between raised CO_2 levels and the presence of Carboniferous Uranium-rich Moomba-Big Lake Granodiorite (Gatehouse, 1986; Wycherley et al., 1999).

3.3 Hydrocarbon Migration

Hydrocarbon generation and expulsion is divided into three phases: (1) early expulsion between the Late Permian and Early Triassic; (2) primary expulsion within the Cretaceous; (3) and a possible secondary expulsion during the Late Cenozoic (Fig. 6) (Lowe-Young et al., 1998; Radke, 2009). These three phases of expulsion coincide with the timing of hydrocarbon migration (Fig. 6c) (Lowe-Young et al., 1998; Radke, 2009). Hydrocarbon generated from Permian source rocks migrated short distances to the vertically stacked overlying or underlying intra-formational reservoirs, or alternatively along deep seated and reactivated basement-involved faults into overlying Eromanga Basin reservoirs (Boreham & Hill, 1998; Gravestock et al., 1998; Radke, 2009). Tertiary hydrocarbon migration through stacked intra-formational seals into overlying reservoirs has also been discussed (Heath et al., 1989; Boult, Lanzilli, Michaelsen, McKirdy, & Ryan, 1998; Gravestock et al., 1998; Hillis et al., 2001; Radke, 2009). Geomechanical modelling of fault reactivation (dilation and shear) through time highlighted the changing conduit potential of individual fault sets as stress conditions changed (Kulikowski et al., 2016c; Kulikowski, 2017; Kulikowski & Amrouch, 2018b). See chapter 10 for more detail.

Secondary hydrocarbon migration from Permian source rocks into overlying Jurassic Eromanga Basin reservoirs has been suggested by numerous authors after observing oil compositions that were not consistent with a Jurassic origin (Heath et al., 1989; Hallmann, Arouri, McKirdy, & Schwark, 2007). The origin of Jurassic oils has been found to be from either: (1) Permian source rocks; (2) Jurassic source rocks; or (3) a combination of the two (Smyth, 1983; Heath et al., 1989; Lowe-Young et al., 1998; Hallmann et al., 2007). In the case of Permian source rock origin, secondary migration of oil was through: (1) permeable fault conduits into shallow Eromanga Basin reservoirs; or (2) through a permeable carrier bed in the up-dip direction towards the flanks of the basin, where overlying Triassic sealing units

effectively pinch-out and allow the oil to migrate into directly overlying reservoir rocks (Heath et al., 1989; Lowe-Young et al., 1998; Borazjani, Kulikowski, Amrouch, & Bedrikovetsky, 2018, 2019). These flank regions host many large producing oil fields (Heath et al., 1989; Borazjani et al., 2018, 2019). In these two migration pathway cases, the oil composition between source and reservoir has shown to be different due to the effects of deep bed filtration (Borazjani et al., 2018, 2019), or water-washing (Heath et al., 1989) of hydrocarbons.

The ability of a fault to act as a potential hydrocarbon conduit can be measured by calculating the Dilation Tendency, or the likelihood of faults to undergo tensile reactivation. Alternatively the likelihood of faults to shear reactivate can be measured by calculating Slip Tendencies. These likelihoods were calculated for four regional fault sets, which were modelled under six unique paleo-stress tensors (Alice Springs Event, Mid-Permian Event, Daralingie Event, Hunter-Bowen Event, Late Cretaceous Event, and Paleogene Event), as well as the present-day stress conditions (Kulikowski et al., 2016c; Kulikowski, 2017; Kulikowski & Amrouch, 2018b). The results of these studies found that early expulsion of hydrocarbons would have preferentially migrated along NE-SW striking high angle (50-70^{o}) faults during the Late Permian and along E-W striking high angle (50-70^{o}) faults during the Late Triassic. Since the critical moment (90 Ma) hydrocarbons would have preferentially migrated along E-W striking high angle (50-70^{o}) faults during the Late Cretaceous and N-S striking high angle (50-70^{o}) faults during the Paleogene. Hydrocarbons generated during the secondary phase, or present-day, would likely be migrating along E-W striking high angle (50-70^{o}) faults or SE-NW strike-slip faults. See Chapter 6.2 for more detail.

3.4 Hydrocarbon Seals and Trap Development

Intra-formational fluvial-lacustrine to lacustrine shales and coal measures form cyclically deposited impermeable seals to underlying reservoirs, while also acting as potential source rocks to overlying reservoirs (Bradshaw, 1993; Gravestock & Jensen-Schmidt, 1998). These vertically stacked intra-formational shales and coals have the highest influence on sealing hydrocarbons within the four-way closing anticlinal traps that are present throughout the basin (Gravestock et al., 1998). The Nappamerri Formation, Roseneath Shale, and Murteree Shale are highly efficient regional seals to the Toolachee, Epsilon, and Patchawarra formations, respectively; however, intra-formational shales hold back hydrocarbon to individual and compartmentalised intra-formational sandstone reservoirs (Gravestock et al., 1998; Gray, 2017; Gray, Daniel, Kaldi, & Kulikowski, 2019). Cretaceous marine sediments and the Late Jurassic Birkhead Formation form regional seals for Jurassic to Early Cretaceous Eromanga Basin reservoirs (Gravestock et al., 1998; Radke, 2009).

The regional Murteree Shale and intra-formational Patchawarra Formation seals are eroded along the western margin of the basin contributing to the significant number of oil discoveries made along the western flank, as oil migrates from the deep sections of the Patchawarra Trough into shallow Eromanga Basin reservoirs (Radke, 2009). Low relief structural closures within the Eromanga Basin are sealed by the regional Birkhead and Wallumbilla formations, facilitating the accumulation of hydrocarbons (Radke, 2009; Kulikowski, Hochwald, Cooke, & Amrouch, 2016b; Kulikowski, Hochwald, & Amrouch, 2018b). A regional polygonal fault system is present within Cretaceous sediments and is observed to occasionally penetrate into the hydrocarbon-rich Murta Member (Fig. 7) (Watterson et al., 2000; Kulikowski, 2017; Kulikowski et al., 2017). Where these normal faults are approximately E-W striking and penetrate into the Murta Member, hydrocarbons may be migrating through permeable fault

conduits into shallow reservoirs, possibly presenting a new exploration strategy (Watterson et al., 2000; Kulikowski et al., 2017).

Insert Fig. 7

Structural trap development occurred as early as the Mid-Permian Event and Late Permian Daralingie Event, coinciding with the early phase of hydrocarbon generation and expulsion (Deighton & Hill, 1998; Kulikowski & Amrouch, 2018a). Key anticlinal traps were developed by two subsequent events; the E-W Hunter-Bowen Event and E-W Late Cretaceous Event (Kulikowski & Amrouch, 2017, 2018a). These two events reactivated basement-involved faults to create broad anticlinal domes within the Permian, and low relief anticlines within Cretaceous sediments prior to the primary phase of hydrocarbon generation and expulsion (Deighton & Hill, 1998). The N-S Paleogene Event (33-23 Ma) may have contributed to a late-stage of structural trap development; however, this occurred significantly after the critical moment in the hydrocarbon system and may have negatively influenced the preservation of existing hydrocarbon accumulations (Lowe-Young et al., 1998; Kulikowski & Amrouch, 2018a, 2018b). Although the majority of accumulations are trapped by anticlines, there does exist an opportunity to begin targeting higher risk stratigraphic pinch-out traps and on-lapping features that are common within the basin, particularly within the hydrocarbon-rich Patchawarra Formation (Apak et al., 1997; Kulikowski, 2017; Kulikowski & Amrouch, 2018a).

3.5 Hydrocarbon Accumulation and Preservation

Hydrocarbons are primarily reservoired within the Tirrawarra Formation, Patchawarra Formation, Epsilon Formation, Daralingie Formation, and Toolachee Formation of the Cooper Basin, and the Hutton Formation and Namur Sandstone of the Eromanga Basin (Kantsler et al., 1984; Alexander et al., 1998; Gravestock et al., 1998; Mackie, 2015). Although these are the dominant oil and gas producers, with the Hutton Sandstone contributing greater than 50% of

oil discoveries (by volume) in the Eromanga Basin, hydrocarbons can be found in virtually all reservoir-quality zones older than the Late Cretaceous (Kantsler et al., 1984; Lowe-Young et al., 1998; Radke, 2009). The majority of Cooper Basin hydrocarbon discoveries are located within the South Australian region, reflecting the significantly greater volume of Permian source rocks (Kantsler et al., 1984; Reynolds et al., 2006). Primary hydrocarbon accumulation commenced during the Late Cretaceous critical moment (90 Ma), with existing fields withstanding the Late Cretaceous Event (95-55 Ma), Paleogene Event (33-23 Ma), and the present-day stress environment (Fig. 6c) (Kantsler et al., 1984; Lowe-Young et al., 1998; Mackie, 2015; Kulikowski & Amrouch, 2017).

The preservation of accumulations appears to be unaffected by these three events, as seismic data shows that basement-involved faults were not reactivated; however, sub-seismic resolution faulting may be possible considering that resolution is not better than 15 m (Kulikowski et al., 2017; Kulikowski and Amrouch, 2018b). Fault reactivation causing less than 15 m of displacement can be sufficient to cause seal breach and facilitate tertiary migration of hydrocarbons, particularly if fault geometries are optimally oriented to tensile reactivate (dilate). Geomechanical modelling of fault reactivation has shown that the most common fault set, NE-SW striking high angle (50-70^{o}), was the most likely to shear reactivate during the four most recent (Daralingie Event, Hunter-Bowen Event, Late Cretaceous Event, Paleogene Event) tectonic events (Kulikowski & Amrouch, 2018b). Under contemporary stresses, SE-NW strike-slip faults are most likely to shear reactivate and must be accurately interpreted because of the high likelihood of interacting with, and complicating, hydraulic fracture stimulations (Pokalai et al., 2016; Pokalai, 2018; Kulikowski et al., 2016c).

4. Geophysics

4.1 Significant Seismic Reflectors

With the majority of Cooper Basin hydrocarbons reservoired within Permian rocks, the near top Toolachee Formation (P-reflector), near top Patchawarra Formation (V-reflector), and middle Patchawarra (VC-reflector) seismic reflectors are most commonly interpreted and associated with regionally consistent coal markers (Kulikowski, 2017). The Cretaceous Cadna-owie Formation reflector (C-reflector) is an easily identifiable and regional strong amplitude reflector (Fig. 8a). Its interpretation provides the structural trap geometry for Jurassic and Cretaceous reservoirs, as well as providing broad insights into the underlying structures. This reflector also shows intermittent normal displacement caused by polygonal faults extending down from the Mackunda Formation (AM-reflector) into the deeper hydrocarbon-rich Murta Member (D-reflector) (Fig. 7). The top Nappamerri Group reflector (N-reflector) shows a similar characteristic to the Cadna-owie Formation reflector, although with variable amplitude due to the erosional boundary that it represents (Fig. 8a). This reflector marks the boundary between the Cooper and Eromanga basins.

Insert Fig. 8

In the area of this study, the top of Permian sedimentation is identified by an abrupt strong amplitude package that represents the fluvial to deltaic Toolachee Formation (P-reflector) (Fig. 8a). The top Patchawarra Formation (V-reflector) is notoriously bland, attributed to the relatively more transitional boundary between the upper Patchawarra Formation and the Murteree Shale (U-reflector) that results in a low acoustic impedance boundary. As such, the stronger amplitude reflector immediately below the top Patchawarra Formation is typically interpreted (Fig. 8a). Within the Patchawarra Formation, the VC30 and VC50 coal measures produce strong amplitude (soft-kick) reflectors; however, the reflectors commonly split and

merge (Fig. 8a). Middle Patchawarra Formation reflectors have been shown to on-lap onto paleo-structures correlating to the Mid-Permian Event (290-270 Ma) (Apak et al., 1997; Kulikowski & Amrouch, 2018a). Below the Permian coal measures, seismic resolution rapidly decays and the interpretation of reflectors and faults becomes difficult (Fig. 8a). The Tirrawarra and Merrimelia formation reflectors are absent in some parts of the basin and require high well control to be interpreted accurately.

Seismic interpretation of the basement (Z-reflector) is again difficult throughout the basin, commonly requiring phantom interpretation through significant fault shadow and decayed amplitude (Fig. 8a). Seismic resolution has been calculated to be upwards of 150 m, in contrast to Cretaceous reflectors that can be between 15-20 m (Kulikowski, 2017; Kulikowski et al., 2017). Recently acquired 3D seismic surveys have much greater resolution below Permian coal measures, with broadband and full-azimuthal seismic data expected to significantly improve the resolution in the near future.

4.2 Seismic Time-to-Depth Conversion Methods

The seismic time-to-depth conversion process can incur large (10’s of feet) errors caused by local velocity anomalies, incorrect well ties, or more commonly from a poor understanding of the near surface velocity variation, or statics. Although errors cannot be removed entirely, selecting the most accurate depth conversion method for the given study area can have noticeable effects. For example, the presence of low relief hydrocarbon-rich structural traps within the Eromanga Basin can depend on the depth conversion method being used (Kulikowski, 2017; Kulikowski et al., 2016b, 2018b). Additionally, fault analysis may lead to incorrect results if seismic data remains in the time-domain, as fault geometries will change once in the depth-domain (Fig. 8b & 8c).

555 Complete seismic volume time-to-depth conversion is often time consuming and not
556 necessary for generating simple reflector maps. As such, time-to-depth conversion is often
557 performed at a mapped level using gridding software, or horizon maths tools built into seismic
558 processing and interpretation software. For the purpose of generating reflector maps, only the
559 interpreted two-way-time (TWT) seismic reflector grid, rather than the seismic volume, is
560 converted. In the simplest sense, the TWT grid is multiplied by a constant velocity to generate
561 a depth grid. Three seismic time-to-depth conversion methods are commonly used within the
562 Cooper-Eromanga basins, including the: (1) pseudo average velocity method (Fig. 9a); (2)
563 time-depth trend method (Fig. 9b); and (3) interval velocity method (Fig. 9c).

564 Insert Fig. 9

565 ***4.2.1 Pseudo Average Velocity Method***

566 The pseudo average velocity (V_a) method is one of the more simple, yet most commonly used,
567 seismic time-to-depth conversion methods within the Cooper-Eromanga basins. This simple
568 approach does not explicitly consider velocity anomalies. Rather, for any given well location
569 and for any given reflector, the depth (Δz: depth in feet) is obtained from well data and the
570 interpreted time (Δt: one-way-time in seconds) obtained from seismic data (Fig. 9a). The ratio
571 of the two measured values provides the V_a at the well location, such that;

572 $$V_a = \frac{\sum_{k=1}^{n} z_k}{\sum_{k=1}^{n} t_k} = \frac{\Delta Z\ (ft)}{\Delta t\ (s)}$$

573 Where k is the k^{th} reflector measured from n well locations. The time-to-depth conversion
574 process involves multiplying the resultant V_a with the seismic data (one-way-time: OWT in
575 seconds), to give depth (ft), such that;

576 $$Depth = V_a * OWT$$

For seismic data that contains an abundance of well control, the V_a for each well location can be averaged to determine the overall mean V_a of the entire survey. Alternatively, the V_a values at each well location can be gridded to produce a spatial contour map of V_a, which can take into account spatial velocity anomalies. The V_a from the surface to the Upper Cretaceous, Cadna-owie Formation, and Top Permian seismic reflectors was measured from 12 3D seismic surveys (Fig. 3b) to give a basin wide V_a value (Fig. 9d). The basin wide V_a from the mean sea level to the: (1) Upper Cretaceous reflector is 2,280 m/s, (2) Cadna-owie Formation reflector is 2,375 m/s; and (3) Top Permian reflector is 2,740 m/s (Fig. 9d). Although simplistic, this method was found to be one of the most accurate in the Cooper-Eromanga basins for converting interpreted reflector surfaces from the time-domain to the depth-domain (Rady, 2006; Kulikowski et al., 2016b, 2018b; Kulikowski, 2017). The accuracy of time-to-depth conversion methods for entire 3D seismic volumes has yet to be explored.

4.2.2 Time-Depth Trend Method

The time-depth (T-D) trend method utilises the relationship between the TWT and depth values for a given reflector, hence is closely related to the pseudo average velocity method. The T-D pairs of various reflectors at a given well location are plotted on a two-way graph and a linear ($y = mx + c$), or occasionally exponential ($y = ax^2 + bx + c$), trend is defined, where *y* is depth, *x* is time, *m* is slope, and *a*, *b*, and *c* are constants (Fig. 9b). The T-D trend equation that defines the distribution is used to directly convert the TWT seismic data to depth. The T-D Trend (Fig. 9e) from the 12 3D seismic surveys (Kulikowski et al., 2017) was found to be approximately;

$$Depth\ (m) = 280.5 * (TWT)^2 + 847.97 * (TWT)$$

Where *TWT* is two-way-time measured in seconds. Not all T-D pairs will plot precisely on this trend, and may create poor well ties. Therefore, when performing a time-to-depth

conversion on a gridded reflector, the resultant depth grid must be tied to the well control precisely by firstly gridding the error between the depth and the time-to-depth converted grid, and secondly subtracting the resultant error correction grid from the time-to-depth converted grid (Kulikowski et al., 2016b, 2018b; Kulikowski, 2017).

This method of time-to-depth conversion is a commonly used method in the Cooper-Eromanga basins, with early work utilising check-shot data and continuous velocity logs to calibrate seismic data. Continuous velocity logs can provide direct input data for velocity models and T-D pairs for key stratigraphic markers. It should be noted, however, that velocities from velocity logs and the velocities used for depth conversion are very different to each other and if used, a conversion factor map needs to be generated. Check-shot data for time-to-depth conversion has somewhat become outdated, with advancements in technology providing more accuracy through vertical seismic profile (VSP) acquisition (Levin & Lynn, 1958; Ganley & Kanasewich, 1980; Hauge, 1981; Balch, Lee, Miller, & Ryder, 1982; Balch & Lee, 1984; Hardage, 1985; Gajewski & Pšenčik, 1990). Check-shot and VSP data are obtained in a similar fashion to seismic data, where a P-wave travel time is measured from the surface to a downhole receiver (Stainsby & Worthington, 1985). In the case of check-shot and VSP data, the receiver is lowered through the borehole at various levels. However, the resolution of VSP data is significantly higher than check-shot data, as the number of borehole receivers can be as dense as every 25 m, in contrast to check-shot data that is only collected at key stratigraphic intervals.

4.2.3 Interval (Layer-Cake) Velocity Method

The interval velocity (V_i) method is used to represent the abrupt vertical changes in velocity evident across significant stratigraphic packages. A look at continuous velocity logs and synthetic seismograms shows that velocities are not constant and can abruptly increase or decrease depending on the rock composition (Al-Chalabi, 1974). The more basic interval

velocity model divides the subsurface into key stratigraphic packages that have unique velocities (V_i), such that the depth can be calculated by;

$$Depth = \sum_{j=1}^{n} V_i(t_{j+1} - t_j)$$

Where *n* is the number of intervals (layers) bound by the j^{th} reflectors, which are measured in the time-domain, *t* (one-way-time), at a given well location.

High velocity cemented calcite zones (CCZ) are present within the Eromanga Basin and can distort the true subsurface image when not incorporated into velocity models (Kulikowski et al., 2016b; Kulikowski, 2017). Precise interval velocity modelling can include these high velocity zones for more accurate seismic depth conversion that consider areal velocity changes. Interval velocity models are also used when anomalous velocities are present within a specific stratal-unit, which can be caused by overpressures, cementation, or the presence of faults and fractures. To capture these areal velocity changes, 3D velocity modelling is recommended.

4.3 Seismic Time-to-Depth Conversion Accuracy

The accuracy of converting post-stack seismic data from the time-domain to the depth-domain has been a significant topic of conversation within the Cooper-Eromanga basins. Inaccurate seismic depth conversion has significant implications for a number of key processes, which include: (1) drilling low relief Jurassic to Cretaceous pseudo-structures that appear in depth converted seismic data due to velocity anomalies; (2) overlooking low relief Jurassic to Cretaceous structural traps that do not appear in depth converted seismic data due to inaccurate velocity modelling; (3) inaccurate economic estimates of new wells that, if depth is underestimated, may require drilling additional 10's of feet that may change the economic feasibility; (4) coring the wrong intervals while drilling; (5) inaccurate reserves calculations that could be under or overestimated; and (6) errors with geomechanical modelling of fault

reactivation, as fault geometries will change and could influence the sealing potential of fault bound accumulations (Hillis, Macklin, & Siffleet, 1995; Lowe-Young et al., 1998; Kulikowski et al., 2016b, 2018b; Kulikowski, 2017).

The historical inaccuracy of seismic depth conversions can be attributed to a number of factors ranging from: (1) known high velocity calcite cemented zones (CCZ); (2) the regional system of Cretaceous polygonal faults that can influence the spatial and temporal velocity; (3) velocity characteristics of fluvially deposited channel sands; and (4) the near surface 'statics' attributed to changes in surface conditions (rocky, regolith, etc.) (Hillis et al., 1995; Lowe-Young et al., 1998; Kulikowski et al., 2016b, 2018b; Kulikowski, 2017). The effect of statics on seismic depth conversion is difficult to constrain, but can be slightly mitigated through one-dimensional (1D) up-hole seismic refraction surveys that deliberately drill shallow wells to target the velocity of the near surface (Igboekwe & Ohaegbuchu, 2011). This technique can accurately measure the velocity at the wellbore, but, as with most wellbore derived data, must be extrapolated to the wider and often kilometre-scale field, which is a large assumption that can influence accuracy. To entirely mitigate the large effect of statics in seismic depth conversion accuracy within the Cooper-Eromanga basins, a method of velocity acquisition targeting the near surface must be investigated.

Refraction statics is another method that captures the near surface velocity variation through the interpretation of shallow refracted seismic reflectors. These interpreted reflectors are used to determine the thickness of shallow low velocity weathered and unconsolidated sediments, which if not corrected for, can create pseudo structures in the deeper seismic data (Farrell and Euwema, 1984). This method can provide high density near surface velocity data that can also be integrated with 1D up-hole data to reduce the effects of statics.

671 At this present moment, much of the work on seismic time-to-depth conversion accuracy in
672 the basins appears to be kept behind closed doors by operating companies. Literature provides
673 only two studies in the Cooper-Eromanga basins that are focused on this topic (Hillis et al.,
674 1995; Kulikowski et al., 2018b), with Hillis et al. (1995) choosing to focus on a small local
675 dataset. The only regional study assessing the depth conversion accuracy in the basin used a
676 statistical approach testing the accuracy of the four most commonly used methods (pseudo
677 average velocity, time-depth trend, kriging with external drift using TWT, and kriging with
678 external drift to tie stacking velocities to average well velocities) by employing a cross-
679 validation, or blind-well test, method (Kulikowski et al., 2018b). An automated looping script
680 was developed to manage the large dataset, comprising 13 3D seismic volumes, 73 interpreted
681 TWT grids, and 729 wells (Kulikowski et al., 2018b). Their results found that although the
682 pseudo average velocity method was the most accurate at a high-level (±24.9 ft), the accuracy
683 of methods changes by 10's of feet depending on the unique dataset and the combination of
684 significant variables (Kulikowski et al., 2018b).

685 The significant variables to the accuracy of depth conversion were: (1) the distance between
686 the well that is being predicted and existing well control; (2) the spatial location within the
687 basin; (3) the reflector of interest; and (4) the location of the well that is being predicted relative
688 to the existing well data envelope (Kulikowski et al., 2018b). Interestingly the number of well
689 controls had a negligible effect on accuracy, but rather the proximity of well controls to the
690 well that is being predicted. The regional study reiterates the argument that depth conversion
691 accuracy in the Cooper-Eromanga basins is a complicated issue that must be further
692 investigated.

693 **4.4 Seismic Data Analysis**

694 Analysis of seismic data through the use of seismic attributes, amplitude versus offset (AVO)
695 analysis, spectral decomposition, and seismic inversion modelling can unlock hidden details
696 that may not be immediately obvious within the amplitude volume. These techniques have
697 become a common tool for exploration and development programs around the world and would
698 be highly beneficial in the fluvially dominated Cooper-Eromanga basins (Fig. 10). Incoherency
699 (coherency or similarity) is a seismic attribute that was first introduced by Bahorich and Farmer
700 (1995) and further developed by Gersztenkorn and Marfurt (1999) and is used to visually
701 emphasise the discrepancy (typically faults) between adjacent seismic traces along a horizon
702 or time-slice (Neves, Zahrani, & Bremkamp, 2004; Mai, Marfurt, & Chávez-Pérez, 2009;
703 Backé, Abul Khair, King, & Holford, 2011; Basir, Javaherian, & Yaraki, 2013). This attribute
704 has been shown to be particularly beneficial when interpreting basement and polygonal faults
705 (Fig. 10b) from the low resolution seismic data typical to the Cooper-Eromanga basins
706 (Kulikowski, 2017; Kulikowski et al., 2017). Curvature is another structural attribute that is
707 defined as the rate of change of the direction of a curve (Roberts, 2001), where significant
708 curvature values are often associated with reflector displacement such as those caused by
709 fractures or faults (Roberts, 2001; Al-Dossary and Marfurt, 2006; Backé et al., 2011; King et
710 al., 2011; Abul Khair, Cooke, King, Hand, & Tingay, 2012; Kulikowski, 2017; Kulikowski,
711 Amrouch, & Burgin, 2018a). This attribute has the potential to constrain the distribution of
712 natural fracture sweet-spots away from one-dimensional well data if carefully applied
713 (Kulikowski, 2017; Kulikowski et al., 2018a).

714 Considering that hydrocarbons are predominantly reservoired within fluvial sandstones in the
715 Cooper-Eromanga basins, displaying the spatial distribution of amplitude along a reflector
716 surface can aid in detecting these strong amplitude reservoirs (Fig. 10a), particularly if
717 associated with characteristic amplitude versus offset (AVO) responses. In some cases, these

reservoirs can verge on being at a sub-seismic resolution scale and can be overlooked in seismic data. The application of spectral decomposition on the seismic volume can assist in detecting hydrocarbons, thin fluvial beds (Fig. 10d), and can also visual enhance small scale faults (Partyka, Gridley, & Lopez, 1999).

Another issue facing explorationists is the discrimination between the signature of thin gas reservoirs and coals in stacked seismic data. Owing to the significant difference in Poisson's ratio between sandstone and coal, the application of AVO analysis to Cooper-Eromanga basins seismic data has provided evidence to suggest that such discrimination is possible and most effective when using a rotated extended elastic impedance attribute in the presence of tuning (Fig. 10c) (Tyiasning and Cooke, 2015).

Insert Fig. 10

5. Contemporary Stress Tensor

Contemporary stress tensors are well constrained in the basin, calculated from borehole breakouts and drilling induced tensile fractures, diagnostic fracture injection tests, and leak off tests (e.g. Hillis, Enever, & Reynolds, 1999; Hillis & Reynolds, 2000, 2003; Reynolds, Coblentz, & Hillis, 2002, 2003; Reynolds et al., 2004, 2006; Reynolds, Mildren, Hillis, Meyer, & Flottmann, 2005; Sandiford, Wallace, & Coblentz, 2004; Nelson, Meyer, Hillis, & Mildren, 2005; Nelson, Hillis, Sandiford, Reynolds, & Mildren, 2006; Müller, Dyksterhuis, & Rey, 2012; Pokalai, Ahmed, Haghighi, & Gonzalez, 2015a; Pokalai, Haghighi, Sarkar, Tyiasning, & Cooke, 2015b; Pokalai et al., 2016; Nelson, Chipperfield, Hillis, Gilbert, & McGowen, 2017a; Nelson et al., 2007b; Pokalai, 2018). The far-field origin of in situ stresses has been explained by Reynolds et al. (2003) to originate from the Tonga-Kermadee subduction zone and the New Zealand collisional boundary. These tectonic stresses are transferred through the upper crust of eastern Australia to give an approximately ESE-WNW maximum horizontal

742 stress within the Cooper-Eromanga basins. The stress regime is dominantly strike-slip, but can
743 transition to a compressional stress regime with increased depth, as the overpressures will
744 decrease the effective vertical stress magnitude more than the effective horizontal stress
745 magnitudes (Reynolds et al., 2006; Cooke et al., 2016). Alternatively, depletion of hydrocarbon
746 reservoirs can reduce pore pressure, which in turn increases the effective vertical stress
747 magnitude (Teufel, Rhett, & Farrell 1991). Given that the effective vertical stress magnitude
748 can become larger than both effective horizontal stress magnitudes through reservoir depletion,
749 the in situ stress can transition into an extensional stress regime (Teufel et al., 1991). This
750 transition between regimes will have implications for late-stage development programs
751 incorporating hydraulic fracturing and infill drilling, as the unexpected stress regime can
752 impact the effectiveness of those programs.

753 For the majority of the basin a strike-slip stress regime is present, with an ESE-WNW oriented
754 maximum principal stress (Fig. 11a); however, local stress perturbations caused by faults can
755 cause stress rotation (Fig. 11b). The magnitude of maximum horizontal stress has been
756 constrained to approximately 41 MPa/km based on a combination of frictional limit theory
757 (Sibson, 1974), drilling induced tensile fractures, and the use of tensile strength and knowledge
758 of horizontal fabrics at the wellbore wall (Reynolds et al., 2005; Nelson et al., 2005; 2007).
759 The vertical principal stress magnitude is dependent on the overburden rock thickness and
760 density, as well as the local pore pressure (Fig. 11c). The range of magnitudes present within
761 the basin for the vertical stress is between approximately 17 and 20 MPa/km (Reynolds et al.,
762 2006; Nelson et al., 2007; Pokalai et al., 2015a; 2016; Pokalai, 2018). As mentioned earlier, a
763 decrease in the pore pressure caused by depletion can increase the effective magnitude of the
764 vertical principal stress. Minimum horizontal stress magnitudes are typically calculated from
765 leak off tests or obtained from the minimum closure pressure during a mini-frac test (Fig. 11c).
766 Within the Cooper-Eromanga basins, the minimum horizontal stress magnitude can vary

767 significantly between approximately 12 and 27 MPa/km and can depend on the interpretation
768 technique used to read closure pressures (Nelson et al., 2007).

769 Insert Fig. 11

770 Equally as important as the principal stress magnitude, the pore pressure gradient can
771 influence the reactivation and development of natural fractures and faults. Increases in pore
772 pressure effectively shift the Mohr's circle to the left, closer to the failure and reactivation
773 envelopes. This effect can be induced by hydraulic fracture stimulation treatments and through
774 gas and water injection wells. Pore pressure within the basin remains at a hydrostatic gradient
775 (0.433 psi/ft) until depths of between 8000 and 8800 ft, where overpressure is first observed
776 and is largely depended on the location (van Ruth & Hillis, 2000; Kulikowski et al., 2016a). A
777 recent study within the basin calculated the effective tectonic strain to be between
778 approximately 400 and 500 microstrains, with strain in the maximum horizontal stress direction
779 being three times greater than that in the minimum horizontal stress direction (Pokalai et al.,
780 2016; Pokalai, 2018).

781 **6. Geomechanical modelling of fault reactivation**

782 **6.1 Theory**

783 Reactivation refers to the movement of faults and fractures under present-day stress
784 conditions and can be analysed by creating a geomechanical model and measuring the shear or
785 tensile (dilation) reactivation potential. A poor understanding of the local and regional stress
786 conditions has tremendous implications for hydrocarbon migration pathway models, hydraulic
787 fracture stimulation treatments, reservoir development, and seal integrity. Faults that are
788 optimally oriented to undergo tensile reactivation, or dilate, can provide permeable conduits
789 for hydrocarbon migration. An increase in pore pressure, through hydraulic fracture stimulation
790 or water/gas injection wells, can facilitate shear or tensile reactivation along pre-existing faults

and fractures. Geomechanical models have also been shown to effectively predict the shear and tensile reactivation potential of faults under paleo-stress conditions, which is beneficial when incorporated with hydrocarbon migration pathway modelling (Kulikowski, 2017; Kulikowski & Amrouch, 2018b).

The Dilation Tendency (T_d) measures the likelihood that faults and fractures will tensile reactive and is governed by the orientation and magnitude of the effective normal stress, $\sigma_n{}'$, acting on a fault plane. The T_d is normalised to the differential stress to give values between zero (low likelihood) and one (high likelihood), where $\sigma_1{}'$ is the maximum effective stress and $\sigma_3{}'$ is the minimum effective stress (Ferrill et al., 1999; Jolie, Moeck, & Faulds, 2015), such that;

$$T_d = \frac{\sigma_1{}' - \sigma_n{}'}{\sigma_1{}' - \sigma_3{}'}$$

Fracture Stability is a measure of the pore pressure required to effectively shift the Mohr's circle to the left and intersect the failure or reactivation envelope for a given fault plane. The relationship between an increase in pore pressure (ΔP_p) and the change in horizontal stress magnitude (ΔS_{Hor}) is such that (Hung and Wu, 2012);

$$\Delta S_{Hor} = \alpha\left(\frac{1-2v}{1-v}\right)\Delta P_p$$

Where α is Biot's coefficient that describes the difference between the total and effective stresses, and v is the Poisson ratio. This equation shows the direct relationship between increasing pore pressure to an increase in the horizontal stress magnitudes. Therefore, the Fracture Stability results are provided as the pore pressure increase required to induce shear reactivation. The Slip Tendency of faults provides a normalised scale of the Fracture Stability, where zero (0) has a low likelihood, and one (1) has a high likelihood of shear reactivating.

The likelihood of faults and fractures to act as conduits can also be measured through the Leakage Factor equation that relates the pore pressure (P_p) with the difference between the normal stress (σ_n) and shear stresses (τ) acting on a given fault plane, such that;

$$Leakage\ Factor = \frac{P_p}{\sigma_n - \tau}$$

The structural stability is assessed for three groups of structural data common to the Cooper-Eromanga basins: (1) Basement Faults; (2) Polygonal Faults; and (3) Natural Fractures.

6.2 Basement Faults

6.2.1 Summary

The majority of the basement-involved faults developed during the early tectonic development of the Australian-Mawson Block (Fig. 4a), where a Pre-Cambrian (650-575 Ma) SE-NW oriented extensional stress regime event created NE-SW striking normal faults and SE-NW strike-slip faults throughout much of Australia (Kuang, 1985; Haines et al., 2001; Apak et al., 1997; Gibson et al., 2013; Kulikowski, 2017; Kulikowski & Amrouch, 2017). These two dominant sets are present throughout the Cooper-Eromanga basins and form close relationships with anticlinal hydrocarbons traps (Fig. 12) and the NE-SW striking GMI and NM ridges (Fig. 3b). Through time, these pre-existing basement-involved faults were repeatedly reactivated by subsequent compressional and strike-slip stress regime events (Apak et al., 1997; Gravestock & Jensen-Schmidt, 1998; Kulikowski, 2017; Kulikowski & Amrouch, 2017, 2018; Kulikowski et al., 2017). Repeated reactivation of pre-existing faults is supported by multiple erosional unconformities and the negligible distribution of low angle compressional faults, albeit up to four compressional events (Mid-Permian Event, Hunter-Bowen Event, Late Cretaceous Event, and Paleogene Event) had affected the region (Kulikowski & Amrouch, 2017). Under Andersonian faulting theory (Anderson, 1951), such compressional events would develop low angle (30^{o}) faults; however, due to the abundance of high angle (60^{o}) normal faults present in the basin (Kulikowski, 2017; Kulikowski & Amrouch, 2017), it would be more stress economic to reactivate existing faults rather than develop new faults.

Insert Fig. 12

The original NE-SW striking normal faults, which are present throughout the basin (Fig. 13a & 13b), are now observed to positively displace reflectors (Apak et al., 1997; Gravestock &

Jensen-Schmidt, 1998; Radke, 2009; Kulikowski, 2017; Kulikowski & Amrouch, 2017, 2018; Kulikowski et al., 2017). Their stratigraphic distribution is often limited to terminating within basement or Middle Permian stratigraphy, and rarely penetrating into younger units (Apak et al., 1997; Gravestock & Jensen-Schmidt, 1998; Radke, 2009; Kulikowski, 2017; Kulikowski & Amrouch, 2017b). Due to the poor seismic resolution below Permian coal measures, detailed fault growth studies (e.g. Giba, Walsh, & Nicole, 2012; Jackson and Rotevatn, 2013; Black, McCormack, Elders, & Robertson, 2017; Robson, 2018; Robson, Holford, King, & Kulikowski, 2018) have not been possible and their interpretation becomes more difficult with depth. The difficulty is also exaggerated when developing fault models from seismic data that remains in the time-domain, as the true fault angle is not being captured (Fig. 8b & 8c). The difference in basement-fault geometry between the time and depth-domains has proven to be problematic for previous researchers that used sparse 2D seismic data, as their work interpreted purely extensional faults, which were later re-interpreted as compressional faulting, and which are now known to be a combination of inverted normal faults, compressional faults and strike-slip faults (e.g. Kuang, 1985; Stanmore, 1989; Apak et al., 1997; Sun, 1997; Gravestock & Jensen-Schmidt, 1998; Radke, 2009; Grant-Woolley et al., 2014; Kulikowski, 2017; Kulikowski & Amrouch, 2017b; Kulikowski et al., 2017).

Insert Fig. 13

The SE-NW strike-slip faults are present throughout the region and have been attributed to reducing reservoir performance through cataclasis, compartmentalisation of reservoirs, and potentially complicating hydraulic fracture stimulation treatments (Grant-Woolley et al., 2014; Kulikowski et al., 2016c). These strike-slip faults appear predominantly within basement and can extend into the hydrocarbon-rich Patchawarra Formation (Apak et al., 1997; Radke, 2009; Kulikowski & Amrouch, 2017b; Kulikowski et al., 2017). This fault set can easily be overlooked in cross-section due to the seismic resolution at basement and must be investigated

in time-slice (or depth-slice) views to observe lateral displacements or linear features. A series of large basin-scale en echelon NNE-SSW strike-slip faults are present in the Patchawarra Trough (Fig. 3a) and form pop-up or positive flower structures that have been developed into highly economic fields. Their presence elsewhere in the basin may be equally as fruitful; however, are yet to be discovered!

6.2.2 Reactivation potential under paleostress evolution

A new approach for assessing the reactivation and dilation potential of faults through time was presented by Kulikowski & Amrouch (2018b), using the Cooper-Eromanga basins as a case study. This approach utilises complete paleo-stress tensors for six events (Kulikowski & Amrouch, 2017) that were obtained through calcite twin stress inversion analysis (Etchecopar, 1984). Calcite twin stress inversion has been used extensively around the world to provide quantitative data on polyphase tectonic events (e.g. Amrouch, Lacombe, Mouthereau & Dissez, 2005; Lacombe, Amrouch, Mouthereau & Dissez, 2007; Amrouch, 2010; Amrouch, Lacombe, Bellahsen, Daniel & Callot, 2010; Amrouch, Beaudoin, Lacombe, Bellahsen, & Daniel, 2011; Beaudoin et al., 2012; Arboit, Amrouch, Collins, King, & Morley, 2015; Arboit, Amrouch, Morley, Collins, & King, 2017; Kulikowski, 2017; Kulikowski and Amrouch, 2017, 2018b; Burgin, Amrouch, Rajabi, Kulikowski, Holford, 2018). Complete paleo-stress tensors form the Cooper-Eromanga basins were integrated with geomechanical models to simulate the stress conditions present during each of the six key stages of basin evolution. Results found that after the critical moment in the Cooper-Eromanga basins petroleum system (90 Ma), E-W (Late Cretaceous Event) and N-S (Paleogene Event) striking high angle (50-70^{o}) faults were most likely to be dilated and acting as permeable hydrocarbon conduits (Fig. 13c). The critical moment defines the major period of hydrocarbon generation, migration and entrapment. This provides critical information that improves hydrocarbon migration pathway models that previously considered faults to have static 2D mechanical properties.

The history of basement fault reactivation is often constrained through fault growth analysis using 3D seismic data (e.g. Williams, Powell, & Cooper, 1989; Childs, Nicol, Walsh, & Watterson, 1996; Baudon & Cartwright, 2008); however, this cannot be performed in regions that have poor seismic resolution. For such regions, including the Cooper-Eromanga basins, the Slip Tendency of faults is calculated using paleo-stress tensors and geomechanical modelling to provide insights into the 4D evolution of fault reactivation. Kulikowski & Amrouch (2018b) measured the Slip Tendency of four major fault sets modelled using the paleo-stress tensors during six tectonic events (Fig. 13d). The results showed that N-S striking high angle (50-70^{o}) faults were most likely to reactivate during the Alice Springs Event, and E-W striking high angle (50-70^{o}) faults likely reactivated during the Mid-Permian Event (Fig. 13d). Since these two events NE-SW striking high angle (50-70^{o}) faults were most likely to shear reactivate under the subsequent Daralingie Event, Hunter-Bowen Event, Late Cretaceous Event and Paleogene Event (Fig. 13d). This is in line with other research suggesting considerable exhumation and erosion along the major NE-SW striking GMI and NM ridges (Kuang, 1985; Apak et al., 1997; Gravestock & Jensen-Schmidt, 1998; Mavromatidis, 2006, 2008; Kulikowski & Amrouch, 2017b).

6.2.3 Reactivation potential under contemporary stress

A case study on the Swan Lake 3D and Dullingari 3D seismic surveys, located adjacent to the GMI and NM ridges, respectively, investigated the reactivation potential of basement-involved faults under contemporary stresses by measuring the Slip Tendency, Dilation Tendency, and Fracture Stability (Kulikowski et al., 2016c). The study analysed four unique fault sets modelled using hydrostatic pressure, in situ stress, and typical rock mechanics parameters from the Cooper Basin.

Results from Kulikowski et al. (2016c) showed that E-W striking faults have the highest Dilation Tendency (0.900) and thus most likely to act as permeable hydrocarbon conduits under the present-day stress (Fig. 13c). The study also identified SE-NW strike-slip faults within both 3D seismic surveys and found that they are most likely to shear reactivate (Fig. 13d). A pore pressure increase of between only 0.5 and 5.0 MPa is required for this fault set to intersect the reactivation curve. Shear reactivation can compartmentalise the reservoir, reduce reservoir properties through cataclasis, complicate hydraulic fracture propagation, and facilitate tertiary migration of hydrocarbons. Therefore, precise seismic interpretation, particularly in depth-slice to observe lateral offsets, must focus on the identification of SE-NW striking strike-slip faults in order to incorporate their presence with the development of hydraulic fracture stimulation and drilling programs.

6.3 Cretaceous Polygonal Fault System

6.3.1 Summary

Layer bound polygonal faults are present within Cretaceous Eromanga Basin marine sediments across the entire basin (Heath et al., 1989; Watterson et al., 2000; Kulikowski, 2017; Kulikowski et al., 2017; Kulikowski & Amrouch, 2017b). These faults were first identified from 2D seismic data (Rumph, 1982; Moore & Pitt, 1984; Newton, 1986; Gilby & Mortimore, 1989; Gorter, Gostin, & Plummer, 1989; Longley, 1989; Scholefield, 1989; Young, Gunther, & Dixon, 1989), with the 3D distribution and regional extent only recently discovered in literature (Oldham & Gibbins, 1995; Watterson et al., 2000; Kulikowski, 2017; Kulikowski et al., 2017). A detailed analysis of polygonal faults within the Lake Hope 3D seismic survey suggests that their development is linked to a density inversion, where a low density and overpressured stratal unit was buried and de-watered by overlying normally pressured and higher density sediments (Watterson et al., 2000). The planar normal faults are mostly contained within the Mackunda Formation, Coorikiana Sandstone, Bulldog Shale and

Wallumbilla Formation; however, larger faults are found to penetrate into the underlying and oil-rich Murta Member (Fig. 7). Maximum throw was found within the Coorikiana Sandstone. The dip angle of faults remains constant along a given fault plane and can range between 44° and 61° (Watterson et al., 2000). This polygonal fault system may present a new hydrocarbon exploration opportunity targeting shallow oil that has migrated from Lower Cretaceous oil-rich reservoirs through permeable polygonal faults (Fig. 7) (Watterson et al., 2000).

The normal displacement across polygonal faults can tilt shallow reservoirs such that low relief structural traps are developed and potentially fault sealing. Low relief structures that are bound by deeply penetrating faults can facilitate the accumulation of oil in shallow reservoirs. This play has yet to be truly tested in this region, but is analogous to the polygonal fault system associated with Tertiary hydrocarbon-rich shales in the North Sea (Cartwright & Lonergan, 1997; Lonergan, Cartwright, & Jolly, 1998). The presence of faults within hydrocarbon reservoirs can have tremendous implications for effective production and development, such as compartmentalisation of the reservoir, tertiary hydrocarbon migration, and complications with hydraulic fracture stimulation treatments. Considering that Lower Cretaceous and Jurassic hydrocarbon reservoirs are currently being explored and developed, an understanding of the geometry, intensity and reactivation potential of the Cretaceous polygonal fault system is highly beneficial.

6.3.2 Reactivation potential under paleostress conditions

This potential new play type was first suggested by Watterson et al. (2000), who suggested the possibility that these faults may be facilitating the tertiary migration of hydrocarbons from known reservoirs to shallow sedimentary rocks. Little literature has since appeared in relation to this exploration opportunity, with the regional extent of this system only recently discovered (Kulikowski, 2017; Kulikowski et al., 2017). The Leakage Factor and Dilation Tendency of

this regional polygonal fault system were modelled to determine the optimum fault geometry required for fluid flow (Kulikowski et al., 2017).

The results show that high dip angle (50-90°) polygonal faults striking 080-260°N and 125-305°N have the largest Leakage Factor, and fault planes with high dip angle (50-90°) striking 105-285°N have the largest Dilation Tendency (Kulikowski et al., 2017). These fault planes are therefore most likely to facilitate the tertiary migration of hydrocarbons from Lower Cretaceous hydrocarbon-rich reservoirs into shallow structures, given that they penetrate below the Cadna-owie Formation into the hydrocarbon-rich Murta Member.

6.4 Natural Fractures

6.4.1 Summary

Natural fractures can provide highly permeable pathways for hydrocarbon production if the local and regional fracture set geometries are known. The strike and dip angle of fracture sets are equally as important for optimising hydrocarbon recovery. Six regionally pervasive conjugate natural fracture sets (Fig. 14a) are present in the Cooper-Eromanga basins (Kulikowski & Amrouch, 2017). The timing of their development, stratigraphic distribution, and spatial intensity has been well constrained (Kulikowski et al., 2016a; Kulikowski, 2017; Kulikowski & Amrouch, 2017). Extrapolation of wellbore derived natural fractures and faults to the wider reservoir has also been investigated by a number of authors (Backé et al., 2011; King et al., 2011; Abul Khair et al., 2012; Abul Khair, Cooke, & Hand, 2013; Abul Khair, Cooke, & Hand, 2015; Kulikowski et al., 2018a), suggesting that upwards of 70% of wellbore fractures are represented in seismic curvature results.

Insert Fig. 14

6.4.2 Natural fractures at the well bore

Low dip angle (30°) conjugate fracture sets striking E-W and N-S are present throughout the stratigraphic column and associated with the Paleogene Event, and the Upper Cretaceous and Hunter-Bowen events, respectively. A third low dip angle conjugate fracture set is present only within the Patchawarra, Tirrawarra, Merrimelia and Basement formations striking NE-SW and associated with the Mid-Permian Event. A vertical conjugate natural fracture set striking NNE-SSW and SE-NW is present only within Basement and developed during the Alice Springs Event. Two additional conjugate natural fracture sets are present throughout the stratigraphic column, striking NE-SW and SE-NW with high dip angles (50-70°), and most likely associated with periods of post-compressional flexural relaxation, or basin sag (Abul Khair et al., 2015; Kulikowski & Amrouch, 2017). The majority of interpreted fractures have high dip angles (50-70°) making the true wellbore fracture intensity of vertical wells difficult to constrain. A comparison between the fracture intensity interpreted from vertical, horizontal and inclined wells would provide more meaningful and representative fracture intensities.

A robust natural fracture study was performed for the Warburton Basin (Sun, 1999) using core, borehole image logs, and dip meter logs. The conclusions present a number of fracture sets; however, their methods relied too heavily on the strike of fractures and did not consider that slight changes in dip angle (20°) can have a different interpretation (Anderson, 1951). For this reason the use of seismic attributes, such as most positive and most negative curvature, can be misleading by only providing the strike of possible fractures and faults. Fracture sets with similar strike direction but different dip angles cannot be distinguished from these seismic trending methods.

Horizontal fractures have also been proposed to exist in the basin, and likely associated with periods of significant exhumation and erosion (Flottmann, Campagna, Hillis, & Warner, 2004; Tyiasning & Cooke, 2016; Cooke et al., 2016). Significant erosion can reduce the vertical stress magnitude and create local compressional stress regimes that can develop tensile horizontal

fractures. These horizontal fractures can complicate hydraulic fracture stimulation treatments by preferentially reactivating and causing rotation of hydraulic fractures into the horizontal plane, which is a common phenomenon in the Cooper-Eromanga basins (Cooke et al., 2016; Pokalai et al., 2016; Pokalai, 2018).

6.4.3 Natural fractures away from the well bore

A common assumption within the petroleum industry is that wellbore data can be extrapolated to the wider reservoir, which assumes that stress conditions, structural data, pore pressures, reservoir properties and characteristic, and other important criteria remain constant. If incorrect, this assumption can lead to obvious implications for exploration and development programs. As the Cooper-Eromanga basins contain low permeability reservoirs, the presence of permeable fracture networks can add great economic value to prospects; however, much of the existing work assumes that one-dimensional borehole data is representative of the wider kilometre-scale fields (Kulikowski et al., 2018a). Recent advancements in seismic acquisition and processing have enabled the use of seismic attributes to provide information away from the wellbore that is otherwise overlooked in the original amplitude volumes.

Curvature analysis is a seismic attribute that has been shown to correlate well with wellbore derived fracture and fault data (e.g. Murray, 1968; Lisle, 1994; Stewart & Podolski, 1998; Hakami, Marfurt, & Al-Dossary, 2004; Al-Dosary & Marfurt, 2006; Chopra & Marfurt, 2007; King et al., 2011; Abul Khair et al., 2012; Kulikowski et al., 2018a). The calculated value for curvature is defined as the rate of change of the direction of a curve (Roberts, 2001), such that for any point (P) the curvature (K) is defined as the rate of change of the dip angle ($d\omega$) with respect to the arc length (dS) (Roberts, 2001). The arc length (dS) is obtained from the osculating circle that has a common tangent to *P* and makes the greatest possible contact with

the curve (Roberts, 2001). The radius of the osculating circle forms the radius of curvature (R); such that in two-dimensions the value for *K* is defined as (Roberts, 2001);

$$K = \frac{d\omega}{dS} = \frac{2\pi}{2\pi R} = \frac{1}{R}$$

Curvature analysis has previously been performed within the Cooper-Eromanga basins (Backé et al., 2011; King et al., 2011; Abul Khair et al., 2012; Kulikowski et al., 2018a) showing a close relationship with the fracture geometry measured at the wellbore (Fig. 14b & 14c), although the density of fracturing can be underestimated in vertical wells (Kulikowski, 2017). As the two major fracture sets present in the basin are high angled (>50º dip), it is statistically less likely that these will be intersected by vertical wells, and may therefore be providing a less than true fracture density. The spatial and temporal distribution of permeable fracture networks away from the wellbore using curvature analysis has shown that high angle E-W and SE-NW striking fractures are highly pervasive and most likely to be permeable under contemporary stresses (Kulikowski et al., 2018a). These E-W and SE-NW striking fracture sets are present in each of the five 3D seismic surveys analysed by Kulikowski et al. (2018a) and were found to increase in intensity along E-W elongate anticlinal structures, which may present an exploration target for future programs. The use of curvature analysis for field development programs that target fracture networks appears invaluable, as it can provide the spatial and temporal distributions of permeable fracture networks in the subsurface away from the wellbore.

6.4.4 Reactivation potential under contemporary stress

Understanding the distribution, geometry, and intensity of permeable fracture networks is an important aspect of development programs in the low permeability Cooper-Eromanga basins. The likelihood of fractures to reactivate and be open to fluid flow is primarily controlled by the contemporary stress conditions relative to the fracture geometry. The contemporary stress in

the Cooper-Eromanga basins has an approximately E-W oriented maximum horizontal stress and is under a strike-slip stress regime, but the orientation can vary by up to 20° and the regime can alternate between a compressional stress regime (Fig. 11c) (e.g. Nelson et al., 2007; Reynolds et al., 2004; King et al., 2011; Abul Khair et al., 2012; Kulikowski et al., 2016c; Pokalai et al., 2016; Pokalai, 2018). This variation of in situ stress has a profound influence on: (1) reactivation potential of fractures and faults; (2) hydraulic fracturing; and (3) infers that geomechanical modelling performed on the basin-scale may not be representative of the field-scale.

King et al. (2011) and Abul Khair et al. (2012) measured the fracture susceptibility of natural fractures on a basin-scale assuming an E-W oriented maximum horizontal stress that alternates between a strike-slip and compressional stress regime. Their study found that NE-SW and SE-NW striking fractures with moderate dip angles are most prone to reactivation (Fig. 14d & 14e). Understanding the shear reactivation potential is important; however, measuring the likelihood of tensile reactivation is equally as important. Kulikowski et al. (2018a) measured the Dilation Tendency of 454 fractures to show that E-W and SE-NW striking high angle (60°) fractures are optimally oriented to dilate and act as potential hydrocarbon conduits under contemporary stresses (Fig. 14f). These sets are regionally pervasive away from the wellbore within the Patchawarra Formation and would form ideal fracture sweet-spots given sufficient intensity (Fig. 14b & 14c).

7. Hydraulic fracturing and well monitoring

Hydraulic fracturing has been performed in the Cooper Basin since 1969 (McGowen, Gilbert, & Samari, 2007). The majority of hydraulic fracturing treatments are focus on the predominately Permian sandstone reservoirs, especially in the tight sand Patchawarra Formation. This formation has low (milliDarcy) permeability and requires multistage hydraulic

fracturing to optimise production and be economically feasible. There is significant gas potential to explore and develop in this area; however, the stress complexity and high pressure and temperature conditions are challenging to effectively execute hydraulic fracturing programs.

During injection and fracture propagation a considerable pressure loss can be observed near the wellbore. This near-wellbore pressure loss (NWBPL) was first discussed by Chipperfield & Britt (2000) and Roberts et al. (2000), who stated that the causes of NWBPL are related to pressure loss within the perforations, and tortuosity within the induced fracture path near the wellbore. Johnson et al. (2002) and Johnson and Greenstreet (2003) discussed pressure dependent leak-off (PDL) and NWBPL in the Cooper Basin and showed the significant impact it can have on production performance. NWBPL is caused by frictional pressure loss at the wellbore and closely related to tortuosity. Four different types of fracture propagation can result from high tortuosity including fracture turning, fracture twisting, multiple fracturing and fracture migration. High NWBPL can therefore complicate the hydraulic fracture process and result in a lower percentage of proppant being placed within the target reservoir (Pokalai et al., 2015a, 2015b; Pokalai, 2018).

When pre-existing natural fractures are present within a reservoir the near-wellbore pressure loss is considerably higher due to the complex interactions that create multiple fractures with tortuous paths. This tortuous path will shear and tensile reactivate pre-existing natural fractures to create a large amount of pressure dependent leak-off. Therefore, pressure dependent leak-off can have both positive and negative impacts. It can increase rock permeability by increasing the stimulated rock volume, while at the same time causing a high near-wellbore pressure drop. However, to have better proppant placement and to maximise the flowback of fracturing fluid, near-wellbore pressure needs to be reduced.

The majority of the Patchawarra Formation consists of thick sand intervals that cycle between coal measures and shale, and is currently exposed to high pressure, high stress, and high temperature conditions. Therefore, the fracturing fluid system and proppant need to be selected in order to suit these conditions. Fracturing fluid is commonly a water-based fluid system within the Cooper-Eromanga basins comprising of either a Linear Gel or a Borate Crosslink Gel that is injected during the pad stage, slurry stage and the flushing stage. Proppant is typically 100 mesh sand and is pumped into the target zone to reduce NWBPL and to bridge-off the PDL. This is followed by the injection of ceramic proppant to provide high fracture conductivity. The perforations that the hydraulic fracture is pumped into are typically made by lowering expendable hollow carrier (EHC) or link guns down the wellbore to perforate the casing completion at the target location. The style of perforating guns is primarily dependant on well completion, with EHC guns commonly used in monobore completions to mitigate rat-hole loss, and link guns are used in conventional completion designs.

Once perforations and hydraulic fracture stimulations are complete and the well begins producing hydrocarbons, there is a significant need for well surveillance and intervention programs due to the harsh subsurface conditions within the Cooper-Eromanga basins. These can range from high temperatures, high pressures, and high CO_2 concentrations, to liquid loading (water in the wellbore) issues that can lead to reduced production (Rigby & Smith, 1981; Wycherley et al., 1999; McGowen et al., 2007; Winterfield, Missikos, Tio, & Dalgety, 2014). Hydrocarbon production can also be inhibited by the development of scale (halite and calcite) within the perforations, where pressure and temperature rapidly decrease causing solutes to precipitate. The CO_2 concentration within the Cooper-Eromanga basins is significantly higher (10-30 v/v%) than the average sedimentary basin (Rigby & Smith, 1981; Wycherley et al., 1999), contributing to the need to mitigate calcite scale through acid treatments, re-perforation, and regular wireline drift and broach intervention programs (Pitkin,

Wedham, McGowen, & Thom, 2012). Salts (NaCl) have also been found to precipitate within perforations originating from salty groundwater invading the reservoir.

Other than causing scale build-up, the invasion of groundwater into the wellbore can also increase the production rate required to lift, and unload, the liquids to surface and can cause liquid loading within the wellbore to effectively stop production (Winterfield et al., 2014). Mitigation techniques for this may include artificial lifts (nitrogen injection), compressor installation to reduce back-pressure, plunger lift systems, injection of foaming agents via micro-strings, installation of siphon strings (or recompletion to small diameter tubing) to reduce the minimum rate to lift liquids, well cycling (pressure build-up), and producing the well to atmospheric pressures for a short period of time to unload liquids (McGowen et al., 2007; Winterfield et al., 2014).

8. Exploration and Development

8.1 Current Programs

Current exploration programs are somewhat simplistic and have remained inline with the original anticlinal theory; identify and drill an anticlinal closure (Apak et al., 1997; Lowe-Young et al., 1998; Morton, 1998; O'Neil, 1998). This approach has generated in excess of 6.5 trillion cubic feet (TCF) of sales gas; however, an estimated 1.6 TCF is remaining to be produced from anticlinal and stratigraphic traps (Mackie, 2015). This estimate does not include the highly prospective unconventional plays (basin centred gas, deep coal, and fractured basement) that have sparked renewed interest in the basin. Oil exploration, now primarily targeting the Jurassic Eromanga Basin reservoirs, has also become highly profitable, generating 520 million barrels (mmbbls) from Jurassic to Cretaceous reservoirs, with an estimated 150 mmbbls of recoverable reserves remaining (Mackie, 2015). Although the majority of oil discovered in the basins is in Jurassic and Cretaceous reservoirs, oil has also been discovered

in the Early Permian Tirrawarra Formation in the Tirrawarra (80% of known Permian oil) and Fly Lake/Brolga fields (Gravestock et al., 1998). Taking into account the number of exploration wells drilled versus new Permian gas field discoveries, the success rate for current exploration programs is approximately 40% (Mackie, 2015). The success of Mesozoic oil exploration wells grew from 12% to 45% after the introduction of 3D seismic data acquisition, illustrating the significance of geophysical advancements in discovering new fields and new play types (Mackie, 2015).

There are currently two major plays in the province; (1) targeting Jurassic Eromanga Basin oil reservoired in anticlinal closures; and (2) targeting Permian Cooper Basin gas reservoired in anticlinal and stratigraphic traps (Lowe-Young et al., 1998; Radke, 2009; Scott et al., 2013; Mackie, 2015). The majority of Jurassic oil is reservoired within the Murta Member, Namur Sandstone, Birkhead Formation, Hutton Sandstone, and Poolowanna Formation given that a structural trap exists (Lowe-Young et al., 1998; Kulikowski, 2017; Kulikowski et al., 2016b, 2017c). It is important to note, however, that, as previous indicated, the presence of these typically low-relief structural traps can depend on the seismic time-to-depth conversion method being used, as the conversion errors can be greater than the structural closure (Lowe-Young et al., 1998; Radke, 2009; Kulikowski et al., 2016b, 2017c; Kulikowski, 2017). Although, some stratigraphic traps have been discovered in the Eromanga Basin sequence that appear to be restricted to the Birkhead Formation sandstone channel faces embedded in floodplain and lacustrine shales. The source of this Jurassic oil in the central portion of the play has been attributed to Permian source rocks migrating vertically through leaky seals or along fault conduits (Lowe-Young et al., 1998; Radke, 2009). Recently, the Eromanga Basin oil play has been extended to the western flank of the Cooper Basin, where major oil exploration and production is currently taking place (Lowe-Young et al., 1998). The western flank oil play primarily targets low relief anticlinal traps within the Jurassic Eromanga Basin reservoirs that

are also charged by Permian source rocks migrating through eroded regional seals on the flank of the basin (Lowe-Young et al., 1998; Radke, 2009).

The anticlinal closures common to the basin are often associated with reactivated basement-involved faults that develop broad structures in the overlying stratigraphy, but they can also be associated with positive flower (pop-up) features that are common in the Patchawarra Trough, or as fault-bound anticlines where large basement-involved faults have reactivated and penetrated through overlying units (Apak et al., 1997; Lowe-Young et al., 1998; Radke, 2009; Scott et al., 2013; Mackie, 2015; Kulikowski, 2017; Kulikowski et al., 2017). The case of fault-bound anticlines is most common along the GMI and NM ridges where the large NE-SW striking high angle (50-70^{o}) faults have shown evidence of relatively more recent reactivation (Apak et al., 1997; Gravestock et al., 1998; Kulikowski and Amrouch, 2018a). These anticlinal traps allow for the accumulation of oil and gas within all reservoir quality sandstones in both the Cooper and Eromanga basins (Kantsler, 1984; Lowe-Young et al., 1998; Alexander et al., 1998; Morton, 1998; Radke, 2009; Scott et al., 2013).

8.2 Future Research and Exploration Programs

As the anticline becomes entirely exploited in this province, companies will transition into the next phase of hydrocarbon exploration targeting technically more challenging plays, such as the basin centred gas play, deep coal measure play, stratigraphic plays, polygonal fault play, and potentially fractured basement play that is juxtaposed to Permian source rocks. Each of these relatively unconventional plays will require a more thorough understanding of the basin. Therefore, as exploration within the Cooper-Eromanga basins becomes more challenging, the collaboration between academic researchers and explorationists will become more integral to exploration success. Much of the regional structural, stratigraphic, and stress framework for the basin has been well constrained in recent times (e.g. Apak et al., 1997; Gravestock &

Jensen-Schmidt, 1998; Hillis et al., 1999, 2001; Reynolds et al., 2002, 2003, 2004, 2005, 2006; Mavromatidis, 2006, 2008; Nelson et al., 2006, 2007a, 2007b; Radke, 2009; Pokalai et al., 2015a, 2015b, 2016; Kulikowski et al., 2016a, 2017; Kulikowski, 2017; Kulikowski & Amrouch, 2017, 2018a, 2018b; Pokalai, 2018); however, there does remain a large volume of research that can directly impact the success of future hydrocarbon exploration and development programs. Additionally, exploration and production companies play an important role in the effective exploitation of Australia's largest onshore hydrocarbon province by testing new concepts and acquiring new data that will promote further research in the basin.

A complete 3D reconstruction of the basin has not yet been completed and would provide valuable information on the fault growth through time. Detailed fault growth analyses are not possible in the basin given the poor seismic resolution at basement; however, with continued improvement in seismic acquisition and processing techniques, a fault growth study may be possible in the future. This may ultimately lead to a complete structural and stratigraphic 3D reconstruction of the basin and provide a 3D view of the temporal and spatial distribution of the three basins (Cooper, Eromanga, and Lake Eyre basins) that overly basement (Warburton Basin). The spatial extent of major unconformities, both local and regional, would also be useful, particularly as oil migration from Permian sources to Eromanga Basin reservoirs relies on the presence of unconformities that have effectively removed regional seals (Lowe-Young et al., 1998). The distribution and magnitude of overpressure has previously been investigated (van Ruth & Hillis, 2000; Hillis et al., 2001; van Ruth, Hillis, Tingate, & Swarbrick, 2003; Kulikowski et al., 2016a); however, the mechanism for overpressure generation in the basin remains questionable and may be investigated by integrating reservoir pressure, vertical stress magnitude, and sonic velocity data (Tingay, Hillis, Swarbrick, Morley, & Damit, 2007). The degree of stress perturbation caused by pre-existing faults should also be investigated in more detail, as local stress rotation does exist (Fig. 11b).

To accurately interpret seismic data, the amplitude volume must be converted from the time-domain to the depth-domain using an appropriate depth conversion method (Kulikowski et al., 2016b, 2017c). The errors associated with seismic depth conversion can be attributed to a number of factors, but these can be somewhat mitigated through a more complete understanding of the near surface velocity variation (statics) and a systematic interpretation of shallow reflectors, which are yet to be explored. Mapping the spatial variation of statics in a form that can be incorporated into velocity modelling would provide more accurate results. Considering that the contemporary stress alternates between a strike-slip and compressional stress regime (Fig. 11c), an understanding of the spatial variation in vertical stress magnitudes (calculated from density logs) would be highly beneficial and, if in a gridded map format, could be used to predict stress regimes across the basin.

Rock mechanics data does exist for key parts of the region but is selectively sampled and not representative of heterogeneities, and can contradict with other works (Abul Khair et al., 2013; Nelson et al., 2007). A detailed study focused on constraining the complete and representative rock mechanics data for the Warburton, Cooper and Eromanga basins would provide more certainty on geomechanical and hydraulic fracture stimulation models. Ideally, future hydraulic fracture stimulation models would incorporate the certain interaction between induced fractures and naturally occurring fractures and faults, with particular attention to SE-NW strike-slip faults that are most likely to reactivate under contemporary stresses (Kulikowski et al., 2016c). These SE-NW strike-slip faults are difficult to interpret in low resolution seismic data, but can reduce reservoir properties through cataclasis, can compartmentalise the reservoir, and contribute to tertiary hydrocarbon migration if reactivated (Grant-Woolley et al., 2014; Kulikowski et al., 2016c). A study investigating the possible relationship between well and reservoir performance with distance to these SE-NW strike-slip faults would provide a better understanding on their effect on production.

Finally, although not directly applicable to academic researchers, operating companies may discover new opportunities and hydrocarbon reserves by testing such concepts as the: (1) fracture basement play; (2) basin centred gas play; (3) hydraulic fracturing of deep coal; (4) polygonal fault system play; (5) targeting stratigraphic traps; (6) cutting-edge use of seismic data (e.g. direct hydrocarbon indicators and other seismic attributes); and (7) cost effective alternatives to optimise production (pad drilling, deviated wells from existing wellbores, deepening old shallow oil wells to target Permian reservoirs, and perforating thin (1-2 feet) gas saturated and pressurised reservoirs that were initially dismissed).

9. Conlusions

This review forms a robust synthesis of recent developments within Australia's largest onshore hydrocarbon province, the Cooper-Eromanga basins. New technologies and software applications have armed researchers with cutting edge analysis techniques and applications that have generated a recent increase in information that was previously not available. The purpose of this study is to provide readers with a holistic insight into the province that includes: (1) a detailed tectonic and stratigraphic evolution; (2) a summary of geomechanical modelling results that predict fault and fracture reactivation (tensile and shear) through time to better understand hydrocarbon migration pathways; (3) a synthesis of the petroleum system processes and elements; (4) the spatial and temporal distributions of permeable natural fracture networks through wellbore and seismic data analysis; (5) common hydraulic fracturing and well surveillance programs contrast with a discussion on the common difficulties and risks; (6) a discussion on the seismic time-to-depth conversion methods that are being used and their individual accuracies and limitations; (7) current and future hydrocarbon exploration and development targets; and (8) a discussion on the future research opportunities that can directly impact the effectiveness of exploration and development programs.

Reviewing the province has highlighted opportunities for future exploration and identified possible research topics that will be fundamental to the success of future exploration and development programs. These future programs will begin to target technically more challenging plays as the anticline becomes entirely exploited and will require a thorough understanding of the province. The methodologies and approaches summarised within this review forms a research framework that can be applied to other hydrocarbon provinces to better understand the dynamic structural geology, tectonic evolution and application of geophysics.

10. ACKNOWLEDGEMENTS

The authors appreciate the financial contribution made by the GeoFrac Consortium, which includes the sponsoring companies: Santos, Beach Energy, Chevron, Halliburton and BG Group (QGC). DUG Insight software (v.4.0, 2016) was used for seismic visualisation, interpretation and analysis.

11. REFERENCES

Abul Khair, H. A., Cooke, D., King, R., Hand, M., & Tingay, M. (2012). Preliminary workflow for subsurface fracture mapping using 3D seismic surveys: A case study from the Cooper Basin, South Australia. In: Geothermal Research Council Conference, Reno, Nevada, 36, 339-350.

Abul Khair, H., Cooke, D., Hand, M. (2013). The effect of present day in situ stresses and paleo-stresses on locating sweet spots in unconventional reservoirs, a case study from Moomba-Big Lake fields, Cooper Basin, South Australia. Journal of Petroleum Exploration and Production Technology, 3(4), 207-221.

Abul Khair, H., Cooke, D., & Hand, M. (2015). Seismic mapping and geomechanical analyses of faults within deep hot granites, a workflow for enhanced geothermal system projects. Geothermics, 53, 46-56.

Al-Chalbi, M. (1974). An analysis of stacking, RMS, average, and interval velocities over a horizontally layered ground. Geophysical Prospecting, 22(3), 458-475.

Al-Dossary, S., & Marfurt, K. J. (2006). 3D volumetric multispectral estimates of reflector curvature and rotation. Geophysics, 71(5), P41-P51.

Alexander, E. M., Gravestock, D. I., Cubitt, C., & Chaney, A. (1998). Lithostratigraphy and environments of deposition. In: Gravestock, D. I., Hibburt, J. E., & Drexel, J. F., (Eds), The Petroleum Geology of South Australia. Vol. 4: Cooper Basin, South Australia. Department of Primary Industries and Resources. Report Book, 98/9, 69-116.

Amrouch, K., Lacombe, O., Mouthereau, F., & Dissez, L. (2005). Quantification of orientations and magnitudes of the late Cenozoic paleostresses in the Zagros folded belt from calcite twin analysis. In Thrust Belts and Foreland Basins, International Meeting, Rueil-Malmaison, 31-35.

Amrouch, K., Lacombe, O., Bellahsen, N., Daniel, J. M., & Callot, J. P. (2010). Stress and strain patterns, kinematics and deformation mechanisms in a basement-cored anticline: Sheep Mountain Anticline, Wyoming. Tectonics, 29, TC1005, doi:10.1029/2009TC002525.

Amrouch, K. (2010). Apport de l'analyse microstructurale à la comprehension des mécanismes de plissement. Exemples de structures plissées aux USA (Wyoming) et en Iran (Zagros). Thèse, Université Pierre et Marie Curie – Paris 6, 2010-03, 477 p.

Amrouch, K., Beaudoin, N., Lacombe, O., Bellahsen, N., & Daniel, J. M. (2011). Paleostress magnitudes in folded sedimentary rocks. Geophysical Research Letters, 38, L17301, doi:10.1029/2011GL048649.

Anderson, E.M. (1951). The Dynamics of Faulting and Dyke Formation with Applications to Britain, Oliver and Boyd, Edinburgh.

Apak, S. N., Stuart, W. J., Lemon, N. M., & Wood, G. (1997). Structural evolution of the Permian-Triassic Cooper Basin, Australia: Relation to hydrocarbon trap styles. AAPG Bulletin, 81, 533-555.

Arboit, F., Amrouch, K., Collins, A. S., King, R., & Morley, C. (2015). Determination of the tectonic evolution from fractures, faults, and calcite twins on the southwestern margin of the Indochina Block. Tectonics, 34, 1576-1599, doi:10.1002/2015TC003876.

Arboit, F., Amrouch, K., Morley, C., Collins, A. S., & King, R. (2017), Palaeostress magnitudes in the Khao Khwang fold-thrust belt, new insights into the tectonic evolution of the Indosinian orogeny in central Thailand. Tectonophysics, 710-711, 266-276, doi:10.1016/j.tecto.2017.01.008.

Backé, G., Abul Khair, H., King, R., & Holford, S. (2011). Fracture mapping and modelling in shale-gas target in the Cooper basin, South Australia. The APPEA Journal, 51, 397-410.

Bahorich and Farmer (1995)

Balch, A. H., Lee, M. W., Miller, J. J., & Ryder, R. T. (1982). The use of vertical seismic profiles in seismic investigations of the earth. Geophysics, 47(6), 906-918.

Balch, A. H., & Lee, M. W. (1984). Vertical Seismic Profiling: Techniques, Applications, and Case Histories. International Human Resources Development Corporation, Boston, 488 p.

Basir, H. M., Javaherian, A., & Yaraki, M. T. (2013). Multi-attribute ant-tracking and neural network for fault detection: A case study of an Iranian oilfield. Journal of Geophysics and Engineering, 10(1), 015009.

Baudon, C., & Cartwright, J. (2008). The kinematics of reactivation of normal faults using high resolution throw mapping. Journal of Structural Geology, 30(8), 1072–1084.

Beaudoin, N., Leprêtre, R., Bellahsen, N., Lacombe, O., Amrouch, K., Callot, J. P., Emmanuel, L., & Daniel, J. M. (2012). Structural and microstructural evolution of the Rattlesnake Mountain Anticline (Wyoming, USA): new insights into the Sevier and Laramide orogenic stress build-up in the Bighorn Basin. Tectonophysics, 576, 20-45.

Boger, S. D., & Miller, J. M. (2004). Terminal suturing of Gondwana and the onset of the Ross–Delamerian Orogeny: the cause and effect of an Early Cambrian reconfiguration of plate motions. Earth and Planetary Science Letters, 219(1), 35-48.

Borazjani, S., Kulikowski, D., Amrouch, K., McCabe, P., & Bedrikovetsky, P. (2018). Composition changes of hydrocarbons during secondary petroleum migration. The APPEA Journal, 58, 784-787.

Borazjani, S., Kulikowski, D., Amrouch, K., & Bedrikovetsky, P. (2019). Composition Changes of Hydrocarbons during Secondary Petroleum Migration (Case Study in Cooper Basin, Australia). Geosciences, 9(2),

Boreham C. J., & Hill A. J. (1998). Source rock distribution and hydrocarbon geochemistry. In: The petroleum geology of South Australia. Vol. 4: Cooper Basin (eds. D.I. Gravestock, J.E. Hibburt and J.F. Drexel), pp 129-142. South Australia. Department of Primary Industries and Resources. Report Book, 98/9.

Boult, P. J., Lanzilli, E., Michaelsen, B. H., McKirdy, D. M., & Ryan, M. J. (1998). A new model for the Hutton/Birkhead reservoir/seal couplet and the associated Birkhead-Hutton (!) petroleum system. The APPEA Journal, 38(1), 724-744.

Bradshaw, M. T. (1993). Australian petroleum systems. PESA Journal 21, 43-53.

Black, M., McCormack, K. D., Elders, C., & Robertson, D. (2017). Extensional fault evolution within the Exmouth Sub-basin, North West Shelf, Australia. Marine and Petroleum Geology, 85, 301-315.

Burgin, H. B., Amrouch, K., Rajabi, M., Kulikowski, D., & Holford, S. P. (2018). Determining paleo-structural environments through natural fracture and calcite twin analyses: a case study in the Otway Basin. The APPEA Journal, 58, 238-254, DOI: 10.1071/AJ17099.

Cartwright, J., & Lonergan, L. (1997). Seismic expression of layer-bound fault systems of the Eromanga and North Sea Basins. Exploration Geophysics, 28(3), 323-331.

Childs, C., Nicol, A., Walsh, J. J., & Watterson, J. (1996). Growth of vertically segmented normal faults. Journal of Structural Geology, 18(12), 1389-1397.

Chipperfield, S. T., & Britt, L. K. (2000). Application of after-closure analysis for improved fracture treatment optimisation: A Cooper Basin case study. In SPE Rocky Mountain Regional/Low-Permeability Reservoirs Symposium and Exhibition. Society of Petroleum Engineers, SPE -60316-MS.

Chopra, S., & Marfurt, K. J. (2007). Volumetric curvature attributes add value to 3D seismic data interpretation. The Leading Edge, 26(7), 856-867.

Collins, A. S., & Pisarevsky, S. A. (2005). Amalgamating eastern Gondwana: the evolution of the Circum-Indian Orogens. Earth-Science Reviews, 71(3), 229-270.

Cooke, D., Tyiasning, S., & Abul Khair, H. (2016). Unexpected behaviors of stimulated fractures in the high-stress Cooper Basin. The Leading Edge, 35(1), 78-84.

Deighton, I., & Hill, A. J., 1998. Thermal and Burial History. In: The petroleum geology of South Australia. Vol. 4: Cooper Basin (eds. D.I. Gravestock, J.E. Hibburt and J.F. Drexel), pp 143-156. South Australia. Department of Primary Industries and Resources. Report Book, 98/9.

Duddy, I. R. (1987) Fission track thermal history assessment of the Eromanga-Cooper Basin: an initial apatite study, In: Gleadow, A. J. W., Duddy, I. R., Green, P. F., & Lovering, J. F. (Eds). End of Grant Technical Report, NERDDC project no. 720.

Elliott, L. G. (1993). Post-Carboniferous tectonic evolution of eastern Australia. APEA Journal, 33, 215-215.

Etchecopar, A. (1984). Étude des états de Contraintes en Tectonique Cassante et Simulation de Déformations Plastiques: Approche Mathématique, the se Doctorates-Sciences, 270 pp., Univ. Sci. et Tech. Du Languedoc, Montpellier, Fr.

Evans, P.R. (1988). The formation of petroleum and geological history of Australia. In: Petroleum in Australia: the first century. APEA Journal, Special Publication, 26-47.

Farrell, R. C., & Euwema, R. N. (1984). Refraction statics. Proceedings of the IEEE, 72(10), 1316-1329.

Ferrill, D. A., Winterle, J., Wittmeyer, G., Sims, D., Colton, S., Armstrong, A., & Morris, A. P. (1999). Stressed rock strains groundwater at Yucca Mountain, Nevada. GSA Today, 9(5), 1-8.

Flottmann, T., Campagna, D. J., Hillis, R., & Warner, D. (2004). Horizontal microfractures and core discing in sandstone reservoirs, Cooper Basin, Australia. In: Eastern Australasian basins symposium II: Petroleum Exploration Society of Australia Special Publication, 689-694.

Gajewski, D., & Pšenčik, I. (1990). Vertical seismic profile synthetics by dynamic ray tracing in laterally varying layered anisotropic structures. Journal of Geophysical Research: Solid Earth, 95(B7), 11301-11315.

Ganley, D. C., & Kanasewich, E. R. (1980). Measurement of absorption and dispersion from check shot surveys. Journal of Geophysical Research: Solid Earth, 85(B10), 5219-5226.

Gallagher, K. L. (1998). The subsidence history and thermal state of the Eromanga and Cooper Basins (Doctoral dissertation. Australian National University.

Gatehouse, C. G., (1986) The geology of the Warburton Basin in South Australia, Australian Journal of Earth Sciences, 33(2), 161-180, doi:10.1080/08120098608729357.

Gersztenkorn, A., & Marfurt, K. J. (1999). Eigenstructure-based coherence computations as an aid to 3-D structural and stratigraphic mapping. Geophysics, 64(5), 1468-1479.

Giba, M., Walsh, J. J., & Nicol, A. (2012). Segmentation and growth of an obliquely reactivated normal fault. Journal of Structural Geology, 39, 253-267.

Gibson, G. M., Totterdell, J. M., White, L. T., Mitchell, C. H., Stacey, A. R., Morse, M. P., & Whitaker, A. (2013). Pre-existing basement structure and its influence on continental rifting and fracture zone development along Australia's southern rifted margin. Journal of the Geological Society, 170(2), 365-377.

Gilby, A. R., & Mortimore, I. R. (1989). The prospects for Eromanga oil accumulations in the northern Cooper Basin region, Australia.

Gorter, J. D., Gostin, V. A., & Plummer, P. S. (1989). The enigmatic subsurface Tookoonooka complex in south-west Queensland: Its impact origin and implications for hydrocarbon accumulations. In: O'Neil, B. J. (Ed), The Cooper and Eromanga Basins, Australia, pp. 441–456. Petroleum Exploration Society of Australia, Society of Petroleum Engineers & Australian Society of Exploration Geophysicists, Adelaide, Australia.

Grant-Woolley, L., Kong, A., Schoemaker, B., Nasreddin, H., Montague, E. T. (2014). Identification of Strike-Slip Faults Provides Insights into the Further Development of Mature

Cooper Basin Fields. In SPE Asia Pacific Oil & Gas Conference and Exhibition, Adelaide, SPE 171492-MS.

Gravestock, D. I., Alexander, E. M., Morton, J. G. G., & Sun, X. (1998). Reservoirs & Seals. In: Gravestock, D. I., Hibburt, J. E., & Drexel, J. F., (Eds), The Petroleum Geology of South Australia. Vol. 4: Cooper Basin, South Australia. Department of Primary Industries and Resources. Report Book, 98/9, 157-180.

Gravestock, D. I., & Jensen-Schmidt, B. (1998). Structural setting. In: Gravestock, D.I., Hibburt, J.E., Drexel, J.F., (Eds), The Petroleum Geology of South Australia. Vol. 4: Cooper Basin, South Australia. Department of Primary Industries and Resources. Report Book, 98/9, 47-68.

Gray, D. R., & Foster, D. A. (2004). Tectonic evolution of the Lachlan Orogen, southeast Australia: historical review, data synthesis and modern perspectives. Australian Journal of Earth Sciences, 51(6), 773-817.

Gray, M. E. (2017). Analytical Techniques for Evaluating Seal Capacity for Carbon Dioxide Storage in Selected Australian Basins (Doctoral dissertation). The Australian School of Petroleum, the University of Adelaide, Adelaide, Australia.

Gray, M. E., Daniel, R., Kaldi, J., Kulikowski, D. (2019). Determining the Accuracy of Pseudo-Capillary Pressure Curves Generated from Nuclear Magnetic Resonance (NMR) Data: The Cooper Basin, Australia. Australian Journal of Earth Sciences, under review.

Green, P. M., Brain, T. J., & John, B. H. (1989). Possible stratigraphic controls on hydrocarbon distribution within the Jurassic-Early Cretaceous rocks, Eromanga Basin, southern Queensland. In: The Cooper and Eromanga Basins, Australia (ed. B. J. O'Neil), pp. 251-264. Petroleum Exploration Society of Australia, Society of Petroleum Engineers, Australian Society of Exploration Geophysicists (S.A. Branches), Adelaide (Proceedings of Cooper and Eromanga Basins Conference).

Haines, P. W., Hand, M., & Sandiford, M. (2001). Palaeozoic synorogenic sedimentation in central and northern Australia: A review of distribution and timing with implications for the evolution of intracontinental orogens. Australian Journal of Earth Sciences, 48, 911-928.

Hakami, A. M., Marfurt, K. J., & Al-Dossary, S. (2004). Curvature attribute and seismic interpretation: Case study from Fort Worth Basin, Texas, USA. In: SEG Technical Program Expanded Abstracts, 544-547.

Hallmann, C. O., Arouri, K. R., McKirdy, D. M., & Schwark, L. (2007). Temporal resolution of an oil charging history–a case study of residual oil benzocarbazoles from the Gidgealpa Field. Organic Geochemistry, 38(9), 1516-1536.

Hardage, B.A. (1985). Vertical seismic profiling. The Leading Edge, 4(11), 59-59.

Hauge, P. S. (1981). Measurements of attenuation from vertical seismic profiles. Geophysics, 46(11), 1548-1558.

Heath, R., McIntyre, S., & Gibbins, N. (1989). A Permian origin for Jurassic reservoired oil in the Eromanga Basin. In: The Cooper and Eromanga Basins, Australia (ed. B. J. O'Neil), pp. 405-416. Petroleum Exploration Society of Australia, Society of Petroleum Engineers,

Australian Society of Exploration Geophysicists (S. A. Branches), Adelaide (Proceedings of Cooper and Eromanga Basins Conference).

Hillis, R. R., Macklin, T. A., & Siffleet, P. (1995). Regional depth-conversion of mapped seismic two-way-times in the Cooper-Eromanga Basins. Exploration Geophysics, 26(2/3), 412-418.

Hillis, R. R., Enever, J. R., & Reynolds, S. D. (1999). In situ stress field of eastern Australia. Australian Journal of Earth Sciences, 46(5), 813-825.

Hillis, R. R., & Reynolds, S. D. (2000). The Australian stress map. Journal of the Geological Society, 157(5), 915-921.

Hillis, R. R., Morton, J. G. G., Warner, D. S., & Penney, R. K. (2001). Deep basin gas: A new exploration paradigm in the Nappamerri Trough, Cooper Basin, South Australia. The APPEA Journal, 41(1), 185-200.

Hillis, R. R., & Reynolds, S. D. (2003). In situ stress field of Australia. Geological Society of America Special Papers, 372, 49-58.

Hoffmann, K. L. (1989). The influence of pre-Jurassic tectonic regimes on the structural development of the southern Eromanga Basin, Queensland. In: The Cooper and Eromanga Basins, Australia (ed. B. J. O'Neil), pp. 315-328. Petroleum Exploration Society of Australia, Society of Petroleum Engineers, Australian Society of Exploration Geophysicists (S.A. Branches), Adelaide (Proceedings of Cooper and Eromanga Basins Conference).

Hung, J. H., & Wu, J. C. (2012). In-situ stress and fault reactivation associated with LNG injection in the Tiechanshan gas field, fold-thrust belt of Western Taiwan. Journal of Petroleum Science and Engineering, 96, 37-48.

Igboekwe, M. U., & Ohaegbuchu, H. E. (2011). Investigation into the weathering layer using up-hole method of seismic refraction. Journal of Geology and Mining Research, 3(3), 73-86.

Jackson, C. A. L., & Rotevatn, A. (2013). 3D seismic analysis of the structure and evolution of a salt-influenced normal fault zone: a test of competing fault growth models. Journal of Structural Geology, 54, 215-234, doi:10.1016/j.jsg.2013.06.012.

Jadoon, Q. K., Roberts, E., Blenkinsop, T., Raphael, A. J., & Shah, S. A. (2016). Mineralogical modelling and petrophysical parameters in Permian gas shales from the Roseneath and Murteree formations, Cooper Basin, Australia. Petroleum Exploration and Development, 43(2), 277-284.

Jenkins, C.C. (1989). Geochemical correlation of source rocks and crude oils from the Cooper and Eromanga basins. In: O'Neil, B.J. (ed.), The Cooper and Eromanga basins, Australia, 525–540.

Johnson, Jr., R. L., Aw, K. P., Ball, D., & Willis, M. (2002). Completion, Perforating and Hydraulic Fracturing Design Changes Yield Success in an Area of Problematic Frac Placement - the Cooper Basin, Australia, SPE 77906. Paper presented at the SPE Asia Pacific Oil and Gas Conference and Exhibition, Melbourne, Australia.

Johnson, Jr., R. L., & Greenstreet, C. W. (2003). Managing Uncertainty Related to Hydraulic Fracturing Modeling in Complex Stress Environments with Pressure-Dependent Leakoff. The

SPE Annual Technical Conference and Exhibition, Denver, Colorado, 5–8 October, SPE-84492.

Johnson, Jr., R. L., Abul Khair, H., Jeffrey, R. G., Meyer, J. J., Stark, C., & Tauchintz, J. (2015). Improving fracture initiation and potential impact on fracture coverage by implementing optimal well planning and drilling methods for typical stress conditions in the Cooper Basin, Central Australia. The APPEA Journal and Conference Proceedings, 55, extended abstract.

Jolie, E., Moeck, I., & Faulds, J. E. (2015). Quantitative structural geological exploration of fault-controlled geothermal systems—A case study from the Basin-and-Range Province, Nevada (USA). Geothermics 54, 54-67.

Kantsler, A. J., Prudence, T. J. C., Cook, A. C., & Zwigulis, M. (1984). Hydrocarbon habitat of the Cooper/Eromanga basin, Australia. In: Petroleum geochemistry and basin evolution (eds. G. Demaison and R. J. Murris), pp 373-390. American Association of Petroleum Geologists Memoir, 35.

King, R., Abul Khair, H., Bailey, A., Backé, G., Holford, S., & Hand, M. (2011). Integration of In-Situ Stress Analysis and Three-Dimensional Seismic Mapping to Understand Fracture Networks in Australian Basins. In: Proceedings from the Australian Geothermal Energy Conference, 16-18 November, Melbourne, Australia, 129-134.

Kuang, K. S. (1985). History and style of Cooper-Eromanga Basin structures. Exploration Geophysics, 16, 245-248.

Kulikowski, D., Cooke, D., Amrouch, K. (2016a). Constraining the distribution and relationship between overpressure, natural fracture density and temperature in the Cooper Basin. The Australian Petroleum Production and Exploration Association Journal, 56, 11-28, doi:10.1071/AJ15002.

Kulikowski, D., Hochwald, C., Cooke, D., & Amrouch, K. (2016b). A Statistical Approach to Assessing Depth Conversion Uncertainty on a Regional Dataset: Cooper-Eromanga Basin, Australia. ASEG-PESA-AIG 2016 Conference, Adelaide. Extended Abstract #200, 484-490, doi:10.1071/aseg2016ab200.

Kulikowski, D., Amrouch, K., & Cooke, D. (2016c). Geomechanical Modelling of Fault Reactivation in the Cooper Basin, Australia. Australian Journal of Earth Sciences, 63(3), 295-314, doi:10.1080/08120099.2016.1212925.

Kulikowski, D. (2017). Modern Structural Analysis of Subsurface Provinces: A Case Study on the Cooper and Eromanga Basins, Australia (Doctoral dissertation). The Australian School of Petroleum, the University of Adelaide, Adelaide, Australia.

Kulikowski, D., & Amrouch, K. (2017). Combining Geophysical Data and Calcite Twin Stress Inversion to Refine the Tectonic History of Subsurface and Offshore Provinces: A Case Study on the Cooper-Eromanga Basin, Australia. Tectonics, 36(3), 515-541, doi:10.1002/2016TC004366.

Kulikowski, D., Amrouch, K., Cooke, D., & Gray, M. E. (2017). Basement Structural Architecture and Hydrocarbon Conduit Potential of Polygonal Faults in the Cooper-Eromanga Basin, Australia. Geophysical Prospecting, in press, doi:10.1111/1365-2478.12531.

Kulikowski, D., & Amrouch, K. (2018a). 3D Seismic Analysis Investigating the Relationship Between Stratigraphic Architecture and Structural Activity in the Intra-cratonic Cooper and Eromanga Basins, Australia. Marine and Petroleum Geology, 91, 381-400.

Kulikowski, D., & Amrouch, K. (2018b). 4D Modelling of Fault Reactivation using Complete Paleo-Stress Tensors from the Cooper-Eromanga Basin, Australia. Australian Journal of Earth Sciences, 65(5), 661-681, DOI: 10.1080/08120099.2018.1465472.

Kulikowski, D., Amrouch, K., & Burgin, H. B. (2018a). Mapping Permeable Subsurface Fracture Networks: A Case Study on the Cooper Basin, Australia. Journal of Structural Geology, 114, 336-345.

Kulikowski, D., Hochwald, C., & Amrouch, K. (2018b). An automated cross-validation method to assess seismic time-to-depth conversion accuracy: A case study on the Cooper-Eromanga Basin, Australia. Geophysical Prospecting, 66(8), 1521-1534

Lacombe, O., Amrouch, K., Mouthereau, F., & Dissez, L. (2007). Calcite twinning constraints on late Neogene stress patterns and deformation mechanisms in the active Zagros collision belt. Geology, 35(3), 263–266.

Levin, F. K., & Lynn, R. D. (1958). Deep-hole geophone studies. Geophysics, 23(4), 639-664.

Lisle, R. J. (1994). Detection of zones of abnormal strains in structures using Gaussian curvature analysis. AAPG bulletin, 78(12), 1811-1819.

Lodwick, B. (2014). Seismic Geomorphology of the Permian Sediments in the Cooper Basin: A Study of the Toolachee Formation in the Nappamerri Trough (Honours dissertation). The Australian School of Petroleum, the University of Adelaide, Adelaide, Australia.

Lonergan, L., Cartwright, J., & Jolly, R. (1998). The geometry of polygonal fault systems in Tertiary mudrocks of the North Sea. Journal of Structural Geology, 20(5), 529-548.

Longley, I. M. (1989). The Talundilly anomaly and its implications for hydrocarbon exploration of Eromanga astroblemes.

Lowe-Young, B. S., Mackie, S. I., & Heath, R. S. (1998). The Cooper-Eromanga Petroleum System, Australia. Investigation of Essential Elements and Processes. AAPG Bulletin, abstract, 82(13).

Mackie, S. (2015). History of Petroleum Exploration and Development in the Cooper and Eromanga Basins. AAPG/SEG International Conference and Exhibition, Melbourne, Australia, Search and Discovery Article #10814.

Mai, H. T., Marfurt, K. J., & Chávez-Pérez, S. (2009). Coherence and volumetric curvatures and their spatial relationship to faults and folds, an example from Chicontepec basin. Proceedings of the Society of Exploration Geophysicists International Exposition and Annual Meeting, Houston, 1063-1067.

Mavromatidis, A. (2006). Burial/exhumation histories for the Cooper-Eromanga Basins and implications for hydrocarbon exploration, Eastern Australia. Basin Research, 18, 351-373.

Mavromatidis, A. (2008). Two layer model of lithospheric compression and uplift/exhumation in an intracratonic setting: an example from the Cooper–Eromanga Basins, Australia. International Journal of Earth Sciences, 97(3). 623-634.

McGowen, J.M., Gilbert, J.V. & Samari, E. (2007). Hydraulic Fracturing Down Under. Hydraulic Fracturing Technology Conference, College station, Texas, 29–31 January, SPE-106051-MS.

Meixner, T. J., Gunn, P. J., Boucher, R. K., Yeates, T. N., Richardson, L. M., & Frears, R. A. (2000). The nature of the basement to the Cooper Basin region, South Australia. Exploration Geophysics, 31. 24-32.

Metcalfe, I. (2013), Gondwana dispersion and Asian accretion: tectonic and palaeogeographic evolution of eastern Tethys. Journal of Asian Earth Sciences, 66, 1-33.

Moore, P. S., & Pitt, G. M. (1984). Cretaceous of the Eromanga Basin—implications for hydrocarbon exploration. The APPEA Journal, 24(1), 358-376.

Morton, J. G. G. (1998). Undiscovered petroleum resources. In: Gravestock, D.I., Hibburt, J.E. and Drexel, J.F. (eds.), The Petroleum Geology of South Australia. Volume 4: Cooper Basin. Report Book 203-09. South Australia: Department of Primary Industries and Resources, pp. 203-210.

Myers, J. S., Shaw, R. D., & Tyler, I. M. (1996). Tectonic evolution of Proterozoic Australia. Tectonics, 15(6), 1431-1446.

Müller, R. D., Dyksterhuis, S., & Rey, P. (2012). Australian paleo-stress fields and tectonic reactivation over the past 100 Ma. Australian Journal of Earth Sciences, 59, 13-28.

Murray, G. H. (1968). Quantitative fracture study-Spanish Pool, McKenzie County, North Dakota. AAPG Bulletin, 52(1), 57-65.

Nelson, E. J., Meyer, J. J., Hillis, R. R., & Mildren, S. D. (2005). Transverse drilling-induced tensile fractures in the West Tuna area, Gippsland Basin, Australia: implications for the in situ stress regime. International Journal of Rock Mechanics and Mining Sciences, 42(3), 361-371.

Nelson, E., Hillis, R., Sandiford, M., Reynolds, S., & Mildren, S. (2006). Present-day state-of-stress of southeast Australia. APPEA journal, 46(1), 283-305.

Nelson, E. J., Chipperfield, S. T., Hillis, R. R., Gilbert, J., & McGowen, J. (2007a). Using geological information to optimize fracture stimulation practices in the Cooper Basin, Australia. Petroleum Geoscience, 13(1), 3-16.

Nelson, E. J., Chipperfield, S. T., Hillis, R. R., Gilbert, J., McGowen, J., & Mildren, S. D. (2007b). The relationship between closure pressures from fluid injection tests and the minimum principal stress in strong rocks. International Journal of Rock Mechanics and Mining Sciences, 44, 787-801.

Neves, F. A., Zahrani, M. S., & Bremkamp, S. W. (2004). Detection of potential fractures and small faults using seismic attributes. The Leading Edge, 23, (9), 903-906.

Newton, C. B. (1986). The Tintaburra oilfield. The APEA Journal, 26, 334-352.

Oldham, A. C., & Gibbins, N. M., (1995). Lake Hope 3D-A case study. Exploration Geophysics, 26, 383-394.

O'Neil, B. J. (1998). History of Petroleum Exploration and Development. In: Gravestock, D.I., Hibburt, J.E. & Drexel, J.F. (eds.), The Petroleum Geology of South Australia. Volume 4: Cooper Basin. South Australia Department of Primary Industries and Resources, Adelaide. Report Book, 1998/9, pp. 7-36.

Partyka, G., Gridley, J., & Lopez, J. (1999). Interpretational applications of spectral decomposition in reservoir characterization. The Leading Edge, 18(3), 353-360.

Pitkin, M. C., Wadham, T. H., McGowen, J. M., & Thom, W. W. (2012, January). Taking the first steps: Stimulating the Nappamerri Trough resource play. In SPE Asia Pacific Oil and Gas Conference and Exhibition. Society of Petroleum Engineers.

Pitt, G. M. (1986). Geothermal gradients, geothermal histories and the timing of thermal maturation in the Eromanga-Cooper Basins, in Contributions to the Geology and Hydrocarbon Potential of the Eromanga Basin. In: Gravestock, D. I., Moore, P. S., & Pitt, G. M. (Eds), pp. 323-351, Special Publication 12, Geological Society of Australia.

Pokalai, K., Fei, Y., Ahmad, M., Haghighi, M., & Gonzalez, M. (2015a). Design and optimisation of multi-stage hydraulic fracturing in a horizontal well in a shale gas reservoir in the Cooper Basin, South Australia. The Australian Petroleum Production and Exploration Association Journal, 55, 1–14.

Pokalai, K., Haghighi, M., Sarkar, S., Tyiasning, S., & Cooke, D. (2015b). Investigation of the Effects of Near-Wellbore Pressure Loss and Pressure Dependent Leakoff on Flowback during Hydraulic Fracturing with Pre-Existing Natural Fractures. SPE/IATMI Asia Pacific Oil and Gas Conference and Exhibition, Nusa Dua, Bali, SPE-176440.

Pokalai, K., Kulikowski, D., Johnson, Jr., R. L., Haghighi, M., & Cooke, D. (2016). Development of a new approach for hydraulic fracturing in tight sand with pre-existing natural fractures. The Australian Petroleum Production and Exploration Association Journal, 56, 225-238.

Pokalai, K. (2018). Simulation and Optimisation of Hydraulic Fracturing and Flowback in Unconventional Reservoirs: A Case Study in the Cooper Basin, South Australia (Doctoral dissertation). The Australian School of Petroleum, the University of Adelaide, Adelaide, Australia.

Powell, T. G., Boreham, C. J., McKirdy, D. M., Michaelsen, B. H., & Summons, R. E. (1989). Petroleum Geochemistry of the Murta Member, Mooga Formation, and associated oils, Eromanga Basin. The APPEA Journal, 29, 114-129.

Radke, B. (2009). Hydrocarbon and Geothermal Prospectivity of Sedimentary Basins in Central Australia; Warburton, Cooper, Pedirka, Galilee, Simpson and Eromanga Basins. Geoscience Australia Record 2009/25.

Reynolds, S. D., Coblentz, D. D., & Hillis, R. R. (2002). Tectonic forces controlling the regional intraplate stress field in continental Australia: Results from new finite element modelling. Journal of Geophysical Research, 107(B7). 2131.

Reynolds, S. D., Coblentz, D. D., & Hillis, R. R. (2003). Influences of plate-boundary forces on the regional intraplate stress field of continental Australia. Geological Society of America Special Papers, 372, 59-70.

Reynolds, S. D., Mildren, S. D., Hillis, R. R., & Meyer, J. J. (2004). The in situ stress field of the Cooper Basin and its implications for hot dry rock geothermal energy development. In PESA Eastern Australasian Basins Symposium II (2004: Adelaide, South Australia).

Reynolds, S. D., Mildren, S. D., Hillis, R. R., Meyer, J. J., & Flottmann, T. (2005). Maximum horizontal stress orientations in the Cooper Basin, Australia. implications for plate-scale tectonics and local stress sources. Geophysical Journal International, 160, 332-343.

Reynolds, S. D., Mildren, S. D., Hillis, R. R., & Meyer, J. J. (2006). Constraining stress magnitudes using petroleum exploration data in the Cooper-Eromanga Basins, Australia. Tectonophysics, 415, 123-140.

Rezaee, M. R., & Sun, X. (2007). Fracture-Filling Cements in the Palaeozoic Warburton Basin, South Australia. Journal of Petroleum Geology, 30(1), 79-90.

Rigby, D., & Smith, J. W. (1981). An isotopic study of gases and hydrocarbons in the Cooper Basin. The APPEA Journal, 21, 222-229.

Roberts, G. A., Chipperfield, S. T., & Miller, W. K. (2000). The evolution of a high near-wellbore pressure loss treatment strategy for the Australian Cooper Basin. In SPE Annual Technical Conference and Exhibition. Society of Petroleum Engineers.

Roberts, A. (2001). Curvature attributes and their application to 3D interpreted horizons. First Break, 19(2), 85-100.

Robson, A. G. (2018). Normal fault growth analysis using 3D seismic datasets located along Australia's southern margin (Doctoral dissertation). School of Physical Sciences, the University of Adelaide, Adelaide, Australia.

Robson, A. G, Holford, S. P., King, R. C., & Kulikowski, D. (2018). Structural evolution of horst and half-graben structures proximal to a transtensional fault system using a 3D seismic dataset from the Shipwreck Trough, offshore Otway Basin, Australia. Marine and Petroleum Geology, 89, 615-634, doi:10.1016/j.marpetgeo.2017.10.028.

Rumph B. (1982) Seismic data from the Eromanga Basin. In: Moore, S. P., & Mount, T. J. (Eds), Eromanga Basin Symposium: Summary Papers, pp. 193. Geological Society of Australia & Petroleum Exploration Society of Australia, Adelaide, Australia.

Sandiford, M., Wallace, M., & Coblentz, D. (2004). Origin of the in situ stress field in south-eastern Australia. Basin Research, 16(3), 325-338.

Scholefield, T. (1989). The stratigraphy and hydrocarbon potential of the northern Eromanga Basin. In: O'Neil, B. J. (Ed), The Cooper and Eromanga Basins, Australia, pp. 417-427. Petroleum Exploration Society of Australia, Society of Petroleum Engineers & Australian Society of Exploration Geophysicists, Adelaide, Australia.

Scott, M. P., Stephens, T., Durant, R., McGowen, J., Thom, W., & Woodroof, R. (2013). Investigating hydraulic fracturing in tight gas sand and shale gas reservoirs in the Cooper Basin. In: SPE Unconventional Resources Conference and Exhibition-Asia Pacific, SPE-167073-MS.

Senior, B. R., Galloway, M. C., Ingram, J. A., & Senior, D. (1968). The geology of the Barrolka, Eromanga, Durham Downs, Thargomindah, Tickalara and Bulloo 1:250,000 Sheet areas, Queensland. Department of National Development, Bureau of Mineral Resources, Geology and Geophysics, Record no. 1968/35.

Sibson, R. H. (1974). Frictional constraints on thrust, wrench and normal faults. Nature, 249(5457), 542-544.

Smyth, M. (1983). Nature of source material for hydrocarbons in Cooper Basin, Australia. AAPG Bulletin, 67(9), 1422-1426.

Stainsby, S. D., & Worthington, M. H. (1985). Q estimation from vertical seismic profile data and anomalous variations in the central North Sea. Geophysics, 50(4), 615-626.

Stanmore, P. J. (1989). Case studies of stratigraphic and fault traps in the Cooper Basin, Australia. In: The Cooper and Eromanga Basins, Australia. Proceedings of the Cooper and Eromanga Basins Conference, Adelaide, 361-369.

Stewart, S. A., & Podolski, R. (1998). Curvature analysis of gridded geological surfaces. Geological Society, London, Special Publications, 127(1), 133-147.

Stuart, W. J. (1976). The genesis of Permian and lower Triassic reservoir sandstones during phases of southern Cooper Basin development. APEA Journal, 16(1), 27-48.

Sun, X. (1997). Structural style of the Warburton Basin and control in the Cooper and Eromanga Basins, South Australia. Exploration Geophysics, 28(3), 333-339.

Sun, X. (1999). Fracture analysis of the Eastern Warburton Basin (Early Paleozoic). South Australia. National Centre for Petroleum Geology and Geophysics. Report Book, 99, 00014.

Teufel, L. W., Rhett, D. W., & Farrell, H. E. (1991). Effect of reservoir depletion and pore pressure drawdown on in situ stress and deformation in the Ekofisk field, North Sea. In: The 32nd US Symposium on Rock Mechanics (USRMS), American Rock Mechanics Association, Rotterdam, 63-72.

Tingay, M., Hillis, R., Swarbrick, R., Morley, C. & Damit, A. (2007). 'Vertically transferred'' overpressures in Brunei: Evidence for a new mechanism for the formation of high magnitude overpressures. Geology, 35, 1023–1026.

Tyiasning, S., & Cooke, D. (2015). A comparison of competing amplitude variation with offset techniques applied to tight gas sand exploration in the Cooper Basin of Australia. Interpretation, 3(3), SZ15-SZ26.

Tyiasning, S., & Cooke, D. (2016). Anisotropy signatures in the Cooper Basin of Australia: Stress versus fractures. Interpretation, 4(2), SE51-SE61.

Van Ruth, P. & Hillis, R. (2000). Estimating pore pressure in the Cooper Basin, South Australia: sonic log method in an uplifted basin. Exploration Geophysics, 31(1/2), 441-447.

Van Ruth, P., Hillis, R., Tingate, P., & Swarbrick, R. (2003). The origin of overpressure in 'old' sedimentary basins: an example from the Cooper Basin, Australia. Geofluids, 3(2), 125-131.

Veevers, J. J., Jones, J. G., & Powell, C. M. (1982). Tectonic framework of Australia's sedimentary basins. APEA Journal, 22(1), 283-300.

Veevers, J. J., & Powell, C. M. (1984). Uluru and Adelaidean regimes, in J. J. Veevers, ed., Phanerozoic earth history of Australia: Oxford, Clarendon Press, p. 329–339.

Watterson, J., Walsh, J., Nicol, A., Nell, P. A. R., & Bretan, P. G. (2000). Geometry and origin of a polygonal fault system. Journal of the Geological Society, 157(1), 151-162.

Williams, G. D., Powell, C. M., & Cooper, M. A. (1989). Geometry and kinematics of inversion tectonics. Geological Society, London, Special Publications, 44(1), 3-15.

Winterfield, C. D., Missikos, J., Tio, R., & Dalgety, B. (2014, October). Application of Closed Loop Control Logic to Optimise End-of-Life Cycling Production in a Mature Gas Field. In SPE Asia Pacific Oil & Gas Conference and Exhibition. Society of Petroleum Engineers.

Wycherley, H., Fleet, A., & Shaw, H. (1999). Some observations on the origins of large volumes of carbon dioxide accumulations in sedimentary basins. Marine and Petroleum Geology, 16(6), 489-494.

Young, I. F., Gunther, L. M., & Dixon, O. (1989). GSQ Thargomindah-3: A stratigraphic test of a “canyon-like” feature near the Tookoonooka complex, Eromanga basin, Queensland. In: O’Neil, B. J. (Ed), The Cooper and Eromanga Basins, Australia. Adelaide: Proceedings of Petroleum Exploration Society of Australia, Society of Petroleum Engineers, Australian Society of Exploration Geophysicists (SA Branches), 457–471.

12. FIGURES

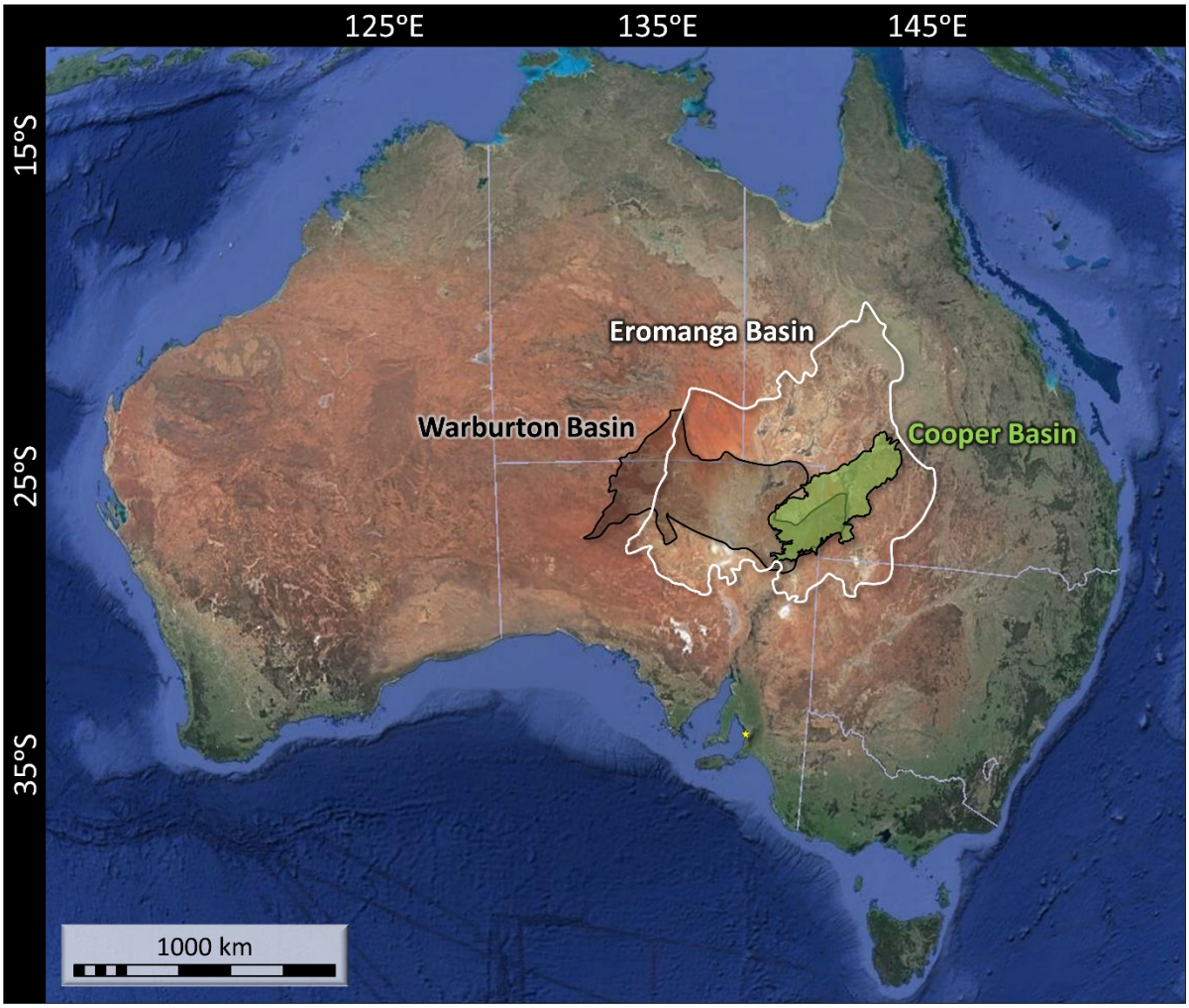

Figure 1. Location of the Warburton, Cooper, and Eromanga basins (after Kulikowski et al., 2016c).

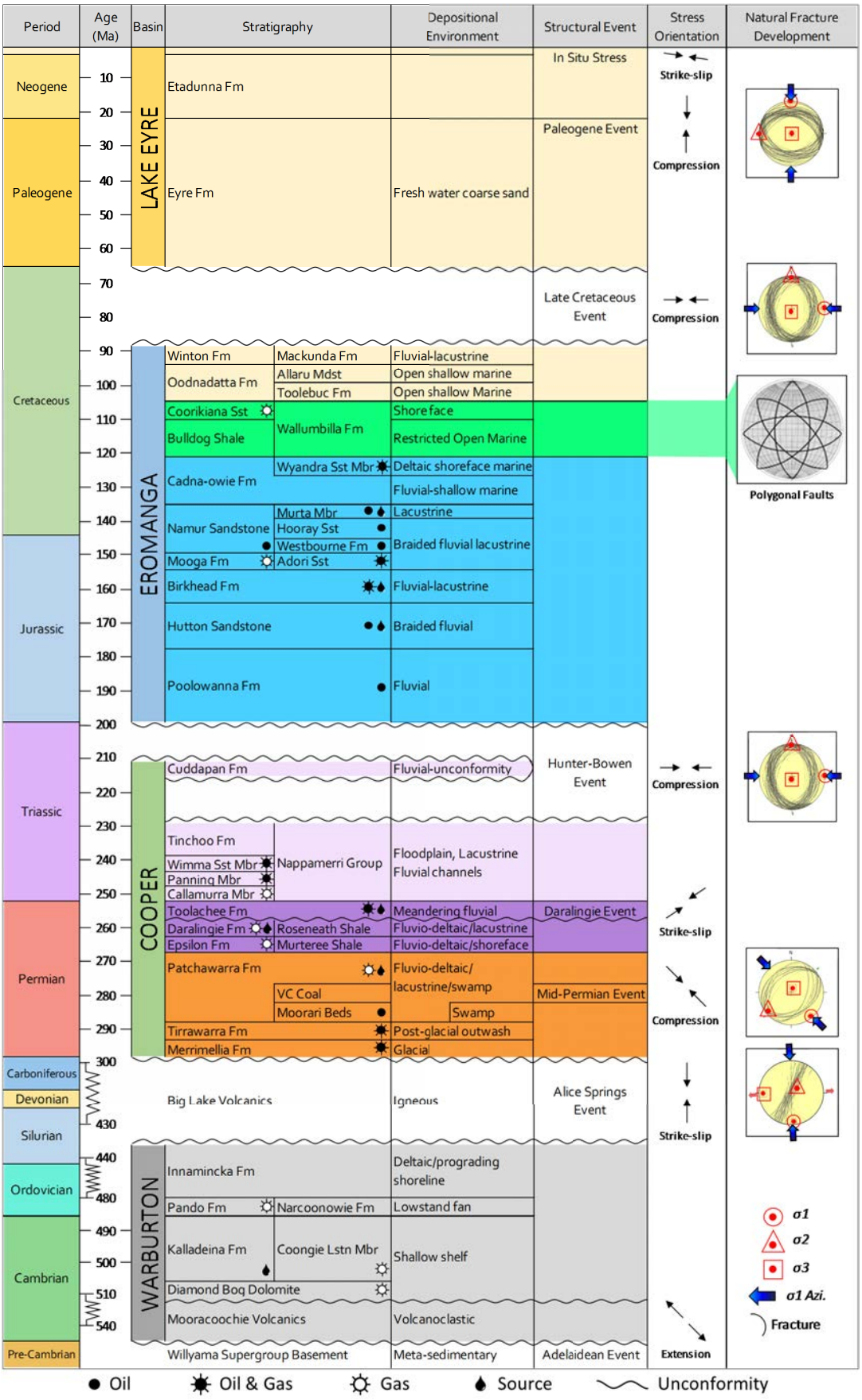

Figure 2. Tectonostratigraphy of the Warburton, Cooper, Eromanga and Lake Eyre basins (after Kulikowski & Amrouch., 2017a).

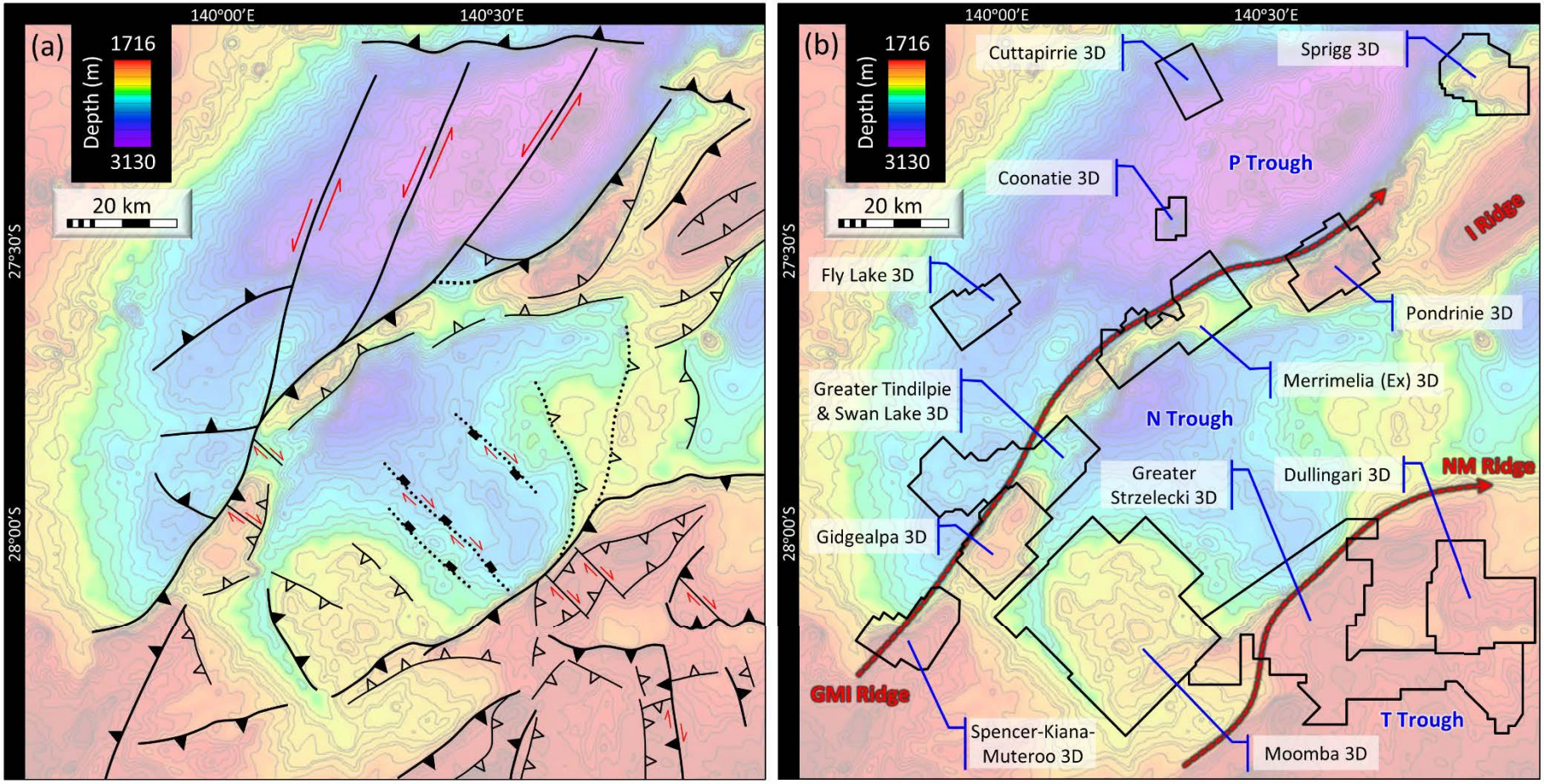

Figure 3. (a) Fault map of the South Australian Cooper-Eromanga basins (after Kulikowski et al., 2017). (b) Location of 12 3D seismic surveys commonly used for research. The location of the Gidgealpa-Merrimelia-Innamincka (GMI) and Nappacoongee-Murteree (NM) ridges, and the Patchawarra (P Trough), Nappamerri (N Trough), and Tenappera (T Trough) troughs are shown (after Kulikowski et al., 2017).

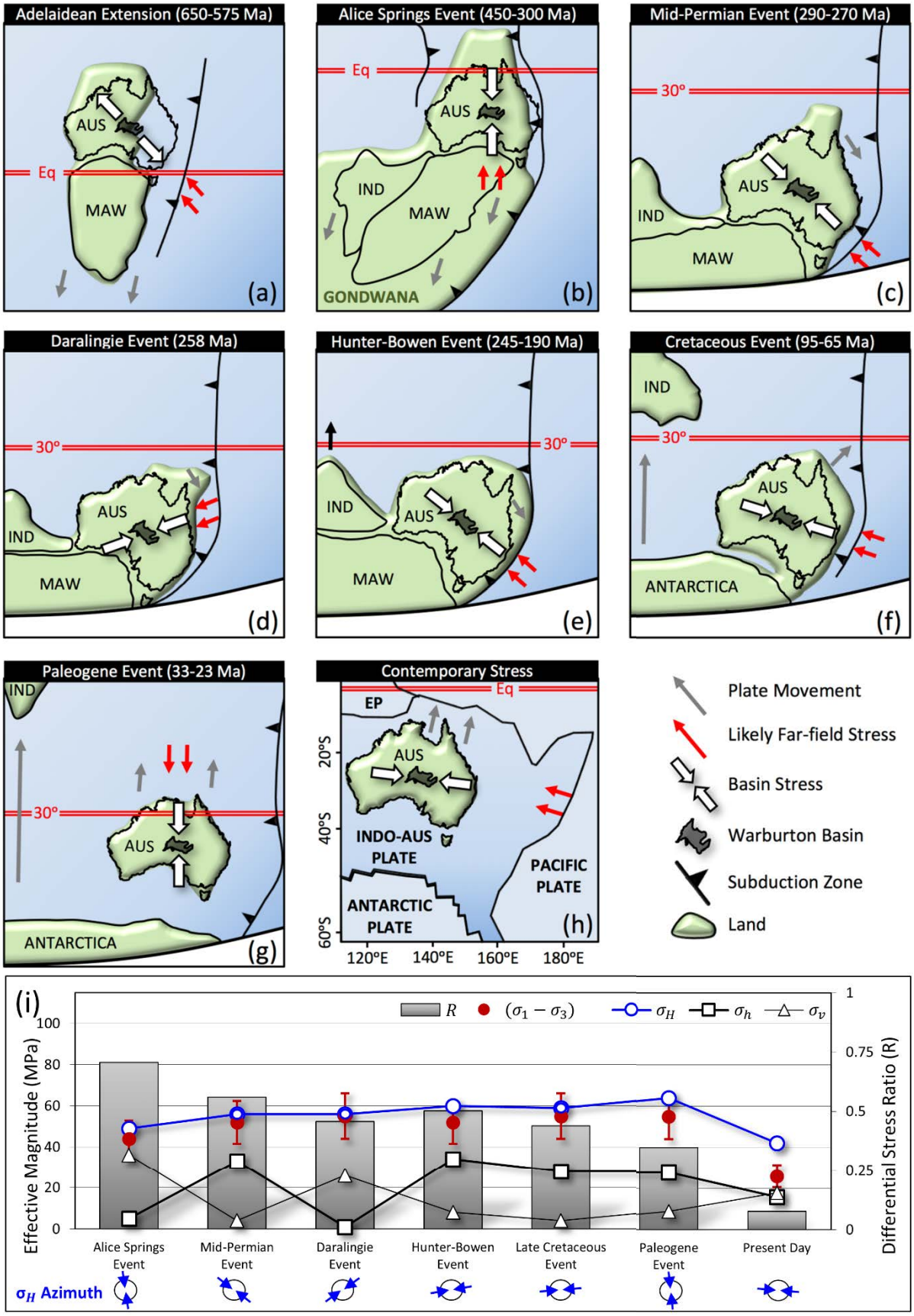
Adelaidean Extension (650-575 Ma)
AUS
Eq
MAW
(a)
Alice Springs Event (450-300 Ma)
Eq
AUS
IND
MAW
GONDWANA
(b)
Mid-Permian Event (290-270 Ma)
30°
AUS
IND
MAW
(c)
Daralingie Event (258 Ma)
30°
AUS
IND
MAW
(d)
Hunter-Bowen Event (245-190 Ma)
30°
IND
AUS
MAW
(e)
Cretaceous Event (95-65 Ma)
IND
30°
AUS
ANTARCTICA
(f)
Paleogene Event (33-23 Ma)
IND
30°
AUS
ANTARCTICA
(g)
Contemporary Stress
Eq
EP
AUS
20°S
40°S
60°S
INDO-AUS PLATE
PACIFIC PLATE
ANTARCTIC PLATE
120°E
140°E
160°E
180°E
(h)
Plate Movement
Likely Far-field Stress
Basin Stress
Warburton Basin
Subduction Zone
Land
(i)
R
$(\sigma_1 - \sigma_3)$
σ_H
σ_h
σ_v
Effective Magnitude (MPa)
Differential Stress Ratio (R)
0
20
40
60
80
100
0
0.25
0.5
0.75
1
Alice Springs Event
Mid-Permian Event
Daralingie Event
Hunter-Bowen Event
Late Cretaceous Event
Paleogene Event
Present Day
σ_H Azimuth

Figure 4. (a)→(h) Geodynamic evolution of Australia with Cooper-Eromanga basins derived stresses through time. (i) Evolution of principal stresses (after Kulikowski & Amrouch, 2017, 2018b).

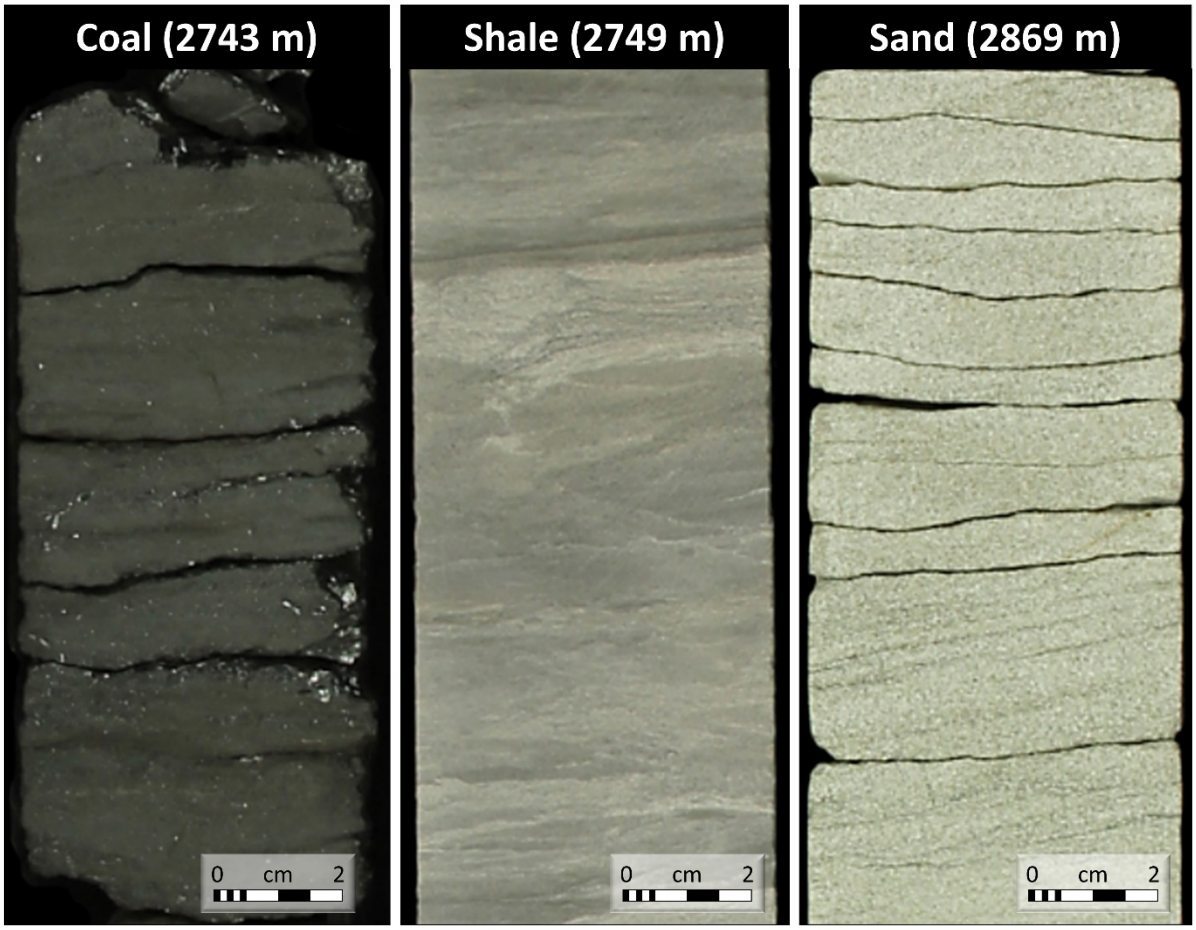

Figure 5. Cyclic lithology variation within the Patchawarra Formation (Core images obtained from Tindilpie 11 well completion report).

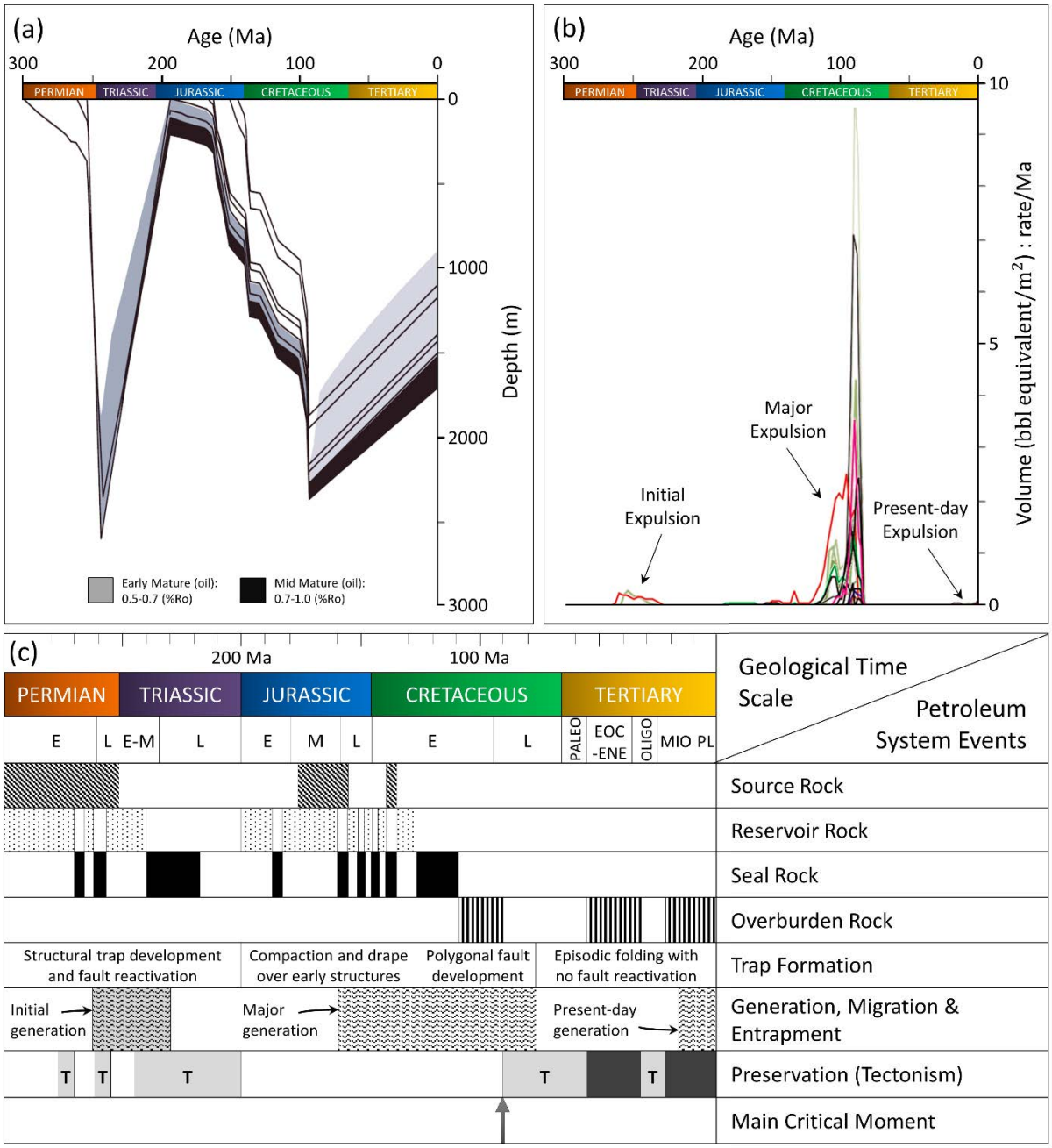

Figure 6. (a) Burial history of Cooper-Eromanga basins (after Mavromatidis, 2006). (b) Gas (per well) and oil expulsion through time (after Deighton & Hill, 2009). (c) Timing of key petroleum system processes (after Lowe-Young et al., 1998).

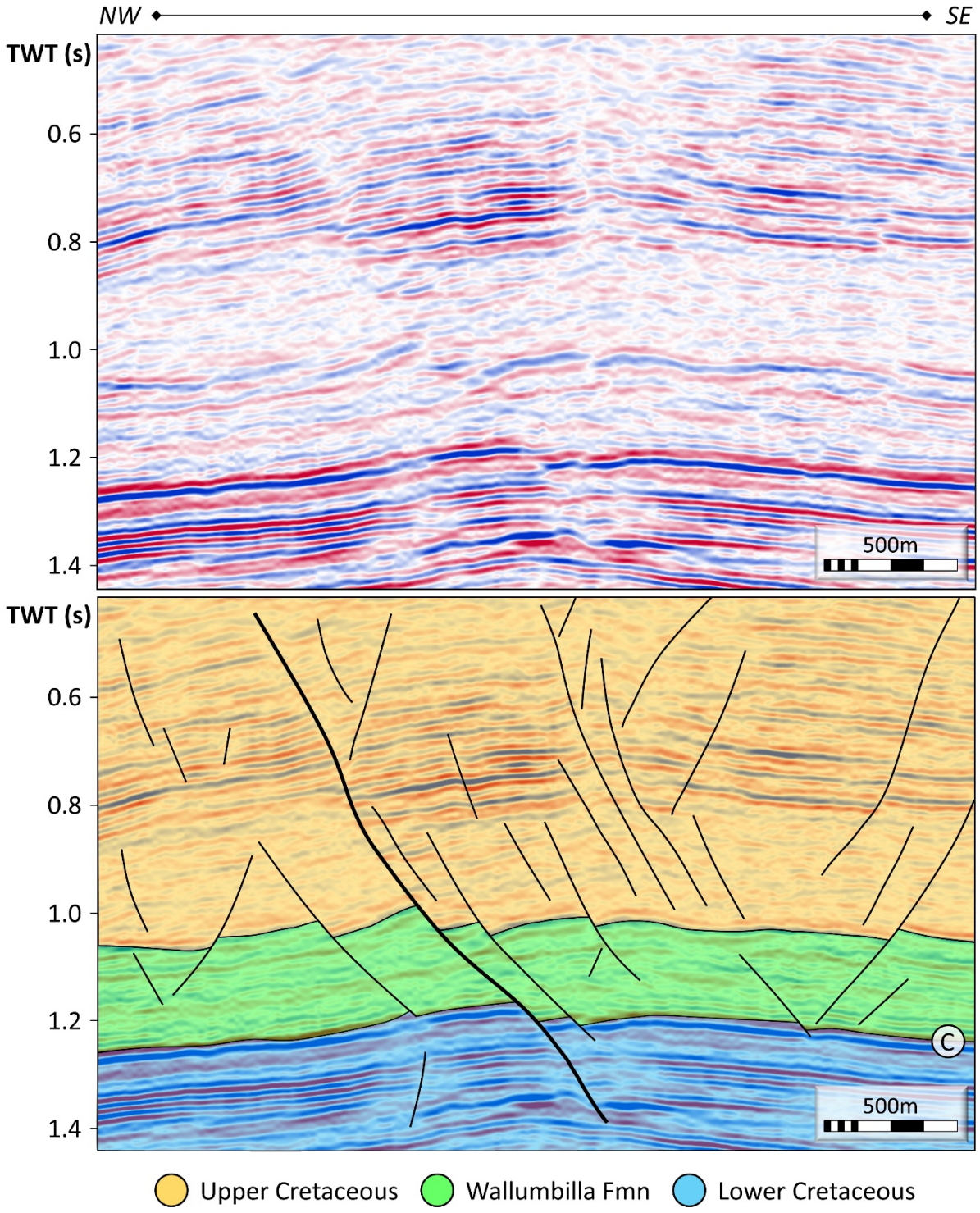

Figure 7. Cross-section from the Spencer-Kiana-Murteree 3D seismic survey (Inline 640) showing the polygonal fault system with large normal faults observed to displace the Cadna-owie Formation reflector and which extend into oil-rich Lower Cretaceous reservoirs (Kulikowski et al., 2017). See Figure 3b for seismic survey location. C-reflector: Cadna-owie Formation.

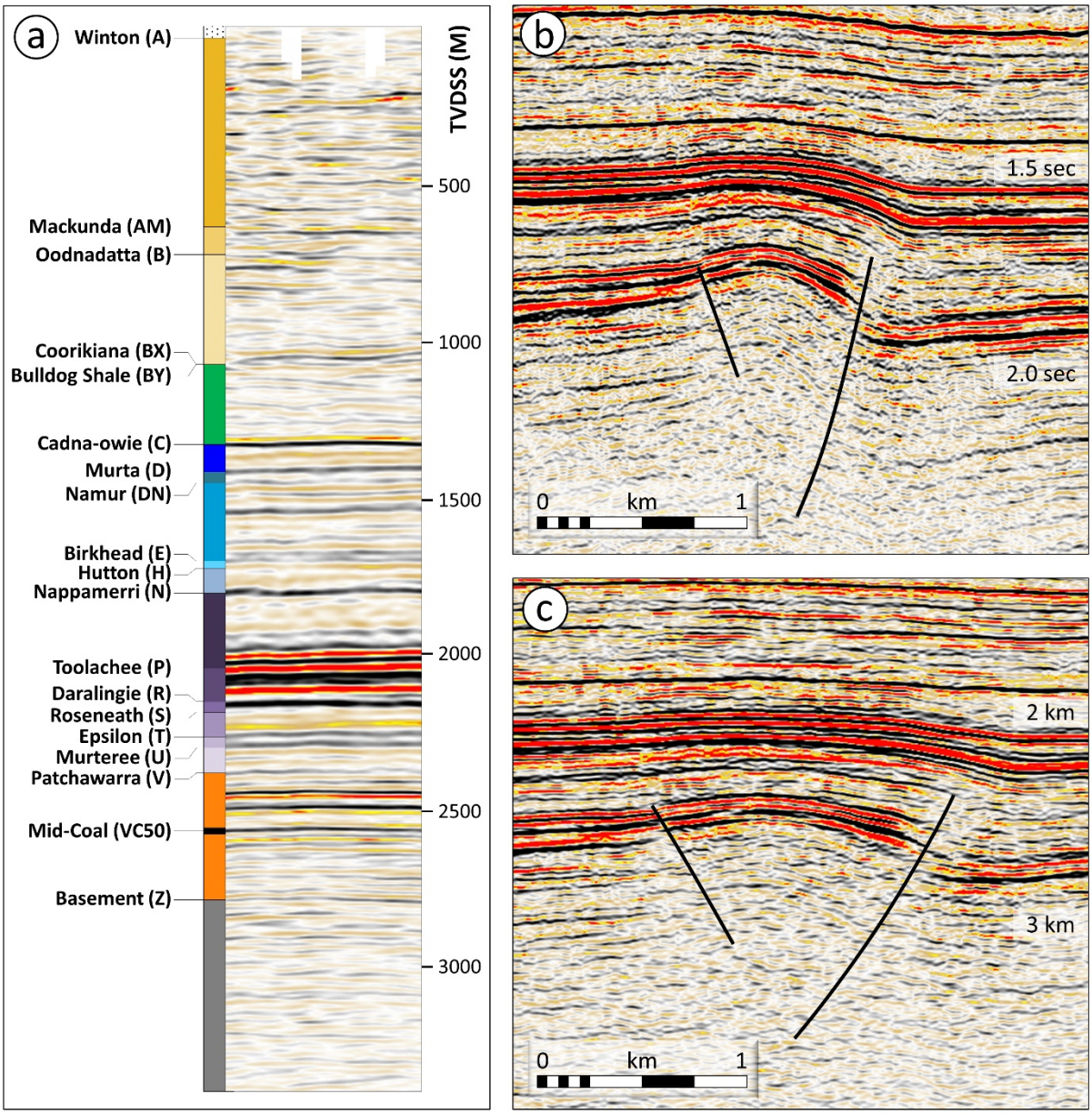

Figure 8. (a) Typical seismic reflection profile showing stratigraphic and seismic markers. The difference in fault geometry when seismic data is in: (b) the time-domain; and (c) the depth-domain. See Figure 2 for stratigraphic names. The markers denote the top of interval.

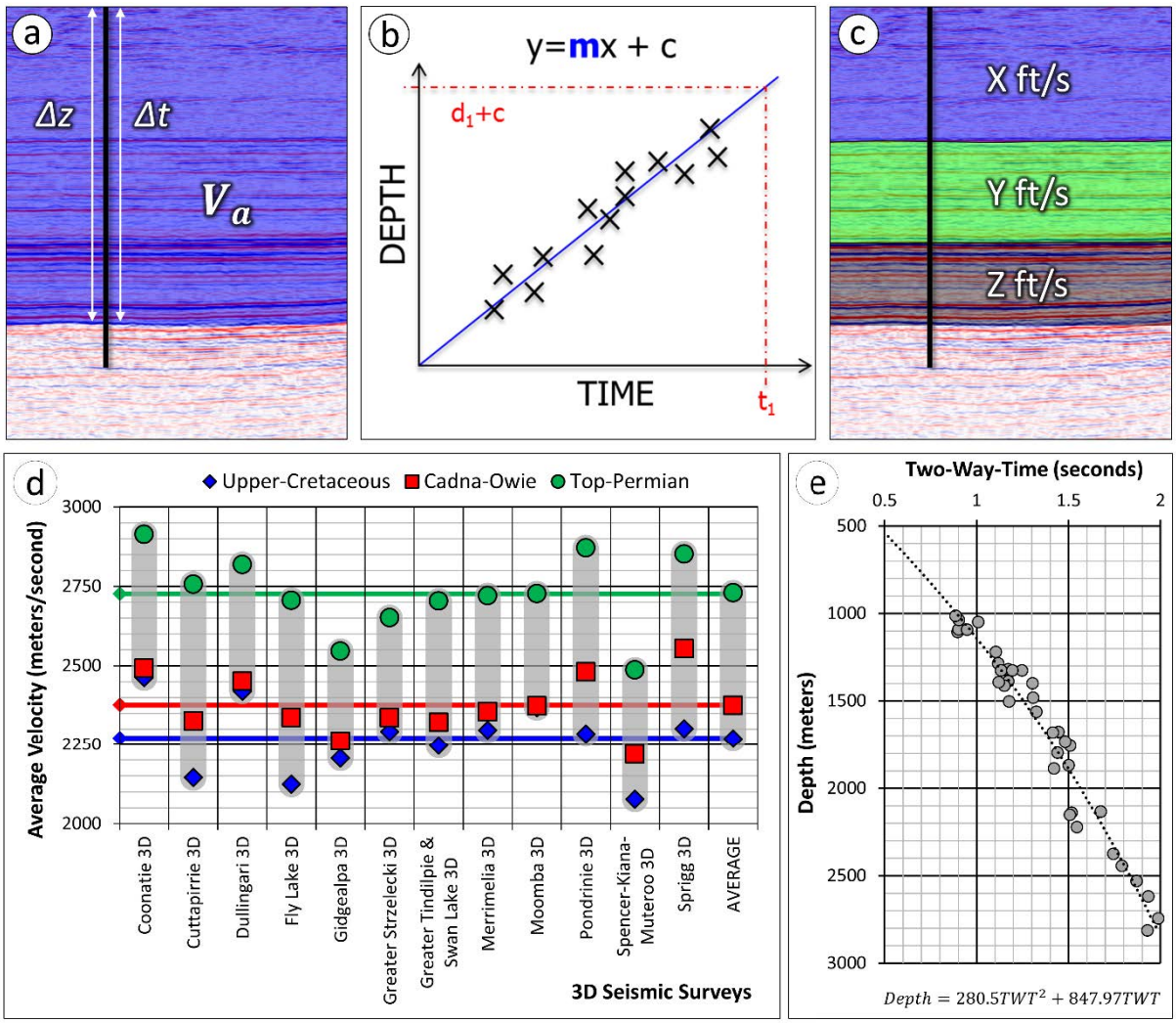

Figure 9. Common seismic time-to-depth conversion methods. (a) Average velocity (V_a) method uses the ratio between depth (from well) and time (from seismic data) for a reflector. (b) Time-depth trend method fits a trend for the time-depth pair data. (c) Interval velocity, or layer-cake, method divides the seismic cross-section into key stratal units and applies different velocities to those layers. (d) Average Velocities for key seismic reflectors. (e) Time-Depth trend obtained from 12 3D seismic surveys (after Kulikowski et al., 2016b, 2017). See Figure 3b for seismic survey location.

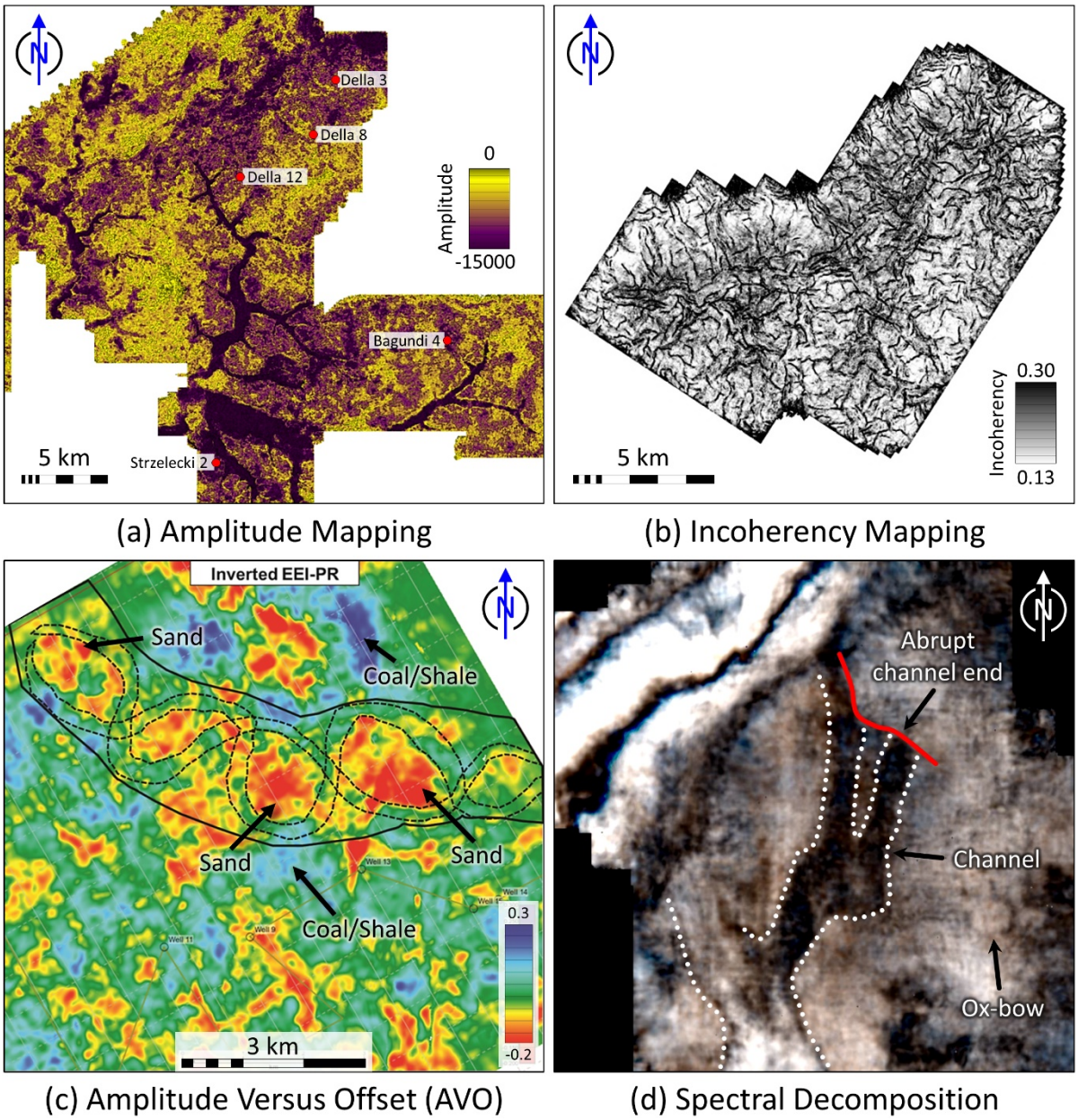

Figure 10. Seismic data analysis techniques beneficial to the fluvial dominated Cooper-Eromanga basins. (a) Amplitudes extracted along reflector surfaces to locate channel systems. Example from Greater Strzelecki 3D showing a large regional channel system (after Kulikowski and Amrouch, 2017); (b) Incoherency analysis along a reflector to identify subtle faults. Example from Spencer-Kiana-Muteroo 3D showing the distribution of polygonal faults along the Upper Cretaceous reflector (after Kulikowski and Amrouch, 2018a); (c) Application of amplitude versus offset (AVO) to differentiate between sandstone and coal measures. The example shows the distribution of sandstone (red-yellow) and shale/coal (green-blue) in the Cooper Basin (after Tyiasning and Cooke, 2015); and (d) Spectral decomposition (colour blending) analysis on the Gaschnitz 3D seismic survey used to delineate the geometry of a fluvial channel and ox-bow feature in the Toolachee Formation, Cooper Basin (Lodwick, 2014).

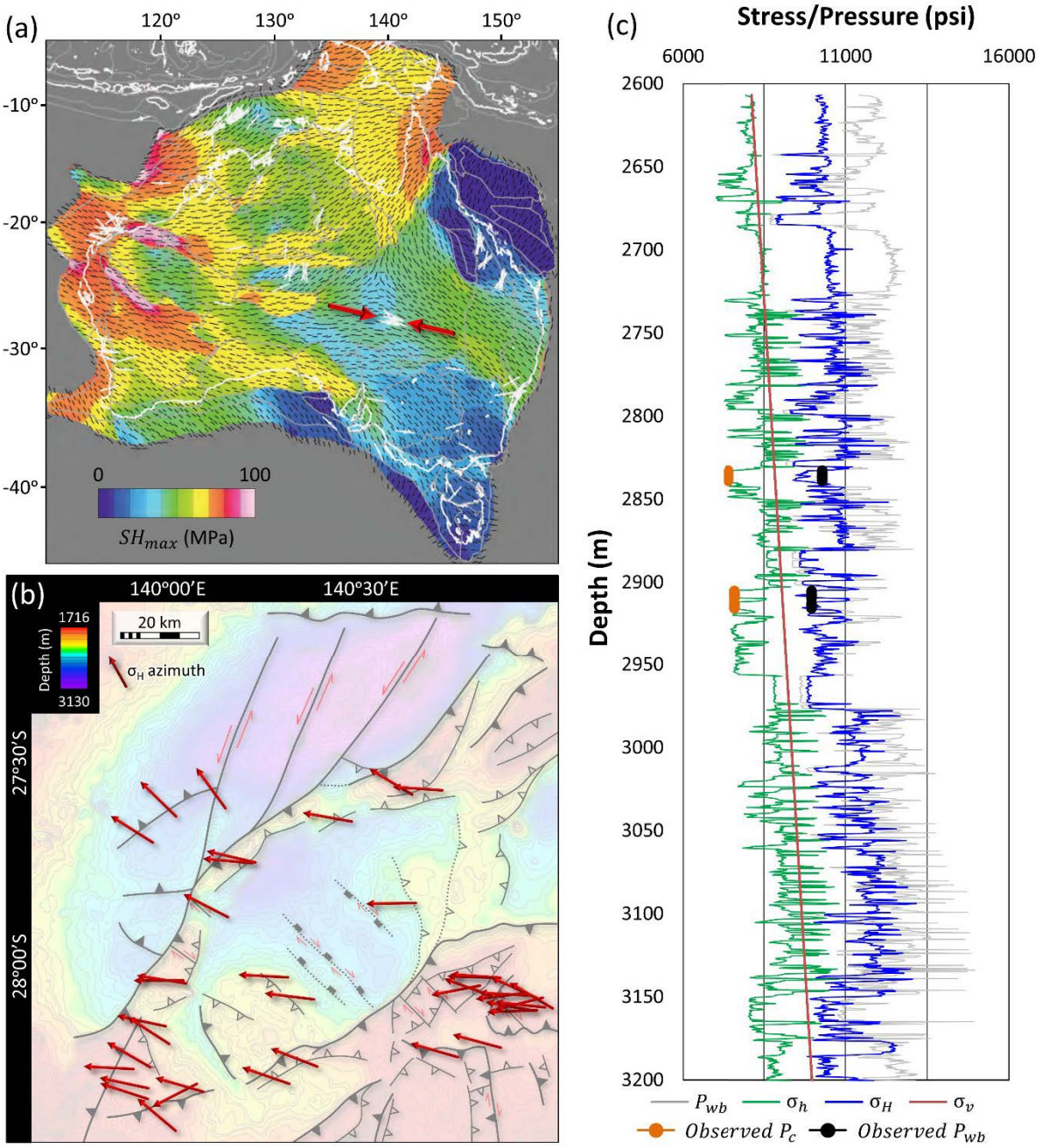

Figure 11. Orientation of the maximum horizontal stress orientation across: (a) Australia (after Müller et al., 2012); and (b) the Cooper-Eromanga basins (after Kulikowski et al., 2017). (c) A typical mechanical earth model for the Patchawarra Formation showing the minimum (σ_h) and maximum (σ_H) horizontal stresses, vertical stress (σ_v), breakdown pressure from logs (P_{wb}) and well test data (observed P_{wb}), and closure pressure (observed P_c) (after Pokalai, 2018). See Figure 4i for the origin of far-field stresses.

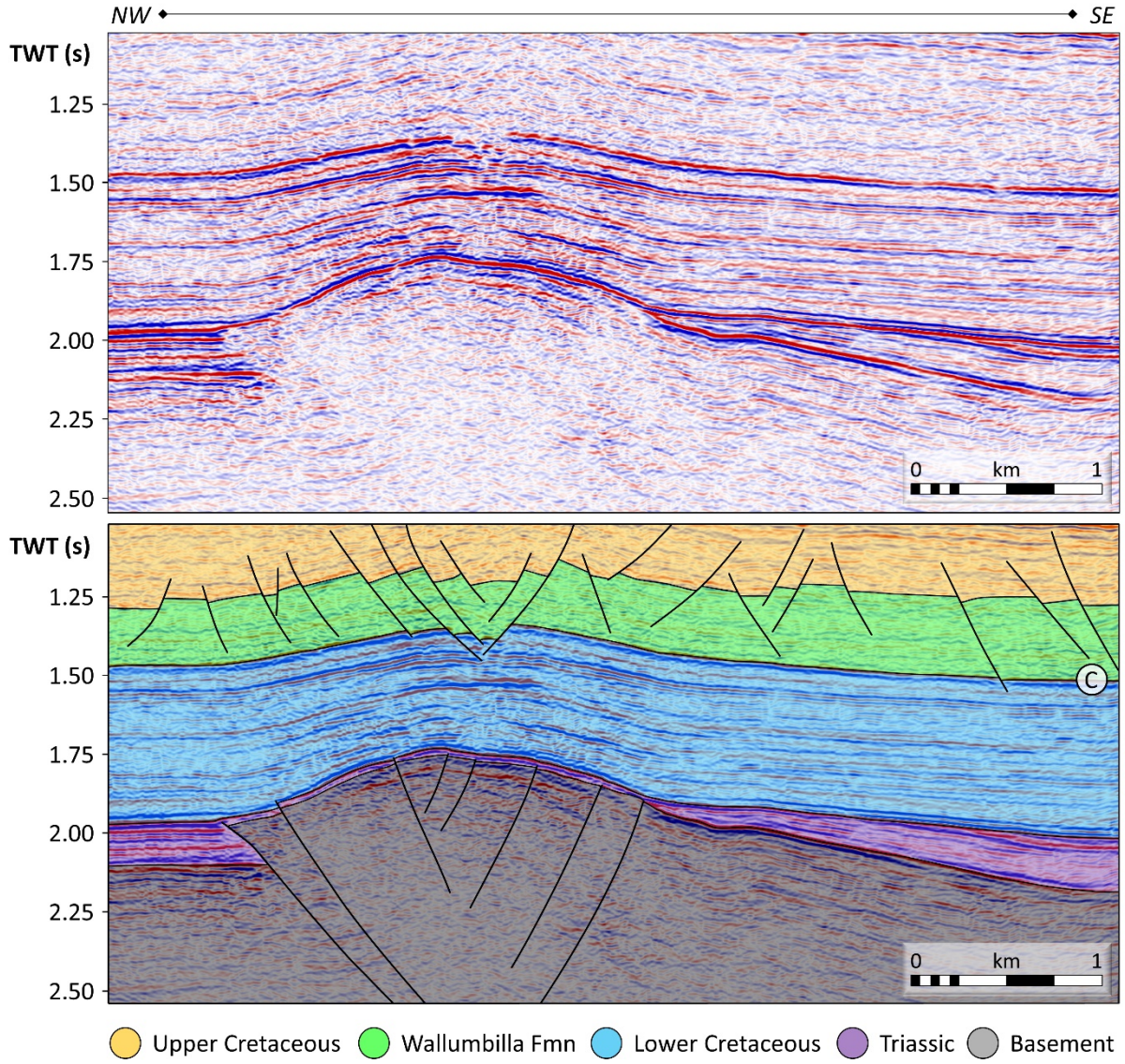

Figure 12. Basement and polygonal faults in the Merrimelia (Extension) 3D seismic survey interpreted along Inline 4295 (Kulikowski et al., 2017). See Figure 3b for seismic survey location. C-reflector: Cadna-owie Formation.

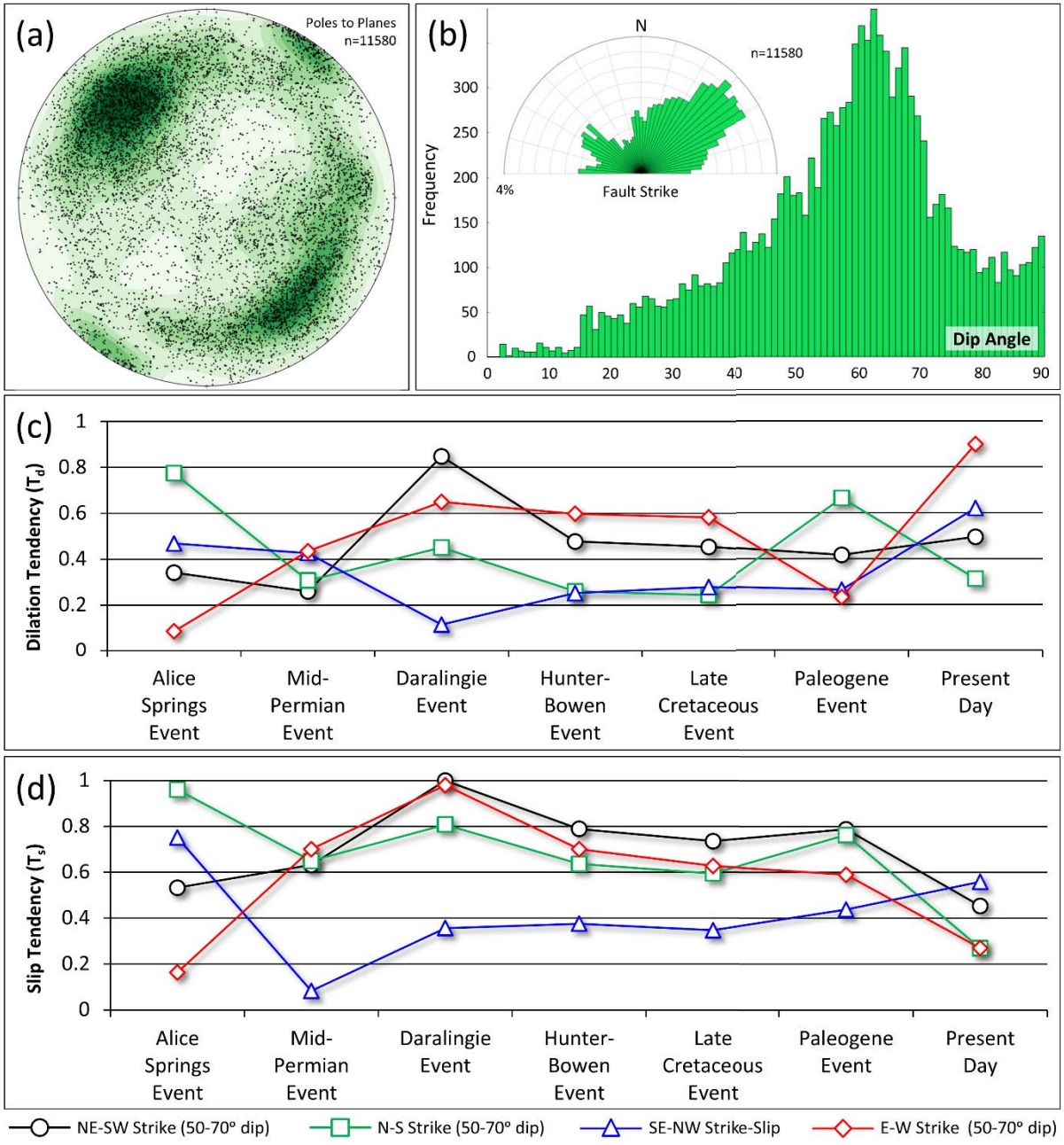

Figure 13. Fault geometry from six 3D seismic surveys (Dullingari 3D, Greater Tindilpie & Swan Lake 3D, Gidgealpa 3D, Greater Strzelecki 3D, Merrimelia (Ext) 3D, and Fly Lake 3D) presented as: (a) poles to planes; and (b) dip and strike (after Kulikowski & Amrouch, 2017a). Reactivation potential of the four most common fault sets measured using the: (c) Dilation Tendency; and (d) Slip Tendency (after Kulikowski & Amrouch, 2018b). See Figure 3 for location of 3D seismic surveys.

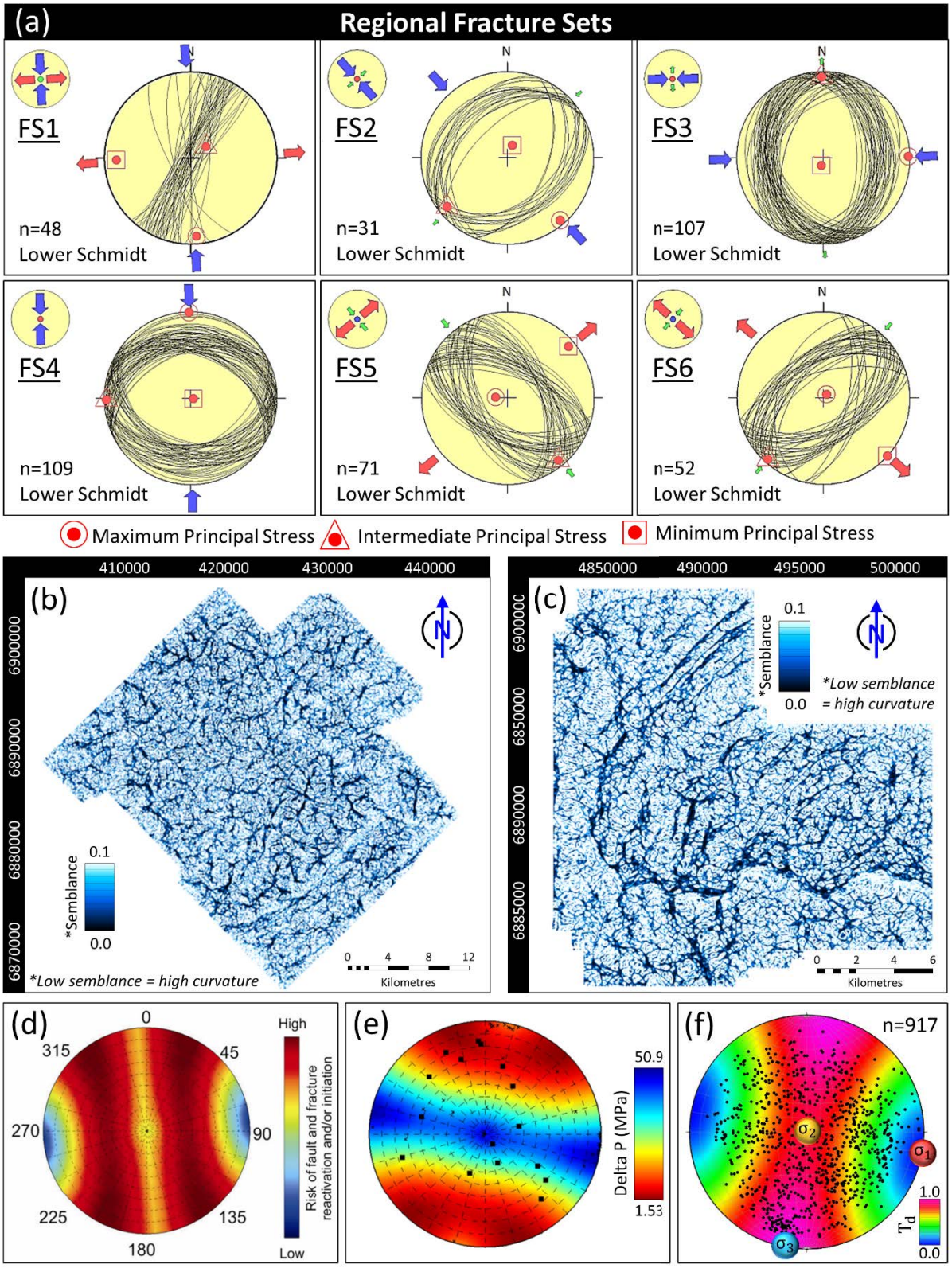

Figure 14. (a) Regional natural fracture sets (Kulikowski & Amrouch, 2017a). Most positive curvature processed into semblance in: (b) Moomba 3D; and (c) Dullingari 3D (Kulikowski et al., 2018a). In situ stress showing: (d) Fracture susceptibility (King et al., 2011); (e) Structural Permeability (Abul Khair et al., 2013); and (f) Dilation Tendency (T_d) (Kulikowski et al., 2017). See Figure 3b for location.

II

Appendix II: Posters and Presentations

In addition to the main body of work within this thesis, a number of spoken and poster presentations were given throughout the three years of candidature.

This poster was presented at the Australian Earth Sciences Convention conference in 2016.

PALEOSTRESS ORIENTATIONS FROM SUBSURFACE AND OUTCROP ANALYSIS IN THE OTWAY BASIN, AUSTRALIA. (Honours Project)

Hugo Burgin, Khalid Amrouch, Mojtaba Rajabi, Simon Holford
The Australian School of Petroleum, University of Adelaide, Adelaide, South Australia, Australia

1. GEOLOGICAL SETTING

Australia's southern, passive margin is believed to have undergone its first extensional event, during the breakup of the super continent Gondwana between 184-145 Ma. This initial phase of rifting is responsible for the formation of the en-echelon series of sedimentary basins straddling its coast line, eg: Bight, Otway and Gippsland. Separation began in the Western Bight Basin, during the Callovian (Mid-Late Jurassic), having propagated east towards the Otway Basin by the Tithonian.

The Otway Basin (Fig.1) is a linear, fault controlled graben that extends on and off shore from the eastern edge of the Duntroon Sub-Basin, south of Kangaroo Island (South Australia), to the western margin of the Bass Basin in Victoria and south into Tasmanian waters. The basin has experienced a number of tectonic events and is structurally complex.

The Structural evolution of the Otway Basin has been widely studied. Although this is the case there continues to be a large degree of uncertainty with respect to the nature of tectonic episodes that have shaped its development. Though many orientations and variations of structural evolution have been proposed, to date no quantitative mechanical data exists to quantify orientations and magnitudes of paleostress regimes within the Basin.

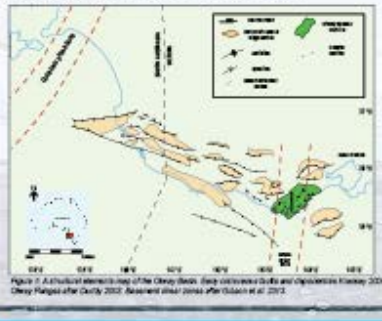

2. METHODOLOGY

The methodology for this study was comprised of a number of:

1) Borehole image log analysis for natural fractures and faults was undertaken within 10 on-shore petroleum wells within the Penola Trough, South Australia.

2) A series of outcrop studies based on identifying natural fracture patterns were completed over a three day field study within the Otway Ranges.

Once identified natural fractures were categorised into eight different sets based upon their degree of dip and dip direction, assigned a conjugate pair and a paleostress regime. Field and well data were analysed seperately using the classification scheme in Table 1.

Additionally, in-situ stress was also calculated using the interpretation of borehole breakouts (BOs) and drilling induced tensile fractures (DITFs).

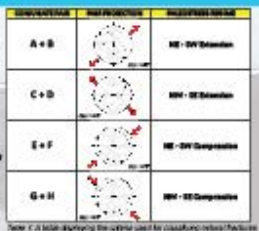

3. RESULTS

Evidence for up to 5 paleo tectonic events was detected from both image log and outcrop analysis (Table 2). No insight into the relative chronology of tectonic events was obtained from well analysis however outcrop studies did reveal that extension orientated NE-SW in all likelyhood preceeded extension orientated NW - SE supporting previous theories suggested by Pelmcek & Cockshell (1994) and Teasdale et al. (2003). This evidence can be seen in figure 6. Additionally both image log analysis and outcrop studies suggested the occurence of a NE - SW orientated compressional event, most likely during the mid - cretaceous. A paleostress regime that to date has not been documented.

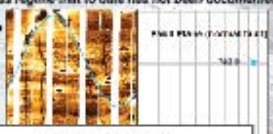

Figure 2: An example of an interpreted fault plane from the image log interpretation of Balnaves 1, within the Eumerella Formation. Displacement of stratigraphic horizons can be observed along the sinusoid.Fault orientation is consistent with NW - SE orientated extension.

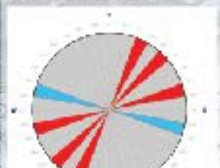

Figure 3: A lower hemisphere projection of identifiable faults from image log interpretation. RED strikes indicate normal faults, BLUE strikes indicate reverse faults.

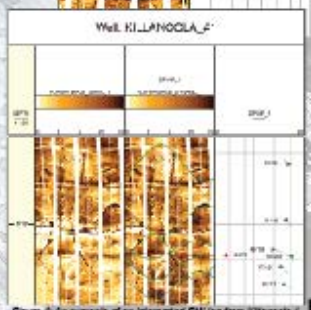

Figure 4: An example of an interpreted FMI log from Killanoola 1 within the Penola Trough, South Australia. Bedding planes appear as red sinusoids and fracture planes appears green sinusoids.

Table 2: A table displaying the orientations of detected paleo tectonic regimes within the specific formations of the study area.

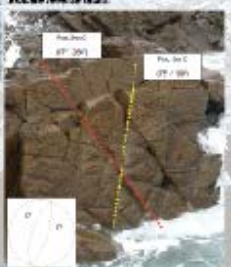

Figure 5: Conjugate fracture pair C and D observed in outcrop along the Great Ocean Road, together the pair form an almost perfect Andersonian example of extension. In this case the orientation of extension was interpreted as NW - SE.

Figure 6: A photograph from the field study showing fracture set C terminating upon fracture set B. From the classification used during this study, this observation implies that NE-SE orientated extension preceeded NW - SE orientated extension.

4. CONCLUSIONS

A number of conclusions can be drawn from the work conducted in this study:

1. Throughout its development the Otway Basin has experienced numerous and extended periods of extension with various orientations.

2. Initial extension within the Otway Basin may have been orientated NE - SW.

3. The Otway Basin may have experienced a compressional event orientated NE - SW during the mid - late Cretaceous Period.

4. Classifying natural fractures - via their degre of dip and dip direction- can provide a largreater insight into the structural evolution of the study area than simply analysing fracture data based upon strike and 2 dimensional orientation.

References

- Gibson, G. M., Totterdell, J. M., White, L. T., Mitchell, C. H., Stacey, A. R., Morse, M. P., & Whitaker, A. (2013). Pre-existing basement structure and its influence on continental rifting and fracture zone development along Australia's southern rifted margin. Journal of the Geological Society, 170(2), 365-377. doi: 10.1144/jgs2012-040
- Krassay, A. A., Cathro, D.L., Ryan, D.J. (2004). A Regional Tectonostratigraphic Framework for the Otway Basin. PESA Eastern Australian Basins Symposium II.
- Pelmcek, D., Cockshell, C. D., Finlayson, D. M., & Hill, R. A. (1994). The Otway Basin: Early Cretaceous Rifting to Miocene Strike Slip. Paper presented at the NOMA/PESA Otway Basin Symposium Abstracts.
- Teasdale, J. P., Ryan, L. L., Stuart-smith, P. G., & Lovibond, M. A. E. T. S. (2003). Structural framework and basin evolution of Australia's southern margin. The APPEA Journal, 43, 19-35.

This poster was presented at the European Geological Union conference in 2017.

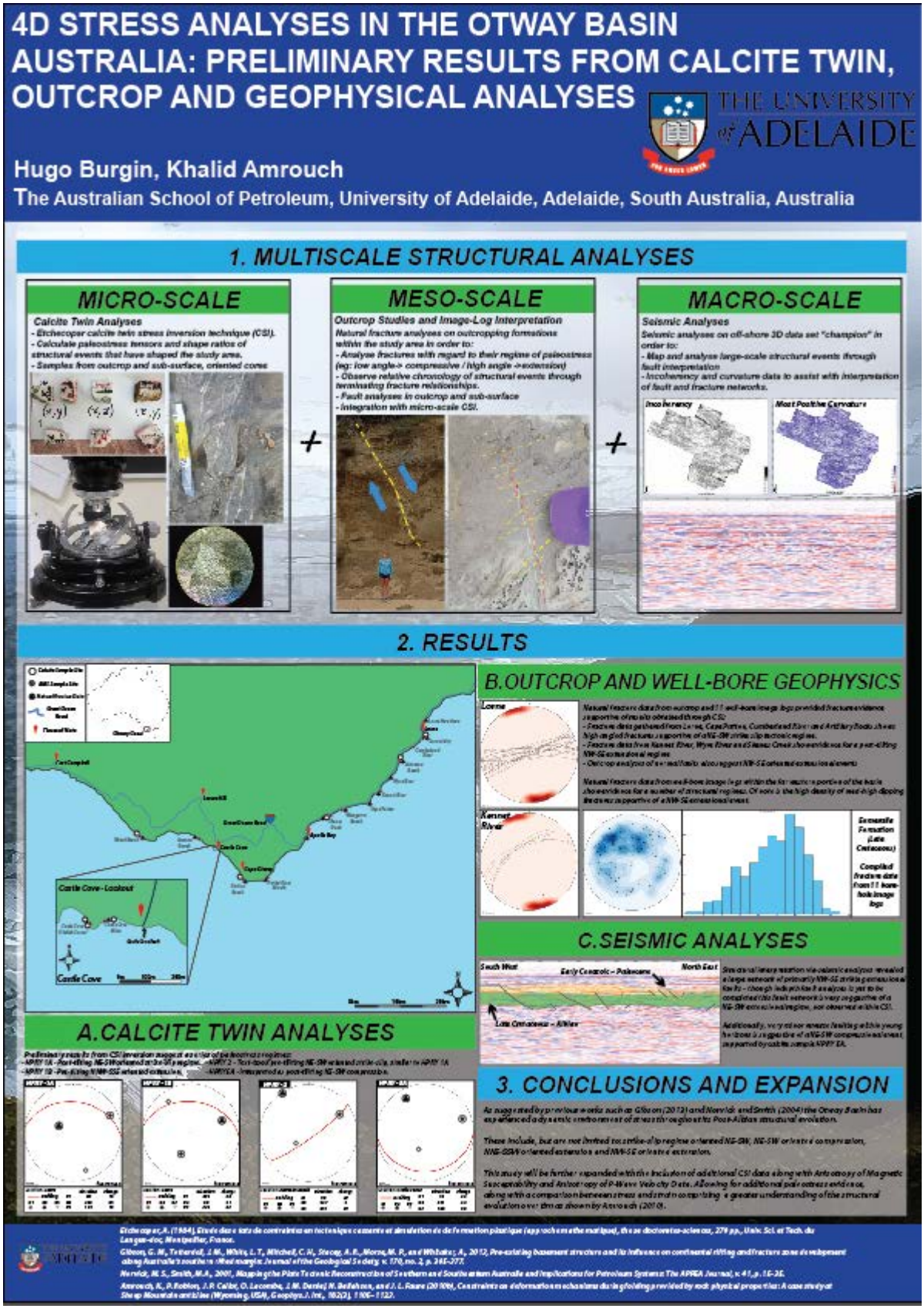

This poster accompanies manuscript 1 and was presented at the APPEA conference in 2018

Determining paleo-structural environments through natural fracture and calcite twin analyses: a case study in the Otway Basin, Australia

Hugo Burgin[1], Khalid Amrouch[1], Mojtaba Rajabi, David Kulikowski[2] and Simon P. Holford[1]

(1) The Australian School of Petroleum, University of Adelaide, Adelaide, South Australia, Australia, (2) Woodside Petroleum, Perth, Australia

Introduction

Paleo-stress inversion is performed on natural fractures and calcite twins from a dataset in the Otway Basin, Australia, to provide insights into the structural history and provide the first quantitative measurement of specific orientations of paleo-stress within the region. The Jurassic to Quaternary Otway Basin (Fig. 1) is a large NW–SE trending sedimentary basin that spans the onshore and offshore parts of South Australia, Victoria and offshore Tasmania. This basin contains hydrocarbon accumulations, geothermal energy potential, and CO2 storage capabilities, all of which require an understanding of subsurface natural fracture distributions and accurate basin development models. Current models show that initial rifting commenced during the Late Jurassic with multiple phases of extension and compression, responsible for the formation of stratigraphic and structural complexities (Norvick and Smith 2001). For the first time the meso- and micro-scale structural history of the Otway Basin is investigated through the 4D analysis of natural fractures obtained from geophysical well data located in the Penola Trough and from outcrop located in the Otway Ranges, with a calcite twin analysis performed on a sample obtained from the Otway Ranges. This study provides valuable information on the: (1) spatial distribution of natural fractures; (2) the temporal distribution of regional natural fracture sets; and (3) constraints on the stress orientation and regime of structural events.

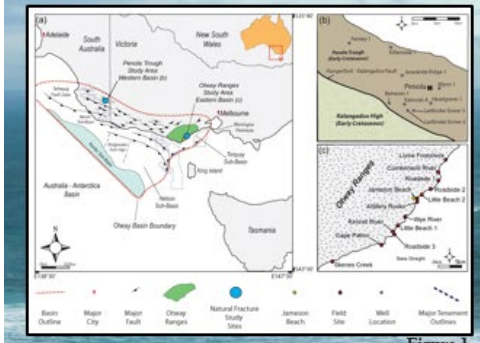

Figure 1

Fig. 1: (a) A map of Australia's southern margin showing the location of the Otway Basin, along with some major structural elements, after Moore et al. (2000) and Krassay et al. (2004). (b) Locations of sub-surface image logs in the Penola Trough. (c) Field sites in the Otway Ranges.

1. Natural Fracture Analysis

Within this study, our interpretation of natural fracture data is based upon the statistical analyses of fracture strike and dip angles, in combination with fracture-bedding relationships. Additionally, the principal stress orientation tool, Win-Tensor (Delvaux and Spemer 2003), was used to constrain the specific sets and assign regional directions of the three principal stresses. Our approach was based upon the fundamental principles of rock failure, with a heavy emphasis on the three Andersonian environments of stress (Anderson 1905) (Fig. 2). The geometry of these regional natural fracture sets are dependent on the relationship between the three principal stresses (σ1, σ 2 and σ 3) and the precise mode of fracturing (I, II or III). An understanding of these fracture geometries, in addition to their relationship with the bedding, allows us to gain insights into the likely stress environment responsible for their development and relative chronology. Results from our fracture analysis are presented in Fig. 3.

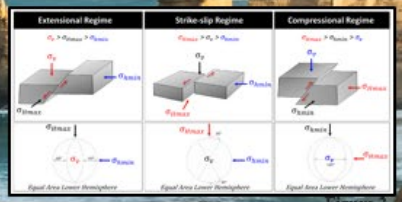

Figure 2

Fig. 2: A schematic diagram showing the three Andersonian stress environments (Anderson 1905) in addition to text book fracture sets formed under their conditions.

Fig. 3: Orientation of the major fracture sets categorised by dip degree and dip direction as part of this study. For well data, these sets include all detected fractures across all penetrated formations with image logs. Field data includes fractures from all 13 localities studied within the Eumeralla Formation. See Fig. 1 for location of wells and field sites.

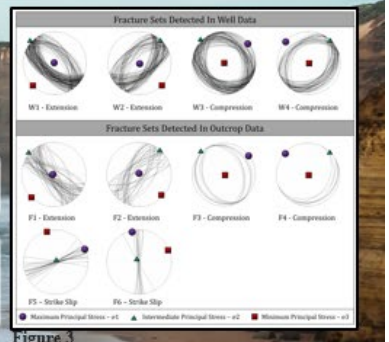

Figure 3

2. Calcite Twin Analysis

Mechanical twinning within calcite (Fig. 4) is a plastic deformation that occurs at low temperatures (25–400°C) and low confining pressures. The process of e-twinning – twinning along the 'e' plane of the crystal lattice – is easily compared with a zone of simple shear. The calcite twin stress inversion technique is similar to the technique used to analyse slickensides on a fault plane (Etcheconar, 1984). The technique consists of developing the best fit tensor for the distribution of twinned and un-twinned e-planes within the sample. Within this study, the use of calcite twin analysis is to: (1) compare the quantitative results with those from natural fracture analysis; and (2) test the regions suitability for more extensive calcite twin analysis. Two possible tensors were produced and are presented in Fig. 5.

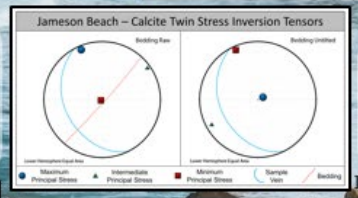

Figure 5

Fig. 5: Lower hemisphere equal area stereonet plots displaying the paleo-stress tensors derived from Etcheconar's (Etcheconar, 1984) calcite twin stress inversion technique (CSIT) measurements at Jameson Beach. See Fig. 1 for location.

Figure 4

Fig. 4: (a) A satellite image (Google Earth 2018) showing the orientation of the vertical bedding within a wave platform at Jameson Beach. The Great Ocean Road can be seen running past on the left (b) A photograph taken in the field showing the sampled vein at Jameson Beach in the Otway Ranges. (c) A universal stage microscope used to measure the spatial orientation of the twinned and un-twinned planes within the crystal and angles of extinction of the calcite crystals. (d) The calcite filled vein – in the Z orientation – from Jameson Beach. The sample is within the Eumeralla Formation

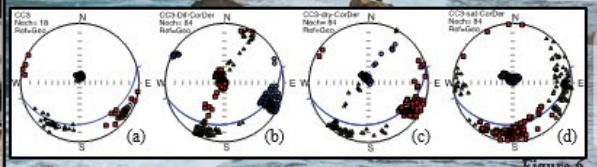

Figure 6

Fig. 6: An example of future work being completed within the basin. lower hemisphere equal area stereonet plots displaying petrophysical data. (a) An example of AMS tensors (b) Differential tensors for APV data (saturated – dry) conditions (c) Example of APV tensors measured with a dry sample (d) Example of APV tensors measured under saturated conditions.

3. Conclusions

Following the analysis of subsurface and outcrop natural fracture data, the structural evolution of both the western and eastern Otway Basin may be considerably more variable and complex than previously thought, especially from the Late Cretaceous until present, which is the most important window for hydrocarbon exploration and production.

- There is natural fracture evidence for multiple paleo-stress regimes including several episodes of extension, strike slip and compression many of them following the deposition of the Eumeralla formation in the Late Cretaceous.
- Calcite twin stress inversion presents two possible stress tensors which both align with natural fracture data
- Strike slip stress regimes may be unique to the eastern Otway Basin.
- Evidence for previously undetected compression oriented NE-SW.
- Calcite within the Eumeralla formation is spartic and well enough deformed presenting a good opportunity for further calcite twin stress inversion studies.

4. Future Work

This project is being expanded as part of a PhD at the Australian School of Petroleum. The goal of future work is to complete a multi-scale structural analysis of stress and strain within the study area. This includes:

- Additional and more detailed field studies within the region.
- The structural analysis of 2D and 3D seismic data within the basin.
- Additional calcite twin stress inversion from outcrop and subsurface samples.
- Petrophysical analysis (AMS and APV) in order to analyse grain-scale deformation (Fig. 6).
- Fault modelling and assessment of present day environments of stress.

References

- Anderson, E. (1905). The dynamics of faulting. The Journal of Geology 14, (3), 254-257.
- Delvaux, D., and Spemer, B. (2003). Stress tensor inversion from fault kinematic indicators and focal mechanism data: the TENSOR program. In New Insights into Structural Interpretation and Modelling (D. Nieuwland Ed.). Geological Society, London, Special Publications, 212: 75-100
- Etcheconar, A. (1984). Etude des états de contraintes en tectonique cassante et simulation de déformations plastiques (Ph.D these). Montpellier, France, Université Montpellier p. 270 p.
- Krassay, A. A., Cathro, D. L., Ryan, D.J. (2004). A Regional Tectonostratigraphic Framework for the Otway Basin. PESA EABS II
- Moore, A. M. G., Shiraj H. M. I. and Norvick M. S. (2000). Deep-water Otway Basin: A New Assessment of the Tectonics and Hydrocarbon Prospectivity. *The APPEA Journal, 40*, 66-85.
- Norvick, M. S., and Smith, M.A. (2000). Mapping the Plate Tectonic Reconstruction of Southern and Southeastern Australia and Implications for Petroleum Systems. The APPEA Journal, 41, 15-35.

This poster accompanies manuscript 2 and will be presented at the APPEA conference in 2019

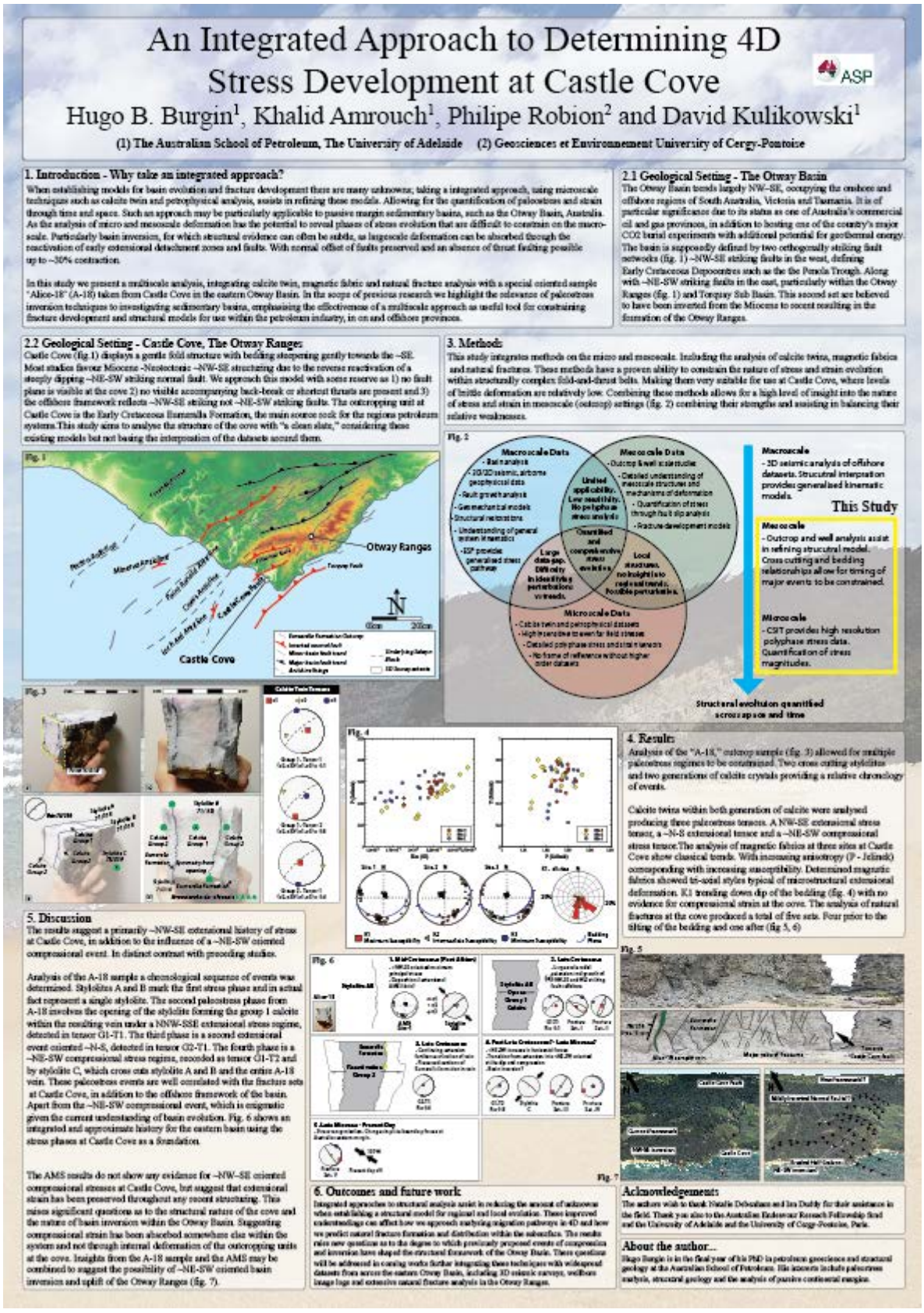

This poster accompanies manuscript 6 and will be presented at the European Geological Union conference in 2017

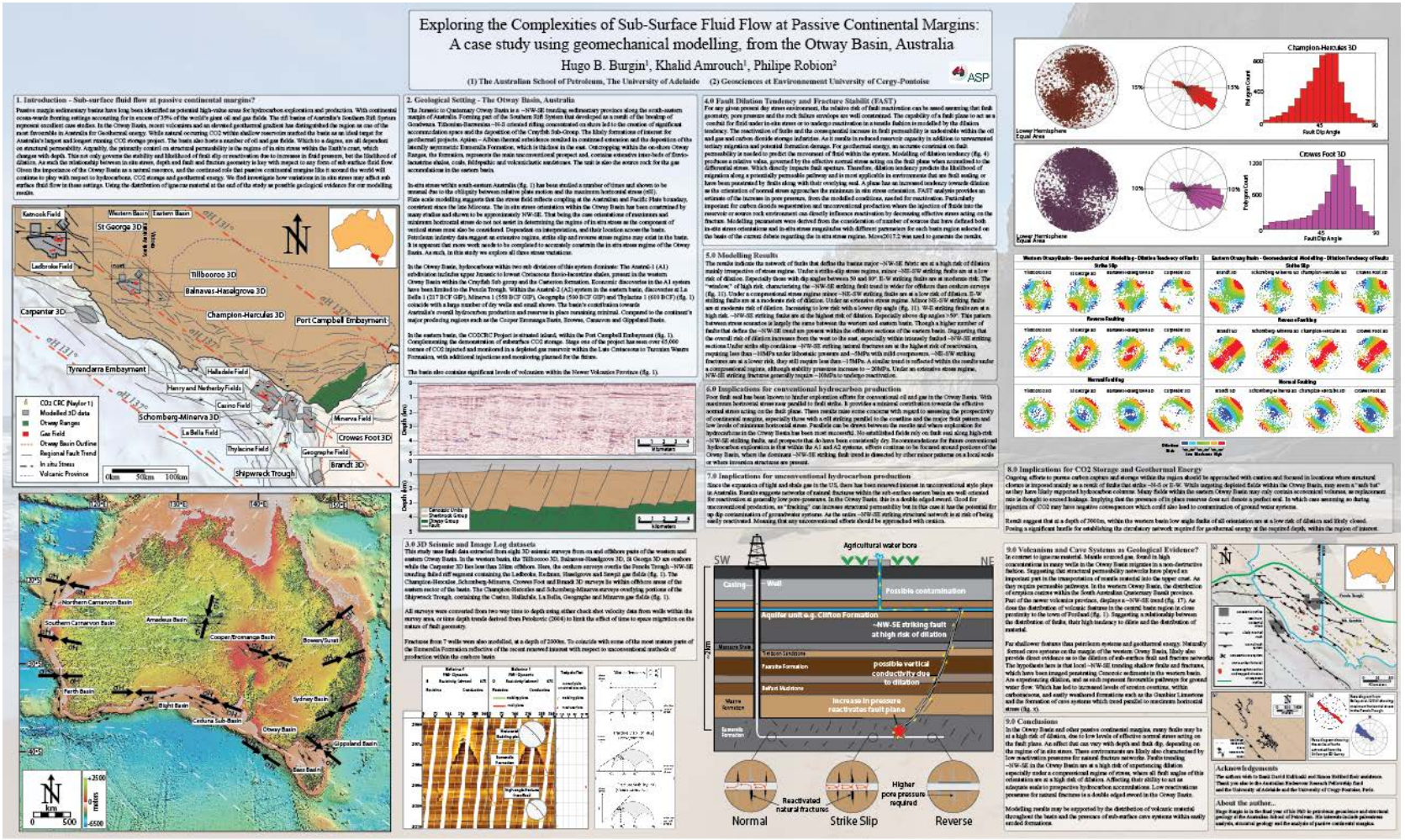

This spoken presentation was presented to colleagues at the Australian School of Petroleum as part of the requirements of the major review for candidature progression.

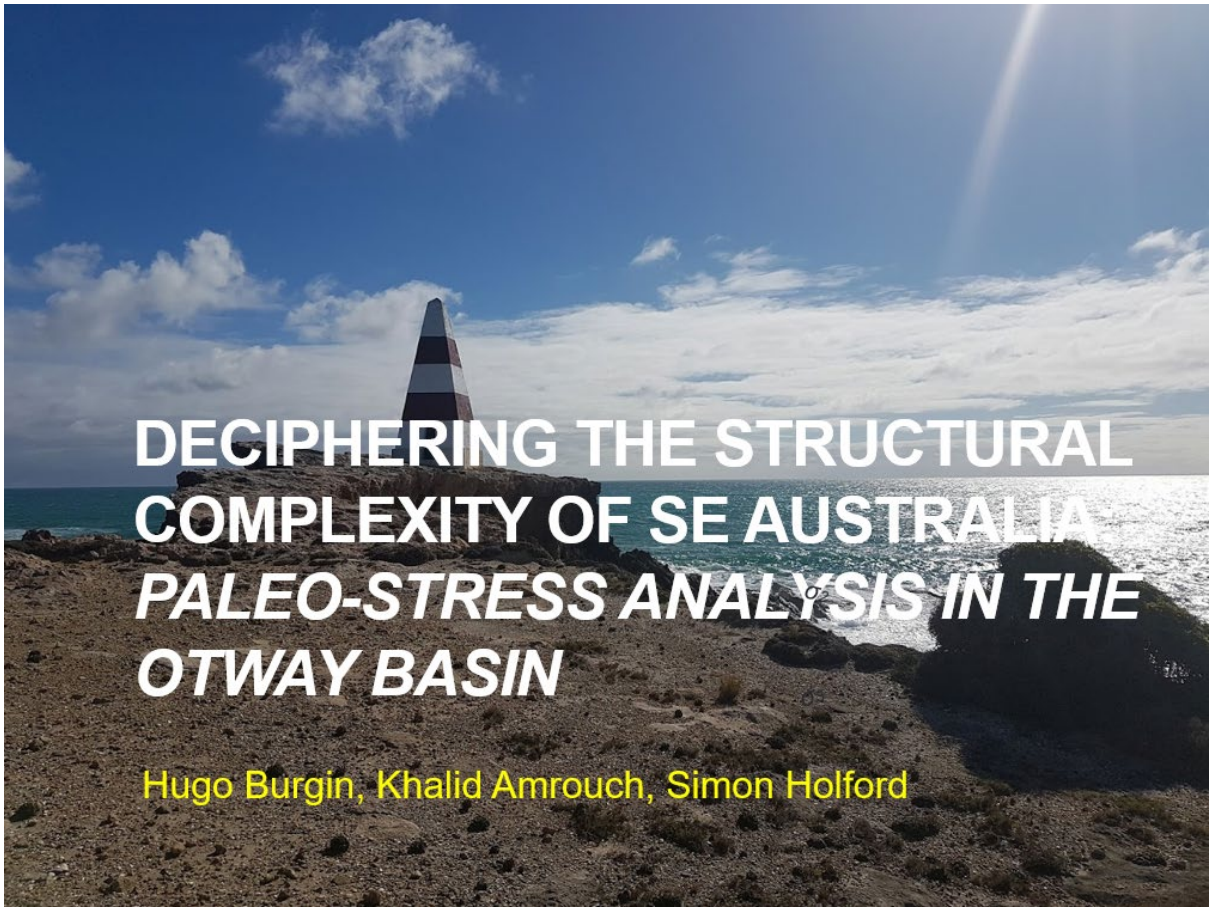

.

This spoken presentation was given to staff at Beach Energy as part of an efforts to actively involve the Australian oil and gas industry in this project.

Multi-Scale Structural Analyses in the Otway Basin

Hugo Burgin
Khalid Amrouch
Simon Holford

ASP
Australian School of Petroleum

THE UNIVERSITY of ADELAIDE

This spoken presentation was given to staff at ExxonMobil as part of the interview process for a secured position as a graduate geoscientist.

Hugo Burgin
Hugo.burgin@adelaide.edu.au

Structural Analyses and Paleo-Stress in the Otway Basin

adelaide.edu.au

ASP
Australian School of Petroleum

Journal of Structural Geology 114 (2018) 336–345

Contents lists available at ScienceDirect

Journal of Structural Geology

journal homepage: www.elsevier.com/locate/jsg

Mapping permeable subsurface fracture networks: A case study on the Cooper Basin, Australia

David Kulikowski*, Khalid Amrouch, Hugo B. Burgin

Australian School of Petroleum, University of Adelaide, North Terrace, 5005, Adelaide, Australia

ARTICLE INFO

Keywords:
Cooper basin
Fracture
Fault
Seismic
Curvature
Geomechanics

ABSTRACT

The spatial distribution of permeable fracture networks is constrained in the subsurface Cooper Basin (Australia) through the integration of most positive curvature (K_+) analysis of five three dimensional (3D) seismic surveys, wellbore fracture data, and geomechanical modelling. The K_+ provides the likely distribution of subsurface extensional fractures based on the stress redistribution along the outer arc of an anticline. These results are reprocessed into the semblance (similarity) attribute to improve the signal-noise ratio prior to being extracted along the gas-rich and low permeability Patchawarra Formation. The subsurface fracture distribution maps show the geometry and density of extensional fractures that have been shown to facilitate fluid migration in this province, particularly those striking SE-NW and E-W, as these are properly oriented to undergo tensile re-activation. The density of these permeable SE-NW and E-W striking fracture sets is predicted to significantly increase along E-W elongate anticlines and may contribute to improved hydrocarbon recovery in this low permeability stratigraphic interval. We show that wellbore fracture data (n = 917) in the Patchawarra Formation presents a close relationship to K_+ results and can be used to generate high density structural data in this basin, with the methodology applicable to other subsurface and offshore provinces.

1. Introduction

Recent developments in three-dimensional (3D) seismic data analysis (Roberts, 2001; Chopra and Marfurt, 2007; Robson, 2017; Robson et al., 2018) have enabled high density structural information to be collected from subsurface and offshore provinces. Fractures detected from the most positive curvature (K_+) seismic attribute have been shown to correlate with outcrop and wellbore data in many provinces (e.g. Murray, 1968; Lisle, 1994; Stewart and Podolski, 1998; Hakami et al., 2004; Al-Dossary and Marfurt, 2006; Chopra and Marfurt, 2007; Bailey et al., 2014), and provides detailed constraints on the distribution of subsurface structures that can be highly beneficial in many industries related to carbon dioxide sequestration, low permeability hydrocarbon production, mining, and geothermal energy. As K_+ does not solely rely on reflector displacement, it can be used to predict the presence of extensional fractures based on the stress redistribution along the outer arc of an anticline (Murray, 1968; Ferrill and Groshong, 1993; Roberts, 2001). Understanding this concept, the distribution of extensional fractures can be selectively predicted. In the hydrocarbon-rich and low permeability Cooper Basin, Australia, these high angled fractures are critically oriented to facilitate fluid migration (Backe et al., 2011; Kulikowski, 2017; Kulikowski and Amrouch, 2017). There, the geometry and distribution of these regionally pervasive fractures are presently derived from wellbore locations, and due to their high angle nature, may not be accurately represented in vertical wellbores.

Using this basin as a case study, this research integrates K_+ analysis, wellbore fracture data, and geomechanical modelling to map the spatial distribution of the regionally pervasive and permeable high ($> 50^0$) angled fractures within the gas-rich and low permeability Patchawarra Formation (Kulikowski and Amrouch, 2017). Five 3D seismic surveys are time-to-depth converted, analysed using the K_+ attribute, processed into semblance attribute volumes to improve the signal-noise ratio before being extracted along the Patchawarra Formation, and finally compared to fracture data derived from 28 wellbores. Geomechanical modelling is incorporated into the methodology to determine the fracture sets that are critically oriented to undergo tensile reactivation and facilitate fluid migration under in-situ stress conditions. The connection between wellbore derived high ($> 50^0$) angle fractures and K_+ results is also discussed for this province. This integrated methodology is carefully applied and can benefit other subsurface or offshore provinces, given adequate geophysical data coverage, to extract important structural data that would otherwise be derived only from sparse wellbore locations.

* Corresponding author.
E-mail addresses: david.kulikowski@adelaide.edu.au (D. Kulikowski), khalid.amrouch@adelaide.edu.au (K. Amrouch), hugo.burgin@adelaide.edu.au (H.B. Burgin).

https://doi.org/10.1016/j.jsg.2018.02.009
Received 19 December 2017; Received in revised form 19 February 2018; Accepted 22 February 2018
Available online 23 February 2018
0191-8141/

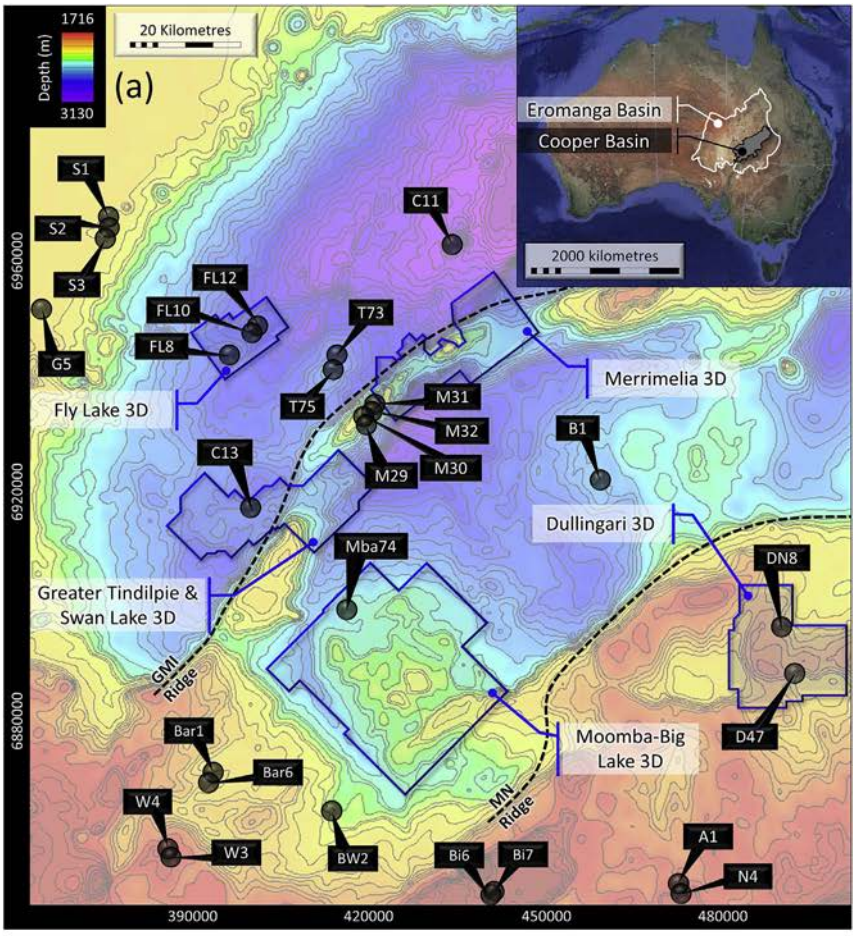

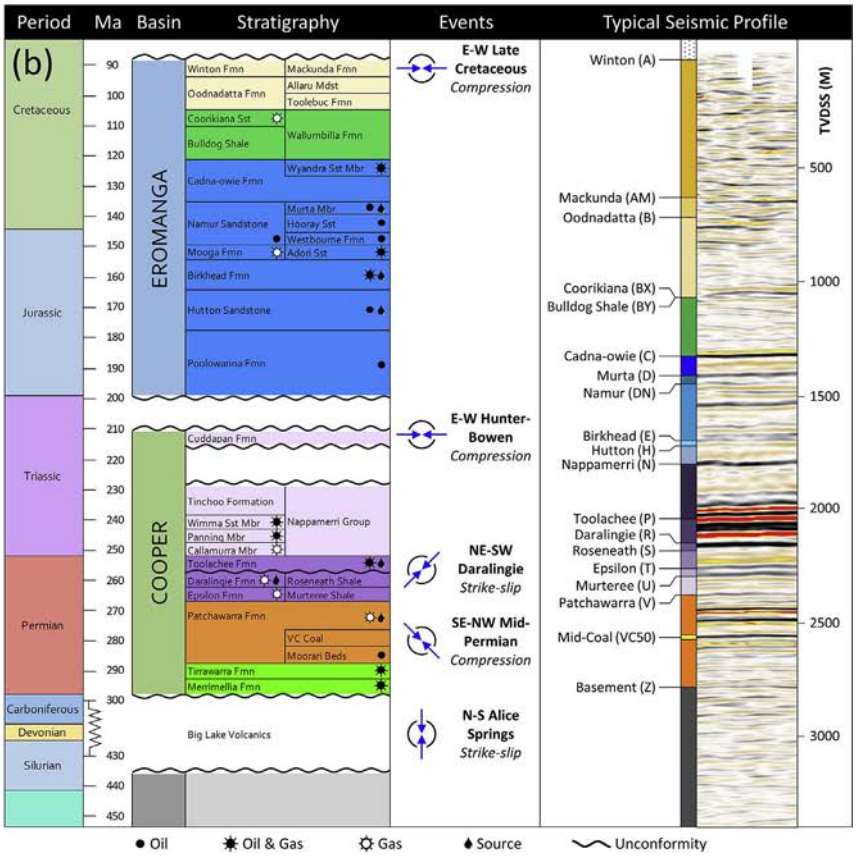

(caption on next page)

Fig. 1. (a) Location of 3D seismic surveys, borehole image logs, and the Gidgealpa-Merrimelia-Innamincka (GMI) and Murteree-Nappacoongee (MN) ridges within the South Australian Cooper Basin. Top Permian depth map shown (Kulikowski and Amrouch, 2017). Inset location of the Eromanga and Cooper basins, Australia (after Kulikowski et al., 2016). GDA94/MGA zone 54 coordinate system used and shown as X-Y locations. (b) Stratigraphic column of the Cooper and Eromanga Basins with a typical seismic reflection profile shown.

2. Geological setting

The Permian to Triassic intra-cratonic Cooper Basin is located in central Australia (Fig. 1a) and is unconformably overlain by the Jurassic to Cretaceous Eromanga Basin (Apak et al., 1997; Alexander et al., 1998). The South Australian portion of this region is defined by the NE-SW striking Gidgealpa-Merrimelia-Innamincka (GMI) and Murteree-Nappacoongee (MN) ridges that bound the NE-SW elongate Patchawarra, Nappamerri and Tenappera troughs (Fig. 1a) (Kulikowski et al., 2018). SE-NW extension during the Adelaidean (650-575 Ma) developed regionally extensive high angled ($> 50^0$) NE-SW striking basement normal faults that created early accommodation space for calcareous and siliciclastic Warburton Basin sediments to be deposited, before being inverted by subsequent compressional and strike-slip stress regime events (Fig. 1b) (Gatehouse, 1986; Apak et al., 1997; Kulikowski and Amrouch, 2017, 2018; Kulikowski et al., 2018).

The unconformity between the Warburton and Cooper basins was created by a N-S strike-slip stress regime belonging to the Carboniferous Alice Springs Event, which was later overlain by Upper Carboniferous glacial sediments (Merrimelia Formation) and Lower Permian braided fluvial sediments (Tirrawarra Formation) (Apak et al., 1997; Kulikowski and Amrouch, 2017). Repeated cycles of sands, shales and coals were deposited during the Middle Permian to form the low permeability and gas-rich Patchawarra Formation (Alexander et al., 1998; Gray, 2017). On-lapping and erosional features are present in the middle Patchawarra Formation along the GMI and MN ridges, and are a result of NW-SE compression during the Mid-Permian Event (Apak et al., 1997; Kulikowski and Amrouch, 2017, 2018). Compression from the Mid-Permian Event gradually eased, forming an east to west transgression, during which the Late Permian Murteree Shale, Epsilon Formation, Roseneath Shale, and Daralingie Formation were deposited (Apak et al., 1997). The Upper Permian Daralingie Formation was later eroded during NE-SW strike-slip stress regime conditions that were associated with the Daralingie Event (Kuang, 1985; Apak et al., 1997; Mavromatidis, 2006; Kulikowski and Amrouch, 2017, 2018). The Late Permian Toolachee Formation and the Triassic Nappamerri Group were deposited under meandering fluvial to deltaic, and floodplain, lacustrine and fluvial channel conditions, respectively (Apak et al., 1997; Alexander et al., 1998), which mark the top of the Cooper Basin stratigraphy.

An E-W compressional stress was present during the Late Triassic Hunter-Bowen Event, which eroded up to 500 m of Nappamerri Group sediments, creating the unconformity between the Cooper and overlying Eromanga basins (Alexander et al., 1998; Mavromatidis, 2006). Jurassic to Cretaceous deposition of Eromanga Basin sediments was uninterrupted, transitioning between fluvial, deltaic, lacustrine and shallow marine conditions (Alexander et al., 1998). Subsequent to this, E-W and N-S compression, associated with the Late Cretaceous Event and Paleogene Event, respectively, created folds and were succeeded by the present-day ESE-WNW strike-slip stress regime (Nelson et al., 2007).

3. Methodology

3.1. Curvature (K) attribute

The value for curvature (K) is the inverse of the radius of the oscillating circle (R) (Eq. (1)) (Roberts, 2001), such that for any point (P) the K is defined as the rate of change of the dip angle ($d\omega$) with respect to the arc length (dS) (Fig. 2a) (Roberts, 2001). The arc length (dS) is obtained from the osculating circle (Fig. 2a) that has a common tangent to P and makes the greatest possible contact with the curve (Roberts, 2001), where in two-dimensions K is defined as;

$$K = \frac{1}{R} \tag{1}$$

This provides unique K values depending on the location along a curve (Fig. 2b). When dealing with 3D data the curvature can be calculated in an infinite number of directions all with unique values. For any P a single intersecting plane normal to the surface that defines the largest absolute curvature value exists, which is termed the maximum curvature (K_{max}) (Roberts, 2001). Perpendicular to this plane, the minimum curvature (K_{min}) value is obtained, which defines the smallest absolute curvature value (Roberts, 2001). The K_{max} and K_{min} attributes are collectively termed the principal curvatures and can be used to derive any curvature value for planes that are normal to the given surface (normal curvature) (Roberts, 2001), such that;

$$K_i = (K_{max})cos^2\delta + (K_{min})sin^2\delta \tag{2}$$

Where δ is the angle between a normal curvature plane (K_i) and the K_{max} plane (Roberts, 2001). The distribution of extensional fractures along the anticlinal traps can be mapped by calculating the most positive curvature (K_+) (Eq. (3)), by incorporating a local quadratic surface with a 3 × 3 grid cell approach (Fig. 2c) (Murray, 1968; Roberts, 2001; Al-Dossary and Marfurt, 2006).

$$K_+ = (a + b) + \sqrt{(a - b)^2 + c^2} \tag{3}$$

where,

$$a = \frac{1}{2}\frac{\delta^2 z}{\delta x^2} = \left(\frac{Z_1 + Z_3 + Z_4 + Z_6 + Z_7 + Z_9}{12\Delta x^2}\right) - \left(\frac{Z_2 + Z_5 + Z_8}{6\Delta x^2}\right) \tag{4}$$

$$b = \frac{1}{2}\frac{\delta^2 z}{\delta y^2} = \left(\frac{Z_1 + Z_2 + Z_3 + Z_7 + Z_8 + Z_9}{12\Delta x^2}\right) - \left(\frac{Z_4 + Z_5 + Z_6}{6\Delta x^2}\right) \tag{5}$$

$$c = \frac{\delta^2 z}{\delta x \delta y} = \left(\frac{Z_3 + Z_7 - Z_1 - Z_9}{4\Delta x^2}\right) \tag{6}$$

Here, Z_i refers to the location of grid nodes along the local quadratic surface and Δx is the distance between grid nodes (Fig. 2c; Roberts, 2001). The equation for K_+ given in Eq. (3) uses the combination of Eqs. (4)–(6) (Roberts, 2001).

The theoretical relationship between K_+ and the presence of extensional fractures is in the stress re-distribution when a stratal-unit (or bed) is folded or bent (i.e. anticline). This folding creates extensional stresses along the outer arc, and compressional stresses in the inner arc (Murray, 1968; Ferrill and Groshong, 1993; Roberts, 2001; Amrouch et al., 2010a, 2010b). As the shape of reflectors can also be affected by mechanism other than folding, such as faulting, erosion, dunes, on-lapping, clinoforms, etc., an understanding of the structural and stratigraphic history of the region must be well understood. As the K_+ analysis predicts the location of fractures along a curved surface, the abrupt curvature associated with faulting is also captured in the results. A detailed fault model is therefore created for each seismic survey to help differentiate between the macro-scale faults and the meso-scale fractures.

3.2. Seismic dataset

The K_+ analysis was performed on five depth converted 3D seismic surveys from the South Australian portion of the Cooper Basin (Fig. 1a). These include the Moomba-Big Lake (acquired 1997), Dullingari (acquired 1997), Merrimelia (extension) (acquired 1998), Greater Tindilpie (GT)-Swan Lake (acquired 2000), and Fly Lake (acquired 2000)

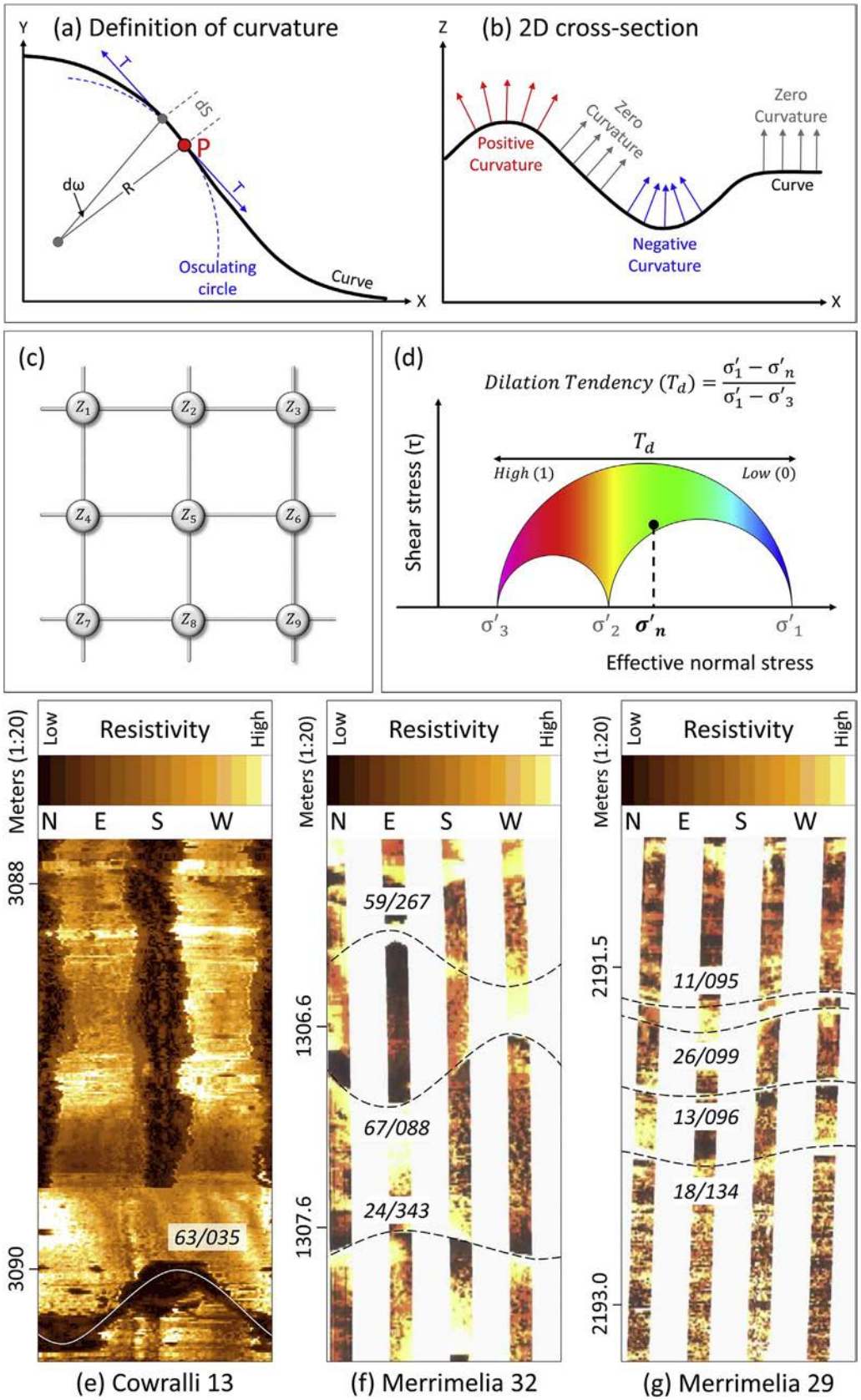

Fig. 2. (a) The definition of curvature where the value for curvature is defined as the rate of change of the direction of a curve, such that for any point (P) the curvature (K) is defined as the rate of change of the dip angle ($d\omega$) with respect to the arc length (dS) (after Roberts, 2001). (b) The change in curvature values along a curve (after Roberts, 2001). (c) Example of a 3 × 3 grid cell containing grid nodes (Z_i) used to compute curvature (Roberts, 2001); (b) The Dilation Tendency (T_d) in terms of maximum (σ'_1), minimum (σ'_3), and normal (σ'_n) effective stresses (Mildren et al., 2005). Conductive (solid line) and resistive (dashed line) natural fractures interpreted in borehole image logs from: (c) Cowralli 13; (d) Merrimelia 32; and (e) Merrimelia 29. See Fig. 1 for location.

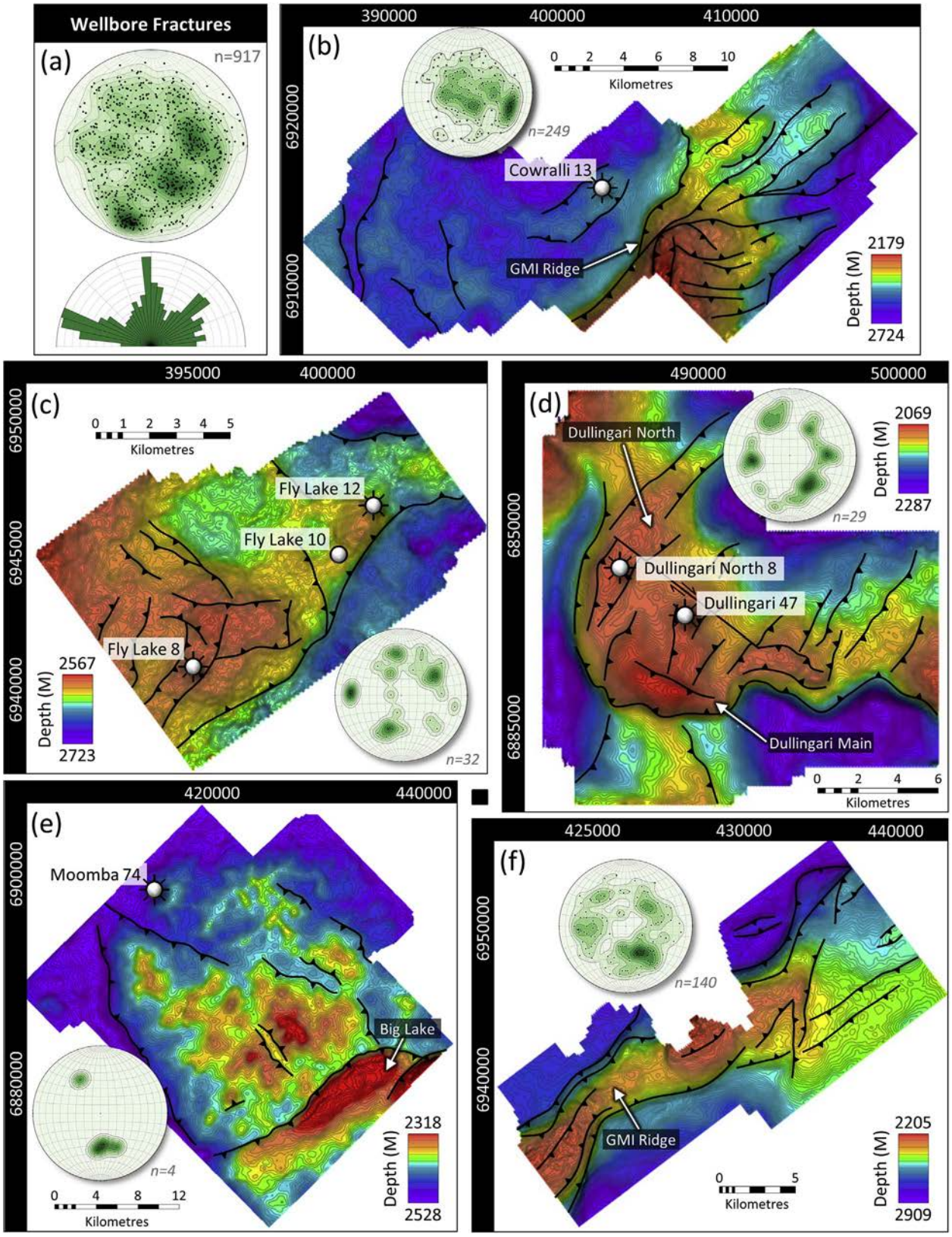

Fig. 3. Basement faults projected onto Top Permian depth maps and the geometry of natural fractures interpreted from image logs in (or adjacent to) the: (a) combined natural fracture data from all wells. See Fig. 1 for seismic survey location. (b) Greater Tindilpie-Swan Lake 3D (after Kulikowski et al., 2018). (c) Fly Lake 3D; (d) Dullingari 3D; (e) Moomba-Big Lake 3D; and (f) Merrimelia (ext) 3D (see Fig. 1 for well location). GDA94/MGA zone 54 coordinate system used and shown as X-Y locations.

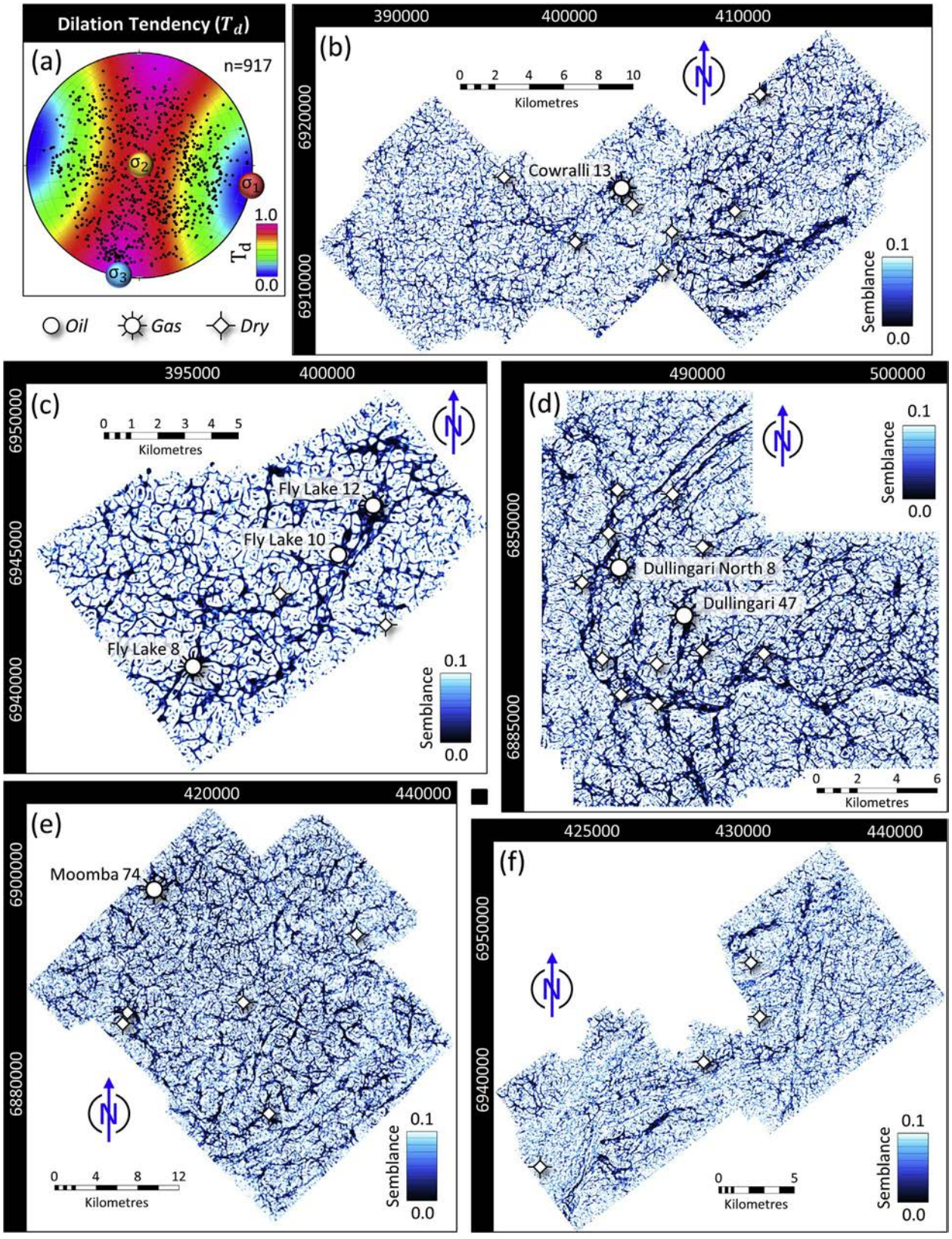

Fig. 4. Most positive curvature displayed as the semblance attribute (zero semblance = fractures) along the Middle Patchawarra Formation in: (a) Dilation Tendency results at 1500 m: equal-area lower hemisphere stereonet with stress data from Nelson et al. (2007). (b) Greater Tindilpie-Swan Lake 3D. (c) Fly Lake 3D; (d) Dullingari 3D; (e) Moomba-Big Lake 3D; and (f) Merrimelia (ext) 3D. See Fig. 1 for location. GDA94/MGA zone 54 coordinate system used and shown as X-Y locations.

3D seismic surveys. A total of 28 borehole image logs were used to measure natural fractures. These vertical wells are present throughout the study area, with 7 wells located within the 3D seismic data, and four wells (Merrimelia 29, 30, 31, and 32) located slightly outside of the Merrimelia (ext) 3D seismic survey (Fig. 1a). Prior to analysis, the seismic data were time-to-depth converted using the average velocity method, which is one of the more accurate methods for the basin (Kulikowski, 2017; Kulikowski et al., 2018). After depth conversion, a 3D subsurface dip field volume was created to provide the dip angle of all reflectors. The five 3D seismic volumes were individually analysed using the K_+ attribute, which was then processed into a semblance (similarity) attribute volume to improve the signal-noise ratio and finally extracted along the Middle Patchawarra Formation reflector. The semblance attribute volume measures the amount of similarity in the seismic curvature results in a local area, highlighting discontinuity trends, such as faults. A half-window vertical distance of 50 m was used, which visually emphasises the curvature results by removing noise (high semblance) and highlighting structural discontinuities (low semblance).

3.3. Dilation Tendency

To determine the likelihood of natural fractures undergoing tensile reactivation, and hence more likely to be hydraulically conductive under in-situ stresses, the Dilation Tendency (T_d) is measured from a geomechanical model using Eq. (8) and illustrated in Fig. 2d (Ferrill et al., 1999; Mildren et al., 2005; Jolie et al., 2015). This attribute is commonly used to determine the reactivation and fluid conduit potential of faults (Barton et al., 1995; Ferrill and Morris, 2003; Jolie et al., 2015; Kulikowski et al., 2016). The T_d is used in preference to measuring the Slip (shear) Tendency, as the latter predicts the shear potential and not the ability of natural fractures to remain open to fluid flow (Ferrill et al., 1999; Mildren et al., 2005). The T_d is governed by the effective normal stress acting on a plane, which directly affects the natural fracture aperture (Ferrill et al., 1999; Mildren et al., 2005). Therefore, the maximum (σ_1'), minimum (σ_3'), and normal (σ_n') effective stresses are used to measure the T_d (Ferrill et al., 1999; Mildren et al., 2005);

$$T_d = \left(\frac{\sigma_1' - \sigma_n'}{\sigma_1' - \sigma_3'} \right) \tag{8}$$

The T_d results are normalised to the differential stress, giving values that range from a maximum of one (high likelihood of tensile reactivation) to a minimum of zero (little to no tensile reactivation). To model the in-situ stress conditions, a present-day maximum horizontal stress orientation of 101°N was used together with a hydrostatic pore pressure gradient, a strike-slip stress regime with a low stress ellipsoid shape ratio (~0.10), and stress magnitude data from Nelson et al. (2007). Importantly, this model does not consider variables such as fracture plane roughness (texture), cementation, pressure variation, or the possibility of crystal bridging, which has been shown to enable fractures to remain open and permeable albeit not preferentially aligned with σ'_1 (Laubach et al., 2004). That being said, this model does show which fractures will be more opened, assuming the same type of fractures with the same parameters and with the same fluid pressures, with the only difference being the geometry. The present-day geomechanical model uses the assumption that hydrostatic pore pressure exists within the case study and is homogenously distributed. This can be an oversimplification and changes in local pore pressure can affect the stability of faults and fractures.

3.4. Borehole image logs

The Cooper Basin is an intra-cratonic subsurface basin, preventing direct measurements from outcrop; therefore, direct natural fracture measurements can only be made from borehole image logs or core. Images of the borehole are generated by measuring the electrical resistivity at the centimetre scale, which can provide information on whether fractures are fluid (conductive and open) or cement (resistive and closed) filled. These methods of obtaining natural fracture data can be selective in the natural fracture sets that are encounter, as high angled sets will be intersected less frequently by vertical wells than the low angle sets. This study uses 28 image logs (Fig. 1a) covering a total length of approximately 7.5 km in vertical wells. Theses were used to measure the natural fracture geometries present across the basin and to then determine which of the fracture sets is critically oriented to undergoes tensile reactivation and facilitate fluid flow (Fig. 2d). Both conductive (open to fluid flow) (Fig. 2e) and resistive (closed to fluid flow) (Fig. 2f and g) natural fractures were interpreted and geomechanically analysed based on the strike and dip angle.

4. Results

Natural fracture data measured from borehole image logs are presented on a stereonet and rose plot to show the regional natural fracture sets (Fig. 3a). The natural fracture data are projected onto the Dilation Tendency results (Fig. 4a) to identify the critically oriented sets.

4.1. Natural fractures at the wellbore

Borehole image log data were interpreted from 28 wells, which included 7 wells present within the 3D seismic data (Fig. 1a). These measured natural fractures (Fig. 3a) were used to: (1) compare the possible variation between the one-dimensional well data and three-dimensional seismic data results; and (2) generate an in-situ geomechanical model to determine the natural fracture geometry critically oriented to undergo tensile reactivation. The wellbore fracture data is dominantly N-S, NE-SW and E-W striking with a large number having a high ($> 50^0$) dip angle (Fig. 3a). This data is also presented for each group of wells that are present within the Greater Tindilpie-Swan Lake (Fig. 3b), Fly Lake (Fig. 3c), Dullingari (Fig. 3d), and Moomba-Big Lake (Fig. 3e) 3D seismic surveys. The fracture data presented for the Merrimelia (extension) 3D seismic survey (Fig. 3f) are located on the southwest border of the seismic survey (Fig. 1a). Important to note is that the statistical likelihood of intersecting high ($> 50^0$) angled fractures is reduced by drilling vertical wells, suggesting that the vertical wells used in this study may be underestimating the true fracture density.

The T_d results found that high angle ($> 50^o$) natural fractures striking 101°N (± 20°) are optimally oriented to dilate ($T_d = 1.0$) and act as potential fluid conduits (Fig. 4a), with natural fractures striking perpendicular to this geometry (011°N strike) being least likely to dilate ($T_d = 0$). This is also observed in borehole image logs, with examples of conductive (open) and resistive (closed) natural fractures presented from Cowralli 13 (Fig. 2e), and Merrimelia 32 (Fig. 2f) and Merrimelia 29 (Fig. 2g), respectively. These results infer that E-W striking high ($> 50^0$) angled natural fractures are critically oriented to undergo tensile reactivation and have potential to improve the hydraulic conductivity of low permeability reservoirs.

4.2. Natural fractures from seismic data

The K_+ results (reprocessed into the semblance attribute) are extracted along the Patchawarra Formation in each of the five seismic surveys (Fig. 4b–f). This allowed the extensional fracture networks to be clearly imaged in the subsurface. An example from the Greater Tindilpie and Swan Lake seismic survey shows the high density of extensional fractures interpreted from the borehole image log, which is reflected in the most positive curvature results (Fig. 5a). A close look at the curvature results (Fig. 5b) shows a dominant N-S strike, which coincides with the mean natural fracture strike interpreted from the

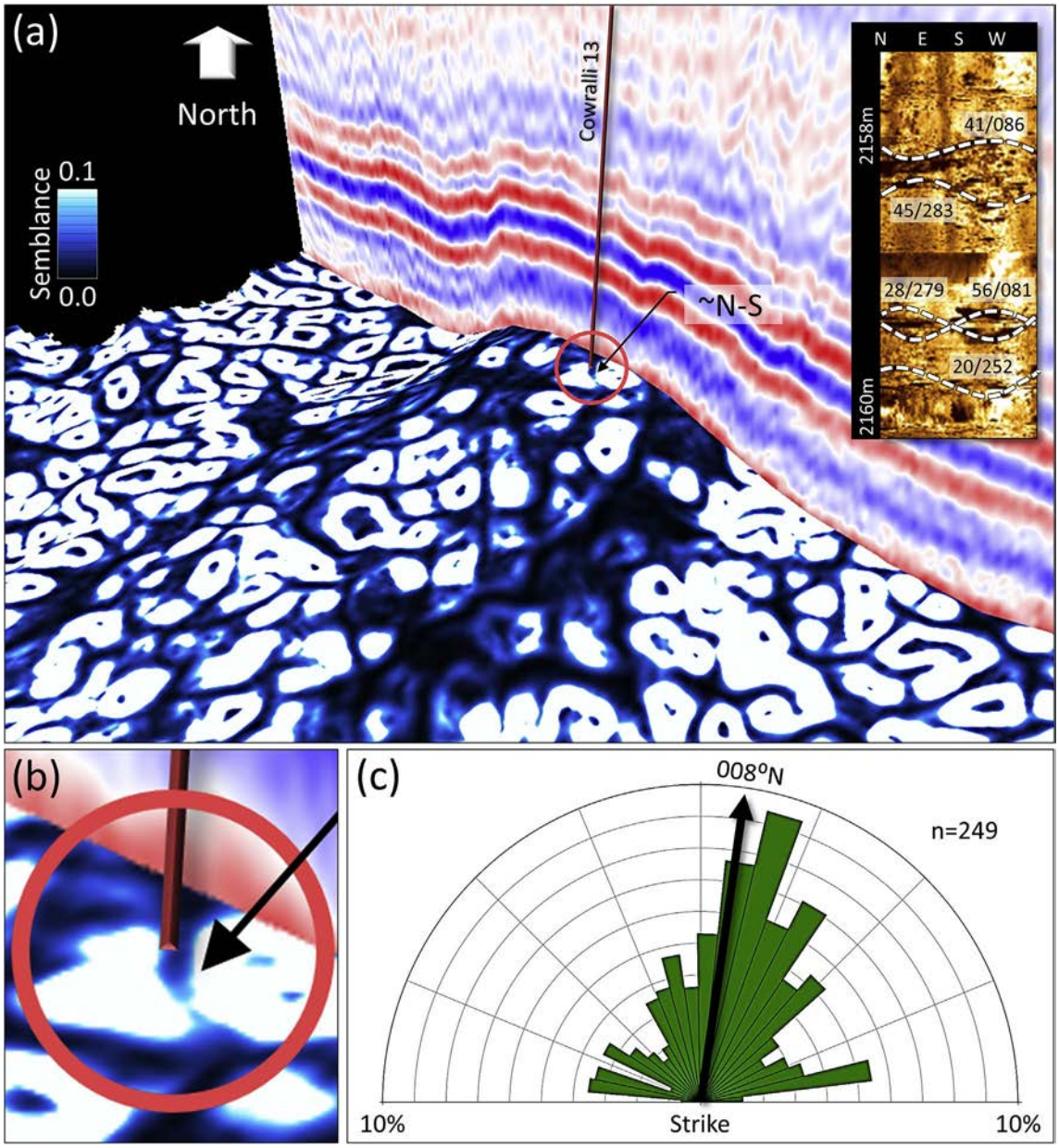

Fig. 5. (a) Seismic curvature (displayed as the semblance attribute) at the Cowralli 13 well location showing N-S striking results correlating well to interpreted N-S striking natural fractures. (b) Zoomed in image of the N-S striking seismic curvature results (displayed as the semblance attribute) at the Cowralli 13 well location. (c) Rose diagram of interpreted natural fractures from the Cowralli 13 borehole image log showing a mean N-S strike direction. See Fig. 1a for location.

borehole image log (Fig. 5c). Other wells that contain high ($> 50^0$) angled fractures also show this expected relationship, whereas wells with a low density of these fractures correspond to poor curvature results. The K_+ results (Fig. 4) also highlight the location of abrupt reflector curvature, or displacement, that is associated with interpreted basement-involved faults (Fig. 3).

4.2.1. Greater Tindilpie-Swan Lake 3D

The Greater Tindilpie-Swan Lake 3D seismic survey contains the Cowralli 13 well, which is located on a subtle NE-SW elongate anticlinal closure on the footwall side of the GMI Ridge (Fig. 3b). The K_+ analysis presents high fracture density (high K_+) within the Cowralli 13 well location, along the NE-SW striking GMI Ridge, and also along the approximately E-W striking splays in the east of the survey (Figs. 3b and 4b). The results present a dominant SE-NW and NE-SW striking network throughout the Middle Patchawarra Formation surface, that increase in density in regions of known basement faults (Figs. 3b and 4b).

4.2.2. Fly Lake 3D

Structural interpretation of Fly lake 3D shows a structural high in the west that is bound from the east by a NE-SW striking fault (Fig. 3c). The K_+ results present lineaments striking NE-SW, E-W, and N-S, with fewer striking SE-NW (Fig. 4c). The results along the Middle Patchawarra Formation show high K_+ values in the northeast of the survey within the vicinity of Fly Lake 10 and Fly Lake 12. Strong K_+ results are also present above known basement faults (Figs. 3c and 4c).

4.2.3. Dullingari 3D

The Dullingari 3D seismic survey contains two well controls; Dullingari North 8 and Dullingari 47, which are in the Dullingari North and Dullingari Main culminations, respectively (Figs. 3d and 4d). The K_+ analysis delineates a NE-SW and SE-NW striking network present throughout the survey (Fig. 4d), with secondary N-S striking features present within the Dullingari Main area (Figs. 3d and 4d). E-W striking K_+ lineaments are found in regions with known E-W striking basement

faults, and increases in density along E-W elongate anticlines (Figs. 3d and 4d). The results along the Middle Patchawarra Formation shows the detailed distribution of structural lineaments, such as the NE-SW striking features in Dullingari North and the saw-tooth-like geometry of the E-W striking fault bounding Dullingari Main from the south (Figs. 3d and 4d).

4.2.4. Moomba-Big Lake 3D

The Moomba 74 borehole image log is located on the outer edge of the Moomba-Big Lake 3D seismic survey, along the flank of a small Permian structure that corresponds to low K_+ (Figs. 3e and 4e). E-W trending K_+ lineaments are present within the Moomba 74 well location, with large SE-NW trending lineaments present elsewhere in the seismic survey that are subparallel to the basement faults (Figs. 3e and 4e). The major NE-SW elongate Big Lake structure is expressed with high K_+ values in the southeast of the survey along the Middle Patchawarra Formation horizon (Figs. 3e and 4e). The K_+ results in this area have a wide distribution of strikes and appears highly complex.

4.2.5. Merrimelia (extension) 3D

Three borehole image logs are located slightly outside of the Merrimelia (extension) 3D seismic survey, but remain along the GMI Ridge (Fig. 1a). The Merrimelia structure is a NE-SW elongate anticline bound from the west by the GMI Ridge fault (Fig. 3f). Significantly high K_+ values are present along this structure and increase to the northeast and southwest (Fig. 4f). The general trend of this dense K_+ network is mostly NE-SW, with secondary N-S, SE-NW, and E-W striking features also present (Fig. 4f). The results present a large N-S striking feature along the Middle Patchawarra Formation in the centre of the survey (Fig. 4f), which coincides with basement faults and an abrupt increase in depth (Fig. 3f).

5. Discussion

Although borehole image logs and cores can provide the natural fracture distribution at the wellbore, assuming this data is representative of the basin can be unrealistic. For one, the sampling of fractures is statistically biased in vertical wells to intersect more low angle fractures than high angle, and coupled with local stress perturbations and lateral changes in geology, the 1D well data can be wholly unrepresentative. An effective means of obtaining high density structural data from subsurface provinces is through the careful application of seismic curvature analysis (e.g. Murray, 1968; Lisle, 1994; Al-Dossary and Marfurt, 2006; Chopra and Marfurt, 2007; Bailey et al., 2014). By understanding that most positive curvature (K_+) analysis selectively presents high ($> 50^o$) angled fractures based on the extensional stress distribution along the outer arc of an anticline, this research is able to constrain the distribution of permeable fracture networks along the gas-rich Patchawarra Formation, Cooper Basin.

Borehole image log interpretation found resistive (closed) natural fractures typically striking N-S and NE-SW with high dip angle ($> 50^o$), with examples shown from Merrimelia 32 (Fig. 2f) and Merrimelia 29 (Fig. 2g). Alternatively, conductive fractures typically strike SE-NW and E-W with high dip angles ($> 50^o$), as shown in Cowralli 13 (Fig. 2e). Regional NE-SW and SE-NW striking faults and fractures have been shown to preferentially shear reactivate under present-day stress (Kulikowski et al., 2016; Kulikowski, 2017); however, it is important to understand whether they will remain open after shearing. We examine this by developing a geomechanical model of the in-situ stress to measure the T_d of fracture sets, with results aligning well with borehole image log interpretation of conductive and resistive fractures, showing that near vertical E-W striking fractures will preferentially dilate ($T_d = 1.0$), as will the pervasive SE-NW striking fracture set ($T_d = 0.7 - 0.8$) (Fig. 4a).

Previous research on the regional natural fracture distribution in the basin found that NE-SW and SE-NW striking high ($> 50^o$) dip angle sets dominate the region and likely developed through extensional stresses (Kulikowski, 2017; Kulikowski and Amrouch, 2017). These fracture sets are present within the Patchawarra Formation together with low angle ($< 30^o$) sets striking NE-SW, N-S, and E-W. The subsurface fracture distributions in each of the five seismic surveys shows a dominant NE-SW and SE-NW strike in the curvature (semblance attribute) results, supporting previous works that suggested their regional presence (Kuang, 1985; Apak et al., 1997; Kulikowski, 2017; Kulikowski and Amrouch, 2017). Amongst this dominant fracture network, N-S and E-W striking lineaments are also identified in each seismic survey. The geomechanical modelling results show that high angled fractures, particularly if striking E-W to SE-NW, are optimally oriented to undergo tensile reactivation. These E-W to SE-NW striking conductive fracture sets are present in each seismic survey and most pervasive within the Fly Lake (Fig. 4c), Dullingari (Fig. 4d), and Moomba-Big Lake (Fig. 4e) 3D seismic surveys. The density of these sets increases rapidly along SE-NW and E-W elongate anticlines, such as those found in the Moomba-Big Lake (Figs. 3e and 4e) and Dullingari (Figs. 3d and 4d) 3D seismic surveys.

Wells that were drilled in regions of high K_+ were found to have an increased number of high ($> 50^o$) angle natural fractures present in the wellbore image logs. This relationship is also found in wells that were drilled in low seismic curvature regions, which have relatively less high ($> 50^o$) angle natural fractures. A low fracture density in the Cooper Basin has previously been described and can potentially be attributed to the inability of vertical wells to intersect the high angled ($> 50^o$) fracture sets that dominate the province (Kulikowski, 2017; Kulikowski and Amrouch, 2017). Seismic K_+ analysis combats this limitation to widely present the fracture density within the five seismic surveys, suggesting that the density may be much higher than previously thought. Once the subsurface distribution of the regionally pervasive and critically oriented high ($> 50^o$) angle E-W and SE-NW striking fractures is defined, these can be exploited and become highly beneficial for many industries including, petroleum, geothermal, and carbon sequestration.

The additional processing of K_+ results into the semblance (similarity) attribute has better defined the fracture networks by improving the signal-noise ratio. High density fracture zones are compared with the location of known dry wells in each of the seismic surveys (Fig. 4), showing a noticeable absence of dry wells from high density locations in all cases. Although drilling within high fracture density zones may not be the single factor involved in a well failing to produce hydrocarbons, it can have a significant impact on the efficiency of hydraulic fracture stimulation treatments and in well design.

The remote sensing of fractures and faults has become an important tool in many industries (e.g. petroleum, geothermal, carbon dioxide capture and storage, hydrology, and mining) because of their potential for enhanced fluid/gas flow. A study that focused on a local area in the Penola Trough, Otway Basin, presented a large 3D subsurface fracture network that appeared to show good connectivity from curvature results; however, through core and image log analysis, and stress modelling, Bailey et al. (2014) concluded that this network was likely to be a poor hydraulic conductor. This reiterated the need for a careful approach when exploiting subsurface fracture networks. Following on from this work, we used the Cooper Basin as a case study to highlight the potential of integrating seismic curvature analysis with wellbore data and geomechanical modelling to constrain the distribution of permeable subsurface fracture networks, that would otherwise be limited to one-dimensional well data. Although we focus on one stratigraphic interval within the basin, future work should consider the changing fracture distribution between stratigraphic intervals and attempt to investigate the vertical persistency of fractures and its relationship to vertical hydraulic conductivity.

The careful application of this approach would be most beneficial to other important subsurface or offshore provinces that have a known regional distribution of high ($> 50^o$) angle extensional fractures and

faults, such as the Otway Basin in Australia (Bailey et al., 2014; Burgin et al., 2018), Piceance Basin in Colorado (Lorenz and Finley, 1991), East Texas Basin in the Gulf of Mexico (Laubach, 1988), Ordos Basin in China (Lianbo and Xiang-Yang, 2009), and frontier basins, such as the Ceduna Sub-basin in Australia (Robson, 2017), the group of basins in offshore Columbia (Beltrán Rivas and Vargas Jiménez, 2014), the Congo Basin in offshore West Africa (Brownfield and Charpentier, 2006), Zagros collision belt (Lacombe et al., 2007), and the Big Horn Basin in Wyoming (Amrouch et al., 2011; Beaudoin et al., 2012).

6. Conclusion

This research uses the intra-cratonic subsurface Cooper Basin (Australia) as a case study to carefully apply an approach that maps the distribution of permeable fracture networks through the integration of most positive curvature (K_+) seismic analysis, wellbore fracture data, and in-situ geomechanical modelling. Five three-dimensional seismic surveys were analysed using the K_+ seismic attribute to constrain the distribution of critically oriented high ($> 50^0$) angle permeable fracture networks within the gas-rich and low permeability Patchawarra Formation. The regionally pervasive high angle ($> 50^o$) SE-NW and E-W striking fracture sets were identified to be critically oriented to undergo tensile reactivation and act as fluid conduits under in-situ stresses. These sets are identified in each of the five seismic surveys and found to increase in density along E-W elongate anticlines. The well fracture data in the Cooper Basin presents a close relationship to K_+ results, which can be important for generating representative high density structural data that would otherwise be restricted to sparse well locations. Careful application of this approach to other subsurface or offshore provinces can provide important high density structural information between sparse one-dimensional well data.

Acknowledgements

We thank the financial contribution made by the GeoFrac Consortium, which includes the sponsoring companies: Santos, Beach Energy, Chevron, Halliburton and BG Group (QGC). Thank you to Midland Valley (MOVE), DownUnder Geosolutions (DUG Insight), and Paradigm (Geolog) for academic licencing. Thank you to Carlos H. Grohmann and Ginaldo A.C. Campanha for the “OpenStereo 0.1.2” stereonet software.

References

Al-Dossary, S., Marfurt, K.J., 2006. 3D volumetric multispectral estimates of reflector curvature and rotation. Geophysics 71 (5), 41–51.
Alexander, E.M., Gravestock, D.I., Cubitt, C., Chaney, A., 1998. Lithostratigraphy and environments of deposition. In: In: Gravestock, D.I., Hibburt, J.E., Drexel, J.F. (Eds.), The Petroleum Geology of South Australia, vol. 4. Cooper Basin, South Australia. Department of Primary Industries and Resources, pp. 69–116 Report Book, 98/9.
Amrouch, K., Lacombe, O., Bellahsen, N., Daniel, J.M., Callot, J.P., 2010a. Stress and strain patterns, kinematics and deformation mechanisms in a basement-cored anticline: sheep Mountain Anticline, Wyoming. Tectonics 29http://dx.doi.org/10.1029/2009TC002525. TC1005.
Amrouch, K., Robion, P., Callot, J.P., Lacombe, O., Daniel, J.M., Bellahsen, N., Faure, J.L., 2010b. Constraints on deformation mechanisms during folding provided by rock physical properties: a case study at Sheep Mountain anticline (Wyoming, USA). Geophys. J. Int. 182 (3), 1105–1123.
Amrouch, K., Beaudoin, N., Lacombe, O., Bellahsen, N., Daniel, J., 2011. Paleostress magnitudes in folded sedimentary rocks. Geophys. Res. Lett. 38 (17). http://dx.doi.org/10.1029/2011GL048649. L17301.
Apak, S.N., Stuart, W.J., Lemon, N.M., Wood, G., 1997. Structural evolution of the permian-triassic Cooper Basin, Australia: relation to hydrocarbon trap styles. AAPG (Am. Assoc. Pet. Geol.) Bull. 81, 533–555.
Backe, G., Khair, H.A., King, R., Holford, S., 2011. Fracture mapping and modelling in shale-gas target in the Cooper basin, South Australia. APPEA J. 51, 397–410.
Bailey, A., King, R.C., Holford, S.P., Sage, J., Backe, G., Hand, M., 2014. Remote sensing of subsurface fractures in the Otway Basin, South Australia. J. Geophys. Res.: Solid Earth 119 (8), 6591–6612. http://dx.doi.org/10.1002/2013JB010843.
Barton, C.A., Zoback, M.D., Moos, D., 1995. Fluid flow along potentially active faults in crystalline rock. Geology 23, 683–686.
Beaudoin, N., Lepretre, R., Bellahsen, N., Lacombe, O., Amrouch, K., Callot, J., Emmanuel, L., Daniel, J., 2012. Structural and microstructural evolution of the rattlesnake mountain anticline (Wyoming, USA): new insights into the sevier and laramide orogenic stress build-up in the Bighorn Basin. Tectonophysics 576–577, 20–45. http://dx.doi.org/10.1016/j.tecto.2012.03.036.
Beltrán Rivas, J.D., Vargas Jiménez, C.A., 2014. Hydrocarbon production scenarios in Colombia. Review of field sizes, hydrocarbon reserves and expectations of conventional and unconventional resources. Earth Sci. Res. J. 18 (1), 77–83.
Brownfield, M.E., Charpentier, R.R., 2006. Geology and Total Petroleum Systems of the West-Central Coastal Province (7203), West Africa. U.S. Geological Survey Bulletin 2207-B.
Burgin, H.B., Amrouch, K., Rajabi, M., Kulikowski, D., Holford, S.P., 2018. Determining structural environments through natural fracture and calcite twin analysis: a case study in the Otway Basin. APPEA J. 58 (accepted).
Chopra, S., Marfurt, K., 2007. Curvature attribute applications to 3D surface seismic data. Lead. Edge 26 (4), 404–414.
Ferrill, D.A., Groshong, R.H., 1993. Kinematic model for the curvature of the northern Subalpine Chain, France. J. Struct. Geol. 15 (3–5), 523–541.
Ferrill, D.A., Winterle, J., Wittmeyer, G., Sims, D., Colton, S., Armstrong, A., Morris, A.P., 1999. Stressed rock strains groundwater at Yucca Mountain, Nevada. GSA Today (Geol. Soc. Am.) 9 (5), 1–8.
Ferrill, D.A., Morris, A.P., 2003. Dilational normal faults. J. Struct. Geol. 25, 183–196.
Gatehouse, C.G., 1986. The geology of the Warburton Basin in South Australia. Aust. J. Earth Sci. 33 (2), 161–180.
Gray, M.E., 2017. Analytical Techniques for Evaluating Seal Capacity for Carbon Dioxide Storage in Selected Australian Basins (Doctoral dissertation). The Australian School of Petroleum, the University of Adelaide, Adelaide, Australia.
Hakami, A.M., Marfurt, K.J., Al-Dossary, S., 2004. Curvature attribute and seismic interpretation: case study from Fort Worth Basin, Texas, USA. In: 2004 SEG Annual Meeting. Society of Exploration Geophysicists.
Jolie, E., Moeck, I., Faulds, J.E., 2015. Quantitative structural geological exploration of fault-controlled geothermal systems—a case study from the Basin-and-Range Province, Nevada (USA). Geothermics 54, 54–67.
Kuang, K.S., 1985. History and style of Cooper-Eromanga Basin structures. Explor. Geophys. 16, 245–248.
Kulikowski, D., Amrouch, K., Cooke, D., 2016. Geomechanical modelling of fault reactivation in the Cooper Basin, Australia. Aust. J. Earth Sci. 63 (3), 295–314. http://dx.doi.org/10.1080/08120099.2016.1212925.
Kulikowski, D., 2017. Modern Structural Analysis of Subsurface Provinces: a Case Study on the Cooper and Eromanga Basins, Australia (Doctoral dissertation). The Australian School of Petroleum, the University of Adelaide, Adelaide, Australia.
Kulikowski, D., Amrouch, K., 2017. Combining geophysical data and calcite twin stress inversion to refine the tectonic history of subsurface and offshore provinces: a case study on the Cooper-Eromanga Basin, Australia. Tectonics 36 (3), 515–541. http://dx.doi.org/10.1002/2016TC004366.
Kulikowski, D., Amrouch, K., 2018. 3D seismic analysis investigating the relationship Between stratigraphic architecture and structural activity in the intra-cratonic cooper and Eromanga Basins, Australia. Mar. Petrol. Geol. 91, 381–400. http://dx.doi.org/10.1016/j.marpetgeo.2018.01.019.
Kulikowski, D., Amrouch, K., Cooke, D., Gray, M.E., 2018. Basement structural architecture and hydrocarbon conduit potential of polygonal faults in the Cooper-Eromanga Basin, Australia. Geophys. Prospect. 66 (2), 366–396. http://dx.doi.org/10.1111/1365-2478.12531.
Lacombe, O., Amrouch, K., Mouthereau, F., Dissez, L., 2007. Calcite twinning constraints on late Neogene stress patterns and deformation mechanisms in the active Zagros collision belt. Geology 35 (3), 263–266. http://dx.doi.org/10.1130/G23173A.1.
Laubach, S.E., 1988. Subsurface fractures and their relationship to stress history in East Texas Basin sandstone. Tectonophysics 156 (1/2), 37–49.
Laubach, S.E., Olson, J.E., Gale, J.F., 2004. Are open fractures necessarily aligned with maximum horizontal stress? Earth Planet Sci. Lett. 222 (1), 191–195.
Lianbo, Z., Xiang-Yang, L., 2009. Fractures in sandstone reservoirs with ultra-low permeability: a case study of the upper triassic Yanchang Formation in the Ordos Basin, China. AAPG (Am. Assoc. Pet. Geol.) Bull. 93 (4), 461–477.
Lisle, R.J., 1994. Detection of zones of abnormal strains in structures using Gaussian curvature analysis. AAPG (Am. Assoc. Pet. Geol.) Bull. 78 (12), 1811–1819.
Lorenz, J.C., Finley, S.J., 1991. Regional fractures II: Fracturing of mesaverde reservoirs in the Piceance Basin, Colorado. AAPG (Am. Assoc. Pet. Geol.) Bull. 75 (11), 1738–1757.
Mavromatidis, A., 2006. Burial/exhumation histories for the Cooper-Eromanga Basins and implications for hydrocarbon exploration, Eastern Australia. Basin Res. 18, 351–373.
Mildren, S.D., Hillis, R.R., Dewhurst, D.N., Lyon, P.J., Meyer, J.J., Boult, P.J., 2005. FAST: a new technique for geomechanical assessment of the risk of reactivation-related breach of fault seals. In: In: Boult, P., Kaldi, J. (Eds.), Evaluating Fault and Cap Rock Seals, vol. 2. AAPG Hedberg Series, Barossa Valley, South Australia, pp. 73–85.
Murray, G.H., 1968. Quantitative fracture study-Spanish pool, McKenzie county, North Dakota. AAPG (Am. Assoc. Pet. Geol.) Bull. 52 (1), 57–65.
Nelson, E.J., Chipperfield, S.T., Hillis, R.R., Gilbert, J., McGowen, J., 2007. Using geological information to optimize fracture stimulation practices in the Cooper Basin, Australia. Petrol. Geosci. 13 (1), 3–16.
Roberts, A., 2001. Curvature attributes and their application to 3D interpreted horizons. First Break 19 (2), 85–100.
Robson, A.G., 2017. Normal fault Growth Analysis Using 3D Seismic Datasets Located along Australia's Southern Margin (Doctoral dissertation). School of Physical Sciences, the University of Adelaide, Adelaide, Australia.
Robson, A.G., Holford, S.P., King, R.C., Kulikowski, D., 2018. Structural evolution of horst and half-graben structures proximal to a transtensional fault system determined using 3D seismic data from the Shipwreck Trough, offshore Otway Basin, Australia. Mar. Petrol. Geol. 89, 615–634. http://dx.doi.org/10.1016/j.marpetgeo.2017.10.028.
Stewart, S.A., Podolski, R., 1998. Curvature analysis of gridded geological surfaces. Geol. Soc. Lond. Spec. Publ. 127 (1), 133–147.

Appendix I.II: Co-Authored Manuscript 2

The intracratonic Cooper and Eromanga Basins, Australia: A Comprehensive Review

The finalised version of this manuscript will be submitted to the *Australian Journal of Earth Science.*

As with section I.I while based in the Cooper Basin, in central Australia. This manuscript draws on many of the elements fundamental to the main body of this thesis.

Much of the new contributions to the framework of the basin within the manuscript were made using the same approach as applied within the preceding pages of this thesis.

This study is further testament to what can be achieved when a multiscale approach to basin analysis is completed. Comprehensively summarising many geological aspects of the basin and its structural evolution.

The intracratonic Cooper and Eromanga Basins, Australia: A Comprehensive Review

David **Kulikowski**[a] (drdavidkulikowski@gmail.com)
Khalid **Amrouch**[a] (khalid.amrouch@adelaide.edu.au)
Kunakorn **Pokalai**[a] (kunakorn.pokalai@adelaide.edu.au)
Steve I. **Mackie**[b] (steve.mackie@geosimconsulting.com.au)
Michael E. **Gray**[a] (michael.gray2@woodside.com.au)
Hugo B. **Burgin**[a] (hugo.burgin@adelaide.edu.au)

[a]Australian School of Petroleum, University of Adelaide, North Terrace, 5005, Adelaide, Australia.

[b]Geosim Consulting Pty Ltd, 112b Sydenham Rd, Norwood, 5067, Adelaide, Australia.

Citation: Kulokowski, D., Amrouch, K., Pokalai, K., Mackie, S. I., Gray, M. and **Burgin H. B**. (2019) The intracratonic Cooper and Eromanga Basins, Australia: A Comprehensive Review (in – prep)

Abstract

This review focuses on integrating old literature with present-day models to provide a modern summary of Australia's largest onshore hydrocarbon province, the Cooper-Eromanga basins, with a focus on structural geology and geophysics. A rapid rise in cutting-edge research has been facilitated by exploration companies transitioning away from the nearly extinct anticlinal theory, to technically more challenging plays within the basin. The purpose of this review is to provide new and existing operating companies, and researchers, with a summary of the recent research developments, together with the fundamentals of the basin, to ensure that the tremendous unconventional hydrocarbon potential is effectively explored for and appropriately developed. A modern tectonostratigraphic evolution model is presented alongside the stress magnitude, regime and orientation of the six events that have affected the province (N-S Carboniferous Alice Springs Event; SE-NW Mid-Permian Event; NE-SW Late Permian Daralingie Event; E-W Triassic Hunter-Bowen Event; E-W Late Cretaceous Event; N-S Paleogene Event). Integration of these complete paleo-stress tensors with geomechanical models has constrained the dynamic reactivation (shear and tensile) of faults through time to find that since the critical moment (90 Ma), N-S and E-W striking high angle (50-70^{o}) faults were most likely to facilitate hydrocarbon migration. These form the major topics of discussion; however, the temporal and spatial distribution of natural fractures away from the wellbore, seismic time-to-depth conversion methods and accuracies, petroleum systems elements and processes, current and future exploration programs, common hydraulic fracturing and well surveillance programs, and recommendations for future research are also discussed. The methodologies, cutting-edge research and novel approaches presented here form a framework that can be applied to other hydrocarbon provinces around the world while also providing a knowledge platform for this highly prospective hydrocarbon province.

1. Introduction

The Cooper-Eromanga basins are Australia's largest onshore hydrocarbon province (Fig. 1) and have been producing oil and gas from tight reservoirs since the first natural gas discovery at Gidgealpa in 1963 (Gravestock, Alexander, Morton & Sun, 1998; Radke, 2009; Mackie, 2015). The basins are oil and gas saturated and require the simplest of structural traps, an anticline, for effective petroleum accumulation and preservation (Apak, Stuart, Lemon & Wood, 1997; Gravestock et al., 1998; Mackie, 2015). As such, much of the early research has focused on basic structural interpretation of sparse two-dimensional (2D) seismic data that remained in the time-domain, with the primary focus of identifying these anticlinal closures (e.g. Senior, Galloway, Ingram, & Senior, 1968; Stuart, 1976; Veevers, Jones & Powell, 1982; Kuang, 1985; Stanmore, 1989; Elliot, 1993; Apak et al., 1997; Sun, 1997; Gravestock & Jensen-Schmidt, 1998). The lack of detailed research has been further compounded by the limited exposure of rocks at surface, particularly within the South Australian portion of the basin, which has ultimately restricted much of the research to wellbore derived data. However, recent advancements in seismic data acquisition and processing, coupled with novel software applications and approaches, have enabled researchers to better constrain the structural geology and tectonic evolution of the Cooper-Eromanga basins. A detailed and modern synthesis of this prospective province, with a focus on the structural geology and geophysics, will provide fundamental and up to date understandings that will benefit future hydrocarbon exploration and development programs and highlight the present-day research gaps that can be further investigated.

The significantly reduced seismic resolution below Permian coal measures has made research difficult in the past. As a result, the structural and stratigraphic evolution of the province has received conflicting arguments through time, evolving from original models that display normal faults (Gravestock & Jensen-Schmidt, 1998), followed by researchers interpreting the

same structures as reverse faults (Kuang, 1985; Apak et al., 1997; Sun, 1997), to most recent studies that have presented evidence for extensive, compressional, and strike-slip faulting (Radke, 2009; Grant-Wooley, Kong, Schoemaker, Nasreddin & Montague, 2014; Kulikowski, Amrouch & Cooke, 2016c; Kulikowski, 2017; Kulikowski, Amrouch, Cooke & Gray, 2017; Kulikowski & Amrouch, 2017, 2018a, 2018b). These models are discussed and integrated with recent research to provide a modern tectonostratigraphic evolution model, which includes paleo-stress orientations, magnitudes and stress regimes that have affected the province through time.

This transition of structural models can also be linked to the improvement, and the use, of seismic time-to-depth conversion methods, which can have a significant impact on: (1) the true measurable fault dip angle; (2) the presence or absence of shallow low relief structures; and (3) pseudo structures resulting from high or low velocity heterogeneities. To promote the use and accuracy of high resolution 3D seismic data in future research, we describe the most commonly used seismic time-to-depth conversion methods, discuss their individual limitations and accuracies, identify the key seismic reflectors, and highlight the importance of accurate seismic time-to-depth conversion for future hydrocarbon exploration and research purposes.

Similarly, the improvement of petrophysics, drilling, and hydraulic fracture stimulation technologies has fostered exciting new research on geomechanics, optimisation of drilling programs, and in modelling the intrinsic relationship between hydraulic fracture stimulations and pre-existing natural fractures and faults (Chipperfield & Britt, 2000; Roberts, Chipperfield, & Miller, 2000; Johnson, Aw, Ball, & Willis, 2002; Johnson and Greenstreet, 2003; McGowen, Gilbert, & Samari, 2007; Scott et al., 2013; Johnson et al., 2015; Pokalai, Kulikowski, Johnson, Haghighi, & Cooke, 2016; Pokalai, 2018). Understanding the growth of hydraulic fractures, both temporally and spatially away from the wellbore, has been a strongly debated topic within the province (Scott et al., 2013; Cooke et al., 2015). The high stress environment, the effect of

pre-existing natural fractures, the influence of near wellbore pressure loss, and the complexity of intra-formational heterogeneity have contributed to ineffective hydraulic fracture programs in the past (Scott et al., 2013; Cooke, Tyiasning, & Abul Khair, 2016; Pokalai et al., 2016; Pokalai, 2018). These issues, together with current hydraulic fracturing practises and well surveillance programs, are discussed to provide fundamental background information for companies, both existing and new, that are investing in the basin.

This recent influx of high quality detailed research has been driven by the transition to a more technically challenging hydrocarbon exploration strategy. Few undrilled anticlinal traps remain within the basin, facilitating the shift to technically more challenging exploration that is focused on identifying new targets such as stratigraphic traps, basin centred gas, deep coals and polygonal fault related accumulations (Lowe-Young, Mackie, & Heath, 1998; Morton, 1998; Watterson, Walsh, Nicol, Nell, & Bretan, 2000; Hillis, Morton, Warner, & Penney, 2001; Radke, 2009; Mackie, 2015). This paradigm shift has tremendous opportunities for new investors and existing companies targeting hydrocarbons within this prolific basin. To facilitate this transition, the purpose of this research is to collate and critically discuss published works and integrate the key findings into a single document that provides: (1) a modern tectonostratigraphic evolution model; (2) a summary of geomechanical modelling results that predict fault and fracture reactivation (tensile and shear) through time to better understand hydrocarbon migration pathways; (3) a synthesis of the petroleum system processes and elements; (4) the spatial and temporal distributions of permeable natural fracture networks; (5) common hydraulic fracturing and well surveillance programs contrasted with the common difficulties and risks; (6) a discussion of the seismic time-to-depth conversion methods that are being used and their accuracies and limitations; (7) current and future hydrocarbon exploration and development targets; and (8) a discussion on the future research opportunities that can impact the success of future hydrocarbon programs.

This review collates and integrates previous research with modern understandings that can be disseminated within companies operating in the Cooper-Eromanga basins, Australia. The detailed methodologies, cutting-edge research and novel approaches form a research framework that can be applied to other subsurface or offshore provinces around the world.

Insert Fig. 1

2. Modern tectonostratigraphic evolution model

Unique to this province, the Silurian to Cambrian Warburton Basin, Triassic to Permian Cooper Basin, Cretaceous to Jurassic Eromanga Basin, and Paleogene to Quaternary Lake Eyre Basin are separated in time by regional unconformities that were developed through successive reactivation of pre-existing faults (Fig. 2) (Kantsler, Prudence, Cook, & Zwigulis, 1984; Bradshaw, 1993; Apak, 1997; Gravestock & Jensen-Schmidt, 1998; Mavromatidis, 2006). These vertically stacked basins have unique spatial extents and unique stratigraphy and hydrocarbon potential. The Warburton Basin is considered basement within this region and consists of volcanic, shallow shelf, deltaic and prograding shoreline deposits (Gatehouse, 1986). The Cooper Basin is the most hydrocarbon-rich, with a large volume of Permian coals that cycle with intra-formational sandstone and shale (Kantsler et al., 1984; Apak et al., 1997; Alexander, Gravestock, Cubitt, & Chaney, 1998). The Cooper Basin consists mostly of sediments deposited by fluvial, lacustrine, and swamp conditions. The Eromanga Basin is also hydrocarbon-rich with many of the present-day exploration programs targeting oil-rich Jurassic and Early Cretaceous sediments primarily along the western flank of the basin (Heath, McIntyre, & Gibbins, 1989). The depositional environment during this time transitioned from fluvial, lacustrine, deltaic, shoreface marine, and open shallow marine, with fluvial conditions returning to deposit one of the youngest and thickest units of the Eromanga Basin; the Winton

Formation (Lowe-Young et al. 1998). The Lake Eyre Basin is presently exposed at surface with no hydrocarbon potential.

The Permian coals are the major hydrocarbon source rock of the basin, and increase in thickness in the South Australian portion of the basin. As such, the major exploration and development targets are located within South Australia (Reynolds, Mildren, Hillis, & Meyer, 2004, 2006; Mackie, 2015). This portion of the basin contains two NE-SW striking ridges; the Gidgealpa-Merrimelia-Innamincka (GMI) Ridge and the Nappacoongee-Murteree (NM) Ridge (Fig. 3b) (Kuang, 1985; Apak et al., 1997; Gravestock & Jensen-Schmidt, 1998; Kulikowski, 2017). These prominent ridges form the major hydrocarbon fields in this sector of the basin and also separate the NE-SW elongate Patchawarra, Nappamerri and Tenappera troughs (Fig. 3). In the following sections, the structural and stratigraphic evolution of this intra-cratonic region will be discussed, with emphasis on the most up-to-date research.

Insert Fig. 2

Insert Fig. 3

2.1 Pre-Cambrian Extension (650-575 Ma)

During the Late Proterozoic much of the world's landmass was submerged by ocean with a relatively small landmass exposed at surface, consisting of portions of what is now Antarctica, India, South Africa, Congo, and the western portion of Australia (Fig. 4a) (Myers, Shaw, Tyler, 1996; Boger & Miller, 2003; Collins & Pisarevsky, 2005; Kulikowski and Amrouch, 2017). The ancient Australian landmass was in a similar geometry to present-day; slightly rotated in a clockwise direction and bisected in an NNE-SSW direction by the paleo-tectonic plate boundary (Myers et al., 1996; Boger & Miller, 2003; Collins & Pisarevsky, 2005). This boundary is now referred to as the Tasman Line that separates the younger land mass in eastern Australia from the rest of the continent (Haines, Hand, & Sandiford, 2001). Rifting within the

Panthalassic Ocean, east of the ancient plate, began in the Late Proterozoic (650 Ma) in an approximately SE-NW direction. This regional rifting event affected the then Centralian Superbasin as well as the Warburton Basin, developing SE-NW striking strike-slip faults and NE-SW striking normal faults within the Igneous Meta-sedimentary Willyama Supergroup (Veevers & Powell, 1984; Evan, 1988; Apak et al., 1997). These basin- to continent-scale SE-NW strike-slip faults are present within many other Australian provinces (Myers et al., 1996; Gibson et al., 2013).

Deep fault development during the Early Cambrian was concurrent with exhumation of the Mooracoochie Volcanics, which marks the base of the Warburton Basin stratigraphy (Gatehouse, 1986; Sun, 1997; Meixner et al., 2000). Continued extension developed accommodation space for the deposition of shallow shelf sediments that became the Diamond Bog Dolomite (~510 Ma), Coongie Limestone Member (~505-497 Ma), and Kalladeina Formation (~508-485 Ma) (Gatehouse, 1986). As relative sea levels rose, the depositional environment transitioned into low-stand fan, deltaic, and prograding shoreline, which deposited the Narcoonowie Formation (~490 Ma), Pando Formation (~488 Ma), and Innamincka Formation (~485-435 Ma) (Gatehouse, 1986; Rezaee & Sun, 2007). Regional erosion of the upper Innamincka Formation represents the unconformable boundary to the overlying Permian to Triassic Cooper Basin.

Insert Fig. 4

2.2 Carboniferous Alice Springs Event (450-300 Ma)

The Alice Springs Event (ASE) has had a significant influence on the tectonic development of central and northern Australia (Haines et al., 2001). Its effect has been recorded in a number of petroleum basins and structural provinces, including the Amadeus, Ngalia, Georgina, Wiso, Officer, and Warburton basins, as well as the Arunta and Musgrave inliers (Haines et al., 2001).

Calcite twin, natural fracture and fault data from within the South Australian portion of the Warburton Basin has constrained this regional tectonic event to have occurred under a strike-slip stress regime with maximum principal stress in an N-S direction in this region (Fig. 4b) (Kulikowski & Amrouch, 2017). The effective maximum principal stress magnitude was also calculated (49 MPa) through calcite twin stress inversion (Fig. 4i) (Kulikowski & Amrouch, 2018b). Geomechanical modelling of fault reactivation under this paleo-stress tensor identified N-S and NE-SW striking high angle (50-70^{o}), and SE-NW striking strike-slip faults to be the most likely to reactivate (Kulikowski & Amrouch, 2018b). A NNE-SSW and SE-NW striking vertical conjugate natural fracture set was developed during this event and is present only within the Warburton Basin stratigraphy (Kulikowski & Amrouch, 2017).

As mentioned earlier, the stratigraphy of this region contains a regional unconformity that separates the Warburton and Cooper basins and is a result of basement fault reactivation, exhumation and erosion of upper Warburton Basin sediments. Carboniferous Big Lake Granodiorite was also exhumed during this event in local regions south of the GMI Ridge and provides elevated contemporary temperature gradients due to their high uranium content (Meixner et al., 2000; Kulikowski, Cooke, & Amrouch, 2016a). The Australian continent remained connected to Antarctica during this time and exposed to plate scale glaciation (Collins & Pisarevsky, 2005; Gray & Foster, 2004; Metcalfe, 2013).

As the continent began to escape glaciation during the Late Carboniferous to Early Permian, the glacial Merrimelia Formation (~290 Ma) was deposited onto the regional unconformity, marking the base of the Cooper Basin. The overlying Tirrawarra Formation (~287 Ma) was deposited in a postglacial outwash to braided fluvial depositional environment (Lowe-Young et al., 1998; Mavromatidis, 2006). The Tirrawarra Formation is produced for oil, albeit being deeper and under higher temperatures and pressures than the gas-rich middle to upper Permian and Triassic reservoirs (Gravestock et al., 1998). The depositional environment transitioned

into fluvio-deltaic, lacustrine and swamp during the middle Permian, and deposited repeated cycles of sandstone, shale, and coal to compose the predominantly gas-rich Patchawarra Formation (~285-260 Ma) (Kantsler et al., 1984; Apak et al., 1997; Alexander et al., 1998).

2.3 Mid-Permian Event (290-270 Ma)

During deposition of the Patchawarra Formation, intra-formational on-lapping is observed from seismic data along paleo-structural highs, which are more often than not also the present-day structures (Apak et al., 1997; Gravestock & Jensen-Schmidt, 1998). On-lap is observed between 273 and 270 Ma, inferring that structural highs were present during the Mid-Permian and limited the accommodation space (Apak et al., 1996; Kulikowski & Amrouch, 2017, 2018a). Seismic interpretation aligns with stress inversion of calcite twin, natural fracture and fault data, which demonstrate a compressional SE-NW oriented event with an effective maximum principal stress magnitude of 56 MPa (Fig. 4i) (Kulikowski & Amrouch, 2017, 2018b). The far-field stresses likely originated from the approximately NE-SW to N-S striking subduction line along the eastern margin of Australia (Fig. 4c). The paleo-stress conditions likely reactivated E-W, NE-SW and N-S striking high angle (50-70^{o}) faults and developed a regional NE-SW striking low dip angle (30^{o}) conjugate natural fracture set within the Patchawarra, Tirrawarra and Merrimelia formations and also within basement (Kulikowski, 2017; Kulikowski & Amrouch, 2017, 2018b).

As compression from the short lived Mid-Permian Event eased, the upper Patchawarra Formation became finer grained and more shale dominated (Apak et al., 1997). An east to west transgression ended the deposition of the Patchawarra Formation, transitioning into a shoreface and lacustrine dominated environment that deposited the Murteree Shale (~264 Ma), Epsilon Formation (~262 Ma), Roseneath Shale (~260 Ma), and Daralingie Formation (~258 Ma) (Bradshaw, 1993; Apak et al., 1997; Gravestock & Jensen-Schmidt, 1998; Lowe-Young et al.,

1998; Mavromatidis, 2006). The Roseneath-Epsilon-Murteree (REM) stratal unit represents the major shale gas play in the region with total organic carbon (TOC) values ranging between 1.0 and 4.1% (Jadoon, Roberts, Blenkinsop, Raphael, & Shah, 2016).

2.4 Late Permian Daralingie Event (258 Ma)

Following the deposition of the Daralingie Formation, an erosional unconformity was first identified in 2D seismic data (Apak et al., 1996) and later confirmed through calcite twin stress inversion analysis (Kulikowski, 2017; Kulikowski & Amrouch, 2017). This SE-NW oriented strike-slip stress regime event recorded an effective maximum principal stress magnitude of approximately 56 MPa (Fig. 4i) that reactivated NE-SW striking high angle (50-70^{o}) faults (Kulikowski & Amrouch, 2018b). This event is most notable along the NE-SW striking GMI and NM ridges, as a significant portion of the Daralingie Formation was eroded from these areas (Kuang, 1985; Apak et al. 1997; Mavromatidis, 2006). New fracture and fault development was absent during this time, with the stress preferentially accommodated along pre-existing faults (Kulikowski et al., 2017). The far-field stress was likely related to the N-S striking subduction zone east of Australia during this time (Fig. 4d) (Kulikowski & Amrouch, 2017).

2.5 Upper Triassic Hunter-Bowen Event (245-190 Ma)

Post-compressional flexural relaxation, or sag, followed the Daralingie Event and generated accommodation space for the deposition of the Toolachee Formation (~250 Ma) that consists of sands, shales and coals deposited under meandering fluvial to deltaic conditions (Kantsler et al. 1984; Apak et al. 1997; Lowe-Young et al., 1998). The depositional environment transitioned to a floodplain, lacustrine and fluvial channel system in the Triassic, depositing the Nappamerri Group, which includes the Callamurra Member (~245 Ma), Panning Member (~243 Ma), Wimma Sandstone Member (~241 Ma), Tinchoo Formation (~238 Ma), and the

Cuddapan Formation (~210 Ma) (Kantsler et al., 1984; Apak et al., 1997; Alexander et al., 1998; Lowe-Young et al., 1998; Mavromatidis, 2006). The early Nappamerri Group was likely charged with oil and gas from the underlying Toolachee Formation, and perhaps along fault conduits from the deeper early Permian source rocks (Lowe-Young et al., 1998).

A regional erosional unconformity is carved into the upper Tinchoo Formation and the majority of the Cuddapan Formation, which is only present in local areas of the basin (Lowe-Young et al., 1998). This unconformity separates the Cooper and Eromanga basins and marks the timing of the Hunter-Bowen Event. The maximum principal stress was horizontal and in an E-W direction (Fig. 4e) (Kuang, 1985; Apak et al., 1997; Gravestock & Jensen-Schmidt, 1998; Kulikowski & Amrouch, 2017). The regional erosional boundary was first interpreted from 2D seismic data (Kuang, 1985; Apak et al., 1997) and later confirmed through calcite twin stress inversion, and natural fracture and fault stress inversion (Kulikowski & Amrouch, 2017). Calcite twin stress inversion results identified an E-W oriented compressional event with an effective maximum principal stress magnitude of 60 MPa (Fig. 4i) corresponding to the Hunter-Bowen Event (Kulikowski & Amrouch, 2017, 2018b). Geomechanical modelling using this stress tensor identified that NE-SW striking high angle (50-70^{o}) faults were most likely to shear reactivate at this time (Kulikowski & Amrouch, 2018b). Reactivation of predominantly this fault set exhumed and eroded up to 500 meters of Nappamerri Group sediments (Apak et al., 1997; Kantsler et al., 1983; Alexander et al., 1998; Mavromatidis, 2006).

2.6 Late Cretaceous Event (95-55 Ma)

As the Hunter-Bowen Event subsided, flexural relaxation generated accommodation space and a fluvial depositional environment transcended, which deposited the Poolowanna Formation (~200-180 Ma) onto the regional unconformity (Green, Brain, & John, 1989;

Hoffman, 1989; Lowe-Young et al., 1998). Tectonic quiescence continued with the deposition of the braided fluvial Hutton Sandstone (~178-160 Ma), fluvial to lacustrine Birkhead Formation (~157 Ma), and braided fluvial to lacustrine Adori Sandstone (~152 Ma) (Lowe-Young et al., 1998). The braided fluvial to lacustrine depositional environment continued in the region, depositing the Namur Sandstone (~152-140 Ma), Westbourne Formation (~150 Ma), and the oil-rich Murta Member (~140 Ma) (Lowe-Young et al., 1998). Jurassic units contain abundant oil (and gas) reservoirs at a shallower depth than Permian reservoirs, and currently primarily targeted on the western flank of the Cooper Basin (Heath et al., 1989).

The depositional environment transitioned into fluvial to shallow marine conditions and deposited the Cadna-owie Formation (~140-126 Ma) (Lowe-Young et al., 1998). The overlying Wyandra Sandstone Member (~125 Ma) was deposited under deltaic to shoreface marine conditions and contains some oil and gas potential (Lowe-Young et al., 1998). Following this, the Bulldog Shale (~125-108 Ma) and Wallumbilla Formation (~125-104 Ma) were deposited in restricted open marine conditions, which transitioned into a shoreface depositional environment to deposit the Coorikiana Sandstone (~105 Ma), in which some gas discoveries have been recently made (Lowe-Young et al., 1998). Shallow open marine conditions developed and deposited the Oodnadatta Formation (~104-98 Ma), Toolebuc Formation (~103 Ma), and Allaru Mudstone (~100 Ma) (Lowe-Young et al., 1998). Finally, the Winton Formation (~97-93 Ma) and Mackunda Formation (~97 Ma) were deposited by fluvial-lacustrine conditions to mark the final period of sediment deposition within the Eromanga Basin (Lowe-Young et al., 1998). These Middle to Late Cretaceous marine sediments also host the regionally extensive polygonal fault system that presents a new target for future exploration (Watterson et al., 2000). The critical moment in the Cooper-Eromanga basins hydrocarbon system, which marks the time of major hydrocarbon generation, migration, accumulation and preservation, occurred around 90 Ma (Lowe-Young, et al., 1998).

The Winton and Mackunda formations were significantly eroded following their exhumation by the E-W Late Cretaceous compressional Event (Fig. 4f) (e.g. Kuang, 1985; Green et al., 1989; Hoffman, 1989; Apak et al., 1997; Gravestock & Jensen-Schmidt, 1998; Lowe-Young et al., 1998; Mavromatidis, 2006; Kulikowski & Amrouch, 2017, 2018a). Folding related to pre-existing NE-SW striking faults, rather than reactivation, facilitated the development of this erosional boundary, which separates the Eromanga and Lake Eyre basins (Fig. 2). An effective maximum principal stress magnitude of 59 MPa was measured from calcite twin stress inversion analysis (Fig. 4i) (Kulikowski & Amrouch, 2018b). N-S striking low angle (30^{o}) conjugate natural fractures were developed during this time (Kulikowski & Amrouch, 2017). Considering that this event occurred during and after the critical moment, understanding the dilation and shear tendency of faults is vital for accurate migration pathway modelling. Under these stress conditions, E-W and NE-SW striking high angle (60^{o}) faults were the most likely to act as hydrocarbon conduits (Kulikowski & Amrouch, 2018b).

2.7 Paleogene Event (33-23 Ma)

During deposition of the Lake Eyre Basin, which is presently at surface, an N-S oriented Paleogene compressional event developed E-W striking low angle (30^{o}) conjugate natural fractures throughout the stratigraphic column (Kulikowski & Amrouch, 2017). This event is attributed to the northwards movement of the Australian plate (Fig. 4g). The effective maximum principal stress magnitude of this event was calculated from calcite twin stress inversion analysis and found to be 64 MPa (Fig. 4i) (Kulikowski & Amrouch, 2018b). Interestingly, this event does not appear to have reactivated or developed faults; however, N-S and NE-SW striking high angle (50-70^{o}) faults are considered to have been likely to dilate and act as permeable hydrocarbon conduits (Kulikowski & Amrouch, 2018b).

3. Petroleum Systems Elements

3.1 Hydrocarbon Source Rocks

Hydrocarbons in the Cooper Basin are principally sourced from intra-formational Permian coals and Permian to Jurassic carbonaceous shales, and reservoired within fluvial sandstones (Fig. 5) (Boreham & Hill, 1998). The petroleum system is largely gas saturated with small volumes of liquids found in localised areas (Kantsler et al., 1984). As such, the isotopic composition of intra-formational coals and carboniferous shales indicates fresh water origin and dominated by high order plants (Kantsler et al., 1984; Boreham & Hill, 1998). The Toolachee, Daralingie, Epsilon and Patchawarra formations contain an average total organic content (TOC) of 3.9% and 6.9 kg/tonne of hydrocarbon (Smyth, 1983; Boreham and Hill, 1998). The most organic-rich source rock is within the Toolachee Formation, averaging 214 kg/tonne (Hydrogen index) across the Cooper Basin (Boreham & Hill, 1998). Liquid hydrocarbon yields are low in Permian reservoirs due to high vitrinite and inertinite (Type III kerogens) composition in shale and coal measures, and are absent within the over mature Nappamerri Trough, which contributes only dry gas (Kantsler et al., 1984; Boreham & Hill, 1998).

Insert Fig. 5

The hydrocarbon source for the overlying Eromanga Basin is more uncertain, and likely to be sourced from: (1) non-marine Jurassic aged rocks (Powell et al., 1989; Lowe-Young et al., 1998); (2) Permian shales and coals with migration through reactivated faults (Heath et al., 1989; Lowe-Young et al., 1998); and (3) a combination of both Jurassic and Permian source rocks (Fig. 6c) (Kantsler et al., 1984; Jenkins, 1989; Lowe-Young et al., 1998). Jurassic aged units contain oil and gas; however, only gas has been discovered in Cretaceous aged reservoirs in the Strzelecki, Packsaddle and Nappacoongee regions (Kantsler et al., 1984). Permian aged

source rocks are currently within the gas window, with Jurassic to Cretaceous source rocks currently at peak oil generation in the deep basin centres (Kantsler et al., 1984).

Insert Fig. 6

3.2 Hydrocarbon Generation

Permian and Triassic source rocks reached the hydrocarbon generation window as early as the Permian to Middle Triassic during maximum burial (Fig. 6), and peaked during a secondary sag period in the Middle Cretaceous (Deighton & Hill, 1998; Mavromatidis, 2006). Relatively minor hydrocarbon generation and expulsion commenced in the Permian to Middle Triassic, before peaking in the Middle to Late Cretaceous and potentially continues today (Fig. 6a & 6b) (Pitt, 1986; Duddy, 1987; Gallagher, 1988; Lowe-Young et al., 1998; Mavromatidis, 2006; Deighton & Hill, 2009). Minor volumes of hydrocarbons were also generated in the Nappamerri Trough during the Permian, and, given sufficient residual kerogen, the effect of Late Tertiary elevated temperatures and Tertiary deposition may have led to secondary (late-stage) hydrocarbon generation and expulsion in certain parts of the basin (Fig. 6b) (Deighton & Hill, 2009).

Although a rare phenomenon, the concentration of carbon dioxide (CO_2) within the Cooper-Eromanga basins is significantly higher (10-30 v/v%) than typical sedimentary basins (Rigby & Smith, 1981; Kantsler et al., 1984; Wycherley, Fleet, & Shaw, 1999). However, the origin remains somewhat questionable, but could be related to: (1) an increase in coal thickness, with regions containing thick coal deposits, such as the Patchawarra Trough, containing the highest CO_2 concentrations; or (2) magmagenesis or metamorphic reactions, which is also supported by the correlation between raised CO_2 levels and the presence of Carboniferous Uranium-rich Moomba-Big Lake Granodiorite (Gatehouse, 1986; Wycherley et al., 1999).

3.3 Hydrocarbon Migration

Hydrocarbon generation and expulsion is divided into three phases: (1) early expulsion between the Late Permian and Early Triassic; (2) primary expulsion within the Cretaceous; (3) and a possible secondary expulsion during the Late Cenozoic (Fig. 6) (Lowe-Young et al., 1998; Radke, 2009). These three phases of expulsion coincide with the timing of hydrocarbon migration (Fig. 6c) (Lowe-Young et al., 1998; Radke, 2009). Hydrocarbon generated from Permian source rocks migrated short distances to the vertically stacked overlying or underlying intra-formational reservoirs, or alternatively along deep seated and reactivated basement-involved faults into overlying Eromanga Basin reservoirs (Boreham & Hill, 1998; Gravestock et al., 1998; Radke, 2009). Tertiary hydrocarbon migration through stacked intra-formational seals into overlying reservoirs has also been discussed (Heath et al., 1989; Boult, Lanzilli, Michaelsen, McKirdy, & Ryan, 1998; Gravestock et al., 1998; Hillis et al., 2001; Radke, 2009). Geomechanical modelling of fault reactivation (dilation and shear) through time highlighted the changing conduit potential of individual fault sets as stress conditions changed (Kulikowski et al., 2016c; Kulikowski, 2017; Kulikowski & Amrouch, 2018b). See chapter 10 for more detail.

Secondary hydrocarbon migration from Permian source rocks into overlying Jurassic Eromanga Basin reservoirs has been suggested by numerous authors after observing oil compositions that were not consistent with a Jurassic origin (Heath et al., 1989; Hallmann, Arouri, McKirdy, & Schwark, 2007). The origin of Jurassic oils has been found to be from either: (1) Permian source rocks; (2) Jurassic source rocks; or (3) a combination of the two (Smyth, 1983; Heath et al., 1989; Lowe-Young et al., 1998; Hallmann et al., 2007). In the case of Permian source rock origin, secondary migration of oil was through: (1) permeable fault conduits into shallow Eromanga Basin reservoirs; or (2) through a permeable carrier bed in the up-dip direction towards the flanks of the basin, where overlying Triassic sealing units

effectively pinch-out and allow the oil to migrate into directly overlying reservoir rocks (Heath et al., 1989; Lowe-Young et al., 1998; Borazjani, Kulikowski, Amrouch, & Bedrikovetsky, 2018, 2019). These flank regions host many large producing oil fields (Heath et al., 1989; Borazjani et al., 2018, 2019). In these two migration pathway cases, the oil composition between source and reservoir has shown to be different due to the effects of deep bed filtration (Borazjani et al., 2018, 2019), or water-washing (Heath et al., 1989) of hydrocarbons.

The ability of a fault to act as a potential hydrocarbon conduit can be measured by calculating the Dilation Tendency, or the likelihood of faults to undergo tensile reactivation. Alternatively the likelihood of faults to shear reactivate can be measured by calculating Slip Tendencies. These likelihoods were calculated for four regional fault sets, which were modelled under six unique paleo-stress tensors (Alice Springs Event, Mid-Permian Event, Daralingie Event, Hunter-Bowen Event, Late Cretaceous Event, and Paleogene Event), as well as the present-day stress conditions (Kulikowski et al., 2016c; Kulikowski, 2017; Kulikowski & Amrouch, 2018b). The results of these studies found that early expulsion of hydrocarbons would have preferentially migrated along NE-SW striking high angle (50-70^{o}) faults during the Late Permian and along E-W striking high angle (50-70^{o}) faults during the Late Triassic. Since the critical moment (90 Ma) hydrocarbons would have preferentially migrated along E-W striking high angle (50-70^{o}) faults during the Late Cretaceous and N-S striking high angle (50-70^{o}) faults during the Paleogene. Hydrocarbons generated during the secondary phase, or present-day, would likely be migrating along E-W striking high angle (50-70^{o}) faults or SE-NW strike-slip faults. See Chapter 6.2 for more detail.

3.4 Hydrocarbon Seals and Trap Development

Intra-formational fluvial-lacustrine to lacustrine shales and coal measures form cyclically deposited impermeable seals to underlying reservoirs, while also acting as potential source rocks to overlying reservoirs (Bradshaw, 1993; Gravestock & Jensen-Schmidt, 1998). These vertically stacked intra-formational shales and coals have the highest influence on sealing hydrocarbons within the four-way closing anticlinal traps that are present throughout the basin (Gravestock et al., 1998). The Nappamerri Formation, Roseneath Shale, and Murteree Shale are highly efficient regional seals to the Toolachee, Epsilon, and Patchawarra formations, respectively; however, intra-formational shales hold back hydrocarbon to individual and compartmentalised intra-formational sandstone reservoirs (Gravestock et al., 1998; Gray, 2017; Gray, Daniel, Kaldi, & Kulikowski, 2019). Cretaceous marine sediments and the Late Jurassic Birkhead Formation form regional seals for Jurassic to Early Cretaceous Eromanga Basin reservoirs (Gravestock et al., 1998; Radke, 2009).

The regional Murteree Shale and intra-formational Patchawarra Formation seals are eroded along the western margin of the basin contributing to the significant number of oil discoveries made along the western flank, as oil migrates from the deep sections of the Patchawarra Trough into shallow Eromanga Basin reservoirs (Radke, 2009). Low relief structural closures within the Eromanga Basin are sealed by the regional Birkhead and Wallumbilla formations, facilitating the accumulation of hydrocarbons (Radke, 2009; Kulikowski, Hochwald, Cooke, & Amrouch, 2016b; Kulikowski, Hochwald, & Amrouch, 2018b). A regional polygonal fault system is present within Cretaceous sediments and is observed to occasionally penetrate into the hydrocarbon-rich Murta Member (Fig. 7) (Watterson et al., 2000; Kulikowski, 2017; Kulikowski et al., 2017). Where these normal faults are approximately E-W striking and penetrate into the Murta Member, hydrocarbons may be migrating through permeable fault

conduits into shallow reservoirs, possibly presenting a new exploration strategy (Watterson et al., 2000; Kulikowski et al., 2017).

Insert Fig. 7

Structural trap development occurred as early as the Mid-Permian Event and Late Permian Daralingie Event, coinciding with the early phase of hydrocarbon generation and expulsion (Deighton & Hill, 1998; Kulikowski & Amrouch, 2018a). Key anticlinal traps were developed by two subsequent events; the E-W Hunter-Bowen Event and E-W Late Cretaceous Event (Kulikowski & Amrouch, 2017, 2018a). These two events reactivated basement-involved faults to create broad anticlinal domes within the Permian, and low relief anticlines within Cretaceous sediments prior to the primary phase of hydrocarbon generation and expulsion (Deighton & Hill, 1998). The N-S Paleogene Event (33-23 Ma) may have contributed to a late-stage of structural trap development; however, this occurred significantly after the critical moment in the hydrocarbon system and may have negatively influenced the preservation of existing hydrocarbon accumulations (Lowe-Young et al., 1998; Kulikowski & Amrouch, 2018a, 2018b). Although the majority of accumulations are trapped by anticlines, there does exist an opportunity to begin targeting higher risk stratigraphic pinch-out traps and on-lapping features that are common within the basin, particularly within the hydrocarbon-rich Patchawarra Formation (Apak et al., 1997; Kulikowski, 2017; Kulikowski & Amrouch, 2018a).

3.5 Hydrocarbon Accumulation and Preservation

Hydrocarbons are primarily reservoired within the Tirrawarra Formation, Patchawarra Formation, Epsilon Formation, Daralingie Formation, and Toolachee Formation of the Cooper Basin, and the Hutton Formation and Namur Sandstone of the Eromanga Basin (Kantsler et al., 1984; Alexander et al., 1998; Gravestock et al., 1998; Mackie, 2015). Although these are the dominant oil and gas producers, with the Hutton Sandstone contributing greater than 50% of

oil discoveries (by volume) in the Eromanga Basin, hydrocarbons can be found in virtually all reservoir-quality zones older than the Late Cretaceous (Kantsler et al., 1984; Lowe-Young et al., 1998; Radke, 2009). The majority of Cooper Basin hydrocarbon discoveries are located within the South Australian region, reflecting the significantly greater volume of Permian source rocks (Kantsler et al., 1984; Reynolds et al., 2006). Primary hydrocarbon accumulation commenced during the Late Cretaceous critical moment (90 Ma), with existing fields withstanding the Late Cretaceous Event (95-55 Ma), Paleogene Event (33-23 Ma), and the present-day stress environment (Fig. 6c) (Kantsler et al., 1984; Lowe-Young et al., 1998; Mackie, 2015; Kulikowski & Amrouch, 2017).

The preservation of accumulations appears to be unaffected by these three events, as seismic data shows that basement-involved faults were not reactivated; however, sub-seismic resolution faulting may be possible considering that resolution is not better than 15 m (Kulikowski et al., 2017; Kulikowski and Amrouch, 2018b). Fault reactivation causing less than 15 m of displacement can be sufficient to cause seal breach and facilitate tertiary migration of hydrocarbons, particularly if fault geometries are optimally oriented to tensile reactivate (dilate). Geomechanical modelling of fault reactivation has shown that the most common fault set, NE-SW striking high angle (50-70^{o}), was the most likely to shear reactivate during the four most recent (Daralingie Event, Hunter-Bowen Event, Late Cretaceous Event, Paleogene Event) tectonic events (Kulikowski & Amrouch, 2018b). Under contemporary stresses, SE-NW strike-slip faults are most likely to shear reactivate and must be accurately interpreted because of the high likelihood of interacting with, and complicating, hydraulic fracture stimulations (Pokalai et al., 2016; Pokalai, 2018; Kulikowski et al., 2016c).

4. Geophysics

4.1 Significant Seismic Reflectors

With the majority of Cooper Basin hydrocarbons reservoired within Permian rocks, the near top Toolachee Formation (P-reflector), near top Patchawarra Formation (V-reflector), and middle Patchawarra (VC-reflector) seismic reflectors are most commonly interpreted and associated with regionally consistent coal markers (Kulikowski, 2017). The Cretaceous Cadna-owie Formation reflector (C-reflector) is an easily identifiable and regional strong amplitude reflector (Fig. 8a). Its interpretation provides the structural trap geometry for Jurassic and Cretaceous reservoirs, as well as providing broad insights into the underlying structures. This reflector also shows intermittent normal displacement caused by polygonal faults extending down from the Mackunda Formation (AM-reflector) into the deeper hydrocarbon-rich Murta Member (D-reflector) (Fig. 7). The top Nappamerri Group reflector (N-reflector) shows a similar characteristic to the Cadna-owie Formation reflector, although with variable amplitude due to the erosional boundary that it represents (Fig. 8a). This reflector marks the boundary between the Cooper and Eromanga basins.

Insert Fig. 8

In the area of this study, the top of Permian sedimentation is identified by an abrupt strong amplitude package that represents the fluvial to deltaic Toolachee Formation (P-reflector) (Fig. 8a). The top Patchawarra Formation (V-reflector) is notoriously bland, attributed to the relatively more transitional boundary between the upper Patchawarra Formation and the Murteree Shale (U-reflector) that results in a low acoustic impedance boundary. As such, the stronger amplitude reflector immediately below the top Patchawarra Formation is typically interpreted (Fig. 8a). Within the Patchawarra Formation, the VC30 and VC50 coal measures produce strong amplitude (soft-kick) reflectors; however, the reflectors commonly split and

merge (Fig. 8a). Middle Patchawarra Formation reflectors have been shown to on-lap onto paleo-structures correlating to the Mid-Permian Event (290-270 Ma) (Apak et al., 1997; Kulikowski & Amrouch, 2018a). Below the Permian coal measures, seismic resolution rapidly decays and the interpretation of reflectors and faults becomes difficult (Fig. 8a). The Tirrawarra and Merrimelia formation reflectors are absent in some parts of the basin and require high well control to be interpreted accurately.

Seismic interpretation of the basement (Z-reflector) is again difficult throughout the basin, commonly requiring phantom interpretation through significant fault shadow and decayed amplitude (Fig. 8a). Seismic resolution has been calculated to be upwards of 150 m, in contrast to Cretaceous reflectors that can be between 15-20 m (Kulikowski, 2017; Kulikowski et al., 2017). Recently acquired 3D seismic surveys have much greater resolution below Permian coal measures, with broadband and full-azimuthal seismic data expected to significantly improve the resolution in the near future.

4.2 Seismic Time-to-Depth Conversion Methods

The seismic time-to-depth conversion process can incur large (10’s of feet) errors caused by local velocity anomalies, incorrect well ties, or more commonly from a poor understanding of the near surface velocity variation, or statics. Although errors cannot be removed entirely, selecting the most accurate depth conversion method for the given study area can have noticeable effects. For example, the presence of low relief hydrocarbon-rich structural traps within the Eromanga Basin can depend on the depth conversion method being used (Kulikowski, 2017; Kulikowski et al., 2016b, 2018b). Additionally, fault analysis may lead to incorrect results if seismic data remains in the time-domain, as fault geometries will change once in the depth-domain (Fig. 8b & 8c).

555 Complete seismic volume time-to-depth conversion is often time consuming and not
556 necessary for generating simple reflector maps. As such, time-to-depth conversion is often
557 performed at a mapped level using gridding software, or horizon maths tools built into seismic
558 processing and interpretation software. For the purpose of generating reflector maps, only the
559 interpreted two-way-time (TWT) seismic reflector grid, rather than the seismic volume, is
560 converted. In the simplest sense, the TWT grid is multiplied by a constant velocity to generate
561 a depth grid. Three seismic time-to-depth conversion methods are commonly used within the
562 Cooper-Eromanga basins, including the: (1) pseudo average velocity method (Fig. 9a); (2)
563 time-depth trend method (Fig. 9b); and (3) interval velocity method (Fig. 9c).

564 Insert Fig. 9

565 ***4.2.1 Pseudo Average Velocity Method***

566 The pseudo average velocity (V_a) method is one of the more simple, yet most commonly used,
567 seismic time-to-depth conversion methods within the Cooper-Eromanga basins. This simple
568 approach does not explicitly consider velocity anomalies. Rather, for any given well location
569 and for any given reflector, the depth (Δz: depth in feet) is obtained from well data and the
570 interpreted time (Δt: one-way-time in seconds) obtained from seismic data (Fig. 9a). The ratio
571 of the two measured values provides the V_a at the well location, such that;

572 $$V_a = \frac{\sum_{k=1}^{n} z_k}{\sum_{k=1}^{n} t_k} = \frac{\Delta Z\ (ft)}{\Delta t\ (s)}$$

573 Where k is the k^{th} reflector measured from n well locations. The time-to-depth conversion
574 process involves multiplying the resultant V_a with the seismic data (one-way-time: OWT in
575 seconds), to give depth (ft), such that;

576 $$Depth = V_a * OWT$$

For seismic data that contains an abundance of well control, the V_a for each well location can be averaged to determine the overall mean V_a of the entire survey. Alternatively, the V_a values at each well location can be gridded to produce a spatial contour map of V_a, which can take into account spatial velocity anomalies. The V_a from the surface to the Upper Cretaceous, Cadna-owie Formation, and Top Permian seismic reflectors was measured from 12 3D seismic surveys (Fig. 3b) to give a basin wide V_a value (Fig. 9d). The basin wide V_a from the mean sea level to the: (1) Upper Cretaceous reflector is 2,280 m/s, (2) Cadna-owie Formation reflector is 2,375 m/s; and (3) Top Permian reflector is 2,740 m/s (Fig. 9d). Although simplistic, this method was found to be one of the most accurate in the Cooper-Eromanga basins for converting interpreted reflector surfaces from the time-domain to the depth-domain (Rady, 2006; Kulikowski et al., 2016b, 2018b; Kulikowski, 2017). The accuracy of time-to-depth conversion methods for entire 3D seismic volumes has yet to be explored.

4.2.2 Time-Depth Trend Method

The time-depth (T-D) trend method utilises the relationship between the TWT and depth values for a given reflector, hence is closely related to the pseudo average velocity method. The T-D pairs of various reflectors at a given well location are plotted on a two-way graph and a linear ($y = mx + c$), or occasionally exponential ($y = ax^2 + bx + c$), trend is defined, where *y* is depth, *x* is time, *m* is slope, and *a*, *b*, and *c* are constants (Fig. 9b). The T-D trend equation that defines the distribution is used to directly convert the TWT seismic data to depth. The T-D Trend (Fig. 9e) from the 12 3D seismic surveys (Kulikowski et al., 2017) was found to be approximately;

$$Depth\ (m) = 280.5 * (TWT)^2 + 847.97 * (TWT)$$

Where *TWT* is two-way-time measured in seconds. Not all T-D pairs will plot precisely on this trend, and may create poor well ties. Therefore, when performing a time-to-depth

conversion on a gridded reflector, the resultant depth grid must be tied to the well control precisely by firstly gridding the error between the depth and the time-to-depth converted grid, and secondly subtracting the resultant error correction grid from the time-to-depth converted grid (Kulikowski et al., 2016b, 2018b; Kulikowski, 2017).

This method of time-to-depth conversion is a commonly used method in the Cooper-Eromanga basins, with early work utilising check-shot data and continuous velocity logs to calibrate seismic data. Continuous velocity logs can provide direct input data for velocity models and T-D pairs for key stratigraphic markers. It should be noted, however, that velocities from velocity logs and the velocities used for depth conversion are very different to each other and if used, a conversion factor map needs to be generated. Check-shot data for time-to-depth conversion has somewhat become outdated, with advancements in technology providing more accuracy through vertical seismic profile (VSP) acquisition (Levin & Lynn, 1958; Ganley & Kanasewich, 1980; Hauge, 1981; Balch, Lee, Miller, & Ryder, 1982; Balch & Lee, 1984; Hardage, 1985; Gajewski & Pšenčik, 1990). Check-shot and VSP data are obtained in a similar fashion to seismic data, where a P-wave travel time is measured from the surface to a downhole receiver (Stainsby & Worthington, 1985). In the case of check-shot and VSP data, the receiver is lowered through the borehole at various levels. However, the resolution of VSP data is significantly higher than check-shot data, as the number of borehole receivers can be as dense as every 25 m, in contrast to check-shot data that is only collected at key stratigraphic intervals.

4.2.3 Interval (Layer-Cake) Velocity Method

The interval velocity (V_i) method is used to represent the abrupt vertical changes in velocity evident across significant stratigraphic packages. A look at continuous velocity logs and synthetic seismograms shows that velocities are not constant and can abruptly increase or decrease depending on the rock composition (Al-Chalabi, 1974). The more basic interval

velocity model divides the subsurface into key stratigraphic packages that have unique velocities (V_i), such that the depth can be calculated by;

$$Depth = \sum_{j=1}^{n} V_i(t_{j+1} - t_j)$$

Where *n* is the number of intervals (layers) bound by the j^{th} reflectors, which are measured in the time-domain, *t* (one-way-time), at a given well location.

High velocity cemented calcite zones (CCZ) are present within the Eromanga Basin and can distort the true subsurface image when not incorporated into velocity models (Kulikowski et al., 2016b; Kulikowski, 2017). Precise interval velocity modelling can include these high velocity zones for more accurate seismic depth conversion that consider areal velocity changes. Interval velocity models are also used when anomalous velocities are present within a specific stratal-unit, which can be caused by overpressures, cementation, or the presence of faults and fractures. To capture these areal velocity changes, 3D velocity modelling is recommended.

4.3 Seismic Time-to-Depth Conversion Accuracy

The accuracy of converting post-stack seismic data from the time-domain to the depth-domain has been a significant topic of conversation within the Cooper-Eromanga basins. Inaccurate seismic depth conversion has significant implications for a number of key processes, which include: (1) drilling low relief Jurassic to Cretaceous pseudo-structures that appear in depth converted seismic data due to velocity anomalies; (2) overlooking low relief Jurassic to Cretaceous structural traps that do not appear in depth converted seismic data due to inaccurate velocity modelling; (3) inaccurate economic estimates of new wells that, if depth is underestimated, may require drilling additional 10's of feet that may change the economic feasibility; (4) coring the wrong intervals while drilling; (5) inaccurate reserves calculations that could be under or overestimated; and (6) errors with geomechanical modelling of fault

reactivation, as fault geometries will change and could influence the sealing potential of fault bound accumulations (Hillis, Macklin, & Siffleet, 1995; Lowe-Young et al., 1998; Kulikowski et al., 2016b, 2018b; Kulikowski, 2017).

The historical inaccuracy of seismic depth conversions can be attributed to a number of factors ranging from: (1) known high velocity calcite cemented zones (CCZ); (2) the regional system of Cretaceous polygonal faults that can influence the spatial and temporal velocity; (3) velocity characteristics of fluvially deposited channel sands; and (4) the near surface 'statics' attributed to changes in surface conditions (rocky, regolith, etc.) (Hillis et al., 1995; Lowe-Young et al., 1998; Kulikowski et al., 2016b, 2018b; Kulikowski, 2017). The effect of statics on seismic depth conversion is difficult to constrain, but can be slightly mitigated through one-dimensional (1D) up-hole seismic refraction surveys that deliberately drill shallow wells to target the velocity of the near surface (Igboekwe & Ohaegbuchu, 2011). This technique can accurately measure the velocity at the wellbore, but, as with most wellbore derived data, must be extrapolated to the wider and often kilometre-scale field, which is a large assumption that can influence accuracy. To entirely mitigate the large effect of statics in seismic depth conversion accuracy within the Cooper-Eromanga basins, a method of velocity acquisition targeting the near surface must be investigated.

Refraction statics is another method that captures the near surface velocity variation through the interpretation of shallow refracted seismic reflectors. These interpreted reflectors are used to determine the thickness of shallow low velocity weathered and unconsolidated sediments, which if not corrected for, can create pseudo structures in the deeper seismic data (Farrell and Euwema, 1984). This method can provide high density near surface velocity data that can also be integrated with 1D up-hole data to reduce the effects of statics.

671 At this present moment, much of the work on seismic time-to-depth conversion accuracy in
672 the basins appears to be kept behind closed doors by operating companies. Literature provides
673 only two studies in the Cooper-Eromanga basins that are focused on this topic (Hillis et al.,
674 1995; Kulikowski et al., 2018b), with Hillis et al. (1995) choosing to focus on a small local
675 dataset. The only regional study assessing the depth conversion accuracy in the basin used a
676 statistical approach testing the accuracy of the four most commonly used methods (pseudo
677 average velocity, time-depth trend, kriging with external drift using TWT, and kriging with
678 external drift to tie stacking velocities to average well velocities) by employing a cross-
679 validation, or blind-well test, method (Kulikowski et al., 2018b). An automated looping script
680 was developed to manage the large dataset, comprising 13 3D seismic volumes, 73 interpreted
681 TWT grids, and 729 wells (Kulikowski et al., 2018b). Their results found that although the
682 pseudo average velocity method was the most accurate at a high-level (±24.9 ft), the accuracy
683 of methods changes by 10's of feet depending on the unique dataset and the combination of
684 significant variables (Kulikowski et al., 2018b).

685 The significant variables to the accuracy of depth conversion were: (1) the distance between
686 the well that is being predicted and existing well control; (2) the spatial location within the
687 basin; (3) the reflector of interest; and (4) the location of the well that is being predicted relative
688 to the existing well data envelope (Kulikowski et al., 2018b). Interestingly the number of well
689 controls had a negligible effect on accuracy, but rather the proximity of well controls to the
690 well that is being predicted. The regional study reiterates the argument that depth conversion
691 accuracy in the Cooper-Eromanga basins is a complicated issue that must be further
692 investigated.

693 **4.4 Seismic Data Analysis**

694 Analysis of seismic data through the use of seismic attributes, amplitude versus offset (AVO)
695 analysis, spectral decomposition, and seismic inversion modelling can unlock hidden details
696 that may not be immediately obvious within the amplitude volume. These techniques have
697 become a common tool for exploration and development programs around the world and would
698 be highly beneficial in the fluvially dominated Cooper-Eromanga basins (Fig. 10). Incoherency
699 (coherency or similarity) is a seismic attribute that was first introduced by Bahorich and Farmer
700 (1995) and further developed by Gersztenkorn and Marfurt (1999) and is used to visually
701 emphasise the discrepancy (typically faults) between adjacent seismic traces along a horizon
702 or time-slice (Neves, Zahrani, & Bremkamp, 2004; Mai, Marfurt, & Chávez-Pérez, 2009;
703 Backé, Abul Khair, King, & Holford, 2011; Basir, Javaherian, & Yaraki, 2013). This attribute
704 has been shown to be particularly beneficial when interpreting basement and polygonal faults
705 (Fig. 10b) from the low resolution seismic data typical to the Cooper-Eromanga basins
706 (Kulikowski, 2017; Kulikowski et al., 2017). Curvature is another structural attribute that is
707 defined as the rate of change of the direction of a curve (Roberts, 2001), where significant
708 curvature values are often associated with reflector displacement such as those caused by
709 fractures or faults (Roberts, 2001; Al-Dossary and Marfurt, 2006; Backé et al., 2011; King et
710 al., 2011; Abul Khair, Cooke, King, Hand, & Tingay, 2012; Kulikowski, 2017; Kulikowski,
711 Amrouch, & Burgin, 2018a). This attribute has the potential to constrain the distribution of
712 natural fracture sweet-spots away from one-dimensional well data if carefully applied
713 (Kulikowski, 2017; Kulikowski et al., 2018a).

714 Considering that hydrocarbons are predominantly reservoired within fluvial sandstones in the
715 Cooper-Eromanga basins, displaying the spatial distribution of amplitude along a reflector
716 surface can aid in detecting these strong amplitude reservoirs (Fig. 10a), particularly if
717 associated with characteristic amplitude versus offset (AVO) responses. In some cases, these

reservoirs can verge on being at a sub-seismic resolution scale and can be overlooked in seismic data. The application of spectral decomposition on the seismic volume can assist in detecting hydrocarbons, thin fluvial beds (Fig. 10d), and can also visual enhance small scale faults (Partyka, Gridley, & Lopez, 1999).

Another issue facing explorationists is the discrimination between the signature of thin gas reservoirs and coals in stacked seismic data. Owing to the significant difference in Poisson's ratio between sandstone and coal, the application of AVO analysis to Cooper-Eromanga basins seismic data has provided evidence to suggest that such discrimination is possible and most effective when using a rotated extended elastic impedance attribute in the presence of tuning (Fig. 10c) (Tyiasning and Cooke, 2015).

Insert Fig. 10

5. Contemporary Stress Tensor

Contemporary stress tensors are well constrained in the basin, calculated from borehole breakouts and drilling induced tensile fractures, diagnostic fracture injection tests, and leak off tests (e.g. Hillis, Enever, & Reynolds, 1999; Hillis & Reynolds, 2000, 2003; Reynolds, Coblentz, & Hillis, 2002, 2003; Reynolds et al., 2004, 2006; Reynolds, Mildren, Hillis, Meyer, & Flottmann, 2005; Sandiford, Wallace, & Coblentz, 2004; Nelson, Meyer, Hillis, & Mildren, 2005; Nelson, Hillis, Sandiford, Reynolds, & Mildren, 2006; Müller, Dyksterhuis, & Rey, 2012; Pokalai, Ahmed, Haghighi, & Gonzalez, 2015a; Pokalai, Haghighi, Sarkar, Tyiasning, & Cooke, 2015b; Pokalai et al., 2016; Nelson, Chipperfield, Hillis, Gilbert, & McGowen, 2017a; Nelson et al., 2007b; Pokalai, 2018). The far-field origin of in situ stresses has been explained by Reynolds et al. (2003) to originate from the Tonga-Kermadee subduction zone and the New Zealand collisional boundary. These tectonic stresses are transferred through the upper crust of eastern Australia to give an approximately ESE-WNW maximum horizontal

742 stress within the Cooper-Eromanga basins. The stress regime is dominantly strike-slip, but can
743 transition to a compressional stress regime with increased depth, as the overpressures will
744 decrease the effective vertical stress magnitude more than the effective horizontal stress
745 magnitudes (Reynolds et al., 2006; Cooke et al., 2016). Alternatively, depletion of hydrocarbon
746 reservoirs can reduce pore pressure, which in turn increases the effective vertical stress
747 magnitude (Teufel, Rhett, & Farrell 1991). Given that the effective vertical stress magnitude
748 can become larger than both effective horizontal stress magnitudes through reservoir depletion,
749 the in situ stress can transition into an extensional stress regime (Teufel et al., 1991). This
750 transition between regimes will have implications for late-stage development programs
751 incorporating hydraulic fracturing and infill drilling, as the unexpected stress regime can
752 impact the effectiveness of those programs.

753 For the majority of the basin a strike-slip stress regime is present, with an ESE-WNW oriented
754 maximum principal stress (Fig. 11a); however, local stress perturbations caused by faults can
755 cause stress rotation (Fig. 11b). The magnitude of maximum horizontal stress has been
756 constrained to approximately 41 MPa/km based on a combination of frictional limit theory
757 (Sibson, 1974), drilling induced tensile fractures, and the use of tensile strength and knowledge
758 of horizontal fabrics at the wellbore wall (Reynolds et al., 2005; Nelson et al., 2005; 2007).
759 The vertical principal stress magnitude is dependent on the overburden rock thickness and
760 density, as well as the local pore pressure (Fig. 11c). The range of magnitudes present within
761 the basin for the vertical stress is between approximately 17 and 20 MPa/km (Reynolds et al.,
762 2006; Nelson et al., 2007; Pokalai et al., 2015a; 2016; Pokalai, 2018). As mentioned earlier, a
763 decrease in the pore pressure caused by depletion can increase the effective magnitude of the
764 vertical principal stress. Minimum horizontal stress magnitudes are typically calculated from
765 leak off tests or obtained from the minimum closure pressure during a mini-frac test (Fig. 11c).
766 Within the Cooper-Eromanga basins, the minimum horizontal stress magnitude can vary

767 significantly between approximately 12 and 27 MPa/km and can depend on the interpretation
768 technique used to read closure pressures (Nelson et al., 2007).

769 Insert Fig. 11

770 Equally as important as the principal stress magnitude, the pore pressure gradient can
771 influence the reactivation and development of natural fractures and faults. Increases in pore
772 pressure effectively shift the Mohr's circle to the left, closer to the failure and reactivation
773 envelopes. This effect can be induced by hydraulic fracture stimulation treatments and through
774 gas and water injection wells. Pore pressure within the basin remains at a hydrostatic gradient
775 (0.433 psi/ft) until depths of between 8000 and 8800 ft, where overpressure is first observed
776 and is largely depended on the location (van Ruth & Hillis, 2000; Kulikowski et al., 2016a). A
777 recent study within the basin calculated the effective tectonic strain to be between
778 approximately 400 and 500 microstrains, with strain in the maximum horizontal stress direction
779 being three times greater than that in the minimum horizontal stress direction (Pokalai et al.,
780 2016; Pokalai, 2018).

781 **6. Geomechanical modelling of fault reactivation**

782 **6.1 Theory**

783 Reactivation refers to the movement of faults and fractures under present-day stress
784 conditions and can be analysed by creating a geomechanical model and measuring the shear or
785 tensile (dilation) reactivation potential. A poor understanding of the local and regional stress
786 conditions has tremendous implications for hydrocarbon migration pathway models, hydraulic
787 fracture stimulation treatments, reservoir development, and seal integrity. Faults that are
788 optimally oriented to undergo tensile reactivation, or dilate, can provide permeable conduits
789 for hydrocarbon migration. An increase in pore pressure, through hydraulic fracture stimulation
790 or water/gas injection wells, can facilitate shear or tensile reactivation along pre-existing faults

and fractures. Geomechanical models have also been shown to effectively predict the shear and tensile reactivation potential of faults under paleo-stress conditions, which is beneficial when incorporated with hydrocarbon migration pathway modelling (Kulikowski, 2017; Kulikowski & Amrouch, 2018b).

The Dilation Tendency (T_d) measures the likelihood that faults and fractures will tensile reactive and is governed by the orientation and magnitude of the effective normal stress, $\sigma_n{}'$, acting on a fault plane. The T_d is normalised to the differential stress to give values between zero (low likelihood) and one (high likelihood), where $\sigma_1{}'$ is the maximum effective stress and $\sigma_3{}'$ is the minimum effective stress (Ferrill et al., 1999; Jolie, Moeck, & Faulds, 2015), such that;

$$T_d = \frac{\sigma_1{}' - \sigma_n{}'}{\sigma_1{}' - \sigma_3{}'}$$

Fracture Stability is a measure of the pore pressure required to effectively shift the Mohr's circle to the left and intersect the failure or reactivation envelope for a given fault plane. The relationship between an increase in pore pressure (ΔP_p) and the change in horizontal stress magnitude (ΔS_{Hor}) is such that (Hung and Wu, 2012);

$$\Delta S_{Hor} = \alpha\left(\frac{1-2v}{1-v}\right)\Delta P_p$$

Where α is Biot's coefficient that describes the difference between the total and effective stresses, and v is the Poisson ratio. This equation shows the direct relationship between increasing pore pressure to an increase in the horizontal stress magnitudes. Therefore, the Fracture Stability results are provided as the pore pressure increase required to induce shear reactivation. The Slip Tendency of faults provides a normalised scale of the Fracture Stability, where zero (0) has a low likelihood, and one (1) has a high likelihood of shear reactivating.

The likelihood of faults and fractures to act as conduits can also be measured through the Leakage Factor equation that relates the pore pressure (P_p) with the difference between the normal stress (σ_n) and shear stresses (τ) acting on a given fault plane, such that;

$$Leakage\ Factor = \frac{P_p}{\sigma_n - \tau}$$

The structural stability is assessed for three groups of structural data common to the Cooper-Eromanga basins: (1) Basement Faults; (2) Polygonal Faults; and (3) Natural Fractures.

6.2 Basement Faults

6.2.1 Summary

The majority of the basement-involved faults developed during the early tectonic development of the Australian-Mawson Block (Fig. 4a), where a Pre-Cambrian (650-575 Ma) SE-NW oriented extensional stress regime event created NE-SW striking normal faults and SE-NW strike-slip faults throughout much of Australia (Kuang, 1985; Haines et al., 2001; Apak et al., 1997; Gibson et al., 2013; Kulikowski, 2017; Kulikowski & Amrouch, 2017). These two dominant sets are present throughout the Cooper-Eromanga basins and form close relationships with anticlinal hydrocarbons traps (Fig. 12) and the NE-SW striking GMI and NM ridges (Fig. 3b). Through time, these pre-existing basement-involved faults were repeatedly reactivated by subsequent compressional and strike-slip stress regime events (Apak et al., 1997; Gravestock & Jensen-Schmidt, 1998; Kulikowski, 2017; Kulikowski & Amrouch, 2017, 2018; Kulikowski et al., 2017). Repeated reactivation of pre-existing faults is supported by multiple erosional unconformities and the negligible distribution of low angle compressional faults, albeit up to four compressional events (Mid-Permian Event, Hunter-Bowen Event, Late Cretaceous Event, and Paleogene Event) had affected the region (Kulikowski & Amrouch, 2017). Under Andersonian faulting theory (Anderson, 1951), such compressional events would develop low angle (30^{o}) faults; however, due to the abundance of high angle (60^{o}) normal faults present in the basin (Kulikowski, 2017; Kulikowski & Amrouch, 2017), it would be more stress economic to reactivate existing faults rather than develop new faults.

Insert Fig. 12

The original NE-SW striking normal faults, which are present throughout the basin (Fig. 13a & 13b), are now observed to positively displace reflectors (Apak et al., 1997; Gravestock &

Jensen-Schmidt, 1998; Radke, 2009; Kulikowski, 2017; Kulikowski & Amrouch, 2017, 2018; Kulikowski et al., 2017). Their stratigraphic distribution is often limited to terminating within basement or Middle Permian stratigraphy, and rarely penetrating into younger units (Apak et al., 1997; Gravestock & Jensen-Schmidt, 1998; Radke, 2009; Kulikowski, 2017; Kulikowski & Amrouch, 2017b). Due to the poor seismic resolution below Permian coal measures, detailed fault growth studies (e.g. Giba, Walsh, & Nicole, 2012; Jackson and Rotevatn, 2013; Black, McCormack, Elders, & Robertson, 2017; Robson, 2018; Robson, Holford, King, & Kulikowski, 2018) have not been possible and their interpretation becomes more difficult with depth. The difficulty is also exaggerated when developing fault models from seismic data that remains in the time-domain, as the true fault angle is not being captured (Fig. 8b & 8c). The difference in basement-fault geometry between the time and depth-domains has proven to be problematic for previous researchers that used sparse 2D seismic data, as their work interpreted purely extensional faults, which were later re-interpreted as compressional faulting, and which are now known to be a combination of inverted normal faults, compressional faults and strike-slip faults (e.g. Kuang, 1985; Stanmore, 1989; Apak et al., 1997; Sun, 1997; Gravestock & Jensen-Schmidt, 1998; Radke, 2009; Grant-Woolley et al., 2014; Kulikowski, 2017; Kulikowski & Amrouch, 2017b; Kulikowski et al., 2017).

Insert Fig. 13

The SE-NW strike-slip faults are present throughout the region and have been attributed to reducing reservoir performance through cataclasis, compartmentalisation of reservoirs, and potentially complicating hydraulic fracture stimulation treatments (Grant-Woolley et al., 2014; Kulikowski et al., 2016c). These strike-slip faults appear predominantly within basement and can extend into the hydrocarbon-rich Patchawarra Formation (Apak et al., 1997; Radke, 2009; Kulikowski & Amrouch, 2017b; Kulikowski et al., 2017). This fault set can easily be overlooked in cross-section due to the seismic resolution at basement and must be investigated

in time-slice (or depth-slice) views to observe lateral displacements or linear features. A series of large basin-scale en echelon NNE-SSW strike-slip faults are present in the Patchawarra Trough (Fig. 3a) and form pop-up or positive flower structures that have been developed into highly economic fields. Their presence elsewhere in the basin may be equally as fruitful; however, are yet to be discovered!

6.2.2 Reactivation potential under paleostress evolution

A new approach for assessing the reactivation and dilation potential of faults through time was presented by Kulikowski & Amrouch (2018b), using the Cooper-Eromanga basins as a case study. This approach utilises complete paleo-stress tensors for six events (Kulikowski & Amrouch, 2017) that were obtained through calcite twin stress inversion analysis (Etchecopar, 1984). Calcite twin stress inversion has been used extensively around the world to provide quantitative data on polyphase tectonic events (e.g. Amrouch, Lacombe, Mouthereau & Dissez, 2005; Lacombe, Amrouch, Mouthereau & Dissez, 2007; Amrouch, 2010; Amrouch, Lacombe, Bellahsen, Daniel & Callot, 2010; Amrouch, Beaudoin, Lacombe, Bellahsen, & Daniel, 2011; Beaudoin et al., 2012; Arboit, Amrouch, Collins, King, & Morley, 2015; Arboit, Amrouch, Morley, Collins, & King, 2017; Kulikowski, 2017; Kulikowski and Amrouch, 2017, 2018b; Burgin, Amrouch, Rajabi, Kulikowski, Holford, 2018). Complete paleo-stress tensors form the Cooper-Eromanga basins were integrated with geomechanical models to simulate the stress conditions present during each of the six key stages of basin evolution. Results found that after the critical moment in the Cooper-Eromanga basins petroleum system (90 Ma), E-W (Late Cretaceous Event) and N-S (Paleogene Event) striking high angle (50-70^{o}) faults were most likely to be dilated and acting as permeable hydrocarbon conduits (Fig. 13c). The critical moment defines the major period of hydrocarbon generation, migration and entrapment. This provides critical information that improves hydrocarbon migration pathway models that previously considered faults to have static 2D mechanical properties.

The history of basement fault reactivation is often constrained through fault growth analysis using 3D seismic data (e.g. Williams, Powell, & Cooper, 1989; Childs, Nicol, Walsh, & Watterson, 1996; Baudon & Cartwright, 2008); however, this cannot be performed in regions that have poor seismic resolution. For such regions, including the Cooper-Eromanga basins, the Slip Tendency of faults is calculated using paleo-stress tensors and geomechanical modelling to provide insights into the 4D evolution of fault reactivation. Kulikowski & Amrouch (2018b) measured the Slip Tendency of four major fault sets modelled using the paleo-stress tensors during six tectonic events (Fig. 13d). The results showed that N-S striking high angle (50-70^{o}) faults were most likely to reactivate during the Alice Springs Event, and E-W striking high angle (50-70^{o}) faults likely reactivated during the Mid-Permian Event (Fig. 13d). Since these two events NE-SW striking high angle (50-70^{o}) faults were most likely to shear reactivate under the subsequent Daralingie Event, Hunter-Bowen Event, Late Cretaceous Event and Paleogene Event (Fig. 13d). This is in line with other research suggesting considerable exhumation and erosion along the major NE-SW striking GMI and NM ridges (Kuang, 1985; Apak et al., 1997; Gravestock & Jensen-Schmidt, 1998; Mavromatidis, 2006, 2008; Kulikowski & Amrouch, 2017b).

6.2.3 Reactivation potential under contemporary stress

A case study on the Swan Lake 3D and Dullingari 3D seismic surveys, located adjacent to the GMI and NM ridges, respectively, investigated the reactivation potential of basement-involved faults under contemporary stresses by measuring the Slip Tendency, Dilation Tendency, and Fracture Stability (Kulikowski et al., 2016c). The study analysed four unique fault sets modelled using hydrostatic pressure, in situ stress, and typical rock mechanics parameters from the Cooper Basin.

Results from Kulikowski et al. (2016c) showed that E-W striking faults have the highest Dilation Tendency (0.900) and thus most likely to act as permeable hydrocarbon conduits under the present-day stress (Fig. 13c). The study also identified SE-NW strike-slip faults within both 3D seismic surveys and found that they are most likely to shear reactivate (Fig. 13d). A pore pressure increase of between only 0.5 and 5.0 MPa is required for this fault set to intersect the reactivation curve. Shear reactivation can compartmentalise the reservoir, reduce reservoir properties through cataclasis, complicate hydraulic fracture propagation, and facilitate tertiary migration of hydrocarbons. Therefore, precise seismic interpretation, particularly in depth-slice to observe lateral offsets, must focus on the identification of SE-NW striking strike-slip faults in order to incorporate their presence with the development of hydraulic fracture stimulation and drilling programs.

6.3 Cretaceous Polygonal Fault System

6.3.1 Summary

Layer bound polygonal faults are present within Cretaceous Eromanga Basin marine sediments across the entire basin (Heath et al., 1989; Watterson et al., 2000; Kulikowski, 2017; Kulikowski et al., 2017; Kulikowski & Amrouch, 2017b). These faults were first identified from 2D seismic data (Rumph, 1982; Moore & Pitt, 1984; Newton, 1986; Gilby & Mortimore, 1989; Gorter, Gostin, & Plummer, 1989; Longley, 1989; Scholefield, 1989; Young, Gunther, & Dixon, 1989), with the 3D distribution and regional extent only recently discovered in literature (Oldham & Gibbins, 1995; Watterson et al., 2000; Kulikowski, 2017; Kulikowski et al., 2017). A detailed analysis of polygonal faults within the Lake Hope 3D seismic survey suggests that their development is linked to a density inversion, where a low density and overpressured stratal unit was buried and de-watered by overlying normally pressured and higher density sediments (Watterson et al., 2000). The planar normal faults are mostly contained within the Mackunda Formation, Coorikiana Sandstone, Bulldog Shale and

Wallumbilla Formation; however, larger faults are found to penetrate into the underlying and oil-rich Murta Member (Fig. 7). Maximum throw was found within the Coorikiana Sandstone. The dip angle of faults remains constant along a given fault plane and can range between 44° and 61° (Watterson et al., 2000). This polygonal fault system may present a new hydrocarbon exploration opportunity targeting shallow oil that has migrated from Lower Cretaceous oil-rich reservoirs through permeable polygonal faults (Fig. 7) (Watterson et al., 2000).

The normal displacement across polygonal faults can tilt shallow reservoirs such that low relief structural traps are developed and potentially fault sealing. Low relief structures that are bound by deeply penetrating faults can facilitate the accumulation of oil in shallow reservoirs. This play has yet to be truly tested in this region, but is analogous to the polygonal fault system associated with Tertiary hydrocarbon-rich shales in the North Sea (Cartwright & Lonergan, 1997; Lonergan, Cartwright, & Jolly, 1998). The presence of faults within hydrocarbon reservoirs can have tremendous implications for effective production and development, such as compartmentalisation of the reservoir, tertiary hydrocarbon migration, and complications with hydraulic fracture stimulation treatments. Considering that Lower Cretaceous and Jurassic hydrocarbon reservoirs are currently being explored and developed, an understanding of the geometry, intensity and reactivation potential of the Cretaceous polygonal fault system is highly beneficial.

6.3.2 Reactivation potential under paleostress conditions

This potential new play type was first suggested by Watterson et al. (2000), who suggested the possibility that these faults may be facilitating the tertiary migration of hydrocarbons from known reservoirs to shallow sedimentary rocks. Little literature has since appeared in relation to this exploration opportunity, with the regional extent of this system only recently discovered (Kulikowski, 2017; Kulikowski et al., 2017). The Leakage Factor and Dilation Tendency of

this regional polygonal fault system were modelled to determine the optimum fault geometry required for fluid flow (Kulikowski et al., 2017).

The results show that high dip angle (50-90°) polygonal faults striking 080-260°N and 125-305°N have the largest Leakage Factor, and fault planes with high dip angle (50-90°) striking 105-285°N have the largest Dilation Tendency (Kulikowski et al., 2017). These fault planes are therefore most likely to facilitate the tertiary migration of hydrocarbons from Lower Cretaceous hydrocarbon-rich reservoirs into shallow structures, given that they penetrate below the Cadna-owie Formation into the hydrocarbon-rich Murta Member.

6.4 Natural Fractures

6.4.1 Summary

Natural fractures can provide highly permeable pathways for hydrocarbon production if the local and regional fracture set geometries are known. The strike and dip angle of fracture sets are equally as important for optimising hydrocarbon recovery. Six regionally pervasive conjugate natural fracture sets (Fig. 14a) are present in the Cooper-Eromanga basins (Kulikowski & Amrouch, 2017). The timing of their development, stratigraphic distribution, and spatial intensity has been well constrained (Kulikowski et al., 2016a; Kulikowski, 2017; Kulikowski & Amrouch, 2017). Extrapolation of wellbore derived natural fractures and faults to the wider reservoir has also been investigated by a number of authors (Backé et al., 2011; King et al., 2011; Abul Khair et al., 2012; Abul Khair, Cooke, & Hand, 2013; Abul Khair, Cooke, & Hand, 2015; Kulikowski et al., 2018a), suggesting that upwards of 70% of wellbore fractures are represented in seismic curvature results.

Insert Fig. 14

6.4.2 Natural fractures at the well bore

Low dip angle (30°) conjugate fracture sets striking E-W and N-S are present throughout the stratigraphic column and associated with the Paleogene Event, and the Upper Cretaceous and Hunter-Bowen events, respectively. A third low dip angle conjugate fracture set is present only within the Patchawarra, Tirrawarra, Merrimelia and Basement formations striking NE-SW and associated with the Mid-Permian Event. A vertical conjugate natural fracture set striking NNE-SSW and SE-NW is present only within Basement and developed during the Alice Springs Event. Two additional conjugate natural fracture sets are present throughout the stratigraphic column, striking NE-SW and SE-NW with high dip angles (50-70°), and most likely associated with periods of post-compressional flexural relaxation, or basin sag (Abul Khair et al., 2015; Kulikowski & Amrouch, 2017). The majority of interpreted fractures have high dip angles (50-70°) making the true wellbore fracture intensity of vertical wells difficult to constrain. A comparison between the fracture intensity interpreted from vertical, horizontal and inclined wells would provide more meaningful and representative fracture intensities.

A robust natural fracture study was performed for the Warburton Basin (Sun, 1999) using core, borehole image logs, and dip meter logs. The conclusions present a number of fracture sets; however, their methods relied too heavily on the strike of fractures and did not consider that slight changes in dip angle (20°) can have a different interpretation (Anderson, 1951). For this reason the use of seismic attributes, such as most positive and most negative curvature, can be misleading by only providing the strike of possible fractures and faults. Fracture sets with similar strike direction but different dip angles cannot be distinguished from these seismic trending methods.

Horizontal fractures have also been proposed to exist in the basin, and likely associated with periods of significant exhumation and erosion (Flottmann, Campagna, Hillis, & Warner, 2004; Tyiasning & Cooke, 2016; Cooke et al., 2016). Significant erosion can reduce the vertical stress magnitude and create local compressional stress regimes that can develop tensile horizontal

fractures. These horizontal fractures can complicate hydraulic fracture stimulation treatments by preferentially reactivating and causing rotation of hydraulic fractures into the horizontal plane, which is a common phenomenon in the Cooper-Eromanga basins (Cooke et al., 2016; Pokalai et al., 2016; Pokalai, 2018).

6.4.3 Natural fractures away from the well bore

A common assumption within the petroleum industry is that wellbore data can be extrapolated to the wider reservoir, which assumes that stress conditions, structural data, pore pressures, reservoir properties and characteristic, and other important criteria remain constant. If incorrect, this assumption can lead to obvious implications for exploration and development programs. As the Cooper-Eromanga basins contain low permeability reservoirs, the presence of permeable fracture networks can add great economic value to prospects; however, much of the existing work assumes that one-dimensional borehole data is representative of the wider kilometre-scale fields (Kulikowski et al., 2018a). Recent advancements in seismic acquisition and processing have enabled the use of seismic attributes to provide information away from the wellbore that is otherwise overlooked in the original amplitude volumes.

Curvature analysis is a seismic attribute that has been shown to correlate well with wellbore derived fracture and fault data (e.g. Murray, 1968; Lisle, 1994; Stewart & Podolski, 1998; Hakami, Marfurt, & Al-Dossary, 2004; Al-Dosary & Marfurt, 2006; Chopra & Marfurt, 2007; King et al., 2011; Abul Khair et al., 2012; Kulikowski et al., 2018a). The calculated value for curvature is defined as the rate of change of the direction of a curve (Roberts, 2001), such that for any point (P) the curvature (K) is defined as the rate of change of the dip angle ($d\omega$) with respect to the arc length (dS) (Roberts, 2001). The arc length (dS) is obtained from the osculating circle that has a common tangent to *P* and makes the greatest possible contact with

the curve (Roberts, 2001). The radius of the osculating circle forms the radius of curvature (R); such that in two-dimensions the value for *K* is defined as (Roberts, 2001);

$$K = \frac{d\omega}{dS} = \frac{2\pi}{2\pi R} = \frac{1}{R}$$

Curvature analysis has previously been performed within the Cooper-Eromanga basins (Backé et al., 2011; King et al., 2011; Abul Khair et al., 2012; Kulikowski et al., 2018a) showing a close relationship with the fracture geometry measured at the wellbore (Fig. 14b & 14c), although the density of fracturing can be underestimated in vertical wells (Kulikowski, 2017). As the two major fracture sets present in the basin are high angled (>50º dip), it is statistically less likely that these will be intersected by vertical wells, and may therefore be providing a less than true fracture density. The spatial and temporal distribution of permeable fracture networks away from the wellbore using curvature analysis has shown that high angle E-W and SE-NW striking fractures are highly pervasive and most likely to be permeable under contemporary stresses (Kulikowski et al., 2018a). These E-W and SE-NW striking fracture sets are present in each of the five 3D seismic surveys analysed by Kulikowski et al. (2018a) and were found to increase in intensity along E-W elongate anticlinal structures, which may present an exploration target for future programs. The use of curvature analysis for field development programs that target fracture networks appears invaluable, as it can provide the spatial and temporal distributions of permeable fracture networks in the subsurface away from the wellbore.

6.4.4 Reactivation potential under contemporary stress

Understanding the distribution, geometry, and intensity of permeable fracture networks is an important aspect of development programs in the low permeability Cooper-Eromanga basins. The likelihood of fractures to reactivate and be open to fluid flow is primarily controlled by the contemporary stress conditions relative to the fracture geometry. The contemporary stress in

the Cooper-Eromanga basins has an approximately E-W oriented maximum horizontal stress and is under a strike-slip stress regime, but the orientation can vary by up to 20° and the regime can alternate between a compressional stress regime (Fig. 11c) (e.g. Nelson et al., 2007; Reynolds et al., 2004; King et al., 2011; Abul Khair et al., 2012; Kulikowski et al., 2016c; Pokalai et al., 2016; Pokalai, 2018). This variation of in situ stress has a profound influence on: (1) reactivation potential of fractures and faults; (2) hydraulic fracturing; and (3) infers that geomechanical modelling performed on the basin-scale may not be representative of the field-scale.

King et al. (2011) and Abul Khair et al. (2012) measured the fracture susceptibility of natural fractures on a basin-scale assuming an E-W oriented maximum horizontal stress that alternates between a strike-slip and compressional stress regime. Their study found that NE-SW and SE-NW striking fractures with moderate dip angles are most prone to reactivation (Fig. 14d & 14e). Understanding the shear reactivation potential is important; however, measuring the likelihood of tensile reactivation is equally as important. Kulikowski et al. (2018a) measured the Dilation Tendency of 454 fractures to show that E-W and SE-NW striking high angle (60°) fractures are optimally oriented to dilate and act as potential hydrocarbon conduits under contemporary stresses (Fig. 14f). These sets are regionally pervasive away from the wellbore within the Patchawarra Formation and would form ideal fracture sweet-spots given sufficient intensity (Fig. 14b & 14c).

7. Hydraulic fracturing and well monitoring

Hydraulic fracturing has been performed in the Cooper Basin since 1969 (McGowen, Gilbert, & Samari, 2007). The majority of hydraulic fracturing treatments are focus on the predominately Permian sandstone reservoirs, especially in the tight sand Patchawarra Formation. This formation has low (milliDarcy) permeability and requires multistage hydraulic

fracturing to optimise production and be economically feasible. There is significant gas potential to explore and develop in this area; however, the stress complexity and high pressure and temperature conditions are challenging to effectively execute hydraulic fracturing programs.

During injection and fracture propagation a considerable pressure loss can be observed near the wellbore. This near-wellbore pressure loss (NWBPL) was first discussed by Chipperfield & Britt (2000) and Roberts et al. (2000), who stated that the causes of NWBPL are related to pressure loss within the perforations, and tortuosity within the induced fracture path near the wellbore. Johnson et al. (2002) and Johnson and Greenstreet (2003) discussed pressure dependent leak-off (PDL) and NWBPL in the Cooper Basin and showed the significant impact it can have on production performance. NWBPL is caused by frictional pressure loss at the wellbore and closely related to tortuosity. Four different types of fracture propagation can result from high tortuosity including fracture turning, fracture twisting, multiple fracturing and fracture migration. High NWBPL can therefore complicate the hydraulic fracture process and result in a lower percentage of proppant being placed within the target reservoir (Pokalai et al., 2015a, 2015b; Pokalai, 2018).

When pre-existing natural fractures are present within a reservoir the near-wellbore pressure loss is considerably higher due to the complex interactions that create multiple fractures with tortuous paths. This tortuous path will shear and tensile reactivate pre-existing natural fractures to create a large amount of pressure dependent leak-off. Therefore, pressure dependent leak-off can have both positive and negative impacts. It can increase rock permeability by increasing the stimulated rock volume, while at the same time causing a high near-wellbore pressure drop. However, to have better proppant placement and to maximise the flowback of fracturing fluid, near-wellbore pressure needs to be reduced.

The majority of the Patchawarra Formation consists of thick sand intervals that cycle between coal measures and shale, and is currently exposed to high pressure, high stress, and high temperature conditions. Therefore, the fracturing fluid system and proppant need to be selected in order to suit these conditions. Fracturing fluid is commonly a water-based fluid system within the Cooper-Eromanga basins comprising of either a Linear Gel or a Borate Crosslink Gel that is injected during the pad stage, slurry stage and the flushing stage. Proppant is typically 100 mesh sand and is pumped into the target zone to reduce NWBPL and to bridge-off the PDL. This is followed by the injection of ceramic proppant to provide high fracture conductivity. The perforations that the hydraulic fracture is pumped into are typically made by lowering expendable hollow carrier (EHC) or link guns down the wellbore to perforate the casing completion at the target location. The style of perforating guns is primarily dependant on well completion, with EHC guns commonly used in monobore completions to mitigate rat-hole loss, and link guns are used in conventional completion designs.

Once perforations and hydraulic fracture stimulations are complete and the well begins producing hydrocarbons, there is a significant need for well surveillance and intervention programs due to the harsh subsurface conditions within the Cooper-Eromanga basins. These can range from high temperatures, high pressures, and high CO_2 concentrations, to liquid loading (water in the wellbore) issues that can lead to reduced production (Rigby & Smith, 1981; Wycherley et al., 1999; McGowen et al., 2007; Winterfield, Missikos, Tio, & Dalgety, 2014). Hydrocarbon production can also be inhibited by the development of scale (halite and calcite) within the perforations, where pressure and temperature rapidly decrease causing solutes to precipitate. The CO_2 concentration within the Cooper-Eromanga basins is significantly higher (10-30 v/v%) than the average sedimentary basin (Rigby & Smith, 1981; Wycherley et al., 1999), contributing to the need to mitigate calcite scale through acid treatments, re-perforation, and regular wireline drift and broach intervention programs (Pitkin,

Wedham, McGowen, & Thom, 2012). Salts (NaCl) have also been found to precipitate within perforations originating from salty groundwater invading the reservoir.

Other than causing scale build-up, the invasion of groundwater into the wellbore can also increase the production rate required to lift, and unload, the liquids to surface and can cause liquid loading within the wellbore to effectively stop production (Winterfield et al., 2014). Mitigation techniques for this may include artificial lifts (nitrogen injection), compressor installation to reduce back-pressure, plunger lift systems, injection of foaming agents via micro-strings, installation of siphon strings (or recompletion to small diameter tubing) to reduce the minimum rate to lift liquids, well cycling (pressure build-up), and producing the well to atmospheric pressures for a short period of time to unload liquids (McGowen et al., 2007; Winterfield et al., 2014).

8. Exploration and Development

8.1 Current Programs

Current exploration programs are somewhat simplistic and have remained inline with the original anticlinal theory; identify and drill an anticlinal closure (Apak et al., 1997; Lowe-Young et al., 1998; Morton, 1998; O'Neil, 1998). This approach has generated in excess of 6.5 trillion cubic feet (TCF) of sales gas; however, an estimated 1.6 TCF is remaining to be produced from anticlinal and stratigraphic traps (Mackie, 2015). This estimate does not include the highly prospective unconventional plays (basin centred gas, deep coal, and fractured basement) that have sparked renewed interest in the basin. Oil exploration, now primarily targeting the Jurassic Eromanga Basin reservoirs, has also become highly profitable, generating 520 million barrels (mmbbls) from Jurassic to Cretaceous reservoirs, with an estimated 150 mmbbls of recoverable reserves remaining (Mackie, 2015). Although the majority of oil discovered in the basins is in Jurassic and Cretaceous reservoirs, oil has also been discovered

in the Early Permian Tirrawarra Formation in the Tirrawarra (80% of known Permian oil) and Fly Lake/Brolga fields (Gravestock et al., 1998). Taking into account the number of exploration wells drilled versus new Permian gas field discoveries, the success rate for current exploration programs is approximately 40% (Mackie, 2015). The success of Mesozoic oil exploration wells grew from 12% to 45% after the introduction of 3D seismic data acquisition, illustrating the significance of geophysical advancements in discovering new fields and new play types (Mackie, 2015).

There are currently two major plays in the province; (1) targeting Jurassic Eromanga Basin oil reservoired in anticlinal closures; and (2) targeting Permian Cooper Basin gas reservoired in anticlinal and stratigraphic traps (Lowe-Young et al., 1998; Radke, 2009; Scott et al., 2013; Mackie, 2015). The majority of Jurassic oil is reservoired within the Murta Member, Namur Sandstone, Birkhead Formation, Hutton Sandstone, and Poolowanna Formation given that a structural trap exists (Lowe-Young et al., 1998; Kulikowski, 2017; Kulikowski et al., 2016b, 2017c). It is important to note, however, that, as previous indicated, the presence of these typically low-relief structural traps can depend on the seismic time-to-depth conversion method being used, as the conversion errors can be greater than the structural closure (Lowe-Young et al., 1998; Radke, 2009; Kulikowski et al., 2016b, 2017c; Kulikowski, 2017). Although, some stratigraphic traps have been discovered in the Eromanga Basin sequence that appear to be restricted to the Birkhead Formation sandstone channel faces embedded in floodplain and lacustrine shales. The source of this Jurassic oil in the central portion of the play has been attributed to Permian source rocks migrating vertically through leaky seals or along fault conduits (Lowe-Young et al., 1998; Radke, 2009). Recently, the Eromanga Basin oil play has been extended to the western flank of the Cooper Basin, where major oil exploration and production is currently taking place (Lowe-Young et al., 1998). The western flank oil play primarily targets low relief anticlinal traps within the Jurassic Eromanga Basin reservoirs that

are also charged by Permian source rocks migrating through eroded regional seals on the flank of the basin (Lowe-Young et al., 1998; Radke, 2009).

The anticlinal closures common to the basin are often associated with reactivated basement-involved faults that develop broad structures in the overlying stratigraphy, but they can also be associated with positive flower (pop-up) features that are common in the Patchawarra Trough, or as fault-bound anticlines where large basement-involved faults have reactivated and penetrated through overlying units (Apak et al., 1997; Lowe-Young et al., 1998; Radke, 2009; Scott et al., 2013; Mackie, 2015; Kulikowski, 2017; Kulikowski et al., 2017). The case of fault-bound anticlines is most common along the GMI and NM ridges where the large NE-SW striking high angle (50-70^{o}) faults have shown evidence of relatively more recent reactivation (Apak et al., 1997; Gravestock et al., 1998; Kulikowski and Amrouch, 2018a). These anticlinal traps allow for the accumulation of oil and gas within all reservoir quality sandstones in both the Cooper and Eromanga basins (Kantsler, 1984; Lowe-Young et al., 1998; Alexander et al., 1998; Morton, 1998; Radke, 2009; Scott et al., 2013).

8.2 Future Research and Exploration Programs

As the anticline becomes entirely exploited in this province, companies will transition into the next phase of hydrocarbon exploration targeting technically more challenging plays, such as the basin centred gas play, deep coal measure play, stratigraphic plays, polygonal fault play, and potentially fractured basement play that is juxtaposed to Permian source rocks. Each of these relatively unconventional plays will require a more thorough understanding of the basin. Therefore, as exploration within the Cooper-Eromanga basins becomes more challenging, the collaboration between academic researchers and explorationists will become more integral to exploration success. Much of the regional structural, stratigraphic, and stress framework for the basin has been well constrained in recent times (e.g. Apak et al., 1997; Gravestock &

Jensen-Schmidt, 1998; Hillis et al., 1999, 2001; Reynolds et al., 2002, 2003, 2004, 2005, 2006; Mavromatidis, 2006, 2008; Nelson et al., 2006, 2007a, 2007b; Radke, 2009; Pokalai et al., 2015a, 2015b, 2016; Kulikowski et al., 2016a, 2017; Kulikowski, 2017; Kulikowski & Amrouch, 2017, 2018a, 2018b; Pokalai, 2018); however, there does remain a large volume of research that can directly impact the success of future hydrocarbon exploration and development programs. Additionally, exploration and production companies play an important role in the effective exploitation of Australia's largest onshore hydrocarbon province by testing new concepts and acquiring new data that will promote further research in the basin.

A complete 3D reconstruction of the basin has not yet been completed and would provide valuable information on the fault growth through time. Detailed fault growth analyses are not possible in the basin given the poor seismic resolution at basement; however, with continued improvement in seismic acquisition and processing techniques, a fault growth study may be possible in the future. This may ultimately lead to a complete structural and stratigraphic 3D reconstruction of the basin and provide a 3D view of the temporal and spatial distribution of the three basins (Cooper, Eromanga, and Lake Eyre basins) that overly basement (Warburton Basin). The spatial extent of major unconformities, both local and regional, would also be useful, particularly as oil migration from Permian sources to Eromanga Basin reservoirs relies on the presence of unconformities that have effectively removed regional seals (Lowe-Young et al., 1998). The distribution and magnitude of overpressure has previously been investigated (van Ruth & Hillis, 2000; Hillis et al., 2001; van Ruth, Hillis, Tingate, & Swarbrick, 2003; Kulikowski et al., 2016a); however, the mechanism for overpressure generation in the basin remains questionable and may be investigated by integrating reservoir pressure, vertical stress magnitude, and sonic velocity data (Tingay, Hillis, Swarbrick, Morley, & Damit, 2007). The degree of stress perturbation caused by pre-existing faults should also be investigated in more detail, as local stress rotation does exist (Fig. 11b).

To accurately interpret seismic data, the amplitude volume must be converted from the time-domain to the depth-domain using an appropriate depth conversion method (Kulikowski et al., 2016b, 2017c). The errors associated with seismic depth conversion can be attributed to a number of factors, but these can be somewhat mitigated through a more complete understanding of the near surface velocity variation (statics) and a systematic interpretation of shallow reflectors, which are yet to be explored. Mapping the spatial variation of statics in a form that can be incorporated into velocity modelling would provide more accurate results. Considering that the contemporary stress alternates between a strike-slip and compressional stress regime (Fig. 11c), an understanding of the spatial variation in vertical stress magnitudes (calculated from density logs) would be highly beneficial and, if in a gridded map format, could be used to predict stress regimes across the basin.

Rock mechanics data does exist for key parts of the region but is selectively sampled and not representative of heterogeneities, and can contradict with other works (Abul Khair et al., 2013; Nelson et al., 2007). A detailed study focused on constraining the complete and representative rock mechanics data for the Warburton, Cooper and Eromanga basins would provide more certainty on geomechanical and hydraulic fracture stimulation models. Ideally, future hydraulic fracture stimulation models would incorporate the certain interaction between induced fractures and naturally occurring fractures and faults, with particular attention to SE-NW strike-slip faults that are most likely to reactivate under contemporary stresses (Kulikowski et al., 2016c). These SE-NW strike-slip faults are difficult to interpret in low resolution seismic data, but can reduce reservoir properties through cataclasis, can compartmentalise the reservoir, and contribute to tertiary hydrocarbon migration if reactivated (Grant-Woolley et al., 2014; Kulikowski et al., 2016c). A study investigating the possible relationship between well and reservoir performance with distance to these SE-NW strike-slip faults would provide a better understanding on their effect on production.

Finally, although not directly applicable to academic researchers, operating companies may discover new opportunities and hydrocarbon reserves by testing such concepts as the: (1) fracture basement play; (2) basin centred gas play; (3) hydraulic fracturing of deep coal; (4) polygonal fault system play; (5) targeting stratigraphic traps; (6) cutting-edge use of seismic data (e.g. direct hydrocarbon indicators and other seismic attributes); and (7) cost effective alternatives to optimise production (pad drilling, deviated wells from existing wellbores, deepening old shallow oil wells to target Permian reservoirs, and perforating thin (1-2 feet) gas saturated and pressurised reservoirs that were initially dismissed).

9. Conlusions

This review forms a robust synthesis of recent developments within Australia's largest onshore hydrocarbon province, the Cooper-Eromanga basins. New technologies and software applications have armed researchers with cutting edge analysis techniques and applications that have generated a recent increase in information that was previously not available. The purpose of this study is to provide readers with a holistic insight into the province that includes: (1) a detailed tectonic and stratigraphic evolution; (2) a summary of geomechanical modelling results that predict fault and fracture reactivation (tensile and shear) through time to better understand hydrocarbon migration pathways; (3) a synthesis of the petroleum system processes and elements; (4) the spatial and temporal distributions of permeable natural fracture networks through wellbore and seismic data analysis; (5) common hydraulic fracturing and well surveillance programs contrast with a discussion on the common difficulties and risks; (6) a discussion on the seismic time-to-depth conversion methods that are being used and their individual accuracies and limitations; (7) current and future hydrocarbon exploration and development targets; and (8) a discussion on the future research opportunities that can directly impact the effectiveness of exploration and development programs.

Reviewing the province has highlighted opportunities for future exploration and identified possible research topics that will be fundamental to the success of future exploration and development programs. These future programs will begin to target technically more challenging plays as the anticline becomes entirely exploited and will require a thorough understanding of the province. The methodologies and approaches summarised within this review forms a research framework that can be applied to other hydrocarbon provinces to better understand the dynamic structural geology, tectonic evolution and application of geophysics.

10. ACKNOWLEDGEMENTS

The authors appreciate the financial contribution made by the GeoFrac Consortium, which includes the sponsoring companies: Santos, Beach Energy, Chevron, Halliburton and BG Group (QGC). DUG Insight software (v.4.0, 2016) was used for seismic visualisation, interpretation and analysis.

11. REFERENCES

Abul Khair, H. A., Cooke, D., King, R., Hand, M., & Tingay, M. (2012). Preliminary workflow for subsurface fracture mapping using 3D seismic surveys: A case study from the Cooper Basin, South Australia. In: Geothermal Research Council Conference, Reno, Nevada, 36, 339-350.

Abul Khair, H., Cooke, D., Hand, M. (2013). The effect of present day in situ stresses and paleo-stresses on locating sweet spots in unconventional reservoirs, a case study from Moomba-Big Lake fields, Cooper Basin, South Australia. Journal of Petroleum Exploration and Production Technology, 3(4), 207-221.

Abul Khair, H., Cooke, D., & Hand, M. (2015). Seismic mapping and geomechanical analyses of faults within deep hot granites, a workflow for enhanced geothermal system projects. Geothermics, 53, 46-56.

Al-Chalbi, M. (1974). An analysis of stacking, RMS, average, and interval velocities over a horizontally layered ground. Geophysical Prospecting, 22(3), 458-475.

Al-Dossary, S., & Marfurt, K. J. (2006). 3D volumetric multispectral estimates of reflector curvature and rotation. Geophysics, 71(5), P41-P51.

Alexander, E. M., Gravestock, D. I., Cubitt, C., & Chaney, A. (1998). Lithostratigraphy and environments of deposition. In: Gravestock, D. I., Hibburt, J. E., & Drexel, J. F., (Eds), The Petroleum Geology of South Australia. Vol. 4: Cooper Basin, South Australia. Department of Primary Industries and Resources. Report Book, 98/9, 69-116.

Amrouch, K., Lacombe, O., Mouthereau, F., & Dissez, L. (2005). Quantification of orientations and magnitudes of the late Cenozoic paleostresses in the Zagros folded belt from calcite twin analysis. In Thrust Belts and Foreland Basins, International Meeting, Rueil-Malmaison, 31-35.

Amrouch, K., Lacombe, O., Bellahsen, N., Daniel, J. M., & Callot, J. P. (2010). Stress and strain patterns, kinematics and deformation mechanisms in a basement-cored anticline: Sheep Mountain Anticline, Wyoming. Tectonics, 29, TC1005, doi:10.1029/2009TC002525.

Amrouch, K. (2010). Apport de l'analyse microstructurale à la comprehension des mécanismes de plissement. Exemples de structures plissées aux USA (Wyoming) et en Iran (Zagros). Thèse, Université Pierre et Marie Curie – Paris 6, 2010-03, 477 p.

Amrouch, K., Beaudoin, N., Lacombe, O., Bellahsen, N., & Daniel, J. M. (2011). Paleostress magnitudes in folded sedimentary rocks. Geophysical Research Letters, 38, L17301, doi:10.1029/2011GL048649.

Anderson, E.M. (1951). The Dynamics of Faulting and Dyke Formation with Applications to Britain, Oliver and Boyd, Edinburgh.

Apak, S. N., Stuart, W. J., Lemon, N. M., & Wood, G. (1997). Structural evolution of the Permian-Triassic Cooper Basin, Australia: Relation to hydrocarbon trap styles. AAPG Bulletin, 81, 533-555.

Arboit, F., Amrouch, K., Collins, A. S., King, R., & Morley, C. (2015). Determination of the tectonic evolution from fractures, faults, and calcite twins on the southwestern margin of the Indochina Block. Tectonics, 34, 1576-1599, doi:10.1002/2015TC003876.

Arboit, F., Amrouch, K., Morley, C., Collins, A. S., & King, R. (2017), Palaeostress magnitudes in the Khao Khwang fold-thrust belt, new insights into the tectonic evolution of the Indosinian orogeny in central Thailand. Tectonophysics, 710-711, 266-276, doi:10.1016/j.tecto.2017.01.008.

Backé, G., Abul Khair, H., King, R., & Holford, S. (2011). Fracture mapping and modelling in shale-gas target in the Cooper basin, South Australia. The APPEA Journal, 51, 397-410.

Bahorich and Farmer (1995)

Balch, A. H., Lee, M. W., Miller, J. J., & Ryder, R. T. (1982). The use of vertical seismic profiles in seismic investigations of the earth. Geophysics, 47(6), 906-918.

Balch, A. H., & Lee, M. W. (1984). Vertical Seismic Profiling: Techniques, Applications, and Case Histories. International Human Resources Development Corporation, Boston, 488 p.

Basir, H. M., Javaherian, A., & Yaraki, M. T. (2013). Multi-attribute ant-tracking and neural network for fault detection: A case study of an Iranian oilfield. Journal of Geophysics and Engineering, 10(1), 015009.

Baudon, C., & Cartwright, J. (2008). The kinematics of reactivation of normal faults using high resolution throw mapping. Journal of Structural Geology, 30(8), 1072–1084.

Beaudoin, N., Leprêtre, R., Bellahsen, N., Lacombe, O., Amrouch, K., Callot, J. P., Emmanuel, L., & Daniel, J. M. (2012). Structural and microstructural evolution of the Rattlesnake Mountain Anticline (Wyoming, USA): new insights into the Sevier and Laramide orogenic stress build-up in the Bighorn Basin. Tectonophysics, 576, 20-45.

Boger, S. D., & Miller, J. M. (2004). Terminal suturing of Gondwana and the onset of the Ross–Delamerian Orogeny: the cause and effect of an Early Cambrian reconfiguration of plate motions. Earth and Planetary Science Letters, 219(1), 35-48.

Borazjani, S., Kulikowski, D., Amrouch, K., McCabe, P., & Bedrikovetsky, P. (2018). Composition changes of hydrocarbons during secondary petroleum migration. The APPEA Journal, 58, 784-787.

Borazjani, S., Kulikowski, D., Amrouch, K., & Bedrikovetsky, P. (2019). Composition Changes of Hydrocarbons during Secondary Petroleum Migration (Case Study in Cooper Basin, Australia). Geosciences, 9(2),

Boreham C. J., & Hill A. J. (1998). Source rock distribution and hydrocarbon geochemistry. In: The petroleum geology of South Australia. Vol. 4: Cooper Basin (eds. D.I. Gravestock, J.E. Hibburt and J.F. Drexel), pp 129-142. South Australia. Department of Primary Industries and Resources. Report Book, 98/9.

Boult, P. J., Lanzilli, E., Michaelsen, B. H., McKirdy, D. M., & Ryan, M. J. (1998). A new model for the Hutton/Birkhead reservoir/seal couplet and the associated Birkhead-Hutton (!) petroleum system. The APPEA Journal, 38(1), 724-744.

Bradshaw, M. T. (1993). Australian petroleum systems. PESA Journal 21, 43-53.

Black, M., McCormack, K. D., Elders, C., & Robertson, D. (2017). Extensional fault evolution within the Exmouth Sub-basin, North West Shelf, Australia. Marine and Petroleum Geology, 85, 301-315.

Burgin, H. B., Amrouch, K., Rajabi, M., Kulikowski, D., & Holford, S. P. (2018). Determining paleo-structural environments through natural fracture and calcite twin analyses: a case study in the Otway Basin. The APPEA Journal, 58, 238-254, DOI: 10.1071/AJ17099.

Cartwright, J., & Lonergan, L. (1997). Seismic expression of layer-bound fault systems of the Eromanga and North Sea Basins. Exploration Geophysics, 28(3), 323-331.

Childs, C., Nicol, A., Walsh, J. J., & Watterson, J. (1996). Growth of vertically segmented normal faults. Journal of Structural Geology, 18(12), 1389-1397.

Chipperfield, S. T., & Britt, L. K. (2000). Application of after-closure analysis for improved fracture treatment optimisation: A Cooper Basin case study. In SPE Rocky Mountain Regional/Low-Permeability Reservoirs Symposium and Exhibition. Society of Petroleum Engineers, SPE -60316-MS.

Chopra, S., & Marfurt, K. J. (2007). Volumetric curvature attributes add value to 3D seismic data interpretation. The Leading Edge, 26(7), 856-867.

Collins, A. S., & Pisarevsky, S. A. (2005). Amalgamating eastern Gondwana: the evolution of the Circum-Indian Orogens. Earth-Science Reviews, 71(3), 229-270.

Cooke, D., Tyiasning, S., & Abul Khair, H. (2016). Unexpected behaviors of stimulated fractures in the high-stress Cooper Basin. The Leading Edge, 35(1), 78-84.

Deighton, I., & Hill, A. J., 1998. Thermal and Burial History. In: The petroleum geology of South Australia. Vol. 4: Cooper Basin (eds. D.I. Gravestock, J.E. Hibburt and J.F. Drexel), pp 143-156. South Australia. Department of Primary Industries and Resources. Report Book, 98/9.

Duddy, I. R. (1987) Fission track thermal history assessment of the Eromanga-Cooper Basin: an initial apatite study, In: Gleadow, A. J. W., Duddy, I. R., Green, P. F., & Lovering, J. F. (Eds). End of Grant Technical Report, NERDDC project no. 720.

Elliott, L. G. (1993). Post-Carboniferous tectonic evolution of eastern Australia. APEA Journal, 33, 215-215.

Etchecopar, A. (1984). Étude des états de Contraintes en Tectonique Cassante et Simulation de Déformations Plastiques: Approche Mathématique, the se Doctorates-Sciences, 270 pp., Univ. Sci. et Tech. Du Languedoc, Montpellier, Fr.

Evans, P.R. (1988). The formation of petroleum and geological history of Australia. In: Petroleum in Australia: the first century. APEA Journal, Special Publication, 26-47.

Farrell, R. C., & Euwema, R. N. (1984). Refraction statics. Proceedings of the IEEE, 72(10), 1316-1329.

Ferrill, D. A., Winterle, J., Wittmeyer, G., Sims, D., Colton, S., Armstrong, A., & Morris, A. P. (1999). Stressed rock strains groundwater at Yucca Mountain, Nevada. GSA Today, 9(5), 1-8.

Flottmann, T., Campagna, D. J., Hillis, R., & Warner, D. (2004). Horizontal microfractures and core discing in sandstone reservoirs, Cooper Basin, Australia. In: Eastern Australasian basins symposium II: Petroleum Exploration Society of Australia Special Publication, 689-694.

Gajewski, D., & Pšenčik, I. (1990). Vertical seismic profile synthetics by dynamic ray tracing in laterally varying layered anisotropic structures. Journal of Geophysical Research: Solid Earth, 95(B7), 11301-11315.

Ganley, D. C., & Kanasewich, E. R. (1980). Measurement of absorption and dispersion from check shot surveys. Journal of Geophysical Research: Solid Earth, 85(B10), 5219-5226.

Gallagher, K. L. (1998). The subsidence history and thermal state of the Eromanga and Cooper Basins (Doctoral dissertation. Australian National University.

Gatehouse, C. G., (1986) The geology of the Warburton Basin in South Australia, Australian Journal of Earth Sciences, 33(2), 161-180, doi:10.1080/08120098608729357.

Gersztenkorn, A., & Marfurt, K. J. (1999). Eigenstructure-based coherence computations as an aid to 3-D structural and stratigraphic mapping. Geophysics, 64(5), 1468-1479.

Giba, M., Walsh, J. J., & Nicol, A. (2012). Segmentation and growth of an obliquely reactivated normal fault. Journal of Structural Geology, 39, 253-267.

Gibson, G. M., Totterdell, J. M., White, L. T., Mitchell, C. H., Stacey, A. R., Morse, M. P., & Whitaker, A. (2013). Pre-existing basement structure and its influence on continental rifting and fracture zone development along Australia's southern rifted margin. Journal of the Geological Society, 170(2), 365-377.

Gilby, A. R., & Mortimore, I. R. (1989). The prospects for Eromanga oil accumulations in the northern Cooper Basin region, Australia.

Gorter, J. D., Gostin, V. A., & Plummer, P. S. (1989). The enigmatic subsurface Tookoonooka complex in south-west Queensland: Its impact origin and implications for hydrocarbon accumulations. In: O'Neil, B. J. (Ed), The Cooper and Eromanga Basins, Australia, pp. 441–456. Petroleum Exploration Society of Australia, Society of Petroleum Engineers & Australian Society of Exploration Geophysicists, Adelaide, Australia.

Grant-Woolley, L., Kong, A., Schoemaker, B., Nasreddin, H., Montague, E. T. (2014). Identification of Strike-Slip Faults Provides Insights into the Further Development of Mature

Cooper Basin Fields. In SPE Asia Pacific Oil & Gas Conference and Exhibition, Adelaide, SPE 171492-MS.

Gravestock, D. I., Alexander, E. M., Morton, J. G. G., & Sun, X. (1998). Reservoirs & Seals. In: Gravestock, D. I., Hibburt, J. E., & Drexel, J. F., (Eds), The Petroleum Geology of South Australia. Vol. 4: Cooper Basin, South Australia. Department of Primary Industries and Resources. Report Book, 98/9, 157-180.

Gravestock, D. I., & Jensen-Schmidt, B. (1998). Structural setting. In: Gravestock, D.I., Hibburt, J.E., Drexel, J.F., (Eds), The Petroleum Geology of South Australia. Vol. 4: Cooper Basin, South Australia. Department of Primary Industries and Resources. Report Book, 98/9, 47-68.

Gray, D. R., & Foster, D. A. (2004). Tectonic evolution of the Lachlan Orogen, southeast Australia: historical review, data synthesis and modern perspectives. Australian Journal of Earth Sciences, 51(6), 773-817.

Gray, M. E. (2017). Analytical Techniques for Evaluating Seal Capacity for Carbon Dioxide Storage in Selected Australian Basins (Doctoral dissertation). The Australian School of Petroleum, the University of Adelaide, Adelaide, Australia.

Gray, M. E., Daniel, R., Kaldi, J., Kulikowski, D. (2019). Determining the Accuracy of Pseudo-Capillary Pressure Curves Generated from Nuclear Magnetic Resonance (NMR) Data: The Cooper Basin, Australia. Australian Journal of Earth Sciences, under review.

Green, P. M., Brain, T. J., & John, B. H. (1989). Possible stratigraphic controls on hydrocarbon distribution within the Jurassic-Early Cretaceous rocks, Eromanga Basin, southern Queensland. In: The Cooper and Eromanga Basins, Australia (ed. B. J. O'Neil), pp. 251-264. Petroleum Exploration Society of Australia, Society of Petroleum Engineers, Australian Society of Exploration Geophysicists (S.A. Branches), Adelaide (Proceedings of Cooper and Eromanga Basins Conference).

Haines, P. W., Hand, M., & Sandiford, M. (2001). Palaeozoic synorogenic sedimentation in central and northern Australia: A review of distribution and timing with implications for the evolution of intracontinental orogens. Australian Journal of Earth Sciences, 48, 911-928.

Hakami, A. M., Marfurt, K. J., & Al-Dossary, S. (2004). Curvature attribute and seismic interpretation: Case study from Fort Worth Basin, Texas, USA. In: SEG Technical Program Expanded Abstracts, 544-547.

Hallmann, C. O., Arouri, K. R., McKirdy, D. M., & Schwark, L. (2007). Temporal resolution of an oil charging history–a case study of residual oil benzocarbazoles from the Gidgealpa Field. Organic Geochemistry, 38(9), 1516-1536.

Hardage, B.A. (1985). Vertical seismic profiling. The Leading Edge, 4(11), 59-59.

Hauge, P. S. (1981). Measurements of attenuation from vertical seismic profiles. Geophysics, 46(11), 1548-1558.

Heath, R., McIntyre, S., & Gibbins, N. (1989). A Permian origin for Jurassic reservoired oil in the Eromanga Basin. In: The Cooper and Eromanga Basins, Australia (ed. B. J. O'Neil), pp. 405-416. Petroleum Exploration Society of Australia, Society of Petroleum Engineers,

Australian Society of Exploration Geophysicists (S. A. Branches), Adelaide (Proceedings of Cooper and Eromanga Basins Conference).

Hillis, R. R., Macklin, T. A., & Siffleet, P. (1995). Regional depth-conversion of mapped seismic two-way-times in the Cooper-Eromanga Basins. Exploration Geophysics, 26(2/3), 412-418.

Hillis, R. R., Enever, J. R., & Reynolds, S. D. (1999). In situ stress field of eastern Australia. Australian Journal of Earth Sciences, 46(5), 813-825.

Hillis, R. R., & Reynolds, S. D. (2000). The Australian stress map. Journal of the Geological Society, 157(5), 915-921.

Hillis, R. R., Morton, J. G. G., Warner, D. S., & Penney, R. K. (2001). Deep basin gas: A new exploration paradigm in the Nappamerri Trough, Cooper Basin, South Australia. The APPEA Journal, 41(1), 185-200.

Hillis, R. R., & Reynolds, S. D. (2003). In situ stress field of Australia. Geological Society of America Special Papers, 372, 49-58.

Hoffmann, K. L. (1989). The influence of pre-Jurassic tectonic regimes on the structural development of the southern Eromanga Basin, Queensland. In: The Cooper and Eromanga Basins, Australia (ed. B. J. O'Neil), pp. 315-328. Petroleum Exploration Society of Australia, Society of Petroleum Engineers, Australian Society of Exploration Geophysicists (S.A. Branches), Adelaide (Proceedings of Cooper and Eromanga Basins Conference).

Hung, J. H., & Wu, J. C. (2012). In-situ stress and fault reactivation associated with LNG injection in the Tiechanshan gas field, fold-thrust belt of Western Taiwan. Journal of Petroleum Science and Engineering, 96, 37-48.

Igboekwe, M. U., & Ohaegbuchu, H. E. (2011). Investigation into the weathering layer using up-hole method of seismic refraction. Journal of Geology and Mining Research, 3(3), 73-86.

Jackson, C. A. L., & Rotevatn, A. (2013). 3D seismic analysis of the structure and evolution of a salt-influenced normal fault zone: a test of competing fault growth models. Journal of Structural Geology, 54, 215-234, doi:10.1016/j.jsg.2013.06.012.

Jadoon, Q. K., Roberts, E., Blenkinsop, T., Raphael, A. J., & Shah, S. A. (2016). Mineralogical modelling and petrophysical parameters in Permian gas shales from the Roseneath and Murteree formations, Cooper Basin, Australia. Petroleum Exploration and Development, 43(2), 277-284.

Jenkins, C.C. (1989). Geochemical correlation of source rocks and crude oils from the Cooper and Eromanga basins. In: O'Neil, B.J. (ed.), The Cooper and Eromanga basins, Australia, 525–540.

Johnson, Jr., R. L., Aw, K. P., Ball, D., & Willis, M. (2002). Completion, Perforating and Hydraulic Fracturing Design Changes Yield Success in an Area of Problematic Frac Placement - the Cooper Basin, Australia, SPE 77906. Paper presented at the SPE Asia Pacific Oil and Gas Conference and Exhibition, Melbourne, Australia.

Johnson, Jr., R. L., & Greenstreet, C. W. (2003). Managing Uncertainty Related to Hydraulic Fracturing Modeling in Complex Stress Environments with Pressure-Dependent Leakoff. The

SPE Annual Technical Conference and Exhibition, Denver, Colorado, 5–8 October, SPE-84492.

Johnson, Jr., R. L., Abul Khair, H., Jeffrey, R. G., Meyer, J. J., Stark, C., & Tauchintz, J. (2015). Improving fracture initiation and potential impact on fracture coverage by implementing optimal well planning and drilling methods for typical stress conditions in the Cooper Basin, Central Australia. The APPEA Journal and Conference Proceedings, 55, extended abstract.

Jolie, E., Moeck, I., & Faulds, J. E. (2015). Quantitative structural geological exploration of fault-controlled geothermal systems—A case study from the Basin-and-Range Province, Nevada (USA). Geothermics 54, 54-67.

Kantsler, A. J., Prudence, T. J. C., Cook, A. C., & Zwigulis, M. (1984). Hydrocarbon habitat of the Cooper/Eromanga basin, Australia. In: Petroleum geochemistry and basin evolution (eds. G. Demaison and R. J. Murris), pp 373-390. American Association of Petroleum Geologists Memoir, 35.

King, R., Abul Khair, H., Bailey, A., Backé, G., Holford, S., & Hand, M. (2011). Integration of In-Situ Stress Analysis and Three-Dimensional Seismic Mapping to Understand Fracture Networks in Australian Basins. In: Proceedings from the Australian Geothermal Energy Conference, 16-18 November, Melbourne, Australia, 129-134.

Kuang, K. S. (1985). History and style of Cooper-Eromanga Basin structures. Exploration Geophysics, 16, 245-248.

Kulikowski, D., Cooke, D., Amrouch, K. (2016a). Constraining the distribution and relationship between overpressure, natural fracture density and temperature in the Cooper Basin. The Australian Petroleum Production and Exploration Association Journal, 56, 11-28, doi:10.1071/AJ15002.

Kulikowski, D., Hochwald, C., Cooke, D., & Amrouch, K. (2016b). A Statistical Approach to Assessing Depth Conversion Uncertainty on a Regional Dataset: Cooper-Eromanga Basin, Australia. ASEG-PESA-AIG 2016 Conference, Adelaide. Extended Abstract #200, 484-490, doi:10.1071/aseg2016ab200.

Kulikowski, D., Amrouch, K., & Cooke, D. (2016c). Geomechanical Modelling of Fault Reactivation in the Cooper Basin, Australia. Australian Journal of Earth Sciences, 63(3), 295-314, doi:10.1080/08120099.2016.1212925.

Kulikowski, D. (2017). Modern Structural Analysis of Subsurface Provinces: A Case Study on the Cooper and Eromanga Basins, Australia (Doctoral dissertation). The Australian School of Petroleum, the University of Adelaide, Adelaide, Australia.

Kulikowski, D., & Amrouch, K. (2017). Combining Geophysical Data and Calcite Twin Stress Inversion to Refine the Tectonic History of Subsurface and Offshore Provinces: A Case Study on the Cooper-Eromanga Basin, Australia. Tectonics, 36(3), 515-541, doi:10.1002/2016TC004366.

Kulikowski, D., Amrouch, K., Cooke, D., & Gray, M. E. (2017). Basement Structural Architecture and Hydrocarbon Conduit Potential of Polygonal Faults in the Cooper-Eromanga Basin, Australia. Geophysical Prospecting, in press, doi:10.1111/1365-2478.12531.

Kulikowski, D., & Amrouch, K. (2018a). 3D Seismic Analysis Investigating the Relationship Between Stratigraphic Architecture and Structural Activity in the Intra-cratonic Cooper and Eromanga Basins, Australia. Marine and Petroleum Geology, 91, 381-400.

Kulikowski, D., & Amrouch, K. (2018b). 4D Modelling of Fault Reactivation using Complete Paleo-Stress Tensors from the Cooper-Eromanga Basin, Australia. Australian Journal of Earth Sciences, 65(5), 661-681, DOI: 10.1080/08120099.2018.1465472.

Kulikowski, D., Amrouch, K., & Burgin, H. B. (2018a). Mapping Permeable Subsurface Fracture Networks: A Case Study on the Cooper Basin, Australia. Journal of Structural Geology, 114, 336-345.

Kulikowski, D., Hochwald, C., & Amrouch, K. (2018b). An automated cross-validation method to assess seismic time-to-depth conversion accuracy: A case study on the Cooper-Eromanga Basin, Australia. Geophysical Prospecting, 66(8), 1521-1534

Lacombe, O., Amrouch, K., Mouthereau, F., & Dissez, L. (2007). Calcite twinning constraints on late Neogene stress patterns and deformation mechanisms in the active Zagros collision belt. Geology, 35(3), 263–266.

Levin, F. K., & Lynn, R. D. (1958). Deep-hole geophone studies. Geophysics, 23(4), 639-664.

Lisle, R. J. (1994). Detection of zones of abnormal strains in structures using Gaussian curvature analysis. AAPG bulletin, 78(12), 1811-1819.

Lodwick, B. (2014). Seismic Geomorphology of the Permian Sediments in the Cooper Basin: A Study of the Toolachee Formation in the Nappamerri Trough (Honours dissertation). The Australian School of Petroleum, the University of Adelaide, Adelaide, Australia.

Lonergan, L., Cartwright, J., & Jolly, R. (1998). The geometry of polygonal fault systems in Tertiary mudrocks of the North Sea. Journal of Structural Geology, 20(5), 529-548.

Longley, I. M. (1989). The Talundilly anomaly and its implications for hydrocarbon exploration of Eromanga astroblemes.

Lowe-Young, B. S., Mackie, S. I., & Heath, R. S. (1998). The Cooper-Eromanga Petroleum System, Australia. Investigation of Essential Elements and Processes. AAPG Bulletin, abstract, 82(13).

Mackie, S. (2015). History of Petroleum Exploration and Development in the Cooper and Eromanga Basins. AAPG/SEG International Conference and Exhibition, Melbourne, Australia, Search and Discovery Article #10814.

Mai, H. T., Marfurt, K. J., & Chávez-Pérez, S. (2009). Coherence and volumetric curvatures and their spatial relationship to faults and folds, an example from Chicontepec basin. Proceedings of the Society of Exploration Geophysicists International Exposition and Annual Meeting, Houston, 1063-1067.

Mavromatidis, A. (2006). Burial/exhumation histories for the Cooper-Eromanga Basins and implications for hydrocarbon exploration, Eastern Australia. Basin Research, 18, 351-373.

Mavromatidis, A. (2008). Two layer model of lithospheric compression and uplift/exhumation in an intracratonic setting: an example from the Cooper–Eromanga Basins, Australia. International Journal of Earth Sciences, 97(3). 623-634.

McGowen, J.M., Gilbert, J.V. & Samari, E. (2007). Hydraulic Fracturing Down Under. Hydraulic Fracturing Technology Conference, College station, Texas, 29–31 January, SPE-106051-MS.

Meixner, T. J., Gunn, P. J., Boucher, R. K., Yeates, T. N., Richardson, L. M., & Frears, R. A. (2000). The nature of the basement to the Cooper Basin region, South Australia. Exploration Geophysics, 31. 24-32.

Metcalfe, I. (2013), Gondwana dispersion and Asian accretion: tectonic and palaeogeographic evolution of eastern Tethys. Journal of Asian Earth Sciences, 66, 1-33.

Moore, P. S., & Pitt, G. M. (1984). Cretaceous of the Eromanga Basin—implications for hydrocarbon exploration. The APPEA Journal, 24(1), 358-376.

Morton, J. G. G. (1998). Undiscovered petroleum resources. In: Gravestock, D.I., Hibburt, J.E. and Drexel, J.F. (eds.), The Petroleum Geology of South Australia. Volume 4: Cooper Basin. Report Book 203-09. South Australia: Department of Primary Industries and Resources, pp. 203-210.

Myers, J. S., Shaw, R. D., & Tyler, I. M. (1996). Tectonic evolution of Proterozoic Australia. Tectonics, 15(6), 1431-1446.

Müller, R. D., Dyksterhuis, S., & Rey, P. (2012). Australian paleo-stress fields and tectonic reactivation over the past 100 Ma. Australian Journal of Earth Sciences, 59, 13-28.

Murray, G. H. (1968). Quantitative fracture study-Spanish Pool, McKenzie County, North Dakota. AAPG Bulletin, 52(1), 57-65.

Nelson, E. J., Meyer, J. J., Hillis, R. R., & Mildren, S. D. (2005). Transverse drilling-induced tensile fractures in the West Tuna area, Gippsland Basin, Australia: implications for the in situ stress regime. International Journal of Rock Mechanics and Mining Sciences, 42(3), 361-371.

Nelson, E., Hillis, R., Sandiford, M., Reynolds, S., & Mildren, S. (2006). Present-day state-of-stress of southeast Australia. APPEA journal, 46(1), 283-305.

Nelson, E. J., Chipperfield, S. T., Hillis, R. R., Gilbert, J., & McGowen, J. (2007a). Using geological information to optimize fracture stimulation practices in the Cooper Basin, Australia. Petroleum Geoscience, 13(1), 3-16.

Nelson, E. J., Chipperfield, S. T., Hillis, R. R., Gilbert, J., McGowen, J., & Mildren, S. D. (2007b). The relationship between closure pressures from fluid injection tests and the minimum principal stress in strong rocks. International Journal of Rock Mechanics and Mining Sciences, 44, 787-801.

Neves, F. A., Zahrani, M. S., & Bremkamp, S. W. (2004). Detection of potential fractures and small faults using seismic attributes. The Leading Edge, 23, (9), 903-906.

Newton, C. B. (1986). The Tintaburra oilfield. The APEA Journal, 26, 334-352.

Oldham, A. C., & Gibbins, N. M., (1995). Lake Hope 3D-A case study. Exploration Geophysics, 26, 383-394.

O'Neil, B. J. (1998). History of Petroleum Exploration and Development. In: Gravestock, D.I., Hibburt, J.E. & Drexel, J.F. (eds.), The Petroleum Geology of South Australia. Volume 4: Cooper Basin. South Australia Department of Primary Industries and Resources, Adelaide. Report Book, 1998/9, pp. 7-36.

Partyka, G., Gridley, J., & Lopez, J. (1999). Interpretational applications of spectral decomposition in reservoir characterization. The Leading Edge, 18(3), 353-360.

Pitkin, M. C., Wadham, T. H., McGowen, J. M., & Thom, W. W. (2012, January). Taking the first steps: Stimulating the Nappamerri Trough resource play. In SPE Asia Pacific Oil and Gas Conference and Exhibition. Society of Petroleum Engineers.

Pitt, G. M. (1986). Geothermal gradients, geothermal histories and the timing of thermal maturation in the Eromanga-Cooper Basins, in Contributions to the Geology and Hydrocarbon Potential of the Eromanga Basin. In: Gravestock, D. I., Moore, P. S., & Pitt, G. M. (Eds), pp. 323-351, Special Publication 12, Geological Society of Australia.

Pokalai, K., Fei, Y., Ahmad, M., Haghighi, M., & Gonzalez, M. (2015a). Design and optimisation of multi-stage hydraulic fracturing in a horizontal well in a shale gas reservoir in the Cooper Basin, South Australia. The Australian Petroleum Production and Exploration Association Journal, 55, 1–14.

Pokalai, K., Haghighi, M., Sarkar, S., Tyiasning, S., & Cooke, D. (2015b). Investigation of the Effects of Near-Wellbore Pressure Loss and Pressure Dependent Leakoff on Flowback during Hydraulic Fracturing with Pre-Existing Natural Fractures. SPE/IATMI Asia Pacific Oil and Gas Conference and Exhibition, Nusa Dua, Bali, SPE-176440.

Pokalai, K., Kulikowski, D., Johnson, Jr., R. L., Haghighi, M., & Cooke, D. (2016). Development of a new approach for hydraulic fracturing in tight sand with pre-existing natural fractures. The Australian Petroleum Production and Exploration Association Journal, 56, 225-238.

Pokalai, K. (2018). Simulation and Optimisation of Hydraulic Fracturing and Flowback in Unconventional Reservoirs: A Case Study in the Cooper Basin, South Australia (Doctoral dissertation). The Australian School of Petroleum, the University of Adelaide, Adelaide, Australia.

Powell, T. G., Boreham, C. J., McKirdy, D. M., Michaelsen, B. H., & Summons, R. E. (1989). Petroleum Geochemistry of the Murta Member, Mooga Formation, and associated oils, Eromanga Basin. The APPEA Journal, 29, 114-129.

Radke, B. (2009). Hydrocarbon and Geothermal Prospectivity of Sedimentary Basins in Central Australia; Warburton, Cooper, Pedirka, Galilee, Simpson and Eromanga Basins. Geoscience Australia Record 2009/25.

Reynolds, S. D., Coblentz, D. D., & Hillis, R. R. (2002). Tectonic forces controlling the regional intraplate stress field in continental Australia: Results from new finite element modelling. Journal of Geophysical Research, 107(B7). 2131.

Reynolds, S. D., Coblentz, D. D., & Hillis, R. R. (2003). Influences of plate-boundary forces on the regional intraplate stress field of continental Australia. Geological Society of America Special Papers, 372, 59-70.

Reynolds, S. D., Mildren, S. D., Hillis, R. R., & Meyer, J. J. (2004). The in situ stress field of the Cooper Basin and its implications for hot dry rock geothermal energy development. In PESA Eastern Australasian Basins Symposium II (2004: Adelaide, South Australia).

Reynolds, S. D., Mildren, S. D., Hillis, R. R., Meyer, J. J., & Flottmann, T. (2005). Maximum horizontal stress orientations in the Cooper Basin, Australia. implications for plate-scale tectonics and local stress sources. Geophysical Journal International, 160, 332-343.

Reynolds, S. D., Mildren, S. D., Hillis, R. R., & Meyer, J. J. (2006). Constraining stress magnitudes using petroleum exploration data in the Cooper-Eromanga Basins, Australia. Tectonophysics, 415, 123-140.

Rezaee, M. R., & Sun, X. (2007). Fracture-Filling Cements in the Palaeozoic Warburton Basin, South Australia. Journal of Petroleum Geology, 30(1), 79-90.

Rigby, D., & Smith, J. W. (1981). An isotopic study of gases and hydrocarbons in the Cooper Basin. The APPEA Journal, 21, 222-229.

Roberts, G. A., Chipperfield, S. T., & Miller, W. K. (2000). The evolution of a high near-wellbore pressure loss treatment strategy for the Australian Cooper Basin. In SPE Annual Technical Conference and Exhibition. Society of Petroleum Engineers.

Roberts, A. (2001). Curvature attributes and their application to 3D interpreted horizons. First Break, 19(2), 85-100.

Robson, A. G. (2018). Normal fault growth analysis using 3D seismic datasets located along Australia's southern margin (Doctoral dissertation). School of Physical Sciences, the University of Adelaide, Adelaide, Australia.

Robson, A. G, Holford, S. P., King, R. C., & Kulikowski, D. (2018). Structural evolution of horst and half-graben structures proximal to a transtensional fault system using a 3D seismic dataset from the Shipwreck Trough, offshore Otway Basin, Australia. Marine and Petroleum Geology, 89, 615-634, doi:10.1016/j.marpetgeo.2017.10.028.

Rumph B. (1982) Seismic data from the Eromanga Basin. In: Moore, S. P., & Mount, T. J. (Eds), Eromanga Basin Symposium: Summary Papers, pp. 193. Geological Society of Australia & Petroleum Exploration Society of Australia, Adelaide, Australia.

Sandiford, M., Wallace, M., & Coblentz, D. (2004). Origin of the in situ stress field in south-eastern Australia. Basin Research, 16(3), 325-338.

Scholefield, T. (1989). The stratigraphy and hydrocarbon potential of the northern Eromanga Basin. In: O'Neil, B. J. (Ed), The Cooper and Eromanga Basins, Australia, pp. 417-427. Petroleum Exploration Society of Australia, Society of Petroleum Engineers & Australian Society of Exploration Geophysicists, Adelaide, Australia.

Scott, M. P., Stephens, T., Durant, R., McGowen, J., Thom, W., & Woodroof, R. (2013). Investigating hydraulic fracturing in tight gas sand and shale gas reservoirs in the Cooper Basin. In: SPE Unconventional Resources Conference and Exhibition-Asia Pacific, SPE-167073-MS.

Senior, B. R., Galloway, M. C., Ingram, J. A., & Senior, D. (1968). The geology of the Barrolka, Eromanga, Durham Downs, Thargomindah, Tickalara and Bulloo 1:250,000 Sheet areas, Queensland. Department of National Development, Bureau of Mineral Resources, Geology and Geophysics, Record no. 1968/35.

Sibson, R. H. (1974). Frictional constraints on thrust, wrench and normal faults. Nature, 249(5457), 542-544.

Smyth, M. (1983). Nature of source material for hydrocarbons in Cooper Basin, Australia. AAPG Bulletin, 67(9), 1422-1426.

Stainsby, S. D., & Worthington, M. H. (1985). Q estimation from vertical seismic profile data and anomalous variations in the central North Sea. Geophysics, 50(4), 615-626.

Stanmore, P. J. (1989). Case studies of stratigraphic and fault traps in the Cooper Basin, Australia. In: The Cooper and Eromanga Basins, Australia. Proceedings of the Cooper and Eromanga Basins Conference, Adelaide, 361-369.

Stewart, S. A., & Podolski, R. (1998). Curvature analysis of gridded geological surfaces. Geological Society, London, Special Publications, 127(1), 133-147.

Stuart, W. J. (1976). The genesis of Permian and lower Triassic reservoir sandstones during phases of southern Cooper Basin development. APEA Journal, 16(1), 27-48.

Sun, X. (1997). Structural style of the Warburton Basin and control in the Cooper and Eromanga Basins, South Australia. Exploration Geophysics, 28(3), 333-339.

Sun, X. (1999). Fracture analysis of the Eastern Warburton Basin (Early Paleozoic). South Australia. National Centre for Petroleum Geology and Geophysics. Report Book, 99, 00014.

Teufel, L. W., Rhett, D. W., & Farrell, H. E. (1991). Effect of reservoir depletion and pore pressure drawdown on in situ stress and deformation in the Ekofisk field, North Sea. In: The 32nd US Symposium on Rock Mechanics (USRMS), American Rock Mechanics Association, Rotterdam, 63-72.

Tingay, M., Hillis, R., Swarbrick, R., Morley, C. & Damit, A. (2007). 'Vertically transferred'' overpressures in Brunei: Evidence for a new mechanism for the formation of high magnitude overpressures. Geology, 35, 1023–1026.

Tyiasning, S., & Cooke, D. (2015). A comparison of competing amplitude variation with offset techniques applied to tight gas sand exploration in the Cooper Basin of Australia. Interpretation, 3(3), SZ15-SZ26.

Tyiasning, S., & Cooke, D. (2016). Anisotropy signatures in the Cooper Basin of Australia: Stress versus fractures. Interpretation, 4(2), SE51-SE61.

Van Ruth, P. & Hillis, R. (2000). Estimating pore pressure in the Cooper Basin, South Australia: sonic log method in an uplifted basin. Exploration Geophysics, 31(1/2), 441-447.

Van Ruth, P., Hillis, R., Tingate, P., & Swarbrick, R. (2003). The origin of overpressure in 'old' sedimentary basins: an example from the Cooper Basin, Australia. Geofluids, 3(2), 125-131.

Veevers, J. J., Jones, J. G., & Powell, C. M. (1982). Tectonic framework of Australia's sedimentary basins. APEA Journal, 22(1), 283-300.

Veevers, J. J., & Powell, C. M. (1984). Uluru and Adelaidean regimes, in J. J. Veevers, ed., Phanerozoic earth history of Australia: Oxford, Clarendon Press, p. 329–339.

Watterson, J., Walsh, J., Nicol, A., Nell, P. A. R., & Bretan, P. G. (2000). Geometry and origin of a polygonal fault system. Journal of the Geological Society, 157(1), 151-162.

Williams, G. D., Powell, C. M., & Cooper, M. A. (1989). Geometry and kinematics of inversion tectonics. Geological Society, London, Special Publications, 44(1), 3-15.

Winterfield, C. D., Missikos, J., Tio, R., & Dalgety, B. (2014, October). Application of Closed Loop Control Logic to Optimise End-of-Life Cycling Production in a Mature Gas Field. In SPE Asia Pacific Oil & Gas Conference and Exhibition. Society of Petroleum Engineers.

Wycherley, H., Fleet, A., & Shaw, H. (1999). Some observations on the origins of large volumes of carbon dioxide accumulations in sedimentary basins. Marine and Petroleum Geology, 16(6), 489-494.

Young, I. F., Gunther, L. M., & Dixon, O. (1989). GSQ Thargomindah-3: A stratigraphic test of a “canyon-like” feature near the Tookoonooka complex, Eromanga basin, Queensland. In: O’Neil, B. J. (Ed), The Cooper and Eromanga Basins, Australia. Adelaide: Proceedings of Petroleum Exploration Society of Australia, Society of Petroleum Engineers, Australian Society of Exploration Geophysicists (SA Branches), 457–471.

12. FIGURES

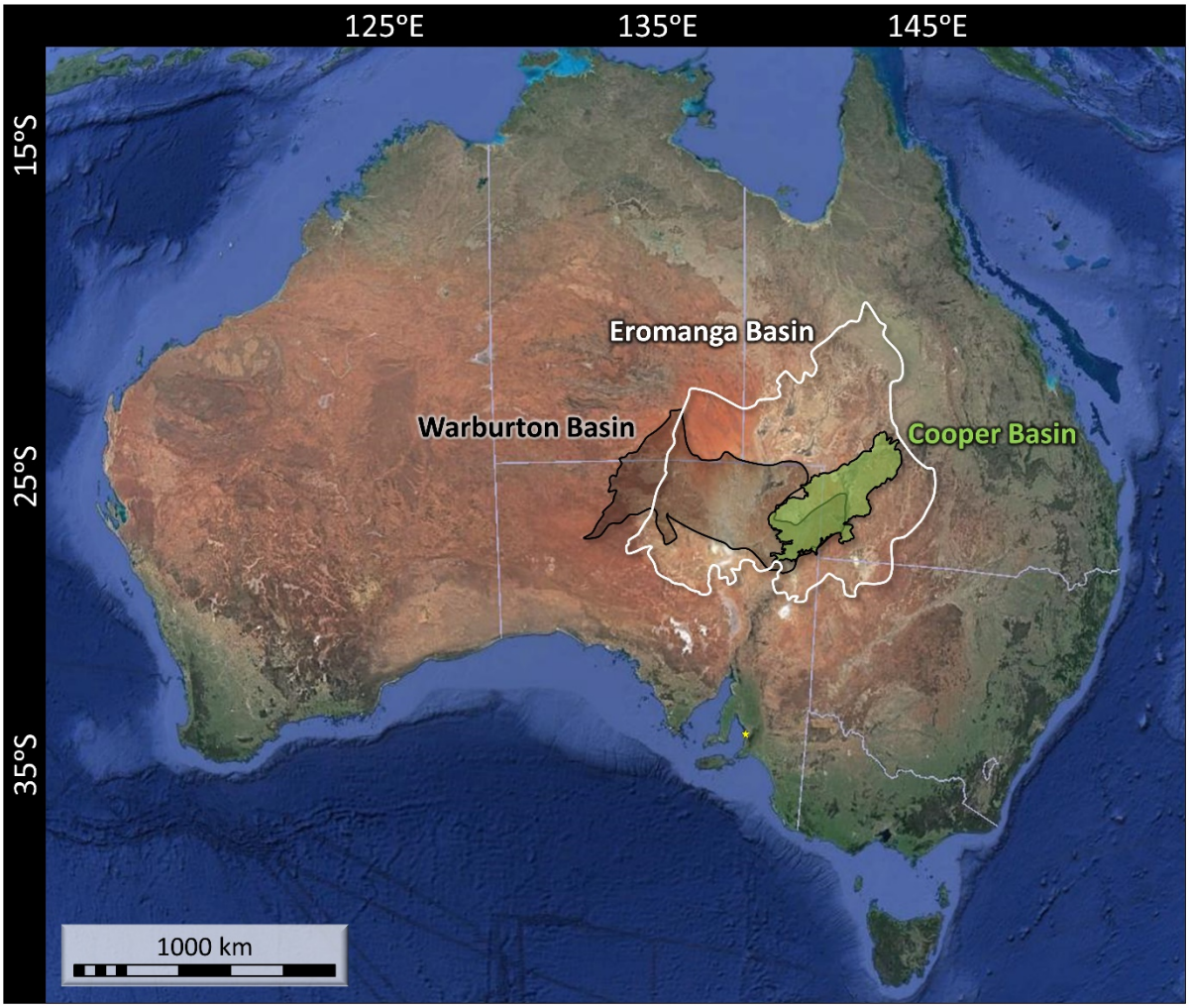

Figure 1. Location of the Warburton, Cooper, and Eromanga basins (after Kulikowski et al., 2016c).

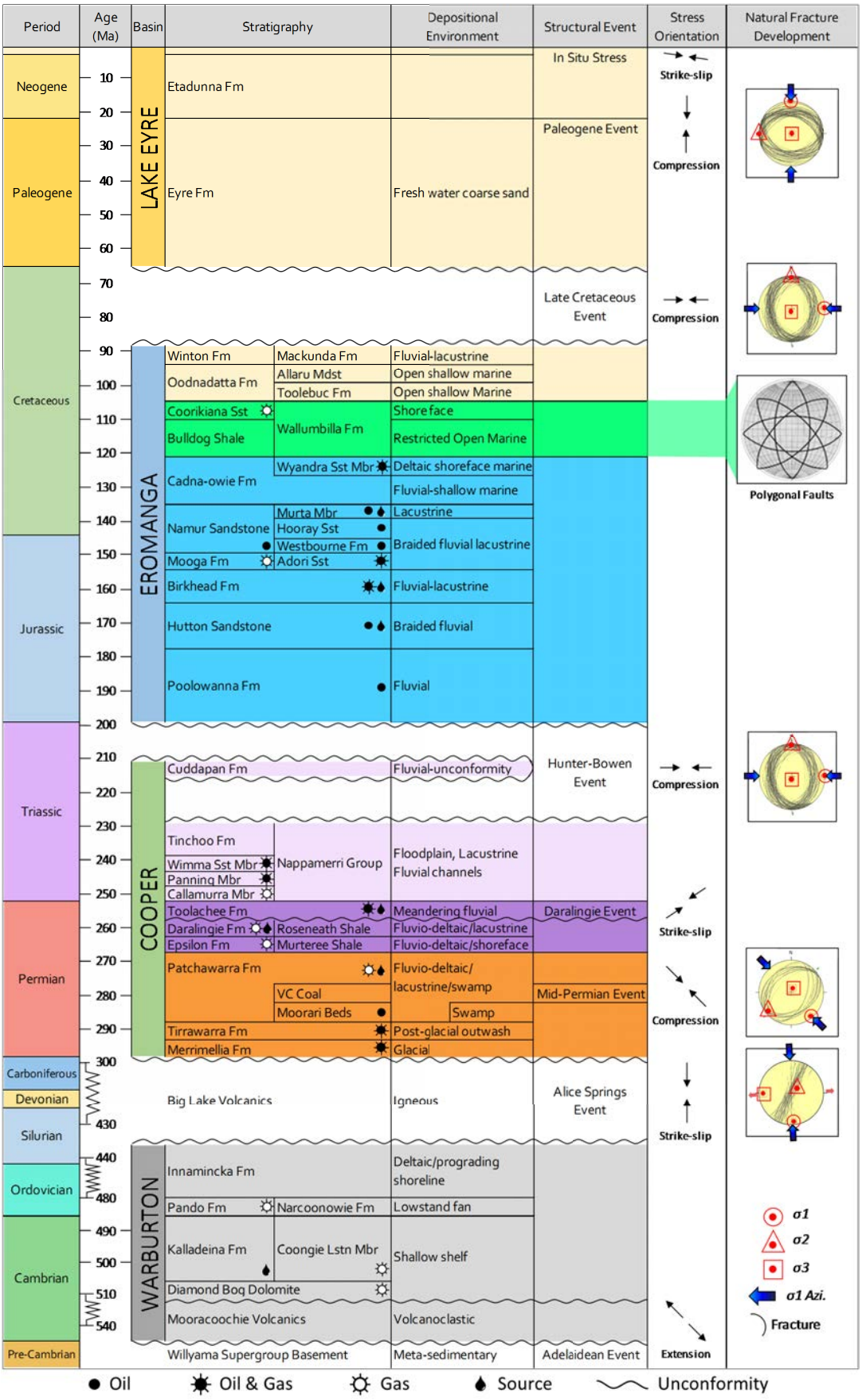

Figure 2. Tectonostratigraphy of the Warburton, Cooper, Eromanga and Lake Eyre basins (after Kulikowski & Amrouch., 2017a).

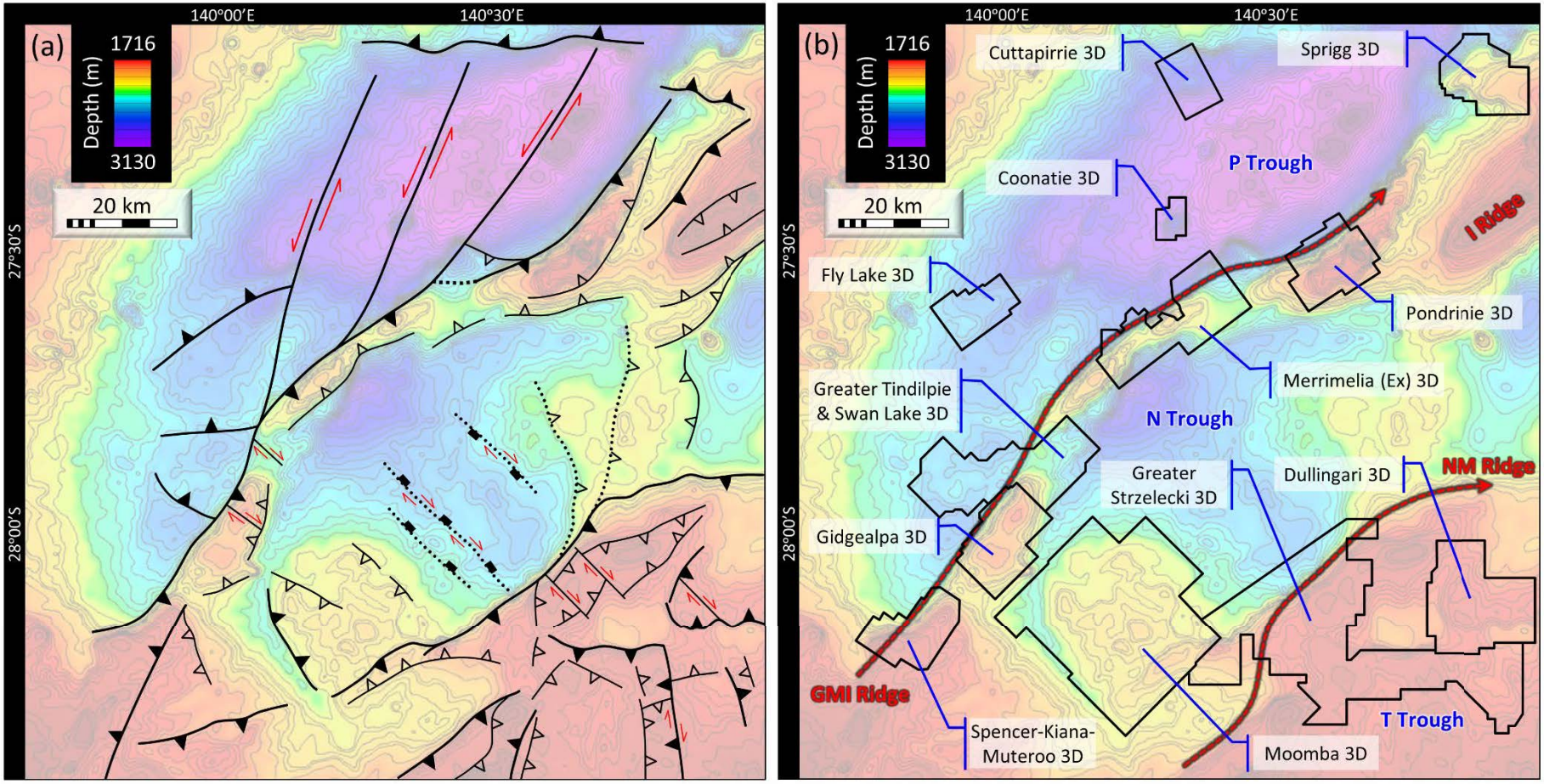

Figure 3. (a) Fault map of the South Australian Cooper-Eromanga basins (after Kulikowski et al., 2017). (b) Location of 12 3D seismic surveys commonly used for research. The location of the Gidgealpa-Merrimelia-Innamincka (GMI) and Nappacoongee-Murteree (NM) ridges, and the Patchawarra (P Trough), Nappamerri (N Trough), and Tenappera (T Trough) troughs are shown (after Kulikowski et al., 2017).

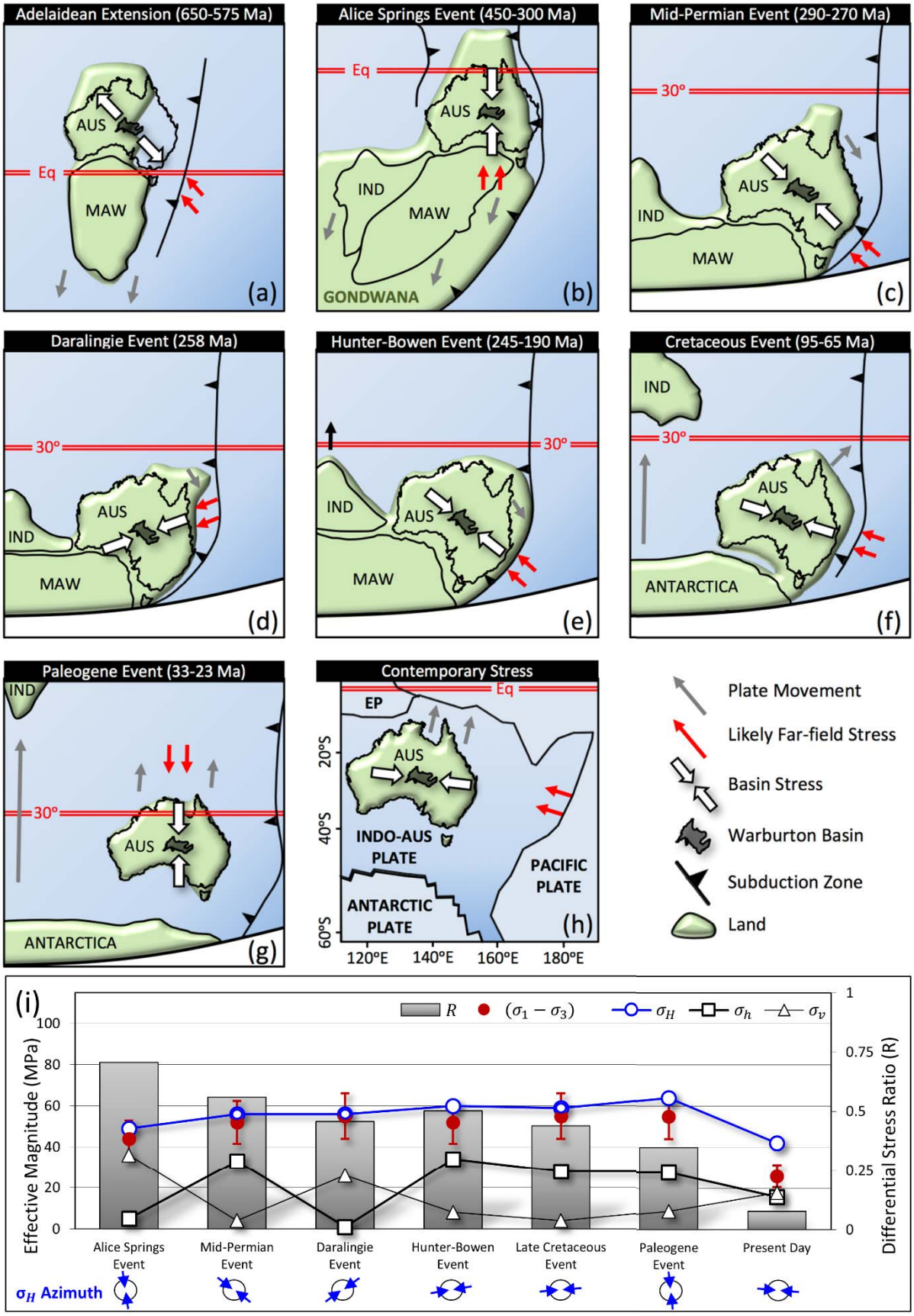
Adelaidean Extension (650-575 Ma)
AUS
Eq
MAW
(a)
Alice Springs Event (450-300 Ma)
Eq
AUS
IND
MAW
GONDWANA
(b)
Mid-Permian Event (290-270 Ma)
30°
AUS
IND
MAW
(c)
Daralingie Event (258 Ma)
30°
AUS
IND
MAW
(d)
Hunter-Bowen Event (245-190 Ma)
30°
IND
AUS
MAW
(e)
Cretaceous Event (95-65 Ma)
IND
30°
AUS
ANTARCTICA
(f)
Paleogene Event (33-23 Ma)
IND
30°
AUS
ANTARCTICA
(g)
Contemporary Stress
Eq
EP
AUS
20°S
40°S
60°S
INDO-AUS PLATE
PACIFIC PLATE
ANTARCTIC PLATE
120°E
140°E
160°E
180°E
(h)
Plate Movement
Likely Far-field Stress
Basin Stress
Warburton Basin
Subduction Zone
Land
(i)
R
$(\sigma_1 - \sigma_3)$
σ_H
σ_h
σ_v
Effective Magnitude (MPa)
Differential Stress Ratio (R)
0
20
40
60
80
100
0
0.25
0.5
0.75
1
Alice Springs Event
Mid-Permian Event
Daralingie Event
Hunter-Bowen Event
Late Cretaceous Event
Paleogene Event
Present Day
σ_H Azimuth

Figure 4. (a)→(h) Geodynamic evolution of Australia with Cooper-Eromanga basins derived stresses through time. (i) Evolution of principal stresses (after Kulikowski & Amrouch, 2017, 2018b).

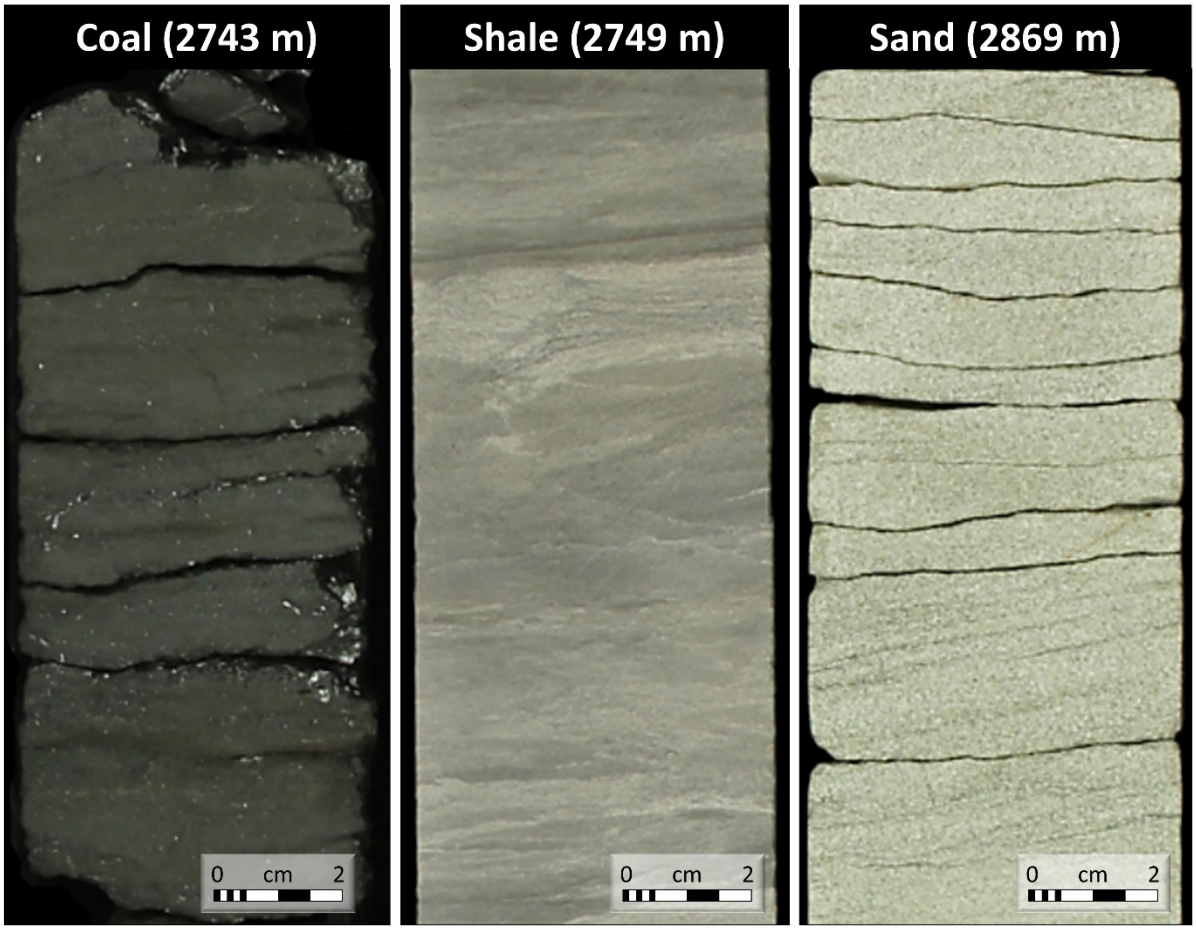

Figure 5. Cyclic lithology variation within the Patchawarra Formation (Core images obtained from Tindilpie 11 well completion report).

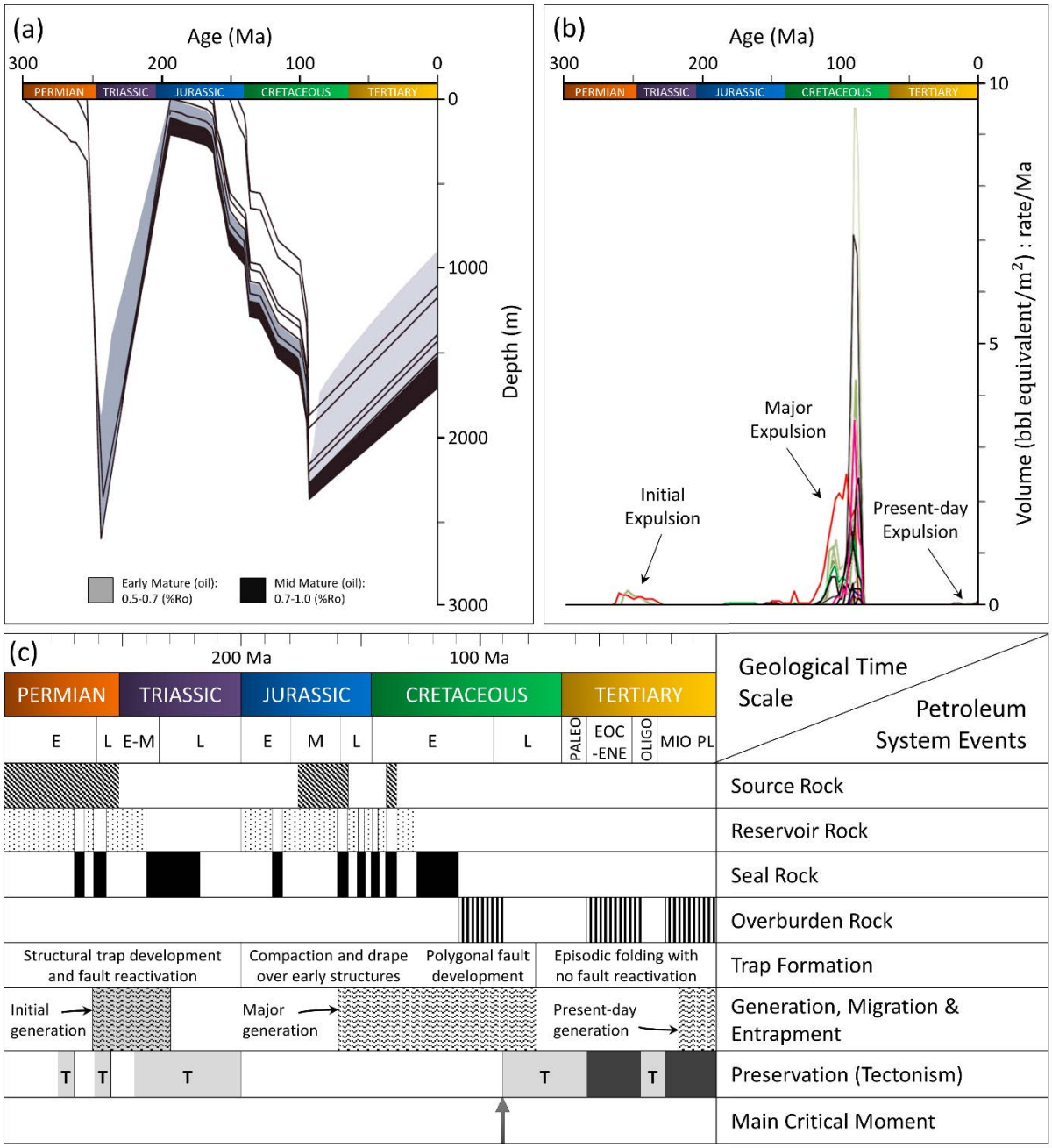

Figure 6. (a) Burial history of Cooper-Eromanga basins (after Mavromatidis, 2006). (b) Gas (per well) and oil expulsion through time (after Deighton & Hill, 2009). (c) Timing of key petroleum system processes (after Lowe-Young et al., 1998).

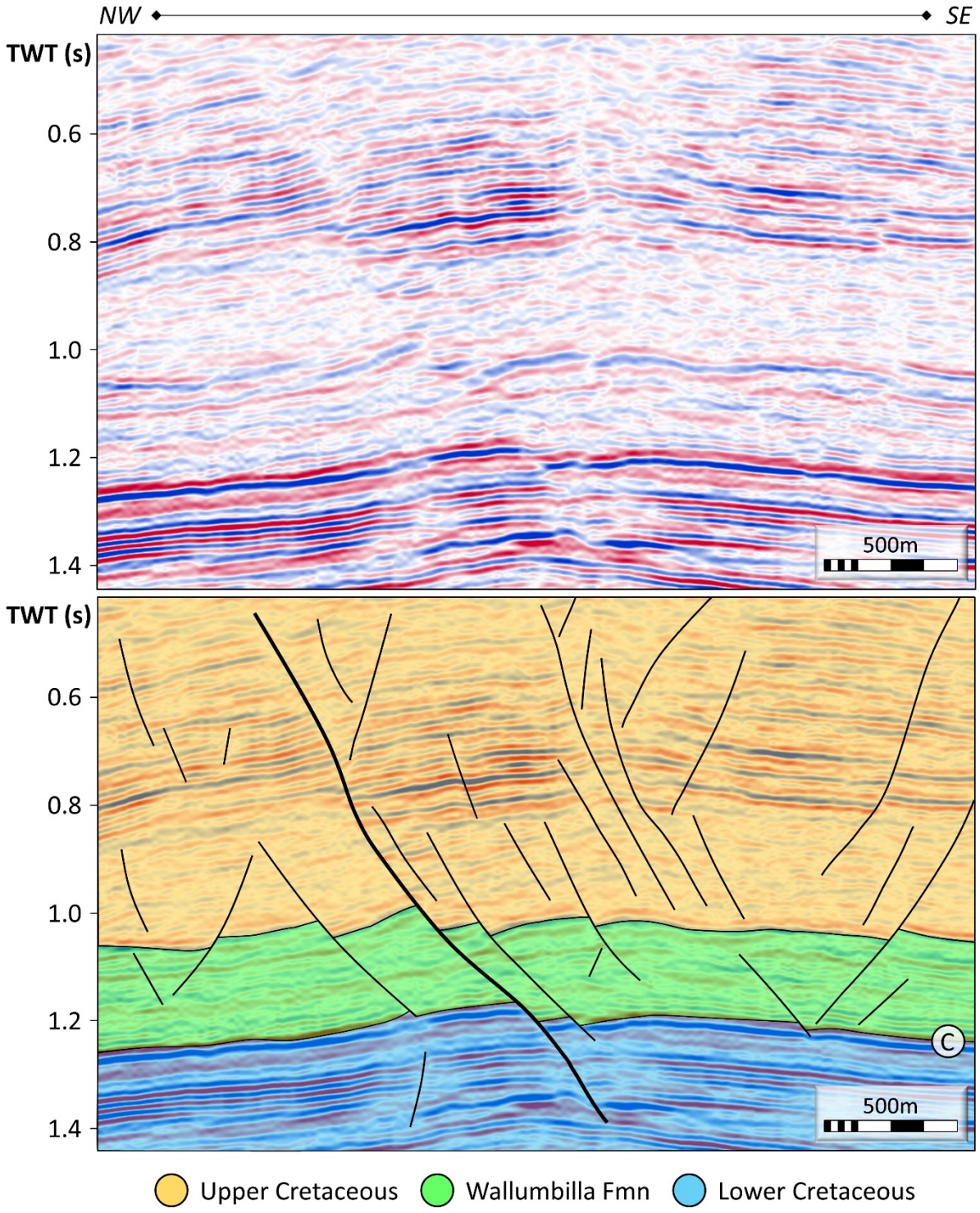

Figure 7. Cross-section from the Spencer-Kiana-Murteree 3D seismic survey (Inline 640) showing the polygonal fault system with large normal faults observed to displace the Cadna-owie Formation reflector and which extend into oil-rich Lower Cretaceous reservoirs (Kulikowski et al., 2017). See Figure 3b for seismic survey location. C-reflector: Cadna-owie Formation.

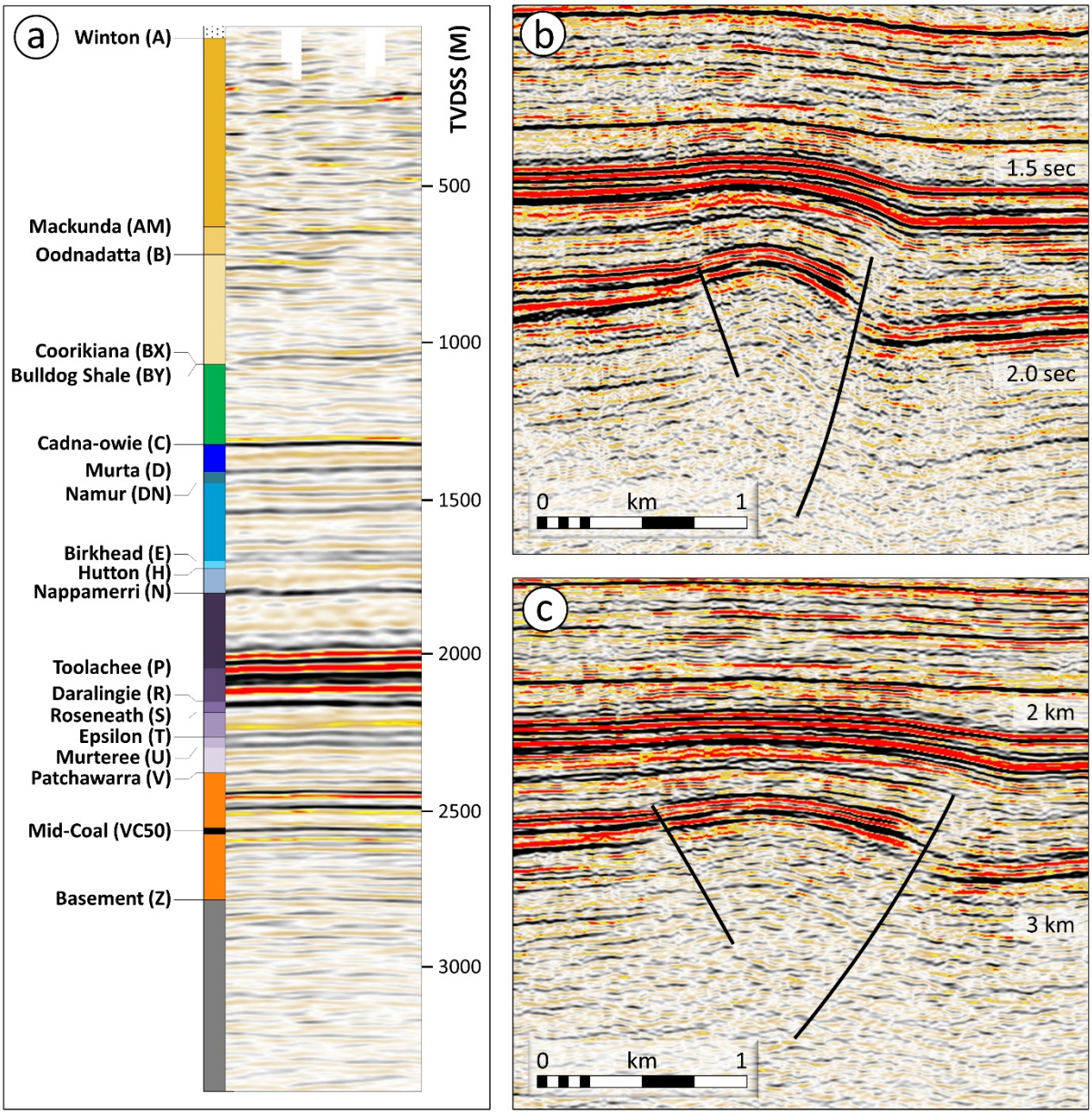

Figure 8. (a) Typical seismic reflection profile showing stratigraphic and seismic markers. The difference in fault geometry when seismic data is in: (b) the time-domain; and (c) the depth-domain. See Figure 2 for stratigraphic names. The markers denote the top of interval.

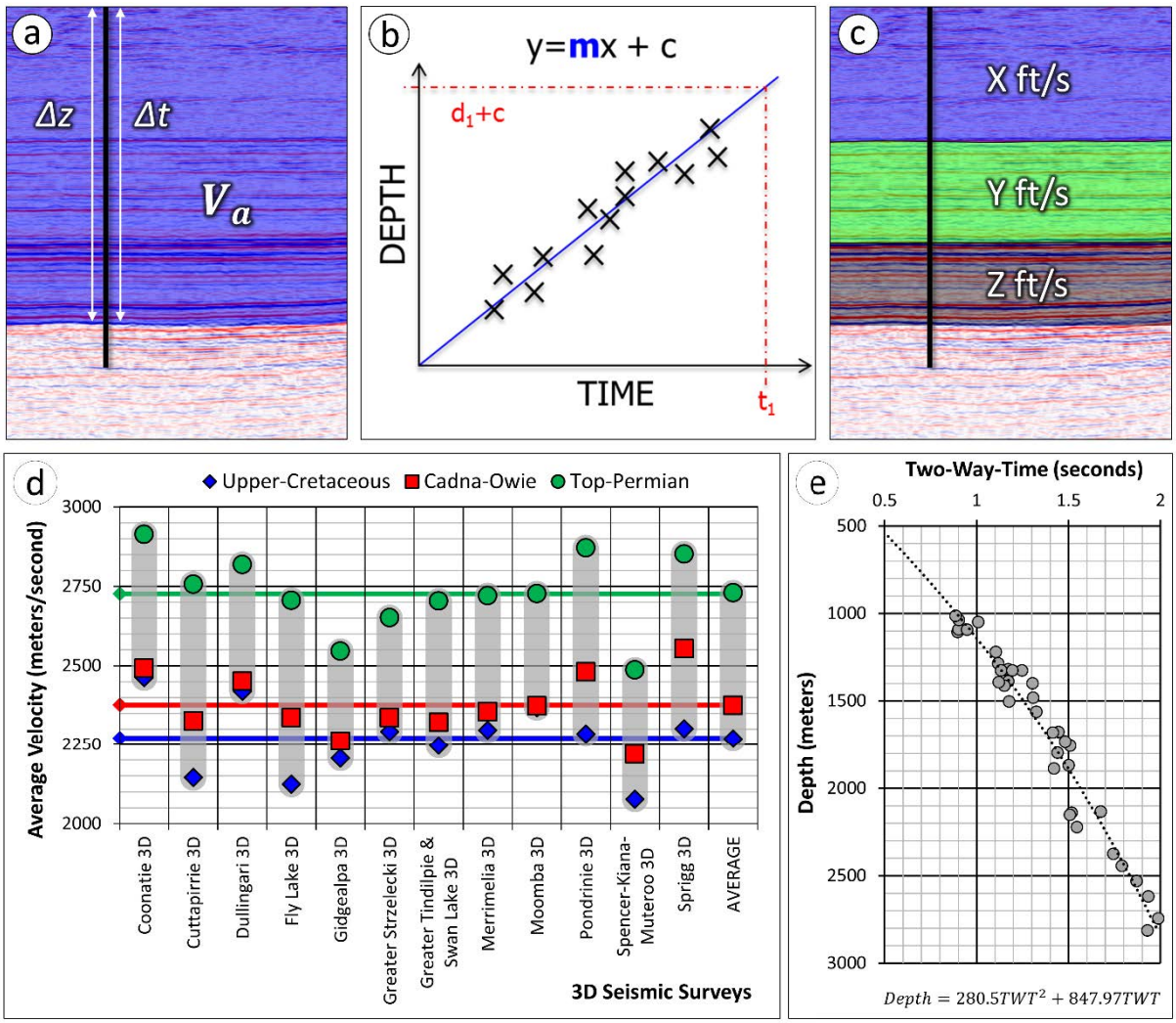

Figure 9. Common seismic time-to-depth conversion methods. (a) Average velocity (V_a) method uses the ratio between depth (from well) and time (from seismic data) for a reflector. (b) Time-depth trend method fits a trend for the time-depth pair data. (c) Interval velocity, or layer-cake, method divides the seismic cross-section into key stratal units and applies different velocities to those layers. (d) Average Velocities for key seismic reflectors. (e) Time-Depth trend obtained from 12 3D seismic surveys (after Kulikowski et al., 2016b, 2017). See Figure 3b for seismic survey location.

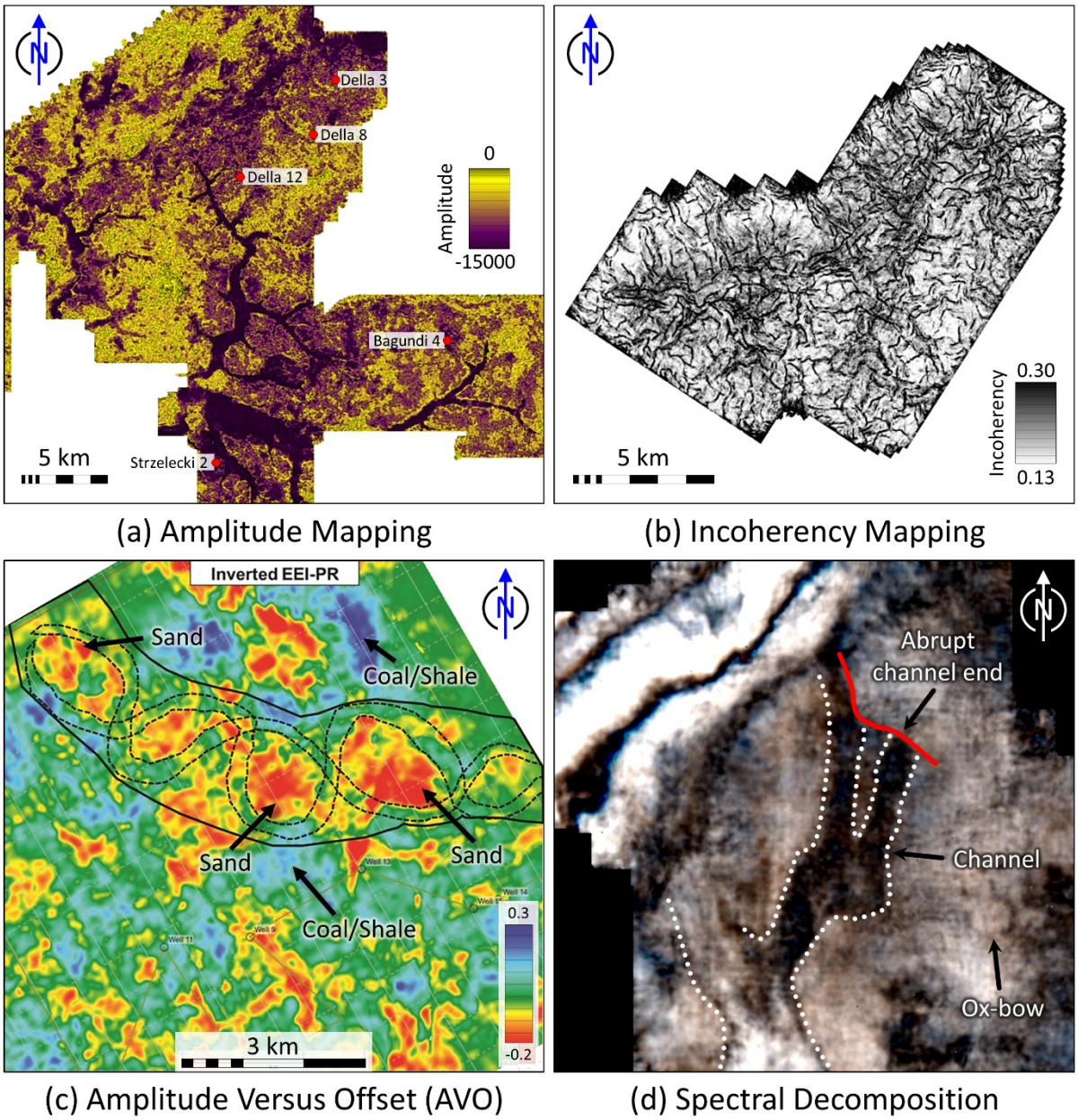

Figure 10. Seismic data analysis techniques beneficial to the fluvial dominated Cooper-Eromanga basins. (a) Amplitudes extracted along reflector surfaces to locate channel systems. Example from Greater Strzelecki 3D showing a large regional channel system (after Kulikowski and Amrouch, 2017); (b) Incoherency analysis along a reflector to identify subtle faults. Example from Spencer-Kiana-Muteroo 3D showing the distribution of polygonal faults along the Upper Cretaceous reflector (after Kulikowski and Amrouch, 2018a); (c) Application of amplitude versus offset (AVO) to differentiate between sandstone and coal measures. The example shows the distribution of sandstone (red-yellow) and shale/coal (green-blue) in the Cooper Basin (after Tyiasning and Cooke, 2015); and (d) Spectral decomposition (colour blending) analysis on the Gaschnitz 3D seismic survey used to delineate the geometry of a fluvial channel and ox-bow feature in the Toolachee Formation, Cooper Basin (Lodwick, 2014).

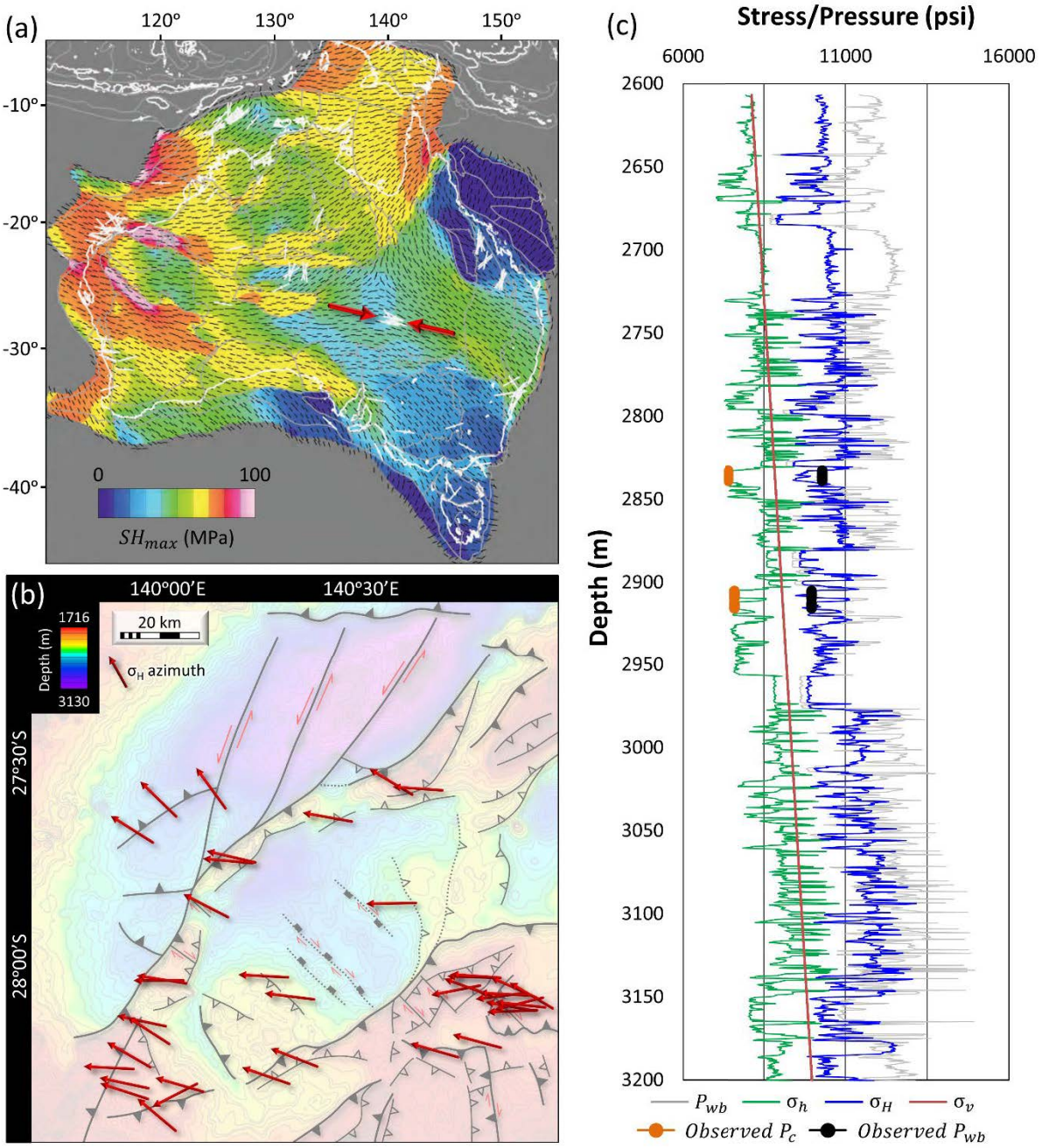

Figure 11. Orientation of the maximum horizontal stress orientation across: (a) Australia (after Müller et al., 2012); and (b) the Cooper-Eromanga basins (after Kulikowski et al., 2017). (c) A typical mechanical earth model for the Patchawarra Formation showing the minimum (σ_h) and maximum (σ_H) horizontal stresses, vertical stress (σ_v), breakdown pressure from logs (P_{wb}) and well test data (observed P_{wb}), and closure pressure (observed P_c) (after Pokalai, 2018). See Figure 4i for the origin of far-field stresses.

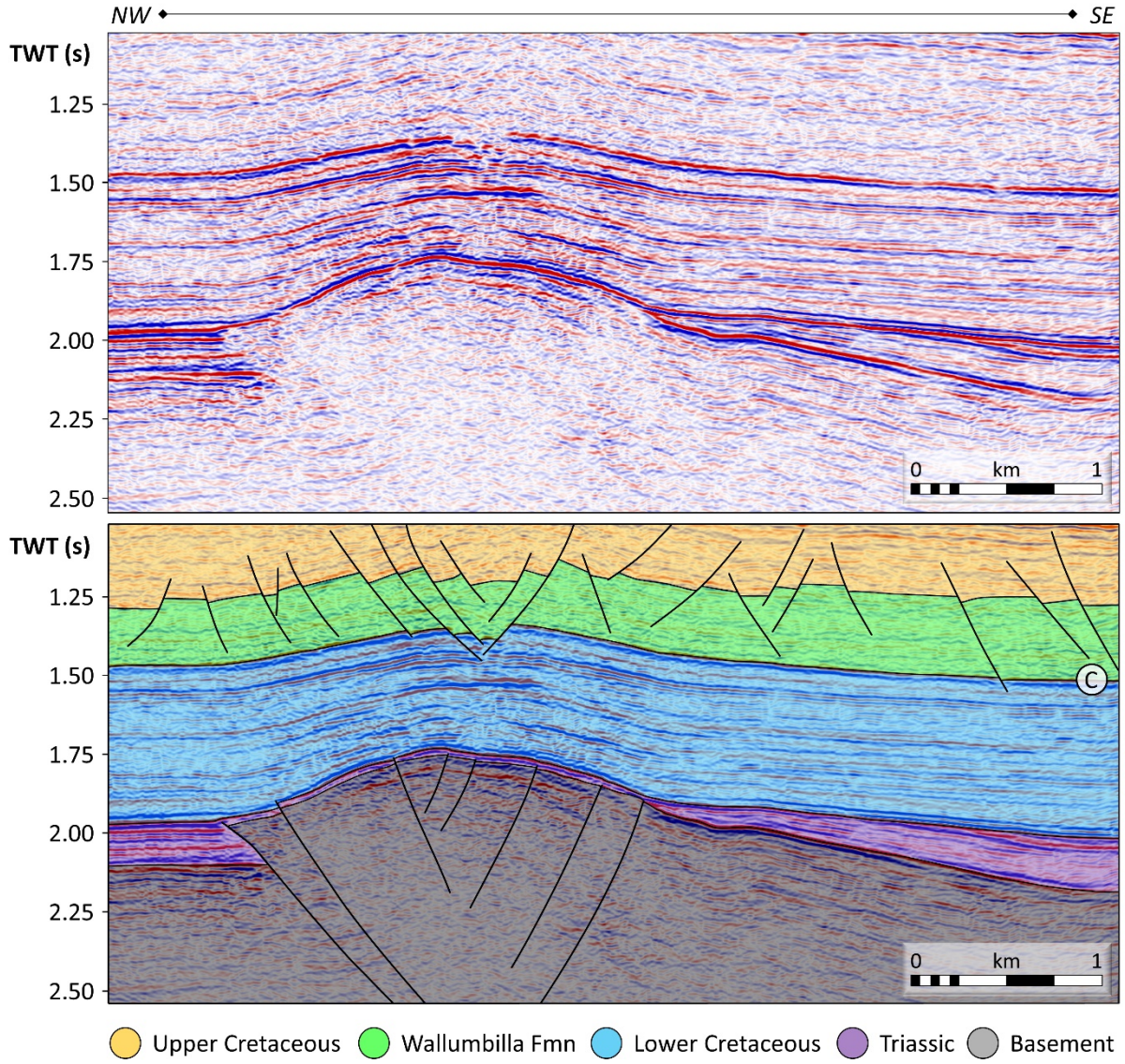

Figure 12. Basement and polygonal faults in the Merrimelia (Extension) 3D seismic survey interpreted along Inline 4295 (Kulikowski et al., 2017). See Figure 3b for seismic survey location. C-reflector: Cadna-owie Formation.

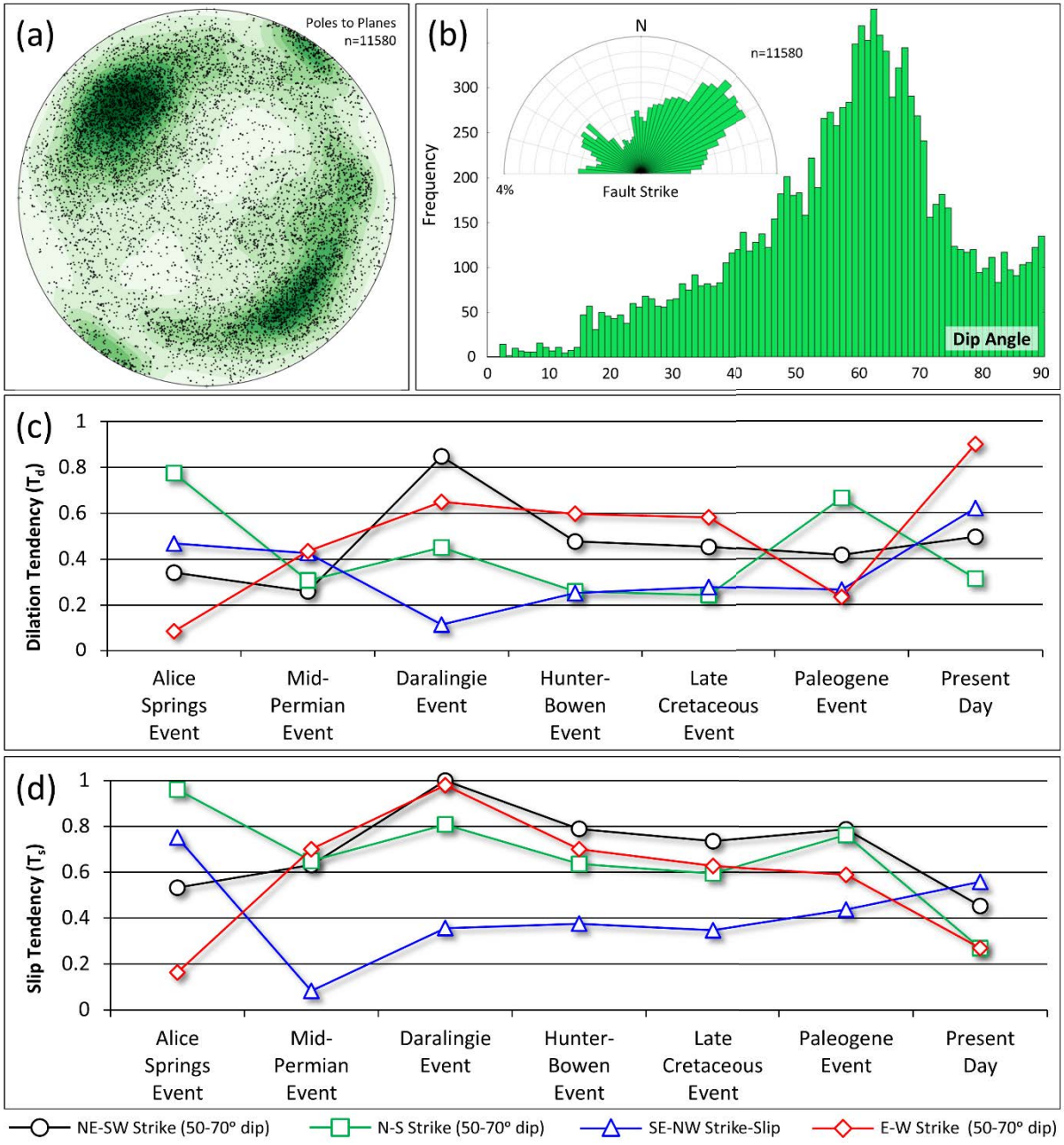

Figure 13. Fault geometry from six 3D seismic surveys (Dullingari 3D, Greater Tindilpie & Swan Lake 3D, Gidgealpa 3D, Greater Strzelecki 3D, Merrimelia (Ext) 3D, and Fly Lake 3D) presented as: (a) poles to planes; and (b) dip and strike (after Kulikowski & Amrouch, 2017a). Reactivation potential of the four most common fault sets measured using the: (c) Dilation Tendency; and (d) Slip Tendency (after Kulikowski & Amrouch, 2018b). See Figure 3 for location of 3D seismic surveys.

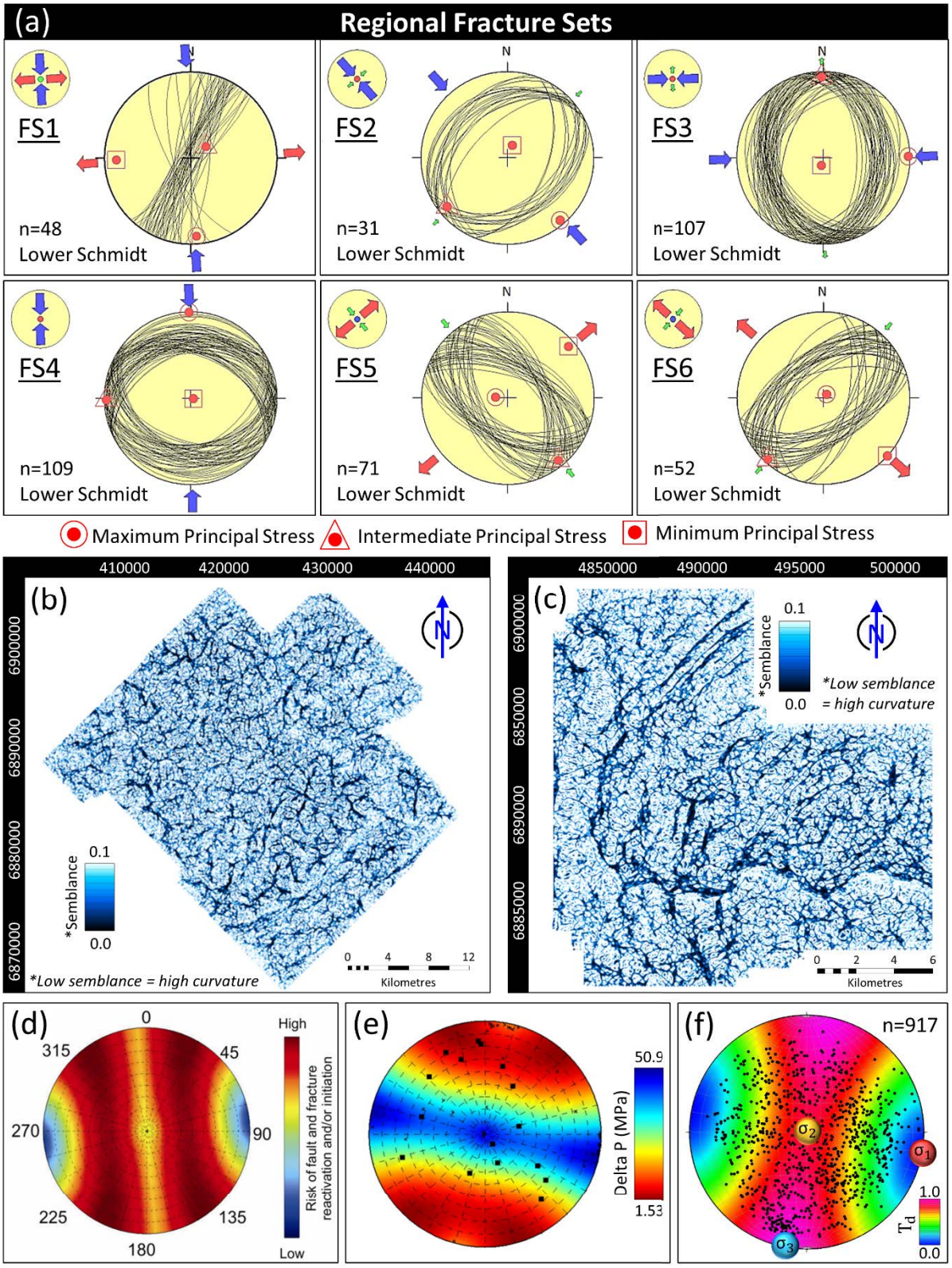

Figure 14. (a) Regional natural fracture sets (Kulikowski & Amrouch, 2017a). Most positive curvature processed into semblance in: (b) Moomba 3D; and (c) Dullingari 3D (Kulikowski et al., 2018a). In situ stress showing: (d) Fracture susceptibility (King et al., 2011); (e) Structural Permeability (Abul Khair et al., 2013); and (f) Dilation Tendency (T_d) (Kulikowski et al., 2017). See Figure 3b for location.

II

Appendix II: Posters and Presentations

In addition to the main body of work within this thesis, a number of spoken and poster presentations were given throughout the three years of candidature.

This poster was presented at the Australian Earth Sciences Convention conference in 2016.

PALEOSTRESS ORIENTATIONS FROM SUBSURFACE AND OUTCROP ANALYSIS IN THE OTWAY BASIN, AUSTRALIA. (Honours Project)

Hugo Burgin, Khalid Amrouch, Mojtaba Rajabi, Simon Holford
The Australian School of Petroleum, University of Adelaide, Adelaide, South Australia, Australia

1. GEOLOGICAL SETTING

Australia's southern, passive margin is believed to have undergone its first extensional event, during the breakup of the super continent Gondwana between 184-145 Ma. This initial phase of rifting is responsible for the formation of the en-echelon series of sedimentary basins straddling its coast line, eg: Bight, Otway and Gippsland. Separation began in the Western Bight Basin, during the Callovian (Mid-Late Jurassic), having propagated east towards the Otway Basin by the Tithonian.

The Otway Basin (Fig.1) is a linear, fault controlled graben that extends on and off shore from the eastern edge of the Duntroon Sub-Basin, south of Kangaroo Island (South Australia), to the western margin of the Bass Basin in Victoria and south into Tasmanian waters. The basin has experienced a number of tectonic events and is structurally complex.

The Structural evolution of the Otway Basin has been widely studied. Although this is the case there continues to be a large degree of uncertainty with respect to the nature of tectonic episodes that have shaped its development. Though many orientations and variations of structural evolution have been proposed, to date no quantitative mechanical data exists to quantify orientations and magnitudes of paleostress regimes within the Basin.

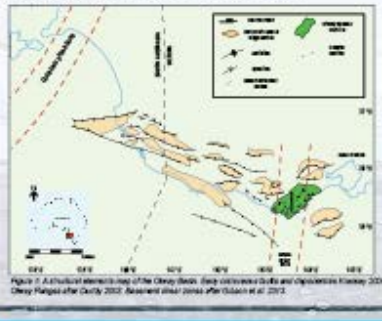

2. METHODOLOGY

The methodology for this study was comprised of a number of:

1) Borehole image log analysis for natural fractures and faults was undertaken within 10 on-shore petroleum wells within the Penola Trough, South Australia.

2) A series of outcrop studies based on identifying natural fracture patterns were completed over a three day field study within the Otway Ranges.

Once identified natural fractures were categorised into eight different sets based upon their degree of dip and dip direction, assigned a conjugate pair and a paleostress regime. Field and well data were analysed seperately using the classification scheme in Table 1.

Additionally, in-situ stress was also calculated using the interpretation of borehole breakouts (BOs) and drilling induced tensile fractures (DITFs).

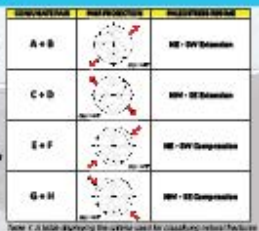

3. RESULTS

Evidence for up to 5 paleo tectonic events was detected from both image log and outcrop analysis (Table 2). No insight into the relative chronology of tectonic events was obtained from well analysis however outcrop studies did reveal that extension orientated NE-SW in all likelyhood preceeded extension orientated NW - SE supporting previous theories suggested by Pelmcek & Cockshell (1994) and Teasdale et al. (2003). This evidence can be seen in figure 6. Additionally both image log analysis and outcrop studies suggested the occurence of a NE - SW orientated compressional event, most likely during the mid - cretaceous. A paleostress regime that to date has not been documented.

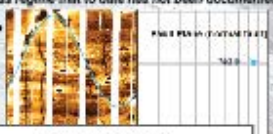

Figure 2: An example of an interpreted fault plane from the image log interpretation of Balnaves 1, within the Eumerella Formation. Displacement of stratigraphic horizons can be observed along the sinusoid.Fault orientation is consistent with NW - SE orientated extension.

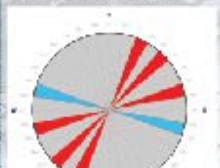

Figure 3: A lower hemisphere projection of identifiable faults from image log interpretation. RED strikes indicate normal faults, BLUE strikes indicate reverse faults.

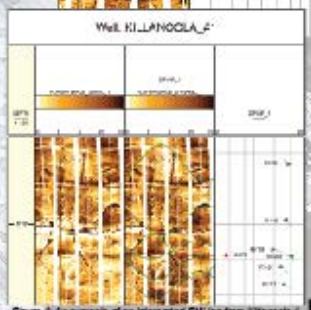

Figure 4: An example of an interpreted FMI log from Killanoola 1 within the Penola Trough, South Australia. Bedding planes appear as red sinusoids and fracture planes appears green sinusoids.

Table 2: A table displaying the orientations of detected paleo tectonic regimes within the specific formations of the study area.

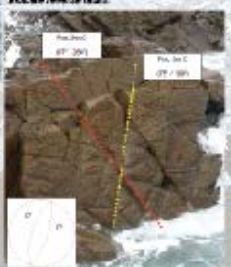

Figure 5: Conjugate fracture pair C and D observed in outcrop along the Great Ocean Road, together the pair form an almost perfect Andersonian example of extension. In this case the orientation of extension was interpreted as NW - SE.

Figure 6: A photograph from the field study showing fracture set C terminating upon fracture set B. From the classification used during this study, this observation implies that NE-SE orientated extension preceeded NW - SE orientated extension.

4. CONCLUSIONS

A number of conclusions can be drawn from the work conducted in this study:

1. Throughout its development the Otway Basin has experienced numerous and extended periods of extension with various orientations.

2. Initial extension within the Otway Basin may have been orientated NE - SW.

3. The Otway Basin may have experienced a compressional event orientated NE - SW during the mid - late Cretaceous Period.

4. Classifying natural fractures - via their degre of dip and dip direction- can provide a largreater insight into the structural evolution of the study area than simply analysing fracture data based upon strike and 2 dimensional orientation.

References

- Gibson, G. M., Totterdell, J. M., White, L. T., Mitchell, C. H., Stacey, A. R., Morse, M. P., & Whitaker, A. (2013). Pre-existing basement structure and its influence on continental rifting and fracture zone development along Australia's southern rifted margin. Journal of the Geological Society, 170(2), 365-377. doi: 10.1144/jgs2012-040
- Krassay, A. A., Cathro, D.L., Ryan, D.J. (2004). A Regional Tectonostratigraphic Framework for the Otway Basin. PESA Eastern Australian Basins Symposium II.
- Pelmcek, D., Cockshell, C. D., Finlayson, D. M., & Hill, R. A. (1994). The Otway Basin: Early Cretaceous Rifting to Miocene Strike Slip. Paper presented at the NOMA/PESA Otway Basin Symposium Abstracts.
- Teasdale, J. P., Ryan, L. L., Stuart-smith, P. G., & Lovibond, M. A. E. T. S. (2003). Structural framework and basin evolution of Australia's southern margin. The APPEA Journal, 43, 19-35.

This poster was presented at the European Geological Union conference in 2017.

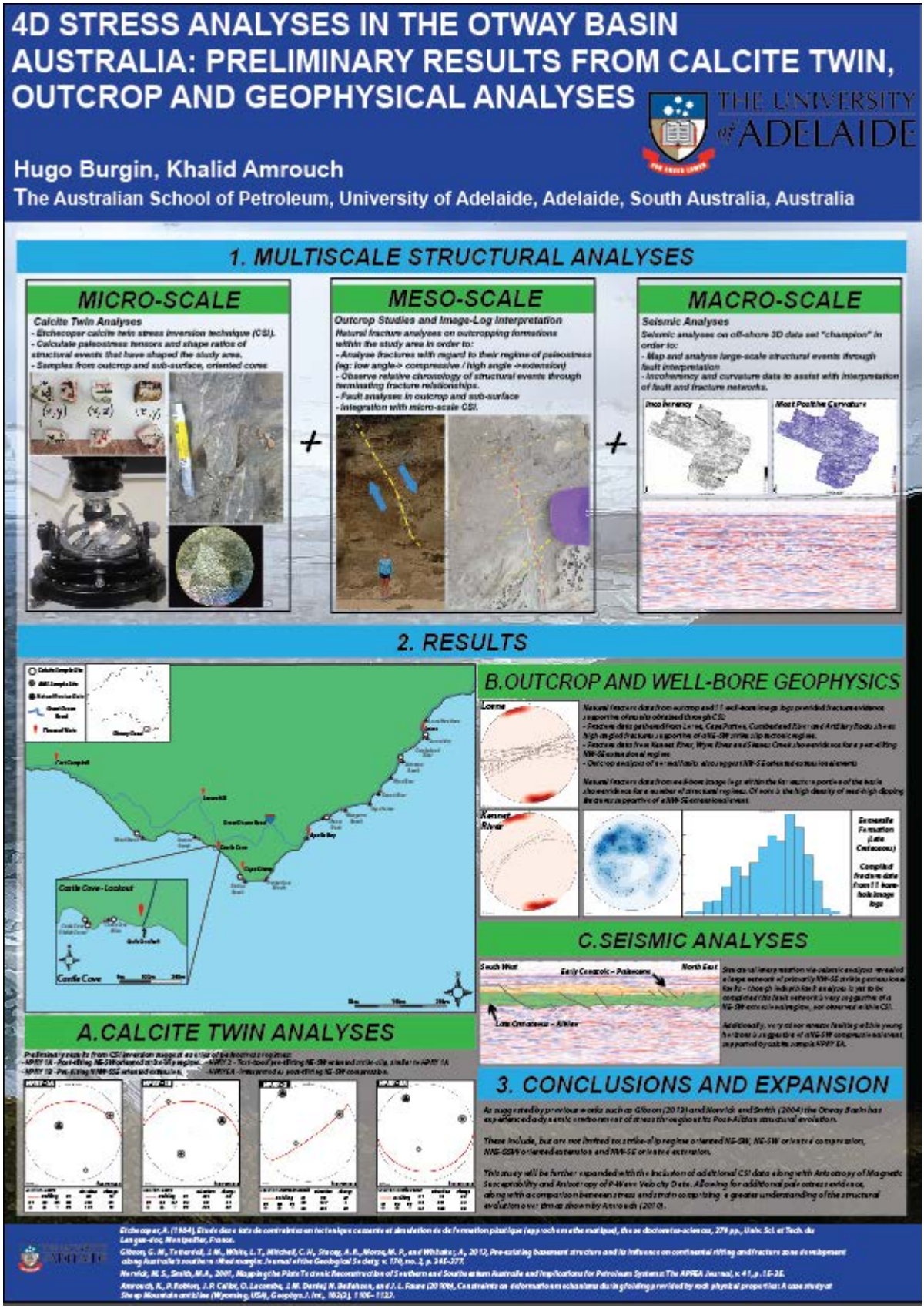

This poster accompanies manuscript 1 and was presented at the APPEA conference in 2018

Determining paleo-structural environments through natural fracture and calcite twin analyses: a case study in the Otway Basin, Australia

Hugo Burgin[1], Khalid Amrouch[1], Mojtaba Rajabi, David Kulikowski[2] and Simon P. Holford[1]

(1) The Australian School of Petroleum, University of Adelaide, Adelaide, South Australia, Australia, (2) Woodside Petroleum, Perth, Australia

Introduction

Paleo-stress inversion is performed on natural fractures and calcite twins from a dataset in the Otway Basin, Australia, to provide insights into the structural history and provide the first quantitative measurement of specific orientations of paleo-stress within the region. The Jurassic to Quaternary Otway Basin (Fig. 1) is a large NW–SE trending sedimentary basin that spans the onshore and offshore parts of South Australia, Victoria and offshore Tasmania. This basin contains hydrocarbon accumulations, geothermal energy potential, and CO2 storage capabilities, all of which require an understanding of subsurface natural fracture distributions and accurate basin development models. Current models show that initial rifting commenced during the Late Jurassic with multiple phases of extension and compression, responsible for the formation of stratigraphic and structural complexities (Norvick and Smith 2001). For the first time the meso- and micro-scale structural history of the Otway Basin is investigated through the 4D analysis of natural fractures obtained from geophysical well data located in the Penola Trough and from outcrop located in the Otway Ranges, with a calcite twin analysis performed on a sample obtained from the Otway Ranges. This study provides valuable information on the: (1) spatial distribution of natural fractures; (2) the temporal distribution of regional natural fracture sets; and (3) constraints on the stress orientation and regime of structural events.

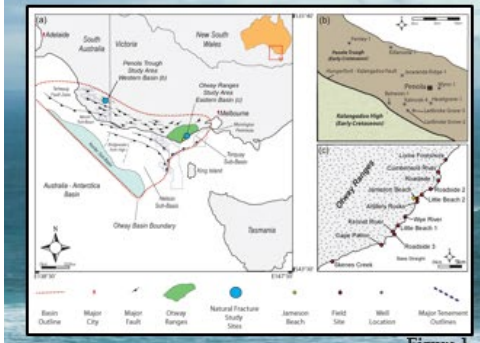

Figure 1

Fig. 1: (a) A map of Australia's southern margin showing the location of the Otway Basin, along with some major structural elements, after Moore et al. (2000) and Krassay et al. (2004). (b) Locations of sub-surface image logs in the Penola Trough. (c) Field sites in the Otway Ranges.

1. Natural Fracture Analysis

Within this study, our interpretation of natural fracture data is based upon the statistical analyses of fracture strike and dip angles, in combination with fracture-bedding relationships. Additionally, the principal stress orientation tool, Win-Tensor (Delvaux and Spemer 2003), was used to constrain the specific sets and assign regional directions of the three principal stresses. Our approach was based upon the fundamental principles of rock failure, with a heavy emphasis on the three Andersonian environments of stress (Anderson 1905) (Fig. 2). The geometry of these regional natural fracture sets are dependent on the relationship between the three principal stresses (σ1, σ 2 and σ 3) and the precise mode of fracturing (I, II or III). An understanding of these fracture geometries, in addition to their relationship with the bedding, allows us to gain insights into the likely stress environment responsible for their development and relative chronology. Results from our fracture analysis are presented in Fig. 3.

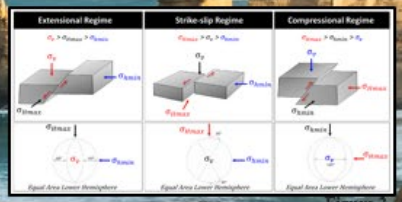

Figure 2

Fig. 2: A schematic diagram showing the three Andersonian stress environments (Anderson 1905) in addition to text book fracture sets formed under their conditions.

Fig. 3: Orientation of the major fracture sets categorised by dip degree and dip direction as part of this study. For well data, these sets include all detected fractures across all penetrated formations with image logs. Field data includes fractures from all 13 localities studied within the Eumeralla Formation. See Fig. 1 for location of wells and field sites.

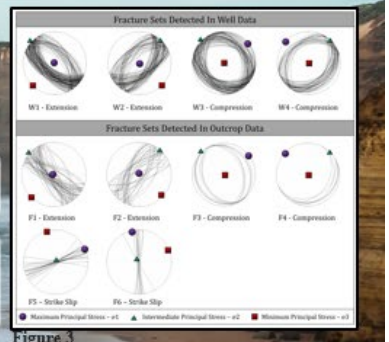

Figure 3

2. Calcite Twin Analysis

Mechanical twinning within calcite (Fig. 4) is a plastic deformation that occurs at low temperatures (25–400°C) and low confining pressures. The process of e-twinning – twinning along the 'e' plane of the crystal lattice – is easily compared with a zone of simple shear. The calcite twin stress inversion technique is similar to the technique used to analyse slickensides on a fault plane (Etcheconar, 1984). The technique consists of developing the best fit tensor for the distribution of twinned and un-twinned e-planes within the sample. Within this study, the use of calcite twin analysis is to: (1) compare the quantitative results with those from natural fracture analysis; and (2) test the regions suitability for more extensive calcite twin analysis. Two possible tensors were produced and are presented in Fig. 5.

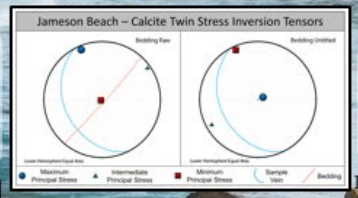

Figure 5

Fig. 5: Lower hemisphere equal area stereonet plots displaying the paleo-stress tensors derived from Etcheconar's (Etcheconar, 1984) calcite twin stress inversion technique (CSIT) measurements at Jameson Beach. See Fig. 1 for location.

Figure 4

Fig. 4: (a) A satellite image (Google Earth 2018) showing the orientation of the vertical bedding within a wave platform at Jameson Beach. The Great Ocean Road can be seen running past on the left (b) A photograph taken in the field showing the sampled vein at Jameson Beach in the Otway Ranges. (c) A universal stage microscope used to measure the spatial orientation of the twinned and un-twinned planes within the crystal and angles of extinction of the calcite crystals. (d) The calcite filled vein – in the Z orientation – from Jameson Beach. The sample is within the Eumeralla Formation

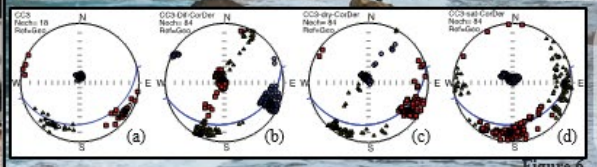

Figure 6

Fig. 6: An example of future work being completed within the basin. lower hemisphere equal area stereonet plots displaying petrophysical data. (a) An example of AMS tensors (b) Differential tensors for APV data (saturated – dry) conditions (c) Example of APV tensors measured with a dry sample (d) Example of APV tensors measured under saturated conditions.

3. Conclusions

Following the analysis of subsurface and outcrop natural fracture data, the structural evolution of both the western and eastern Otway Basin may be considerably more variable and complex than previously thought, especially from the Late Cretaceous until present, which is the most important window for hydrocarbon exploration and production.

- There is natural fracture evidence for multiple paleo-stress regimes including several episodes of extension, strike slip and compression many of them following the deposition of the Eumeralla formation in the Late Cretaceous.
- Calcite twin stress inversion presents two possible stress tensors which both align with natural fracture data
- Strike slip stress regimes may be unique to the eastern Otway Basin.
- Evidence for previously undetected compression oriented NE-SW.
- Calcite within the Eumeralla formation is spartic and well enough deformed presenting a good opportunity for further calcite twin stress inversion studies.

4. Future Work

This project is being expanded as part of a PhD at the Australian School of Petroleum. The goal of future work is to complete a multi-scale structural analysis of stress and strain within the study area. This includes:

- Additional and more detailed field studies within the region.
- The structural analysis of 2D and 3D seismic data within the basin.
- Additional calcite twin stress inversion from outcrop and subsurface samples.
- Petrophysical analysis (AMS and APV) in order to analyse grain-scale deformation (Fig. 6).
- Fault modelling and assessment of present day environments of stress.

References

- Anderson, E. (1905). The dynamics of faulting. The Journal of Geology 14, (3), 254-257.
- Delvaux, D., and Spemer, B. (2003). Stress tensor inversion from fault kinematic indicators and focal mechanism data: the TENSOR program. In New Insights into Structural Interpretation and Modelling (D. Nieuwland Ed.). Geological Society, London, Special Publications, 212: 75-100
- Etcheconar, A. (1984). Etude des états de contraintes en tectonique cassante et simulation de déformations plastiques (Ph.D these). Montpellier, France, Université Montpellier p. 270 p.
- Krassay, A. A., Cathro, D. L., Ryan, D.J. (2004). A Regional Tectonostratigraphic Framework for the Otway Basin. PESA EABS II
- Moore, A. M. G., Shiraj H. M. I. and Norvick M. S. (2000). Deep-water Otway Basin: A New Assessment of the Tectonics and Hydrocarbon Prospectivity. *The APPEA Journal, 40*, 66-85.
- Norvick, M. S., and Smith, M.A. (2000). Mapping the Plate Tectonic Reconstruction of Southern and Southeastern Australia and Implications for Petroleum Systems. The APPEA Journal, 41, 15-35.

This poster accompanies manuscript 2 and will be presented at the APPEA conference in 2019

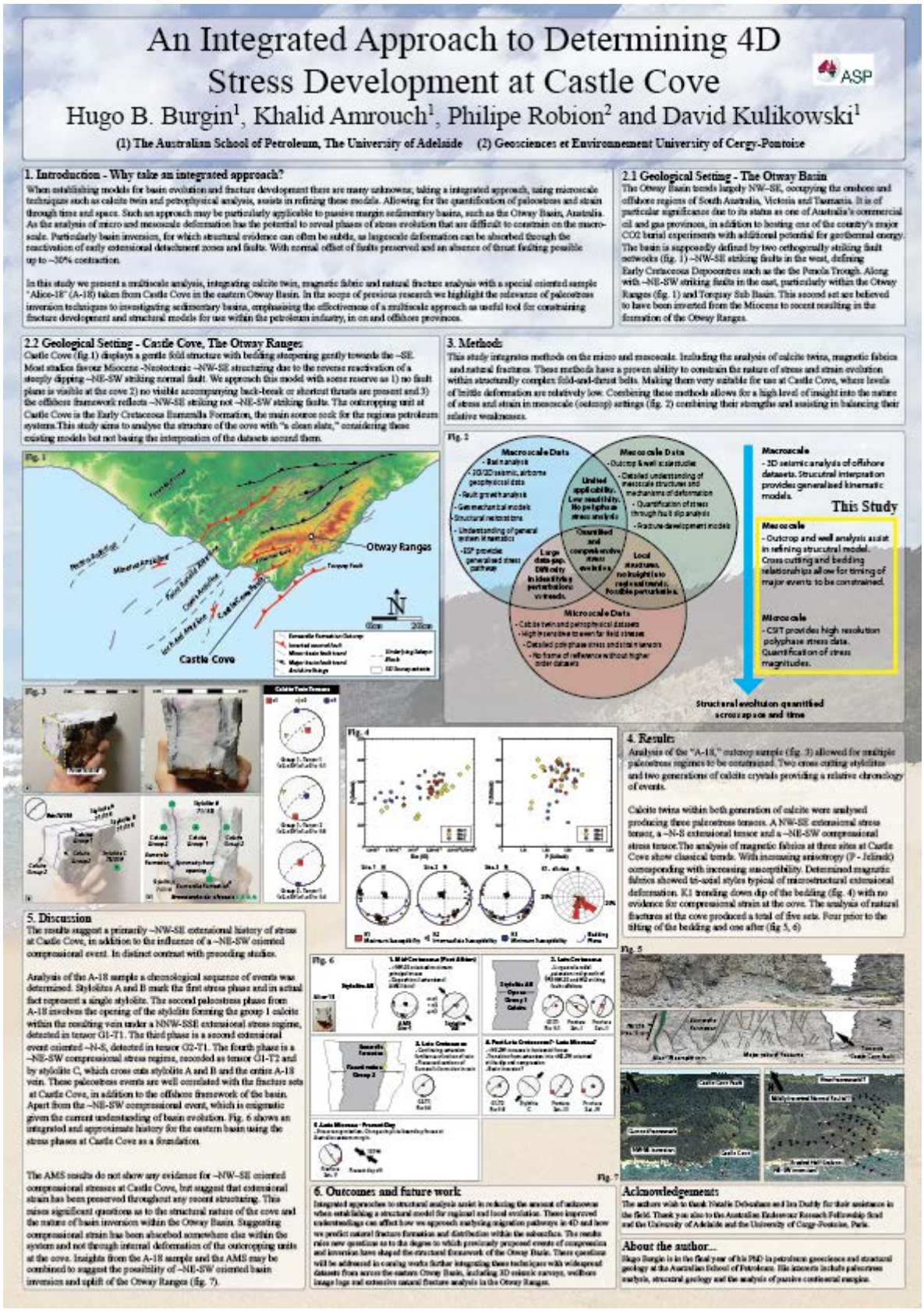

This poster accompanies manuscript 6 and will be presented at the European Geological Union conference in 2017

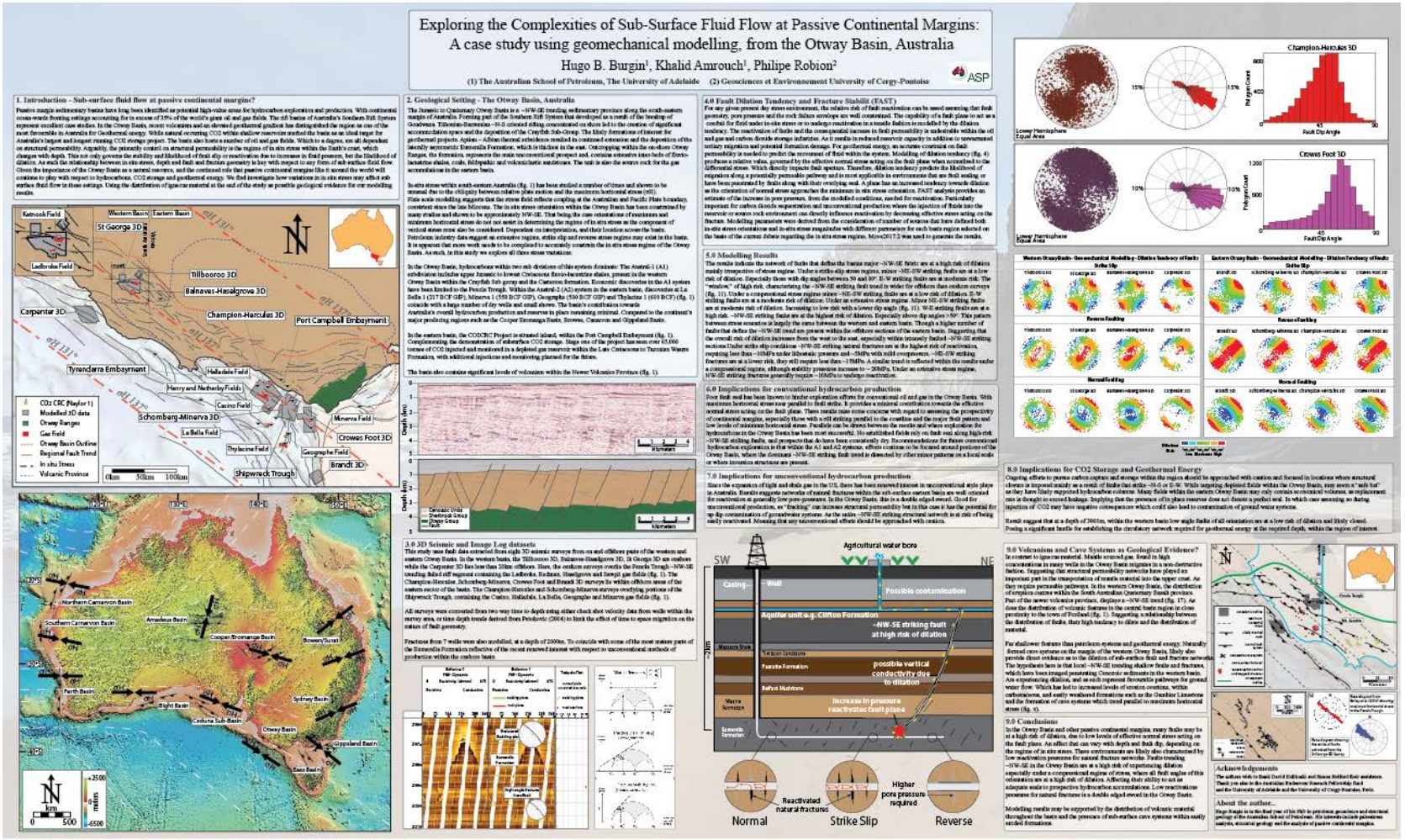

This spoken presentation was presented to colleagues at the Australian School of Petroleum as part of the requirements of the major review for candidature progression.

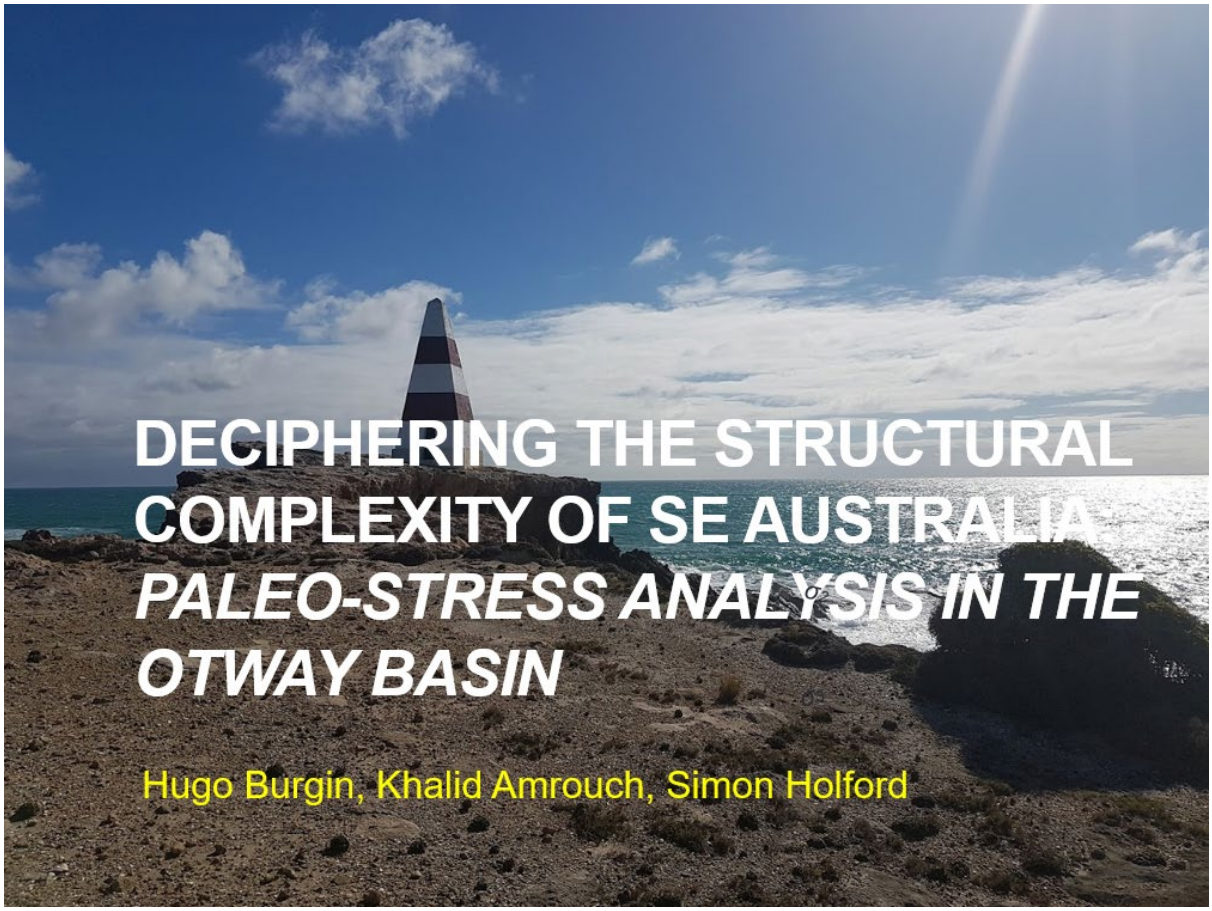

.

This spoken presentation was given to staff at Beach Energy as part of an efforts to actively involve the Australian oil and gas industry in this project.

Multi-Scale Structural Analyses in the Otway Basin

Hugo Burgin
Khalid Amrouch
Simon Holford

ASP
Australian School of Petroleum

THE UNIVERSITY of ADELAIDE

This spoken presentation was given to staff at ExxonMobil as part of the interview process for a secured position as a graduate geoscientist.

Hugo Burgin
Hugo.burgin@adelaide.edu.au

Structural Analyses and Paleo-Stress in the Otway Basin

adelaide.edu.au

ASP
Australian School of Petroleum